AD NUMBER
ADB010053
LIMITATION CHANGES
TO: **Approved for public release; distribution is unlimited.**
FROM: **Distribution authorized to U.S. Gov't. agencies only; Test and Evaluation; MAR 1976. Other requests shall be referred to Air Force Armament Laboratory, ATTN: AFATL/DLMA, Eglin AFB, FL 32543.**
AUTHORITY
USADTC ltr dtd 10 Dec 1979

AEDC-TR-75-125
AFATL-TR-76-23
cy. 1

A COMPILATION OF STATIC STABILITY AND FIN LOADS DATA FOR SLENDER BODY MISSILE MODELS WITH AND WITHOUT TAIL FINS AND WINGS

VOLUME I

PROPULSION WIND TUNNEL FACILITY
ARNOLD ENGINEERING DEVELOPMENT CENTER
AIR FORCE SYSTEMS COMMAND
ARNOLD AIR FORCE STATION, TENNESSEE 37389

March 1976

Final Report for Period March 1968 – March 1973

Distribution limited to U.S. Government agencies only; this report contains information on test and evaluation of military hardware; March 1976; other requests for this document must be referred to Air Force Armament Laboratory (AFATL/DLMA), Eglin Air Force Base, Florida 32543.

Prepared for

AIR FORCE ARMAMENT LABORATORY (AFATL/DLMA)
EGLIN AIR FORCE BASE, FLORIDA 32543

NOTICES

APPROVAL STATEMENT

This technical report has been reviewed and is approved for publication.

FOR THE COMMANDER

John R Taylor

JOHN R. TAYLOR
Analysis & Evaluation
Division
Directorate of Test

Craig E Mahaffy

CRAIG E. MAHAFFY
Colonel, USAF
Director of Test

REPORT DOCUMENTATION PAGE

READ INSTRUCTIONS BEFORE COMPLETING FORM

1. REPORT NUMBER AEDC-TR-75-125 AFATL-TR-76-23 / 2. GOVT ACCESSION NO.	3. RECIPIENT'S CATALOG NUMBER
4. TITLE (and Subtitle) A COMPILATION OF STATIC STABILITY AND FIN LOADS DATA FOR SLENDER BODY MISSILE MODELS WITH AND WITHOUT TAIL FINS AND WINGS - VOLUME I	5. TYPE OF REPORT & PERIOD COVERED Final Report - March 1968 - March 1973
	6. PERFORMING ORG. REPORT NUMBER
7. AUTHOR(s) G. R. Gomillion, ARO, Inc.	8. CONTRACT OR GRANT NUMBER(s)
9. PERFORMING ORGANIZATION NAME AND ADDRESS Arnold Engineering Development Center (XO) Air Force Systems Command Arnold Air Force Station, Tennessee 37389	10. PROGRAM ELEMENT, PROJECT, TASK AREA & WORK UNIT NUMBERS Program Element 62201F
11. CONTROLLING OFFICE NAME AND ADDRESS Air Force Armament Laboratory (AFATL/DLMA) Eglin Air Force Base, Florida 32543	12. REPORT DATE March 1976
	13. NUMBER OF PAGES 534
14. MONITORING AGENCY NAME & ADDRESS (if different from Controlling Office)	15. SECURITY CLASS. (of this report) UNCLASSIFIED
	15a. DECLASSIFICATION/DOWNGRADING SCHEDULE N/A

16. DISTRIBUTION STATEMENT (of this Report) Distribution limited to U.S. Government agencies only; this report contains information on test and evaluation of military hardware; March 1976; other requests for this document must be referred to Air Force Armament Laboratory (AFATL/DLMA), Eglin Air Force Base, Florida 32543.

17. DISTRIBUTION STATEMENT (of the abstract entered in Block 20, if different from Report)

2 Wing bodies -- Stability
3 missiles -- "
4 Fins -- Loads - 5. Control surfaces -

18. SUPPLEMENTARY NOTES

Available in DDC; complete report consists of five volumes.

1.

19. KEY WORDS (Continue on reverse side if necessary and identify by block number)

Martin Generalized Research Model	slender bodies
tables(data)	static stability
guided missiles	fins
models	aerodynamic loading
wing body configurations	control surfaces (Continued)

20. ABSTRACT (Continue on reverse side if necessary and identify by block number)

This document contains a compilation of aerodynamic data for the Martin Generalized Research Model, which is a composite of several body, wing, and tail fin configurations typical of missile applications. The model variations included five body configurations, three wing configurations at various body locations, and 15 tail fin configurations. Static stability and tail fin loads data are presented in tabulated and plotted form for a Mach number range

DD FORM 1 JAN 73 1473 EDITION OF 1 NOV 65 IS OBSOLETE

19. KEY WORDS (Continued)

deflection
transonic flow
supersonic flow
wind tunnel tests

20. ABSTRACT (Continued)

from 0.20 to 4.63 over an angle-of-attack range from -6 to 60 deg and a sideslip angle range from -20 to 20 deg for the body-alone configurations, body-wing configurations, and the body-wing-tail fin configurations. In addition, the tail fin configurations were tested using the reflection plane technique, and the resulting fin loads data are presented for a Mach number range of 0.80 to 2.16 over an angle-of-attack range from 0 to 210 deg. Volume I contains the narrative and selected plotted data.

AFSC
Arnold AFS Tenn

PREFACE

The data presented herein were compiled by the Arnold Engineering Development Center (AEDC), Air Force Systems Command (AFSC), under the sponsorship of the Air Force Armament Laboratory (AFATL), Eglin Air Force Base, Florida. Seven different tests were conducted by three organizations: ARO, Inc. (a subsidiary of Sverdrup & Parcel and Associates, Inc.), contract operator of the AEDC, AFSC, Arnold Air Force Station, Tennessee; Naval Ship Research and Development Center (NSRDC), Bethesda, Maryland; and Langley Research Center (LRC), National Aeronautics and Space Administration (NASA), Langley Air Force Base, Virginia. The data were compiled under ARO Project No. P34A-37A. The author of this report was G. R. Gomillion, ARO, Inc. The manuscript (ARO Control No. ARO-PWT-TR-75-88) was submitted for publication on June 20, 1975.

CONTENTS

ILLUSTRATIONS

Figure | Page

Figure | Page

Figure | Page

TABLES

APPENDIXES
(Under Separate Cover)

1.0 INTRODUCTION

In order to give wider dissemination to the aerodynamic data obtained for the Martin Generalized Research Model at the Arnold Engineering Development Center (AEDC), Aerodynamic Wind Tunnel (4T); the NASA Langley Research Center (LRC), Unitary Plan Wind Tunnel (UPWT); and the Naval Ship Research and Development Center (NSRDC), 7 x 10 Foot Transonic Wind Tunnel (7 x 10), for seven tests during the period March 1968 through March 1973; the Air Force Armament Laboratory (AFATL), Eglin Air Force Base, Florida, requested that AEDC collect, correlate, and publish the data in a consistent format. The basic purpose of this report is to document and catalog all of the valid data obtained on the research model during these tests. For the seven tests, the test facilities and dates are as follows:

Test Number	Facility	Date
1	AEDC-4T	December 1970
2	AEDC-4T	May 1972
3	LRC-UPWT	March 1968
4	LRC-UPWT	April 1970
5	LRC-UPWT	July 1971
6	NSRDC-7X10	October 1968
7	NSRDC-7X10	March 1973

The purpose for testing the Martin Generalized Research Model was to provide data to improve missile aerodynamic methodology and fin design capability. In pursuing the purpose of the testing, the effects of body shape, wing size, wing location, and tail fin planform were investigated. In addition, tail fin loads were measured for various fin deflections with the fins mounted on missile configurations and on a reflection plane. Other studies on the research model included the effects of Reynolds number and of fixing transition. The results of several of the investigations are discussed in Ref. 1 (Test No. 1), Ref. 2 (Test No. 2), Ref. 3 (Test No. 6), and Ref. 4 (Test No. 1), and in addition some of the data presented in this report were included in Ref. 5.

The compiled data in this report are documented with a large portion of the data in plotted form and all the data in tabulated form. Additionally, it should be noted that not all the data obtained on the research model for the seven tests between March 1968 and March 1973 are presented. The data not presented were, for various reasons, believed to be invalid.

Static stability and fin loads data are presented for a Mach number range from 0.20 to 4.63 over an angle-of-attack range from -6 to 60 deg and a sideslip angle range from

-20 to 20 deg for body, body-wing, body-tail, and body-wing-tail configurations. Additional tail fin loads data from the reflection-plane tests are presented for a Mach number range from 0.80 to 2.16 and an angle-of-attack range from 0 to 210 deg.

2.0 APPARATUS

2.1 TEST FACILITIES

2.1.1 Arnold Engineering Development Center (AEDC), Aerodynamic Wind Tunnel (4T)

The AEDC-4T tunnel is a closed-loop, continuous flow, variable-density tunnel in which the Mach number can be varied from 0.1 to 1.3. Also, nozzle blocks can be installed to give nominal Mach numbers of 1.6 and 2.0. At all Mach numbers, the stagnation pressure can be varied from 2 to 26 psia. The test section is 4 ft square and 12.5 ft long with perforated, variable porosity (0.5- to 10-percent open) walls. It is completely enclosed in a plenum chamber from which the air can be evacuated, allowing part of the tunnel airflow to be removed through the perforated walls of the test section.

The model support system consists of a pitch sector, boom, and sting which provide a pitch capability from -11 to 28 deg with respect to the tunnel centerline. The center of rotation is at station 108. In addition, a remote-controlled roll mechanism allows roll angle variations of ±180 deg. A schematic of the test section showing the location of the test model for test No. 1 is shown in Fig. 1. Photographs of the model installation for tests No. 1 and 2 are shown in Fig. 2. A more thorough description of the tunnel may be found in Ref. 6.

2.1.2 Langley Research Center (LRC), Unitary Plan Wind Tunnel (UPWT)

The Unitary Plan Wind Tunnel is a closed-circuit, continuous flow, variable-density, asymmetric sliding-block-type tunnel consisting of two test sections. In one of the test sections the Mach number can be varied from 1.47 to 2.86 and the stagnation pressure can be varied from 3 to 51 psia, whereas for the other test section the Mach number can be varied from 2.29 to 4.63 and the stagnation pressure can be varied from 3 to 142 psia. Each test section is 4 ft square and 7 ft long.

The model support system consists of a pitch sector, boom, and sting which provide a pitch capability from -20 to 20 deg with respect to the tunnel centerline. The center of rotation is located in the test section and may be adjusted over a limited longitudinal range. A more thorough description of the tunnel may be found in Refs. 7, 8, and 9.

2.1.3 Naval Ship Research and Development Center (NSRDC), 7 by 10 Foot Transonic Wind Tunnel (7 x 10)

The NSRDC 7 by 10 Foot Transonic Wind Tunnel is a closed-loop, continuous flow, variable-density tunnel in which the Mach number can be varied from 0.40 to 1.17. The tunnel stagnation pressure can be varied with Mach number and the variation depends on Mach number. The tunnel stagnation pressure range is 4 to 26 psia. The test section is rectangular and measures 7 ft in height, 10 ft in width, and 19 ft in length. The test section is enclosed in a pressure-tight chamber. The floor and ceiling of the test section are slotted and have diffuser flaps at the end of each slot to control flow entry and Mach number.

The model support system consists of a pitch-sideslip sector, boom, and sting which provide remote-control capability in pitch, sideslip, and roll of from -4 to 29 deg, -25 to 25 deg, and -180 to 180 deg, respectively. A more thorough description of the tunnel may be found in Refs. 10, 11, and 12.

2.2 TEST ARTICLES

The test articles, which were furnished by the Martin Marietta Corporation, consisted of five body configurations, three wing configurations, and 15 tail fin configurations. Dimensional sketches in Figs. 3 and 4 show the body and wing configurations, respectively. Photographs of the tail fins are shown in Fig. 5 and tail fin dimensions are shown in Fig. 6. Both wings and tail fins were modified double-wedge airfoils, with leading- and trailing-edge semivertex angles of 4 deg. and slightly rounded (0.015-in. radius) edges. All model dimensions shown in the sketches and used in the data reduction were obtained from the original model drawings; however, when the dimensions of the tail fins were measured, they were, in several cases, different from the drawings. The measured tail fin dimensions are presented in Table 1 for all fins of each tail fin configuration.

For the wing-body configurations, the wings were mounted in the horizontal plane of symmetry with the length, L, defining the axial distance between the model nose and the intersection of the wing leading edge with the body. The tail fins were mounted on the missile body with the four fins in a "plus," cruciform pattern. The tail fins were positioned such that the trailing edge of each fin was in the plane of the model base. The fins could be manually adjusted for deflection angles of 0, ±10, ±20, and ±30 deg.

The tail fins were tested singly mounted on a splitter plate using the reflection plane technique. Sketches and a photograph are presented in Figs. 7 and 8 showing the splitter plate tunnel installation for test No. 2. For test No. 2, the splitter plate included a drive mechanism, shown in Fig. 9, which allowed the fin angle to be changed remotely. This assembly contained a provision for indicating discrete fin angles of 0, 15, 30, 60, 90, 120, 150, and 180 deg. For each discrete fin angle set, the pitch sector angle was varied to obtain the desired angle of attack.

2.3 INSTRUMENTATION

Aerodynamic loads on the complete model were measured with main, six-component, internal, strain-gage balances. In most instances when six-component balance data were obtained, there were four additional three-component, internal, strain-gage balances mounted in the rear section of the model body and used to measure the aerodynamic loads on each tail fin. During the test with the reflection plane, a three-component, strain-gage balance was used to obtain tail fin loads data. For all six-component balance tests one or more base pressures and/or cavity pressures were measured.

3.0 PRESENTATION OF RESULTS

3.1 GENERAL

All main balance data presented have been reduced to coefficient form in the nonrolling axis system. An exception is test No. 6 data which were reduced to coefficient form in the body axis system. When the tail fins are mounted on the missile body, the tail fin data are in an axis system parallel to the missile body axis system; hence, the tail fin normal-force coefficient is based on the force normal to the chordwise plane of the undeflected tail fin, whereas the root bending- and hinge-moment coefficients are referenced to the undeflected tail root chord and hinge lines, respectively. When the tail fin is mounted on the reflection plane, the tail fin data are in the body axis system. All data are correlated into a consistent format with the positive directions of coefficients as shown in Fig. 10. The positive tail fin deflection angles are defined as follows with respect to the unrolled model: tail fins No. 2 and 4, leading edge up; and tail fins No. 1 and 3, leading edge to the right, looking upstream. It should be noted that the tail fin dimensions used in the data reduction are those shown in Fig. 6. The moment reference point (MRP) for the main balance data is located on the body centerline at 50 percent of the model length, and the moment reference point for the fin data is the intersection of the fin hinge line and the fin root chord.

The uncertainties associated with the measured tunnel conditions and aerodynamic coefficients are not available for all the tests. In Tables 2 and 3 are presented the maximum data uncertainties quoted in Refs. 1 and 3 for tests No. 1 and 6, respectively. In Tables 4, 5, and 6, the data uncertainties quoted in Ref. 2 for test No. 2 are presented.

Complete tabulated data are presented in Appendixes A through G, and selected data are presented in plotted form in Figs. 11 through 66. Indexes of the data are presented in Tables 7 through 13. Also, brief discussions of the results of each test are presented in Sections 3.2 through 3.8. The tabulated data, plots, indexes, and discussion are arranged according to test numbers, as identified in Section 1.0.

The indexes list the configurations and the pertinent parameters for each test. The configuration code corresponds to the body, wing, and fin designations of Figs. 3 through 6, with the addition of the notation B0, W0, and F0 to denote absence of the body, wings, or fins, respectively, for the particular configuration. For each test, the data are indexed according to part number. A circled part number in Tables 7 through 13 indicates that data for that part number are presented in plotted form.

The tabulated data presented in the Appendixes include complete data for all part numbers listed in Tables 7 through 13. The data are ordered according to test number and part number, and within each part number, point numbers are used. Reference should be made to the Nomenclature for the definitions of the symbols. Values of coefficients of 9.9999 are used in the tabulations to indicate deletions of erroneous data.

The plots presented in Figs. 11 through 66 were selected to show basic and typical trends. For convenience and for comparison purposes, data for several part numbers are presented on each page, and therefore, the index of figures, at the beginning of the report, should be used to find plotted data of interest.

The data were machine plotted using a curve-fit fairing between data points for tests No. 1 through 5 except for the splitter plate data of test No. 2 which were not faired. Tests No. 6 and 7 data were machine plotted using straight-line fairings between data points. It should also be noted that to improve the quality of production of the plots several data points were deleted from the plots on all the tests. Additionally, all test data, except splitter plate data of test No. 2, and all data of test No. 7, were symboled on every fifth consecutive point. In the case of test No. 2 splitter plate data, only every tenth consecutive point was plotted, and symboled, and in the case of test No. 7 every tenth consecutive point was symboled. In some cases, particularly tests No. 6 and 7, the curves have a rather random appearance because of the scatter and high density of the original data points.

3.2 TEST NUMBER 1

Plotted data for test No. 1 are presented in Figs. 11 through 15, the tabulated data are presented in Appendix A, and the part number summary is presented in Table 7. In test No. 1, data were obtained on the main balance, the four tail fin balances, and the splitter plate balance, but only the main balance data are presented in this report.

The test was conducted in the AEDC-4T Tunnel at a nominal Reynolds number per foot of 2.3 x 10^6. The Mach number range was from 0.8 to 1.3 and the angle-of-attack range was from -3 to 32 deg. Roll angle was not varied and the tail fins were not deflected. Twelve tail fin configurations were tested on the missile body, and body-alone data were obtained for three body configurations.

The details of fixing transition on this test are unknown. In order to provide forebody axial-force coefficients, pressures were measured at two locations at the base of the model and averaged to yield the model base pressure. Some data analysis and additional plotted data can be found in Refs. 1 and 4.

3.3 TEST NUMBER 2

Test No. 2 plotted data are presented in Figs. 16 through 23, the tabulated data are presented in Appendix B, and the part number summary is presented in Table 8. For test No. 2, data are presented for the main balance as well as the four tail fin balances and the splitter plate balance.

The test was conducted in the AEDC-4T Tunnel at a nominal Reynolds number per foot of 2.5 x 10^6. The Mach number range was from 0.80 to 1.30. There were five tail fin configurations tested on the missile body and three tail fin configurations tested on the splitter plate. The angle-of-attack range for the missile was from -2 to 30 deg with the tail fins undeflected throughout the test. The angle-of-attack range of the tail fins mounted on the splitter plate was from 0 to 210 deg.

In addition, a Reynolds number study was conducted using the missile body without tail fins and with tail fins and longitudinal transition strips. With the finned missile configuration, data were obtained with 1/8-in.-wide, No. 60 Carborundum® grit strips along the length of the constant diameter section of the missile body (aft of the missile nose section) equally spaced between the fins on the lee side of the model (Fig. 2c). During this study, the Reynolds number per foot was varied from 0.3 x 10^6 to 4.9 x 10^6 at a Mach number of 0.59.

The pressure was measured at two locations at the base of the missile body and averaged to yield the model base pressure. Some data analysis and additional plotted data can be found in Ref. 2.

3.4 TEST NUMBER 3

Test No. 3 plotted data are presented in Figs. 24 through 27, the tabulated data are presented in Appendix C, and the part number summary is presented in Table 9. For test No. 3, data are presented for the main balance only.

The test was conducted in the LRC-UPWT at a nominal Reynolds number per foot of 3.0×10^6 except as noted. The Mach number was varied from 2.36 to 4.63 and the angle of attack was varied from -4 to 24 deg at model roll angles of 0 and 45 deg. The tail fin deflections were 0 and 20 deg for tail fins No. 1 and 3 and 0 and -20 deg for tail fins No. 2 and 4. There were three tail fin configurations and one wing configuration tested. In addition, data are presented for the case of the tail fins removed.

For all the data, transition was fixed with a 1/16-in.-wide strip of No. 40 sand located 1.2 in. aft of the body nose and 0.4 in. streamwise aft of the tail fin and wing leading edges.

The model cavity pressure was measured and used for the base pressure. In addition, the model orientation was corrected for tunnel flow angularity.

3.5 TEST NUMBER 4

Test No. 4 plotted data are presented in Figs. 28 and 29, the tabulated data are presented in Appendix D, and the part number summary is presented in Table 10. For test No. 4, data are presented for the main balance only.

The test was conducted in the LRC-UPWT at a nominal Reynolds number per foot of 3.0×10^6 except where noted. The Mach number range was from 2.36 to 4.63 and the angle-of-attack range was from -5 to 22 deg at model roll angles of 0 and -90 deg. The tail fin angle deflections were 0 and 20 deg for tail fins No. 1 and 3 and 0 and -20 deg for tail fins No. 2 and 4. There were six tail fin configurations tested.

For all the data, transition was fixed with single-spaced No. 40 sand particles located 1.2 in. aft of the model nose and 0.4 in. streamwise aft of the tail fin leading edges. The pressure was measured at two locations at the base of the missile body and averaged to yield the model base pressure. Also the pressure in the model cavity was measured. The base and cavity pressures were used to compute the forebody axial-force coefficient. In addition, the model orientation was corrected for tunnel flow angularity.

3.6 TEST NUMBER 5

Test No. 5 plotted data are presented in Figs. 30 through 32, the tabulated data are presented in Appendix E, and the part number summary is presented in Table 11. For test No. 5, data are presented for the tail fin configurations mounted on a splitter plate.

The test was conducted in the LRC-UPWT for a Mach number range from 1.50 to 2.16 and an angle-of-attack range from -6 to 28 deg. Ten tail fin configurations were tested on the splitter plate. For all the data, transition was fixed with a 1/16-in.-wide strip of No. 60 sand located 0.4 in. streamwise aft of the fin leading edge.

3.7 TEST NUMBER 6

Test No. 6 plotted data are presented in Figs. 33 through 38, the tabulated data are presented in Appendix F., and the part number summary is presented in Table 12. For test No. 6, data are presented for the main balance as well as the four tail fin balances. It should be noted that C_A and C_{A_B} were not available from test No. 6.

The test was conducted in the NSRDC 7 X 10 tunnel at the nominal Reynolds number per foot of 1.7×10^6. The Mach number was varied from 0.85 to 1.10. The angle of attack was varied from -3 to 31 deg and the sideslip angle from -20 to 20 deg. There were three tail fin configurations and three wing configurations tested. The deflections for tail fins No. 1 and 3 were 0, 10, 20, and 30 deg. Tail fins No. 2 and 4 were not deflected. In addition, body-alone data were obtained.

Transition was fixed, as noted in Ref. 3, with No. 90 grit located 1.0 in. aft of the tail fin and wing leading edges. Some data analysis and additional plotted data can be found in Ref. 3.

3.8 TEST NUMBER 7

Test No. 7 plotted data are presented in Figs. 39 through 66, the tabulated data are presented in Appendix G, and the part number summary is presented in Table 13. For test No. 7, data were obtained on the main balance as well as the four tail fin balances.

The test was conducted in the NSRDC 7 X 10 tunnel at a nominal Reynolds number per foot of 1.7×10^6. The Mach number range was from 0.80 to 1.10 and the angle-of-attack range was from -6 to 60 deg at model roll angles of 0 and 45 deg. The deflections for tail fins No. 1 and 3 were zero, and the deflections for tail fins No. 2 and 4 were 0, -10, -20, and -30 deg. There were seven tail fin configuations tested on the missile body configuration. In addition, body-alone data were obtained.

Whether or not the transition was fixed on this test is unknown. Base pressure measurements were obtained.

REFERENCES

1. Smith, D. K. and German, R. C. "Aerodynamic Characteristics of Low Aspect Ratio Fins at Mach Numbers from 0.80 to 1.30." AEDC-TR-71-74 (AD882989L), April 1971.

2. Whoric, J. M. "Aerodynamic Characteristics of Several Low Aspect Ratio Stabilizer Fins at Mach Numbers from 0.8 to 1.3." AEDC-TR-72-143 (AD903806L), September 1972.

3. Wilkin, F. D. "Missile Tail Effectiveness in Transonic Flow." Master's Thesis, West Virginia University, 1969.

4. Mottinger, T. A. and Washington, W. D. "An Experimental Investigation of Low Aspect Ratio Fins Tested at Transonic Speeds on a Reflection Plane." U.S. Army Missile Command Report No. RD-TM-71-15, July 1971.

5. Fidler, J. E. and Bateman, M. C. "Aerodynamic Methodology (Isolated Fins and Bodies)." U.S. Army Missile Command OR12399, March 1973.

6. Test Facilities Handbook (Tenth Edition). "Propulsion Wind Tunnel Facility, Vol. 4." Arnold Engineering Development Center, May 1974.

7. Manual for Users of the Unitary Plan Wind Tunnel Facilities of the National Advisory Committee for Aeronautics. "The Langley Unitary Plan Wind Tunnel." 1956.

8. Schaefer, W. T., Jr. Characteristics of Major Active Wind Tunnels at the Langley Research Center. "Langley Unitary Plan Wind Tunnel." NASA TMX-1130, July 1965.

9. Pirrello, C. J., Hardin, R. D., Heckart, M. V., and Brown, K. R. An Inventory of Aeronautical Ground Research Facilities, Volume I - Wind Tunnels. "NASA Langley Research Center - Unitary Plan Wind Tunnel." NASA CR-1874, November 1971.

10. Thomas, W. S. "The David Taylor Model Basin 7- by 10-Foot Transonic Wind Tunnel Facility." AERO Report 985, July 1960.

11. Fresh, J. N. The Aerodynamics Laboratory (The First 50 Years). "7- by 10-Foot Transonic Wind Tunnel." AERO Report 1070, January 1964.

12. Pirrello, C. J., Hardin, R. D., Heckart, M. V., and Brown, K. R. An Inventory of Aeronautical Ground Research Facilities, Volume I - Wind Tunnels. "Naval Ship Research and Development Center - 7-Foot by 10-Foot Transonic Wind Tunnel." NASA CR-1874, November 1971.

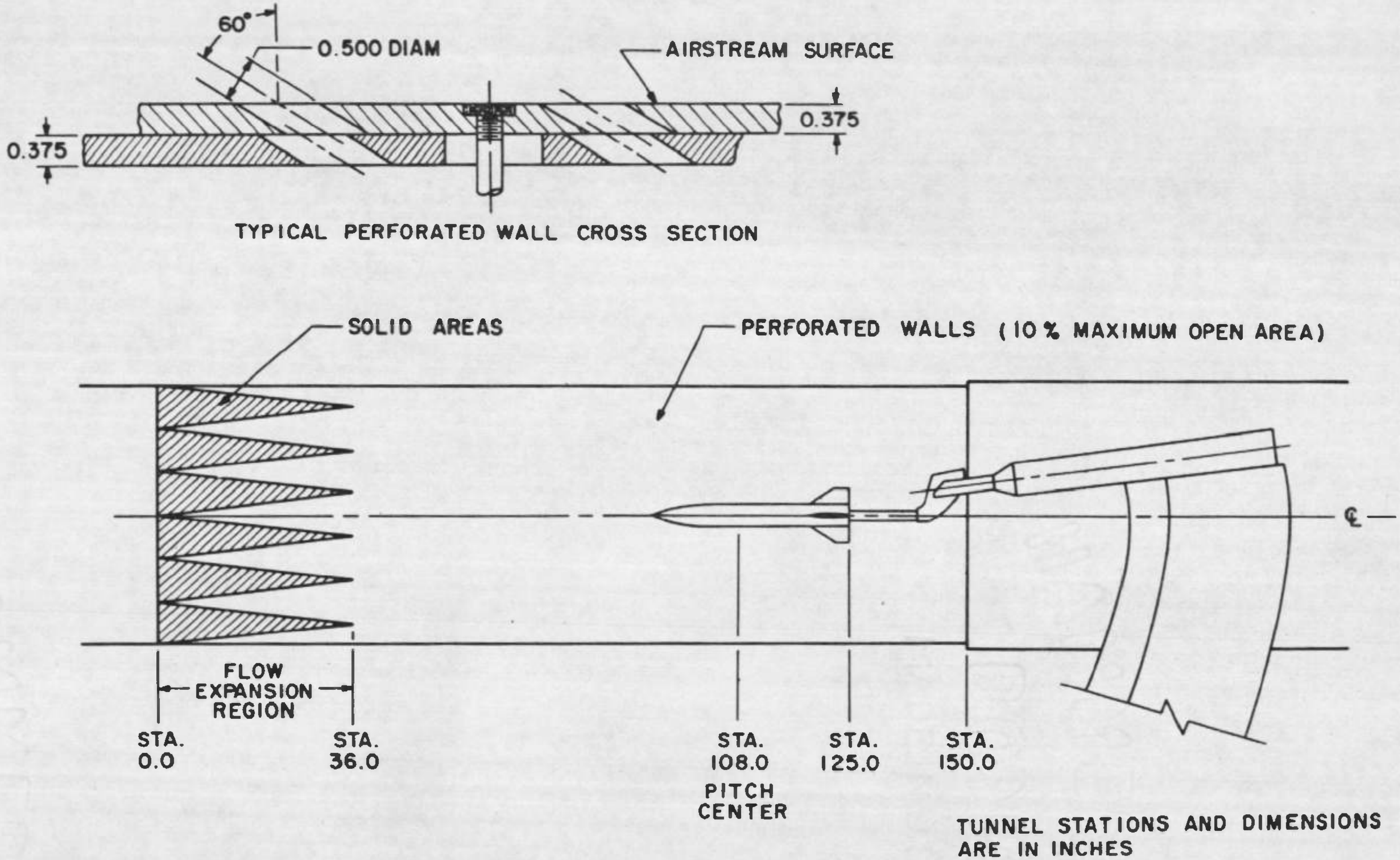

Figure 1. Sketch of test No. 1 model installation.

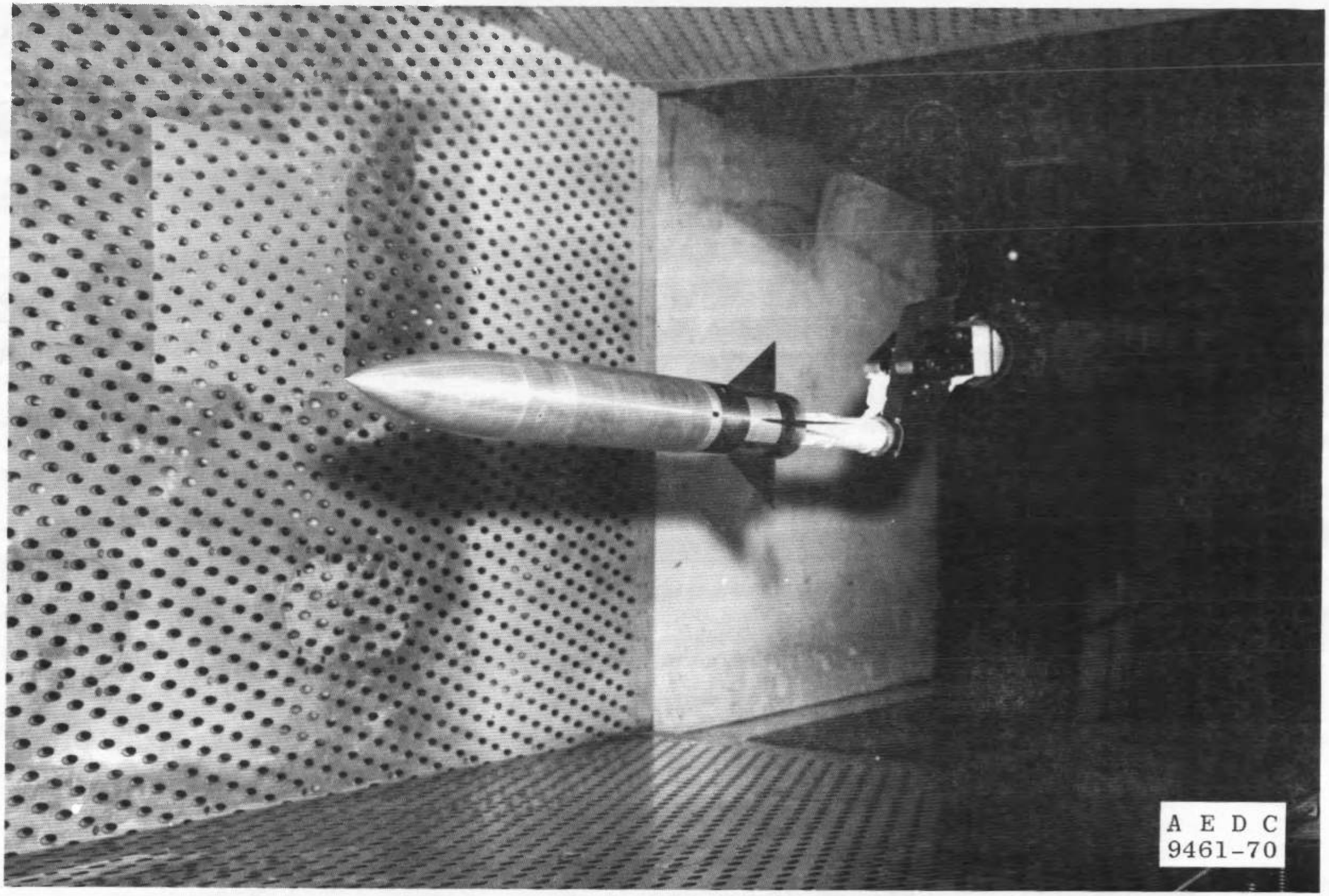

a. Test No. 1, front quarter view
Figure 2. Photographs of model installation in Tunnel 4T.

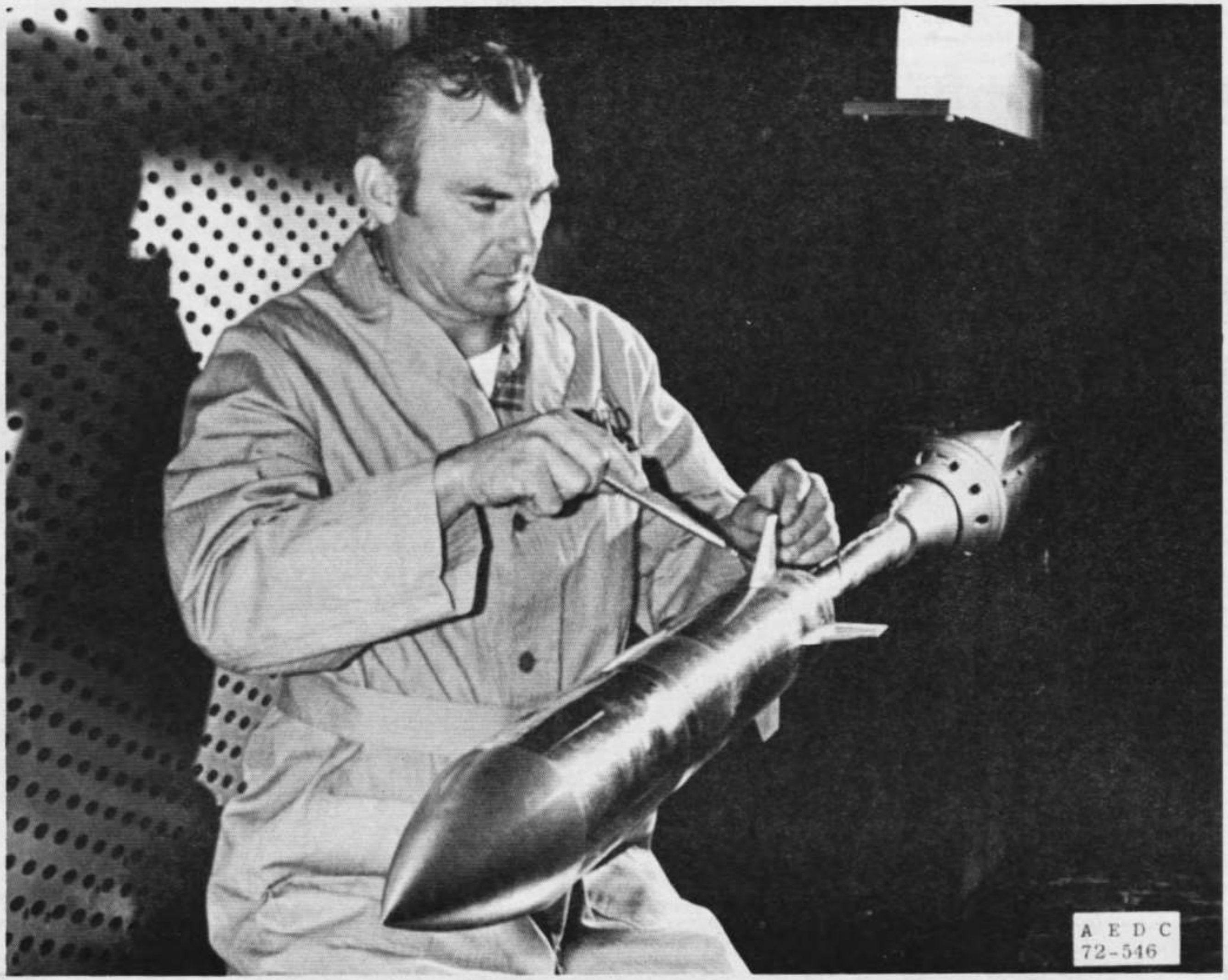

b. Test No. 2, front quarter view
Figure 2. Continued.

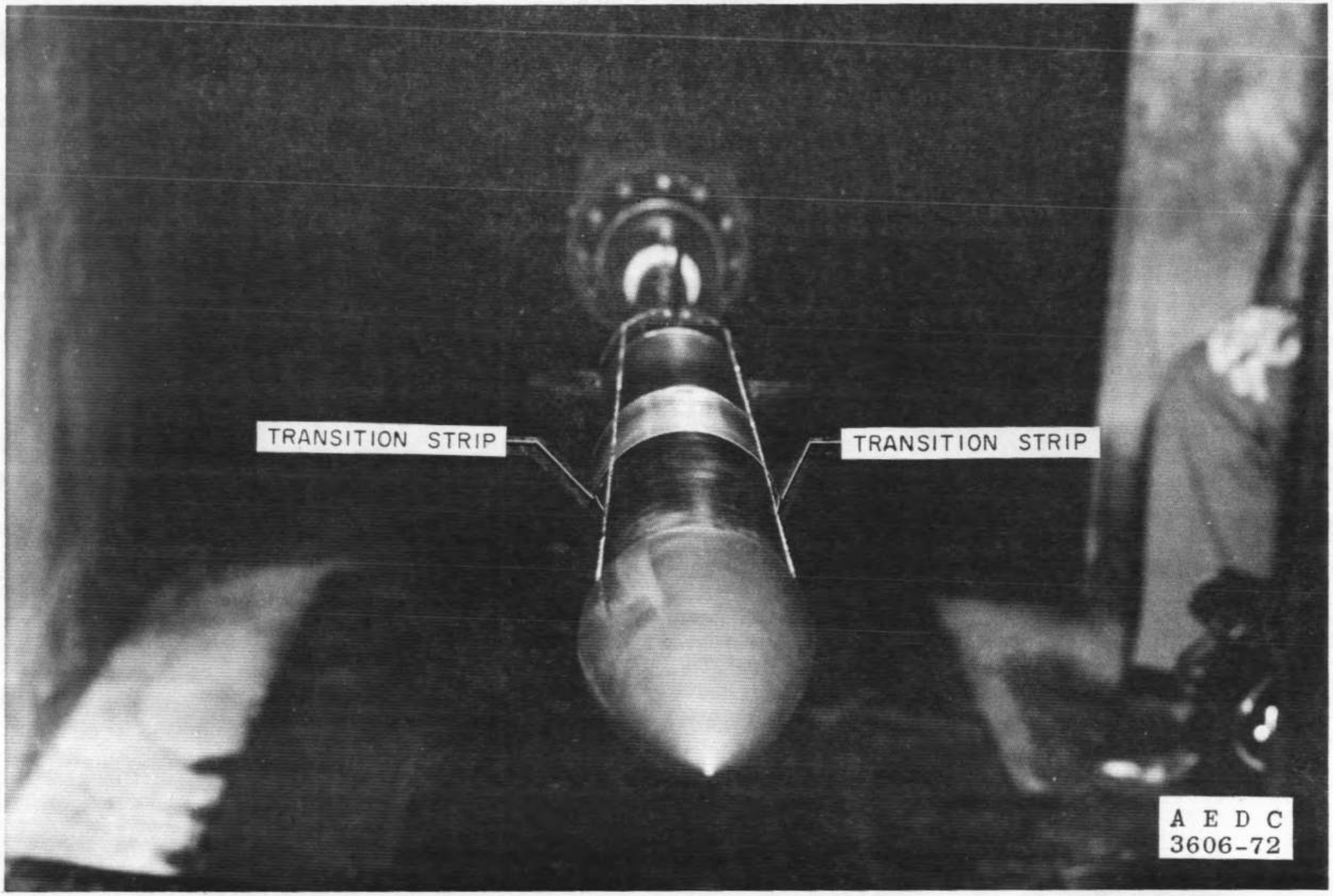

c. Test No. 2, front view showing grit location
Figure 2. Concluded.

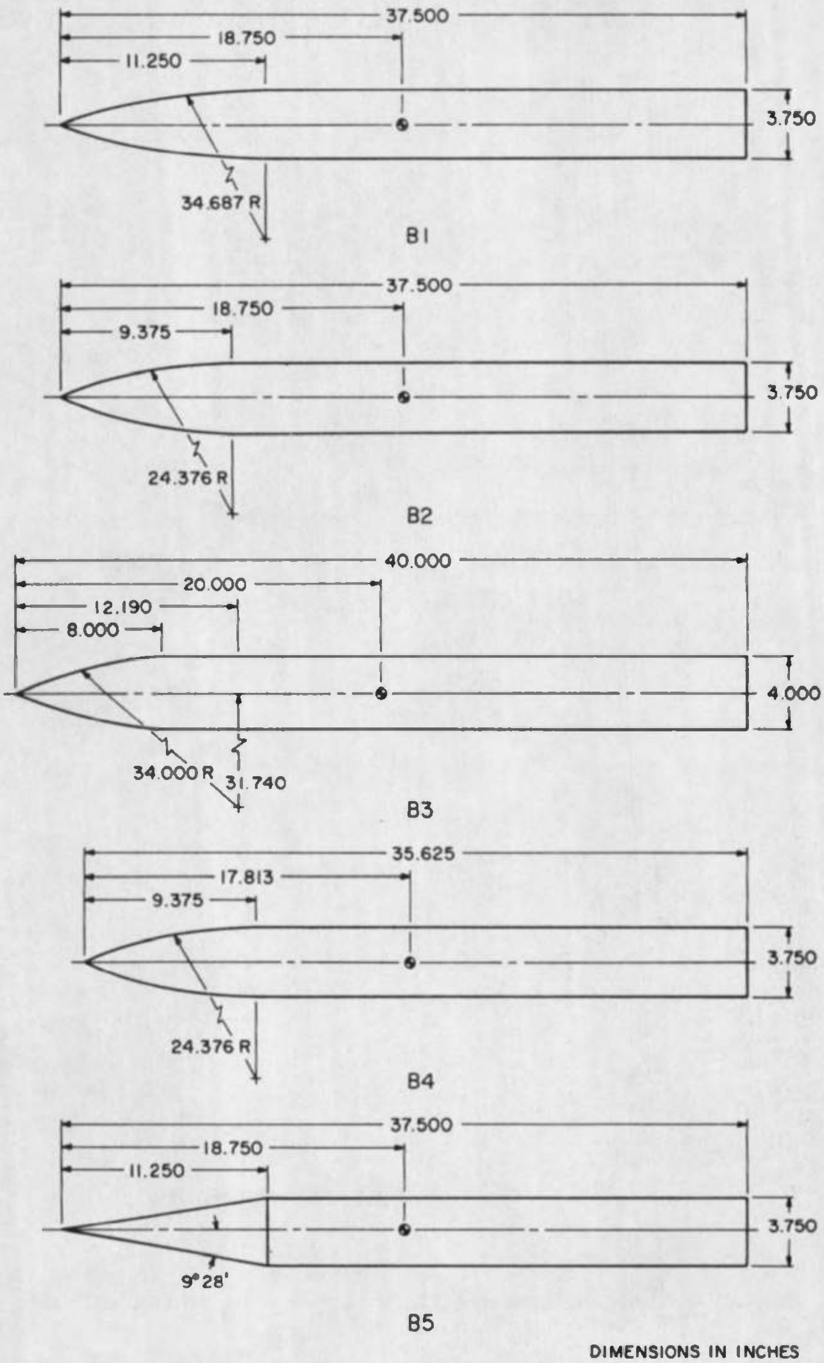

Note: The Body Configuration Shapes are as Follows:
Configurations B1, B2, and B4 are Tangent-Ogive Cylinder.
Configuration B3 is a Secant-Ogive Cylinder.
Configuration B5 is a Cone Cylinder.
⊗ Moment Reference Point.

Figure 3. Dimensional sketch of model body configurations.

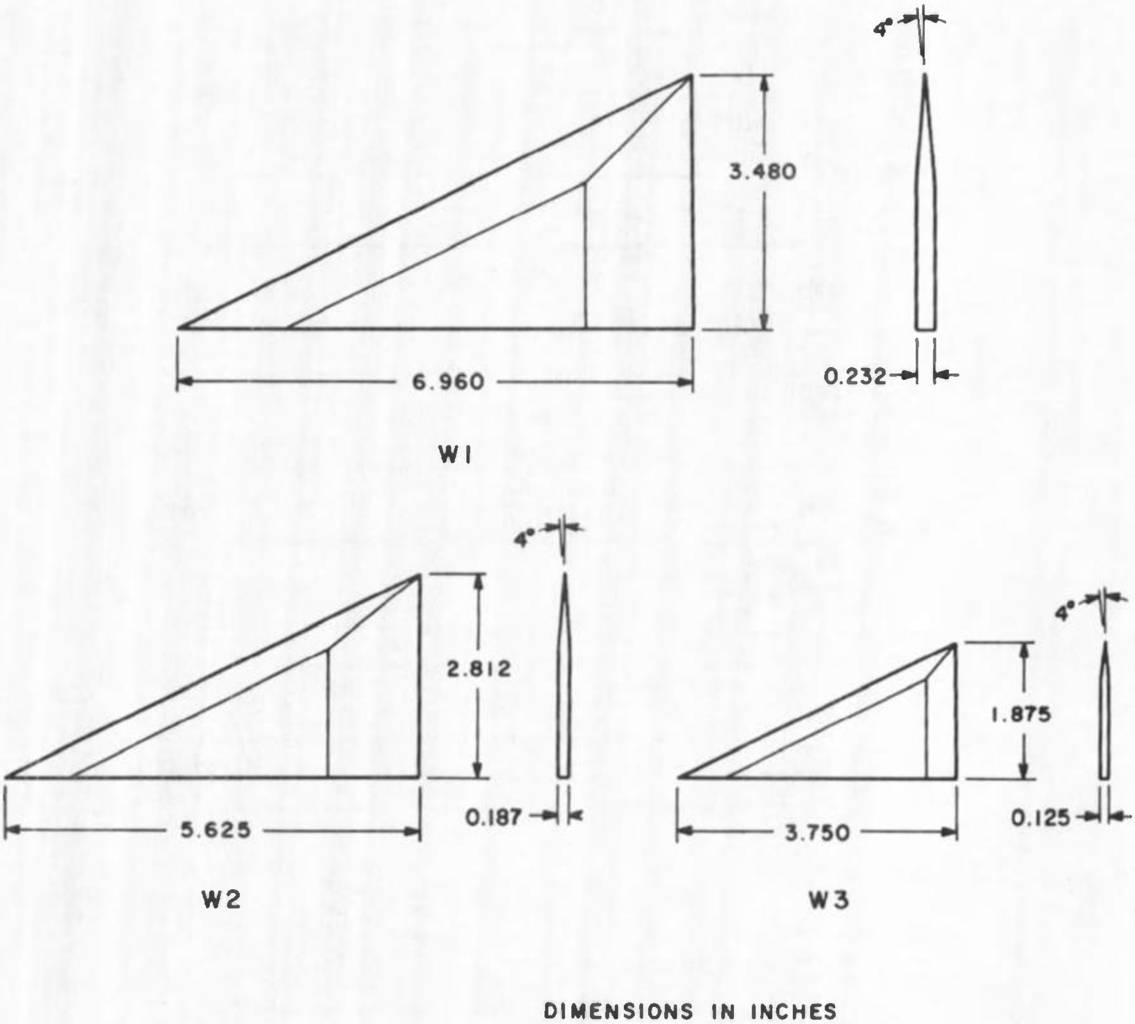

Figure 4. Dimensional sketch of model wing configurations.

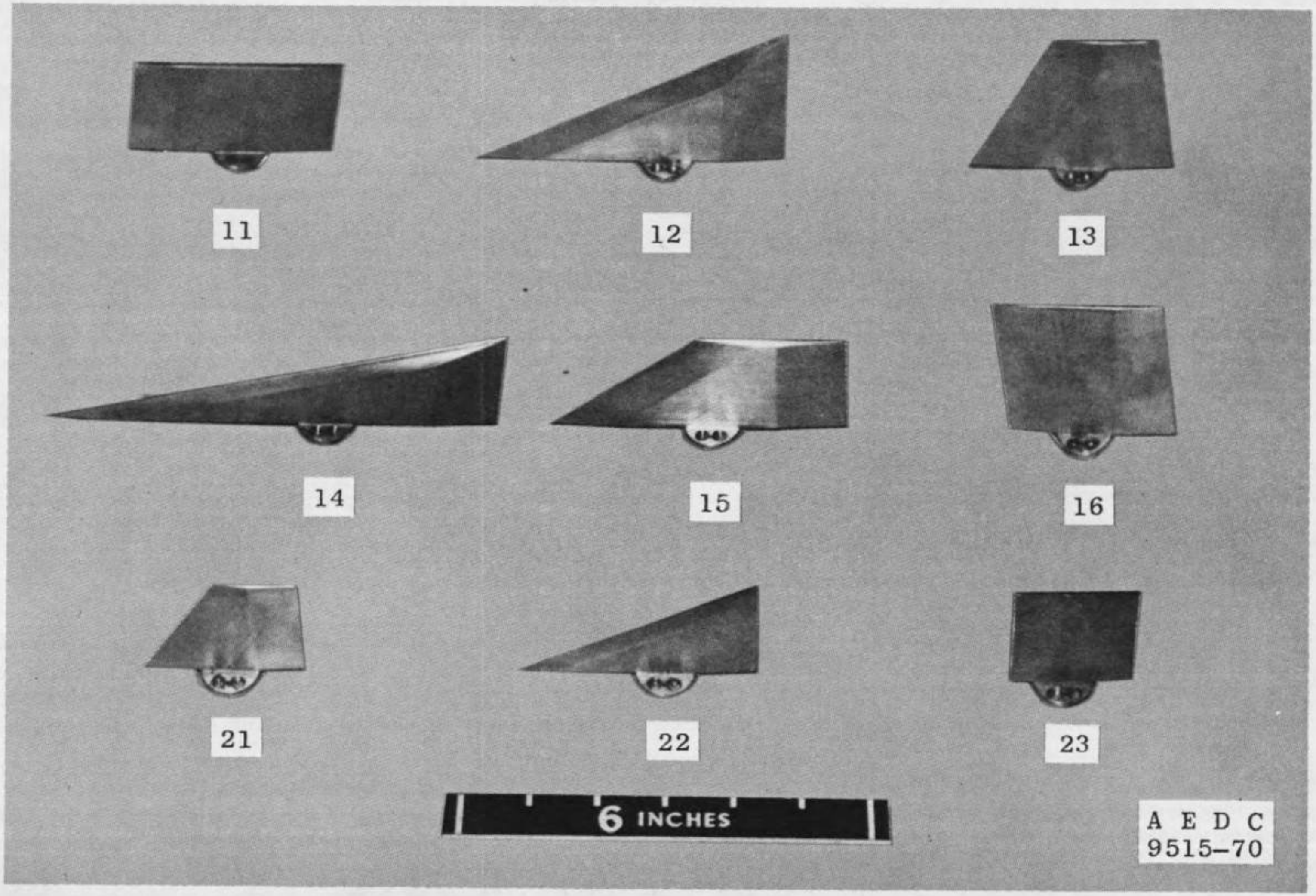

a. Tail fin configurations F11 through F23
Figure 5. Photographs of model tail fin configurations.

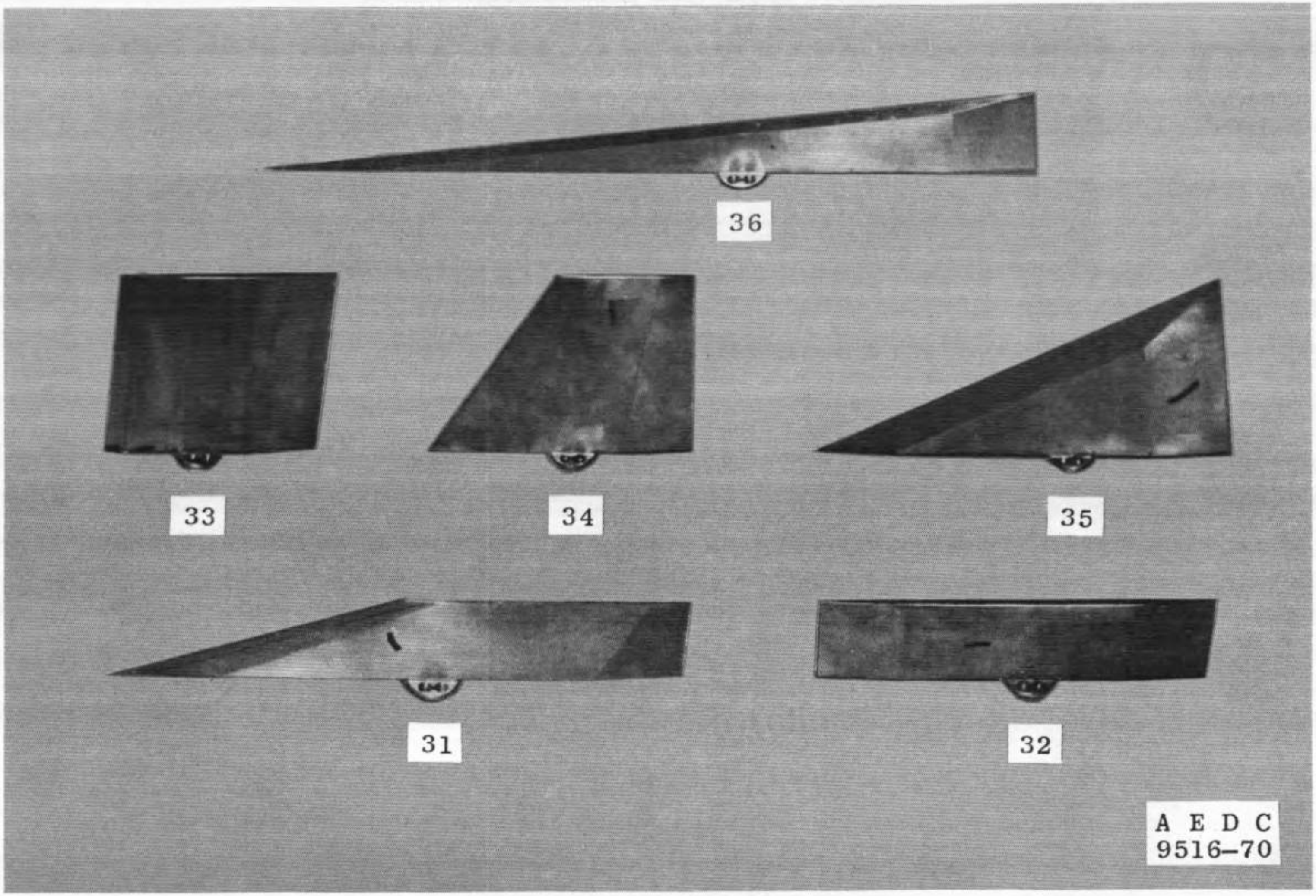

b. Tail fin configurations F31 through F36
Figure 5. Concluded.

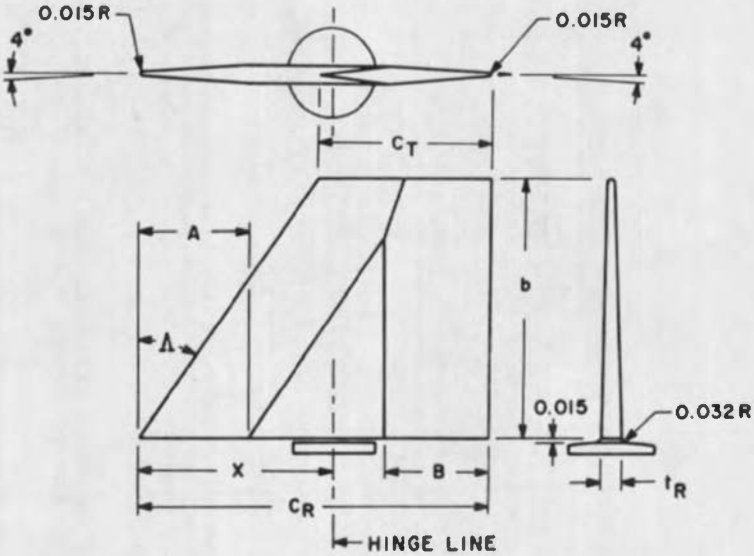

TAIL FIN CONFIG.	S_F ft^2	AR	b in.	λ	Λ	A in.	C_T in.	B in.	C_R in.	X in.	t_R in.
F11	0.04883	0.5	1.875	1.0	0°	0.800	3.750	0.800	3.750	1.687	0.140
F12	0.05492	1.0	2.812	0	63°26'	1.172	0	1.140	5.625	3.487	0.187
F13	0.05488	1.0	2.812	0.5	33°41'	1.158	1.873	1.140	3.747	2.061	0.187
F14	0.04883	0.5	1.875	0	75°57'	1.195	0	1.140	7.500	4.650	0.187
F15	0.04877	0.5	1.875	0.5	53°6'	1.165	2.497	1.140	4.994	2.746	0.187
F16	0.05491	1.0	2.812	1.0	0°	0.800	2.812	0.800	2.812	1.265	0.140
F21	0.02439	1.0	1.874	1.0	0°	0.696	1.874	0.696	1.874	0.843	0.125
F22	0.02441	1.0	1.875	0	63°26'	0.728	0	0.694	3.750	2.325	0.125
F23	0.02505	1.0	1.875	0.5	34°22'	0.713	1.282	0.694	2.565	1.411	0.125
F31	0.09746	0.25	1.875	0.5	69°24'	1.626	4.990	1.587	9.980	5.489	0.250
F32	0.09766	0.25	1.875	1.0	0°	1.587	7.500	1.587	7.500	3.375	0.250
F33	0.13414	1.0	4.395	1.0	0°	1.587	4.395	1.587	4.395	1.978	0.250
F34	0.12784	1.0	4.395	0.5	32°25'	1.606	2.792	1.587	5.585	3.072	0.250
F35	0.13385	1.0	4.395	0	63°23'	1.619	0	1.587	8.771	5.438	0.250
F36	0.09764	0.25	1.875	0	82°52'	1.682	0	1.587	14.998	9.298	0.250

Note: Dimensions of the Tail Fin Configurations from the Original Model Drawings.

Figure 6. Dimensions of the tail fin configurations.

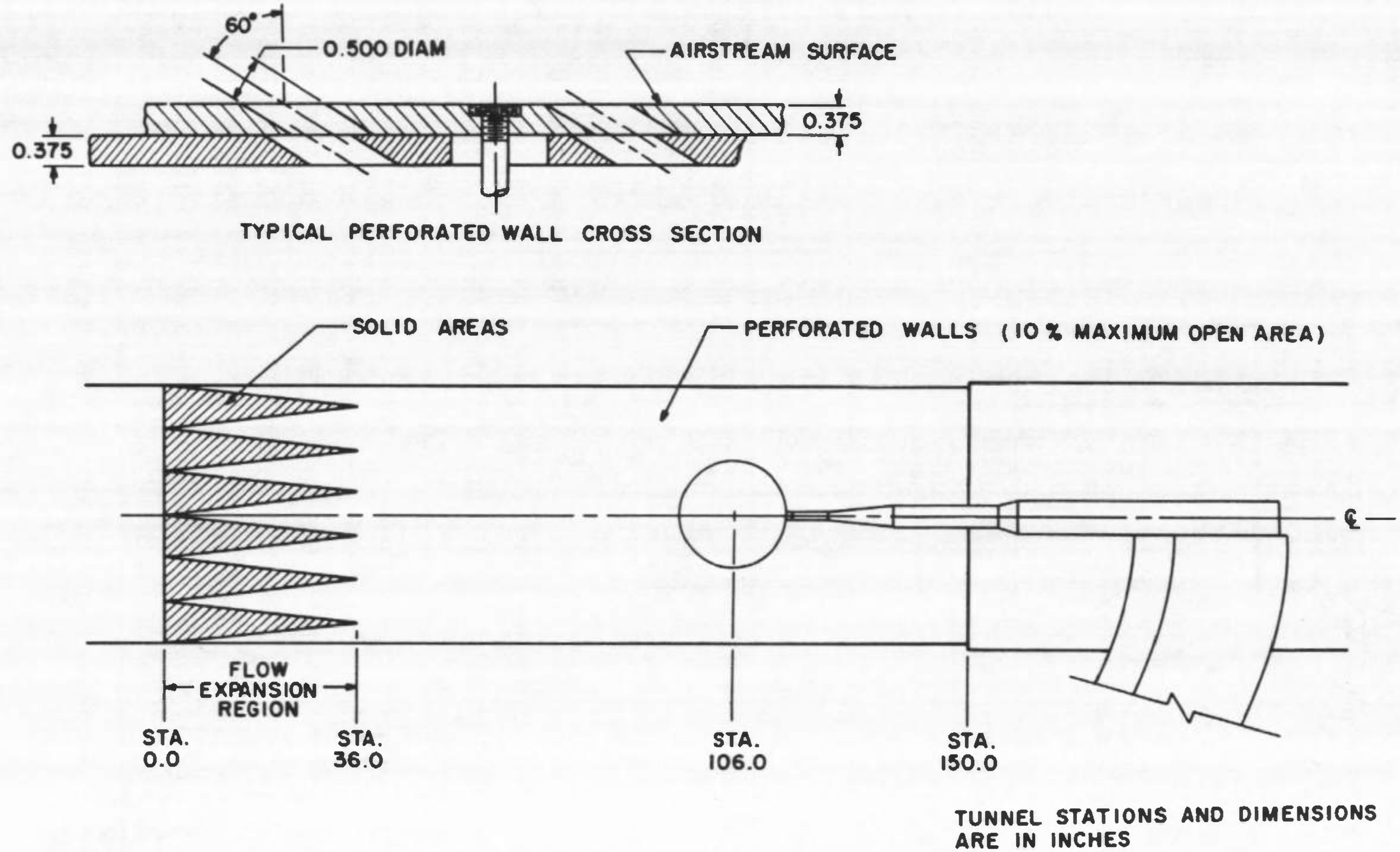

Figure 7. Sketch of test No. 2 splitter plate tunnel installation.

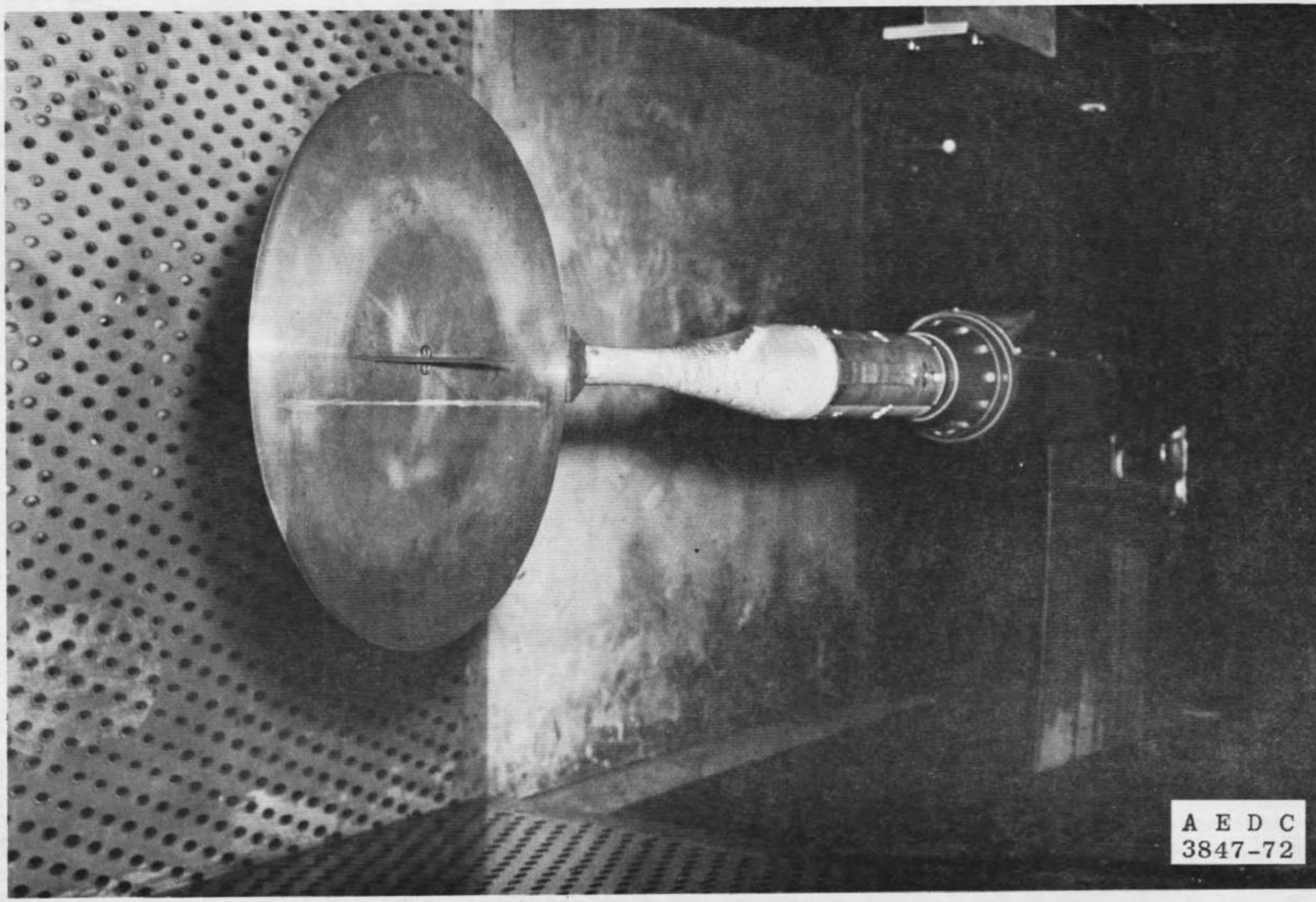

Figure 8. Photograph of test No. 2 splitter plate installation.

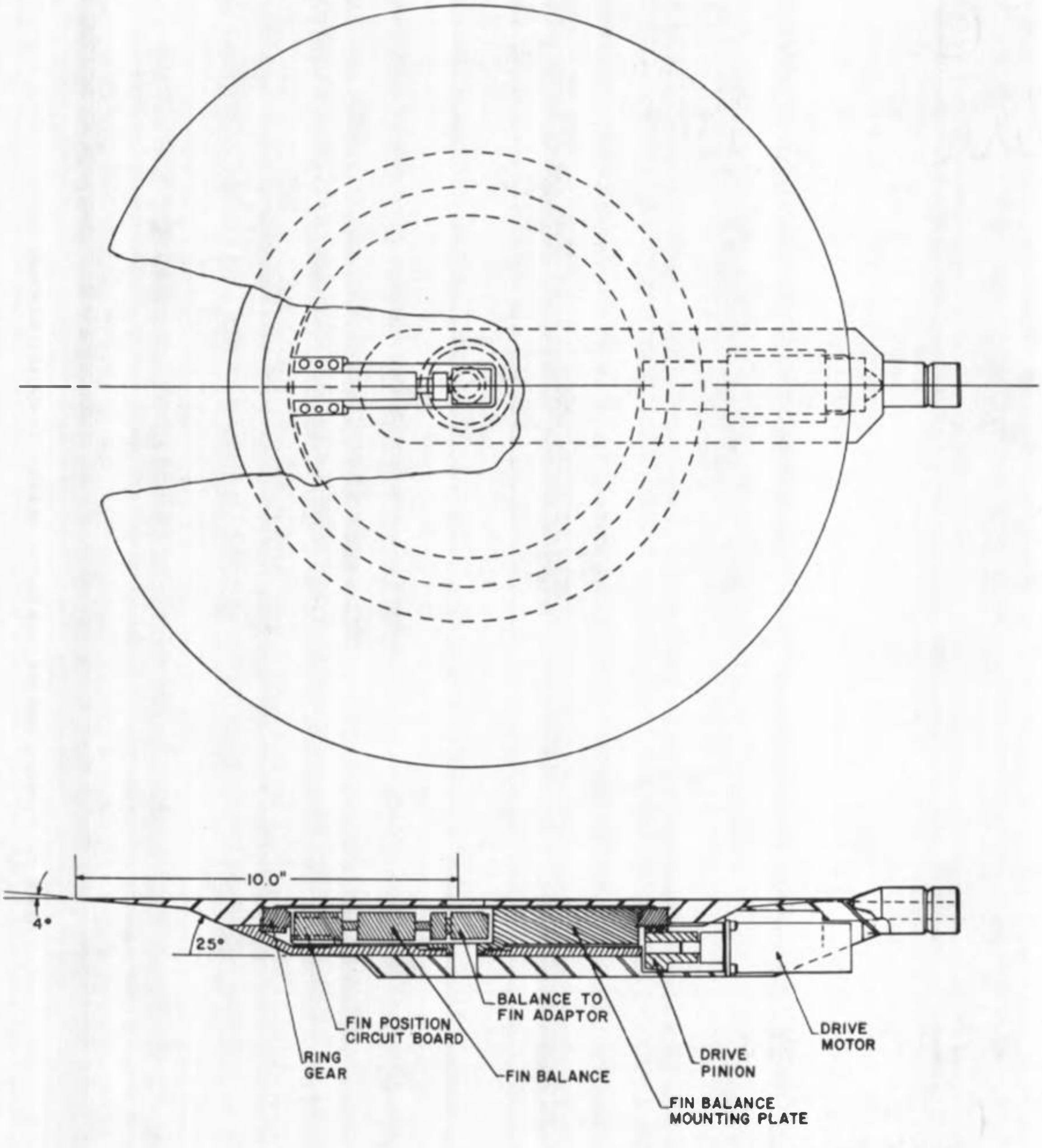

Figure 9. Sketch of splitter plate used in test No. 2.

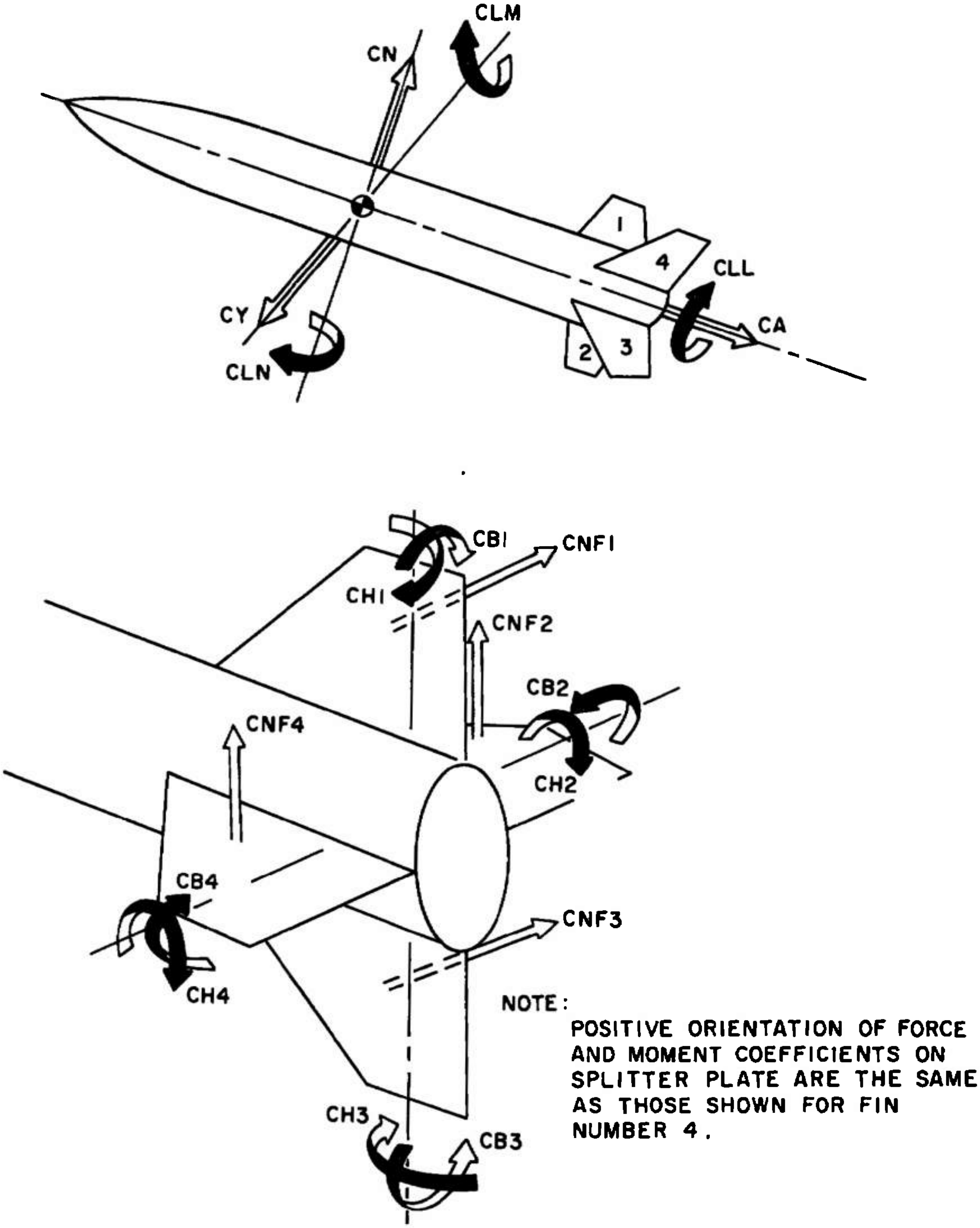

Figure 10. Positive orientations of model aerodynamic coefficients.

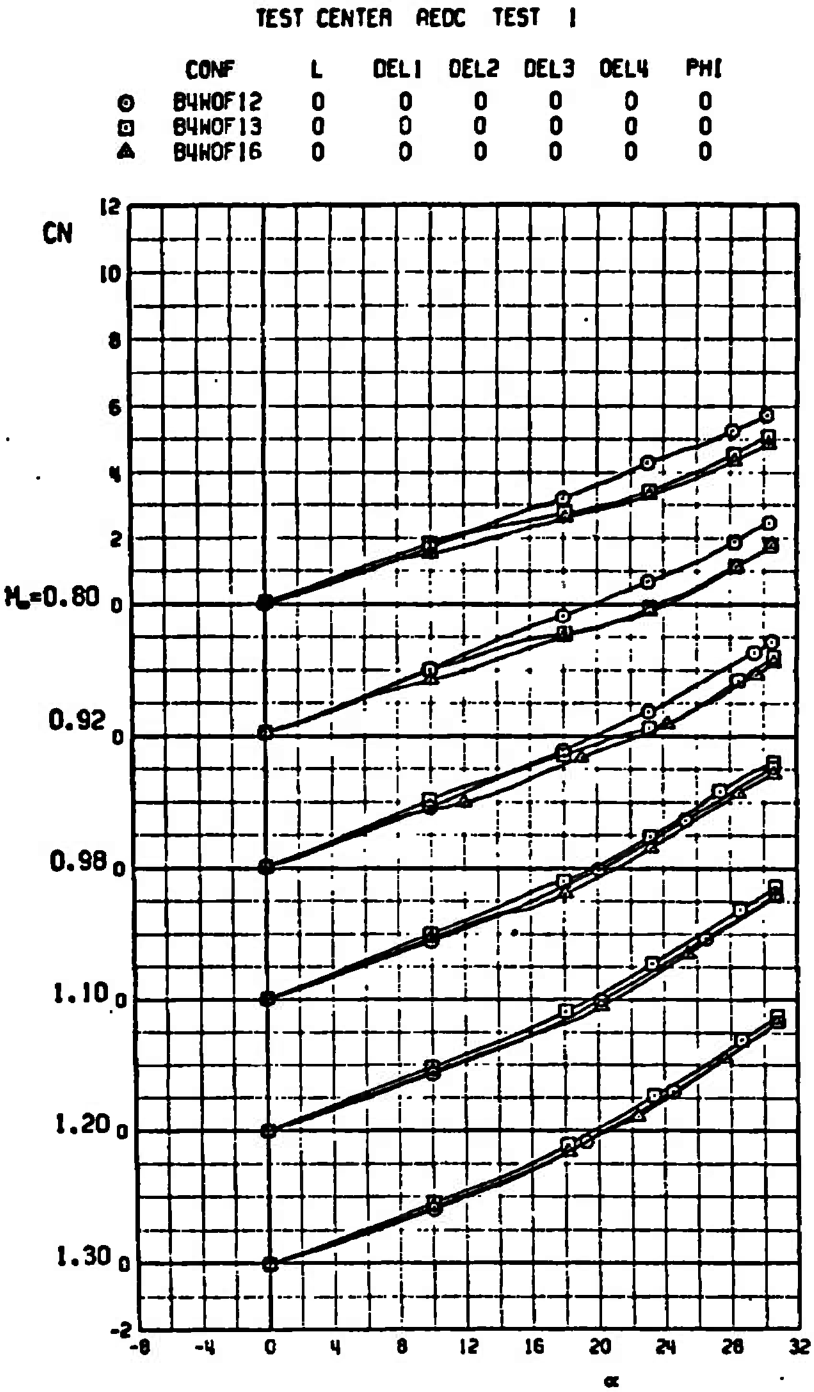

a. CN versus α

Figure 11. Test No. 1, comparison of aerodynamic coefficients of configurations B4W0F12, B4W0F13, and B4W0F16.

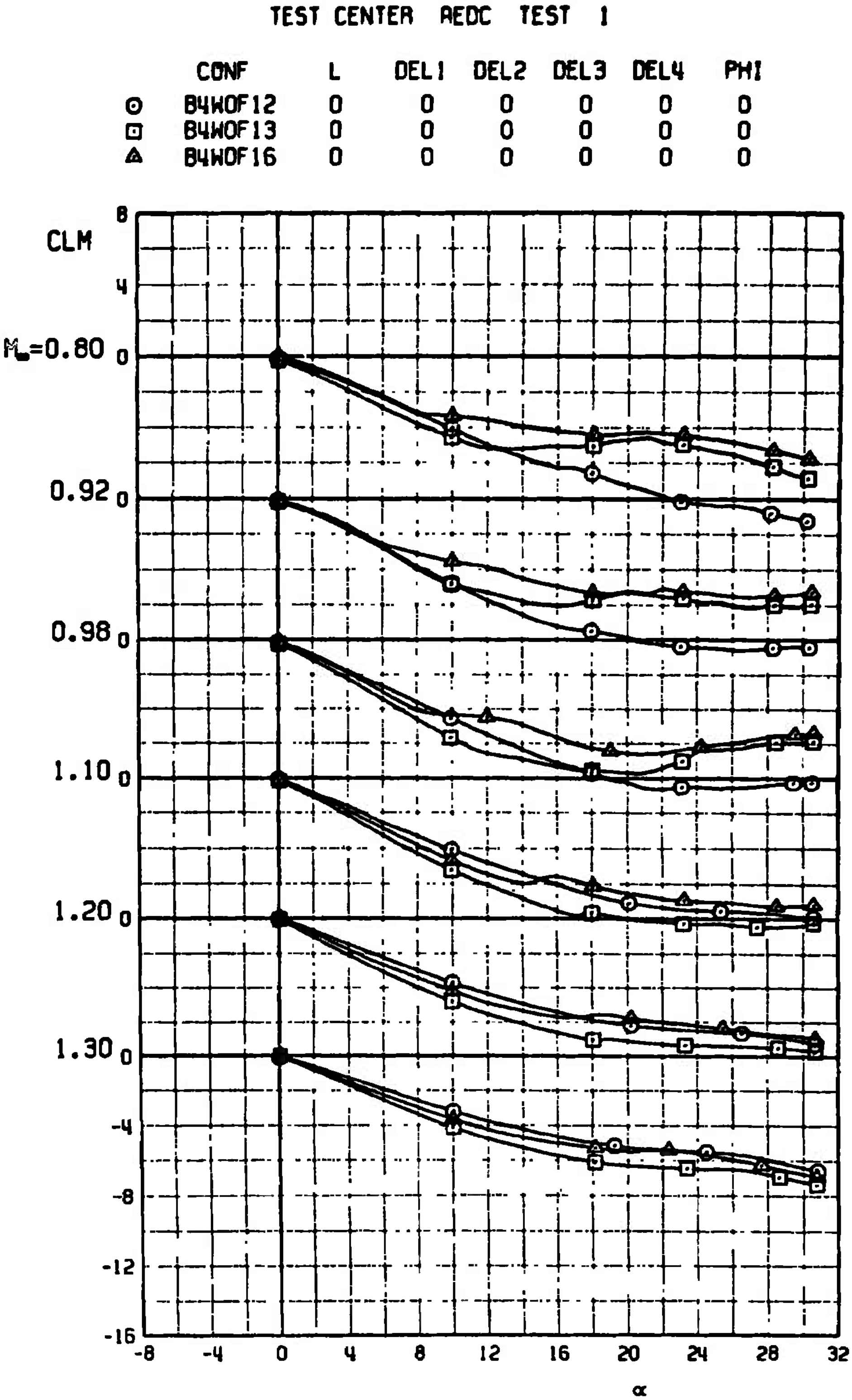

b. CLM versus α
Figure 11. Continued.

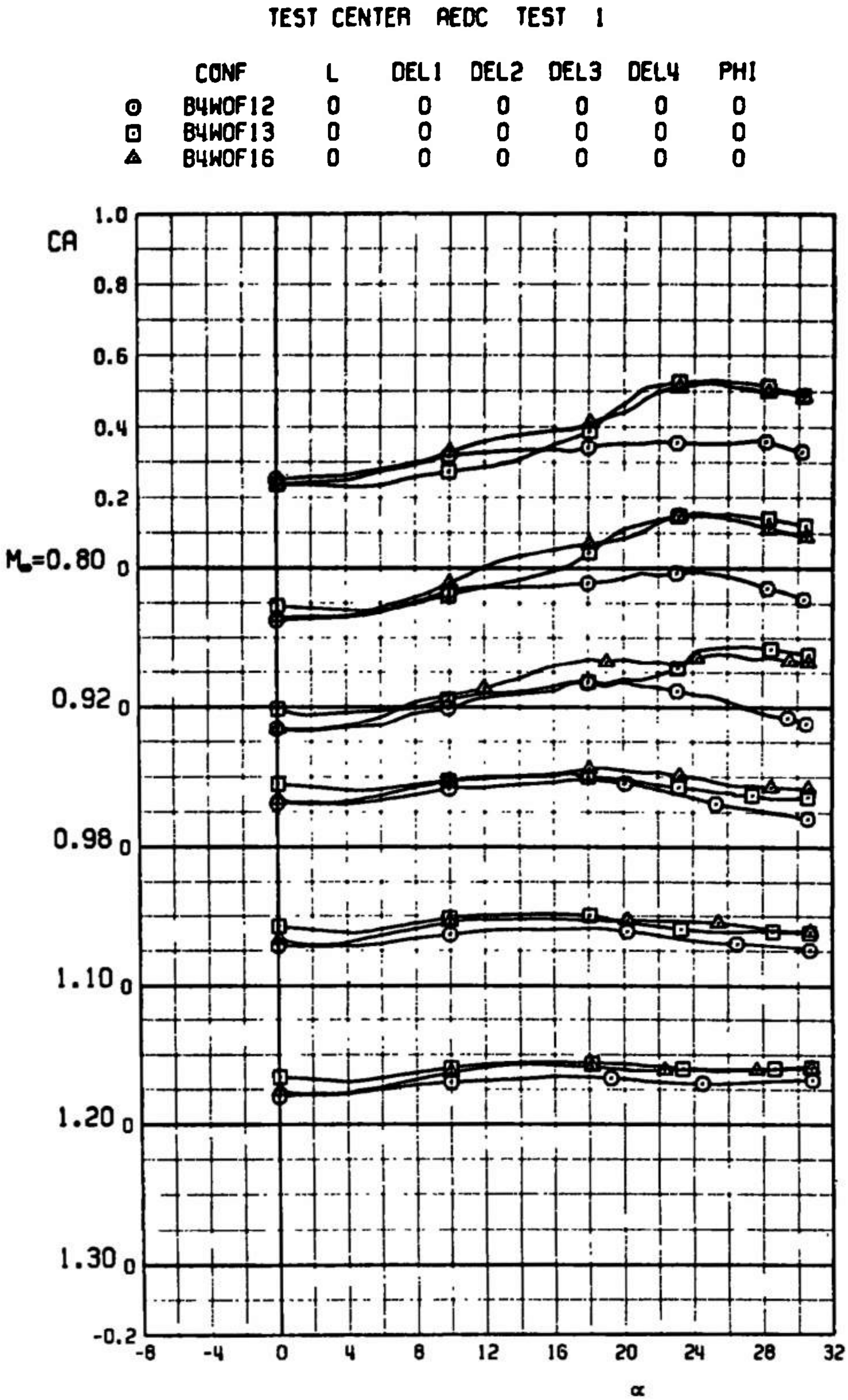

c. CA versus α
Figure 11. Continued.

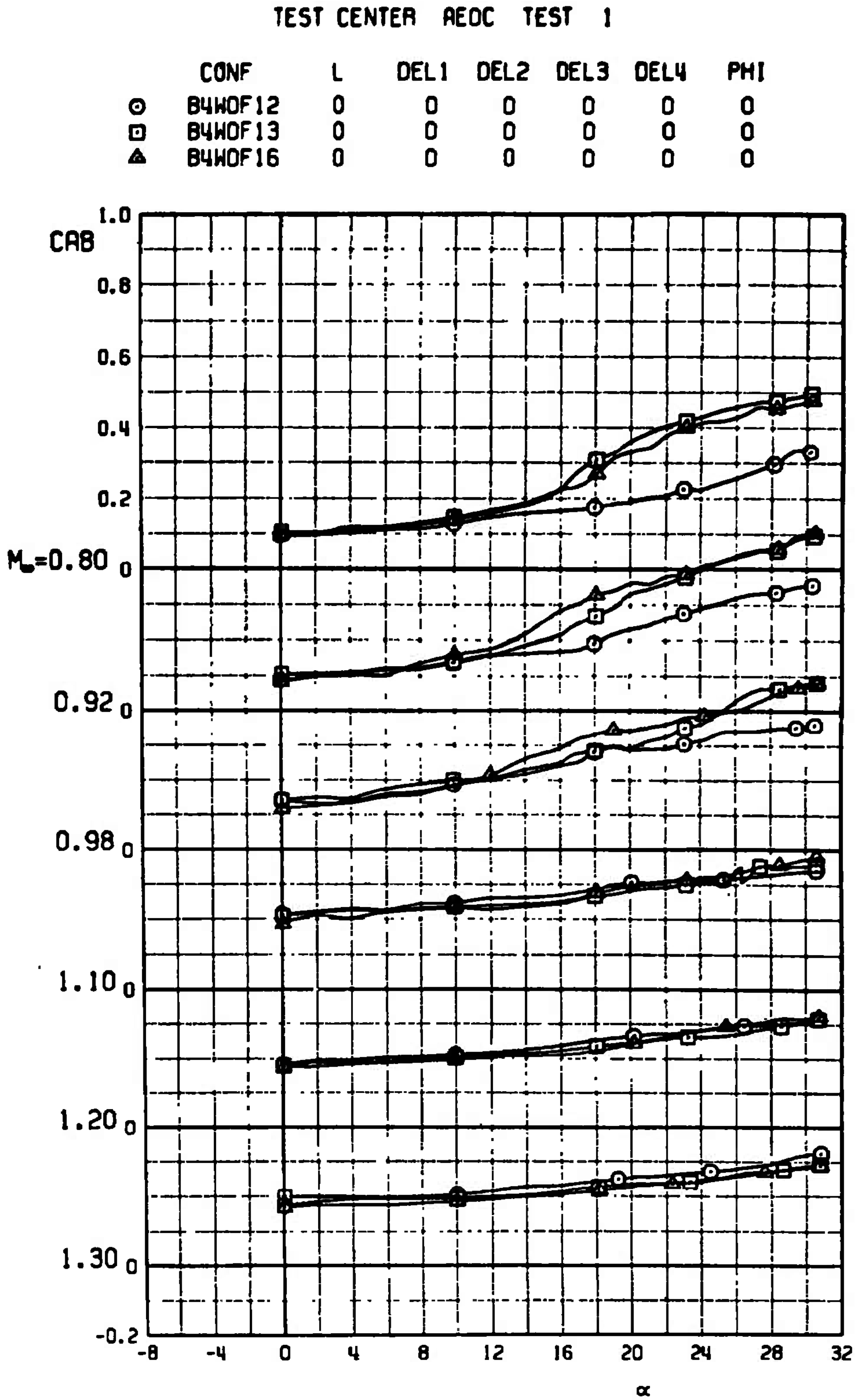

d. CAB versus α
Figure 11. Continued.

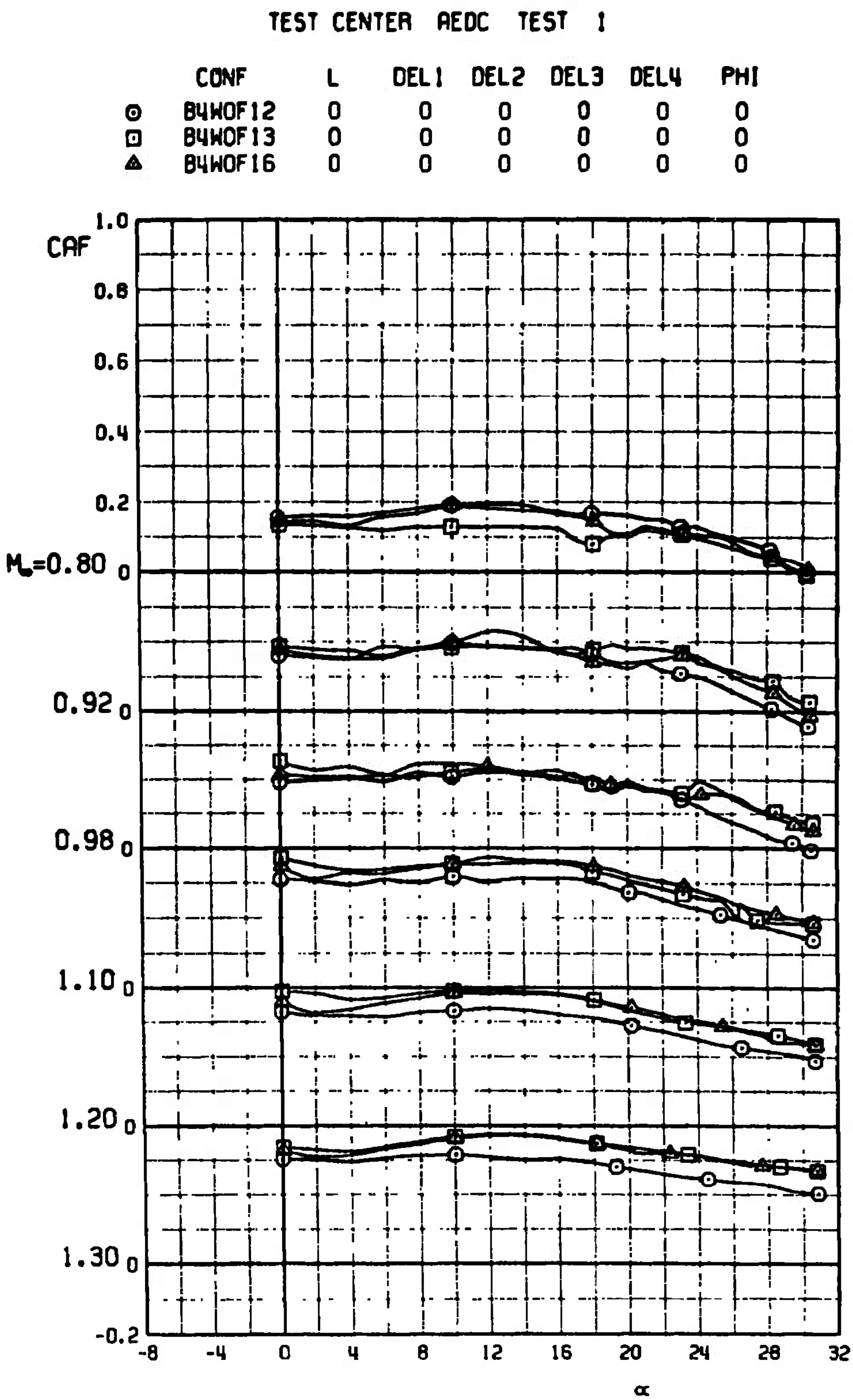

e. CAF versus α

Figure 11. Continued.

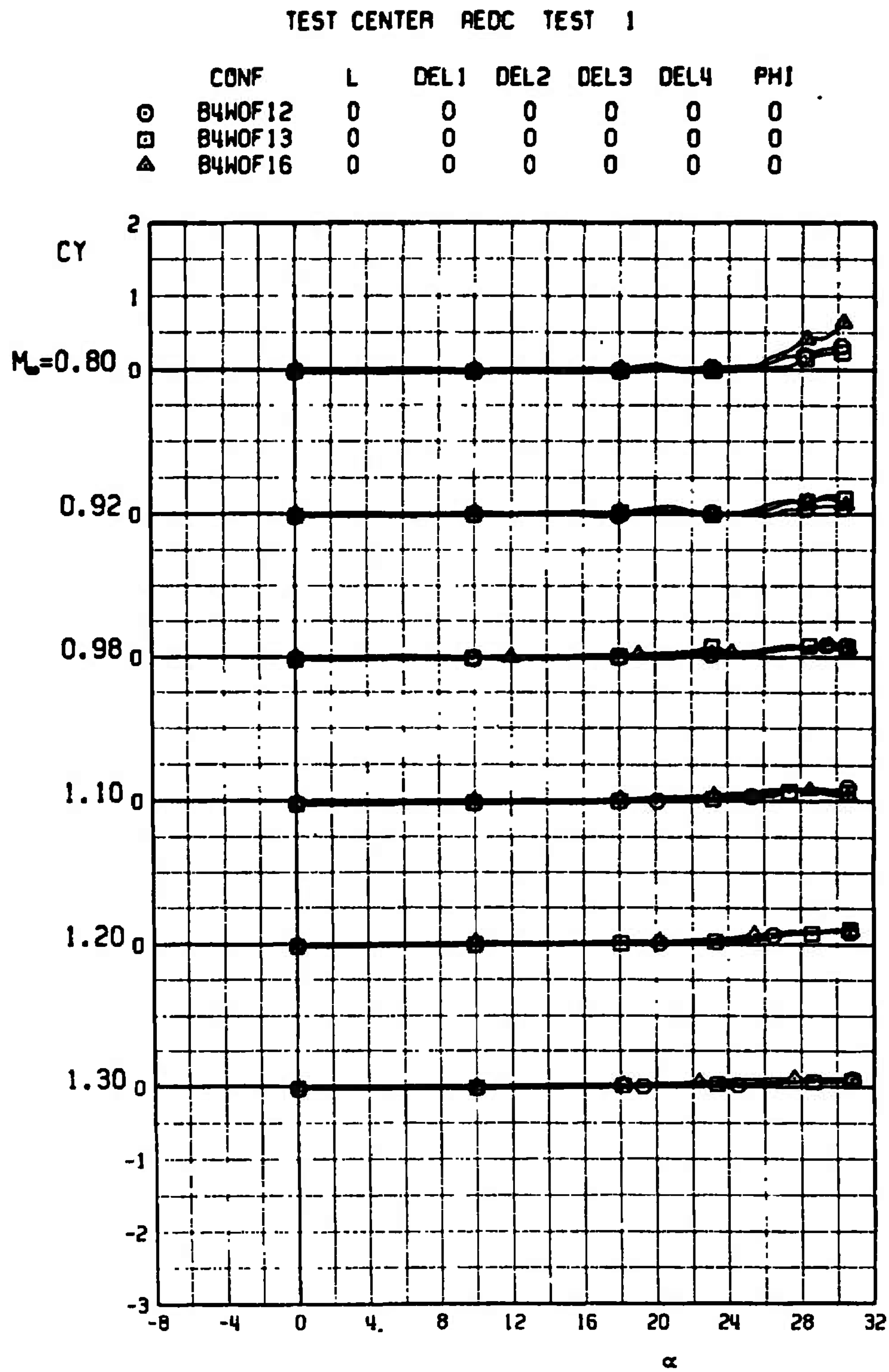

f. CY versus α
Figure 11. Continued.

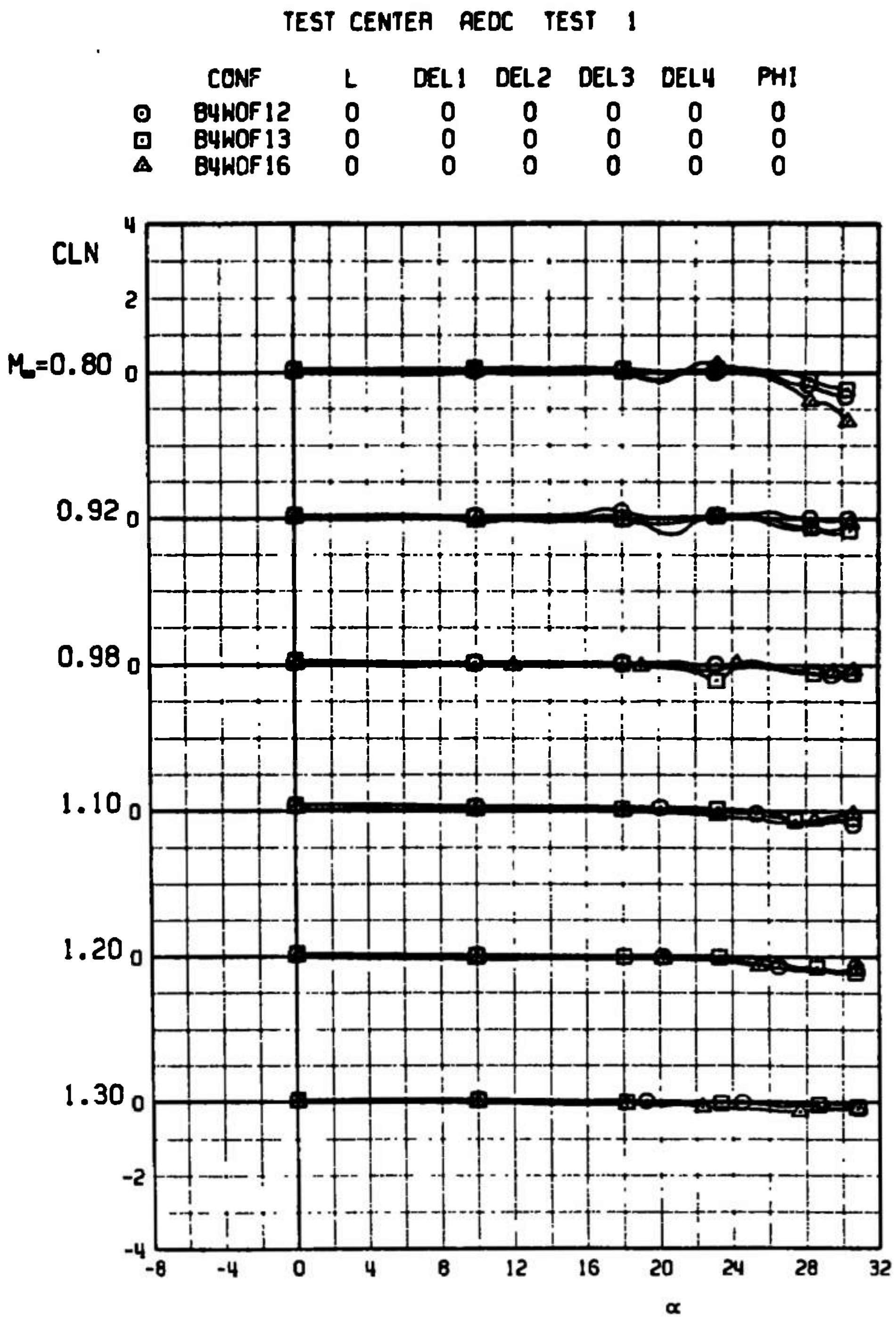

g. CLN versus α
Figure 11. Continued.

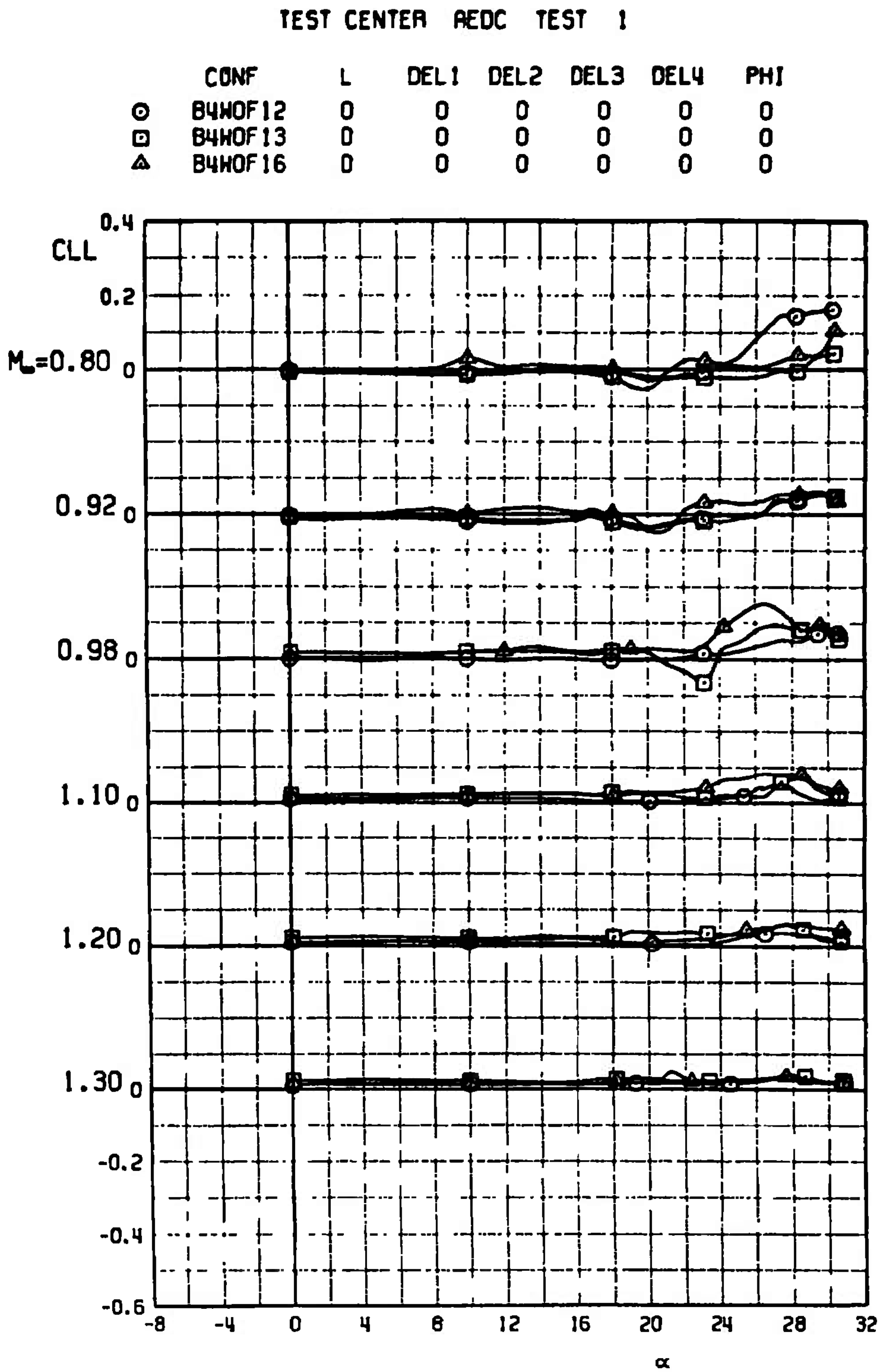

h. CLL versus α
Figure 11. Concluded.

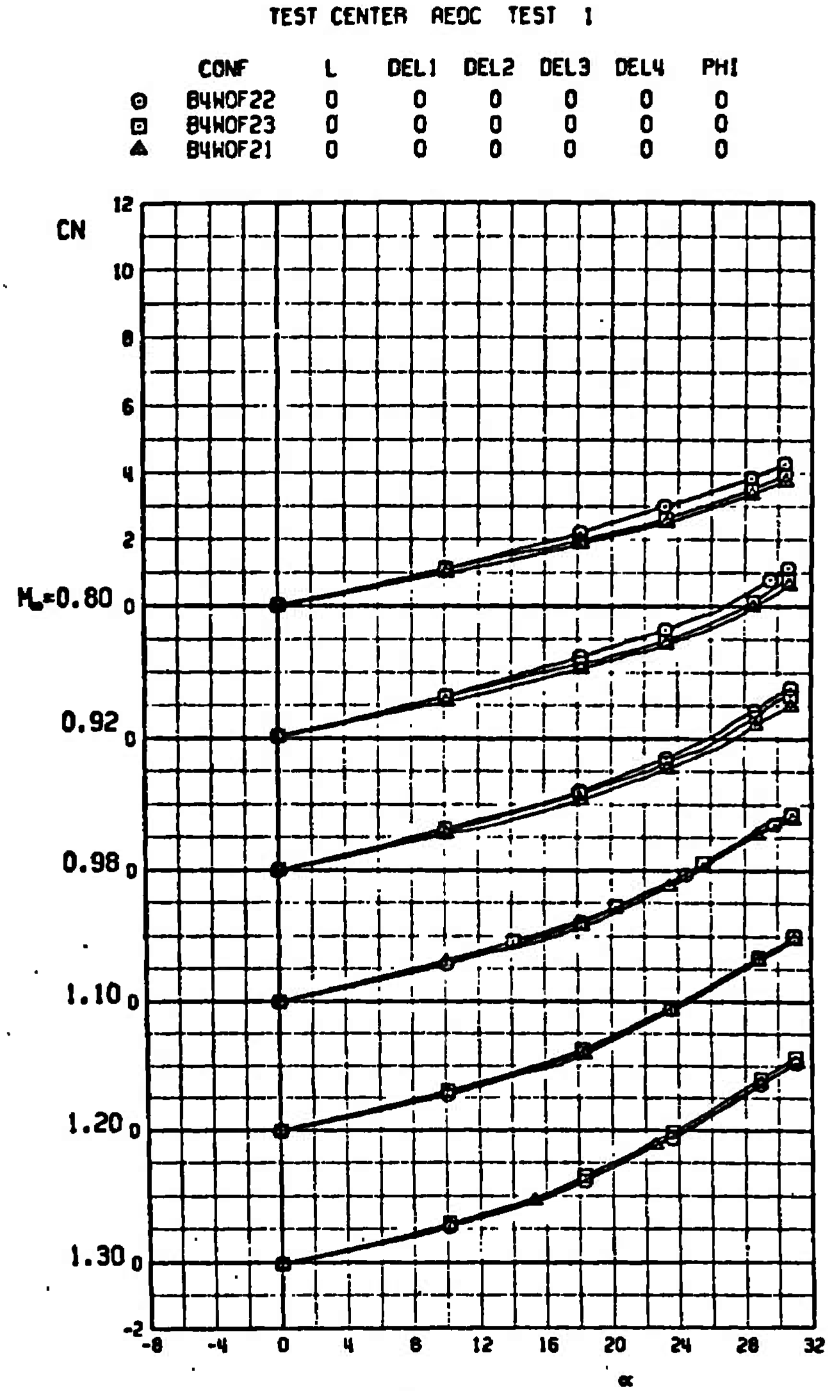

a. CN versus α

Figure 12. Test No. 1, comparison of aerodynamic coefficients of configurations B4W0F22, B4W0F23, and B4W0F21.

TEST CENTER AEDC TEST 1

	CONF	L	DEL1	DEL2	DEL3	DEL4	PHI
⊙	B4W0F22	0	0	0	0	0	0
⊡	B4W0F23	0	0	0	0	0	0
△	B4W0F21	0	0	0	0	0	0

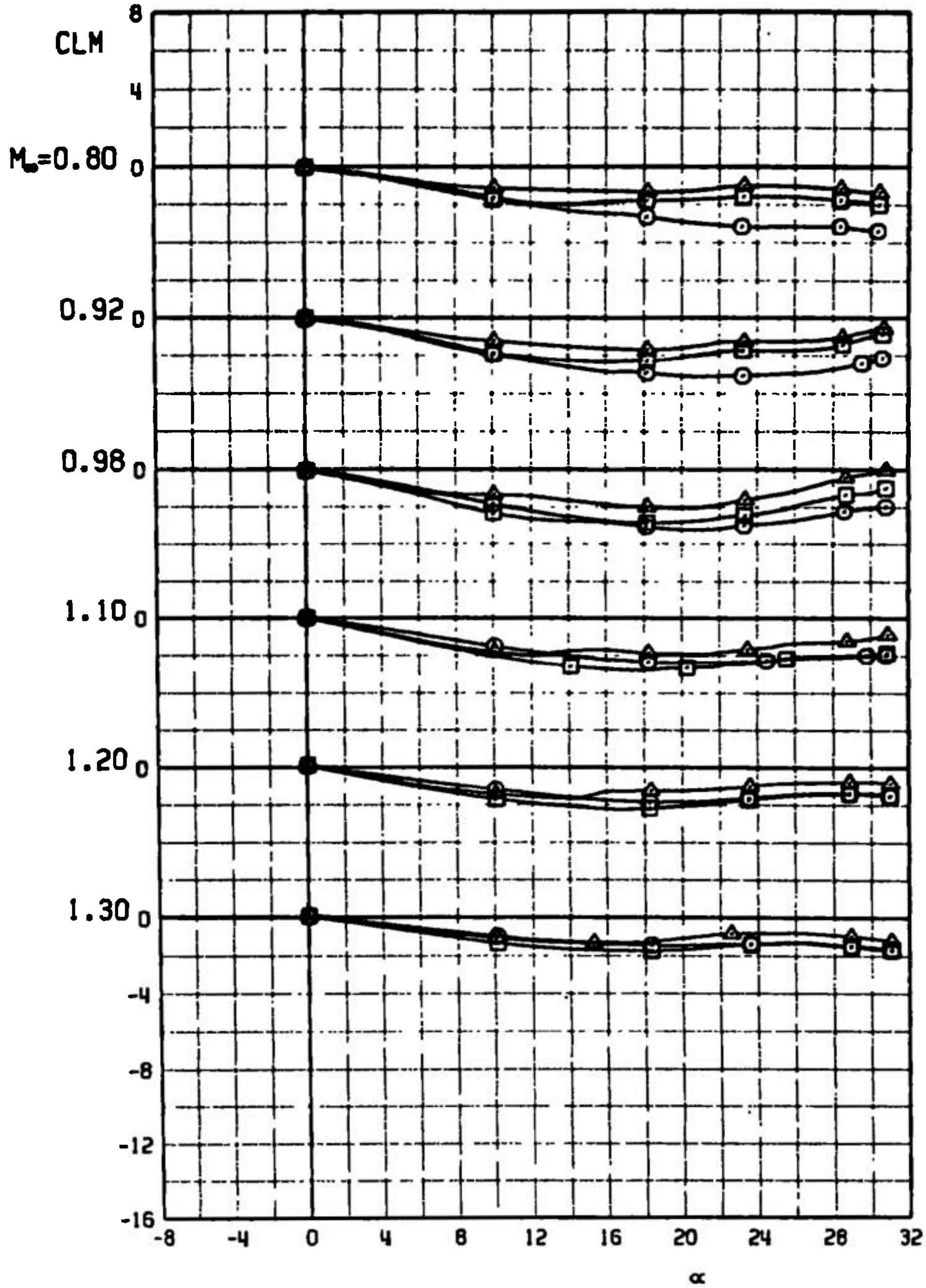

b. CLM versus α
Figure 12. Continued.

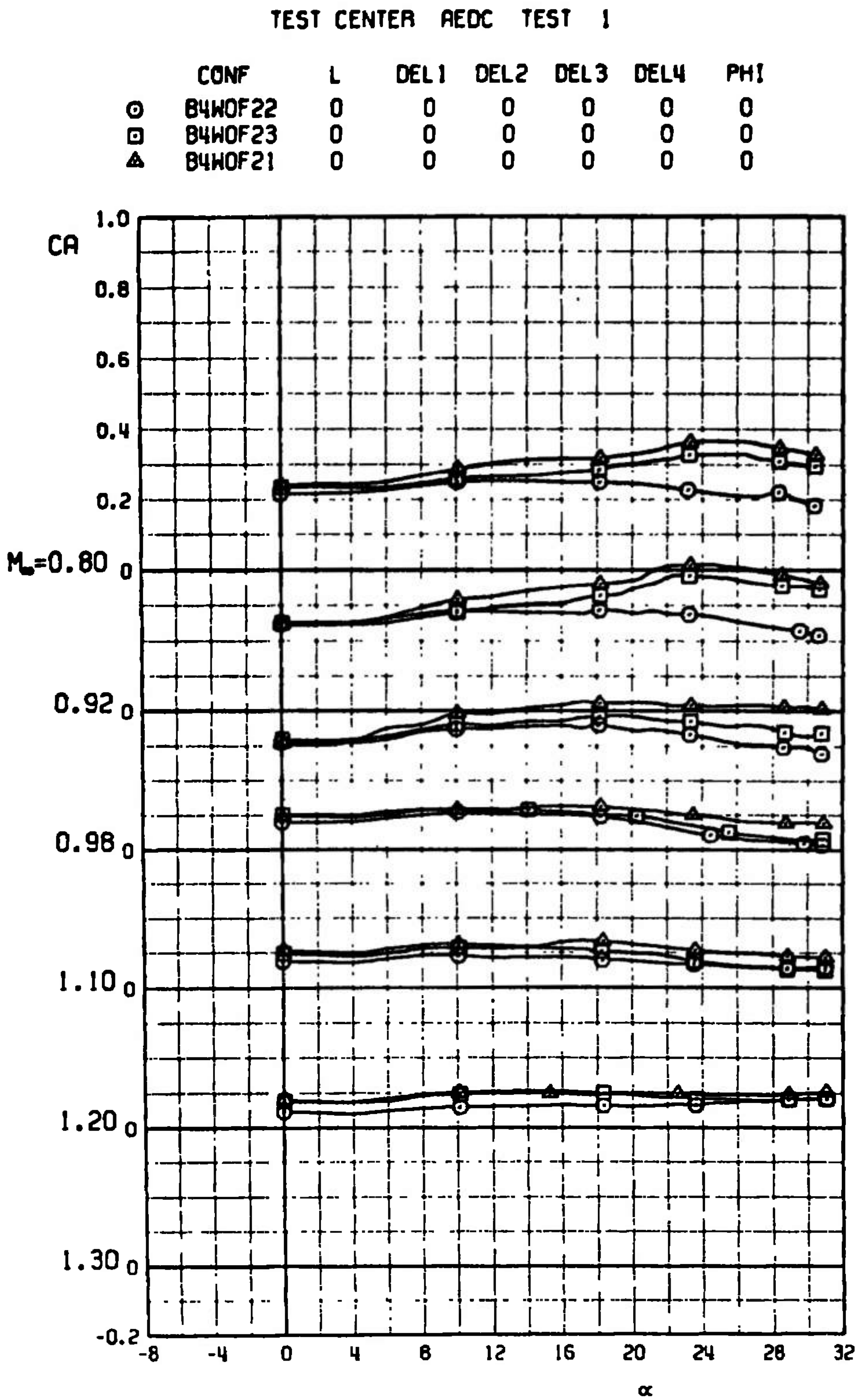

c. CA versus α
Figure 12. Continued.

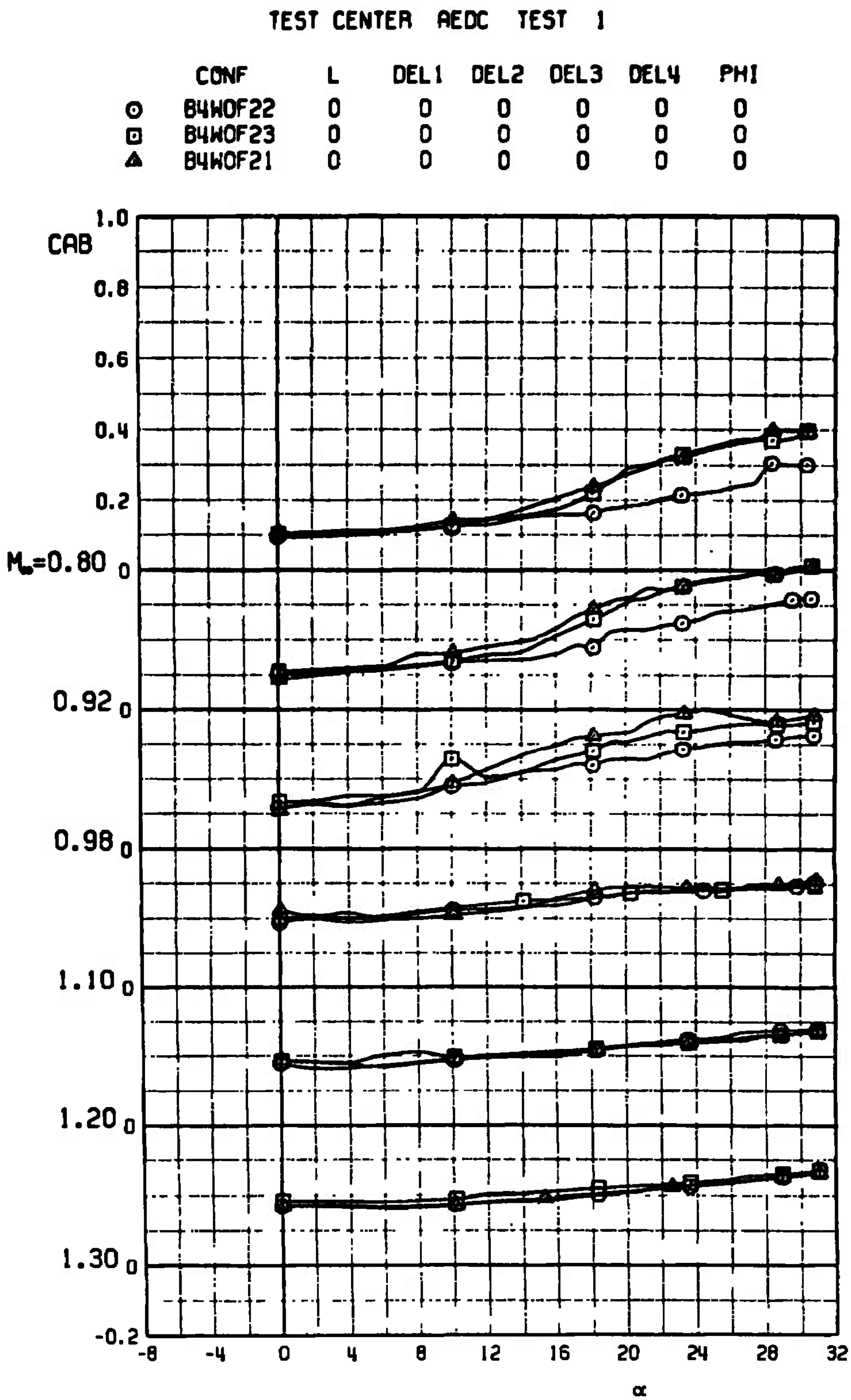

d. CAB versus α
Figure 12. Continued.

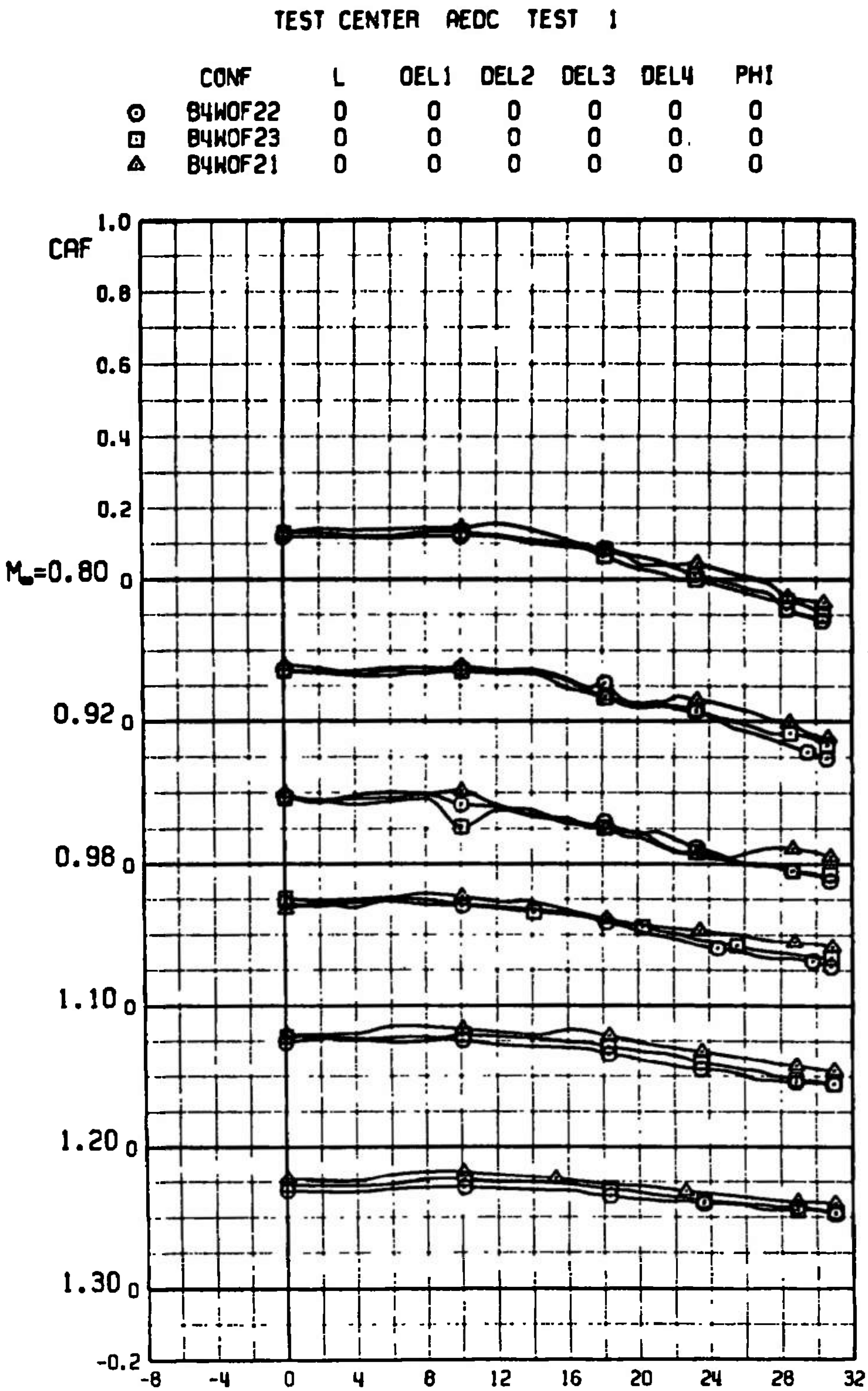

e. CAF versus α
Figure 12. Continued.

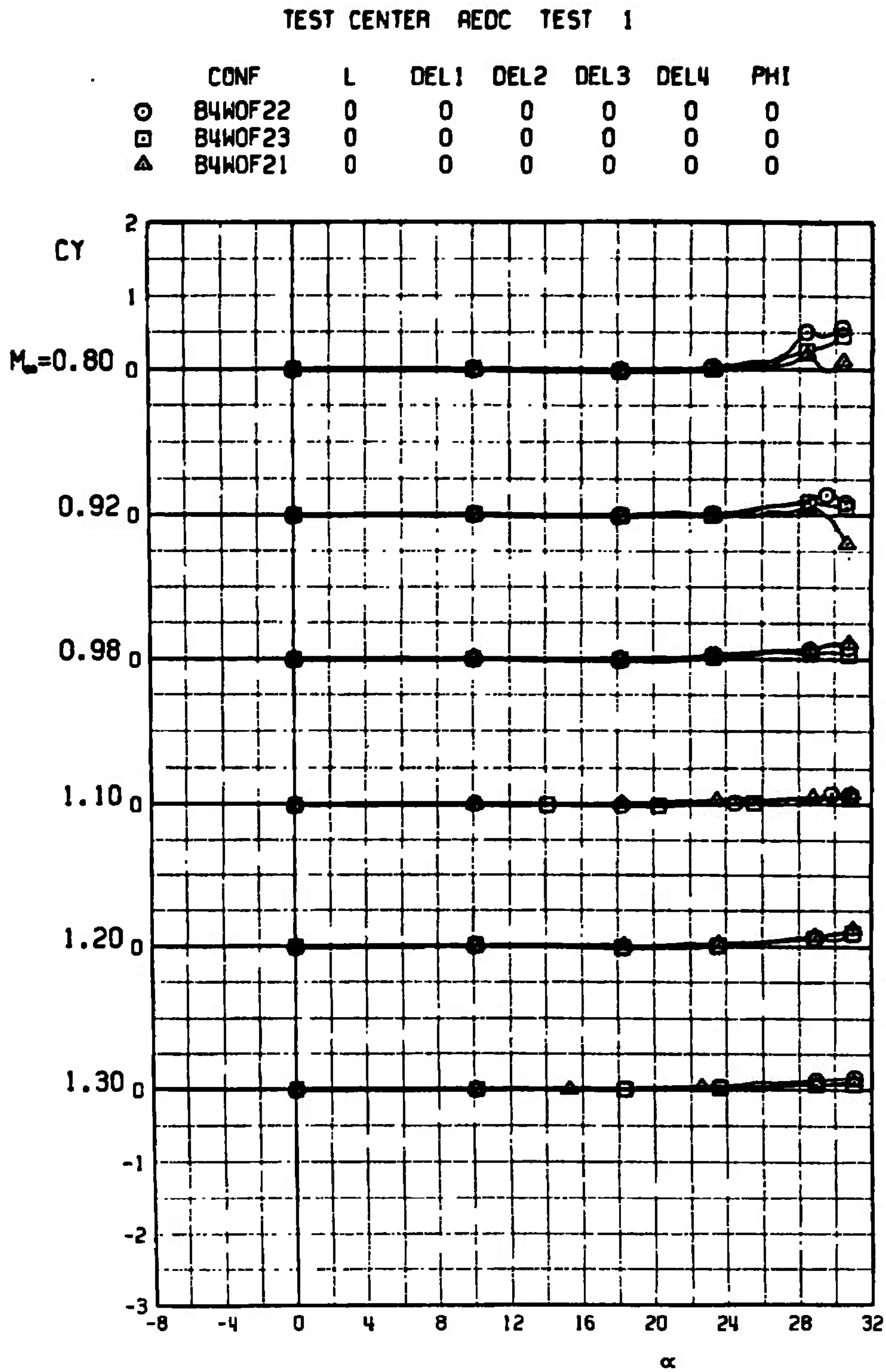

f. CY versus α
Figure 12. Continued.

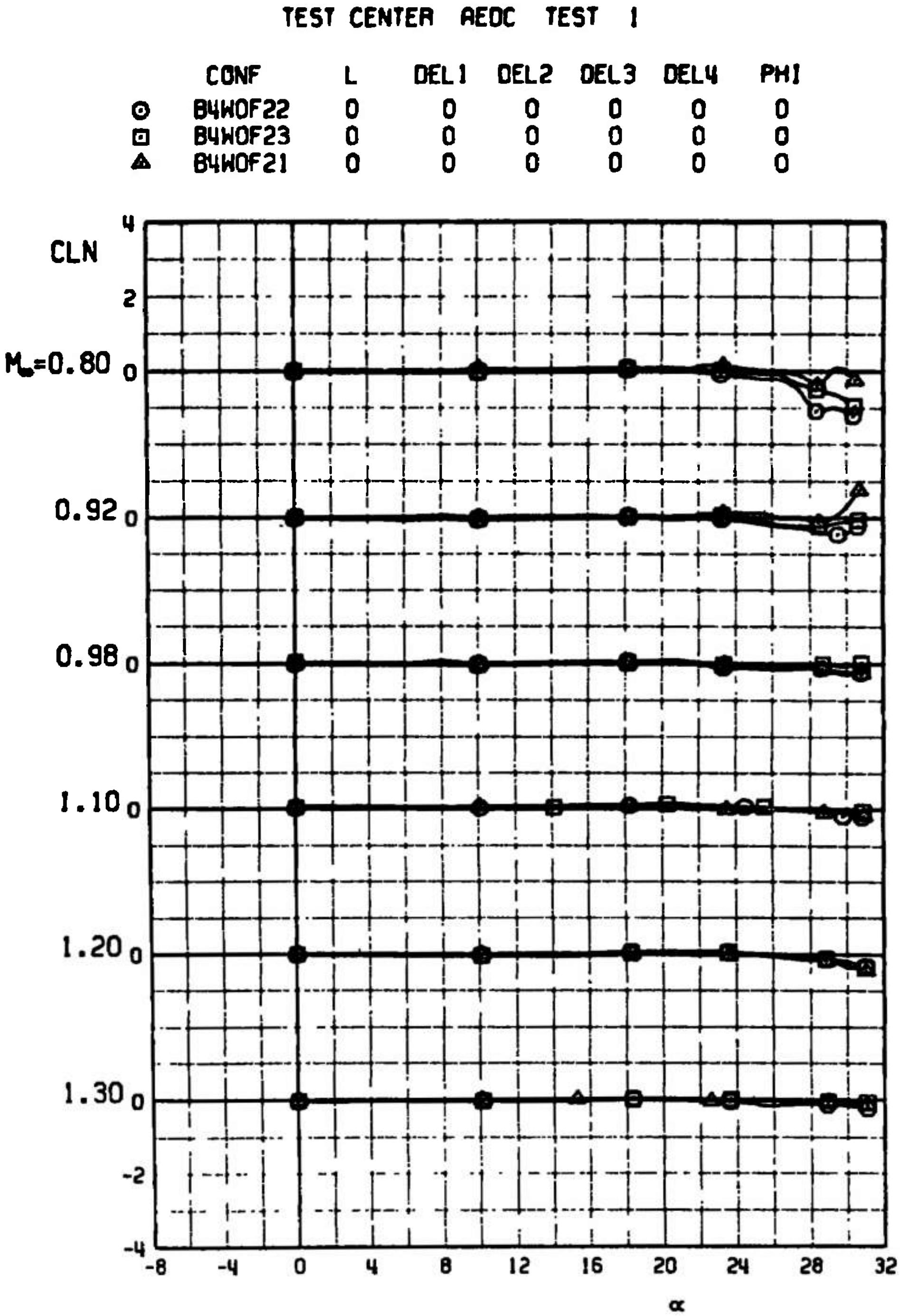

g. CLN versus α
Figure 12. Continued.

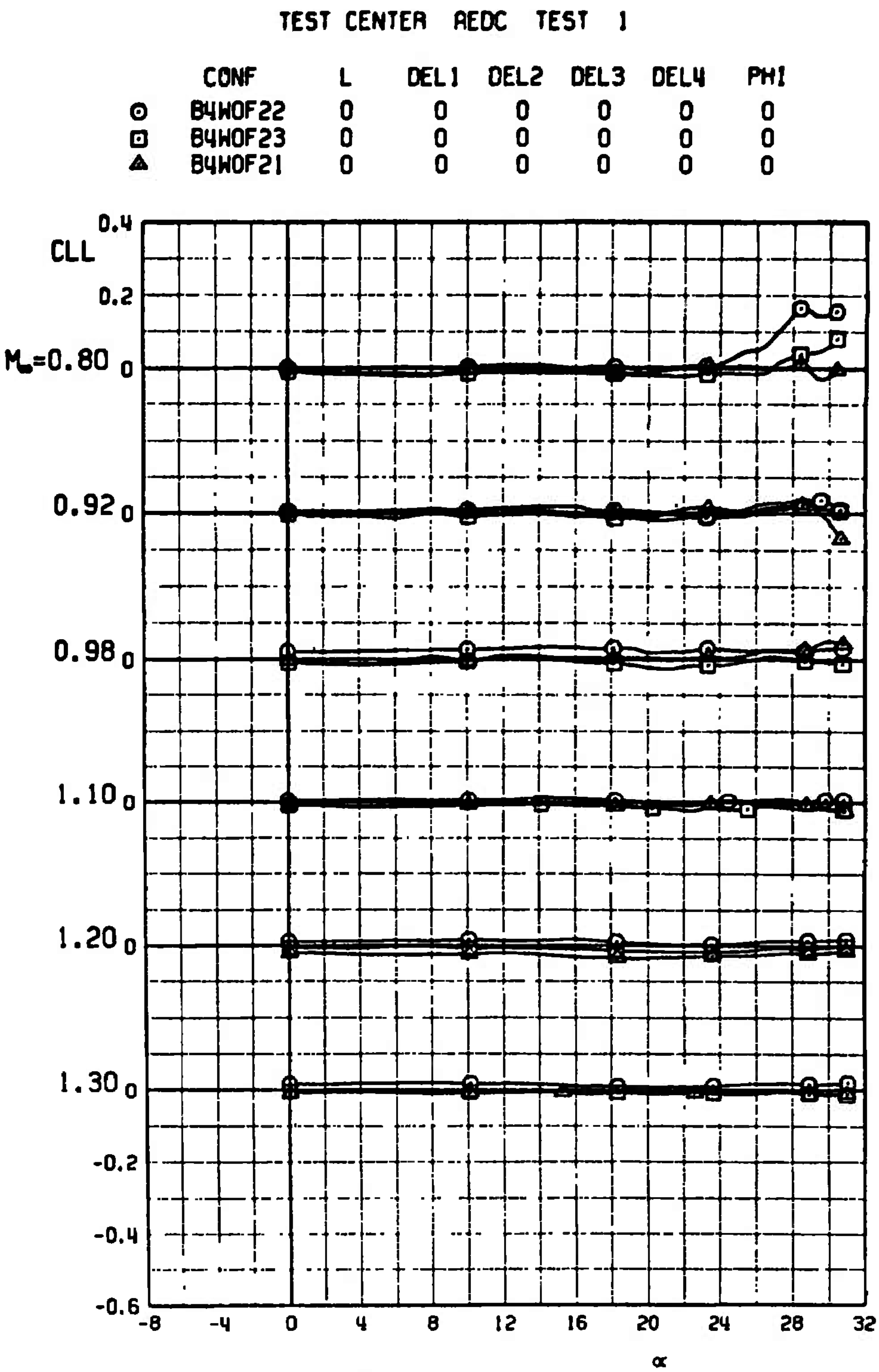

h. CLL versus α
Figure 12. Concluded.

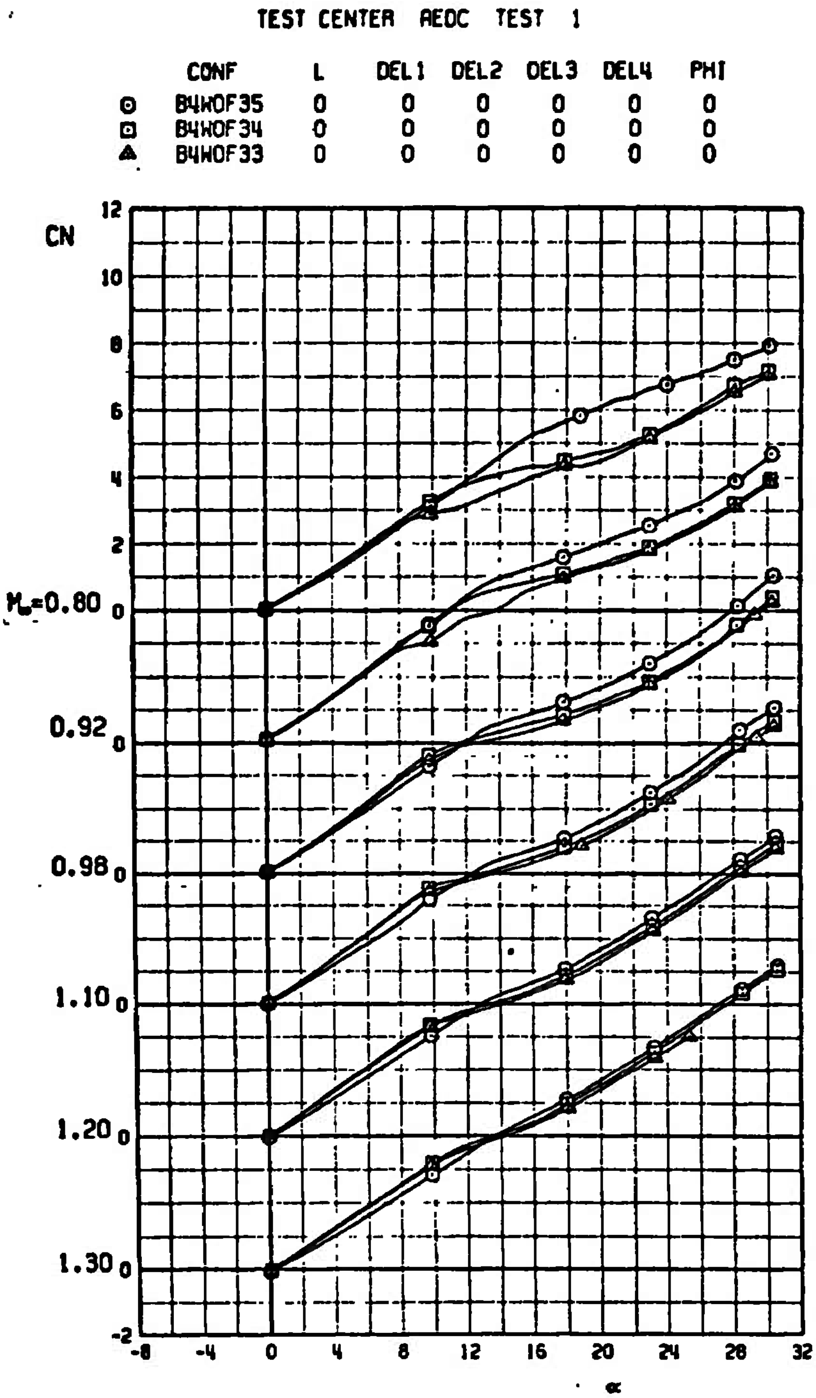

a. CN versus α

Figure 13. Test No. 1, comparison of aerodynamic coefficients of configurations B4W0F35, B4W0F34, and B4W0F33.

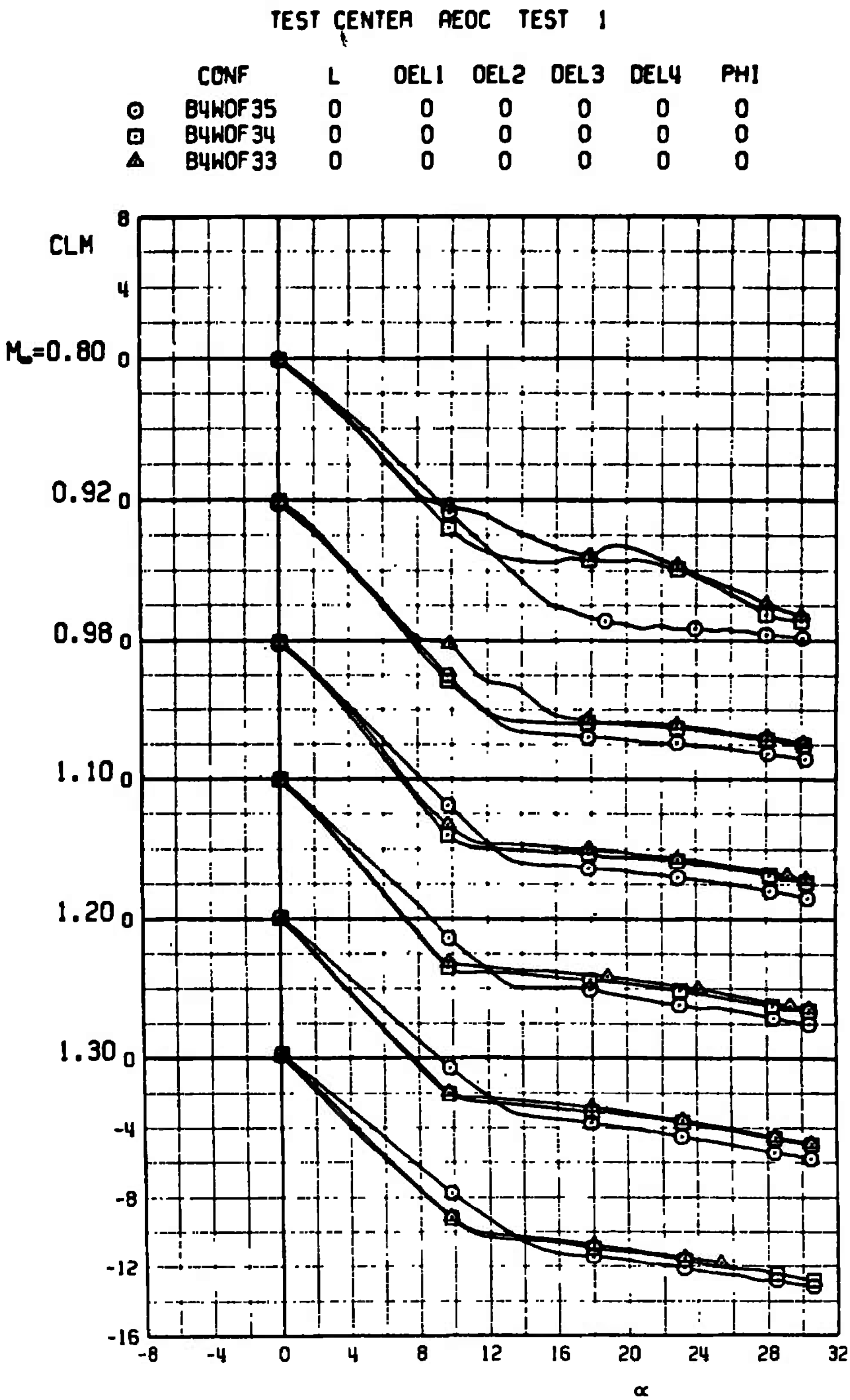

b. CLM versus α
Figure 13. Continued.

TEST CENTER AEDC TEST 1

	CONF	L	DEL1	DEL2	DEL3	DEL4	PHI
⊙	B4WOF35	0	0	0	0	0	0
⊡	B4WOF34	0	0	0	0	0	0
⚠	B4WOF33	0	0	0	0	0	0

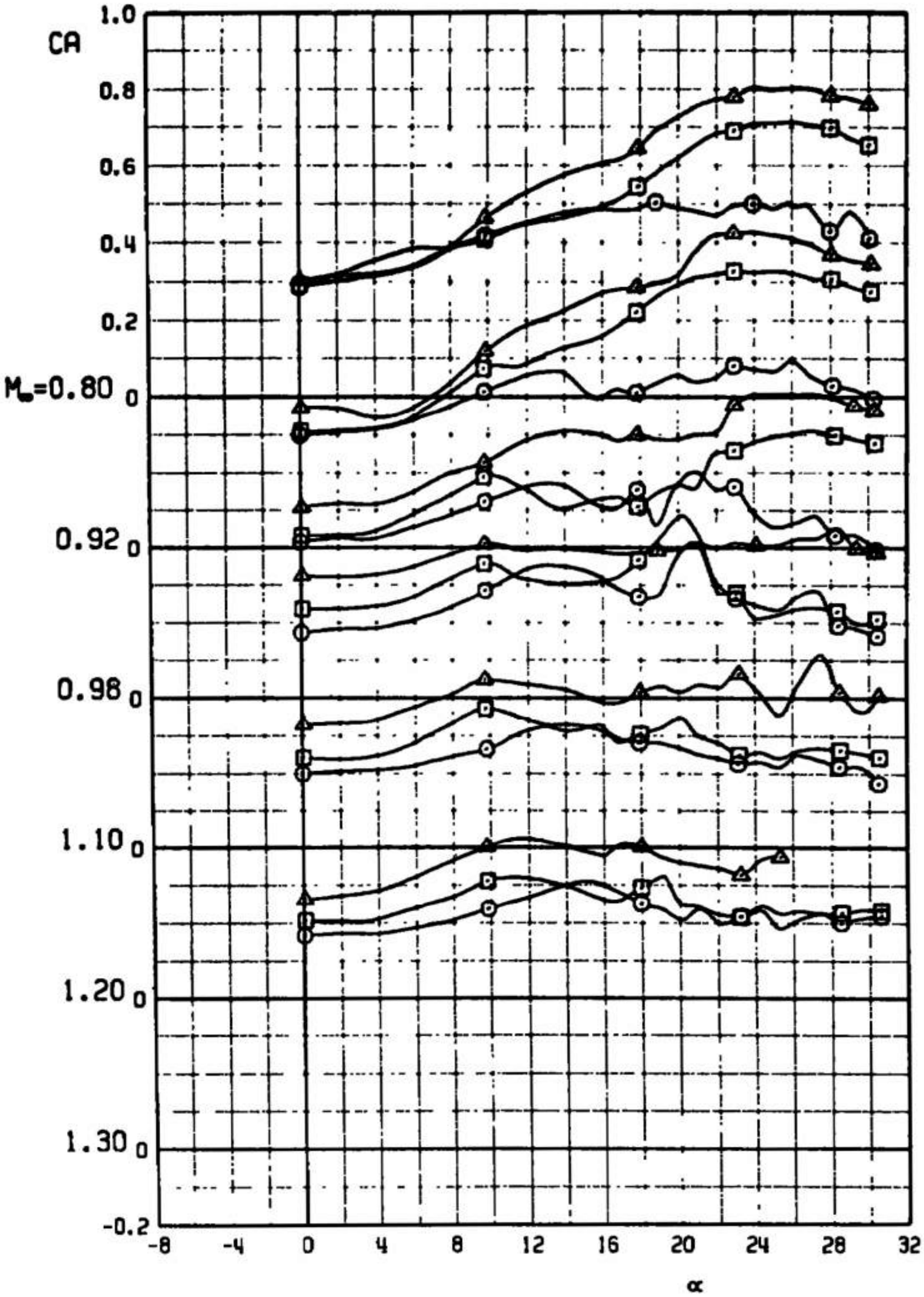

c. CA versus α
Figure 13. Continued.

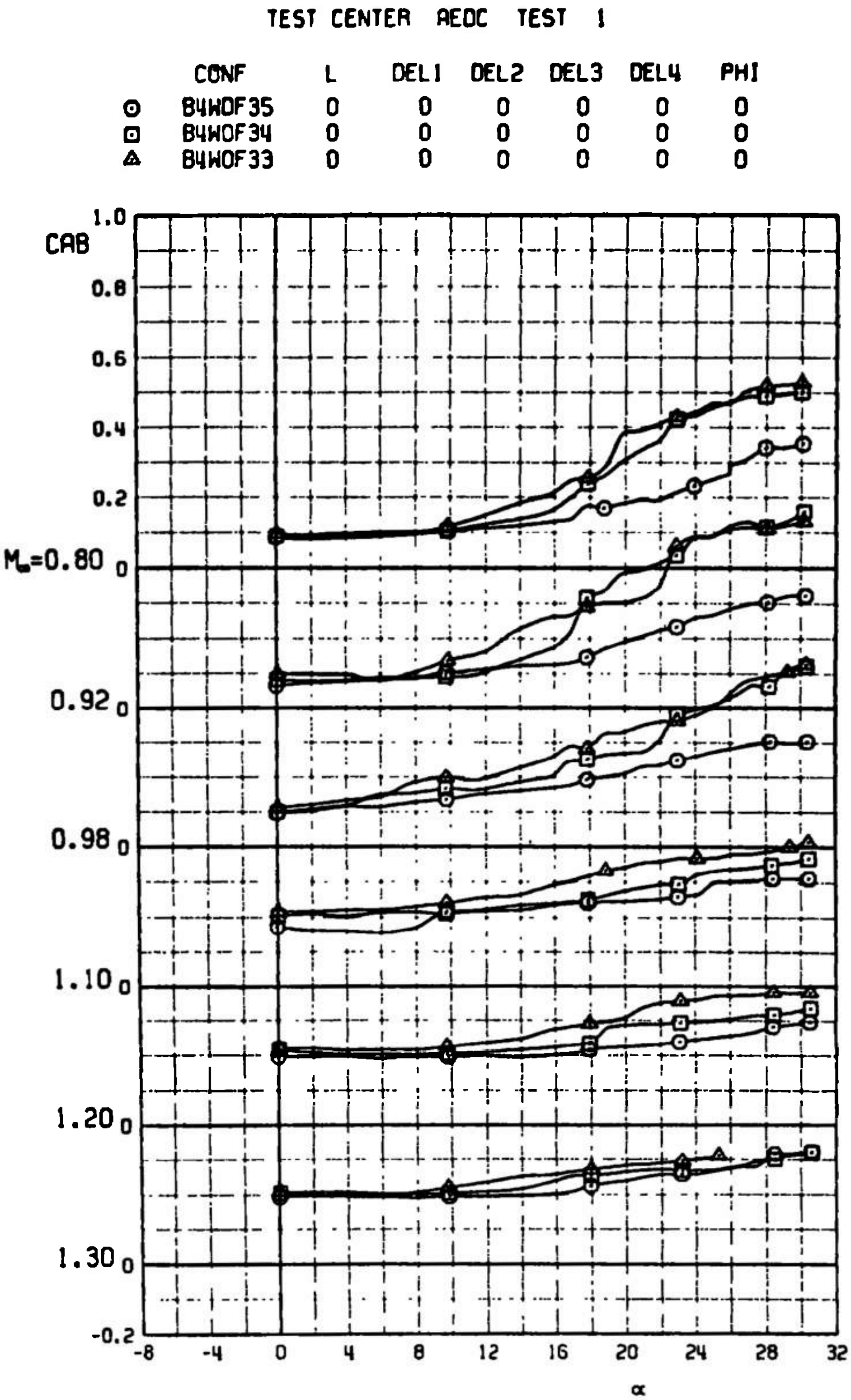

d. CAB versus α
Figure 13. Continued.

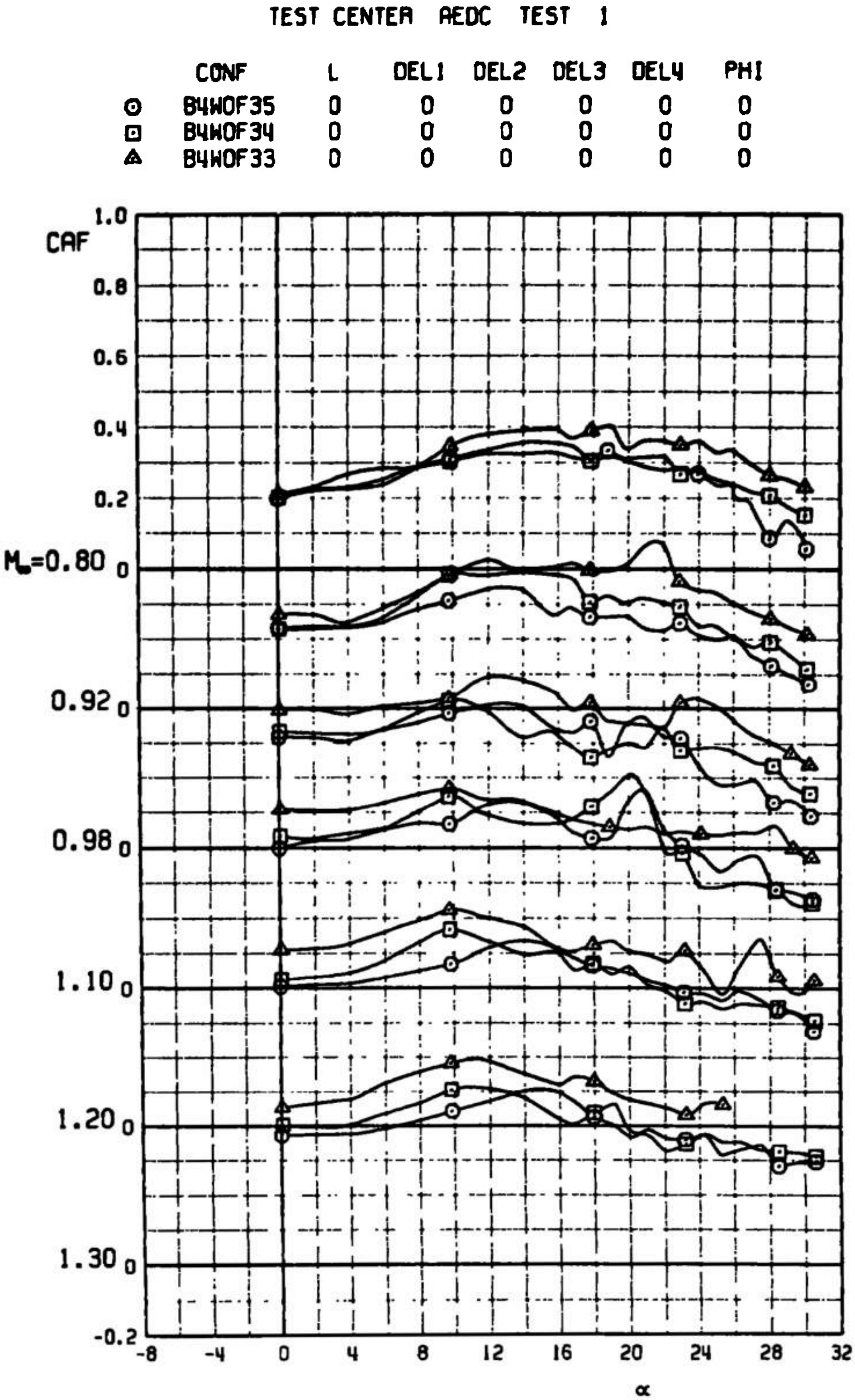

e. CAF versus α
Figure 13. Continued.

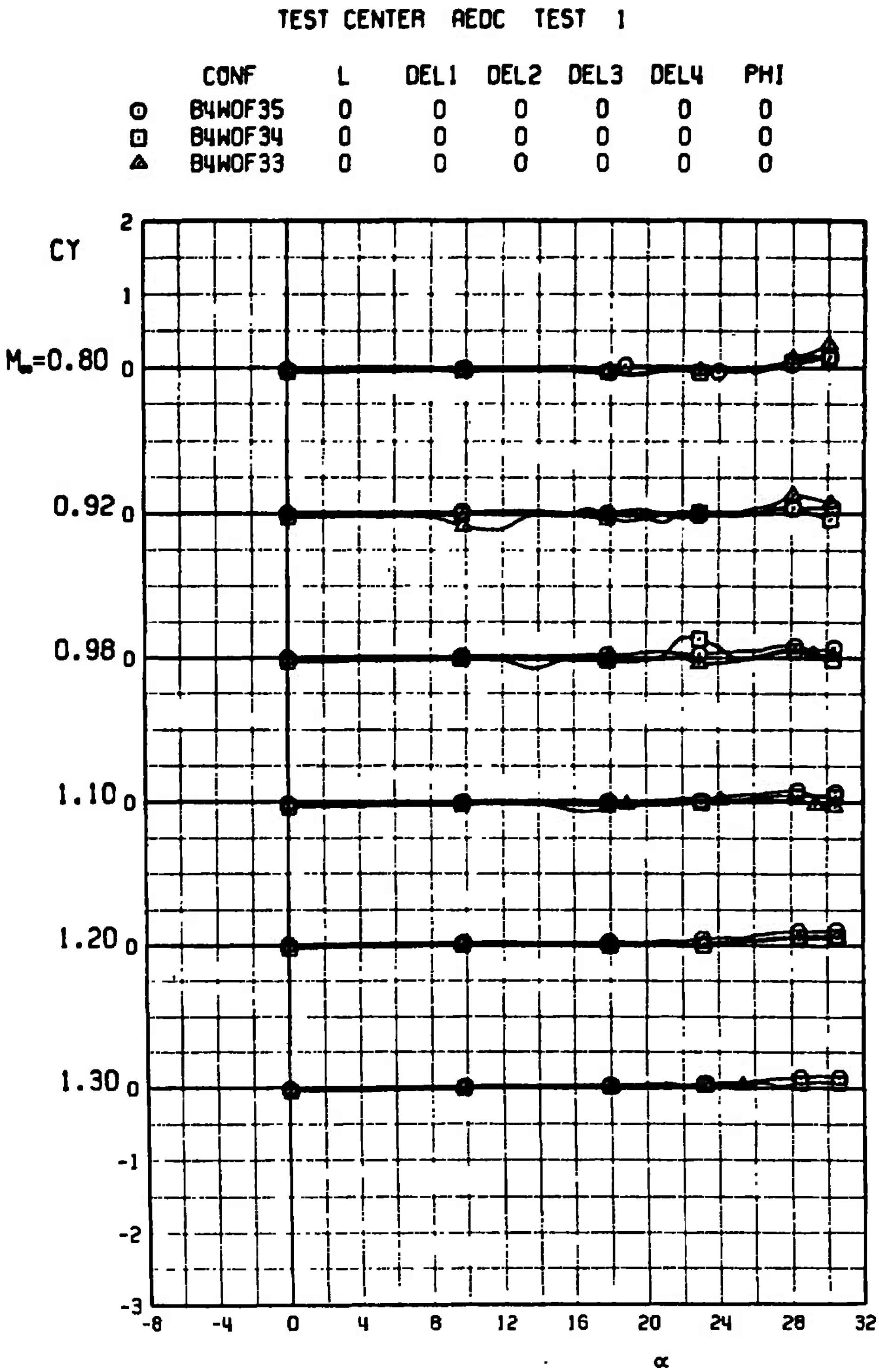

f. CY versus α
Figure 13. Continued.

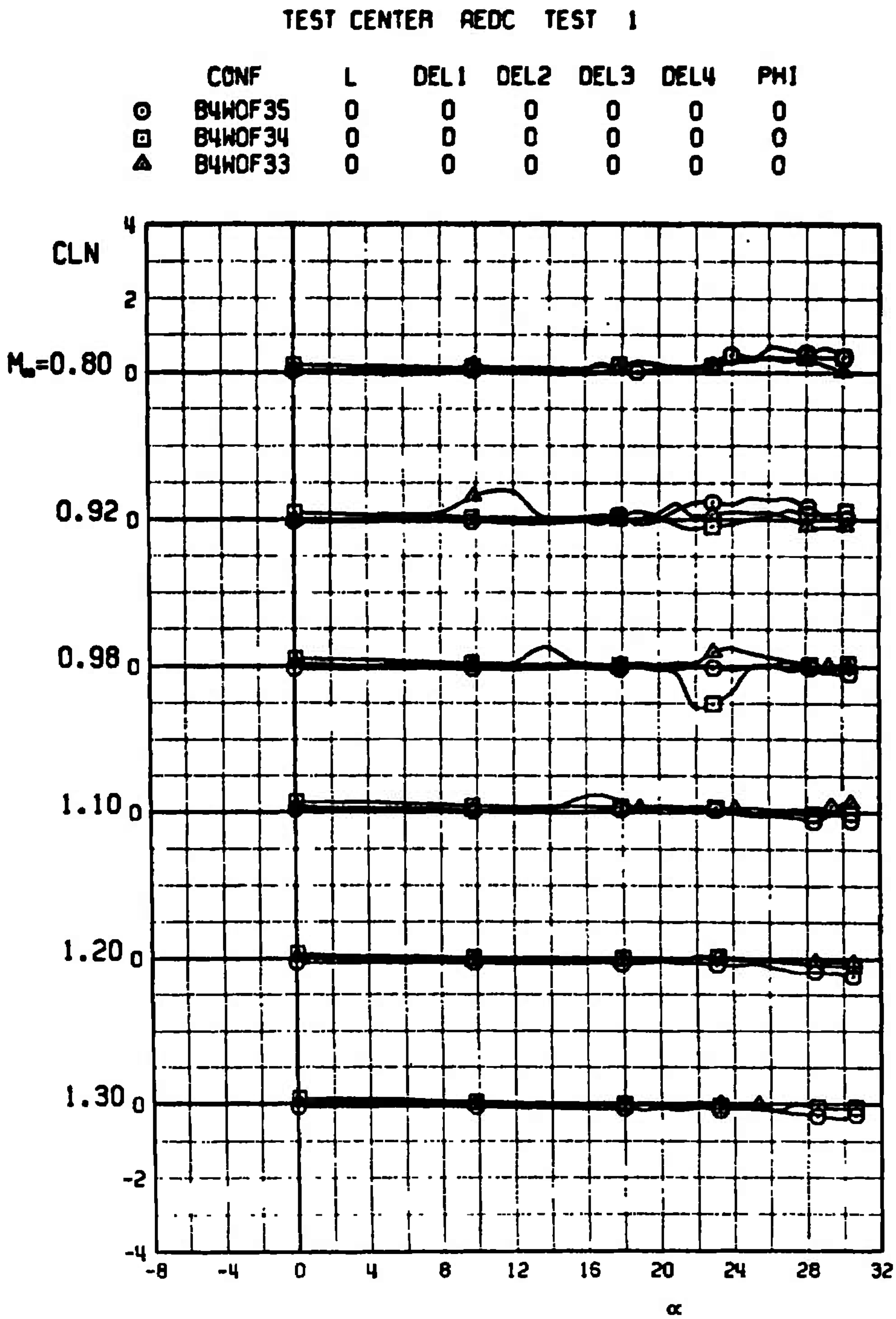

g. CLN versus α
Figure 13. Continued.

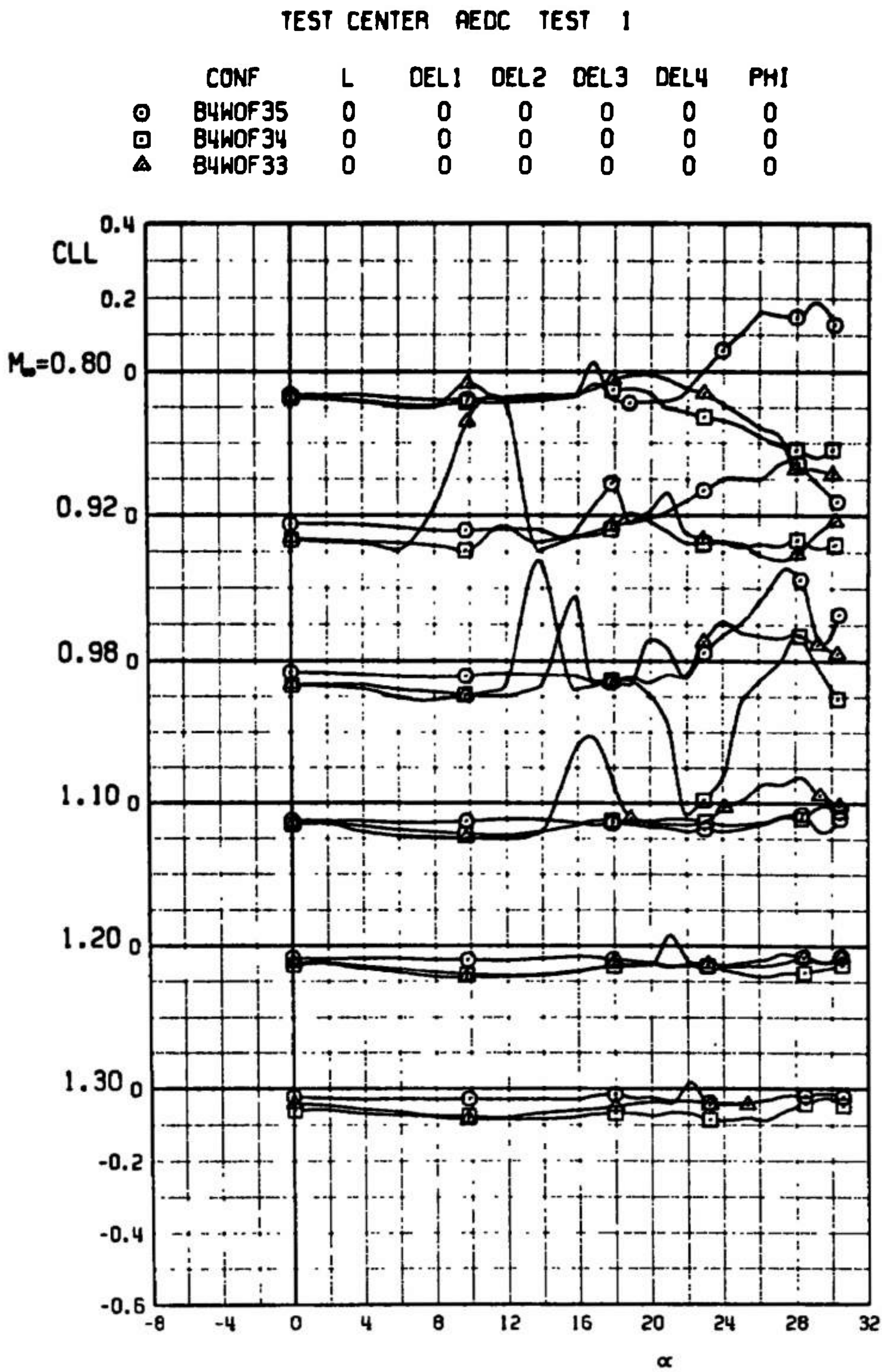

h. CLL versus α
Figure 13. Concluded.

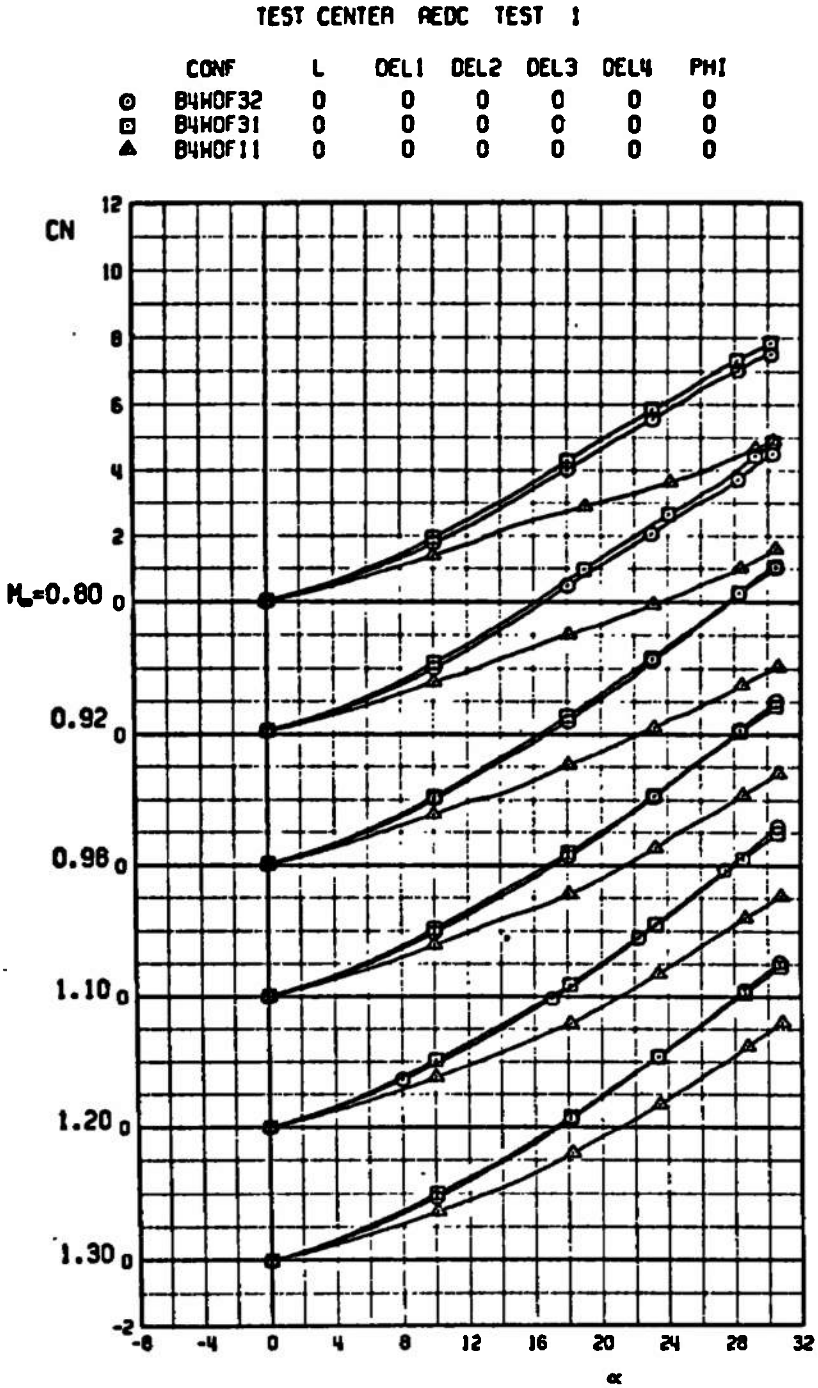

a. CN versus α

Figure 14. Test No. 1, comparison of aerodynamic coefficients of configurations B4W0F32, B4W0F31, and B4W0F11.

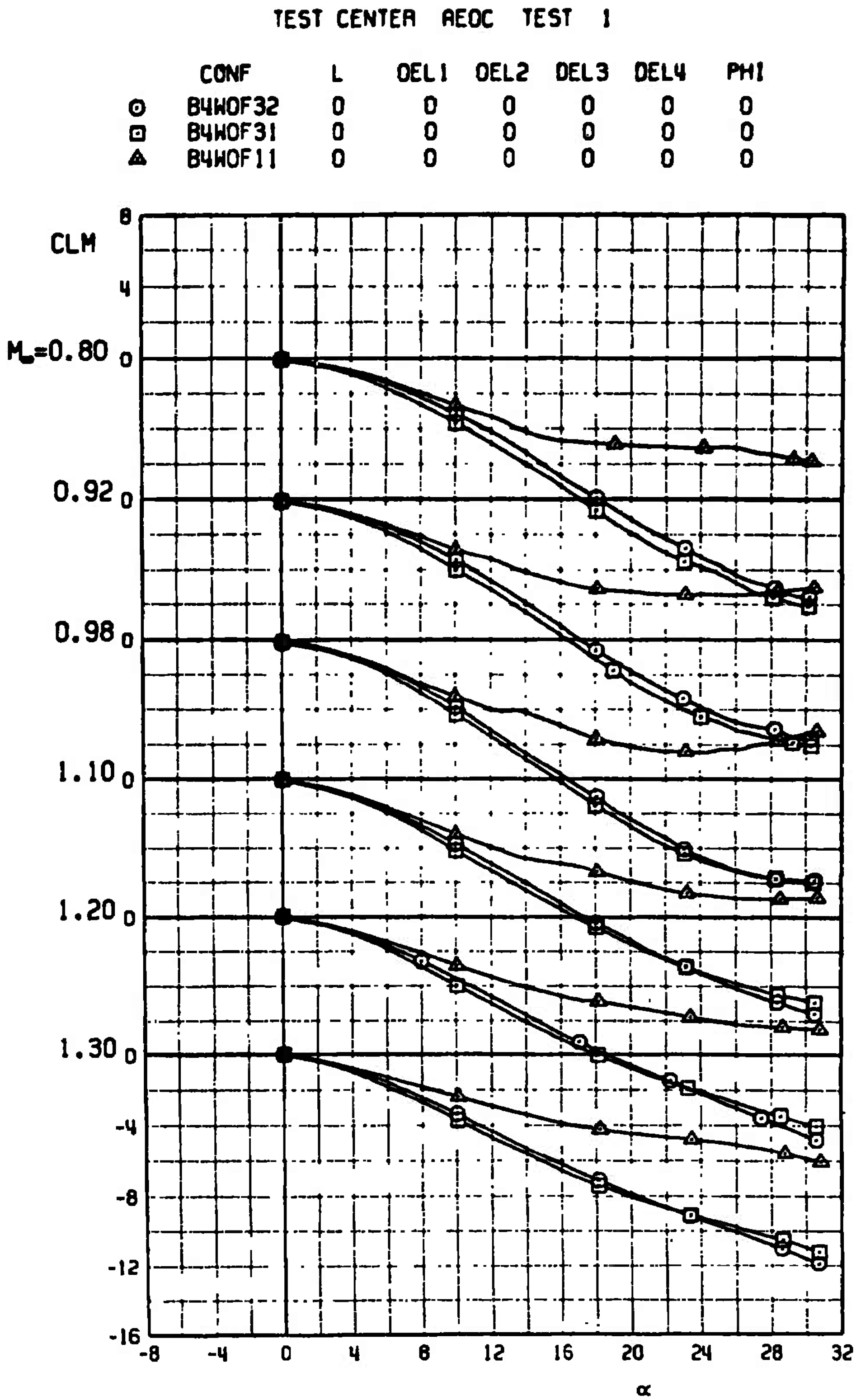

b. CLM versus α
Figure 14. Continued.

TEST CENTER AEDC TEST 1

	CONF	L	DEL1	DEL2	DEL3	DEL4	PHI
⊙	B4W0F32	0	0	0	0	0	0
⊡	B4W0F31	0	0	0	0	0	0
△	B4W0F11	0	0	0	0	0	0

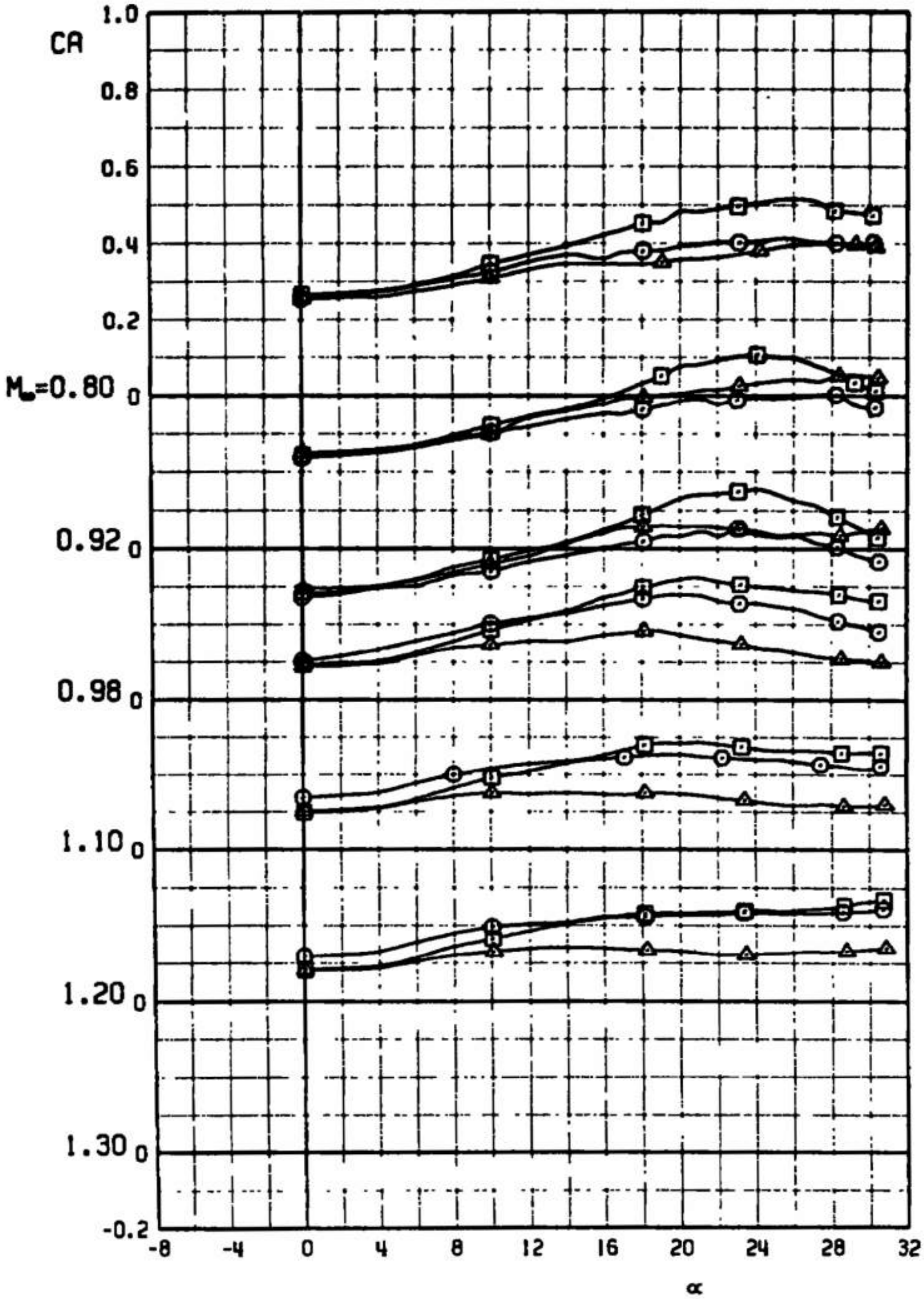

c. CA versus α
Figure 14. Continued.

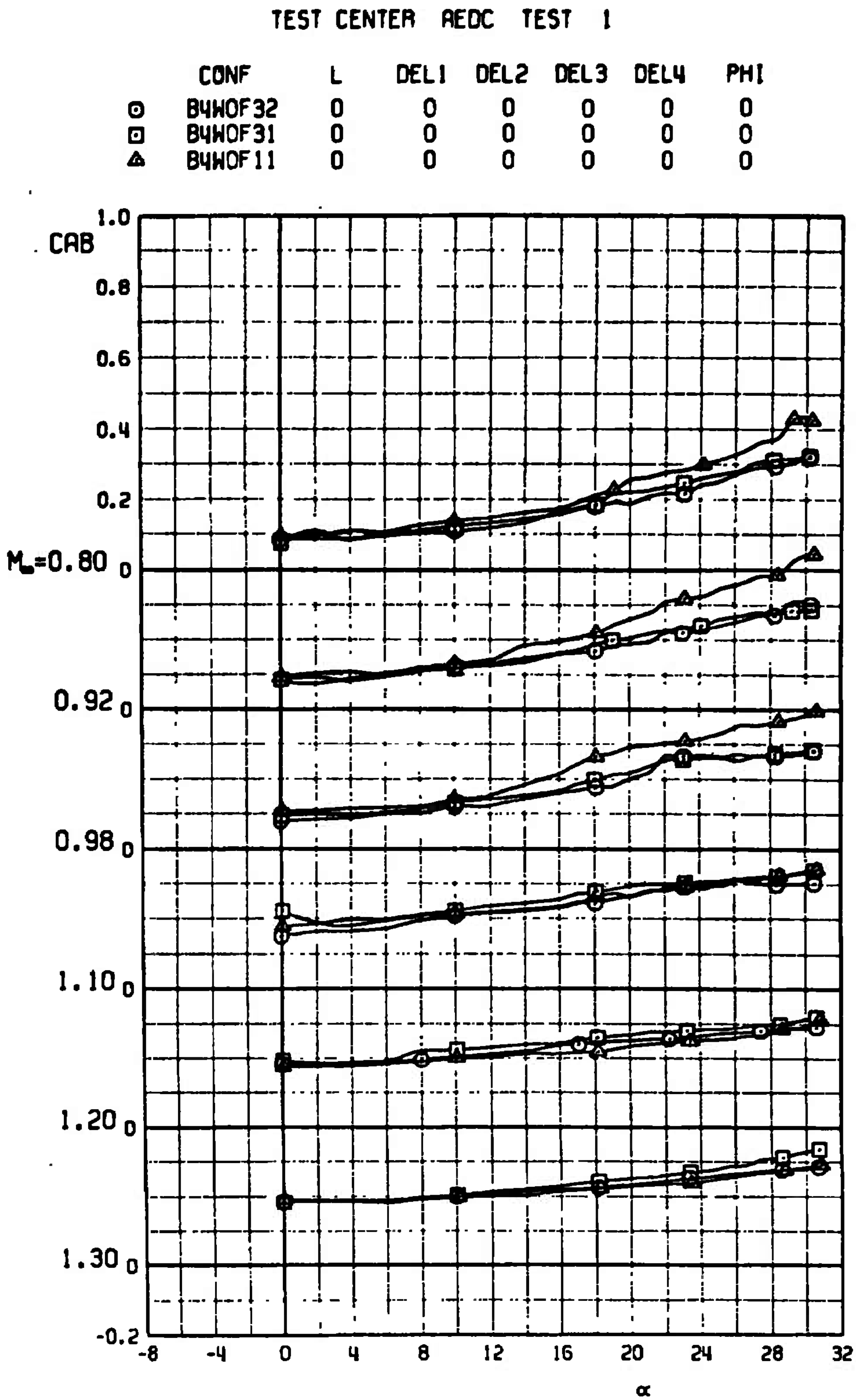

d. CAB versus α
Figure 14. Continued.

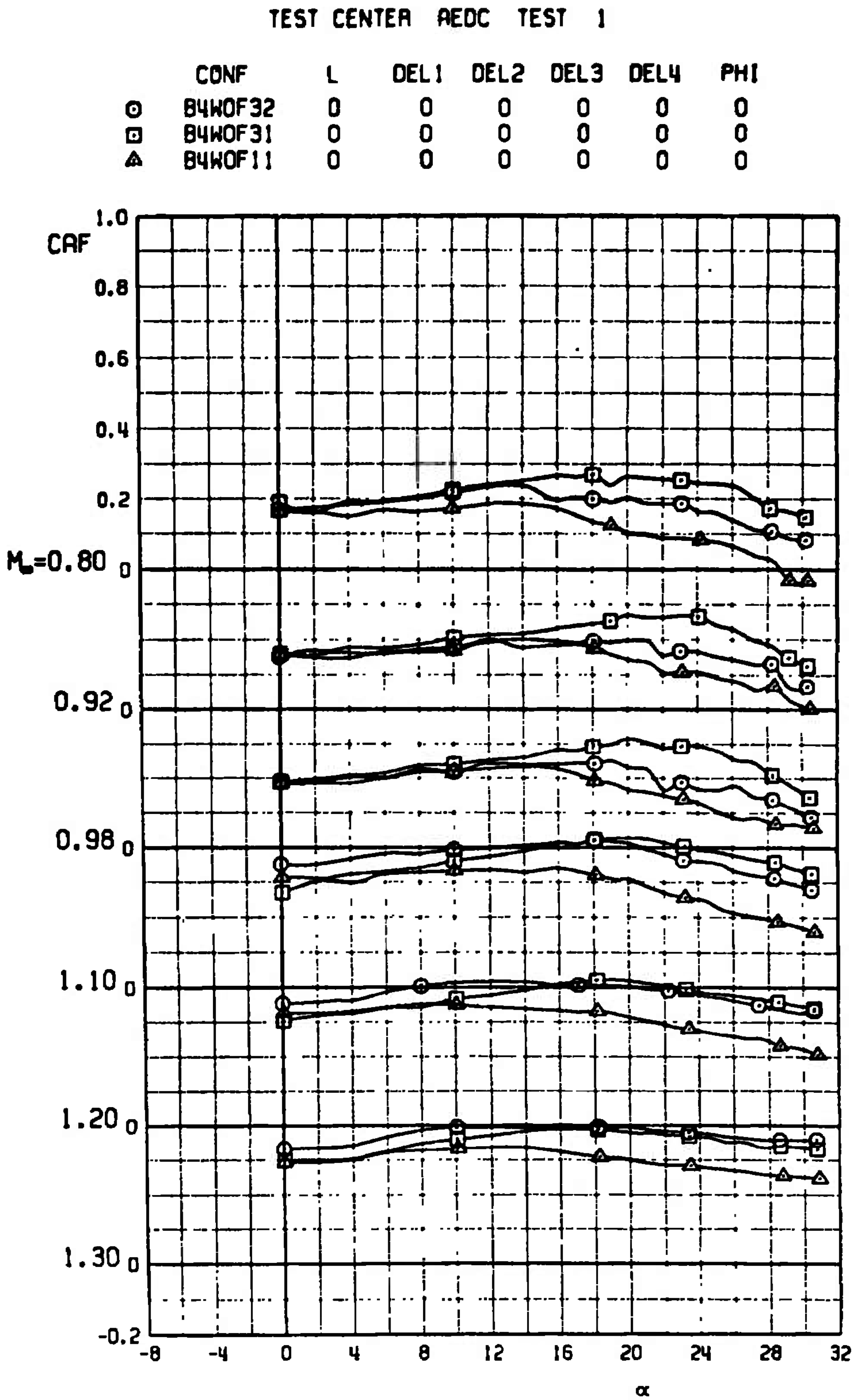

e. CAF versus α
Figure 14. Continued.

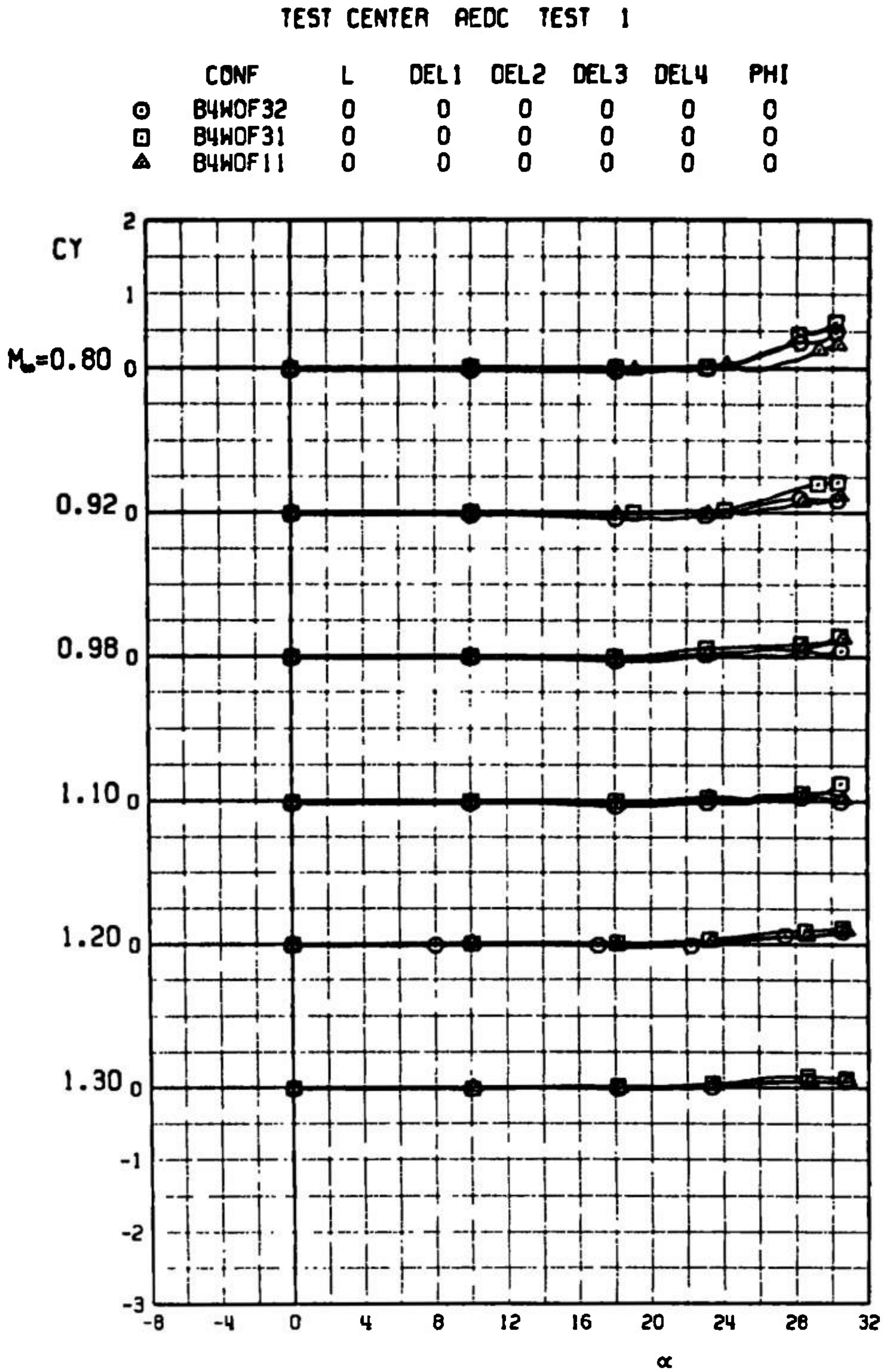

f. CY versus α
Figure 14. Continued.

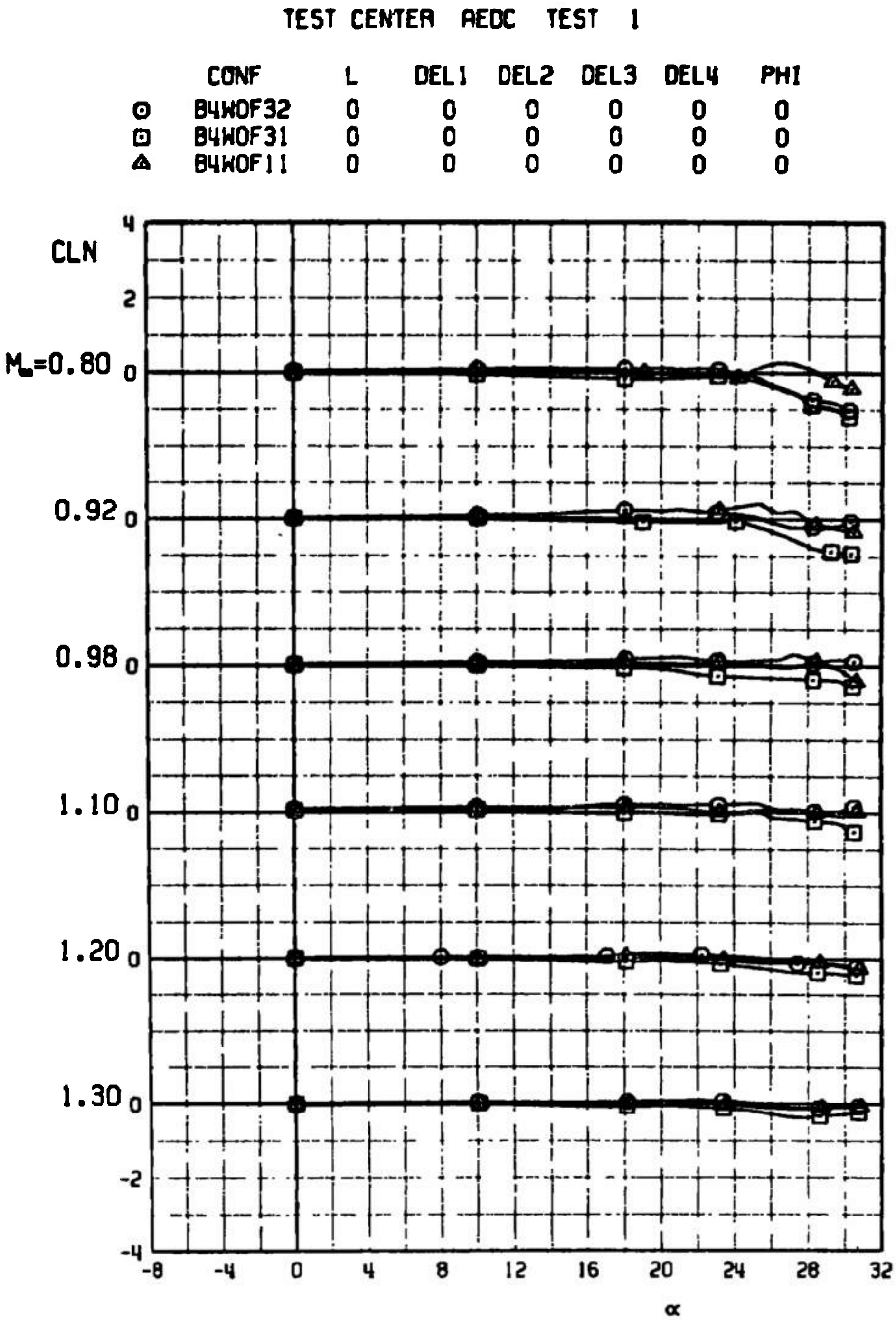

g. CLN versus α
Figure 14. Continued.

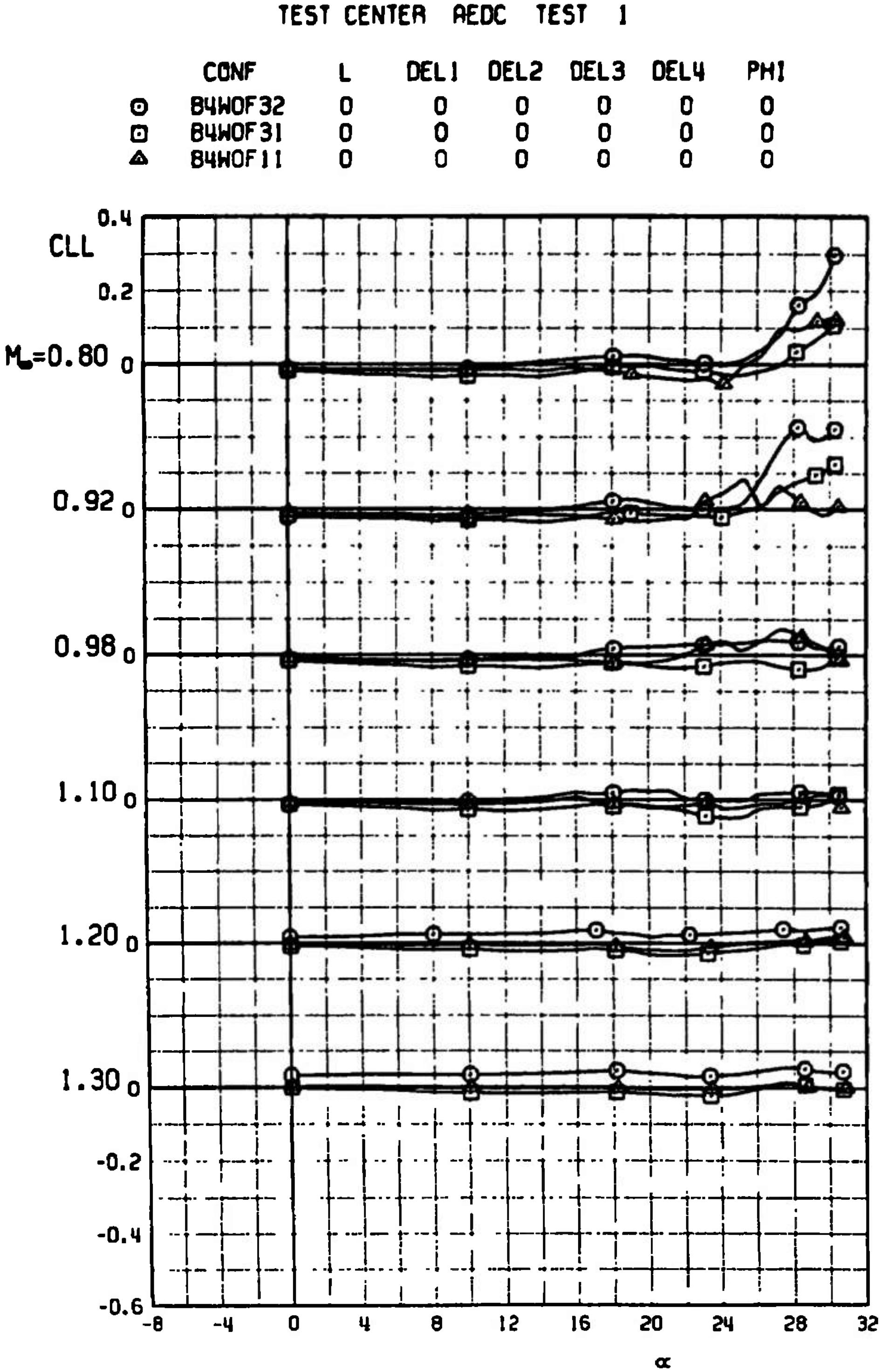

h. CLL versus α
Figure 14. Concluded.

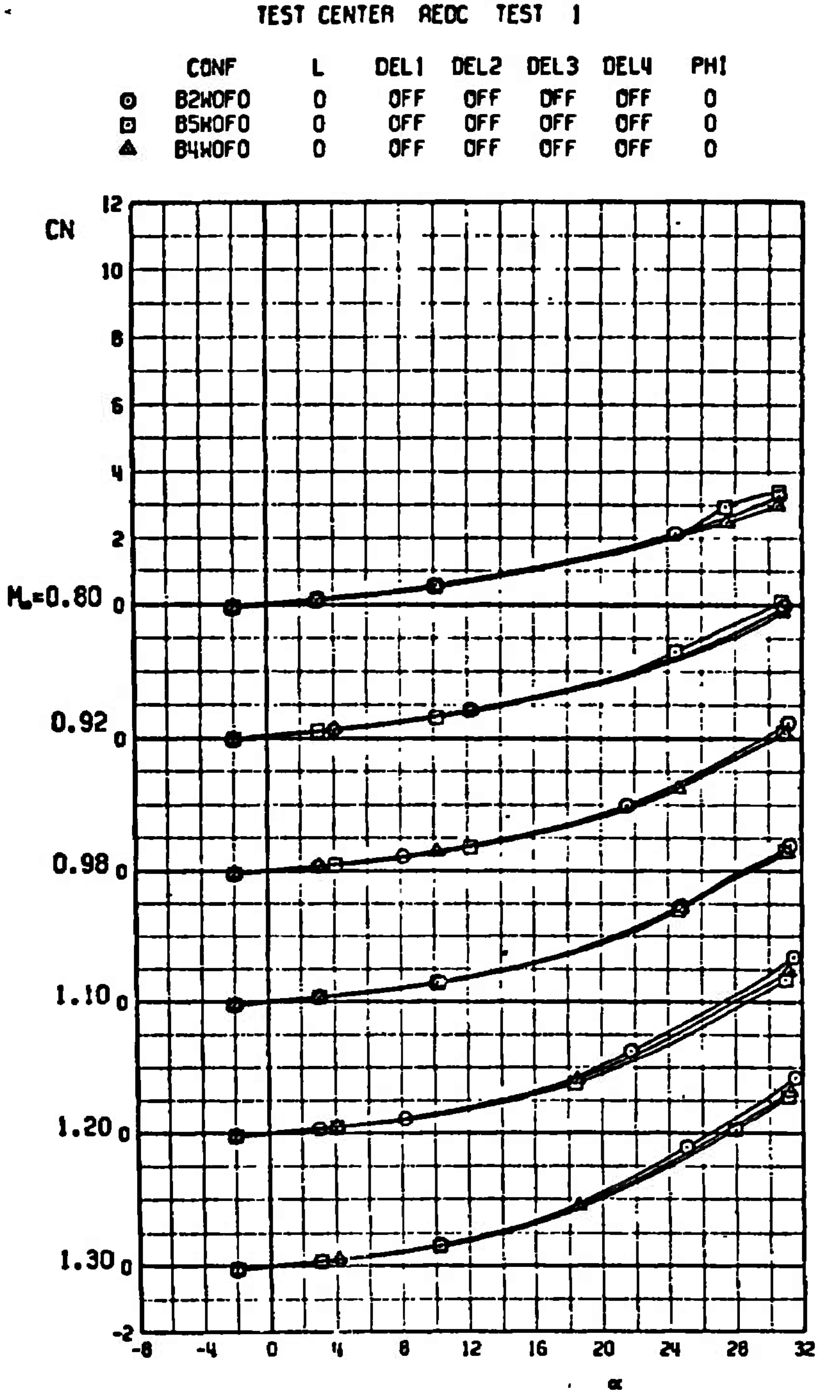

a. CN versus α

Figure 15. Test No. 1, comparison of aerodynamic coefficients of configurations B2W0F0, B5W0F0, and B4W0F0.

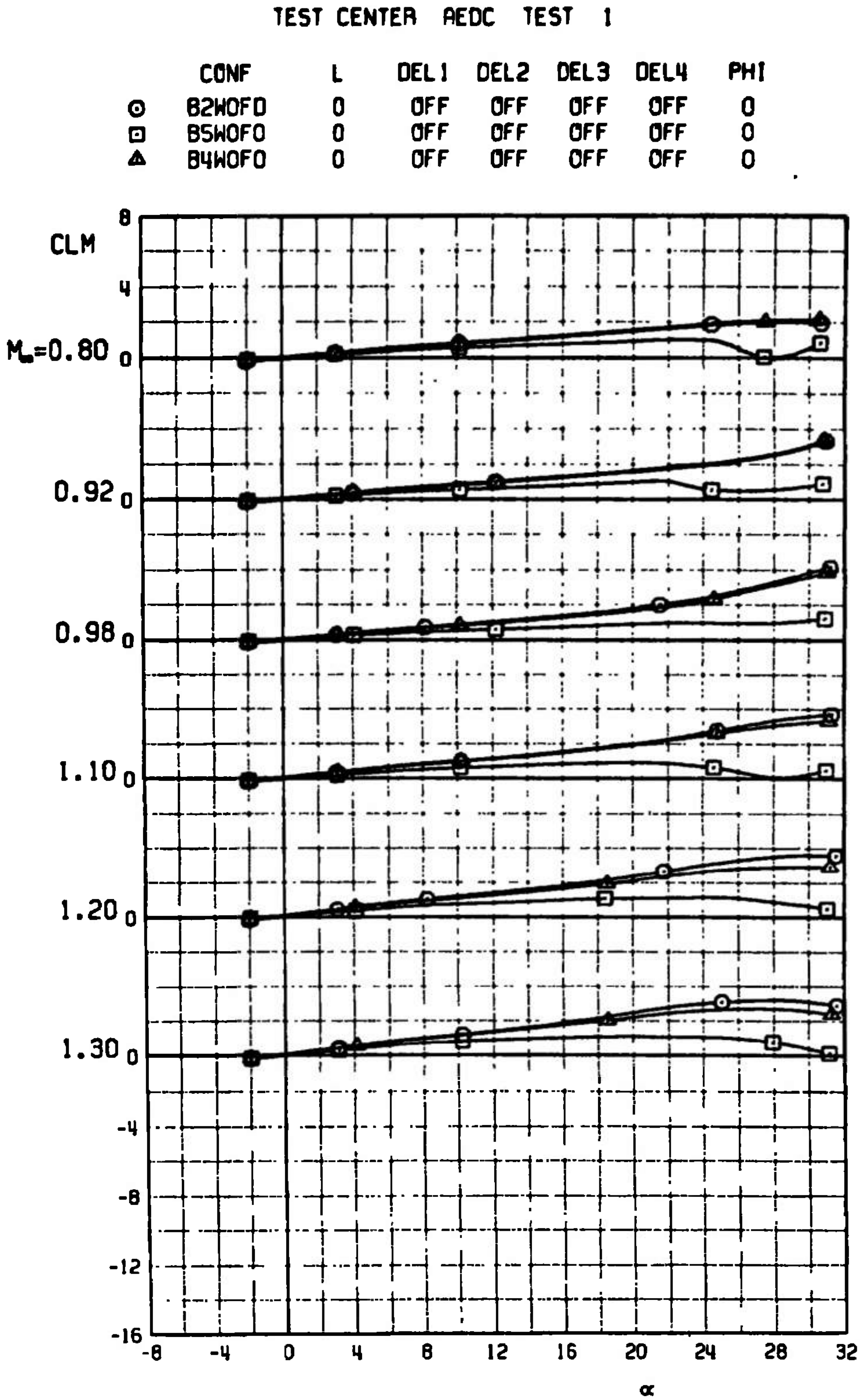

b. CLM versus α
Figure 15. Continued.

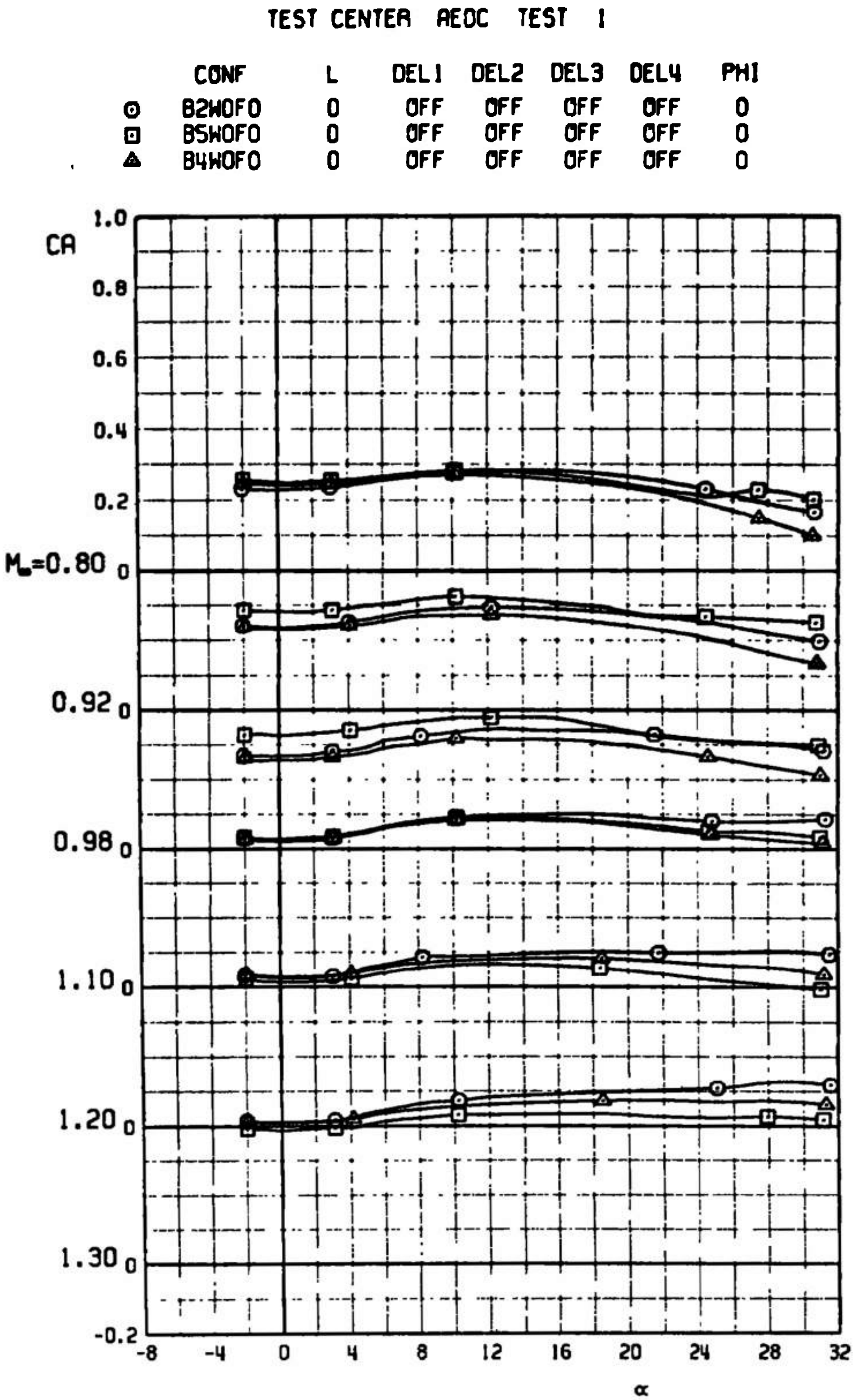

c. CA versus α
Figure 15. Continued.

TEST CENTER AEDC TEST 1

	CONF	L	DEL1	DEL2	DEL3	DEL4	PHI
⊙	B2W0F0	0	OFF	OFF	OFF	OFF	0
⊡	B5W0F0	0	OFF	OFF	OFF	OFF	0
△	B4W0F0	0	OFF	OFF	OFF	OFF	0

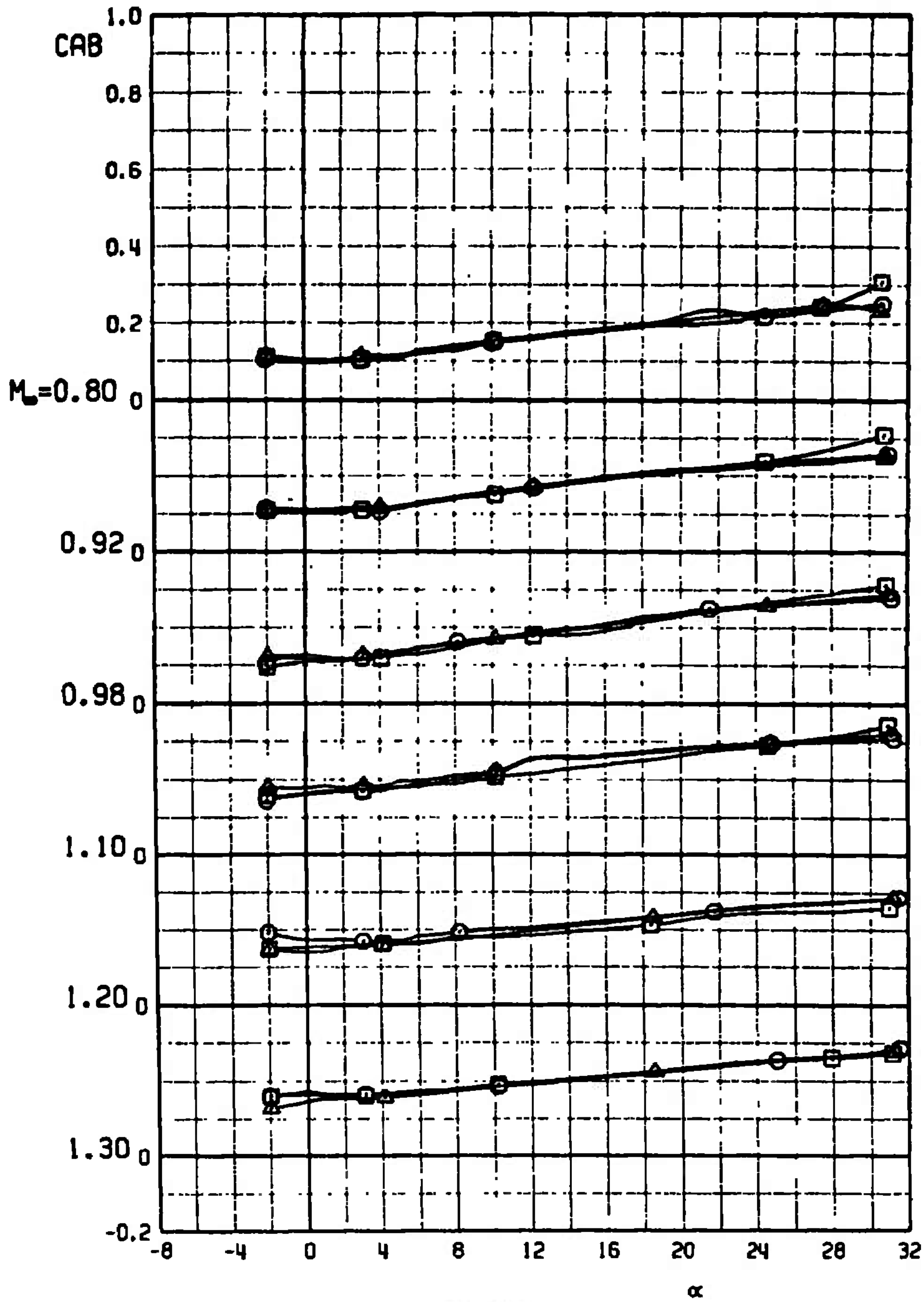

d. CAB versus α
Figure 15. Continued.

TEST CENTER AEDC TEST 1

	CONF	L	DEL1	DEL2	DEL3	DEL4	PHI
⊙	B2WOFO	0	OFF	OFF	OFF	OFF	0
⊡	B5WOFO	0	OFF	OFF	OFF	OFF	0
△	B4WOFO	0	OFF	OFF	OFF	OFF	0

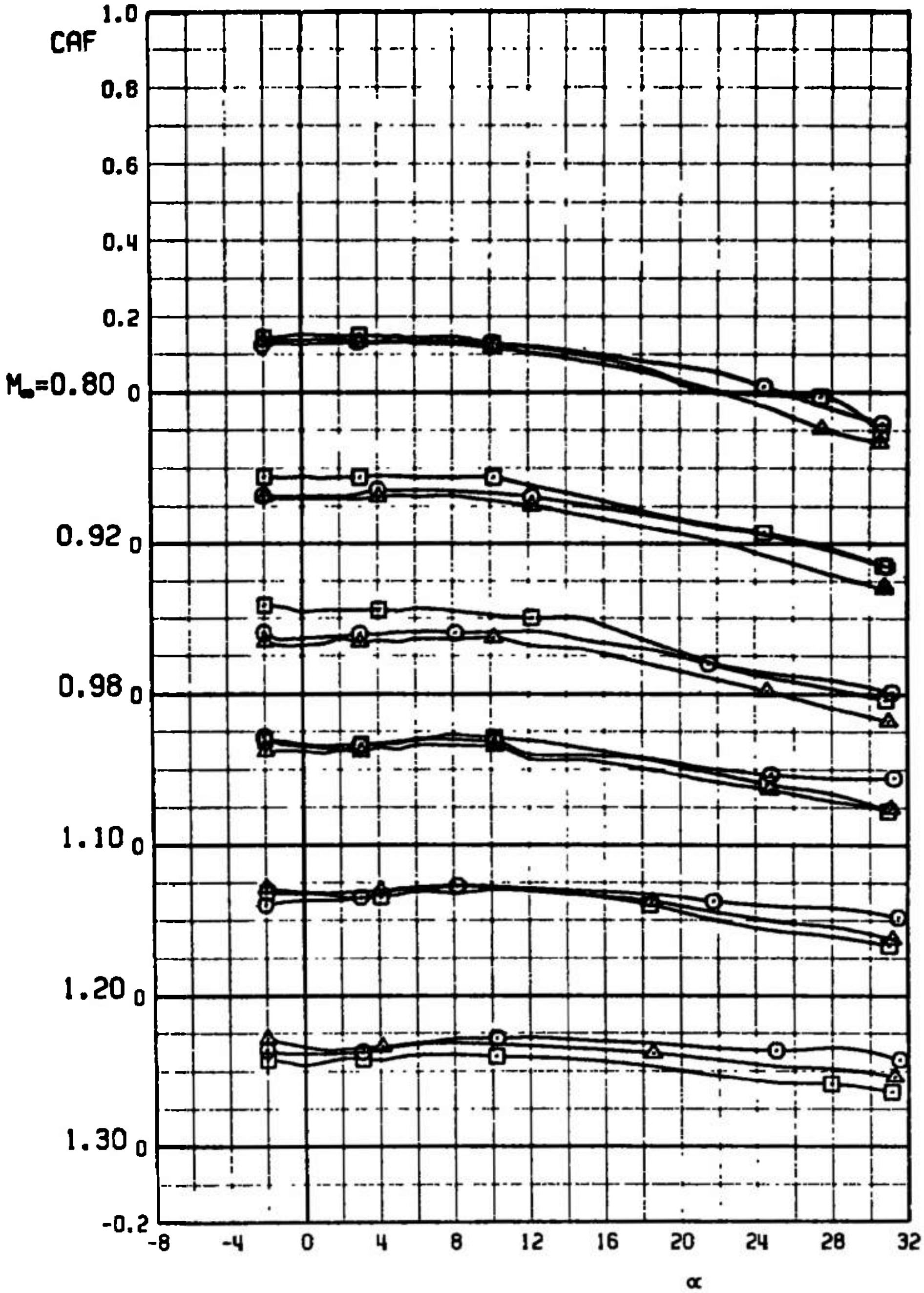

e. CAF versus α
Figure 15. Continued.

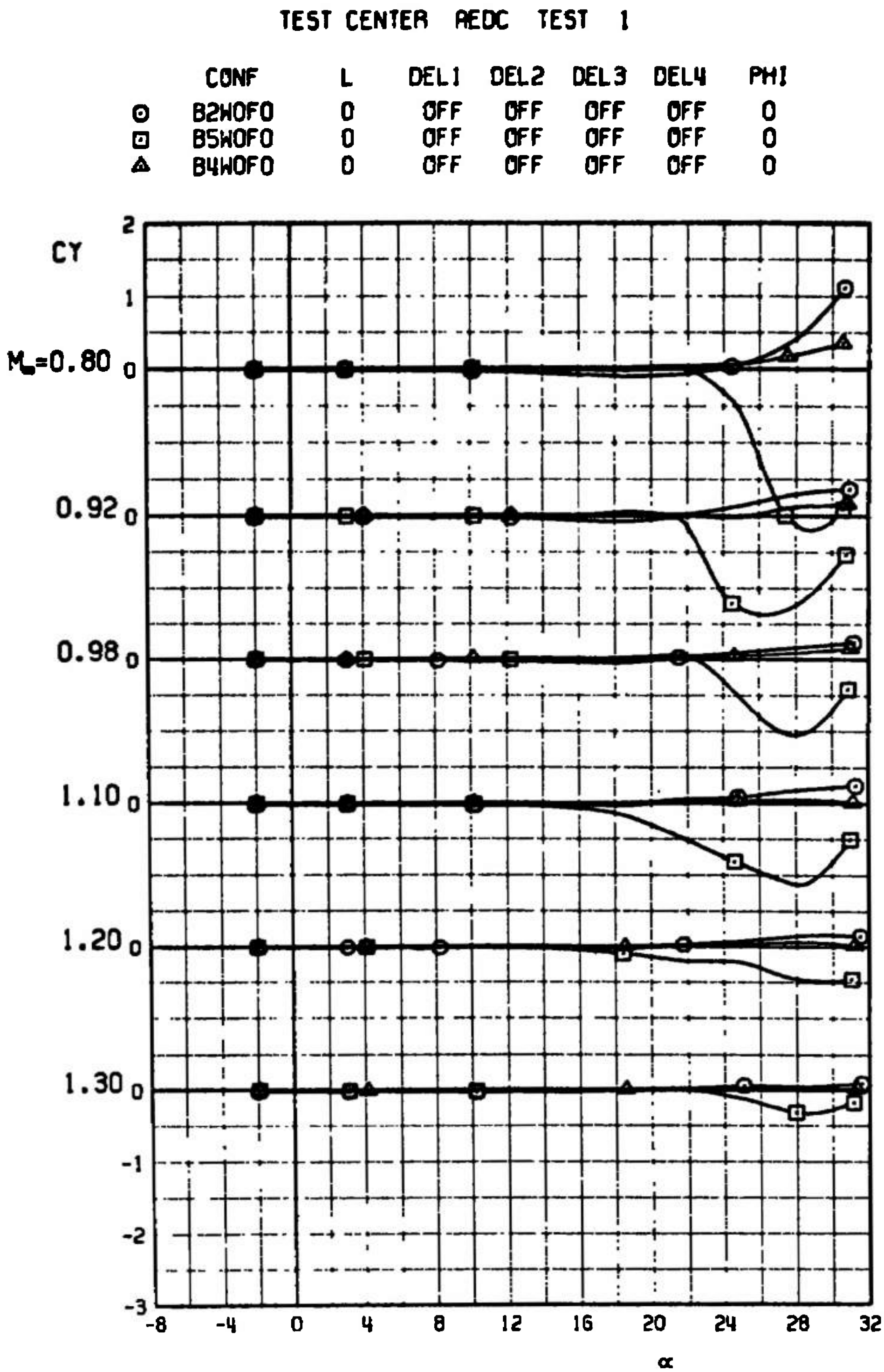

f. CY versus α

Figure 15. Continued.

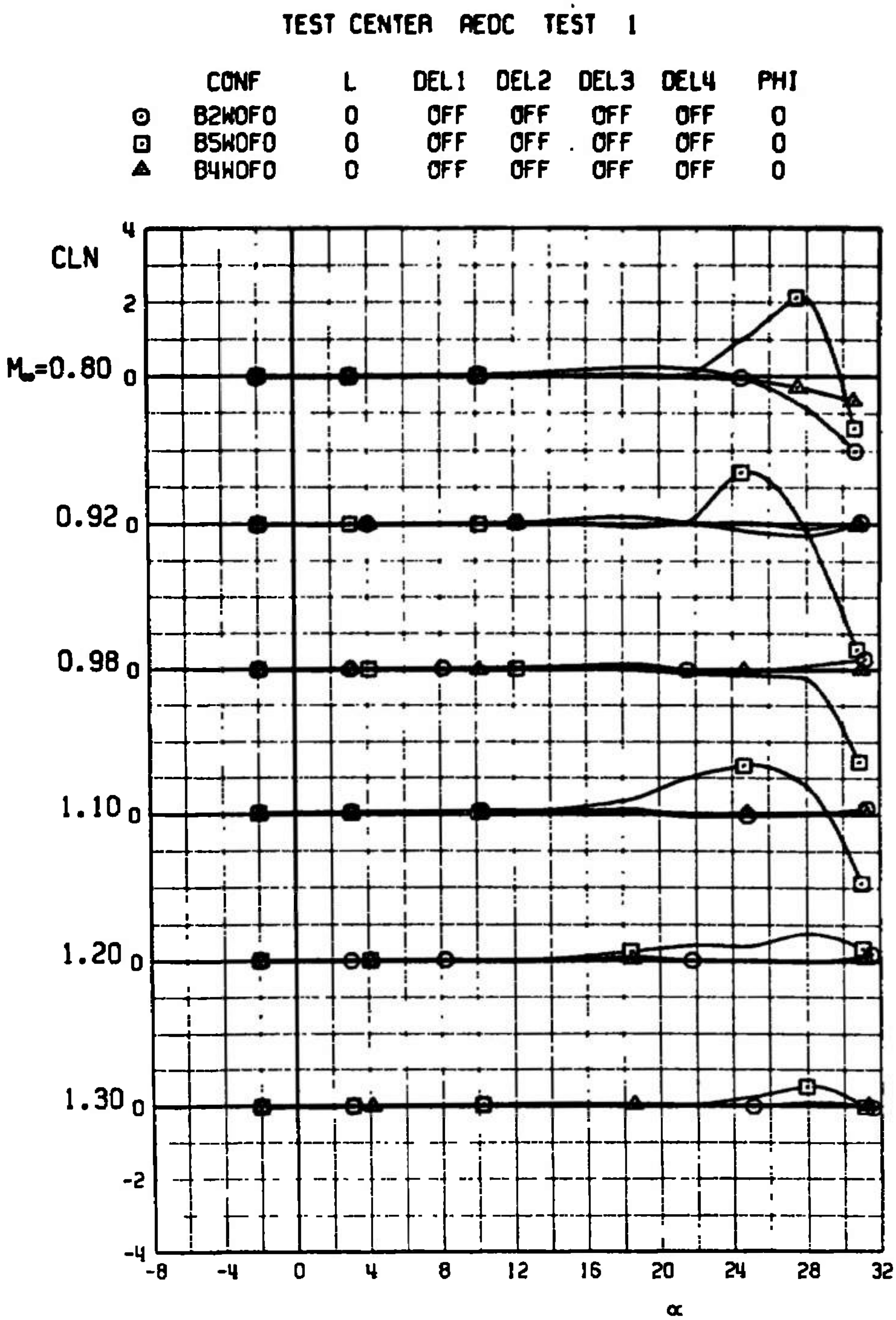

g. CLN versus *α*
Figure 15. Continued.

TEST CENTER AEDC TEST 1

	CONF	L	DEL1	DEL2	DEL3	DEL4	PHI
⊙	B2W0F0	0	OFF	OFF	OFF	OFF	0
⊡	B5W0F0	0	OFF	OFF	OFF	OFF	0
△	B4W0F0	0	OFF	OFF	OFF	OFF	0

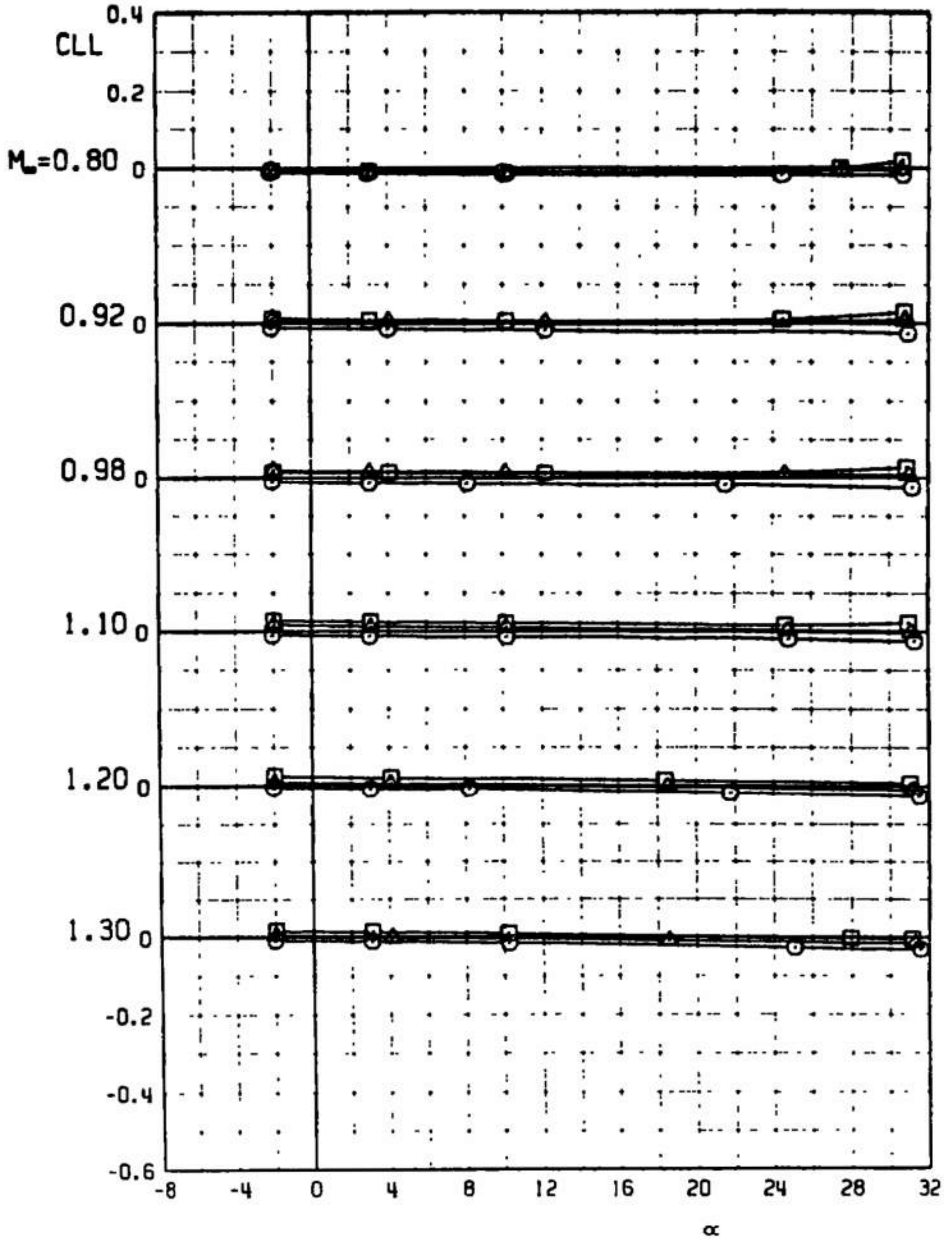

h. CLL versus α
Figure 15. Concluded.

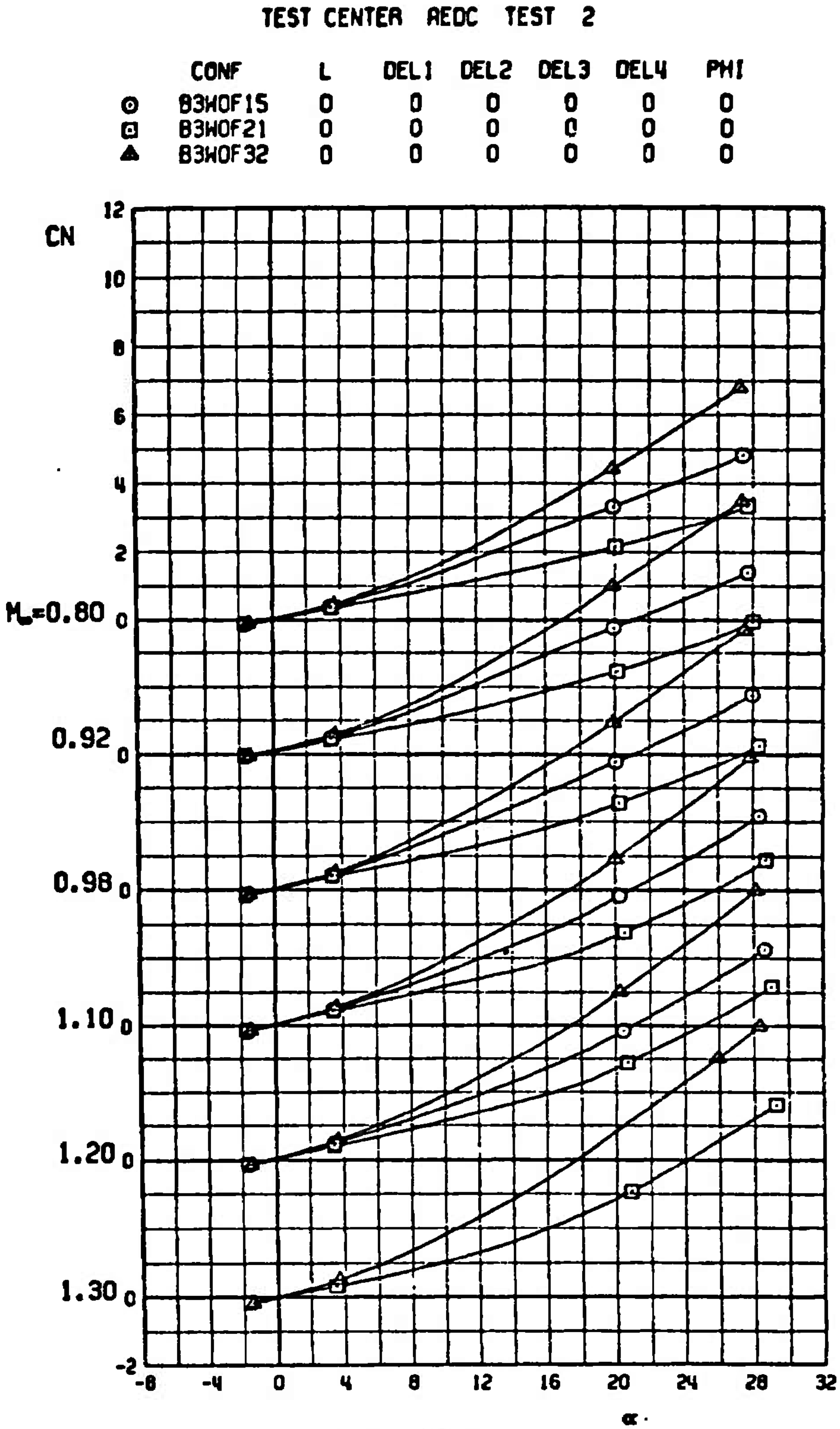

a. CN versus α

Figure 16. Test No. 2, comparison of aerodynamic coefficients of configurations B3W0F15, B3W0F21, and B3W0F32.

TEST CENTER AEDC TEST 2

	CONF	L	DEL1	DEL2	DEL3	DEL4	PHI
⊙	B3W0F15	0	0	0	0	0	0
⊡	B3W0F21	0	0	0	0	0	0
△	B3W0F32	0	0	0	0	0	0

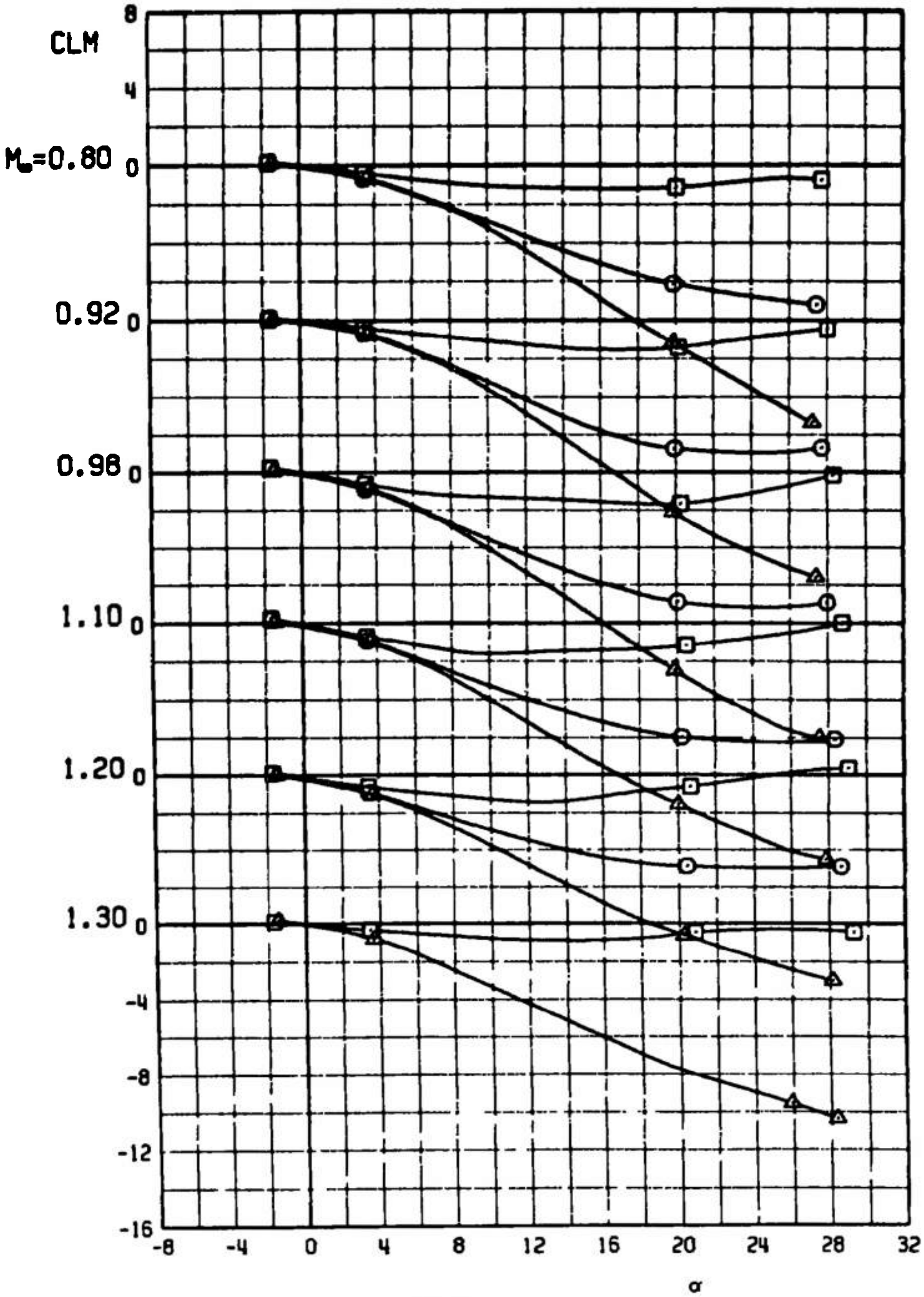

b. CLM versus α

Figure 16. Continued.

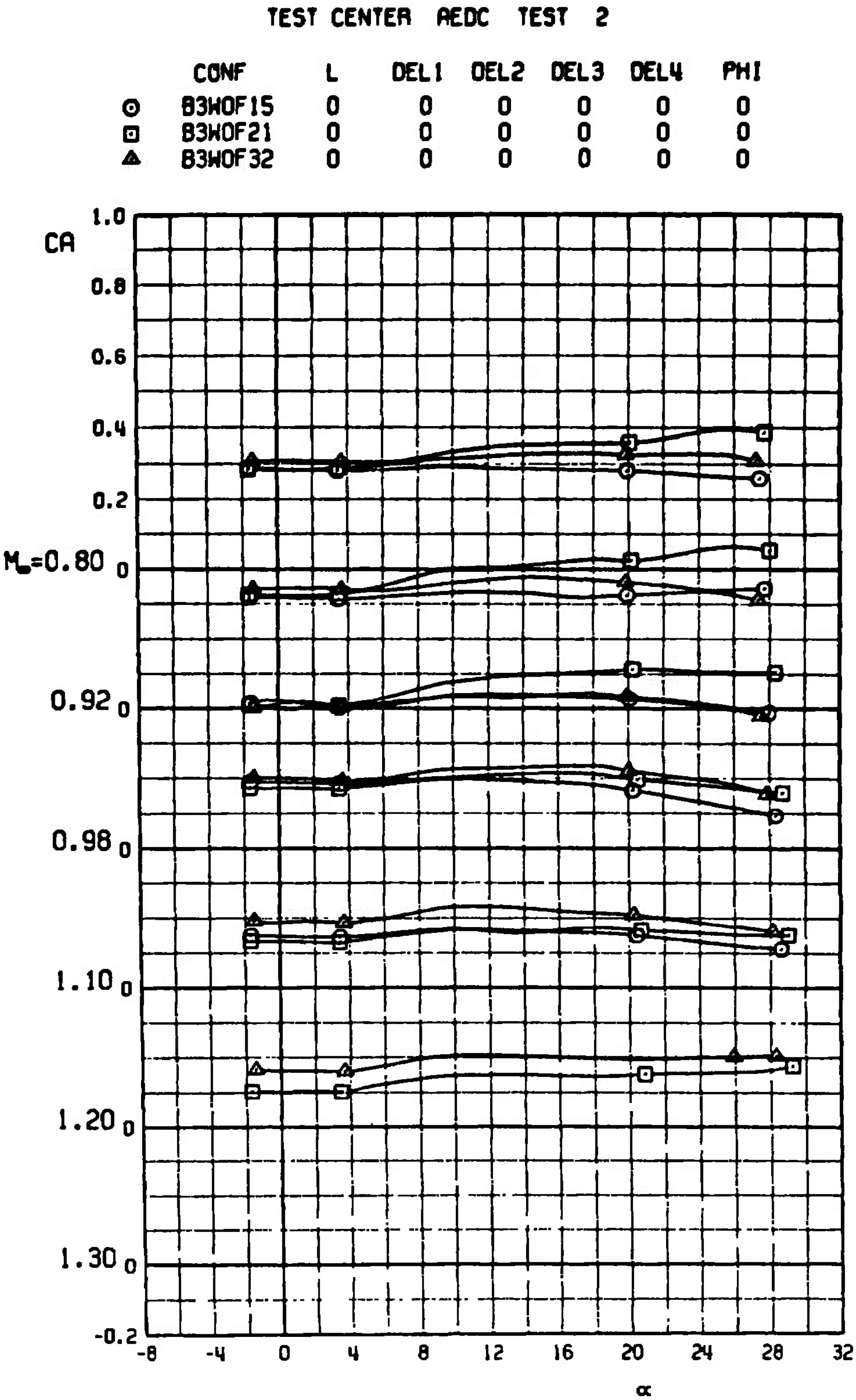

c. CA versus α
Figure 16. Continued.

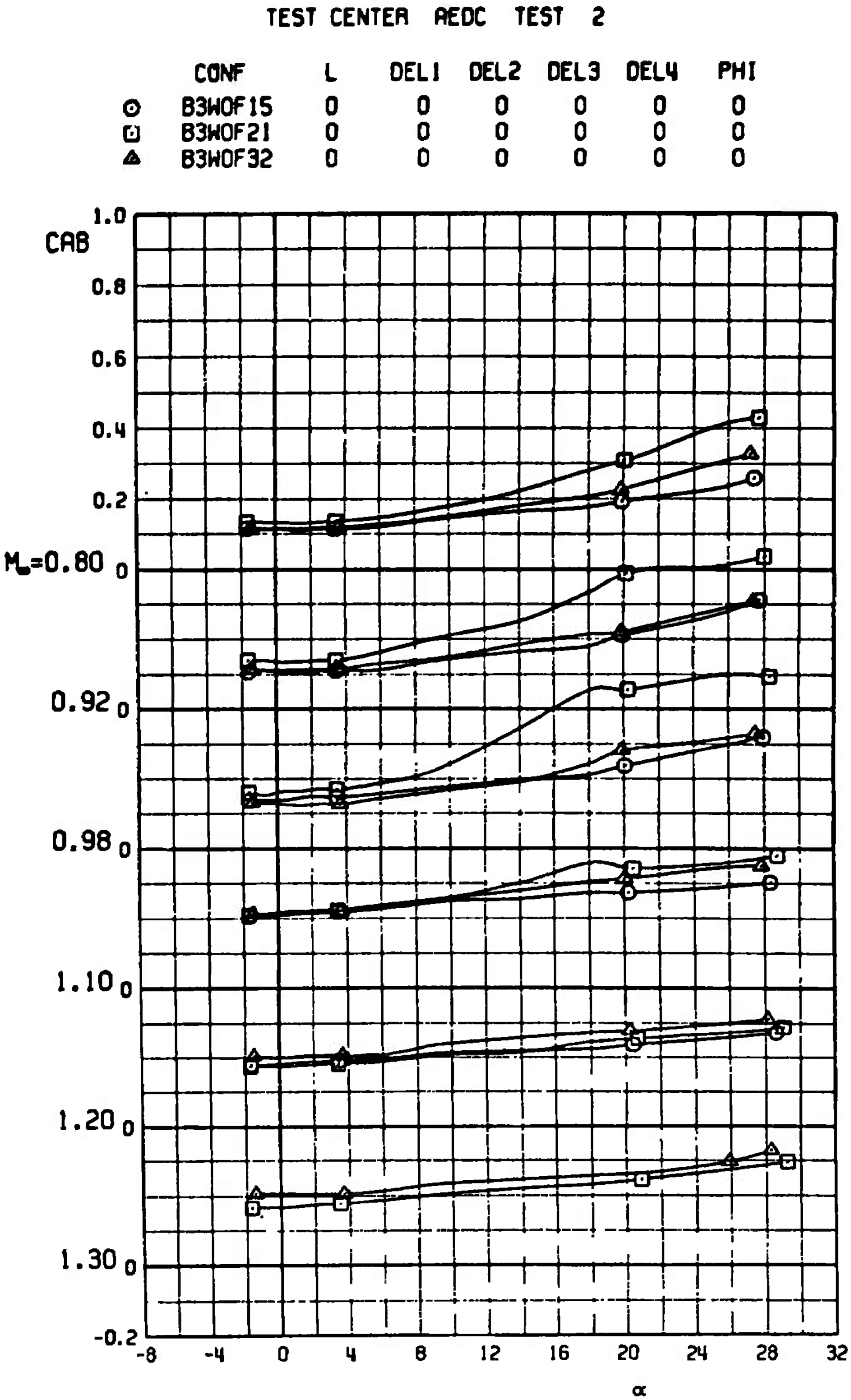

d. CAB versus α

Figure 16. Continued.

TEST CENTER AEDC TEST 2

	CONF	L	DEL1	DEL2	DEL3	DEL4	PHI
⊙	B3WOF15	0	0	0	0	0	0
⊡	B3WOF21	0	0	0	0	0	0
⚠	B3WOF32	0	0	0	0	0	0

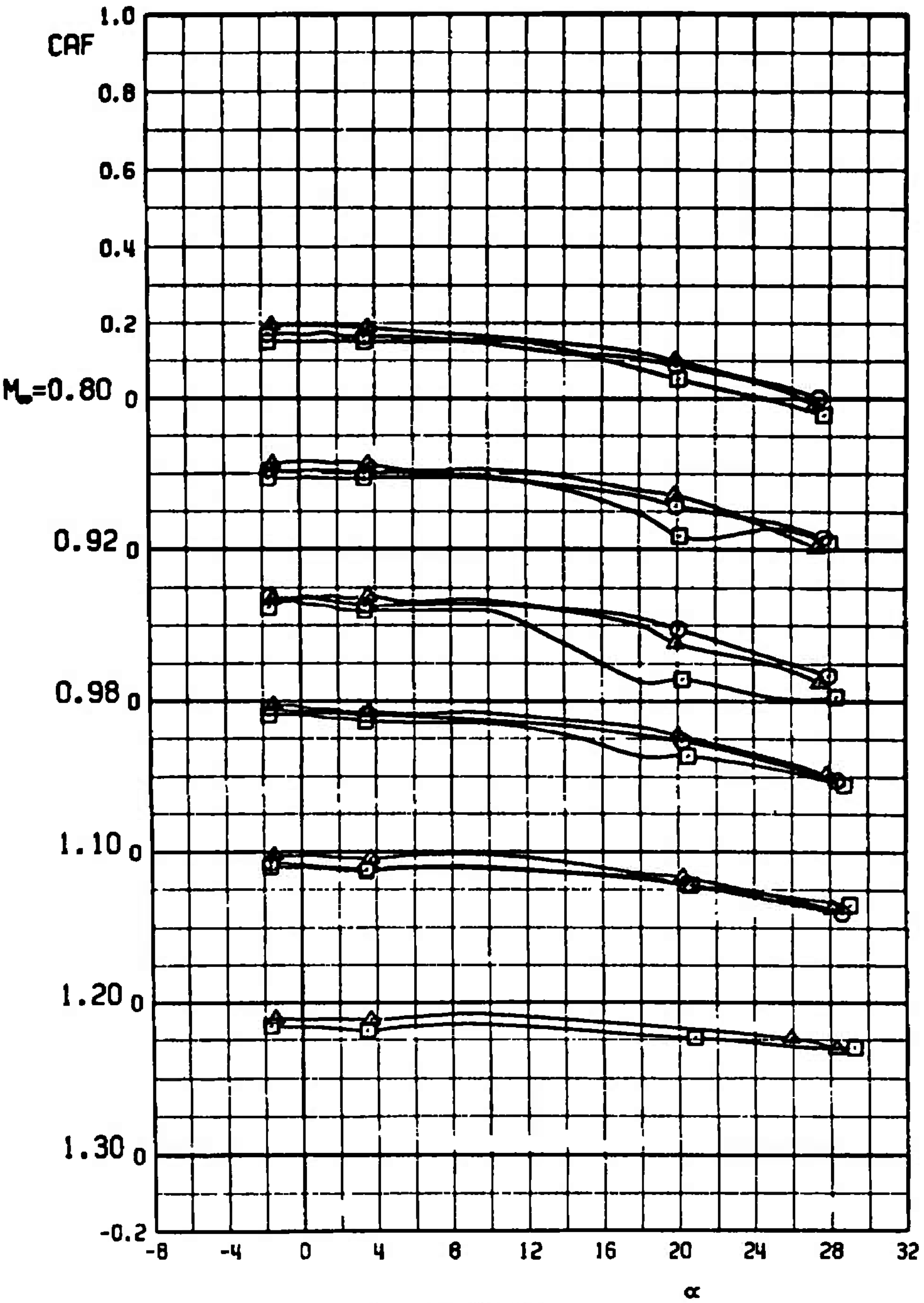

e. CAF versus α
Figure 16. Continued.

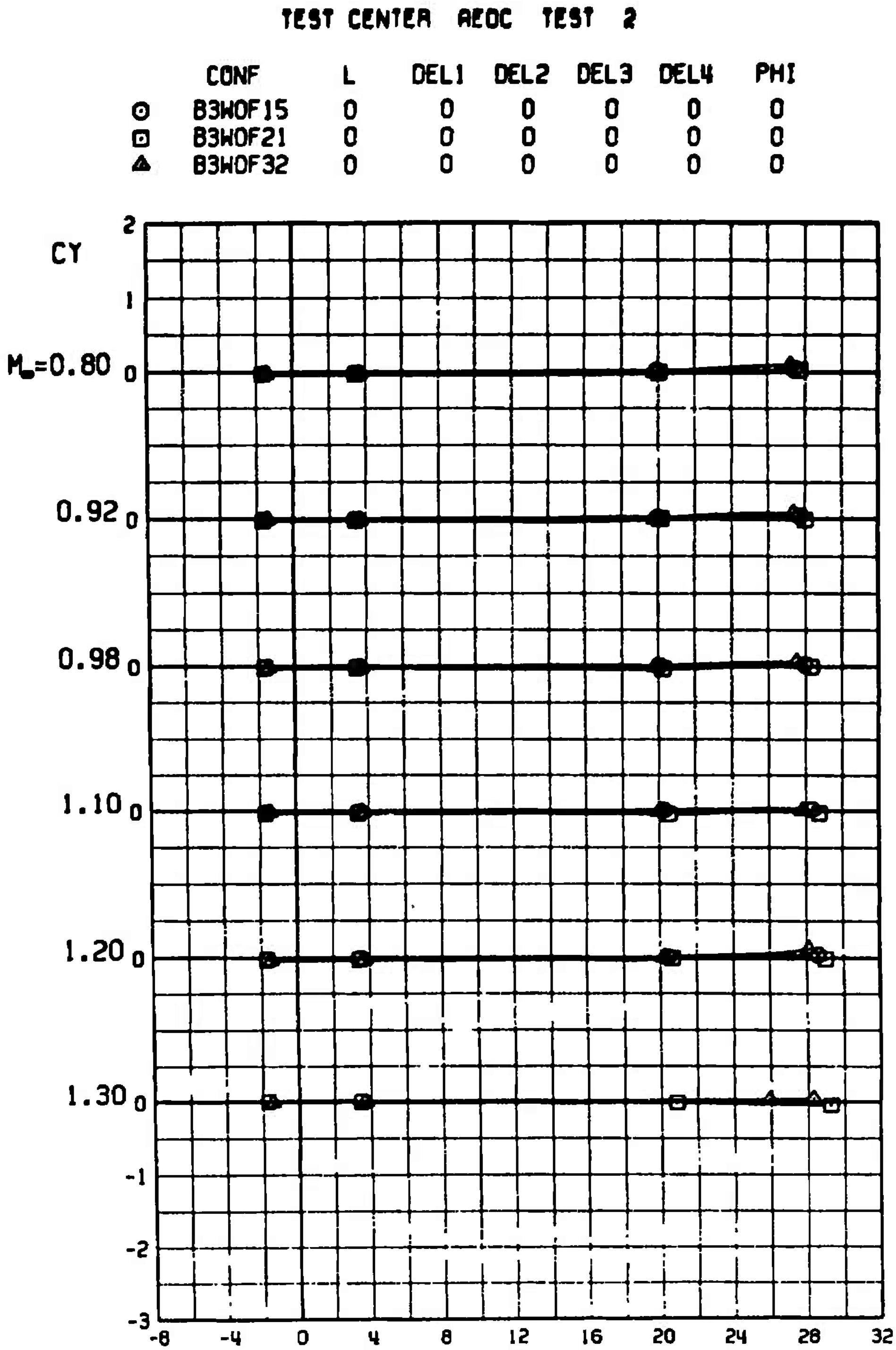

f. CY versus α
Figure 16. Continued.

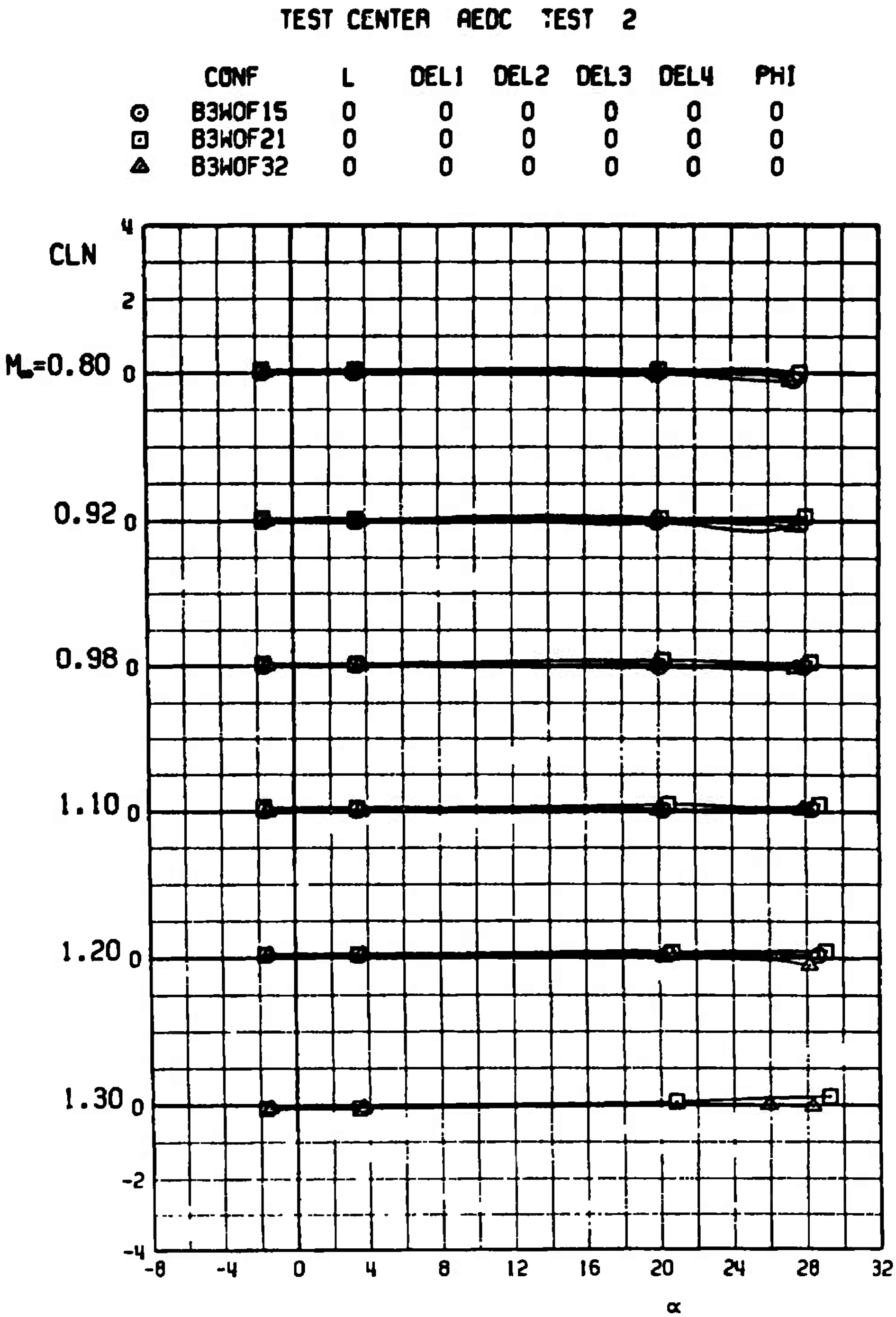

g. CLN versus α
Figure 16. Continued.

TEST CENTER AEDC TEST 2

	CONF	L	DEL1	DEL2	DEL3	DEL4	PHI
⊙	B3W0F15	0	0	0	0	0	0
⊡	B3W0F21	0	0	0	0	0	0
△	B3W0F32	0	0	0	0	0	0

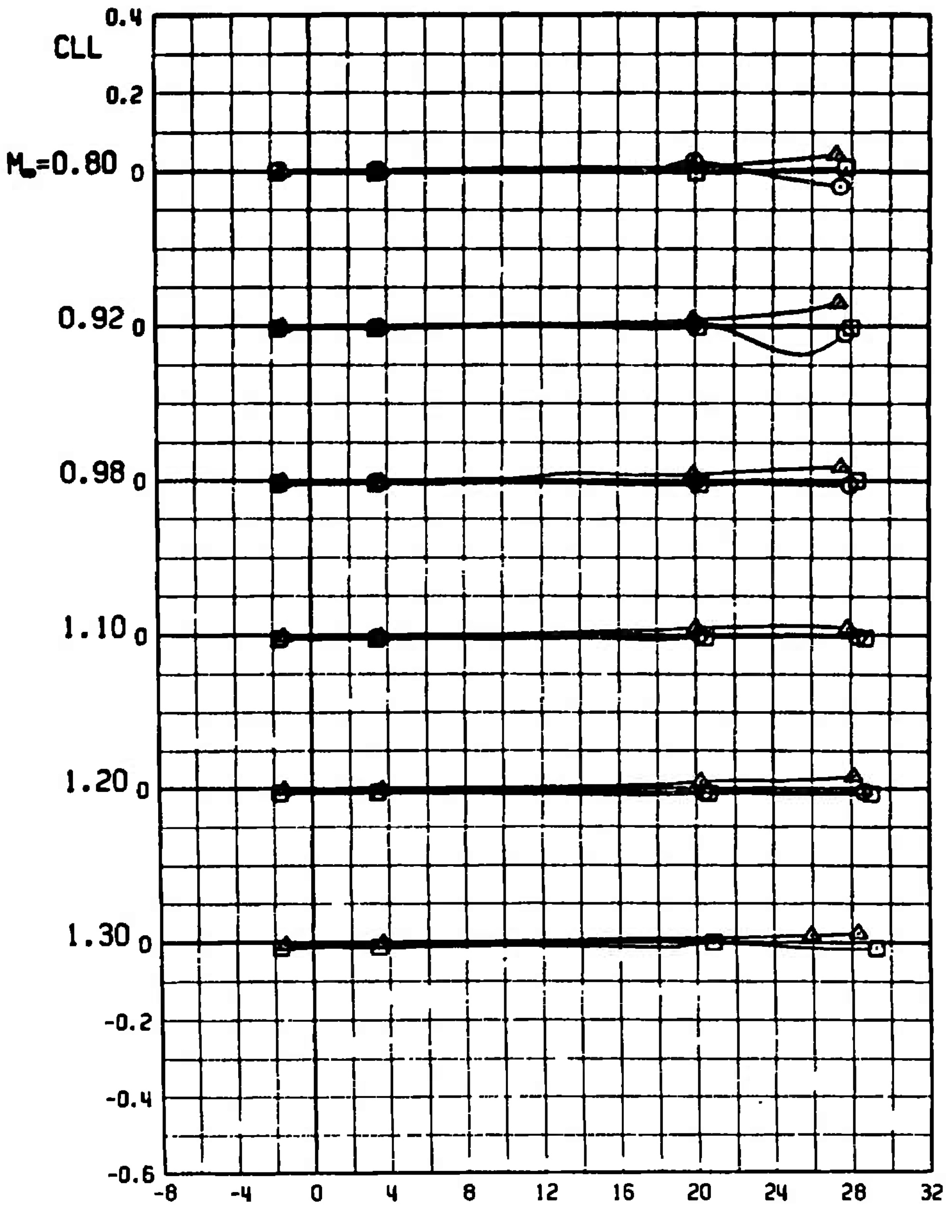

h. CLL versus α
Figure 16. Continued.

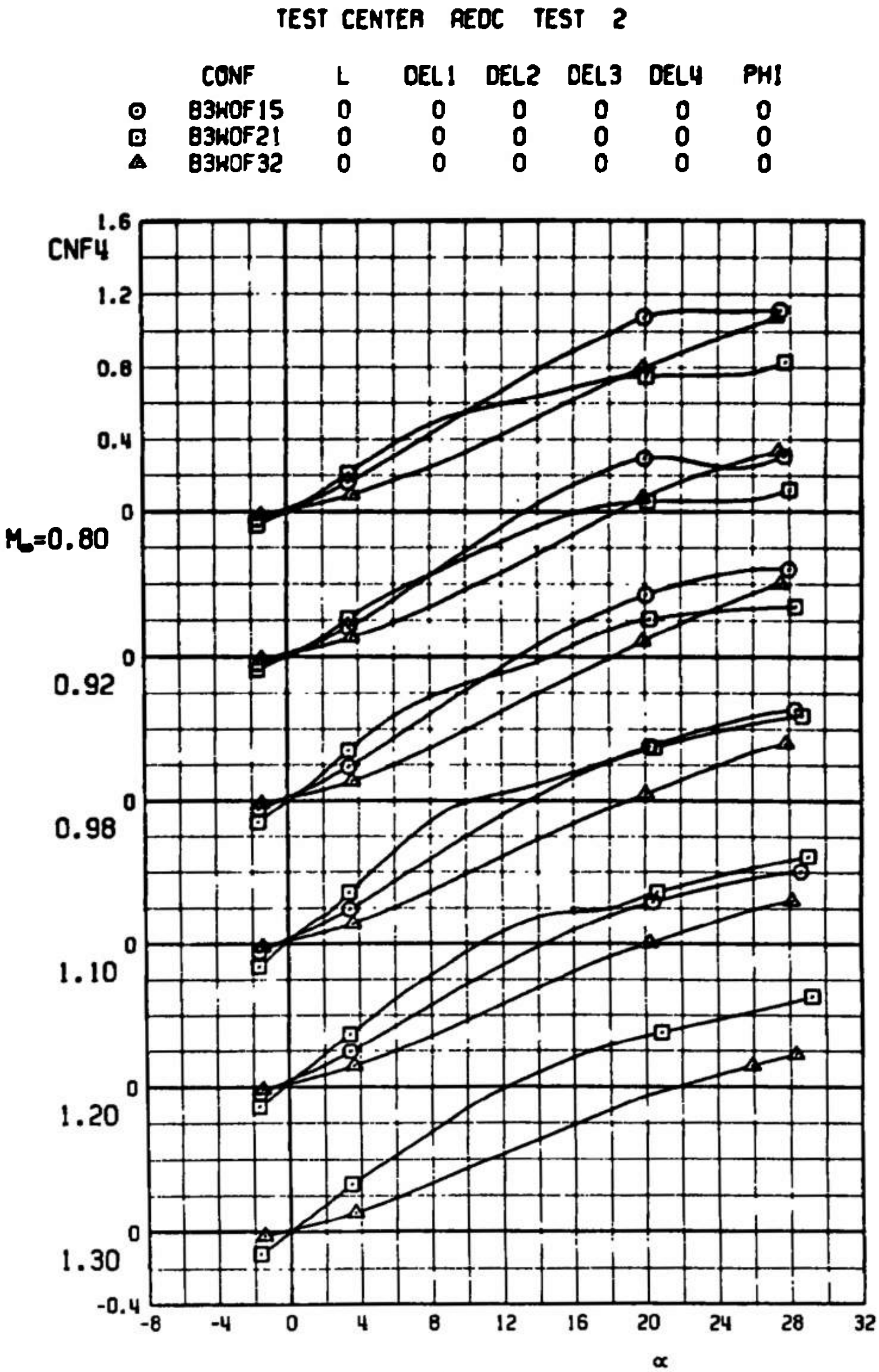

i. CNF4 versus α
Figure 16. Continued.

TEST CENTER AEDC TEST 2

	CONF	L	DEL1	DEL2	DEL3	DEL4	PHI
⊙	B3W0F15	0	0	0	0	0	0
⊡	B3W0F21	0	0	0	0	0	0
△	B3W0F32	0	0	0	0	0	0

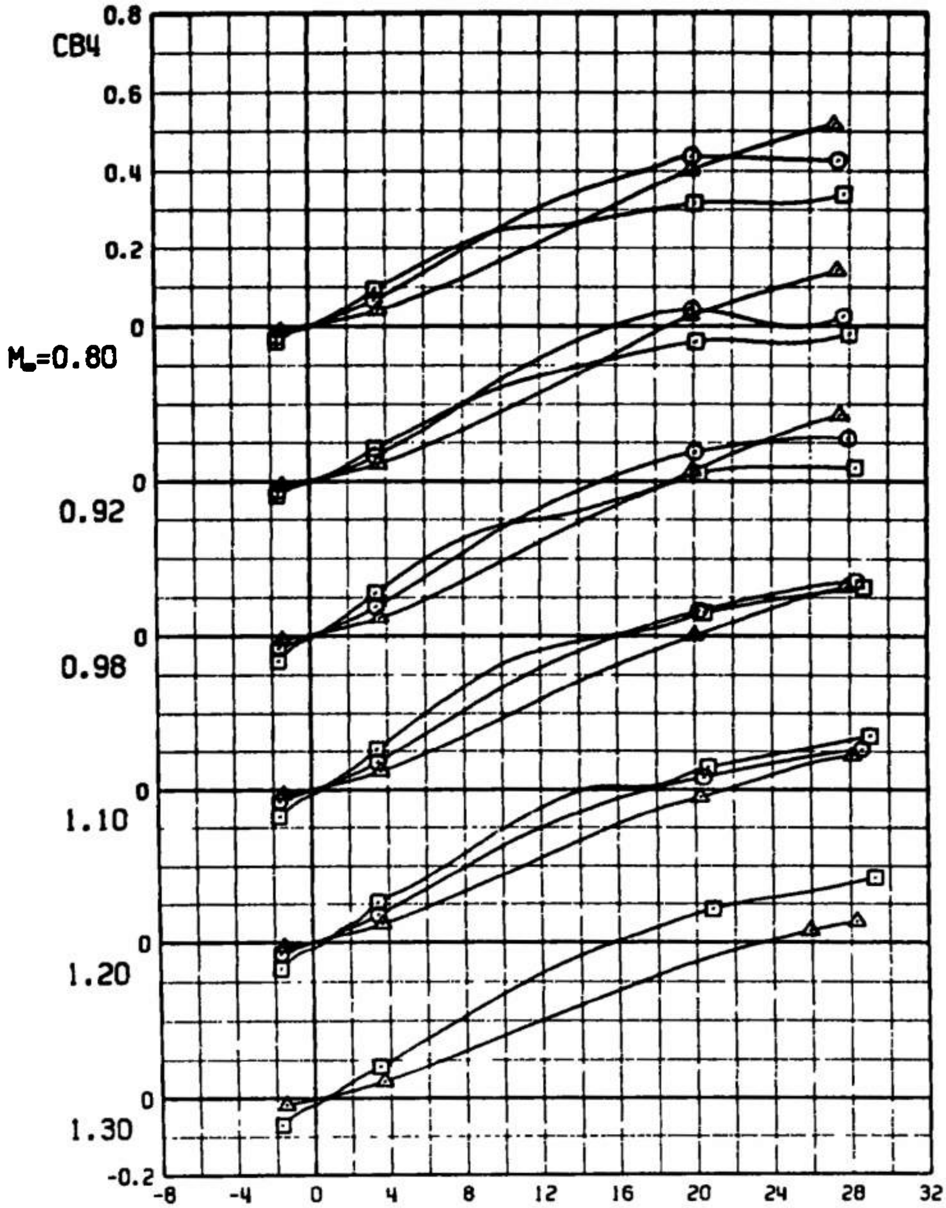

j. CB4 versus α

Figure 16. Continued.

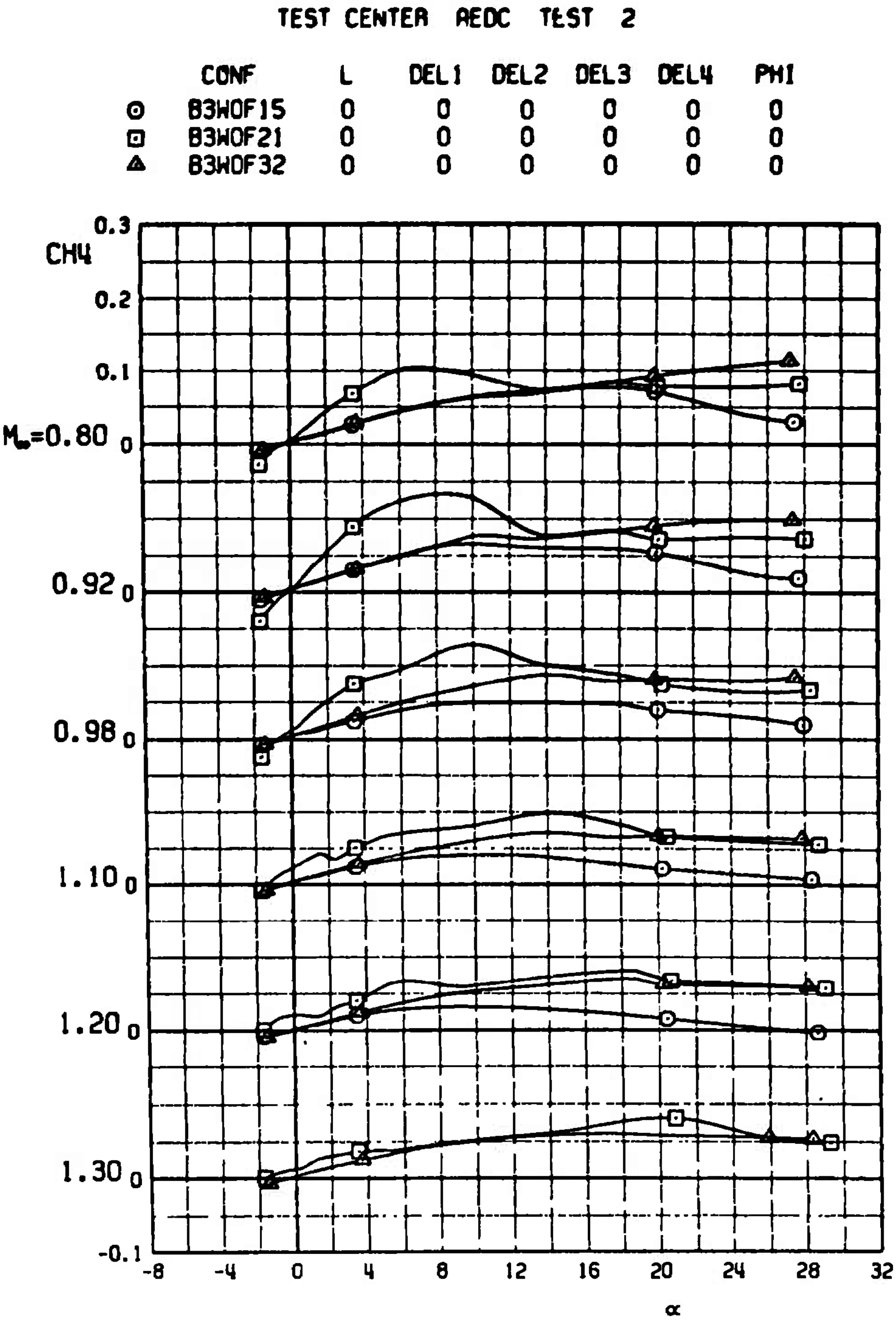

k. CH4 versus α
Figure 16. Concluded.

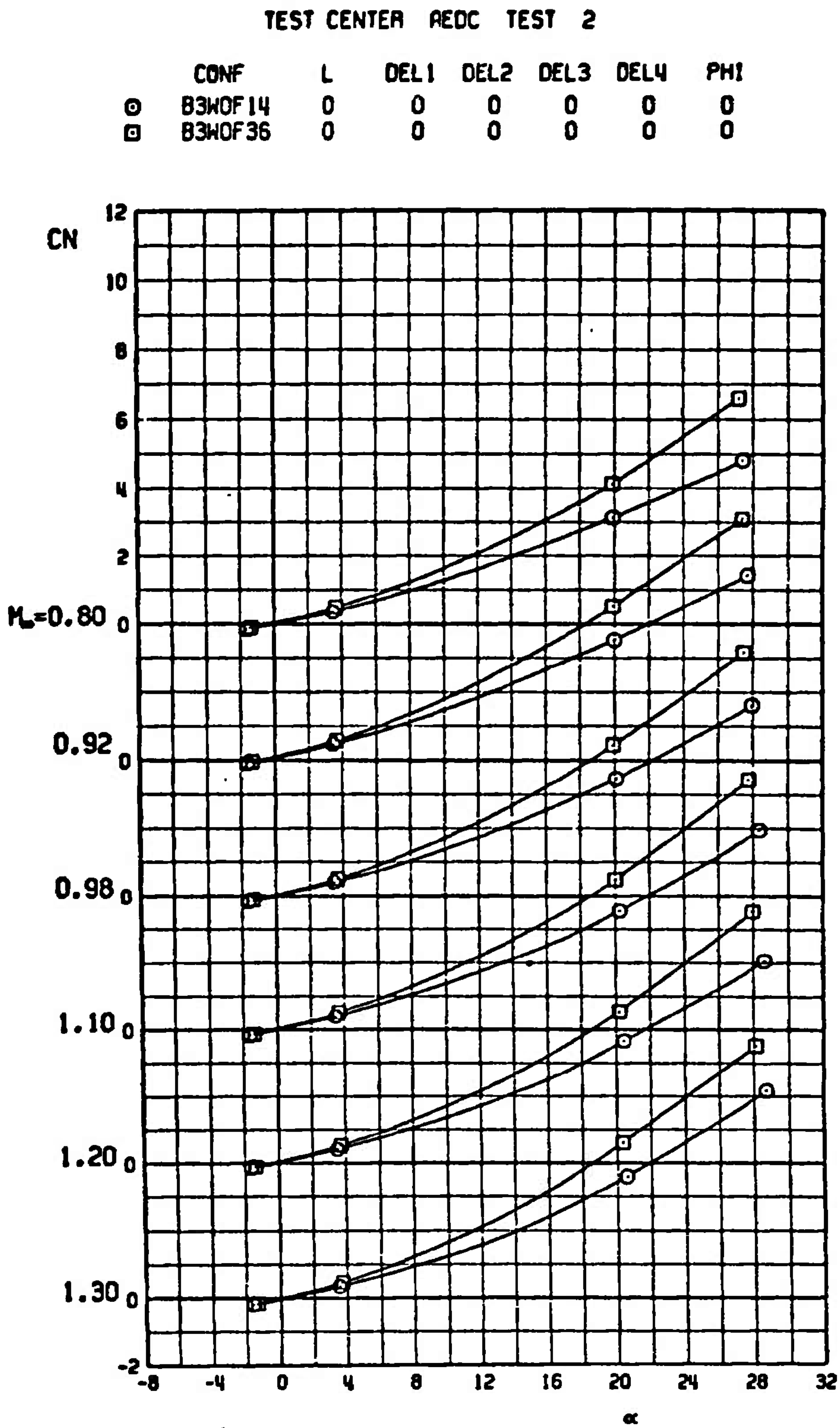

a. CN versus α

Figure 17. Test No. 2, comparison of aerodynamic coefficients of configurations B3W0F14 and B3W0F36.

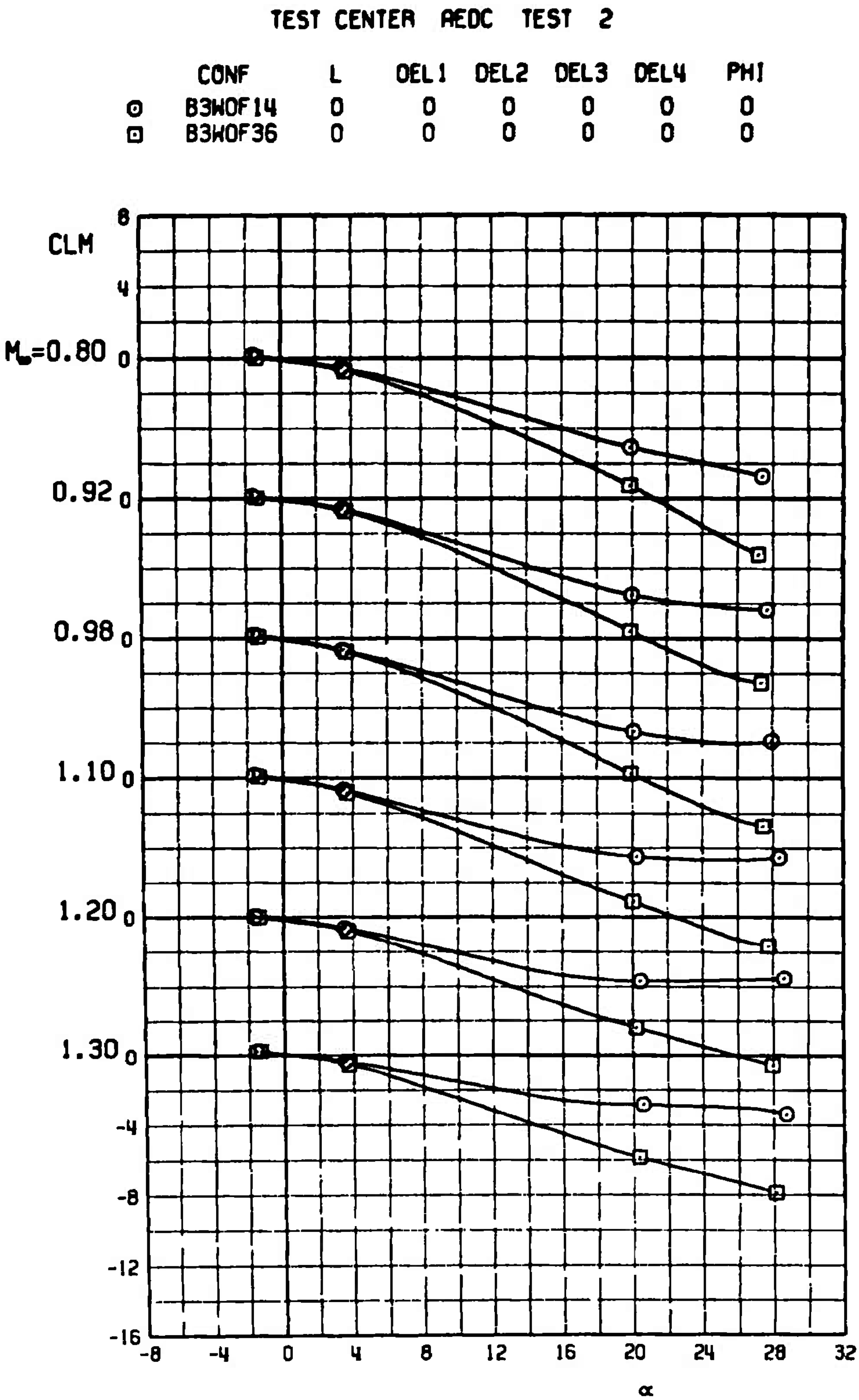

b. CLM versus α
Figure 17. Continued.

TEST CENTER AEDC TEST 2

	CONF	L	DEL1	DEL2	DEL3	DEL4	PHI
⊙	B3W0F14	0	0	0	0	0	0
⊡	B3W0F36	0	0	0	0	0	0

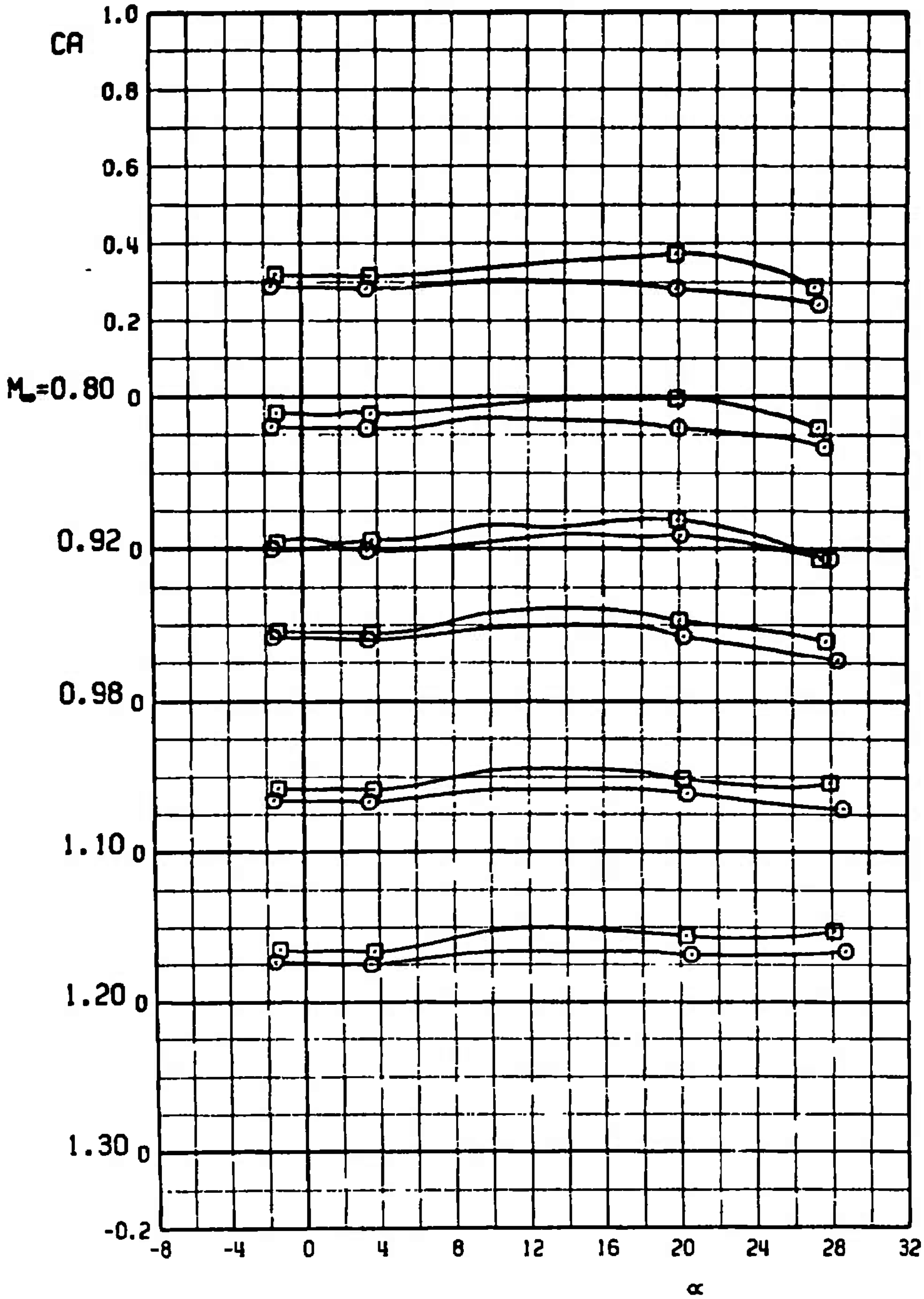

c. CA versus α

Figure 17. Continued.

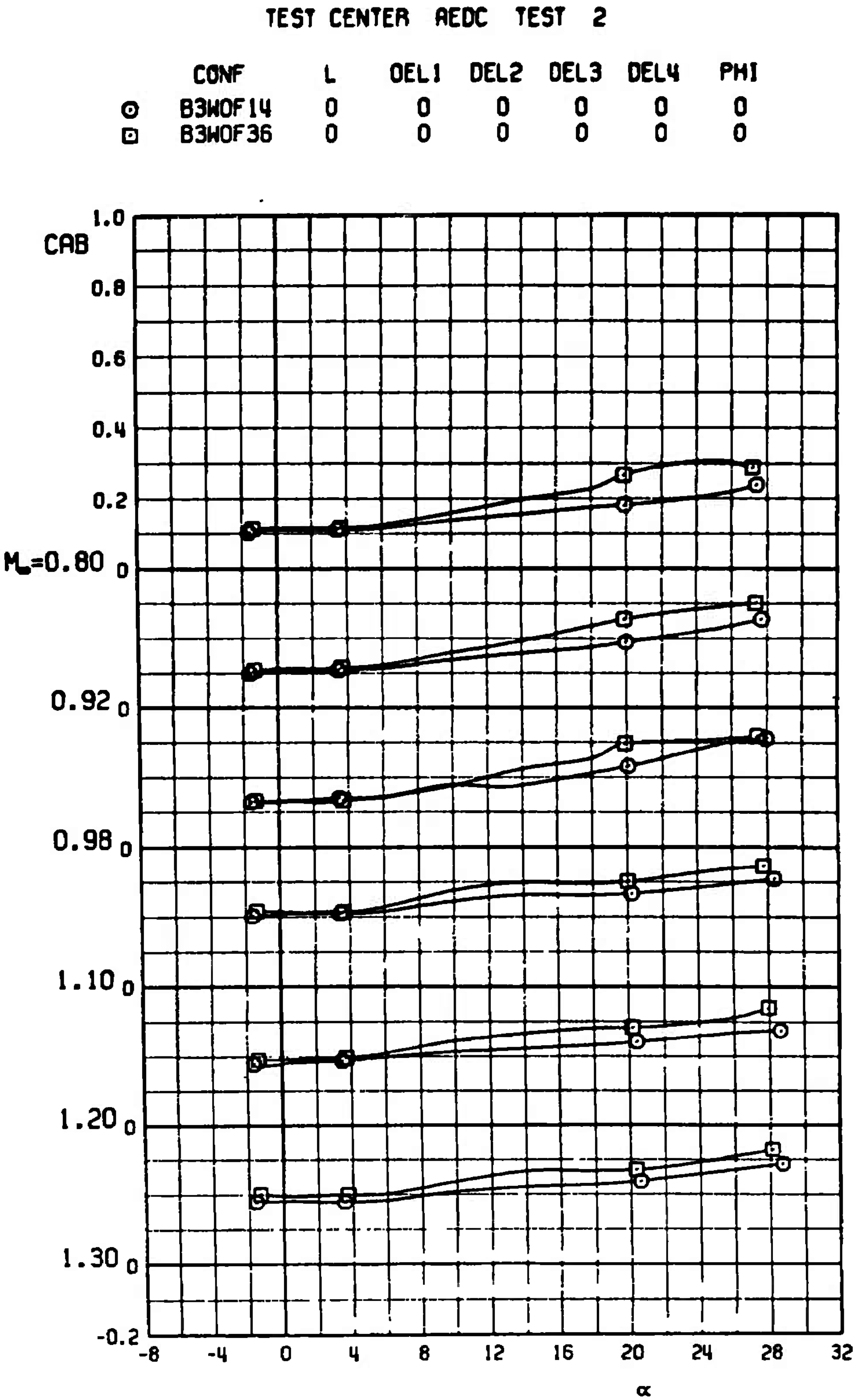

d. CAB versus α
Figure 17. Continued.

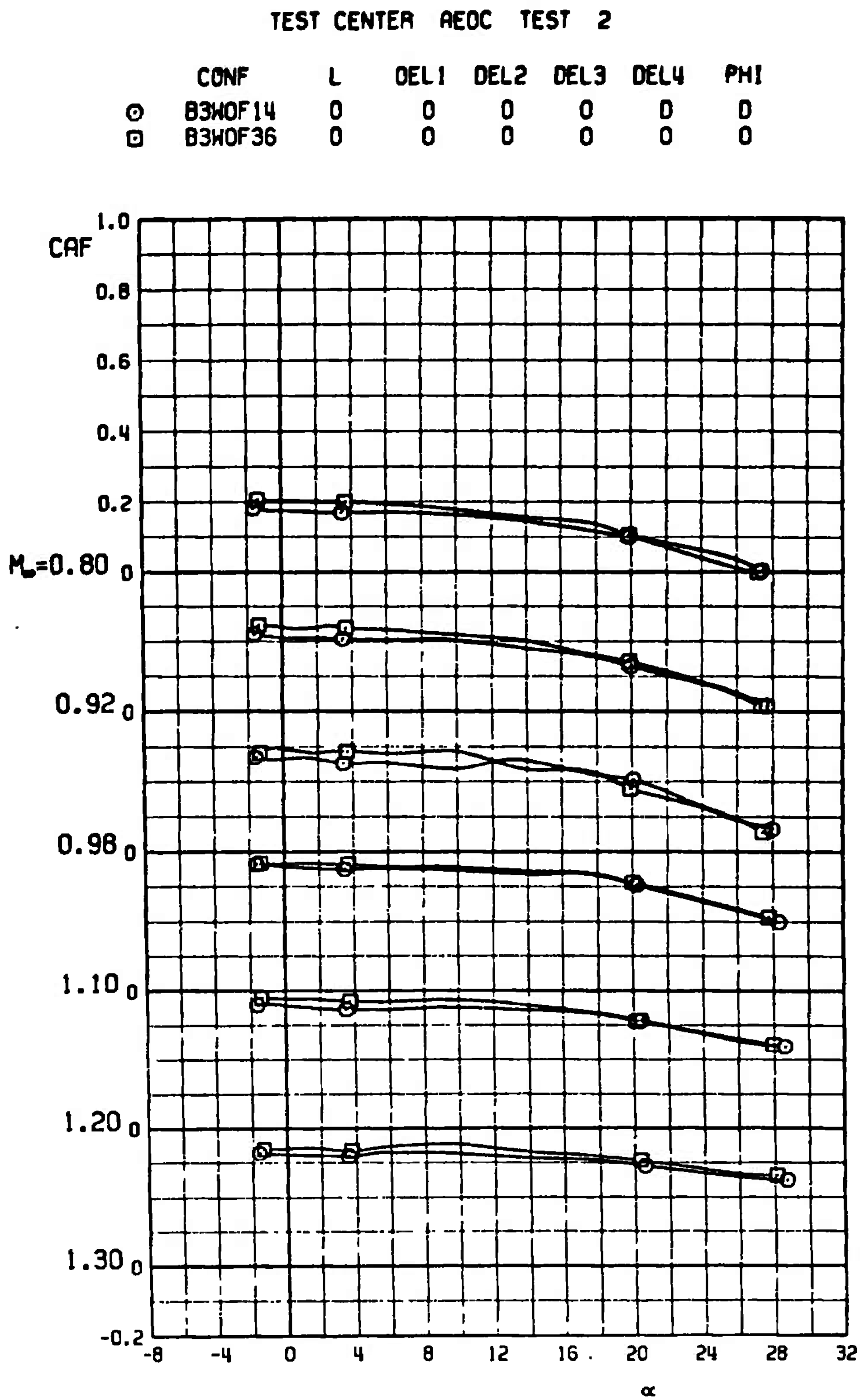

e. CAF versus α

Figure 17. Continued.

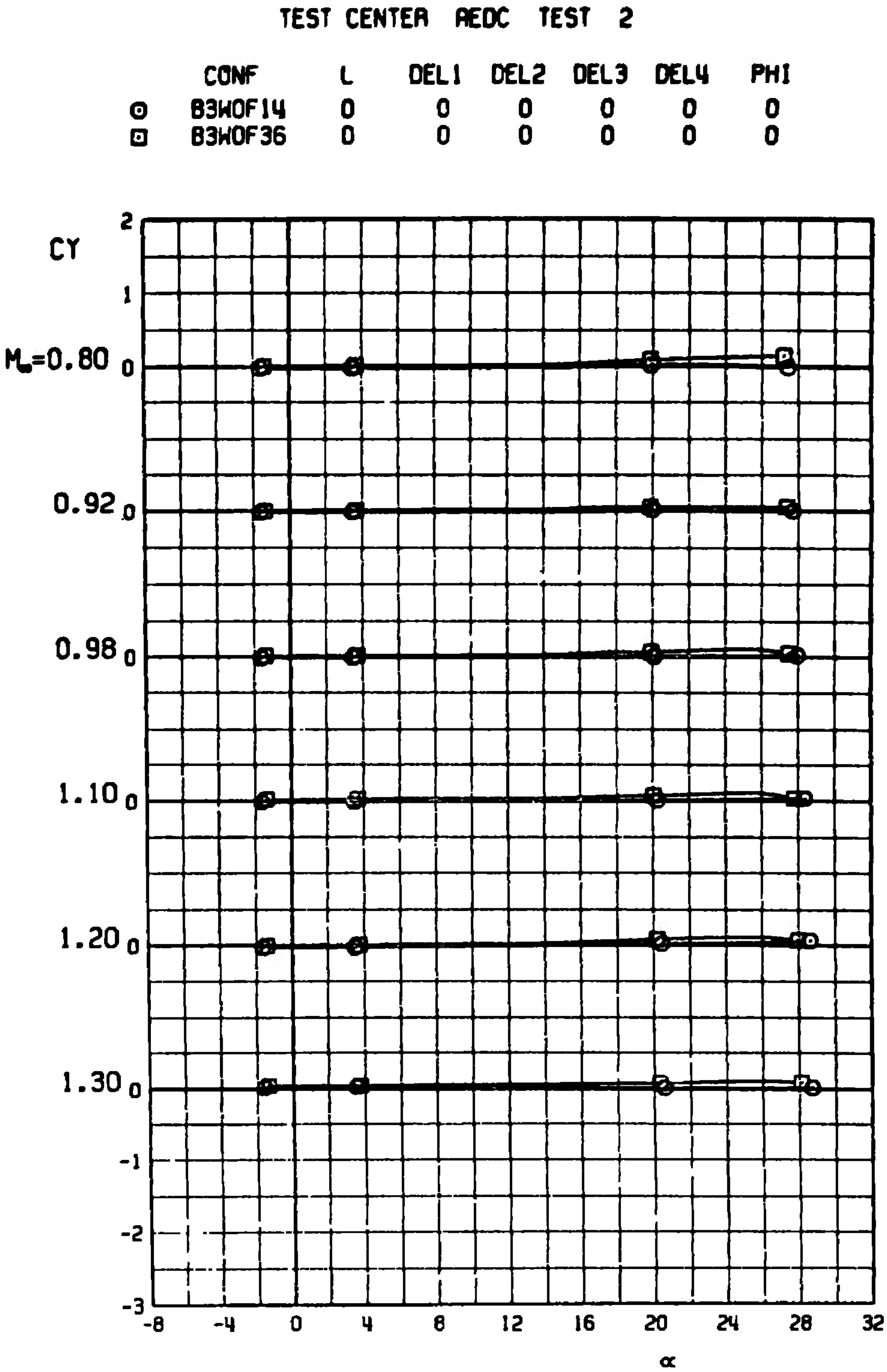

f. CY versus α
Figure 17. Continued.

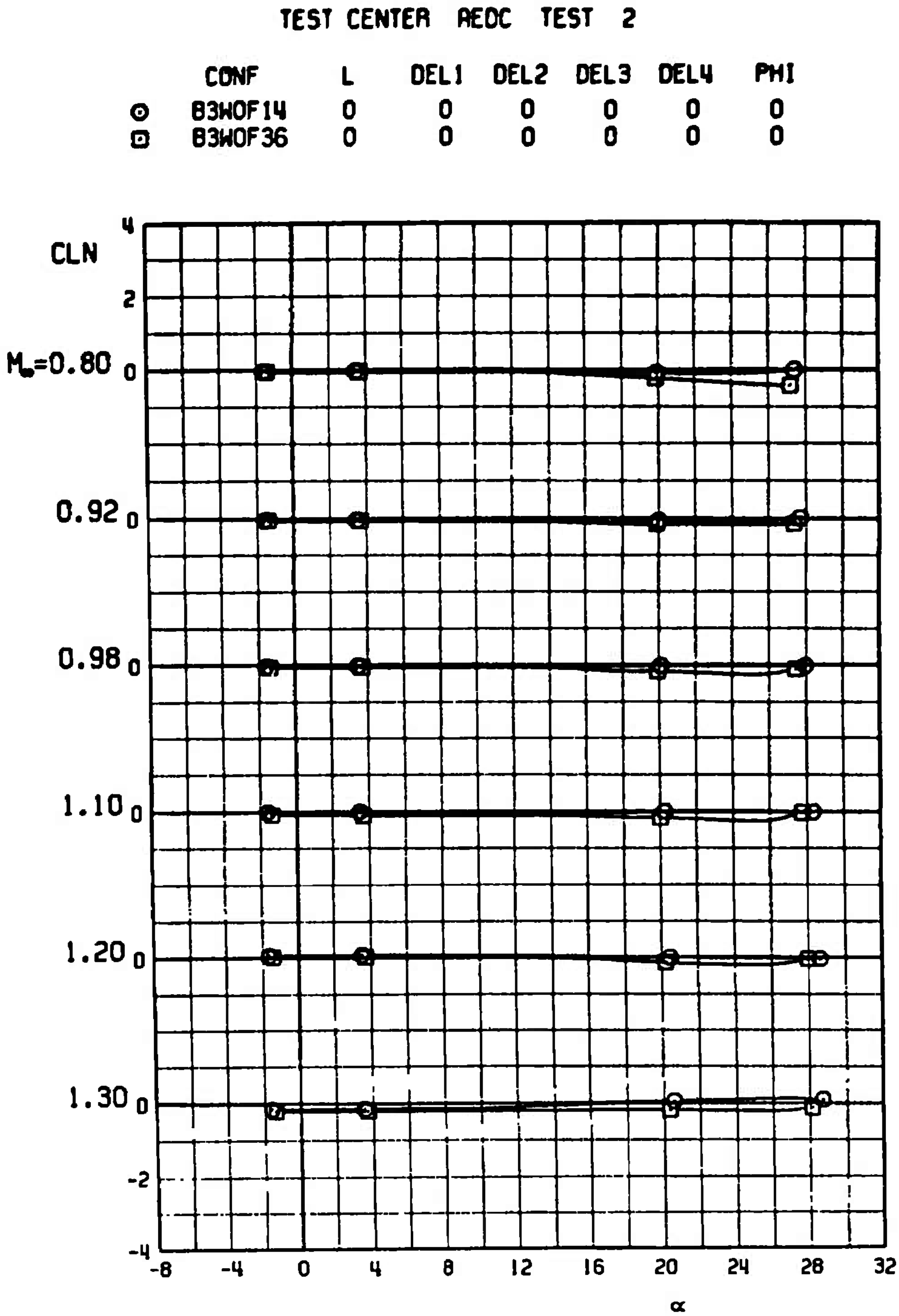

g. CLN versus α
Figure 17. Continued.

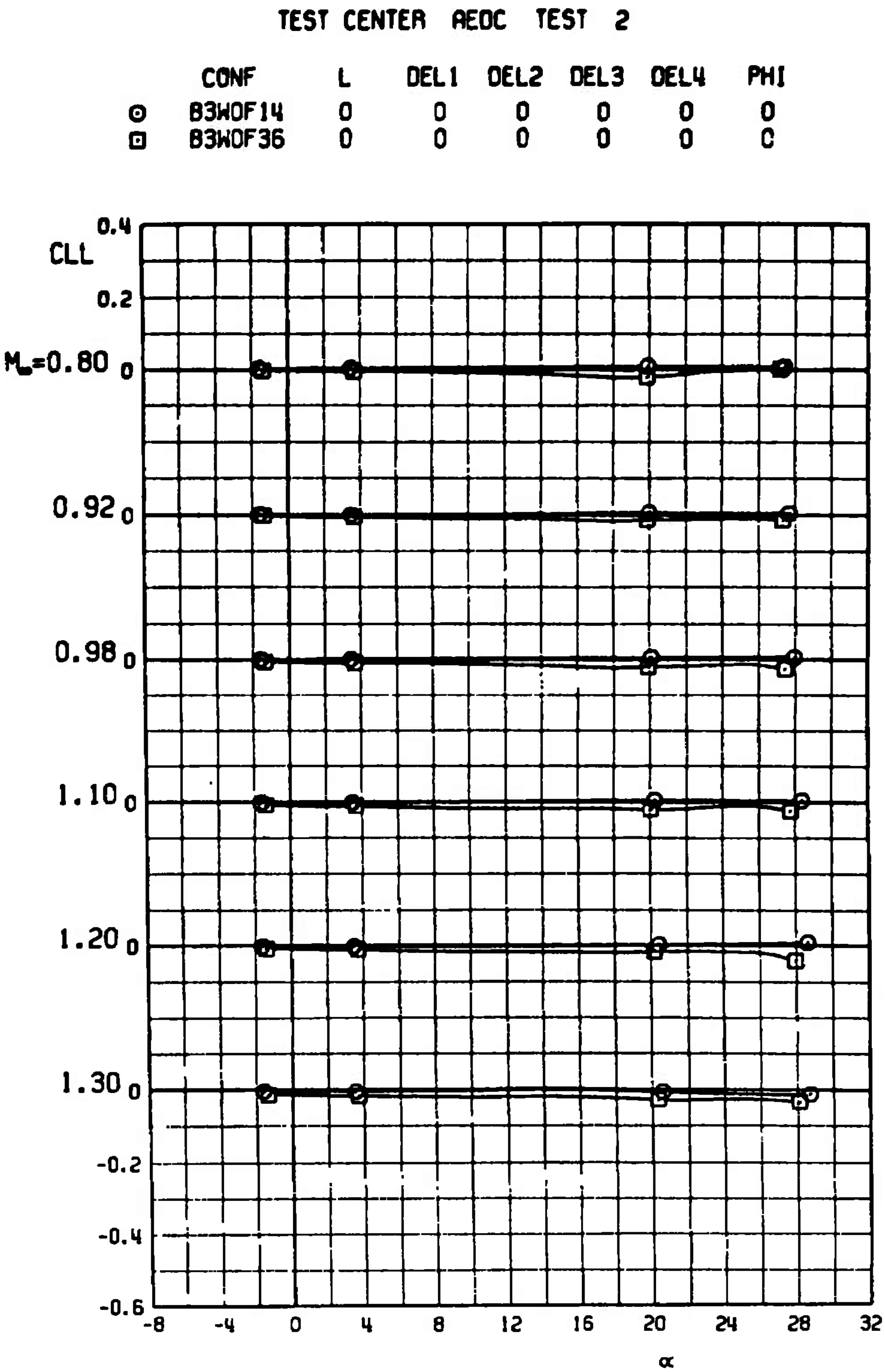

h. CLL versus α
Figure 17. Continued.

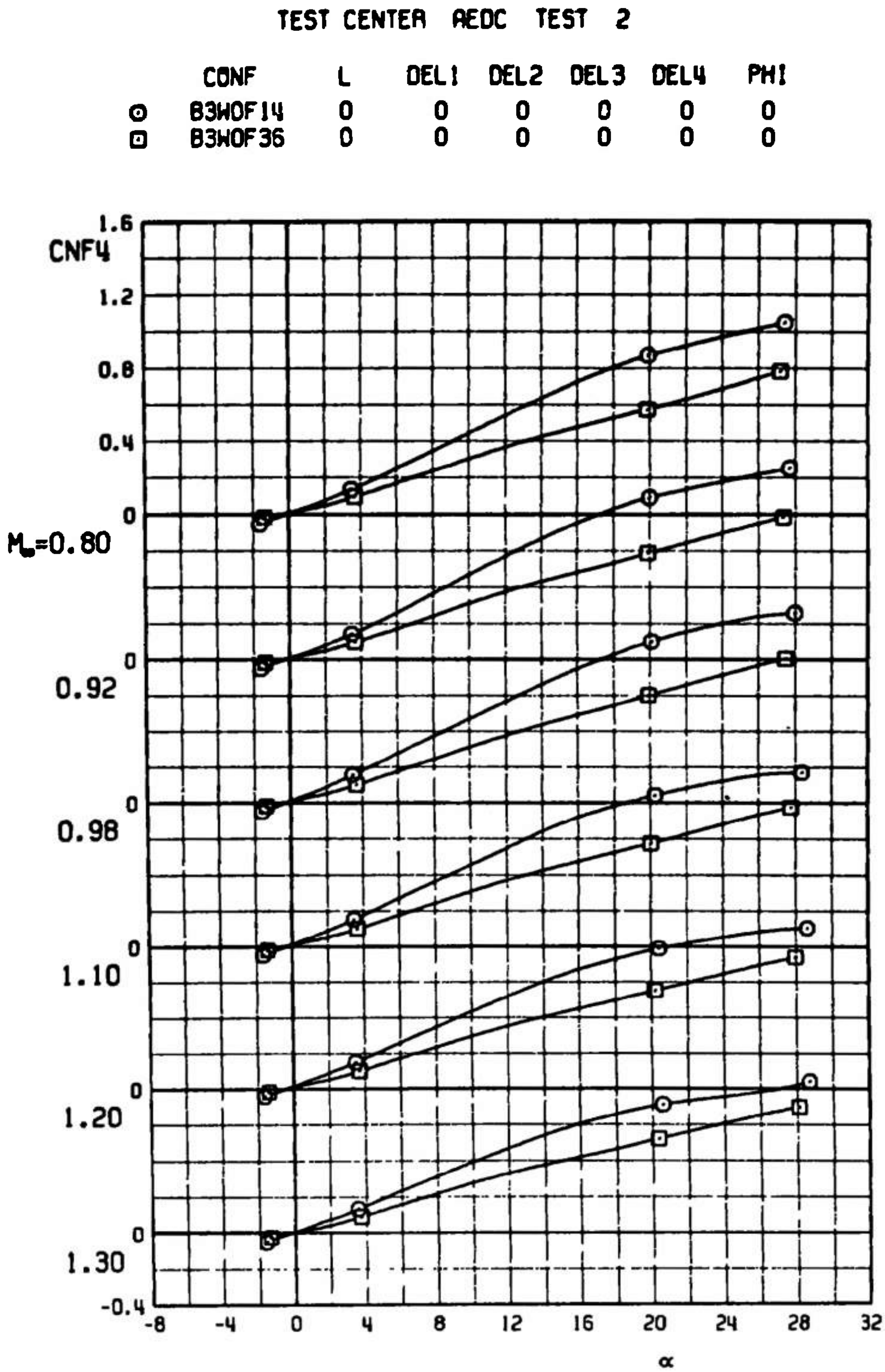

i. CNF4 versus α

Figure 17. Continued.

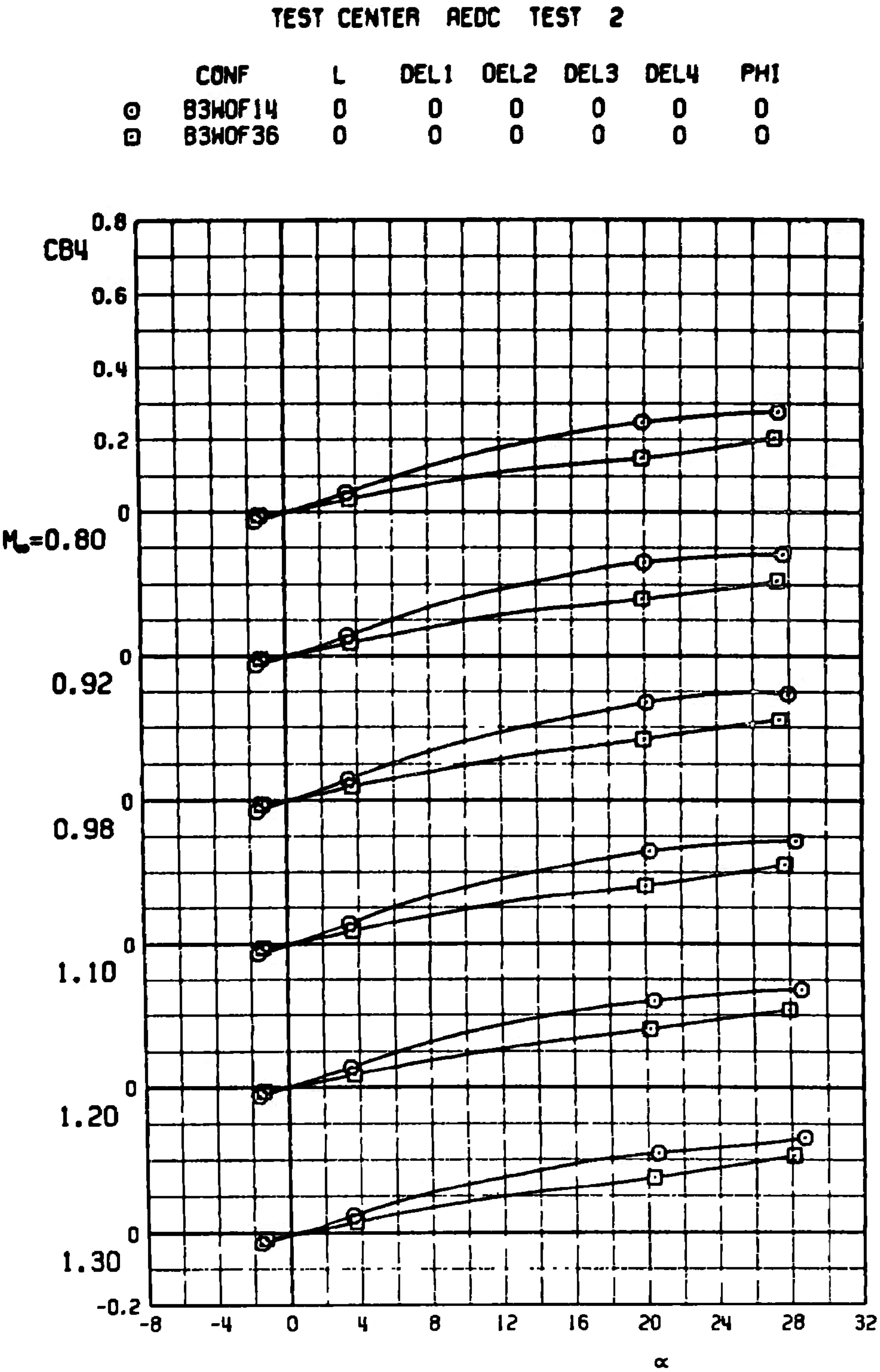

j. CB4 versus α
Figure 17. Continued.

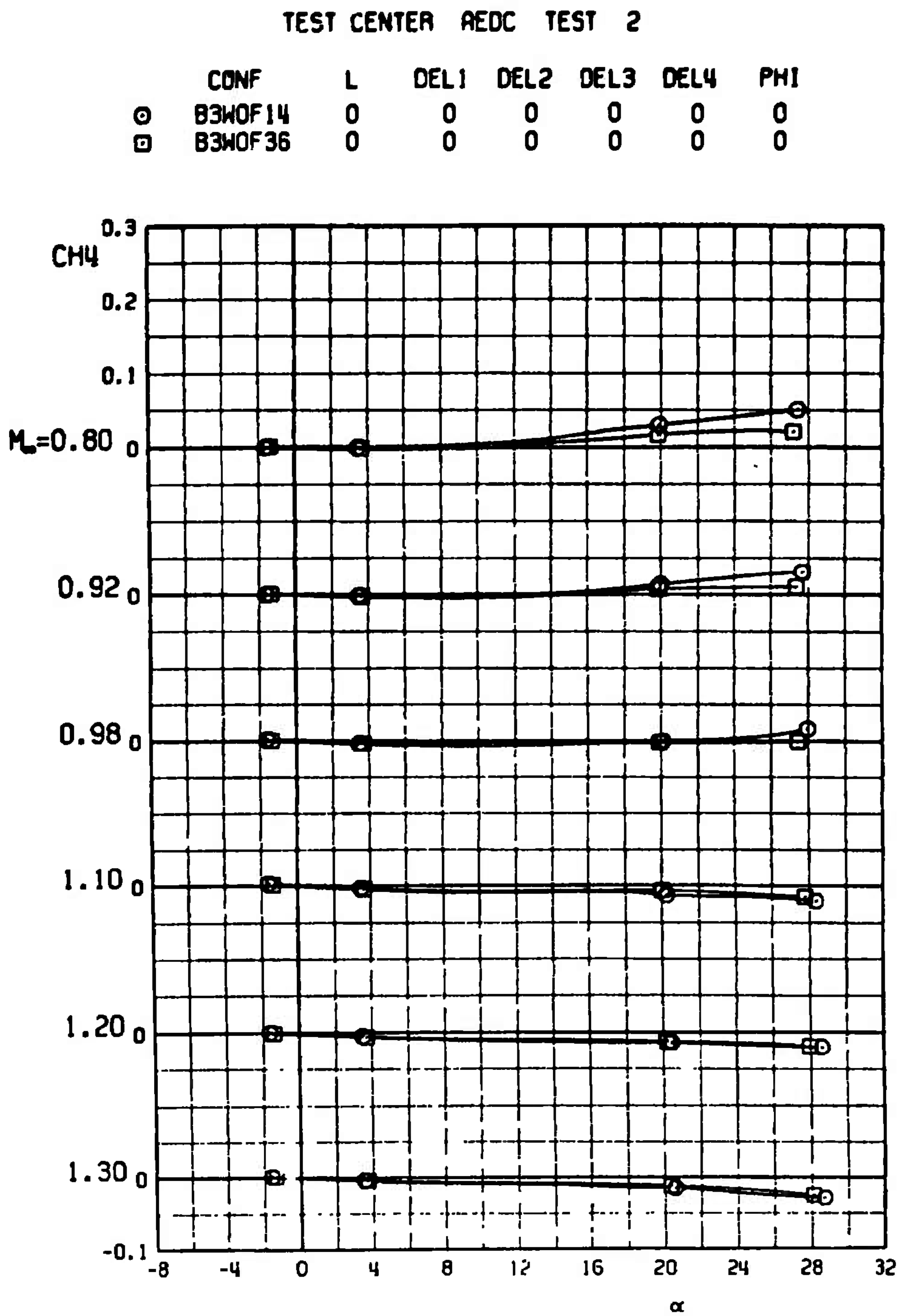

k. CH4 versus α

Figure 17. Concluded.

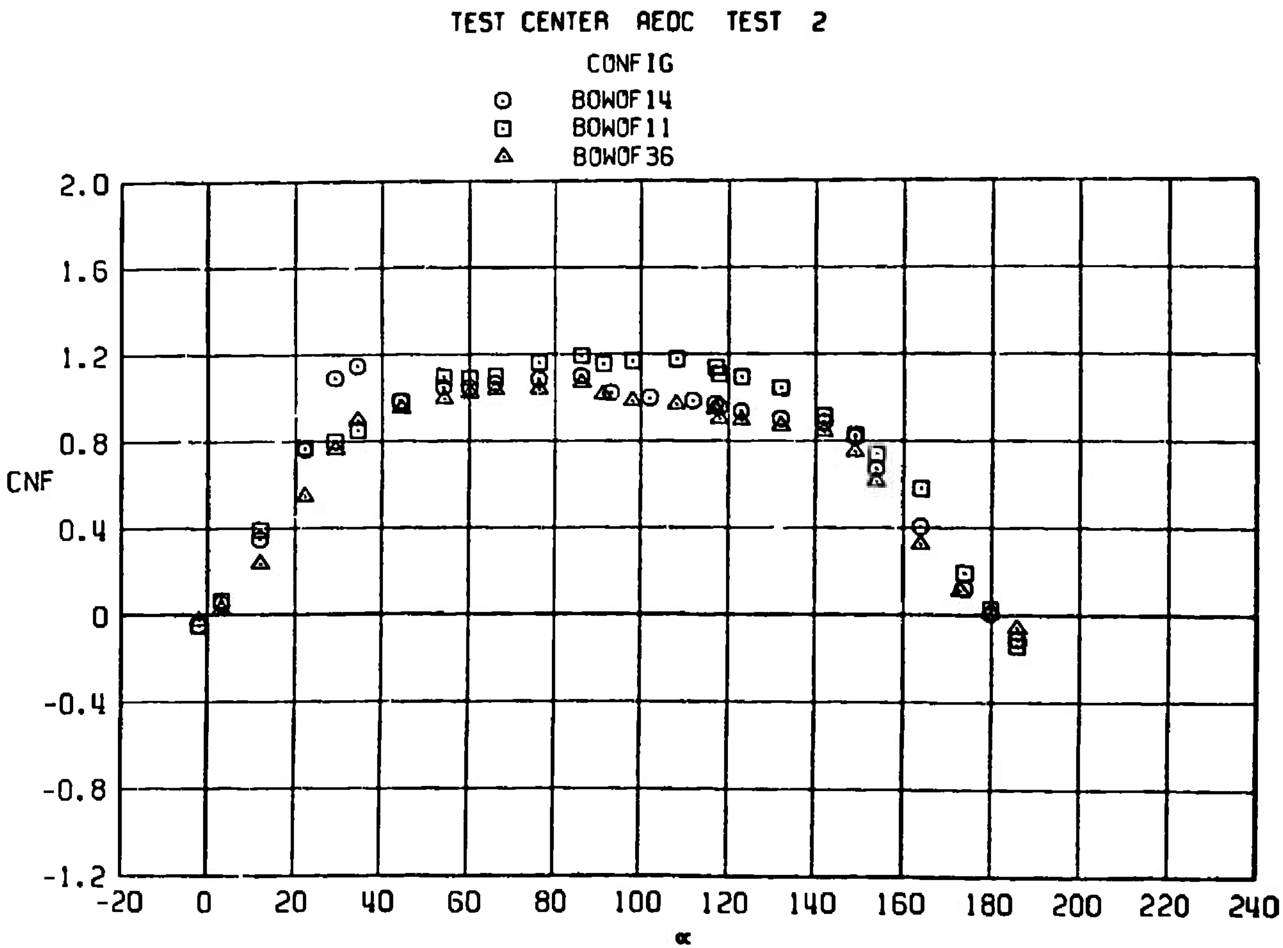

a. CN versus α

Figure 18. Test No. 2, comparison of aerodynamic coefficients of configurations B0W0F14, B0W0F11, and B0W0F36 at $M_\infty = 0.8$.

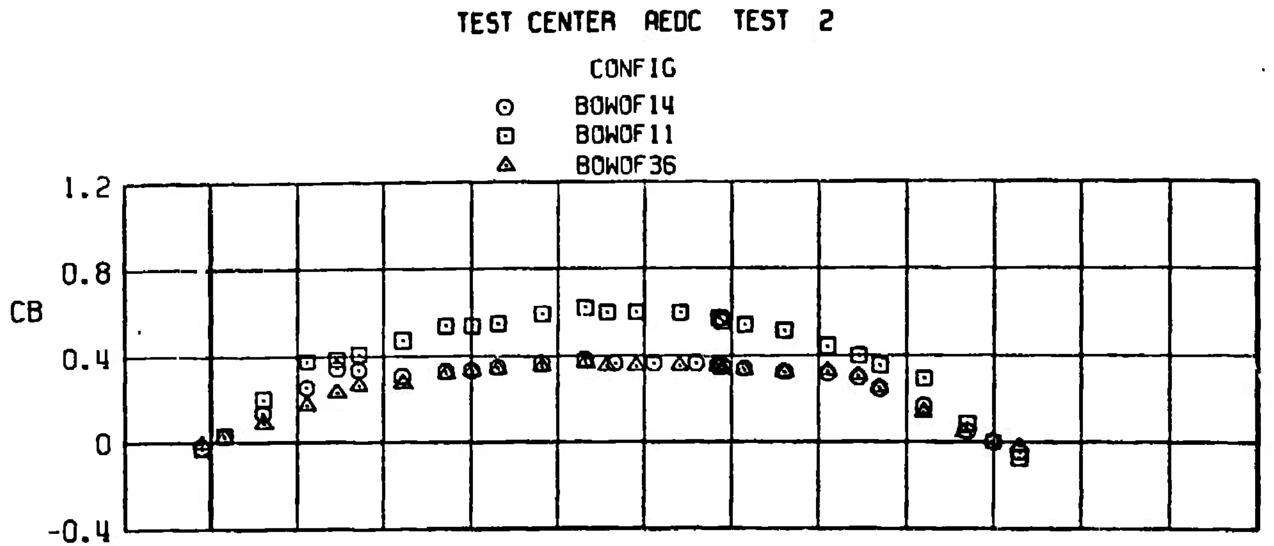

b. CB versus α

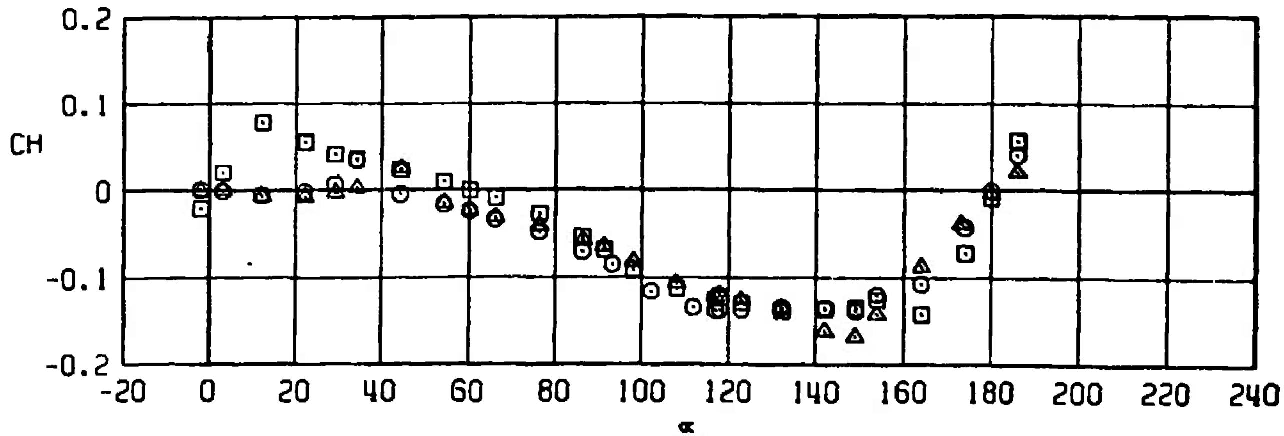

c. CH versus α

Figure 18. Concluded.

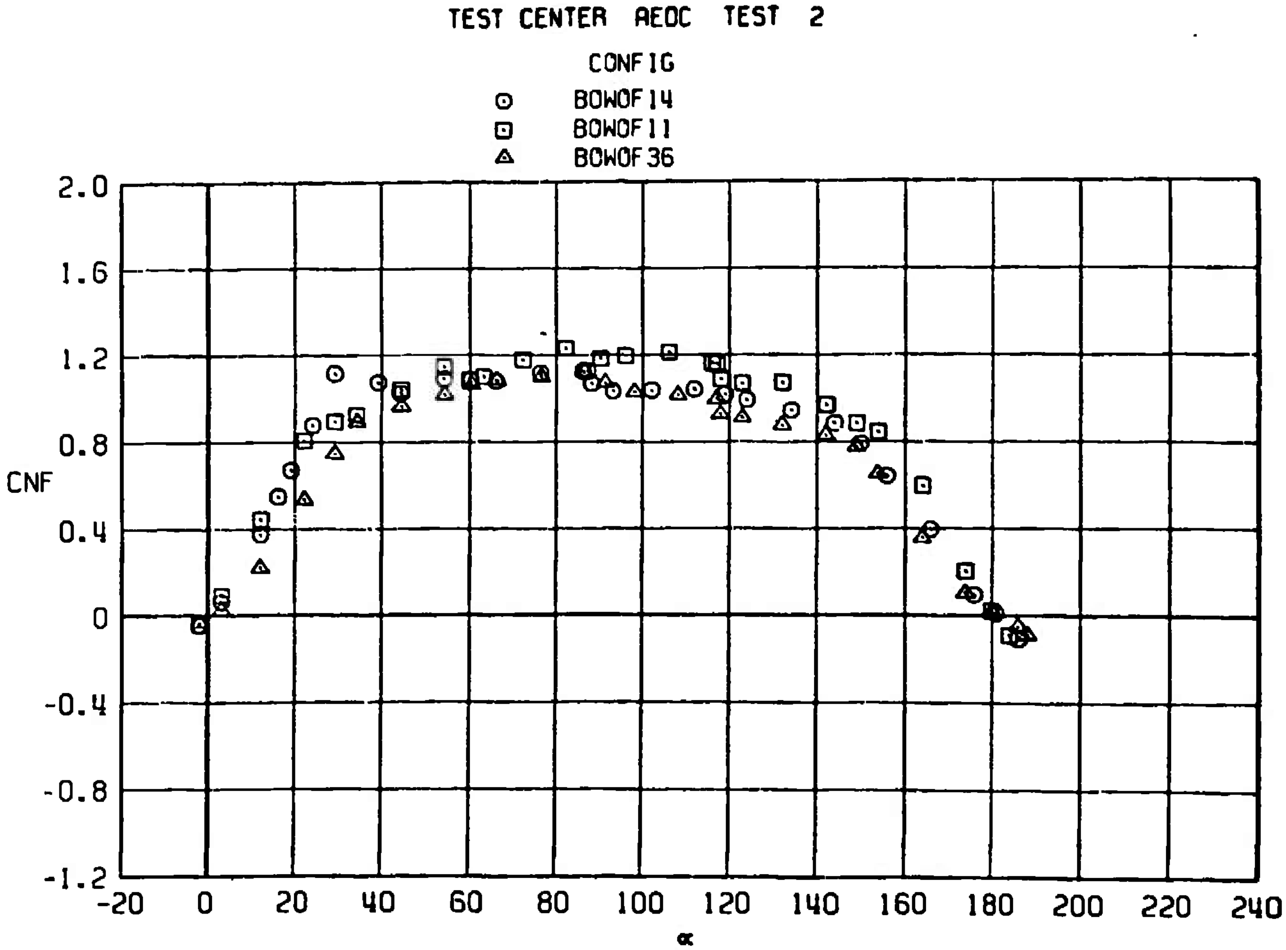

a. CNF versus α

Figure 19. Test No. 2, comparison of aerodynamic coefficients of configurations B0W0F14, B0W0F11, and B0W0F36 at $M_\infty = 0.92$.

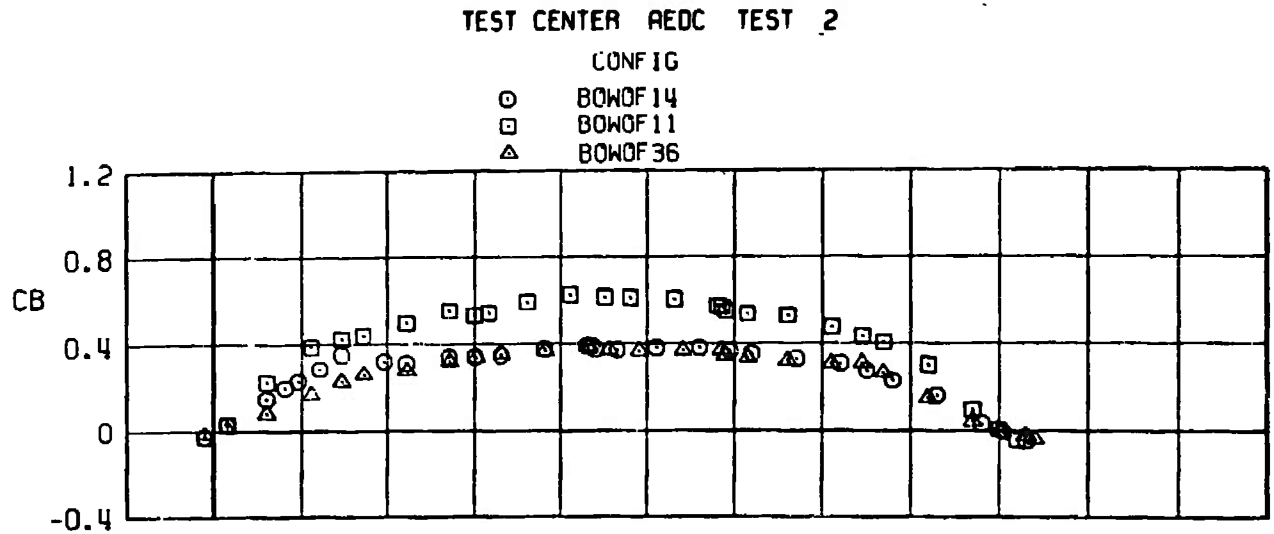

b. CB versus α

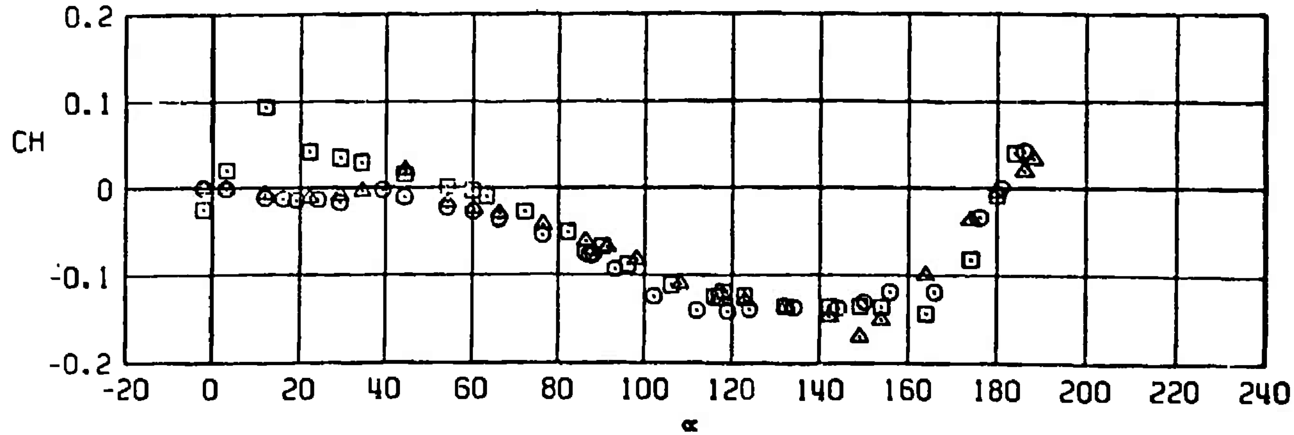

c. CH versus α

Figure 19. Concluded.

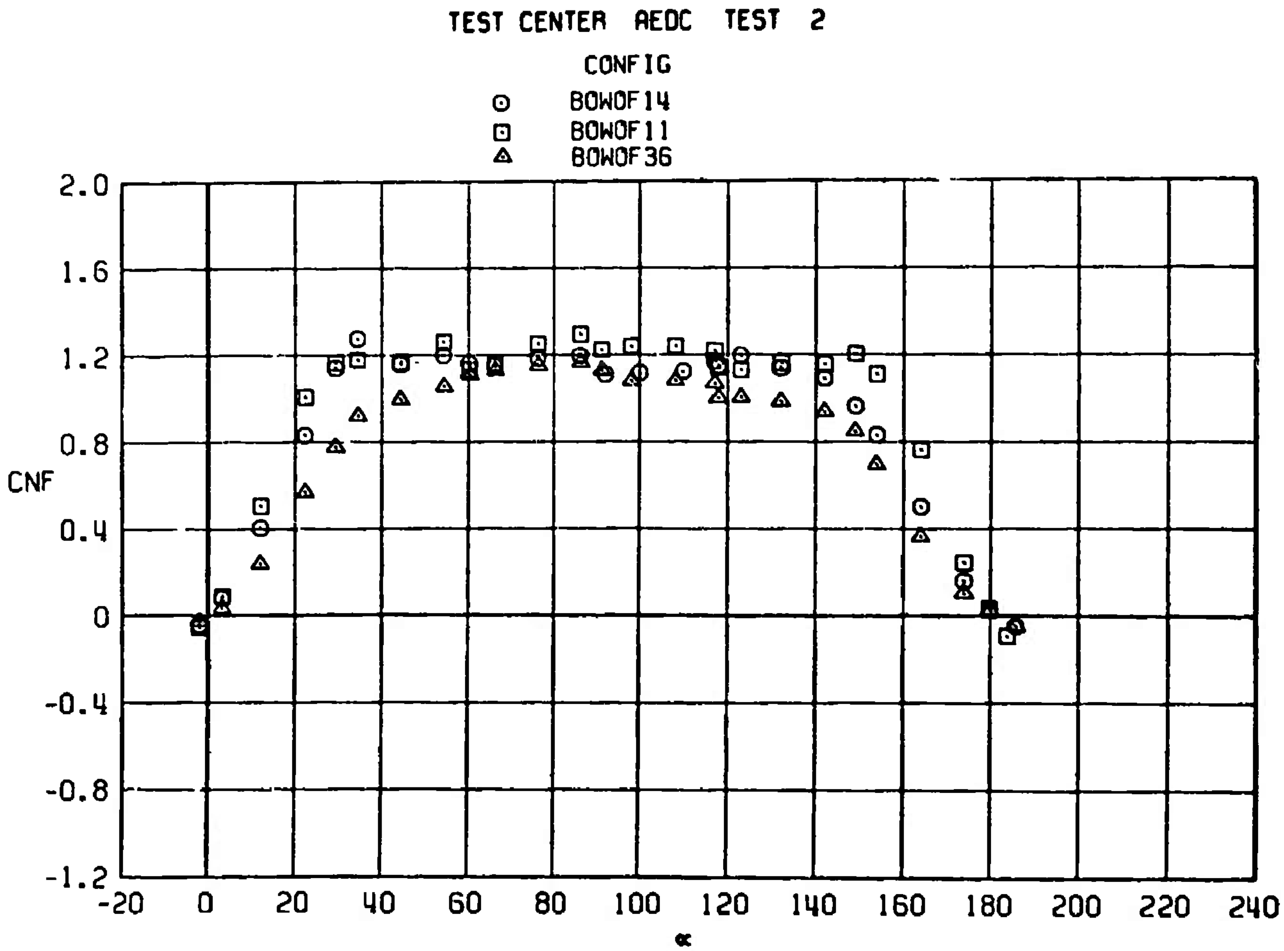

a. CNF versus α

Figure 20. Test No. 2, comparison of aerodynamic coefficients of configurations B0W0F14, B0W0F11, and B0W0F36 at $M_\infty = 0.98$.

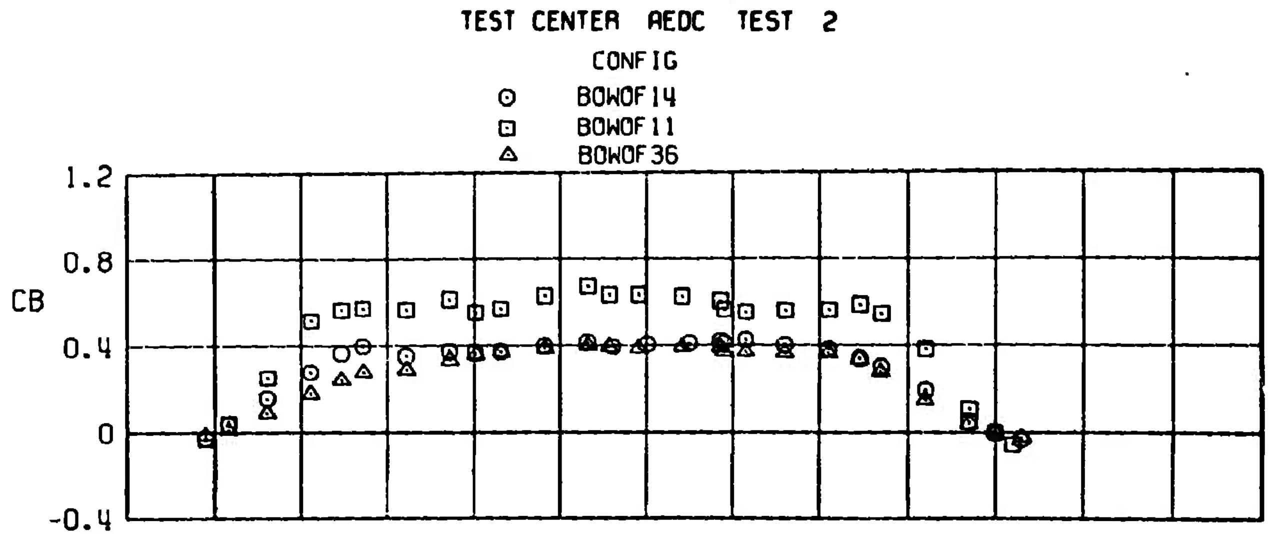

b. CB versus α

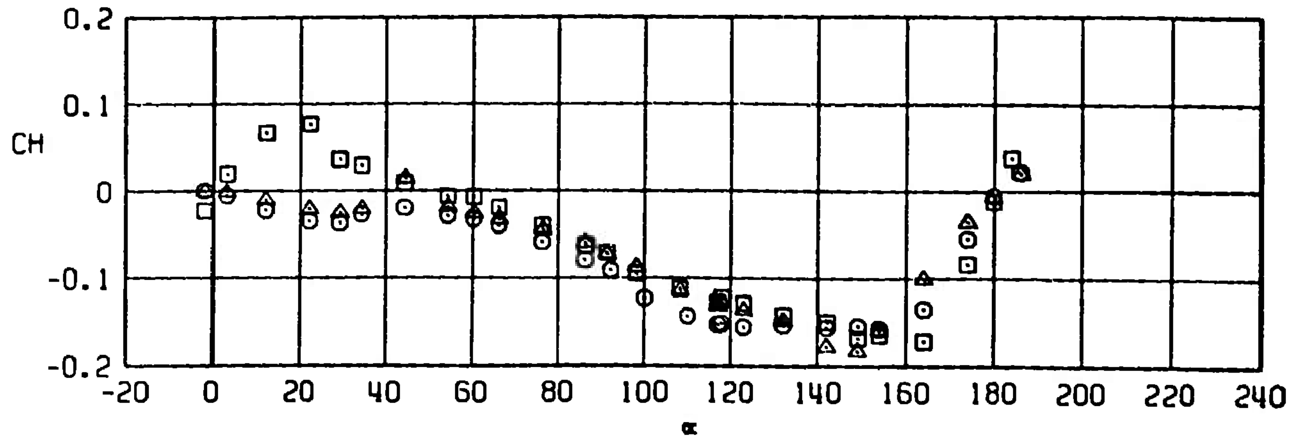

c. CH versus α

Figure 20. Concluded.

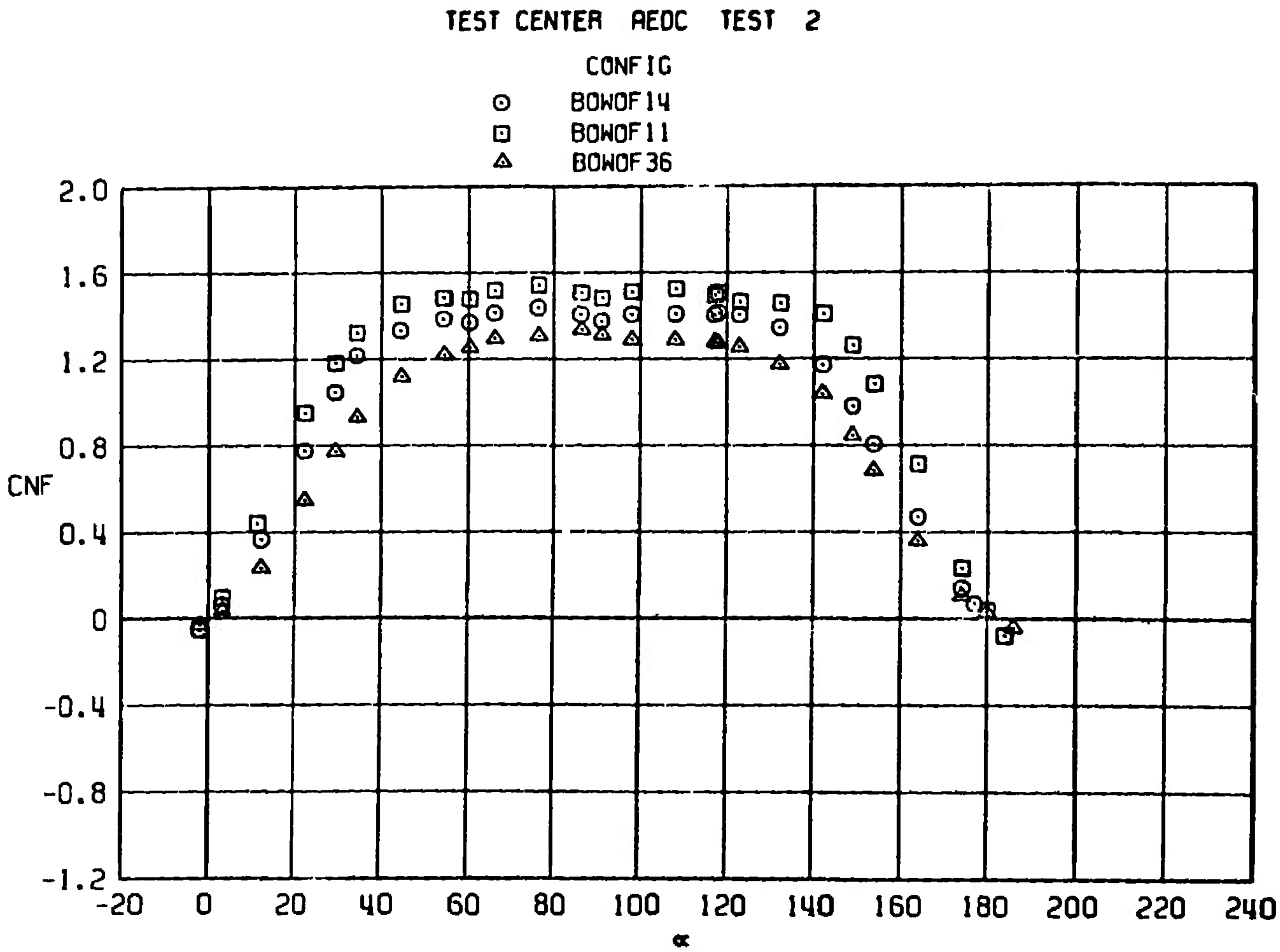

a. CNF versus α

Figure 21. Test No. 2, comparison of aerodynamic coefficients of configurations B0W0F14, B0W0F11, and B0W0F36 at M_∞ = 1.1.

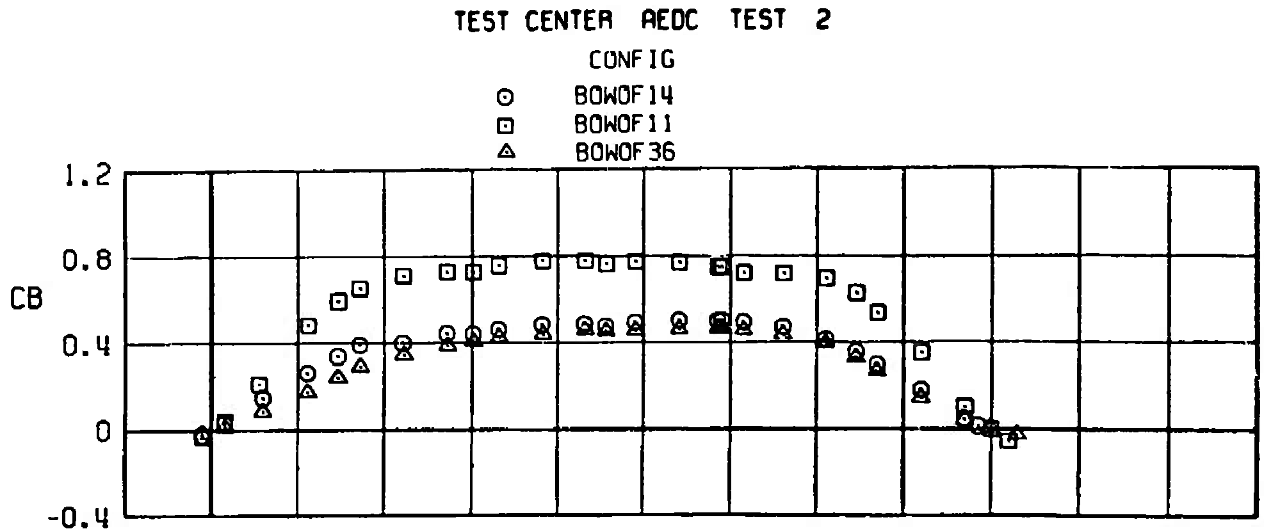

b. CB versus α

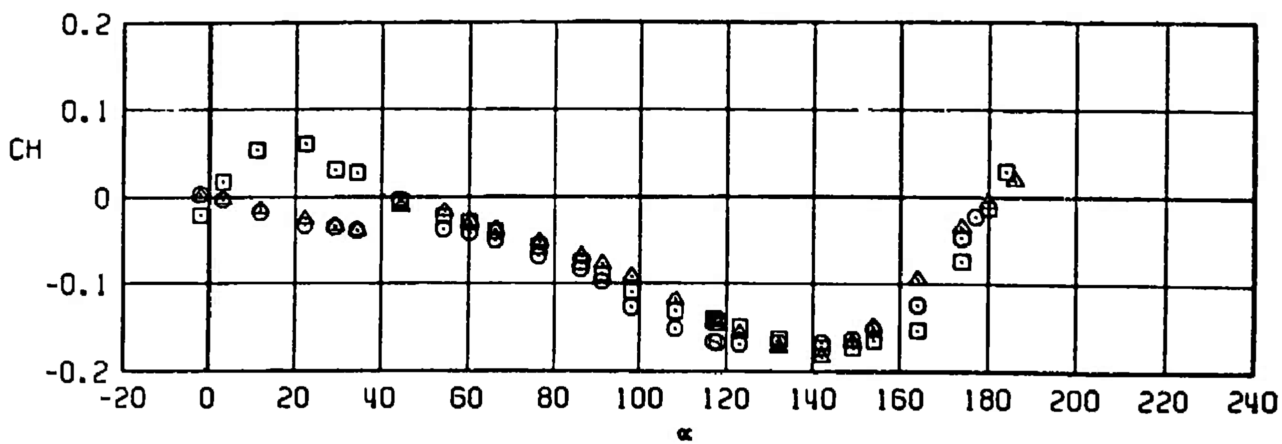

c. CH versus α

Figure 21. Concluded.

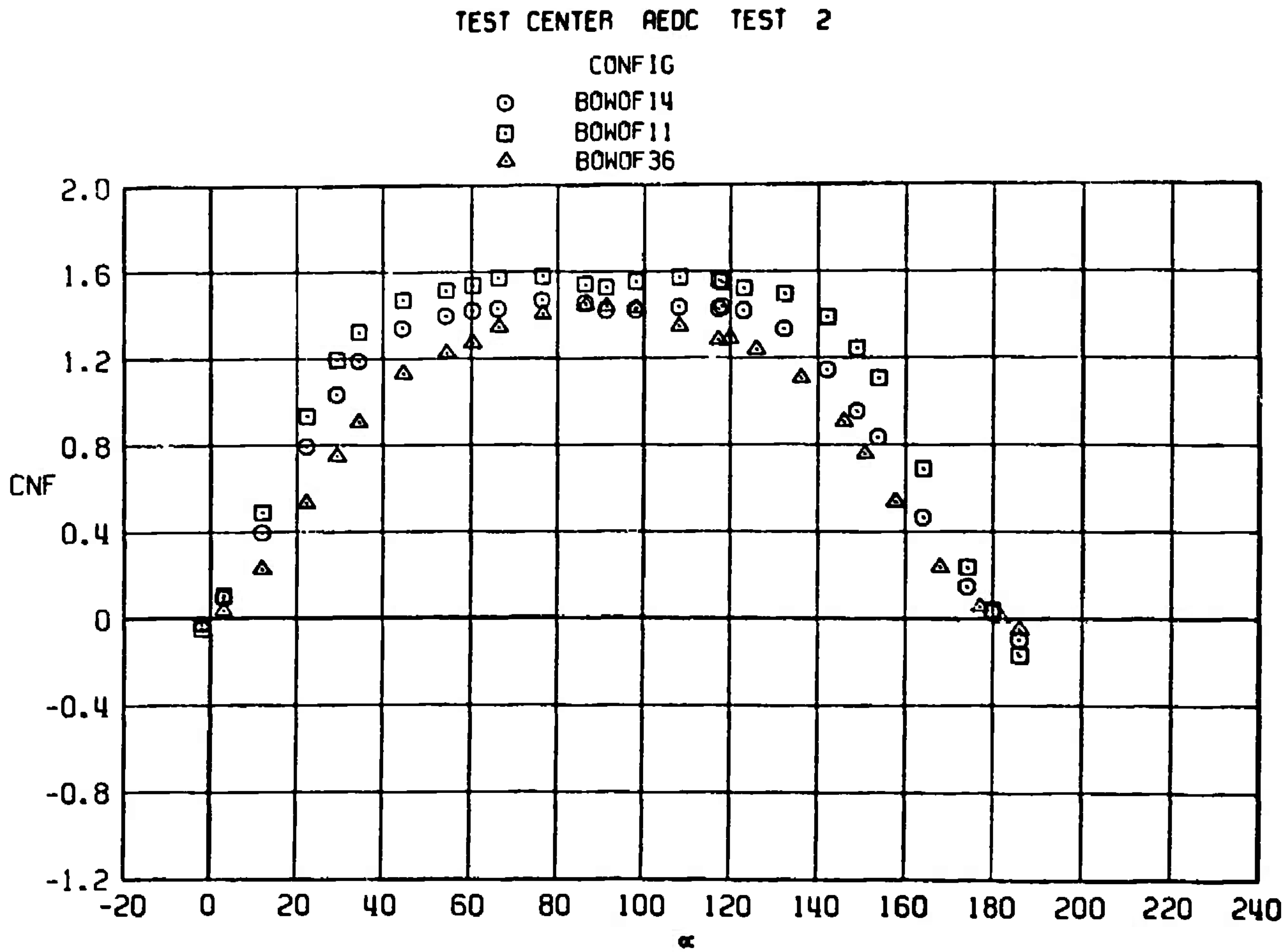

a. CNF versus α

Figure 22. Test No. 2, comparison of aerodynamic coefficients of configurations B0W0F14, B0W0F11, and B0W0F36 at M_∞ = 1.2.

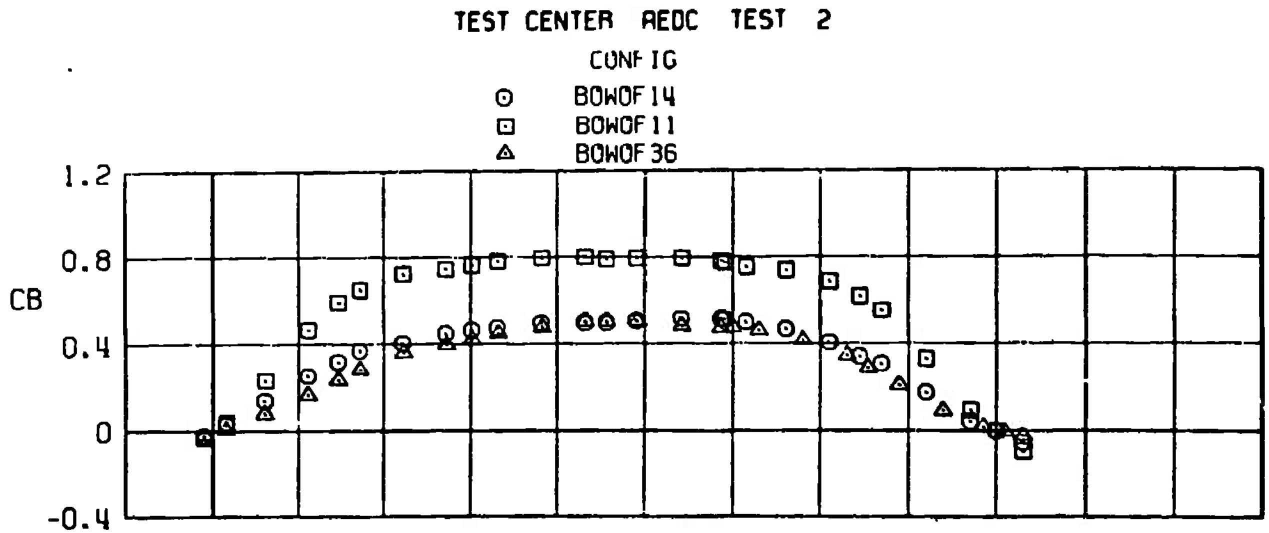

b. CB versus α

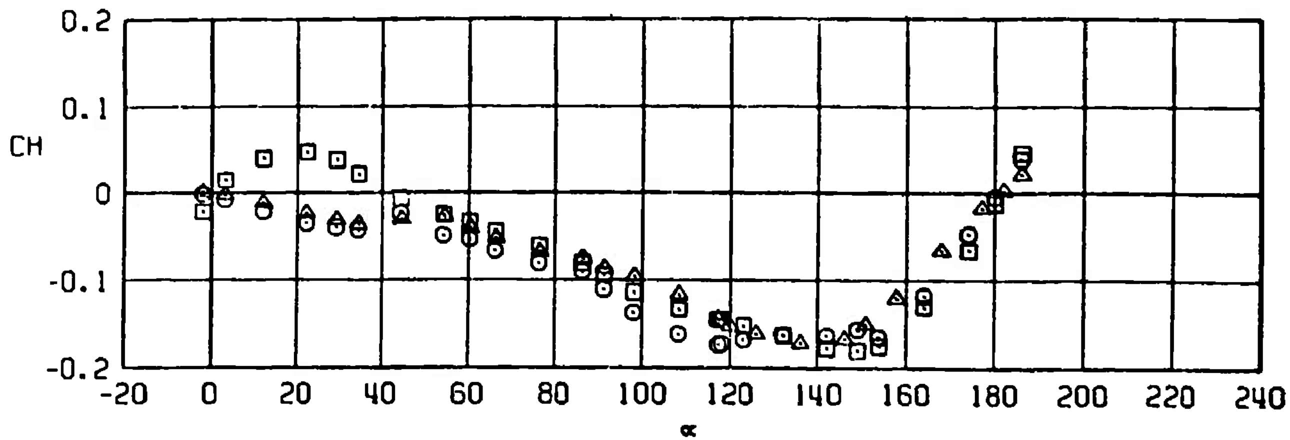

c. CH versus α

Figure 22. Concluded.

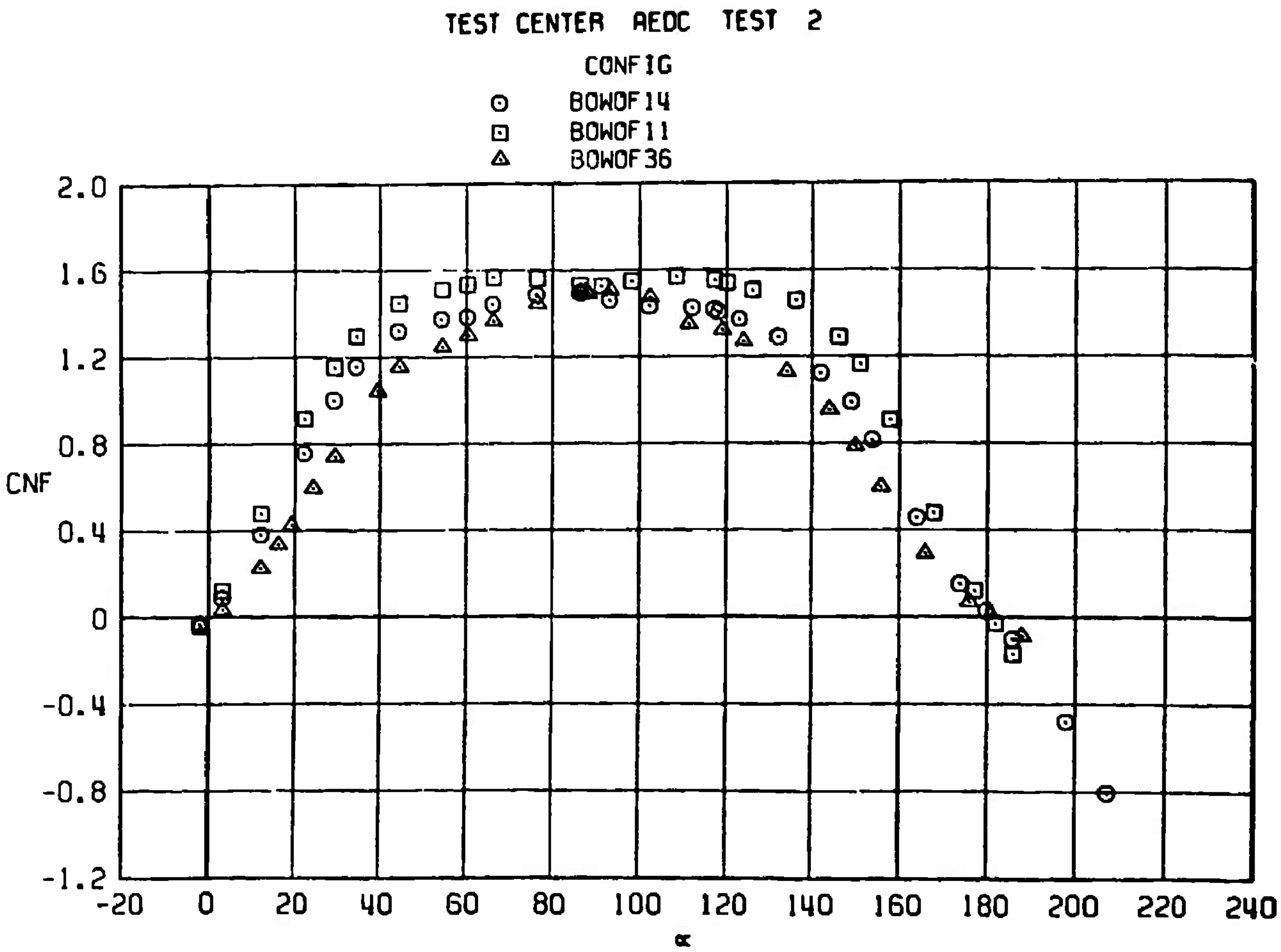

a. CNF versus α

Figure 23. Test No. 2, comparison of aerodynamic coefficients of configurations B0W0F14, B0W0F11, and B0W0F36 at $M_\infty = 1.3$.

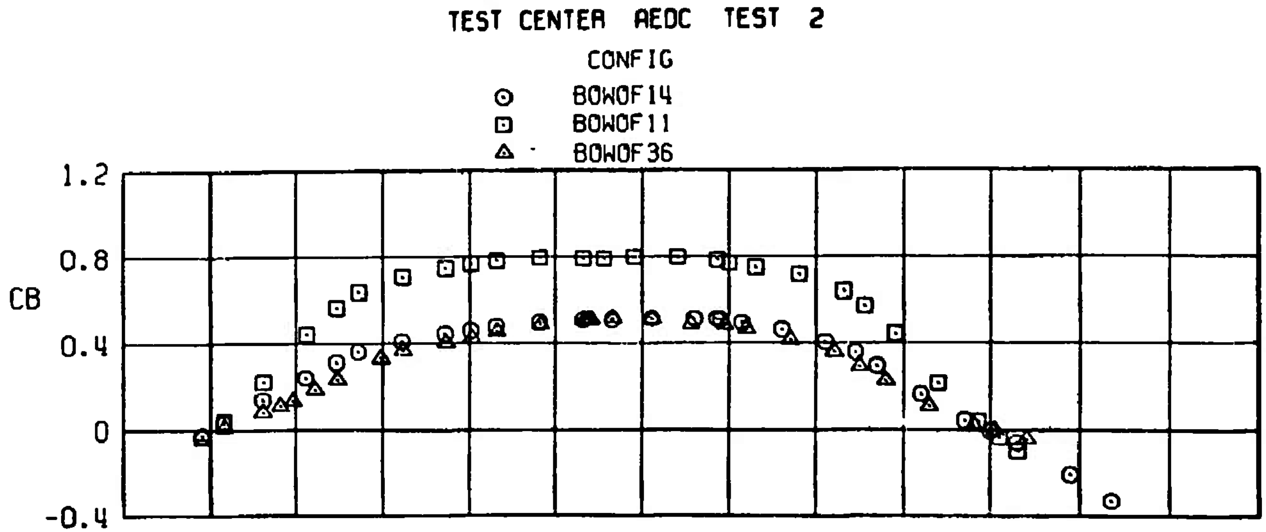

b. CB versus α

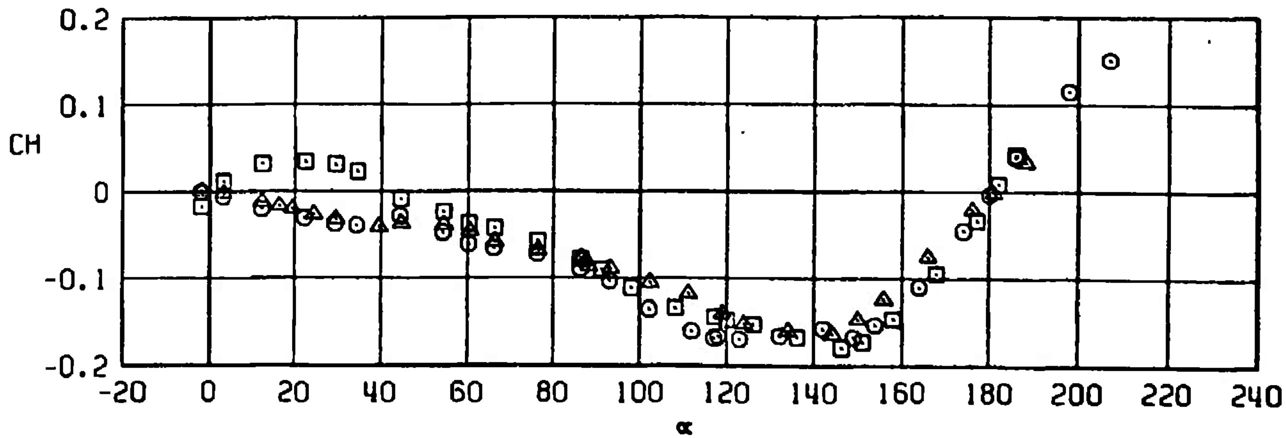

c. CH versus α

Figure 23. Concluded.

TEST CENTER LRC TEST 3

	CONF	L	DEL1	DEL2	DEL3	DEL4	PHI
⊙	B1W0F35	0	0	0	0	0	0
⊡	B1W0F35	0	0	0	0	0	45

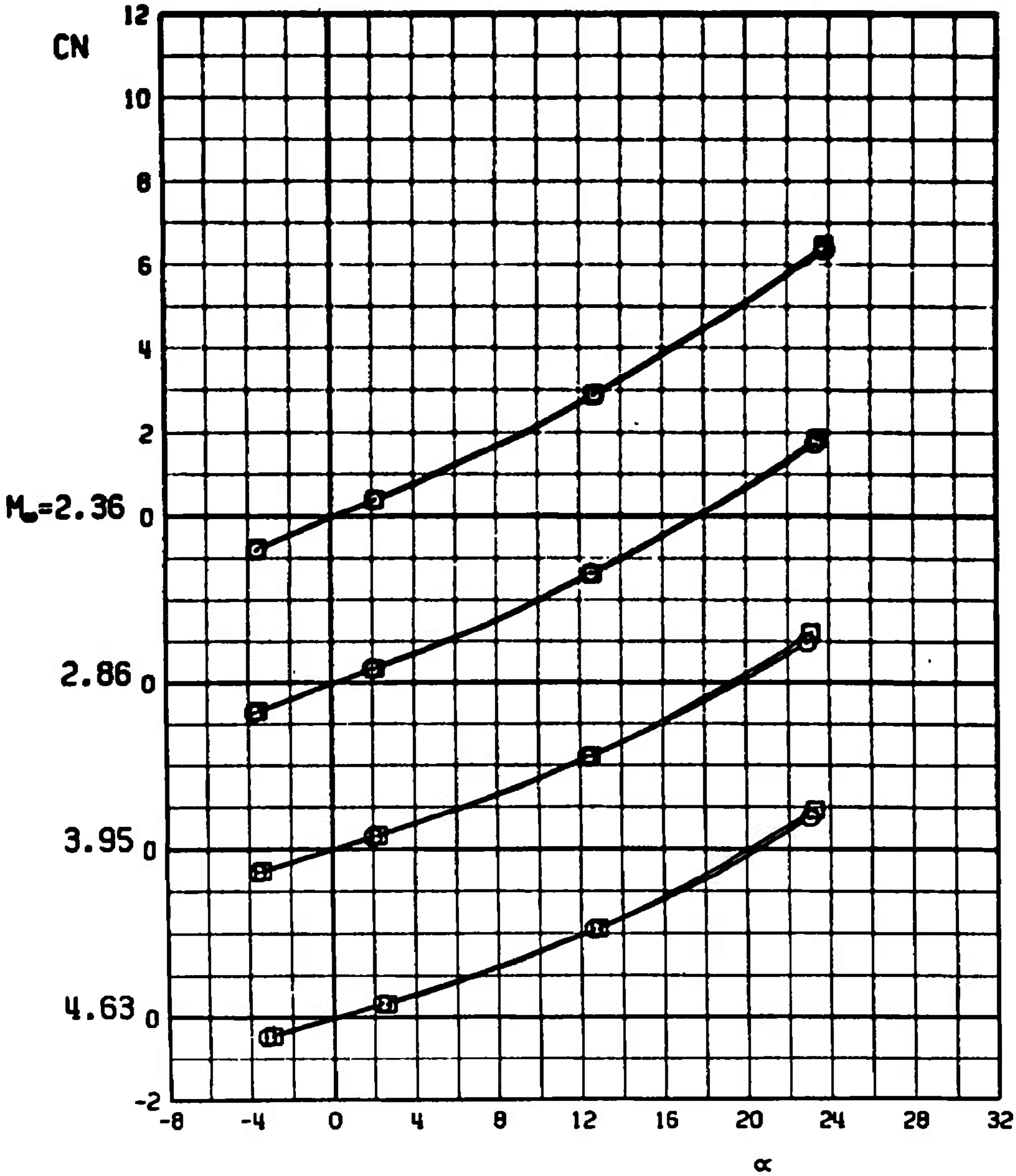

a. CN versus α

Figure 24. Test No. 3, comparison of aerodynamic coefficients of configuration B1W0F35 at roll angles of 0 and 45 deg.

TEST CENTER LRC TEST 3

	CONF	L	DEL1	DEL2	DEL3	DEL4	PHI
⊙	B1W0F35	0	0	0	0	0	0
⊡	B1W0F35	0	0	0	0	0	45

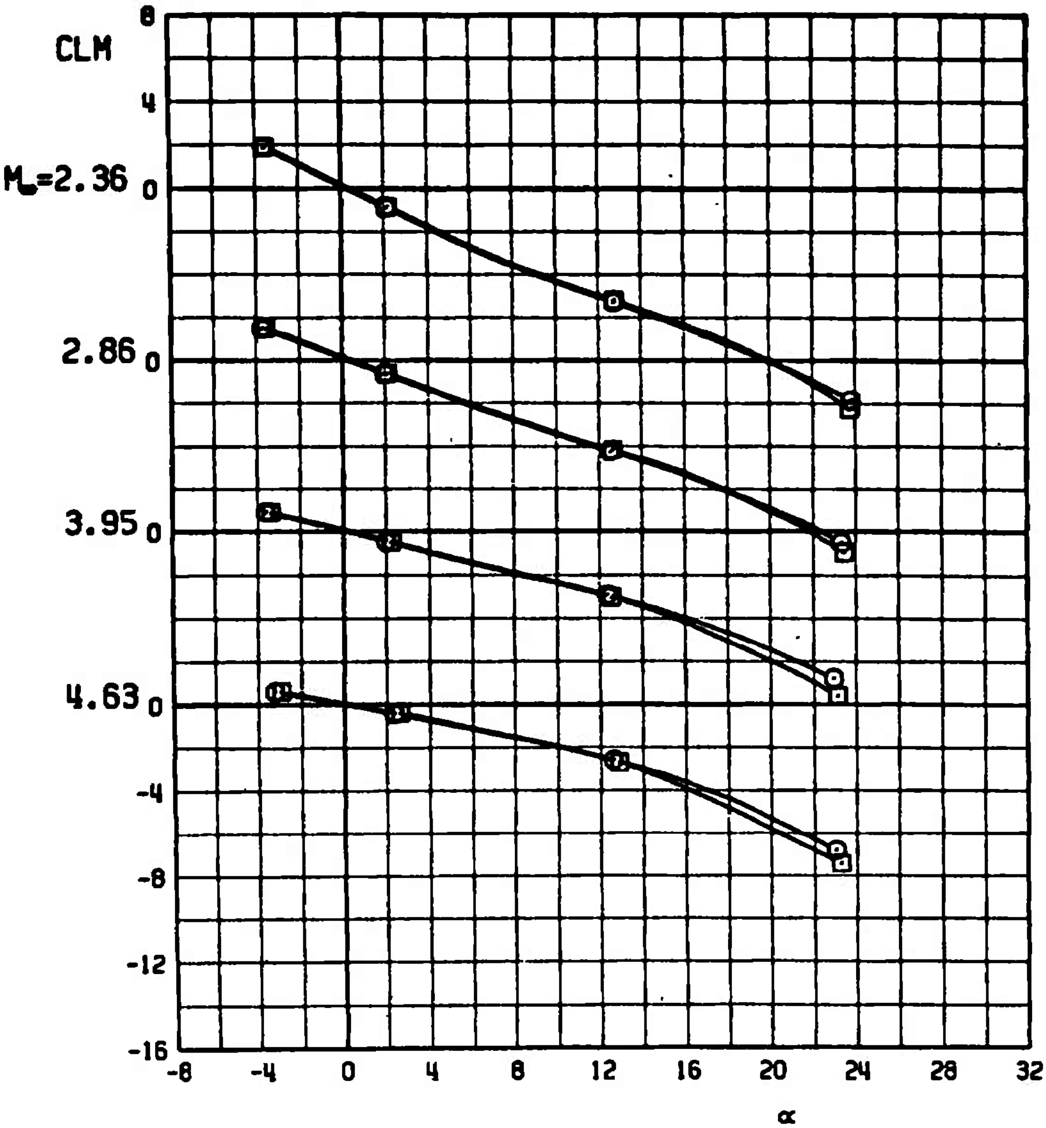

b. CLM versus α
Figure 24. Continued.

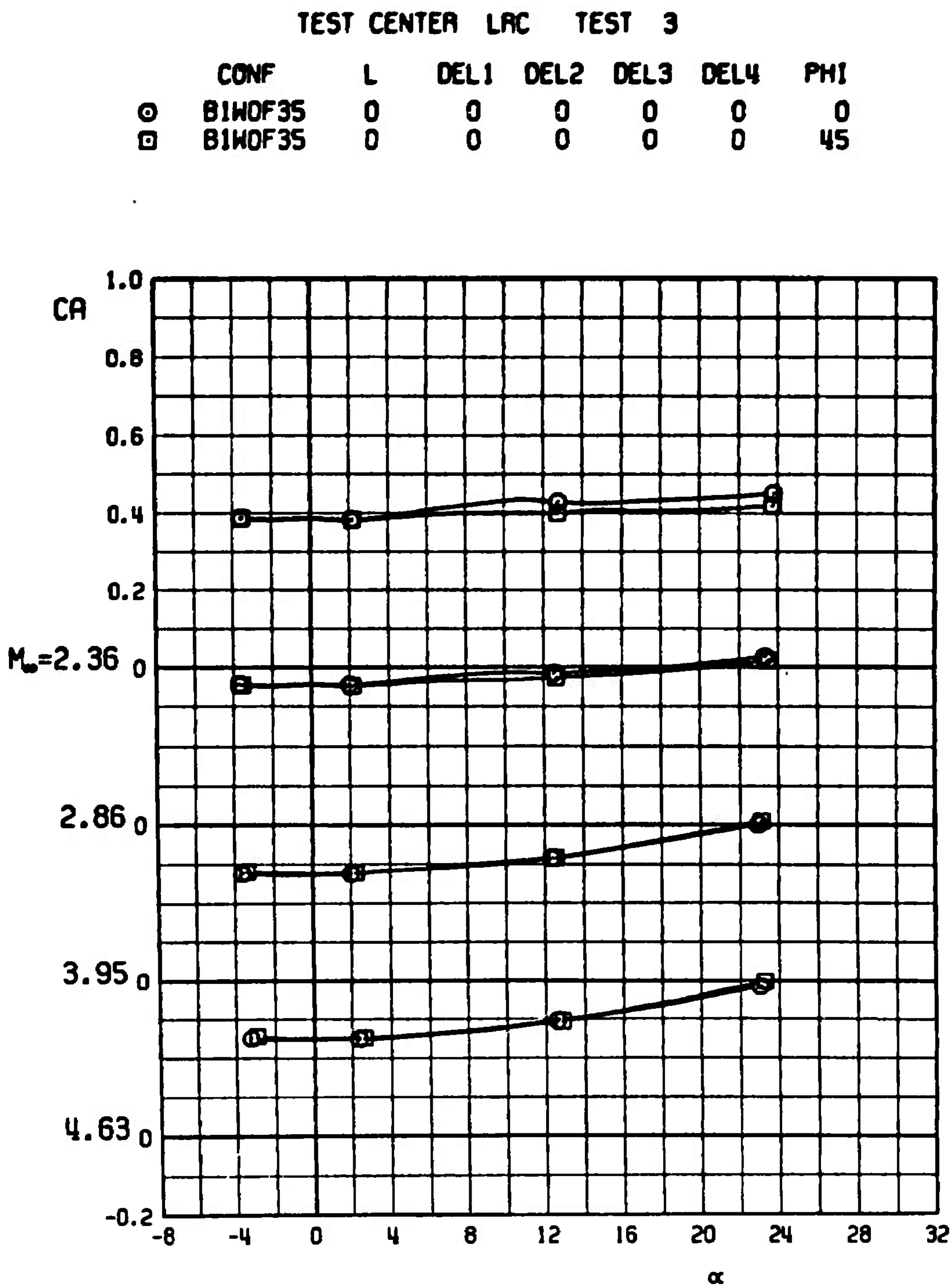

c. CA versus α
Figure 24. Continued.

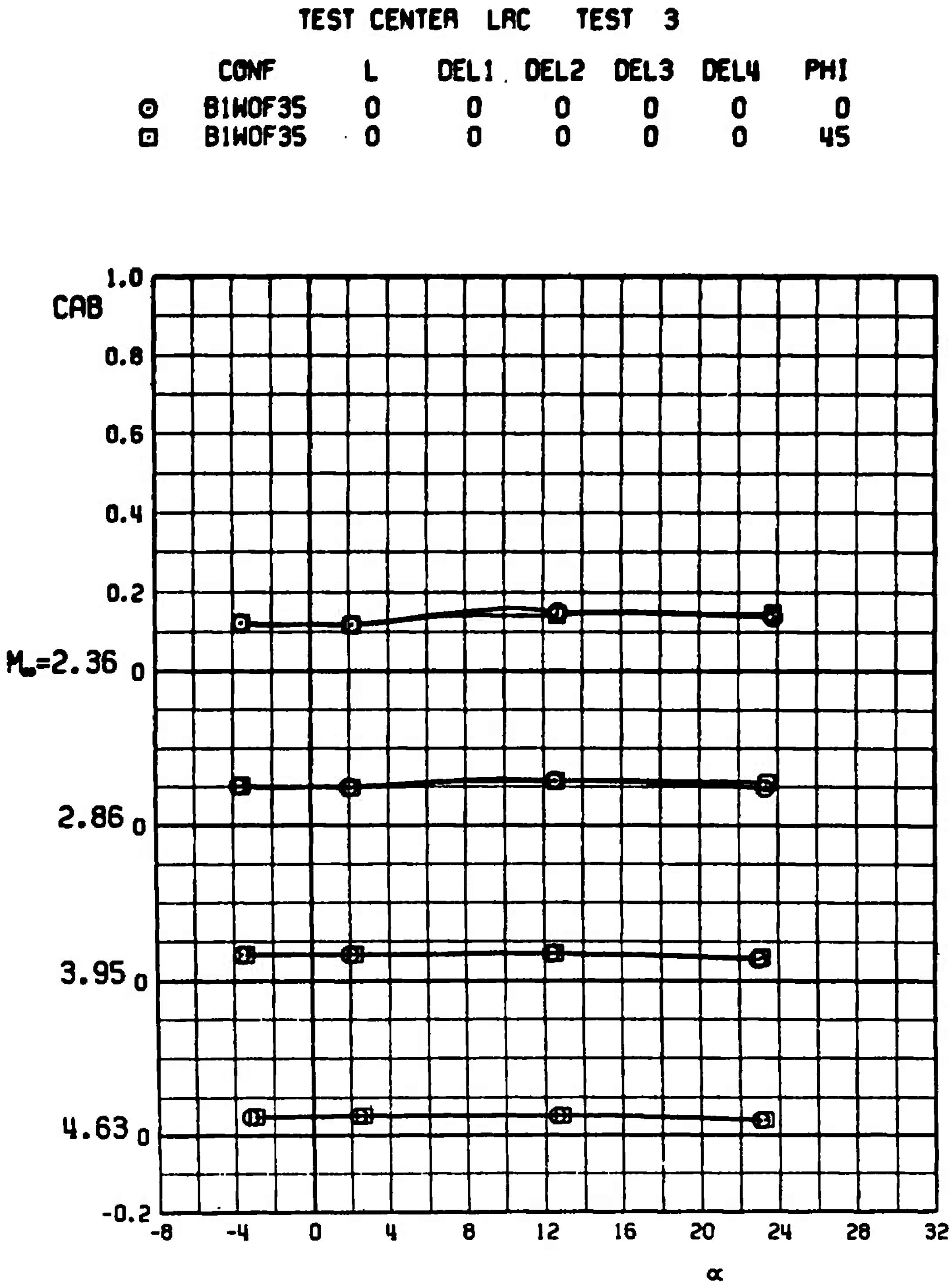

d. CAB versus a
Figure 24. Continued.

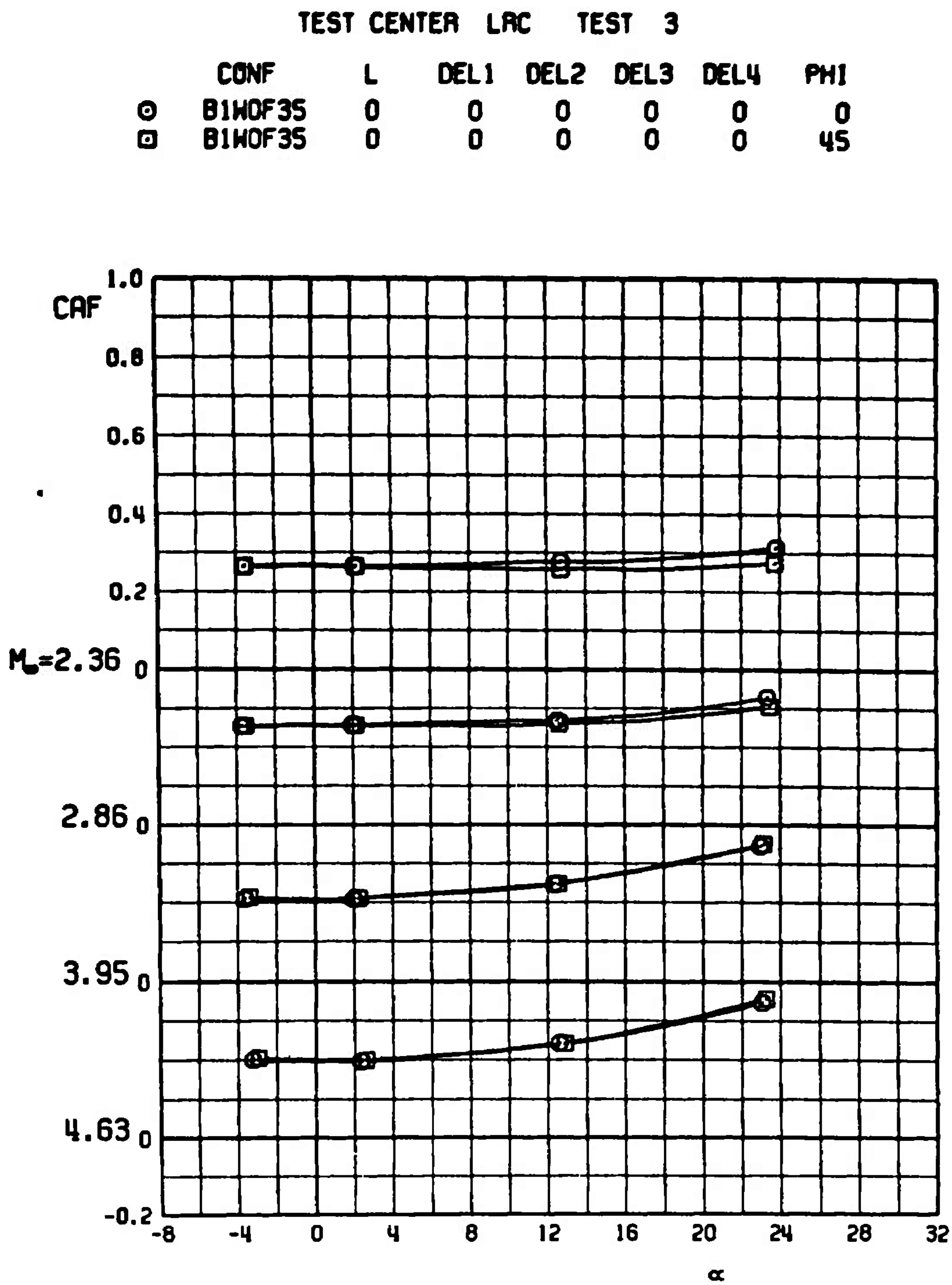

e. CAF versus α
Figure 24. Continued.

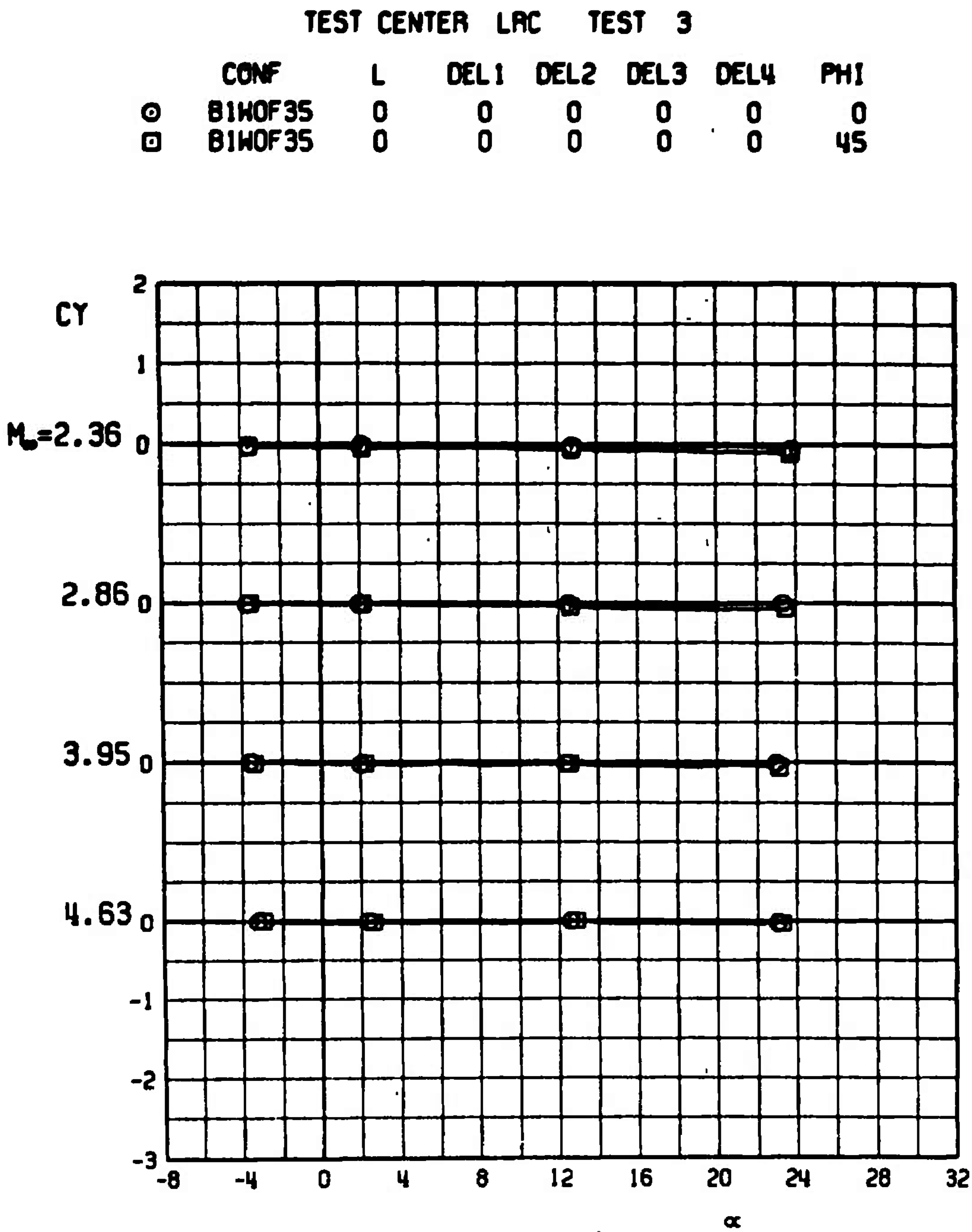

f. CY versus α
Figure 24. Continued.

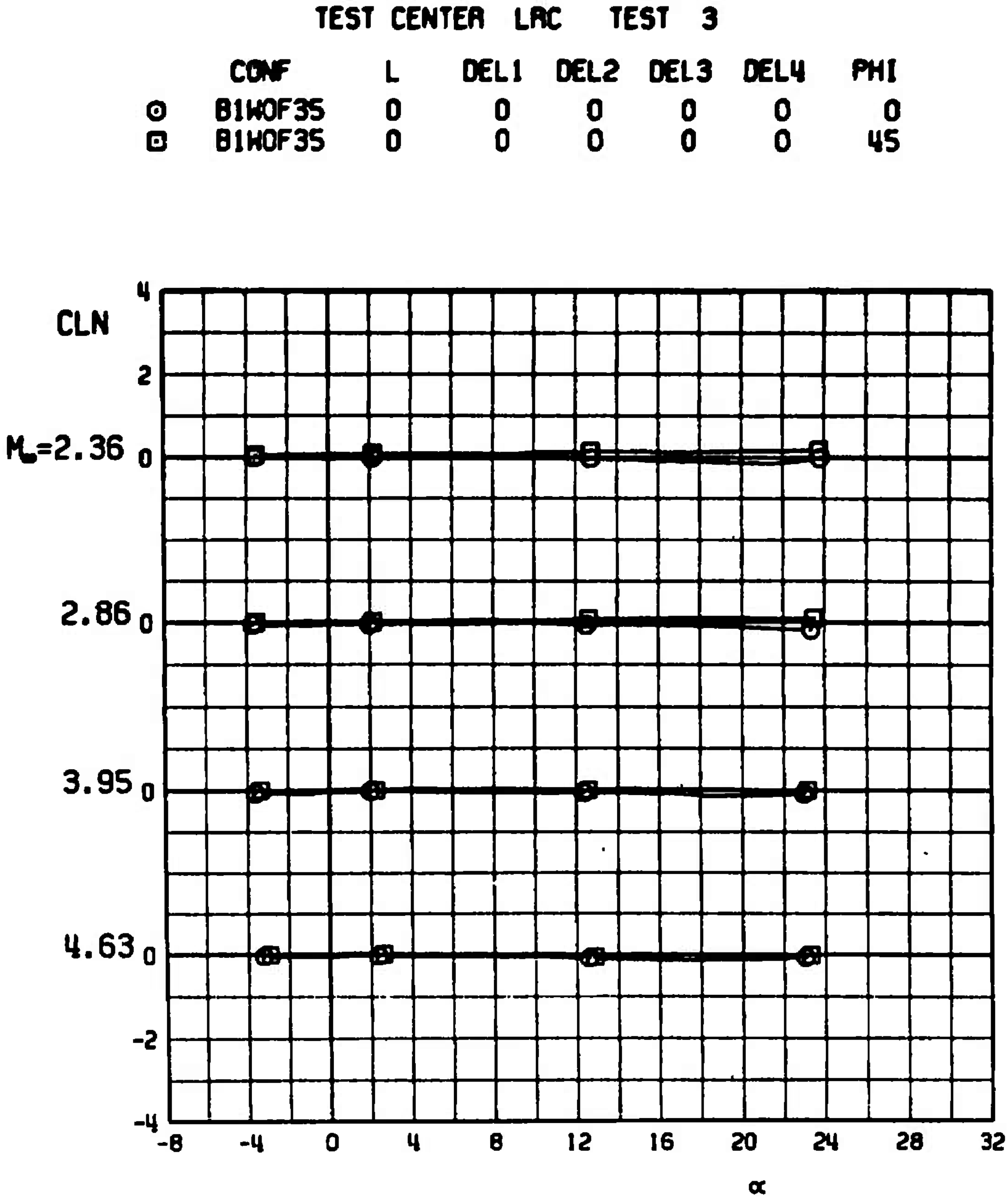

g. CLN versus α
Figure 24. Continued.

TEST CENTER LRC TEST 3

	CONF	L	DEL1	DEL2	DEL3	DEL4	PHI
⊙	B1WOF35	0	0	0	0	0	0
⊡	B1WOF35	0	0	0	0	0	45

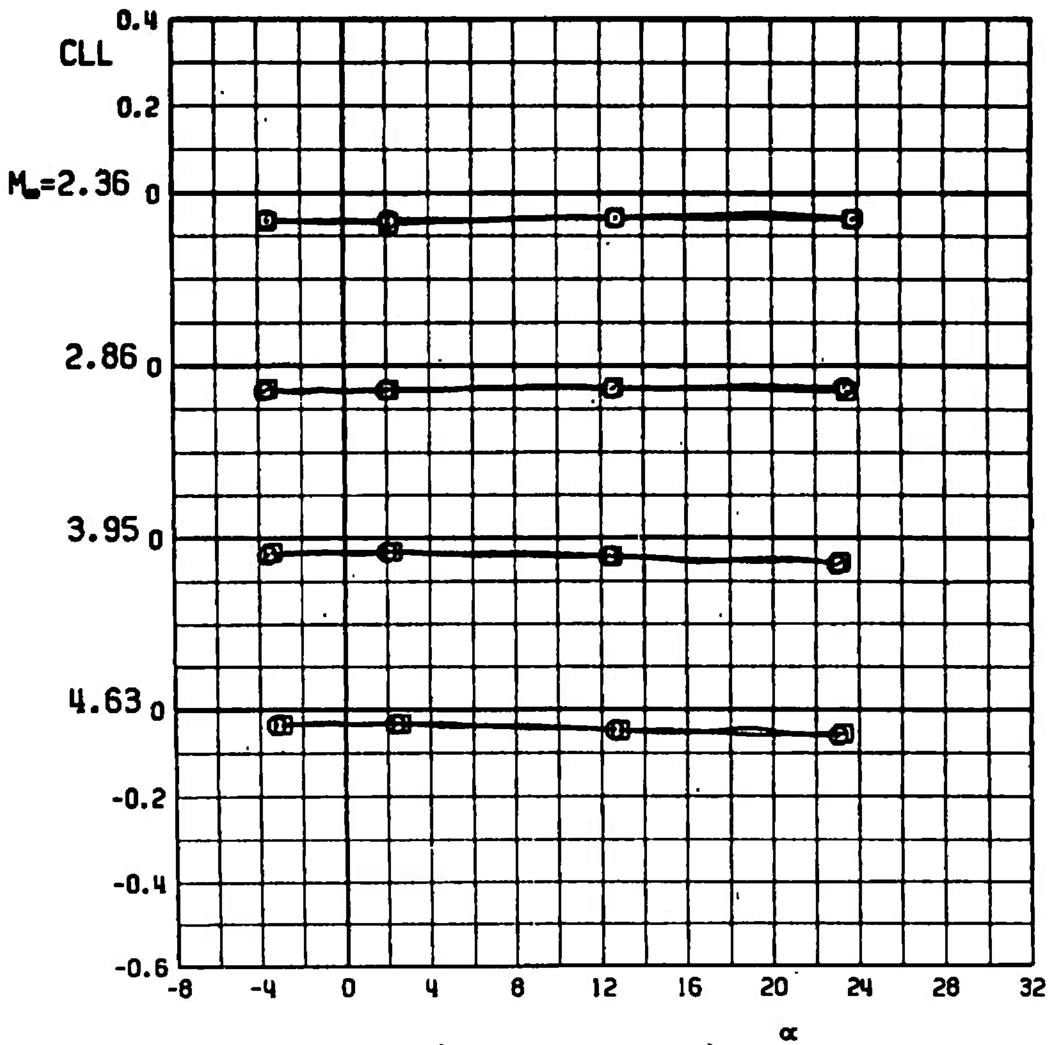

h. CLL versus α
Figure 24. Concluded.

TEST CENTER LRC TEST 3

	CONF	L	DEL1	DEL2	DEL3	DEL4	PHI
⊙	B1W0F33	0	0	0	0	0	0
⊡	B1W0F33	0	0	0	0	0	45

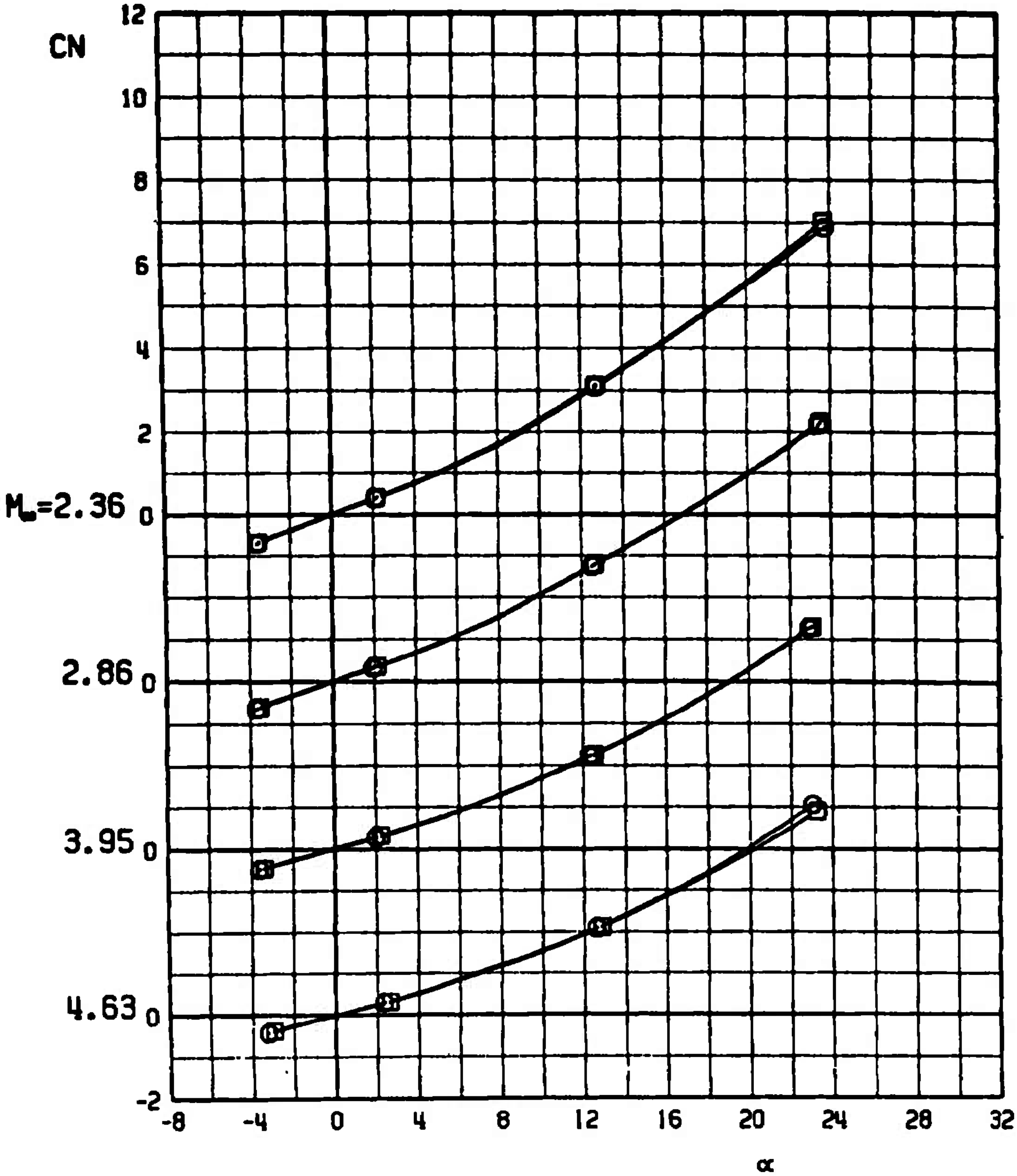

a. CN versus α

Figure 25. Test No. 3, comparison of aerodynamic coefficients of configuration B1W0F33 at roll angles of 0 and 45 deg.

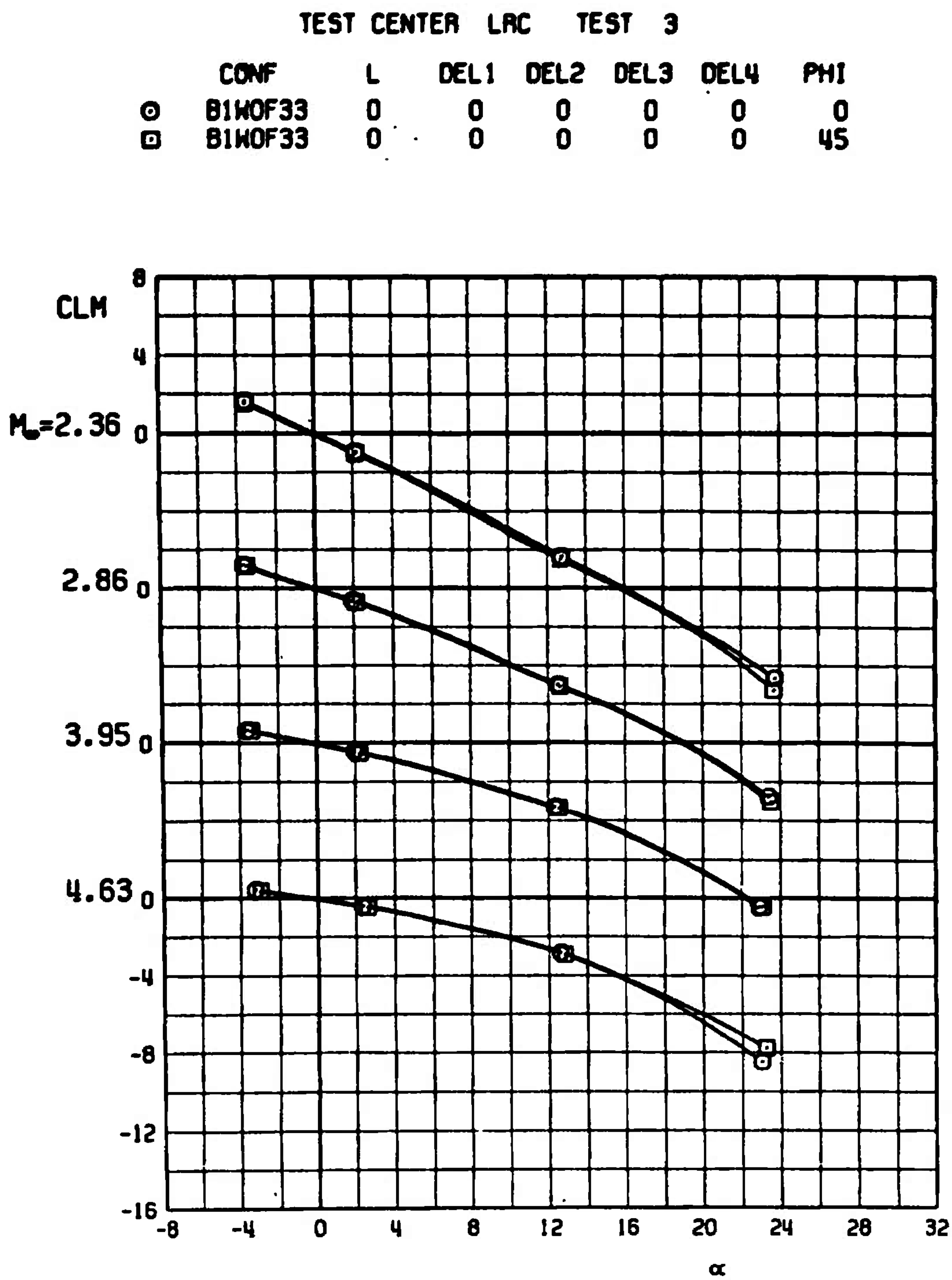

b. CLM versus α
Figure 25. Continued.

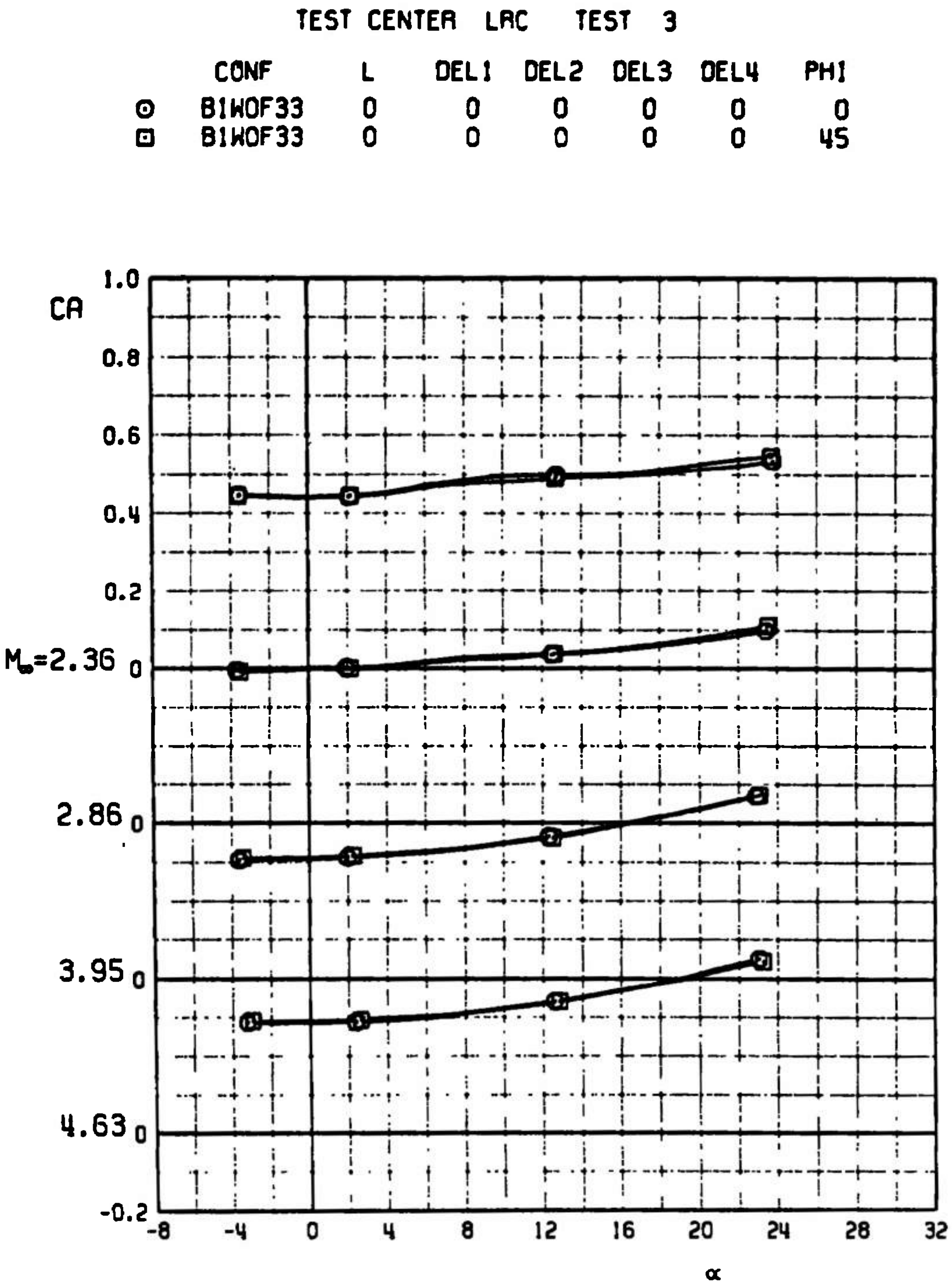

c. CA versus α
Figure 25. Continued.

TEST CENTER. LRC   TEST 3

	CONF	L	DEL1	DEL2	DEL3	DEL4	PHI
⊙	B1W0F33	0	0	0	0	0	0
⊡	B1W0F33	0	0	0	0	0	45

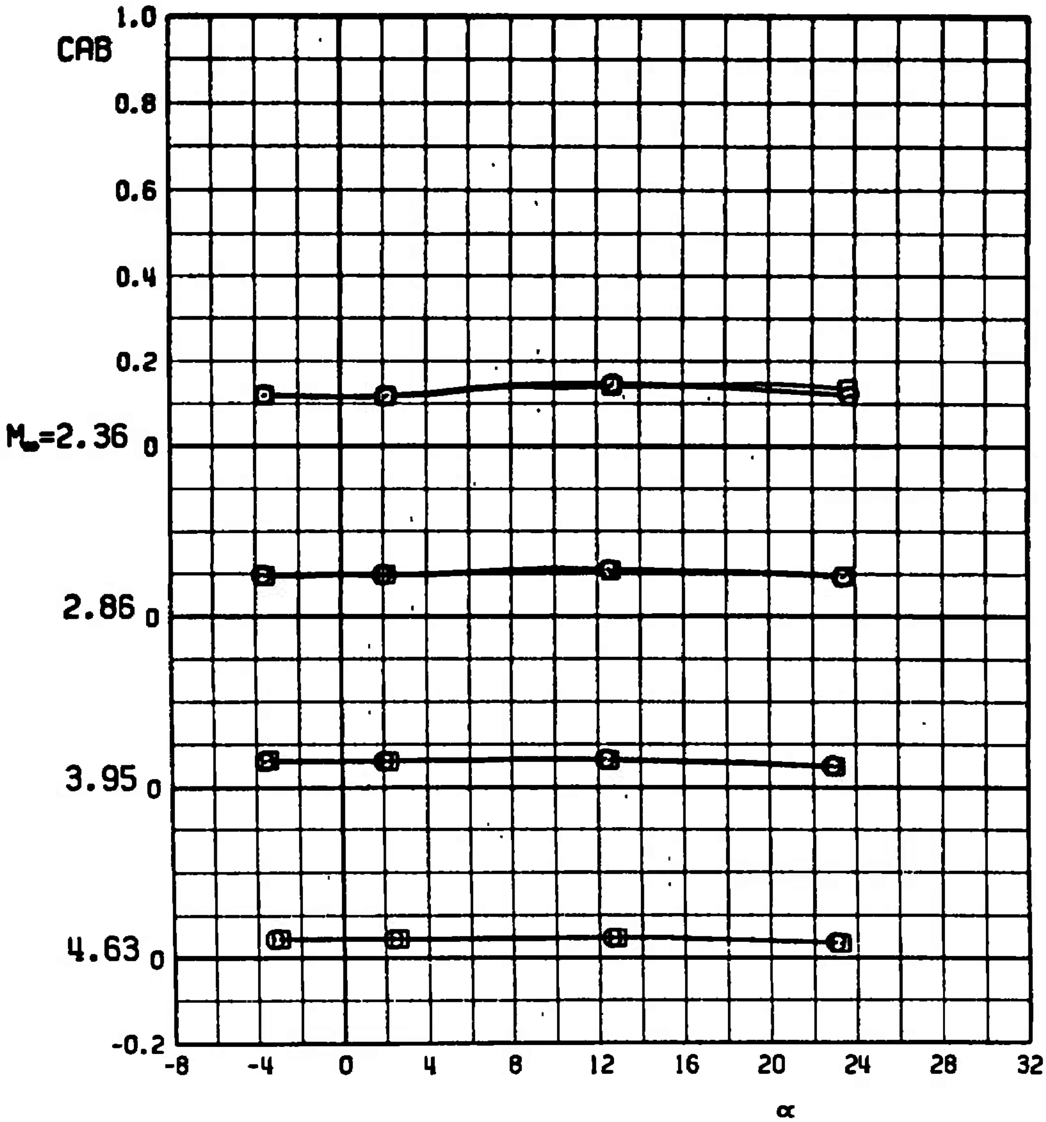

d. CAB versus α
Figure 25. Continued.

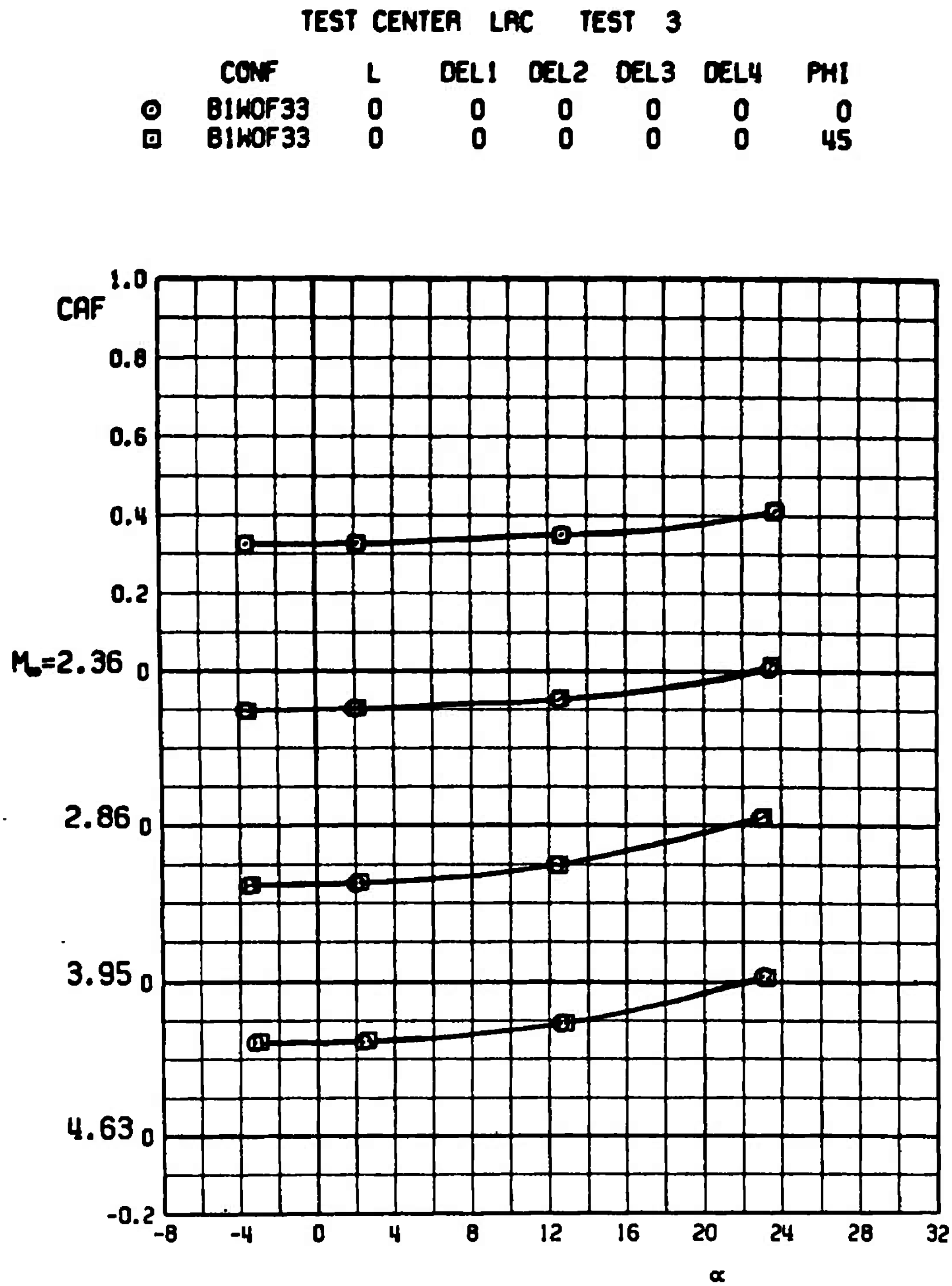

e. CAF versus α
Figure 25. Continued.

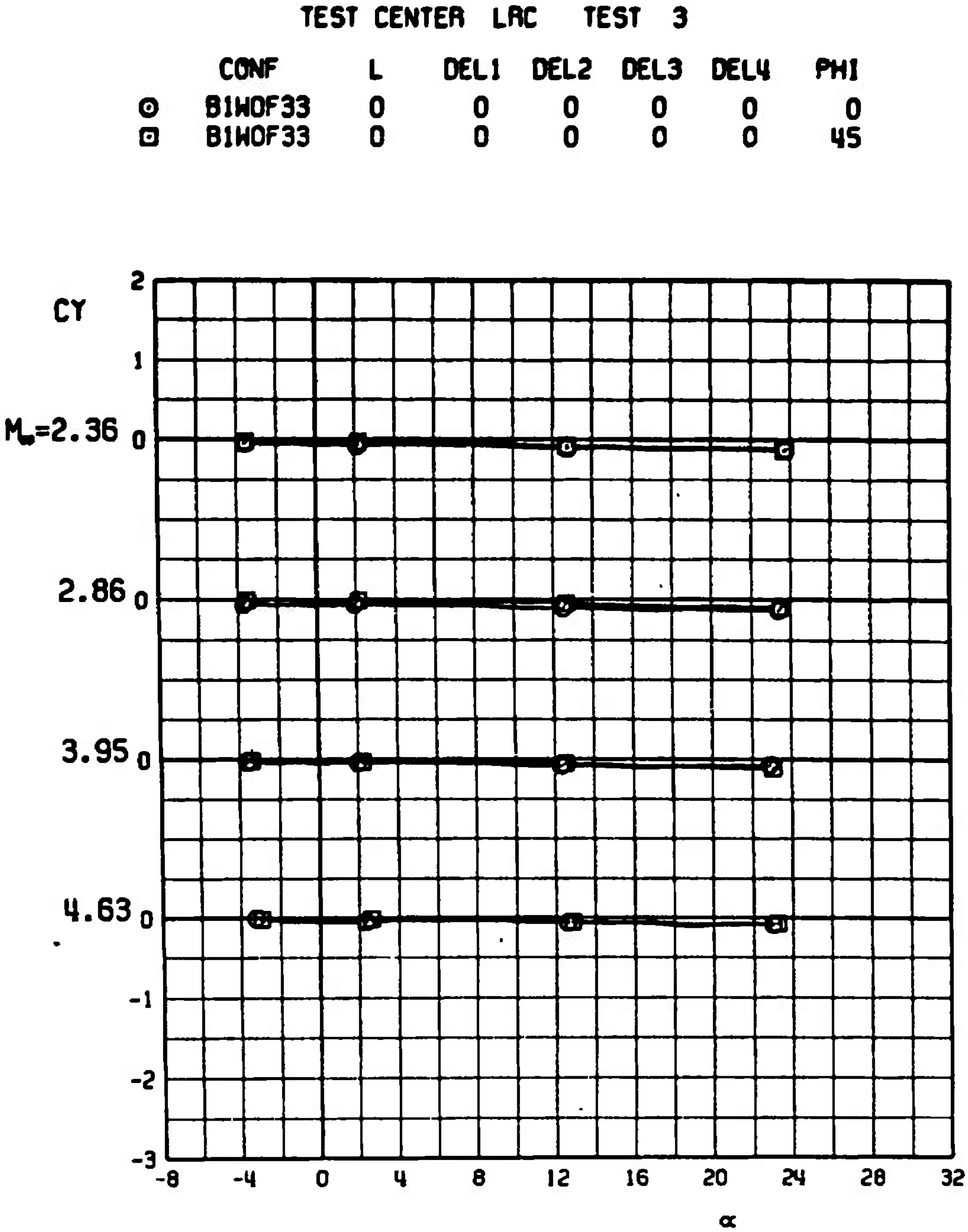

f. CY versus α
Figure 25. Continued.

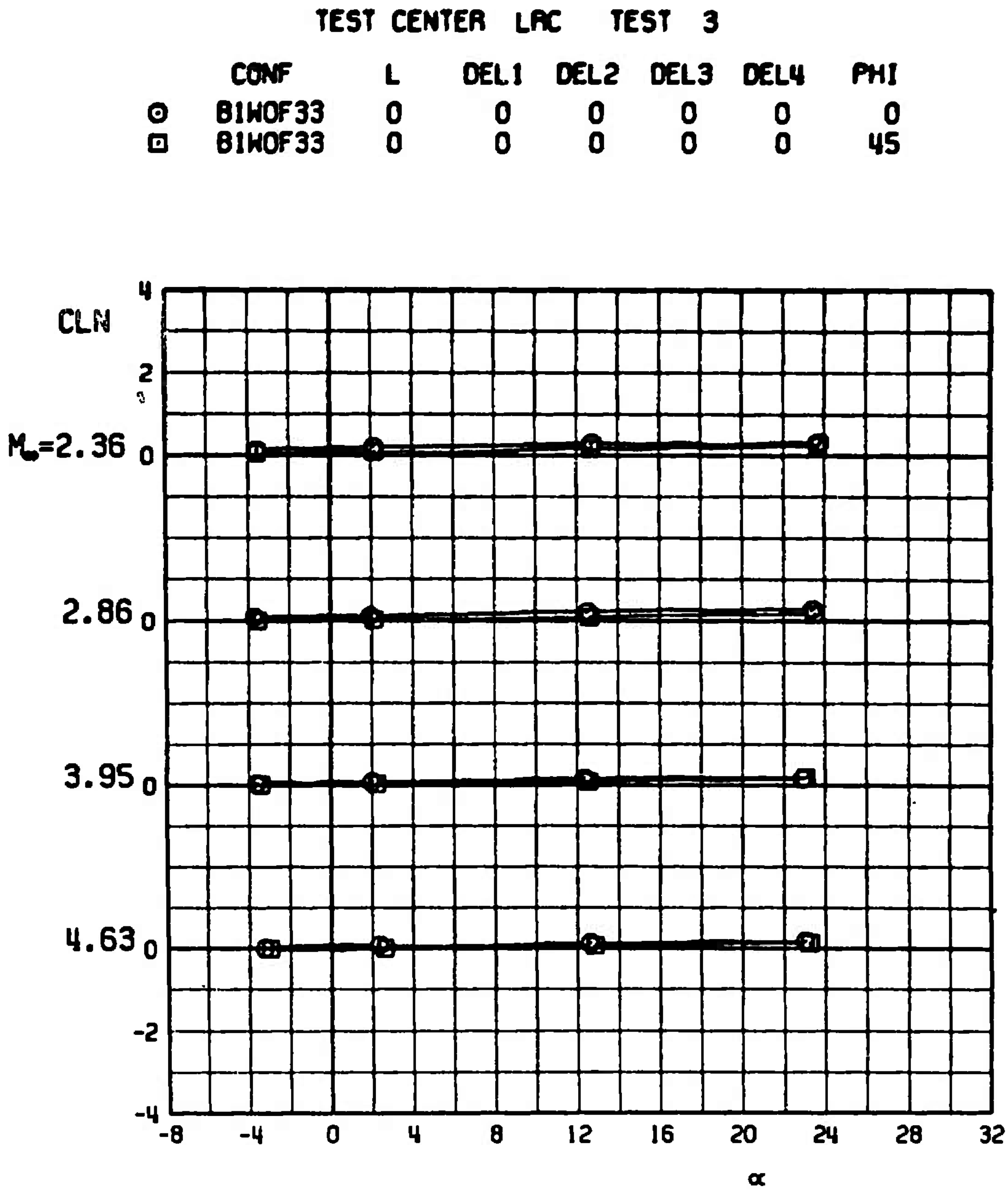

g. CLN versus α

Figure 25. Continued.

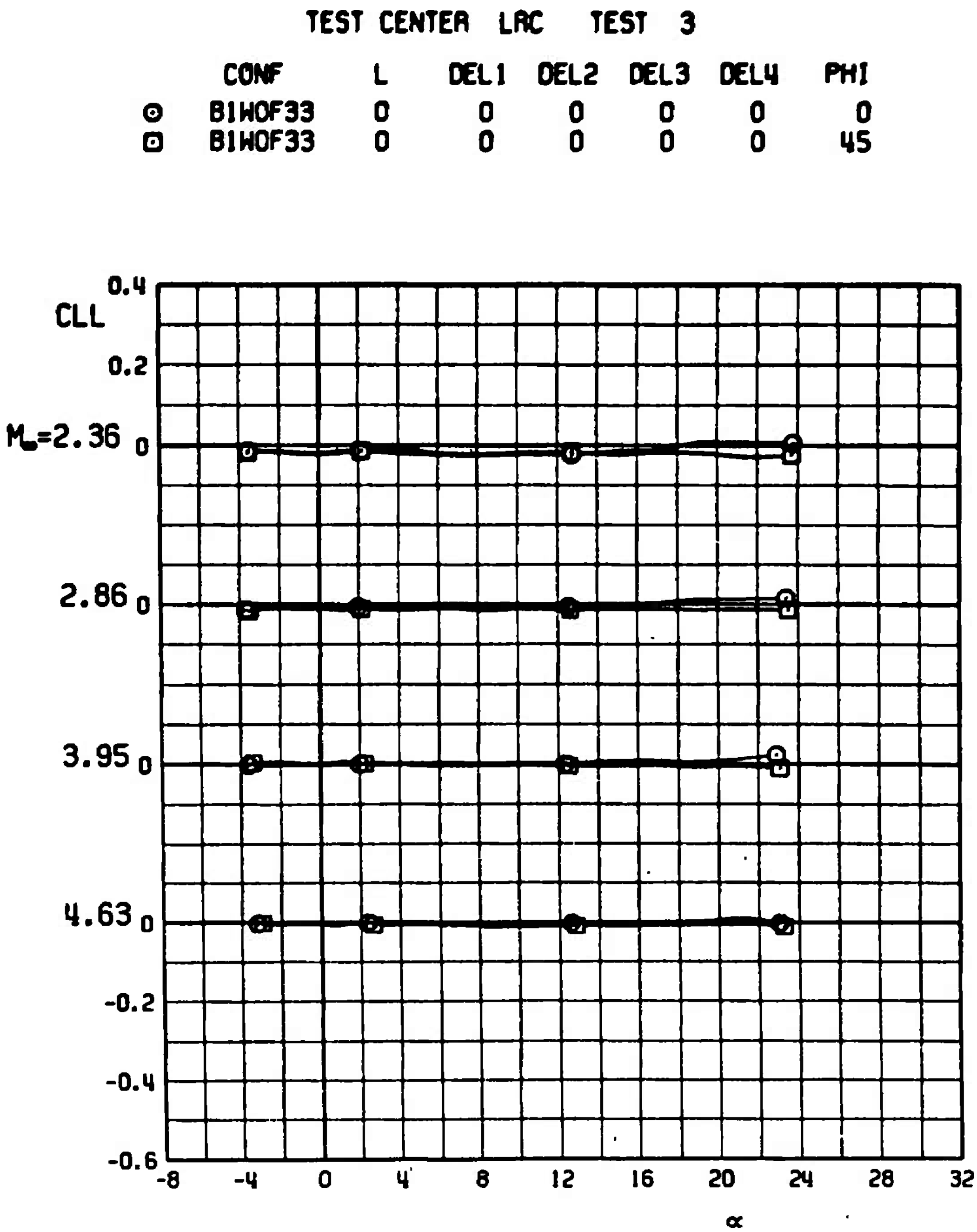

h. CLL versus α
Figure 25. Concluded.

TEST CENTER LRC TEST 3

	CONF	L	DEL1	DEL2	DEL3	DEL4	PHI
⊙	B1W0F34	0	0	0	0	0	0
⊡	B1W0F34	0	0	0	0	0	45

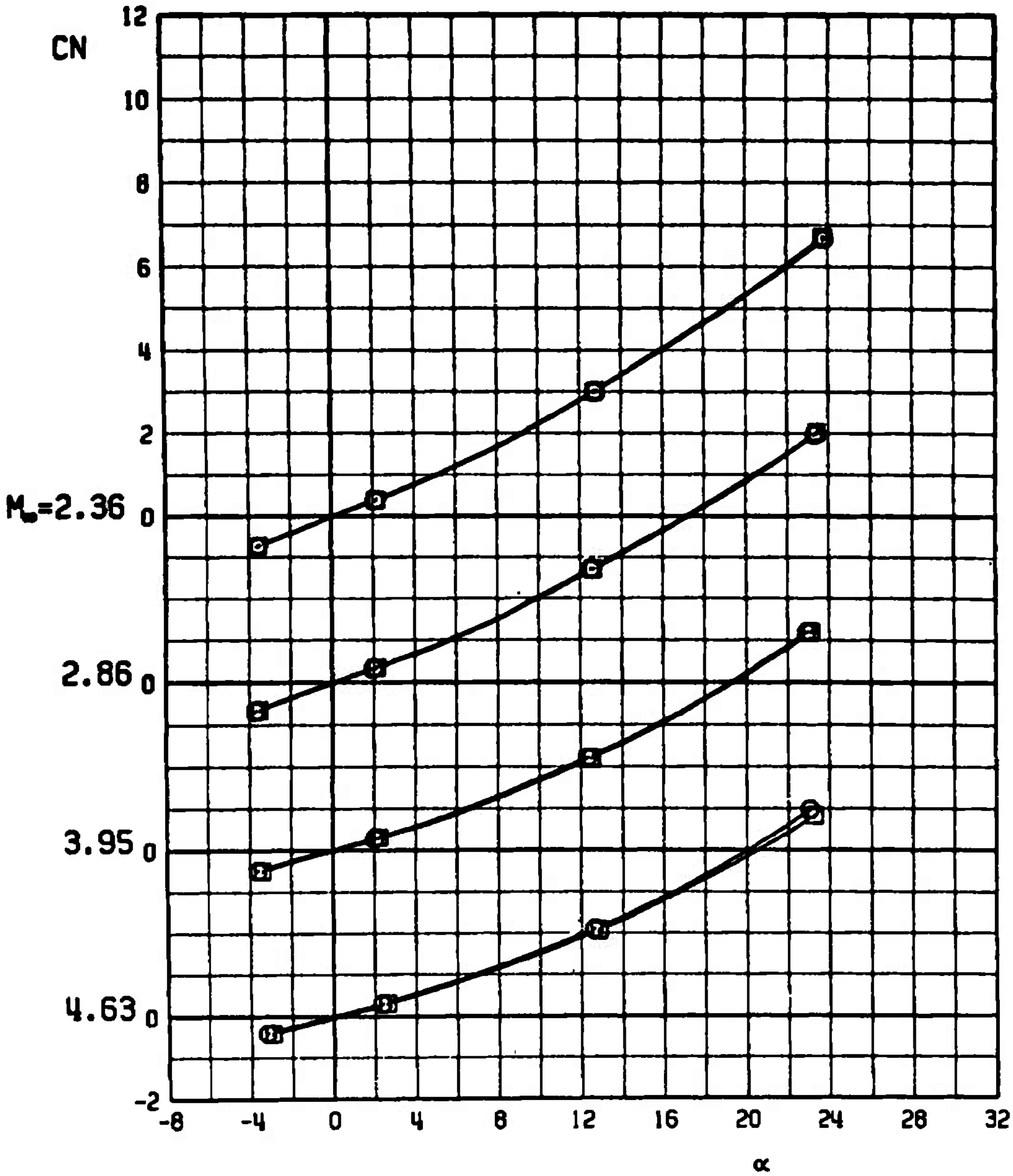

a. CN versus α

Figure 26. Test No. 3, comparison of aerodynamic coefficients of configuration B1W0F34 at roll angles of 0 and 45 deg.

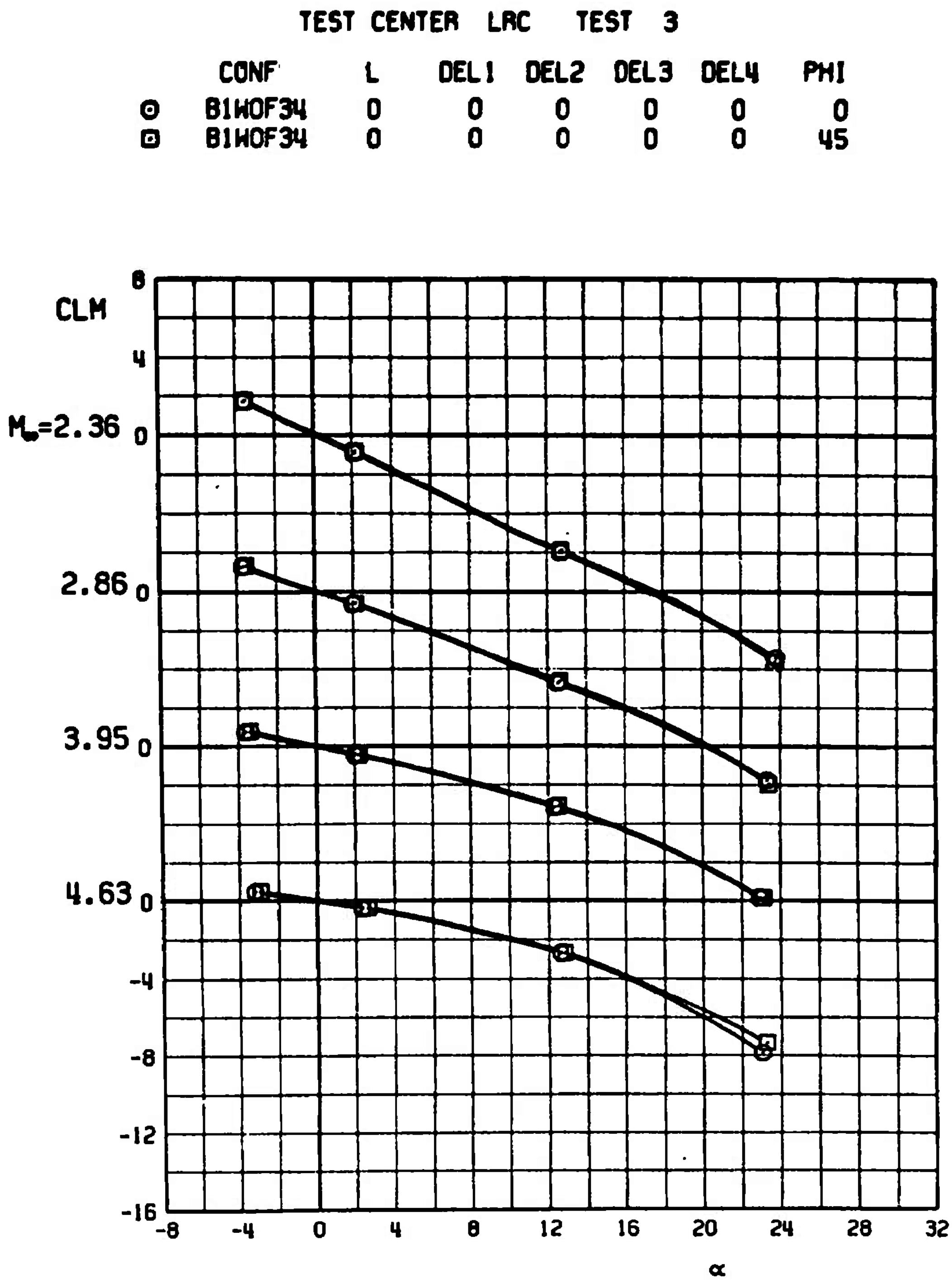

b. CLM versus α
Figure 26. Continued.

TEST CENTER LRC TEST 3

	CONF	L	DEL1	DEL2	DEL3	DEL4	PHI
⊙	B1W0F34	0	0	0	0	0	0
⊡	B1W0F34	0	0	0	0	0	45

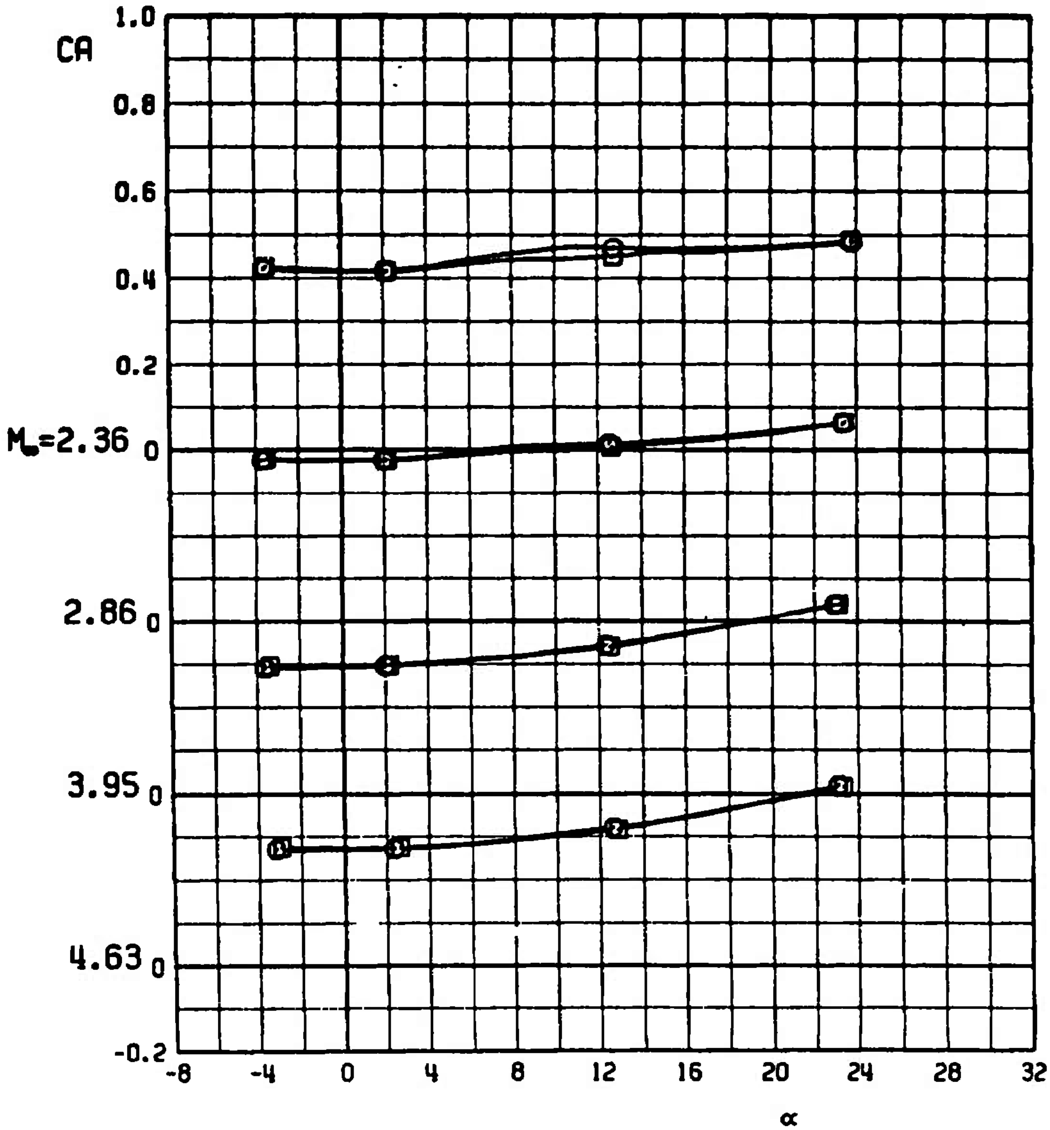

c. CA versus α
Figure 26. Continued.

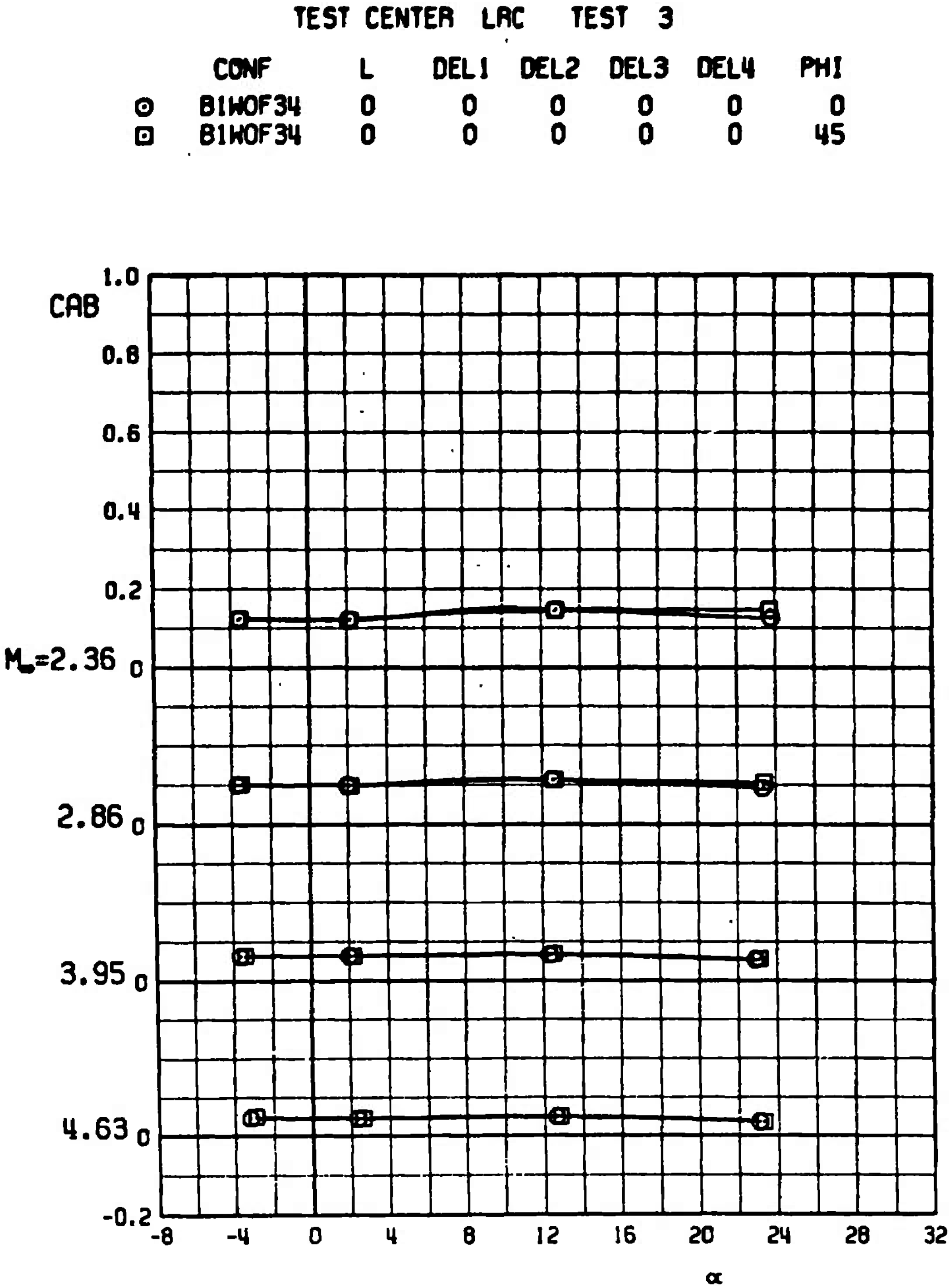

d. CAB versus α
Figure 26. Continued.

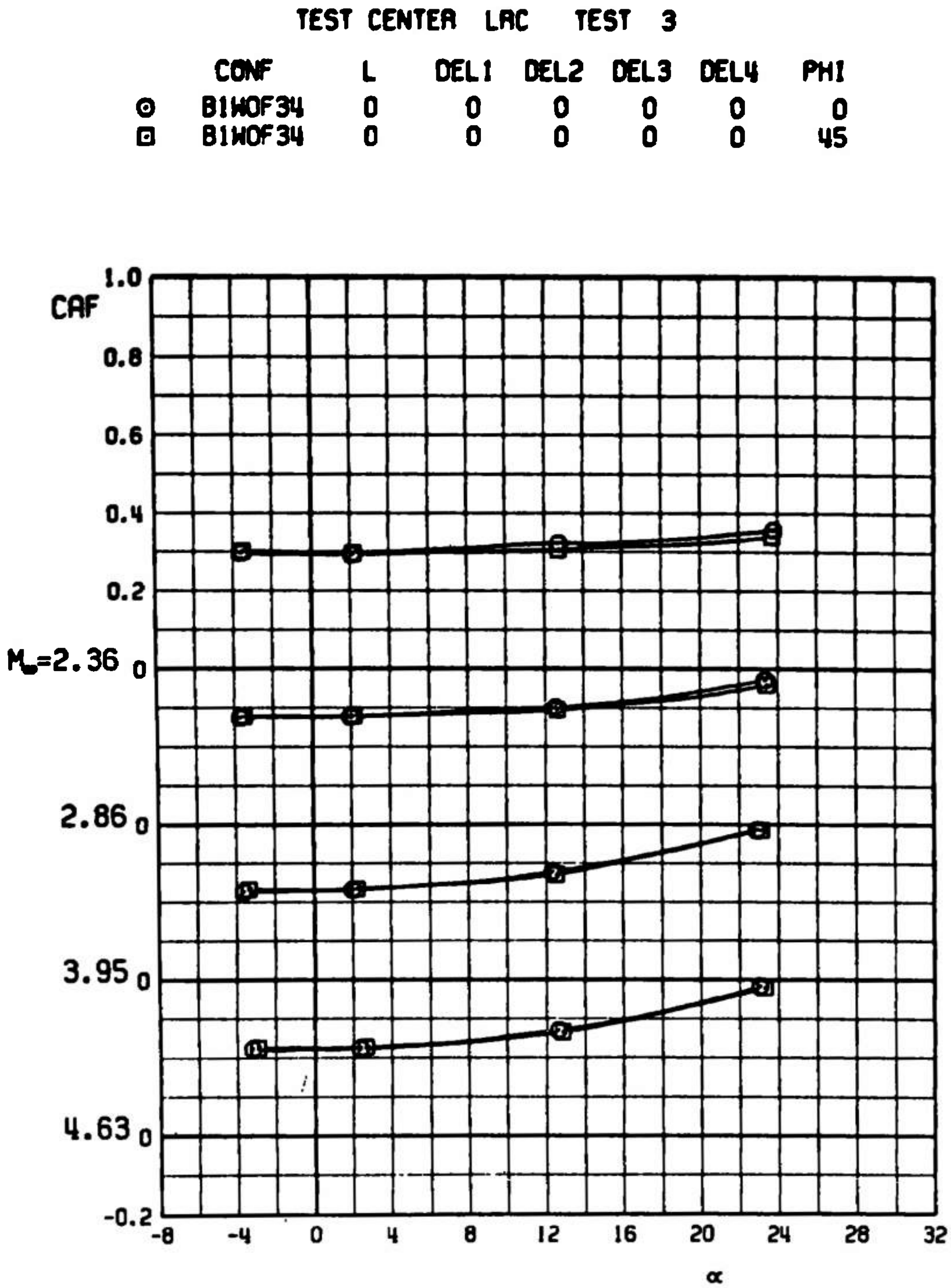

e. CAF versus α
Figure 26. Continued.

TEST CENTER LRC TEST 3

	CONF	L	DEL1	DEL2	DEL3	DEL4	PHI
⊙	B1W0F34	0	0	0	0	0	0
⊡	B1W0F34	0	0	0	0	0	45

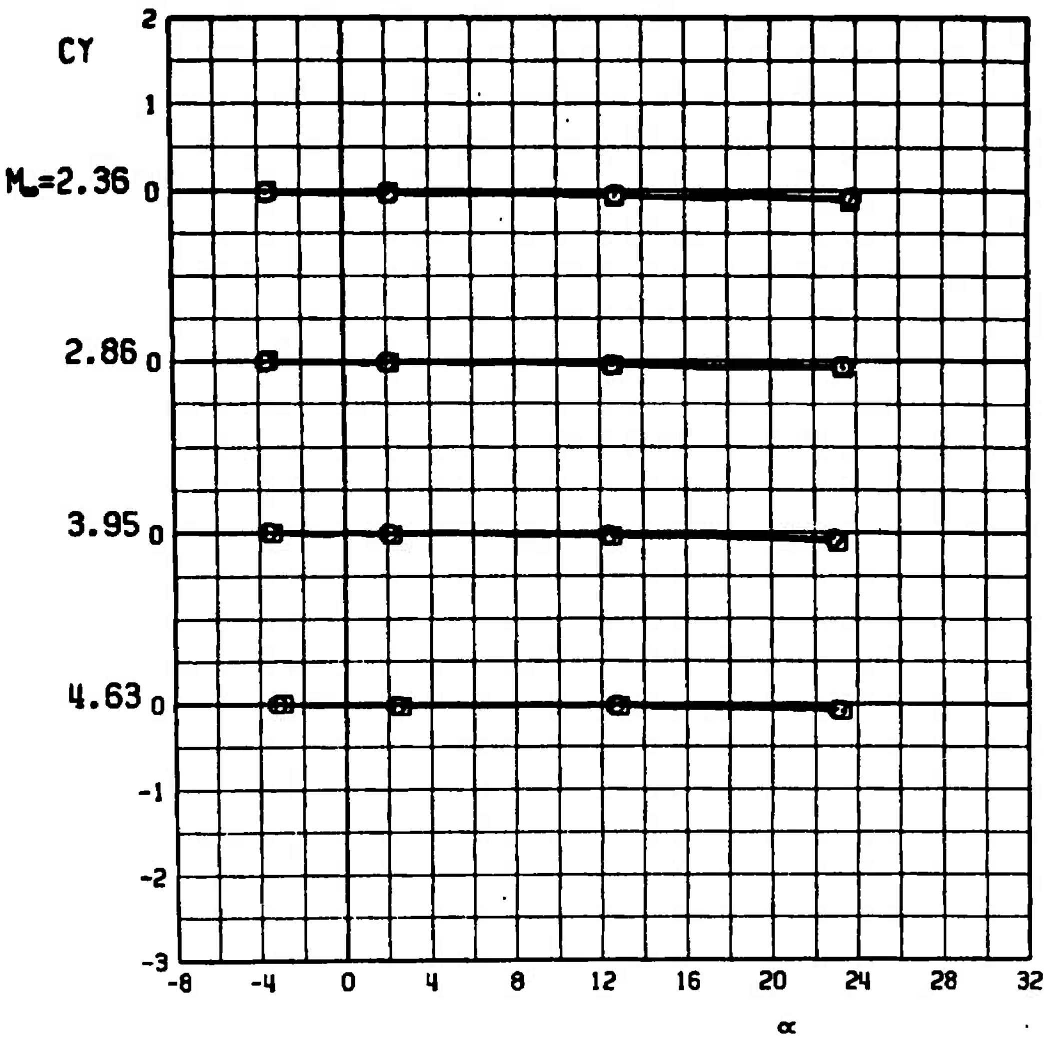

f. CY versus α
Figure 26. Continued.

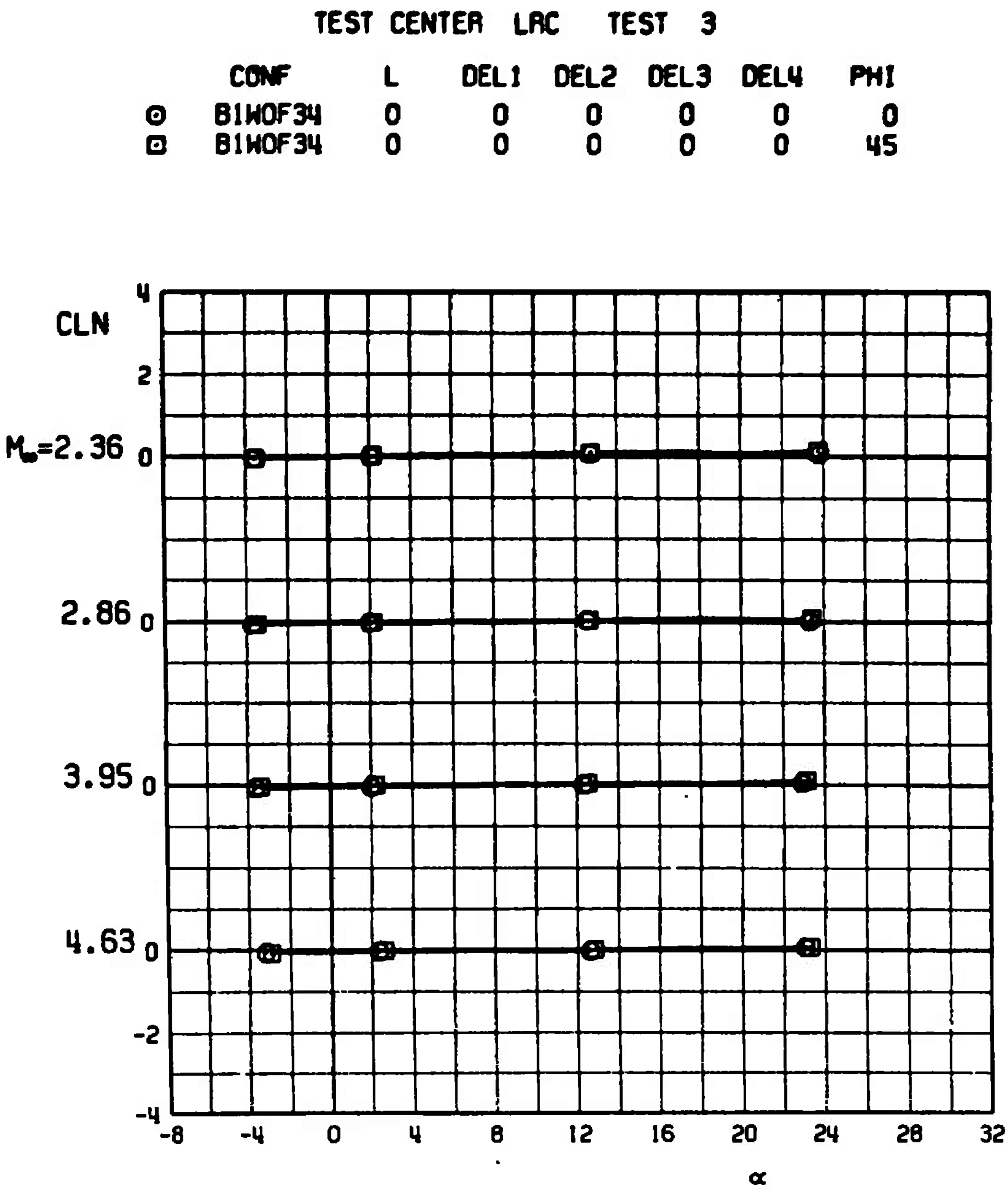

g. CLN versus α
Figure 26. Continued.

TEST CENTER LRC TEST 3

	CONF	L	DEL1	DEL2	DEL3	DEL4	PHI
⊙	B1W0F34	0	0	0	0	0	0
⊡	B1W0F34	0	0	0	0	0	45

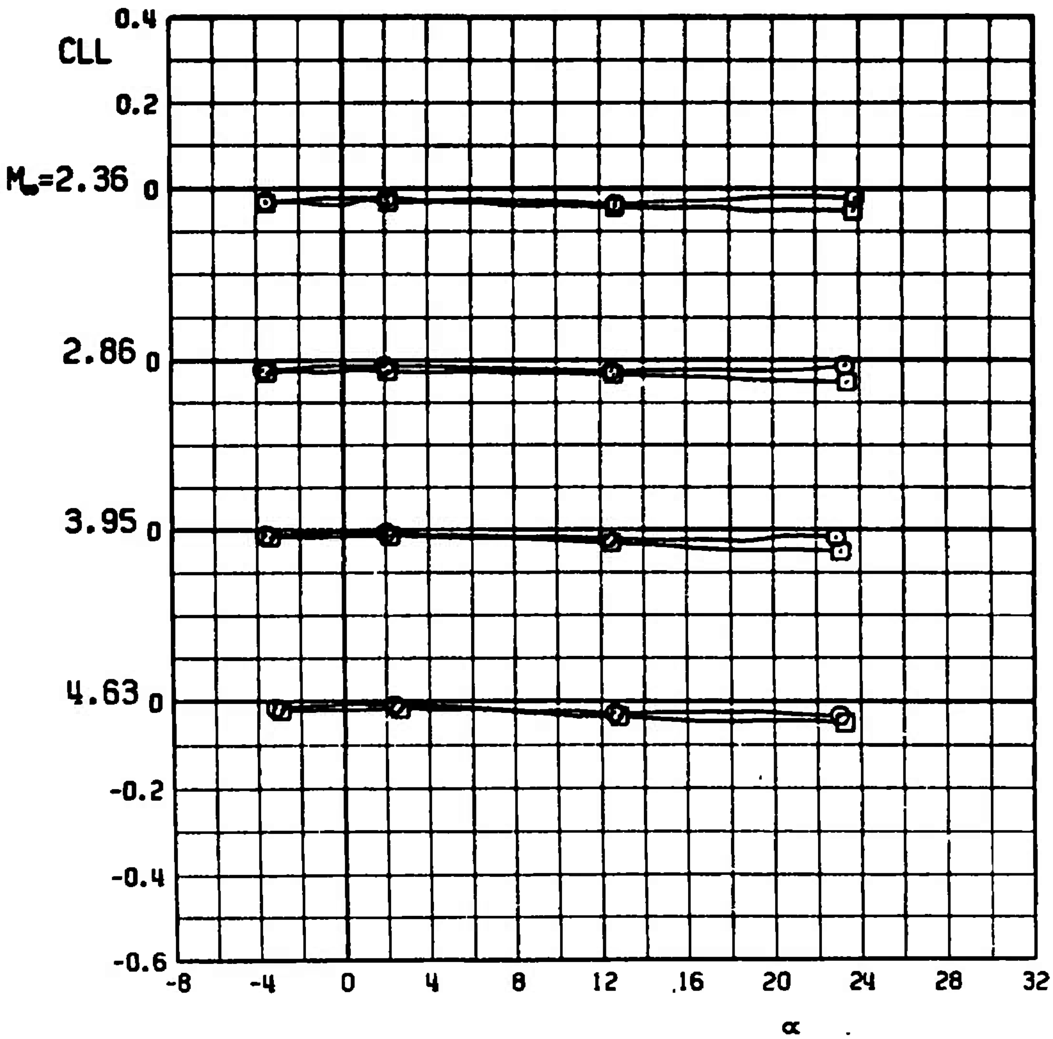

h. CLL versus α
Figure 26. Concluded.

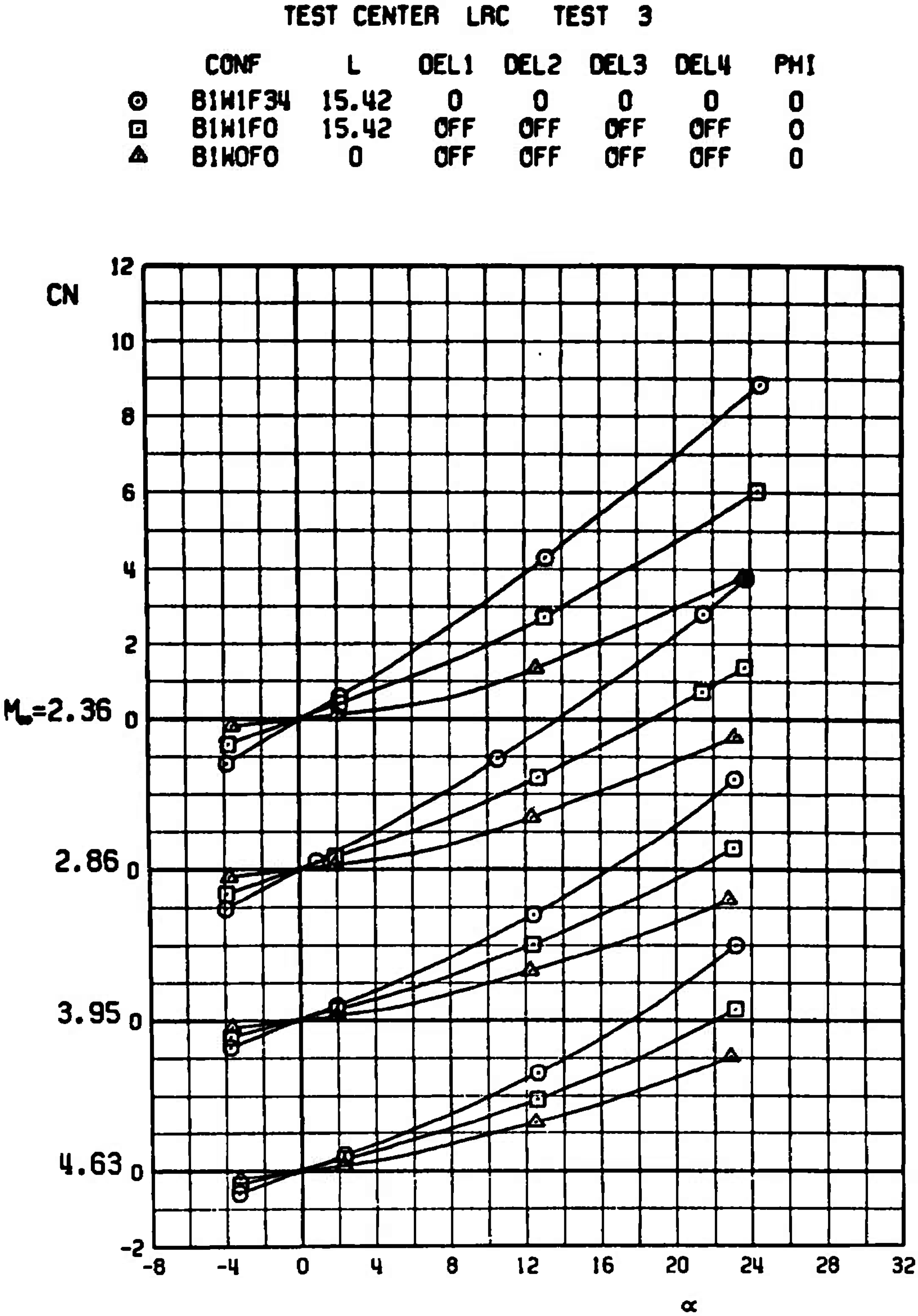

a. CN versus α

Figure 27. Test No. 3, comparison of aerodynamic coefficients of configurations B1W1F34, B1W1F0, and B1W0F0.

TEST CENTER LRC TEST 3

	CONF	L	DEL1	DEL2	DEL3	DEL4	PHI
⊙	B1W1F34	15.42	0	0	0	0	0
⊡	B1W1F0	15.42	OFF	OFF	OFF	OFF	0
▲	B1W0F0	0	OFF	OFF	OFF	OFF	0

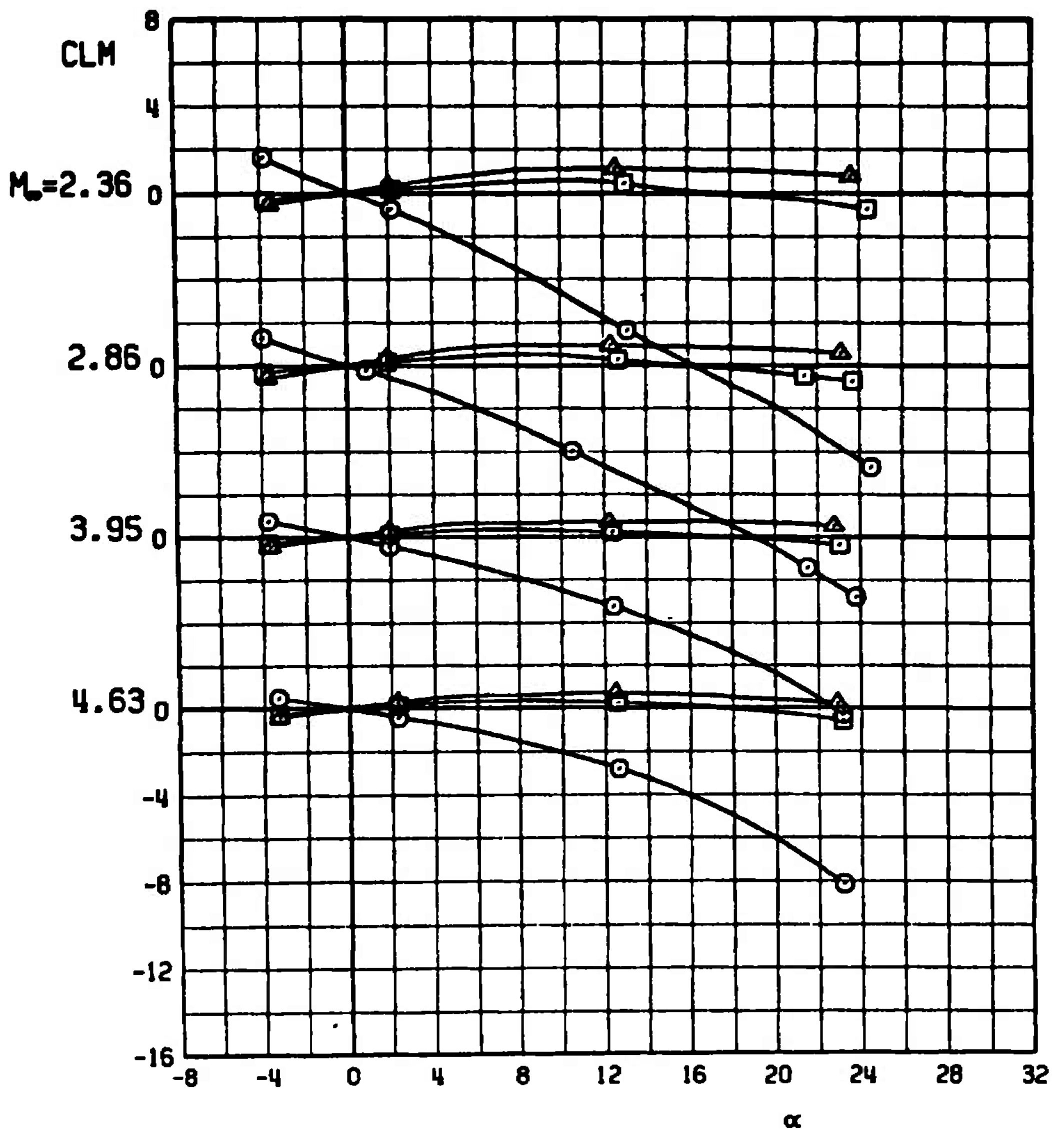

b. CLM versus α
Figure 27. Continued.

TEST CENTER LRC TEST 3

	CONF	L	DEL1	DEL2	DEL3	DEL4	PHI
⊙	B1W1F34	15.42	0	0	0	0	0
⊡	B1W1F0	15.42	OFF	OFF	OFF	OFF	0
△	B1W0F0	0	OFF	OFF	OFF	OFF	0

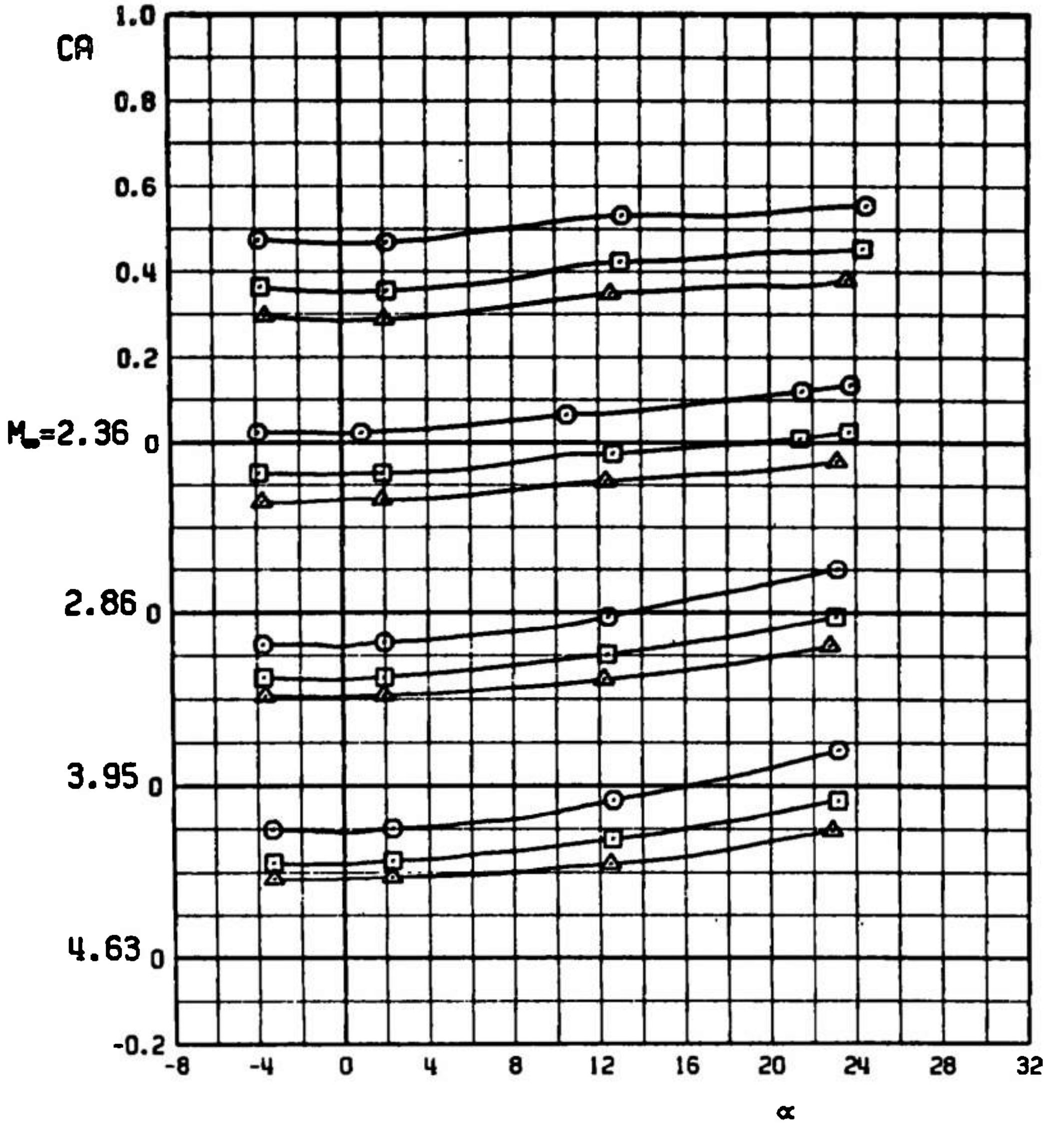

c. CA versus α

Figure 27. Continued.

TEST CENTER LRC TEST 3

	CONF	L	DEL1	DEL2	DEL3	DEL4	PHI
⊙	B1W1F34	15.42	0	0	0	0	0
⊡	B1W1F0	15.42	OFF	OFF	OFF	OFF	0
△	B1W0F0	0	OFF	OFF	OFF	OFF	0

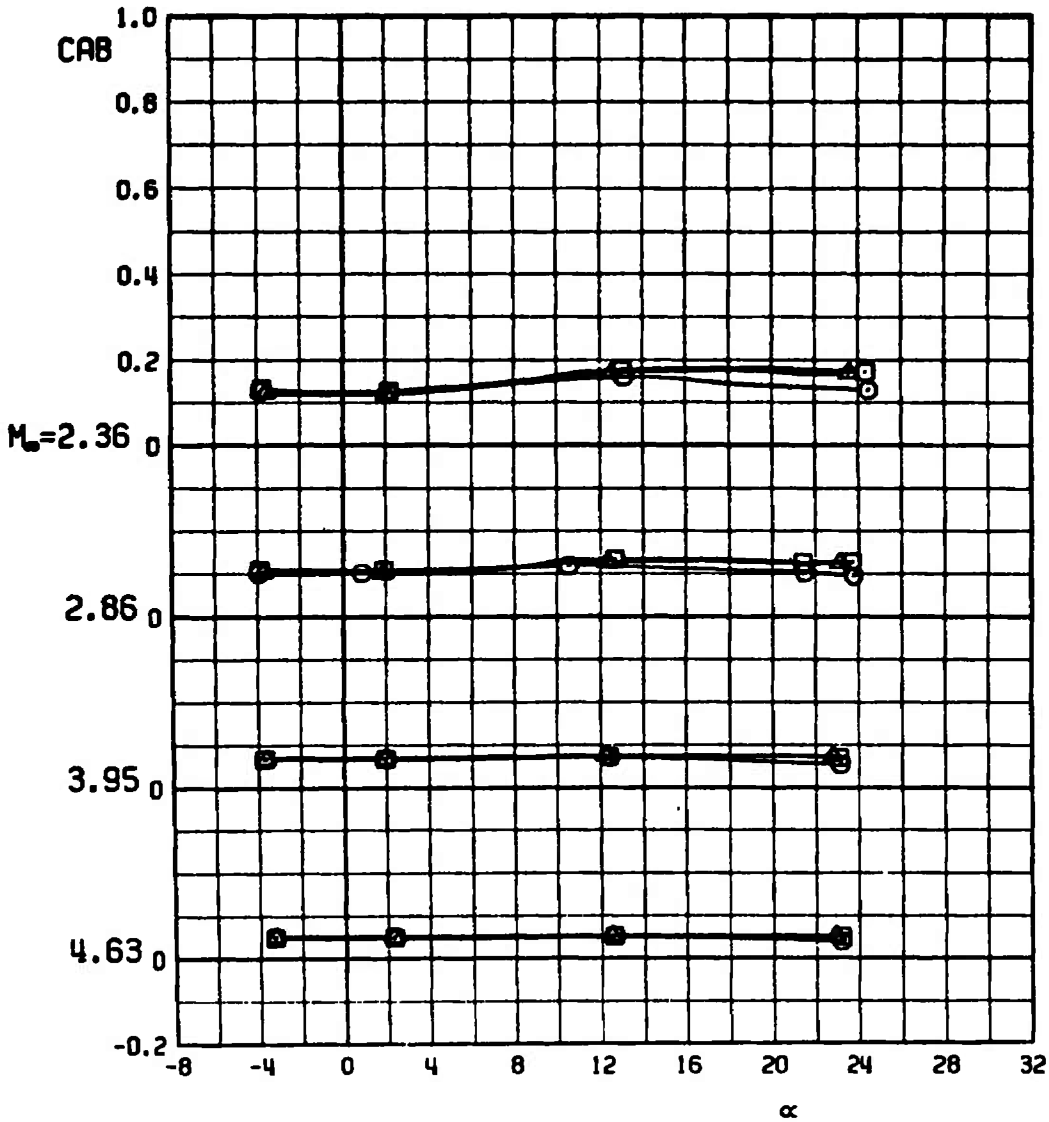

d. CAB versus α

Figure 27. Continued.

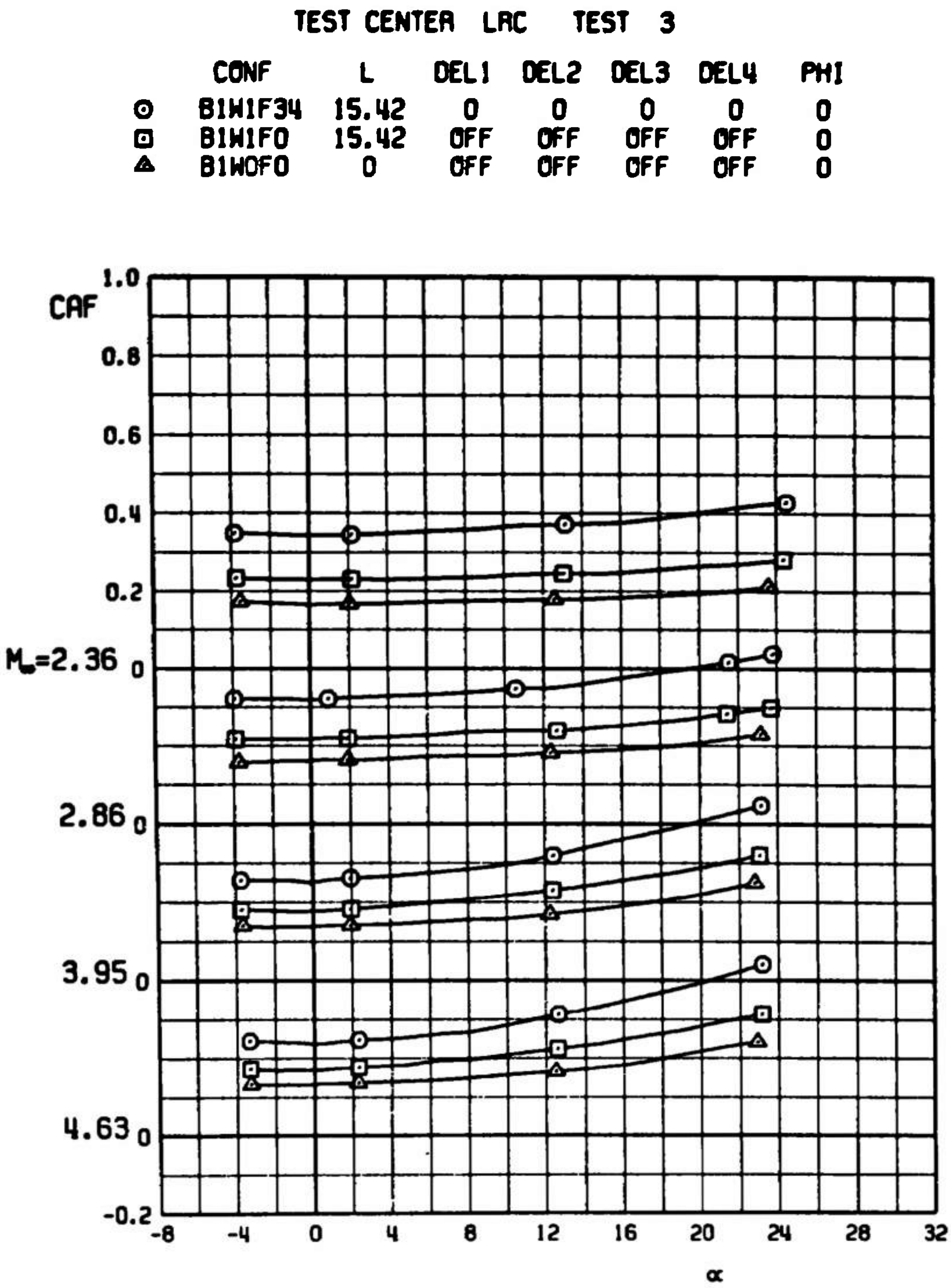

e. CAF versus α
Figure 27. Continued.

TEST CENTER LRC TEST 3

	CONF	L	DEL1	DEL2	DEL3	DEL4	PHI
⊙	B1W1F34	15.42	0	0	0	0	0
⊡	B1W1F0	15.42	OFF	OFF	OFF	OFF	0
▲	B1W0F0	0	OFF	OFF	OFF	OFF	0

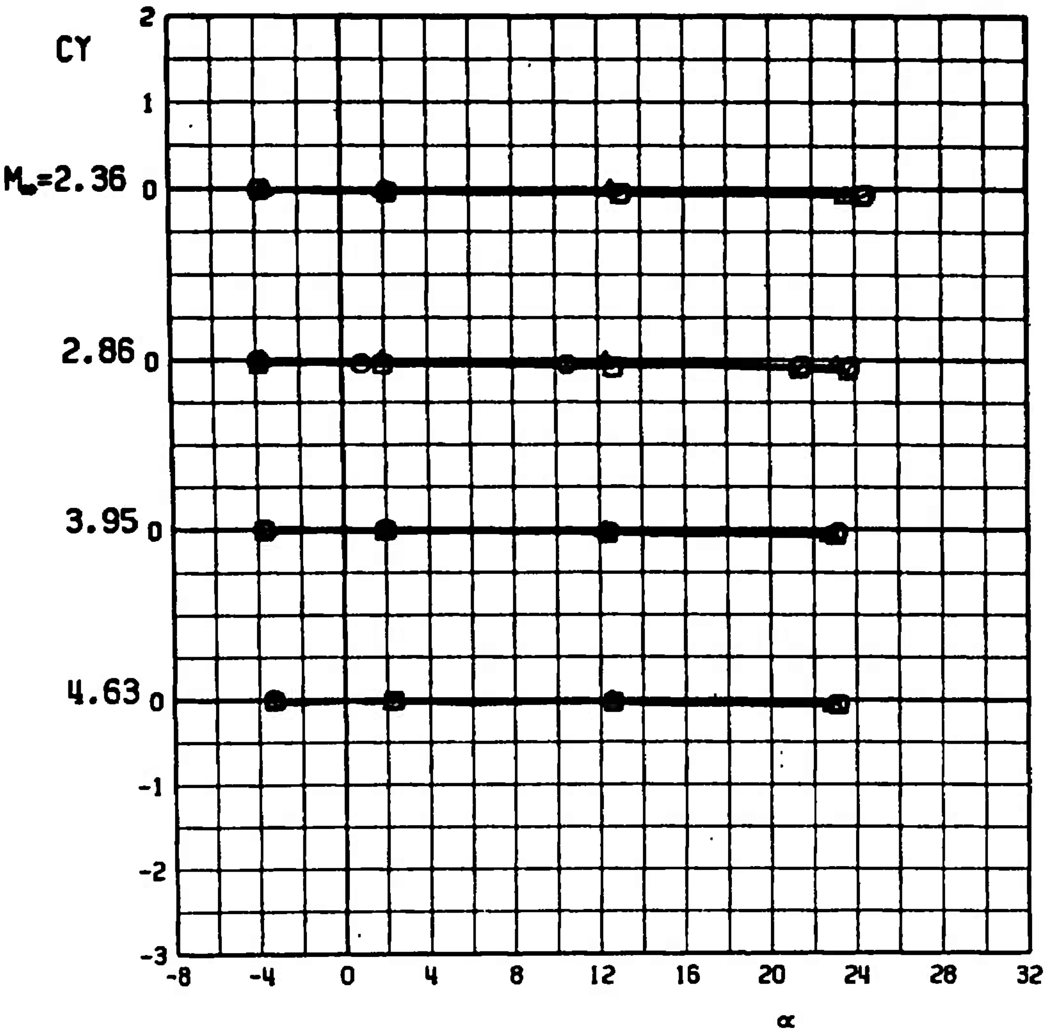

f. CY versus α
Figure 27. Continued.

TEST CENTER LRC TEST 3

	CONF	L	DEL1	DEL2	DEL3	DEL4	PHI
⊙	B1W1F34	15.42	0	0	0	0	0
⊡	B1W1F0	15.42	OFF	OFF	OFF	OFF	0
⚠	B1W0F0	0	OFF	OFF	OFF	OFF	0

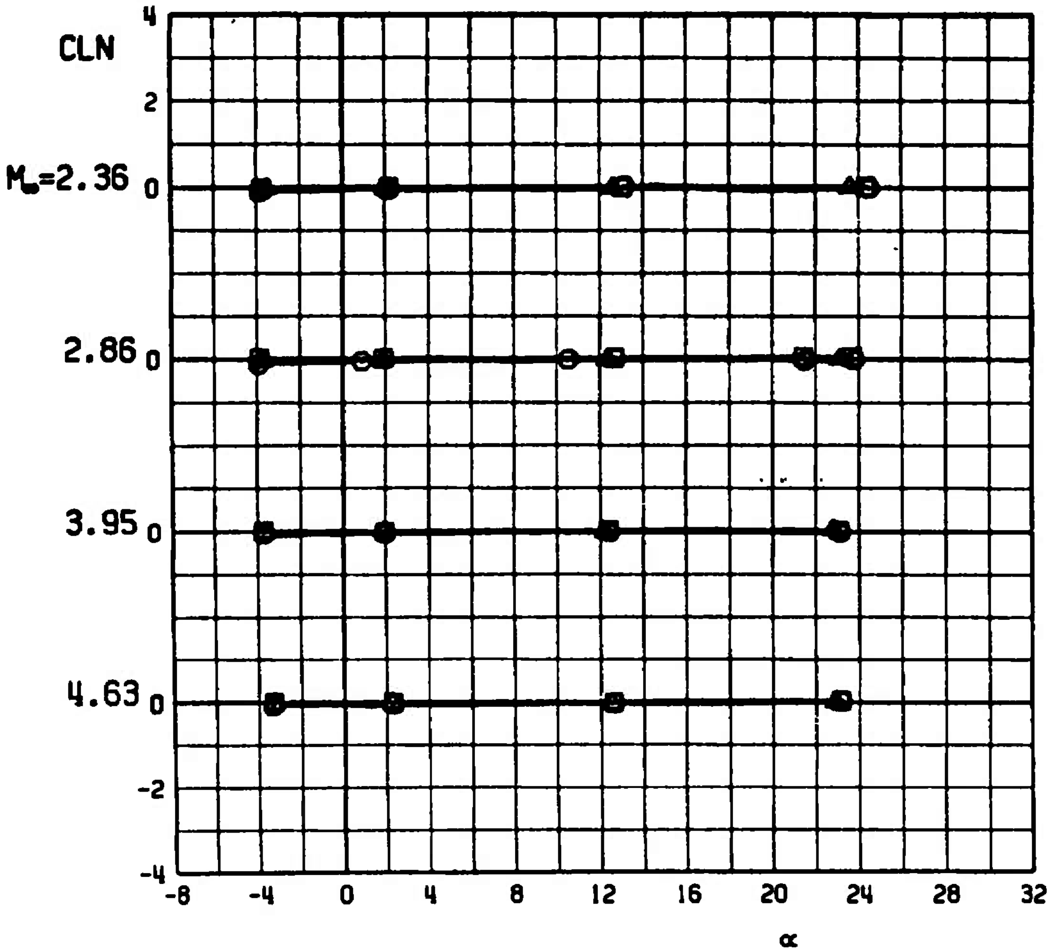

g. CLN versus α
Figure 27. Continued.

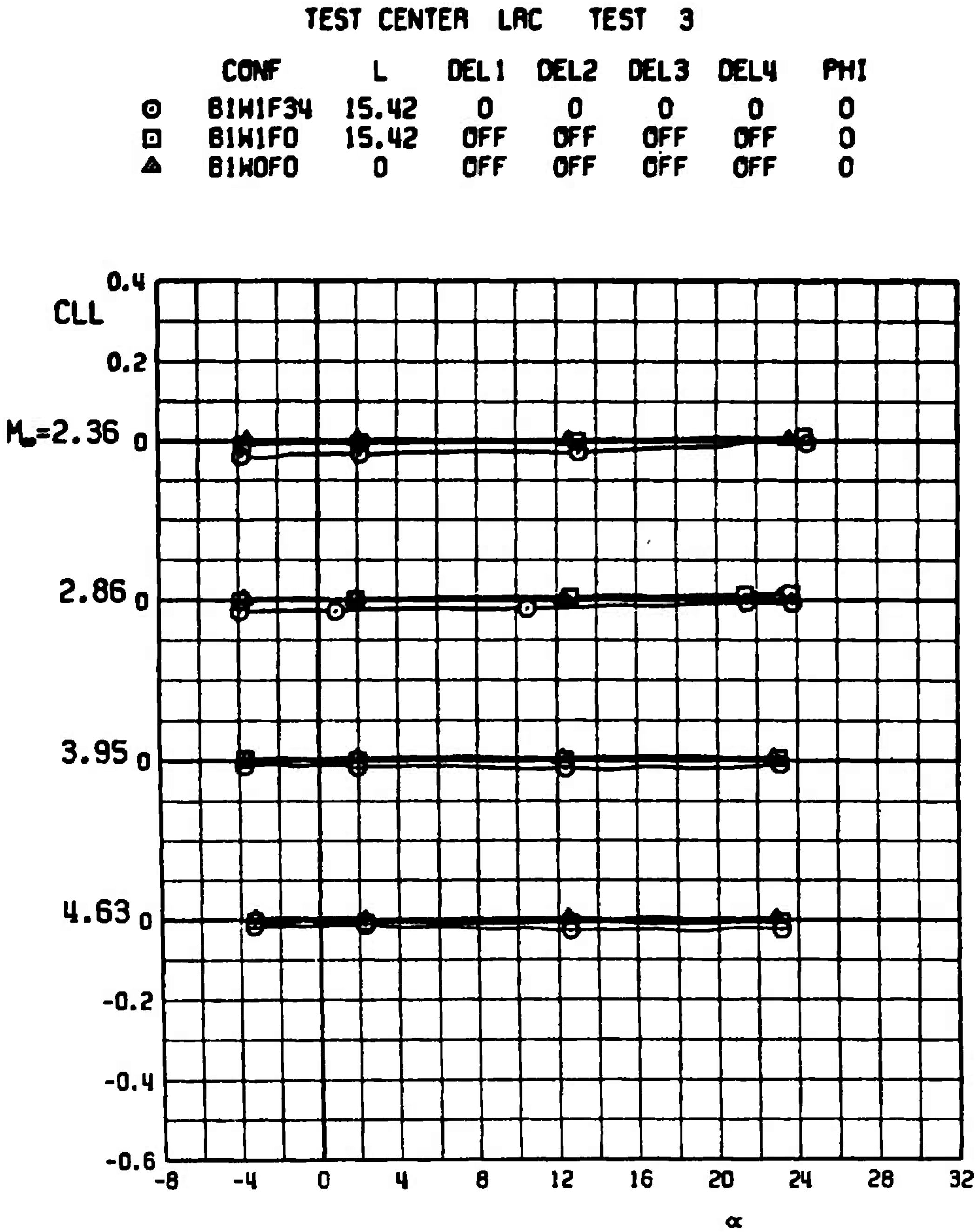

h. CLL versus α
Figure 27. Concluded.

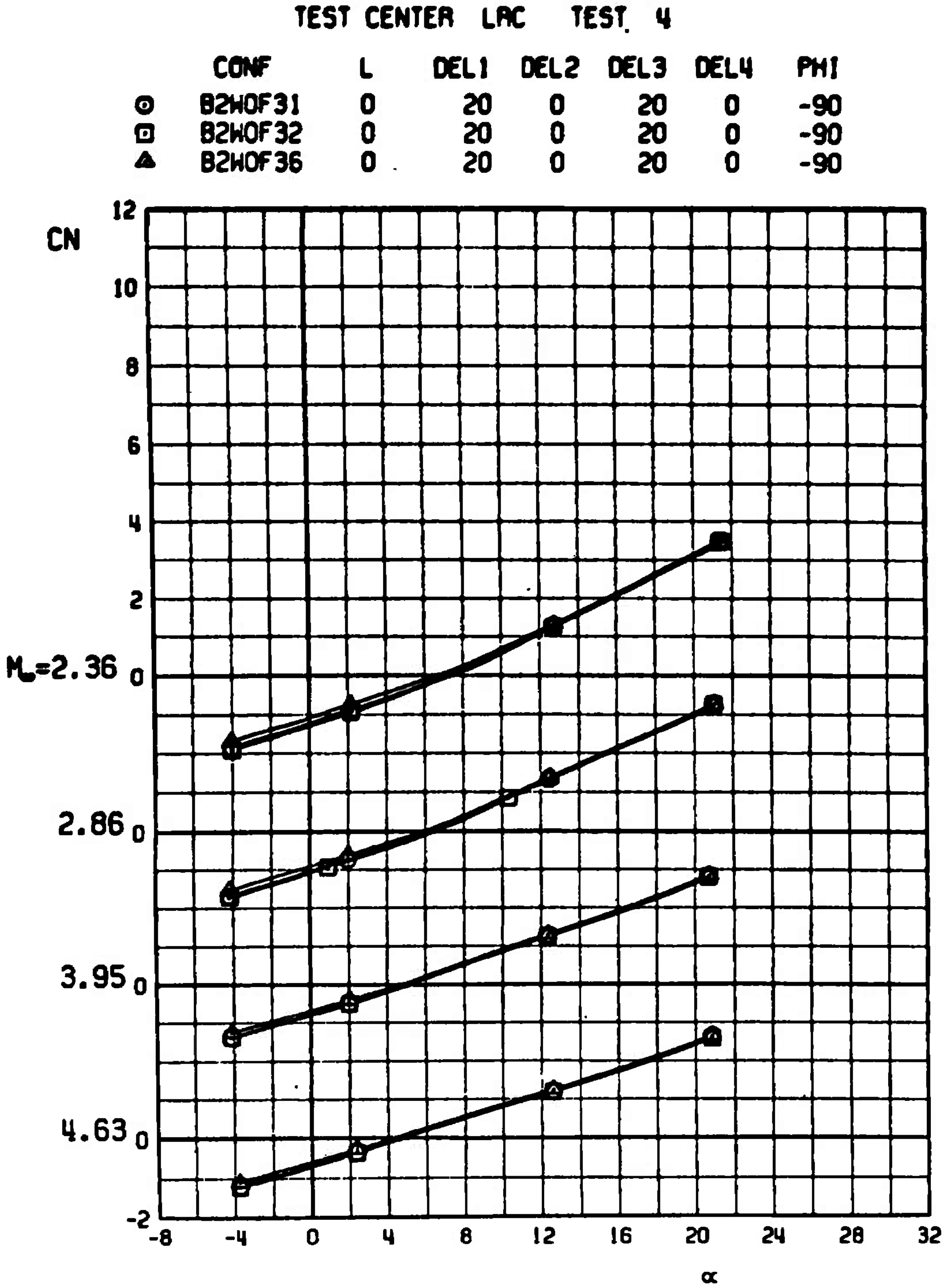

a. CN versus α

Figure 28. Test No. 4, comparison of aerodynamic coefficients of configurations B2W0F31, B2W0F32, and B2W0F36 at a model roll angle of -90 deg and deflections for fins No. 1 and 3 of 20 deg and fins No. 2 and 4 of 0 deg.

TEST CENTER LRC TEST 4

	CONF	L	DEL1	DEL2	DEL3	DEL4	PHI
⊙	B2W0F31	0	20	0	20	0	-90
⊡	B2W0F32	0	20	0	20	0	-90
△	B2W0F36	0	20	0	20	0	-90

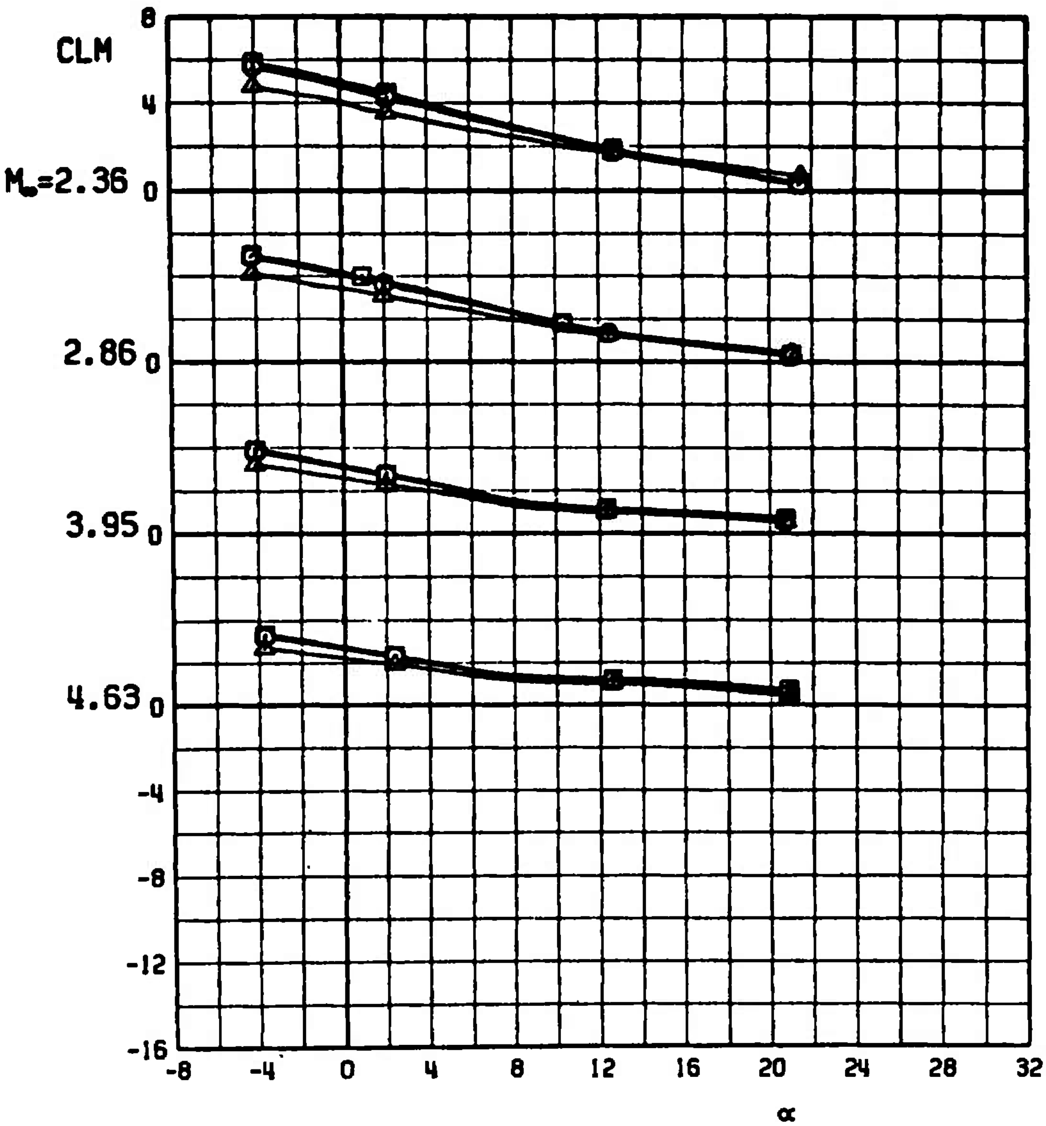

b. CLM versus α
Figure 28. Continued.

TEST CENTER LRC TEST 4

	CONF	L	DEL1	DEL2	DEL3	DEL4	PHI
⊙	B2W0F31	0	20	0	20	0	-90
⊡	B2W0F32	0	20	0	20	0	-90
△	B2W0F36	0	20	0	20	0	-90

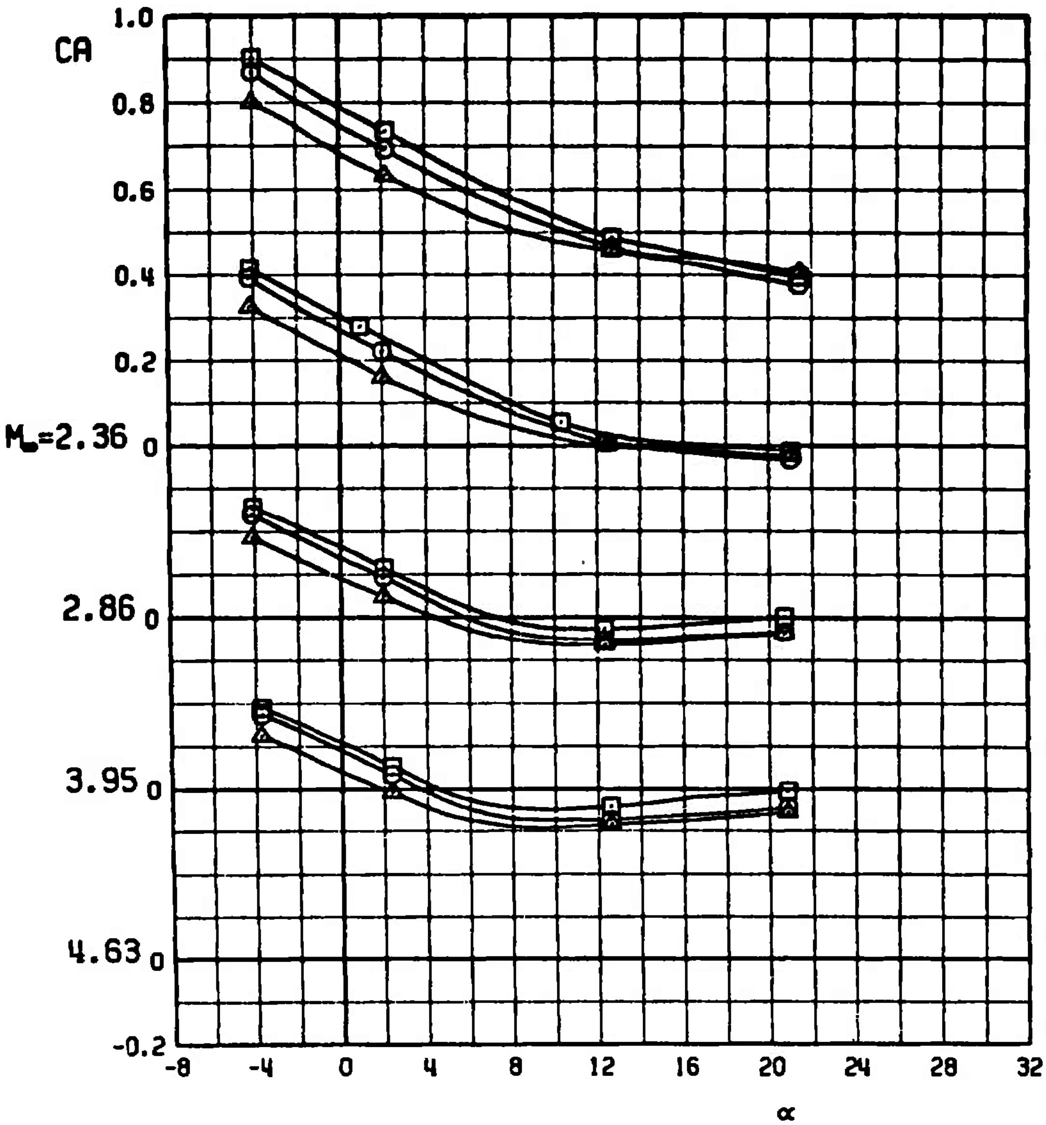

c. CA versus α

Figure 28. Continued.

TEST CENTER LRC TEST 4

	CONF	L	DEL1	DEL2	DEL3	DEL4	PHI
⊙	B2W0F31	0	20	0	20	0	-90
⊡	B2W0F32	0	20	0	20	0	-90
△	B2W0F36	0	20	0	20	0	-90

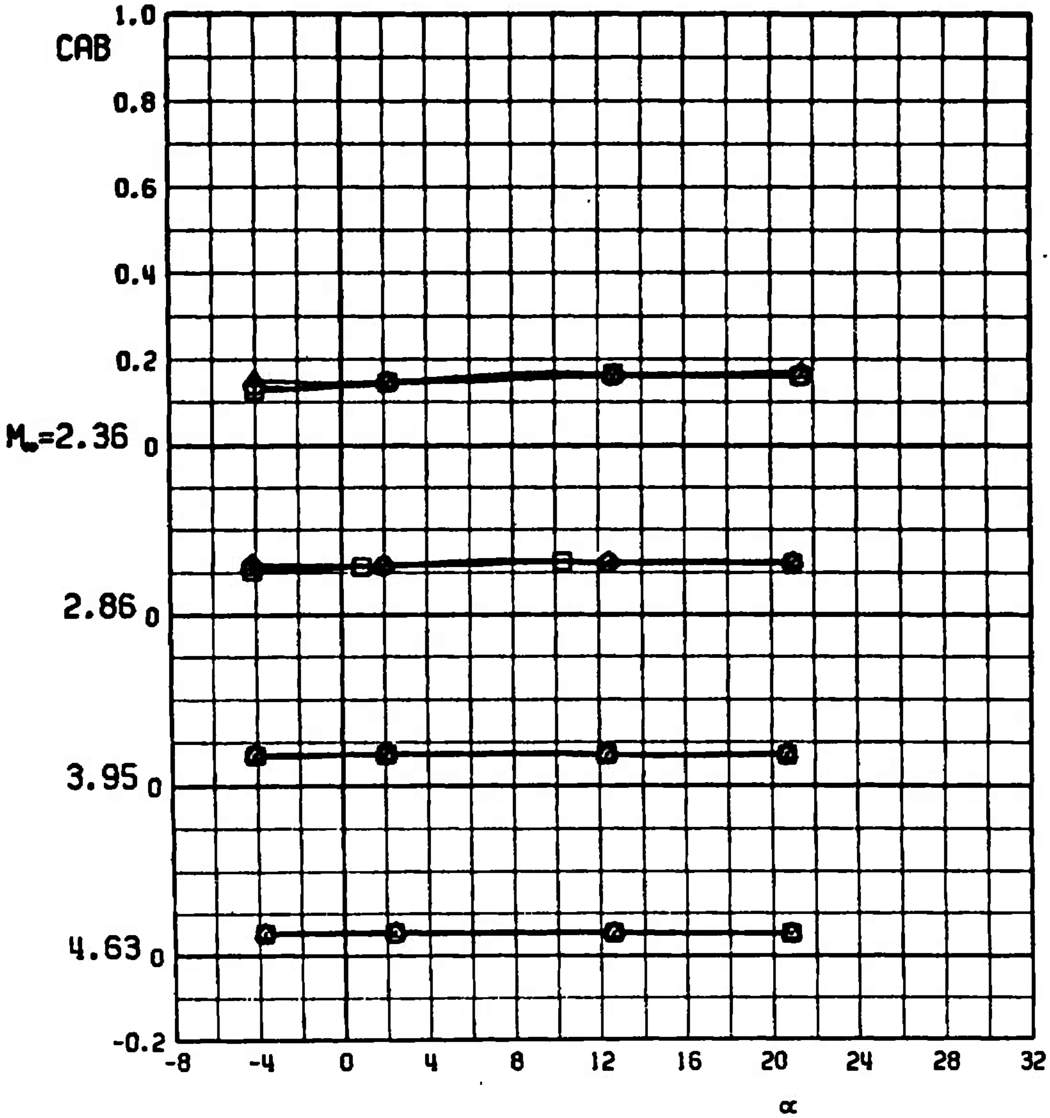

d. CAB versus a
Figure 28. Continued.

TEST CENTER LRC TEST 4

	CONF	L	DEL1	DEL2	DEL3	DEL4	PHI
⊙	B2WOF31	0	20	0	20	0	-90
⊡	B2WOF32	0	20	0	20	0	-90
△	B2WOF36	0	20	0	20	0	-90

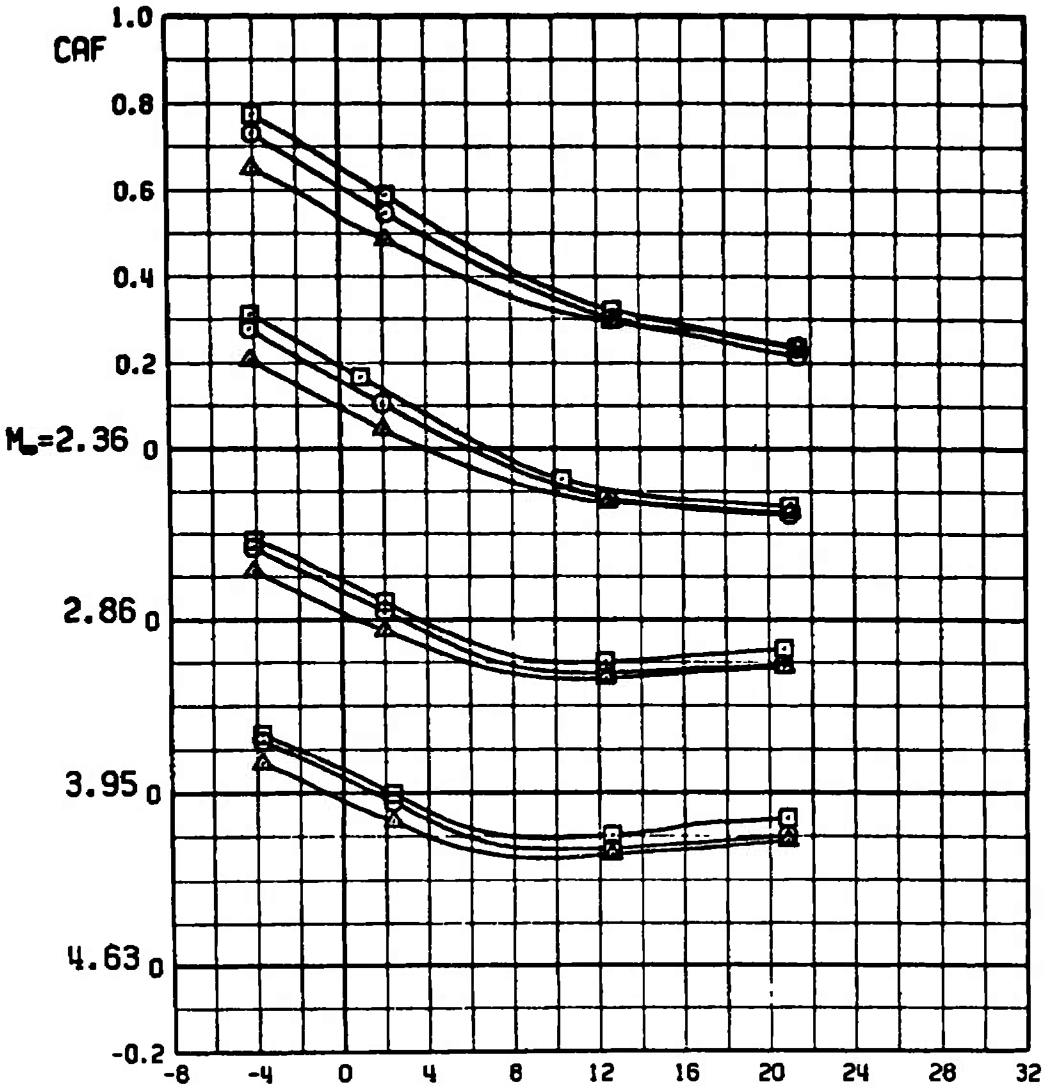

e. CAF versus α
Figure 28. Continued.

TEST CENTER LRC TEST 4

	CONF	L	DEL1	DEL2	DEL3	DEL4	PHI
⊙	B2W0F31	0	20	0	20	0	-90
⊡	B2W0F32	0	20	0	20	0	-90
▲	B2W0F36	0	20	0	20	0	-90

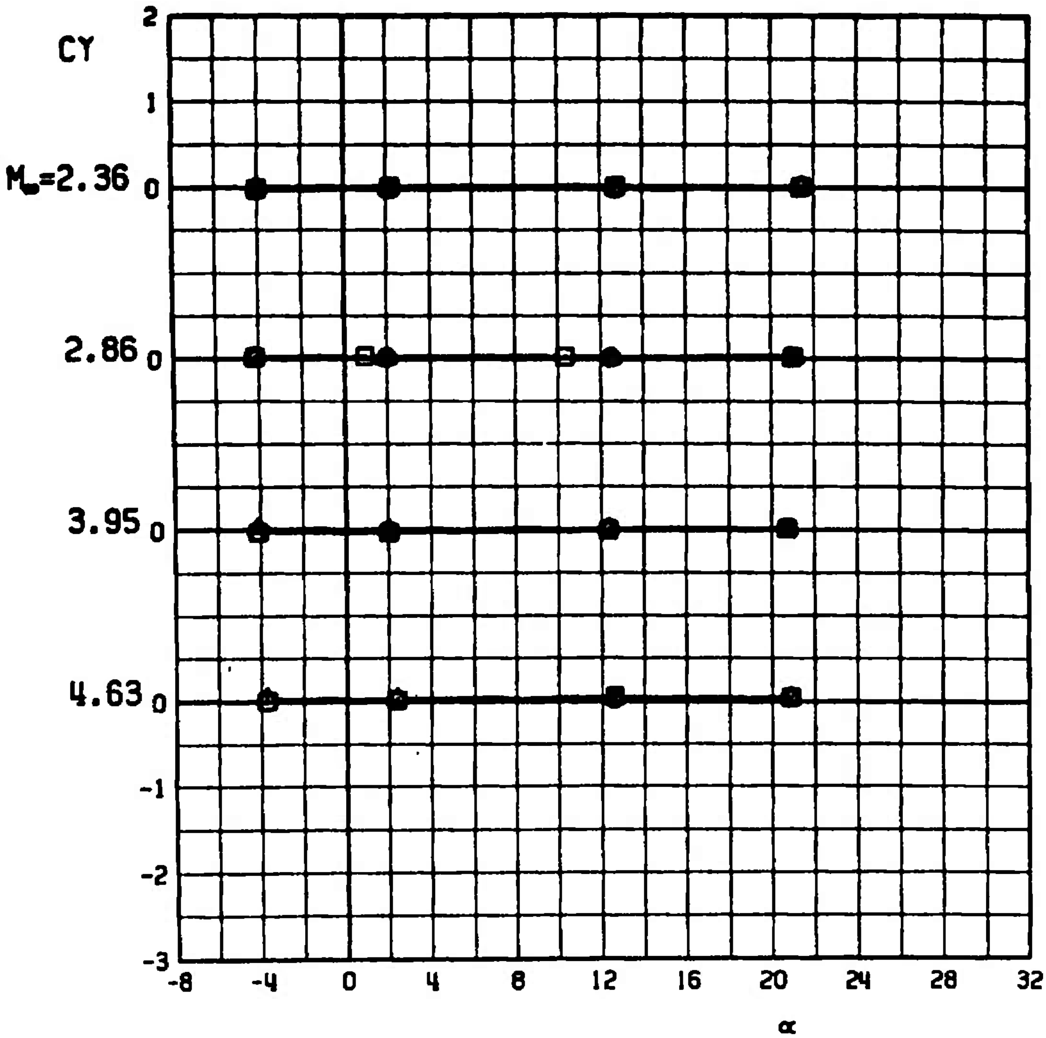

f. CY versus α
Figure 28. Continued.

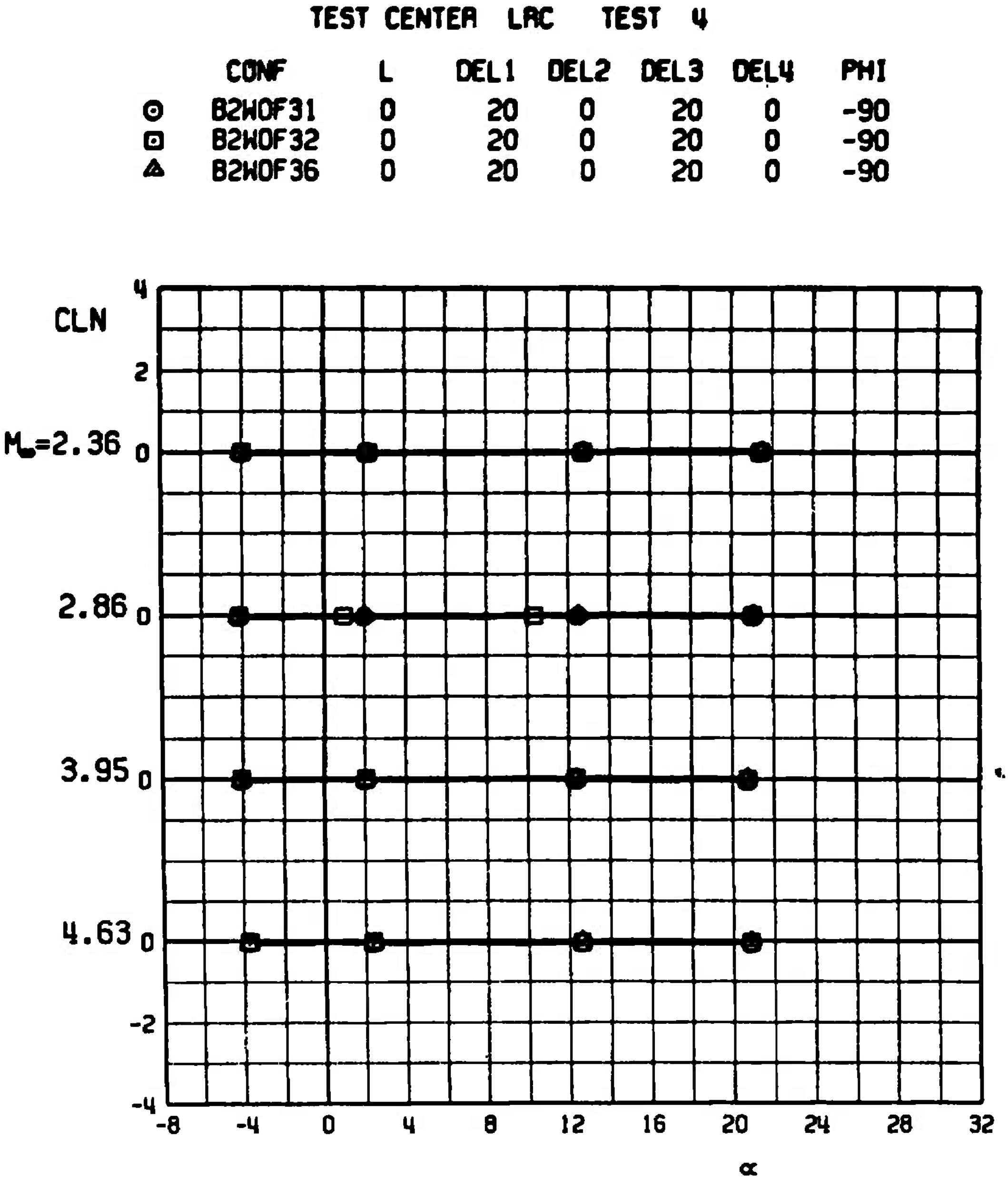

g. CLN versus α
Figure 28. Continued.

TEST CENTER LRC TEST 4

	CONF	L	DEL1	DEL2	DEL3	DEL4	PHI
⊙	B2W0F31	0	20	0	20	0	-90
⊡	B2W0F32	0	20	0	20	0	-90
△	B2W0F36	0	20	0	20	0	-90

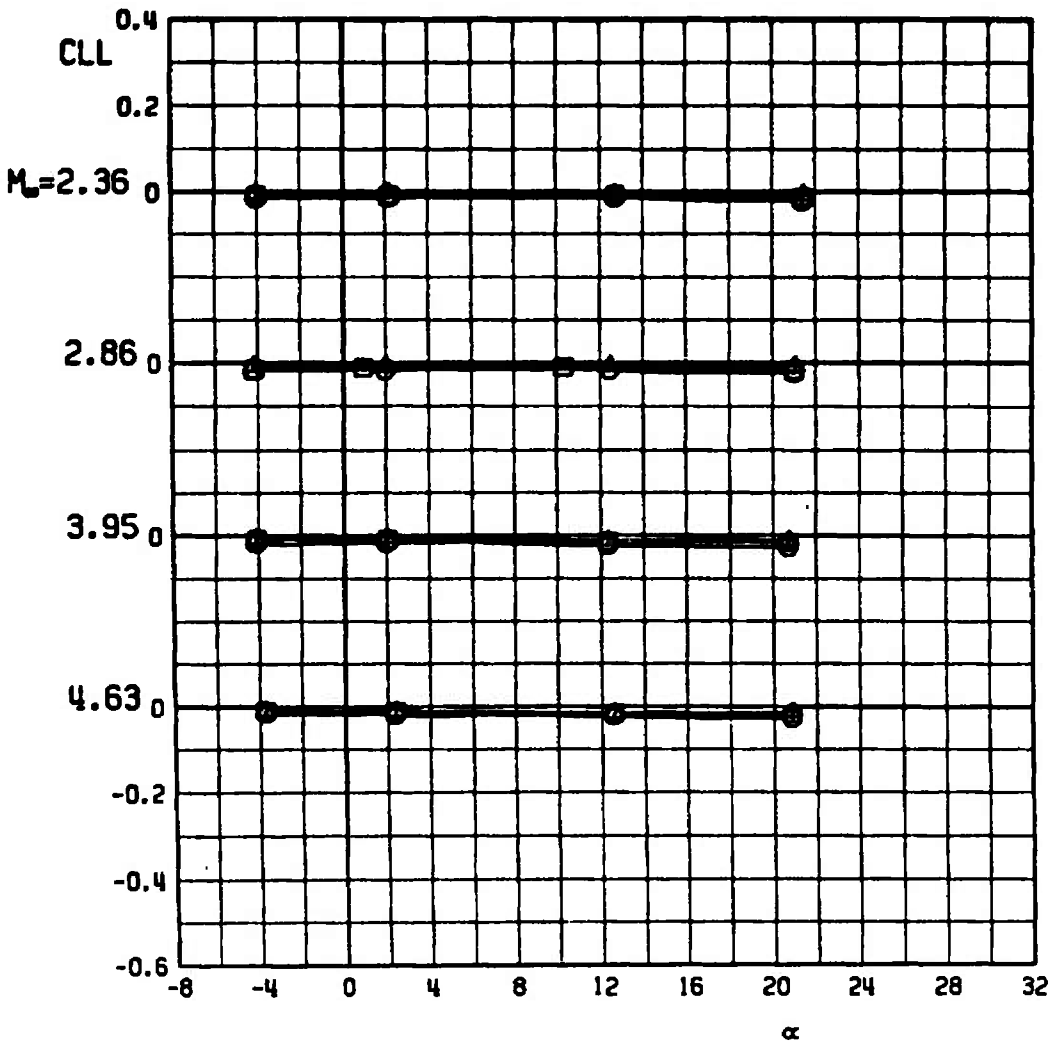

h. CLL versus α
Figure 28. Concluded.

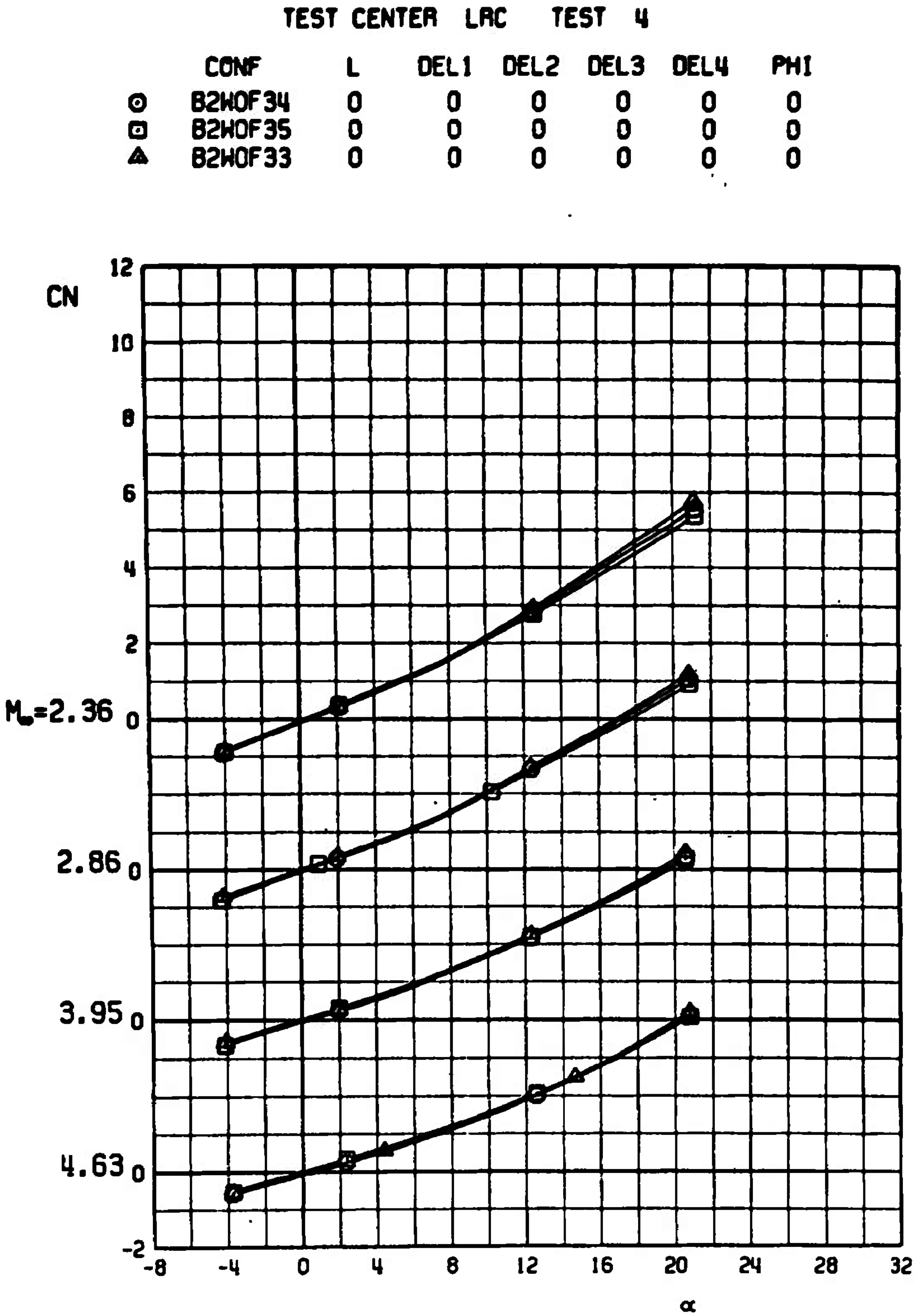

a. CN versus α

Figure 29. Test No. 4, comparison of aerodynamic coefficients of configurations B2W0F34, B2W0F35, and B2W0F33.

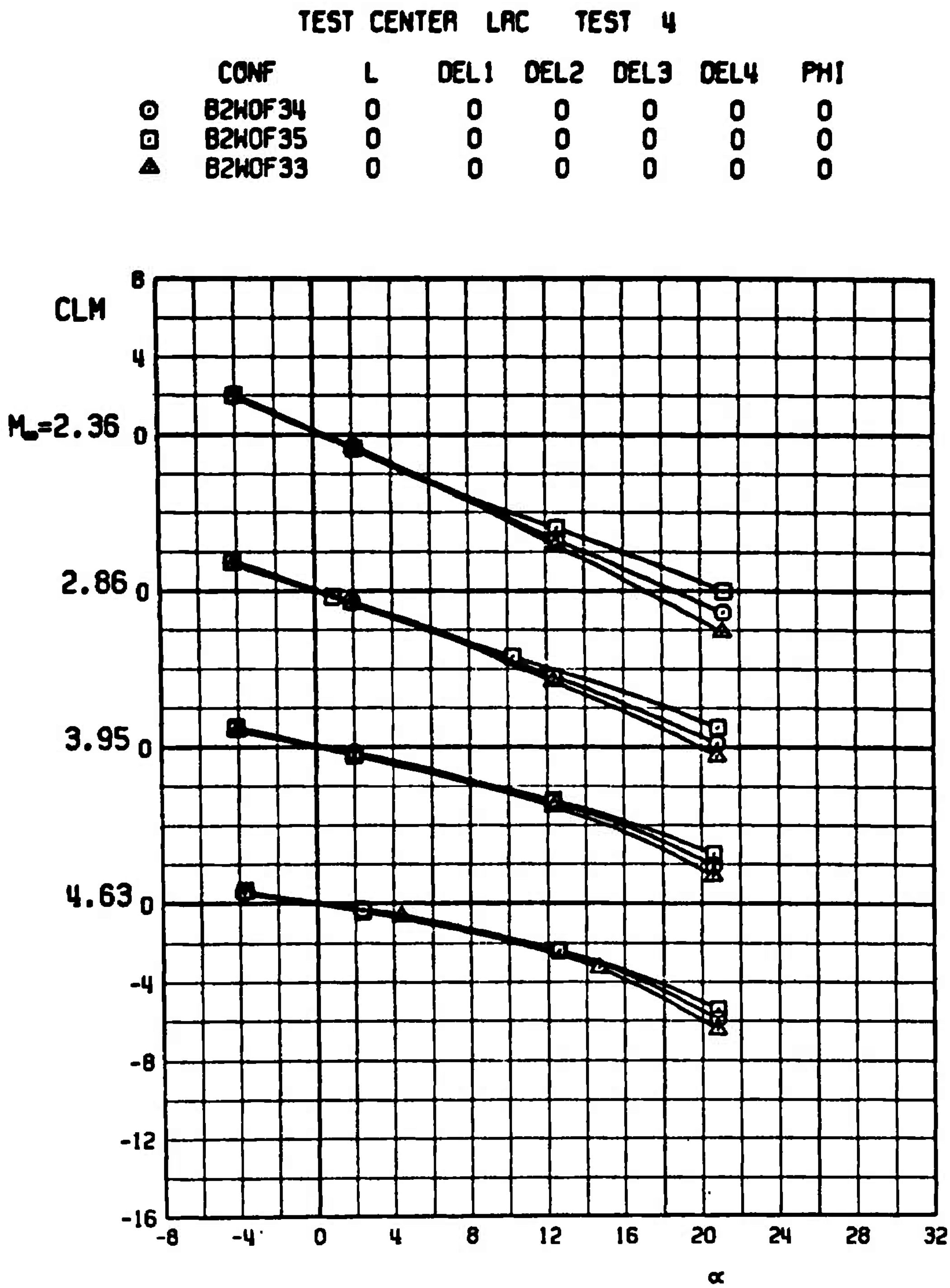

b. CLM versus α
Figure 29. Continued.

TEST CENTER LRC TEST 4

	CONF	L	DEL1	DEL2	DEL3	DEL4	PHI
⊙	B2WOF34	0	0	0	0	0	0
⊡	B2WOF35	0	0	0	0	0	0
▲	B2WOF33	0	0	0	0	0	0

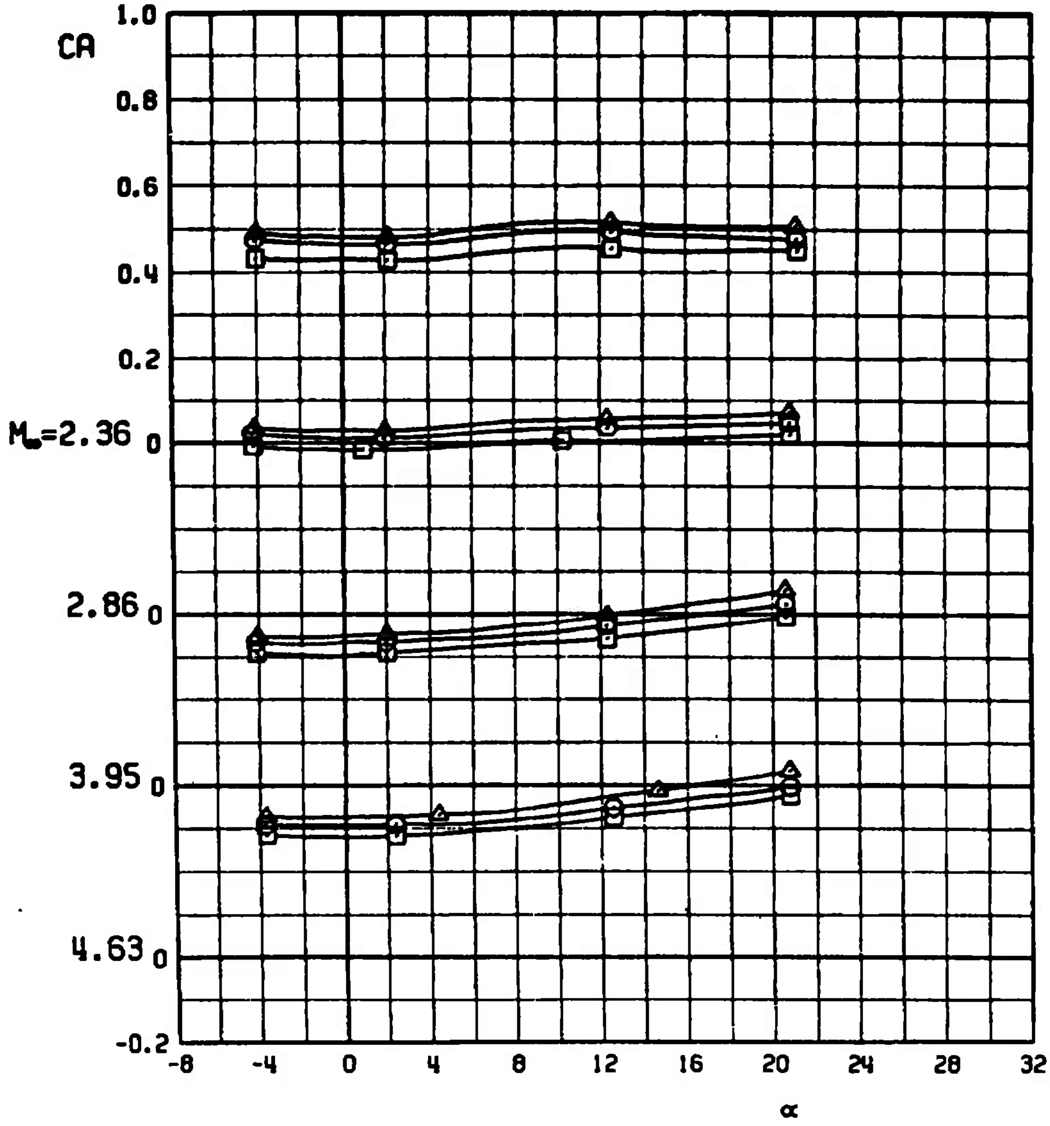

c. CA versus α
Figure 29. Continued.

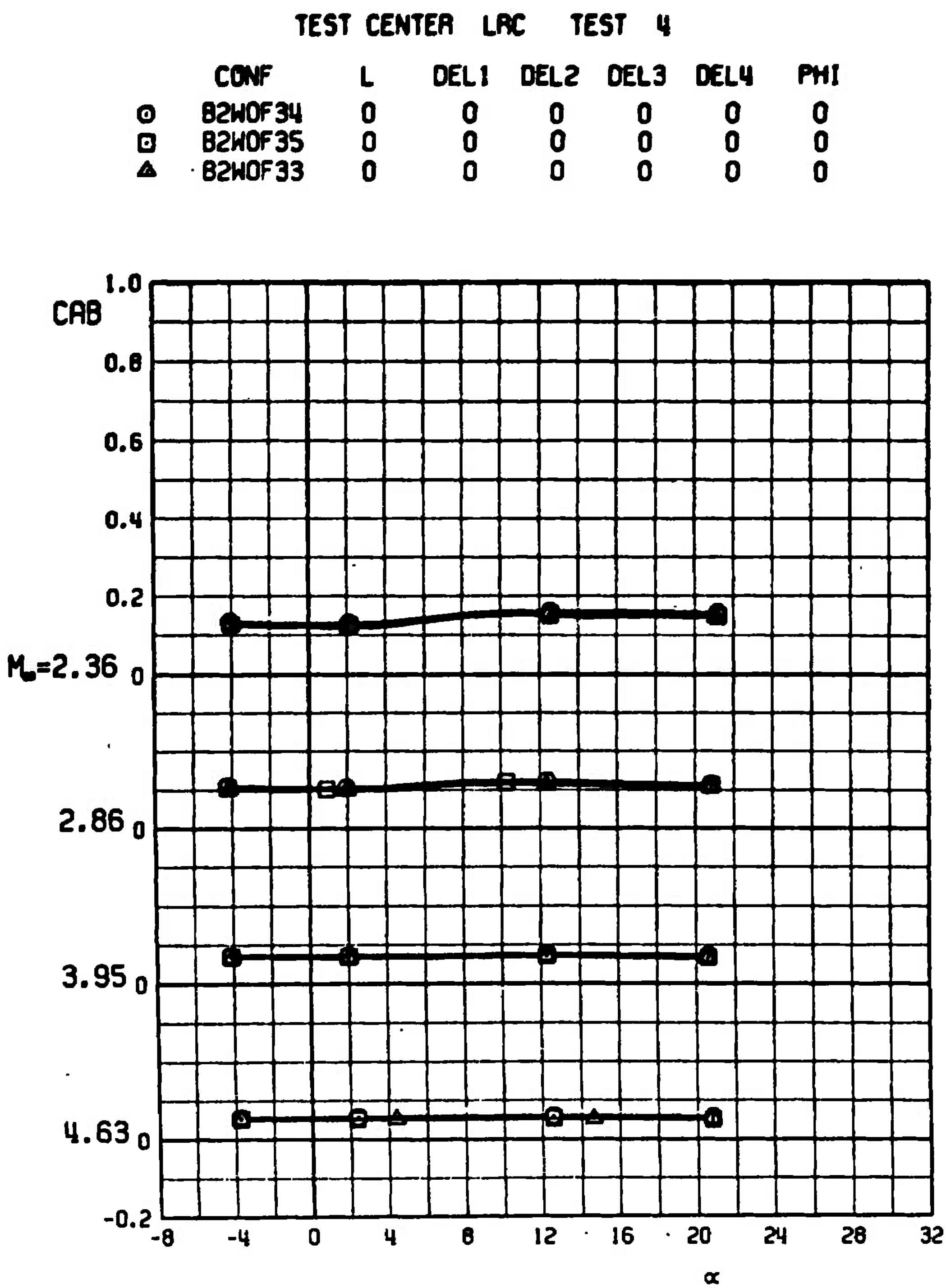

d. CAB versus α

Figure 29. Continued.

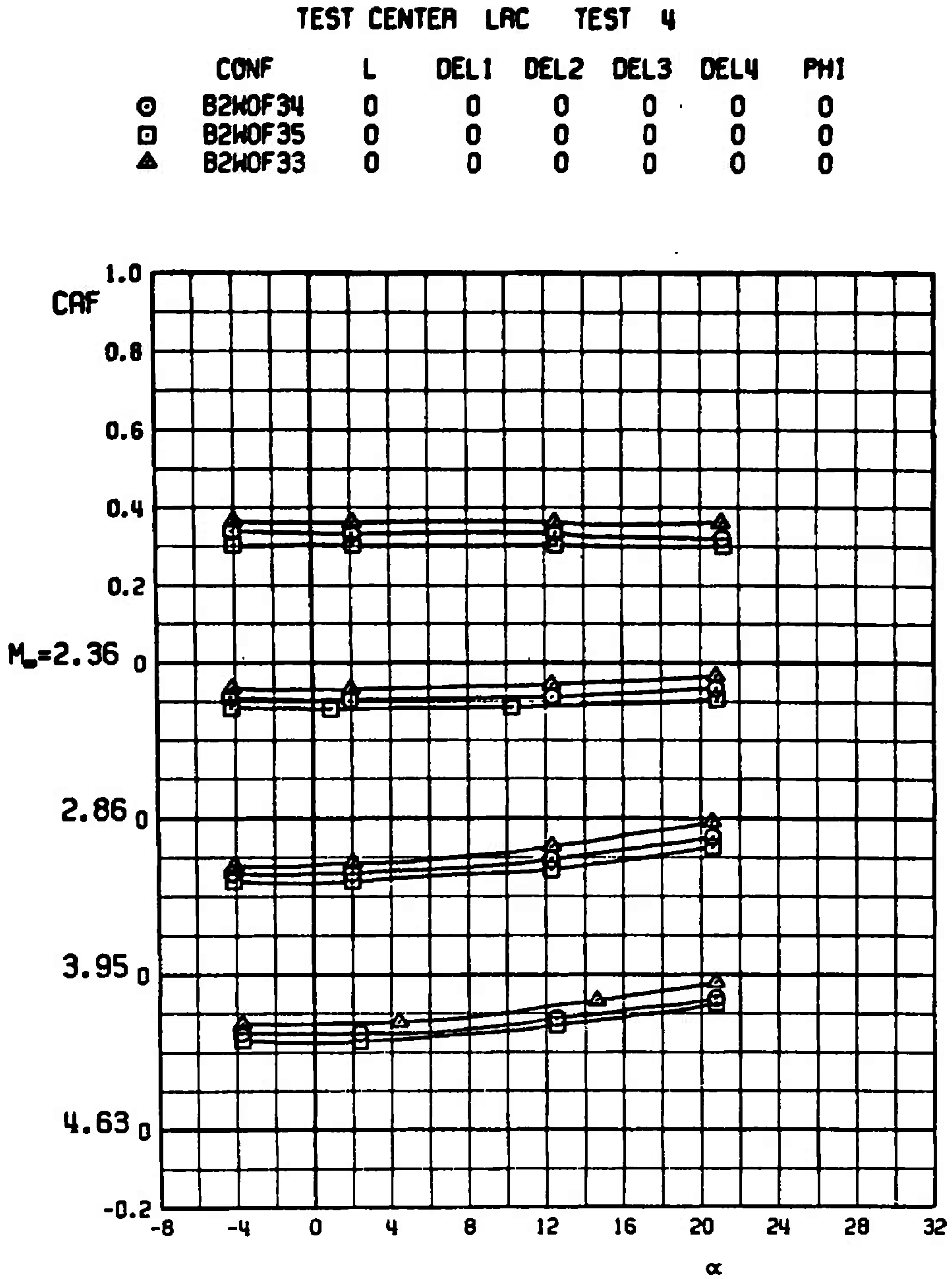

e. CAF versus α
Figure 29. Continued.

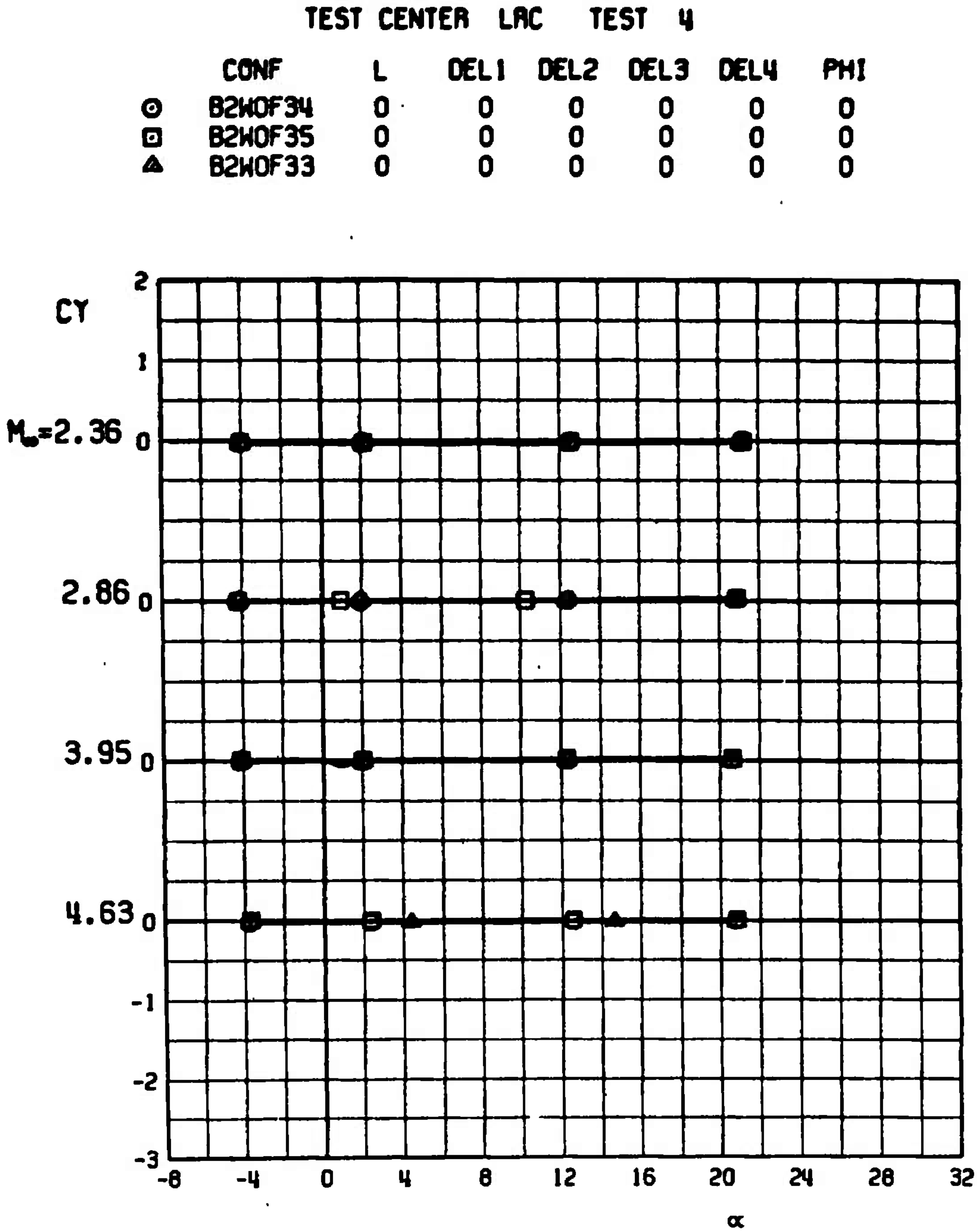

f. CY versus α

Figure 29. Continued.

TEST CENTER LRC TEST 4

	CONF	L	DEL1	DEL2	DEL3	DEL4	PHI
⊙	B2W0F34	0	0	0	0	0	0
⊡	B2W0F35	0	0	0	0	0	0
△	B2W0F33	0	0	0	0	0	0

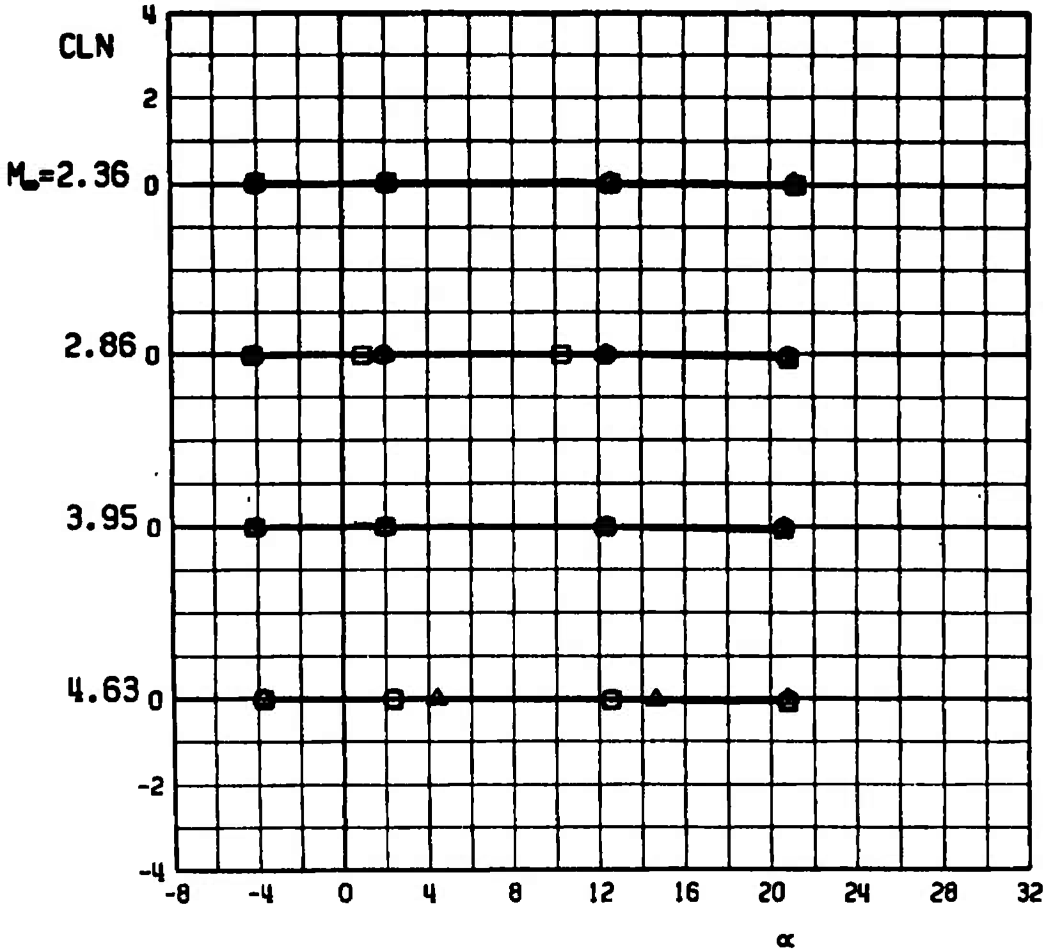

g. CLN versus α
Figure 29. Continued.

TEST CENTER LRC TEST 4

	CONF	L	DEL1	DEL2	DEL3	DEL4	PHI
⊙	B2W0F34	0	0	0	0	0	0
⊡	B2W0F35	0	0	0	0	0	0
△	B2W0F33	0	0	0	0	0	0

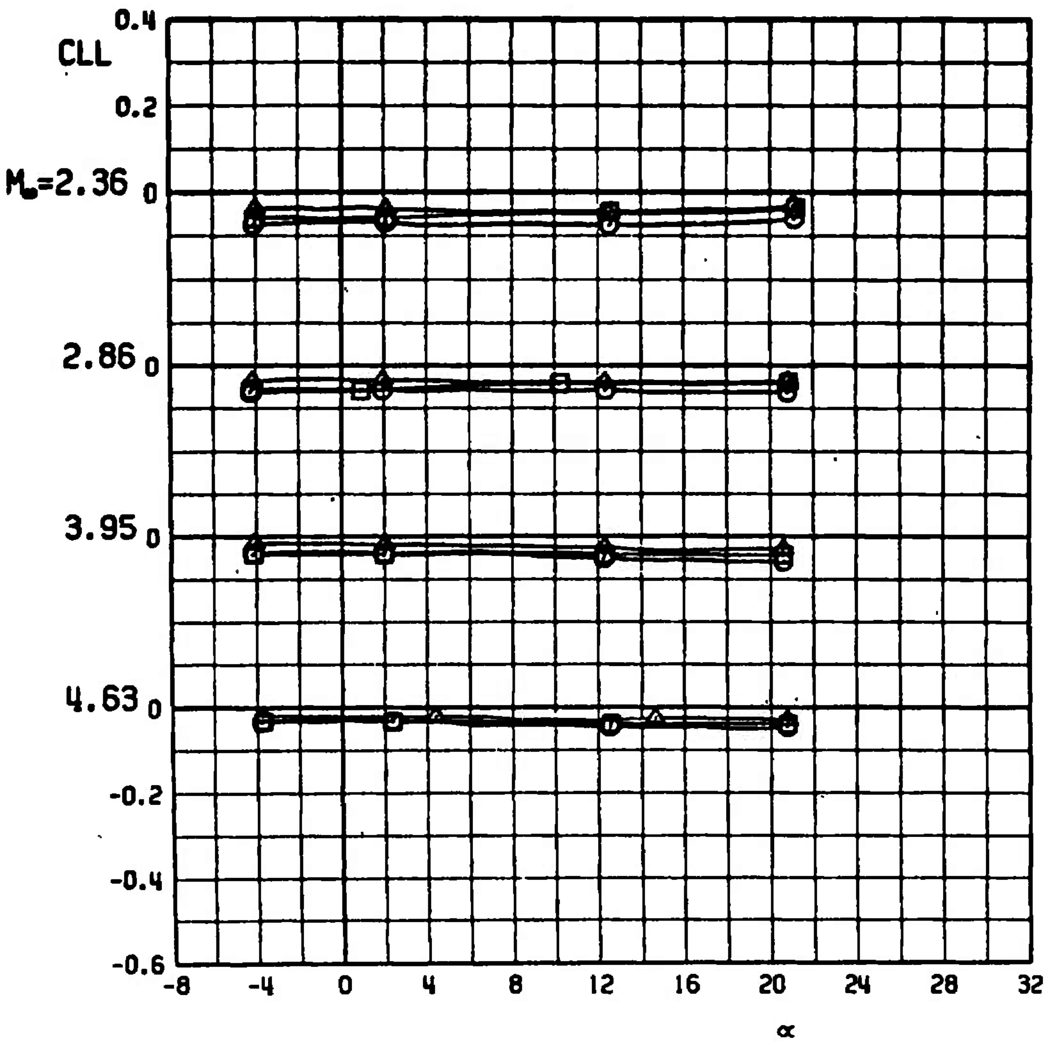

h. CLL versus α
Figure 29. Concluded.

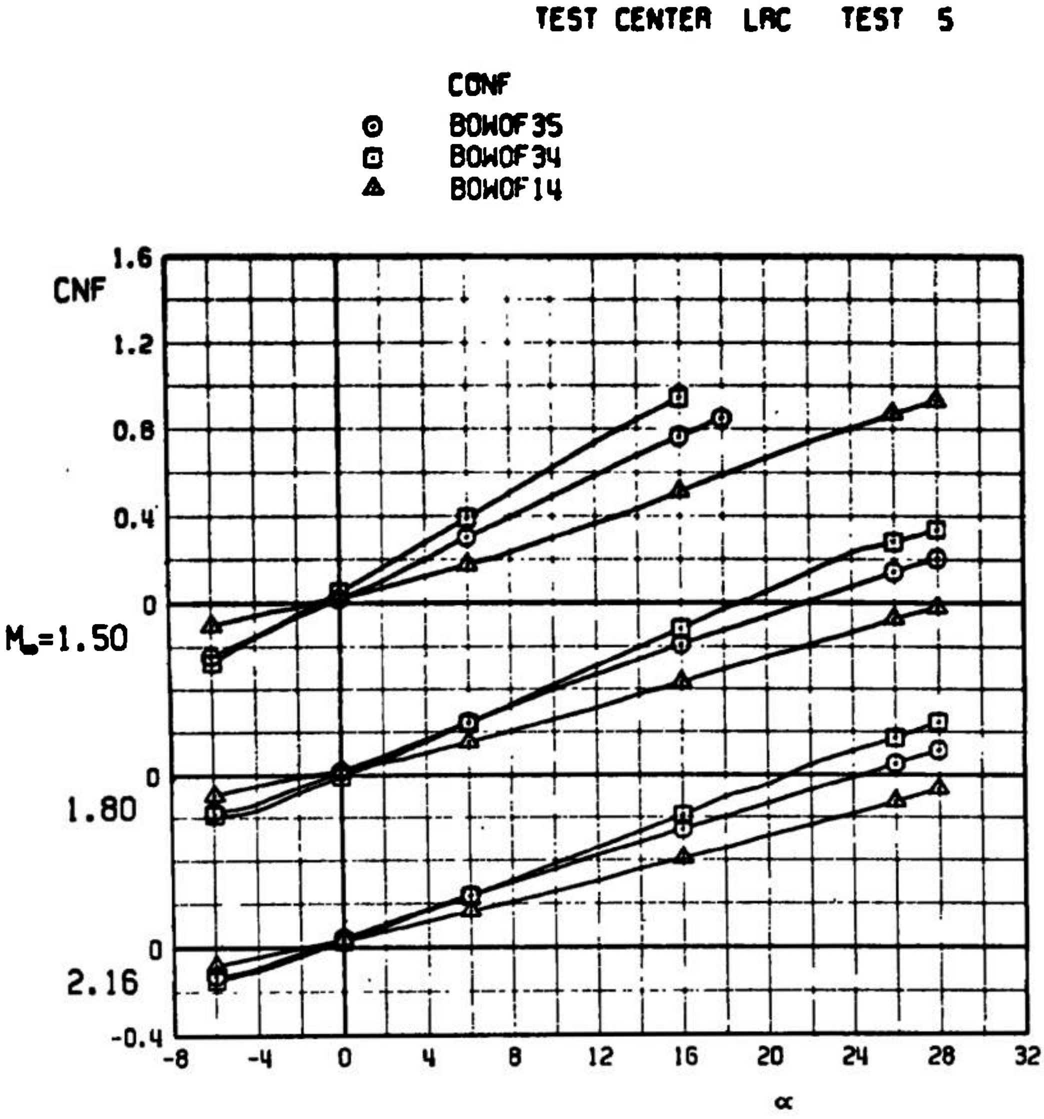

a. CNF versus α

Figure 30. Test No. 5, comparison of aerodynamic coefficients of configurations B0W0F35, B0W0F34, and B0W0F14.

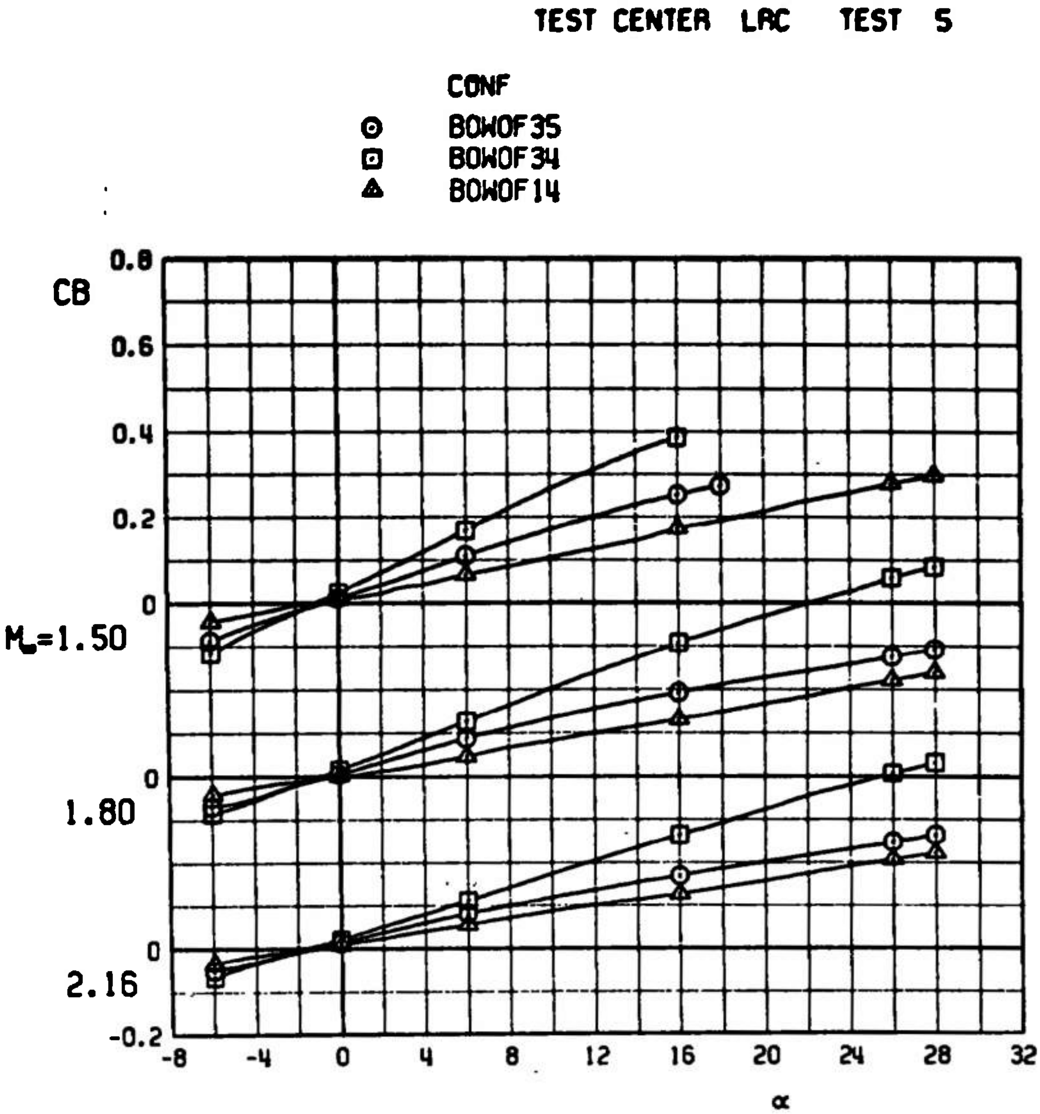

b. CB versus α
Figure 30. Continued.

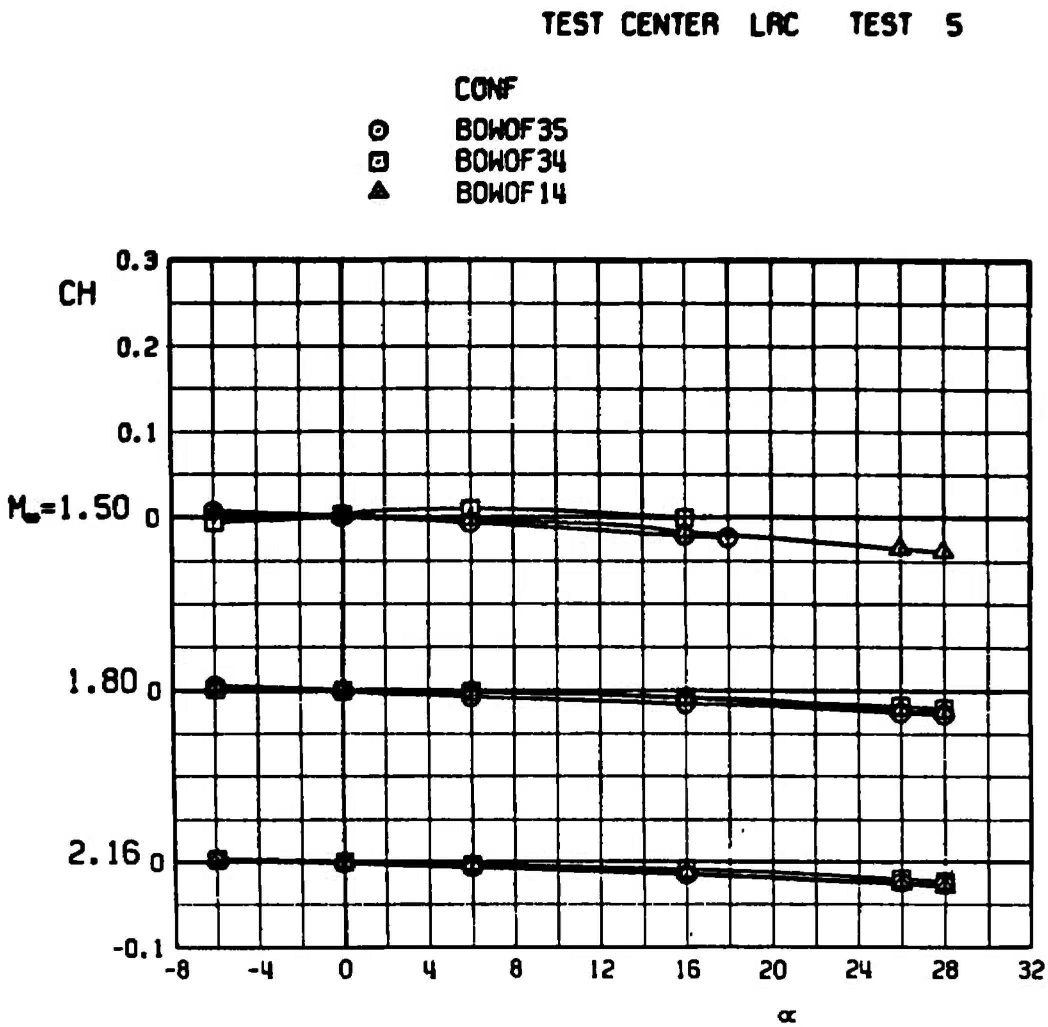

c. CH versus α
Figure 30. Concluded.

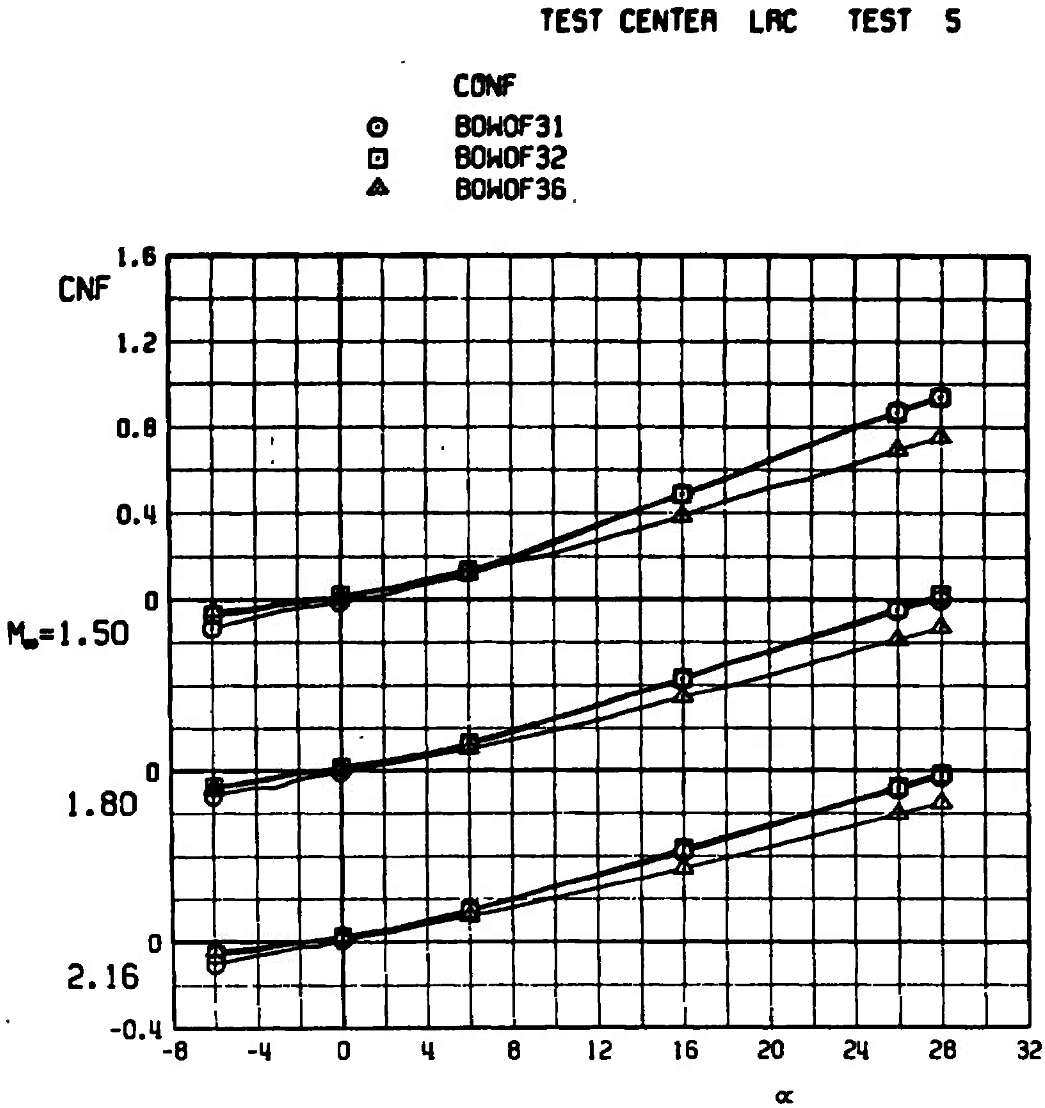

a. CNF versus α

Figure 31. Test No. 5, comparison of aerodynamic coefficients of configurations B0W0F31, B0W0F32, and B0W0F36.

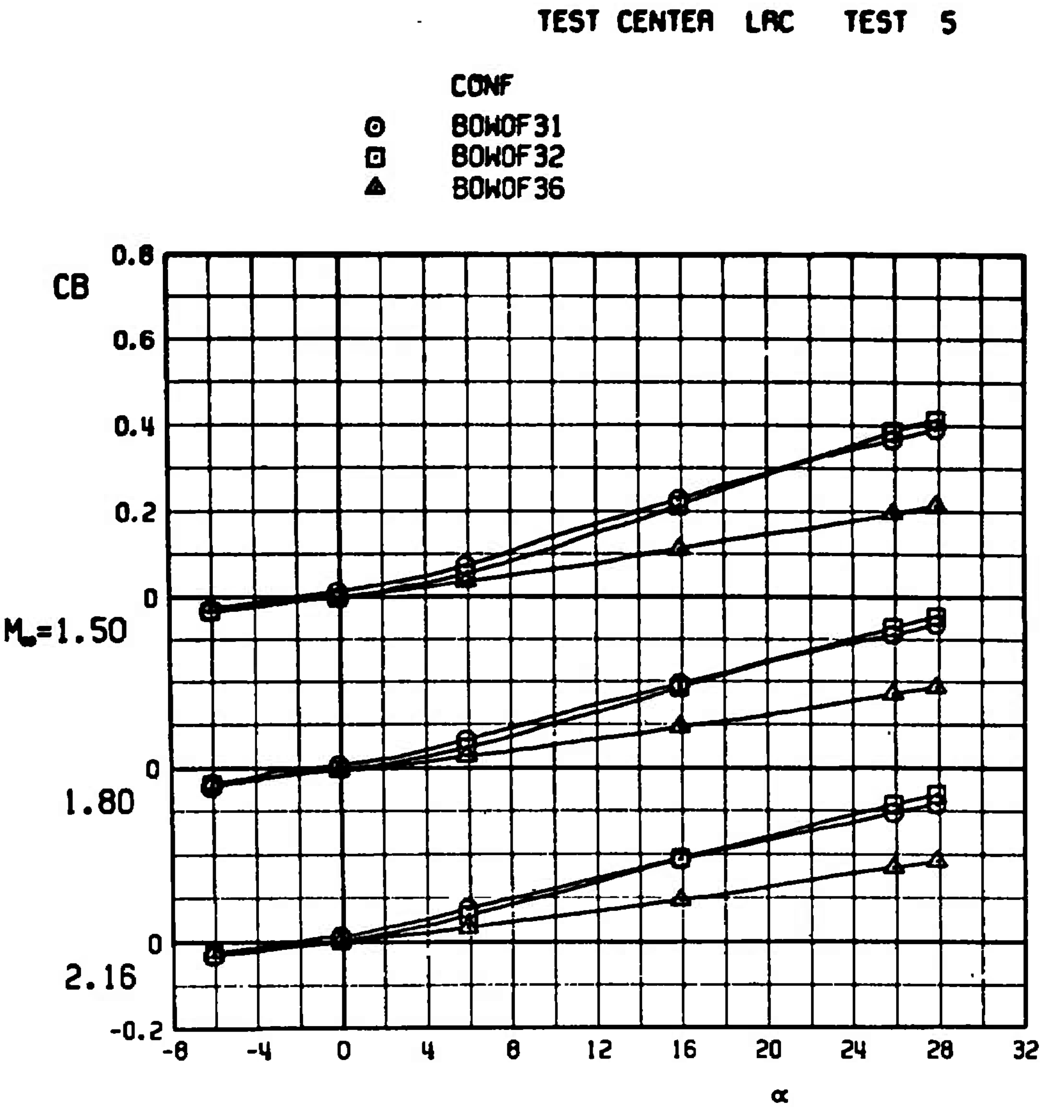

b. CB versus α
Figure 31. Continued.

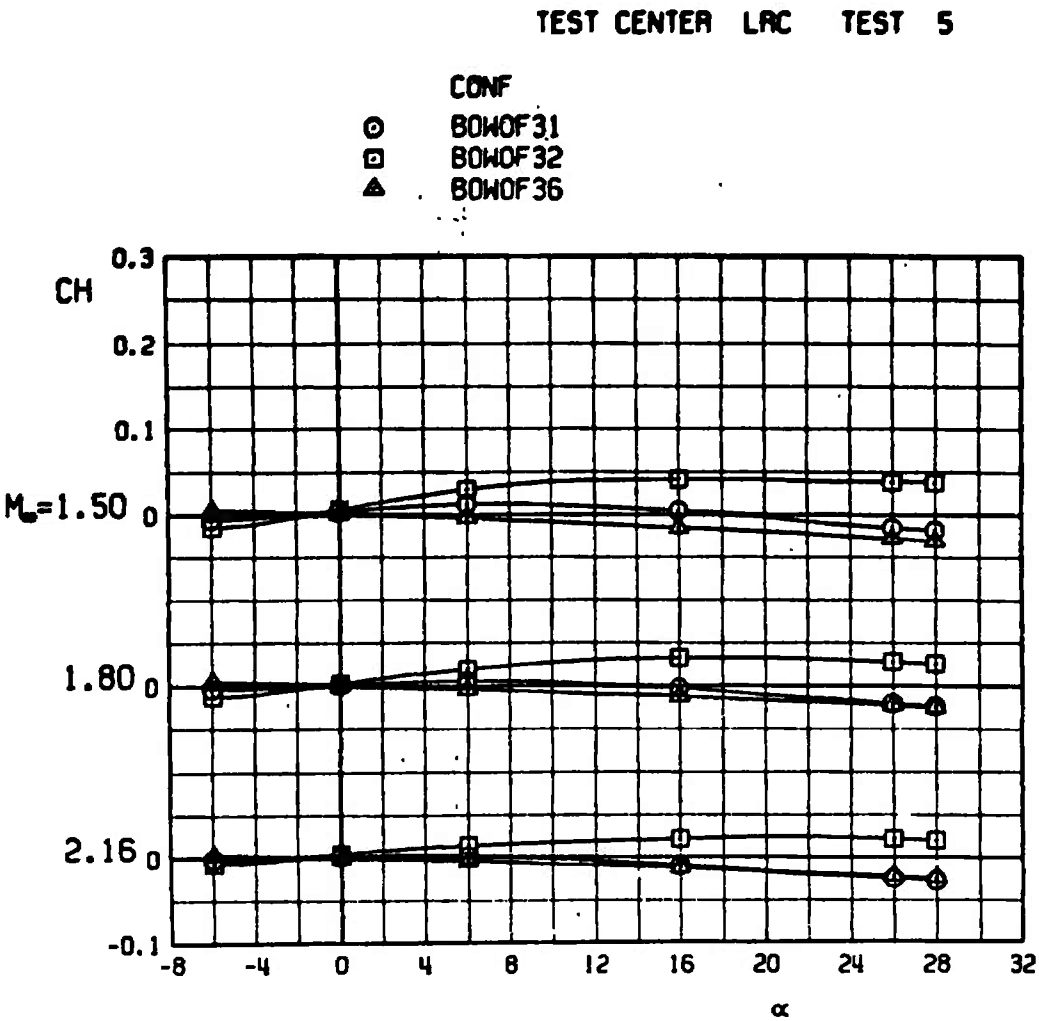

c. CH versus α
Figure 31. Concluded.

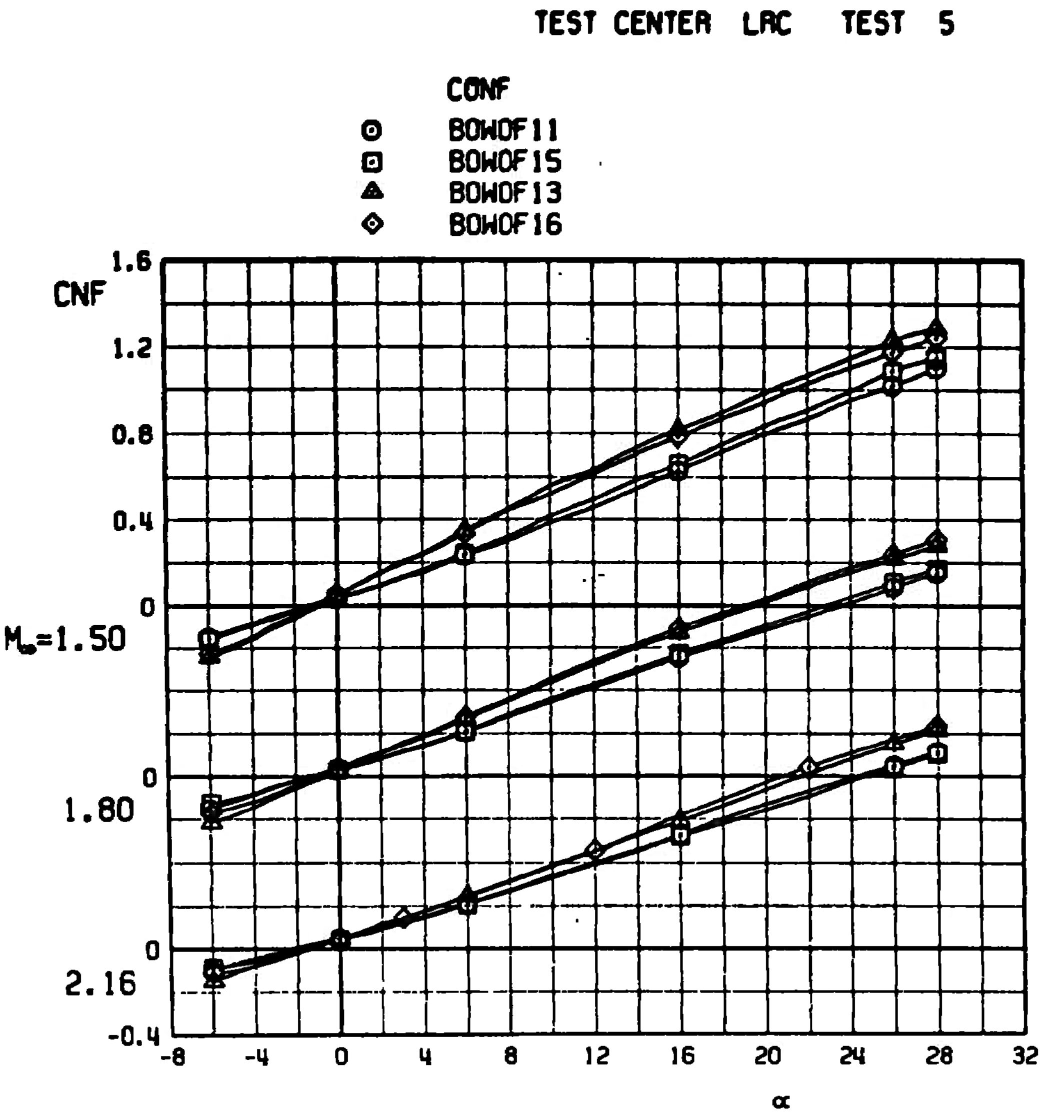

a. CNF versus α

Figure 32. Test No. 5, comparison of aerodynamic coefficients of configurations B0W0F11, B0W0F15, B0W0F13, and B0W0F16.

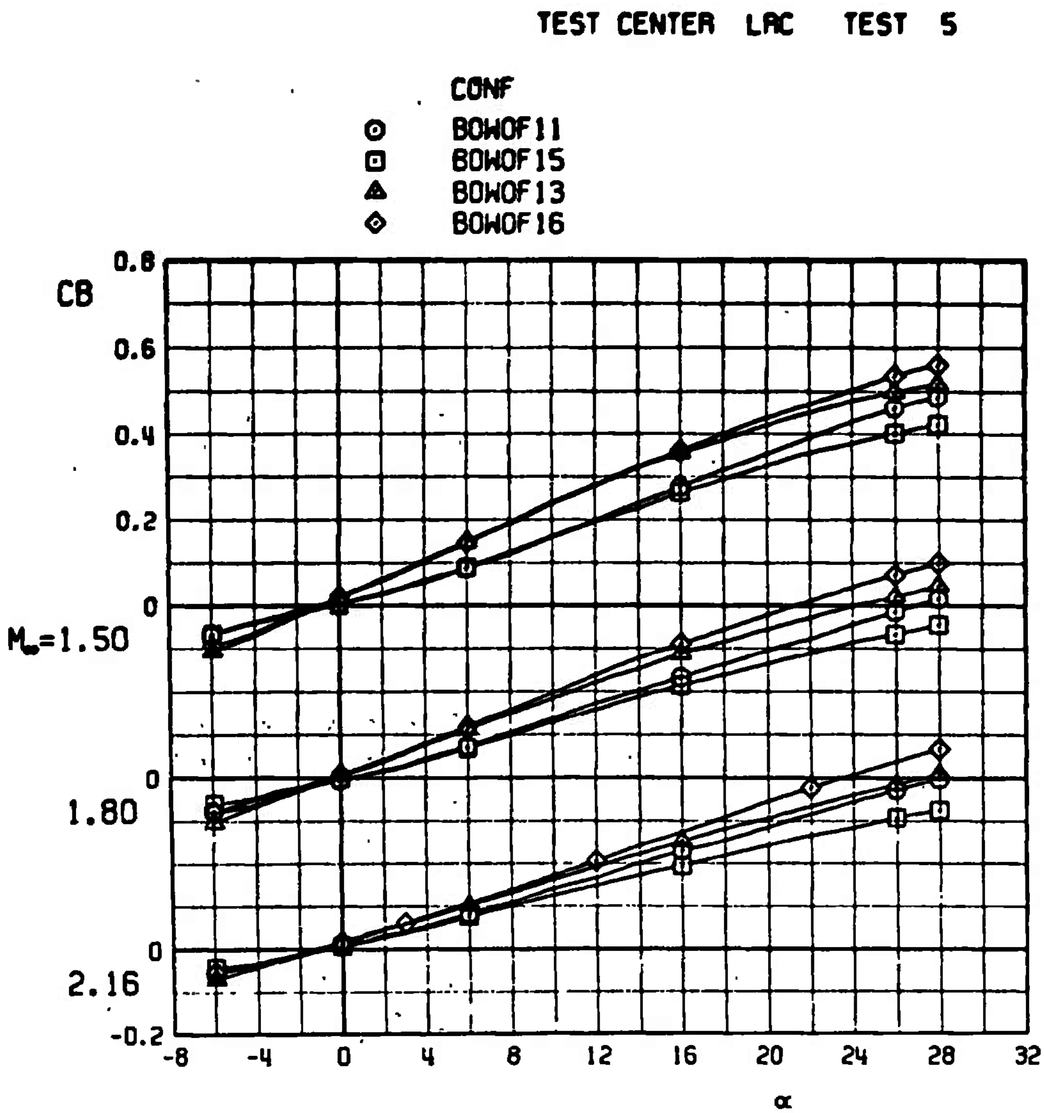

b. CB versus α
Figure 32. Continued.

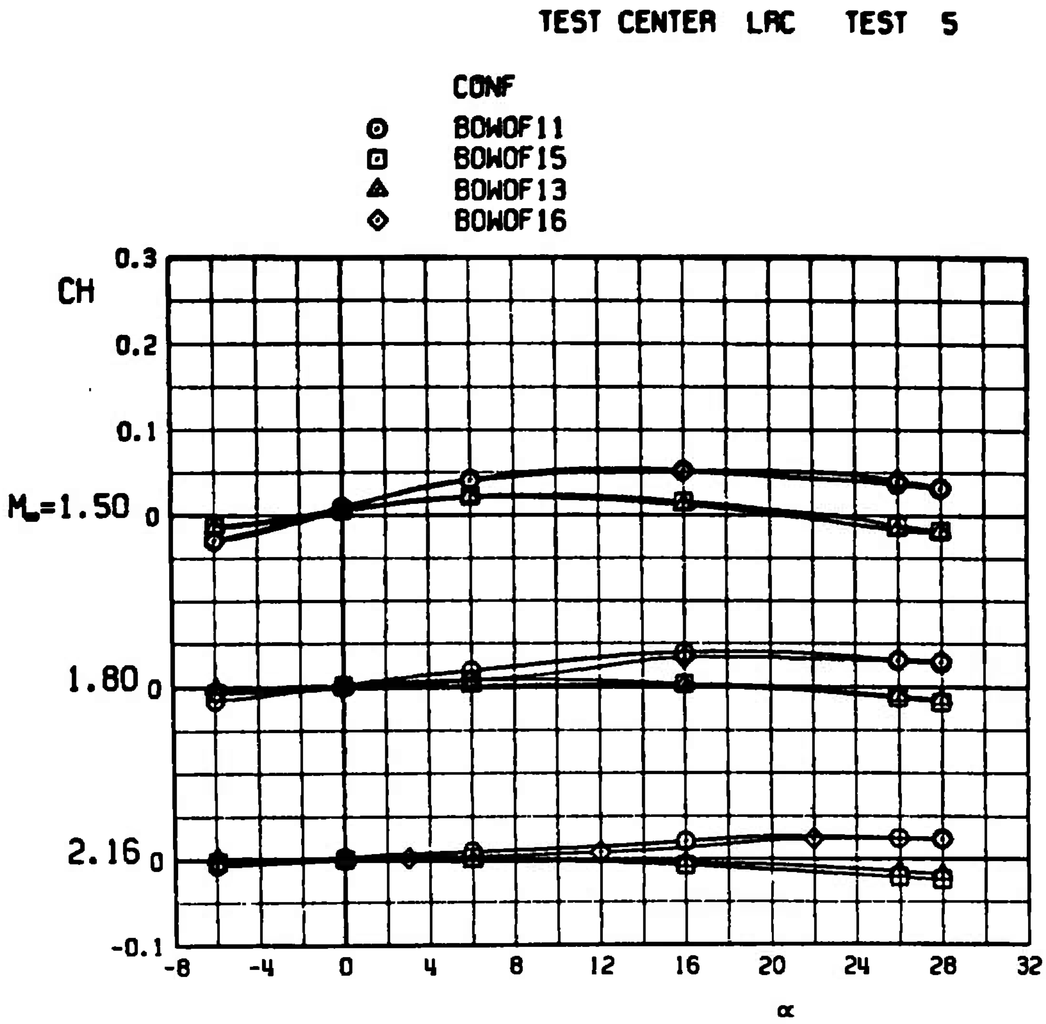

c. CH versus α
Figure 32. Concluded.

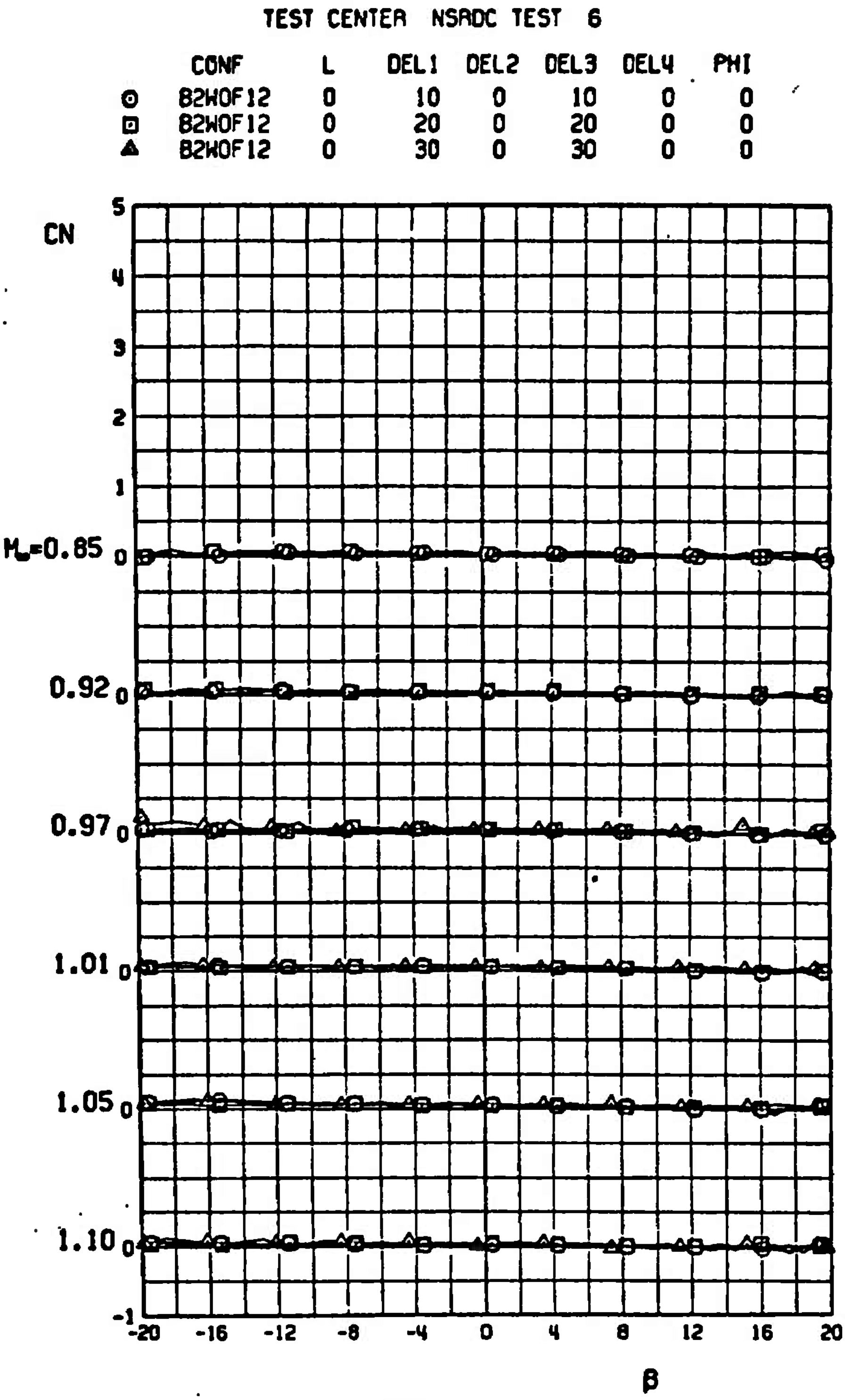

a. CN versus β

Figure 33. Test No. 6, comparison of aerodynamic coefficients of configuration B2W0F12 for various deflections of tail fins No. 1 and 3.

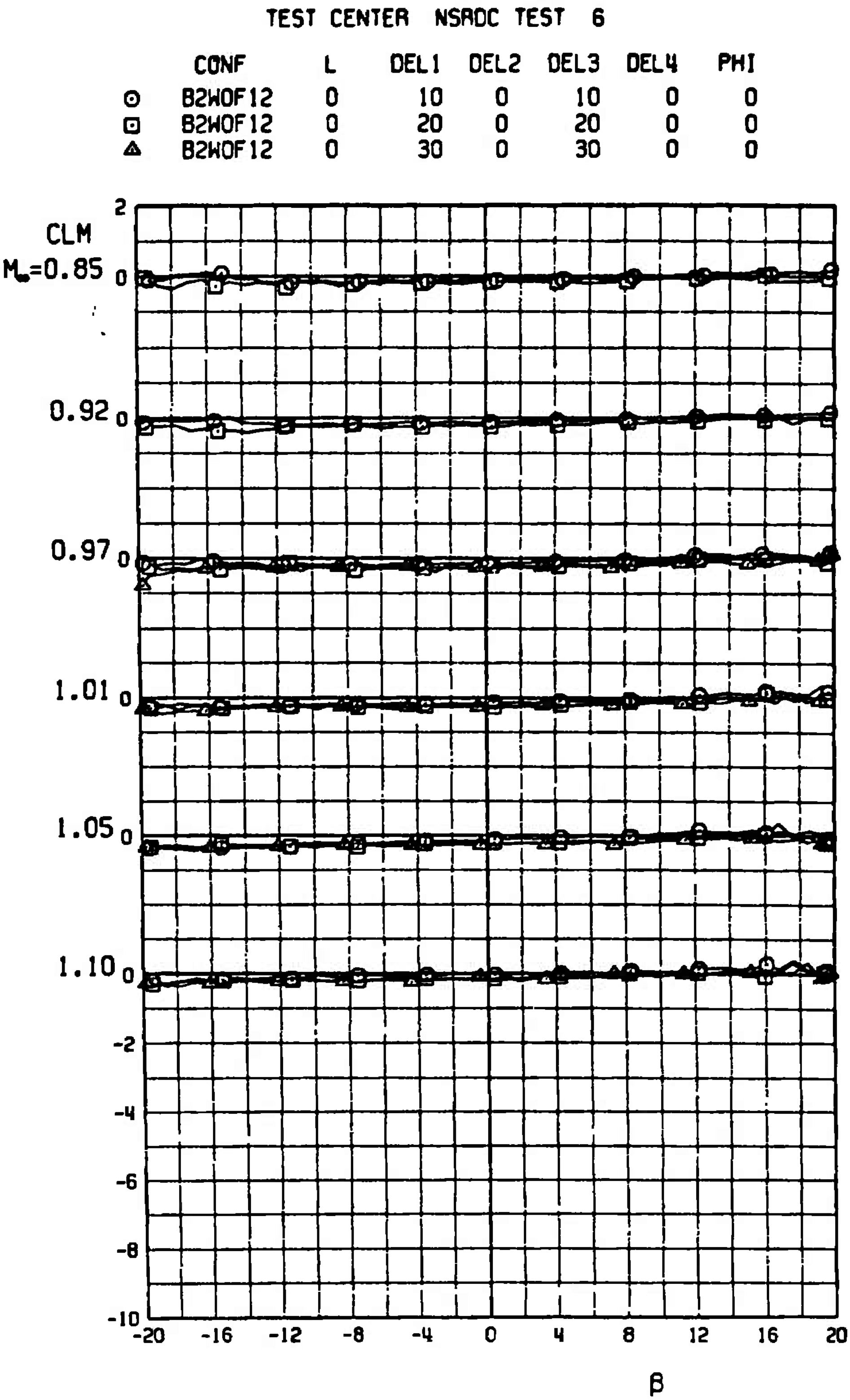

b. CLM versus β
Figure 33. Continued.

TEST CENTER NSRDC TEST 6

	CONF	L	DEL1	DEL2	DEL3	DEL4	PHI
⊙	B2WOF12	0	10	0	10	0	0
⊡	B2WOF12	0	20	0	20	0	0
△	B2WOF12	0	30	0	30	0	0

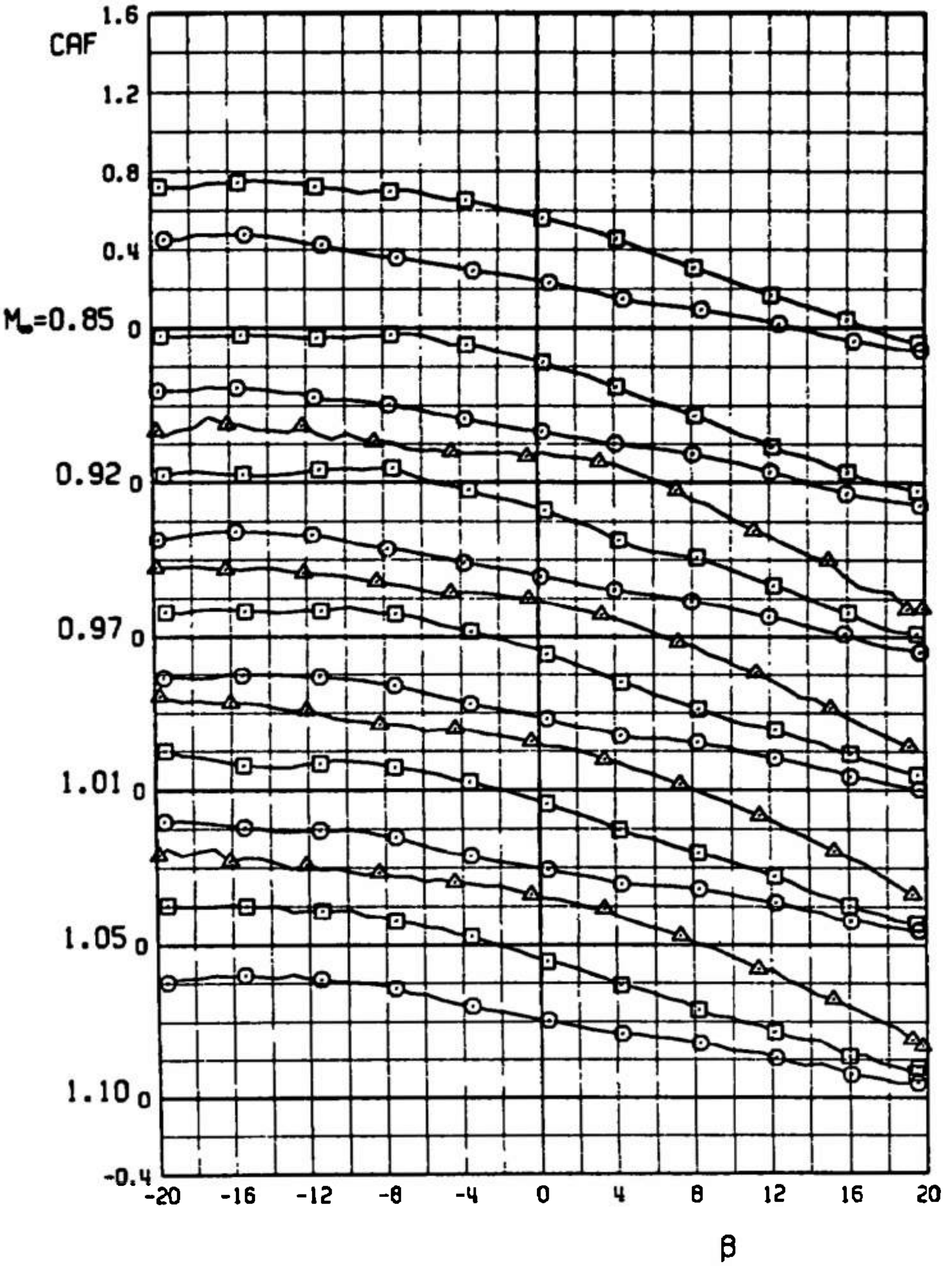

c. CAF versus β

Figure 33. Continued.

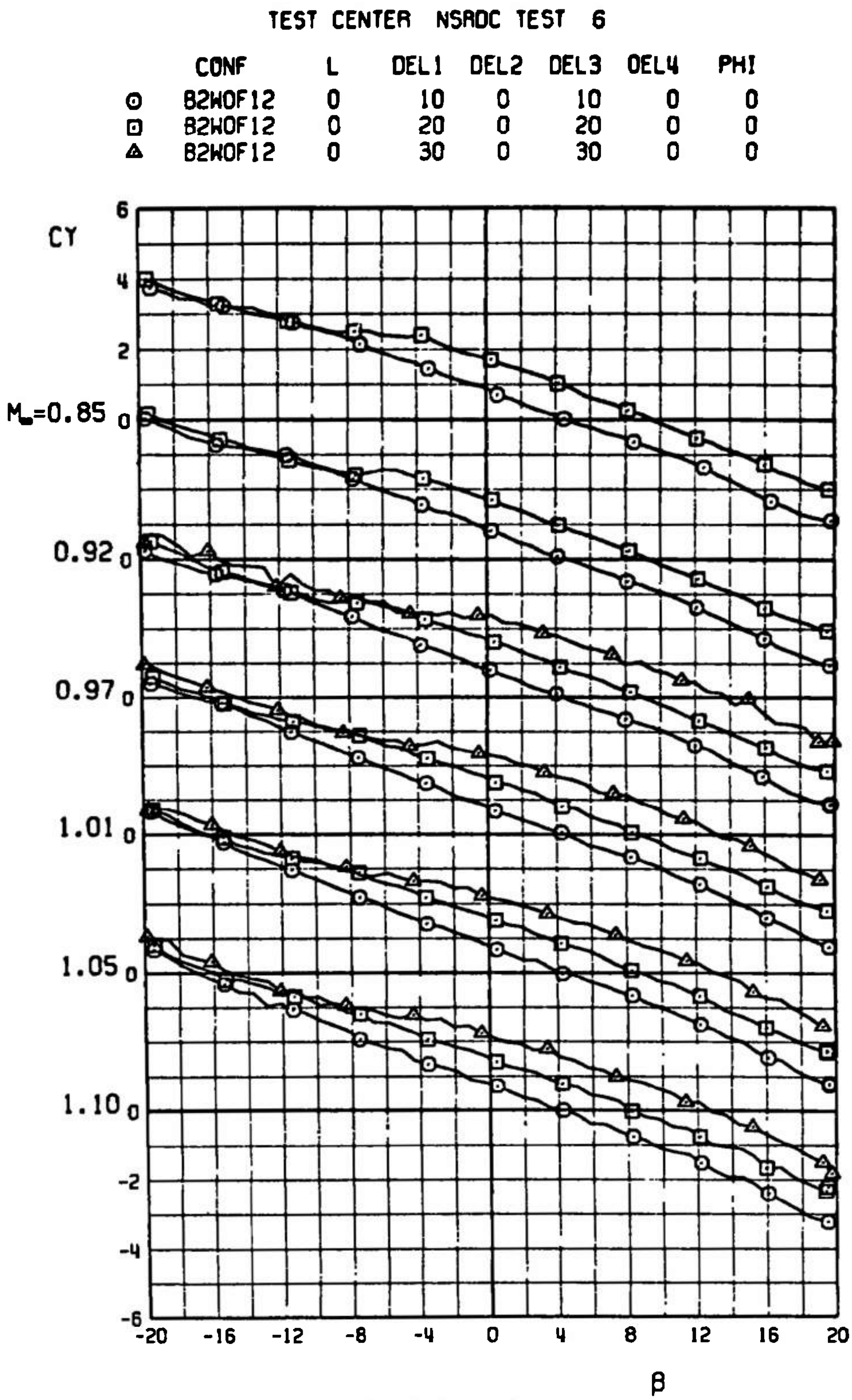

d. CY versus β
Figure 33. Continued.

TEST CENTER NSRDC TEST 6

	CONF	L	DEL1	DEL2	DEL3	DEL4	PHI
⊙	B2W0F12	0	10	0	10	0	0
⊡	B2W0F12	0	20	0	20	0	0
△	B2W0F12	0	30	0	30	0	0

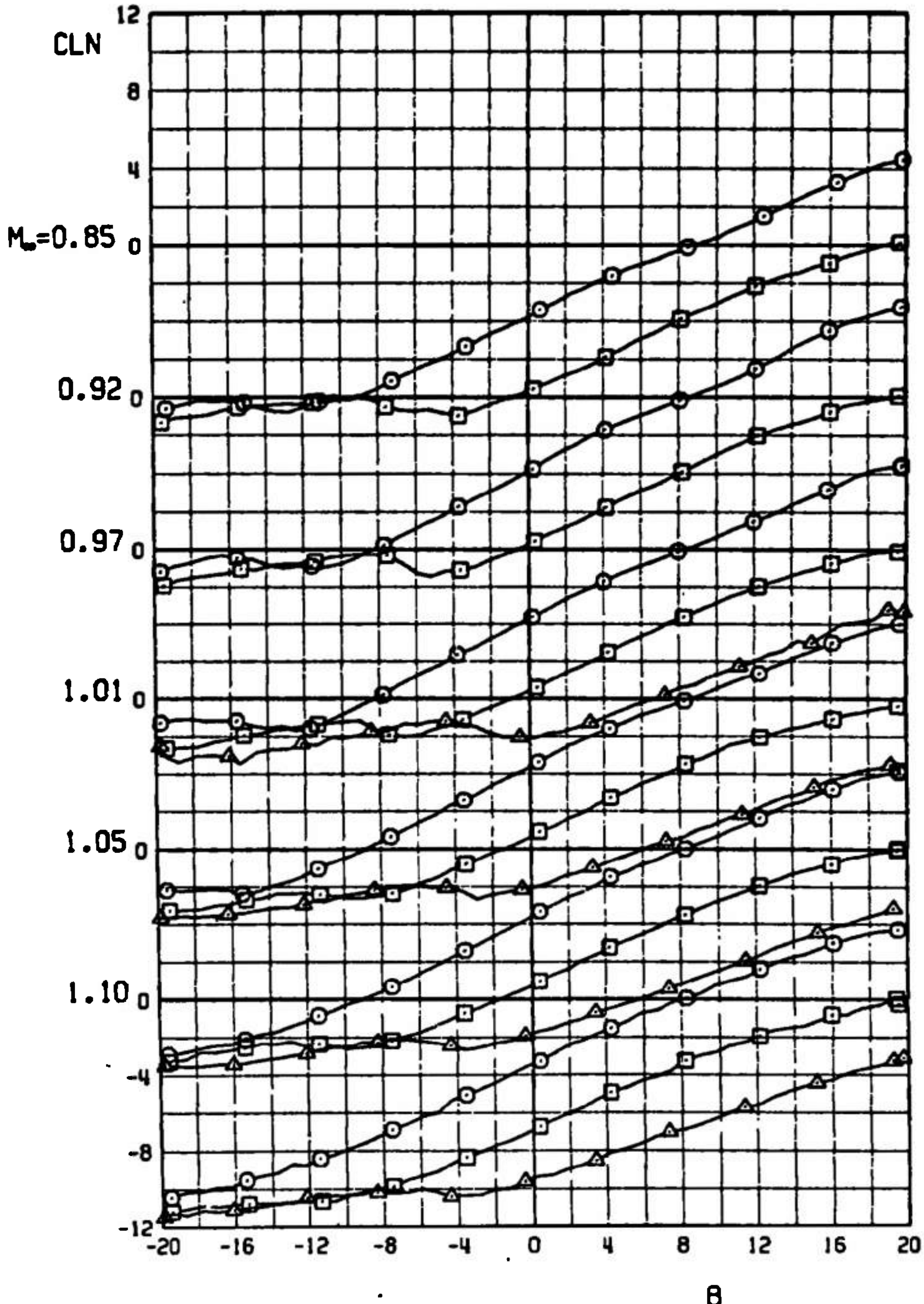

e. CLN versus β
Figure 33. Continued.

TEST CENTER NSRDC TEST 6

	CONF	L	DEL1	DEL2	DEL3	DEL4	PHI
⊙	B2WOF12	0	10	0	10	0	0
⊡	B2WOF12	0	20	0	20	0	0
△	B2WOF12	0	30	0	30	0	0

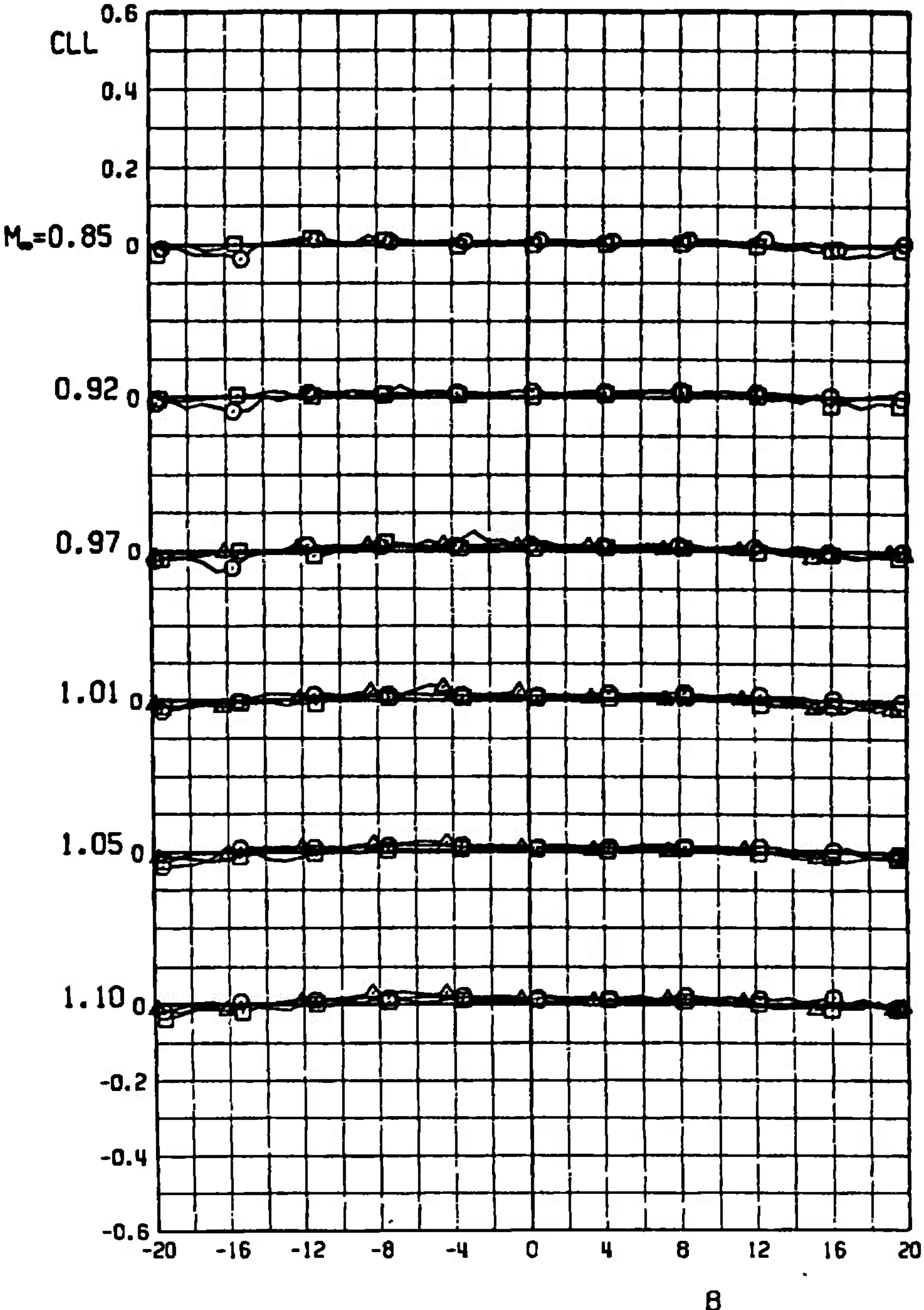

f. CLL versus β
Figure 33. Continued.

TEST CENTER NSRDC TEST 6

	CONF	L	DEL1	DEL2	DEL3	DEL4	PHI
⊙	B2W0F12	0	10	0	10	0	0
⊡	B2W0F12	0	20	0	20	0	0
▲	B2W0F12	0	30	0	30	0	0

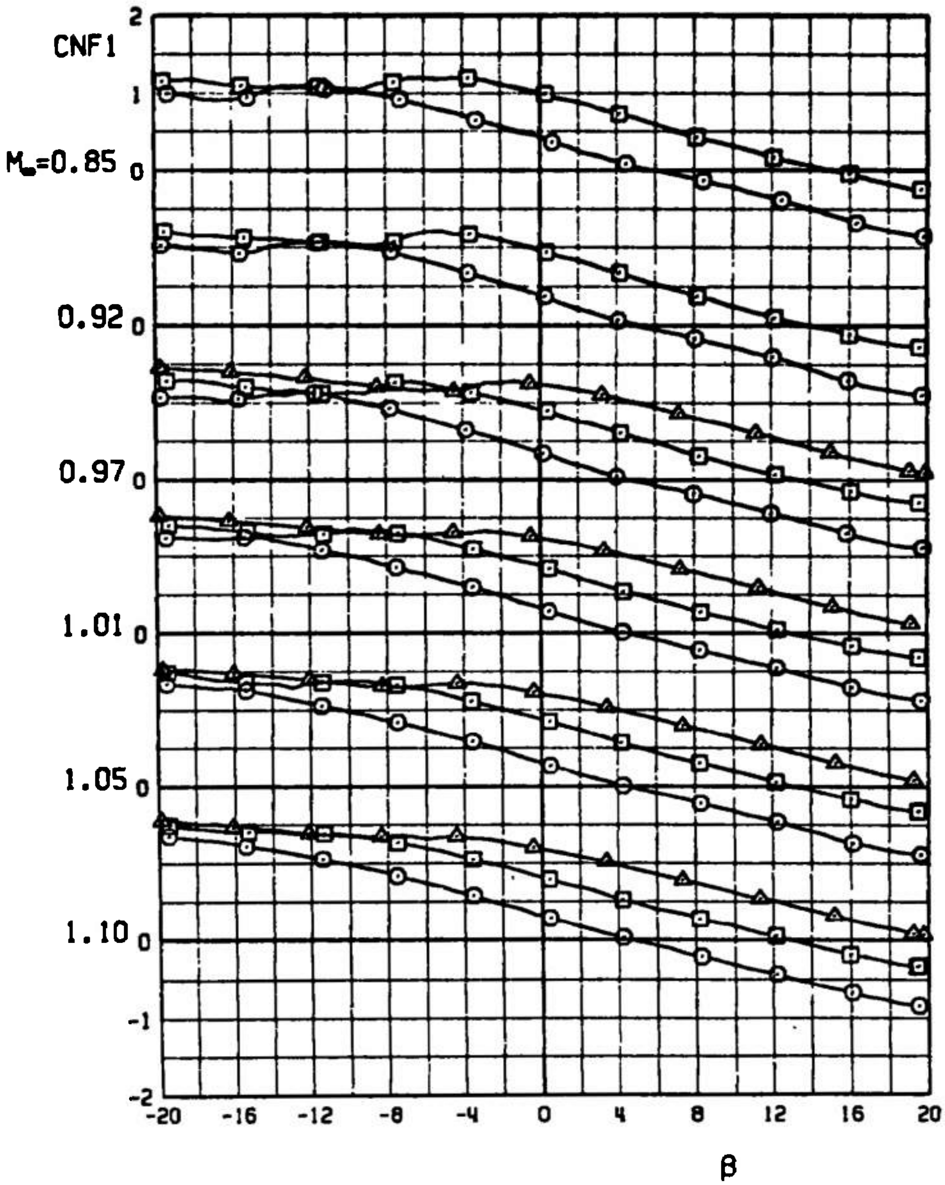

g. CNF1 versus β
Figure 33. Continued.

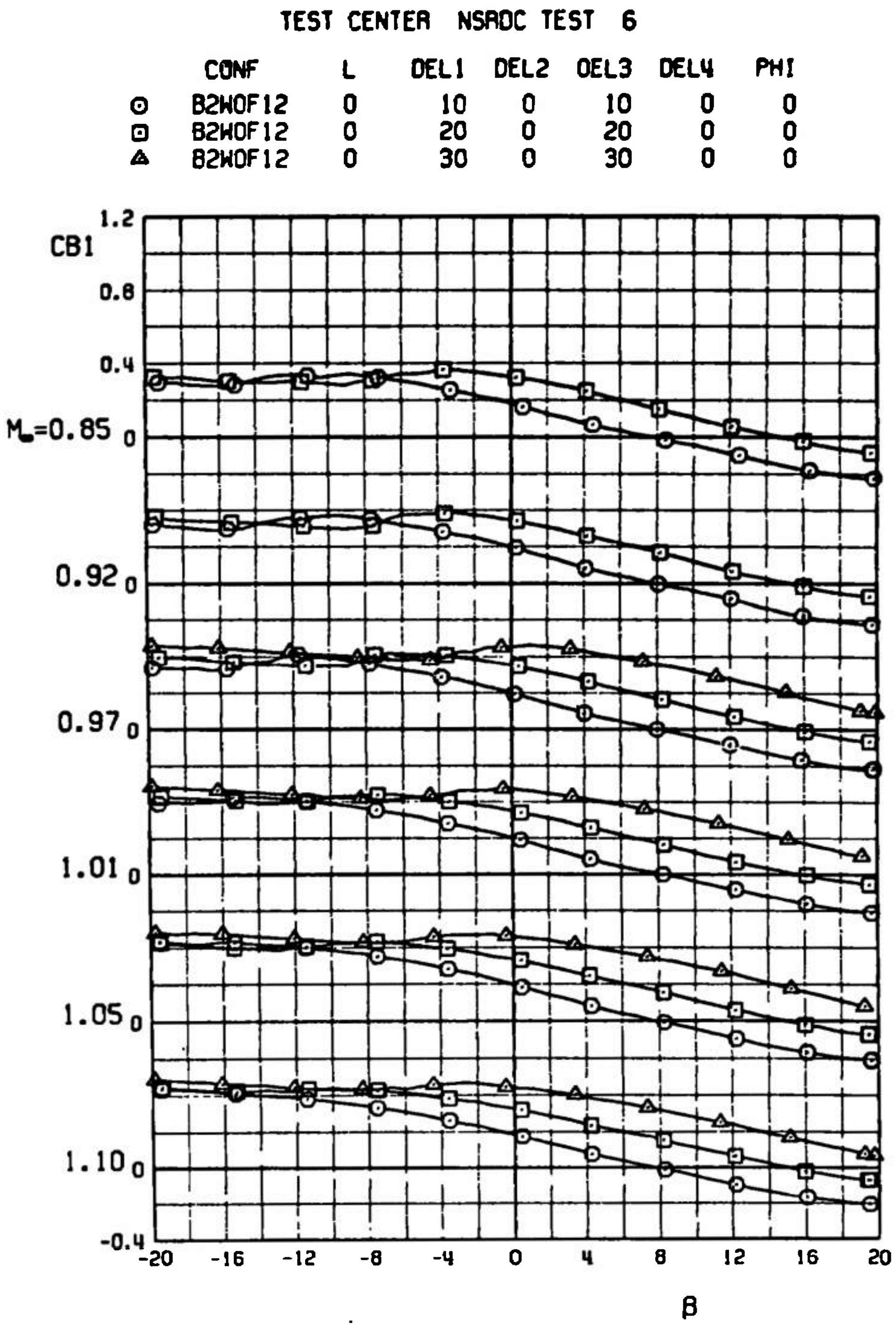

h. CB1 versus β
Figure 33. Continued.

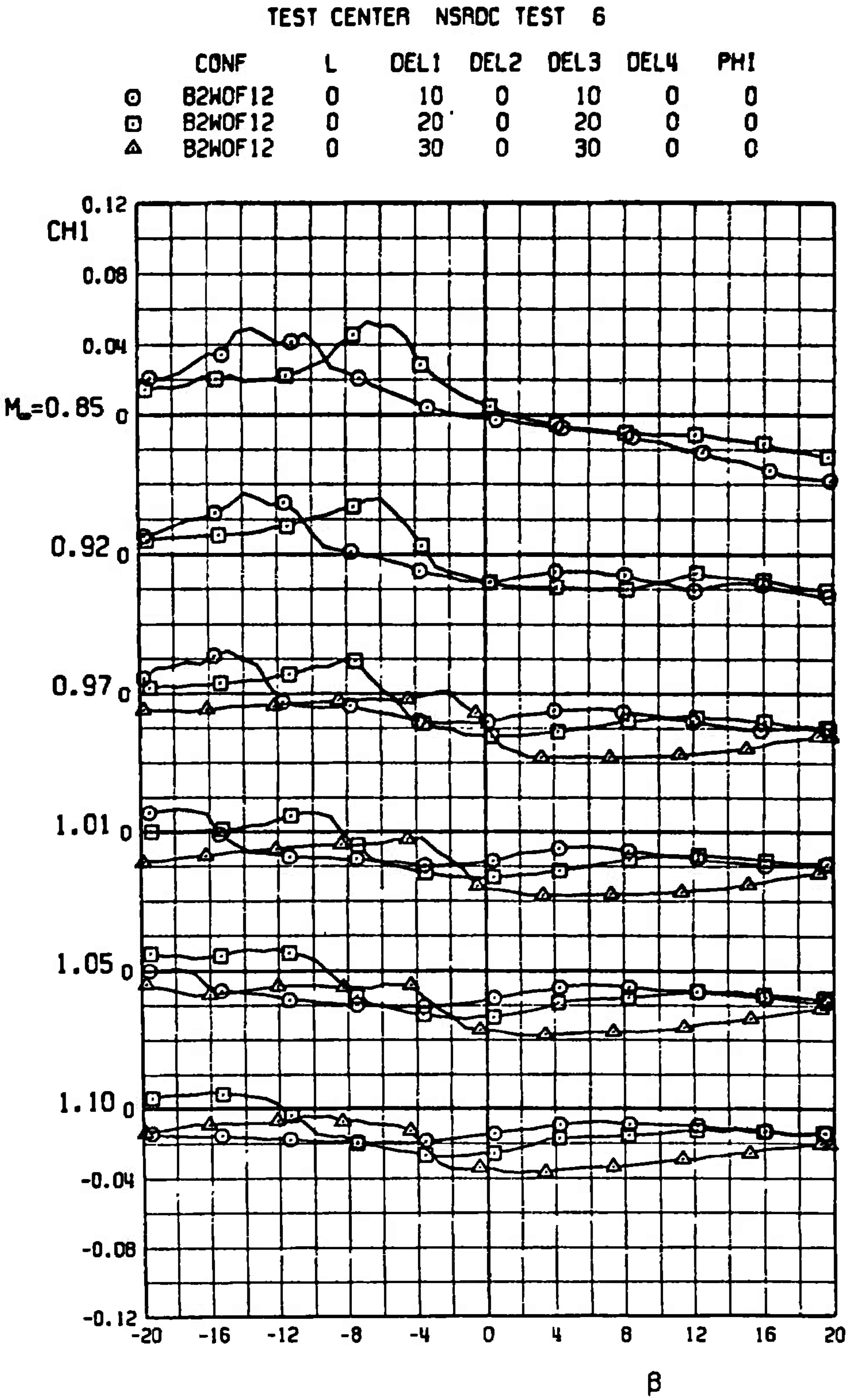

i. CH1 versus β
Figure 33. Concluded.

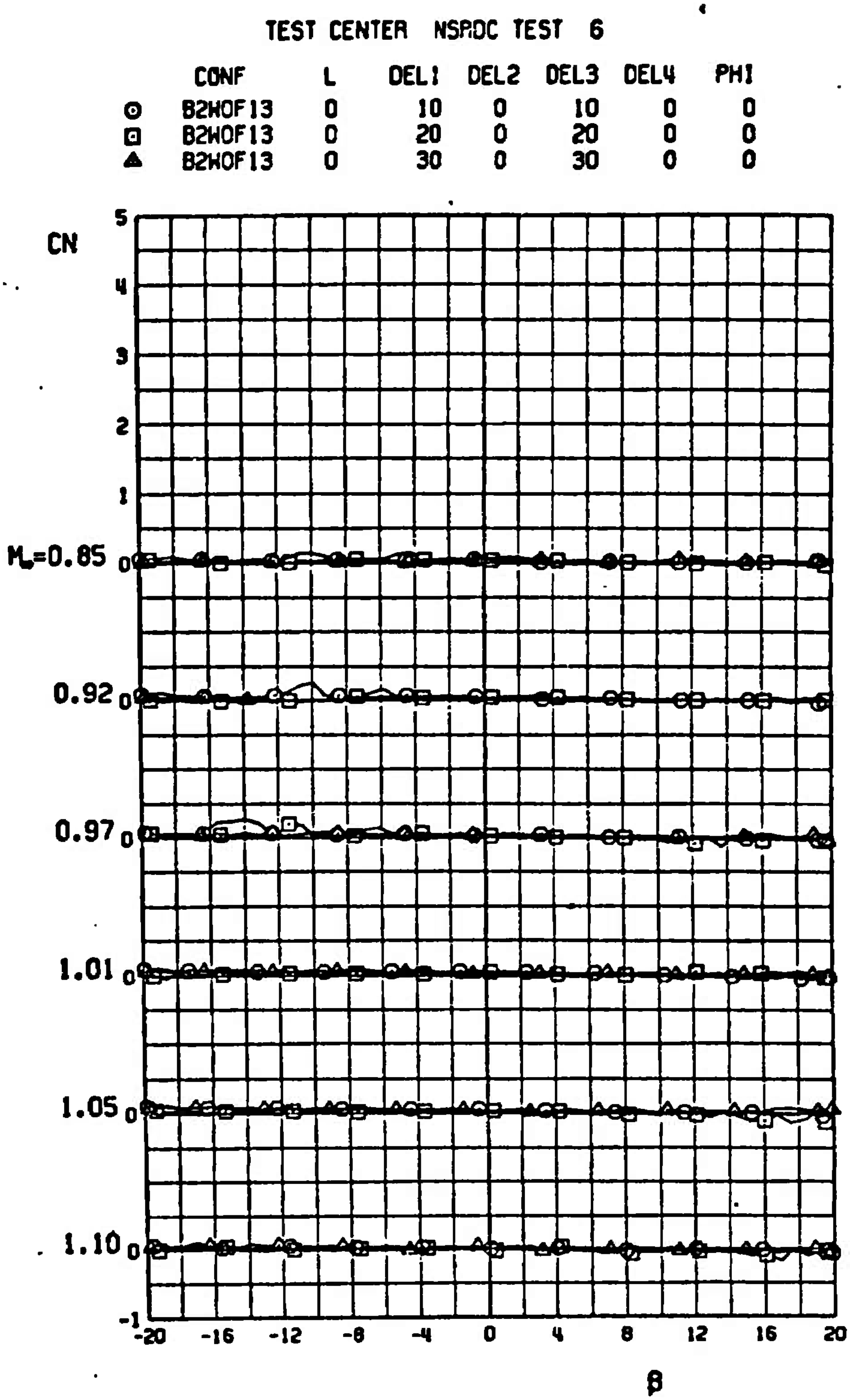

a. CN versus β

Figure 34. Test No. 6, comparison of aerodynamic coefficients of configuration B2W0F13 for various deflections of tail fins No. 1 and 3.

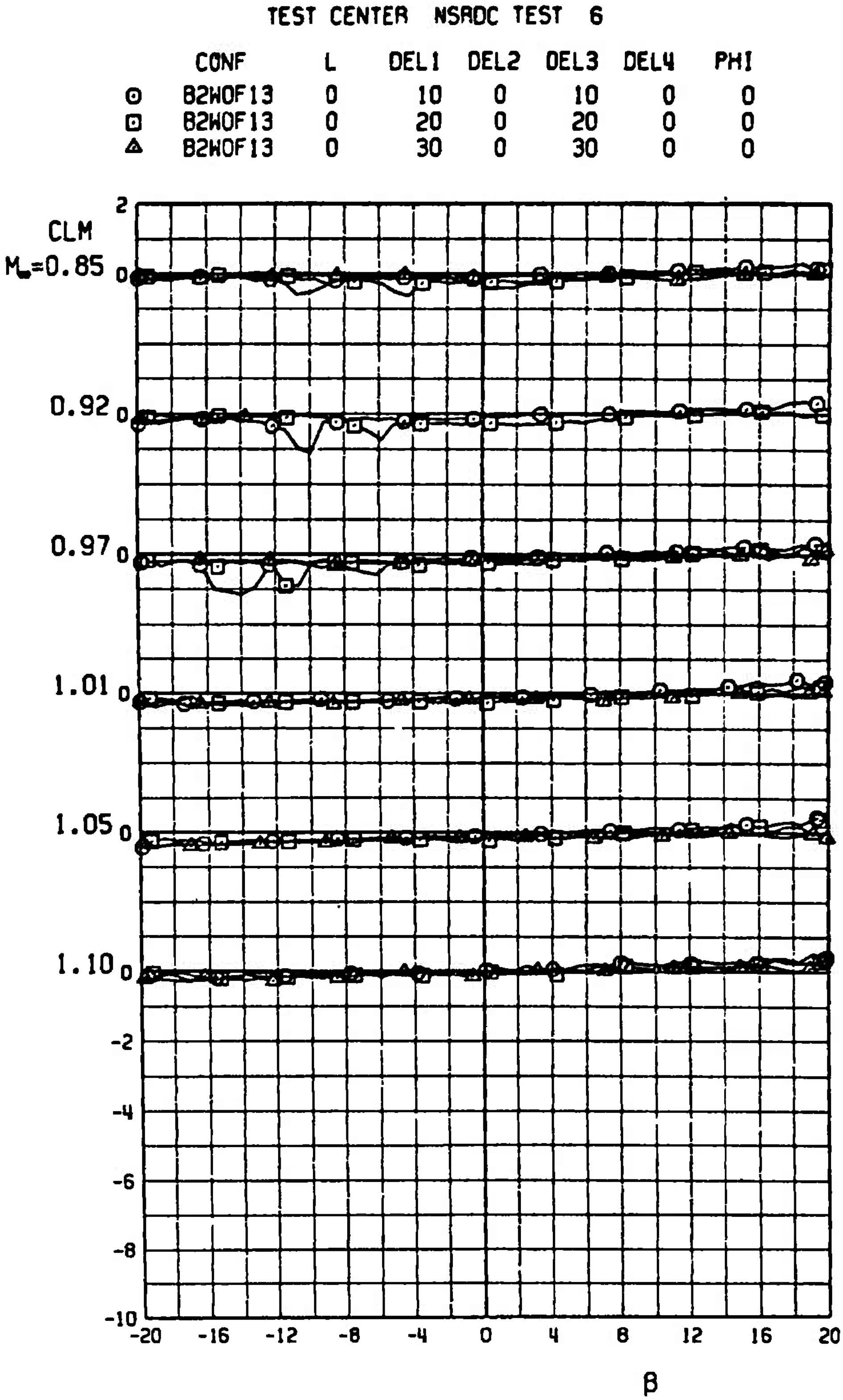

b. CLM versus β
Figure 34. Continued.

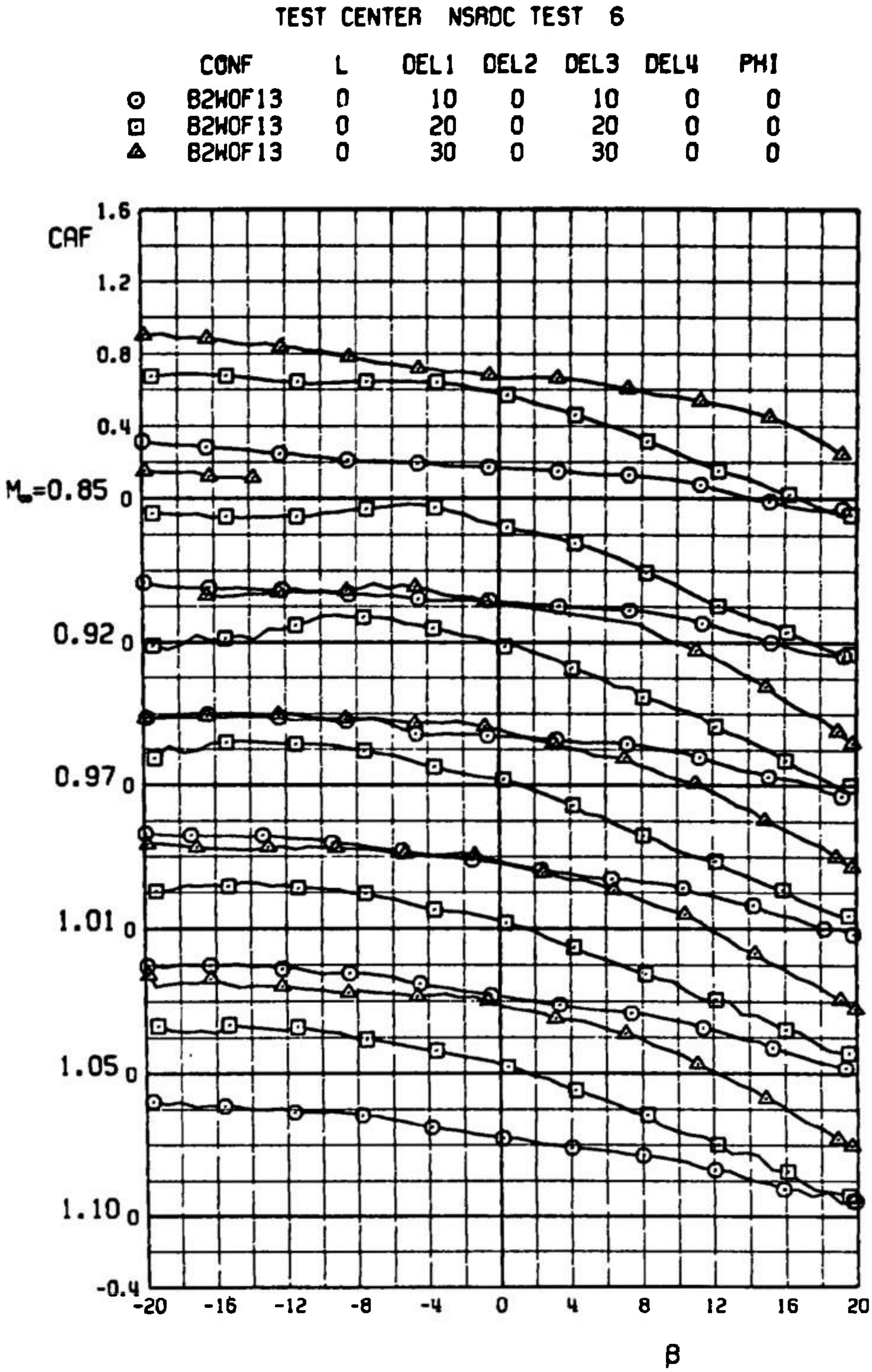

c. CAF versus β
Figure 34. Continued.

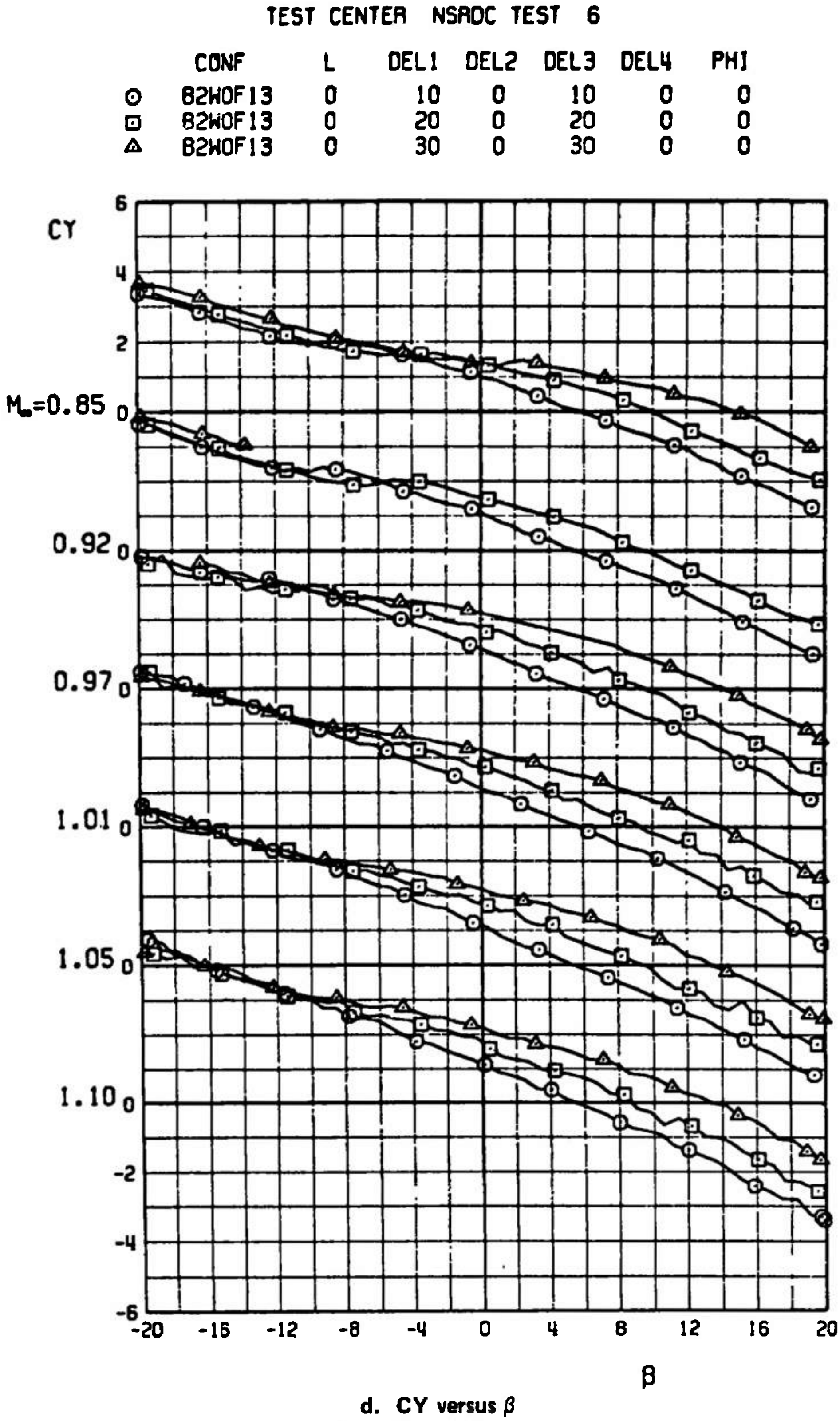

d. CY versus β
Figure 34. Continued.

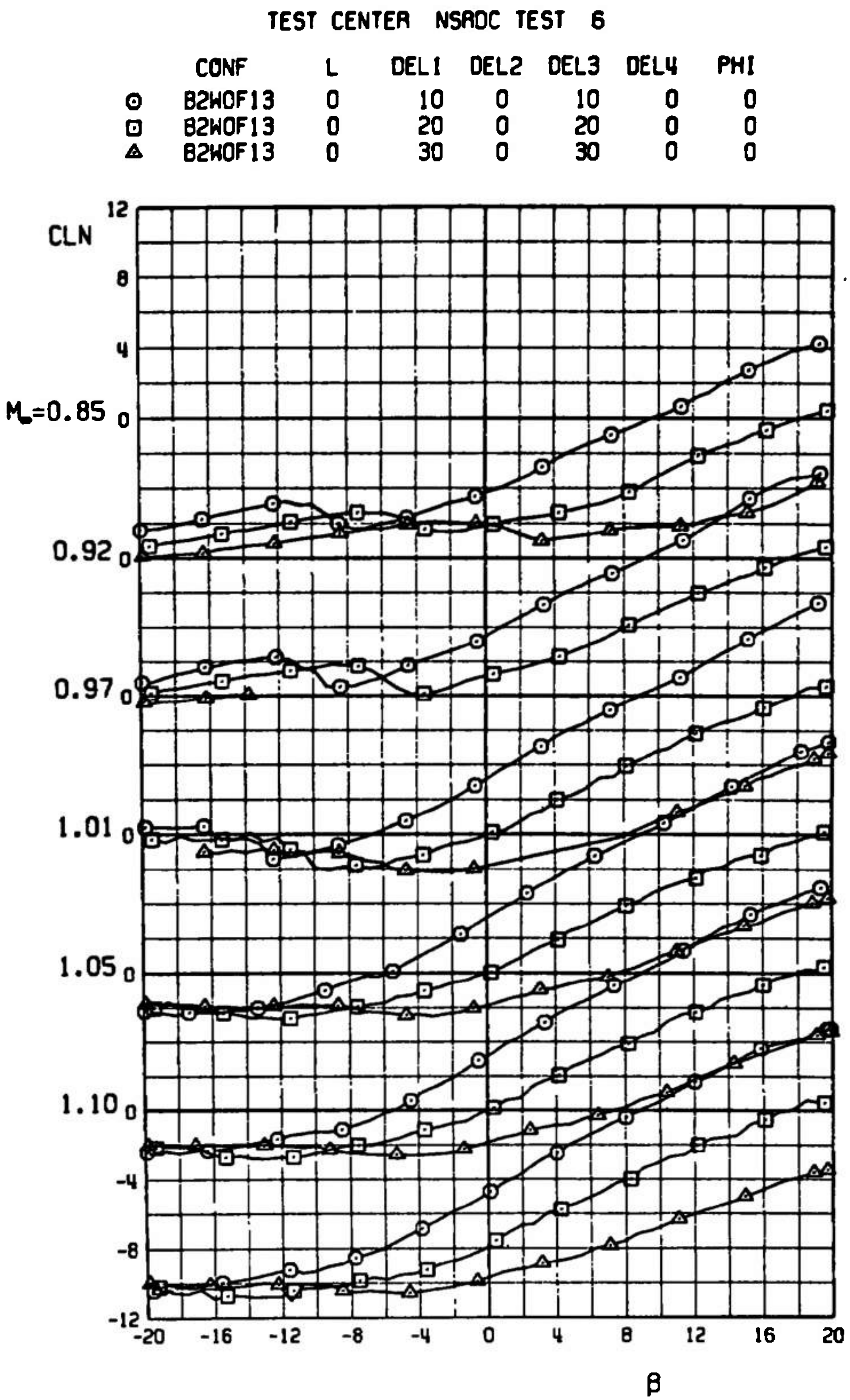

e. CLN versus β
Figure 34. Continued.

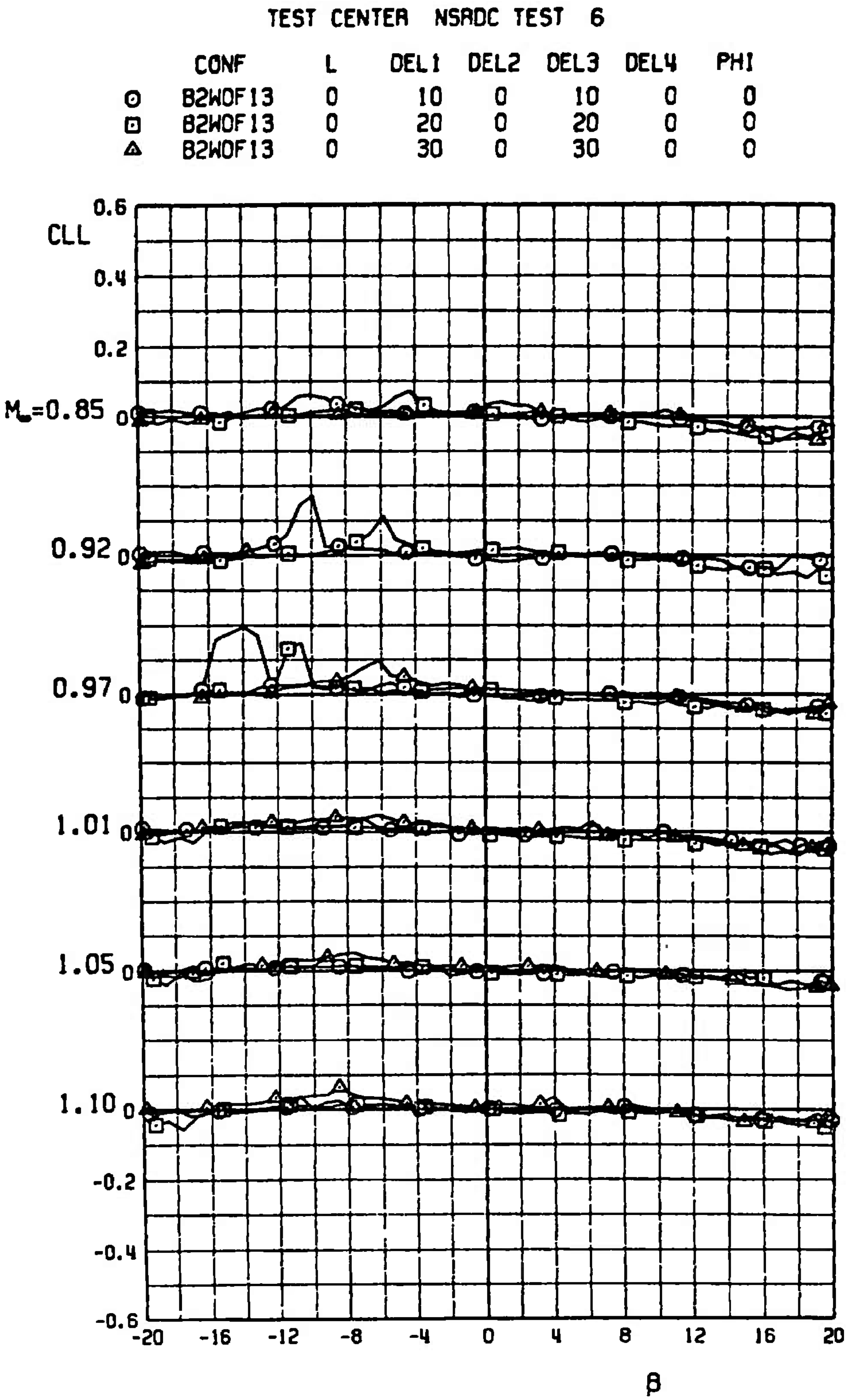

f. CLL versus β
Figure 34. Continued.

TEST CENTER NSRDC TEST 6

	CONF	L	DEL1	DEL2	DEL3	DEL4	PHI
⊙	B2WOF13	0	10	0	10	0	0
⊡	B2WOF13	0	20	0	20	0	0
△	B2WOF13	0	30	0	30	0	0

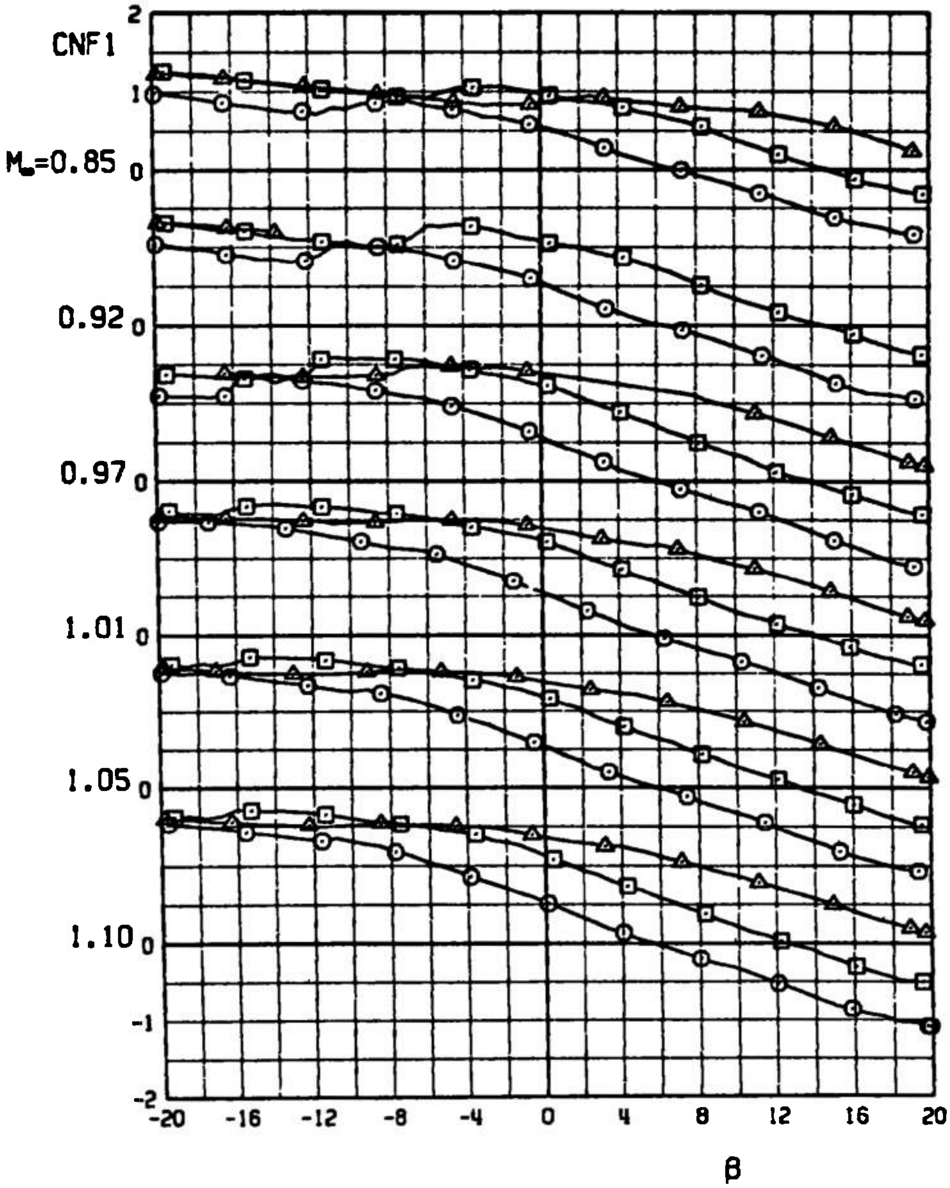

g. CNF1 versus β
Figure 34. Continued.

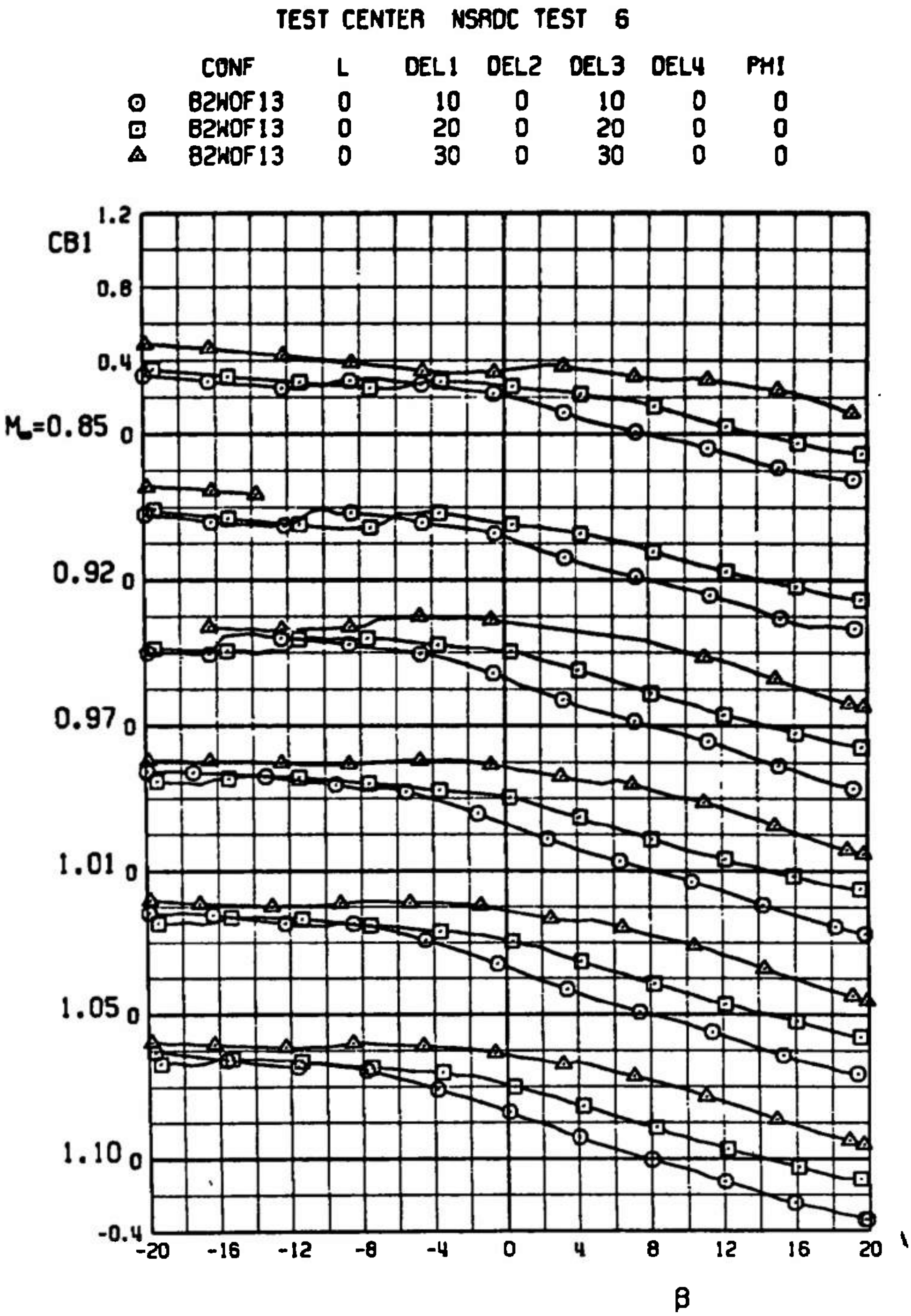

h. CB1 versus β
Figure 34. Continued.

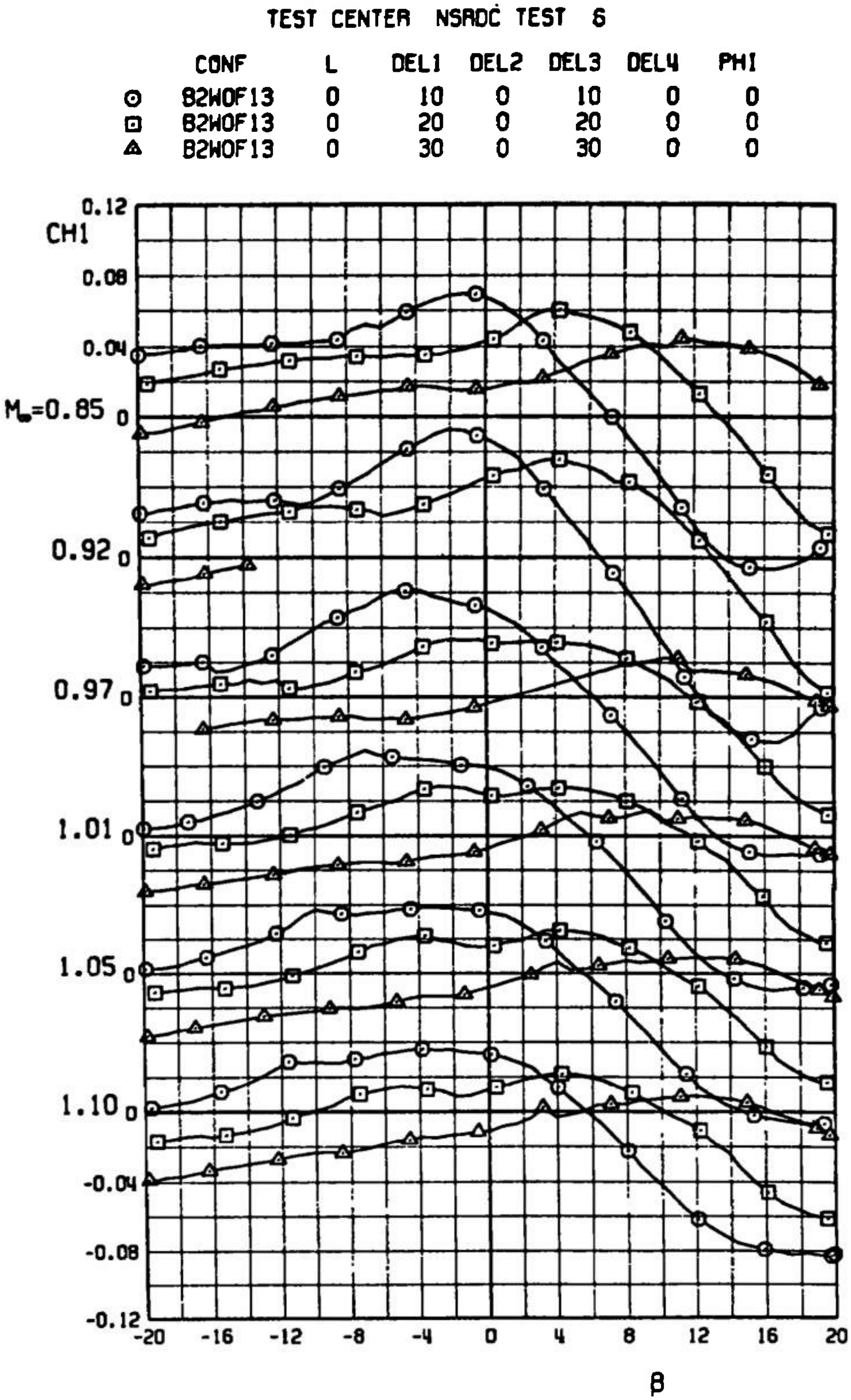

i. CH1 versus β
Figure 34. Concluded.

TEST CENTER NSRDC TEST 6

	CONF	L	DEL1	DEL2	DEL3	DEL4	PHI
⊙	B2W0F16	0	10	0	10	0	0
⊡	B2W0F16	0	20	0	20	0	0
▲	B2W0F16	0	30	0	30	0	0

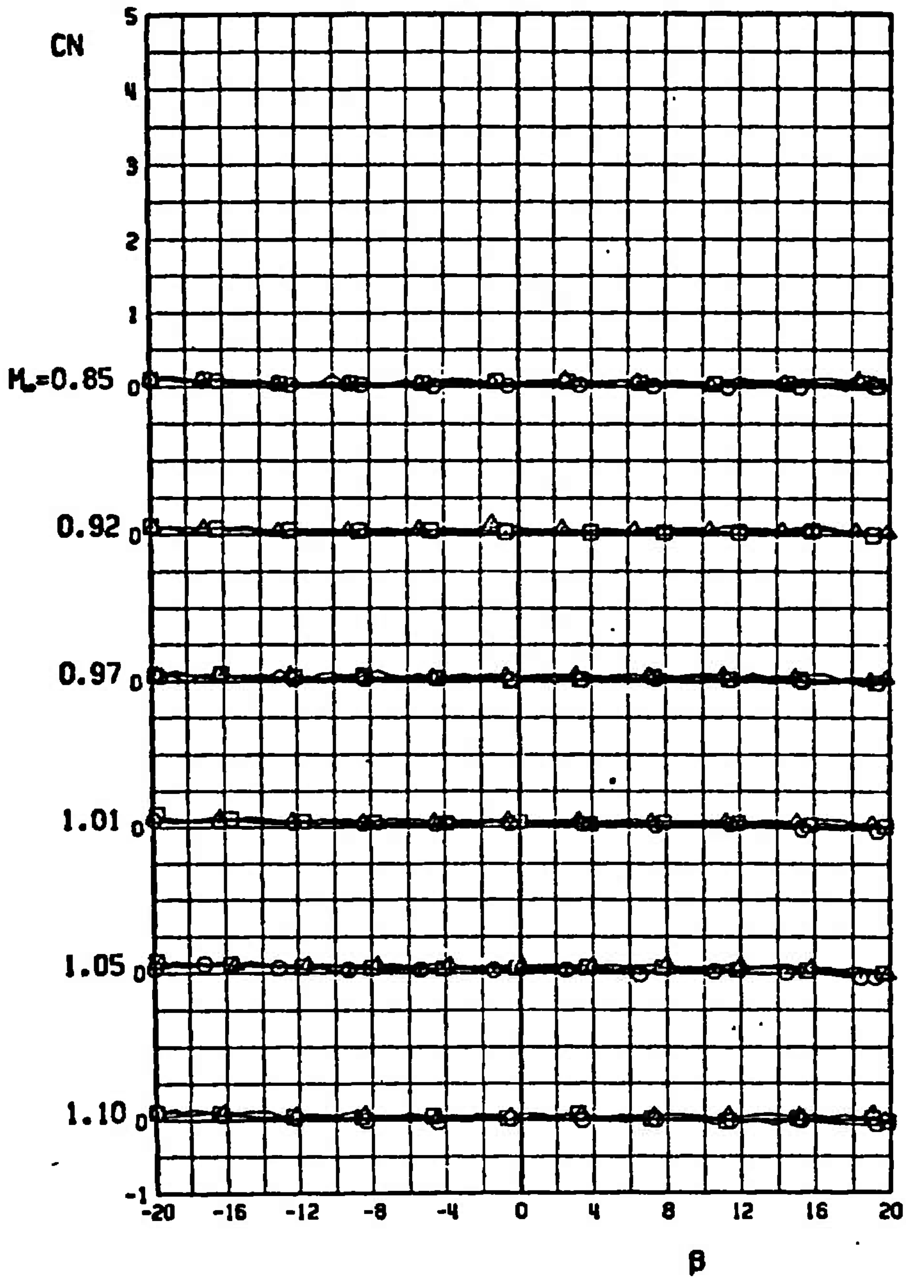

a. CN versus β

Figure 35. Test No. 6, comparison of aerodynamic coefficients of configuration B2W0F16 for various deflections of tail fins No. 1 and 3.

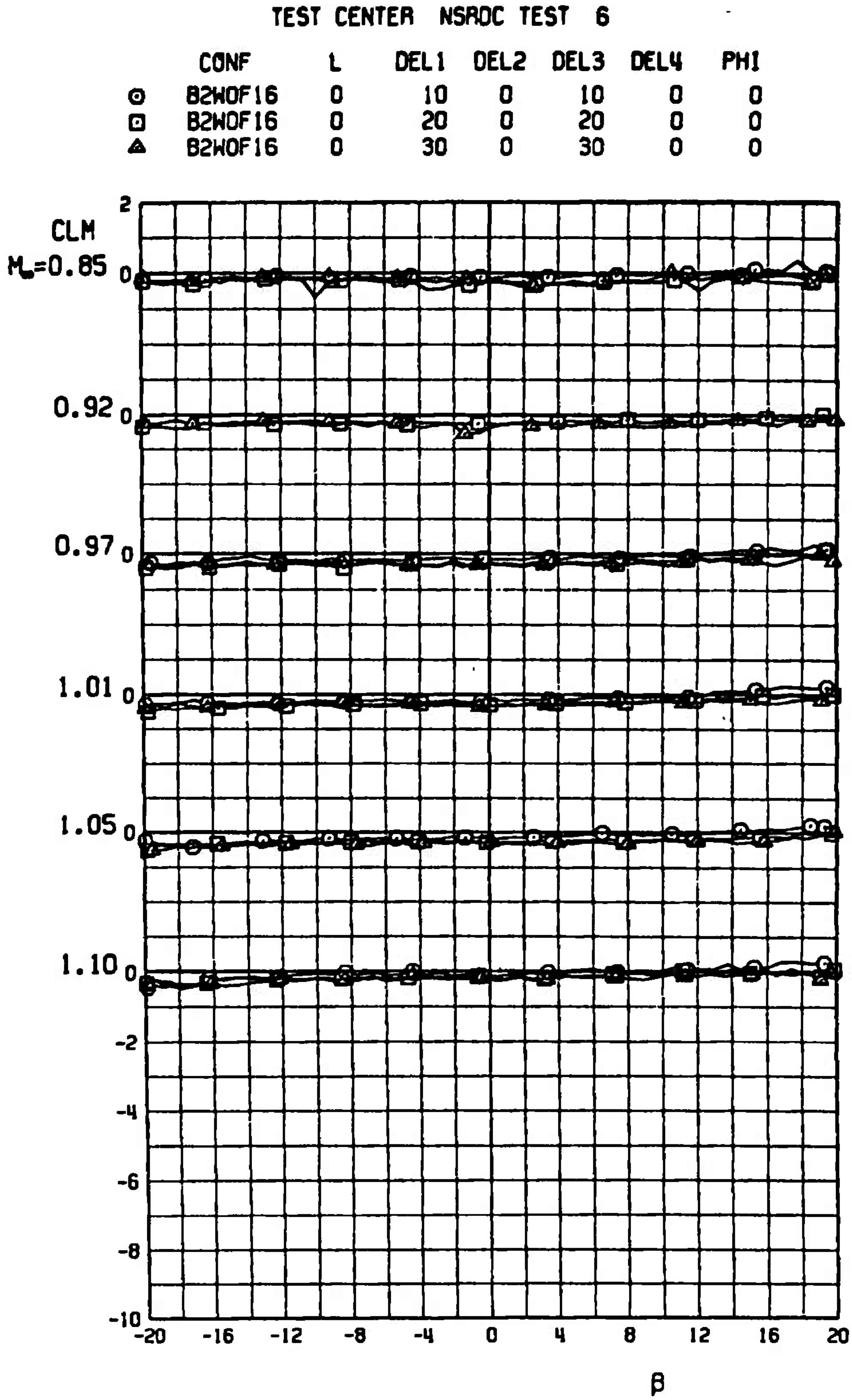

b. CLM versus β
Figure 35. Continued.

TEST CENTER NSRDC TEST 6

	CONF	L	DEL1	DEL2	DEL3	DEL4	PHI
⊙	B2W0F16	0	10	0	10	0	0
⊡	B2W0F16	0	20	0	20	0	0
△	B2W0F16	0	30	0	30	0	0

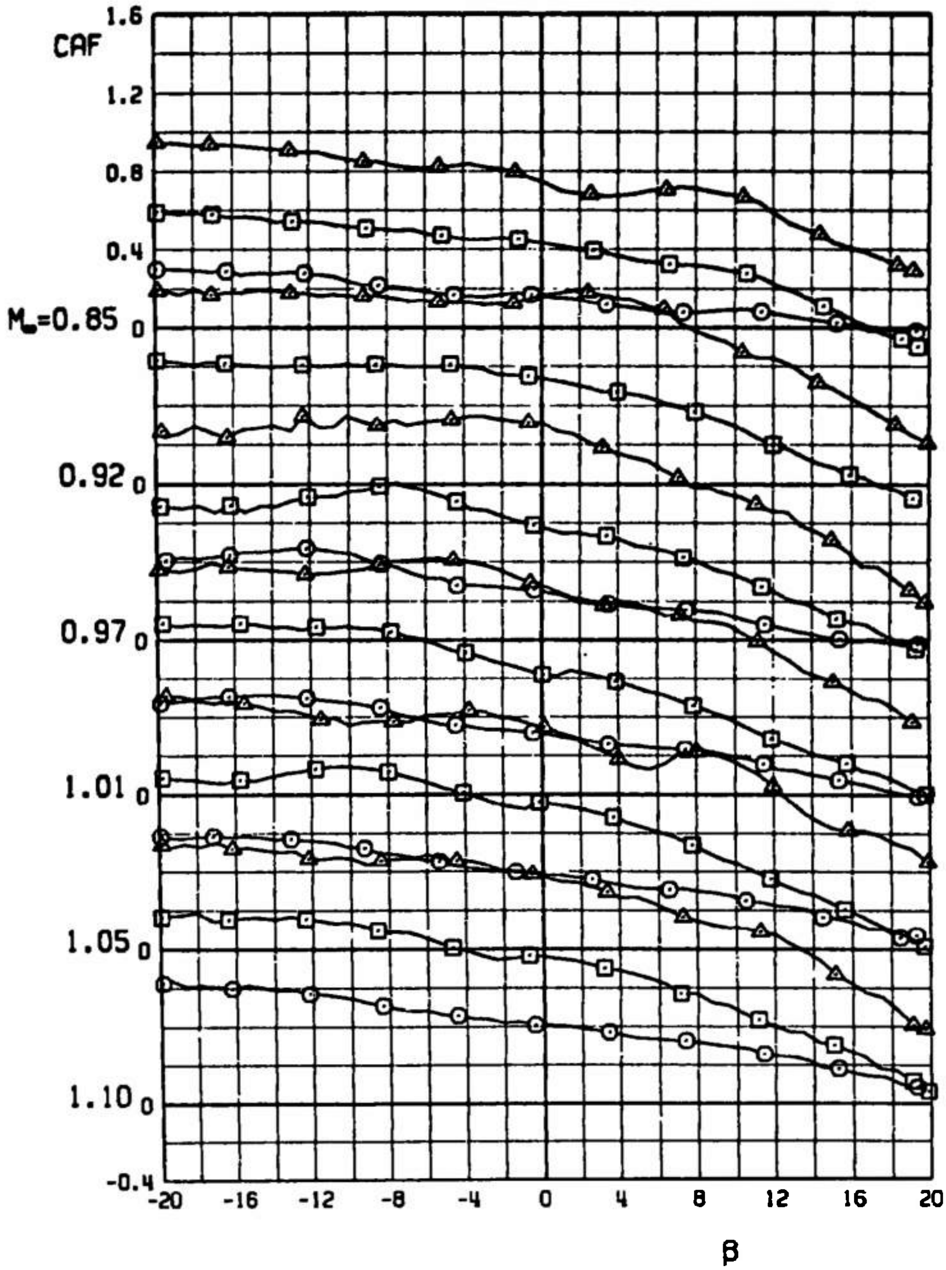

c. CAF versus β
Figure 35. Continued.

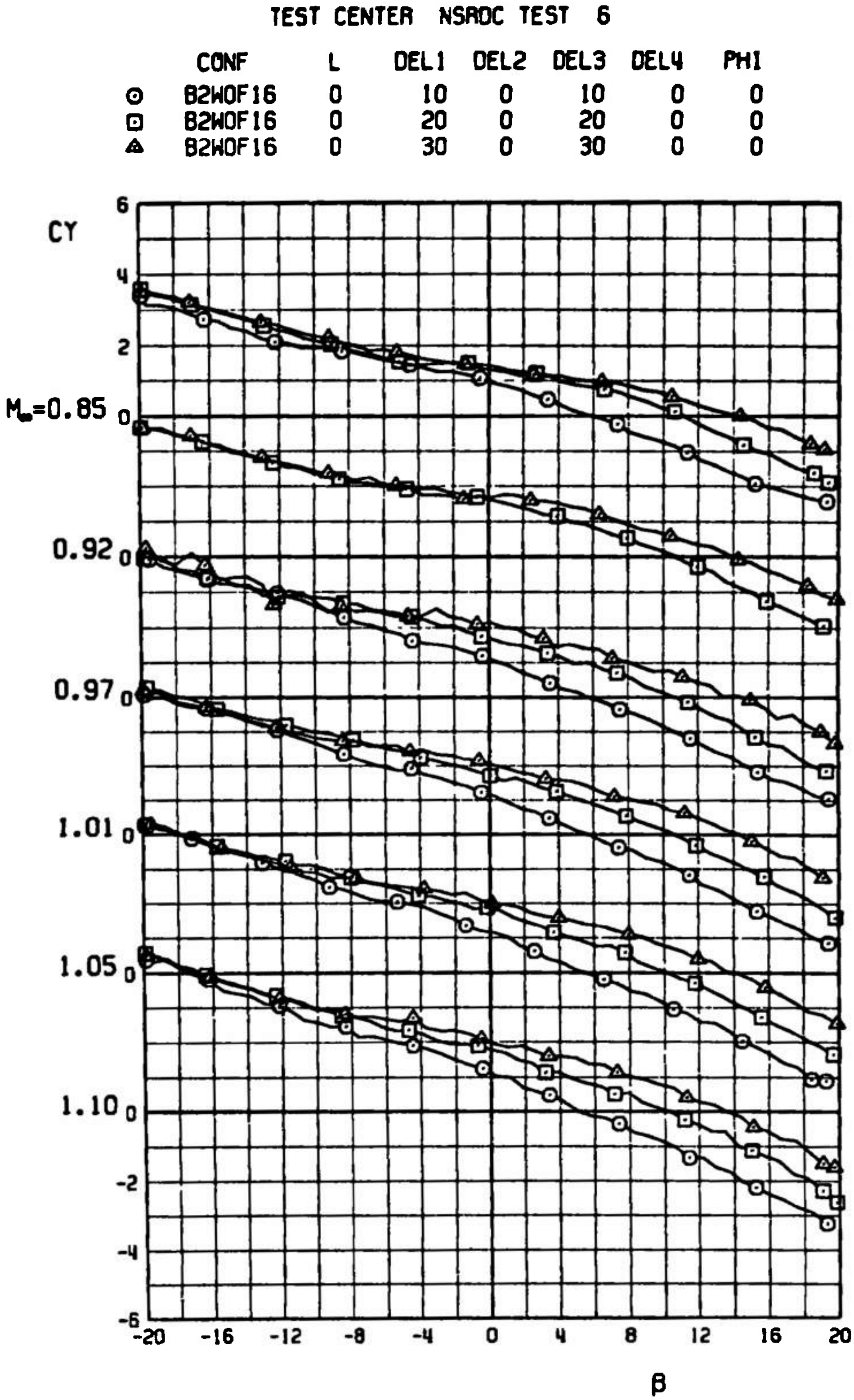

d. CY versus β
Figure 35. Continued.

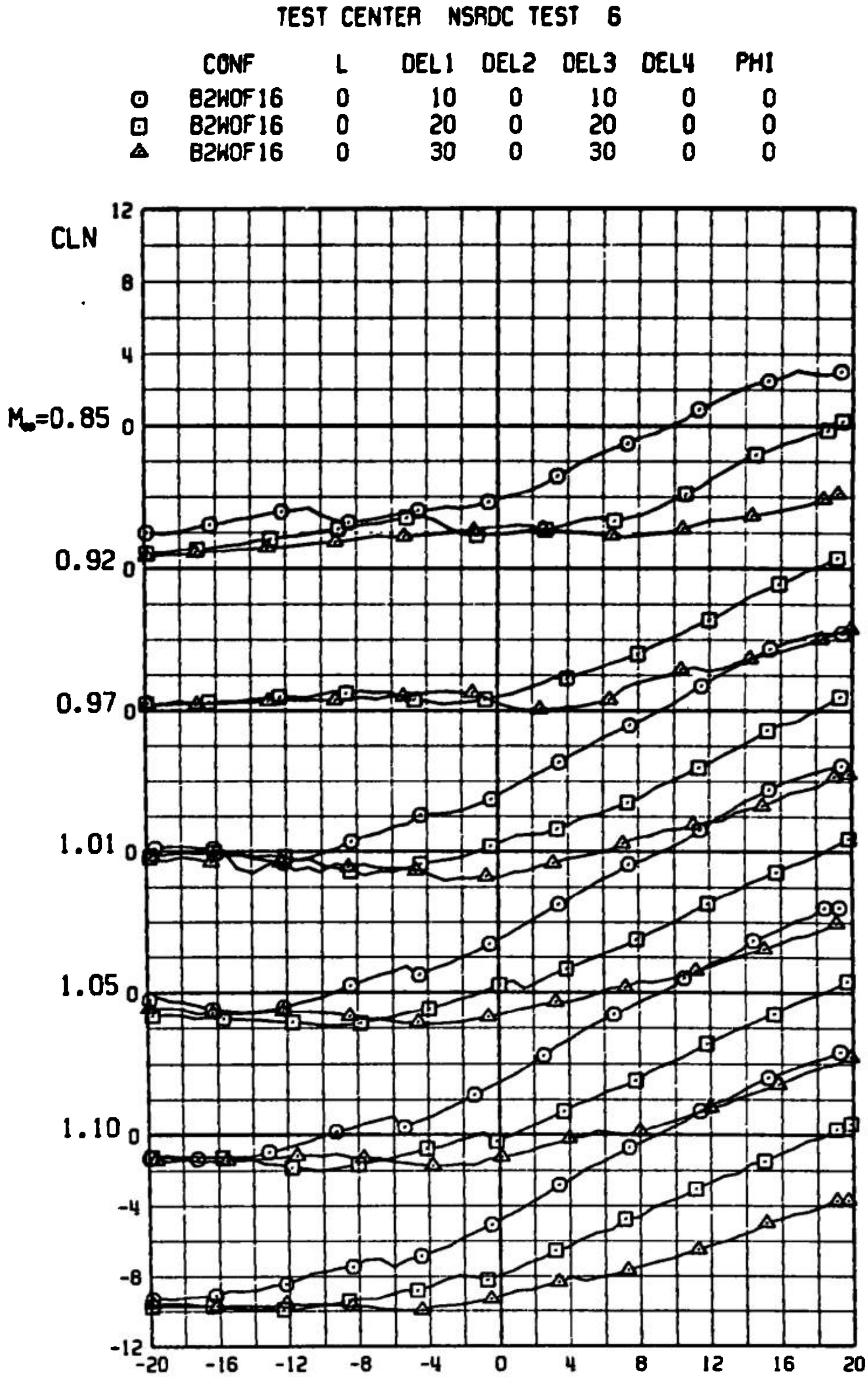

e. CLN versus β

Figure 35. Continued.

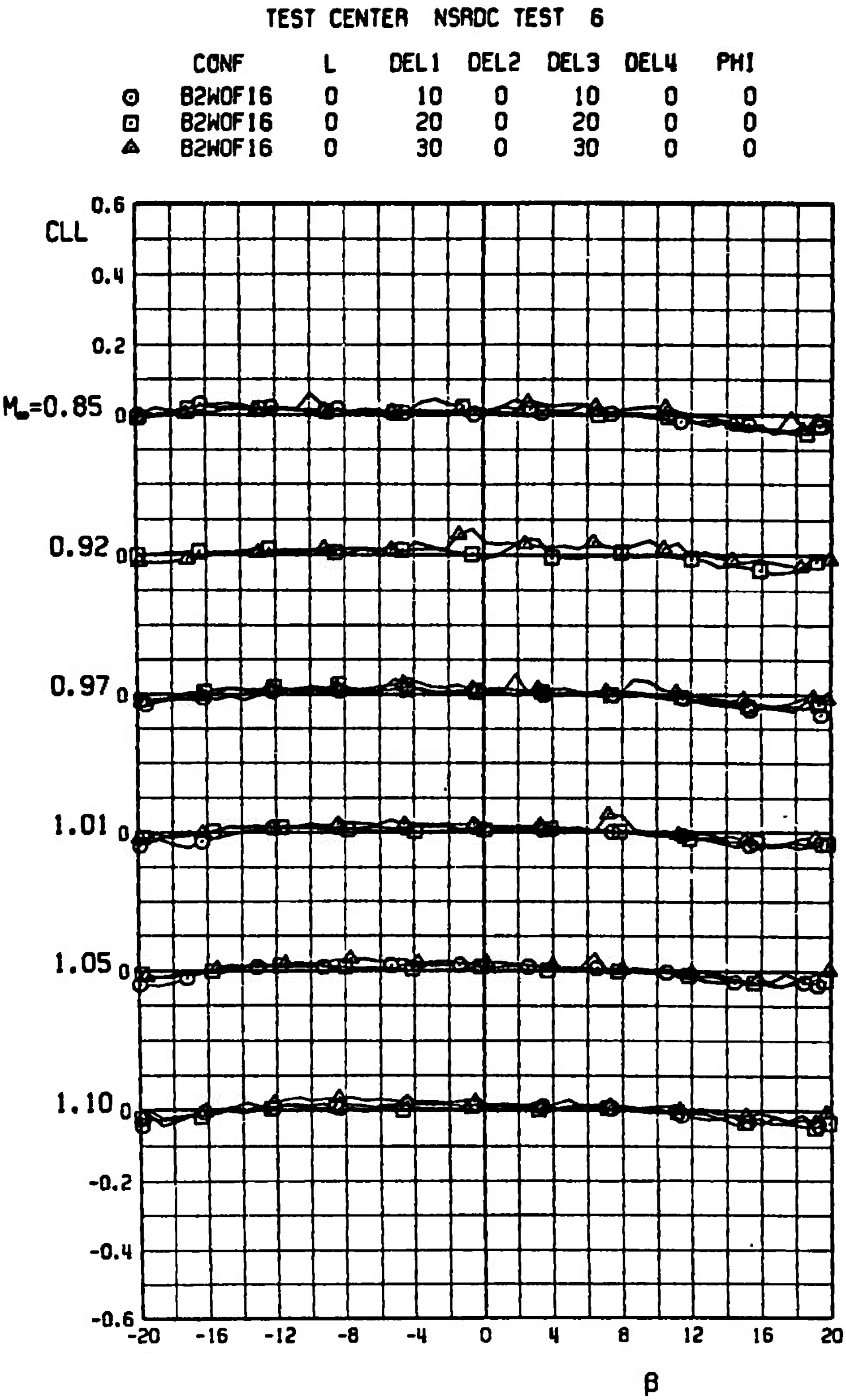

f. CLL versus β
Figure 35. Continued.

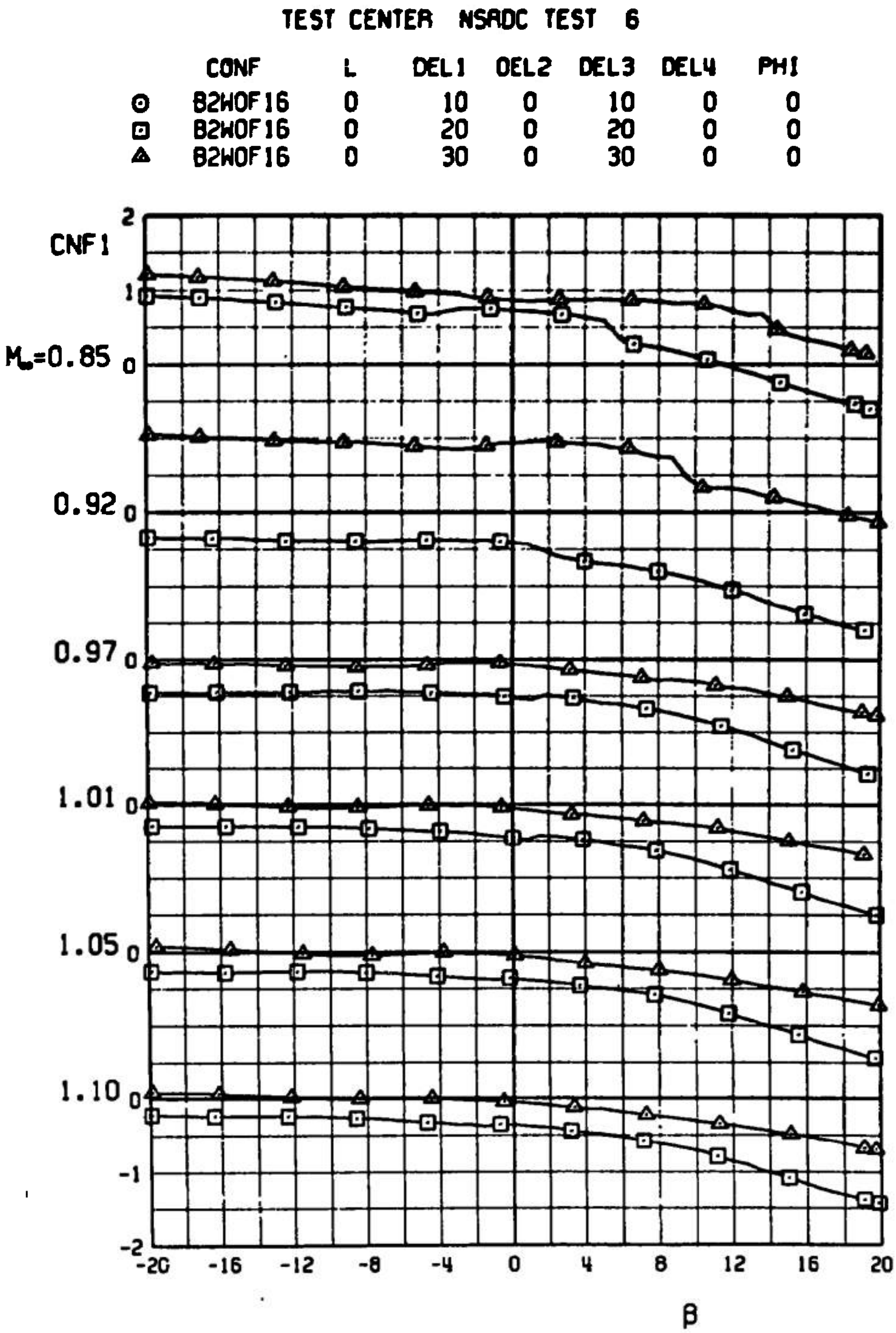

g. CNF1 versus β
Figure 35. Continued.

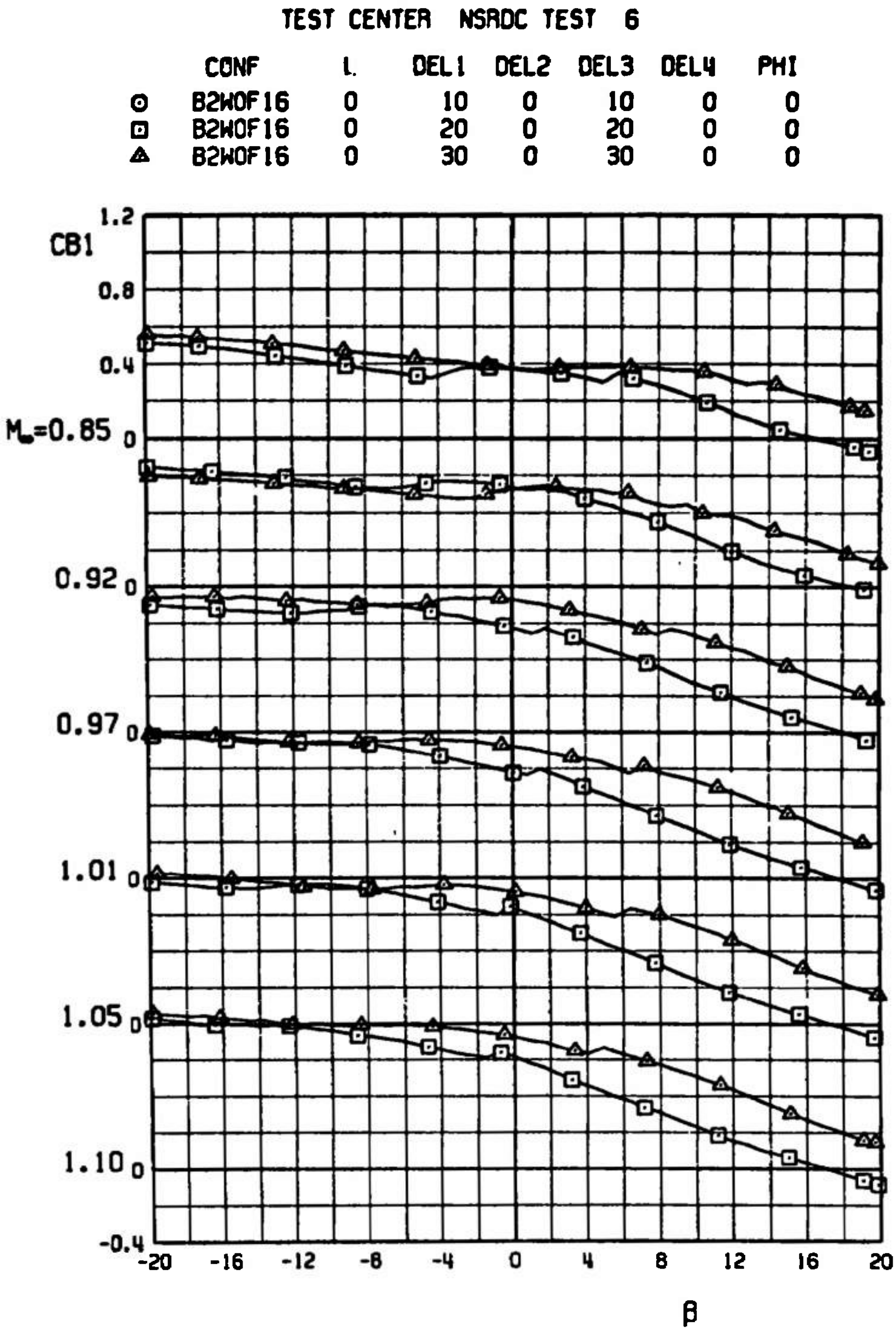

h. CB1 versus β
Figure 35. Continued.

TEST CENTER NSROC TEST 6

	CONF	L	DEL1	DEL2	DEL3	DEL4	PHI
⊙	B2W0F16	0	10	0	10	0	0
⊡	B2W0F16	0	20	0	20	0	0
△	B2W0F16	0	30	0	30	0	0

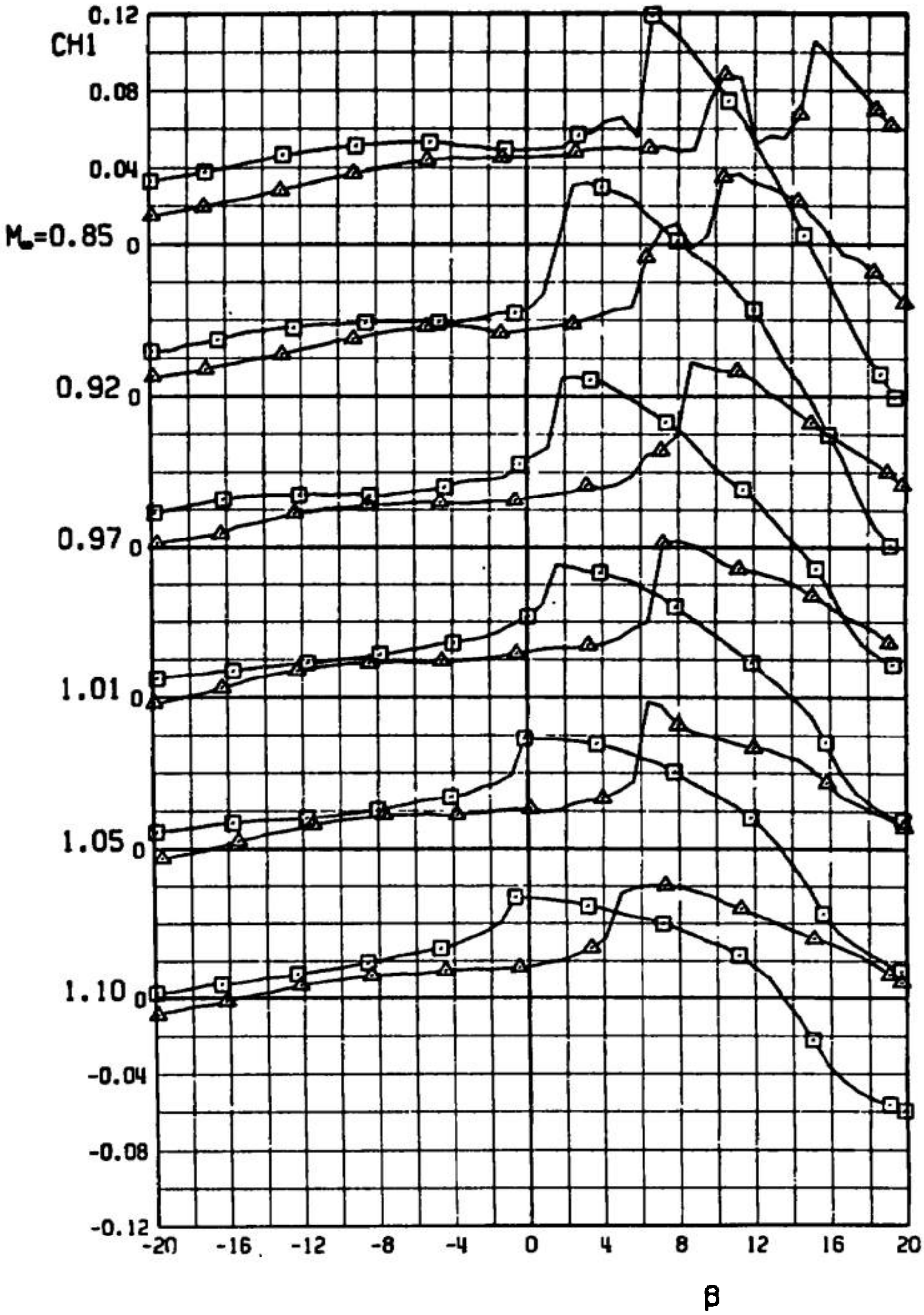

i. CH1 versus β

Figure 35. Concluded.

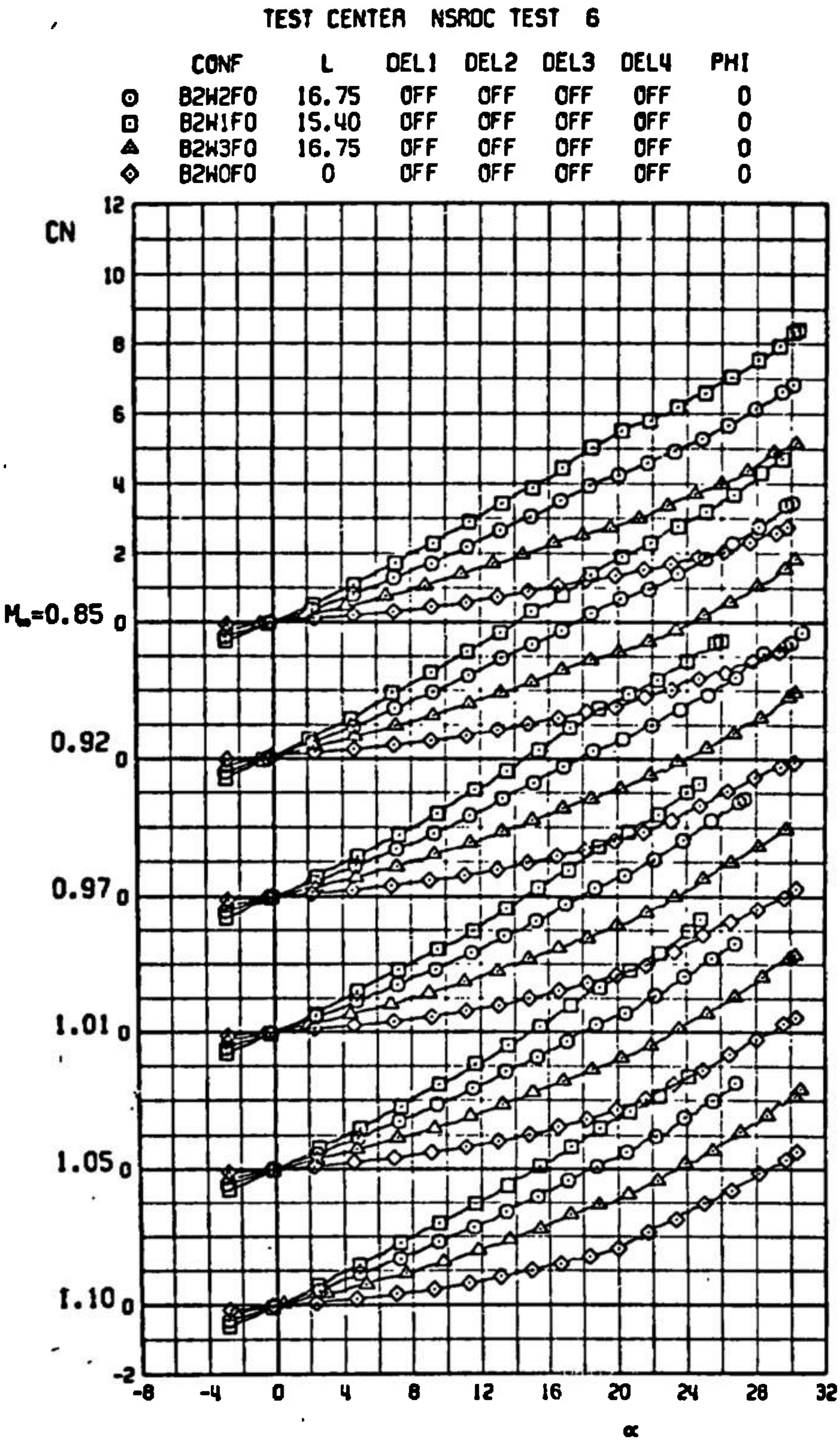

a. CN versus α

Figure 36. Test No. 6, comparison of aerodynamic coefficients of configurations B2W2F0, L = 16.75; B2W1F0, L = 15.40; B2W3F0, L = 16.75; and B2W0F0, L = 0.

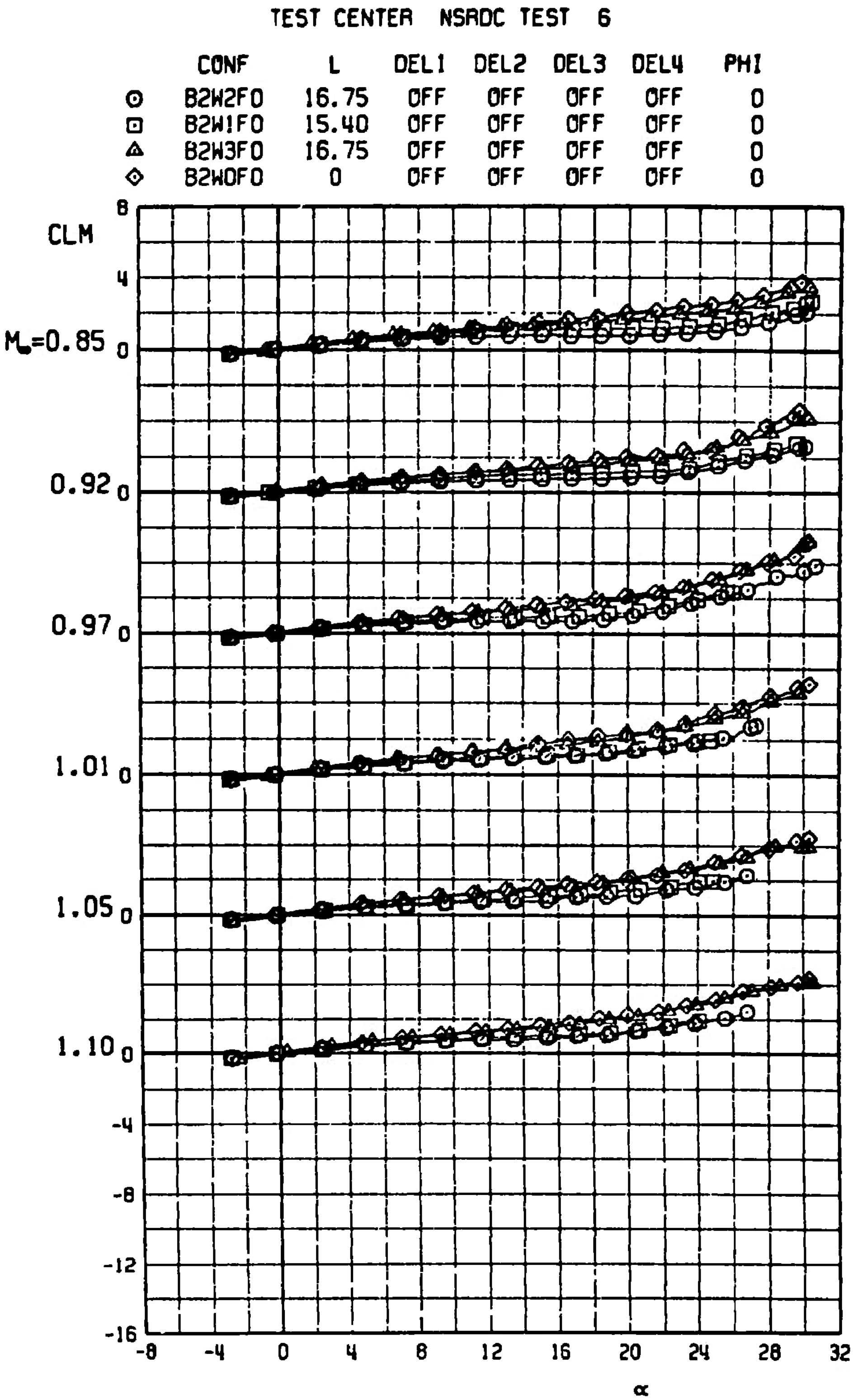

b. CLM versus α
Figure 36. Continued.

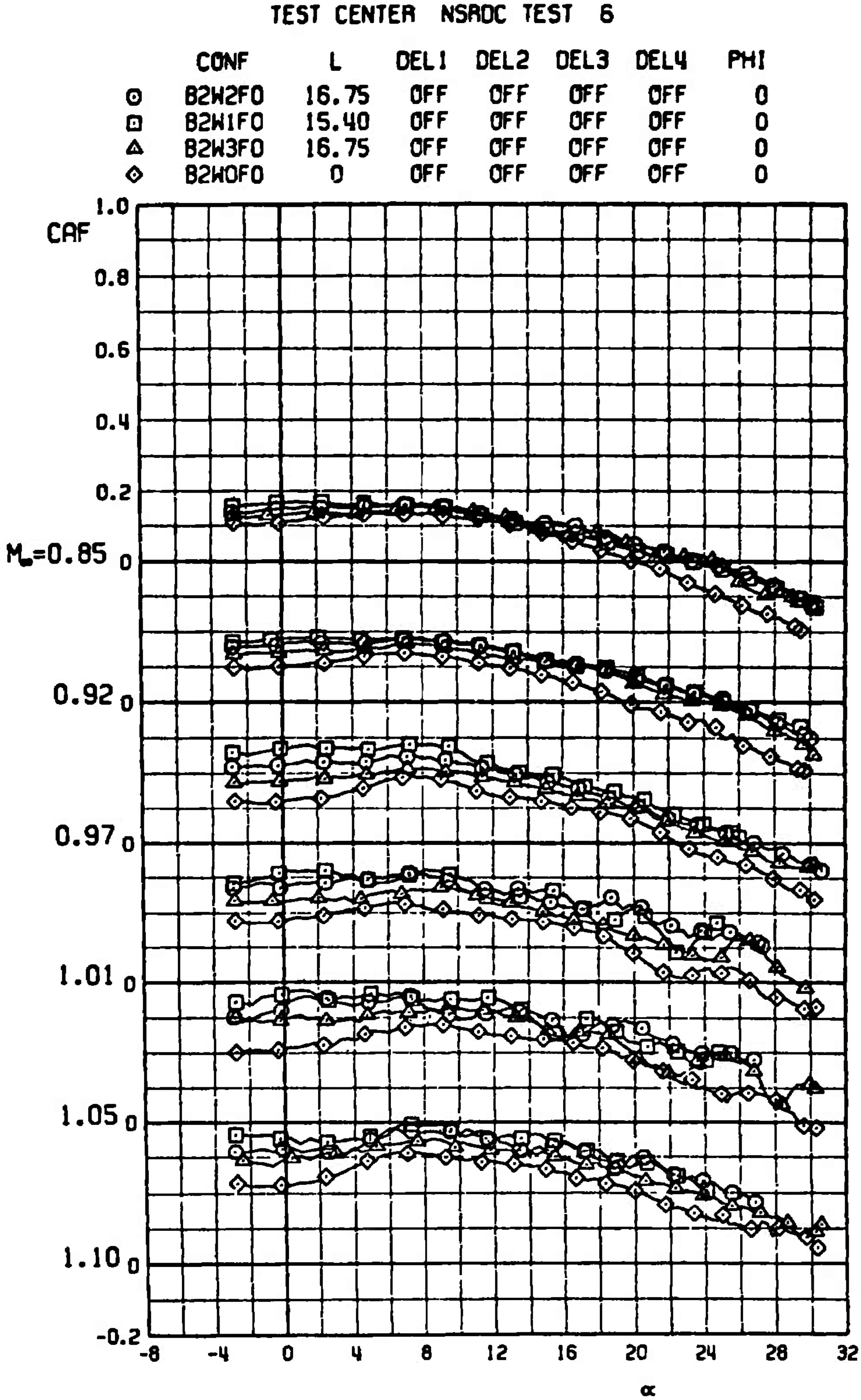

c. CAF versus α
Figure 36. Continued.

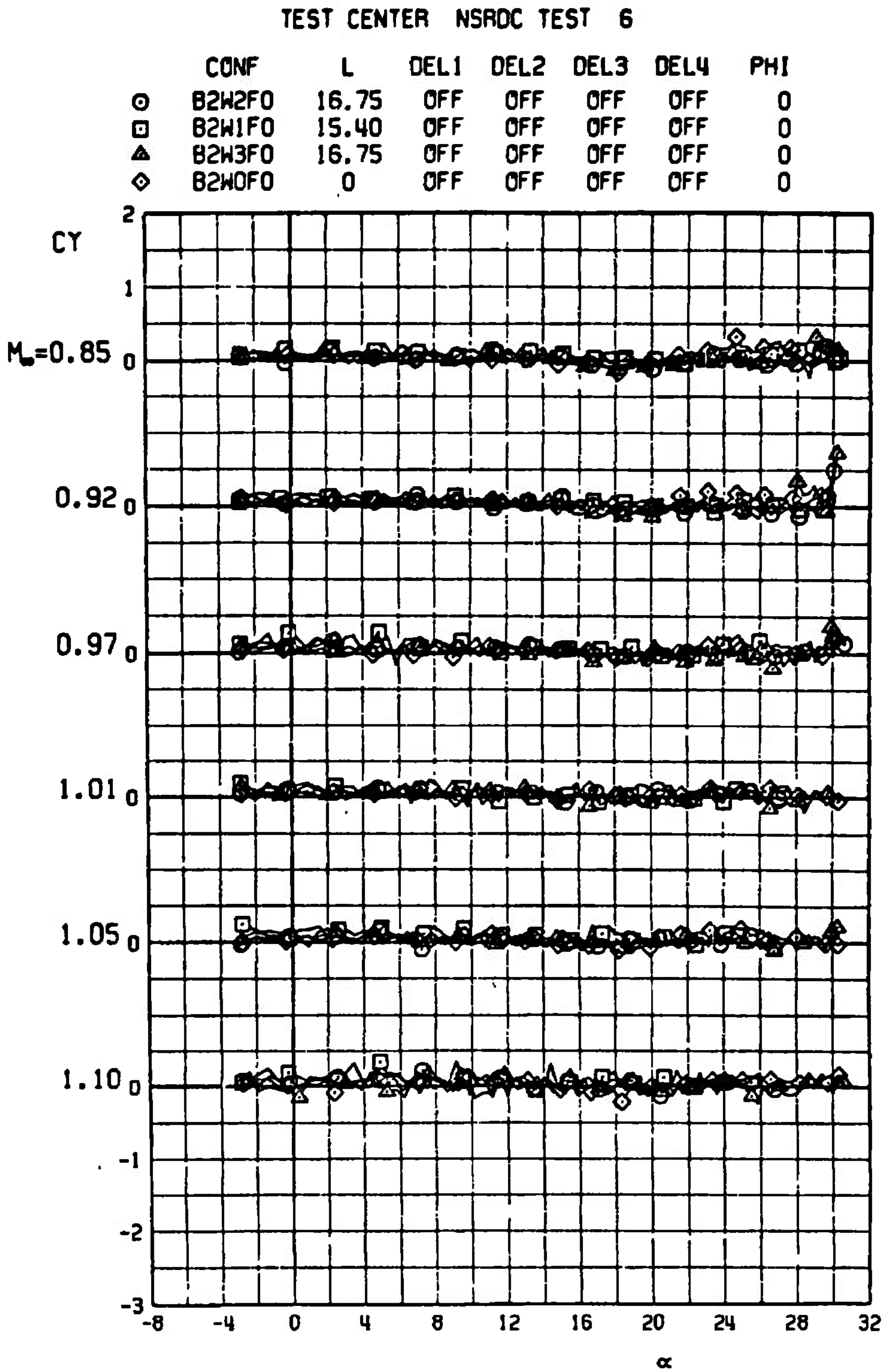

d. CY versus α
Figure 36. Continued.

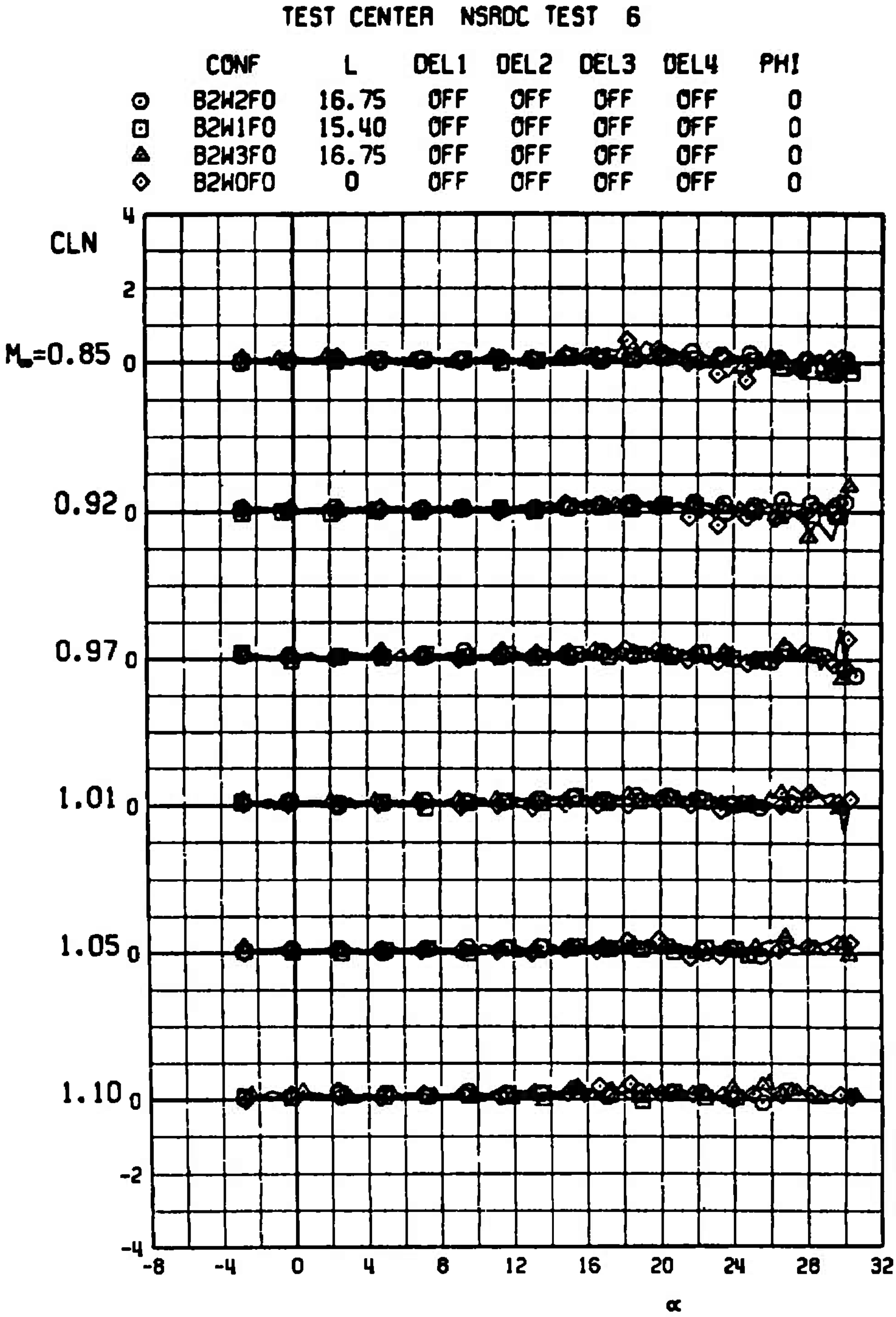

e. CLN versus *α*
Figure 36. Continued.

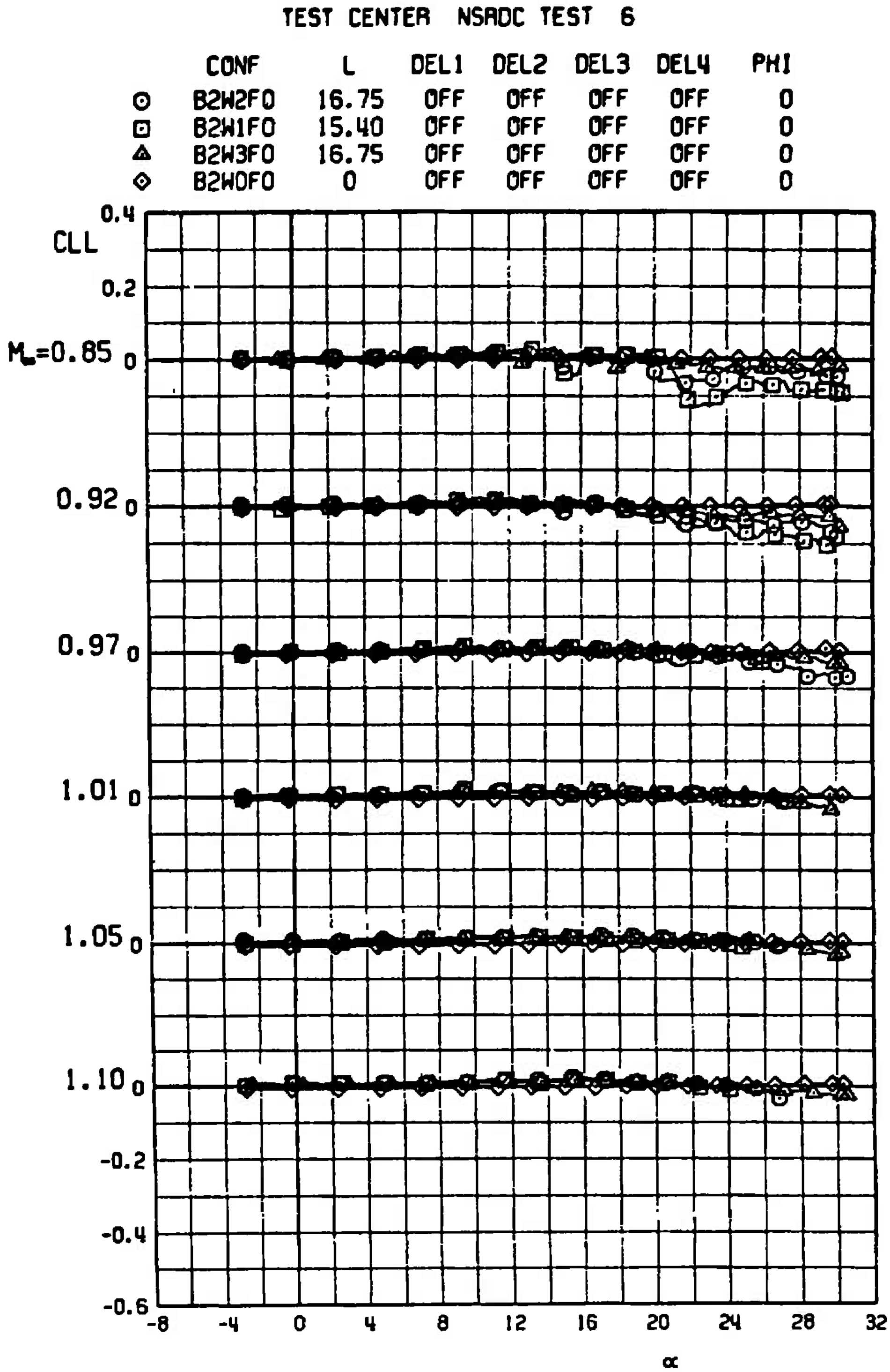

f. CLL versus α

Figure 36. Concluded.

TEST CENTER NSRDC TEST 6

	CONF	L	DEL1	DEL2	DEL3	DEL4	PHI
⊙	B2W3F12	16.75	0	0	0	0	0
⊡	B2W2F12	16.75	0	0	0	0	0
△	B2W1F12	15.40	0	0	0	0	0

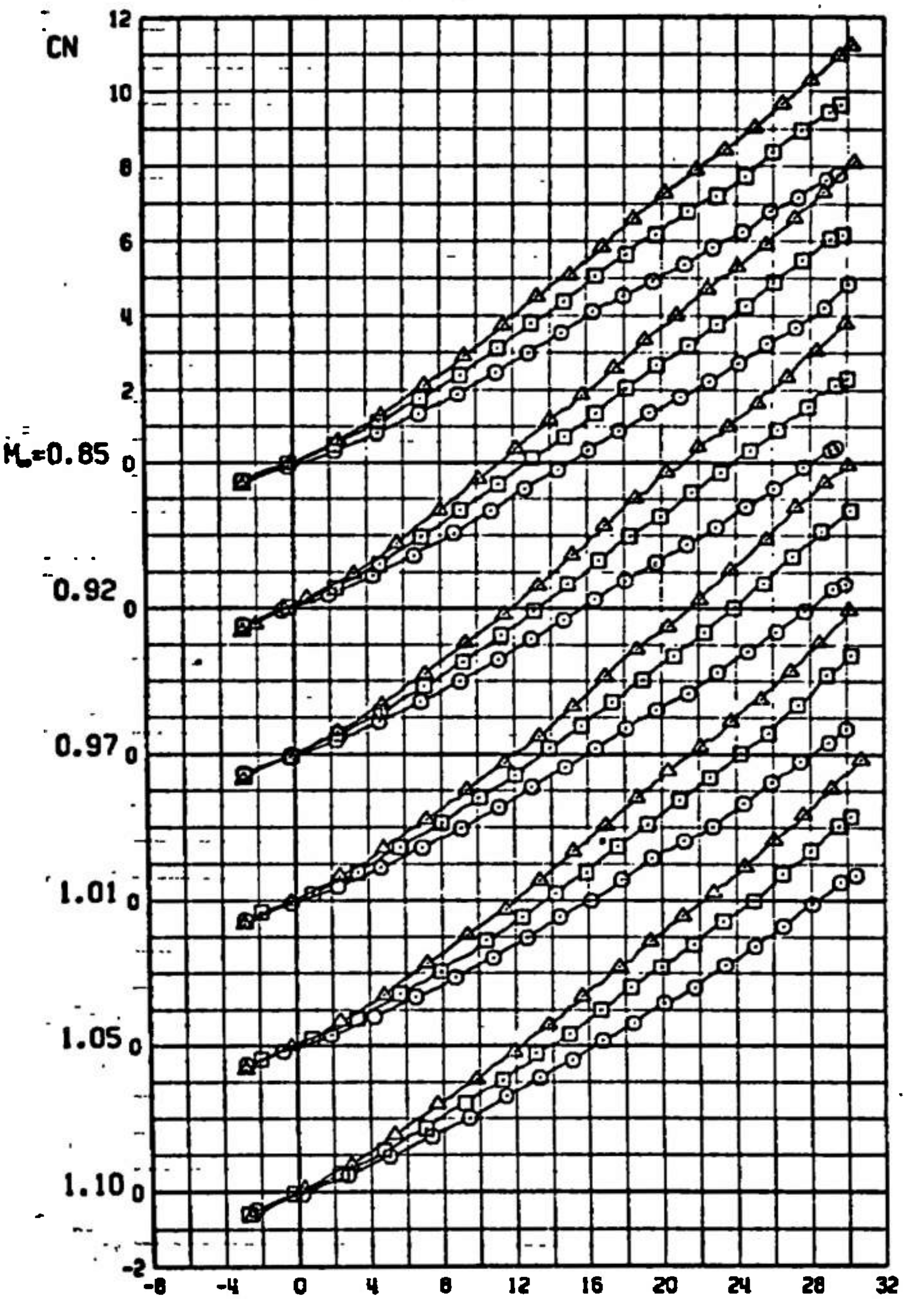

a. CN versus α

Figure 37. Test No. 6, comparison of aerodynamic coefficients of configurations B2W3F12, L = 16.75; B2W2F12, L = 16.75; and B2W1F12, L = 15.40.

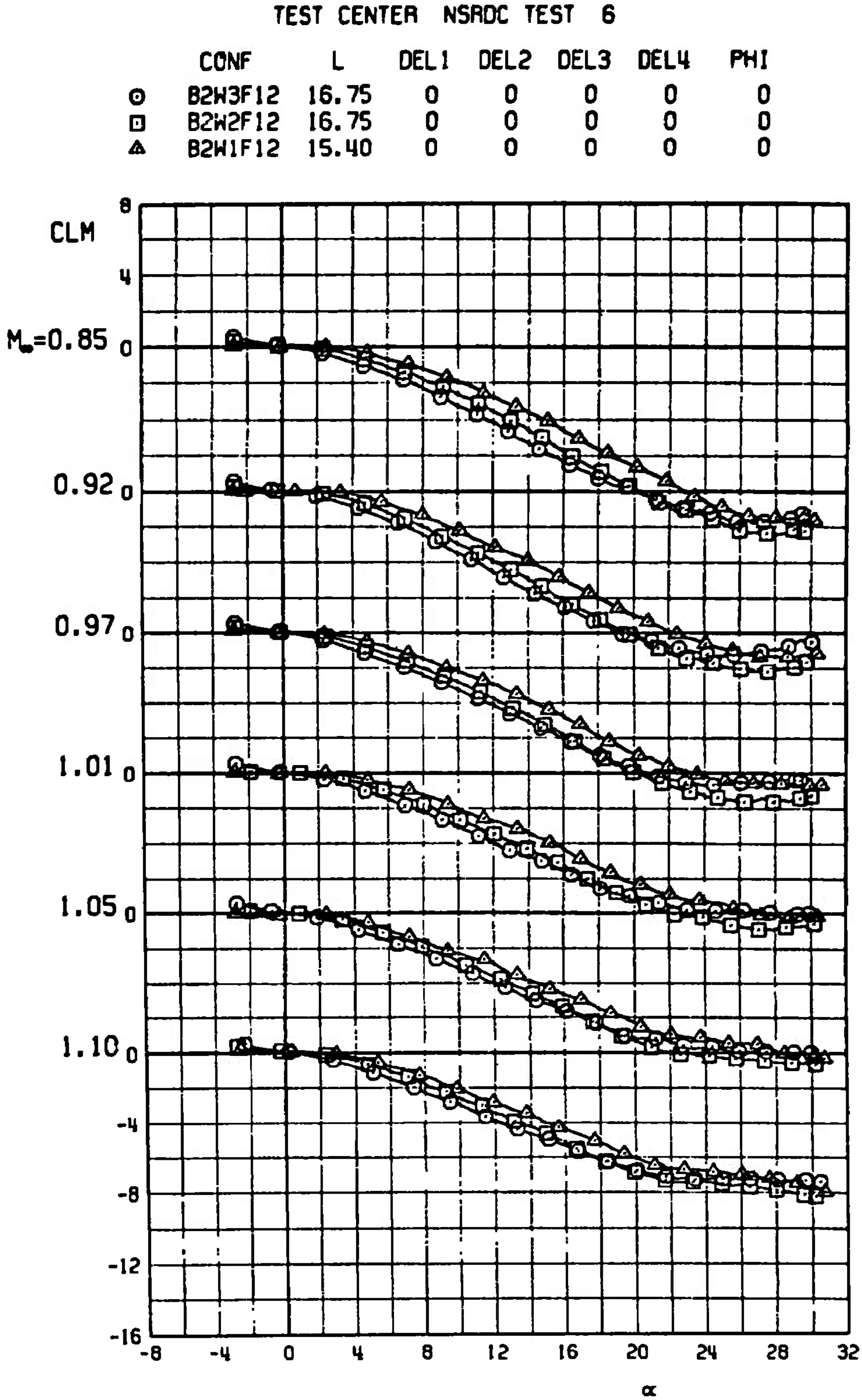

b. CLM versus α
Figure 37. Continued.

TEST CENTER NSRDC TEST 6

	CONF	L	DEL1	DEL2	DEL3	DEL4	PHI
⊙	B2W3F12	16.75	0	0	0	0	0
⊡	B2W2F12	16.75	0	0	0	0	0
△	B2W1F12	15.40	0	0	0	0	0

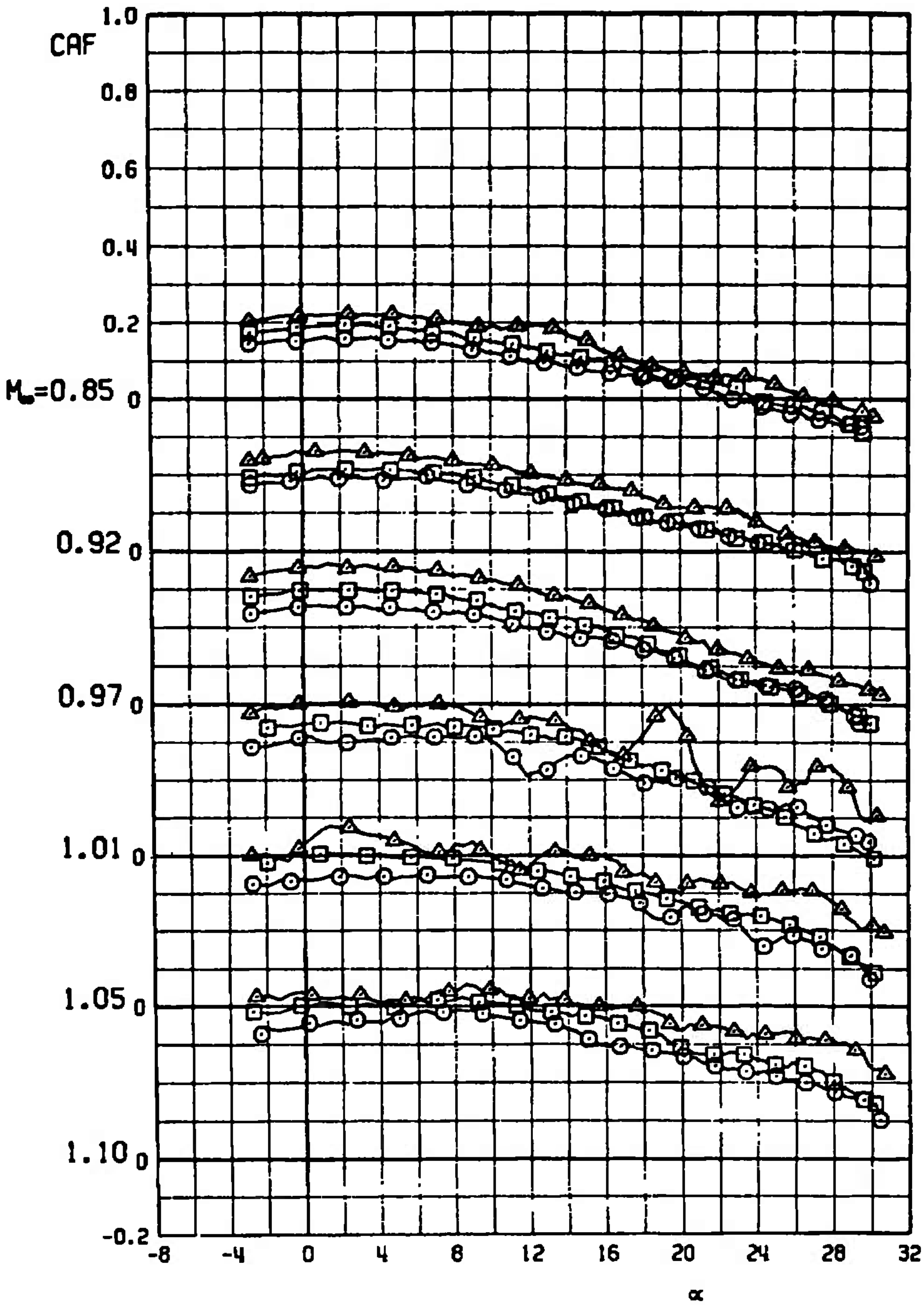

c. CAF versus α
Figure 37. Continued.

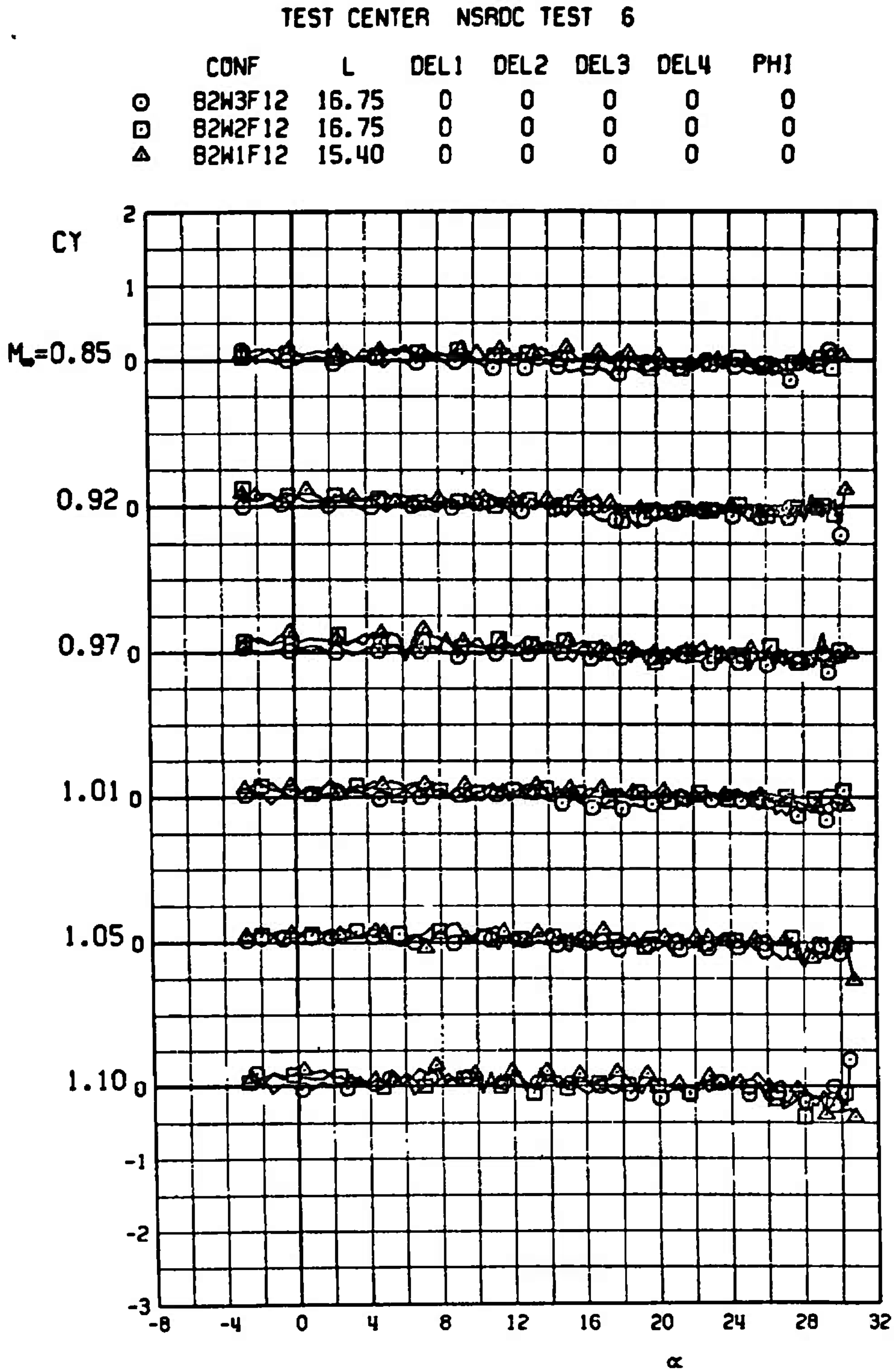

d. CY versus α
Figure 37. Continued.

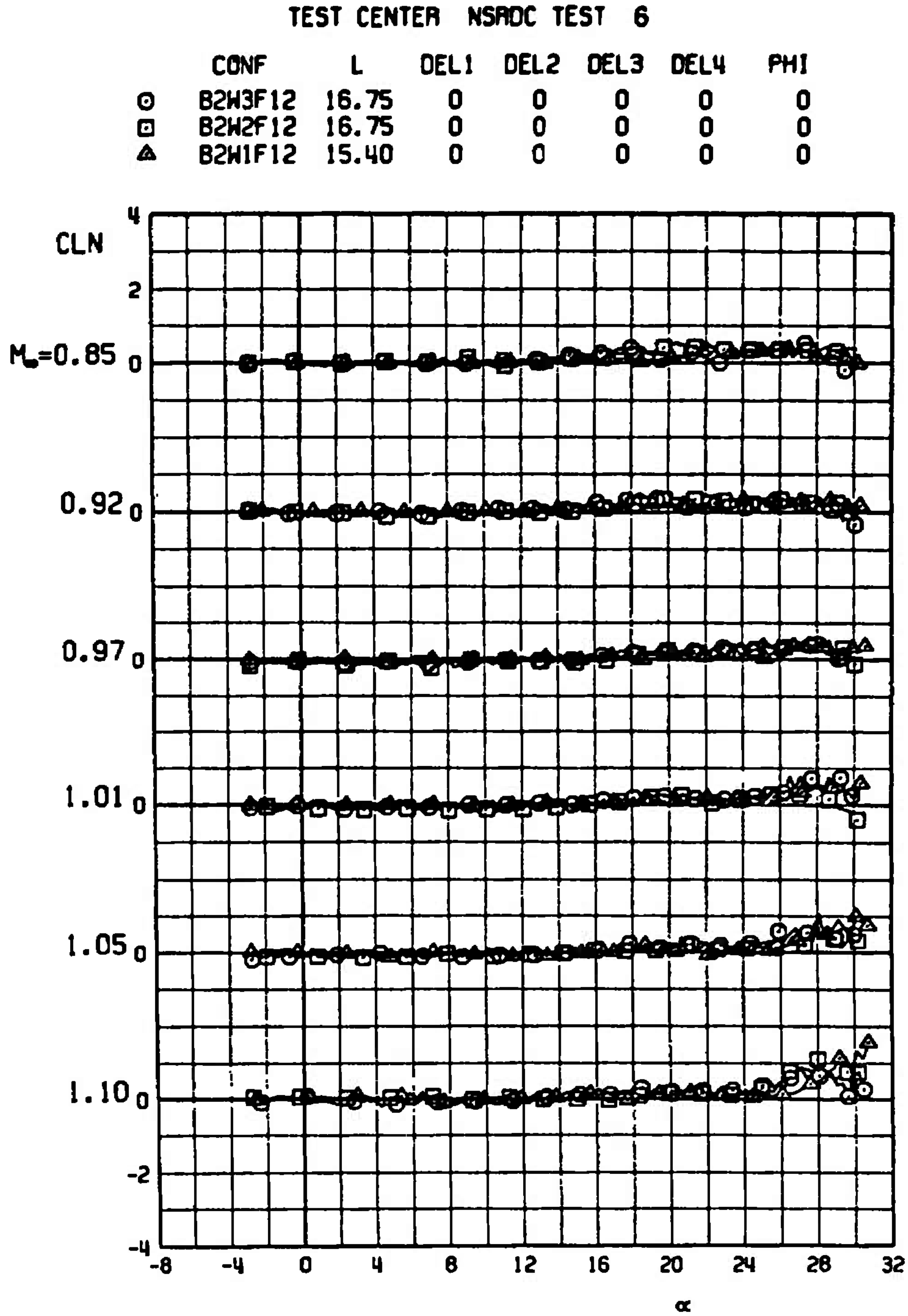

e. CLN versus α
Figure 37. Continued.

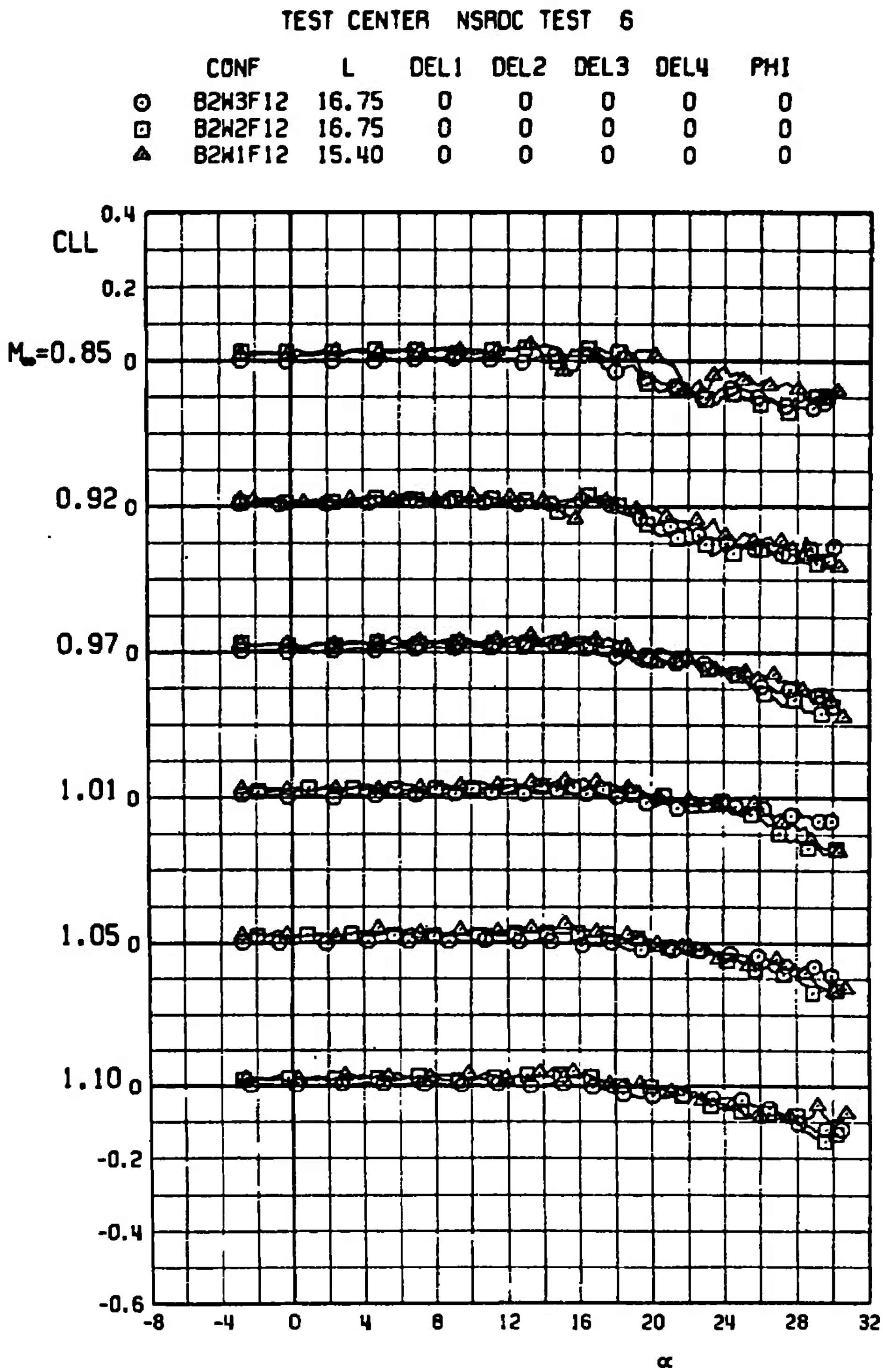

f. CLL versus α
Figure 37. Continued.

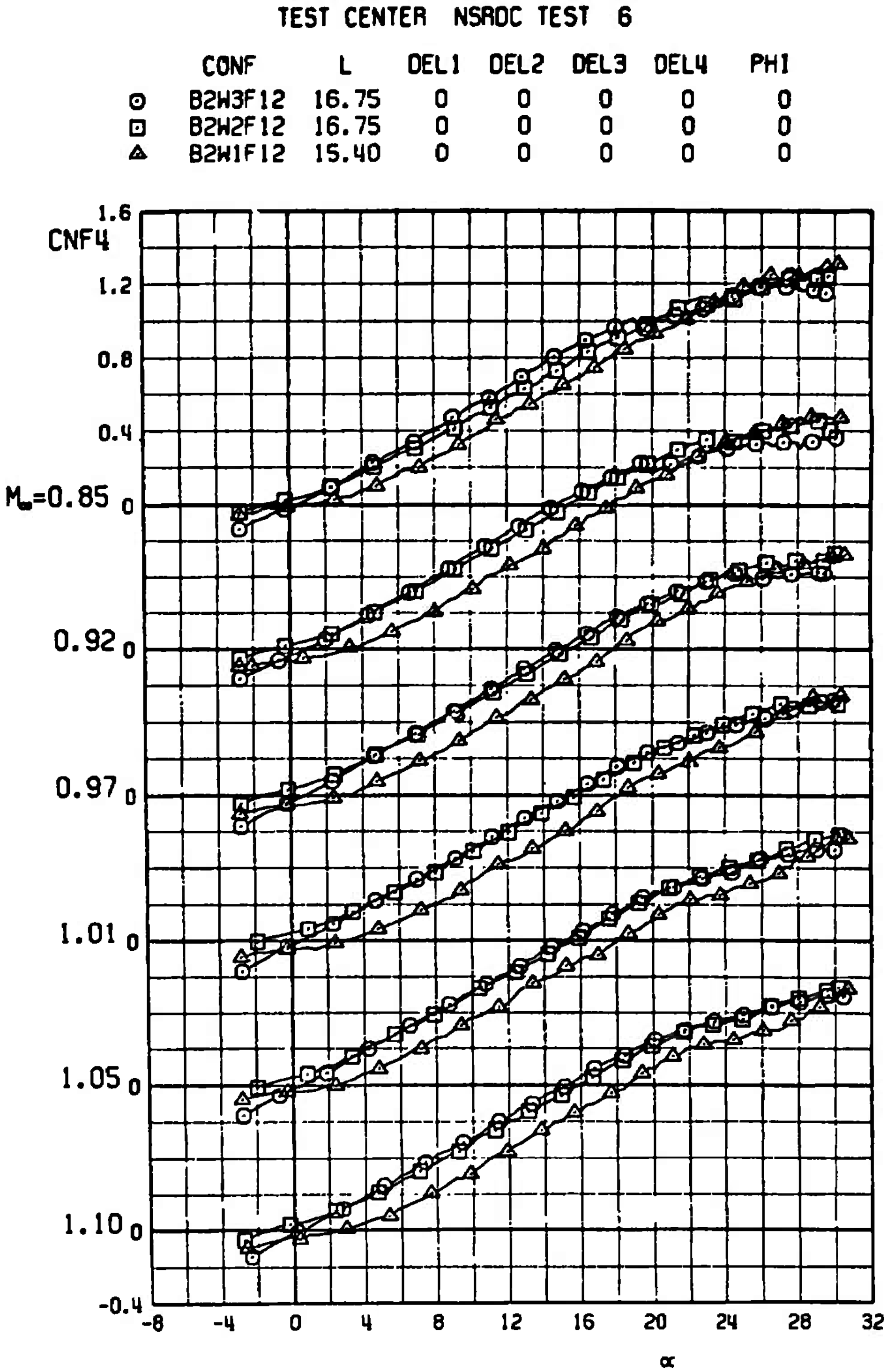

g. CNF4 versus α

Figure 37. Continued.

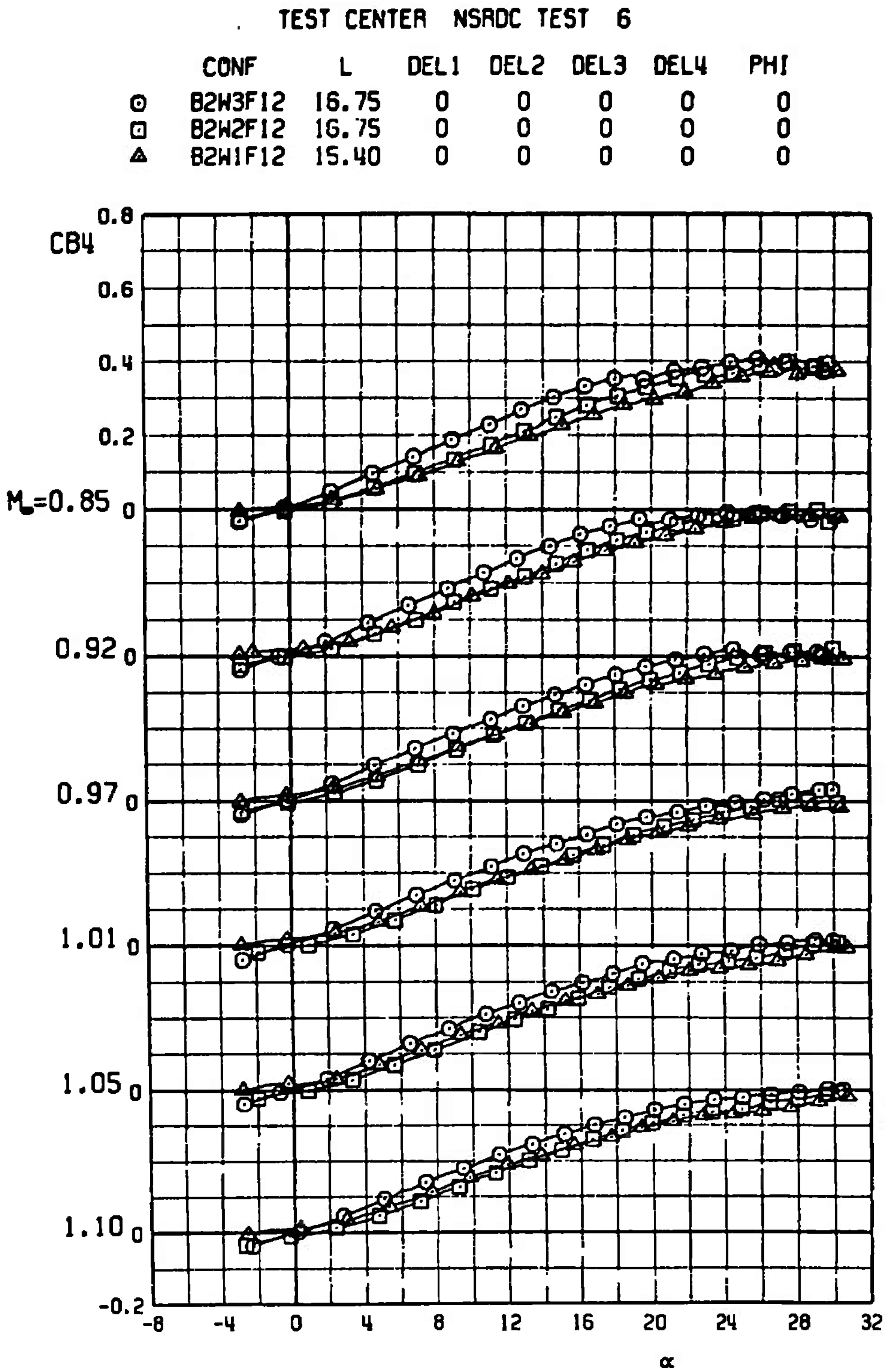

h. CB4 versus α
Figure 37. Continued.

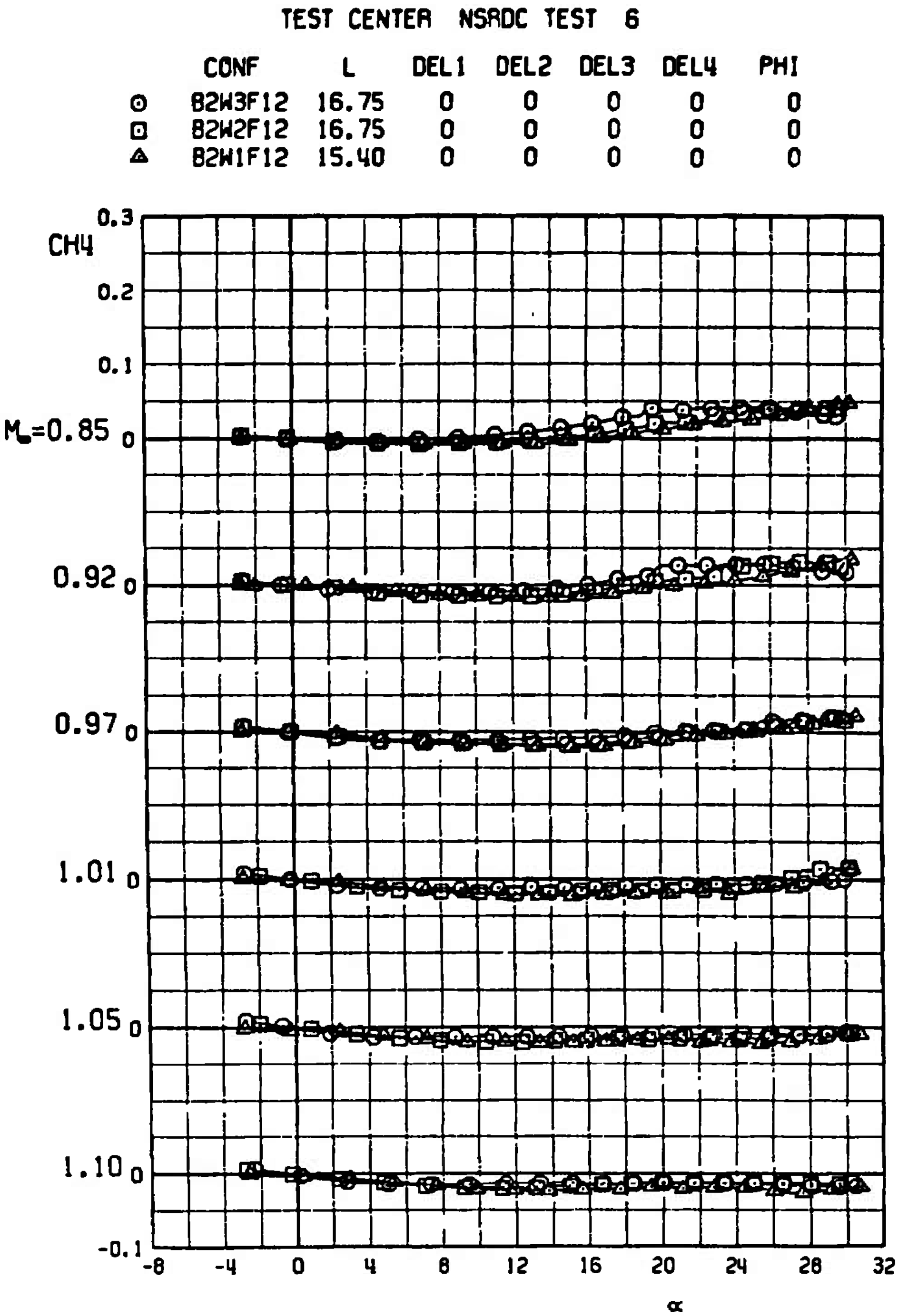

i. CH4 versus α
Figure 37. Concluded.

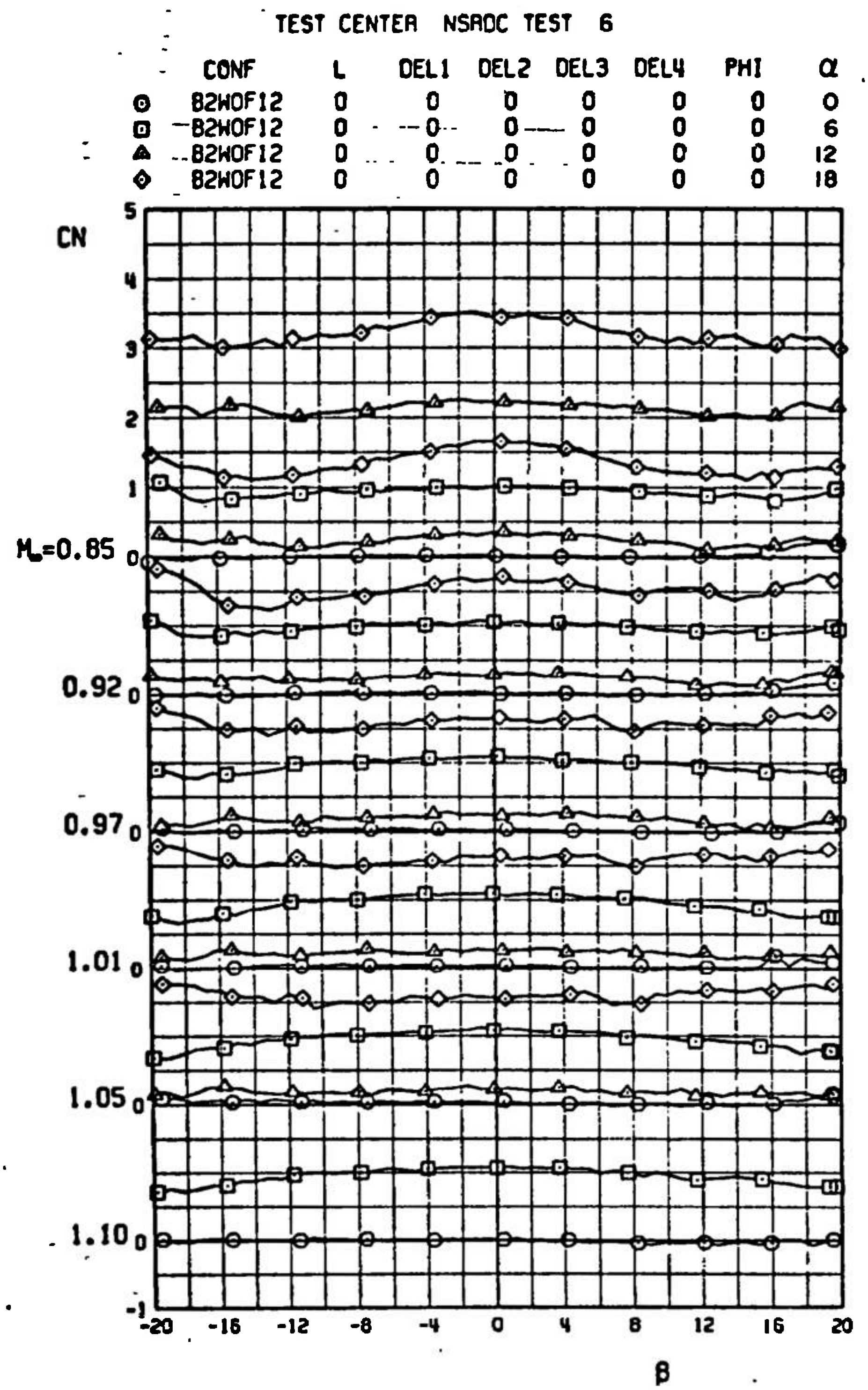

a. CN versus α

Figure 38. Test No. 6, comparison of aerodynamic coefficients of configuration B2W0F12 for combinations of α and β settings.

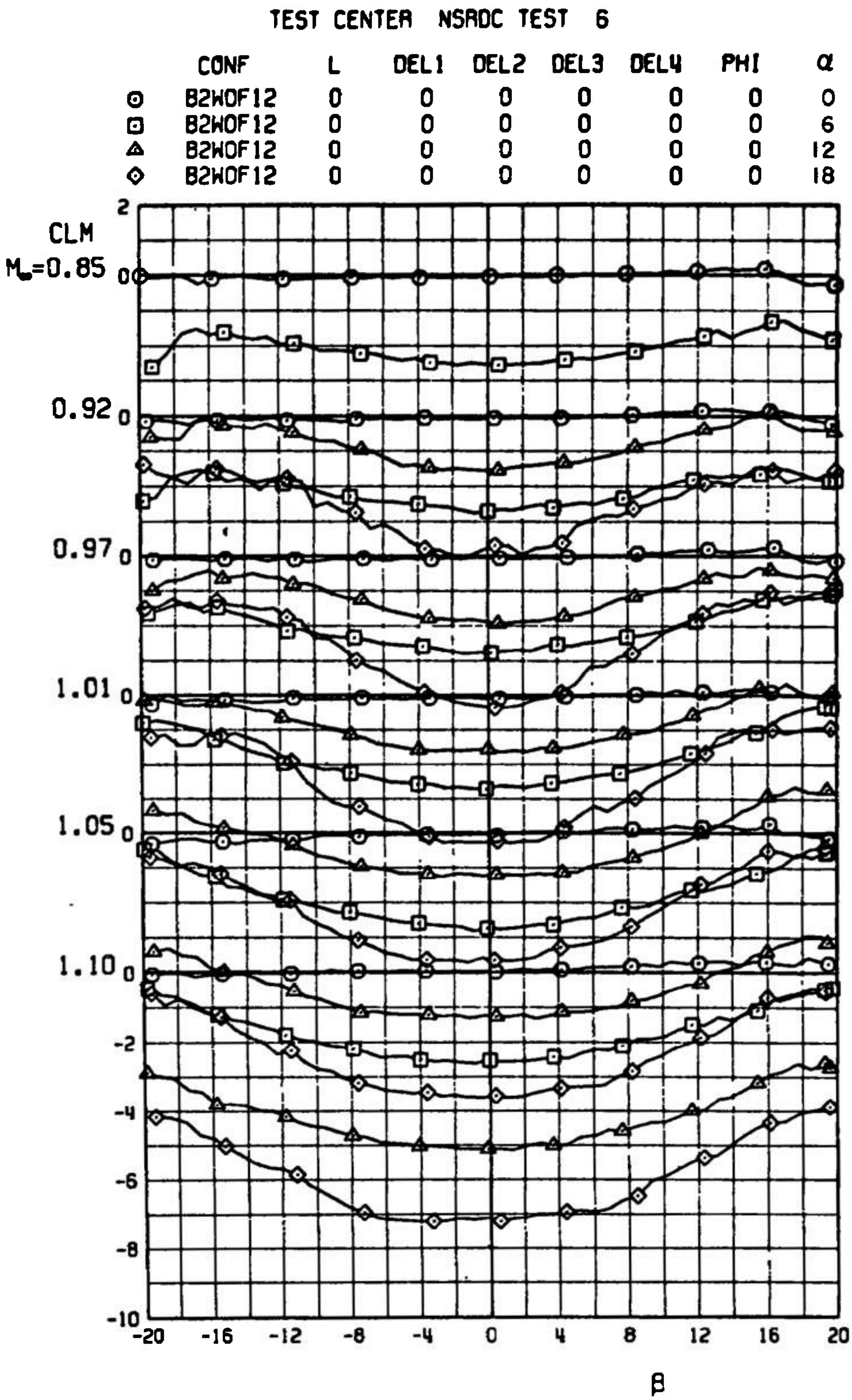

b. CLM versus α
Figure 38. Continued.

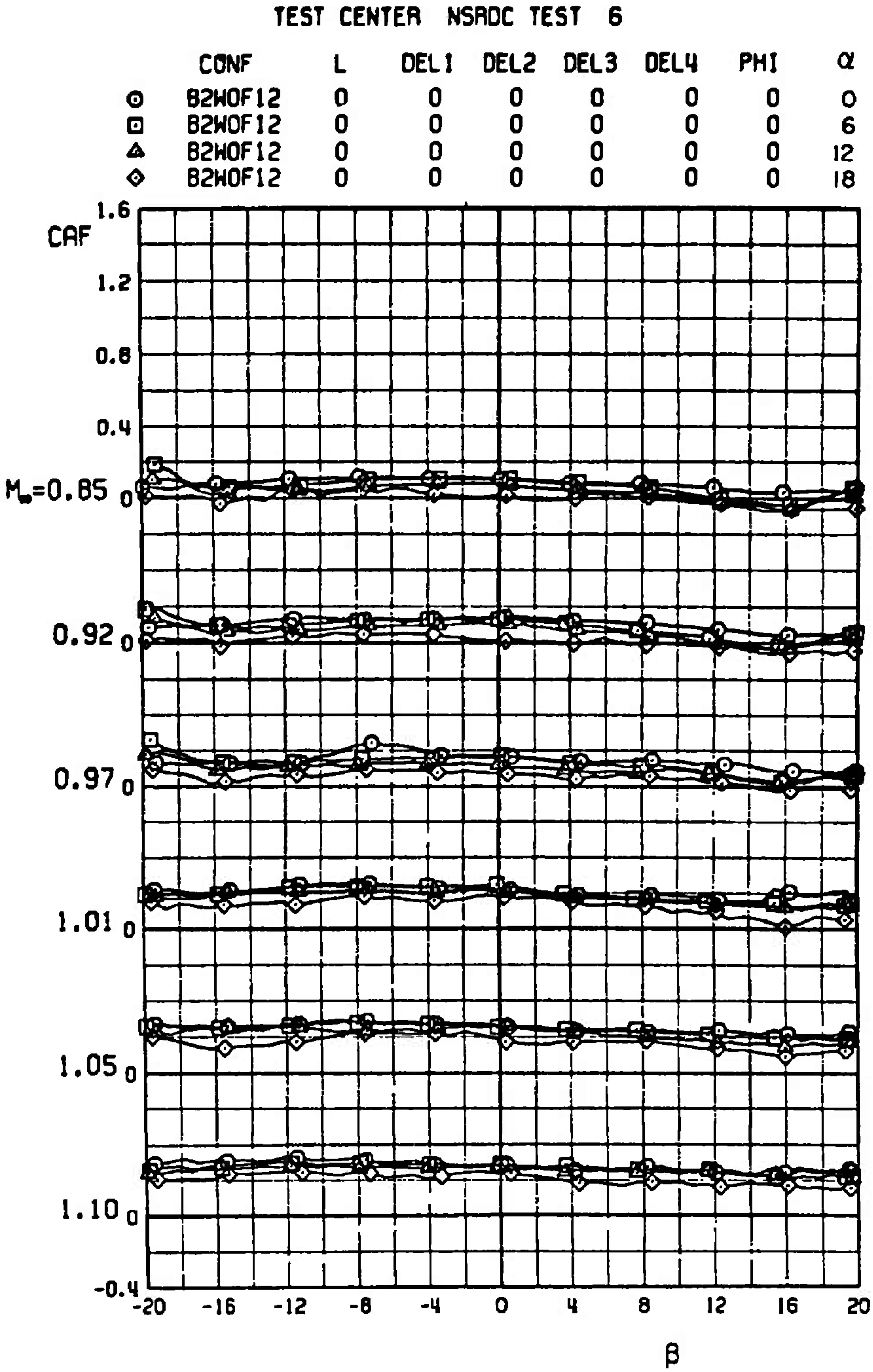

c. CAF versus β
Figure 38. Continued.

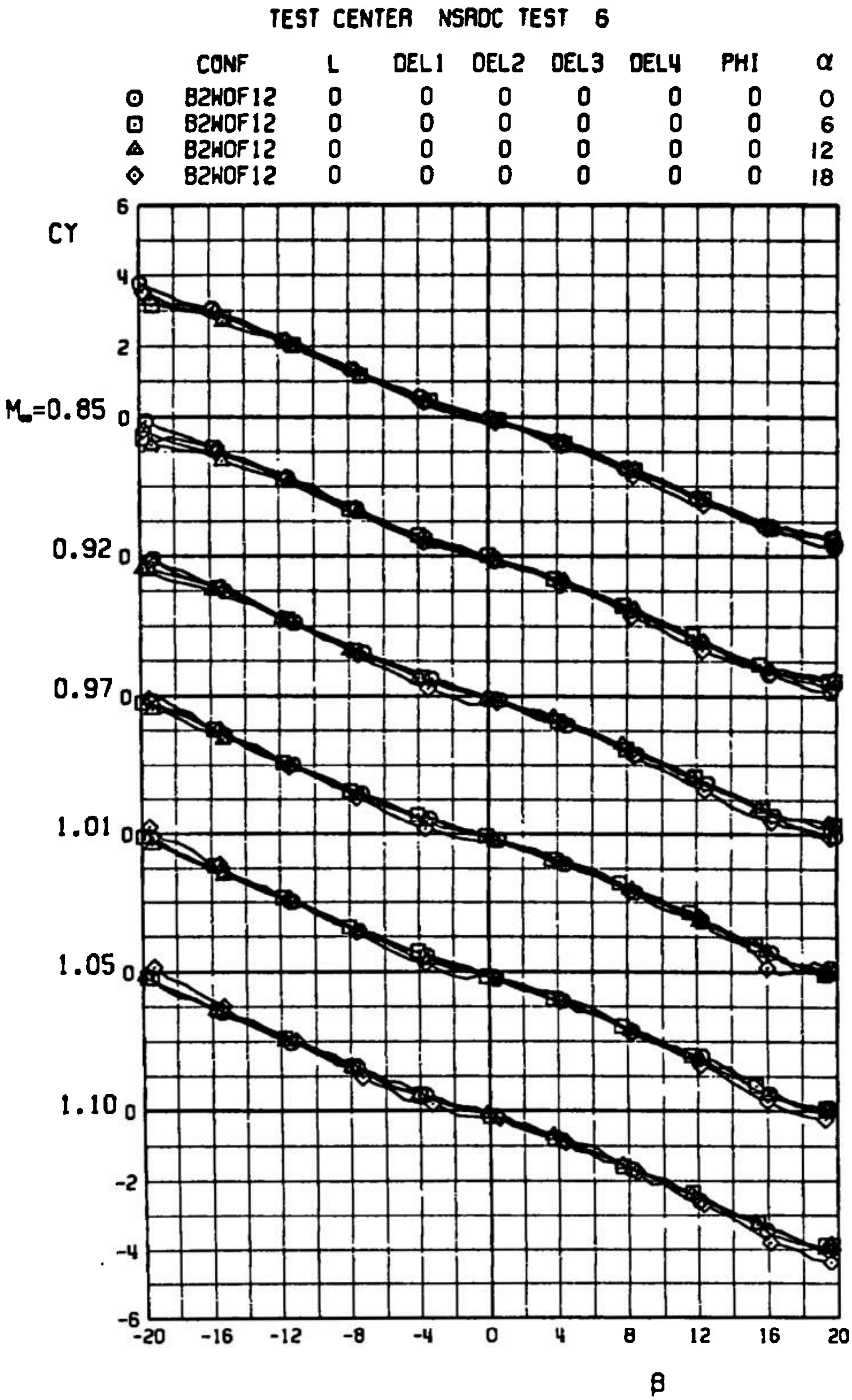

d. CY versus β
Figure 38. Continued.

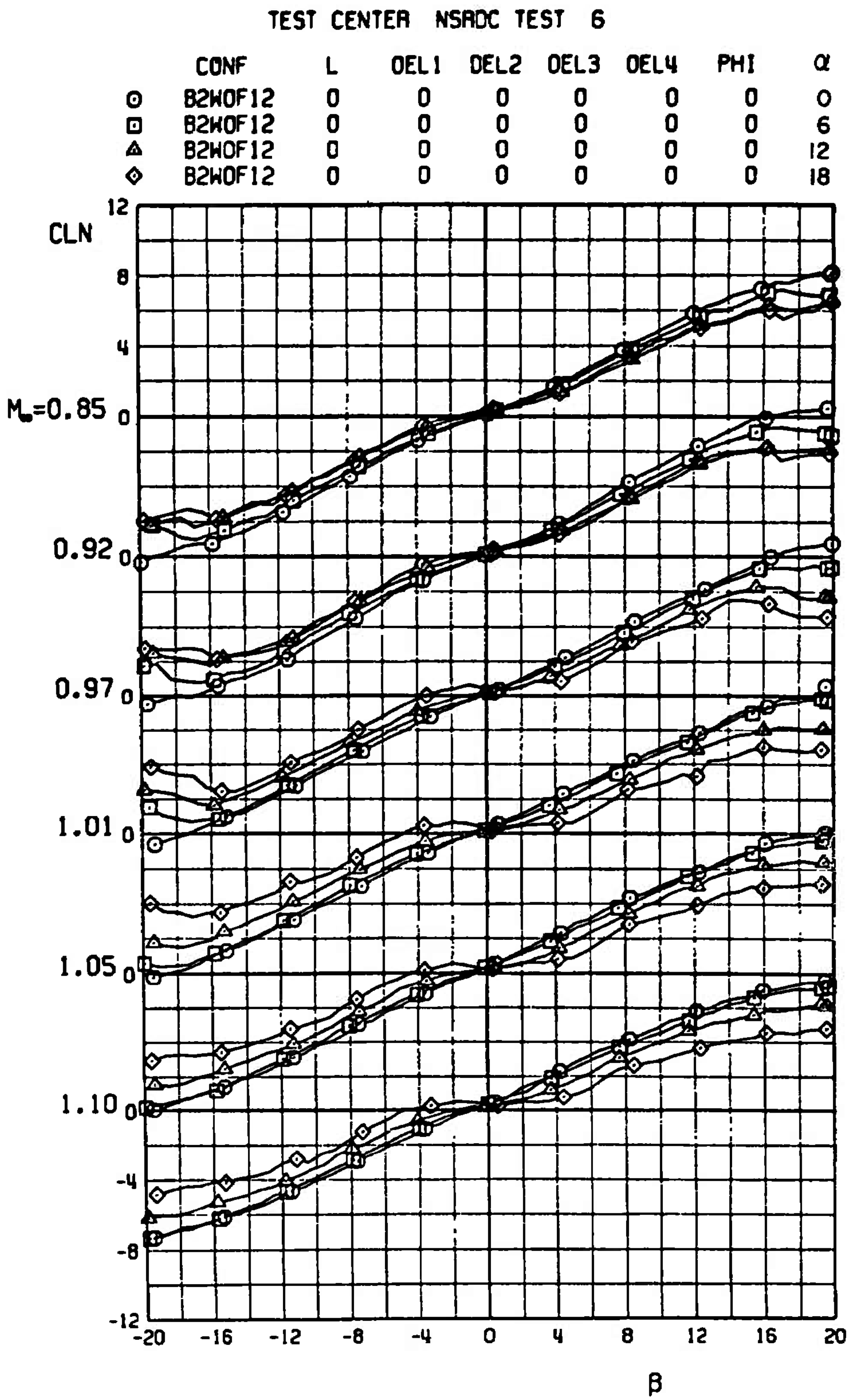

e. CLN versus β
Figure 38. Continued.

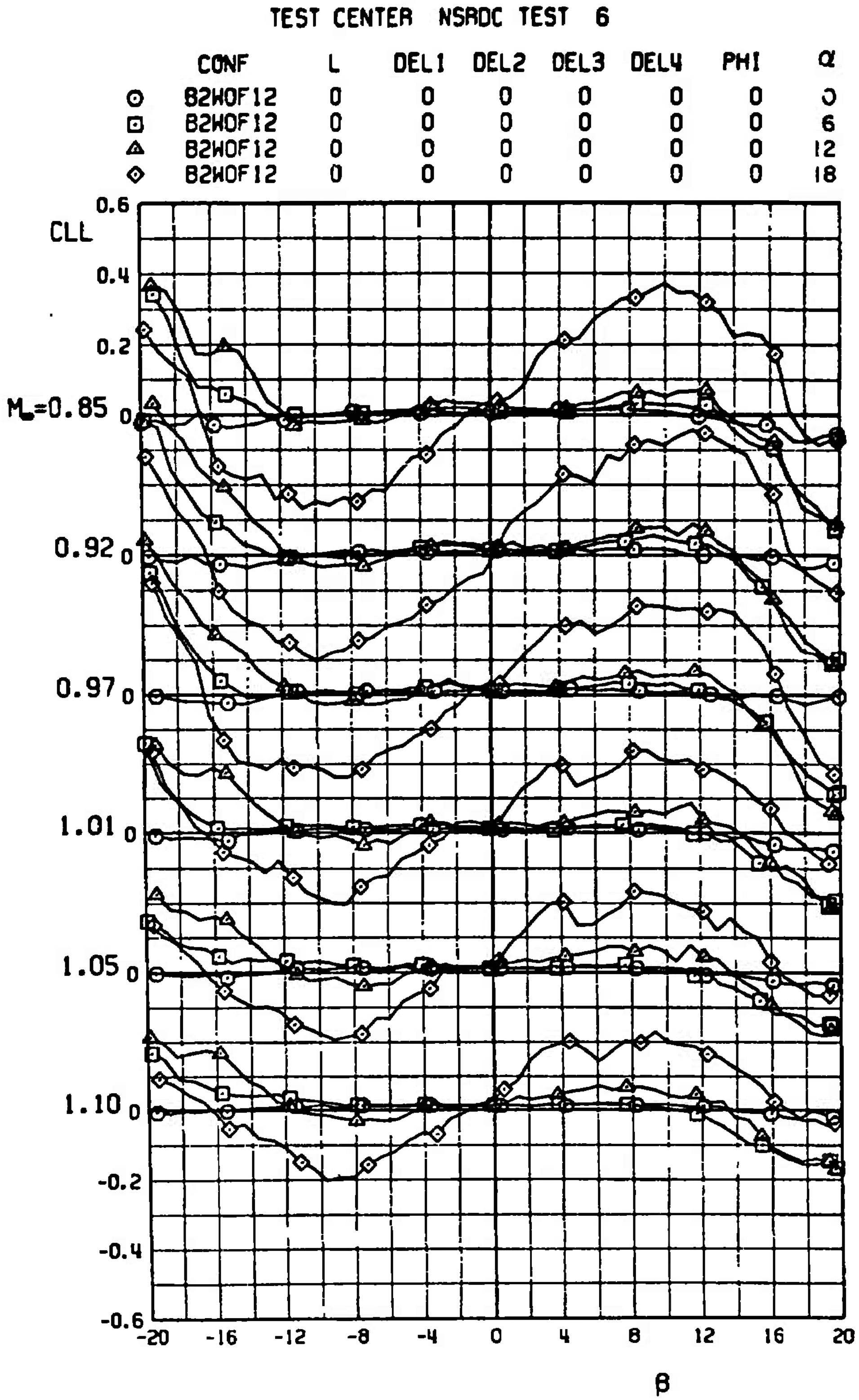

f. CLL versus β
Figure 38. Continued.

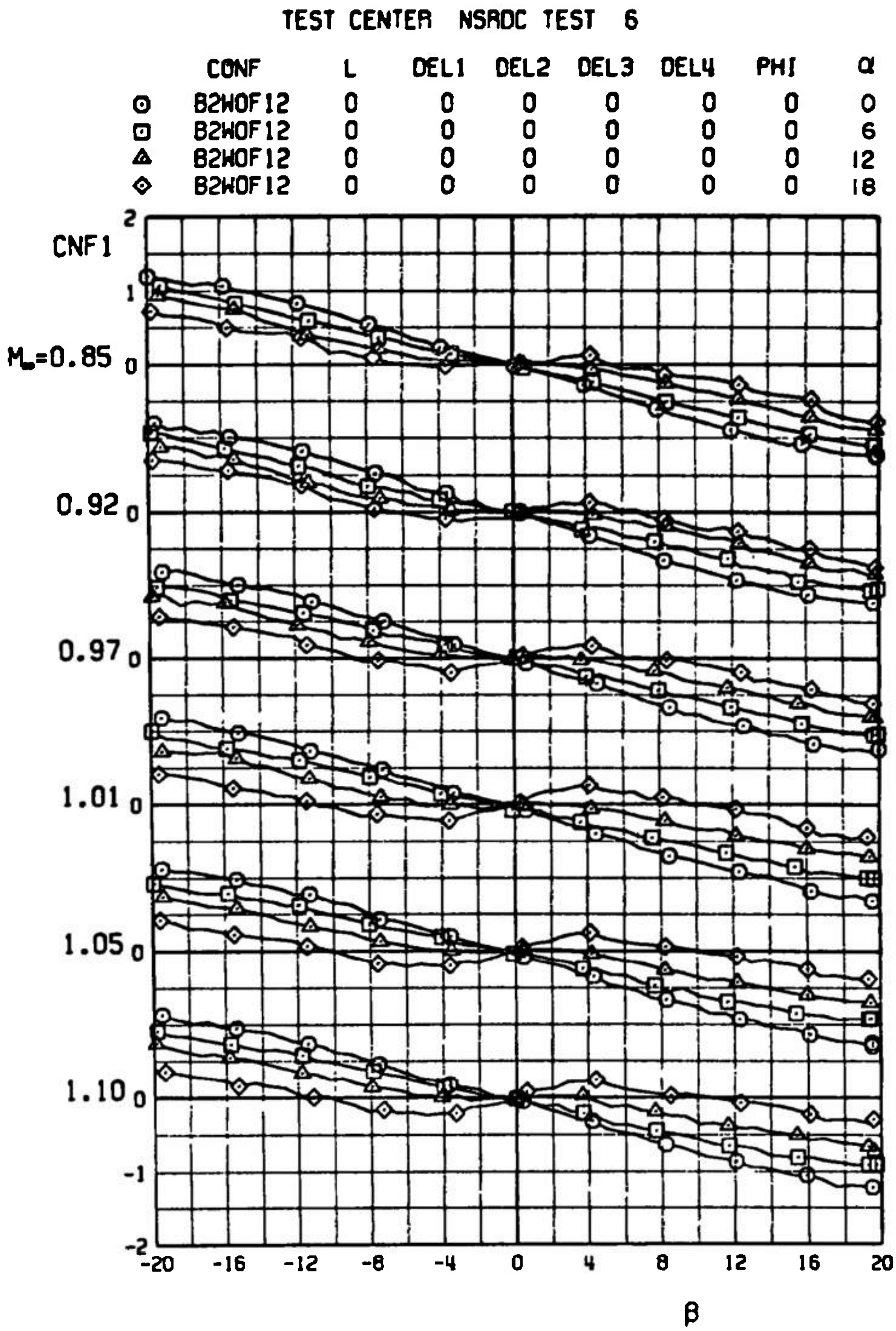

g. CNF1 versus β
Figure 38. Continued.

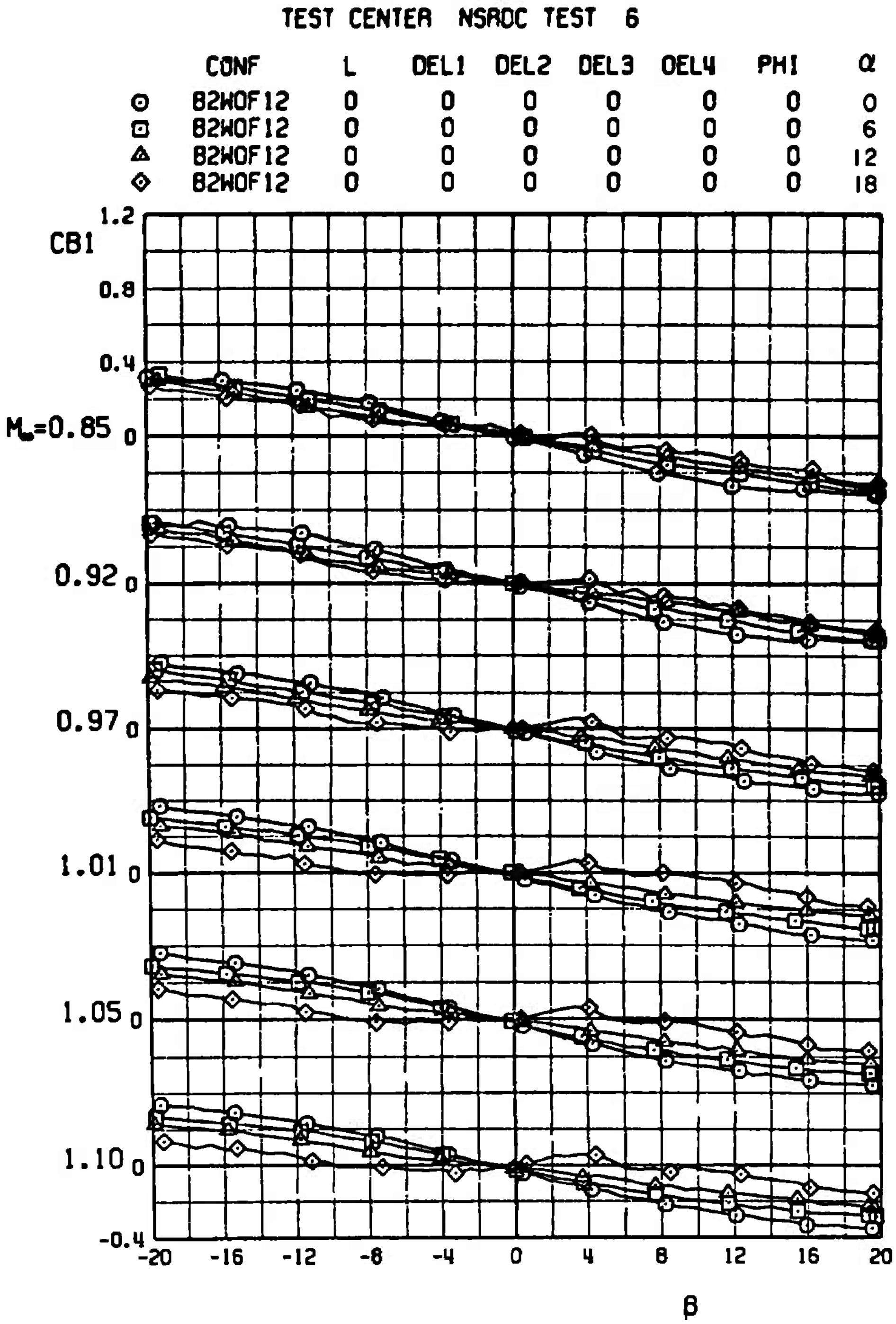

h. CB1 versus β
Figure 38. Continued.

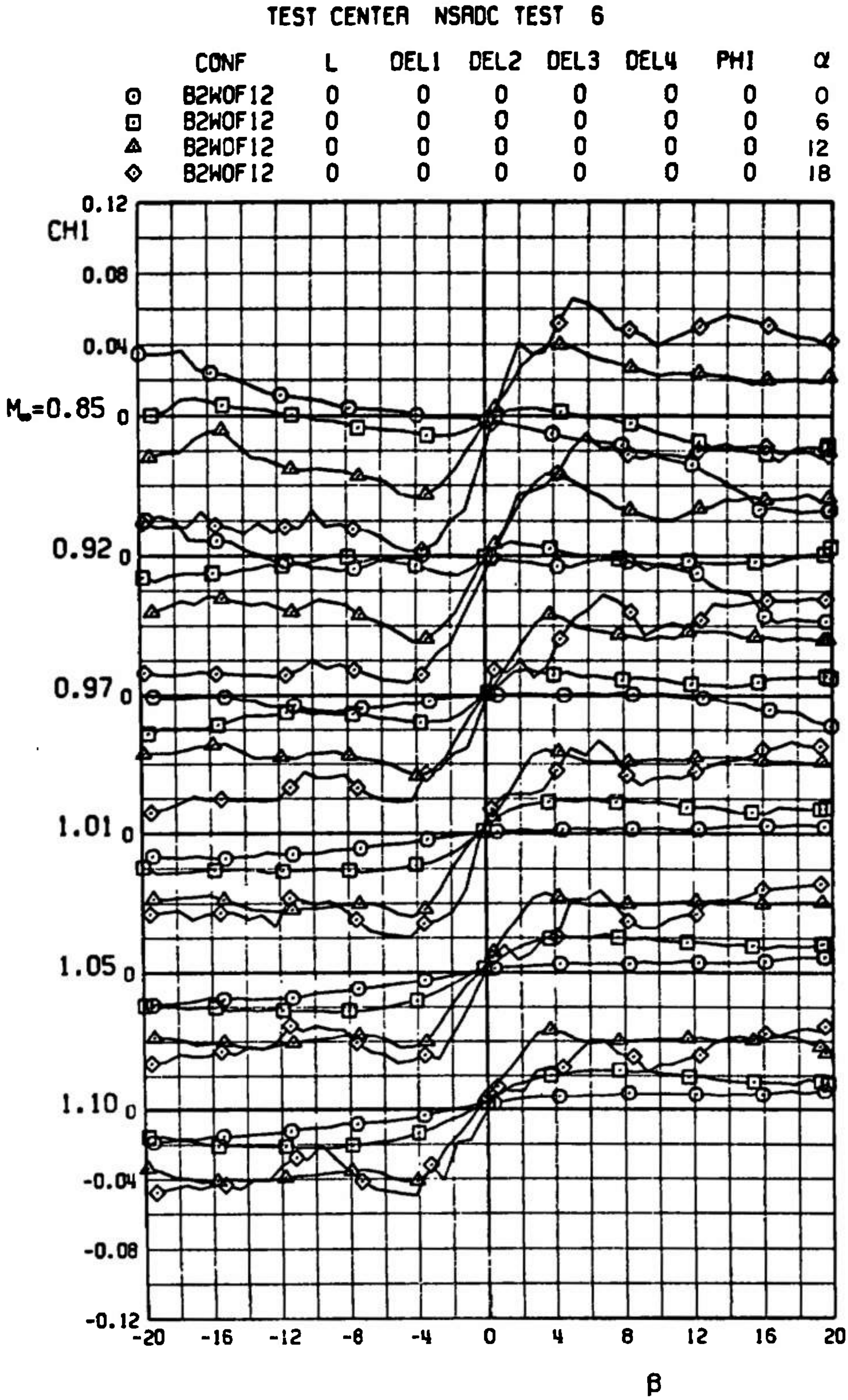

i. CH1 versus β

Figure 38. Concluded.

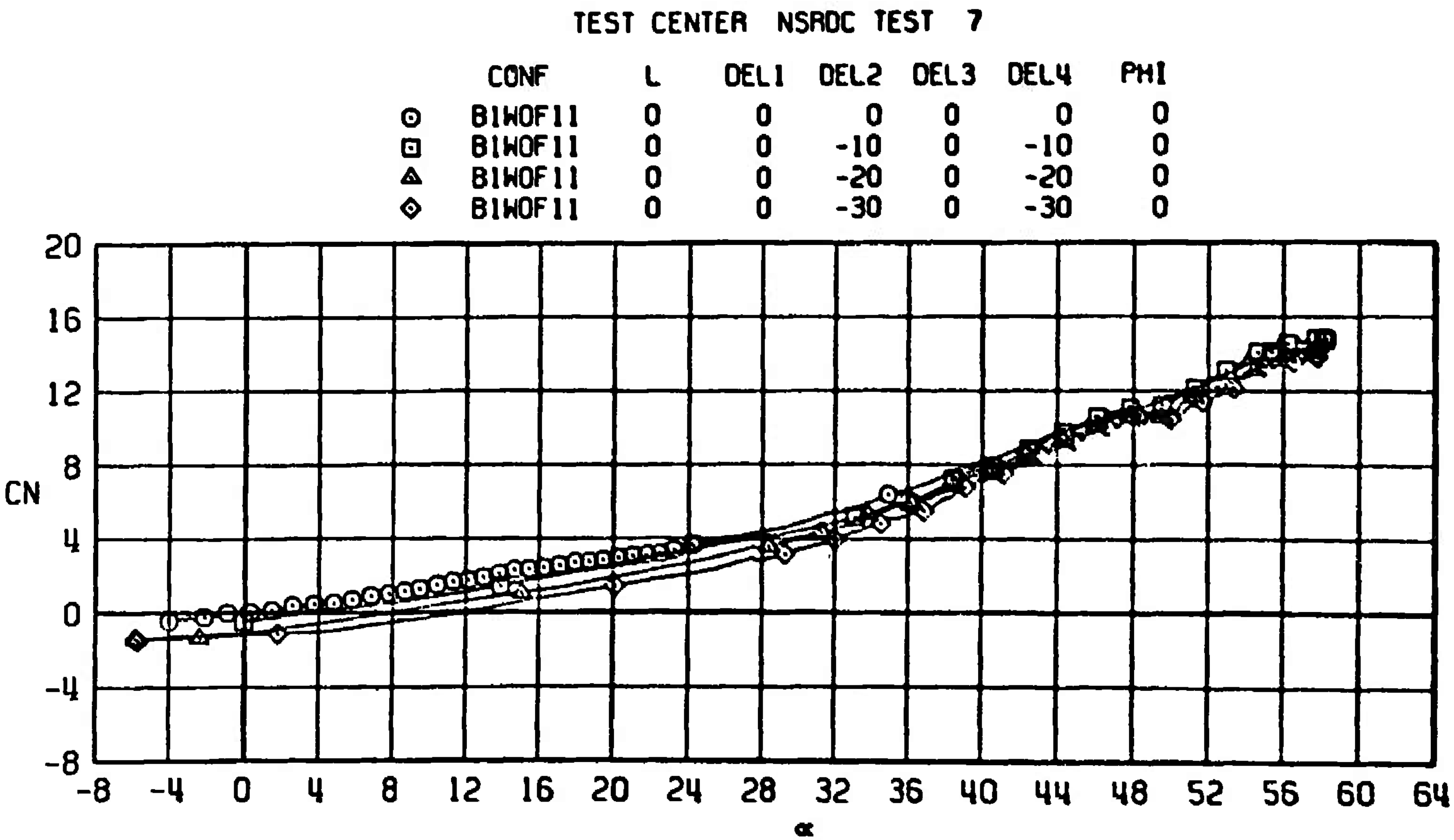

a. CN versus α

Figure 39. Test No. 7, comparison of aerodynamic coefficients of configuration B1W0F11 for various deflections of tail fins No. 2 and 4 at $M_\infty = 0.8$.

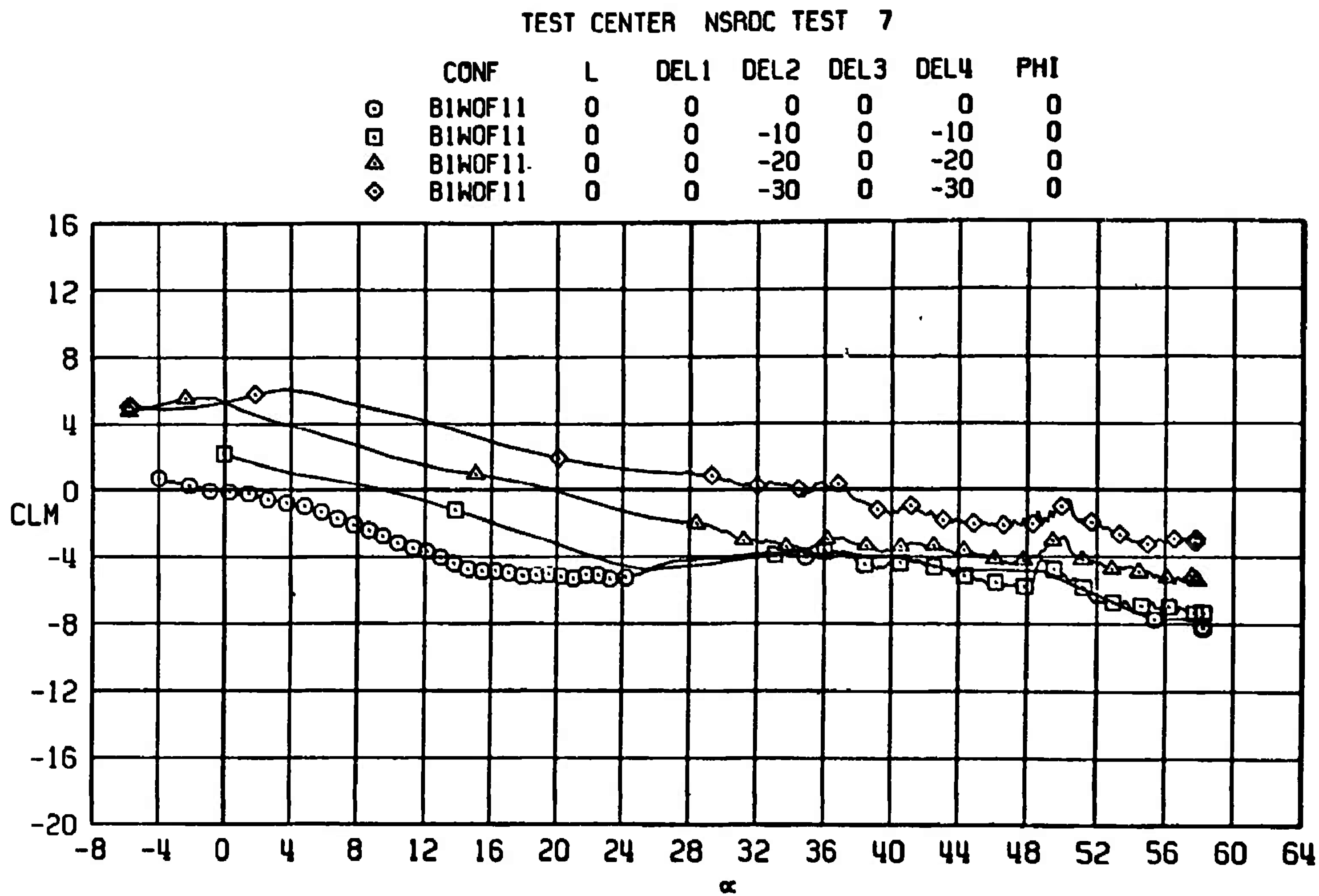

b. CLM versus α
Figure 39. Continued.

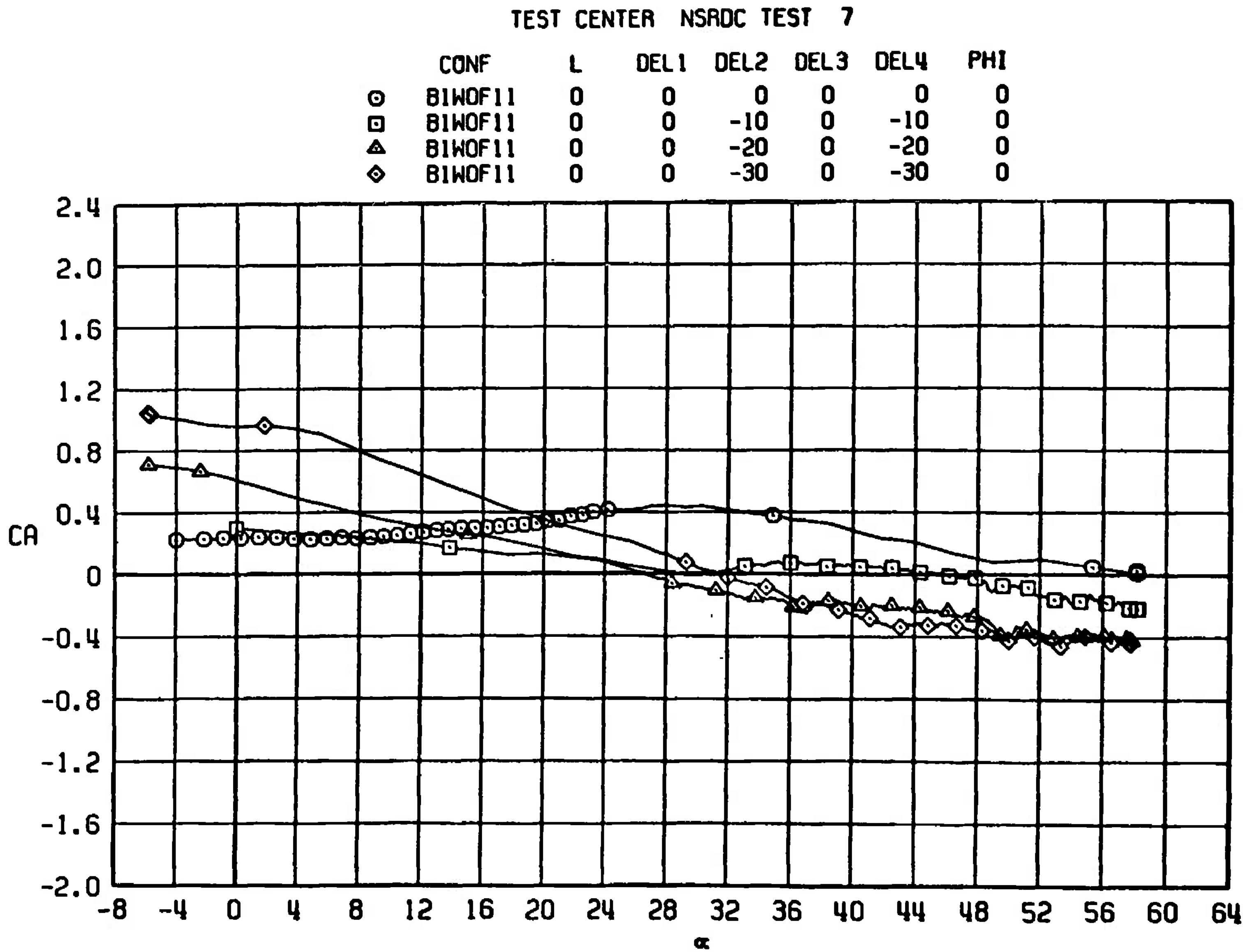

c. CA versus α

Figure 39. Continued.

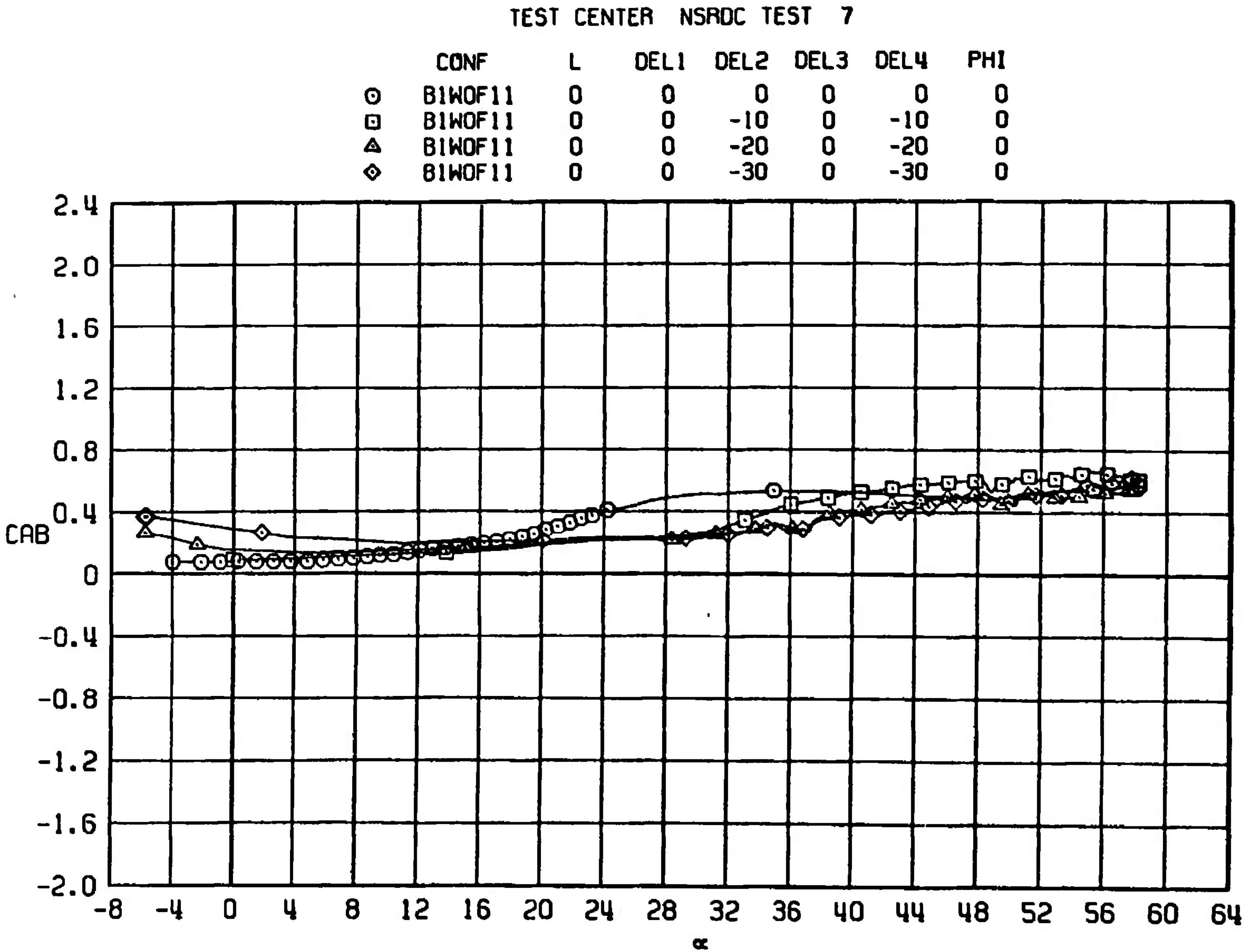

d. CAB versus α
Figure 39. Continued.

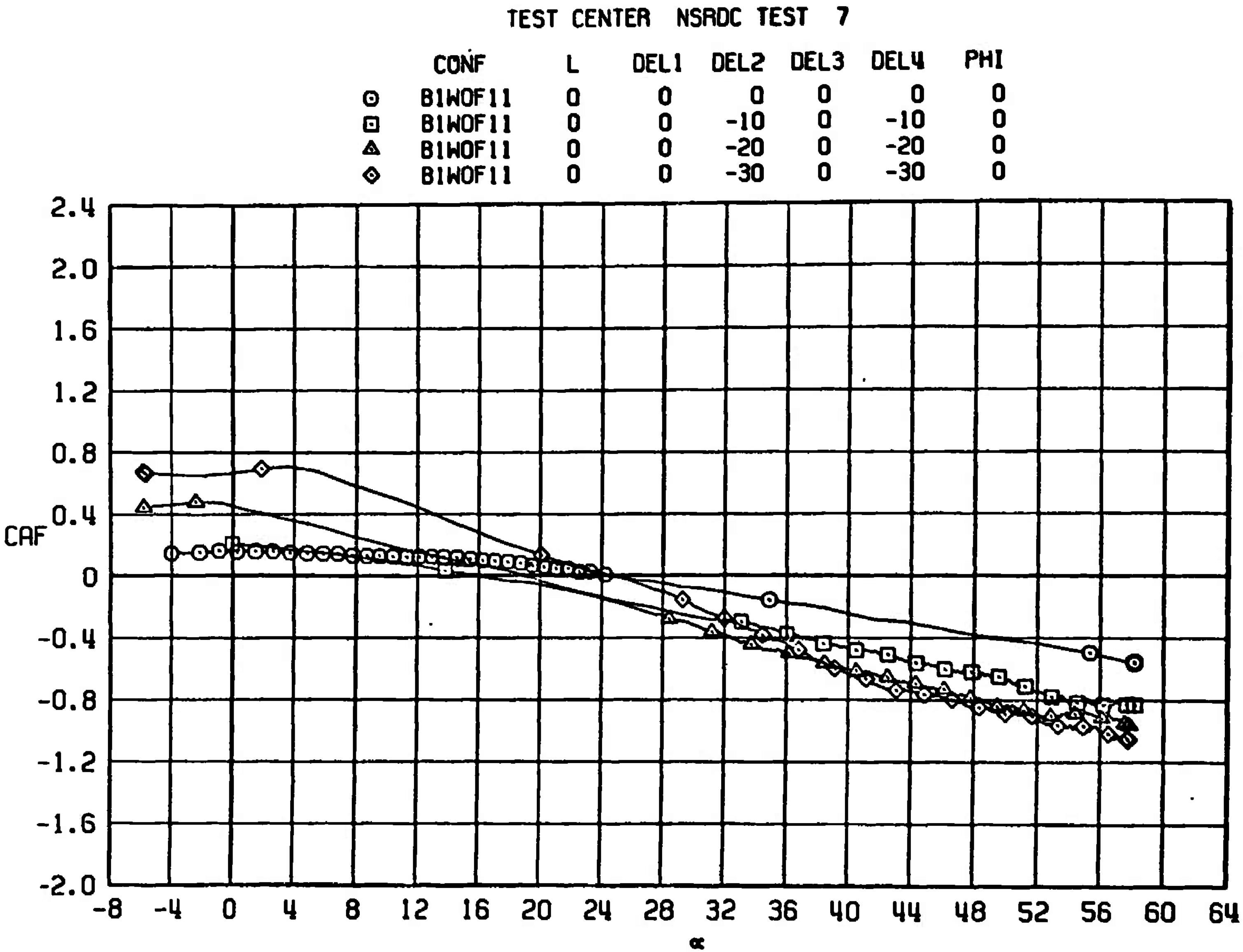

e. CAF versus α

Figure 39. Continued.

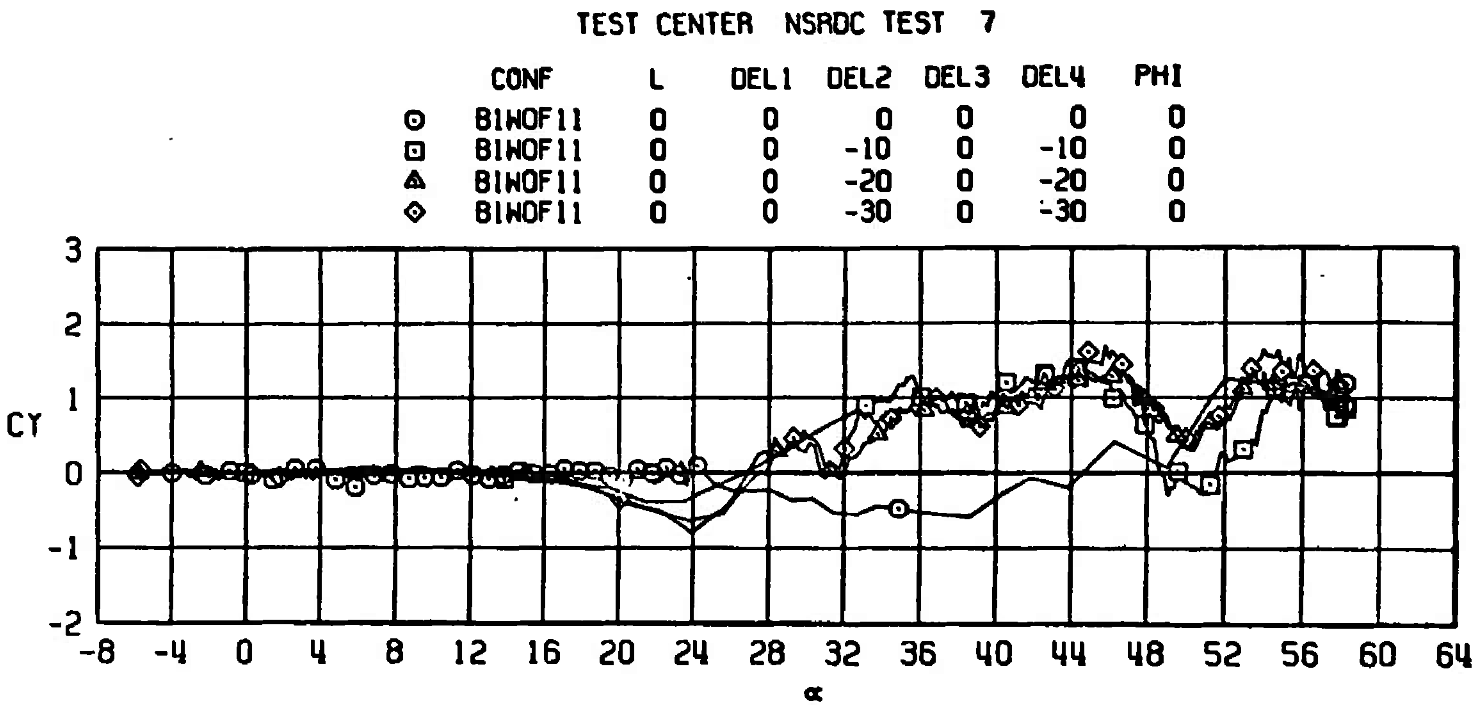

f. CY versus α
Figure 39. Continued.

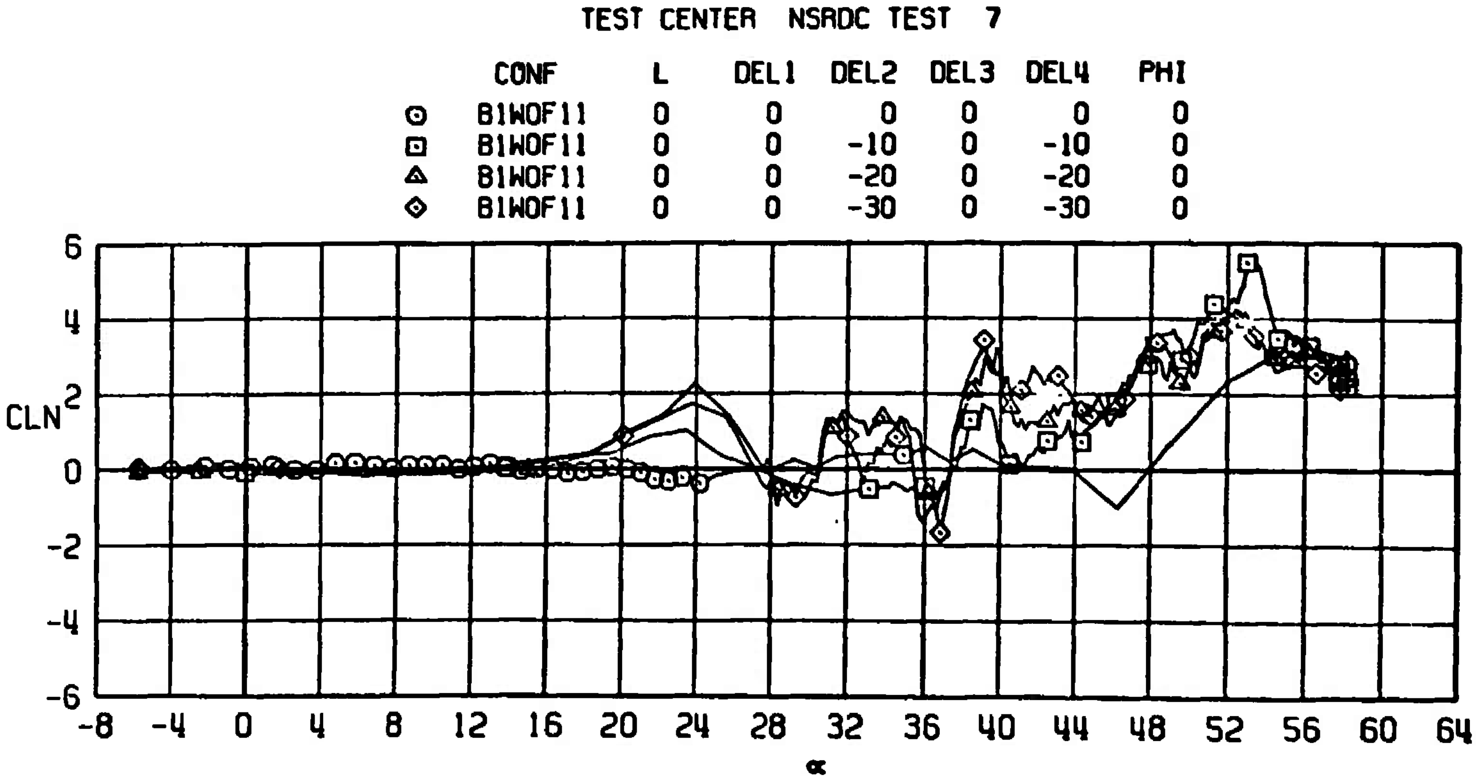

g. CLN versus α
Figure 39. Continued.

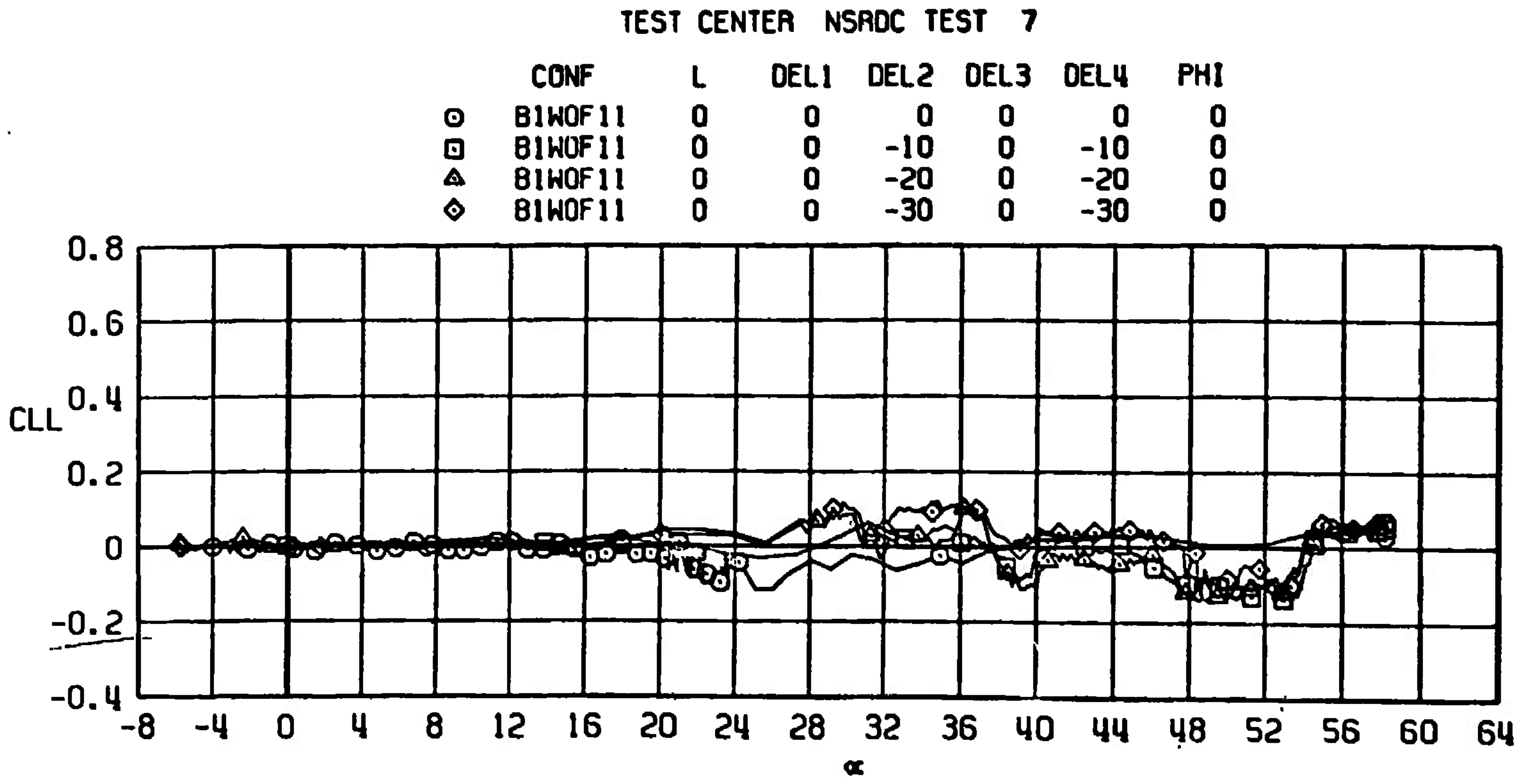

h. CLL versus α
Figure 39. Continued.

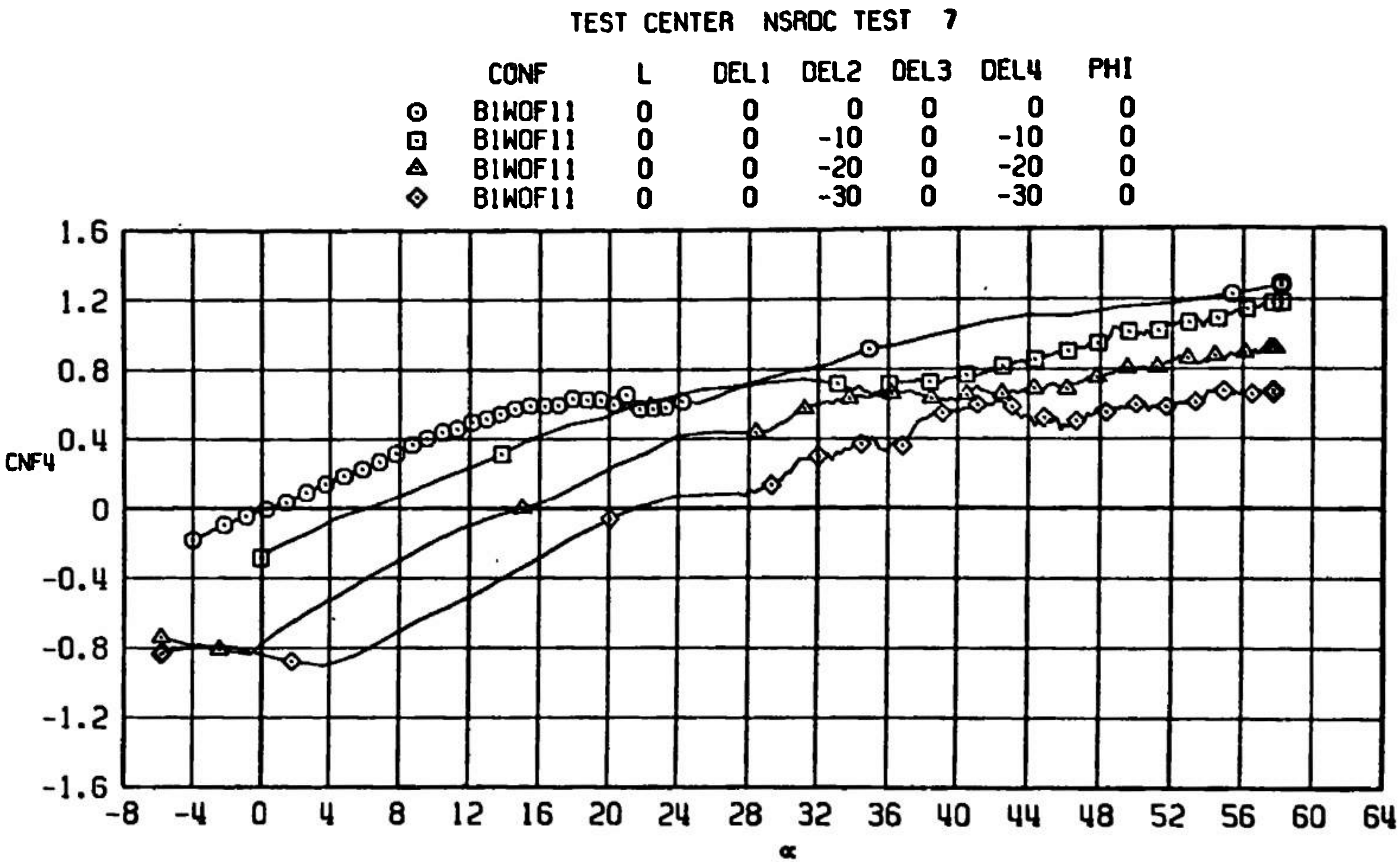

i. CNF4 versus α
Figure 39. Continued.

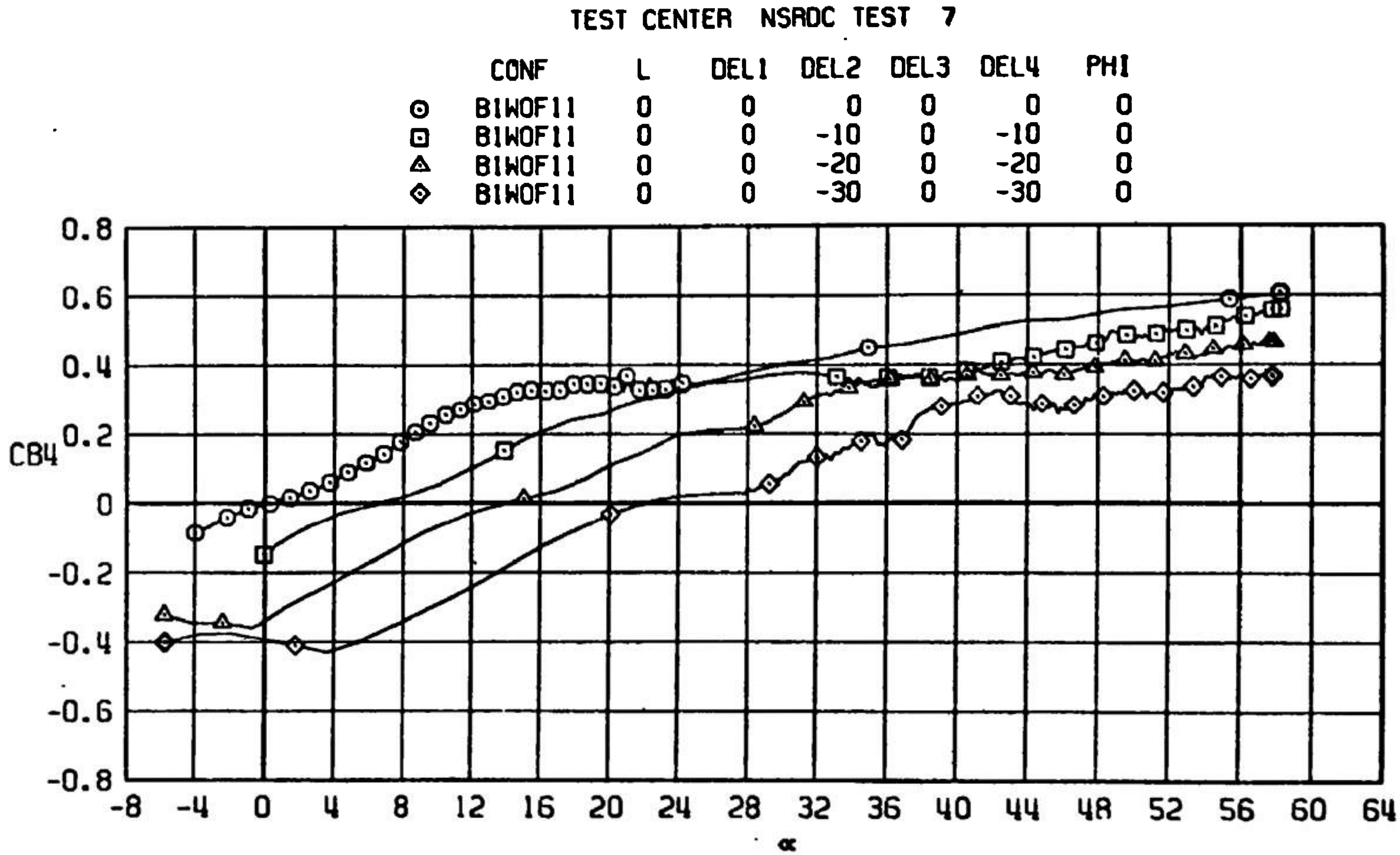

j. CB4 versus α
Figure 39. Continued.

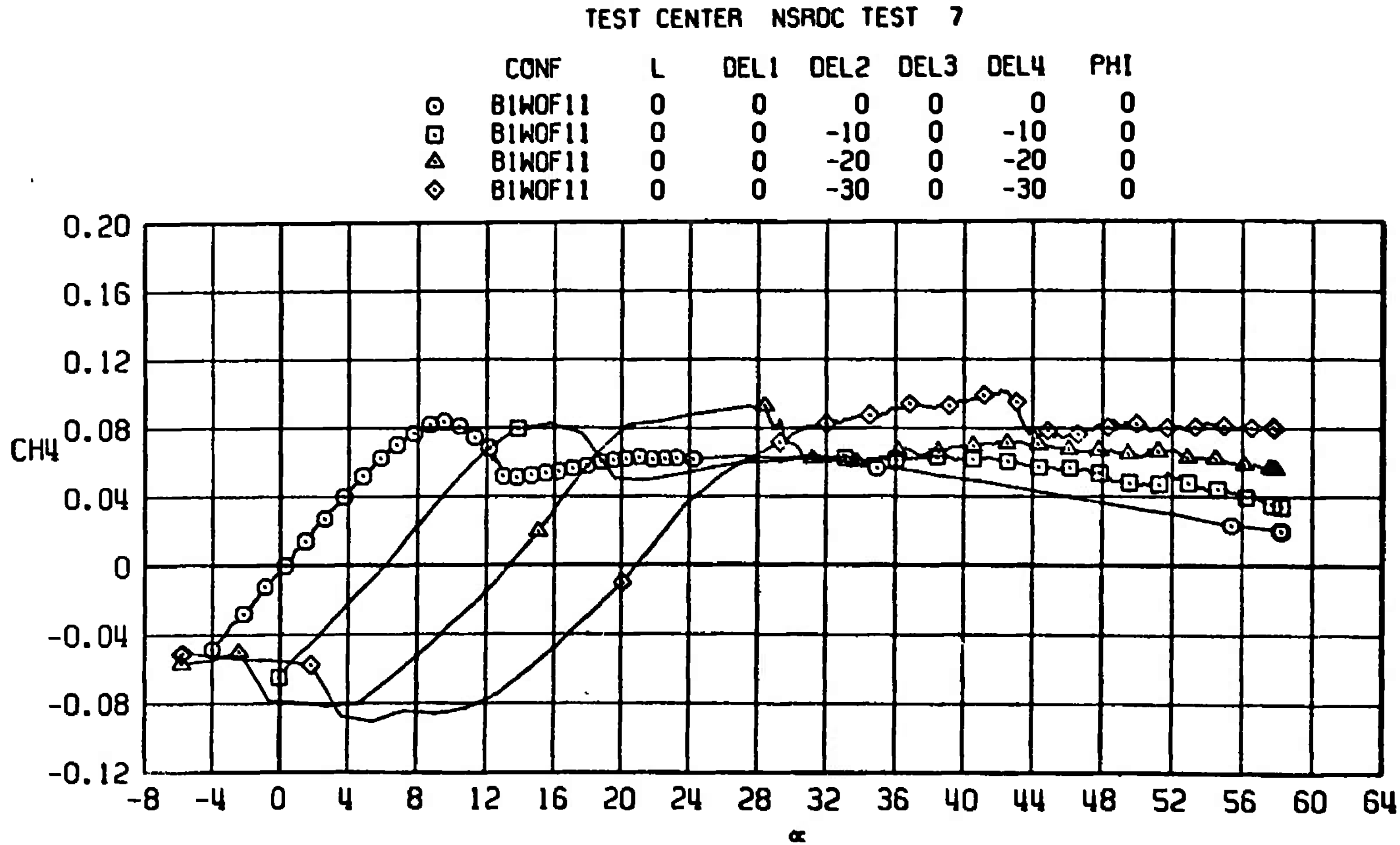

k. CH4 versus α

Figure 39. Concluded.

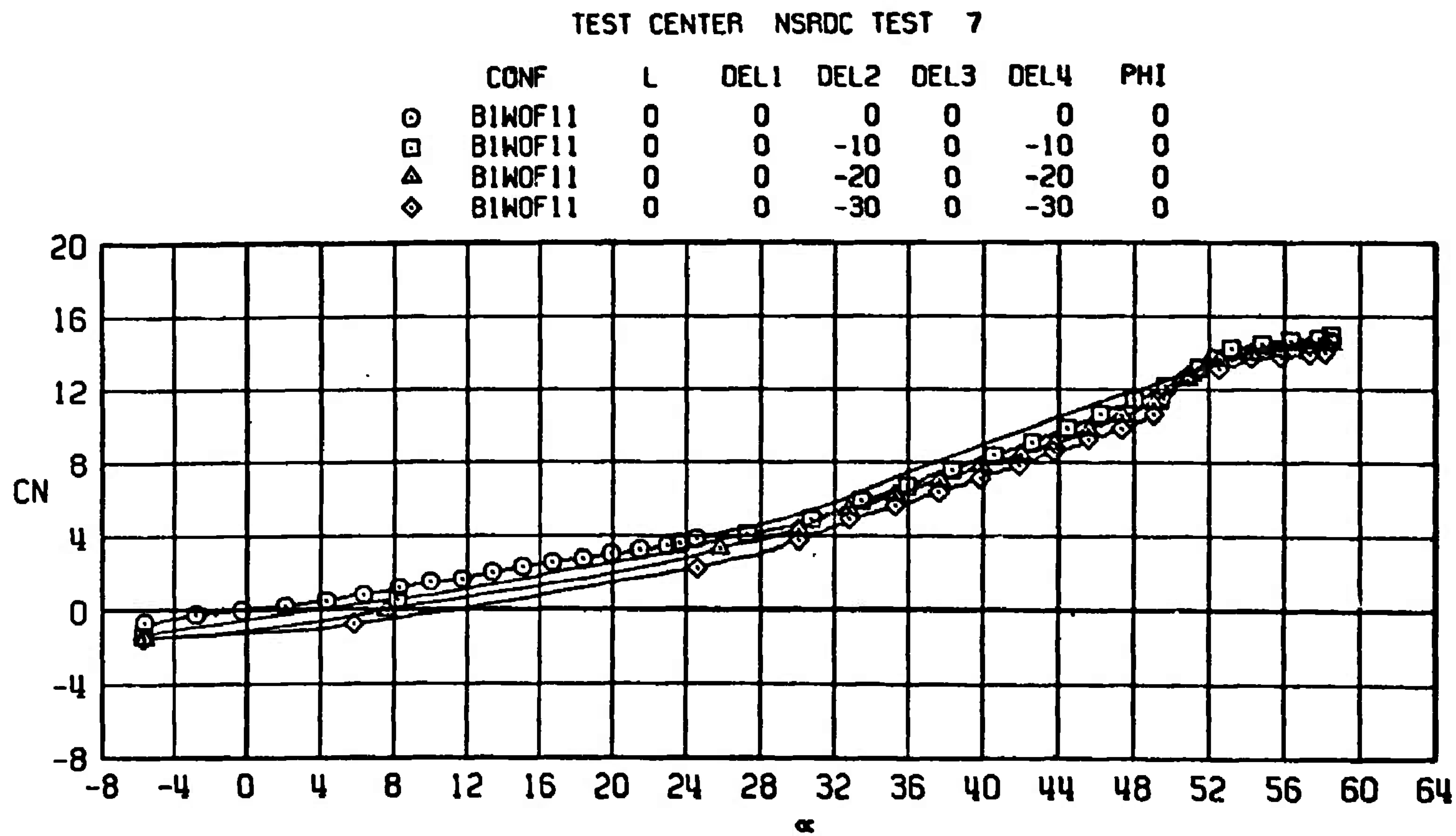

a. CN versus α

Figure 40. Test No. 7, comparison of aerodynamic coefficients of configuration B1W0F11 for various deflections of tail fins No. 2 and 4 at M_∞ = 0.9.

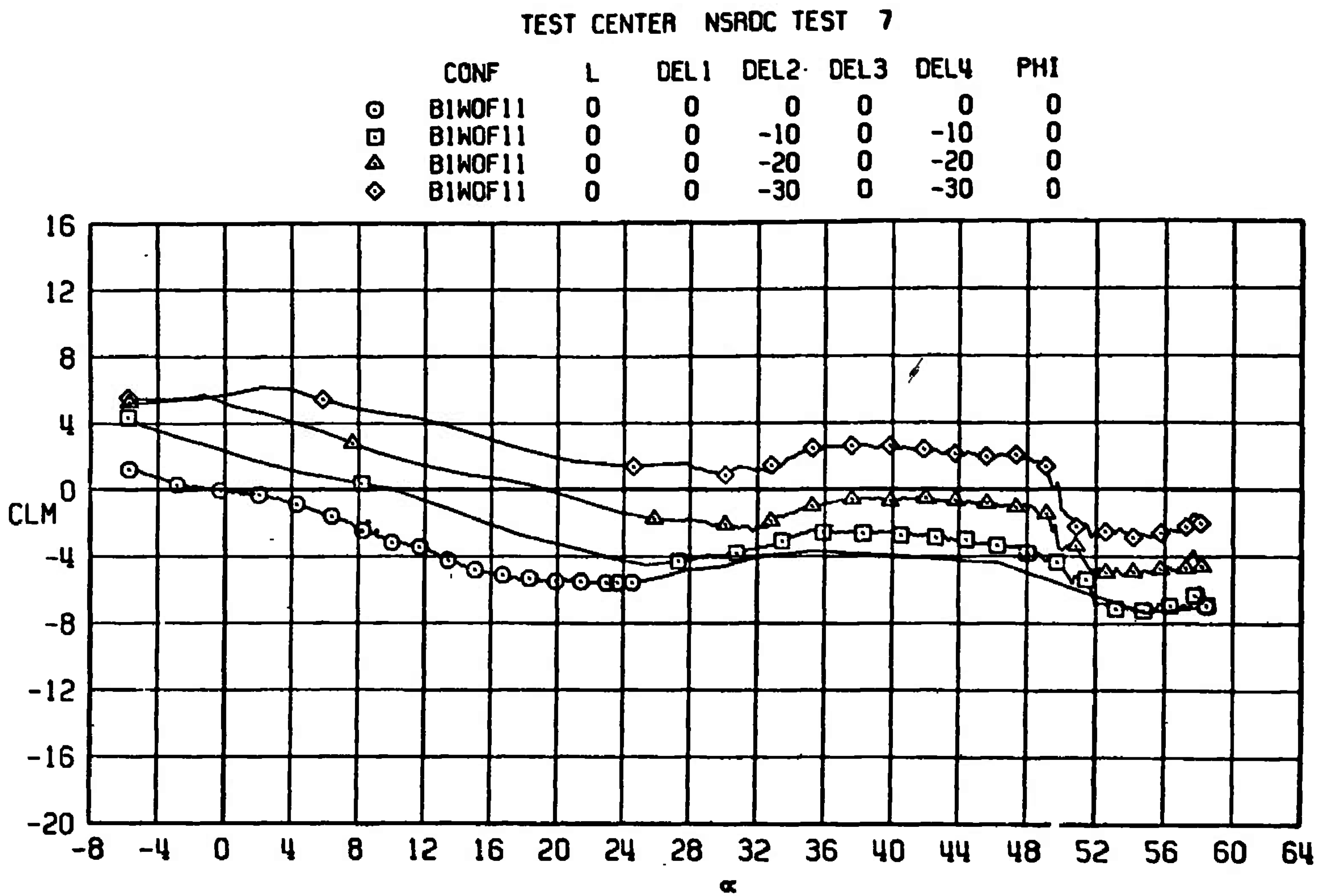

b. CLM versus α

Figure 40. Continued.

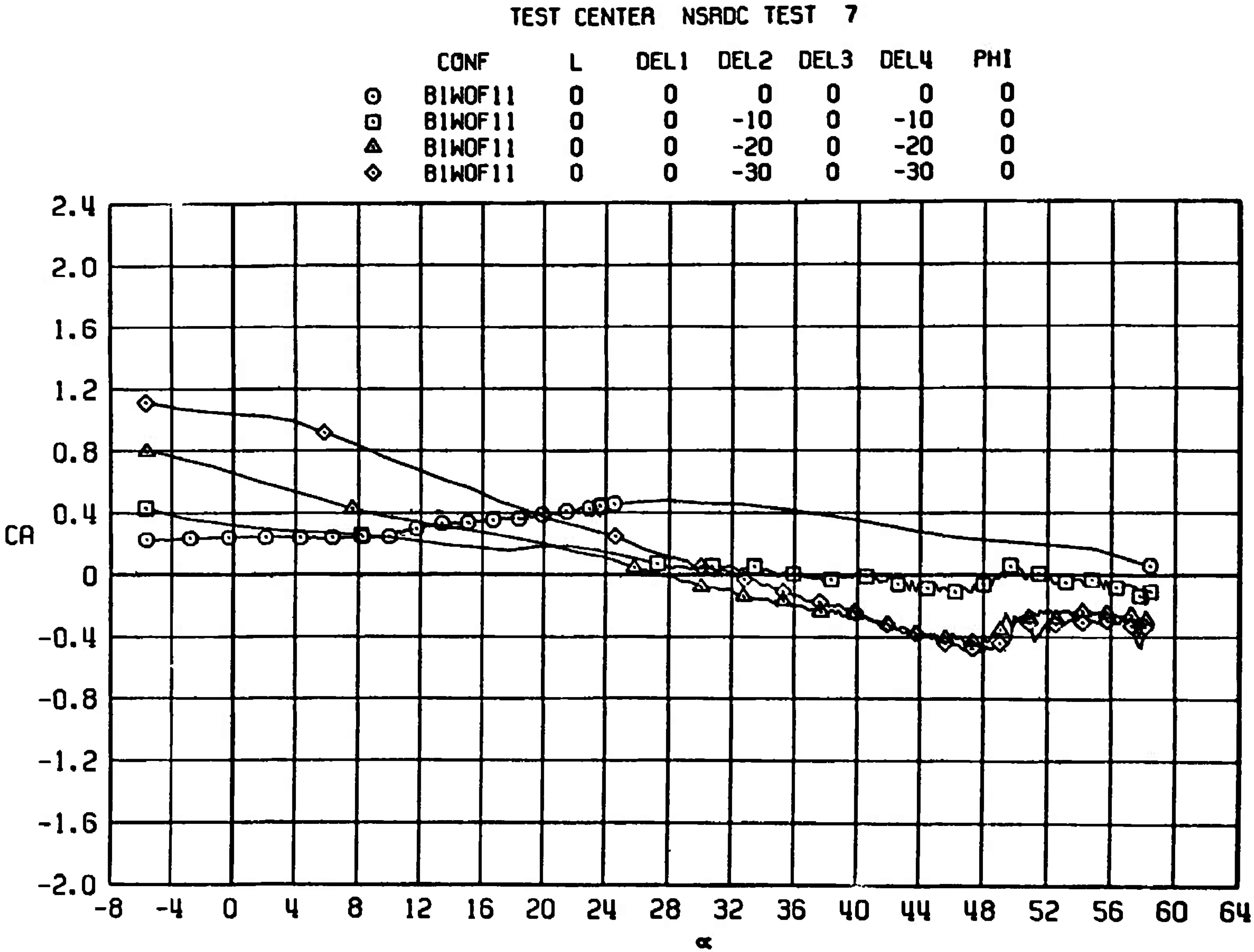

c. CA versus α

Figure 40. Continued.

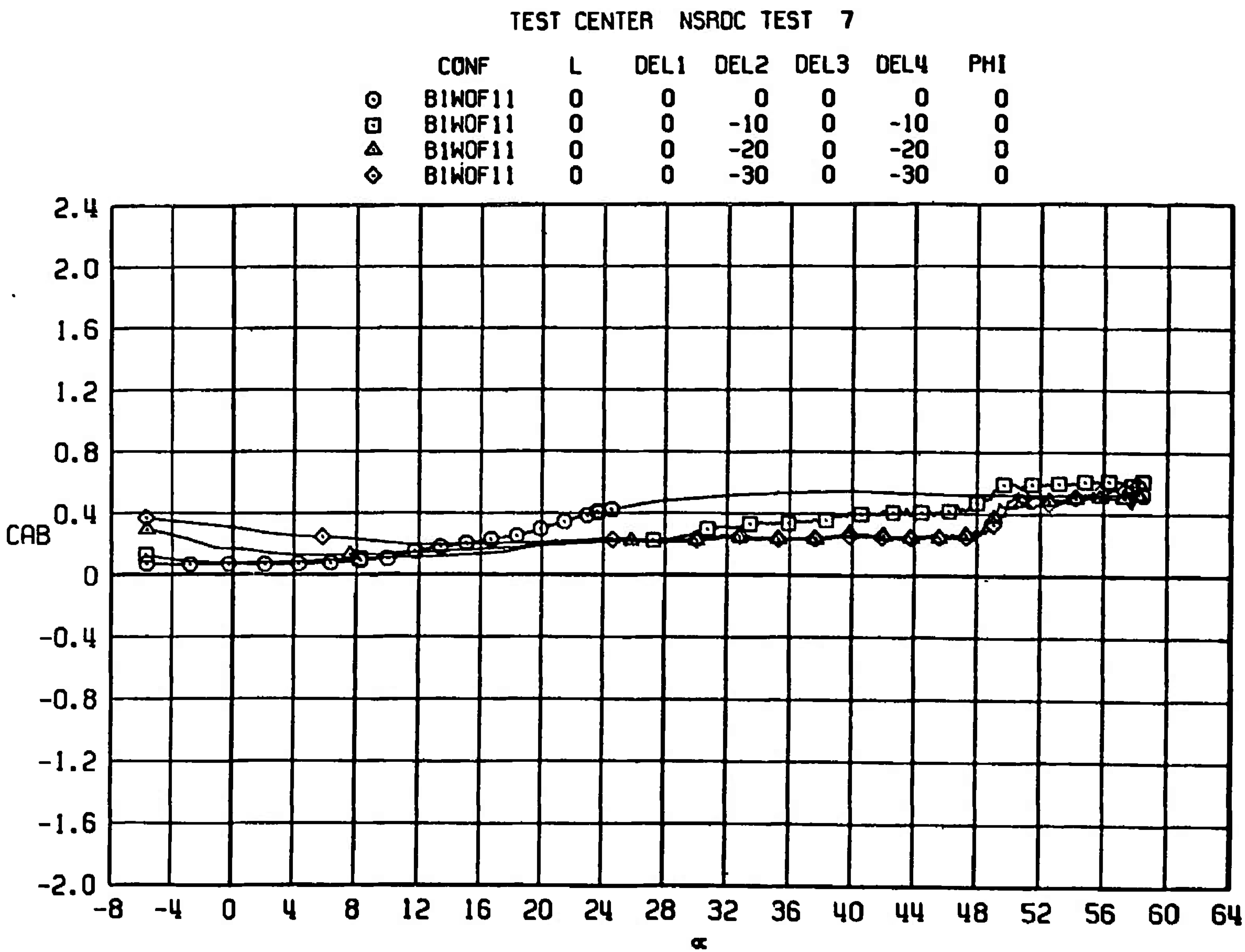

d. CAB versus α
Figure 40. Continued.

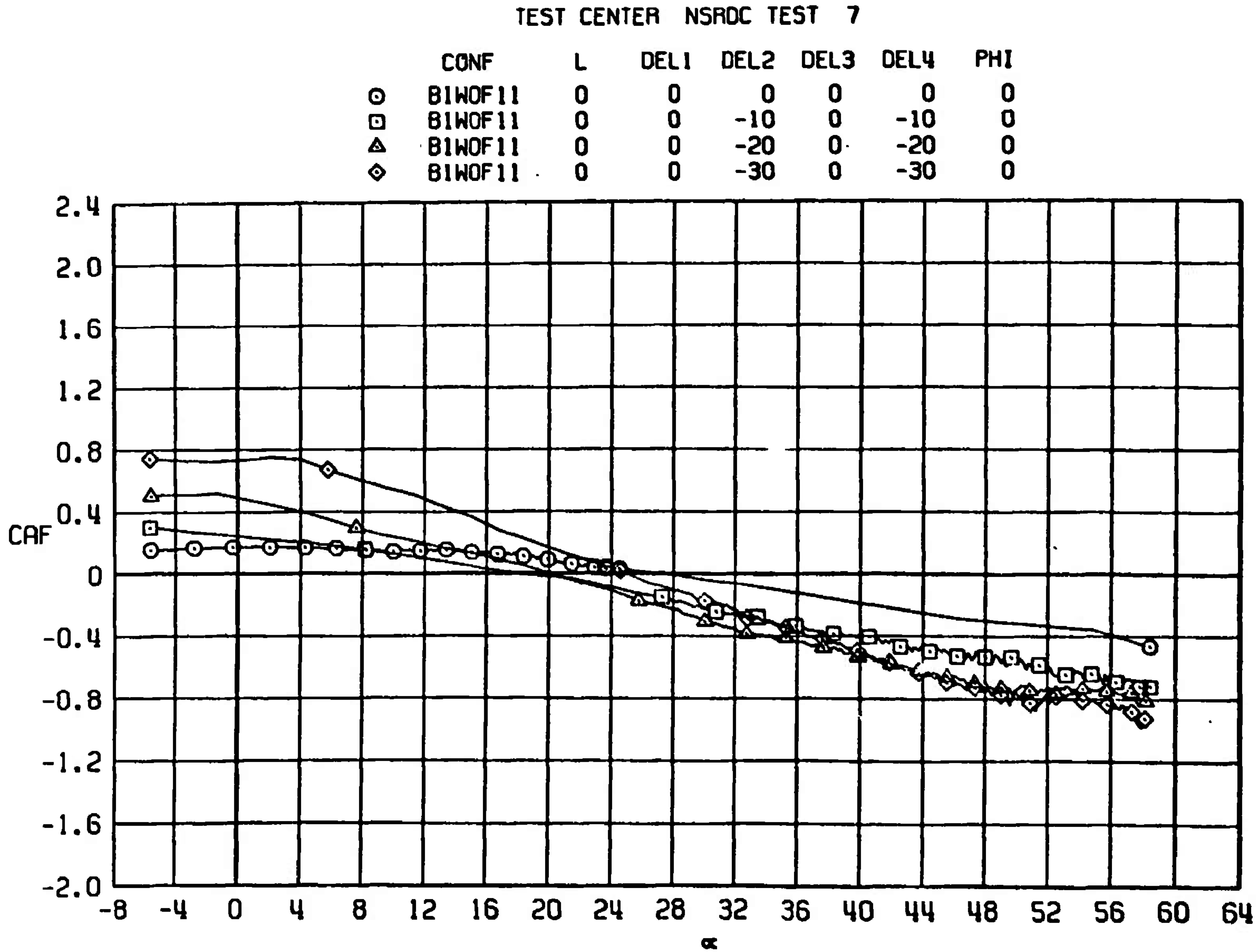

e. CAF versus α
Figure 40. Continued.

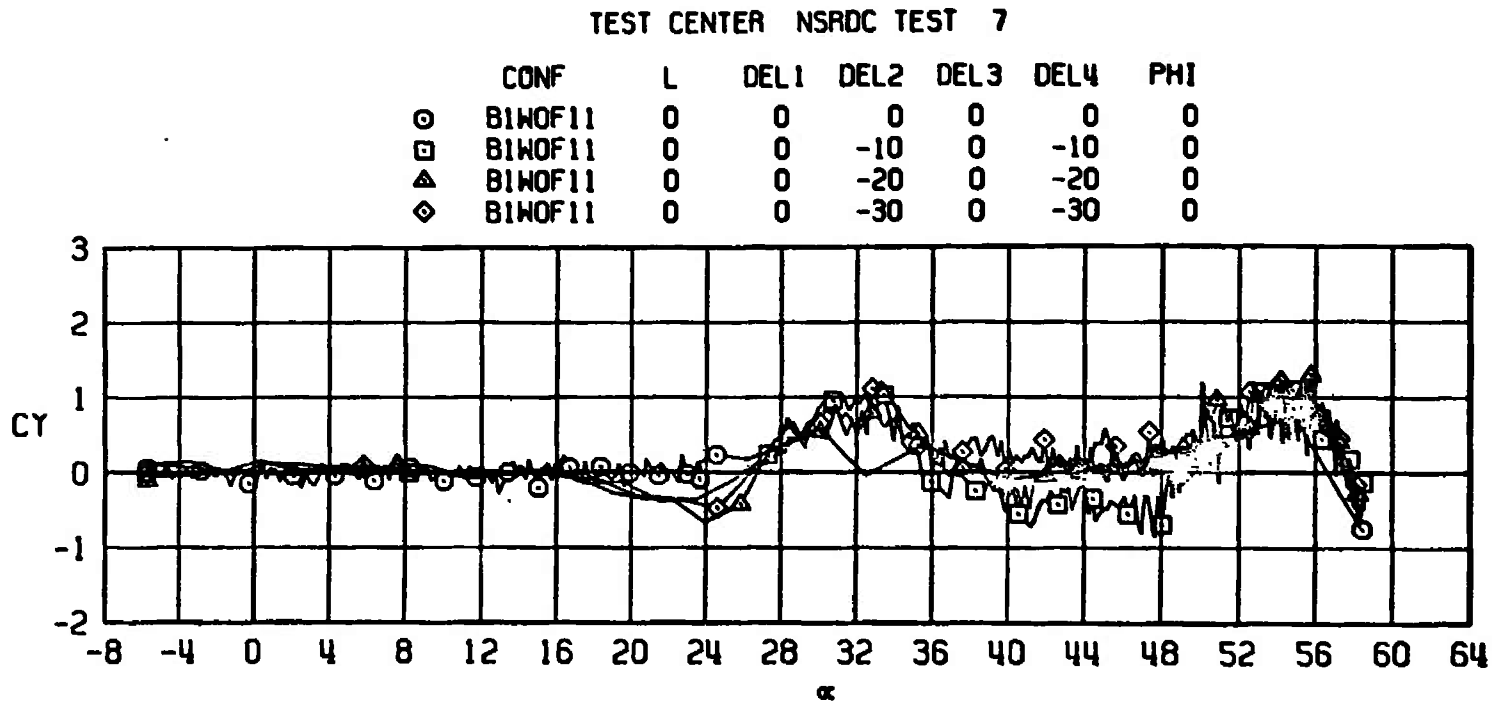

f. CY versus α
Figure 40. Continued.

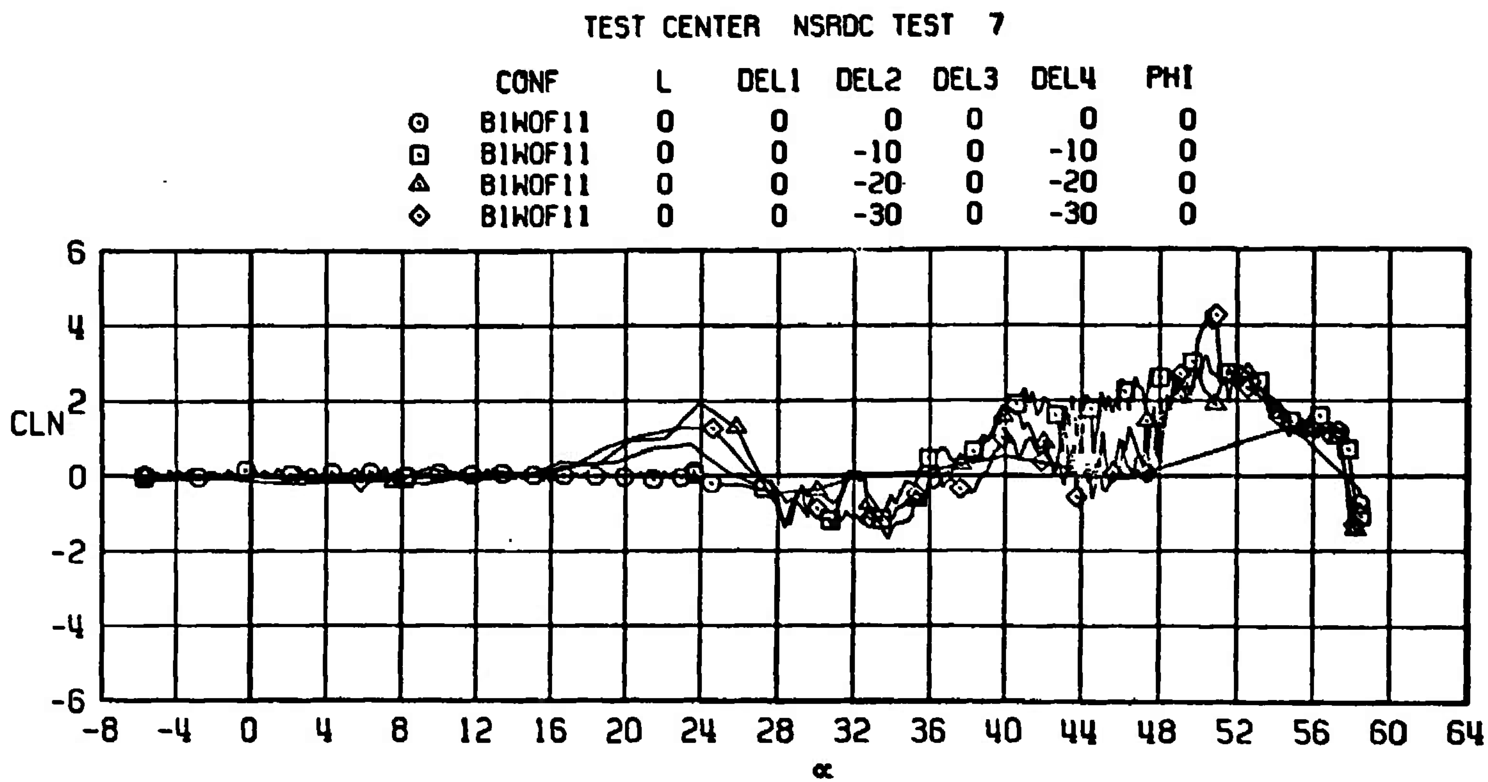

g. CLN versus α
Figure 40. Continued.

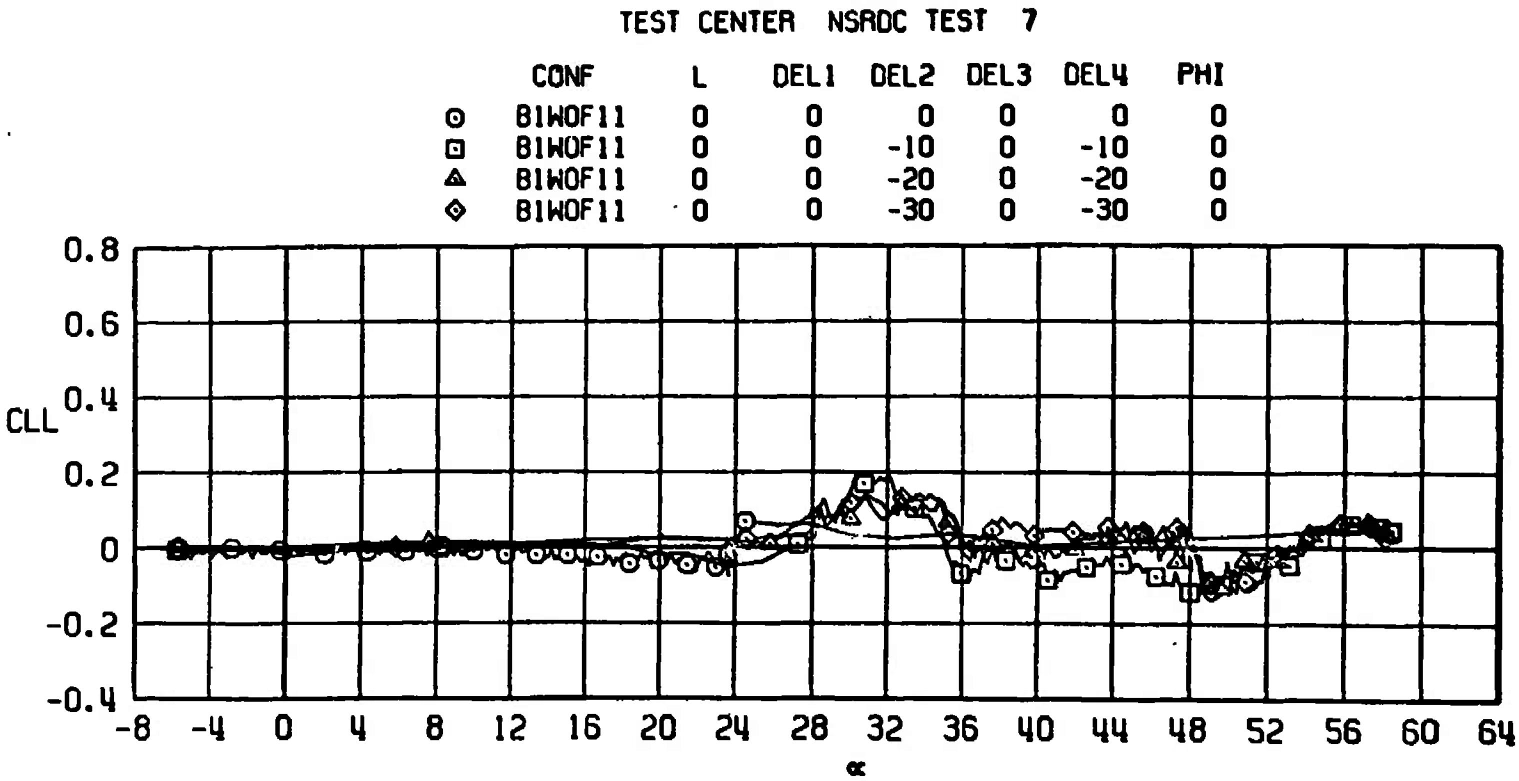

h. CLL versus a

Figure 40. Continued.

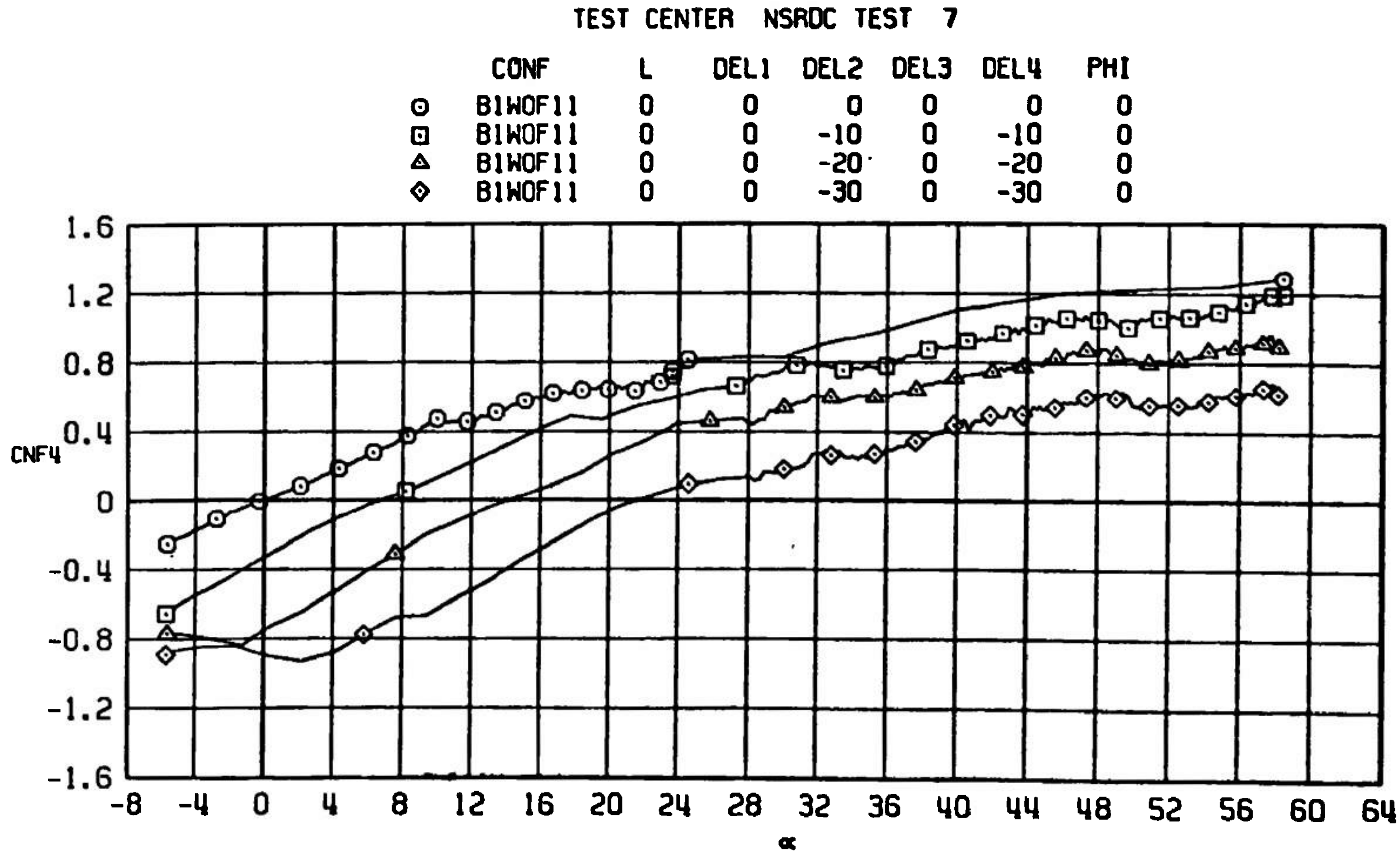

i. CNF4 versus α
Figure 40. Continued.

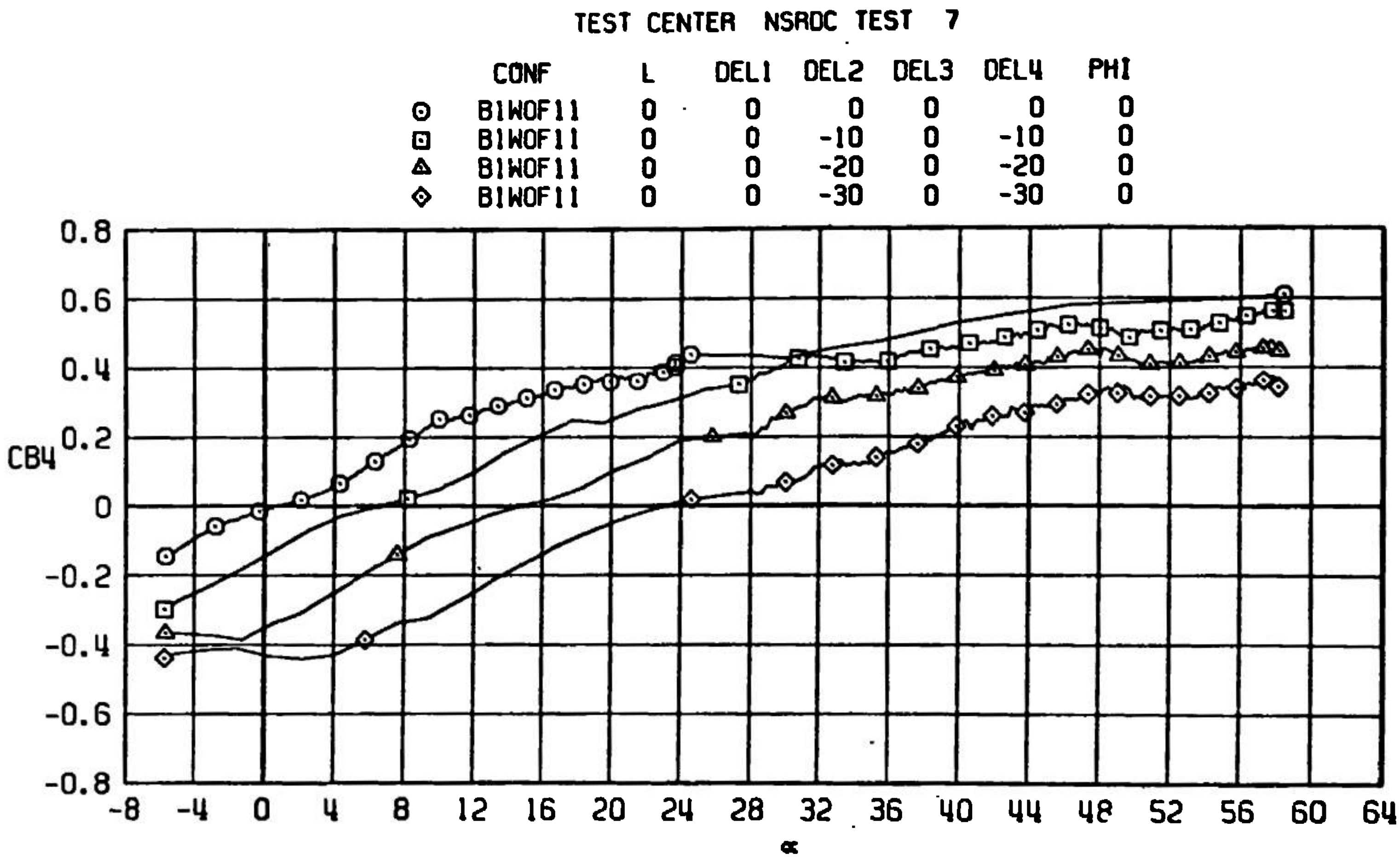

j. CB4 versus α

Figure 40. Continued.

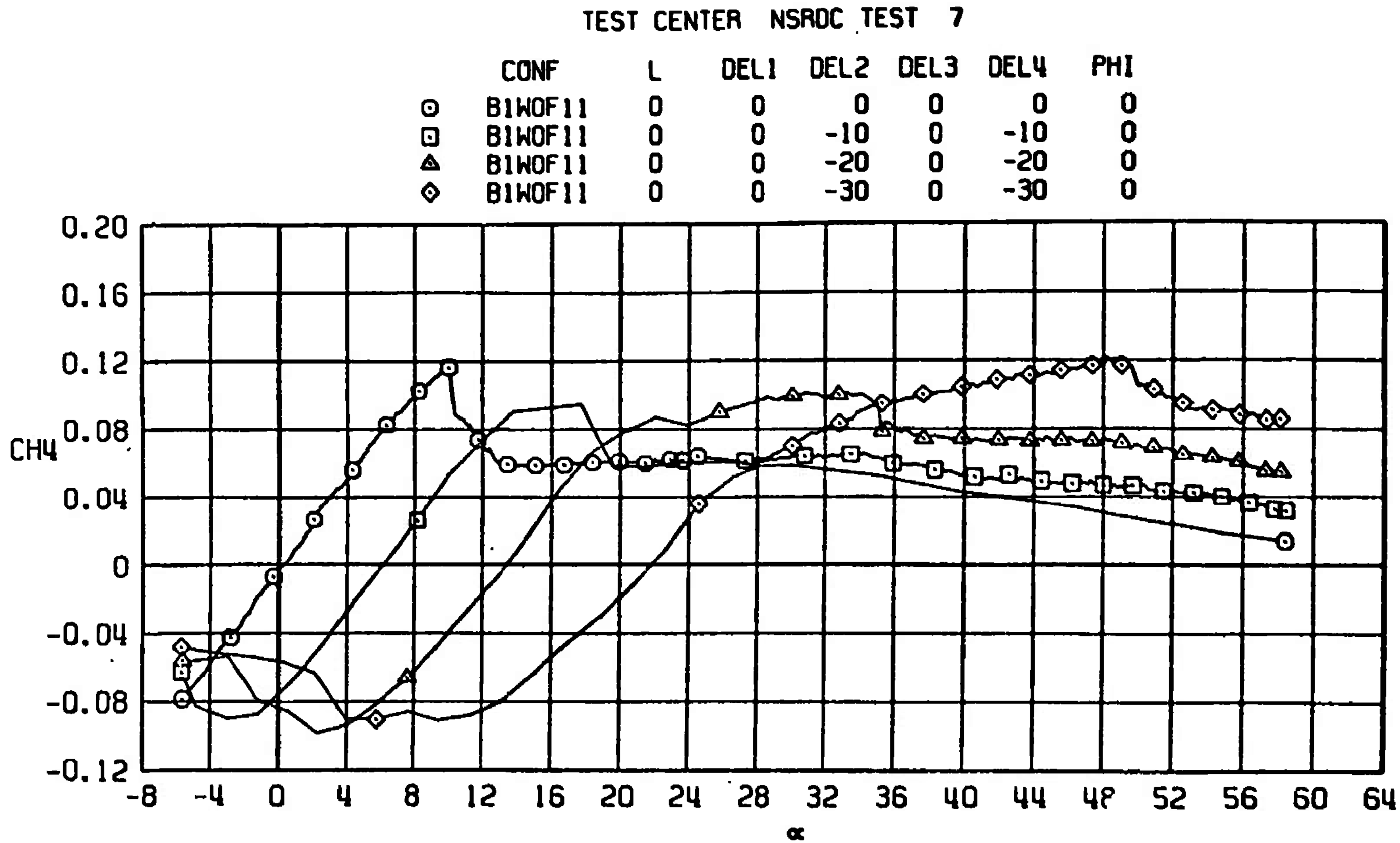

k. CH4 versus α

Figure 40. Concluded.

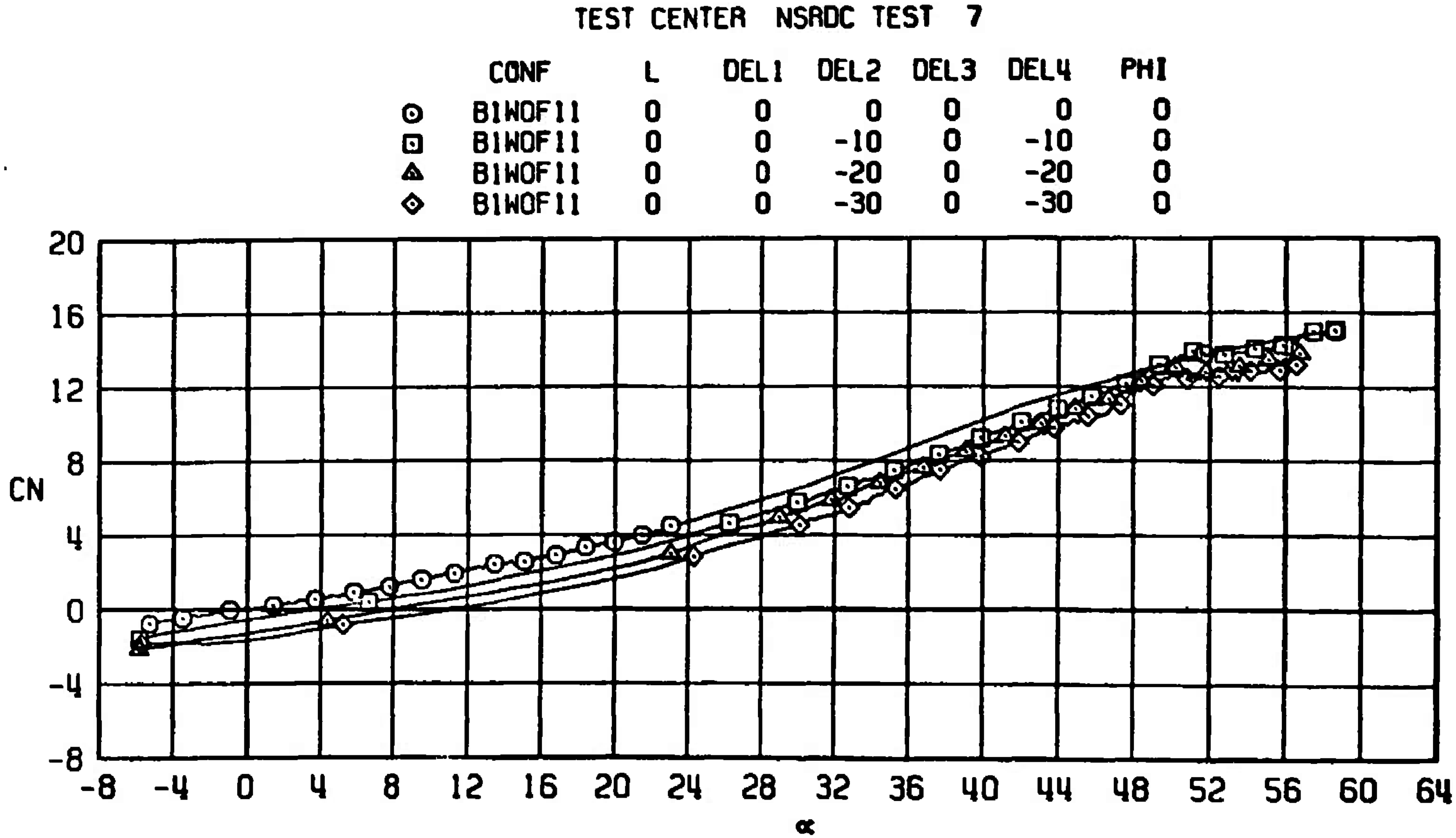

a. CN versus α

Figure 41. Test No. 7, comparison of aerodynamic coefficients of configuration B1W0F11 for various deflections of tail fins No. 2 and 4 at M_∞ = 1.0.

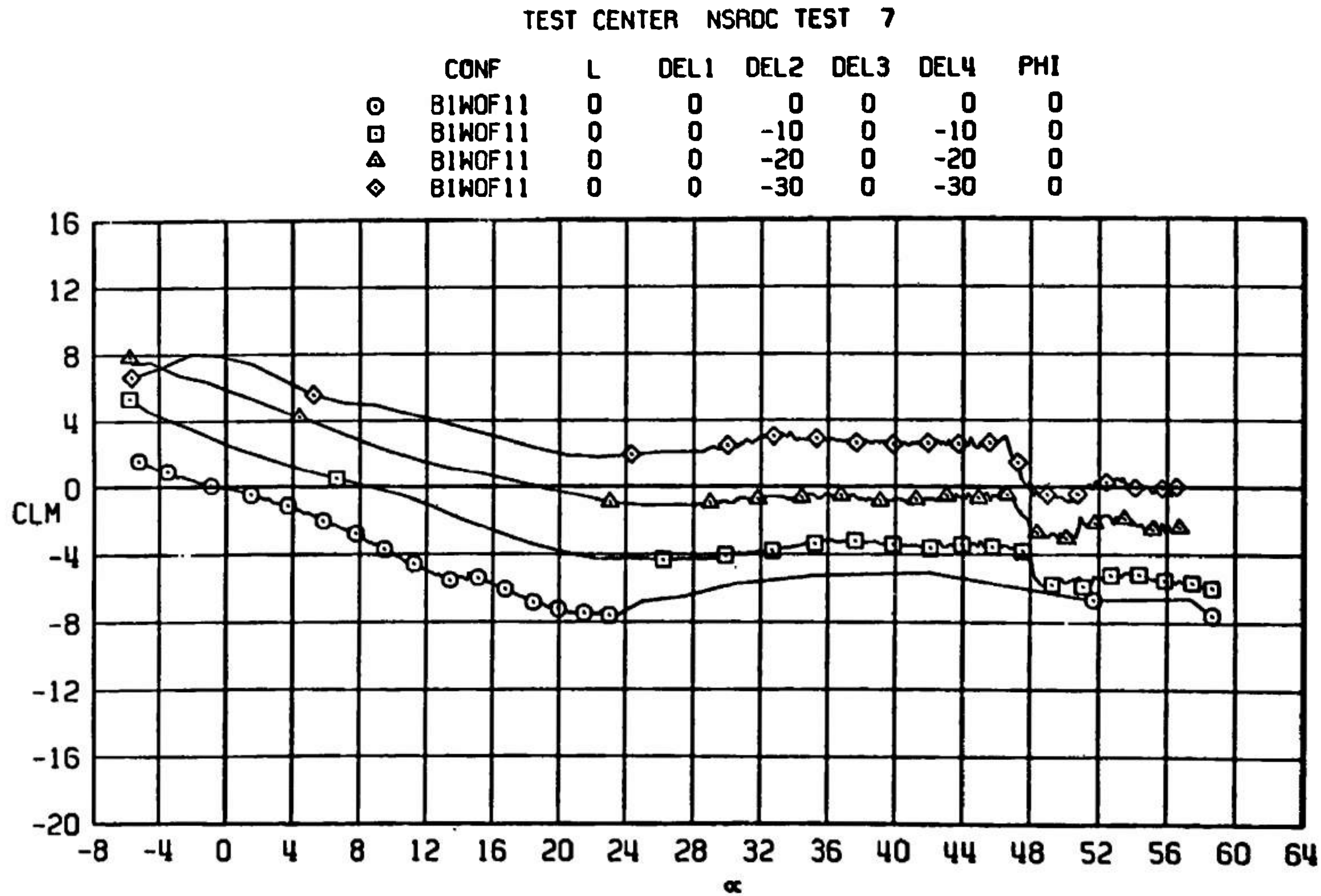

b. CLM versus α
Figure 41. Continued.

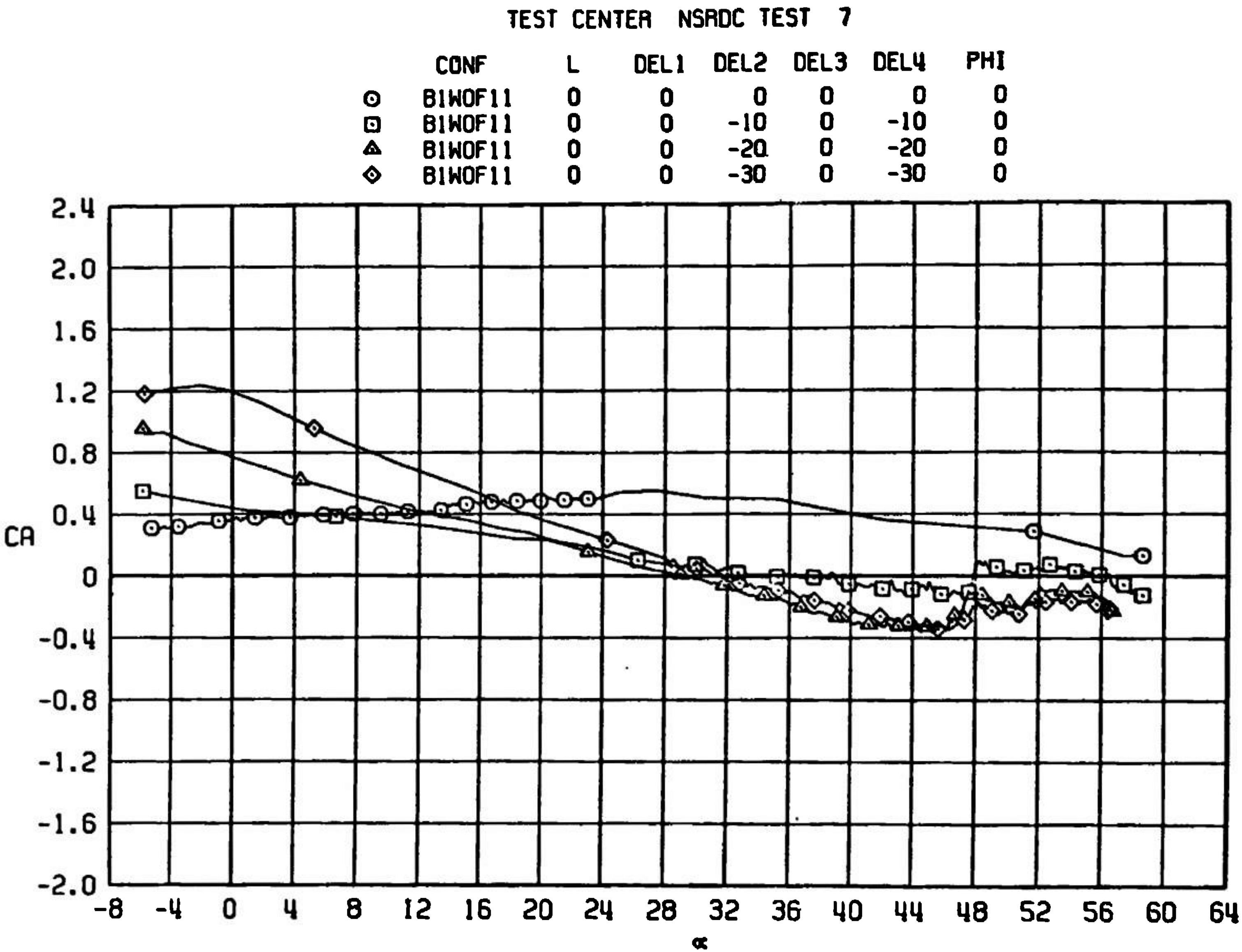

c. CA versus a
Figure 41. Continued.

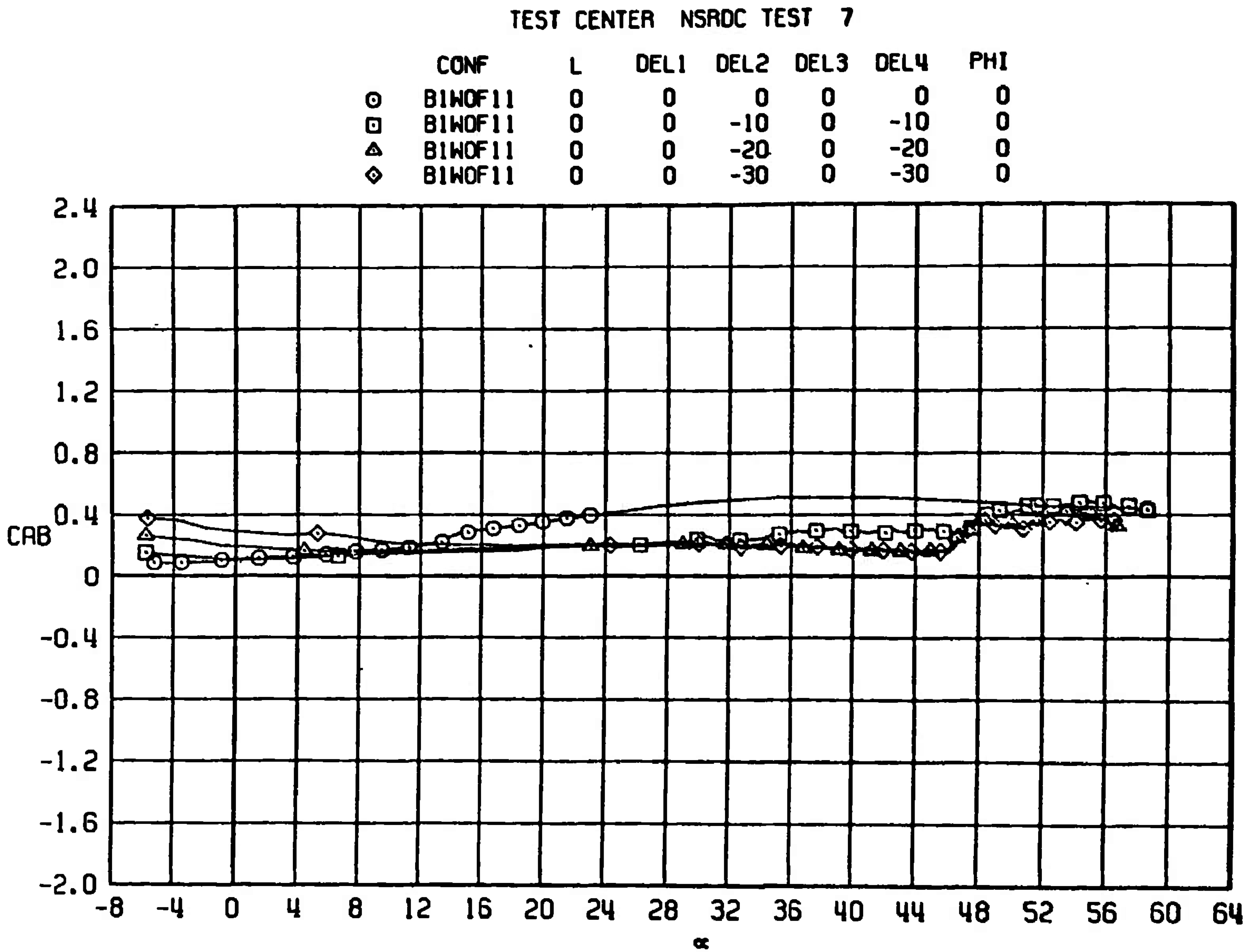

d. CAB versus α

Figure 41. Continued.

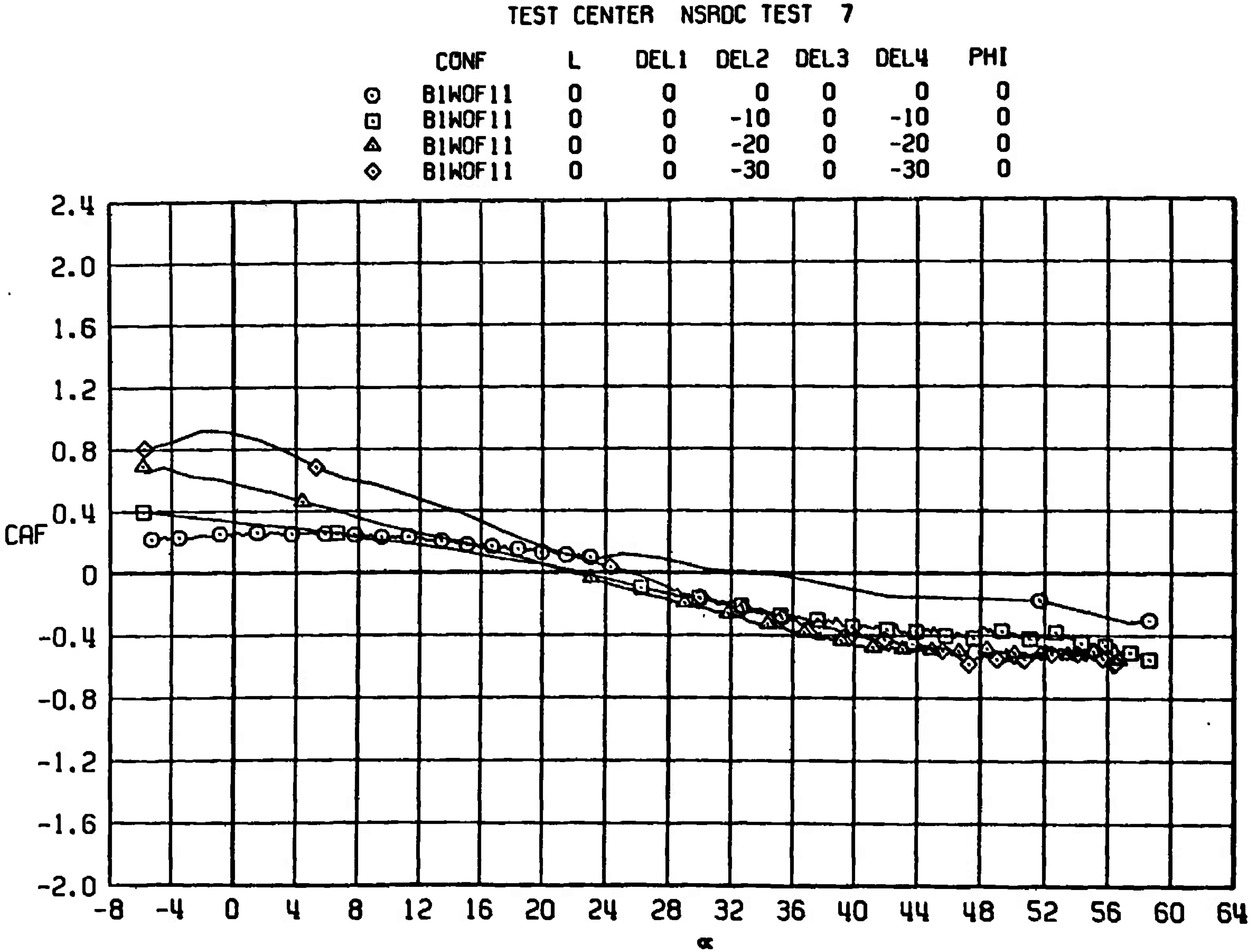

e. CAF versus α
Figure 41. Continued.

TEST CENTER NSRDC TEST 7

	CONF	L	DEL1	DEL2	DEL3	DEL4	PHI
⊙	B1W0F11	0	0	0	0	0	0
⊡	B1W0F11	0	0	-10	0	-10	0
⚠	B1W0F11	0	0	-20	0	-20	0
◈	B1W0F11	0	0	-30	0	-30	0

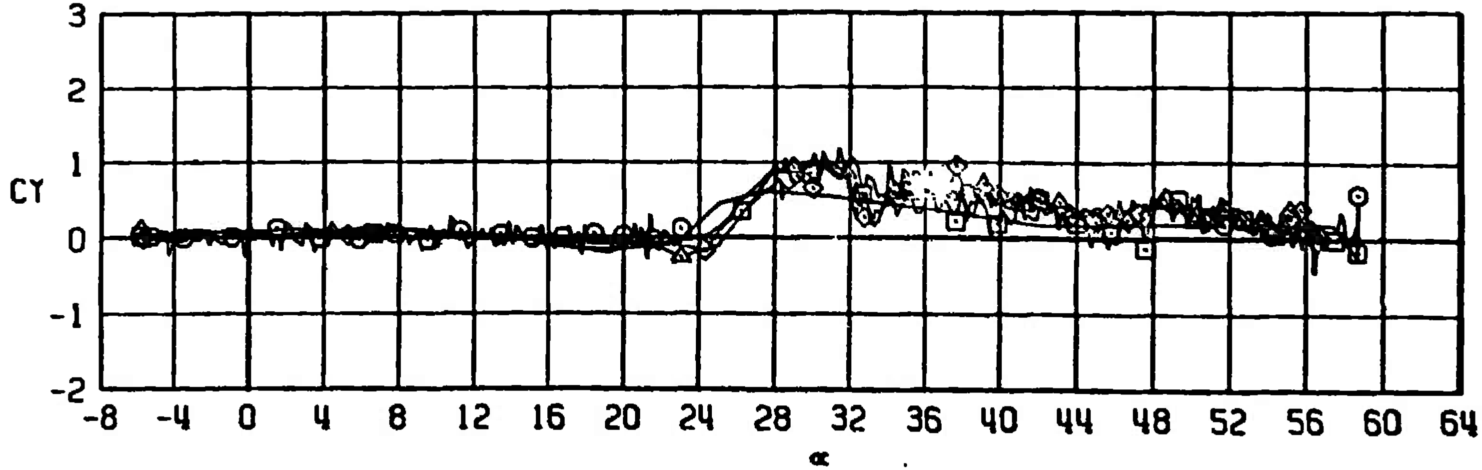

f. CY versus α

Figure 41. Continued.

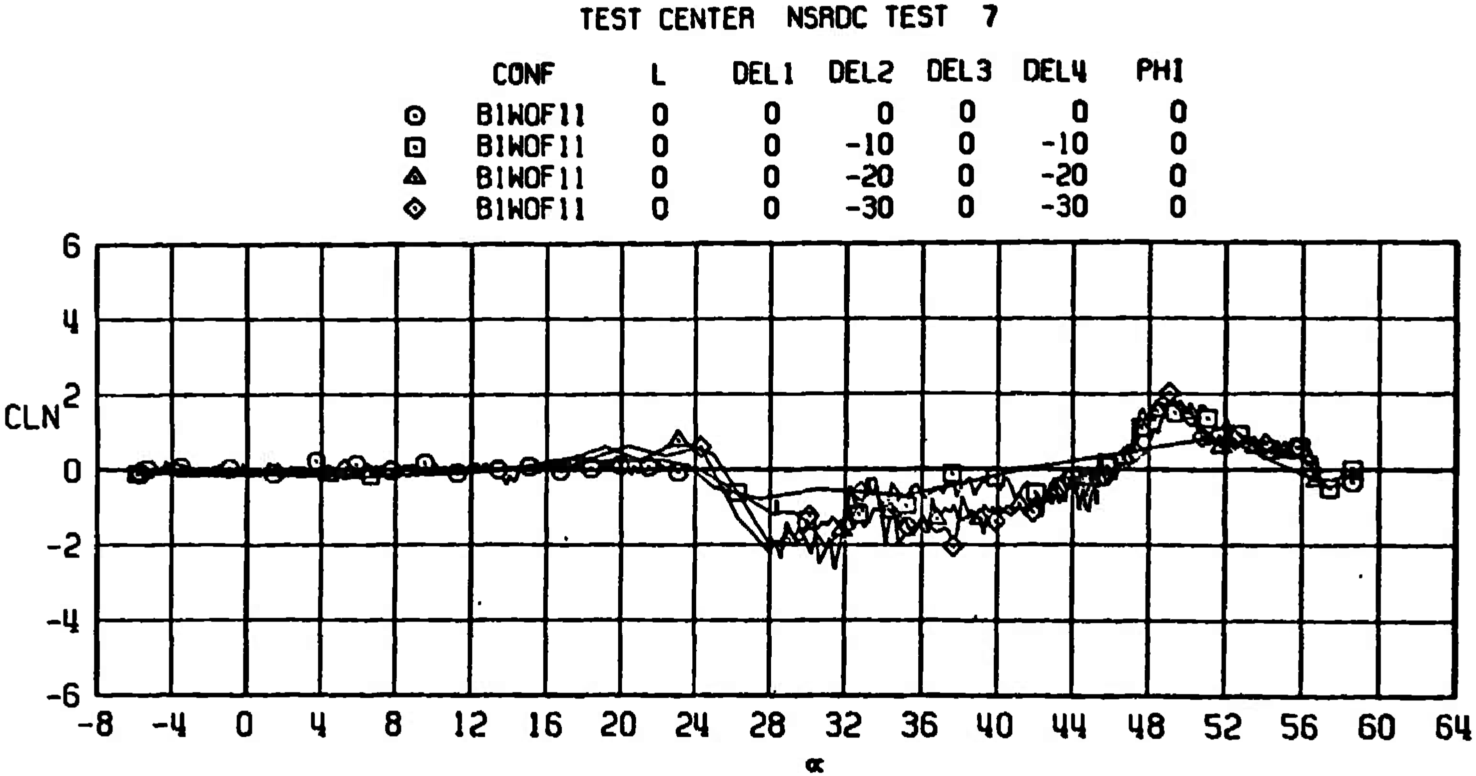

g. CLN versus a
Figure 41. Continued.

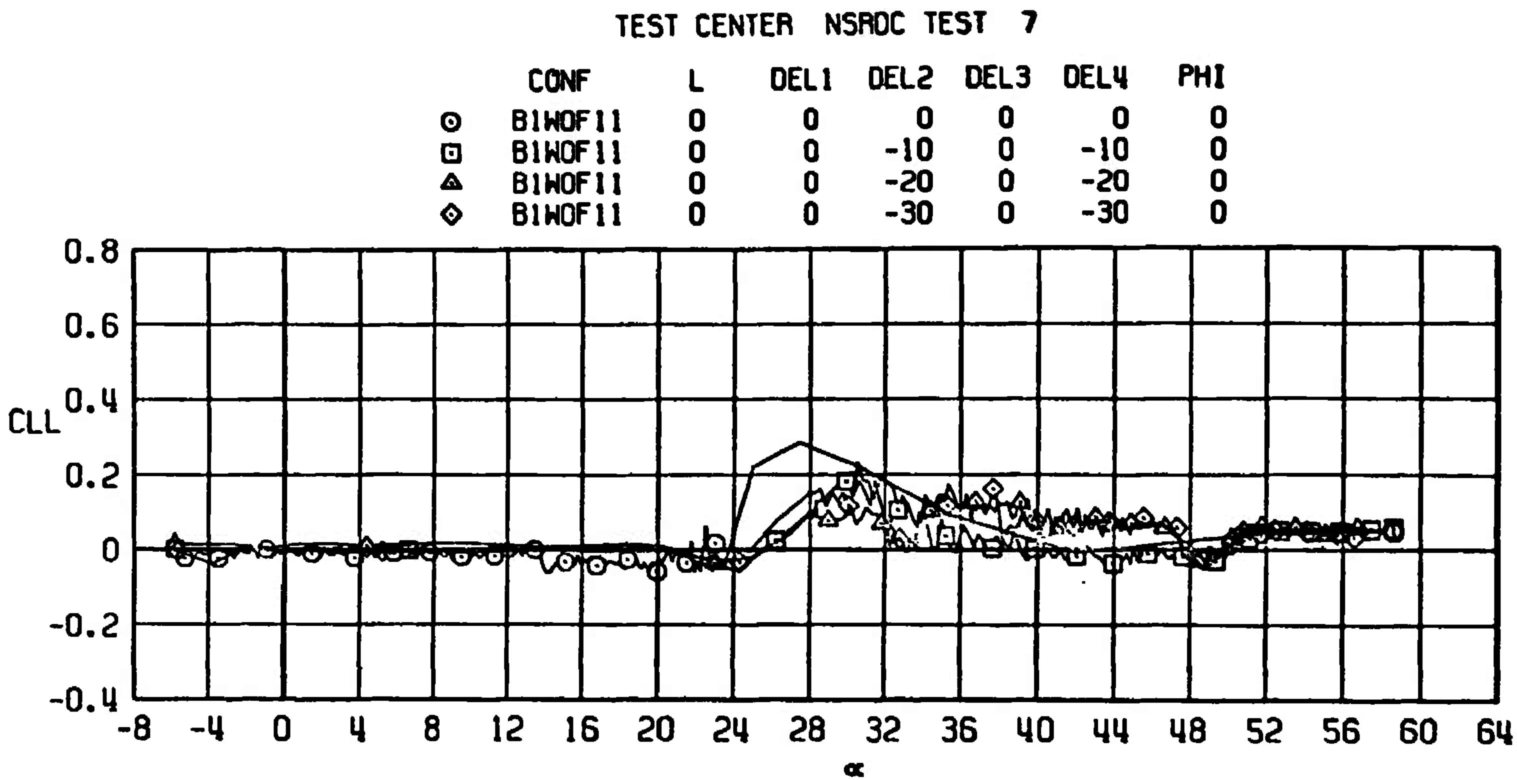

h. CLL versus α
Figure 41. Continued.

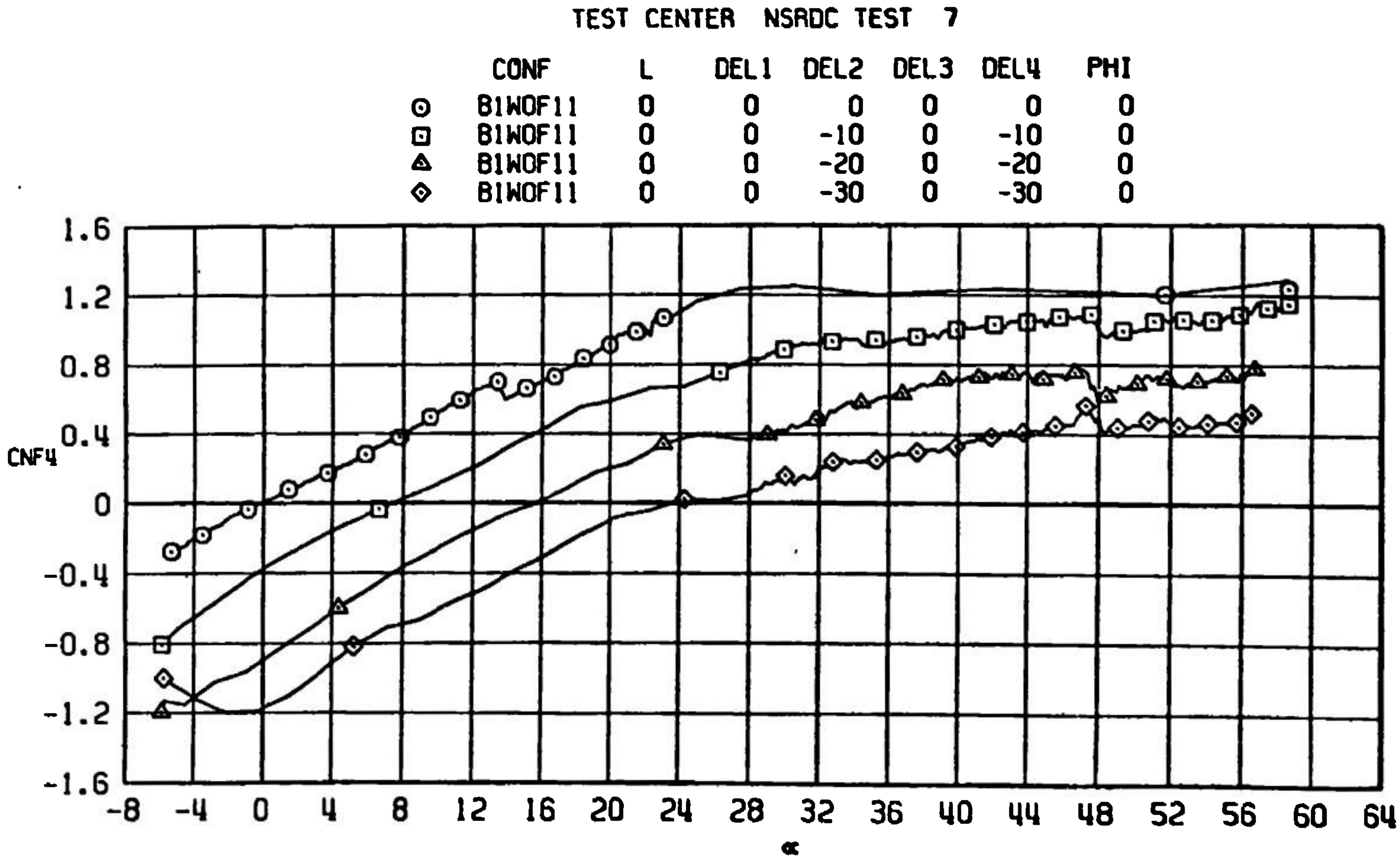

i. CNF4 versus α
Figure 41. Continued.

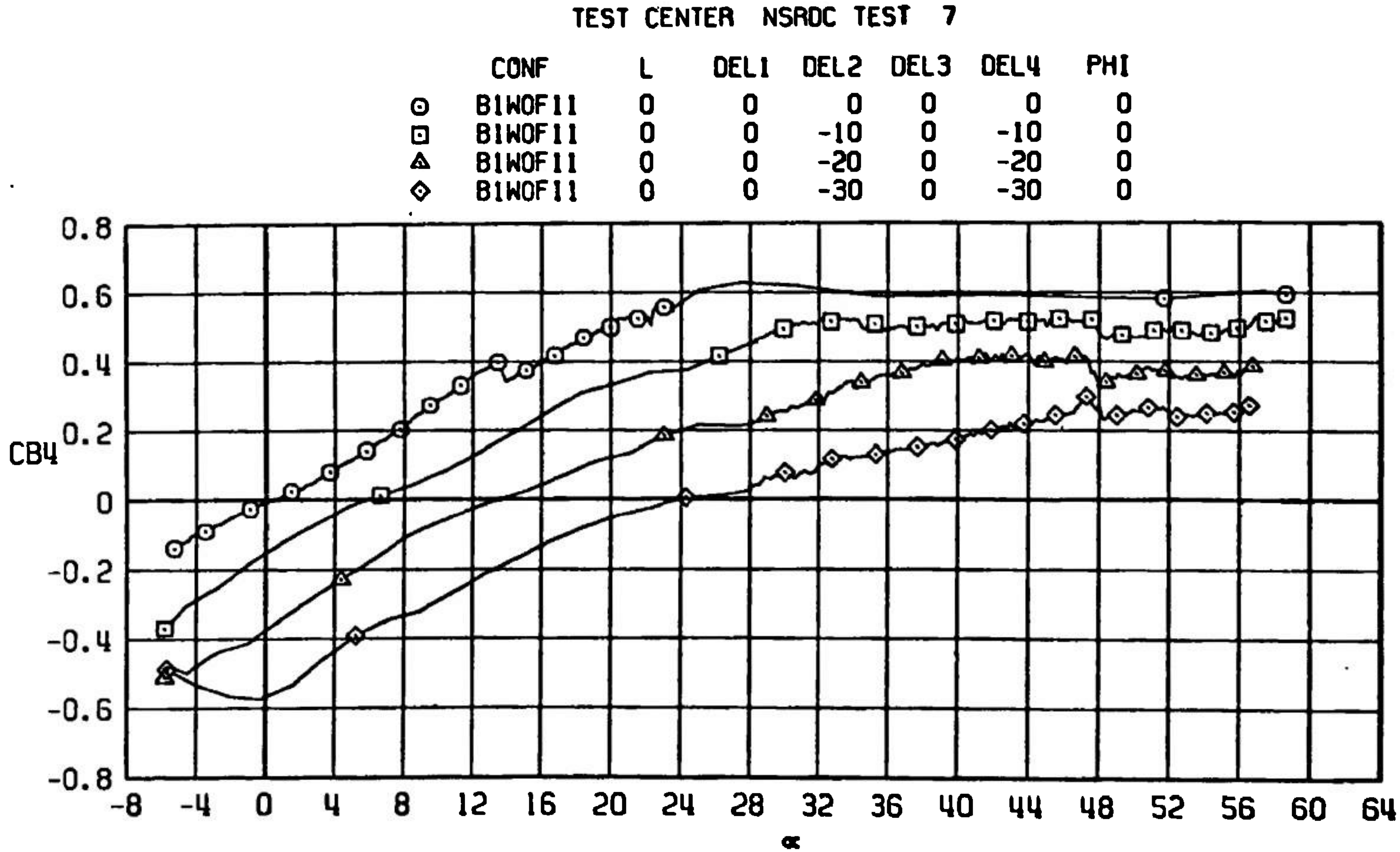

j. CB4 versus α
Figure 41. Continued.

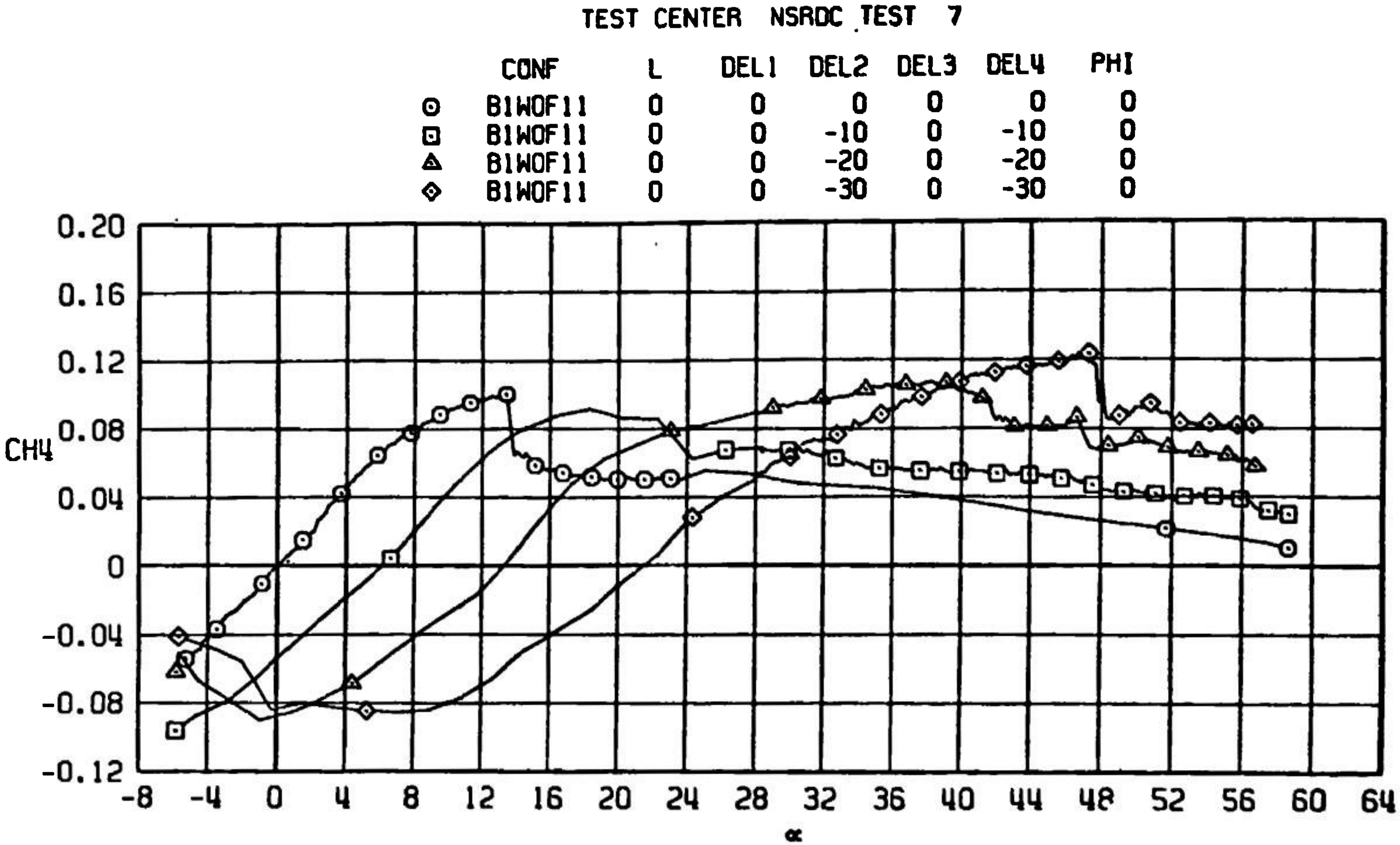

k. CH4 versus α
Figure 41. Concluded.

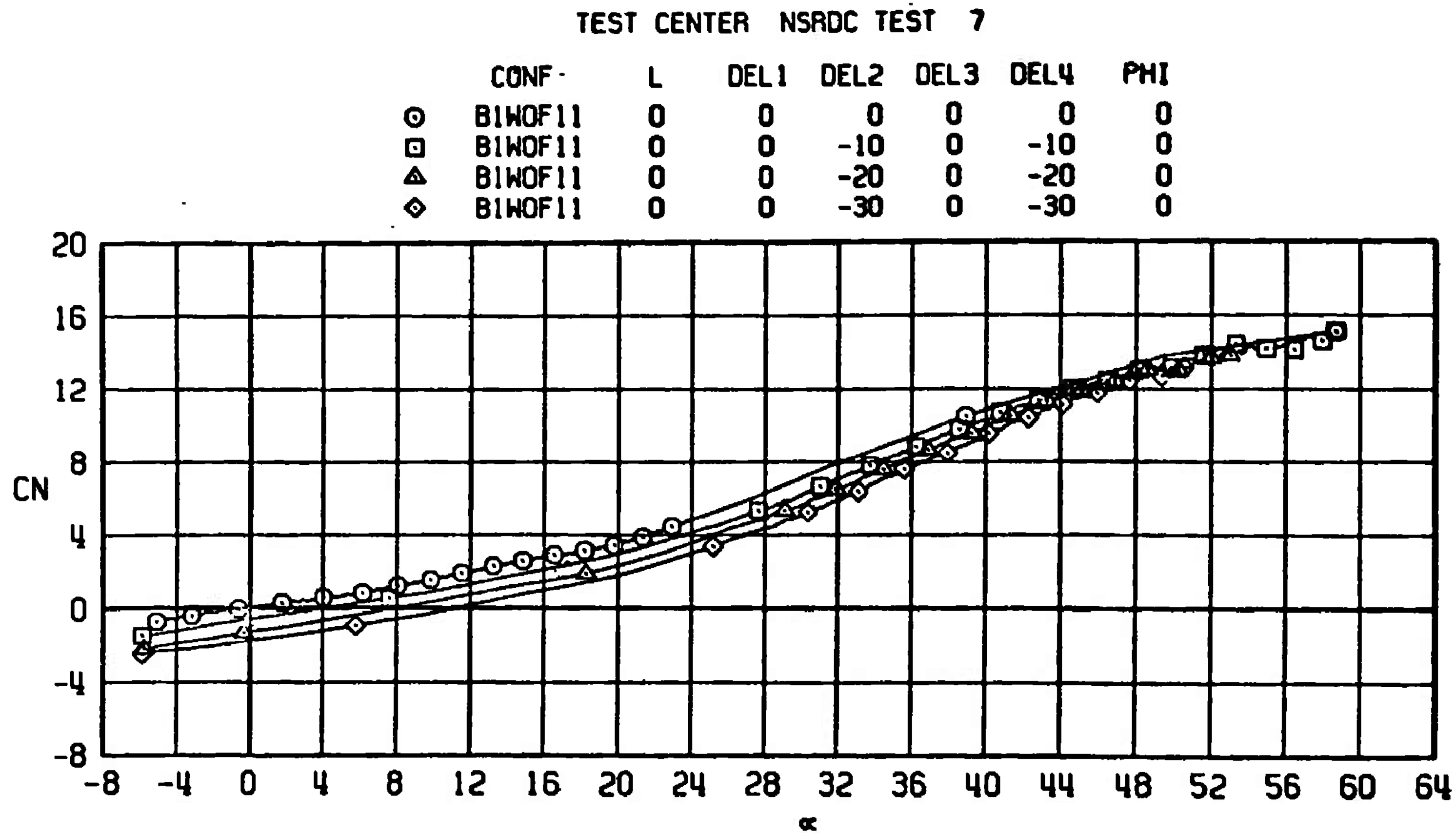

a. CN versus α

Figure 42. Test No. 7, comparison of aerodynamic coefficients of configuration B1W0F11 for various deflections of tail fins No. 2 and 4 at M_∞ = 1.1.

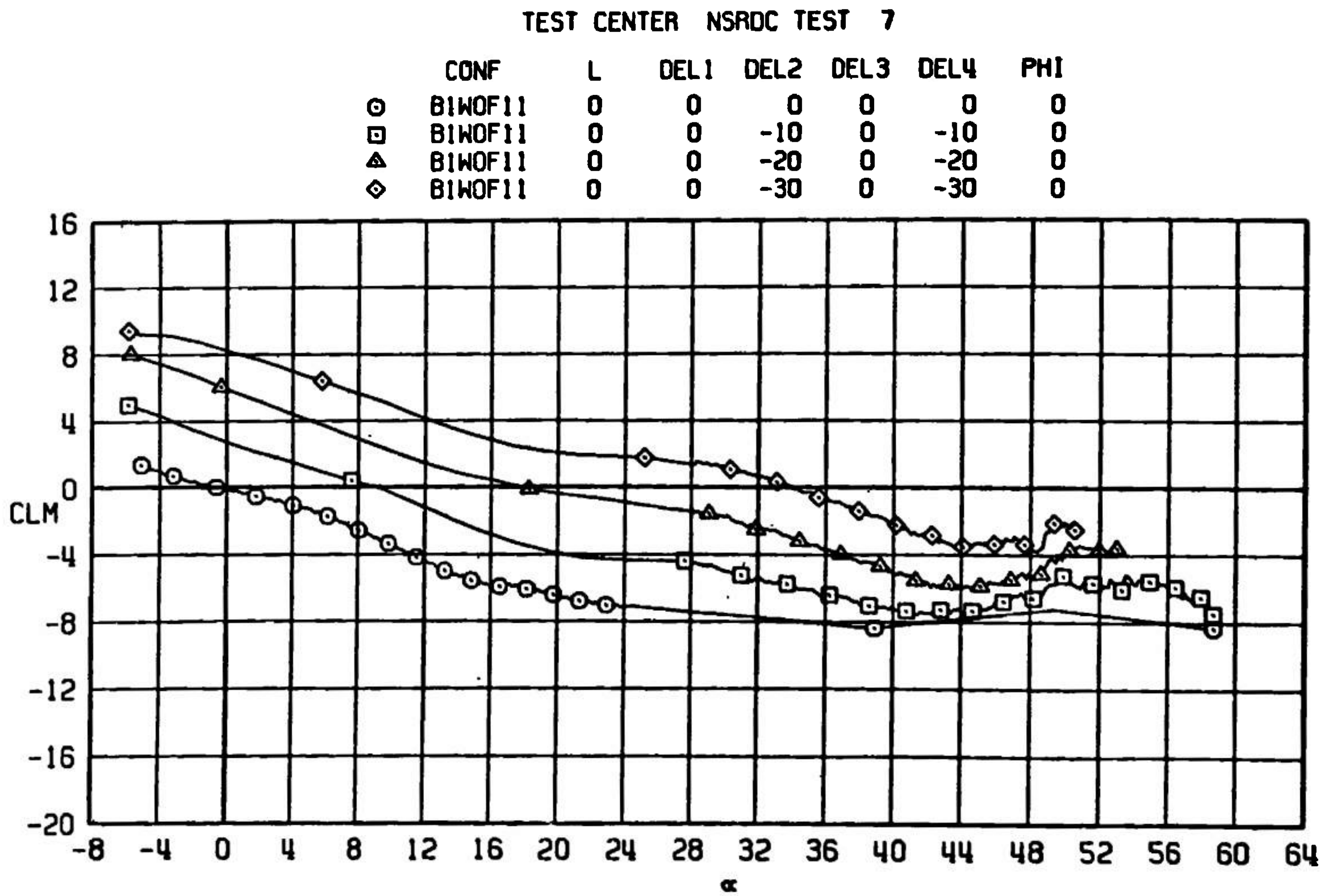

b. CLM versus α
Figure 42. Continued.

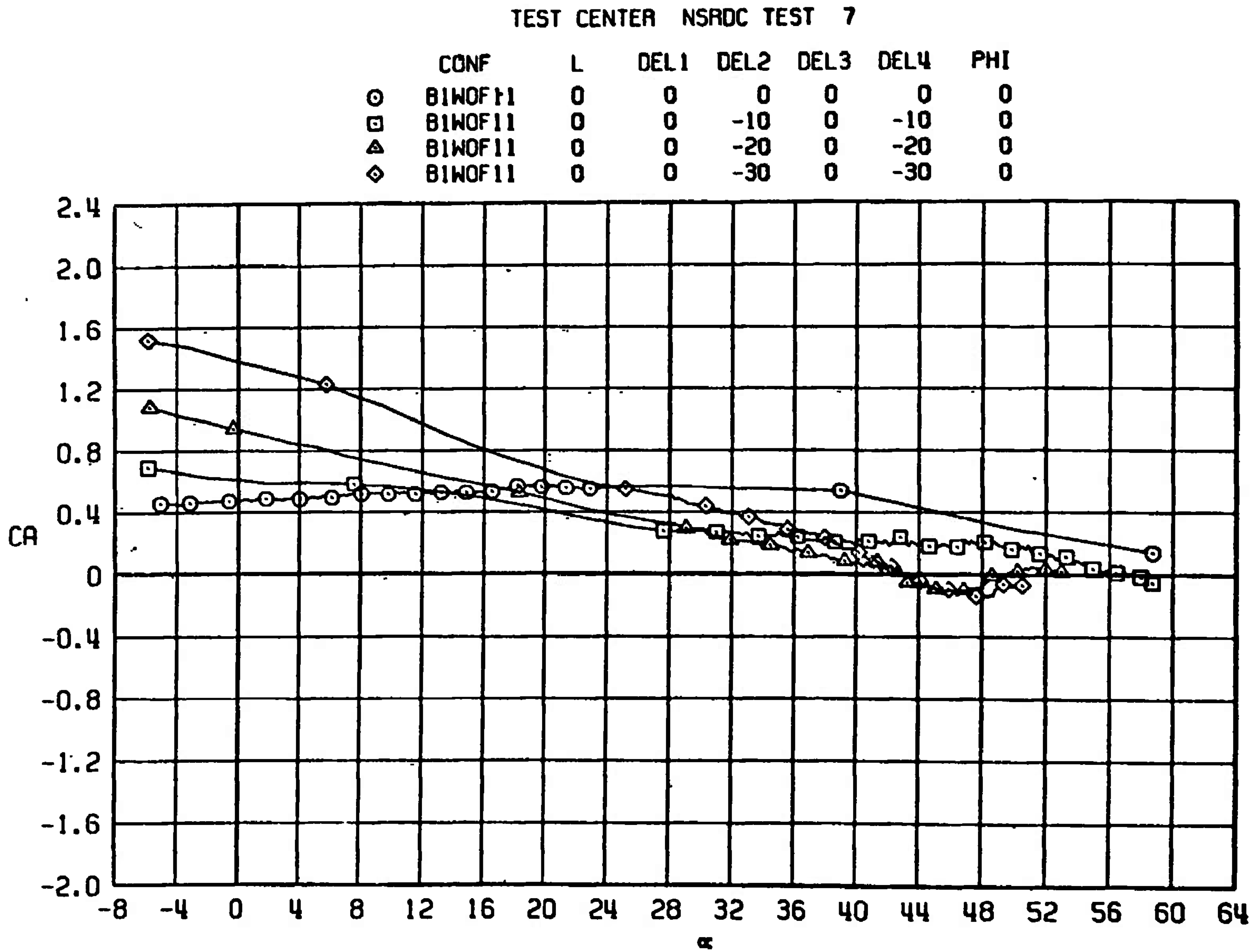

c. CA versus α

Figure 42. Continued.

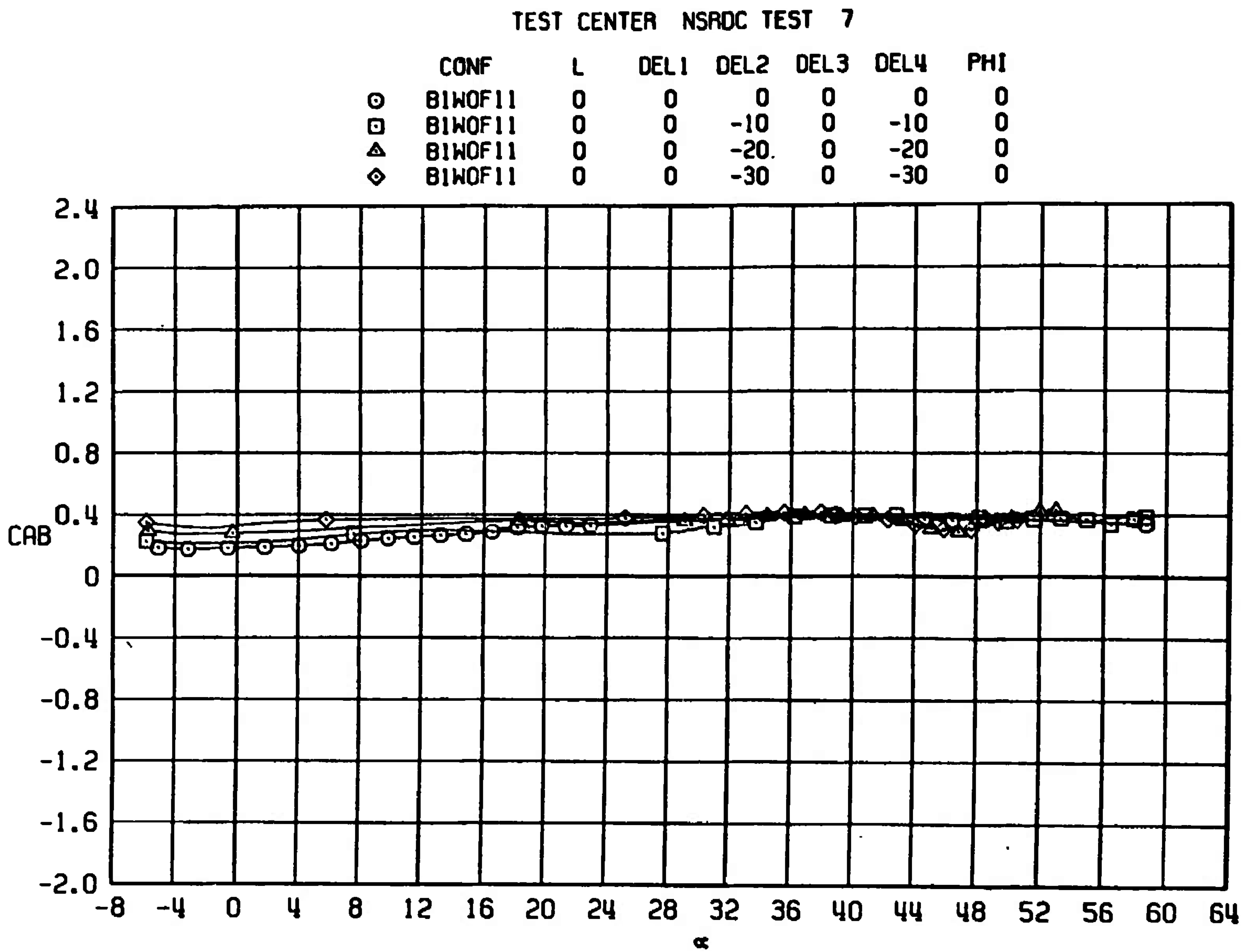

d. CAB versus α
Figure 42. Continued.

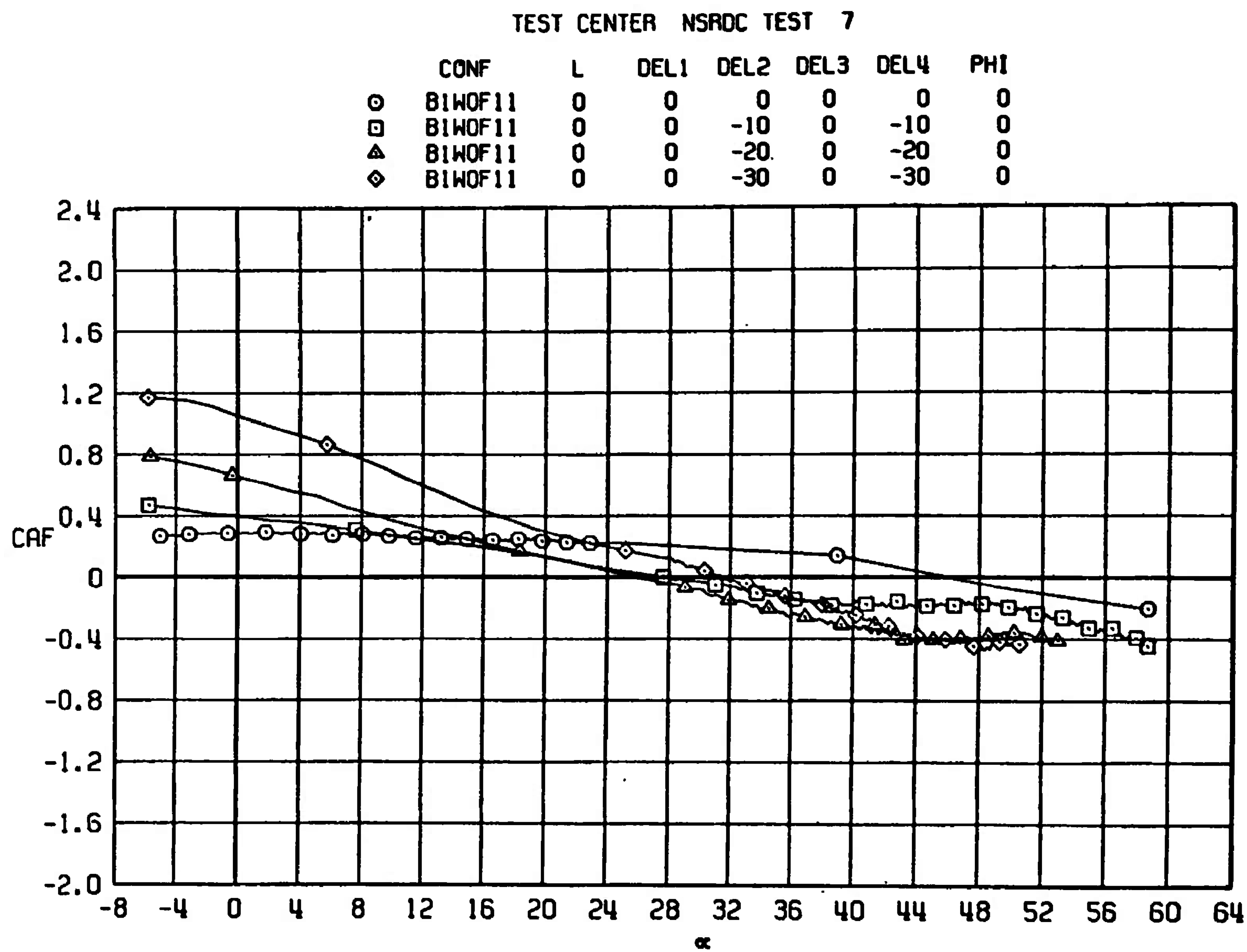

e. CAF versus α

Figure 42. Continued.

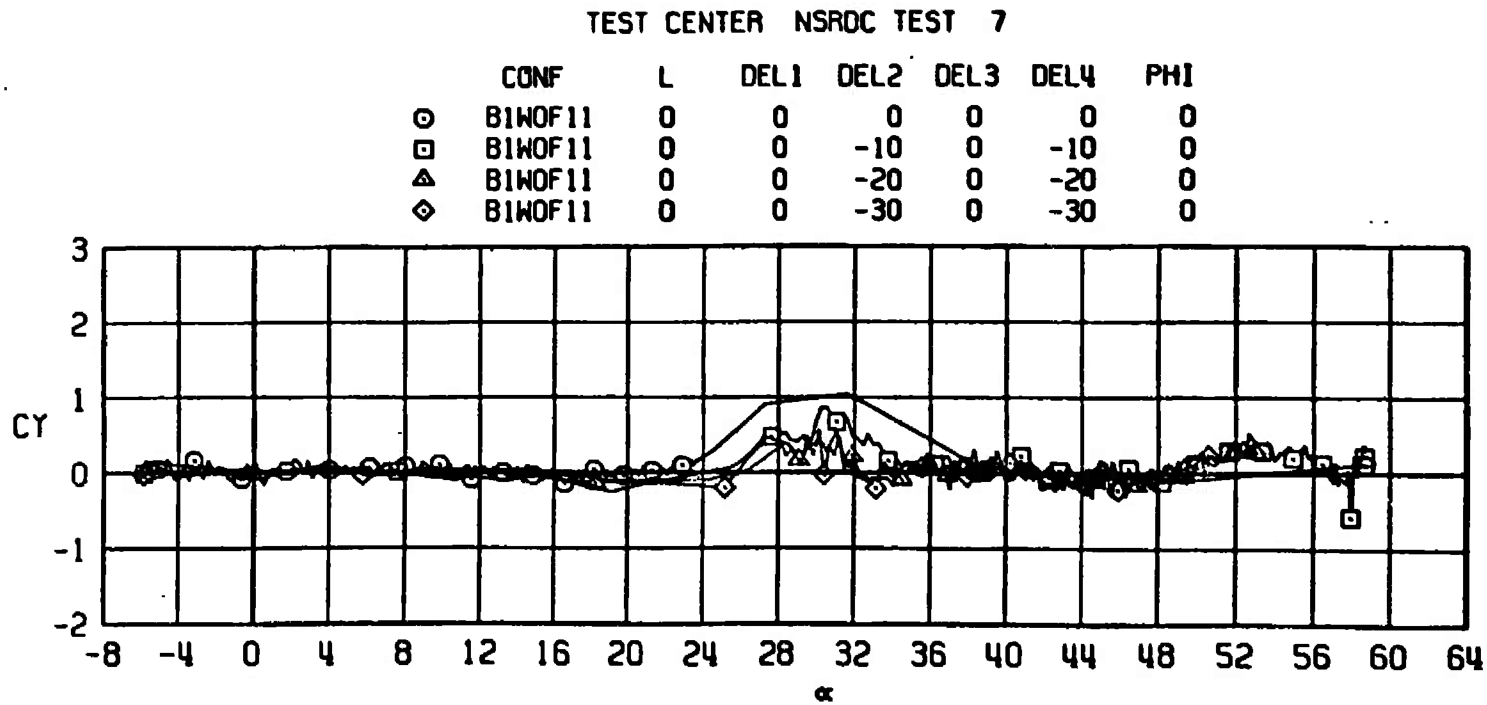

f. CY versus α
Figure 42. Continued.

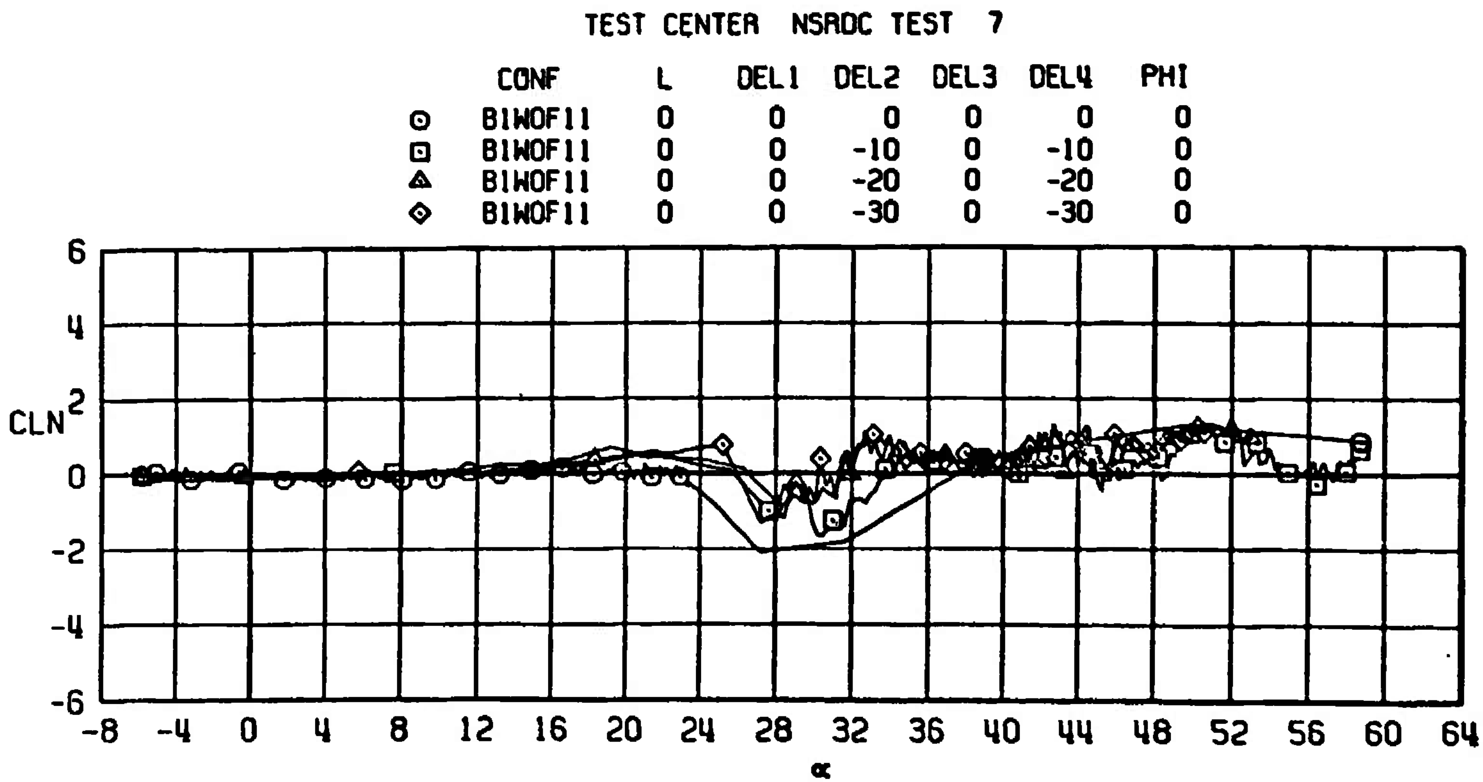

g. CLN versus α
Figure 42. Continued.

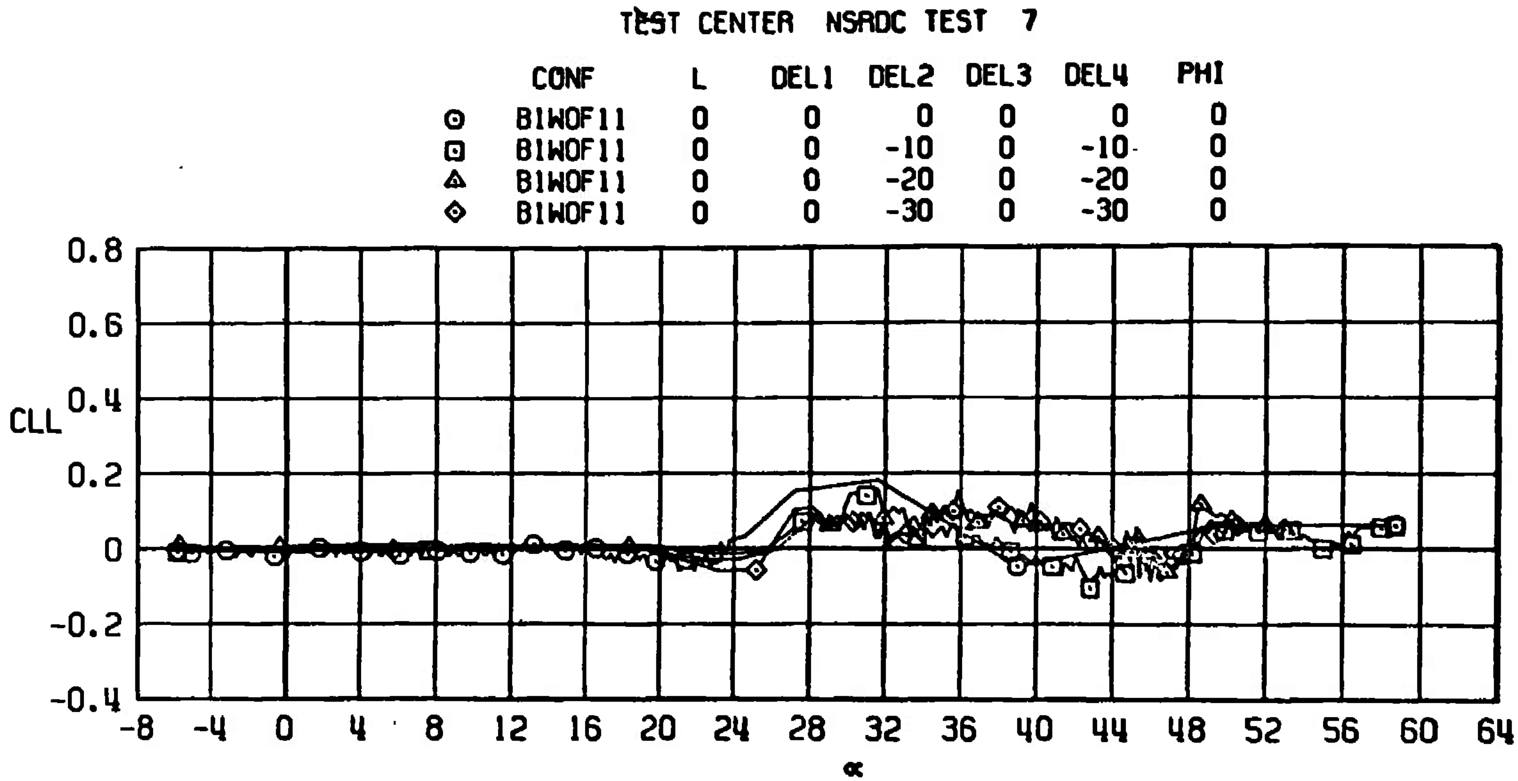

h. CLL versus α
Figure 42. Continued.

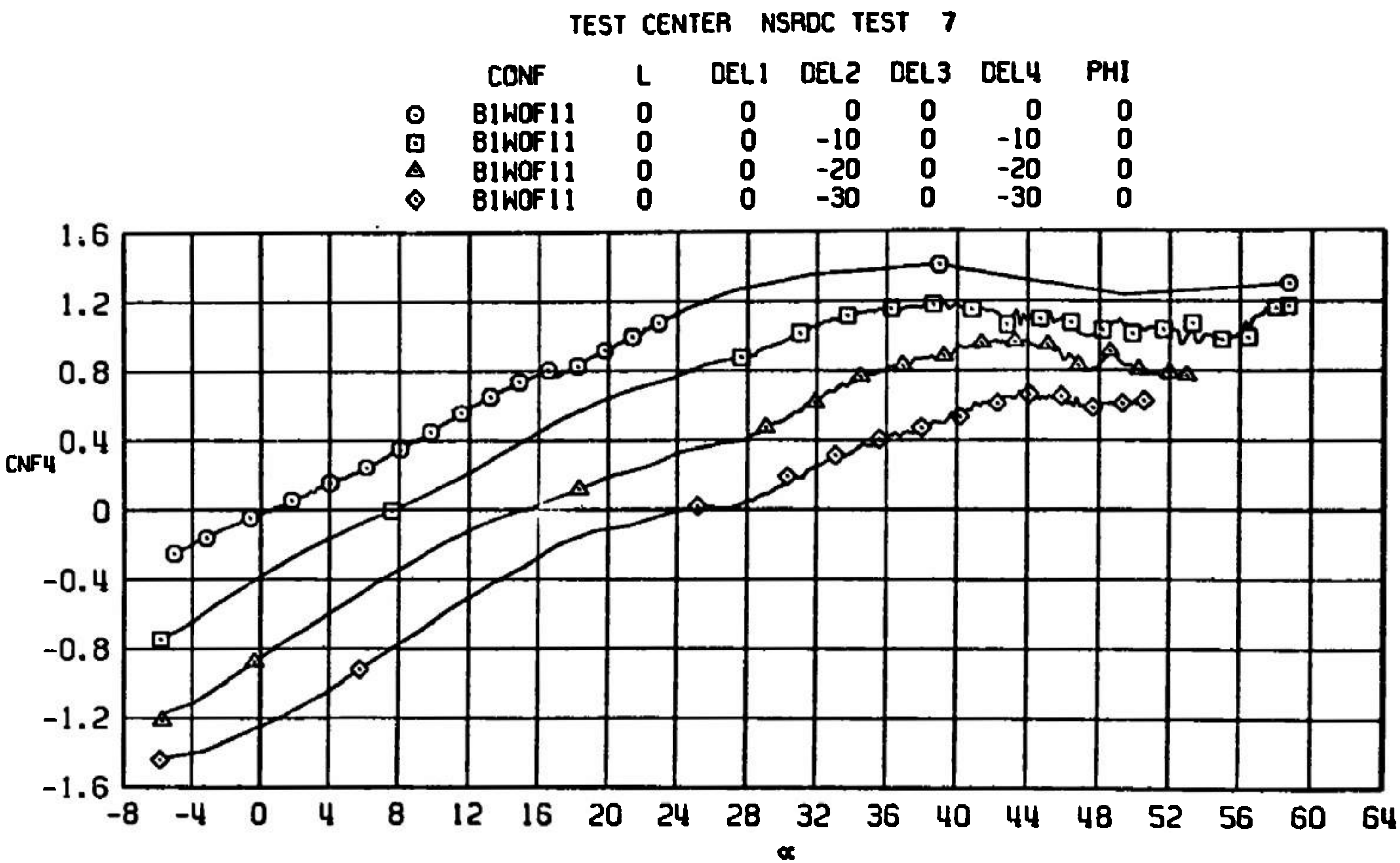

i. CNF4 versus α

Figure 42. Continued.

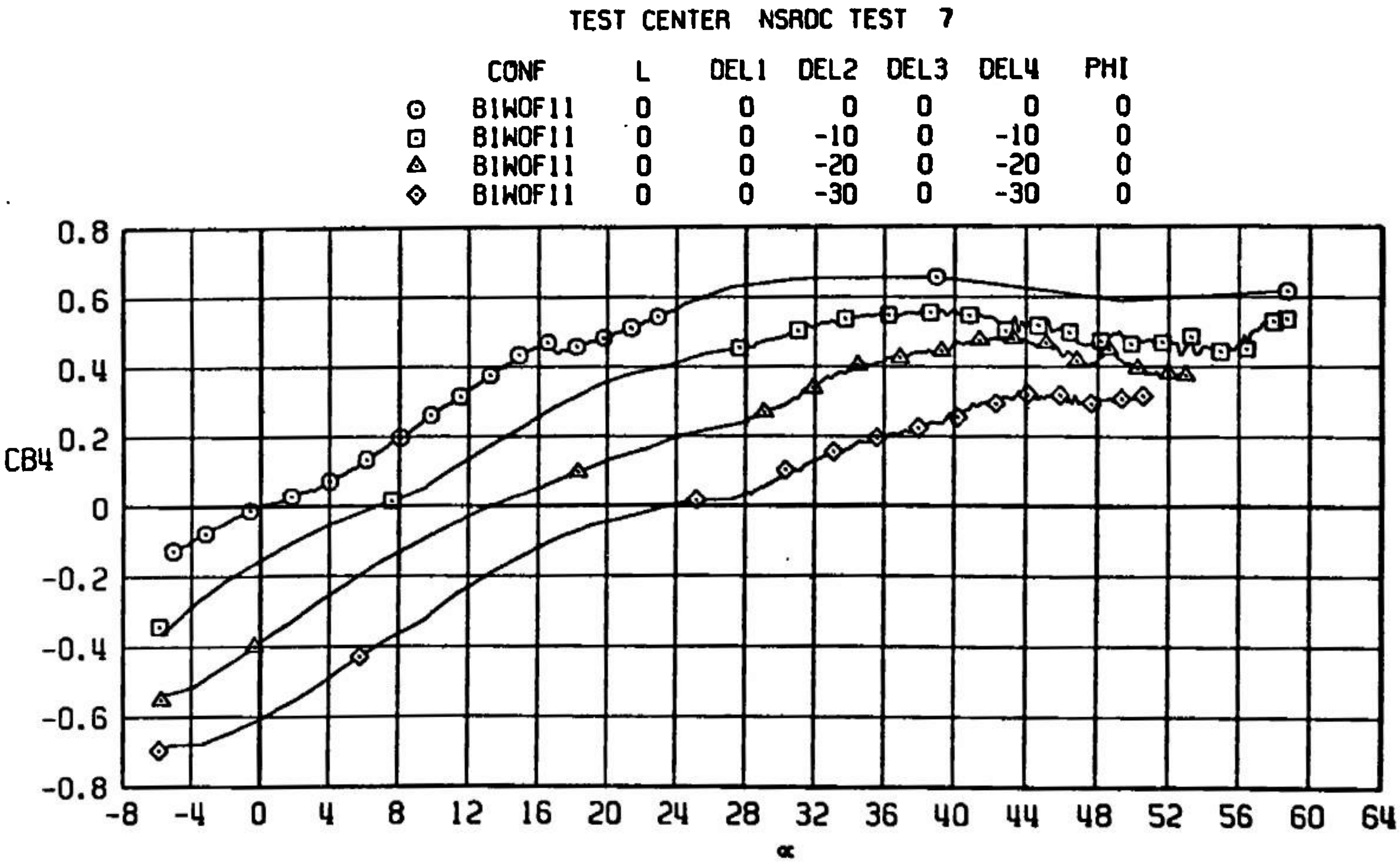

j. CB4 versus α
Figure 42. Continued.

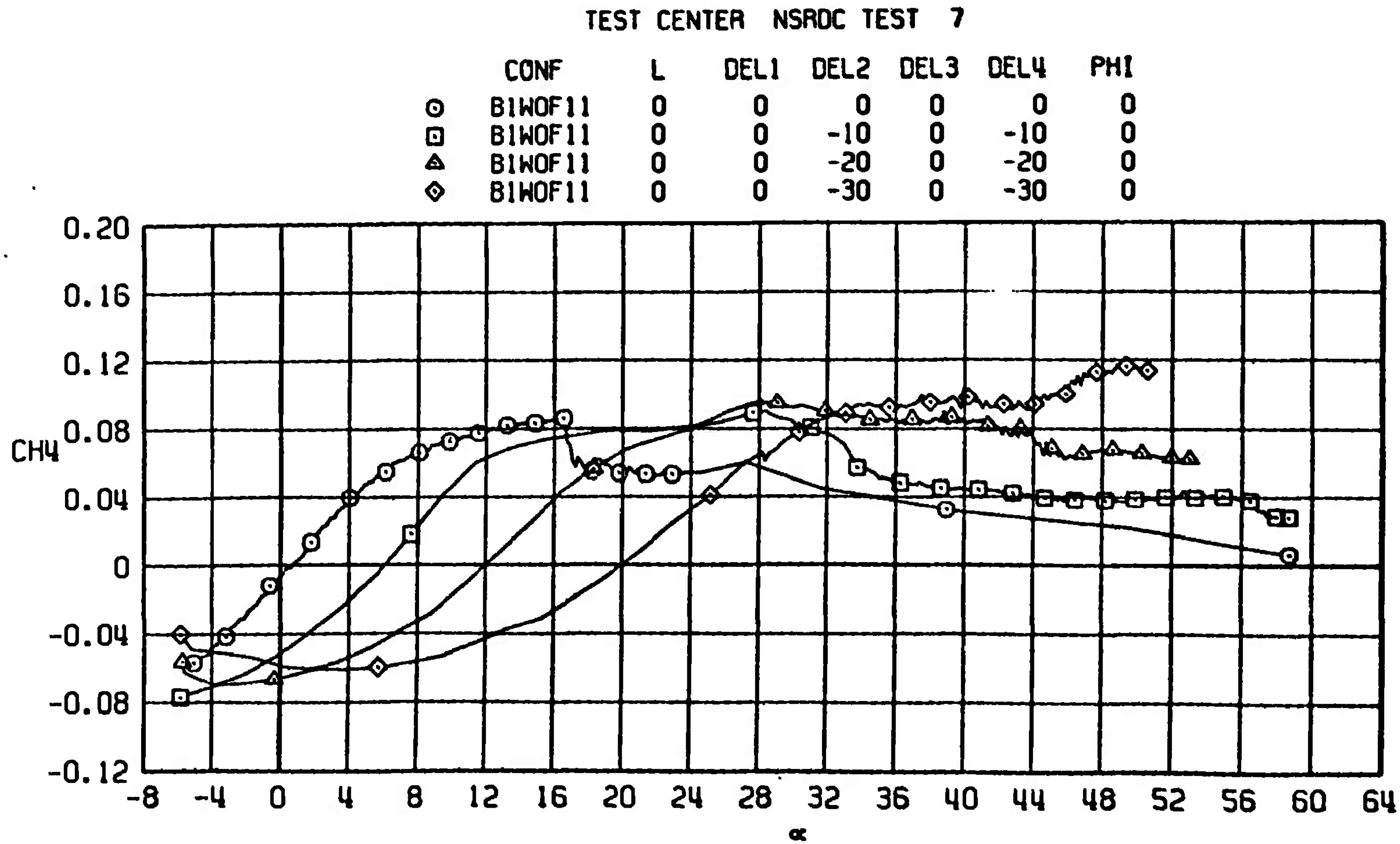

k. CH4 versus α
Figure 42. Concluded.

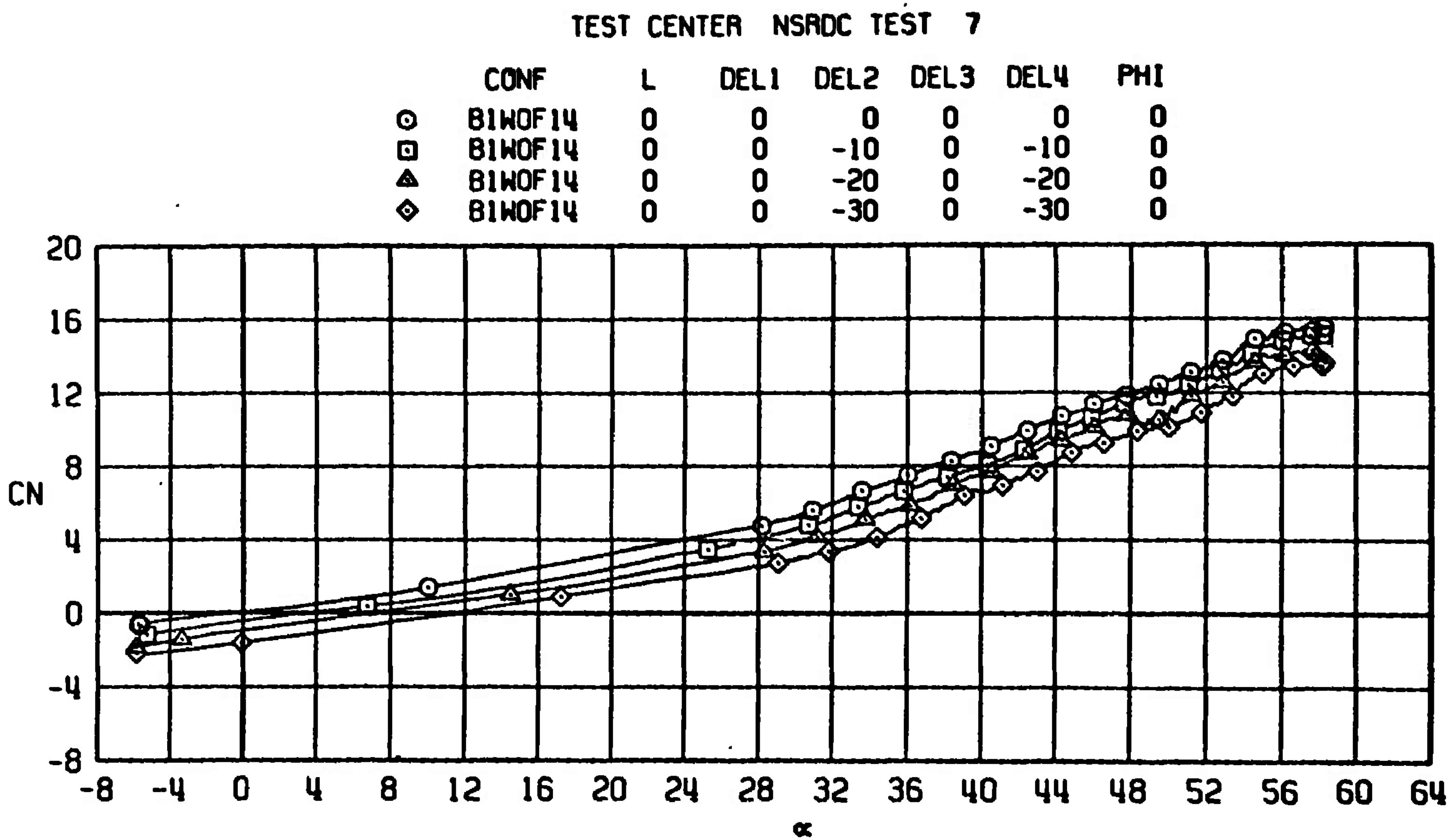

a. CN versus α

Figure 43. Test No. 7, comparison of aerodynamic coefficients of configuration B1W0F14 for various deflections of tail fins No. 2 and 4 at $M_\infty = 0.8$.

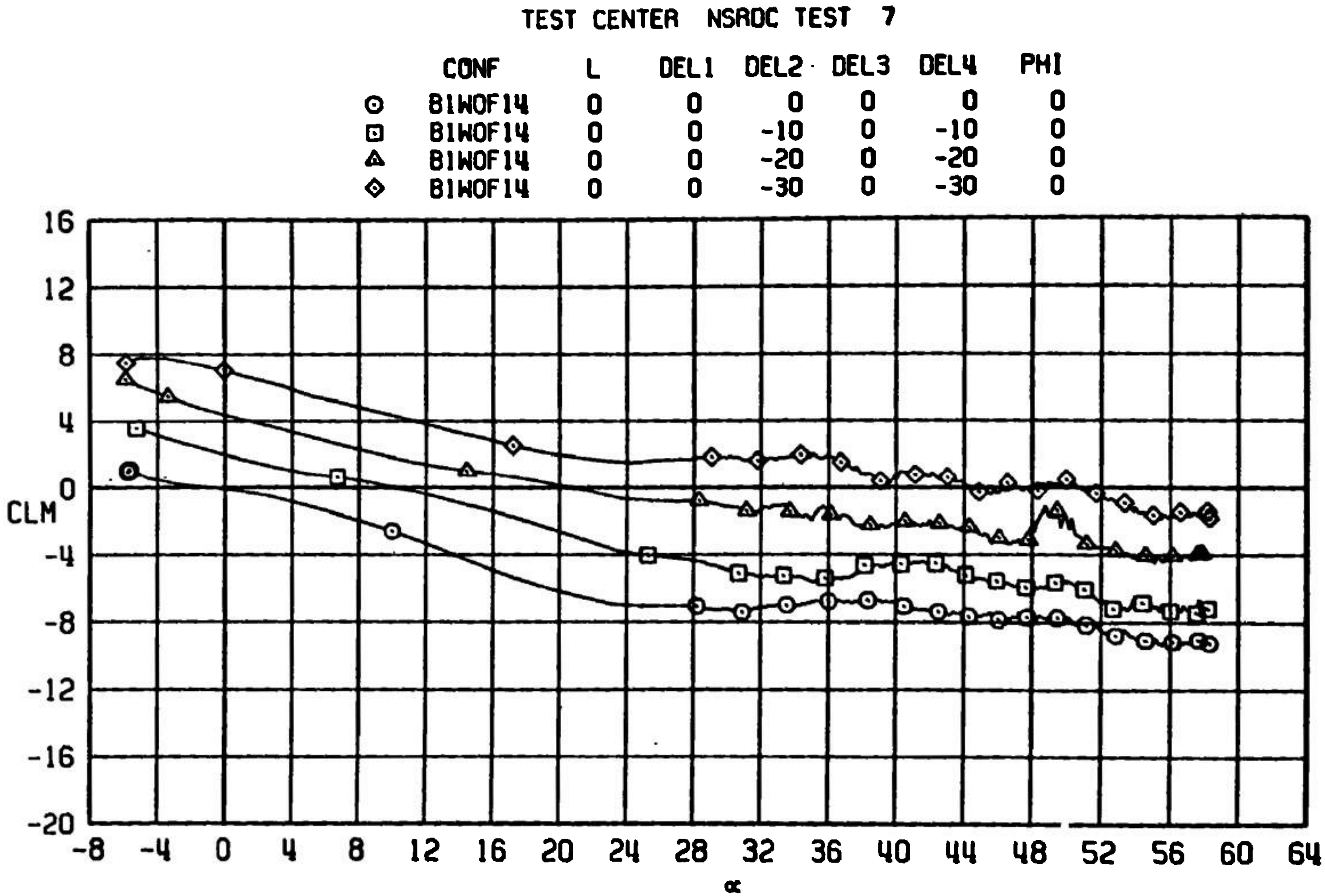

b. CLM versus α
Figure 43. Continued.

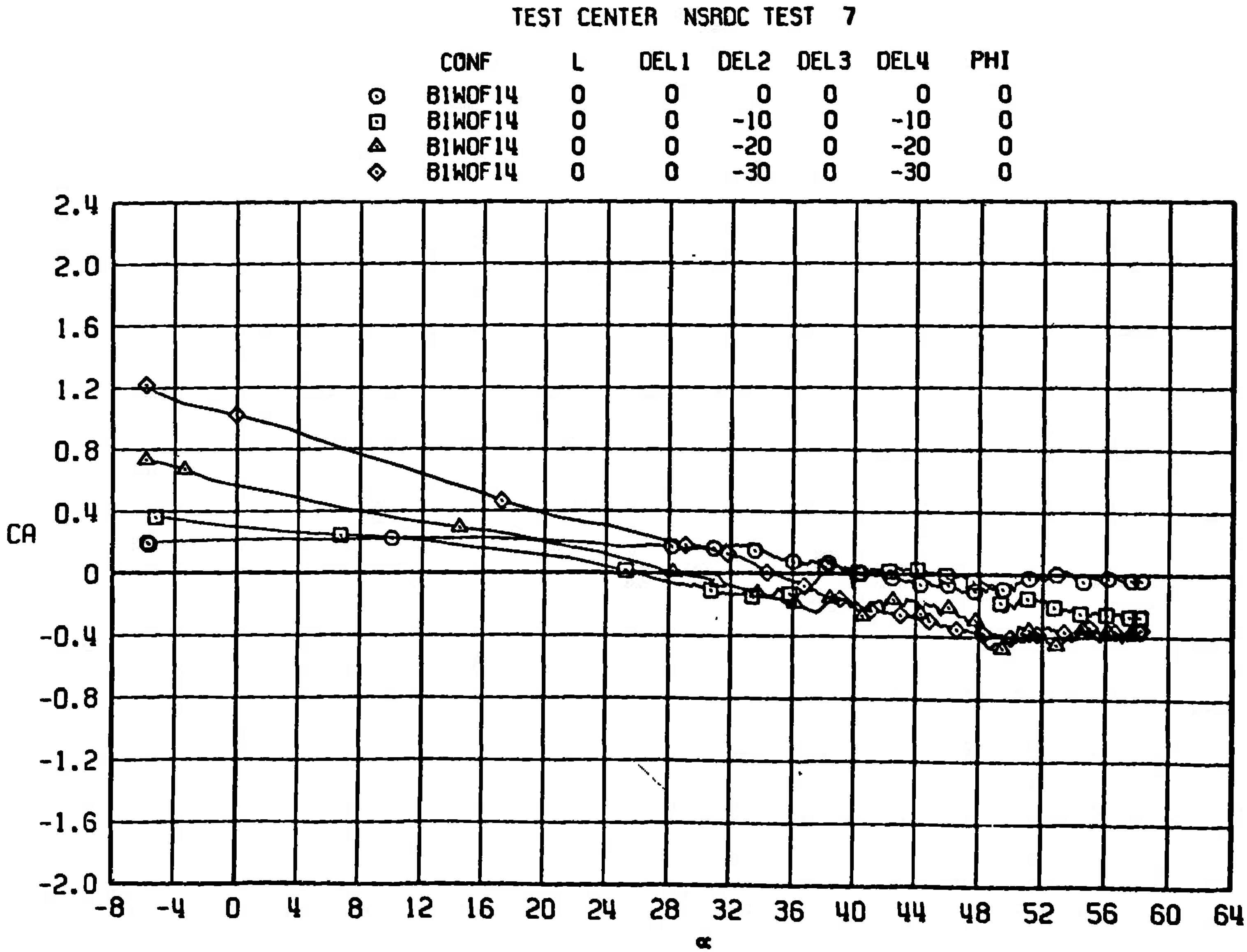

c. CA versus a
Figure 43. Continued.

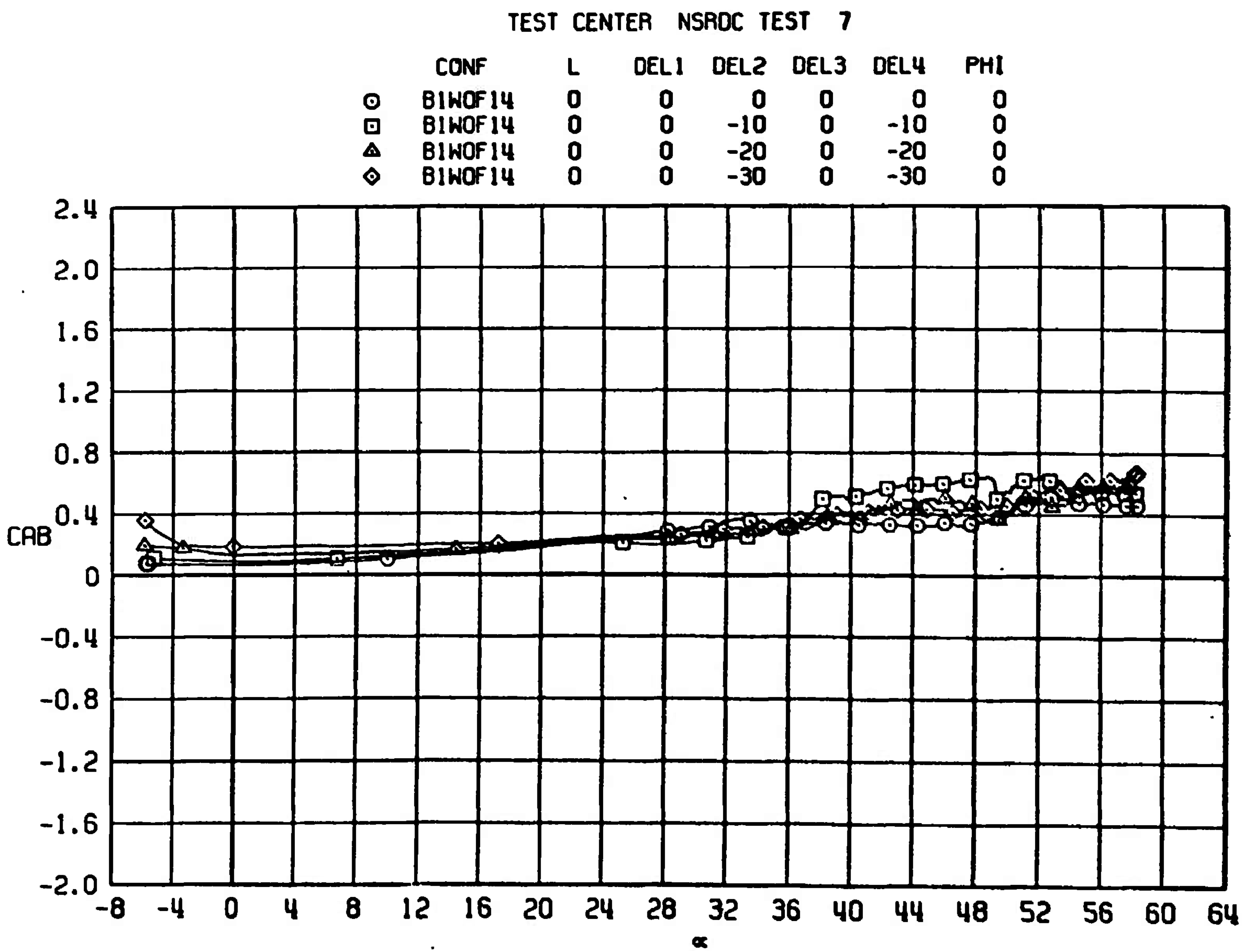

d. CAB versus α
Figure 43. Continued.

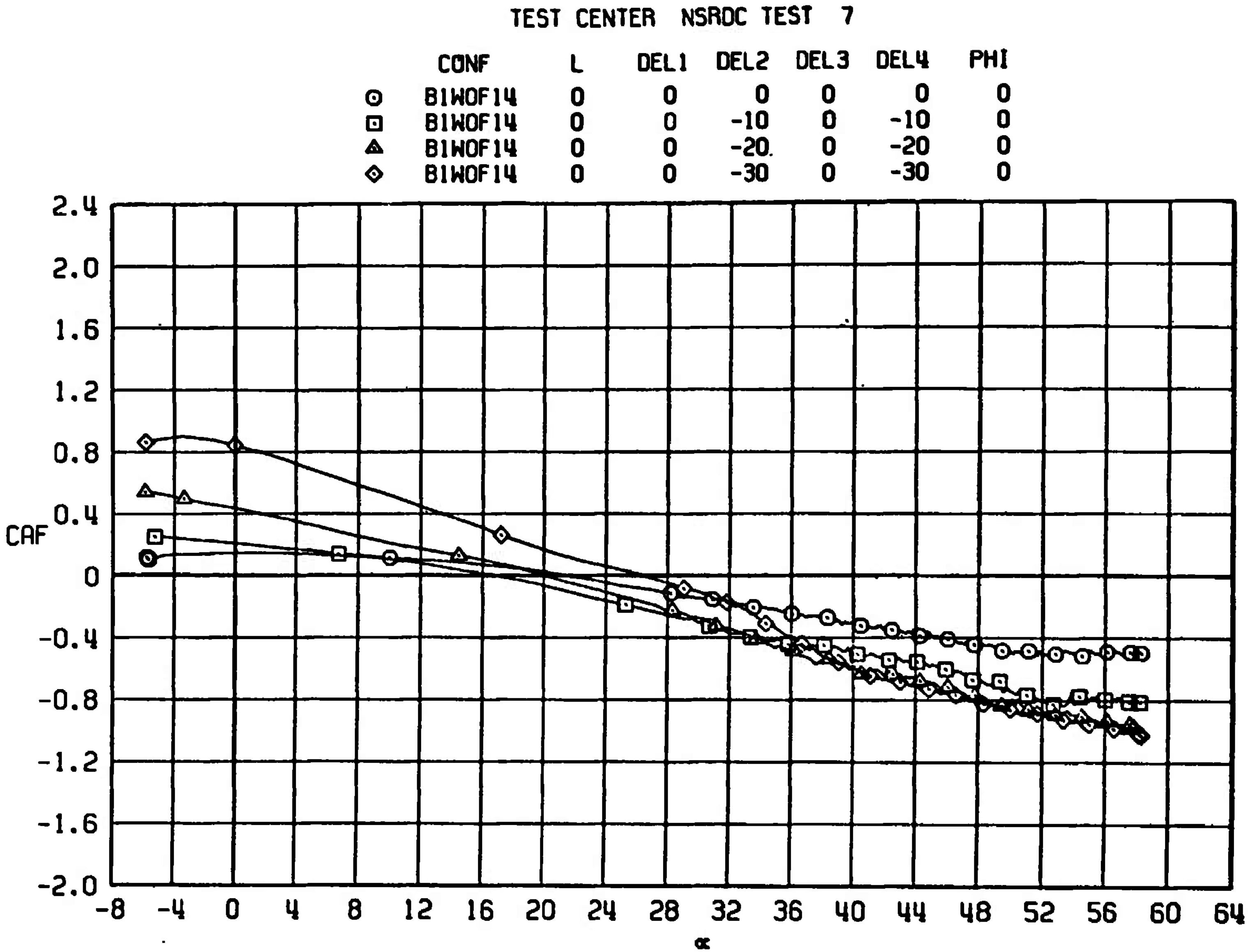

e. CAF versus α
Figure 43. Continued.

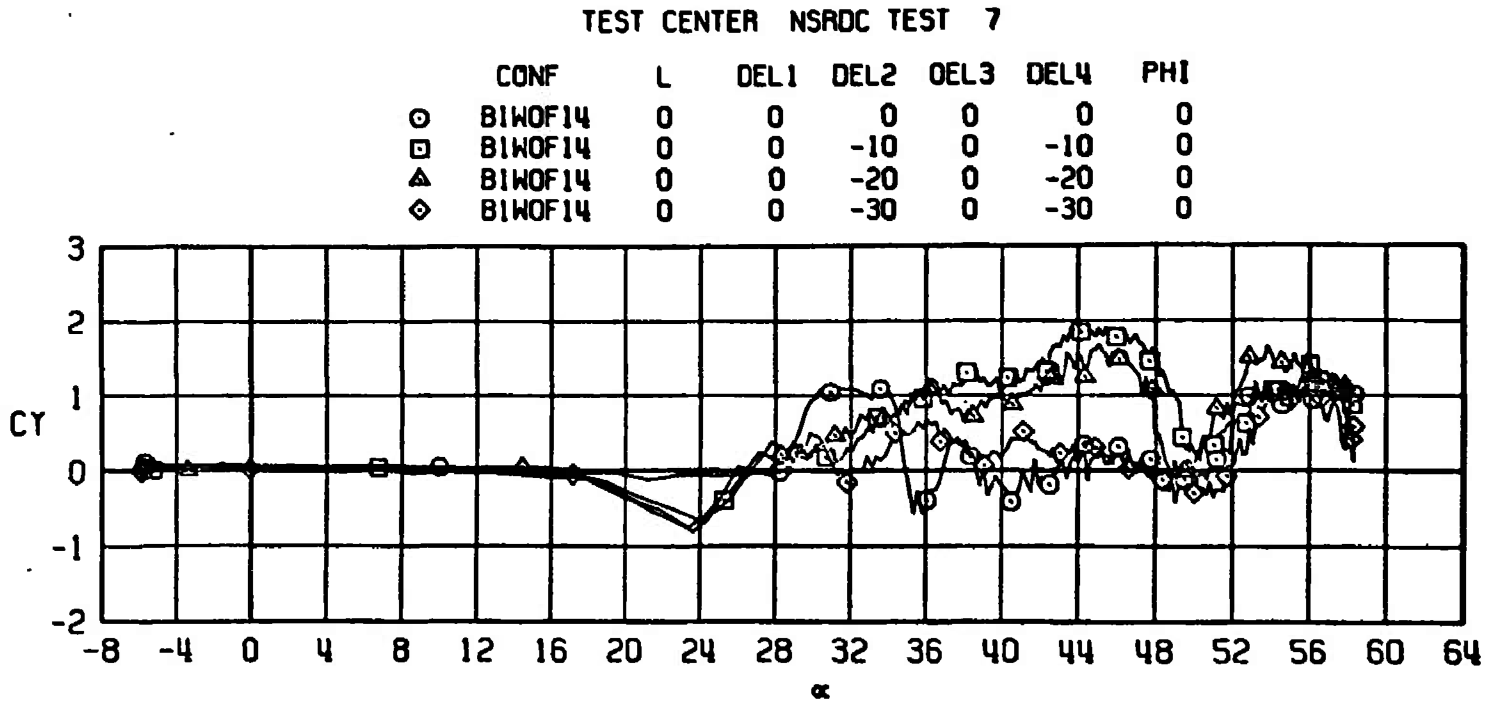

f. CY versus α
Figure 43. Continued.

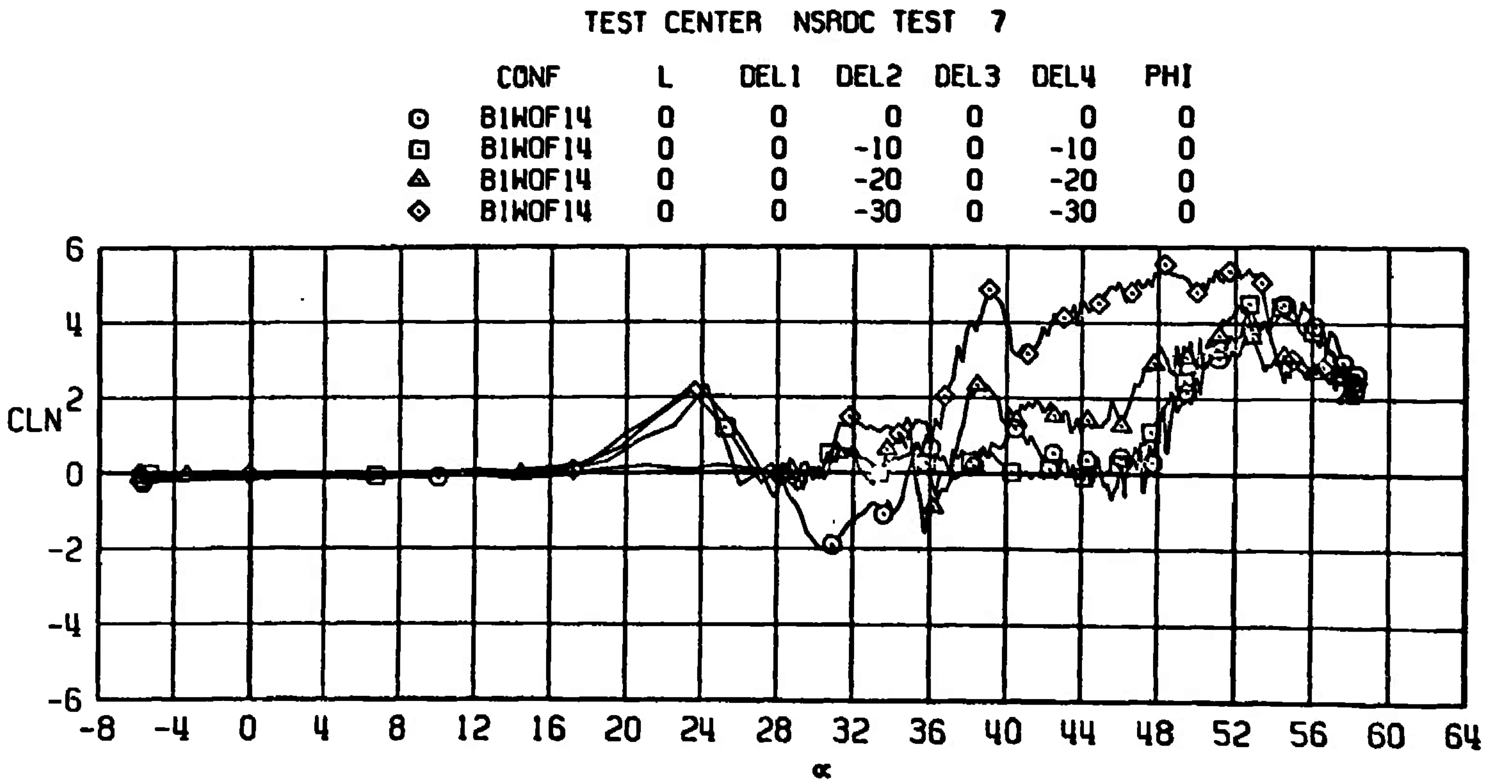

g. CLN versus α

Figure 43. Continued.

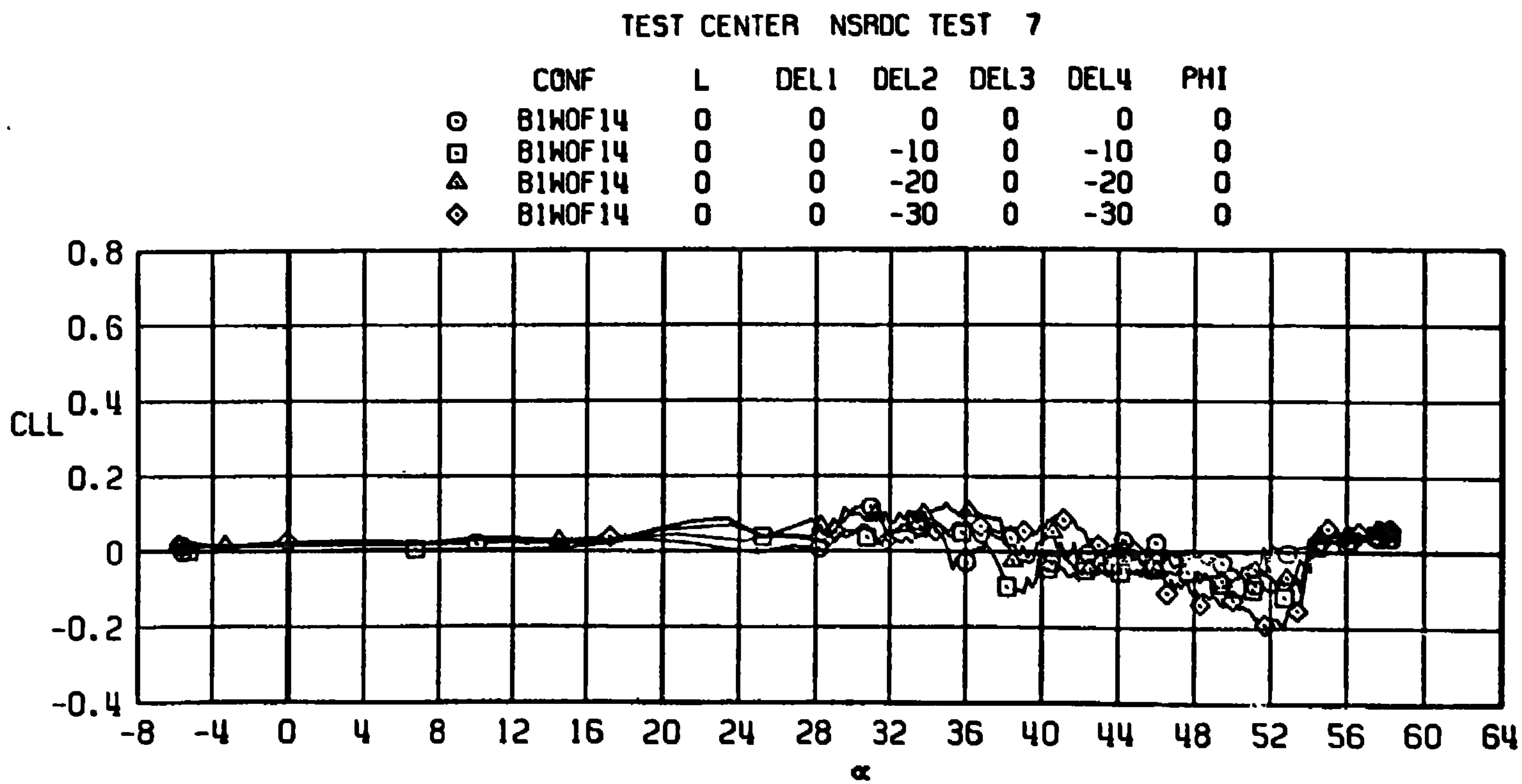

h. CLL versus α

Figure 43. Continued.

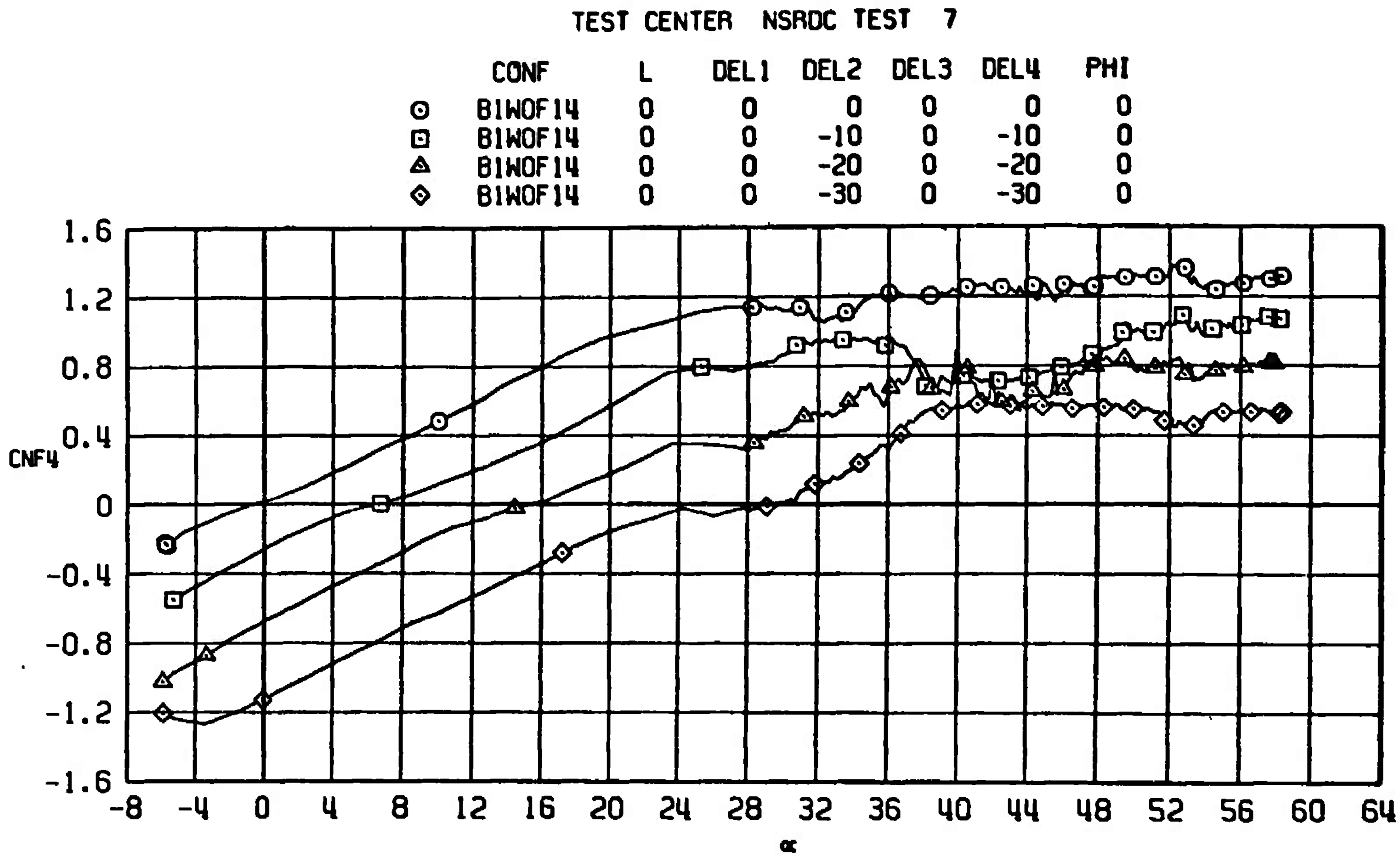

i. CNF4 versus α
Figure 43. Continued.

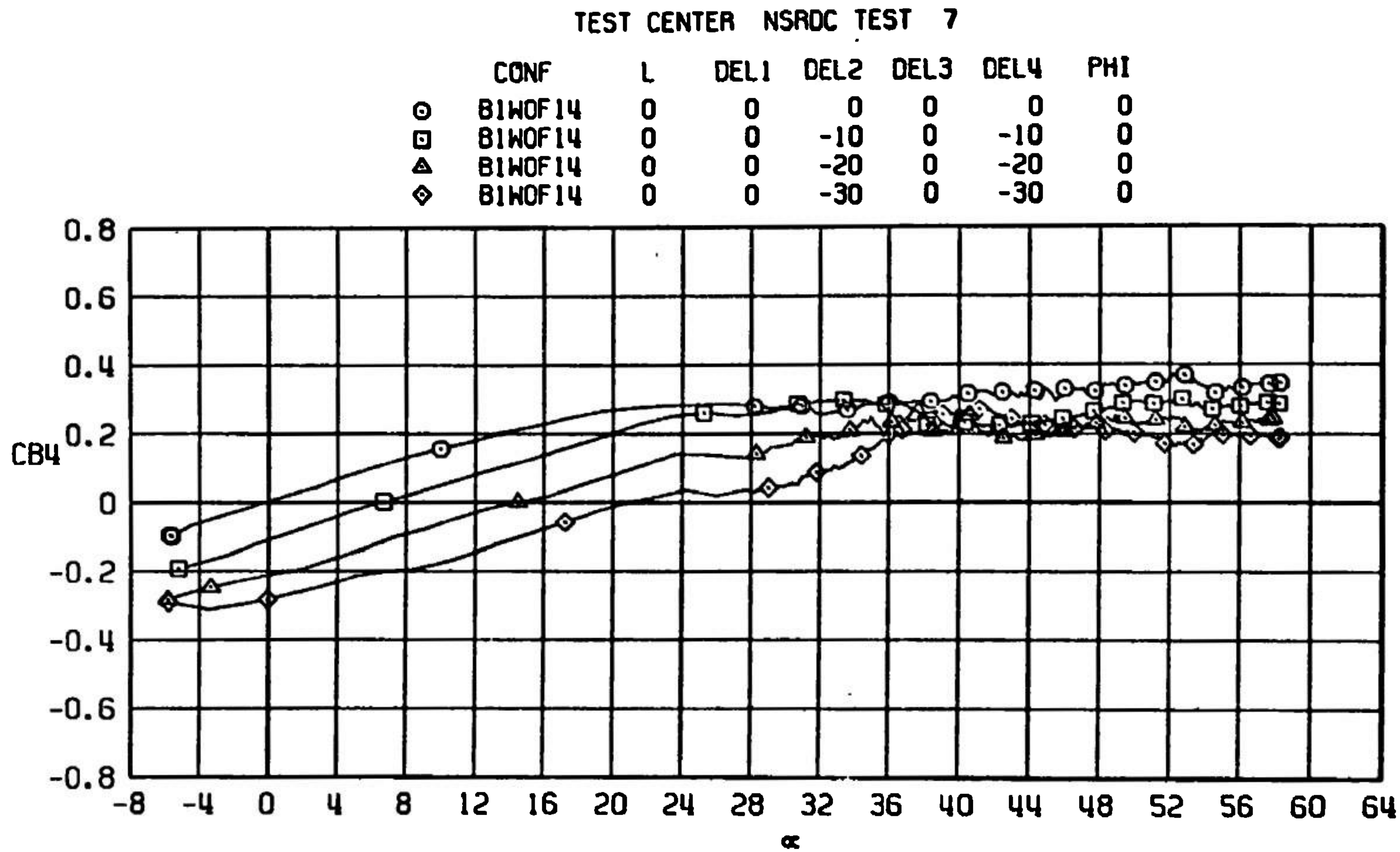

j. CB4 versus α

Figure 43. Continued.

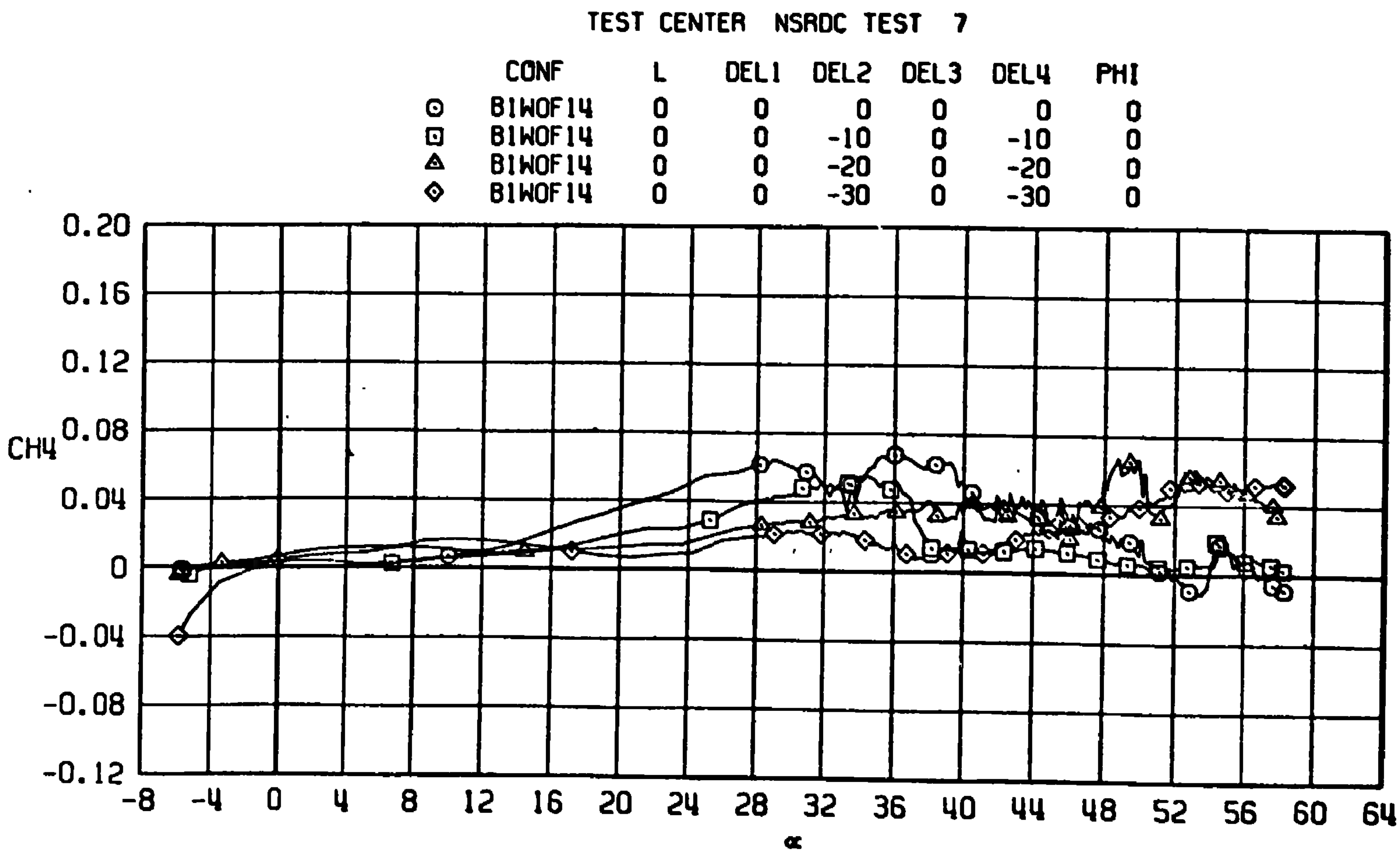

k. CH4 versus α
Figure 43. Concluded.

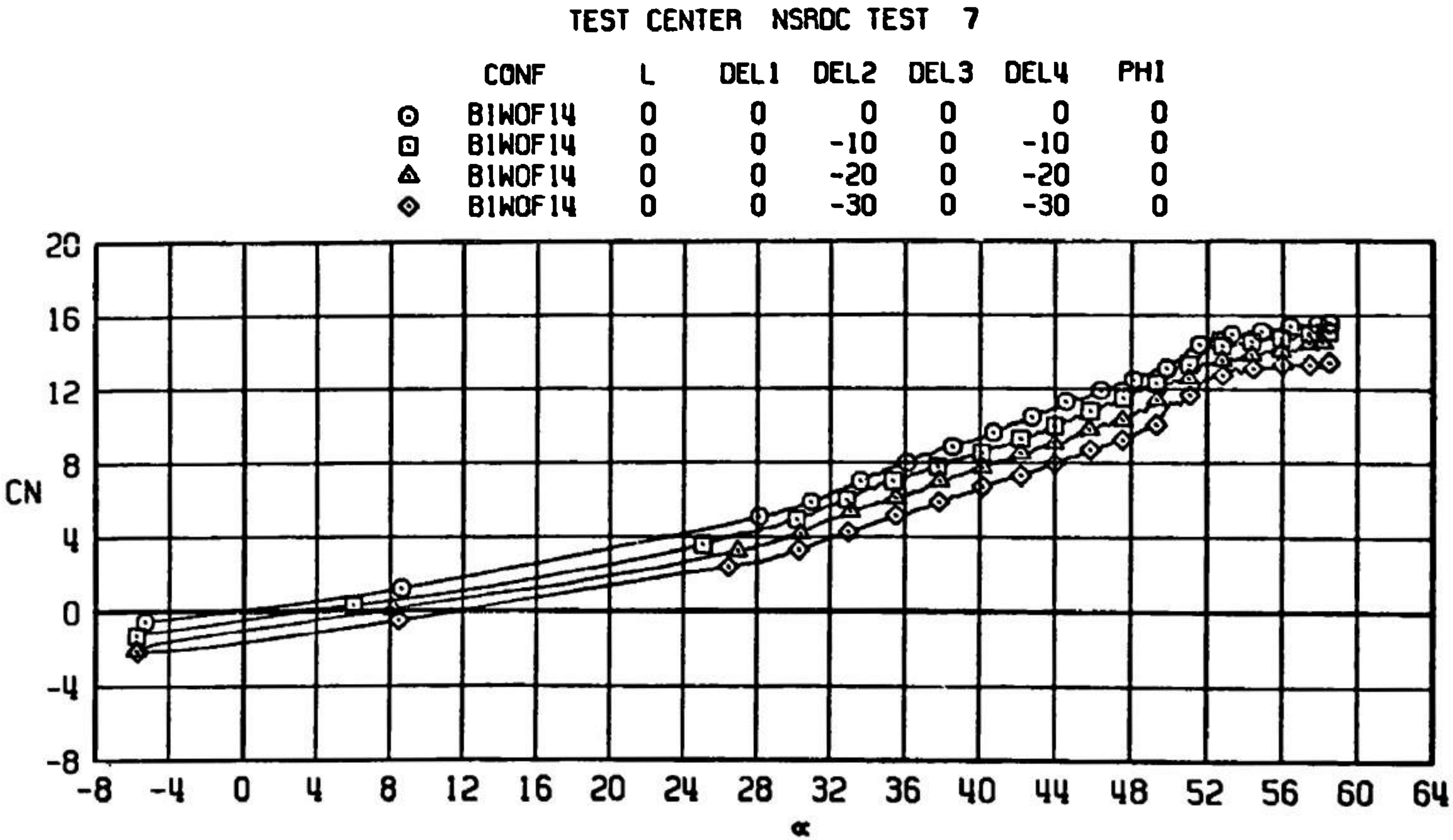

a. CN versus α

Figure 44. Test No. 7, comparison of aerodynamic coefficients of configuration B1W0F14 for various deflections of tail fins No. 2 and 4 at $M_\infty = 0.9$.

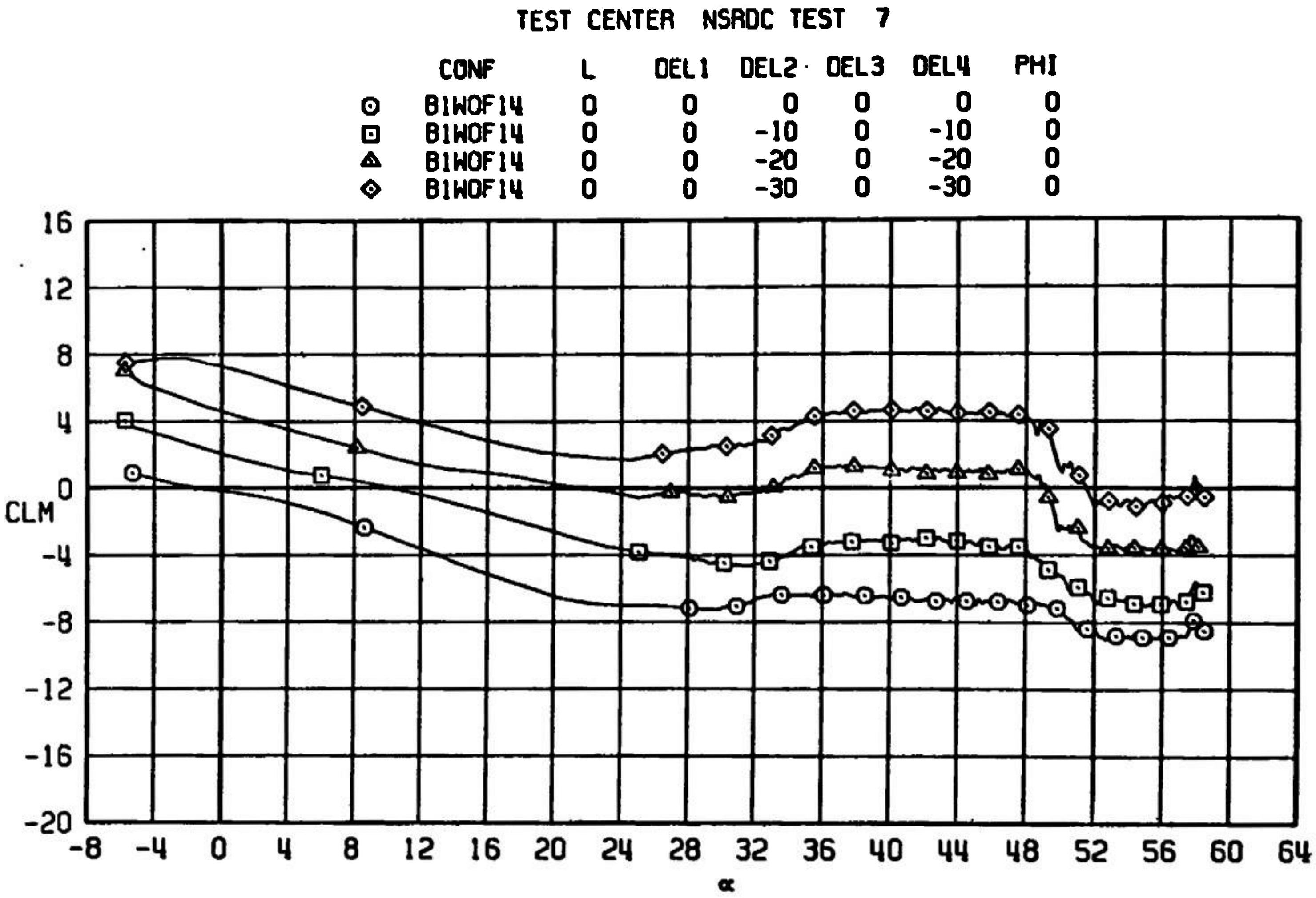

b. CLM versus α
Figure 44. Continued.

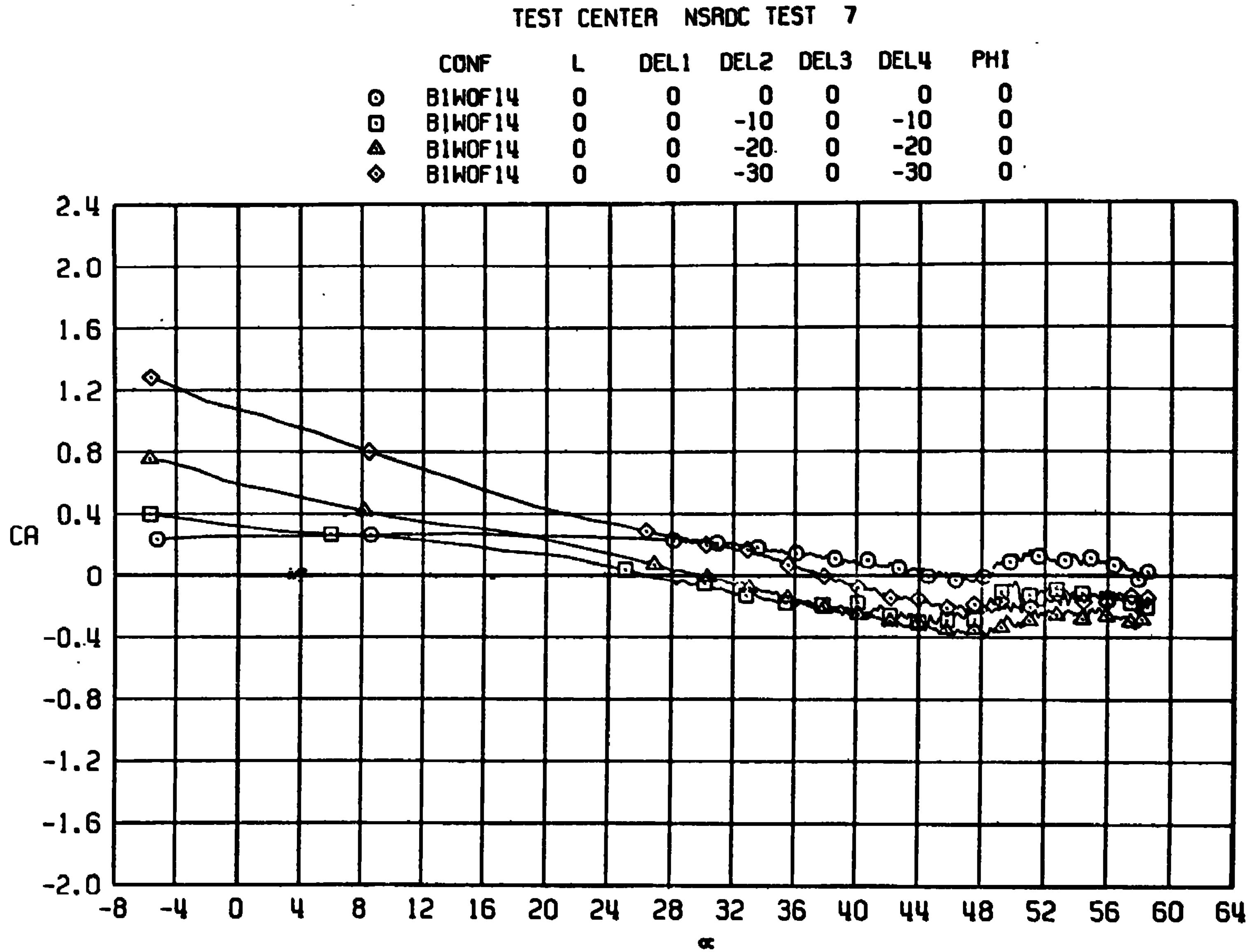

c. CA versus α
Figure 44. Continued.

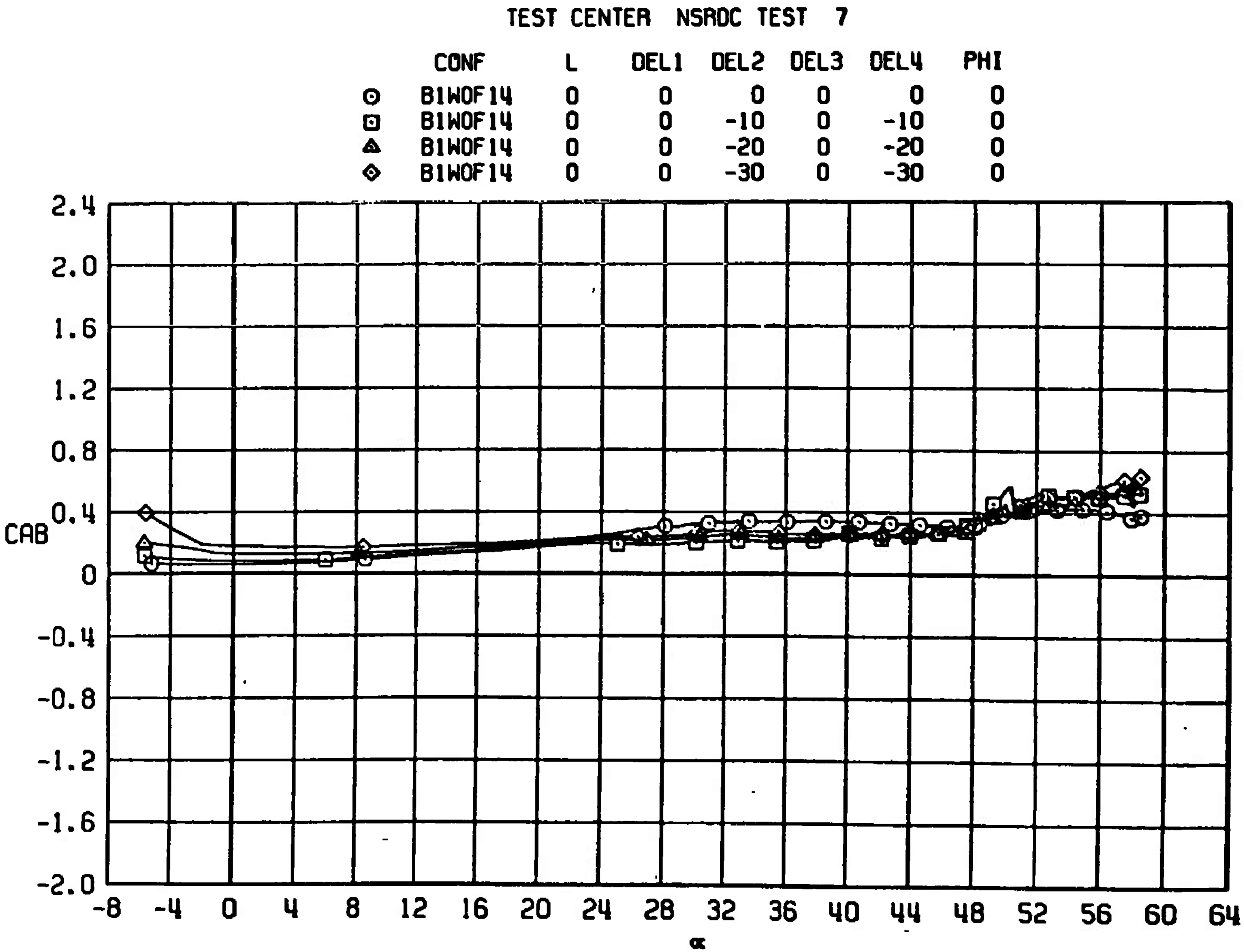

d. CAB versus α
Figure 44. Continued.

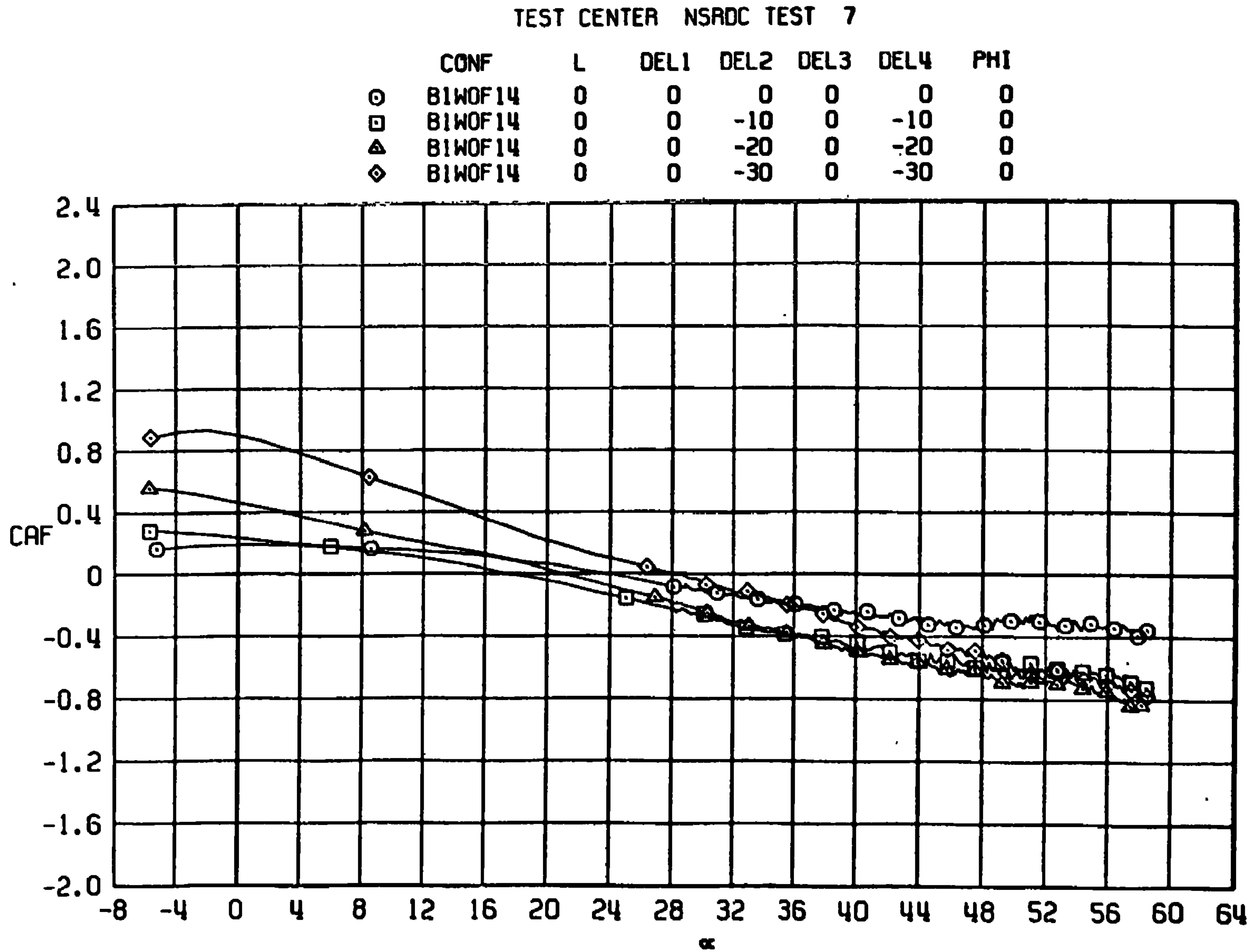

e. CAF versus α
Figure 44. Continued.

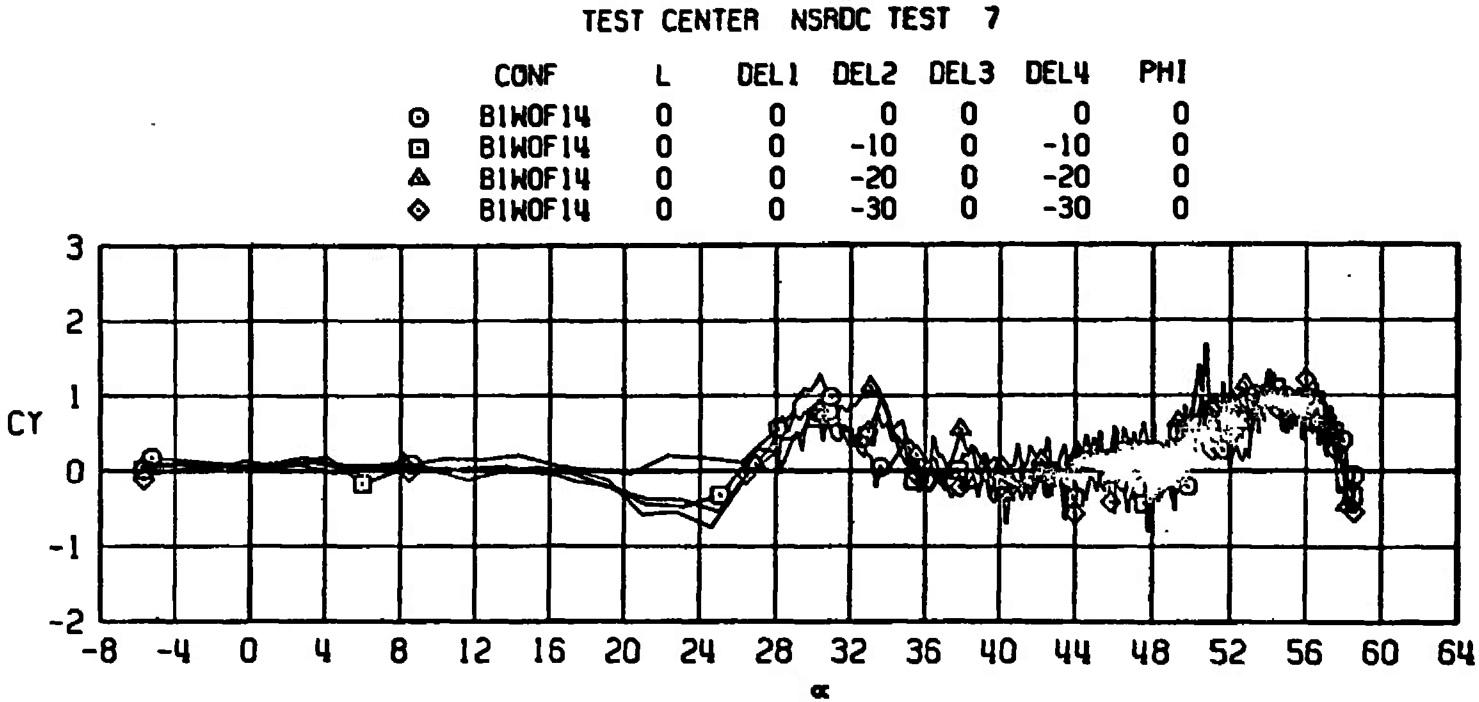

f. CY versus α
Figure 44. Continued.

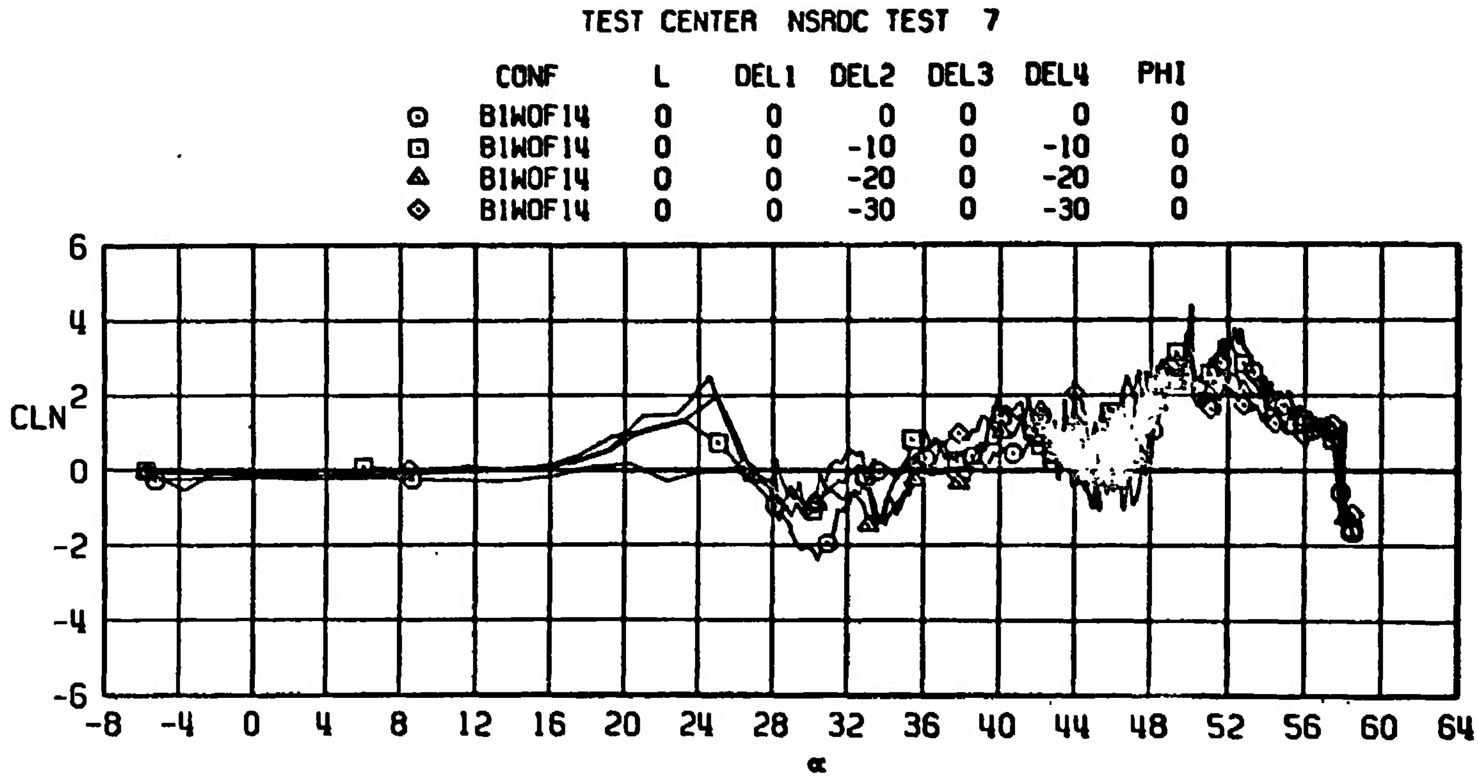

g. CLN versus α
Figure 44. Continued.

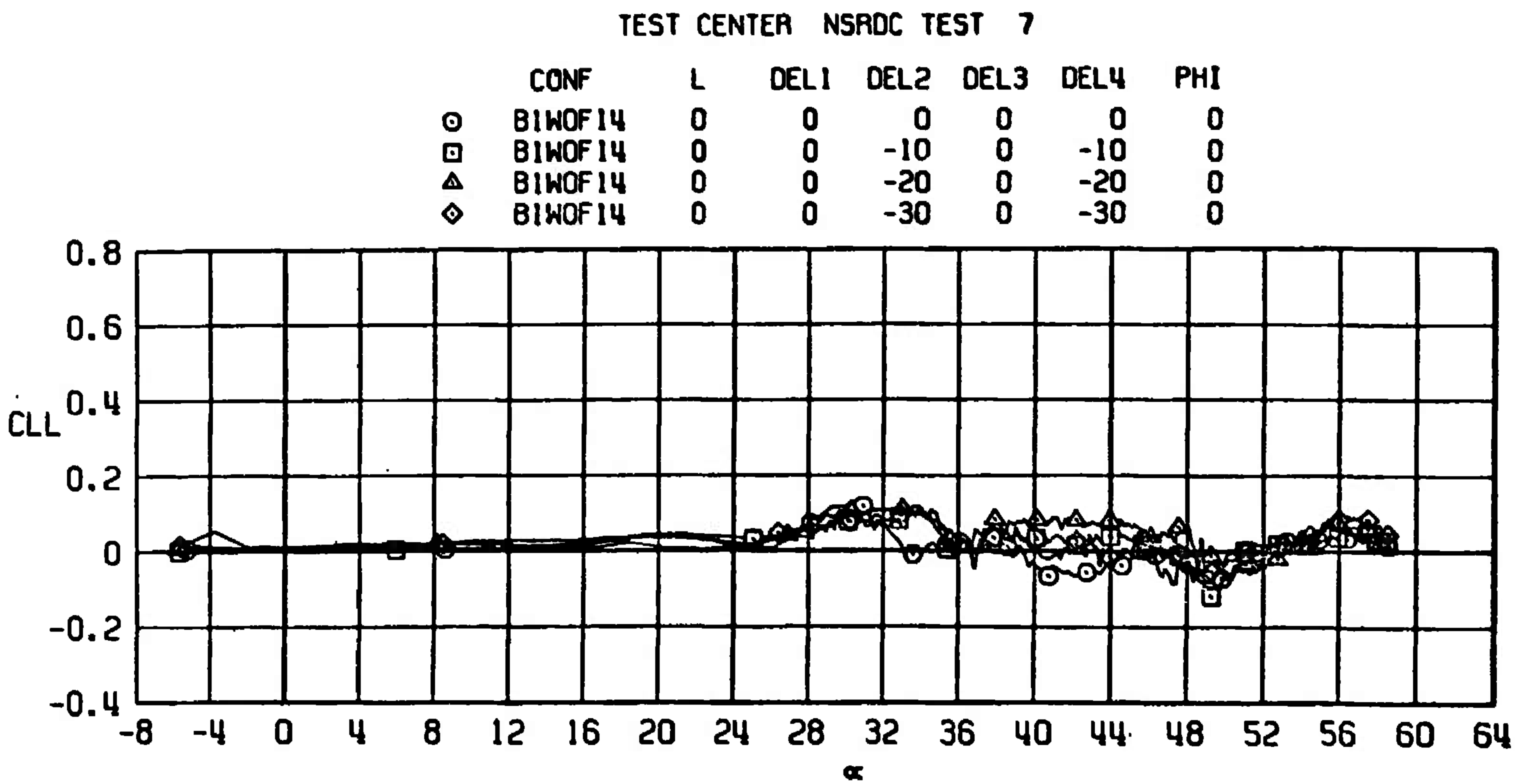

h. CLL versus α
Figure 44. Continued.

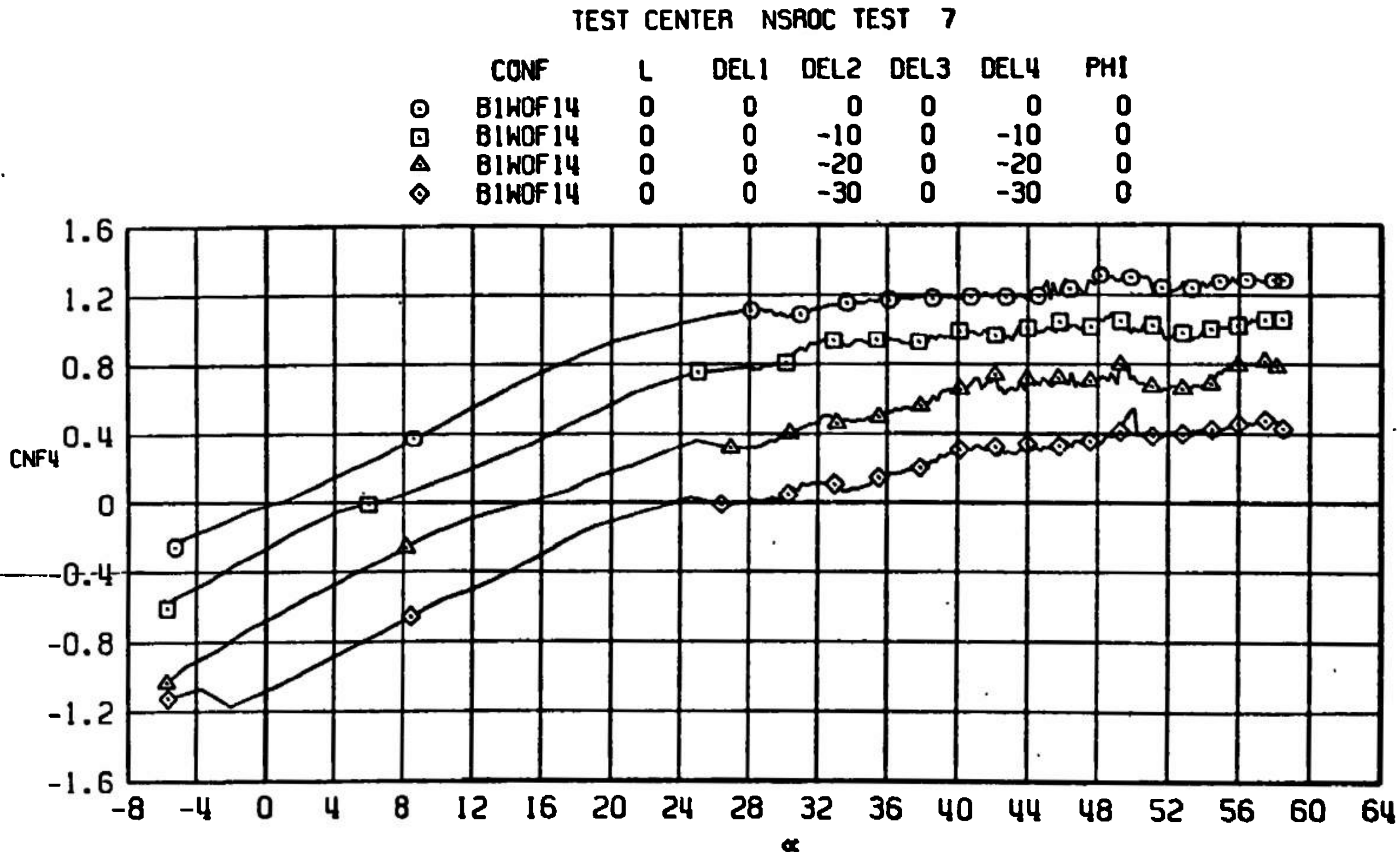

i. CNF4 versus α

Figure 44. Continued.

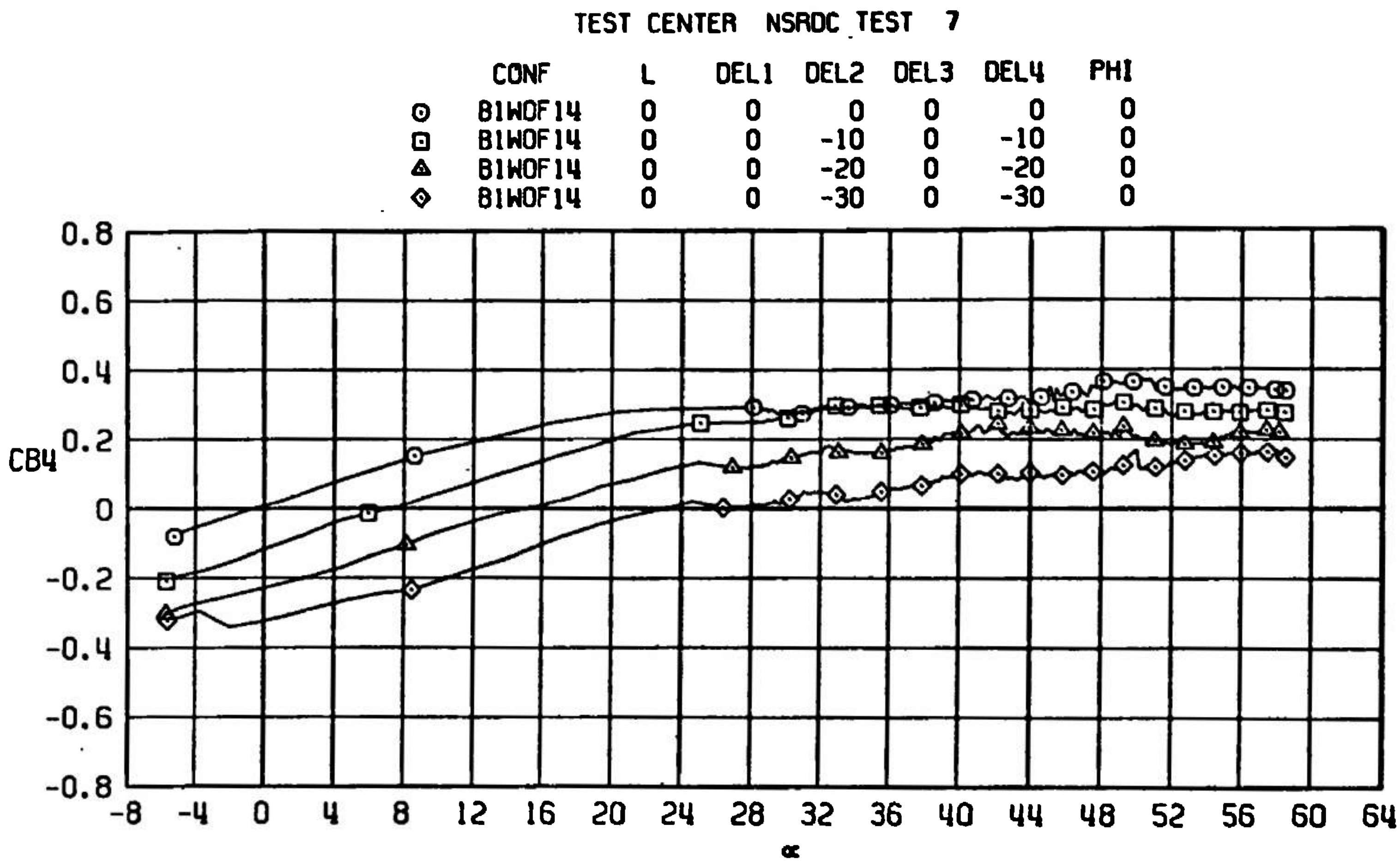

j. CB4 versus α

Figure 44. Continued.

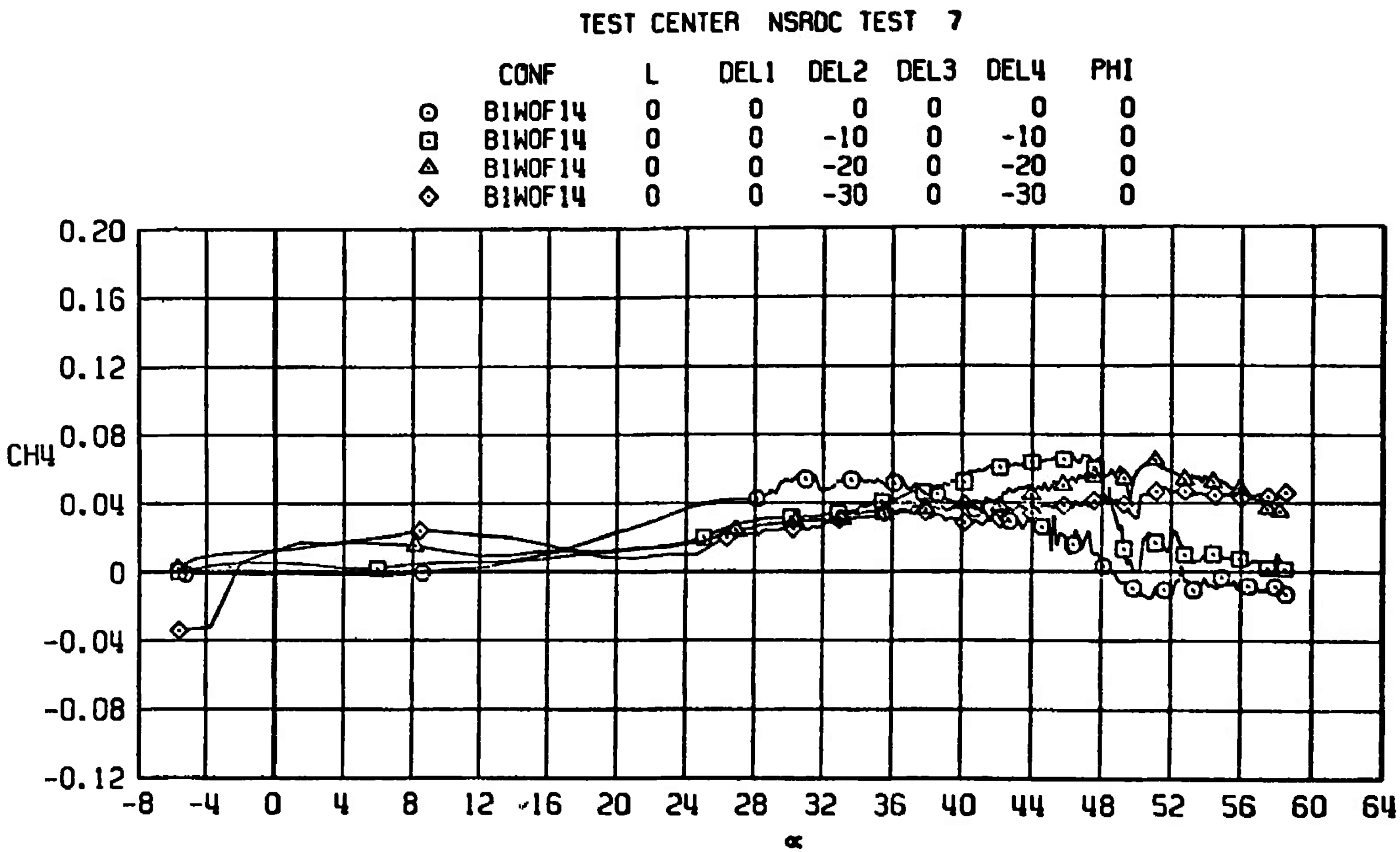

k. CH4 versus α
Figure 44. Concluded.

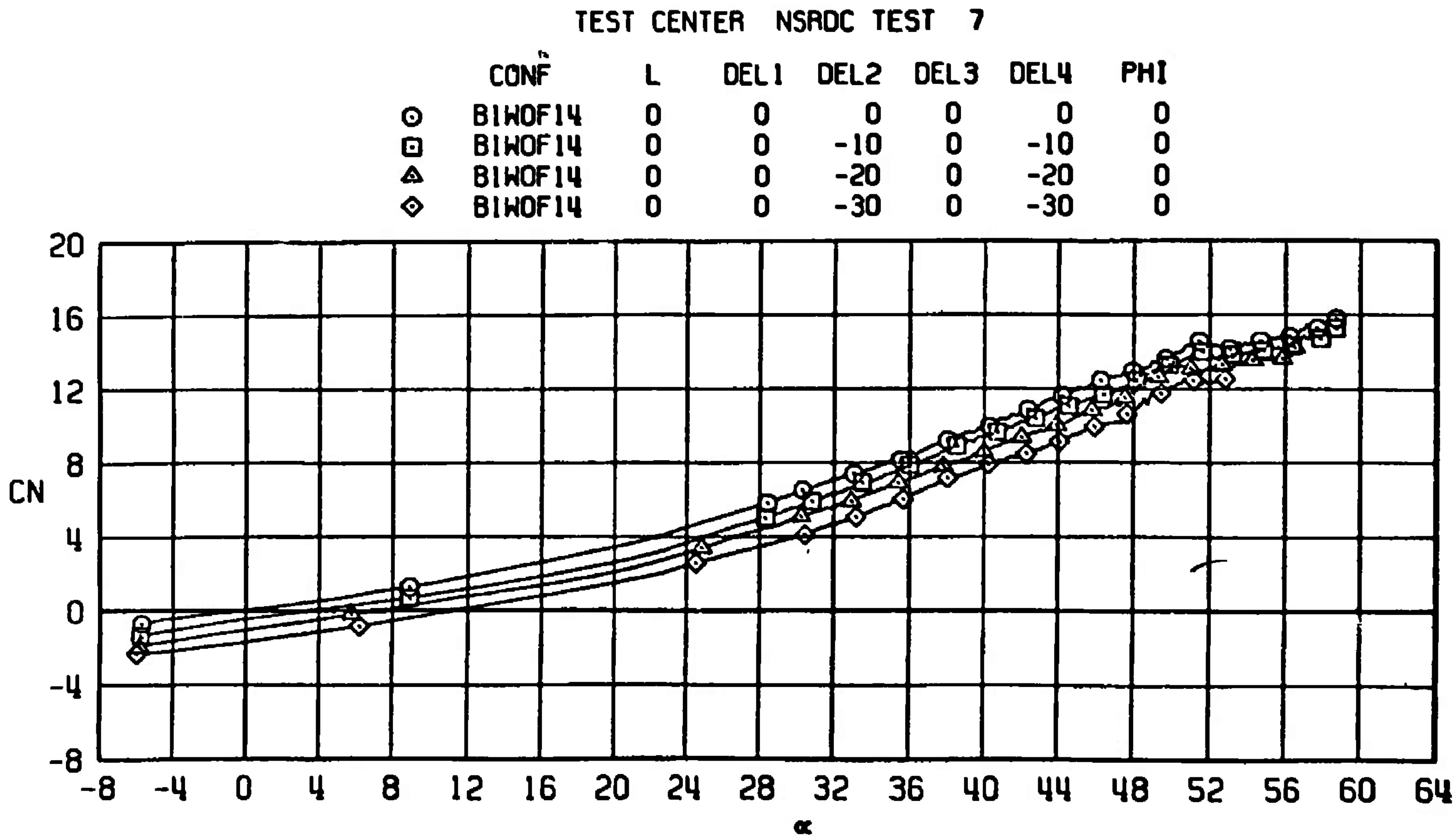

a. CN versus α

Figure 45. Test No. 7, comparison of aerodynamic coefficients of configuration B1W0F14 for various deflections of tail fins No. 2 and 4 at $M_\infty = 1.0$.

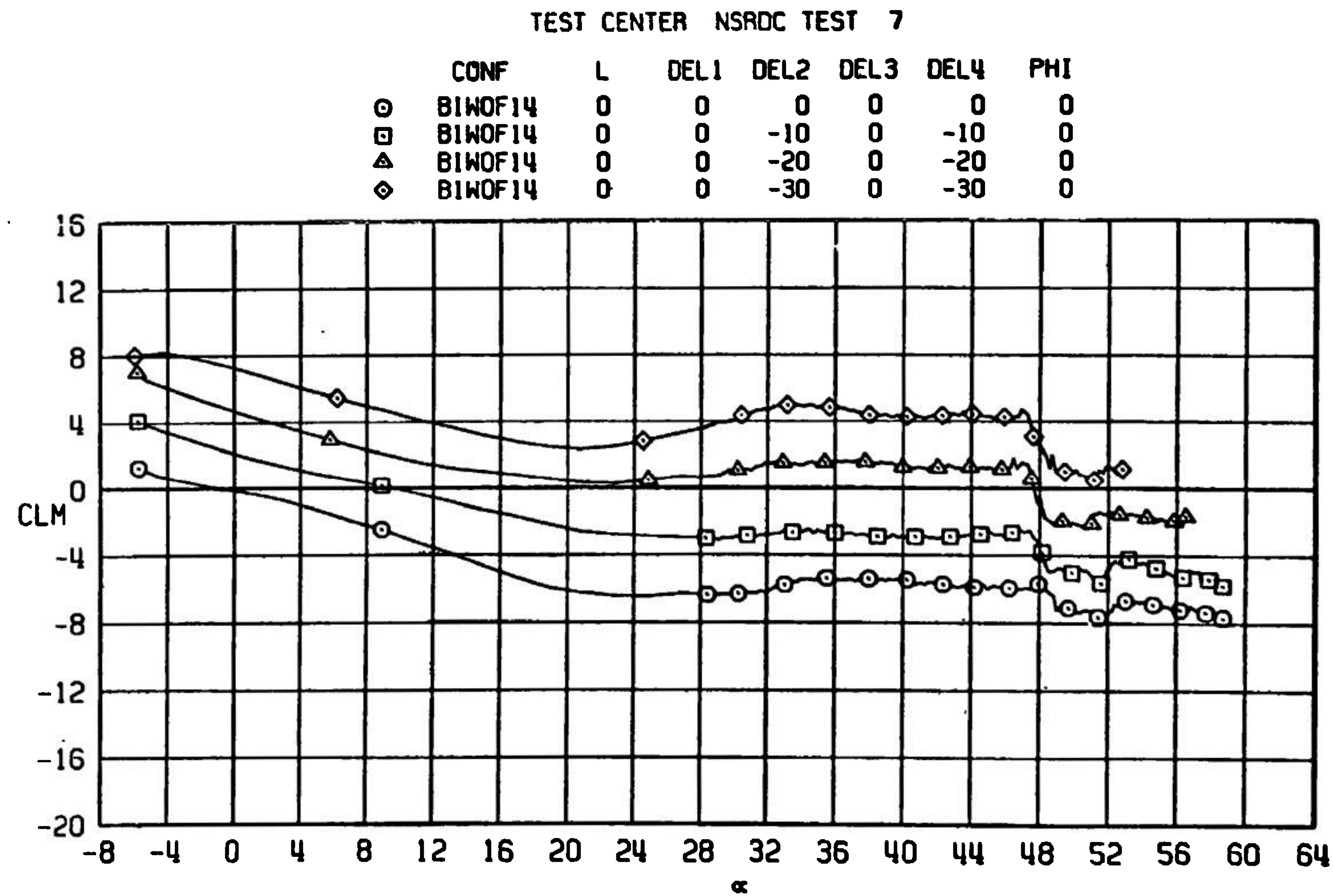

b. CLM versus α
Figure 45. Continued.

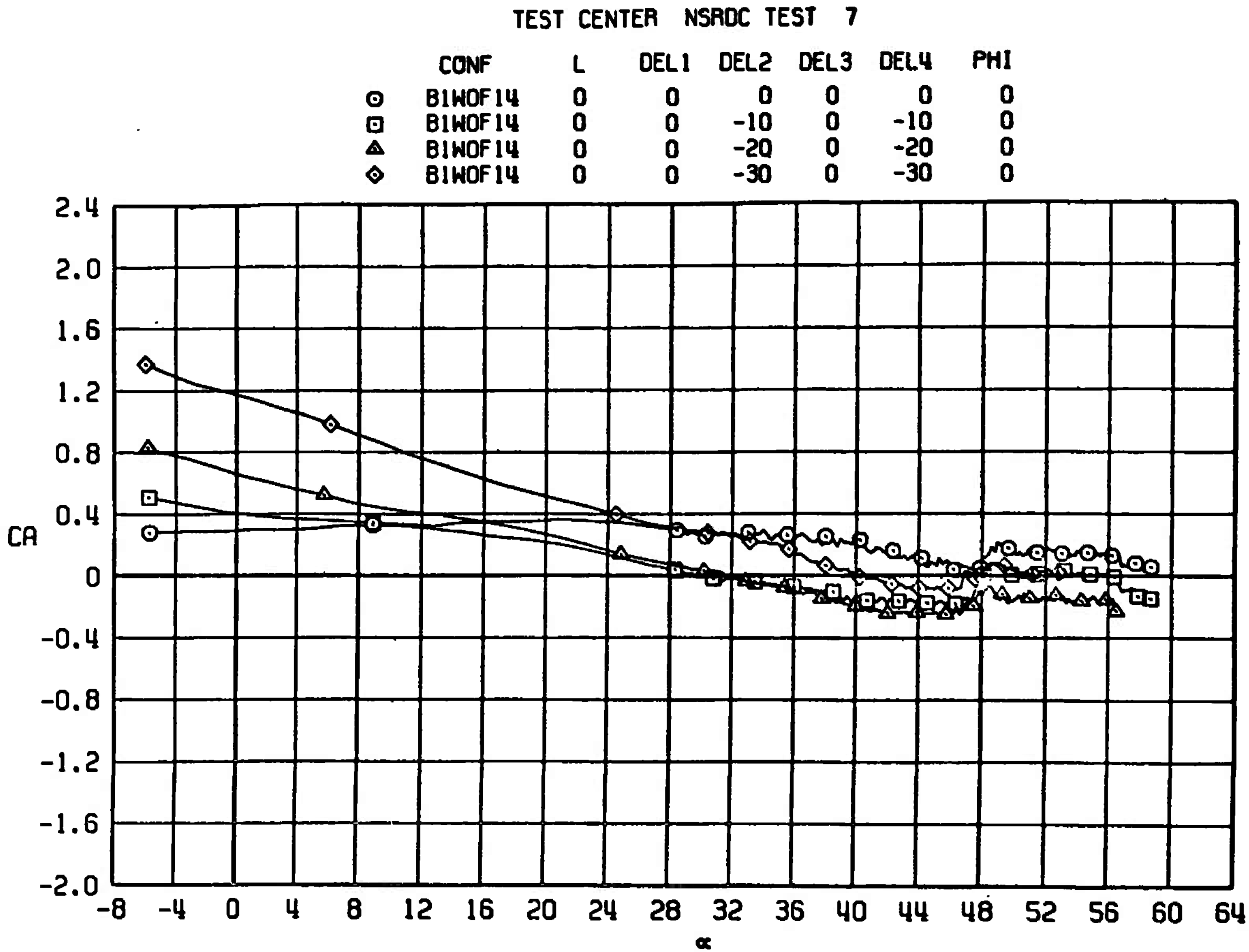

c. CA versus *a*
Figure 45. Continued.

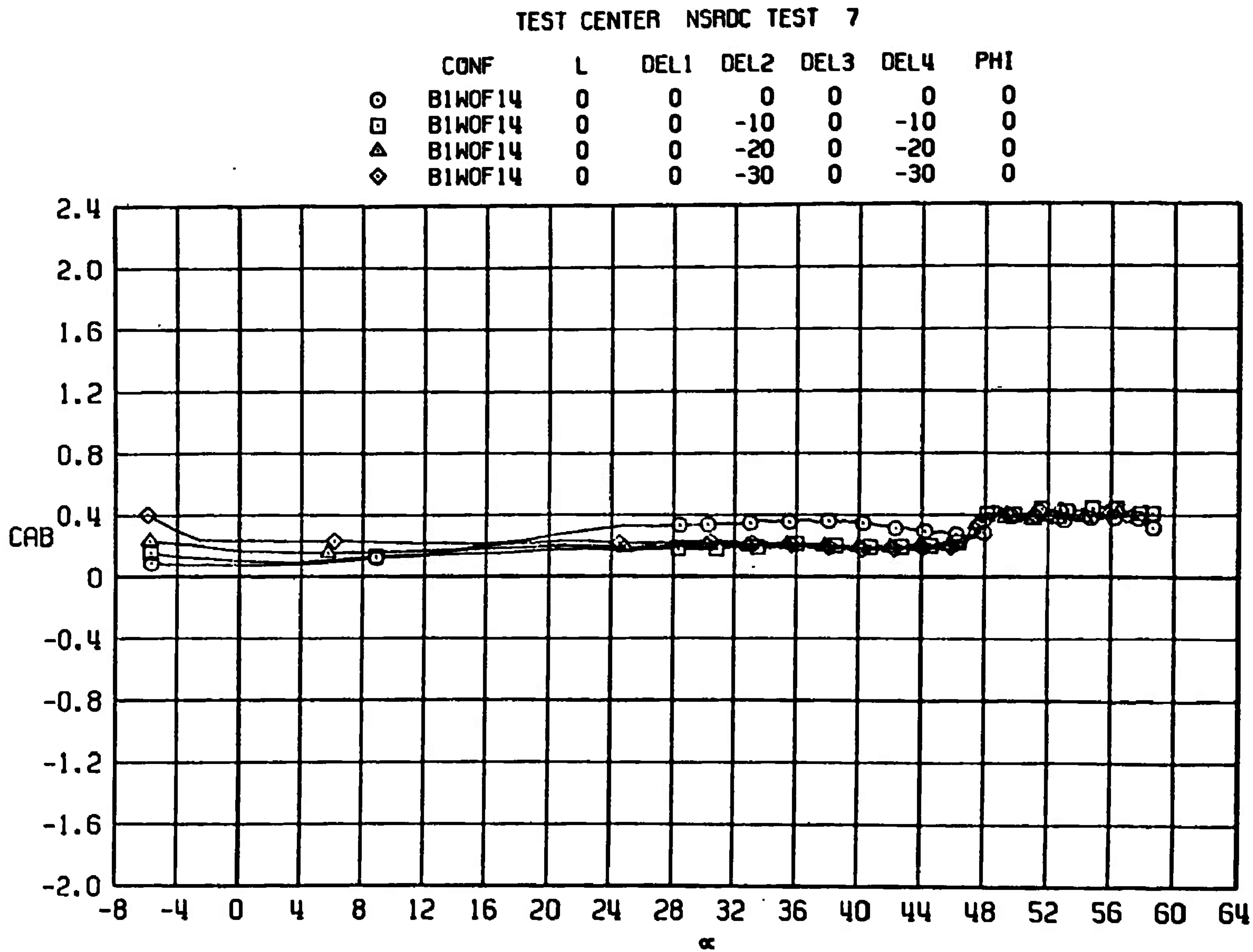

d. CAB versus α
Figure 45. Continued.

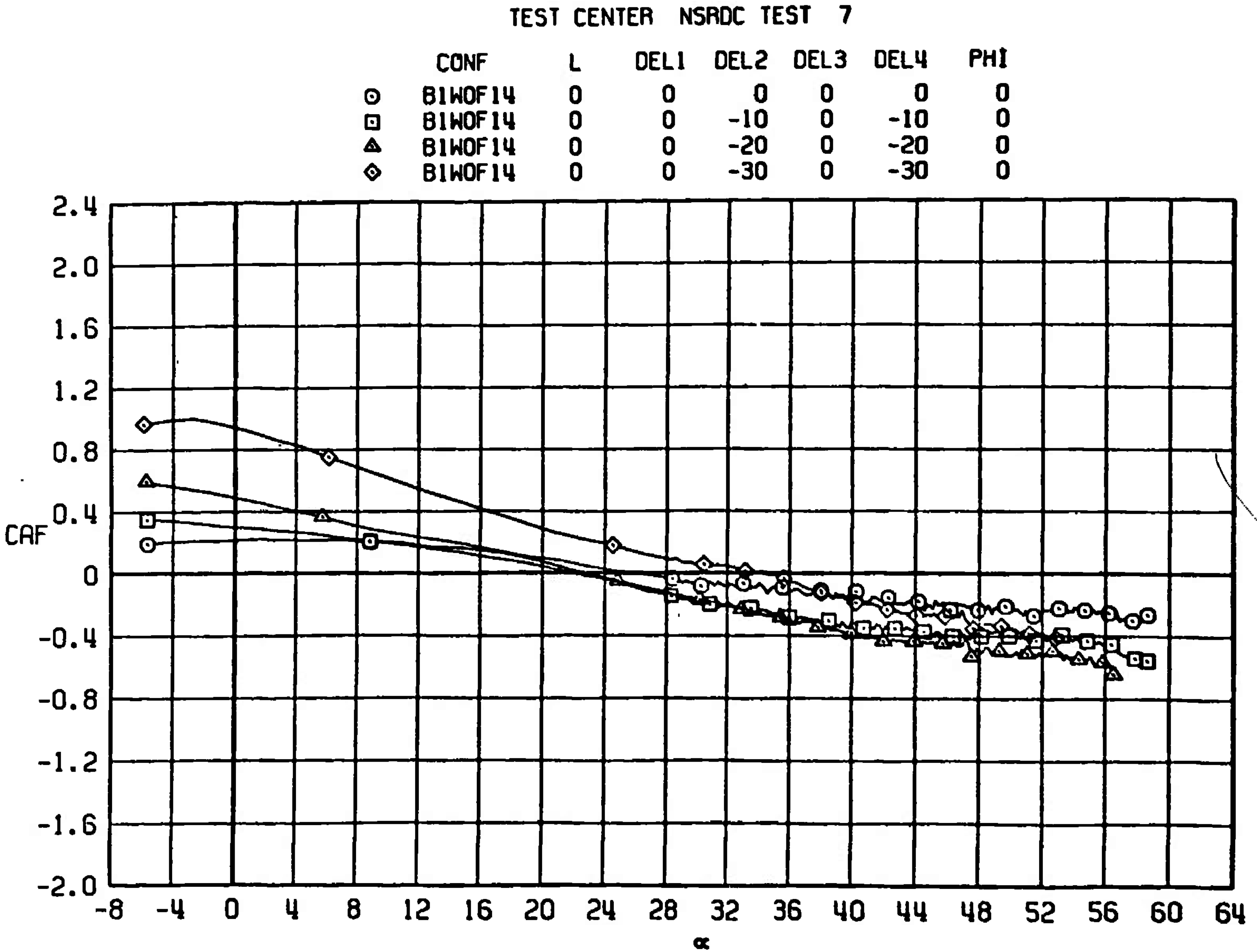

e. CAF versus α
Figure 45. Continued.

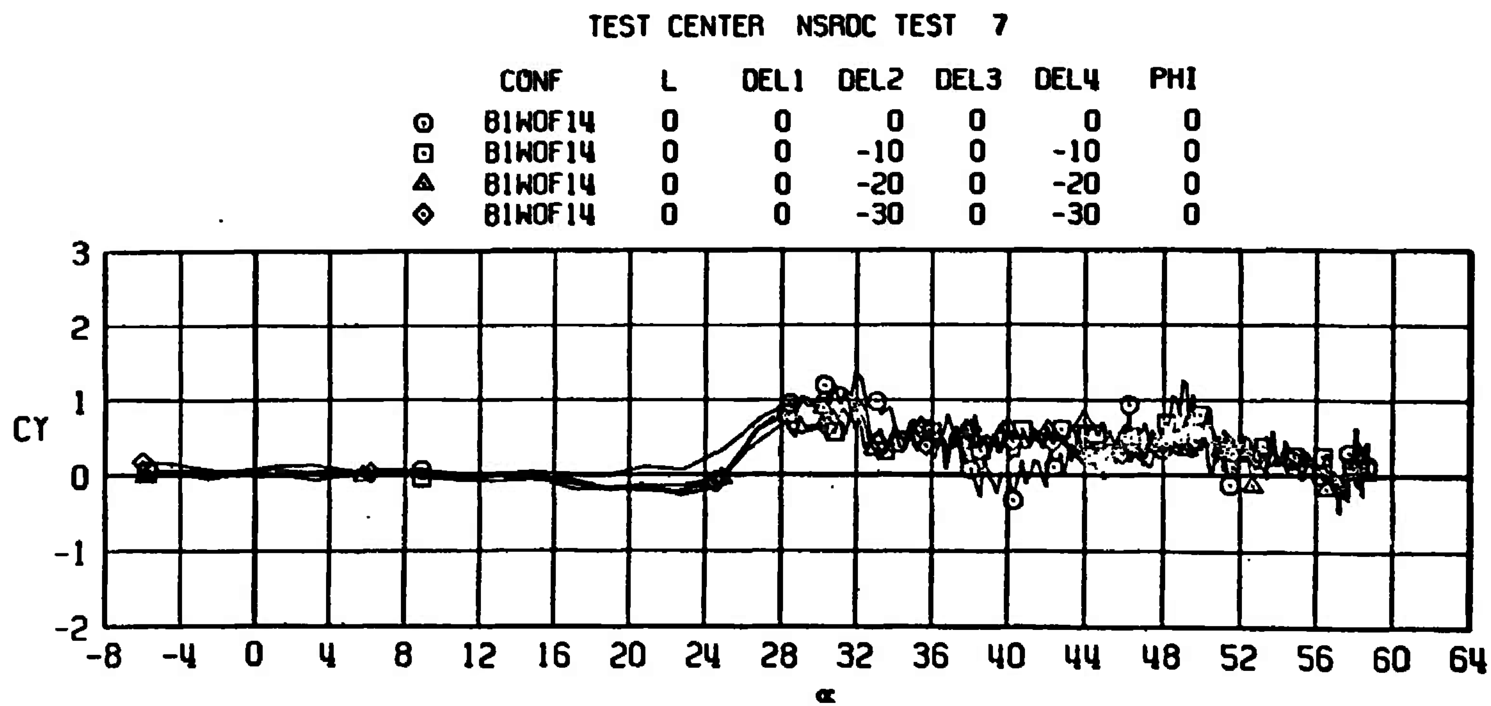

f. CY versus α
Figure 45. Continued.

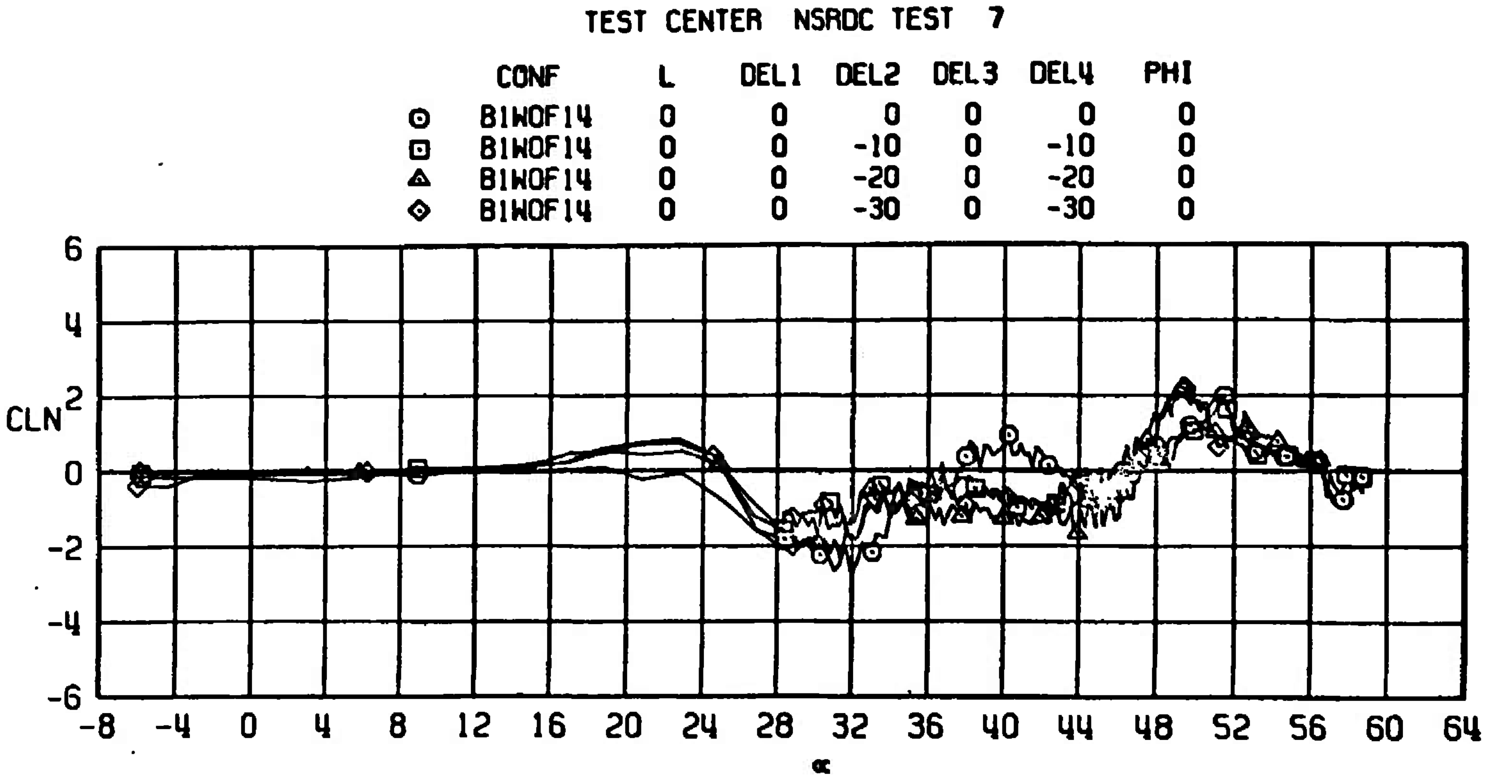

g. CLN versus α
Figure 45. Continued.

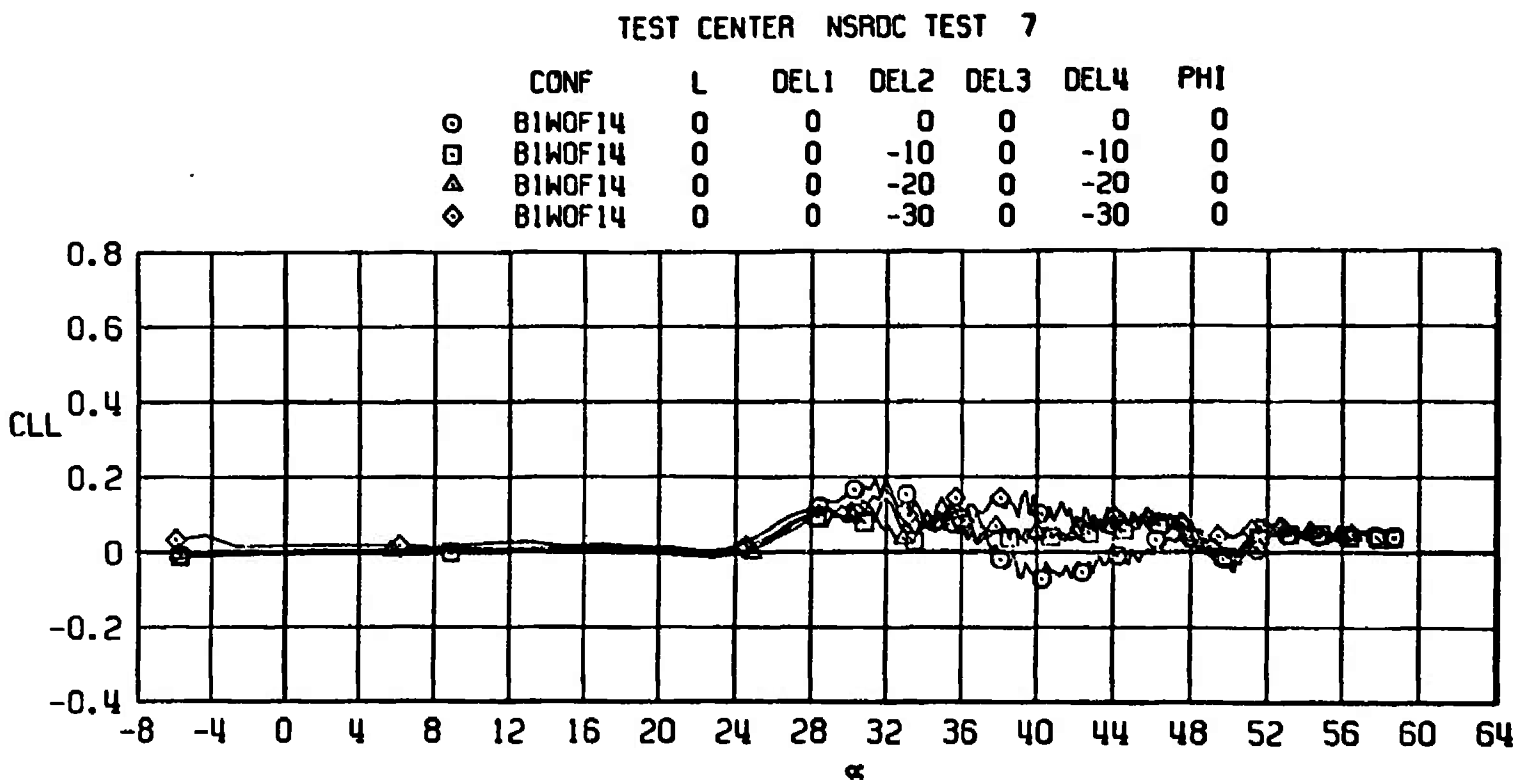

h. CLL versus α
Figure 45. Continued.

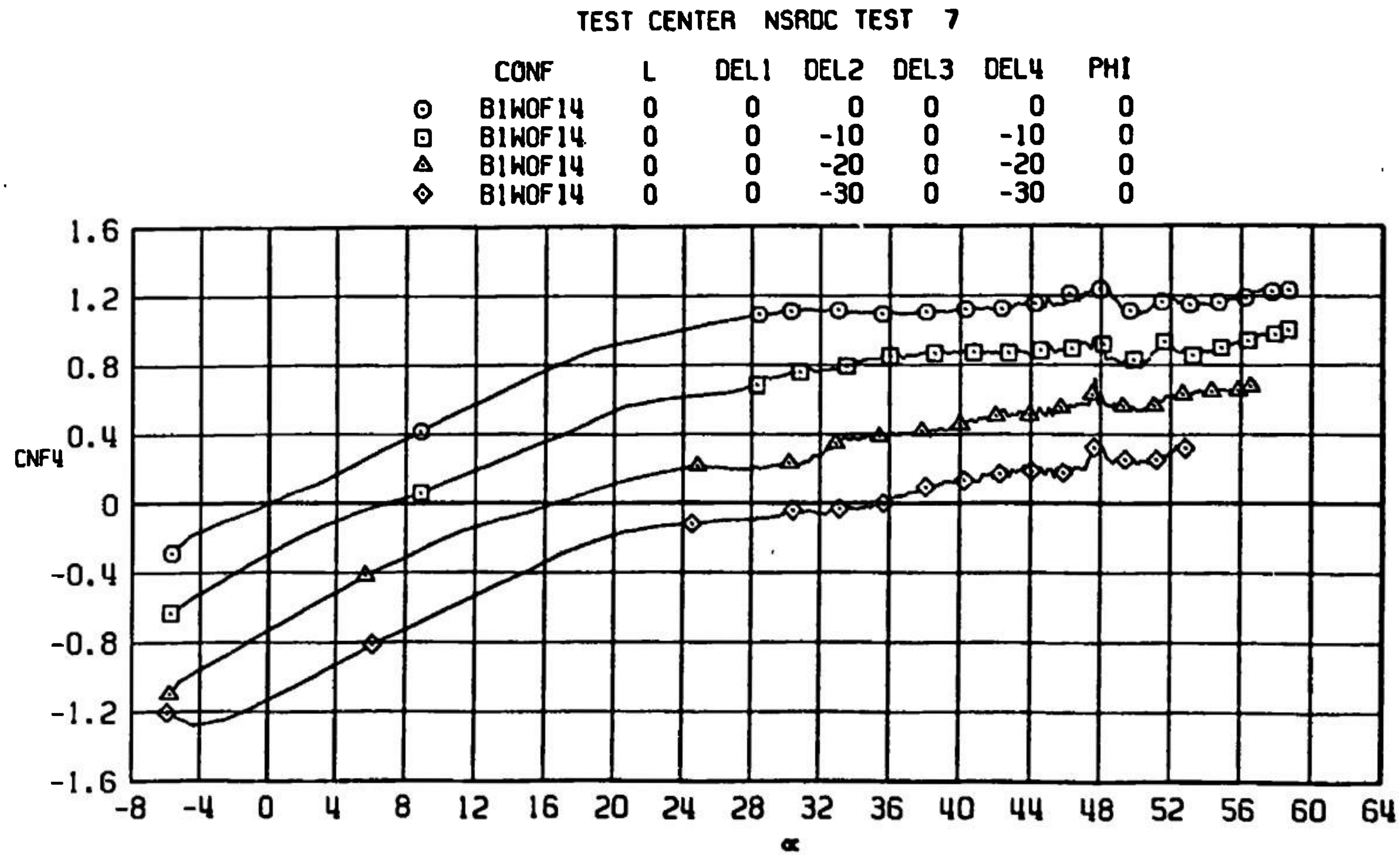

i. CNF4 versus α
Figure 45. Continued.

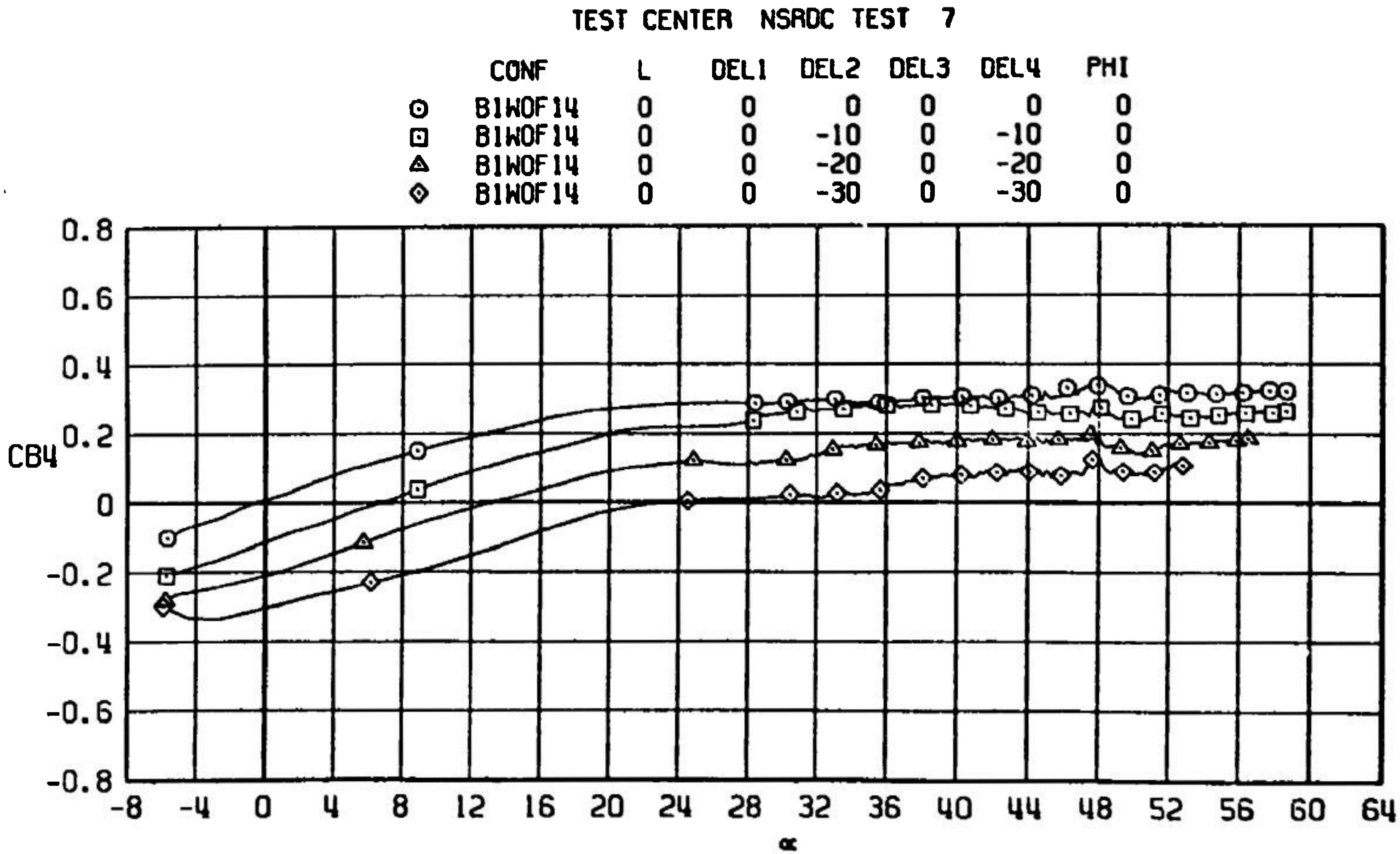

j. CB4 versus α
Figure 45. Continued.

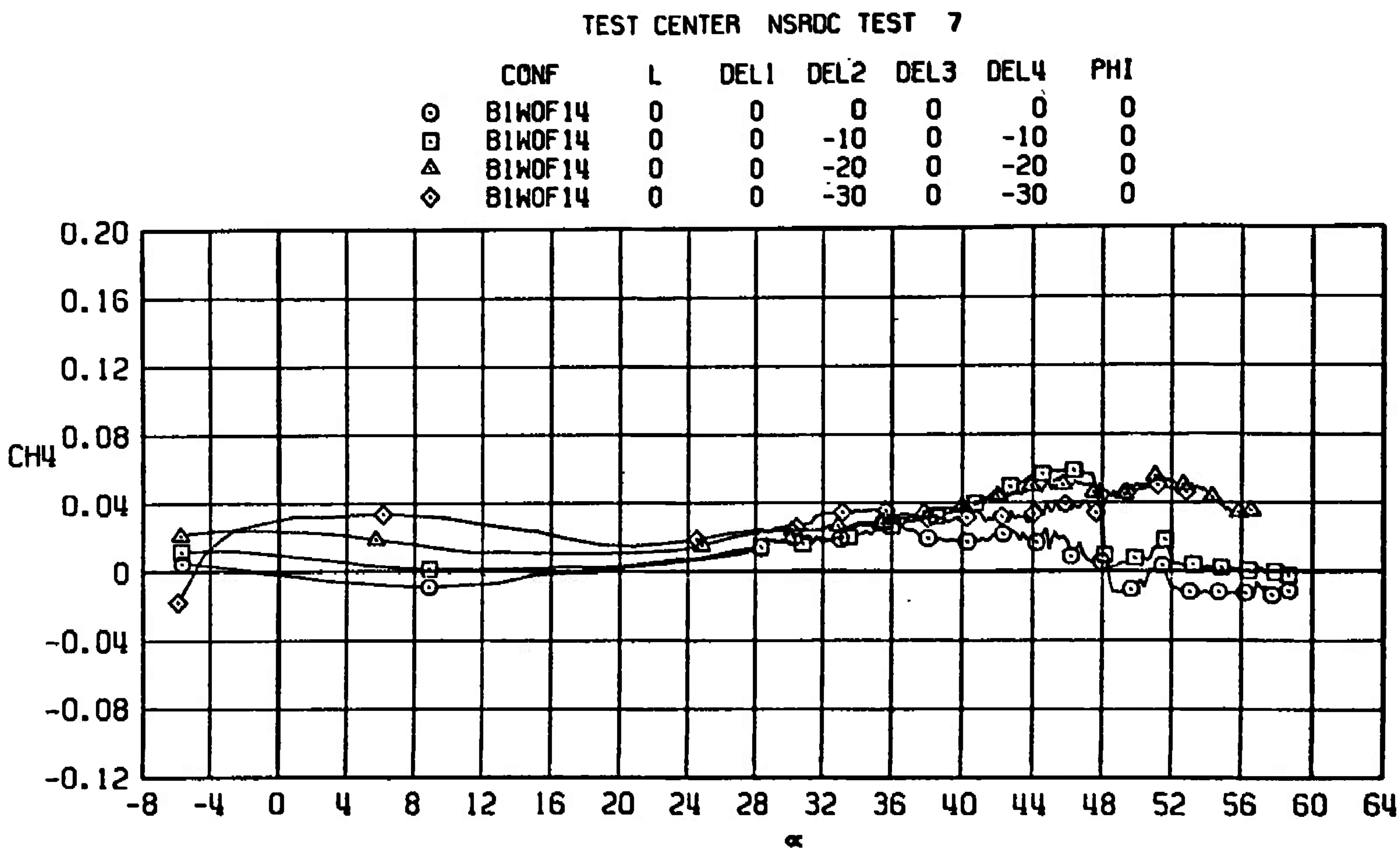

k. CH4 versus α
Figure 45. Concluded.

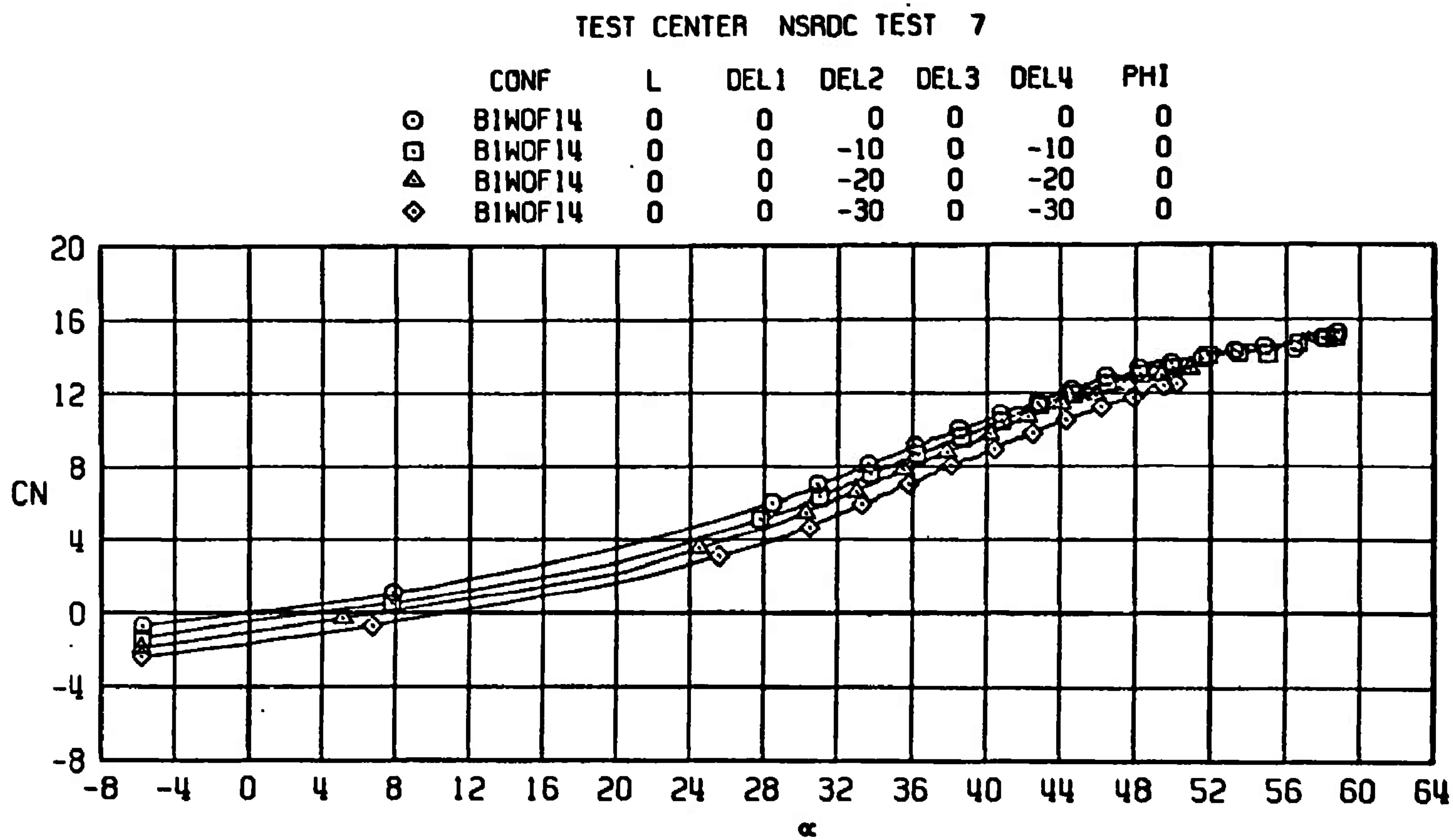

a. CN versus α

Figure 46. Test No. 7, comparison of aerodynamic coefficients of configuration B1W0F14 for various deflections of tail fins No. 2 and 4 at $M_\infty = 1.1$.

TEST CENTER NSRDC TEST 7

	CONF	L	DEL1	DEL2	DEL3	DEL4	PHI
⊙	B1W0F14	0	0	0	0	0	0
⊡	B1W0F14	0	0	-10	0	-10	0
△	B1W0F14	0	0	-20	0	-20	0
◇	B1W0F14	0	0	-30	0	-30	0

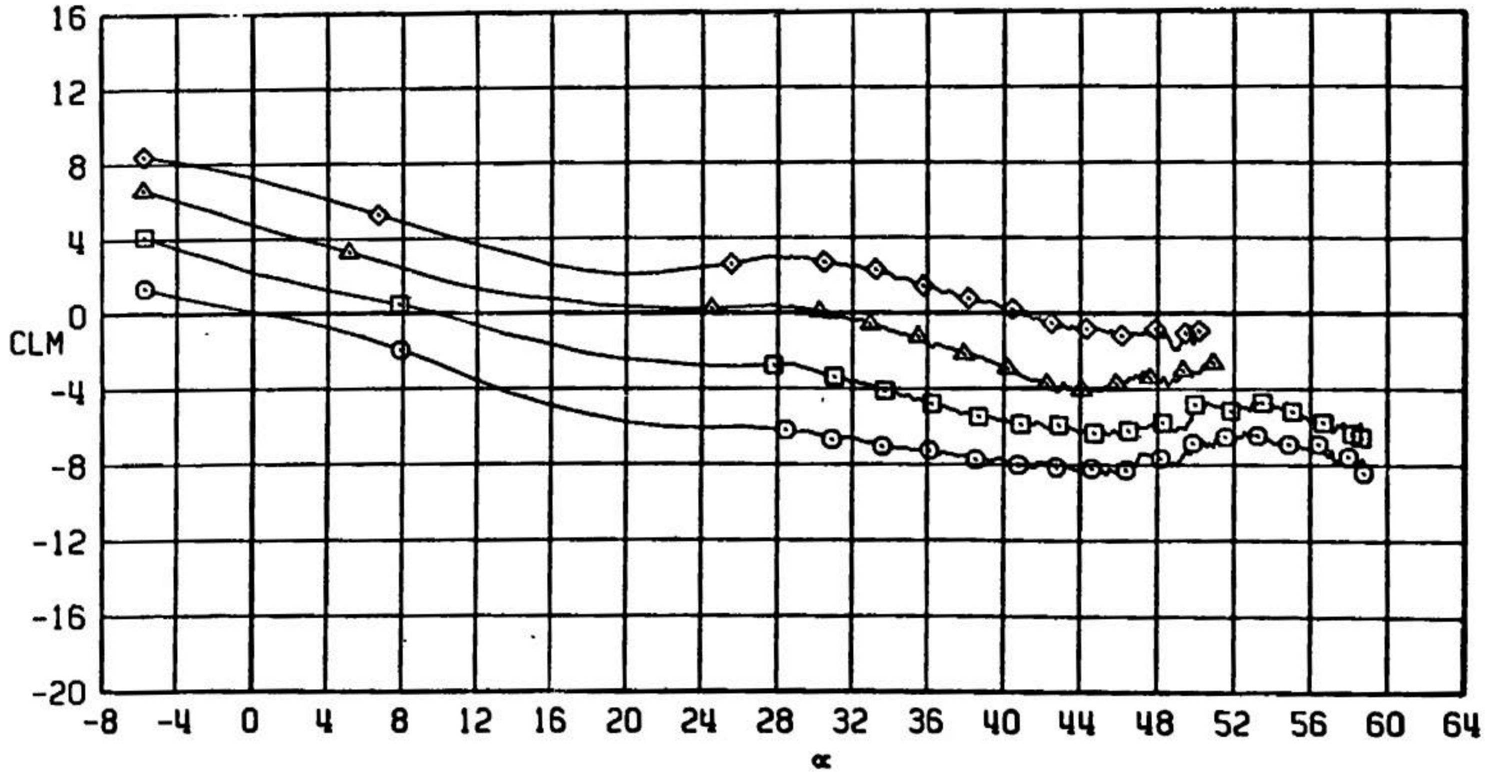

b. CLM versus α

Figure 46. Continued.

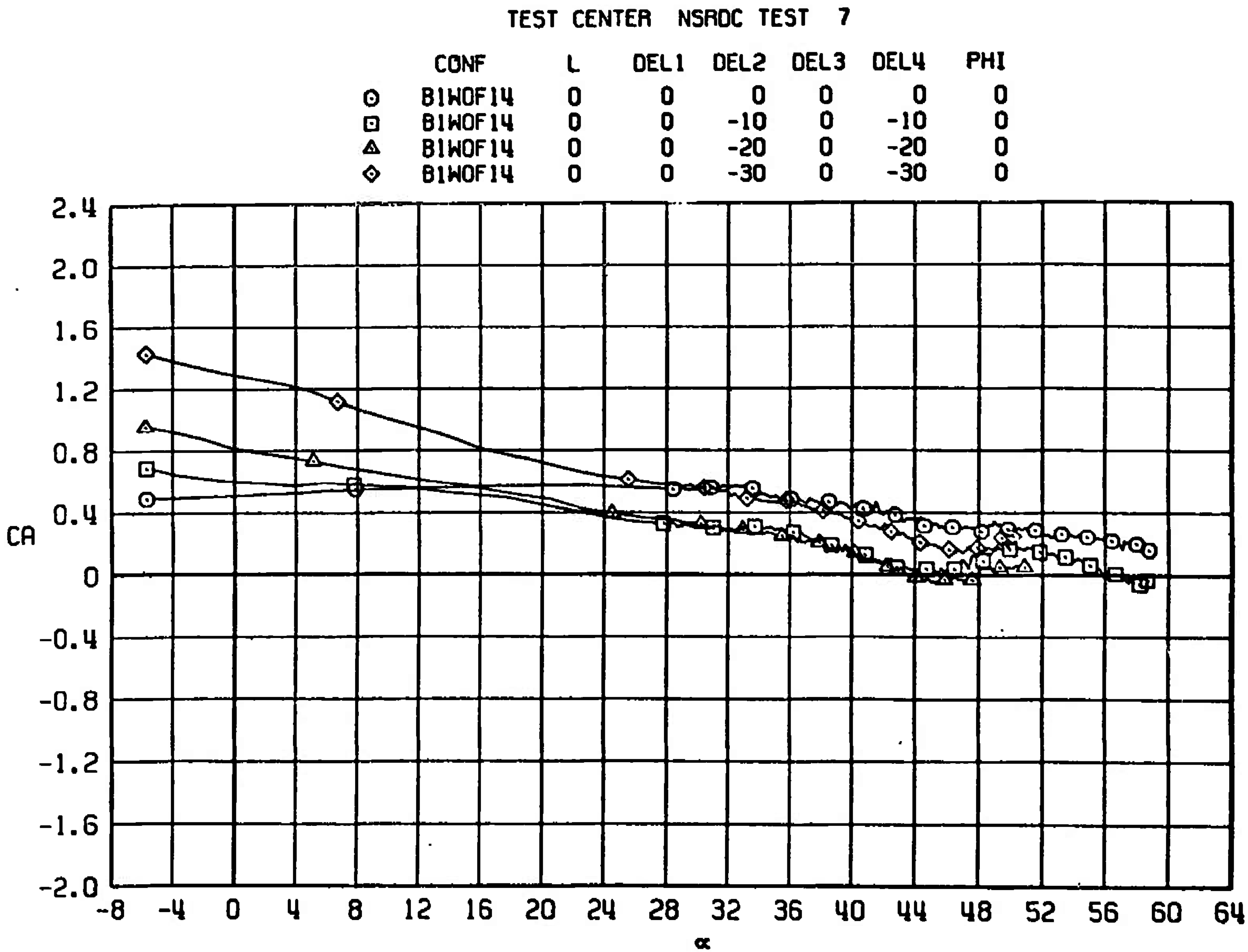

c. CA versus α

Figure 46. Continued.

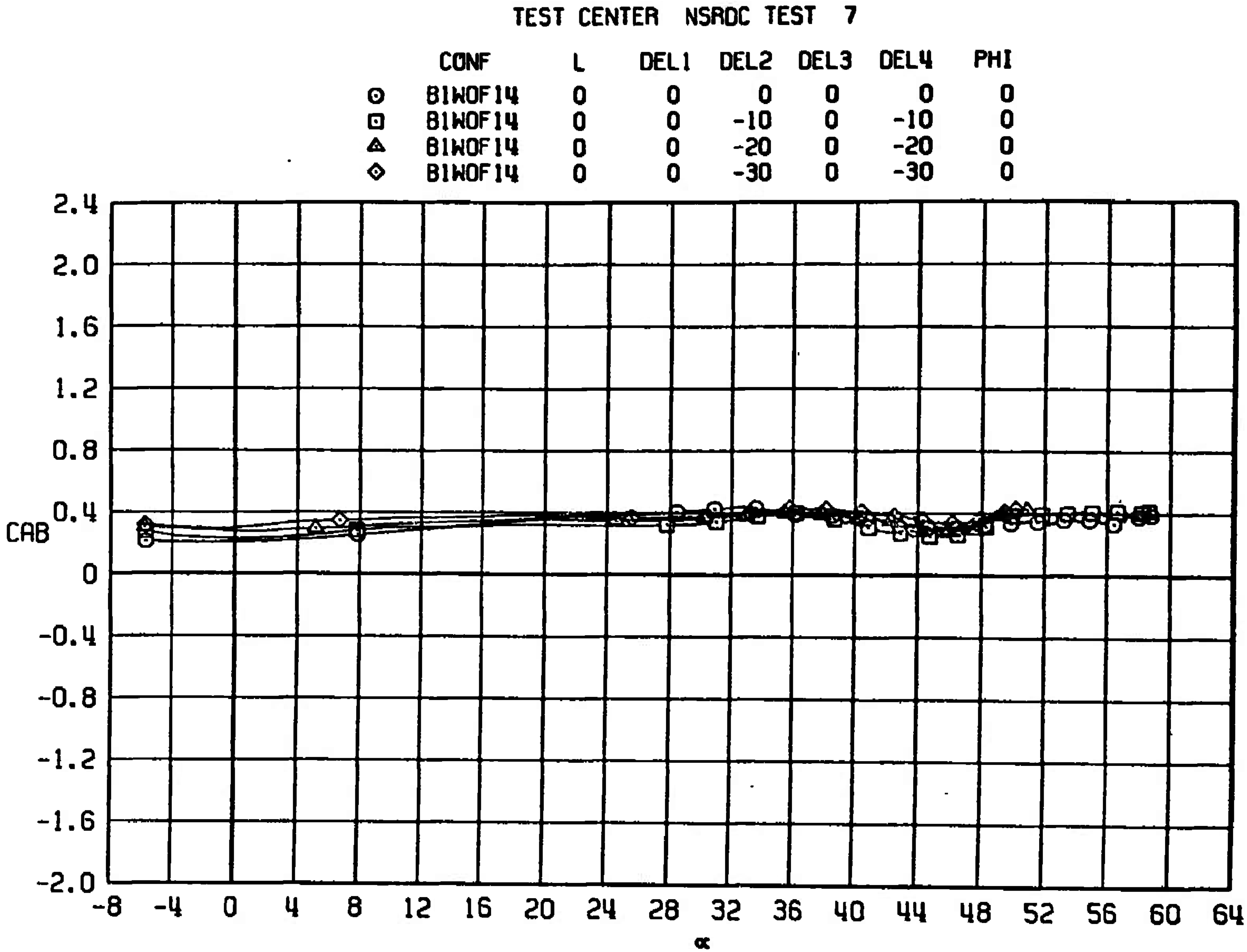

d. CAB versus a
Figure 46. Continued.

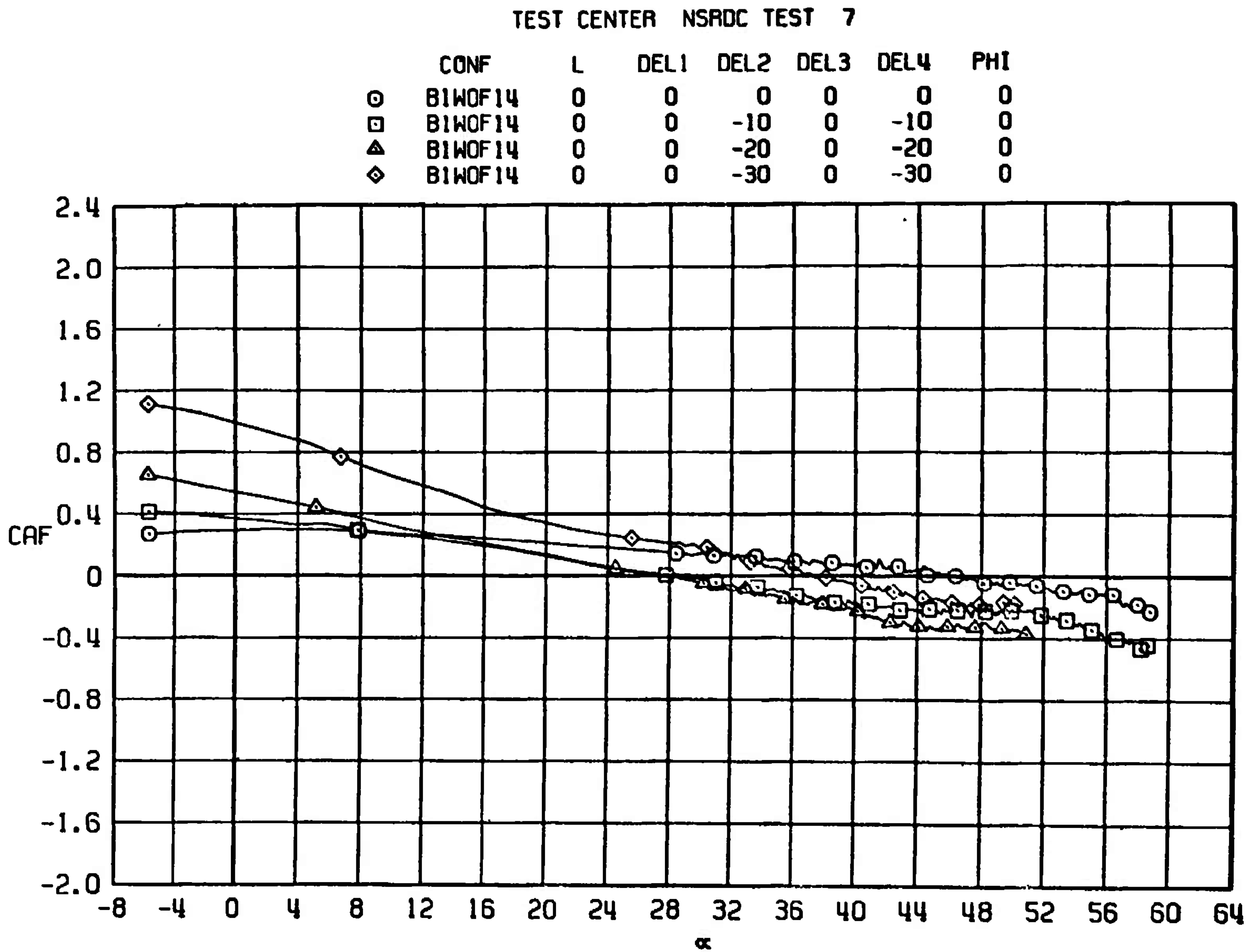

e. CAF versus α

Figure 46. Continued.

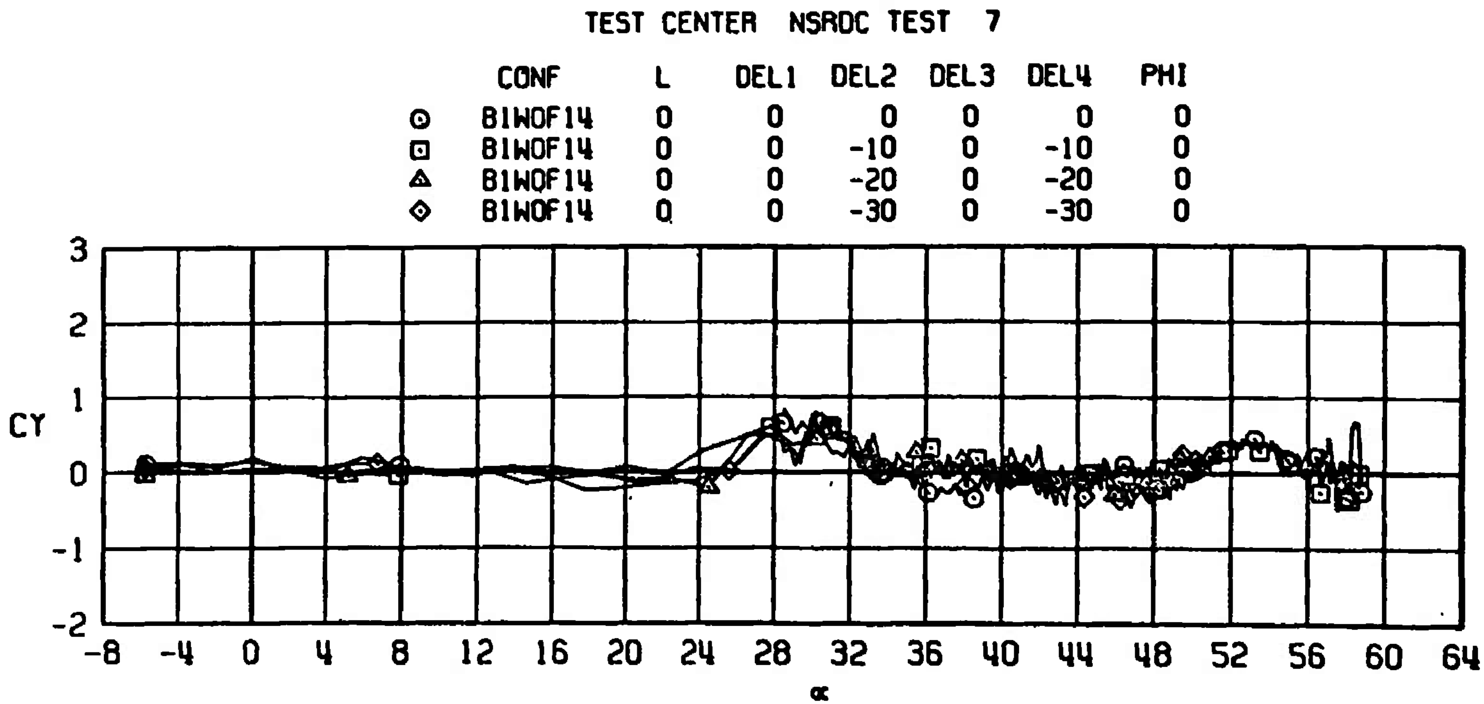

f. CY versus α
Figure 46. Continued.

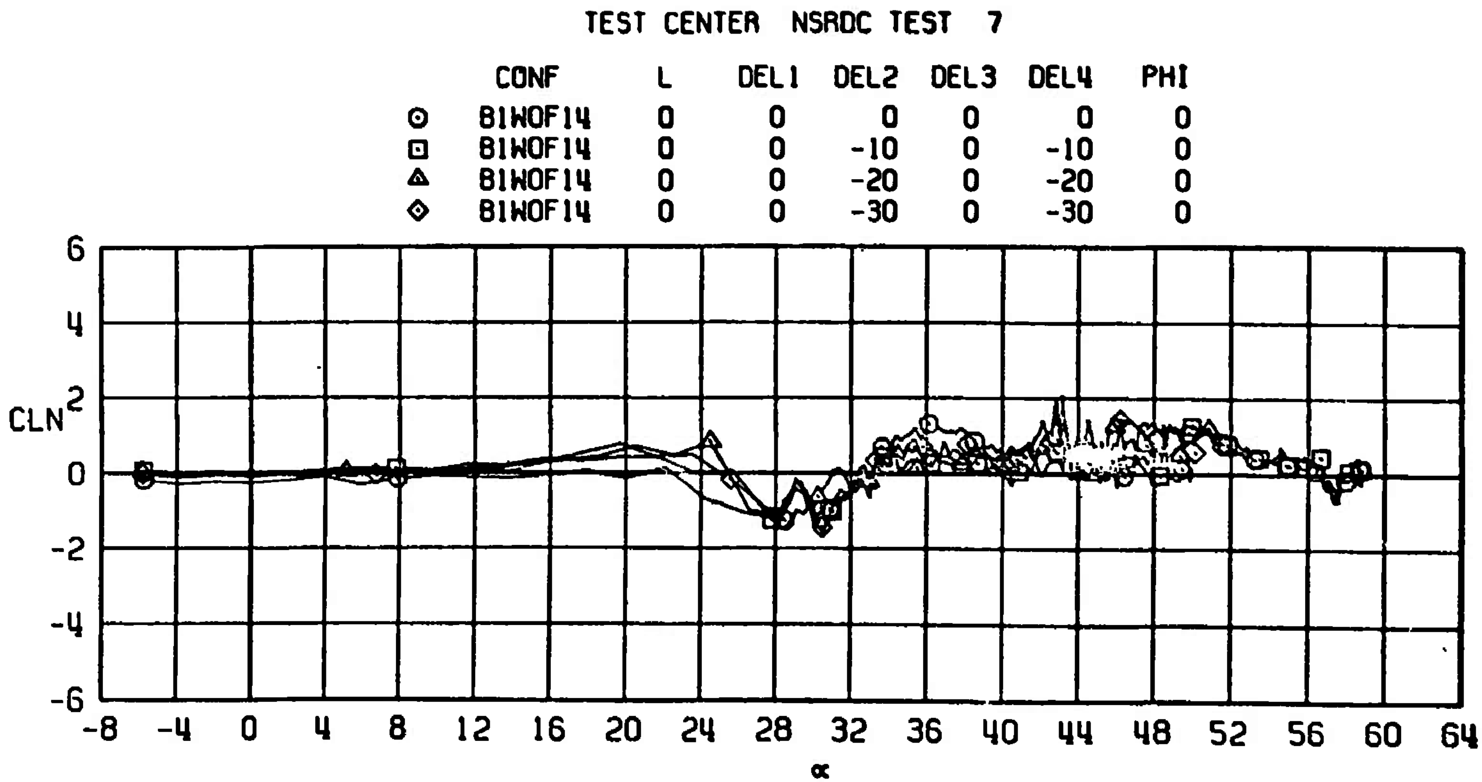

g. CLN versus α
Figure 46. Continued.

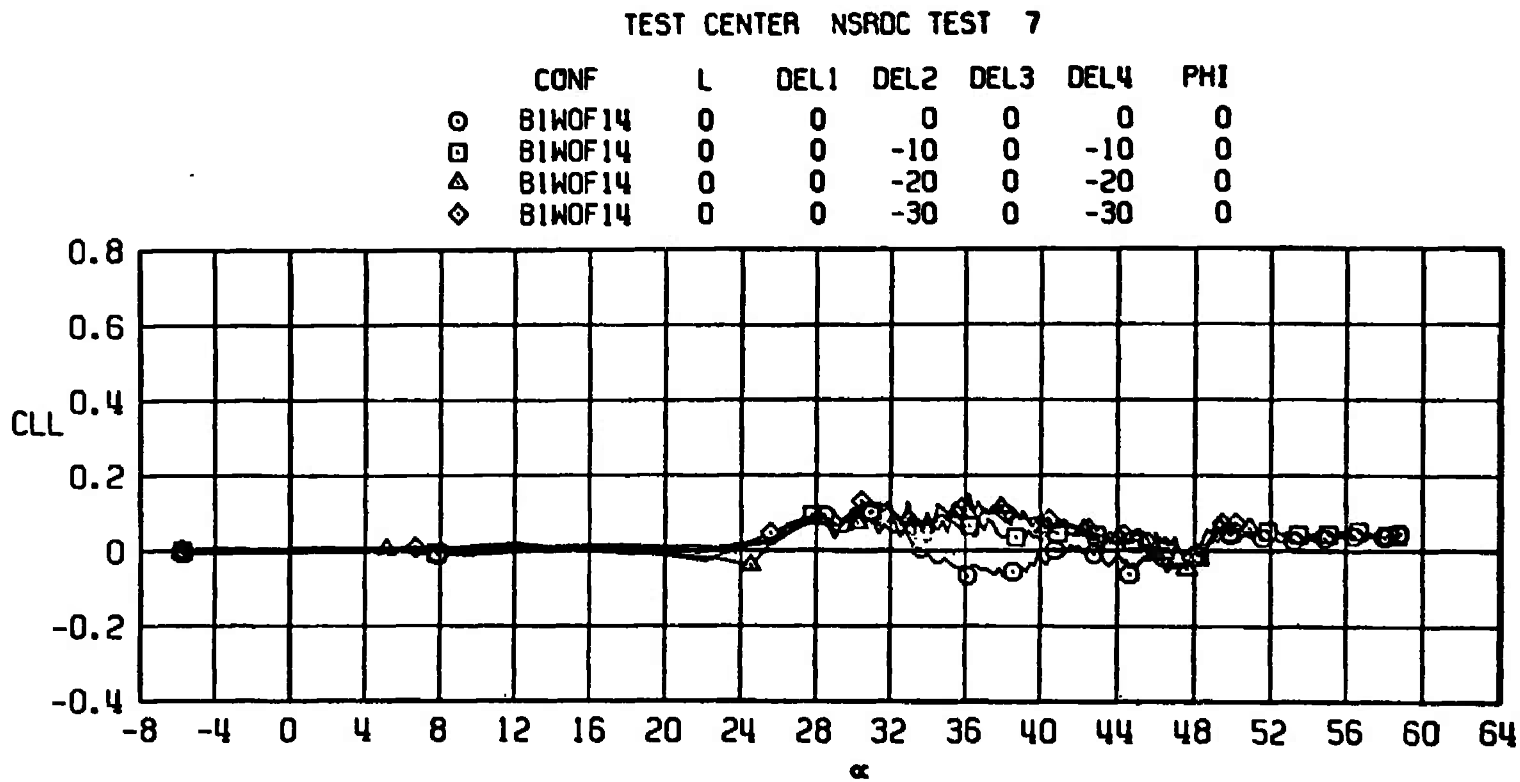

h. CLL versus α

Figure 46. Continued.

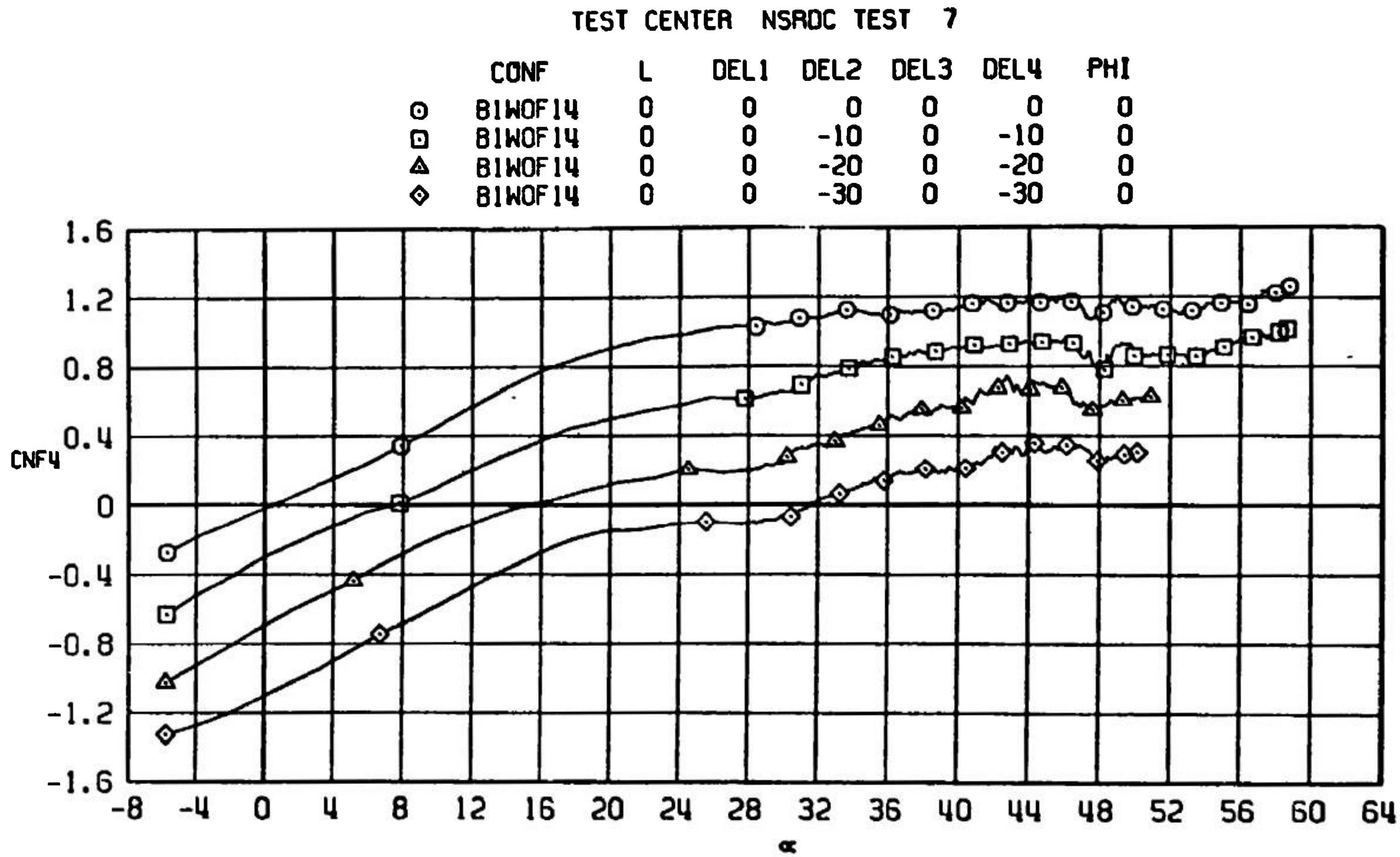

i. CNF4 versus α

Figure 46. Continued.

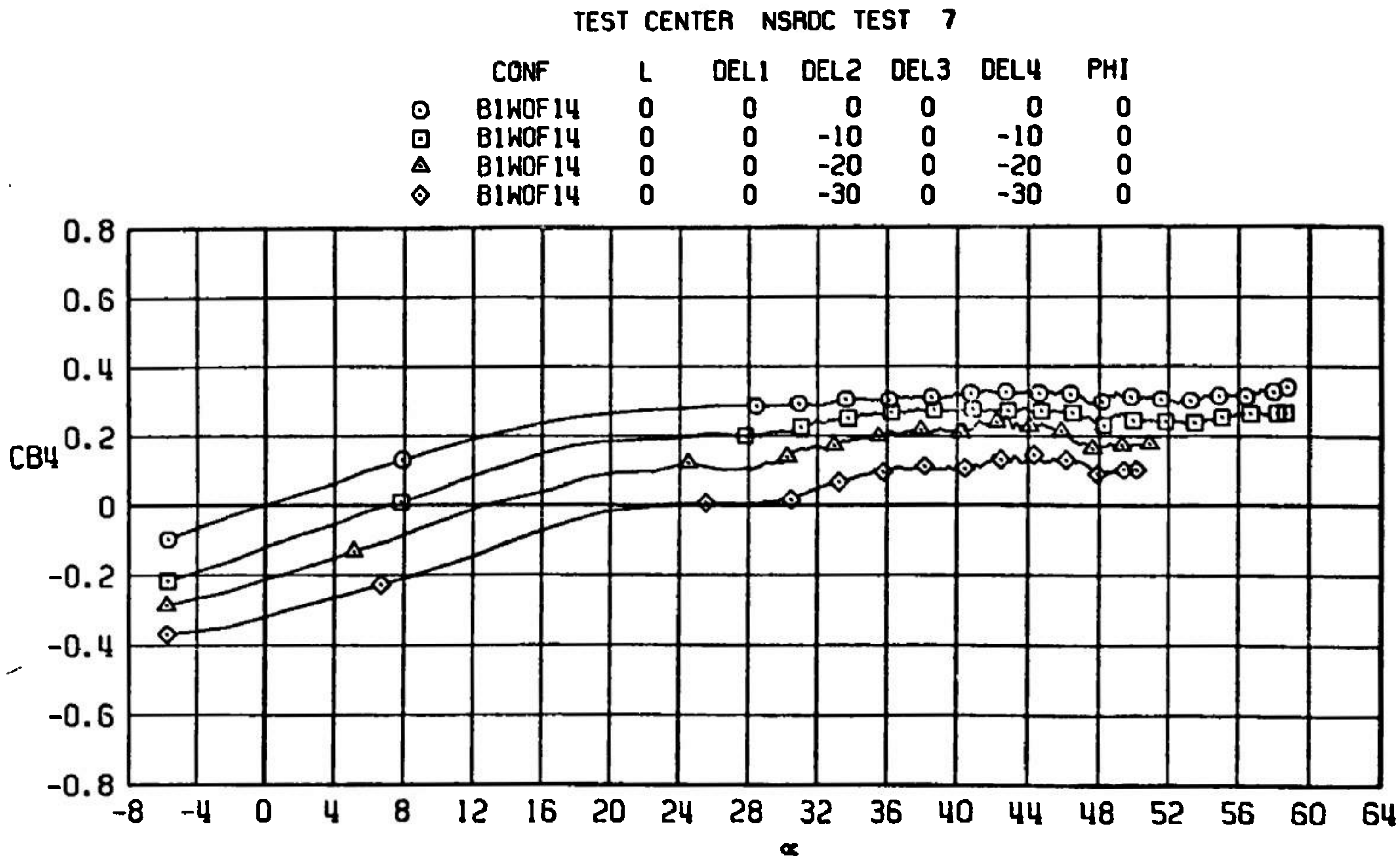

j. CB4 versus α
Figure 46. Continued.

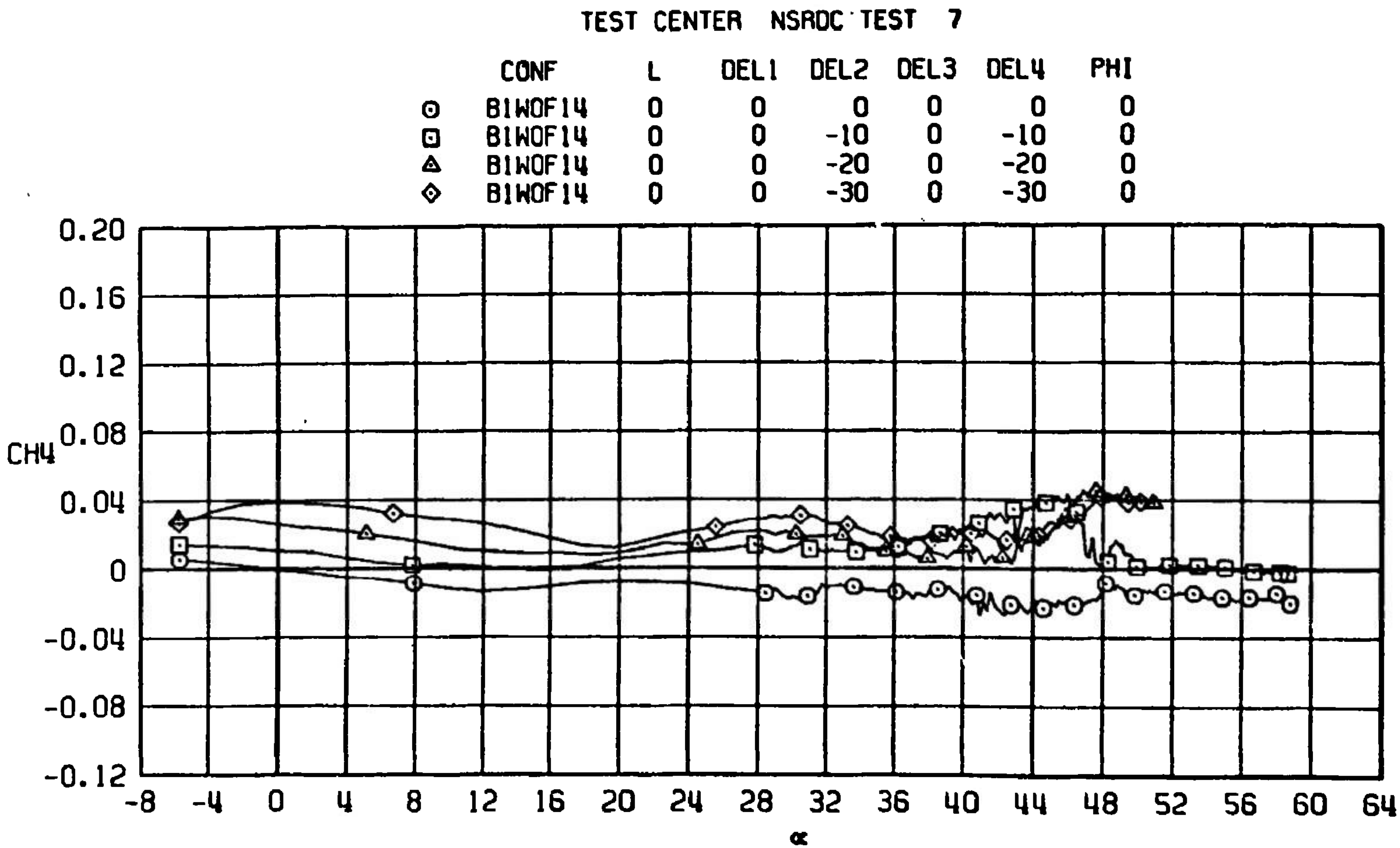

k. CH4 versus α
Figure 46. Concluded.

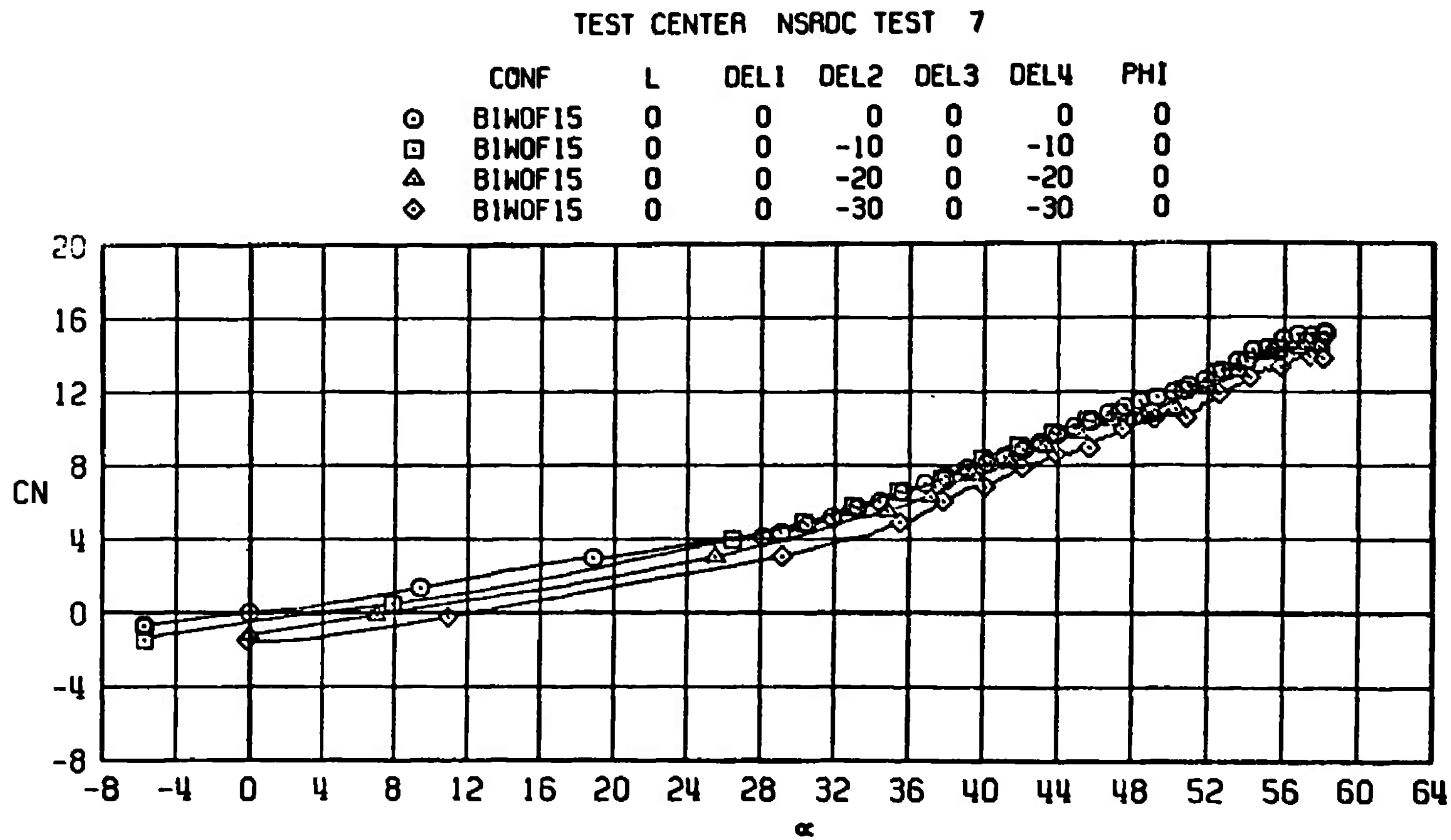

a. CN versus α

Figure 47. Test No. 7, comparison of aerodynamic coefficients of configuration B1W0F15 for various deflections of tail fins No. 2 and 4 at M_∞ = 0.8.

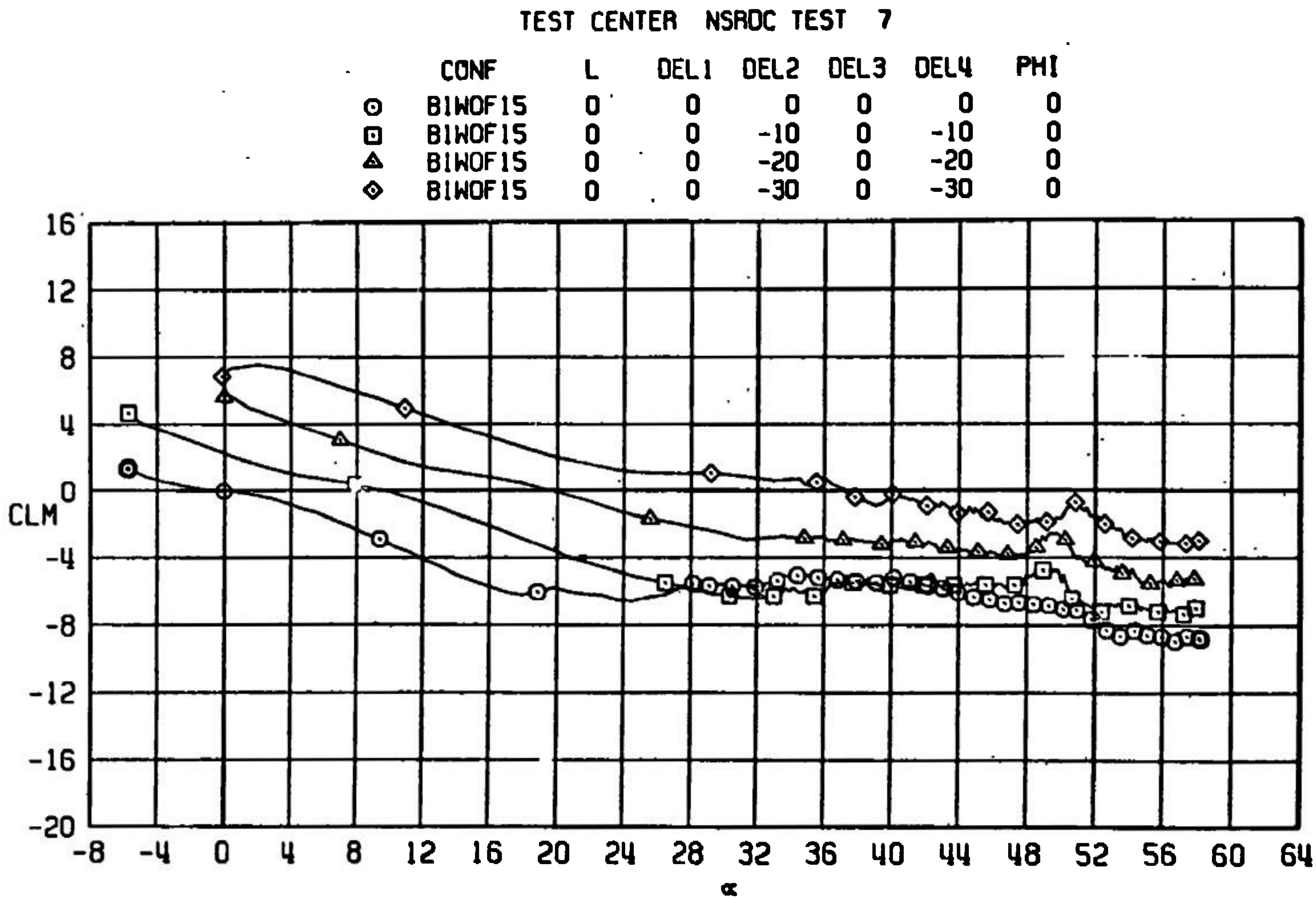

b. CLM versus α
Figure 47. Continued.

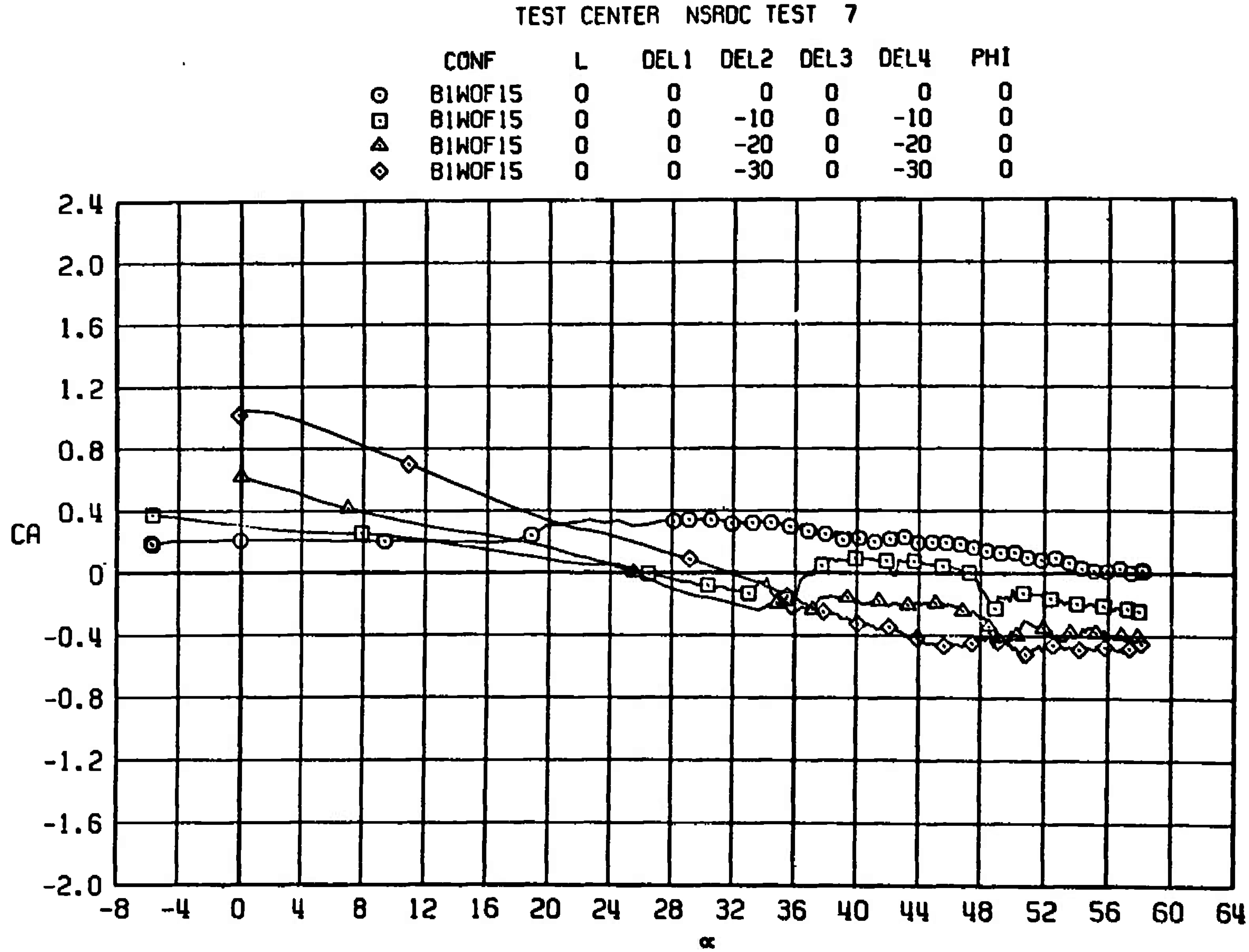

c. CA versus α
Figure 47. Continued.

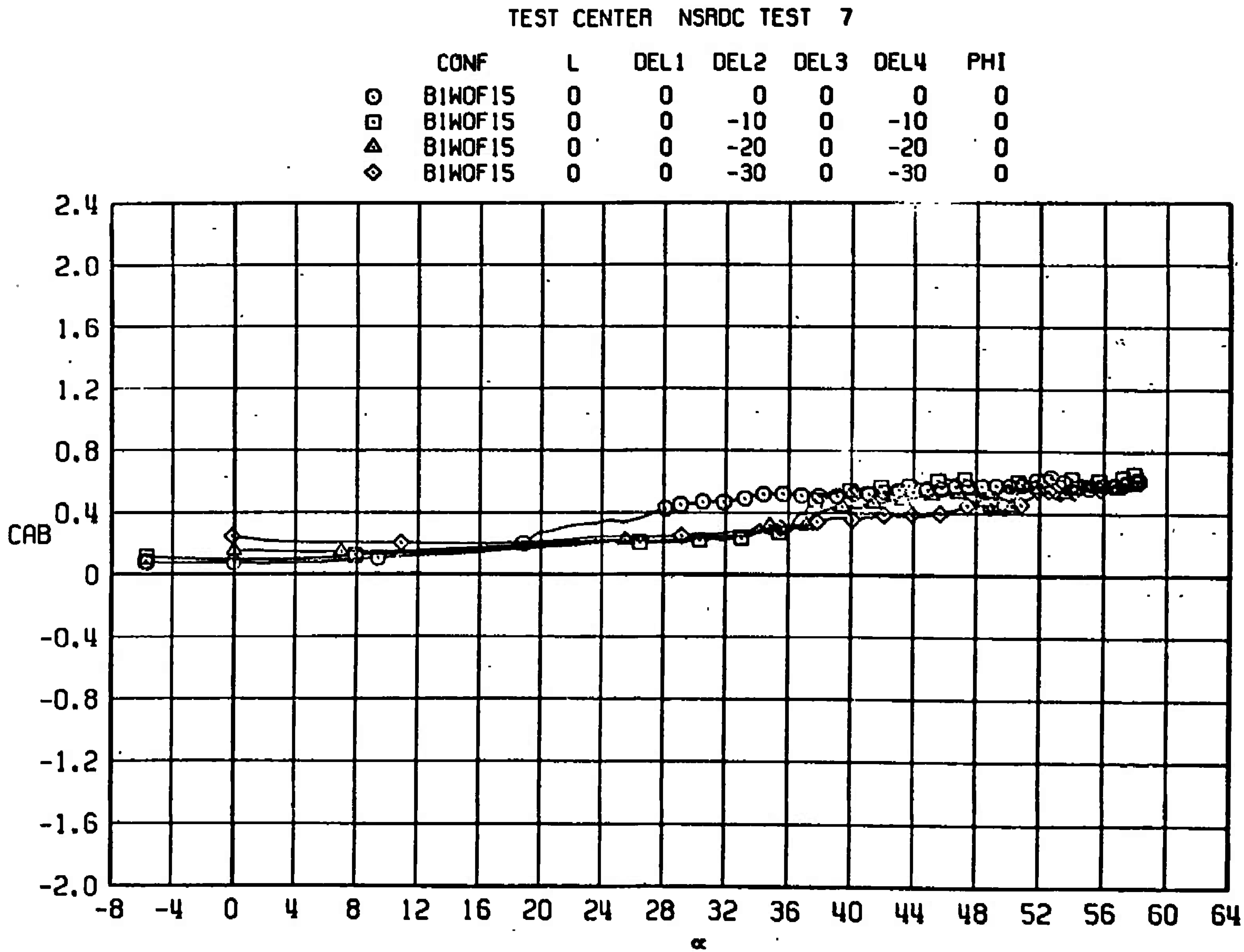

d. CAB versus α
Figure 47. Continued.

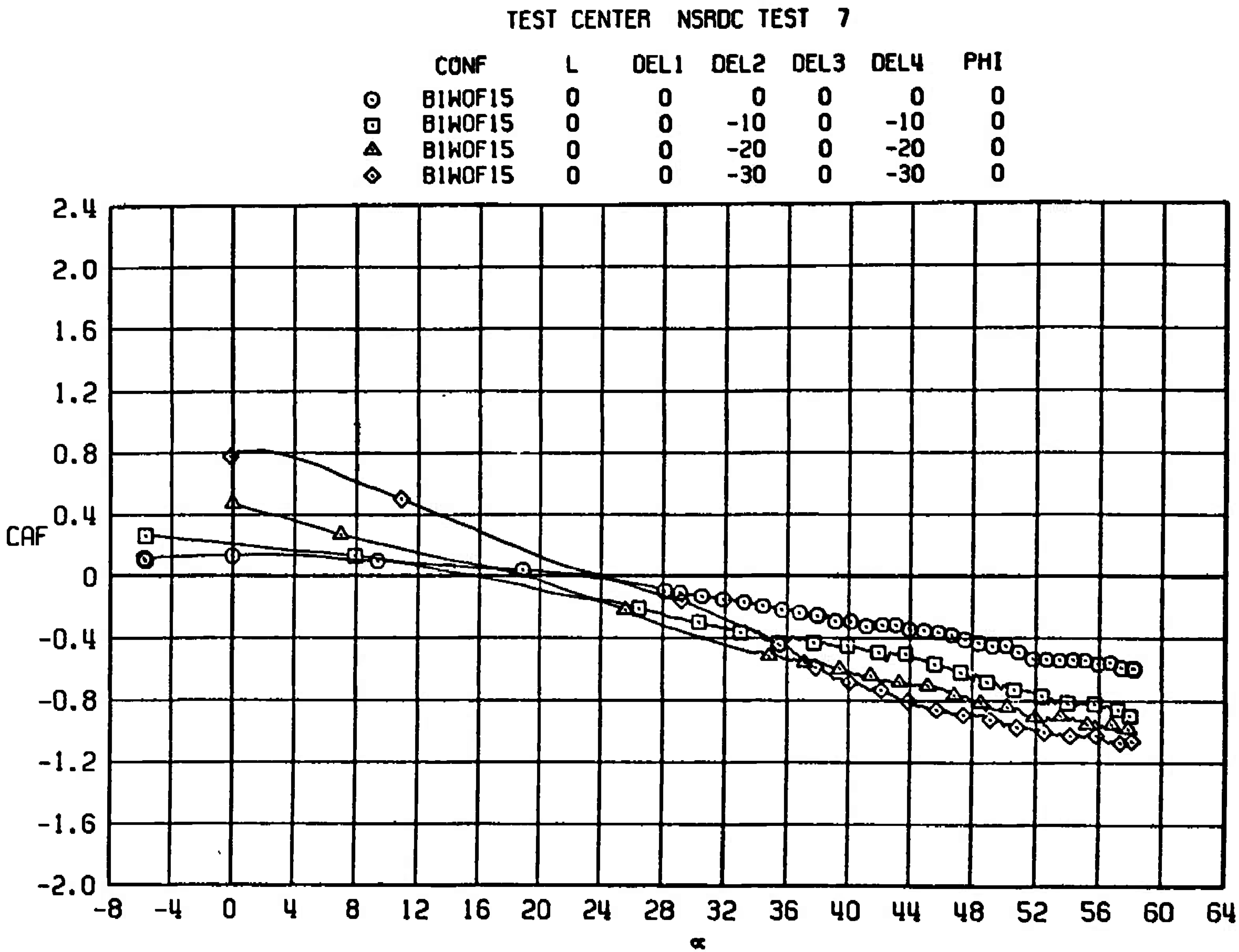

e. CAF versus α
Figure 47. Continued.

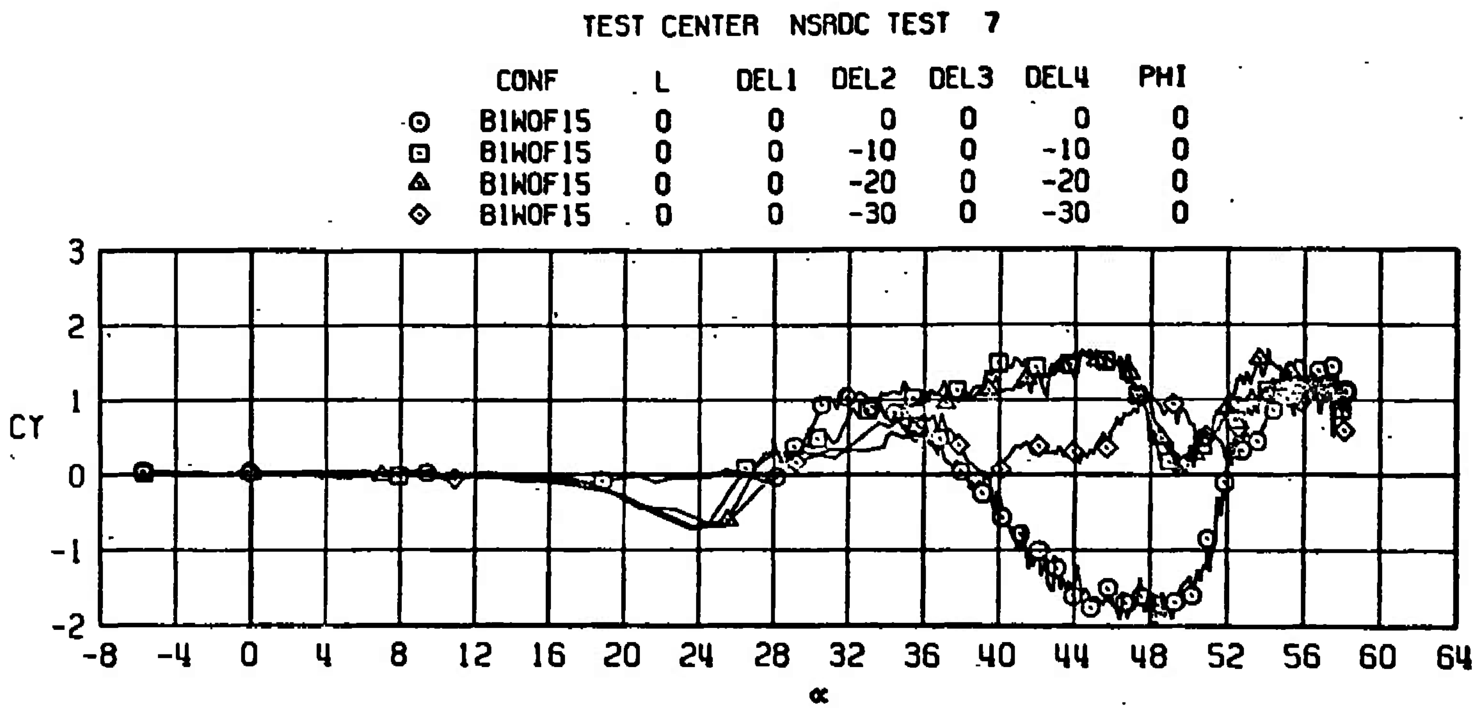

f. CY versus α
Figure 47. Continued.

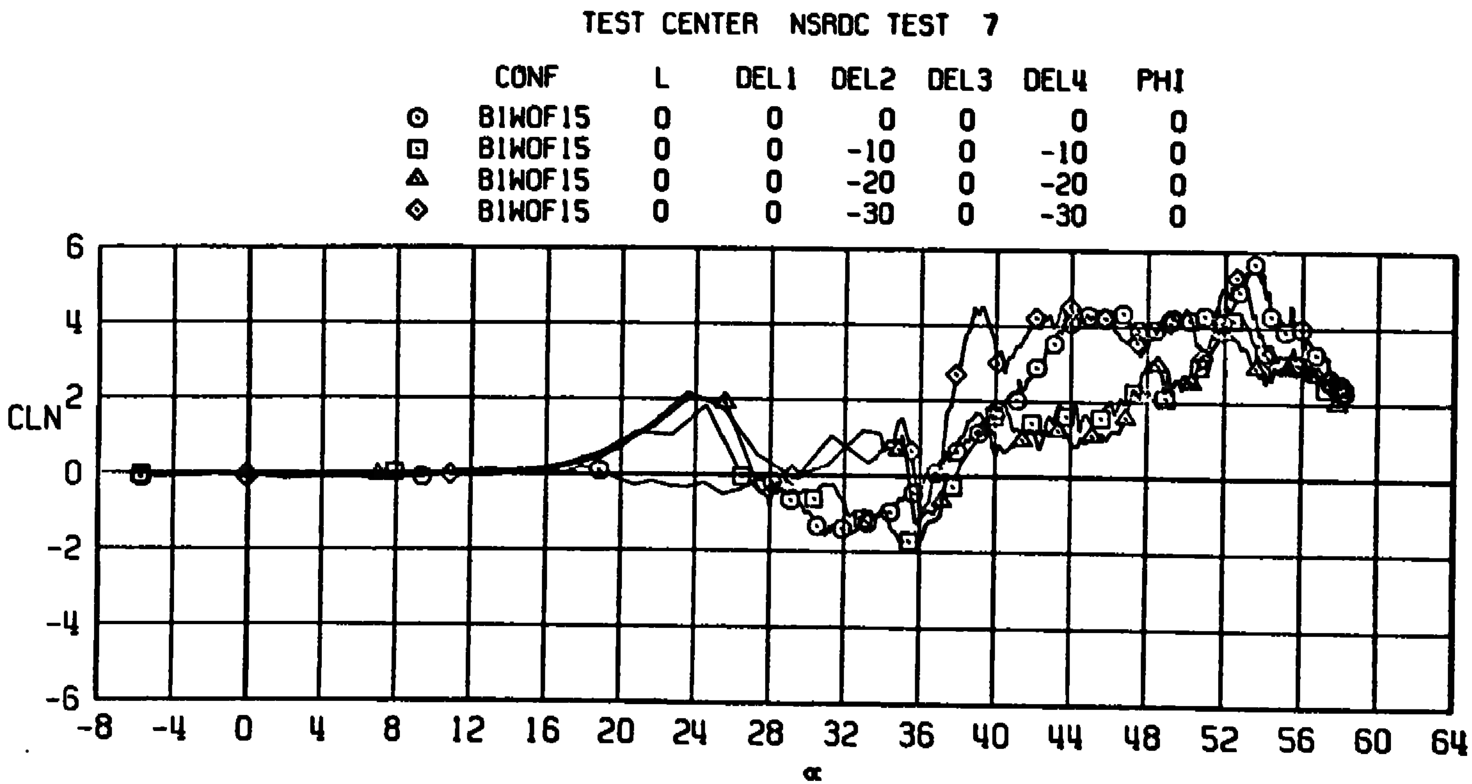

g. CLN versus *α*
Figure 47. Continued.

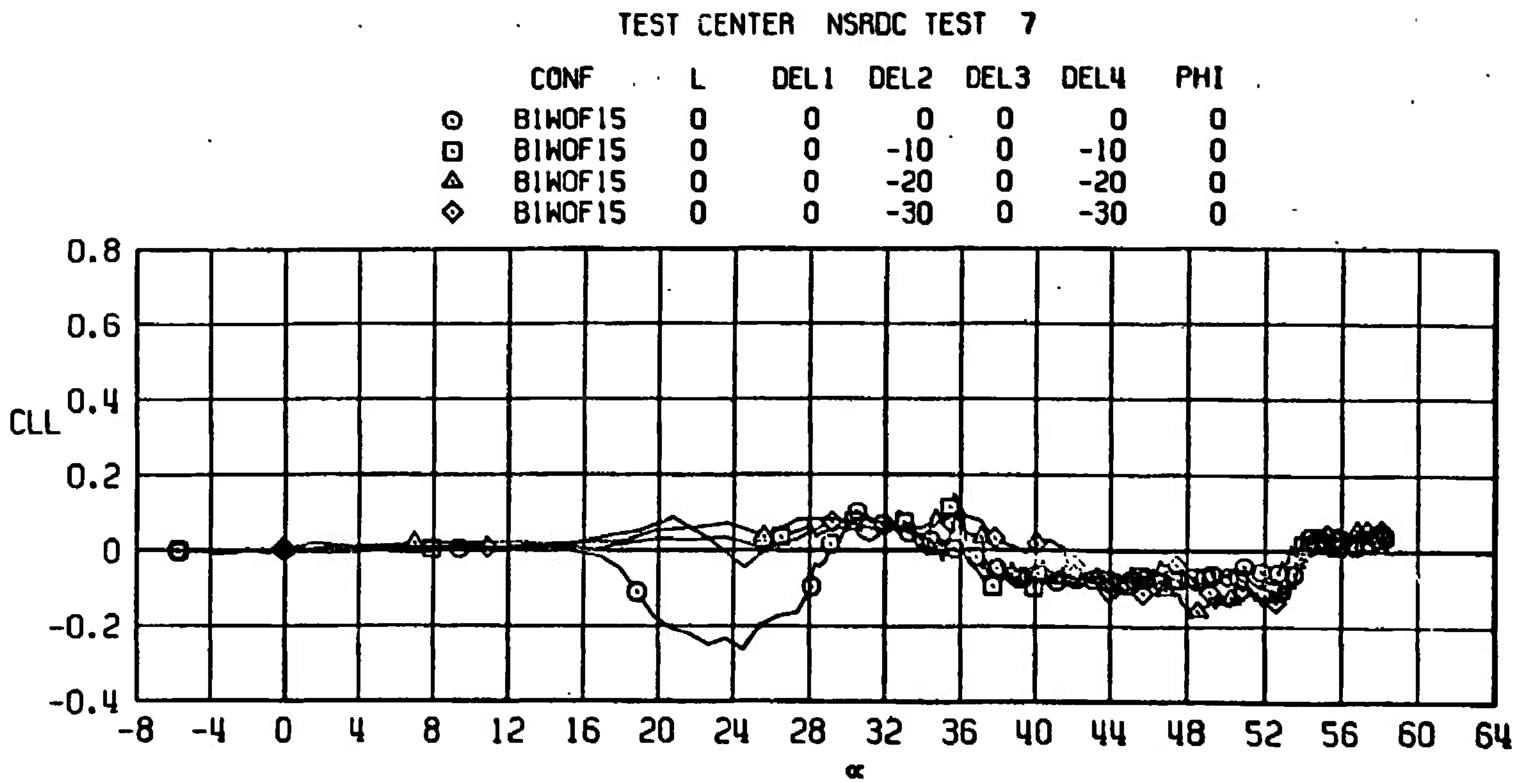

h. CLL versus α
Figure 47. Continued.

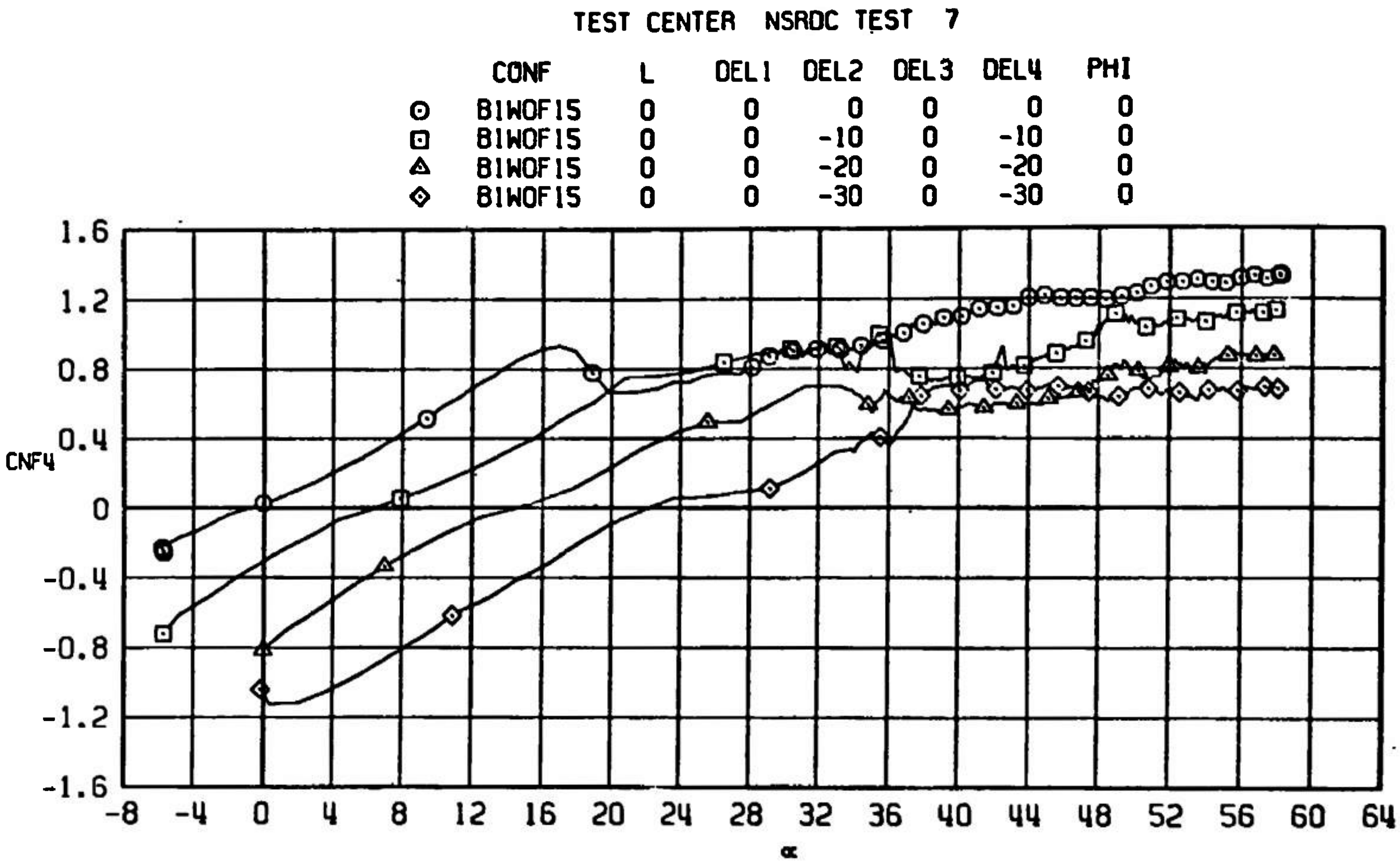

i. CNF4 versus α
Figure 47. Continued.

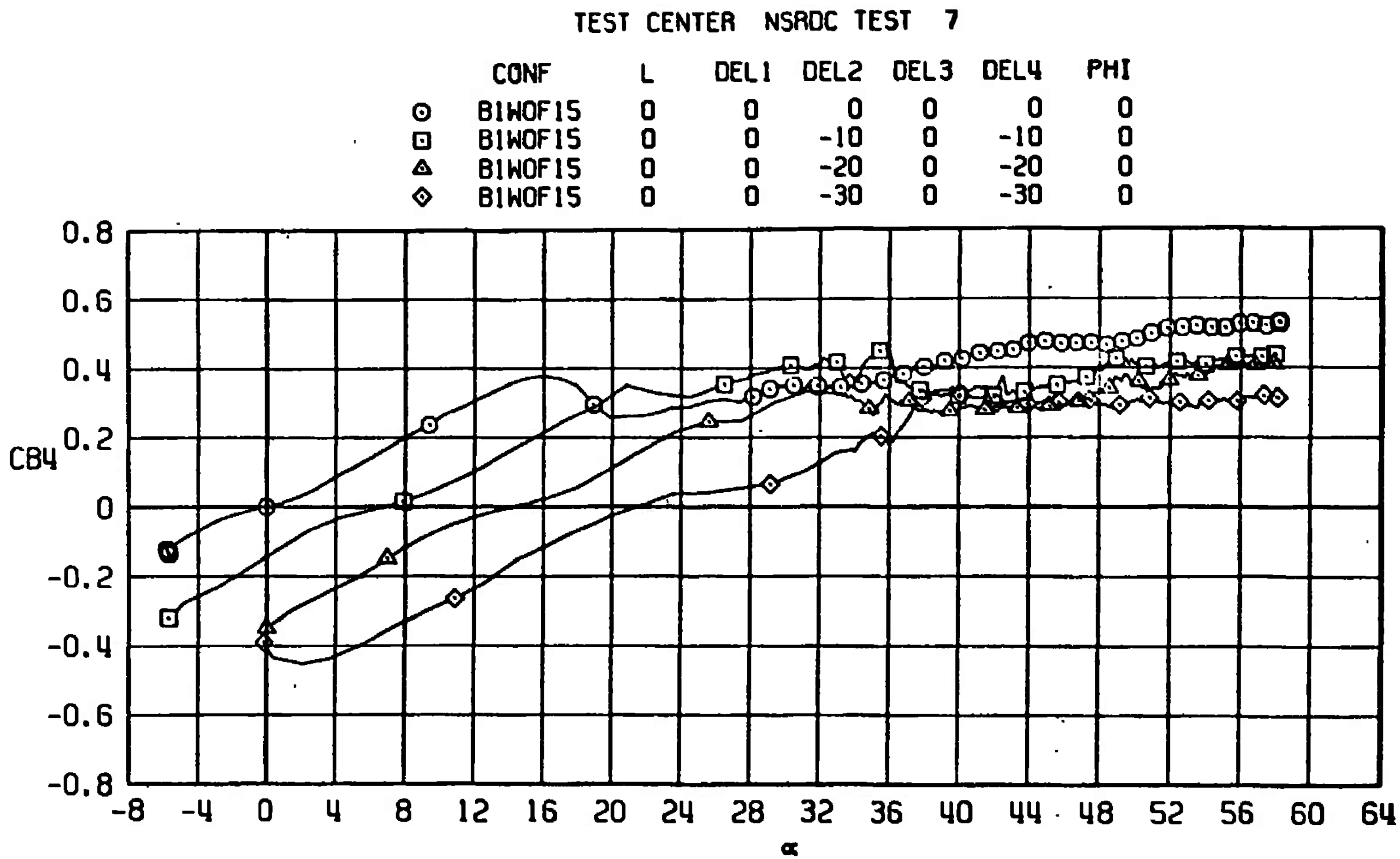

j. CB4 versus α
Figure 47. Continued.

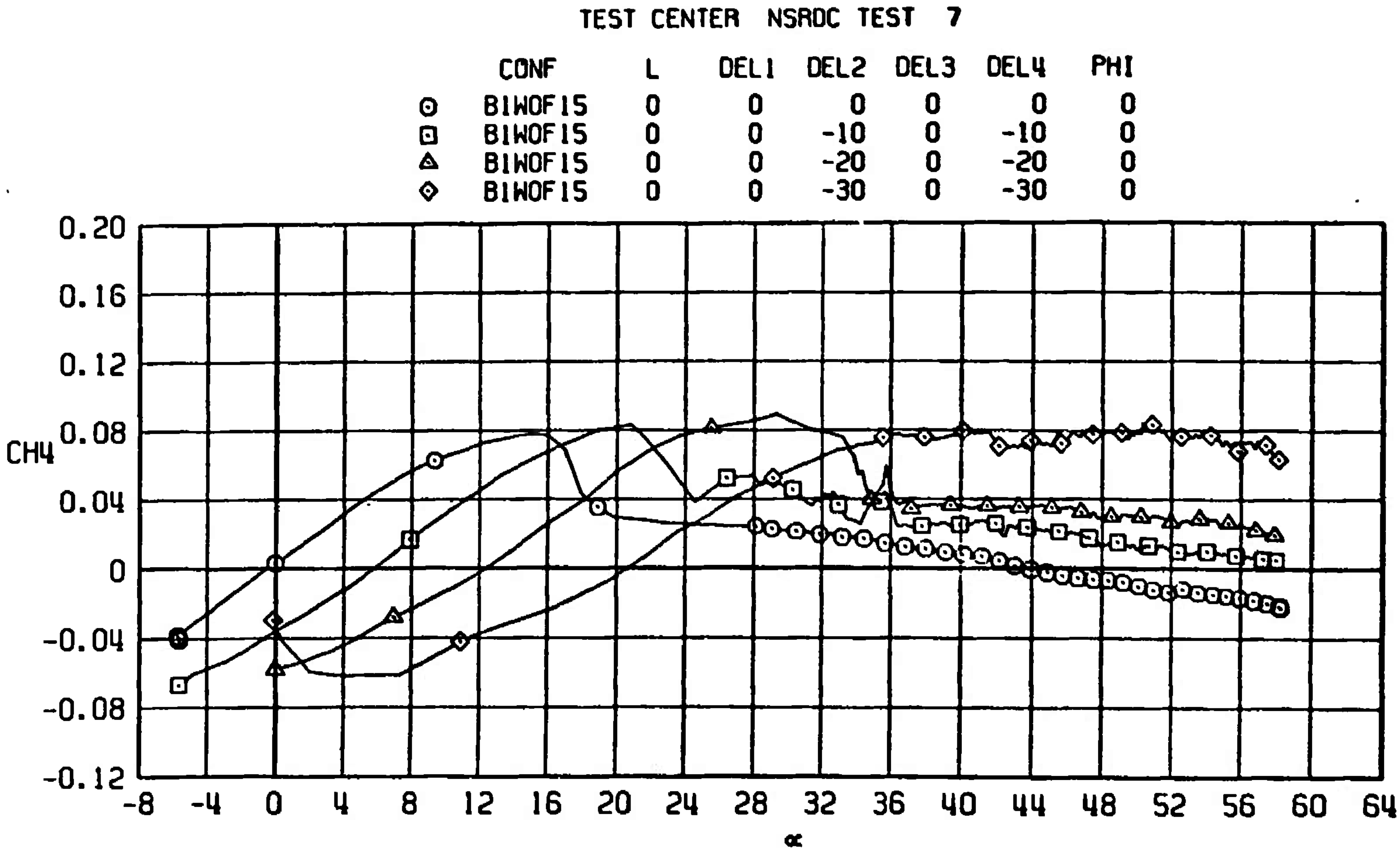

k. CH4 versus α
Figure 47. Continued.

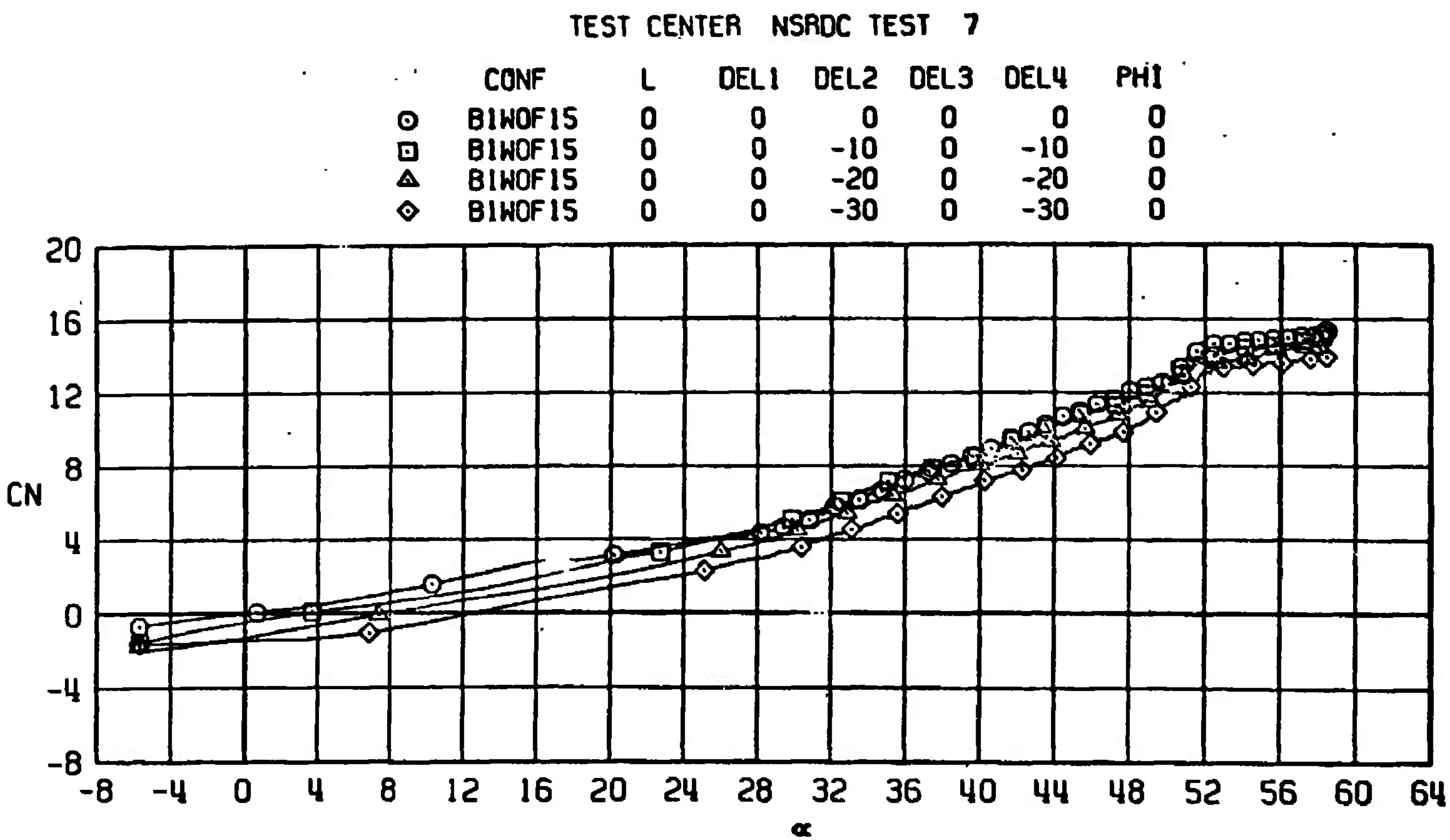

a. CN versus α

Figure 48. Test No. 7, comparison of aerodynamic coefficients of configuration B1W0F15 for various deflections of tail fins No. 2 and 4 at $M_\infty = 0.9$.

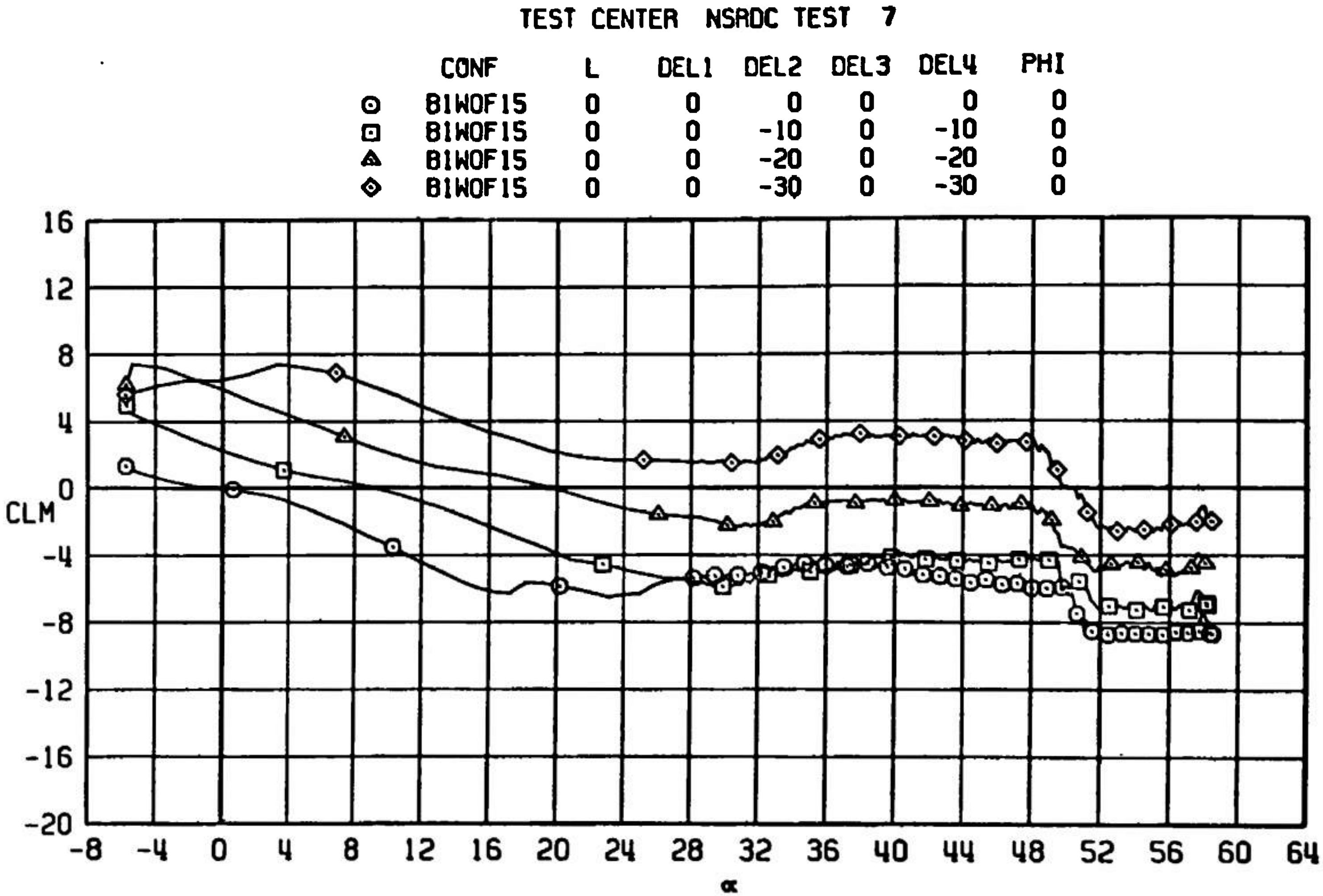

b. CLM versus α
Figure 48. Continued.

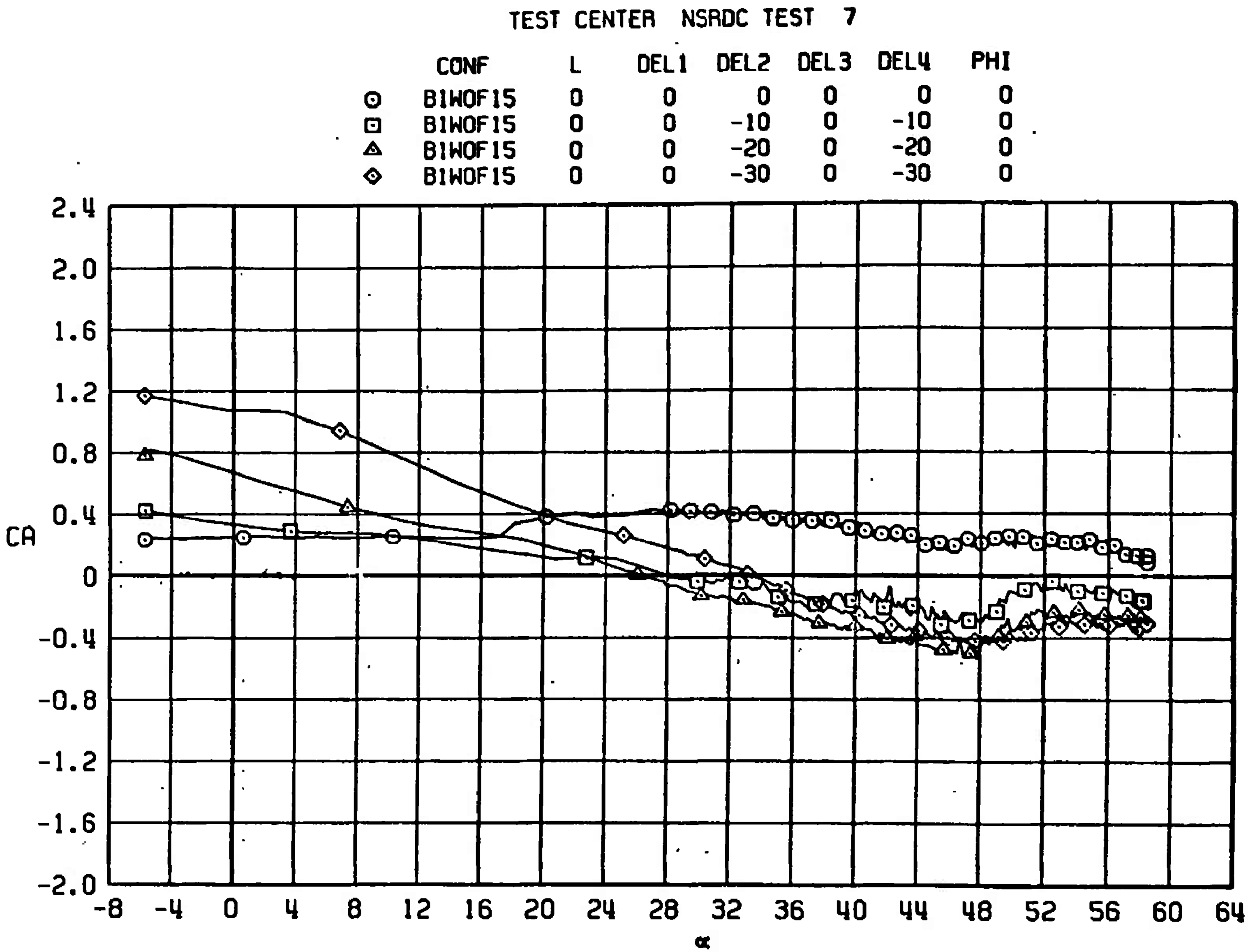

c. CA versus α

Figure 48. Continued.

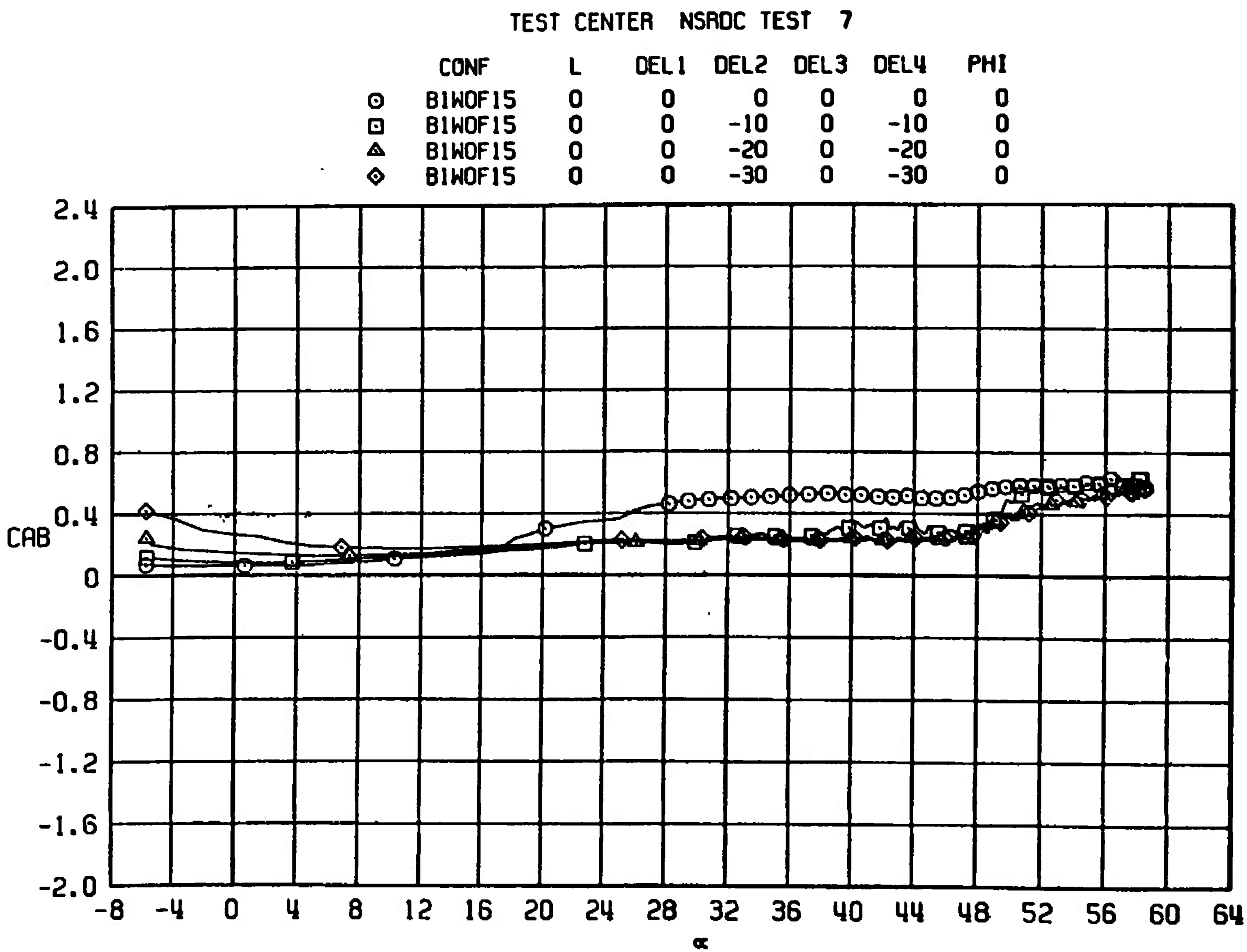

d. CAB versus α
Figure 48. Continued.

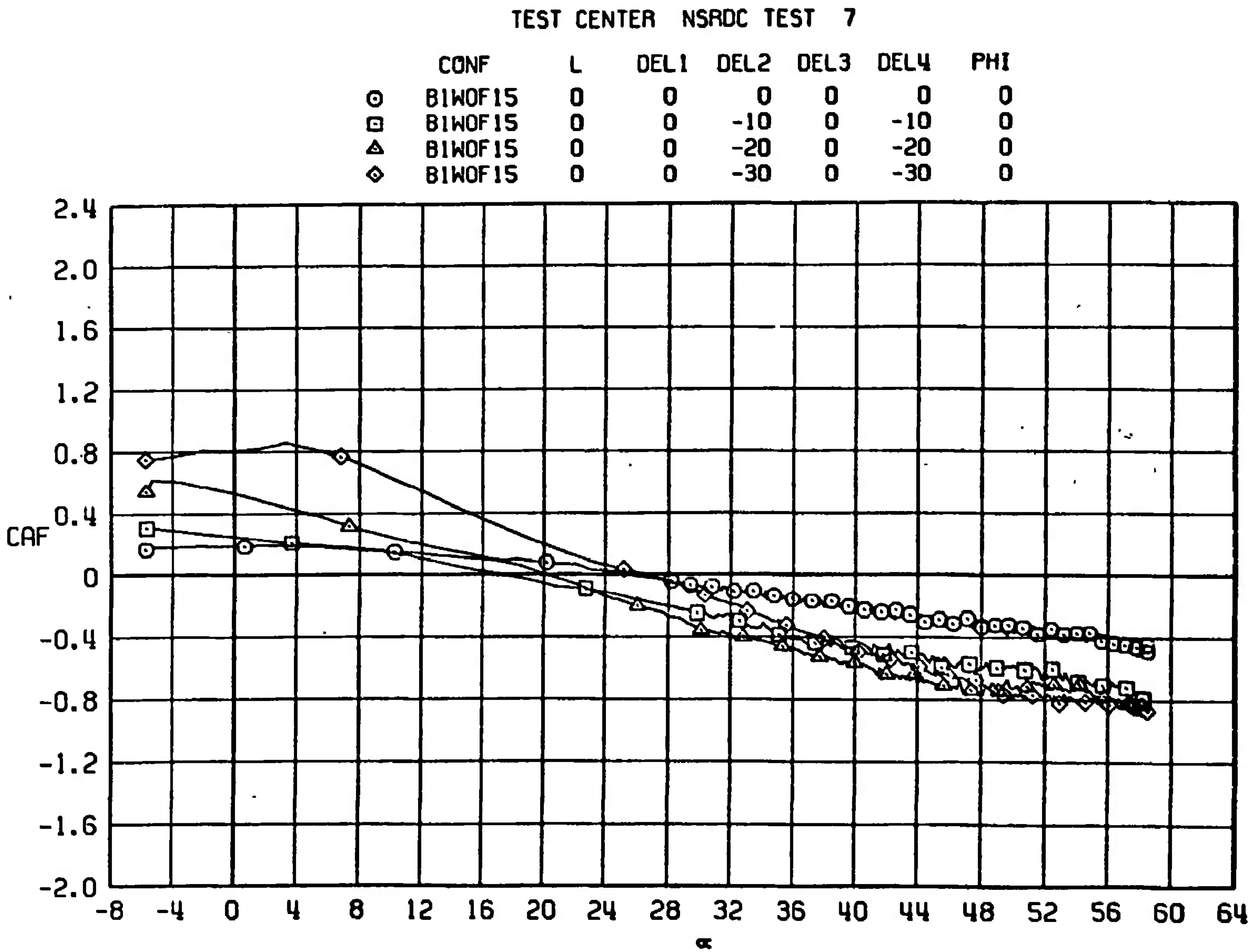

e. CAF versus α

Figure 48. Continued.

TEST CENTER NSRDC TEST 7

	CONF	L	DEL1	DEL2	DEL3	DEL4	PHI
⊙	B1W0F15	0	0	0	0	0	0
⊡	B1W0F15	0	0	-10	0	-10	0
△	B1W0F15	0	0	-20	0	-20	0
◇	B1W0F15	0	0	-30	0	-30	0

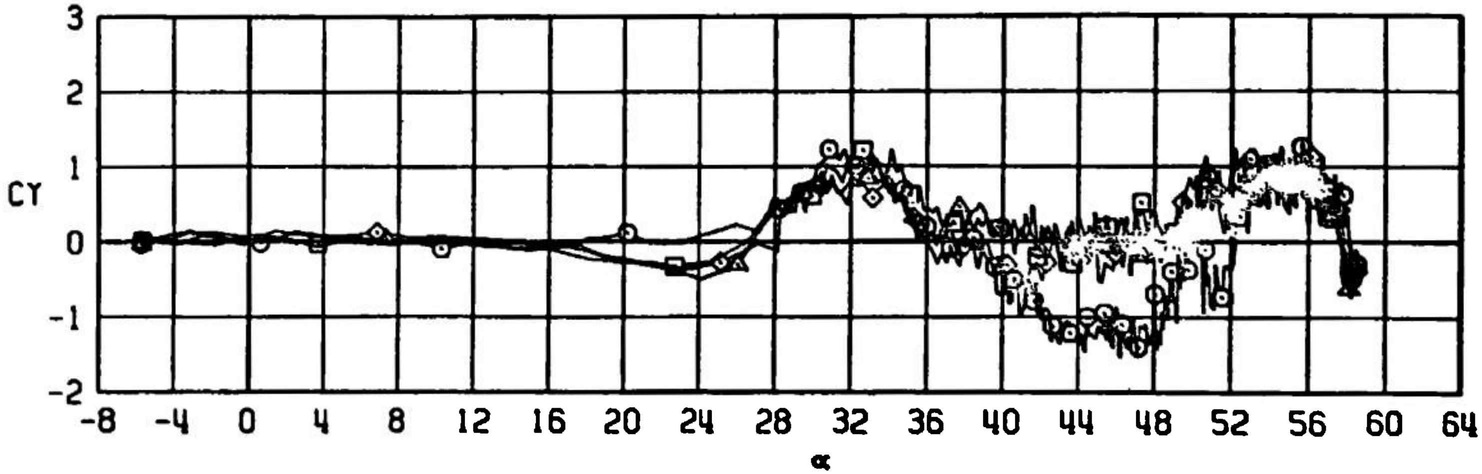

f. CY versus α
Figure 48. Continued.

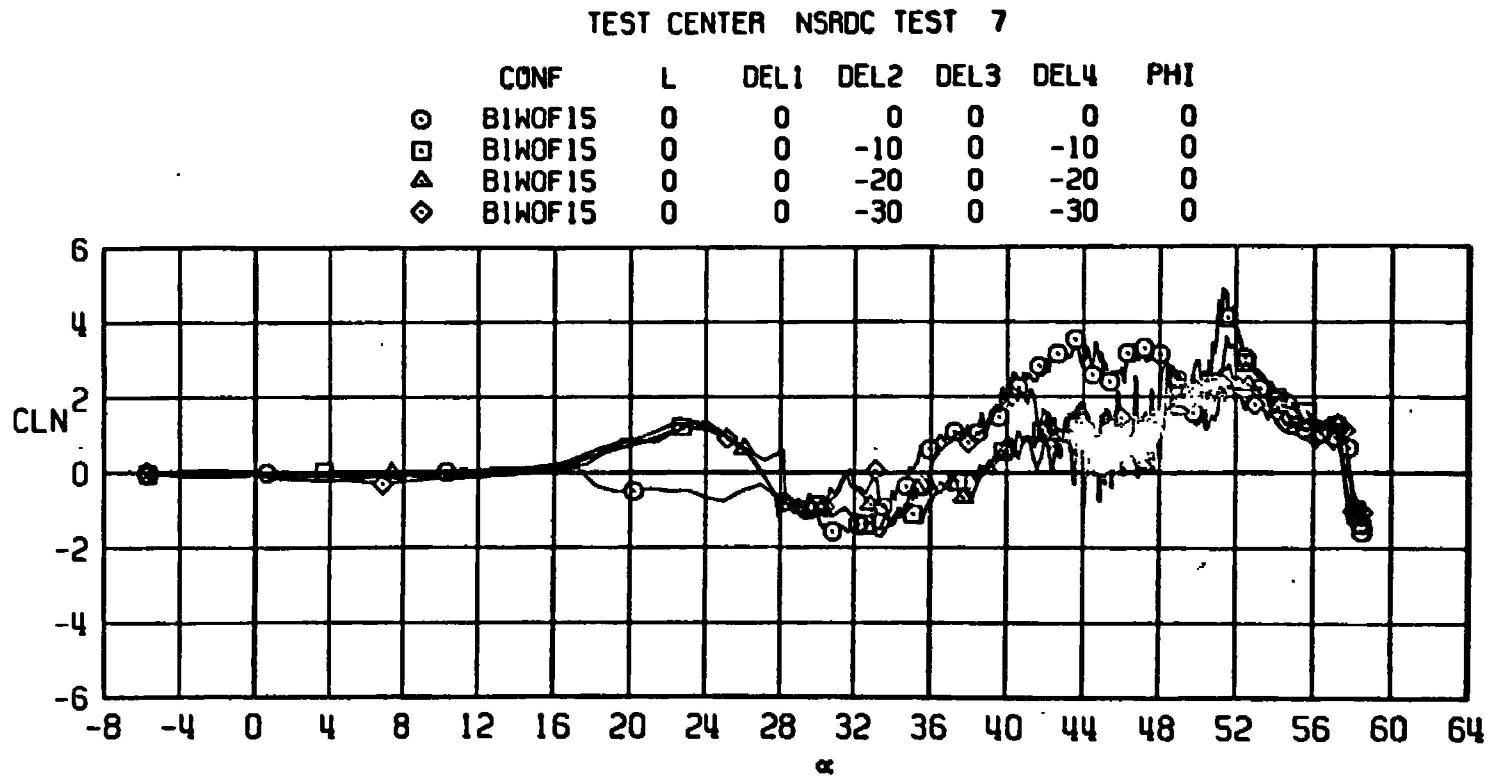

g. CLN versus α
Figure 48. Continued.

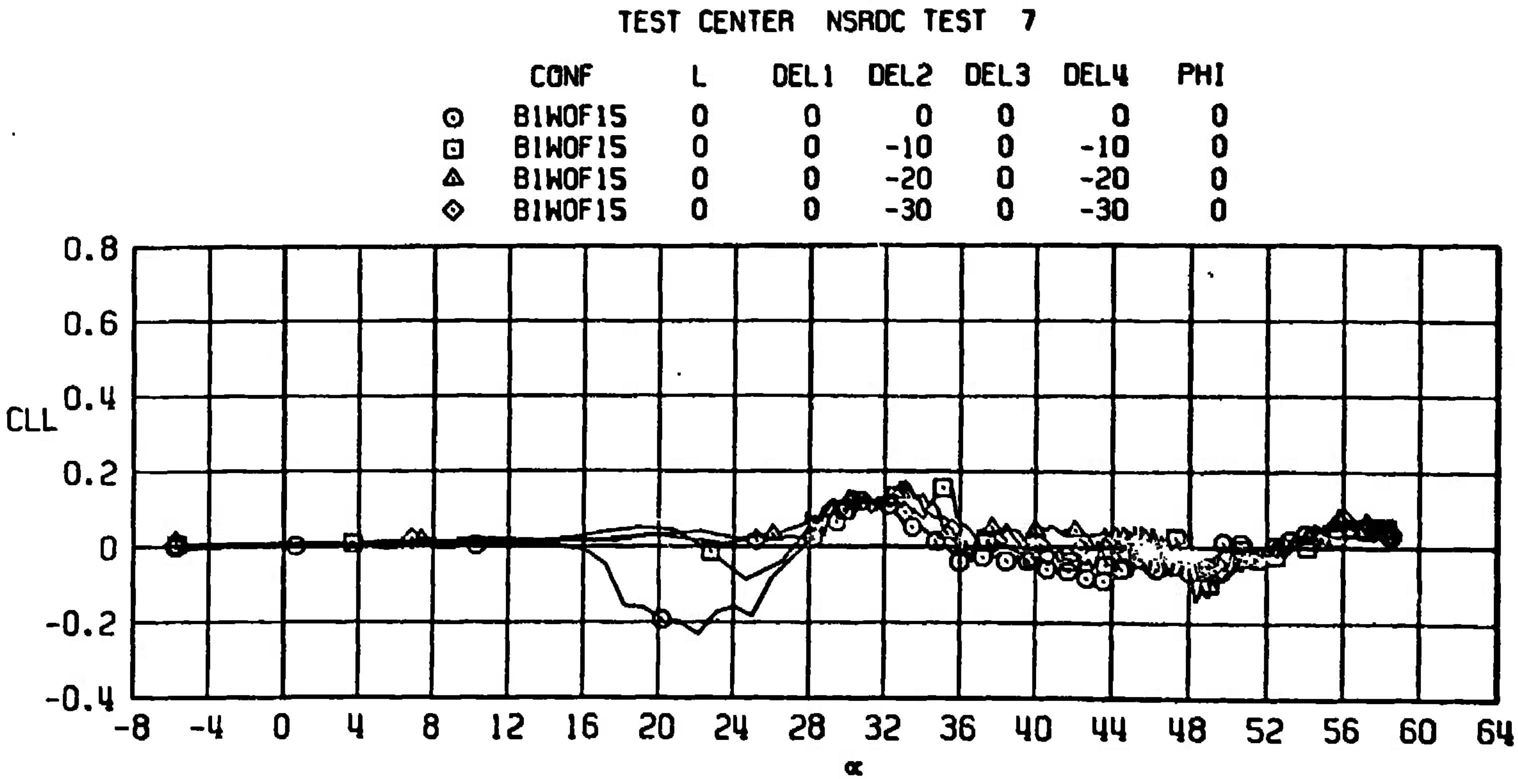

h. CLL versus α
Figure 48. Continued.

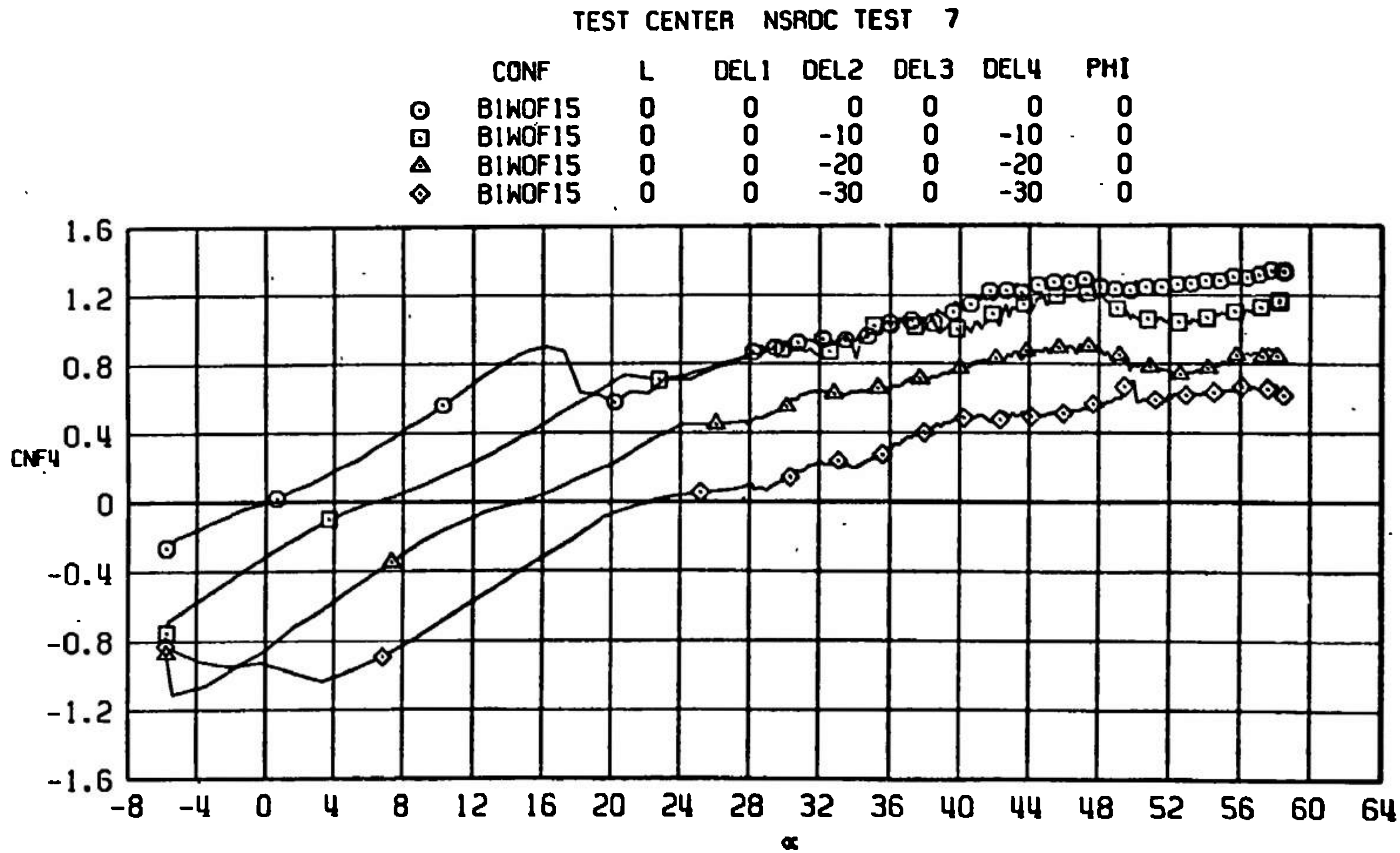

i. CNF4 versus α
Figure 48. Continued.

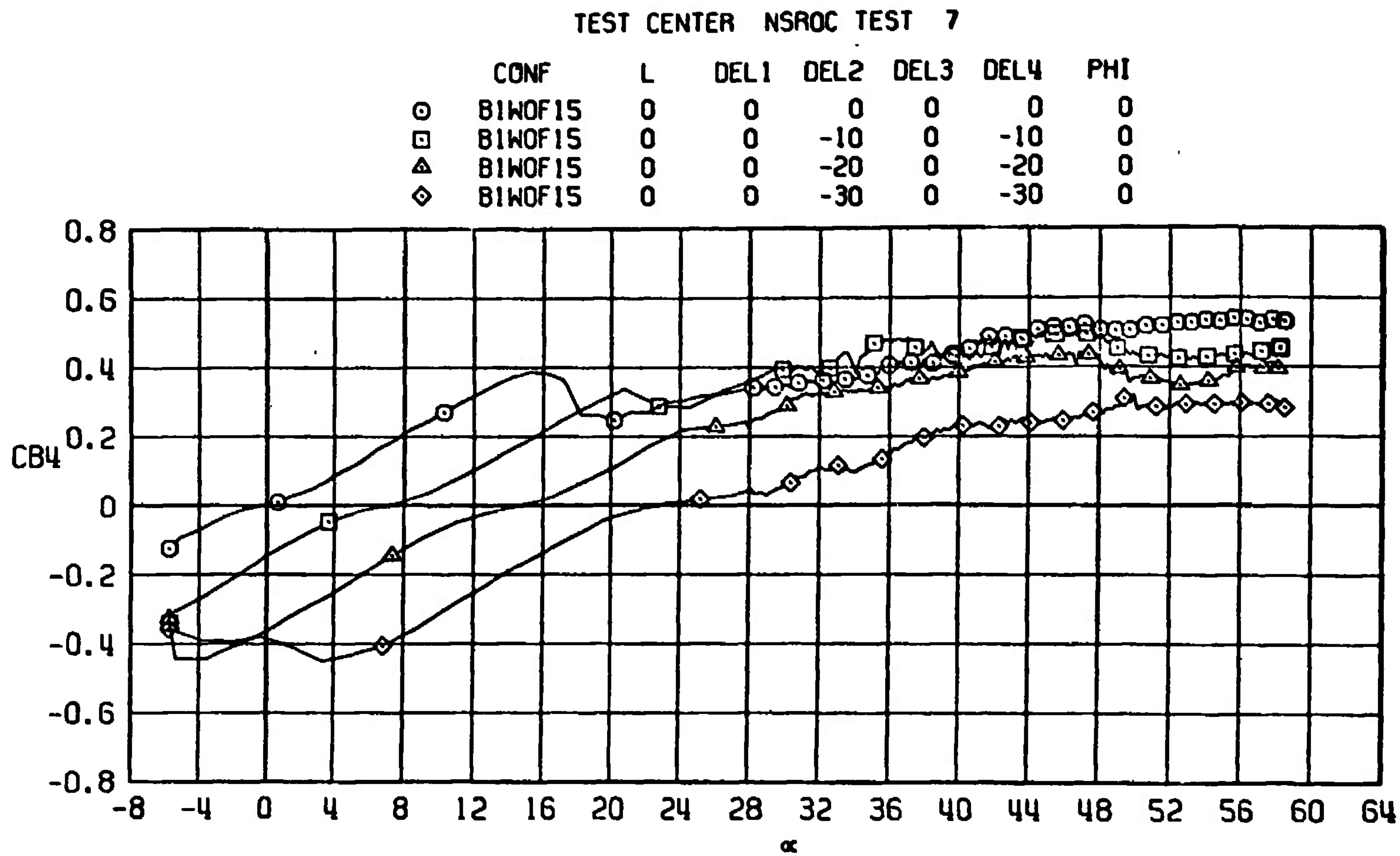

j. CB4 versus α

Figure 48. Continued.

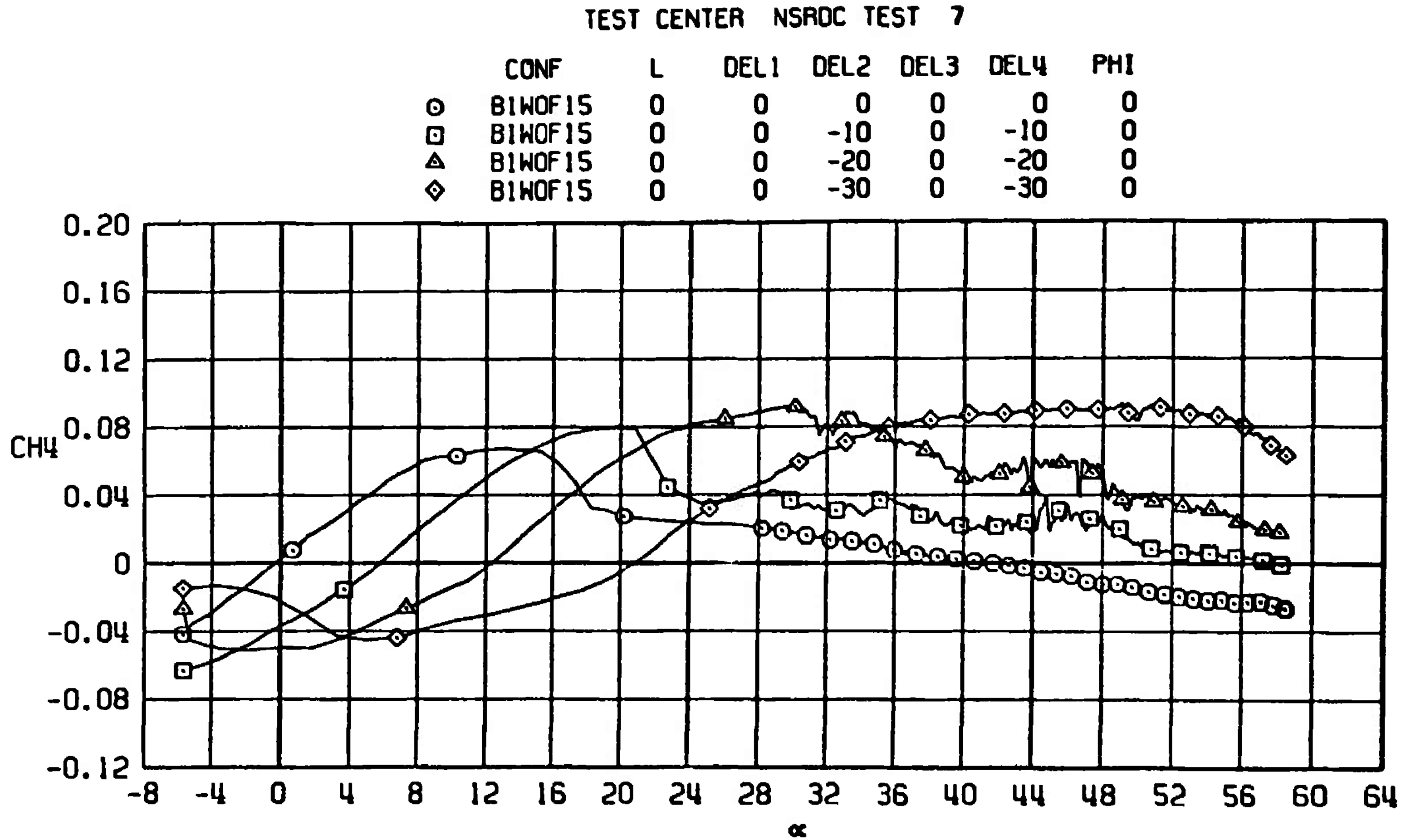

k. CH4 versus α
Figure 48. Concluded.

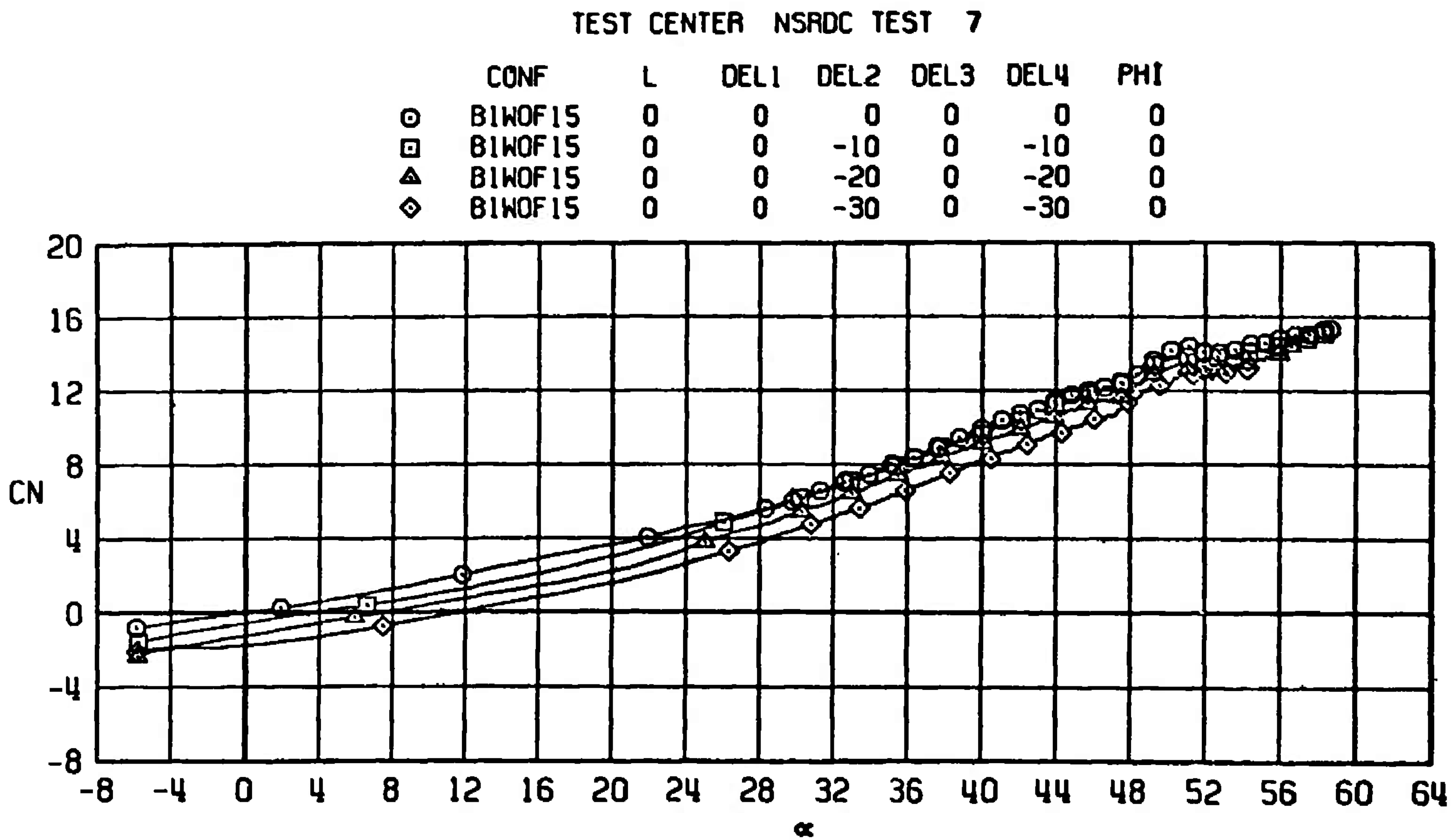

a. CN versus α

Figure 49. Test No. 7, comparison of aerodynamic coefficients of configuration B1W0F15 for various deflections of tail fins No. 2 and 4 at M_∞ = 1.0.

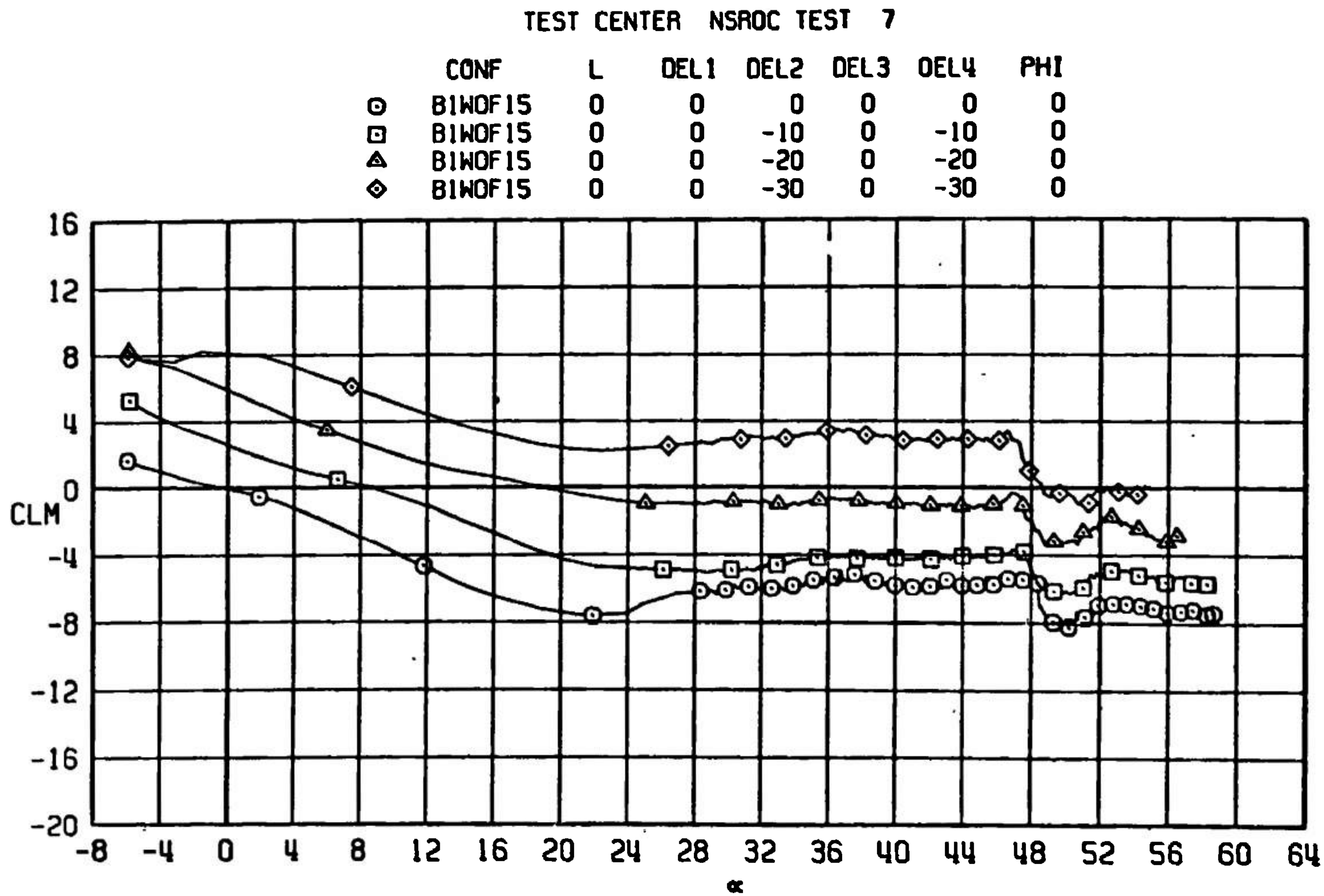

b. CLM versus α

Figure 49. Continued.

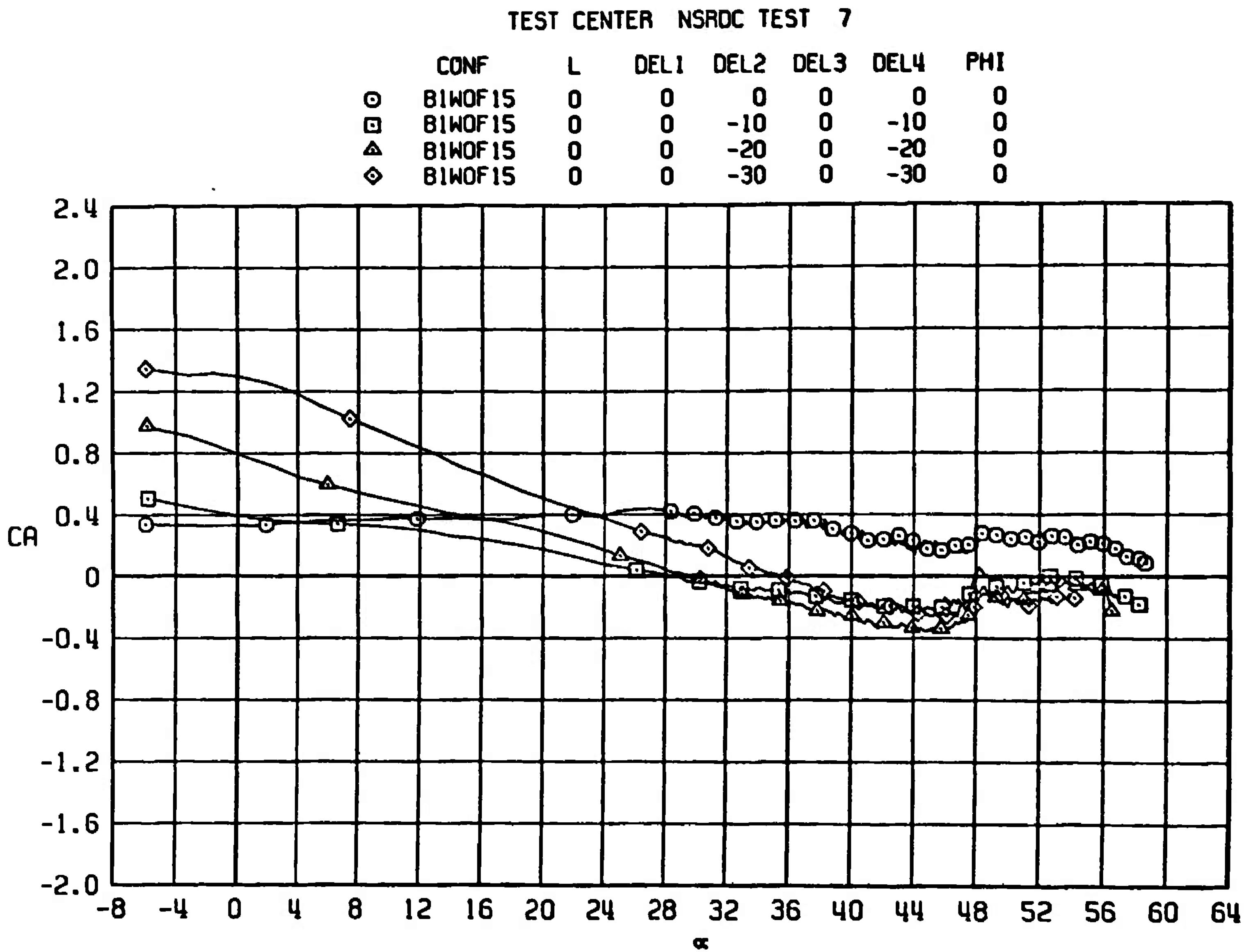

c. CA versus α

Figure 49. Continued.

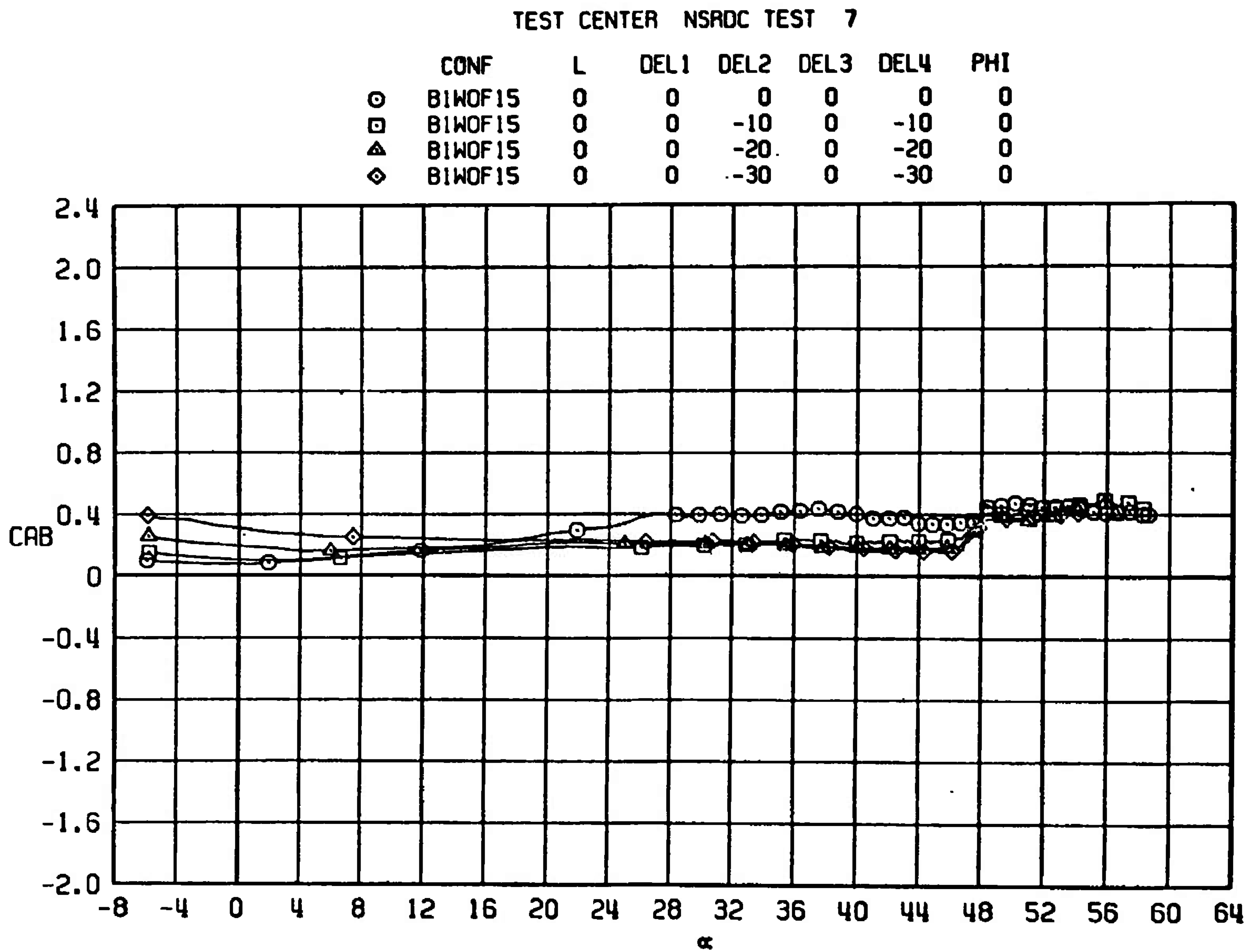

d. CAB versus α

Figure 49. Continued.

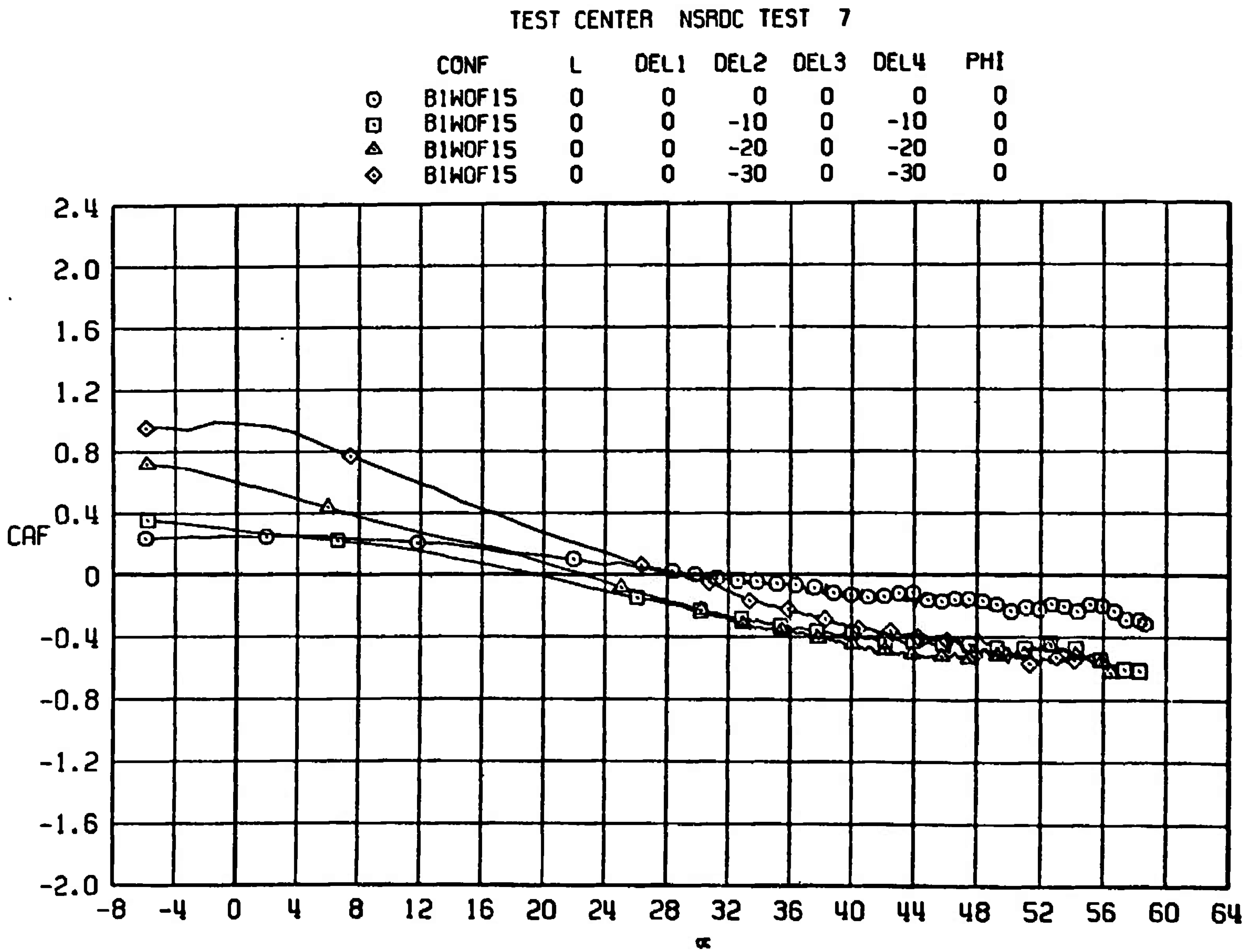

e. CAF versus α
Figure 49. Continued.

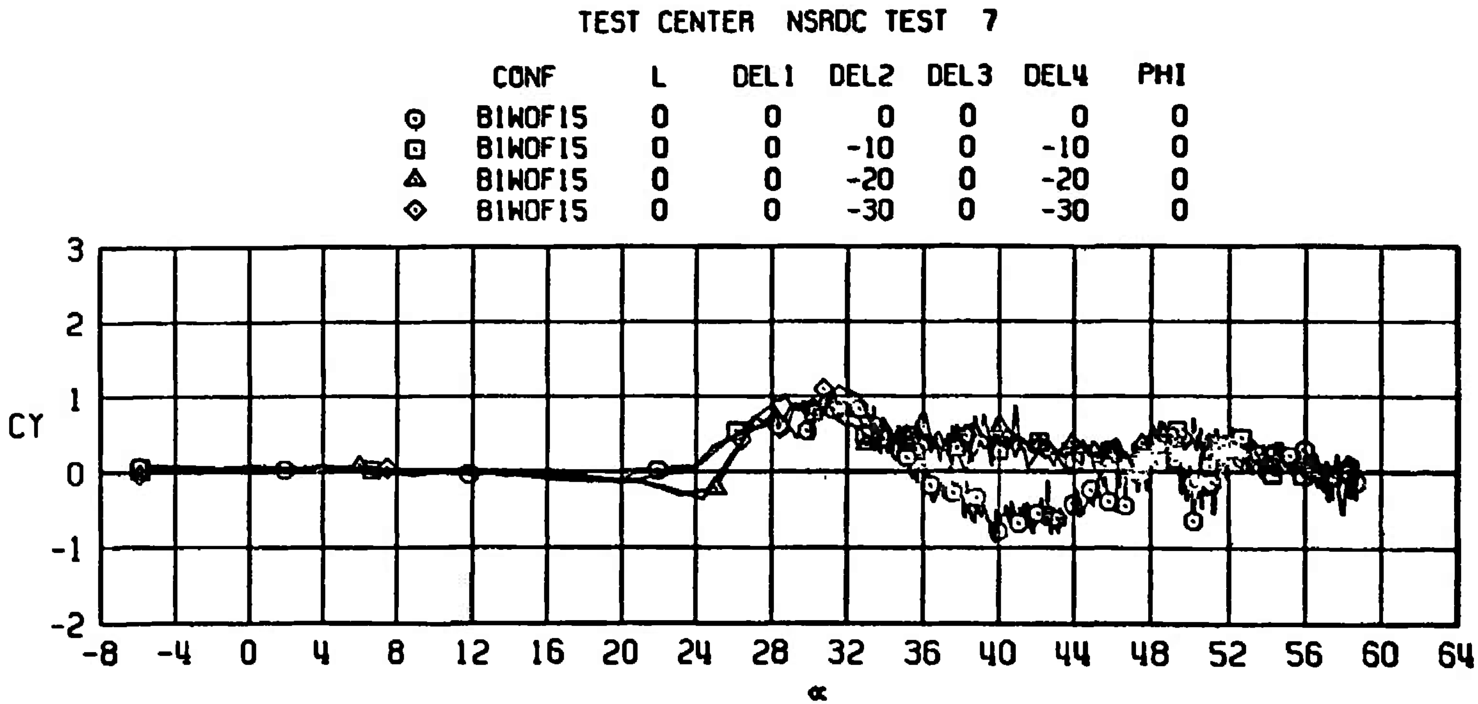

f. CY versus α
Figure 49. Continued.

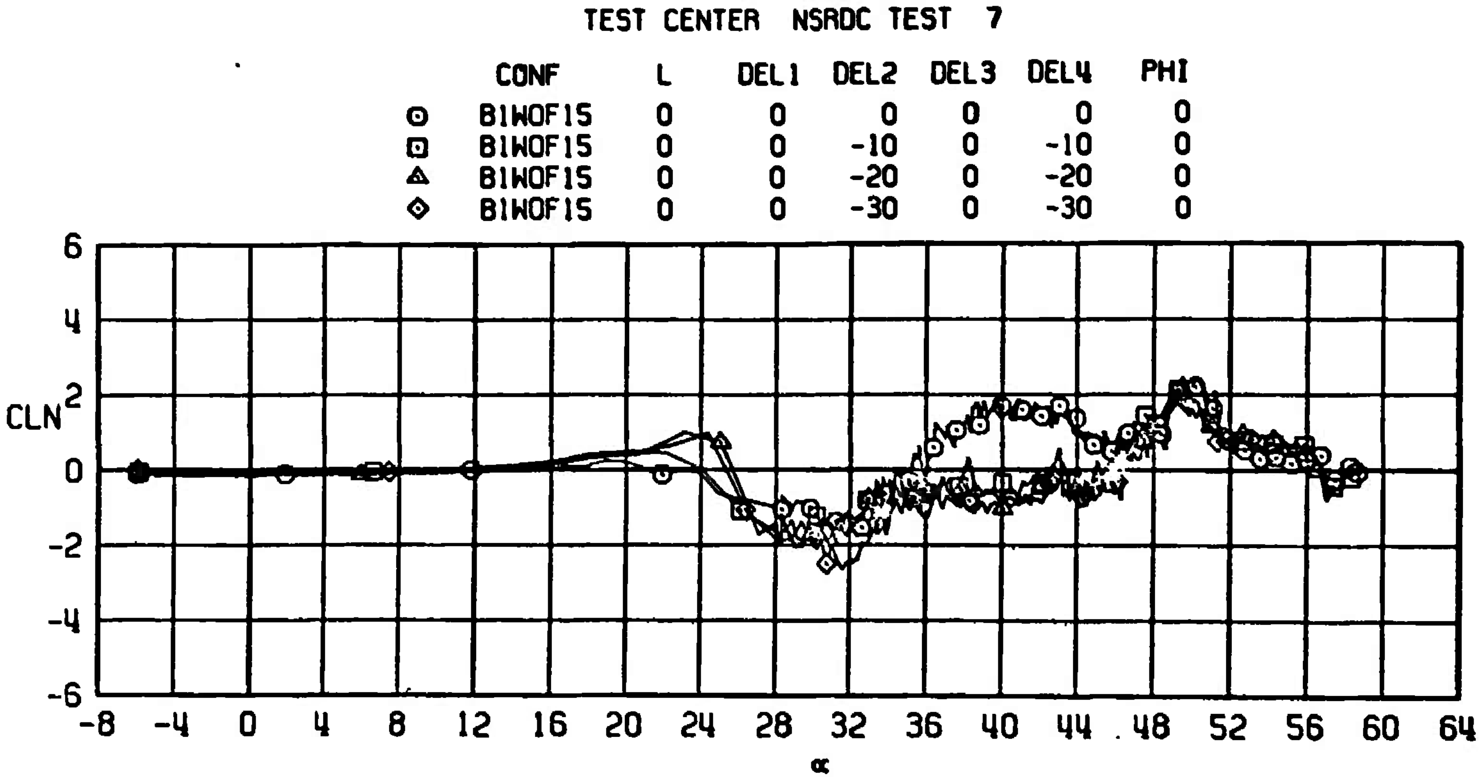

g. CLN versus α
Figure 49. Continued.

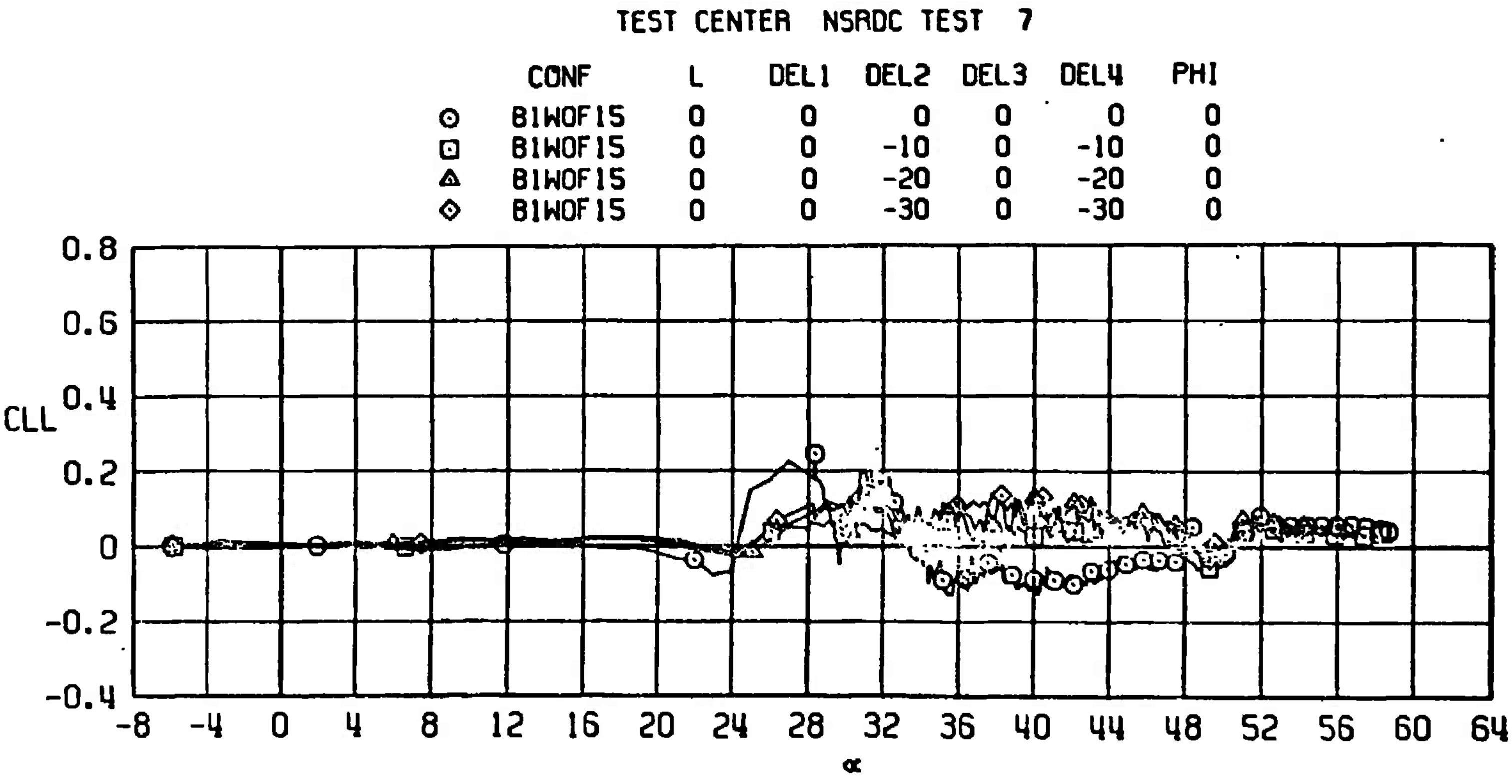

h. CLL versus α
Figure 49. Continued.

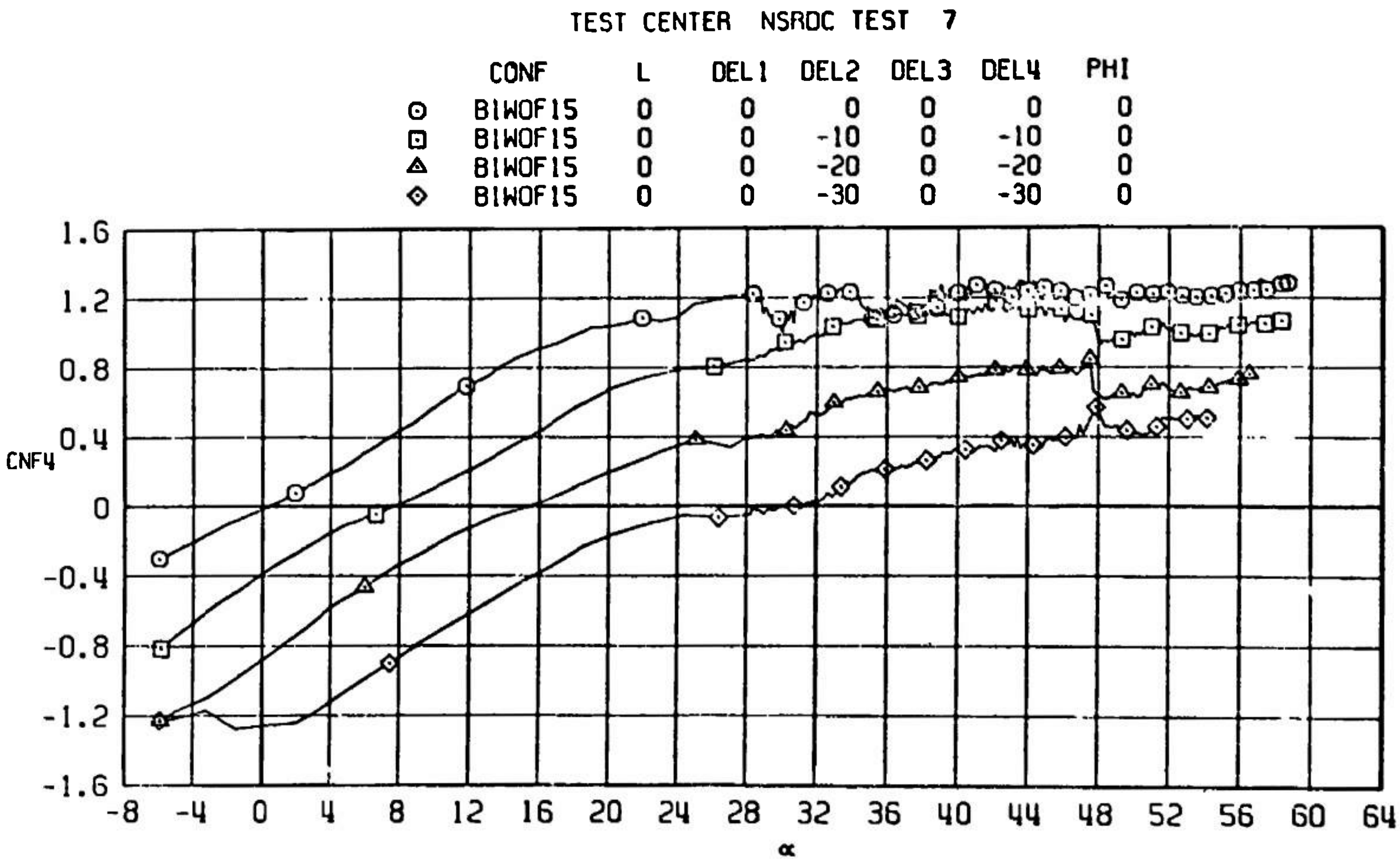

i. CNF4 versus α
Figure 49. Continued.

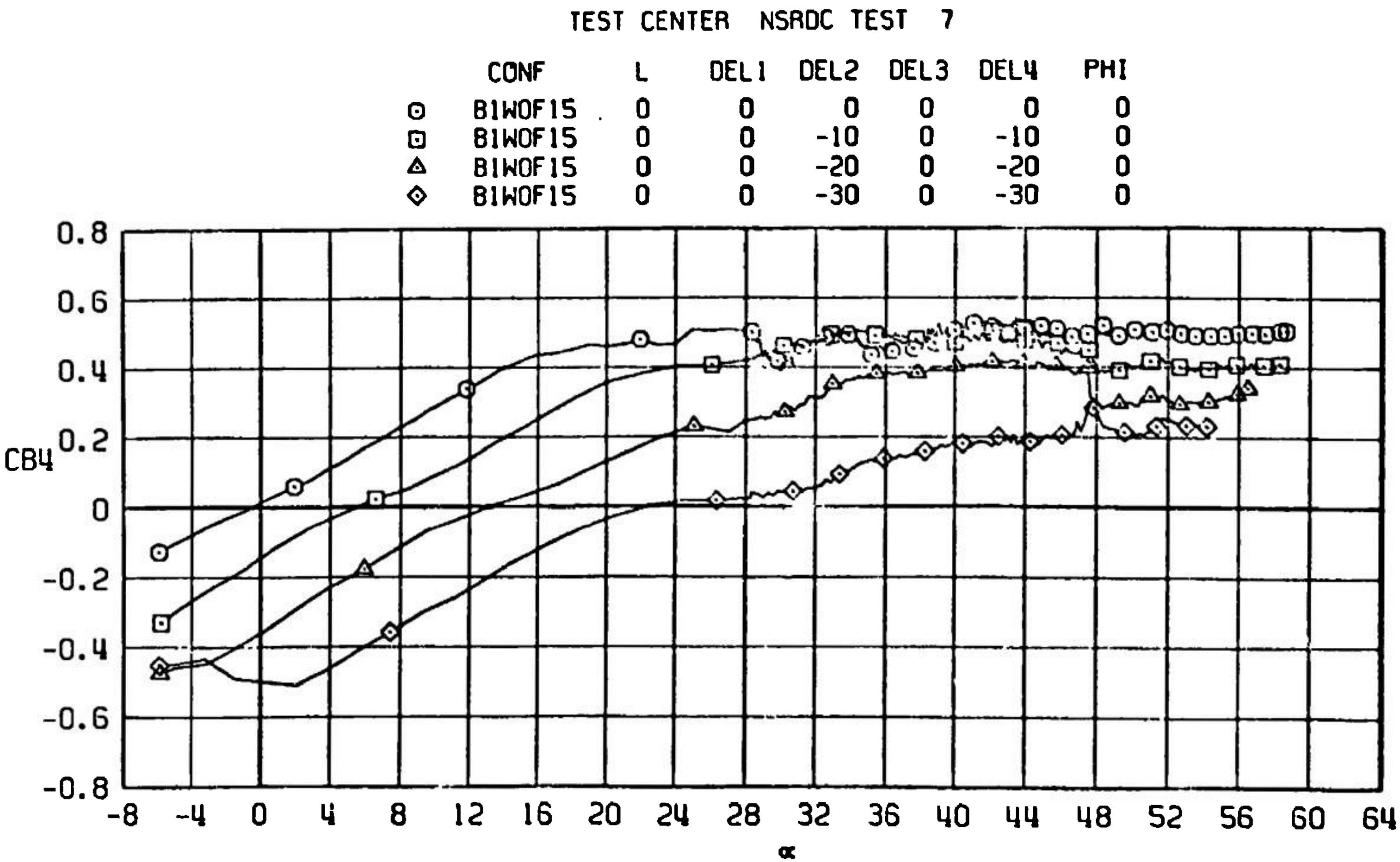

j. CB4 versus α
Figure 49. Continued.

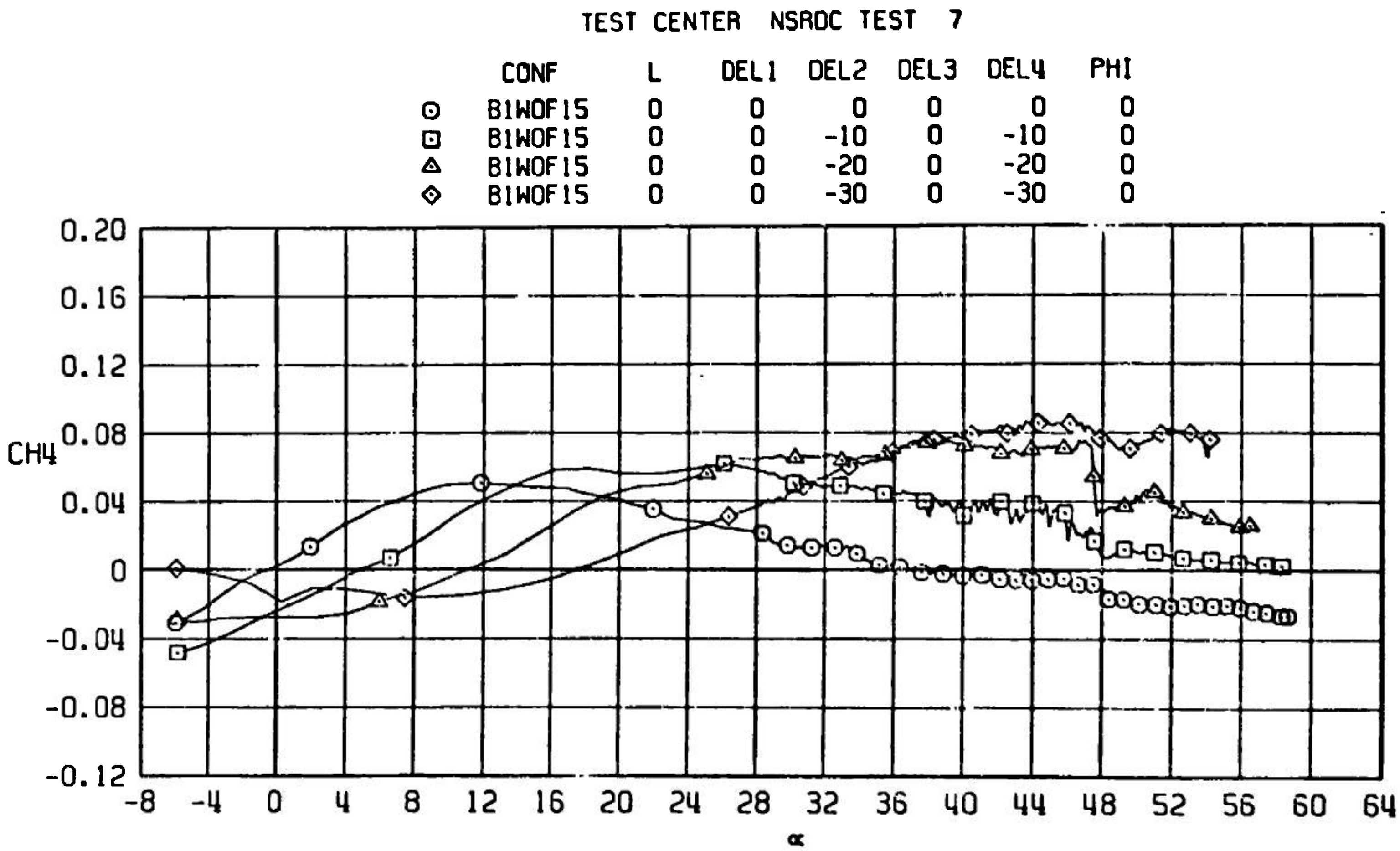

k. CH4 versus α
Figure 49. Concluded.

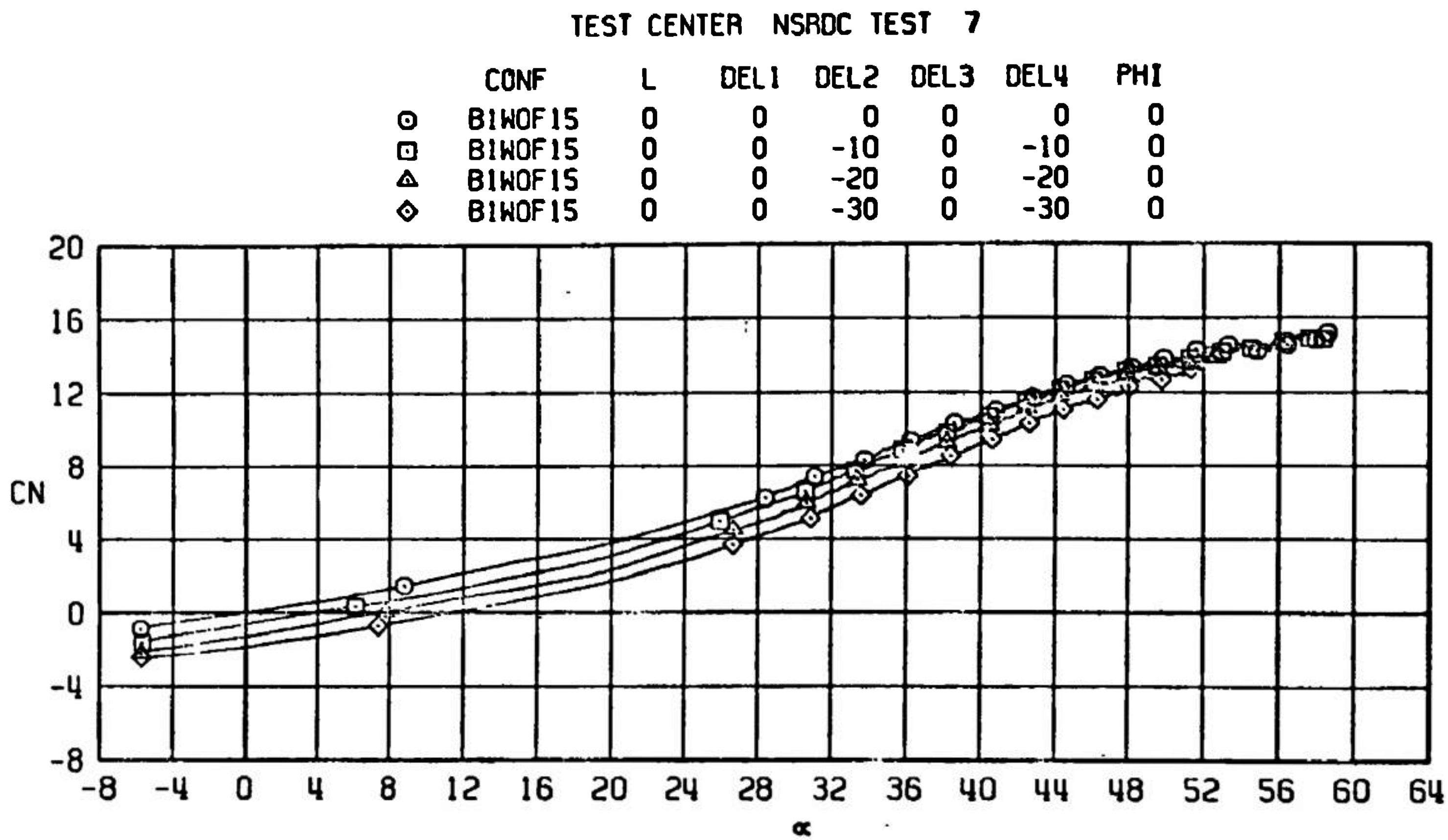

a. CN versus α

Figure 50. Test No. 7, comparison of aerodynamic coefficients of configuration B1W0F15 for various deflections of tail fins No. 2 and 4 at $M_\infty = 1.1$.

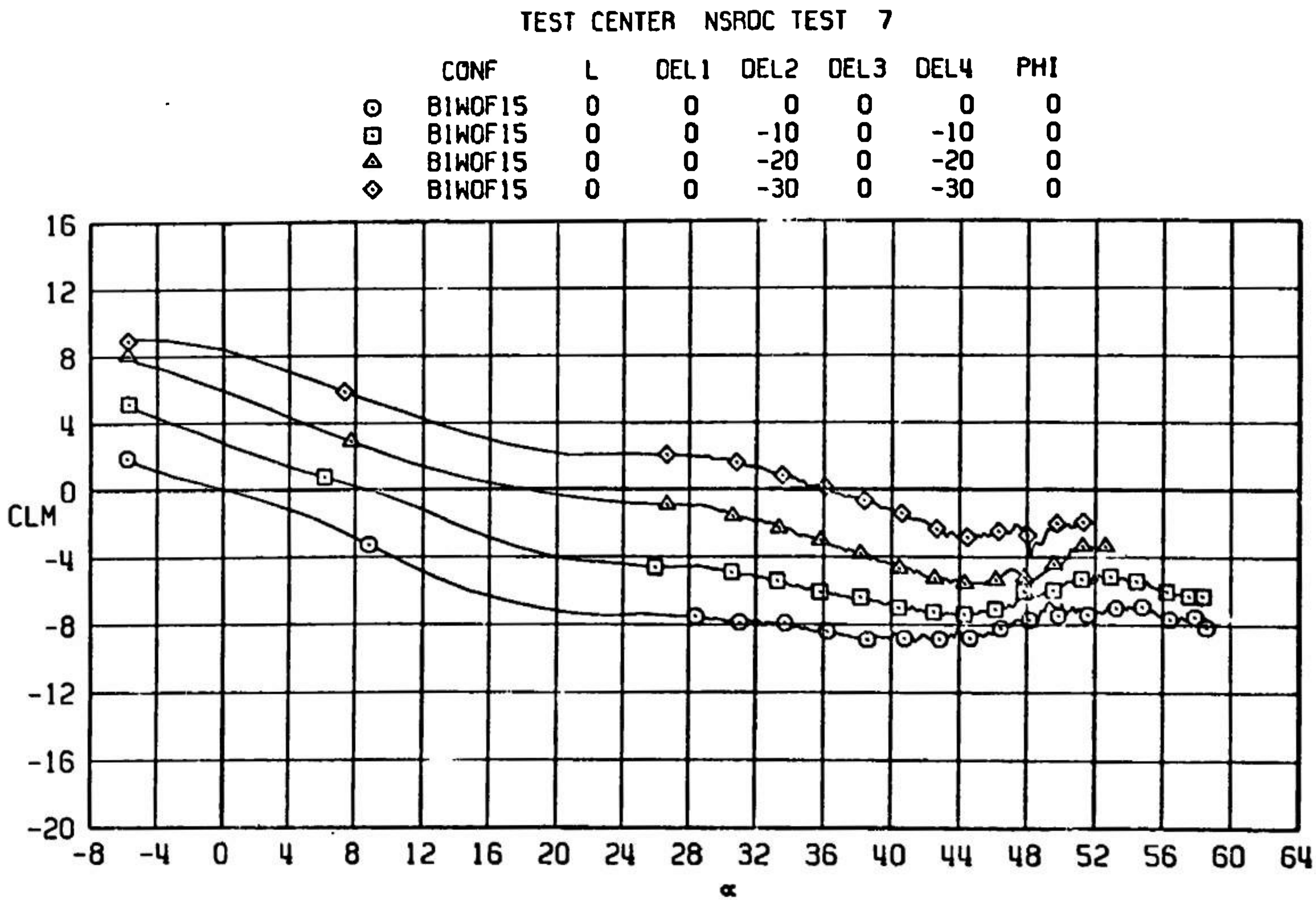

b. CLM versus α
Figure 50. Continued.

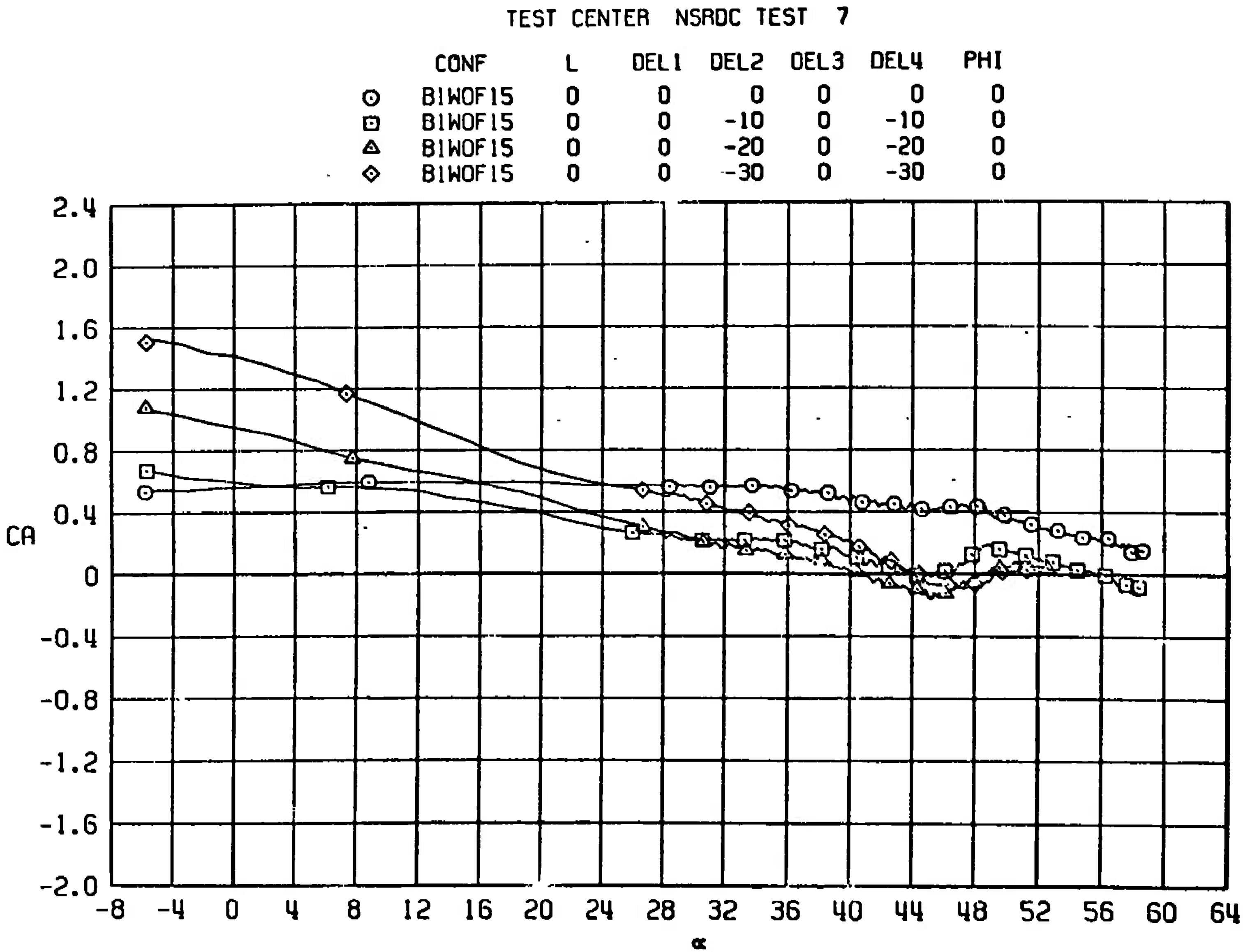

c. CA versus α
Figure 50. Continued.

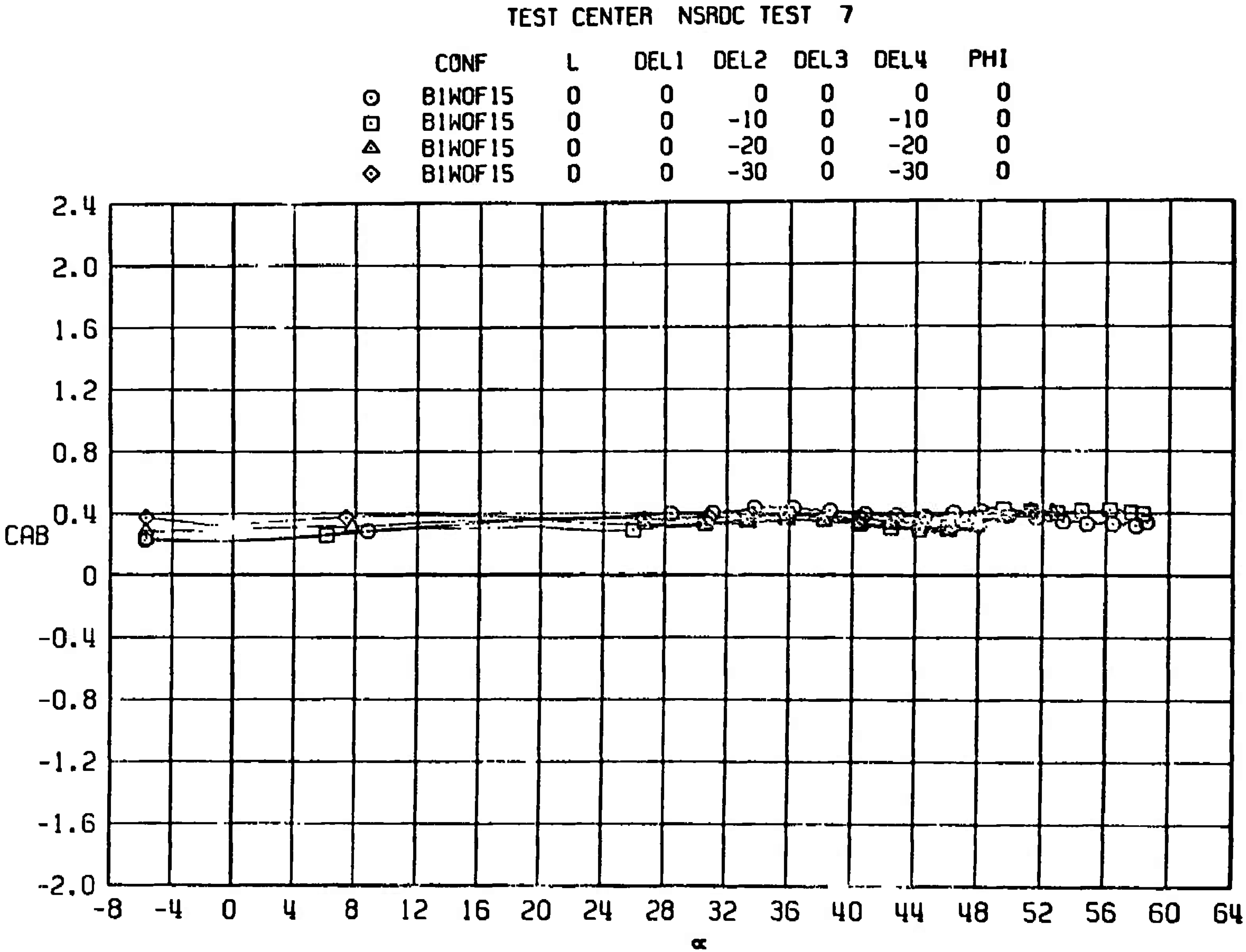

d. CAB versus α
Figure 50. Continued.

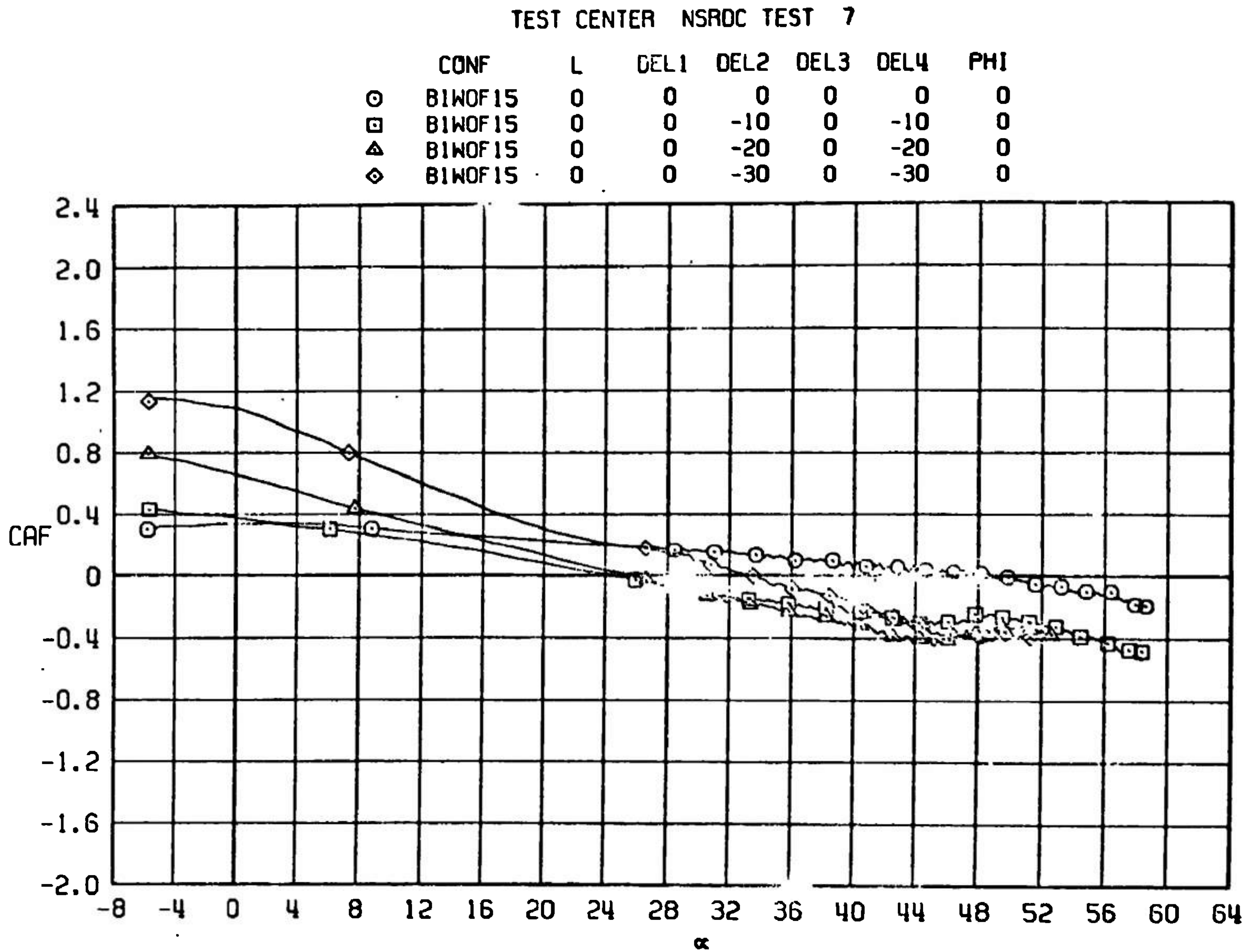

e. CAF versus α

Figure 50. Continued.

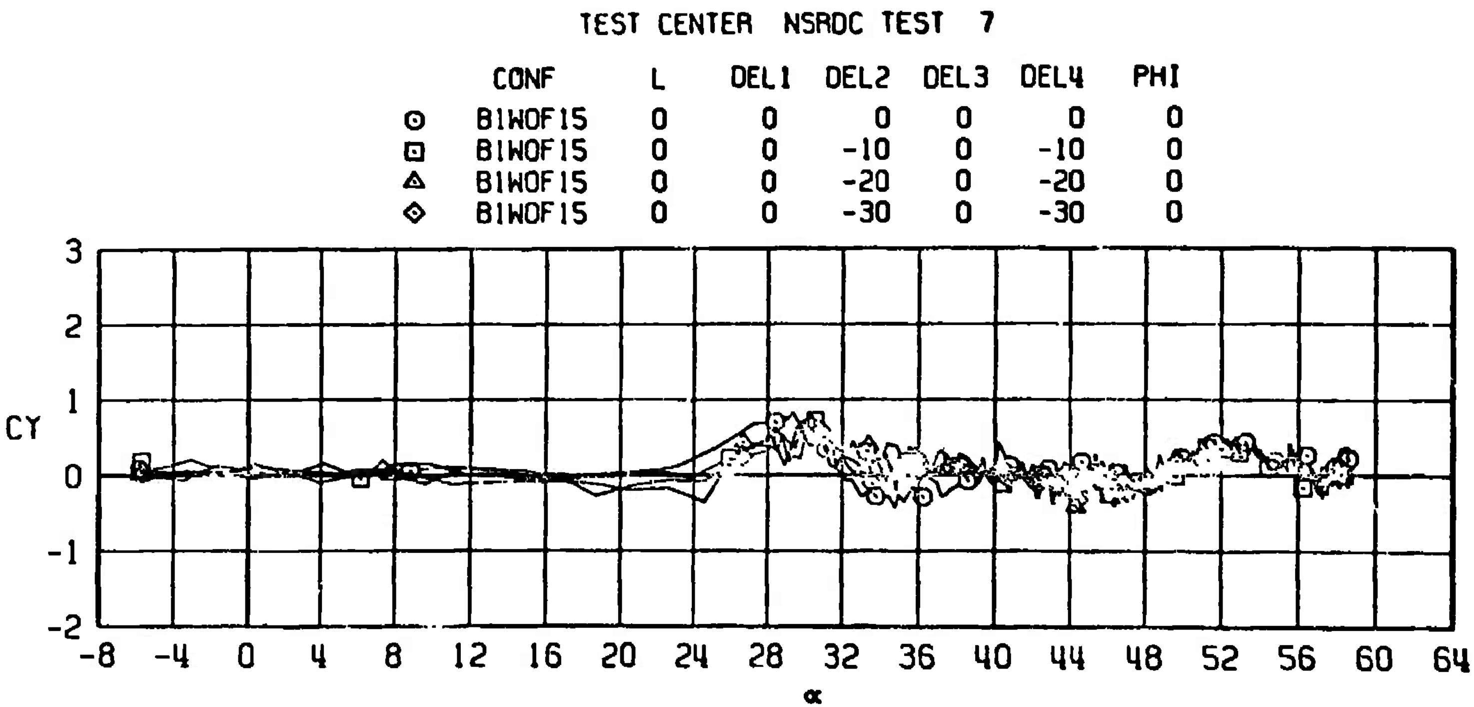

f. CY versus α
Figure 50. Continued.

TEST CENTER NSRDC TEST 7

	CONF	L	DEL1	DEL2	DEL3	DEL4	PHI
⊙	B1WOF15	0	0	0	0	0	0
⊡	B1WOF15	0	0	-10	0	-10	0
⚠	B1WOF15	0	0	-20	0	-20	0
◈	B1WOF15	0	0	-30	0	-30	0

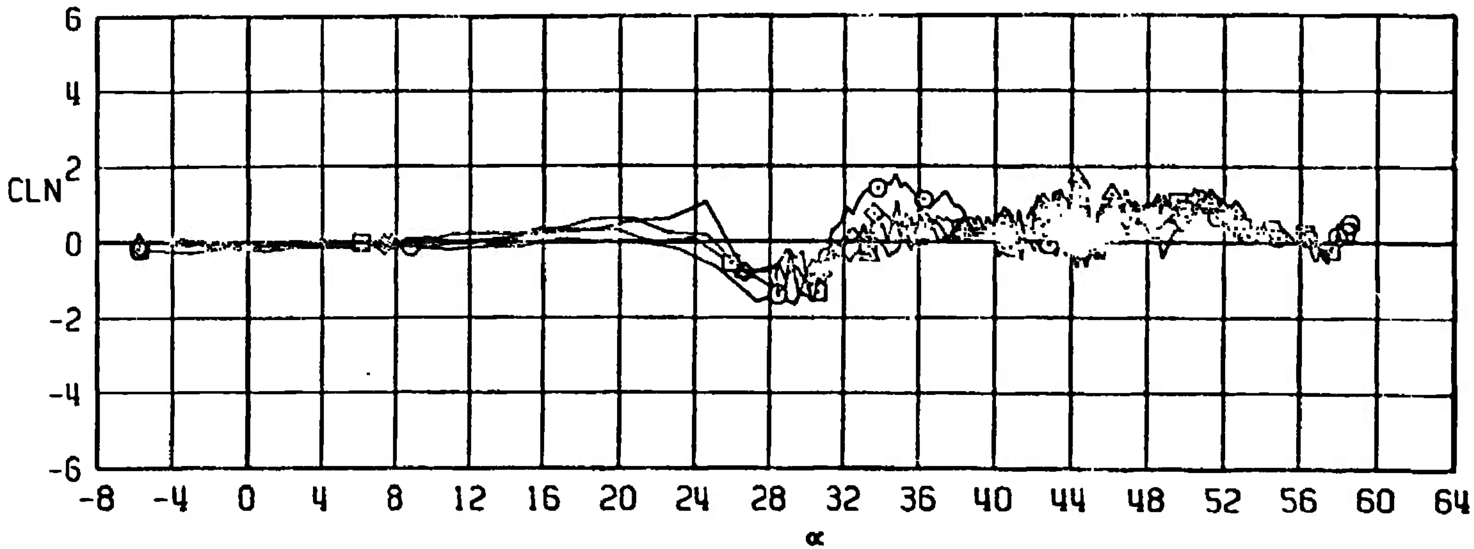

g. CLN versus α
Figure 50. Continued.

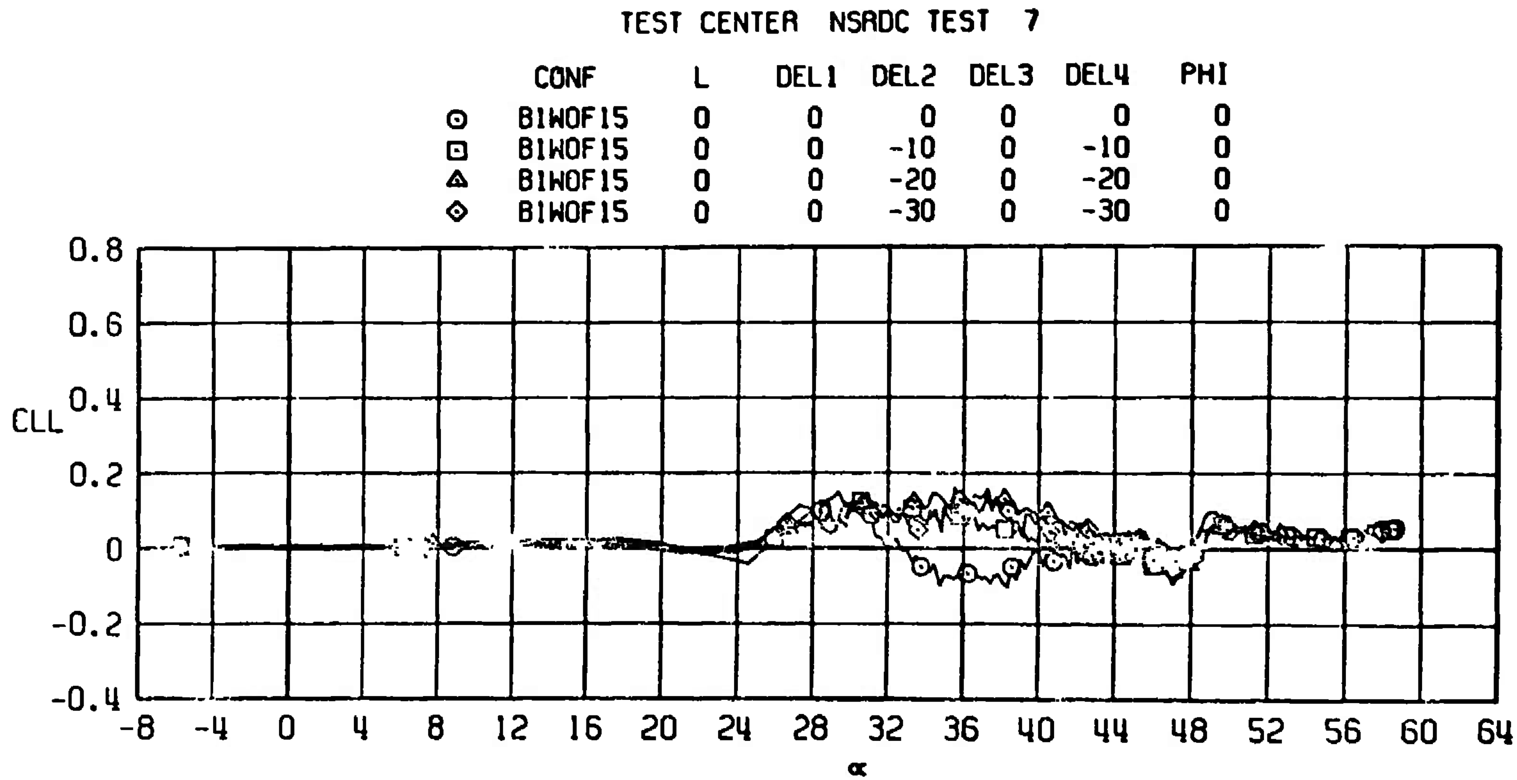

h. CLL versus α
Figure 50. Continued.

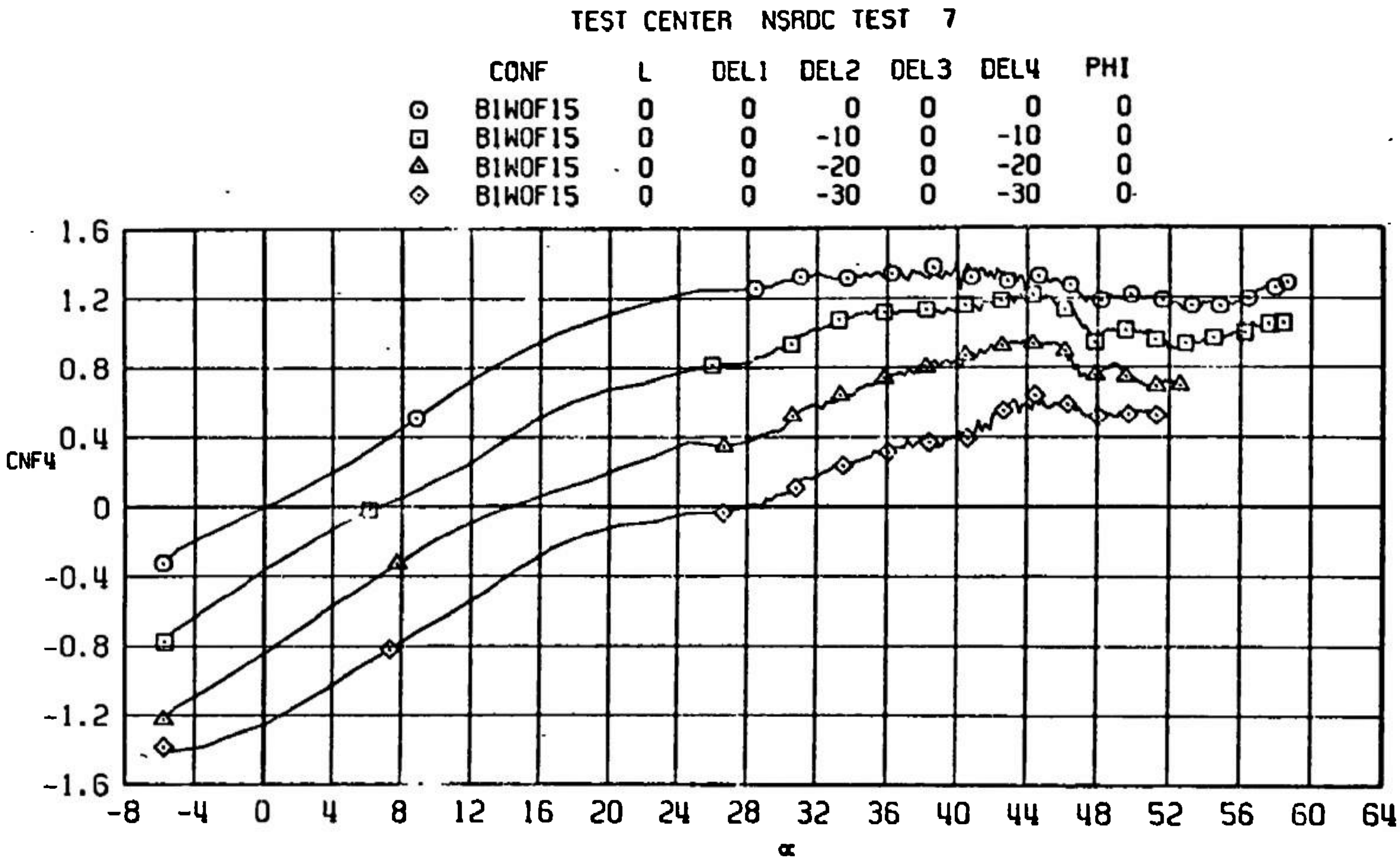

i. CNF4 versus α
Figure 50. Continued.

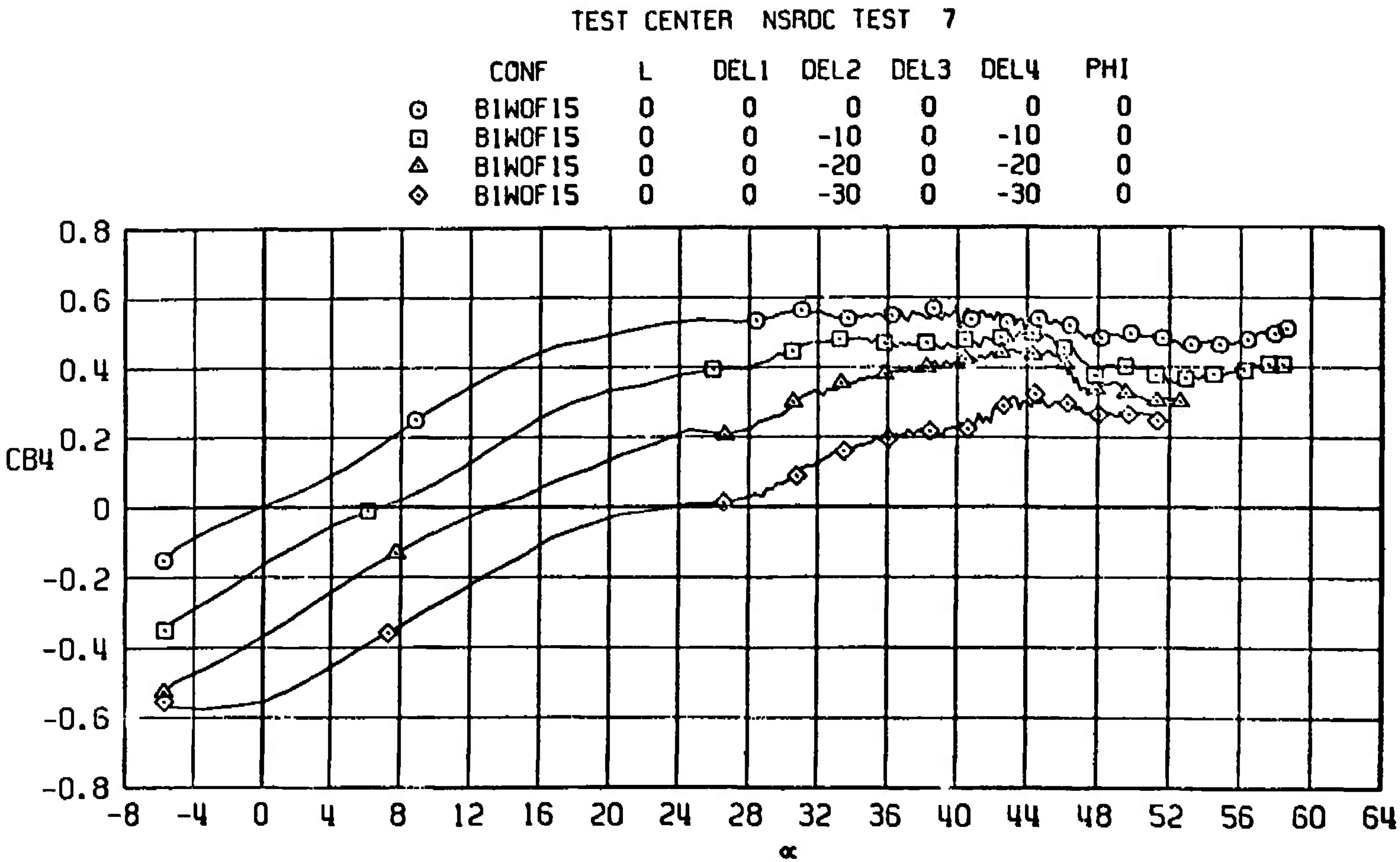

j. CB4 versus α

Figure 50. Continued.

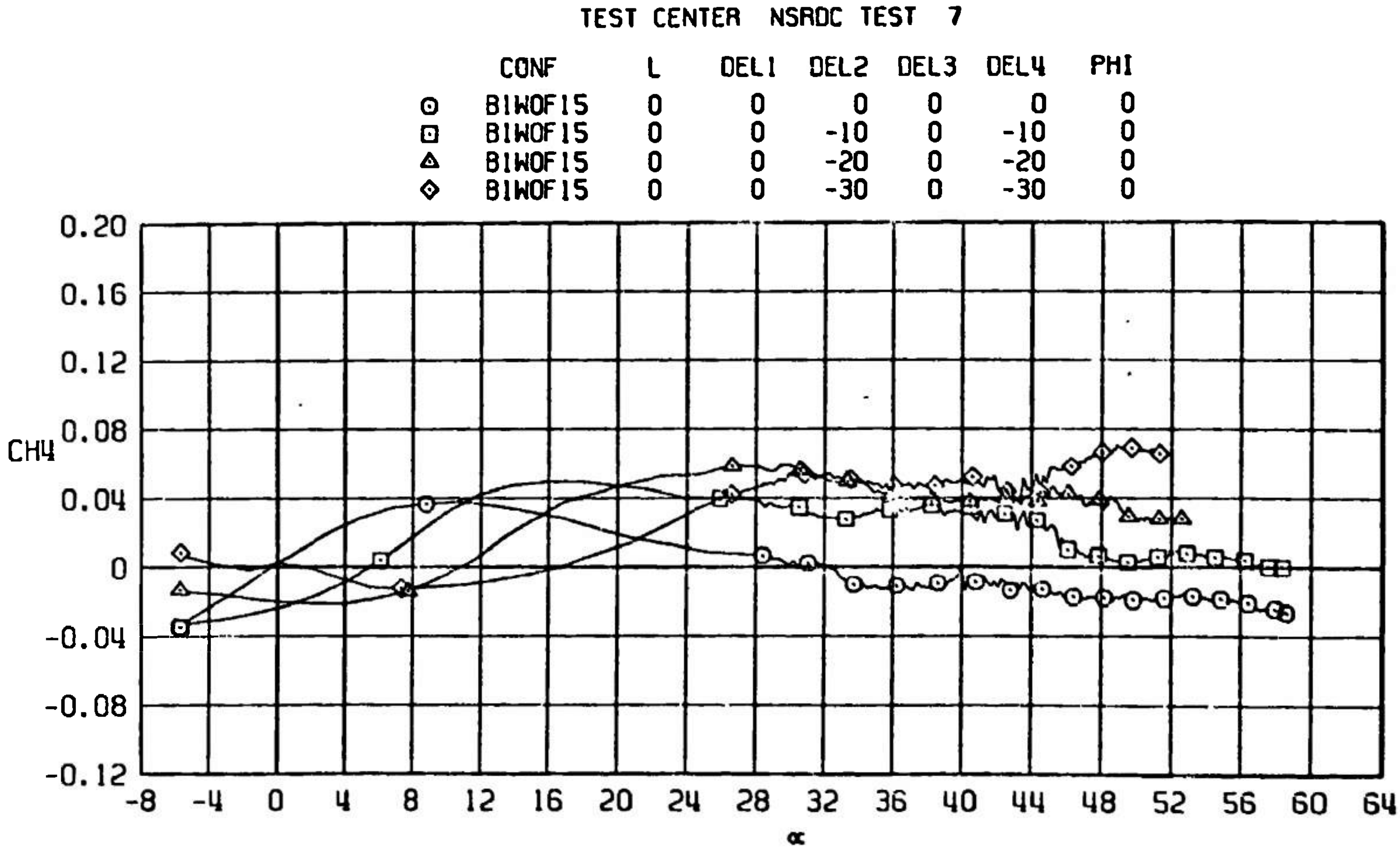

k. CH4 versus α
Figure 50. Concluded.

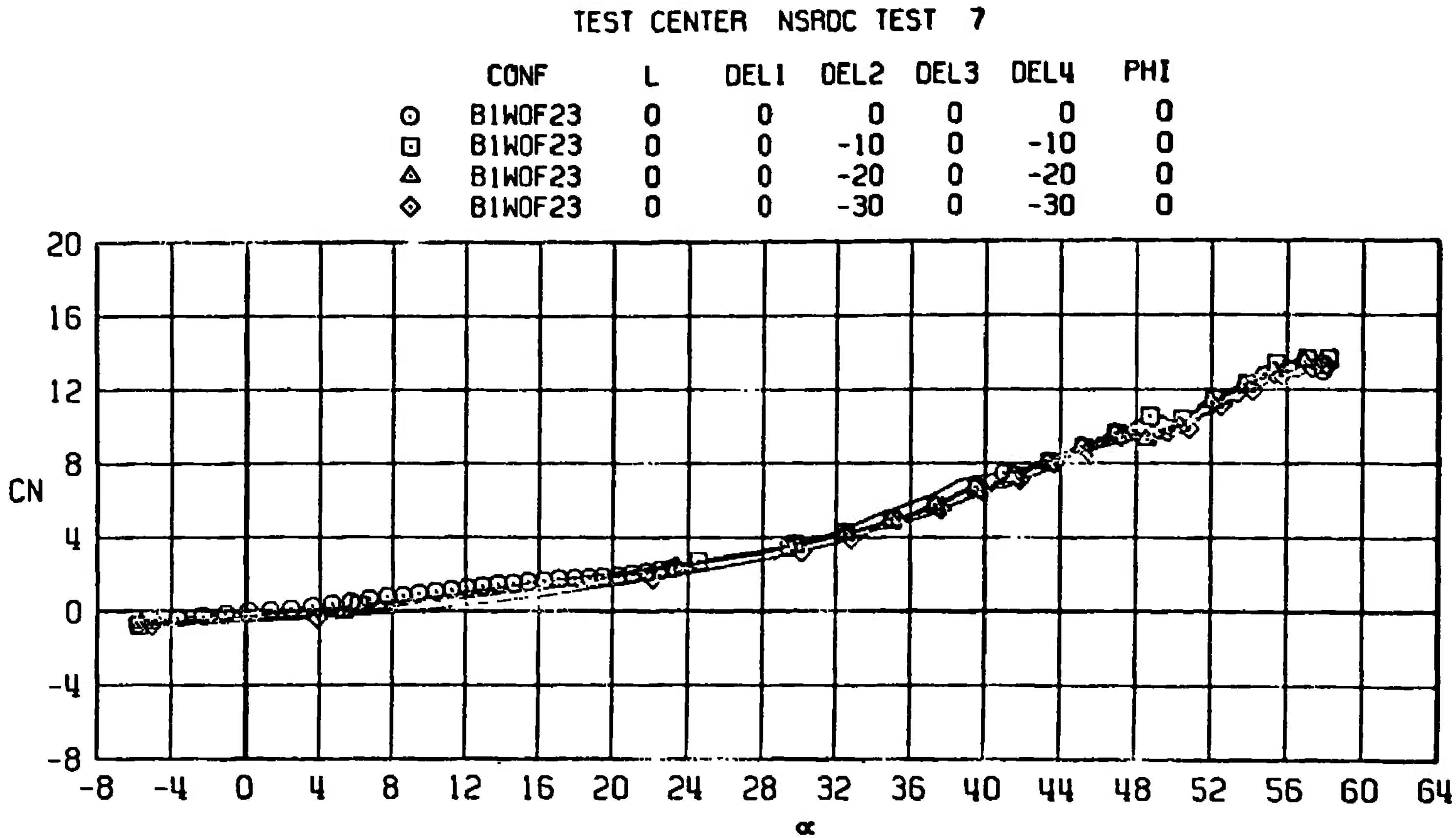

a. CN versus α

Figure 51. Test No. 7, comparison of aerodynamic coefficients of configuration B1W0F23 for various deflections of tail fins No. 2 and 4 at $M_{\infty} = 0.8$.

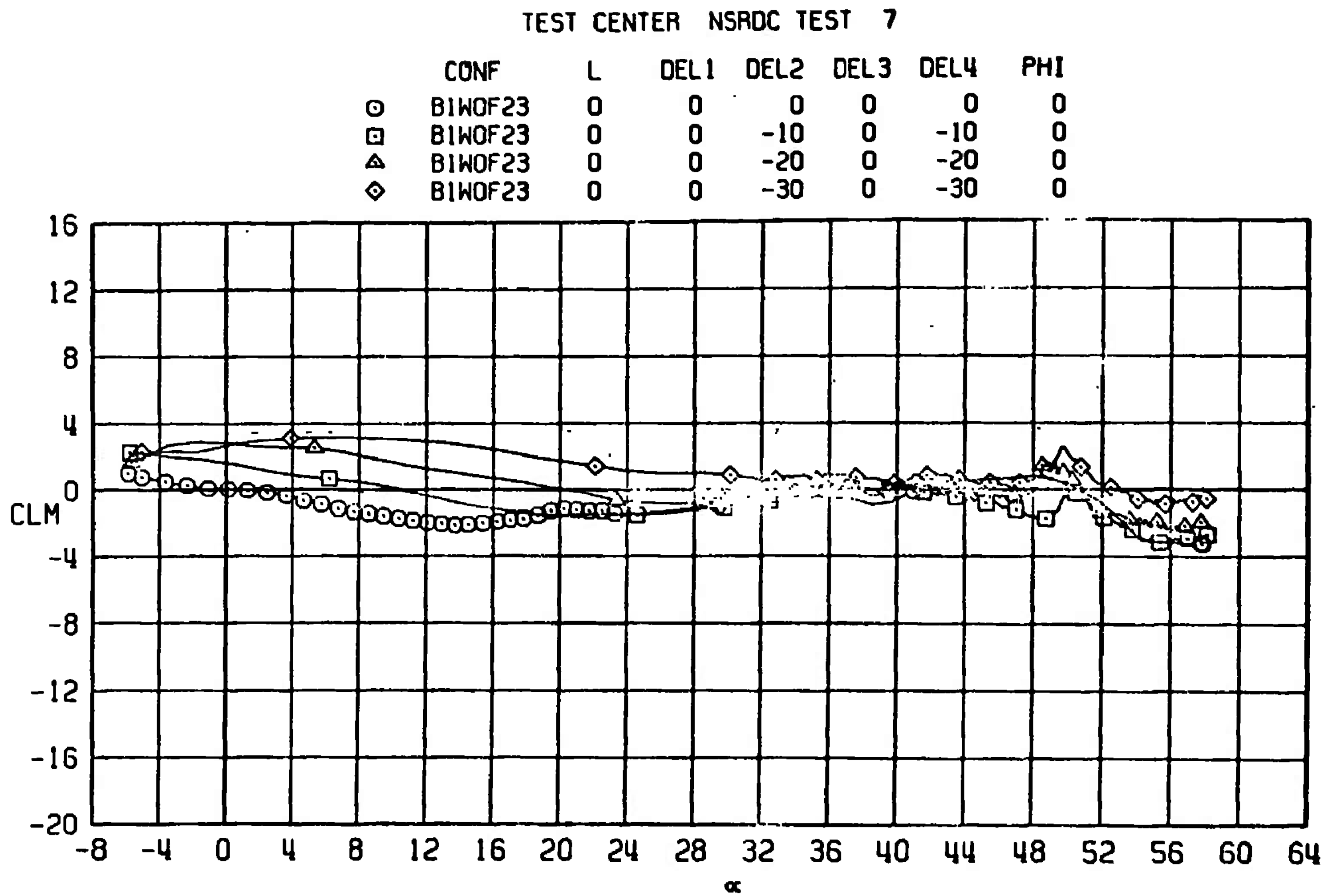

b. CLM versus α
Figure 51. Continued.

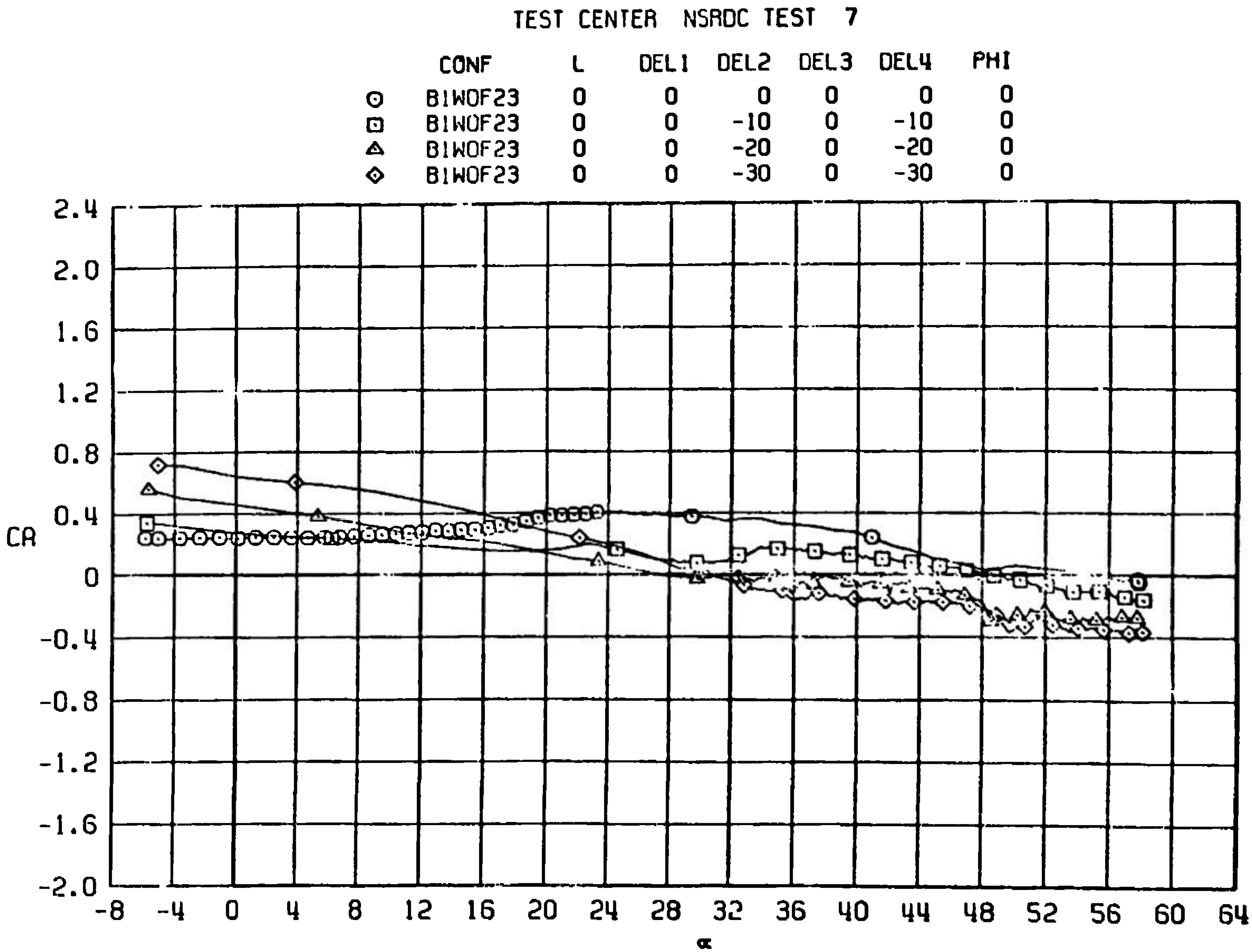

c. CA versus α
Figure 51. Continued.

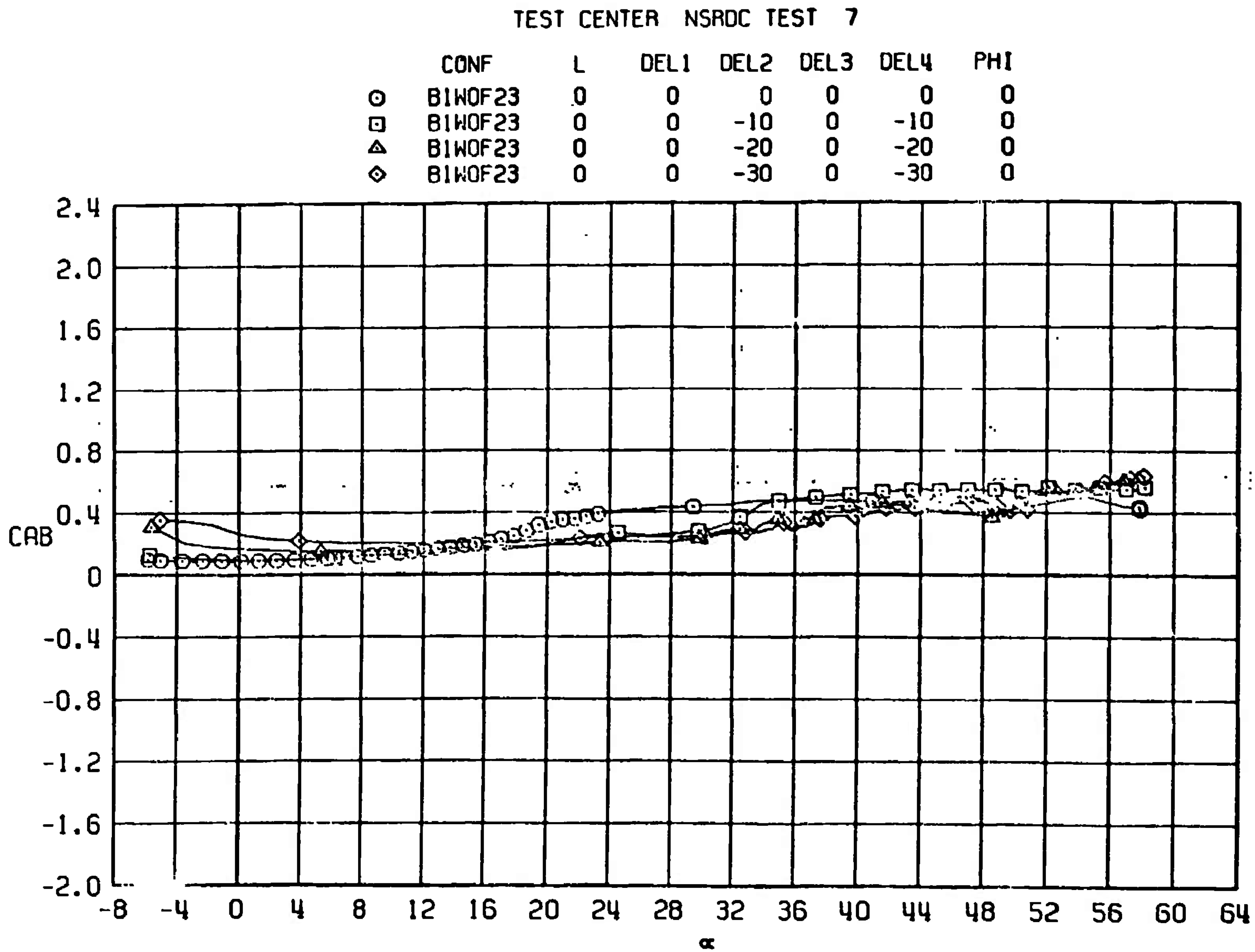

d. CAB versus α

Figure 51. Continued.

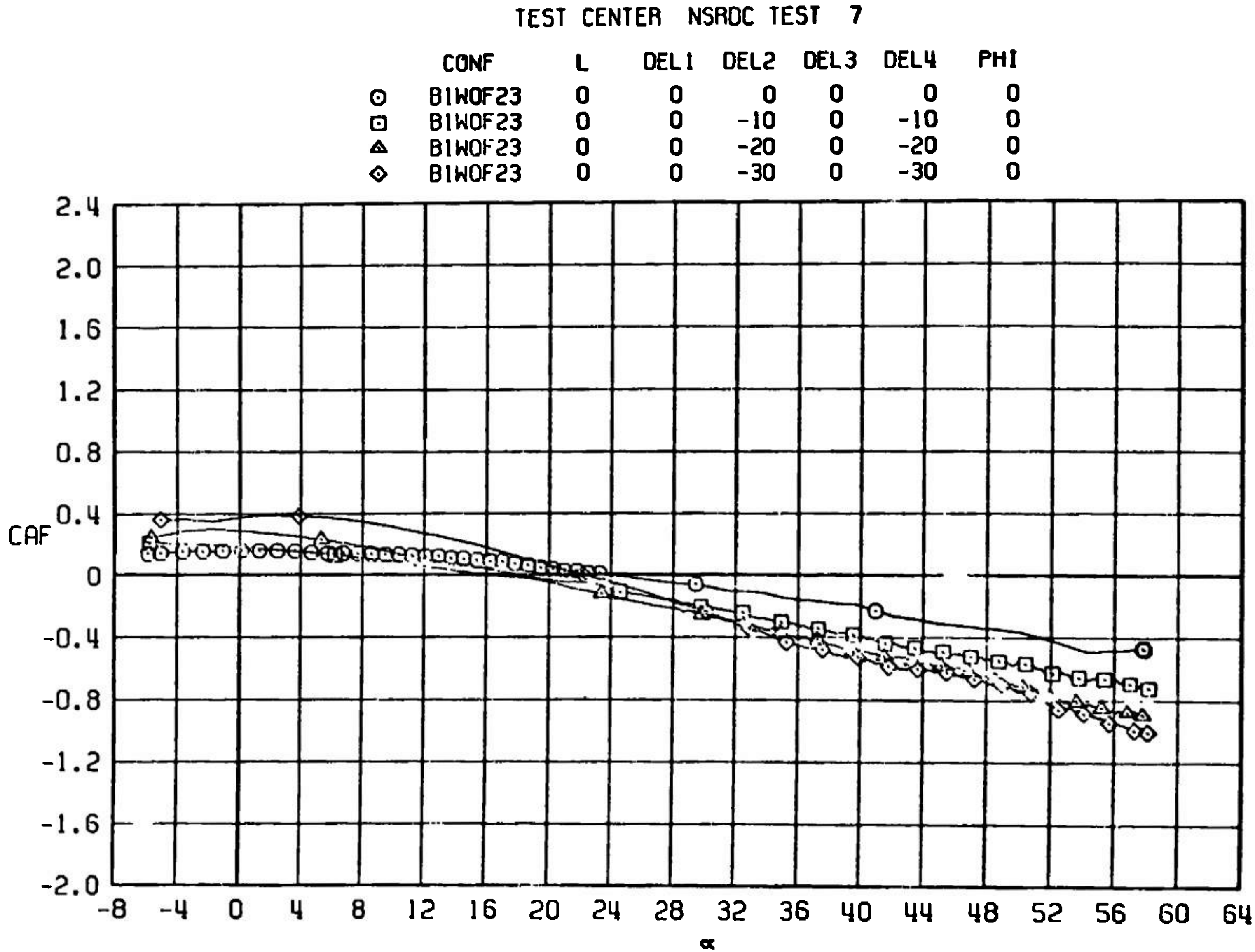

e. CAF versus α
Figure 51. Continued.

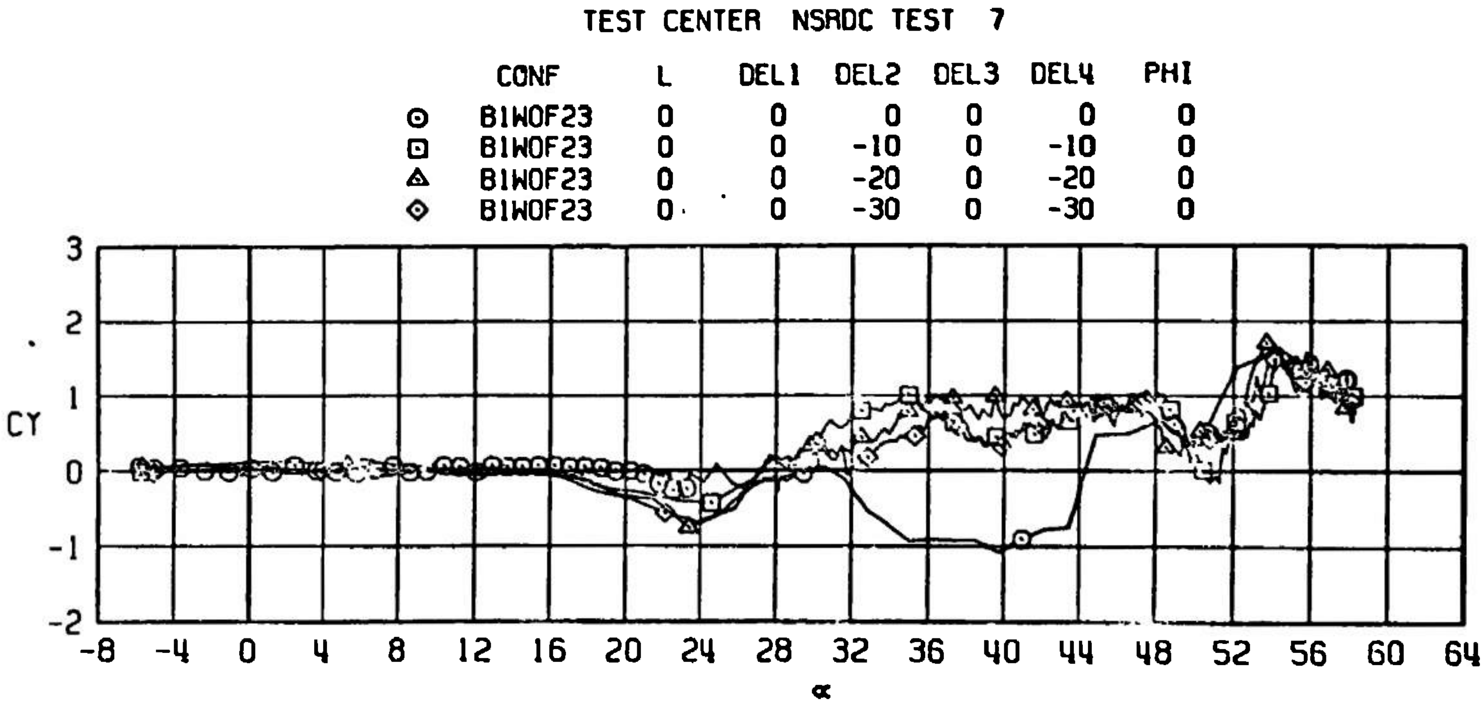

f. CY versus α
Figure 51. Continued.

TEST CENTER NSRDC TEST 7

	CONF	L	DEL1	DEL2	DEL3	DEL4	PHI
⊙	B1W0F23	0	0	0	0	0	0
⊡	B1W0F23	0	0	-10	0	-10	0
△	B1W0F23	0	0	-20	0	-20	0
◇	B1W0F23	0	0	-30	0	-30	0

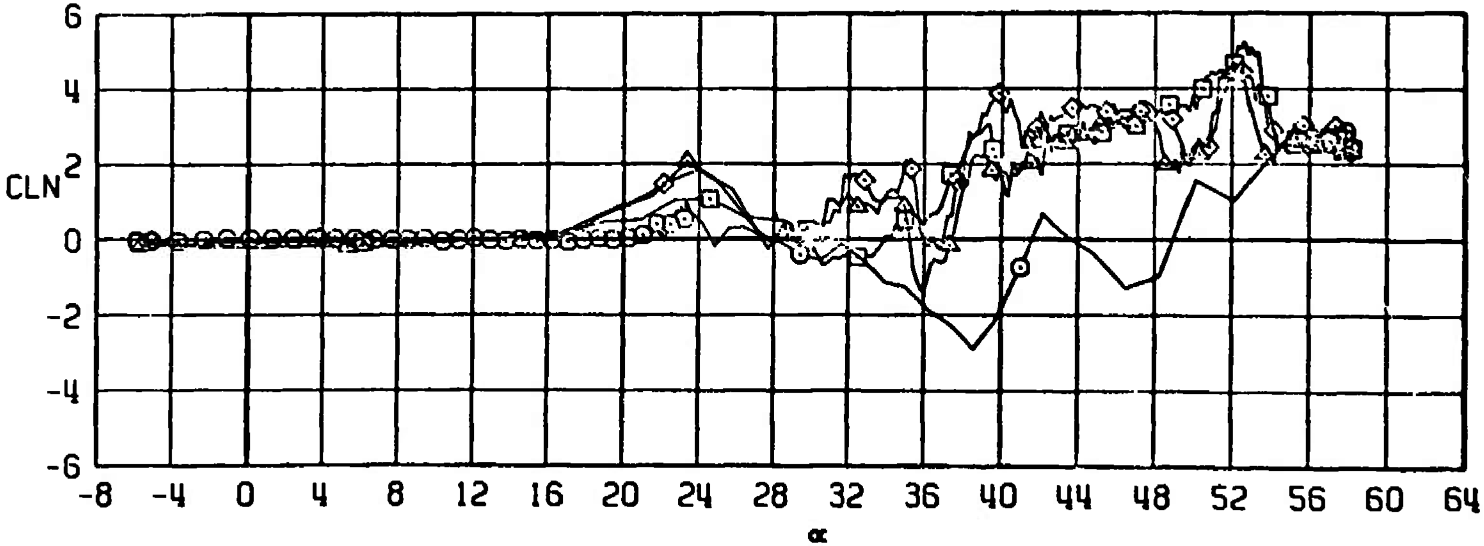

g. CLN versus α
Figure 51. Continued.

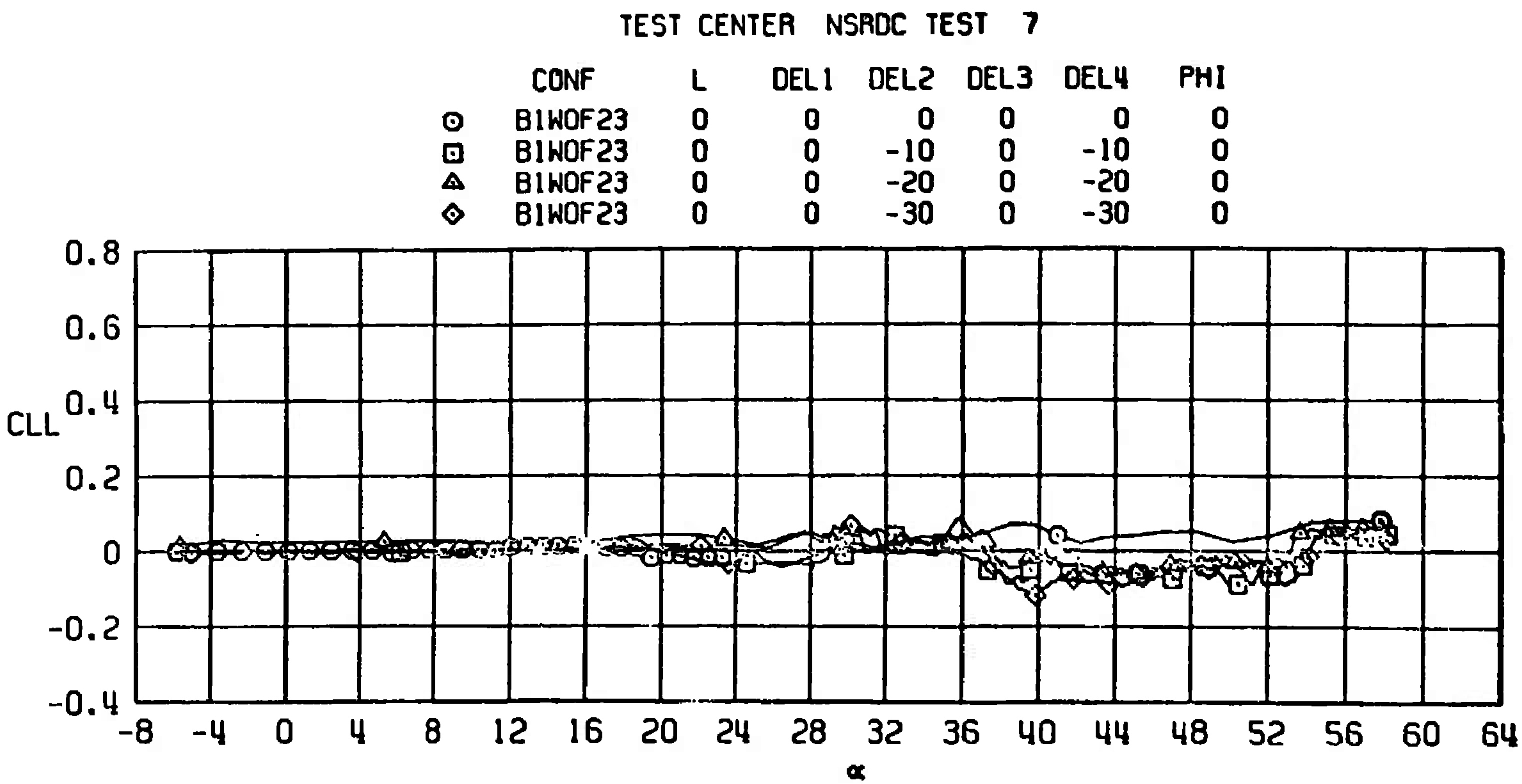

h. CLL versus α
Figure 51. Continued.

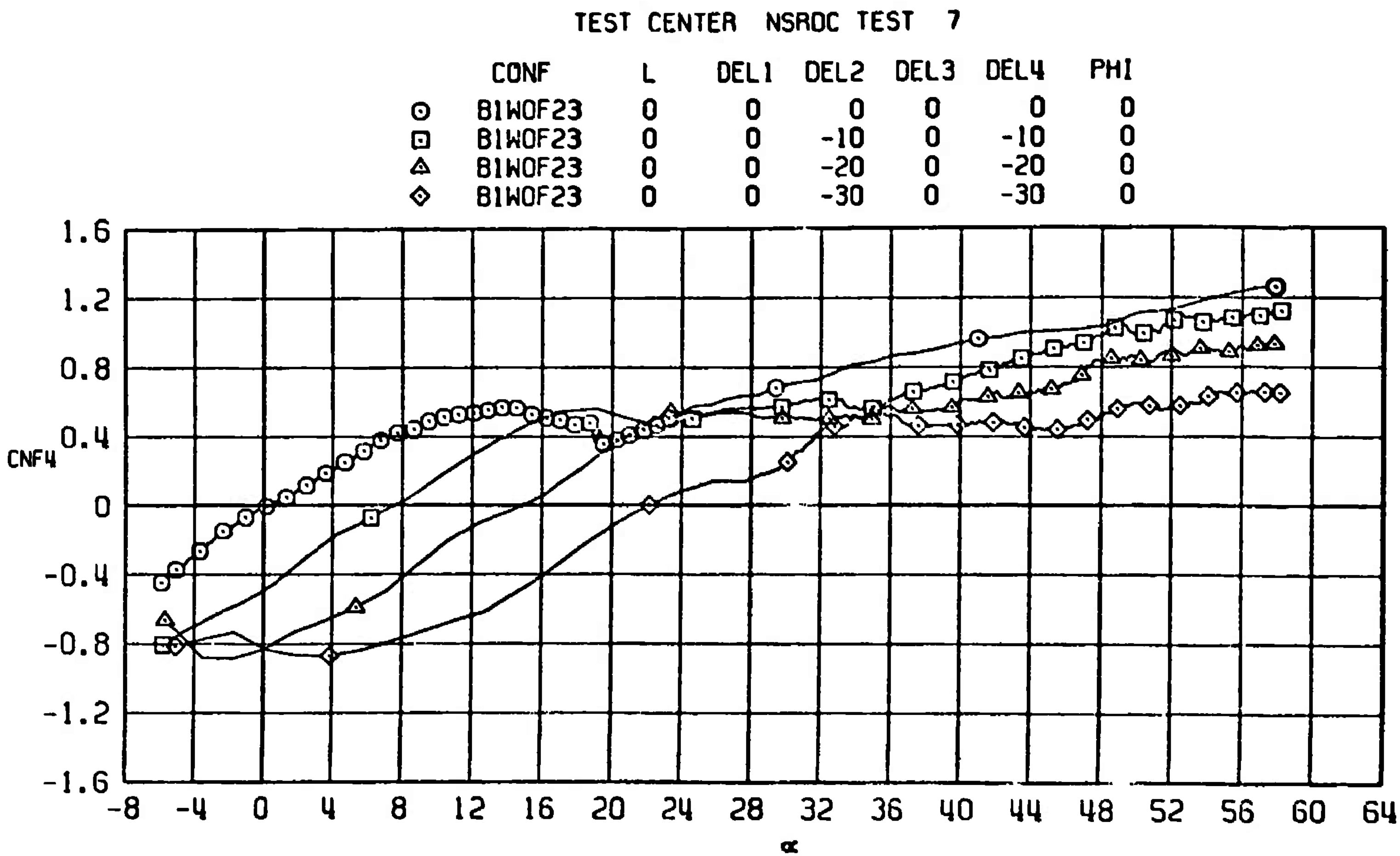

i. CNF4 versus α
Figure 51. Continued.

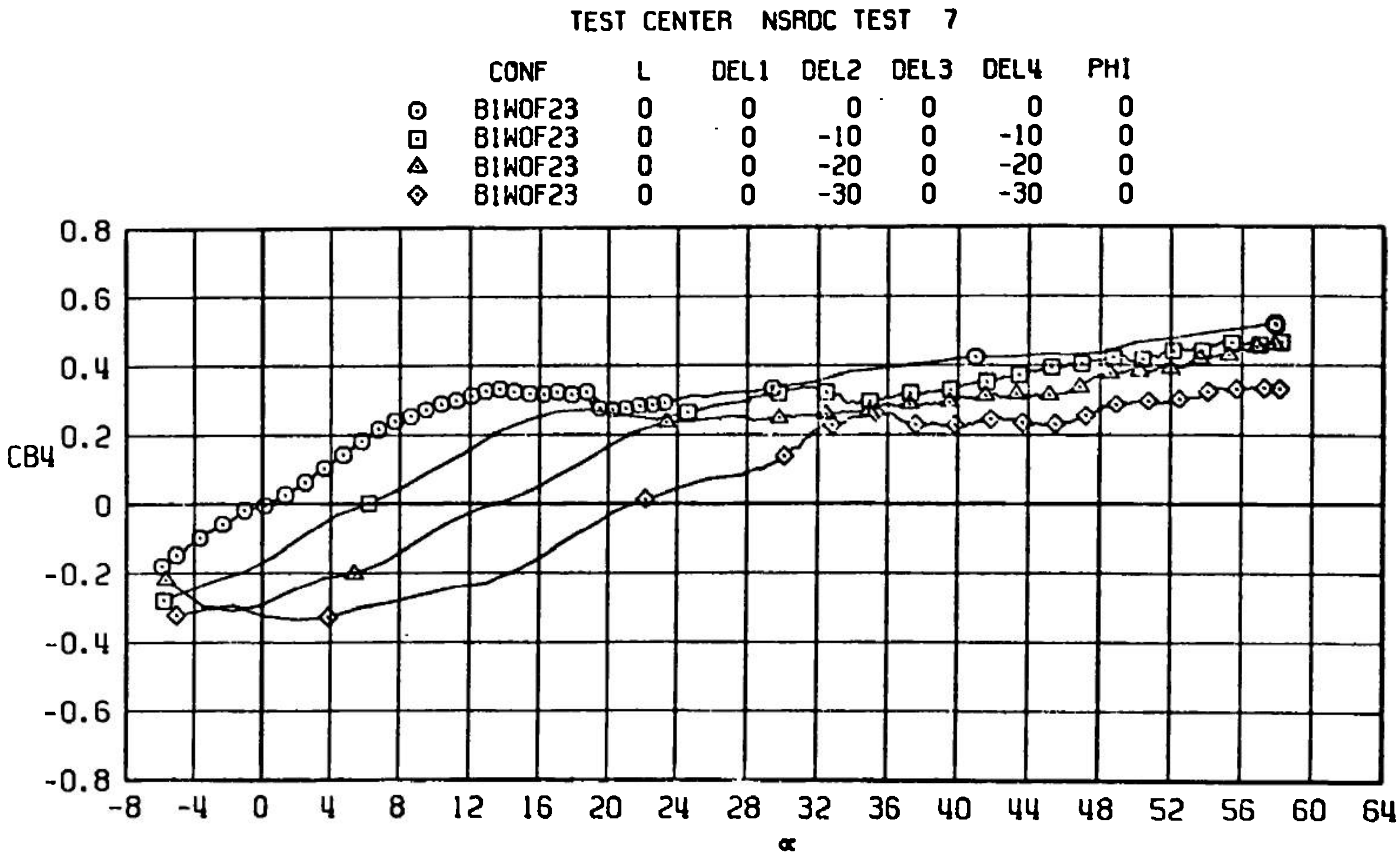

j. CB4 versus α
Figure 51. Continued.

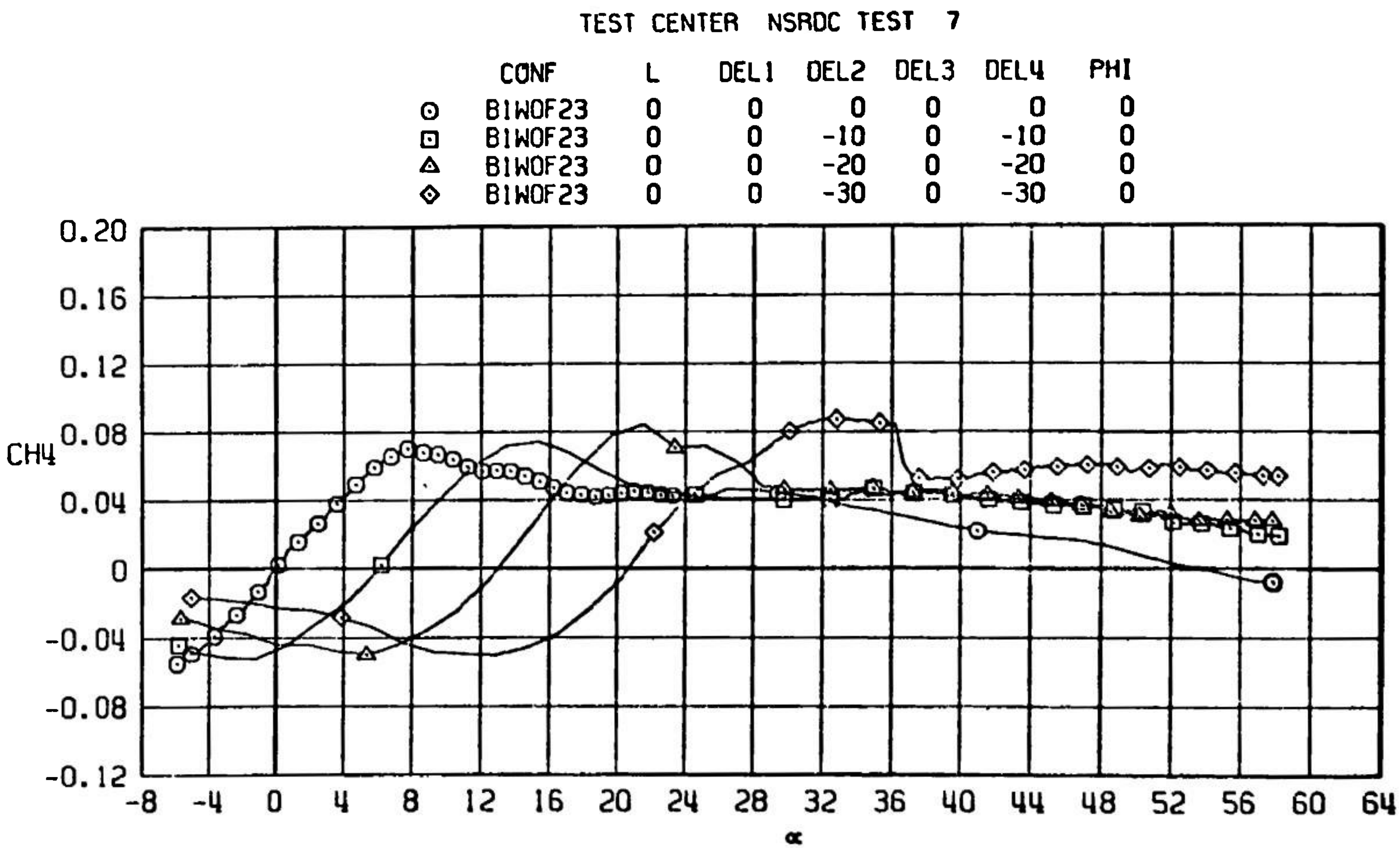

k. CH4 versus α

Figure 51. Concluded.

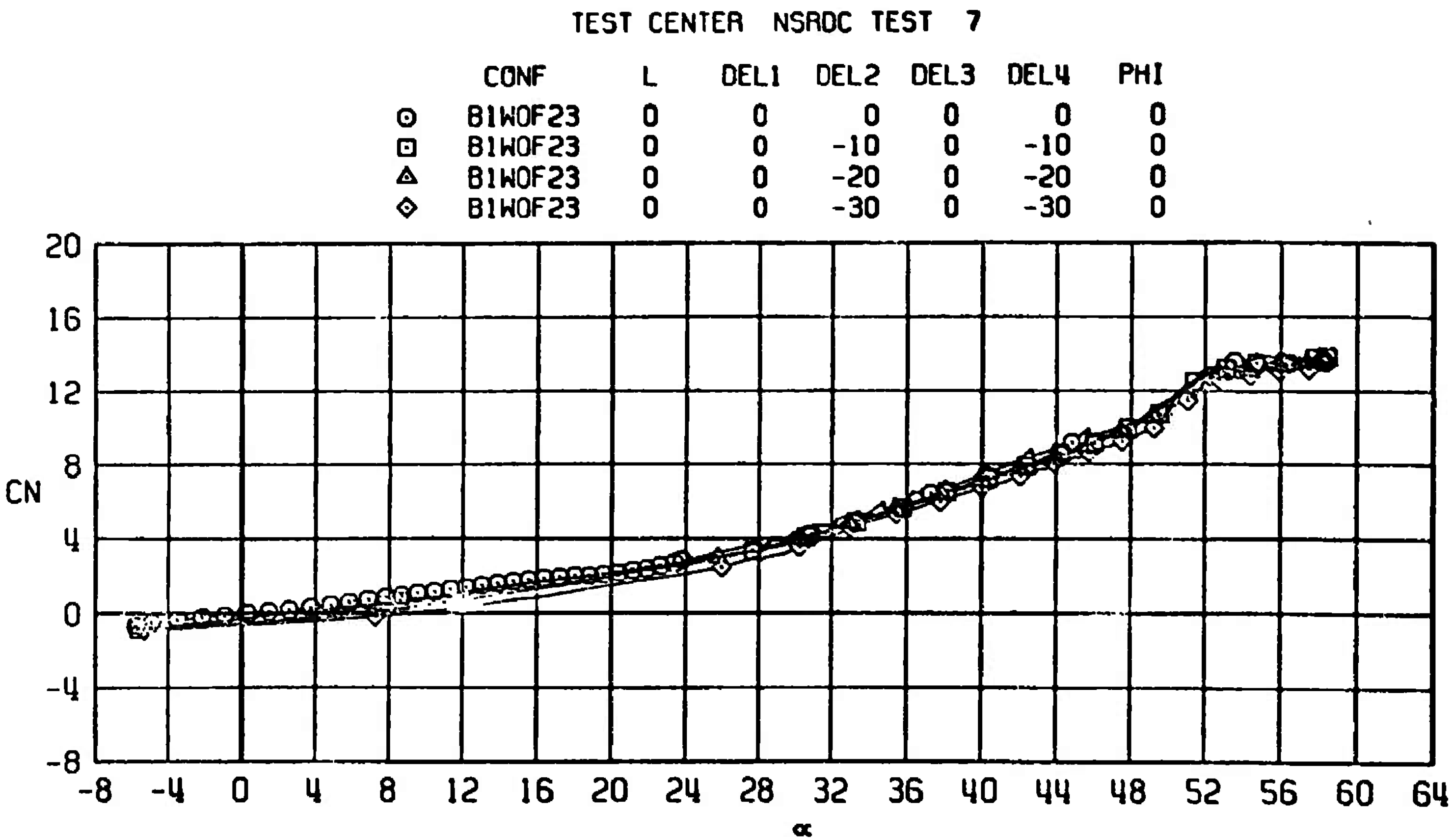

a. CN versus α

Figure 52. Test No. 7, comparison of aerodynamic coefficients of configuration B1W0F23 for various deflections of tail fins No. 2 and 4 at M_∞ = 0.9.

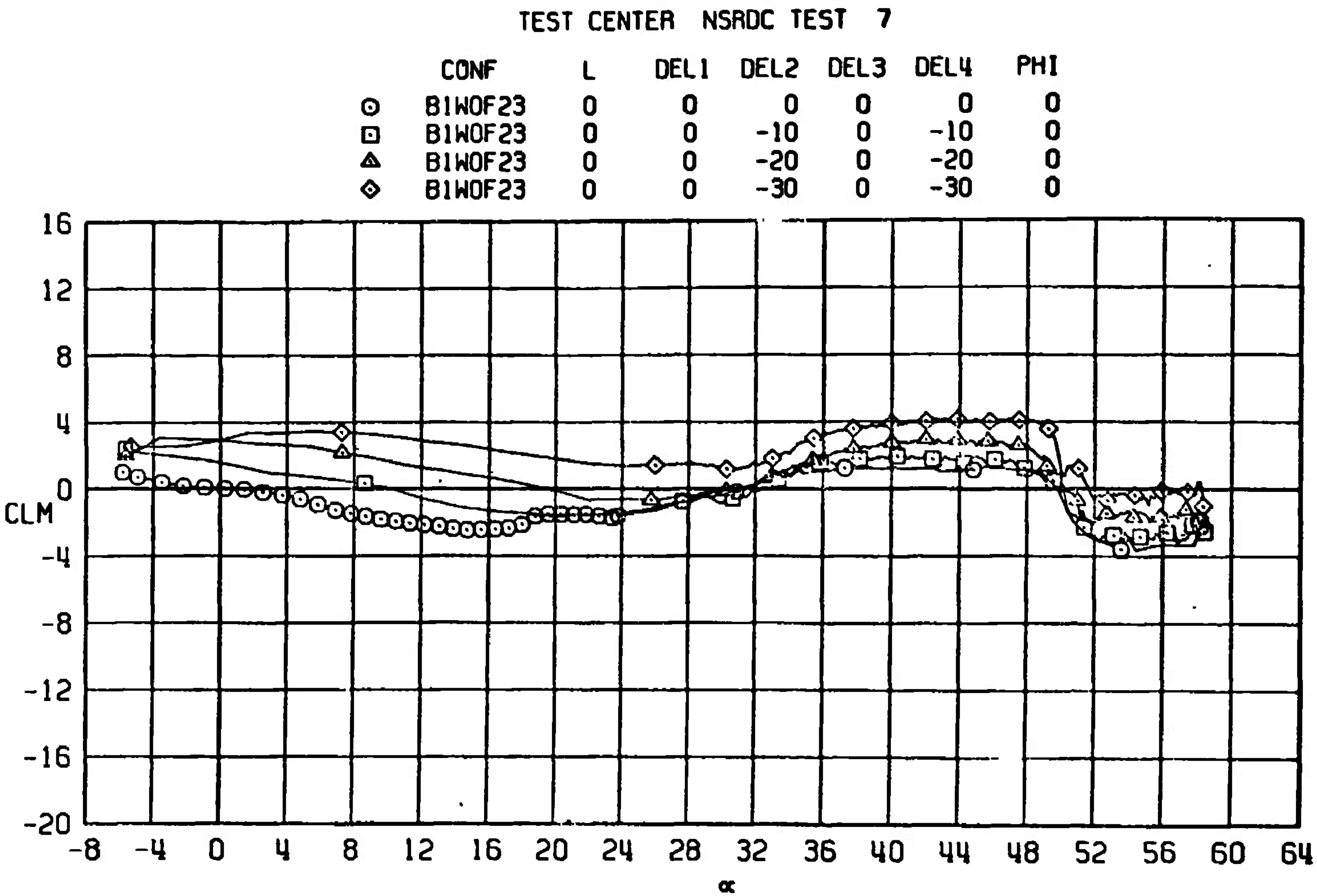

b. CLM versus α
Figure 52. Continued.

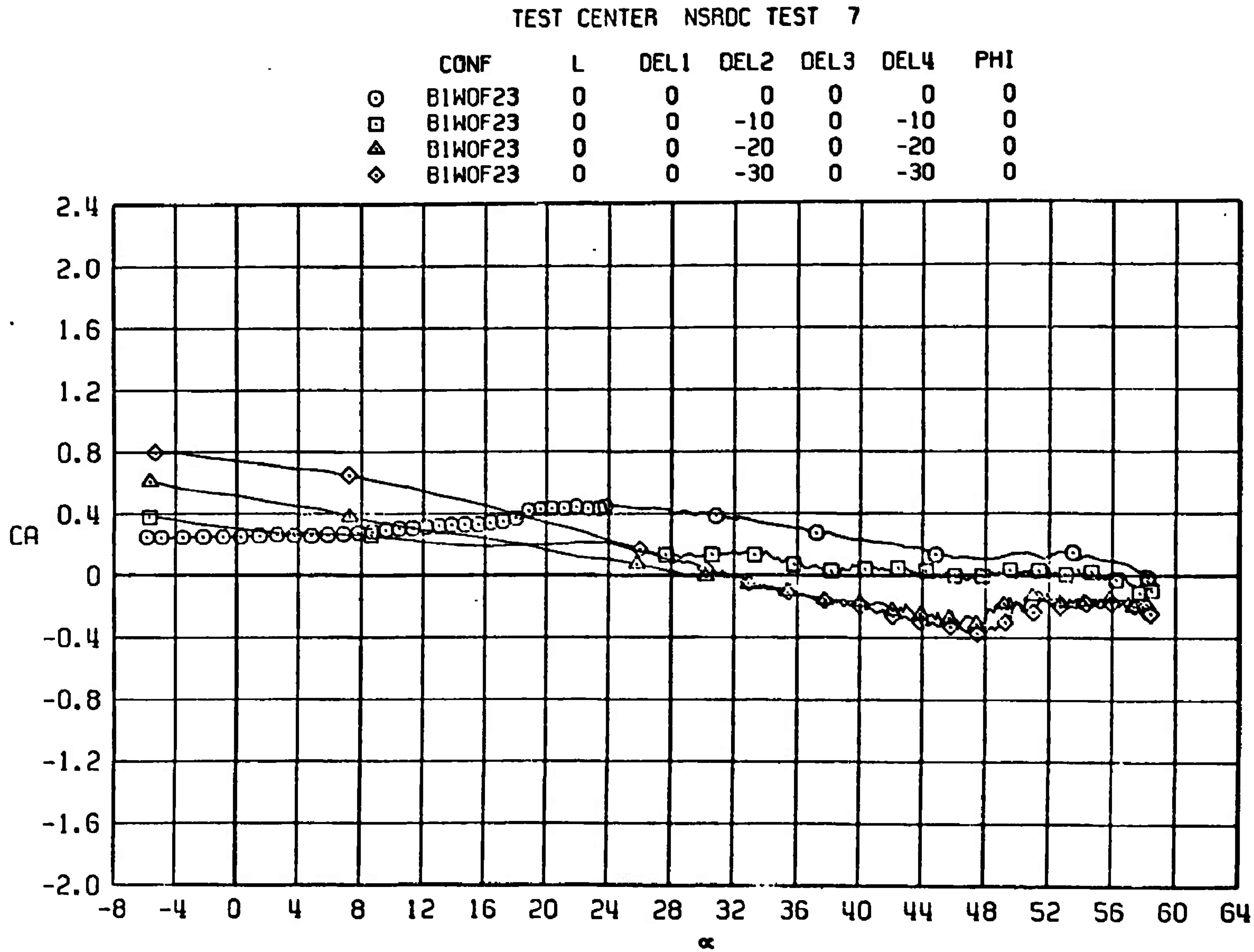

c. CA versus α

Figure 52. Continued.

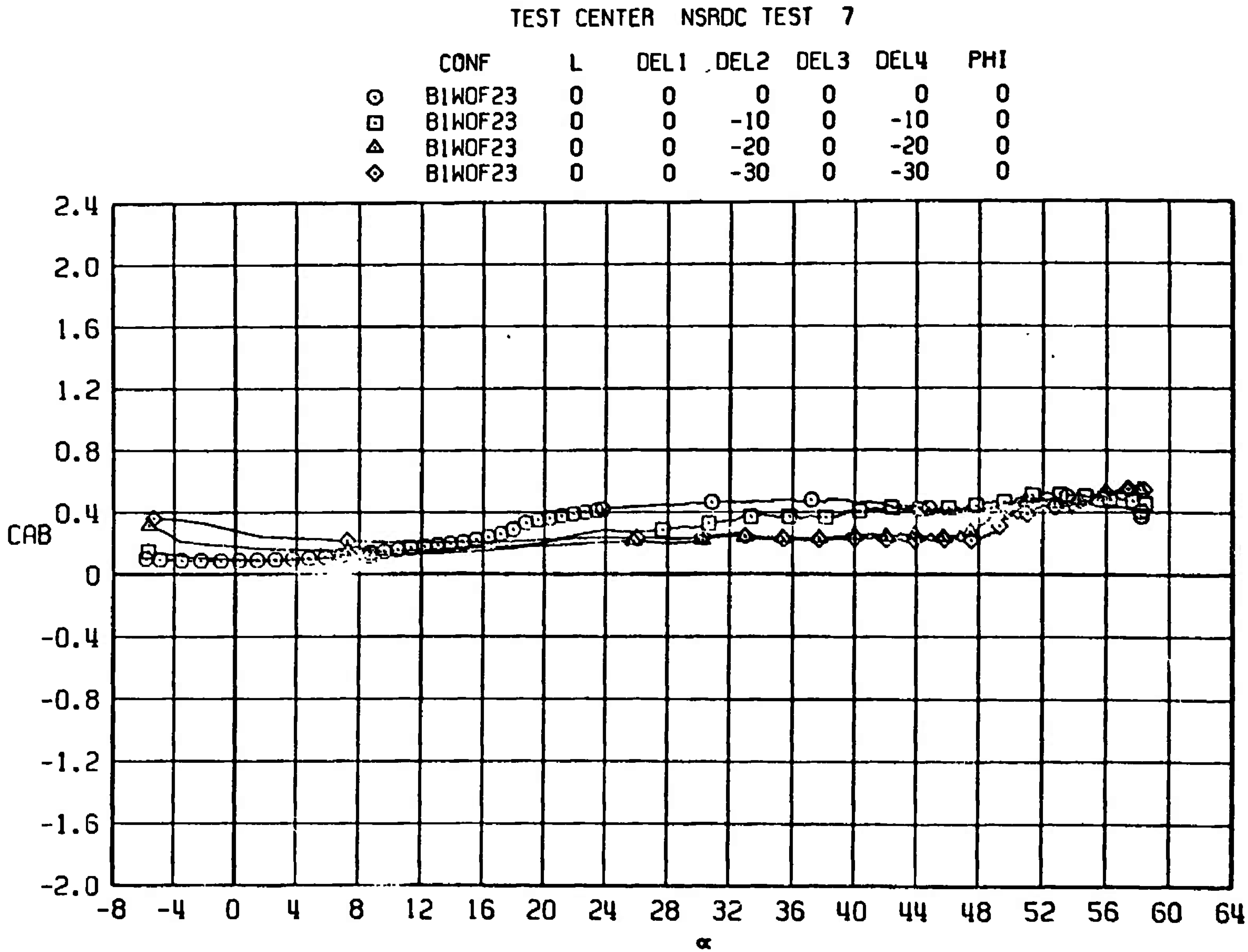

d. CAB versus α
Figure 52. Continued.

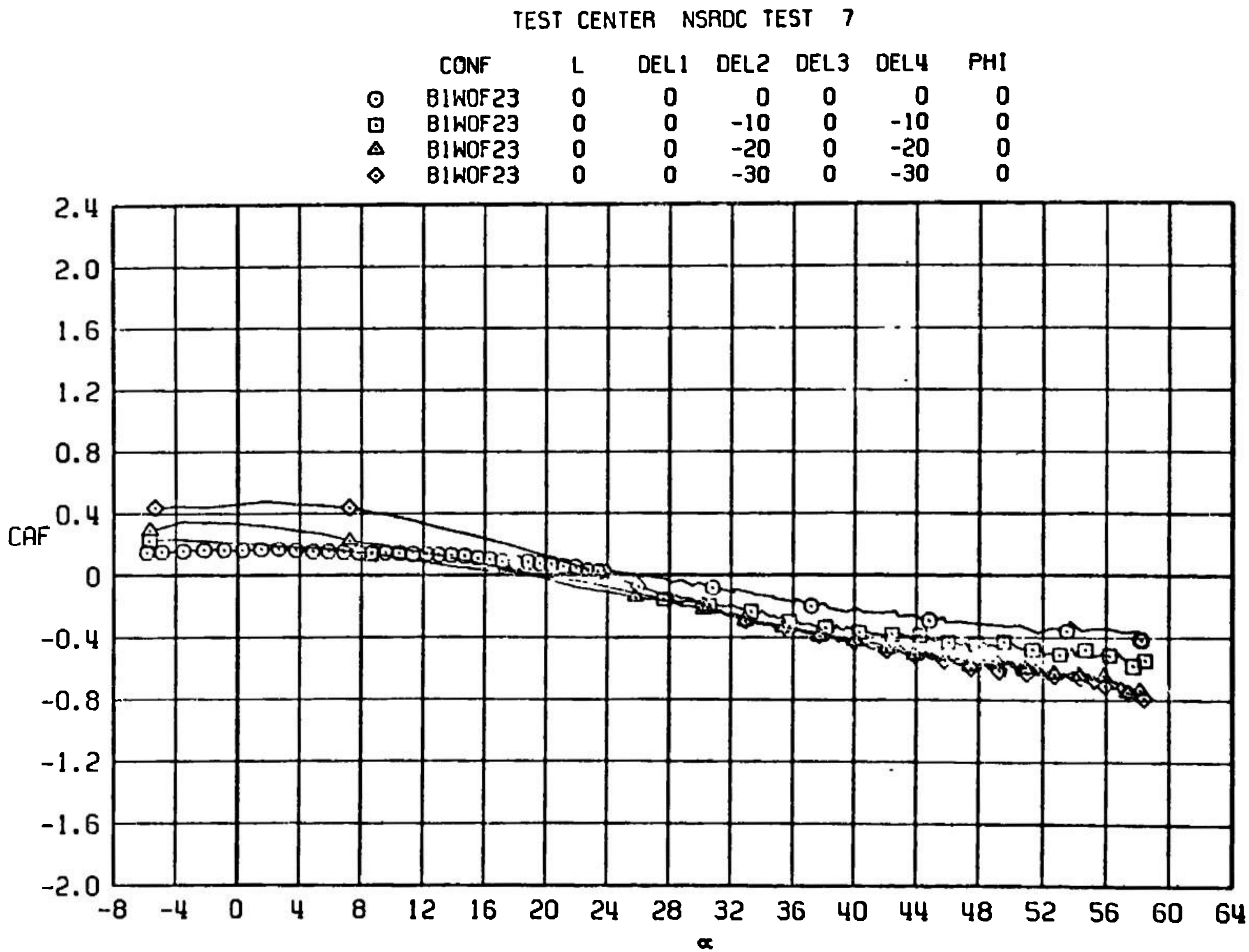

e. CAF versus α
Figure 52. Continued.

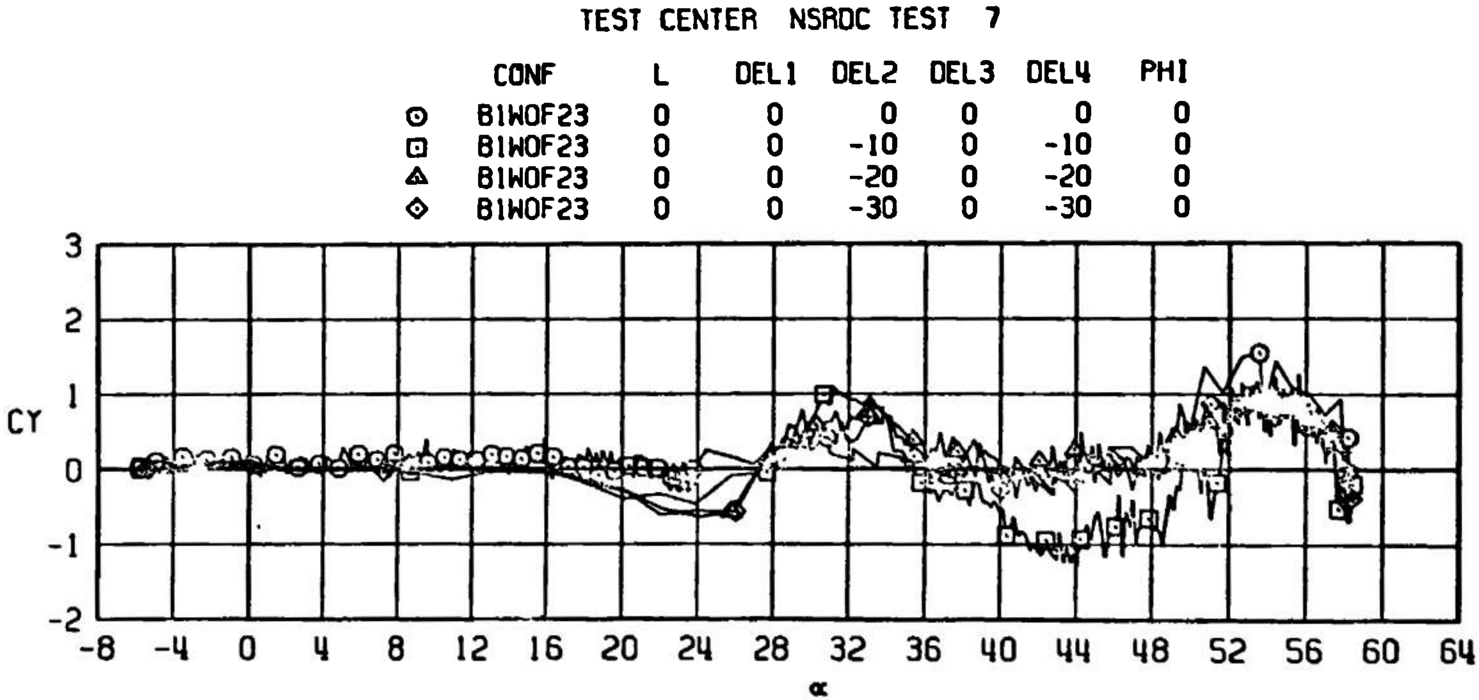

f. CY versus α

Figure 52. Continued.

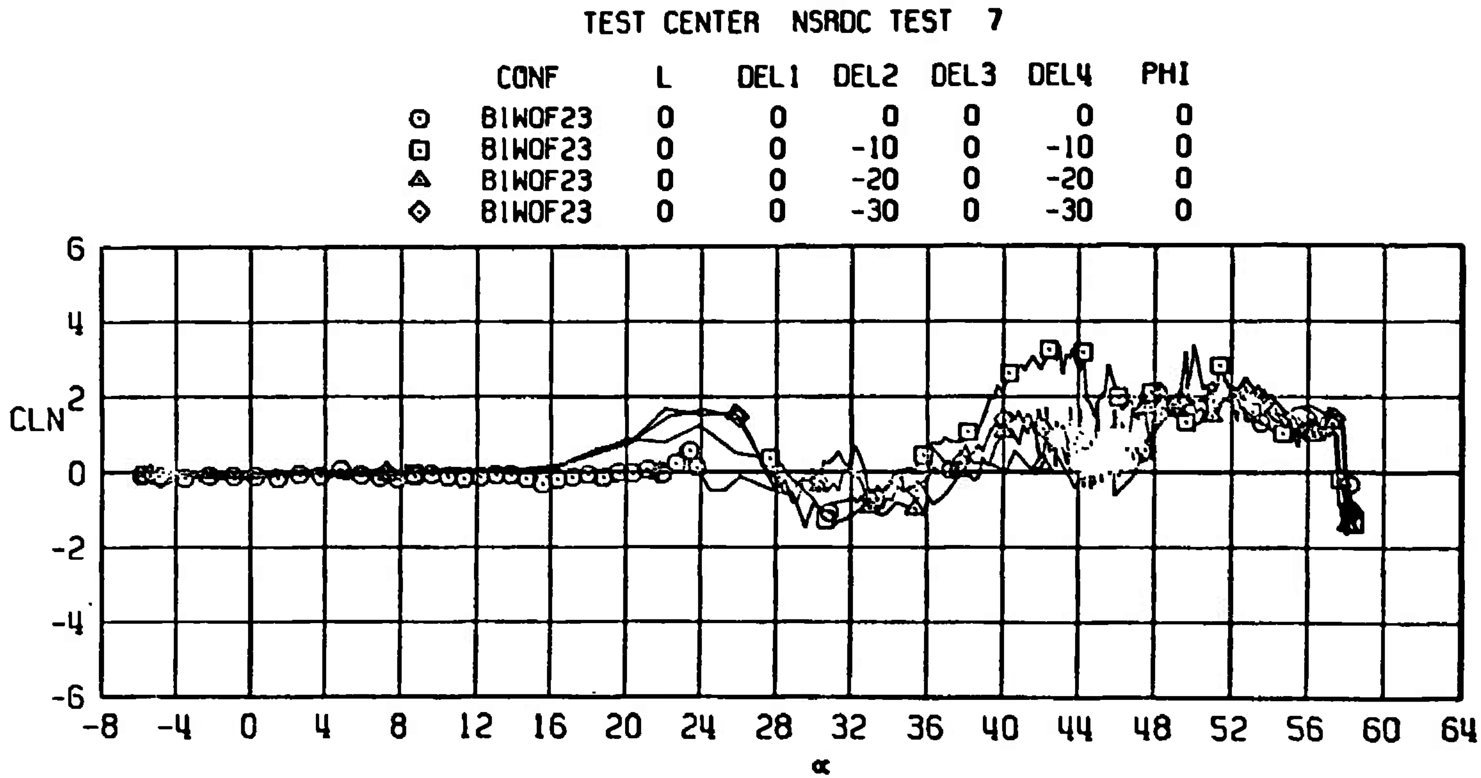

g. CLN versus α
Figure 52. Continued.

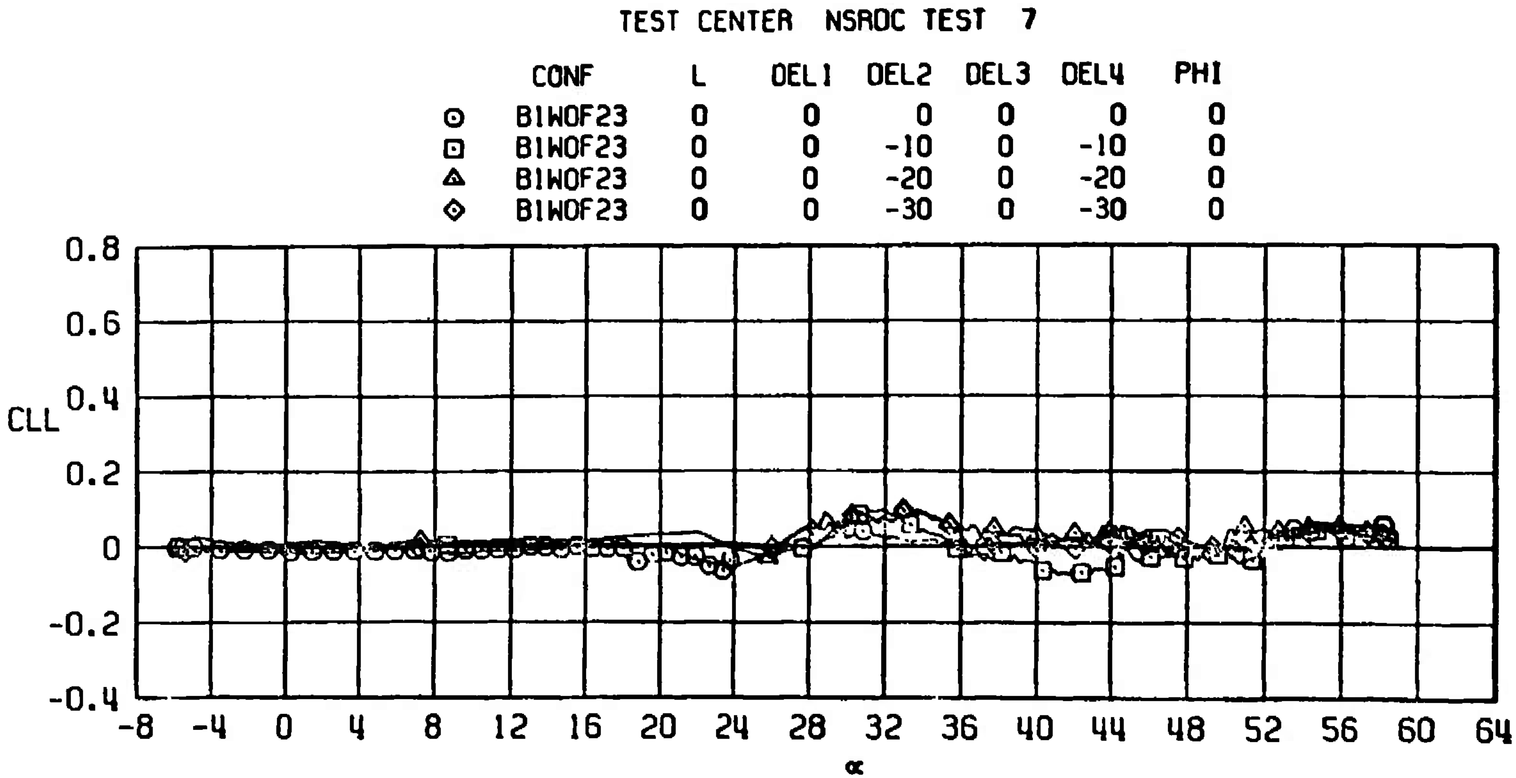

h. CLL versus α
Figure 52. Continued.

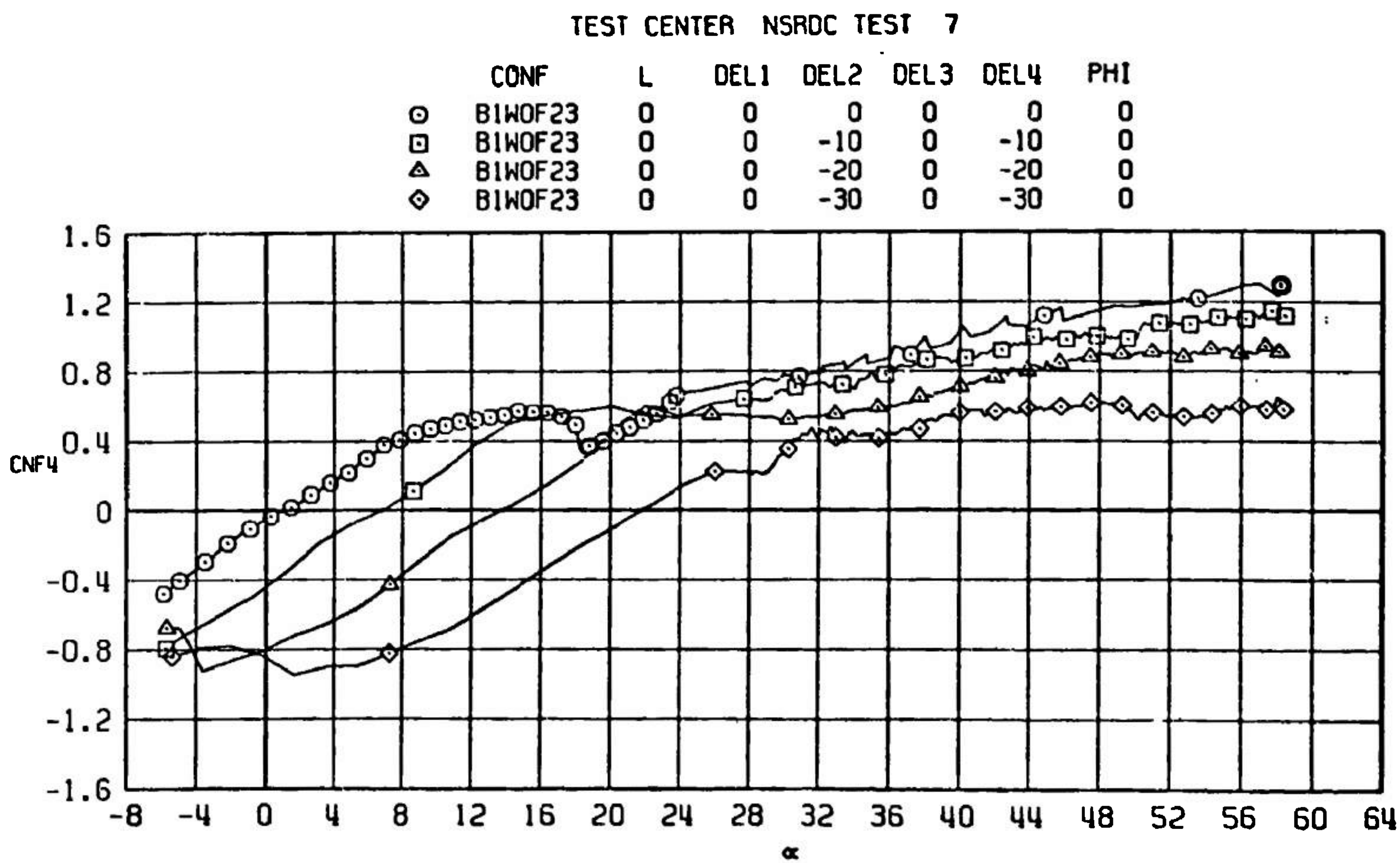

i. CNF4 versus α
Figure 52. Continued.

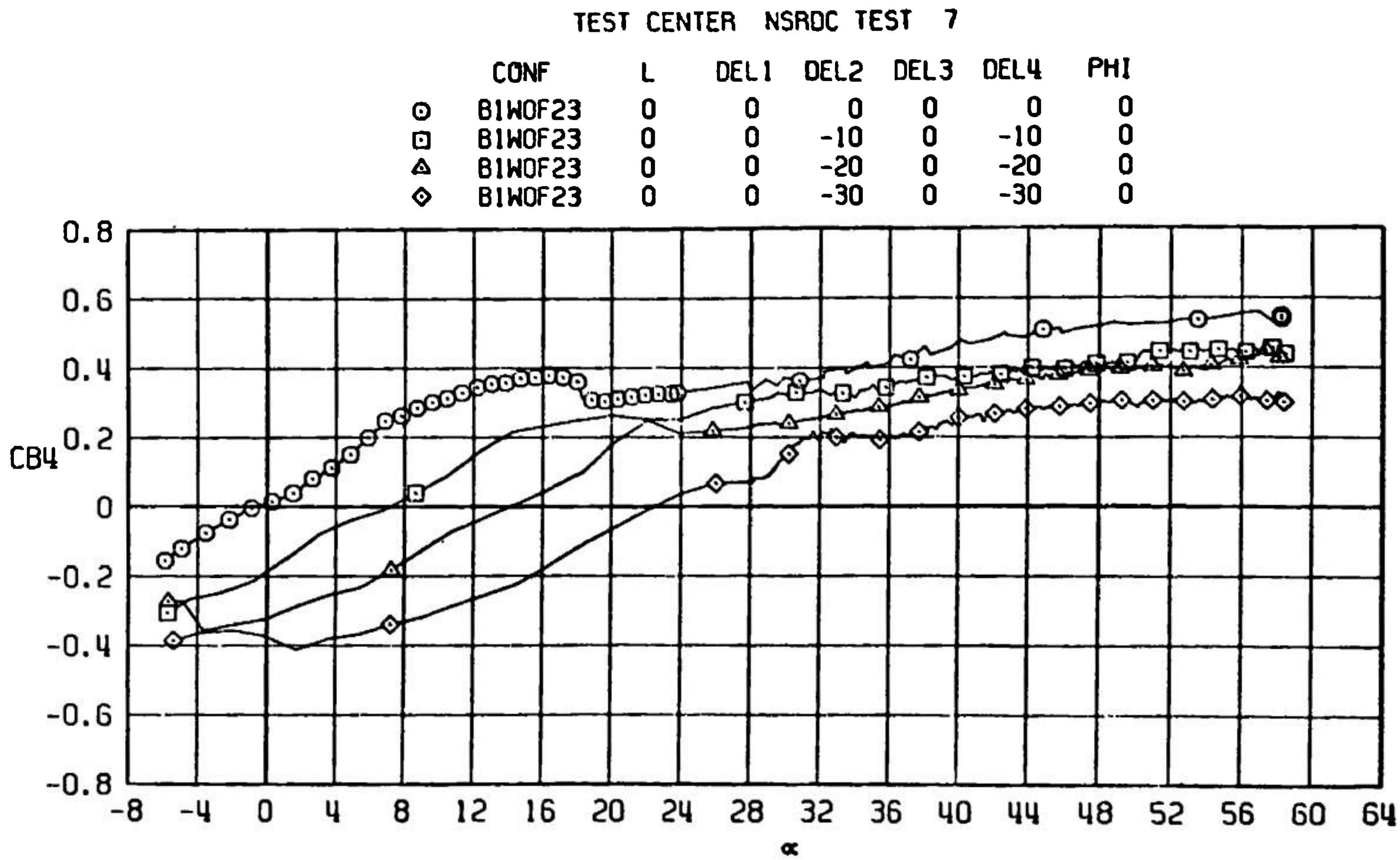

j. CB4 versus α

Figure 52. Continued.

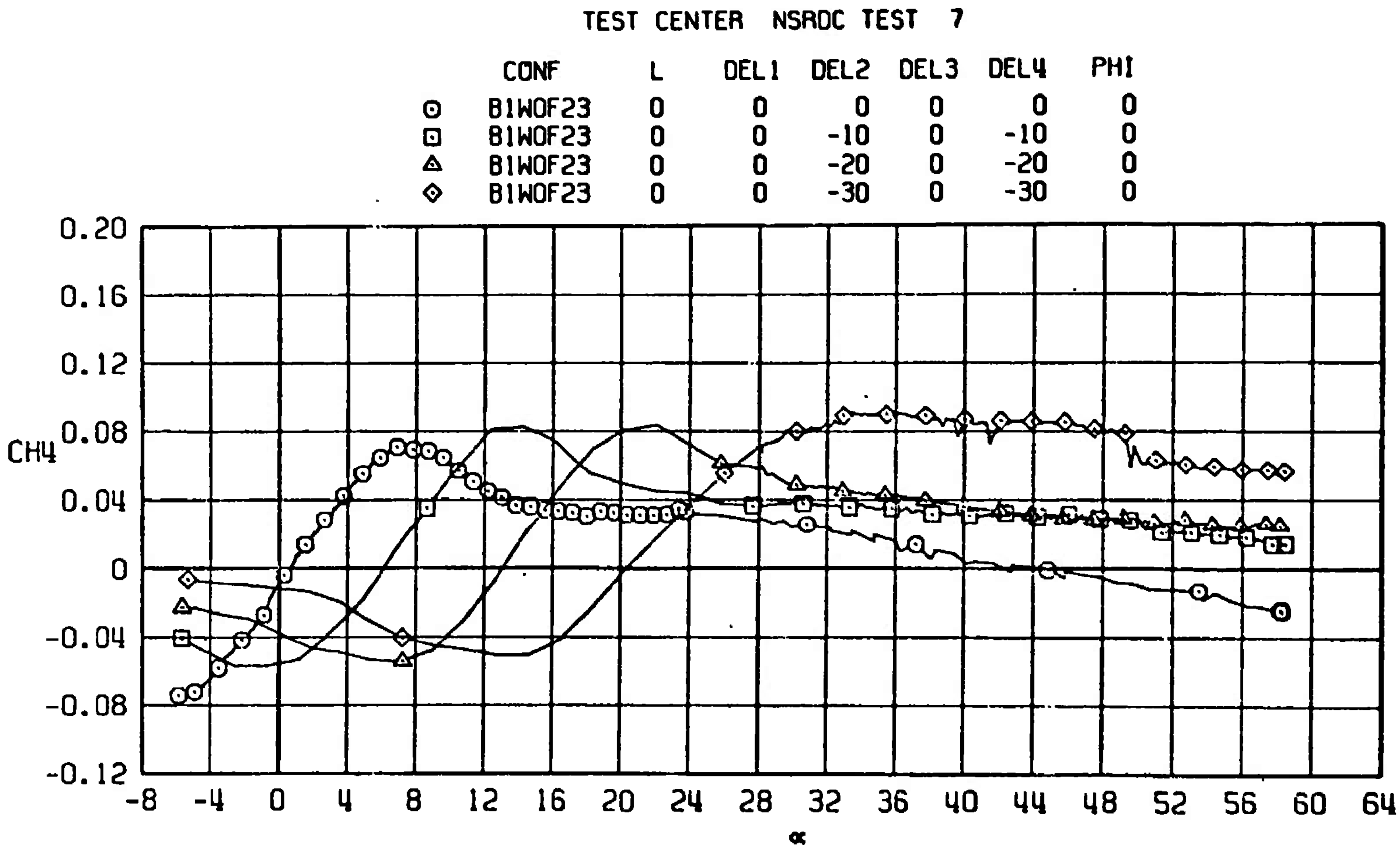

k. CH4 versus α
Figure 52. Concluded.

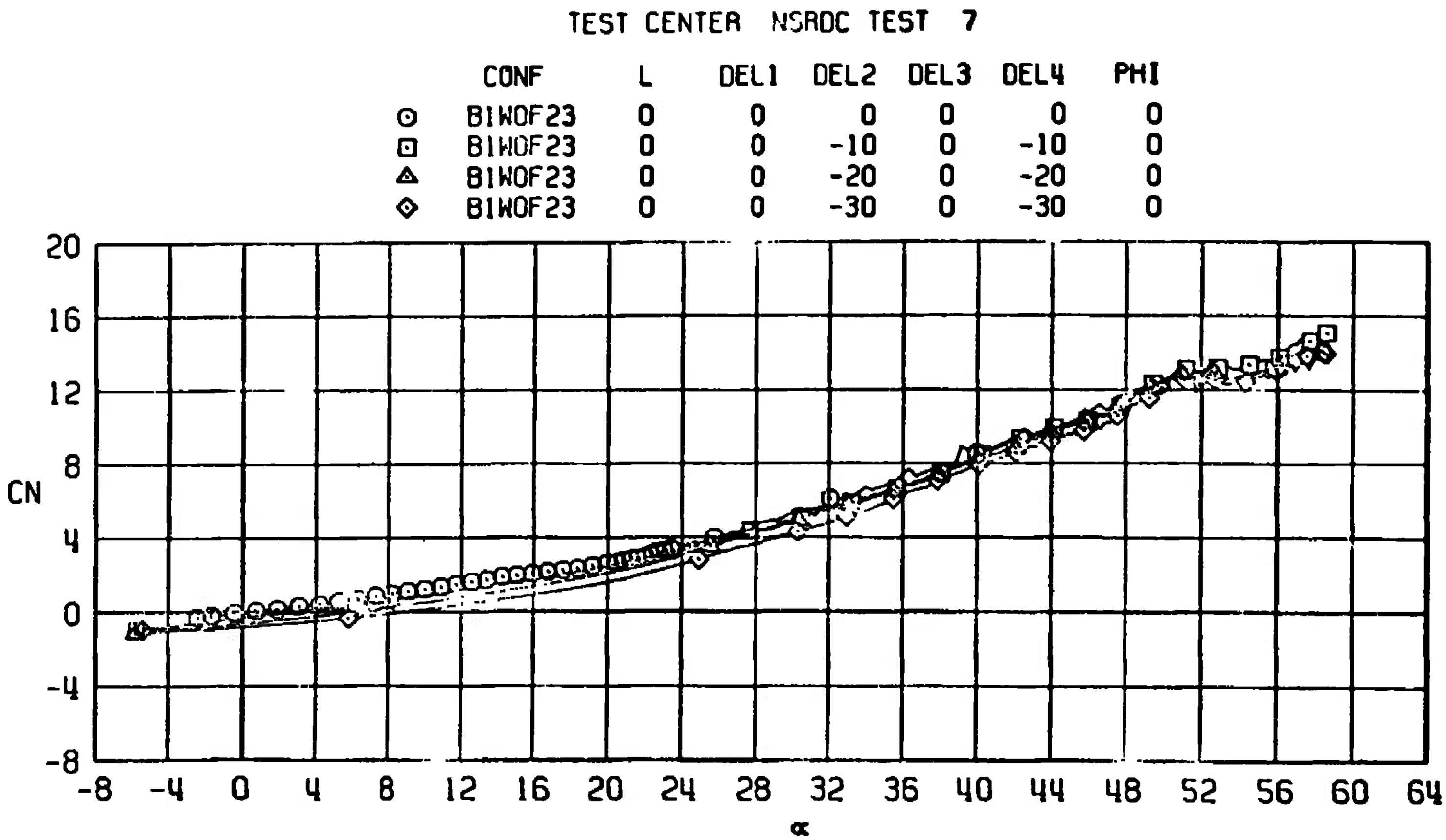

a. CN versus α

Figure 53. Test No. 7, comparison of aerodynamic coefficients of configuration B1W0F23 for various deflections of tail fins No. 2 and 4 at $M_\infty = 1.0$.

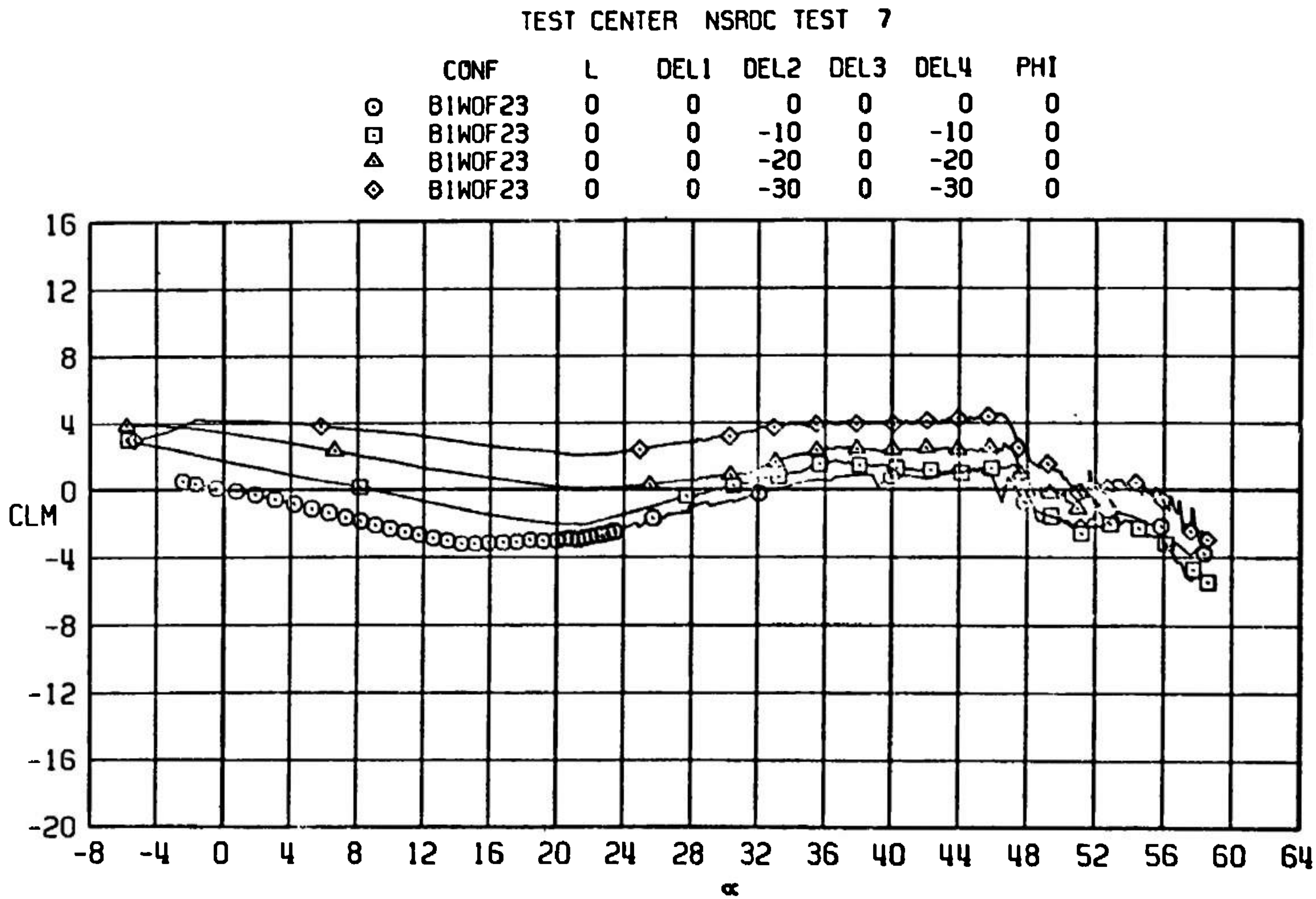

b. CLM versus α

Figure 53. Continued.

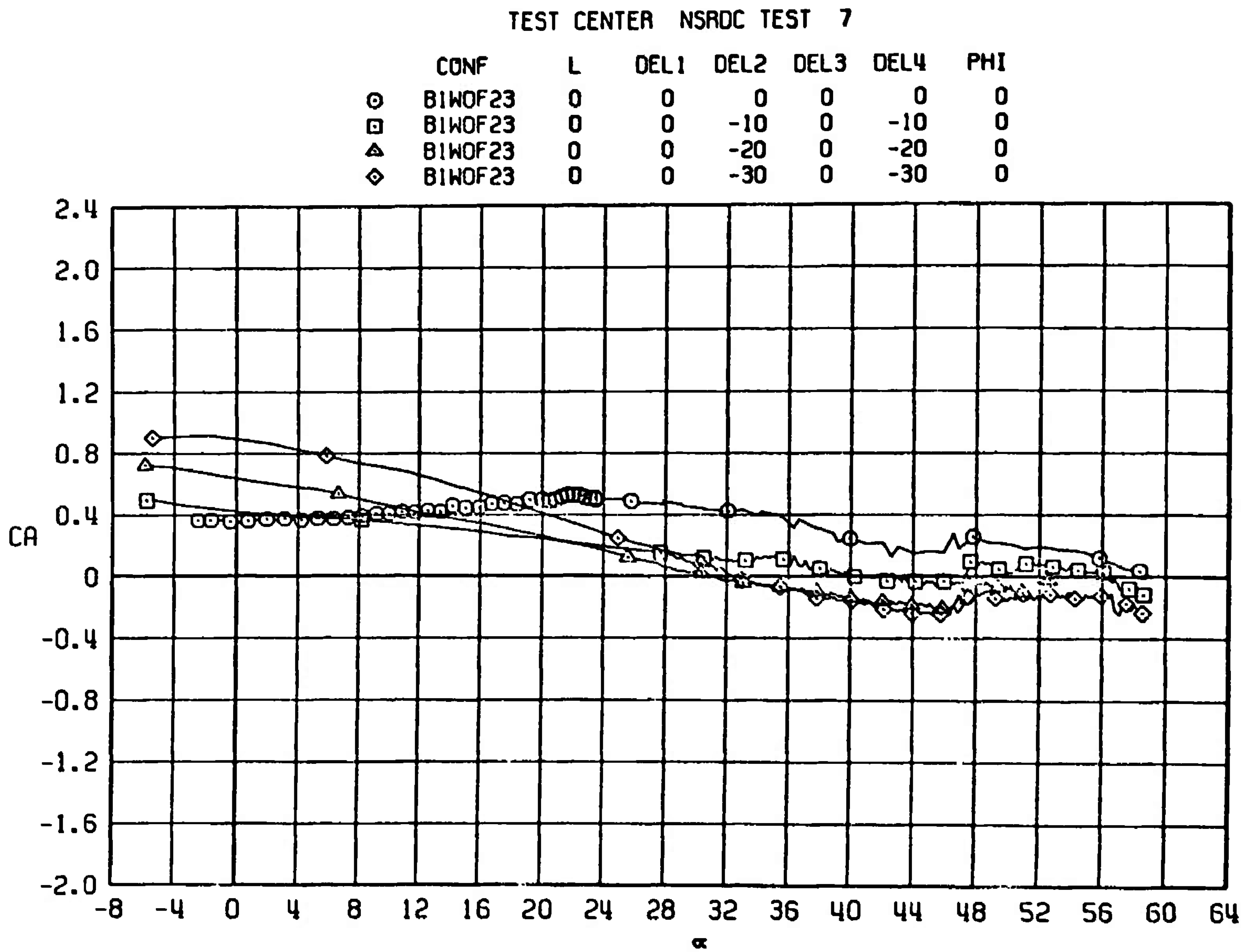

c. CA versus α

Figure 53. Continued.

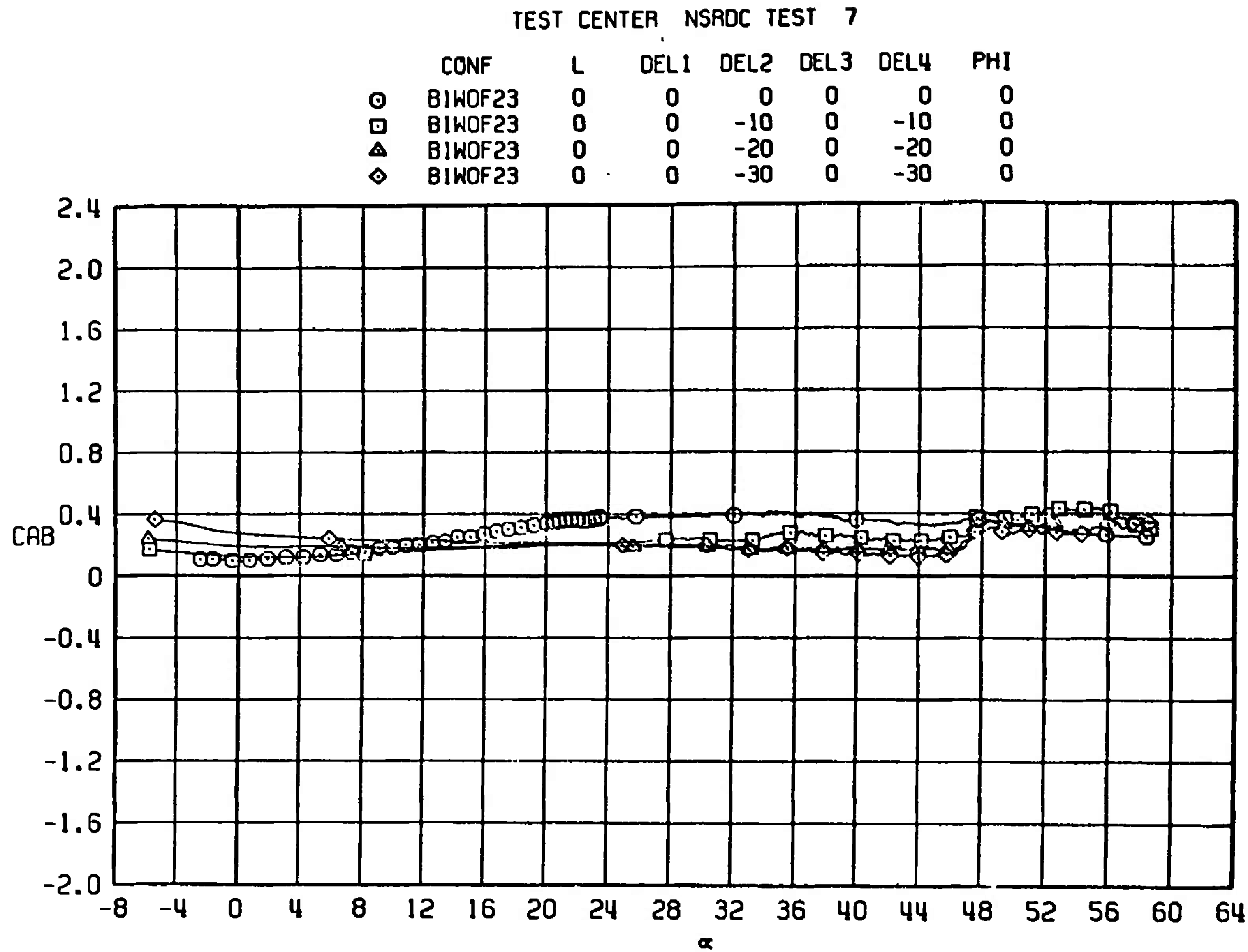

d. CAB versus α

Figure 53. Continued.

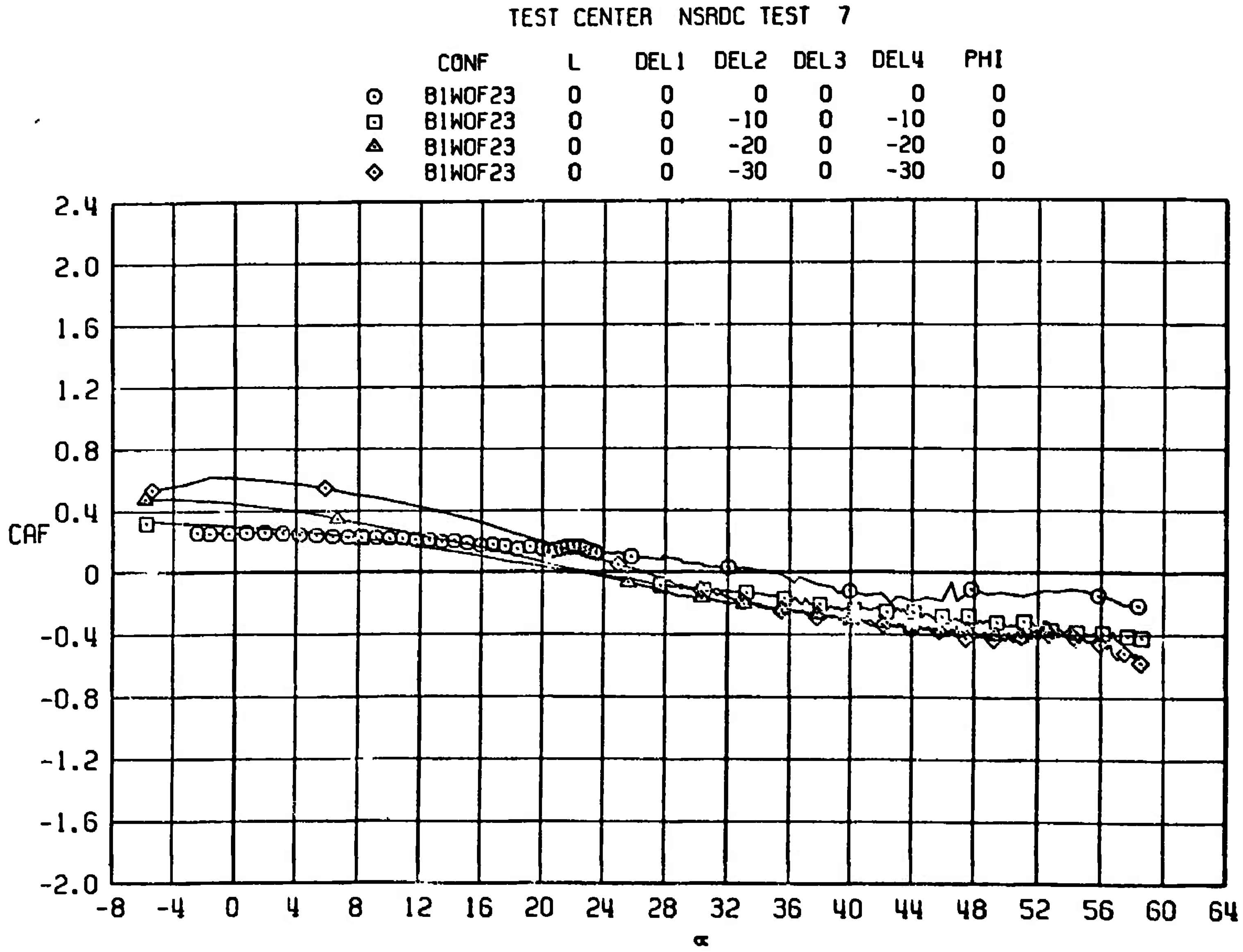

e. CAF versus α
Figure 53. Continued.

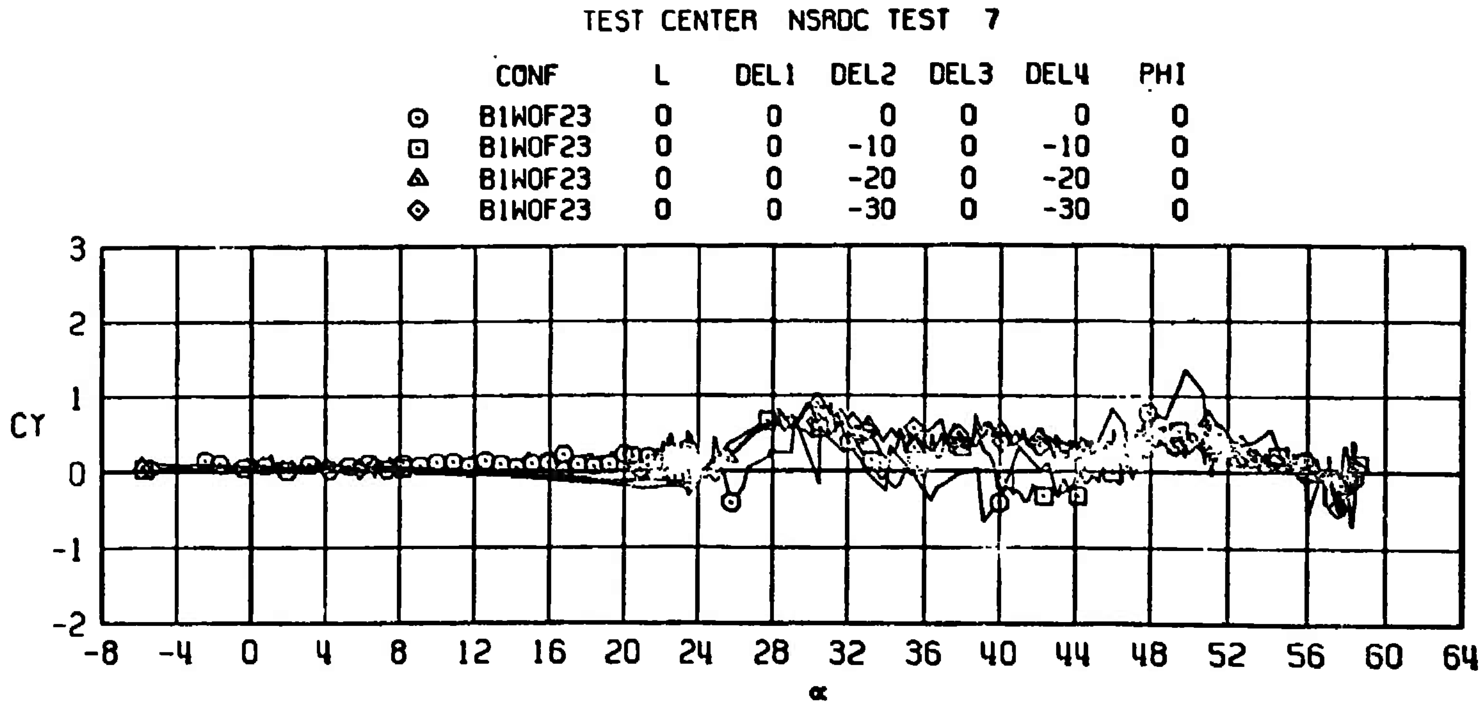

f. CY versus α
Figure 53. Continued.

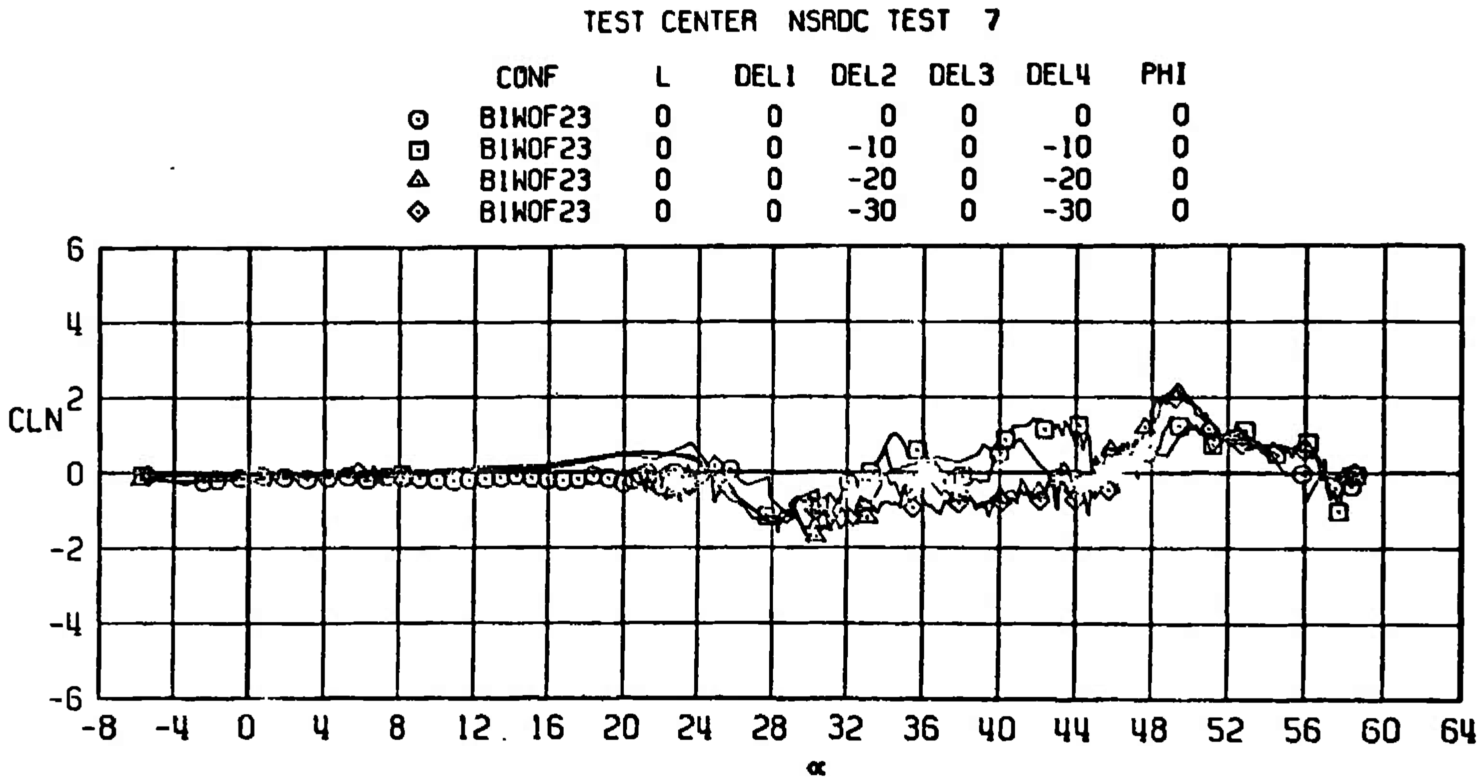

g. CLN versus α

Figure 53. Continued.

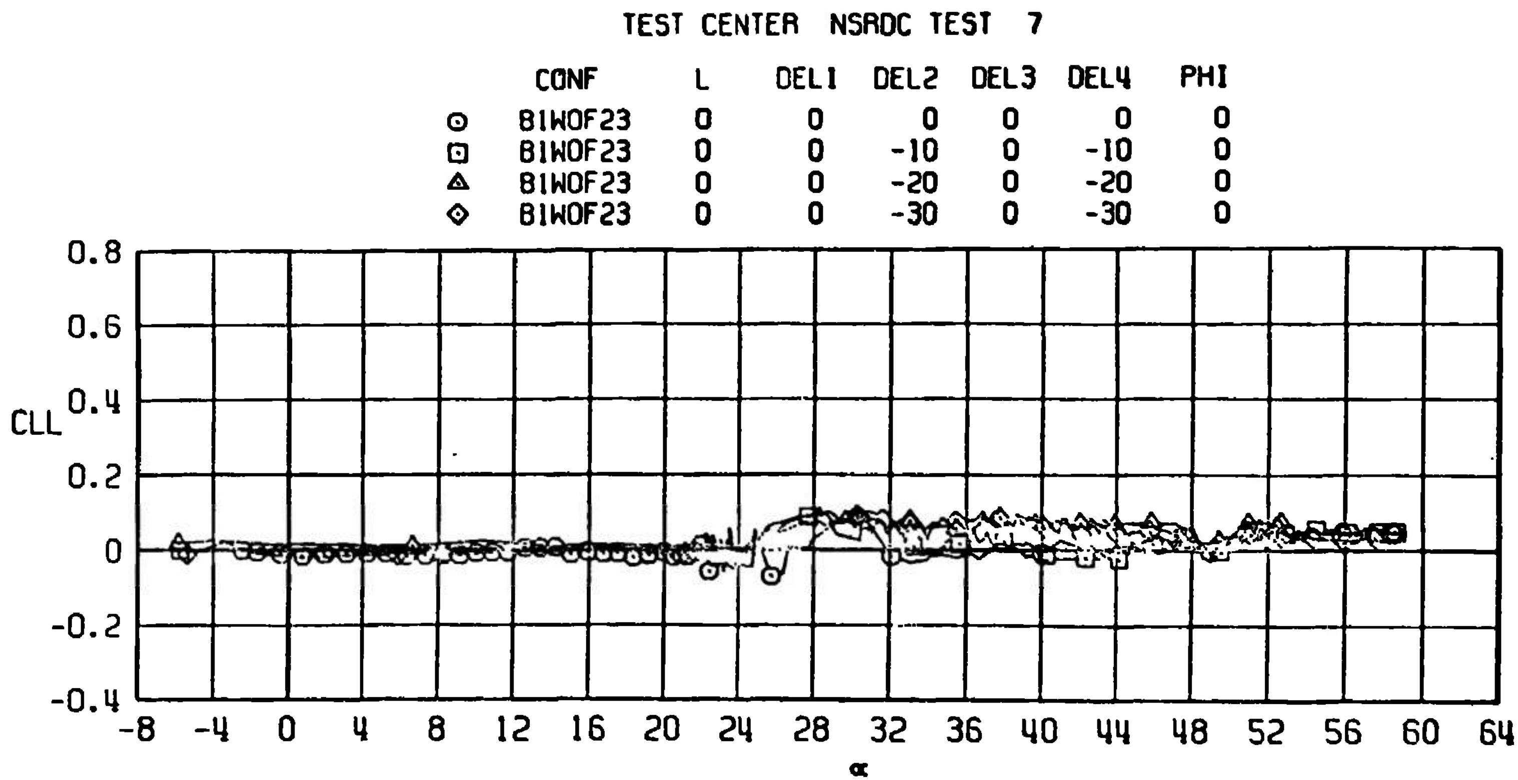

h. CLL versus α

Figure 53. Continued.

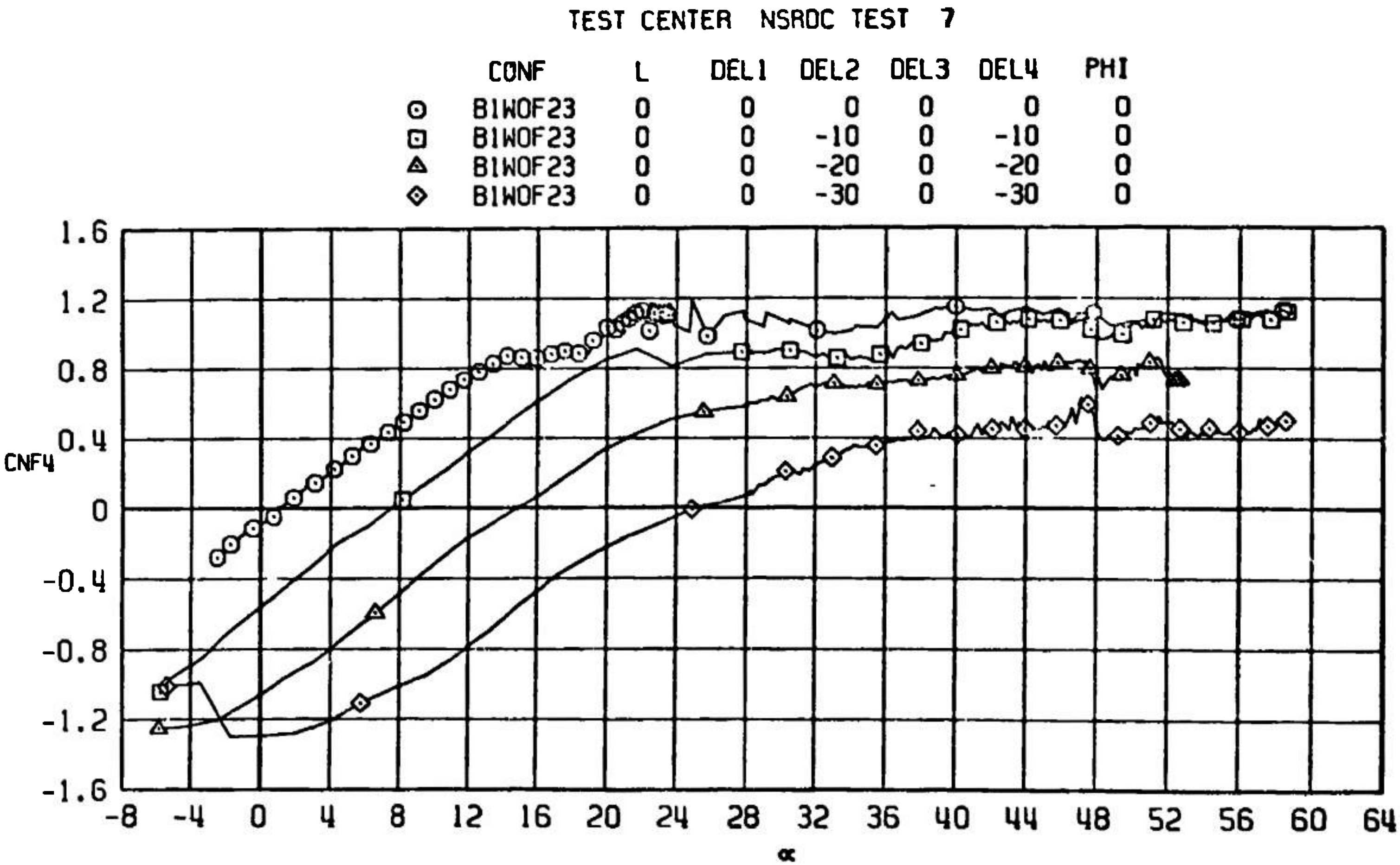

i. CNF4 versus α

Figure 53. Continued.

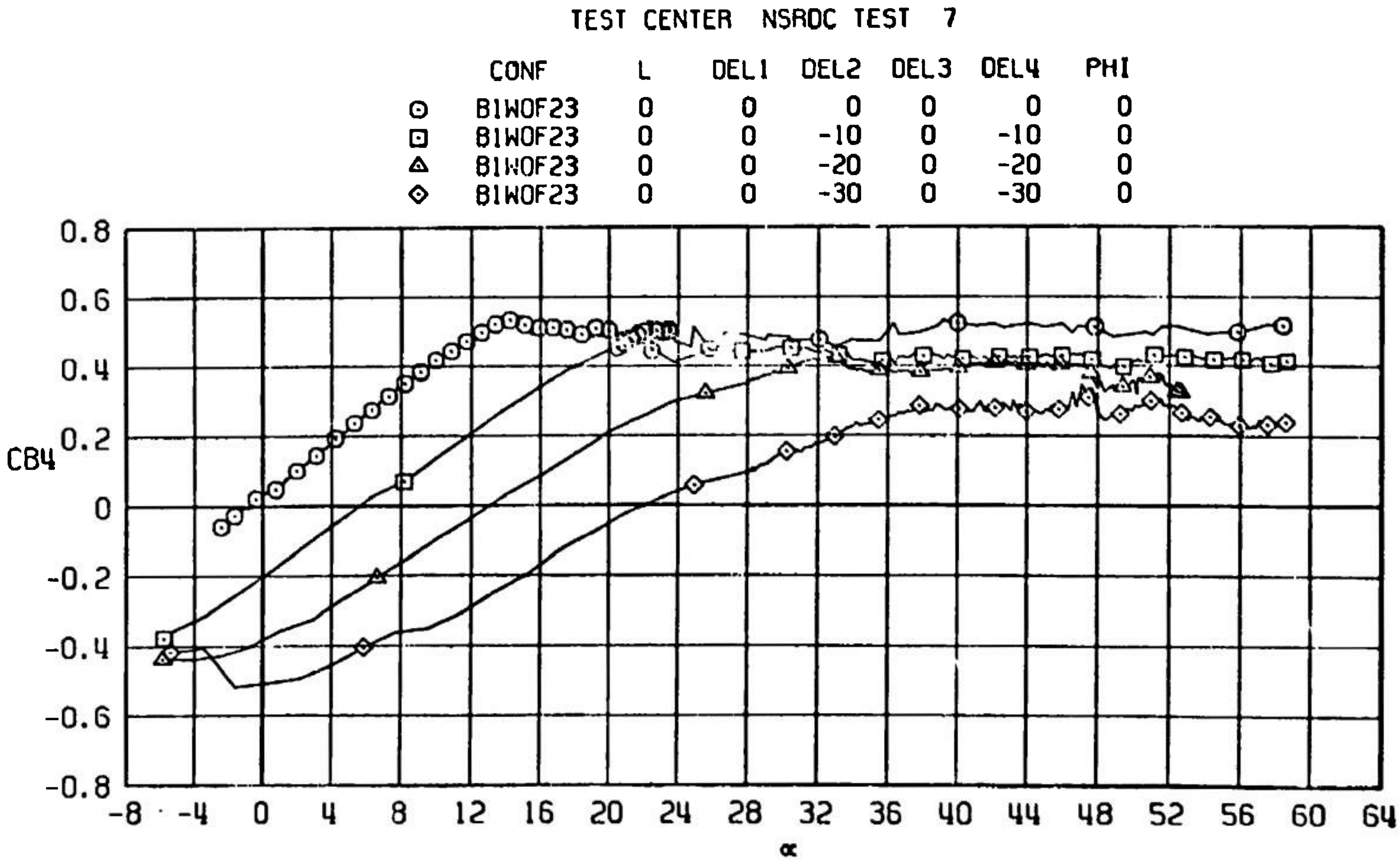

j. CB4 versus α
Figure 53. Continued.

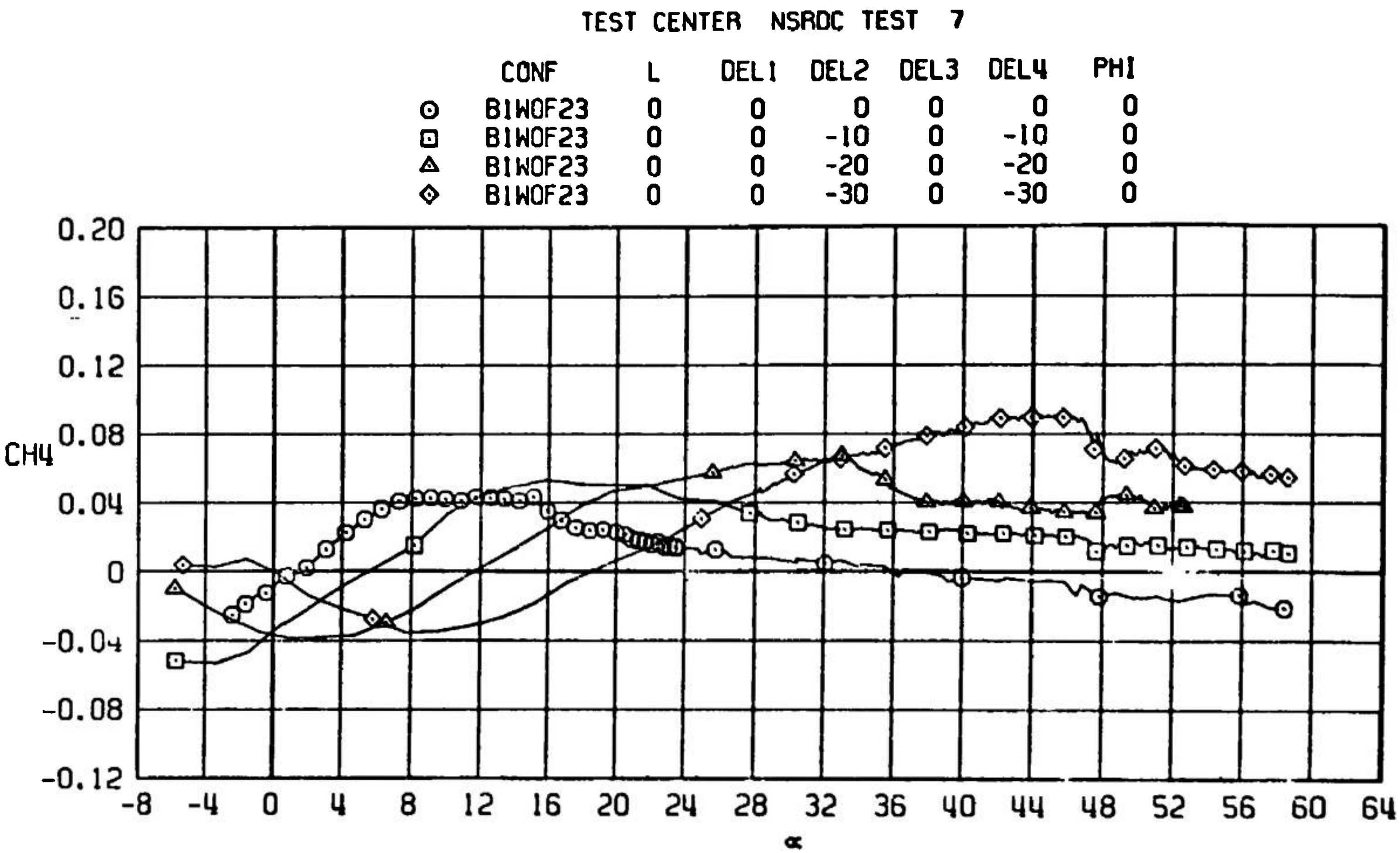

k. CH4 versus α

Figure 53. Concluded.

TEST CENTER NSRDC TEST 7

	CONF	L	DEL1	DEL2	DEL3	DEL4	PHI
⊙	B1W0F23	0	0	0	0	0	0
⊡	B1W0F23	0	0	-10	0	-10	0
△	B1W0F23	0	0	-20	0	-20	0
◇	B1W0F23	0	0	-30	0	-30	0

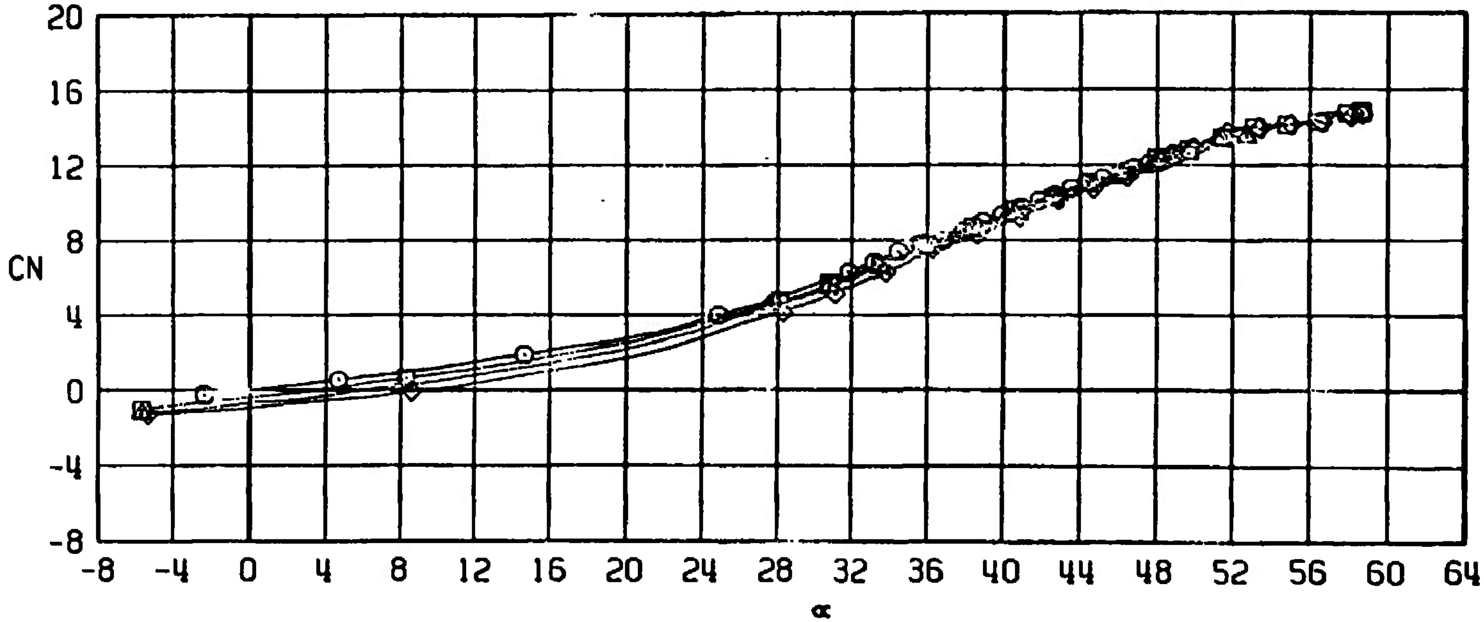

a. CN versus α

Figure 54. Test No. 7, comparison of aerodynamic coefficients of configuration B1W0F23 for various deflections of tail fins No. 2 and 4 at M_∞ = 1.1.

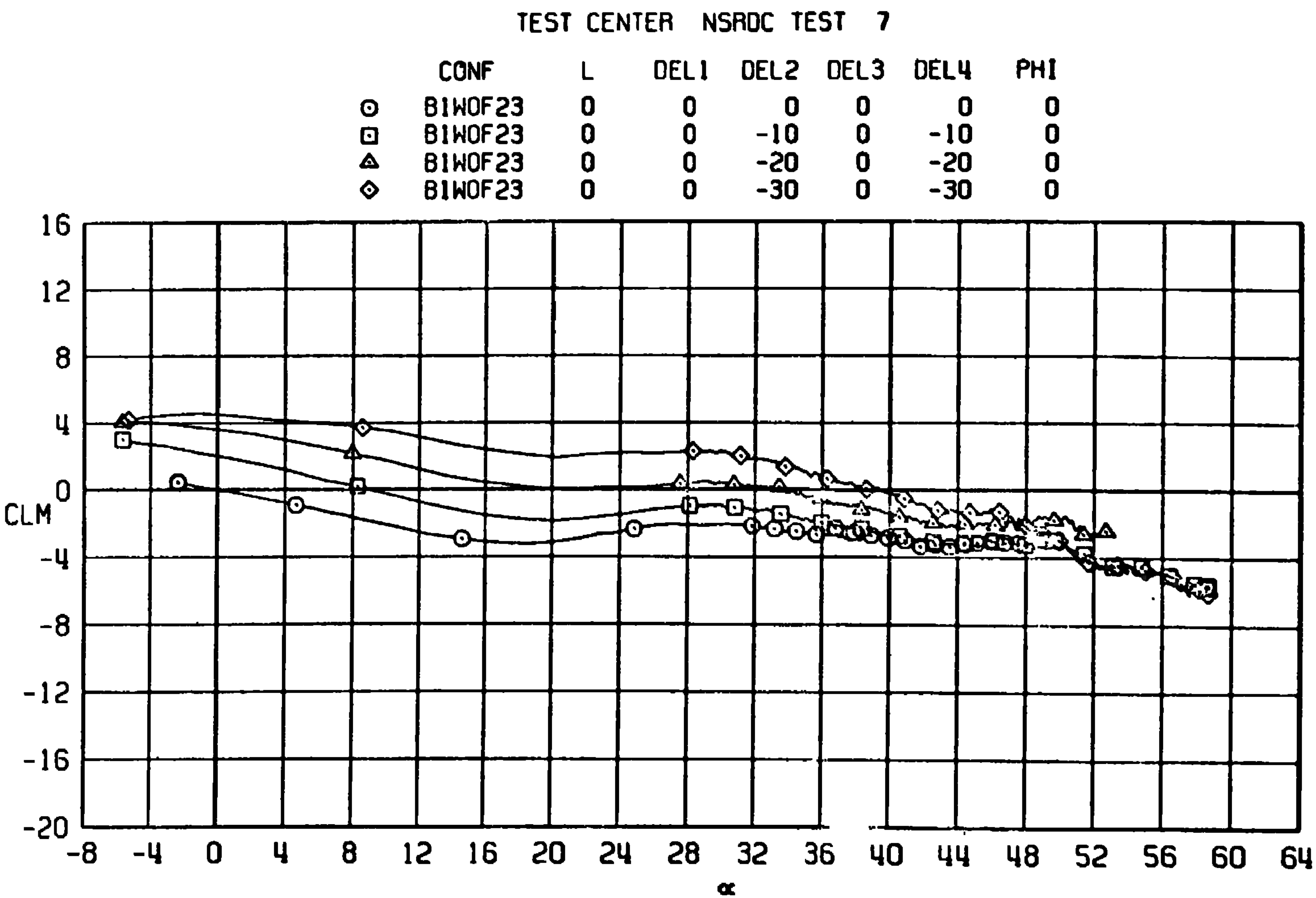

b. CLM versus α

Figure 54. Continued.

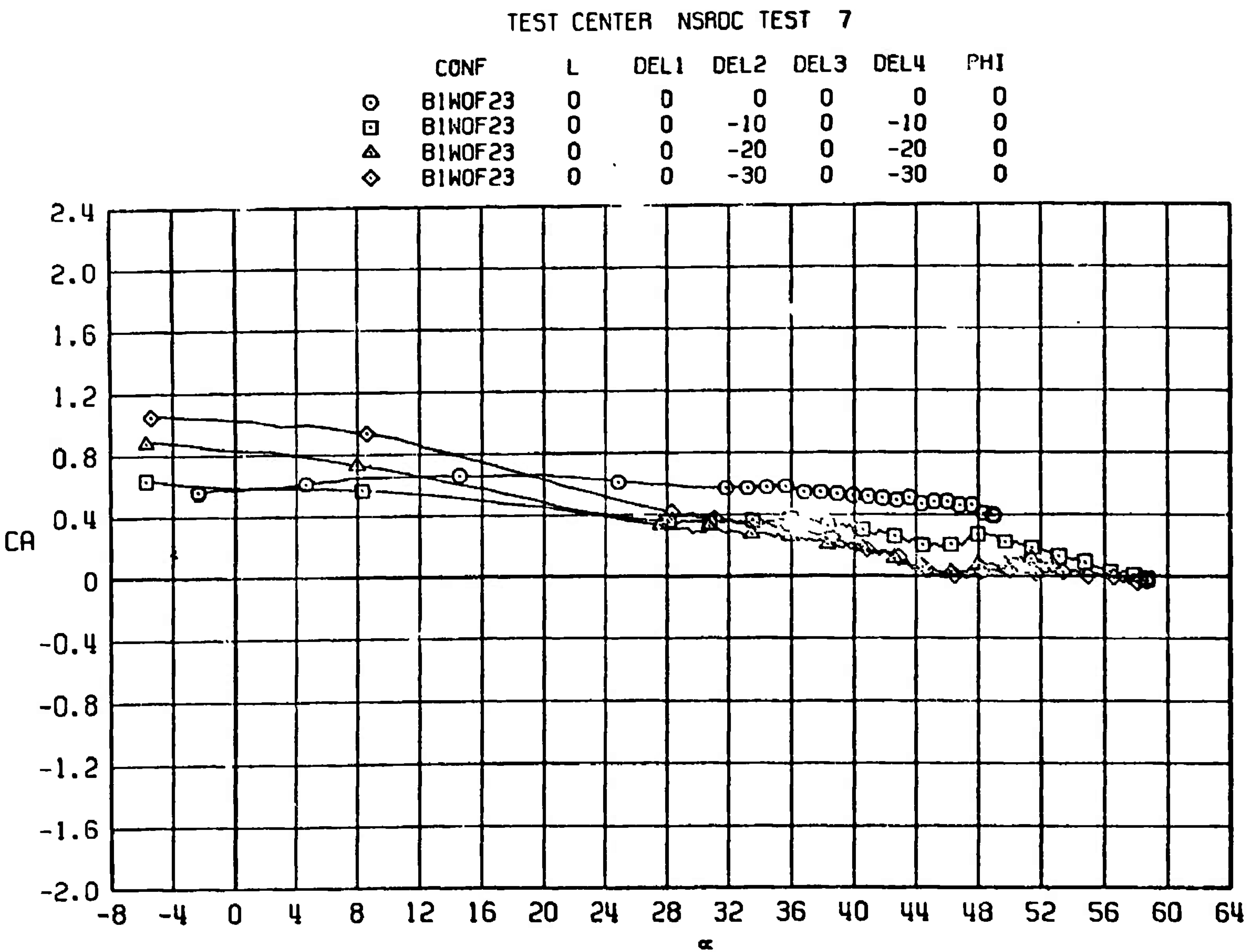

c. CA versus α
Figure 54. Continued.

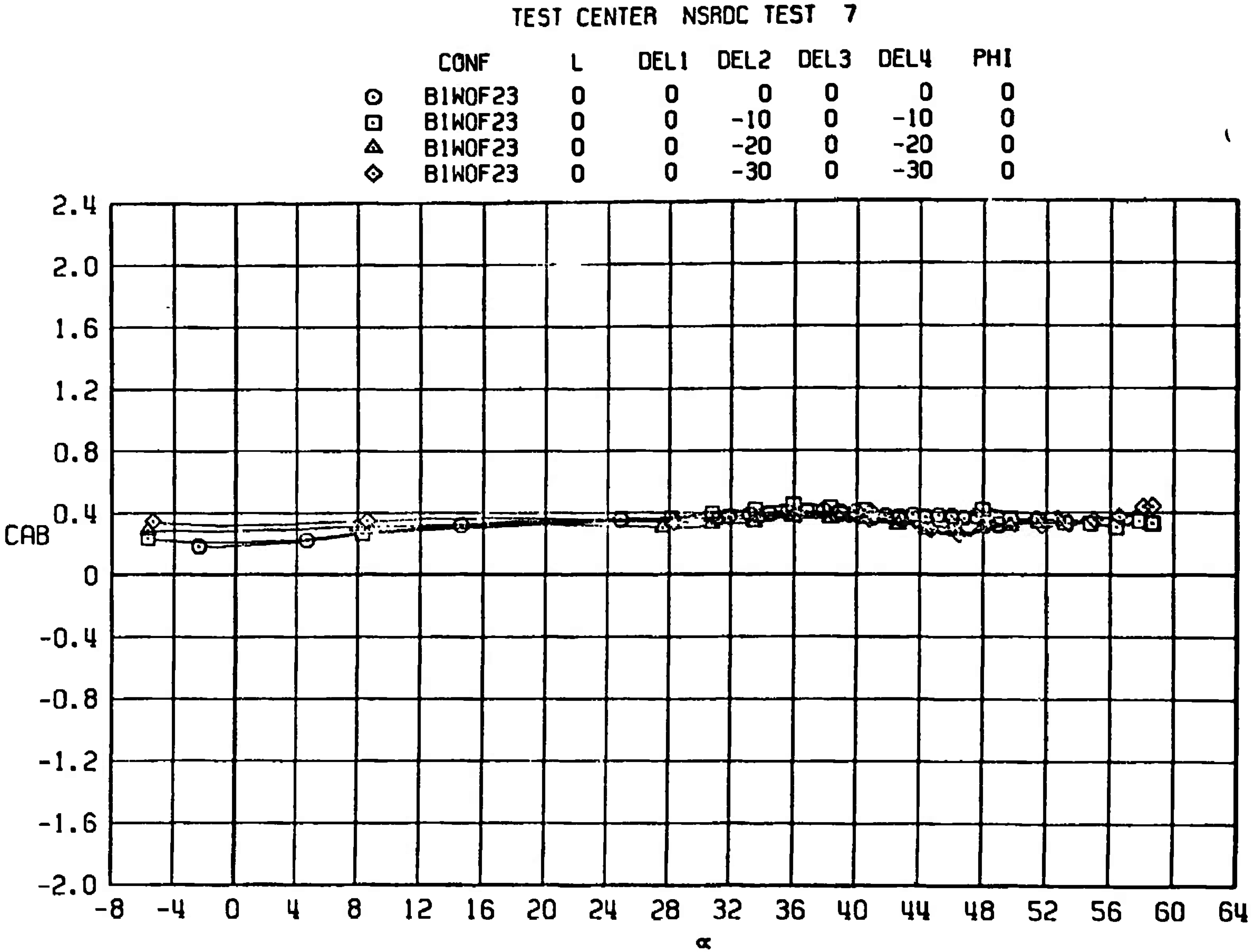

d. CAB versus α

Figure 54. Continued.

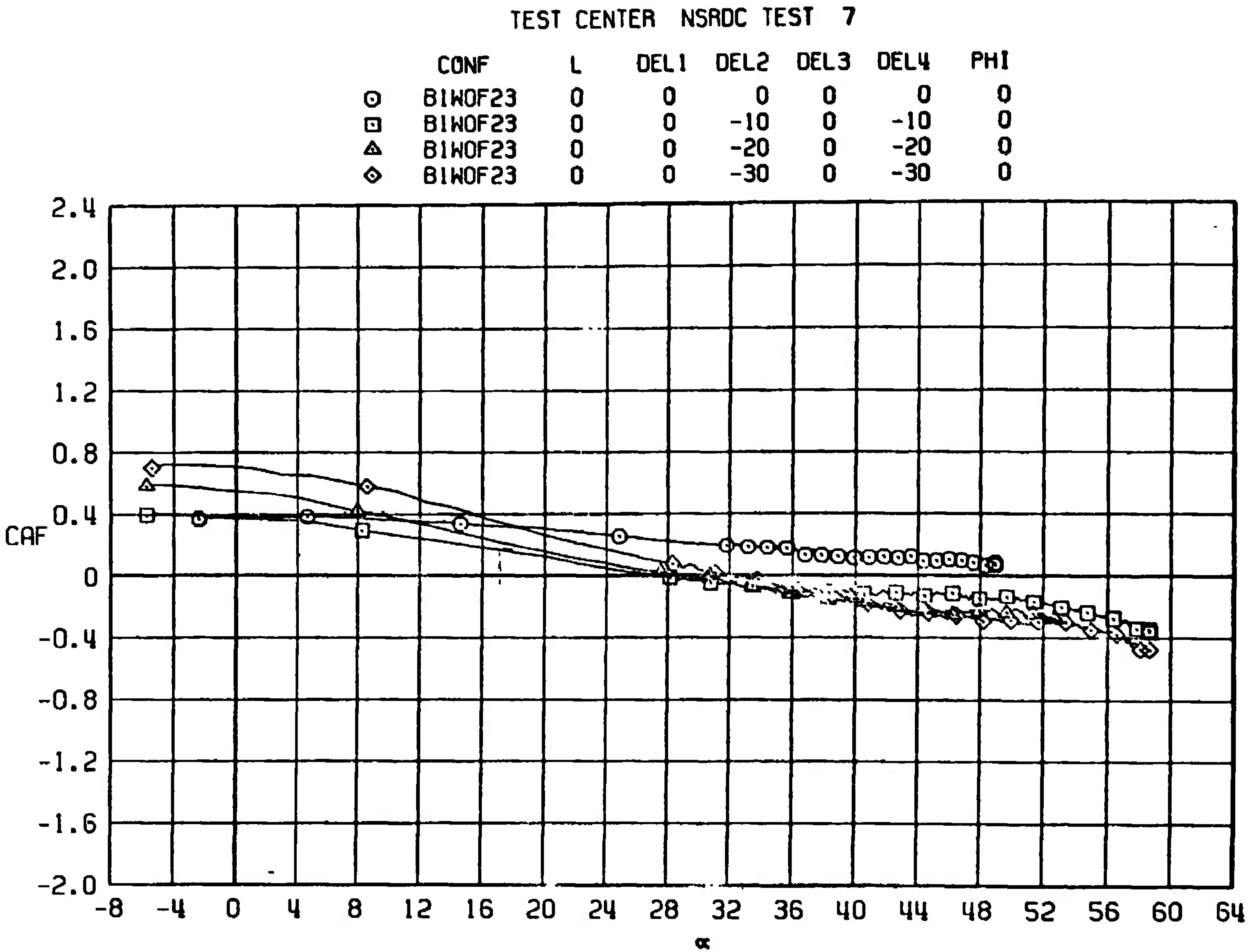

e. CAF versus α
Figure 54. Continued.

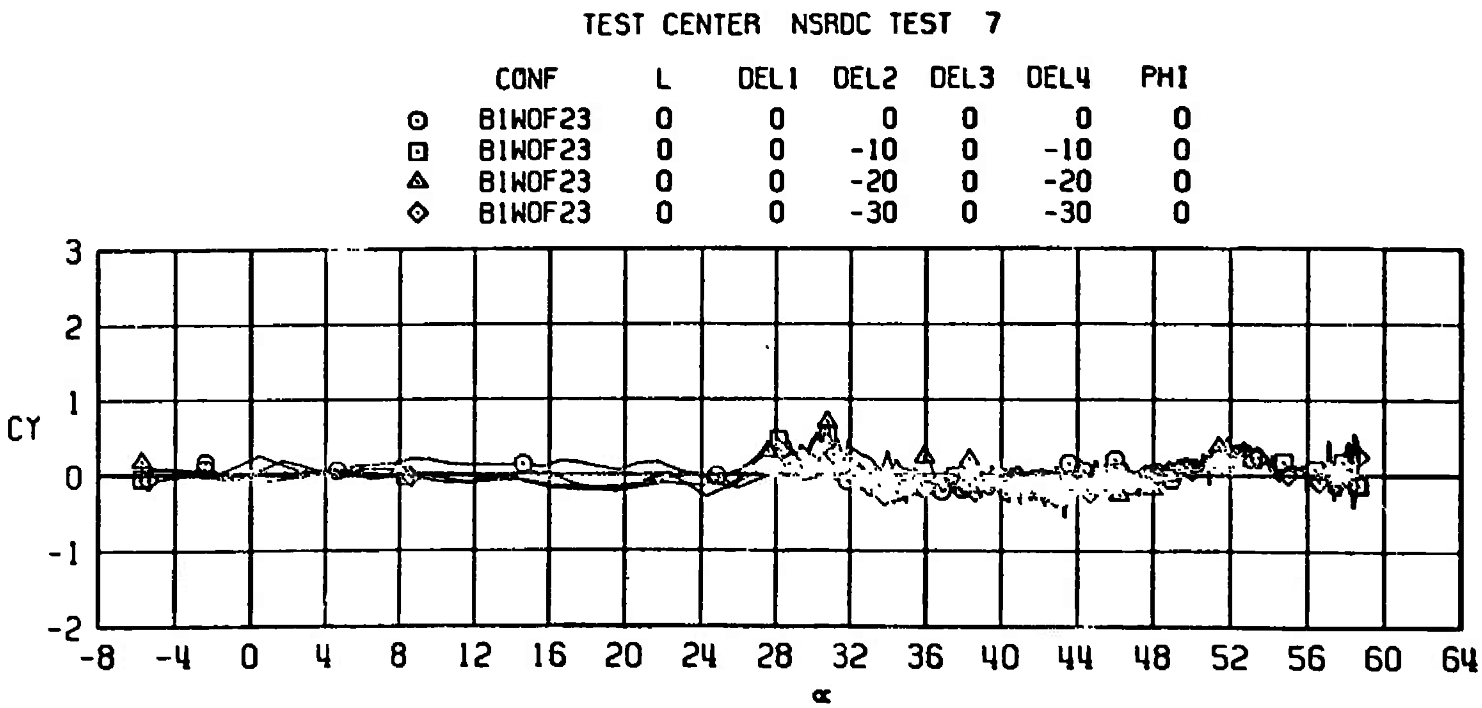

f. CY versus α

Figure 54. Continued.

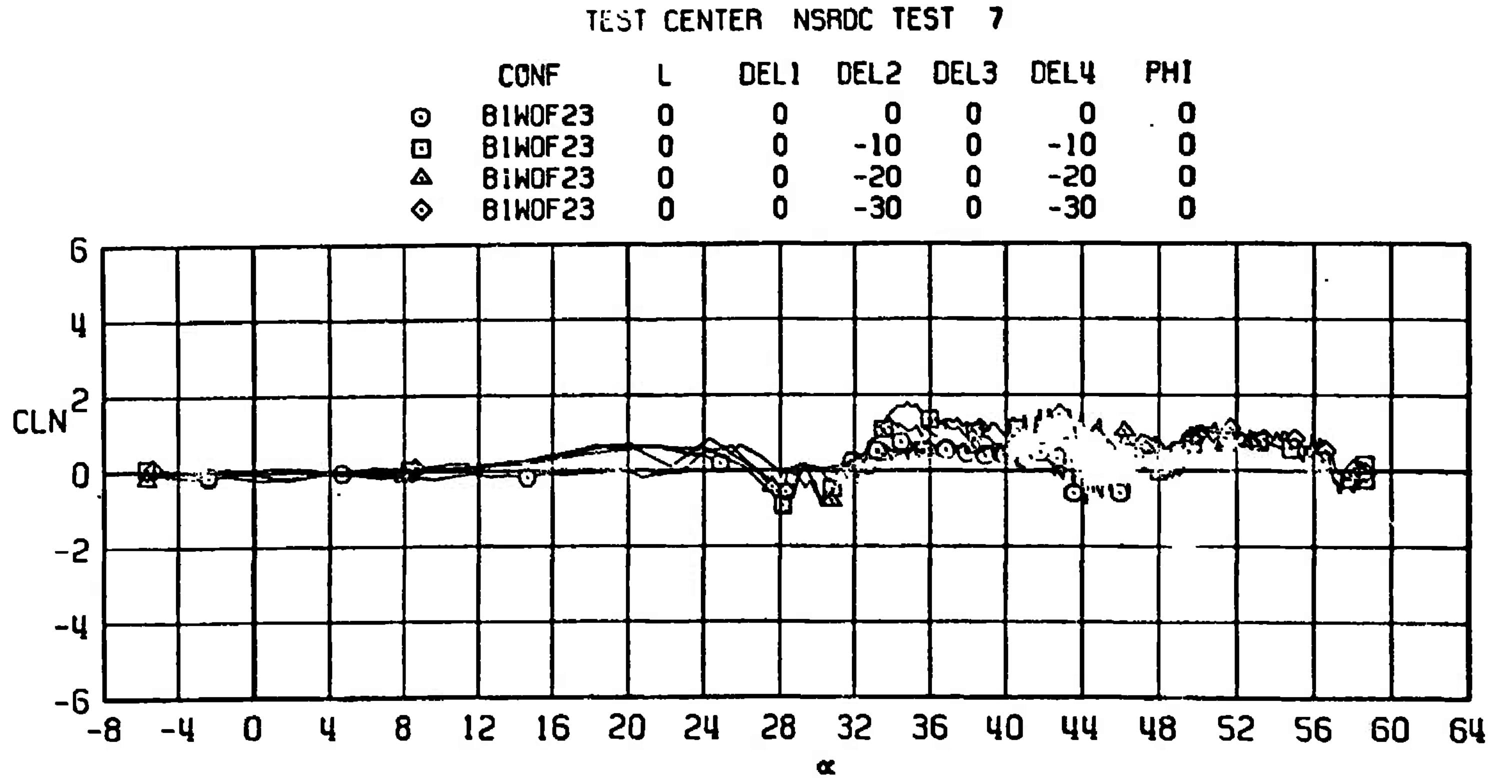

g. CLN versus α
Figure 54. Continued.

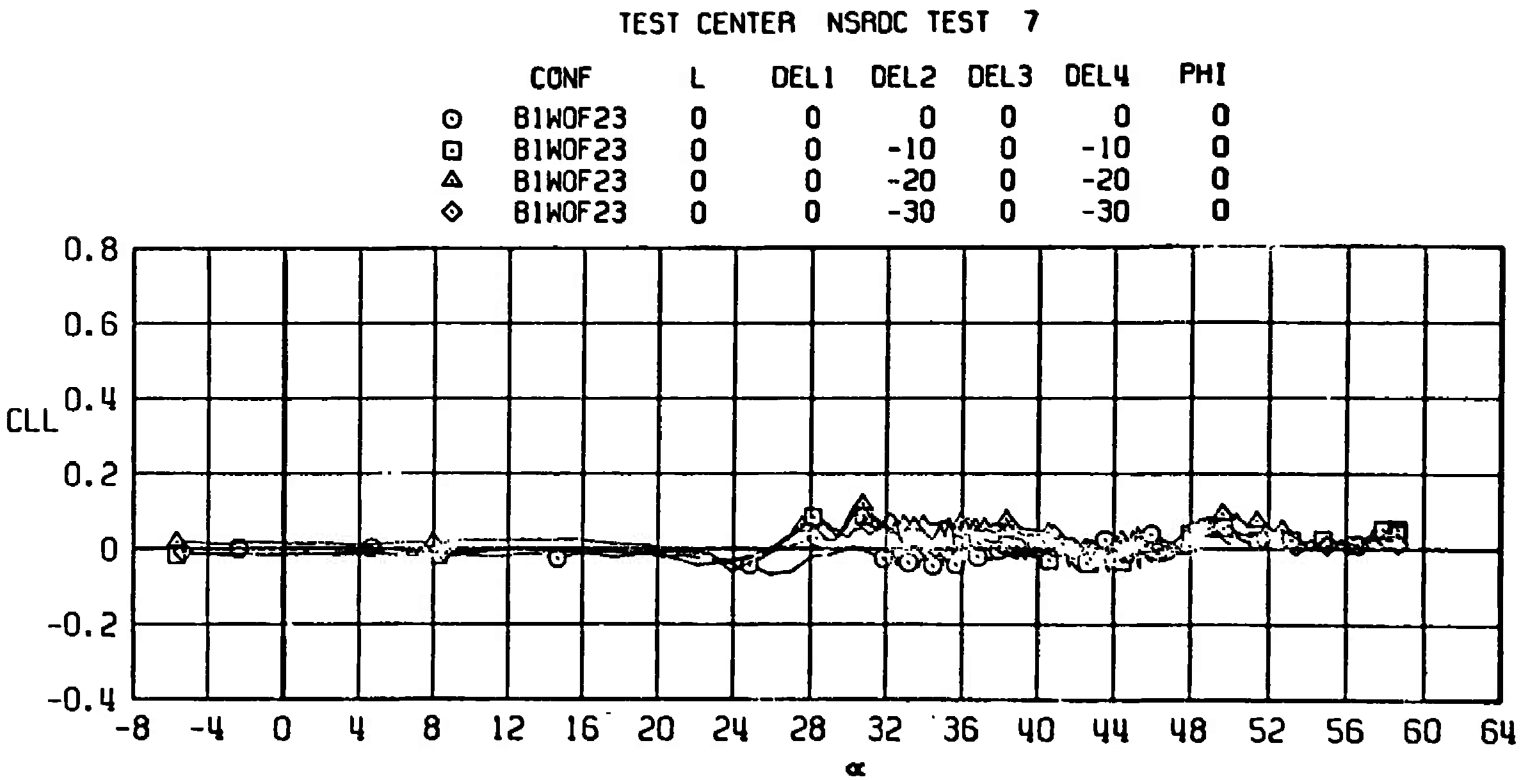

h. CLL versus α

Figure 54. Continued.

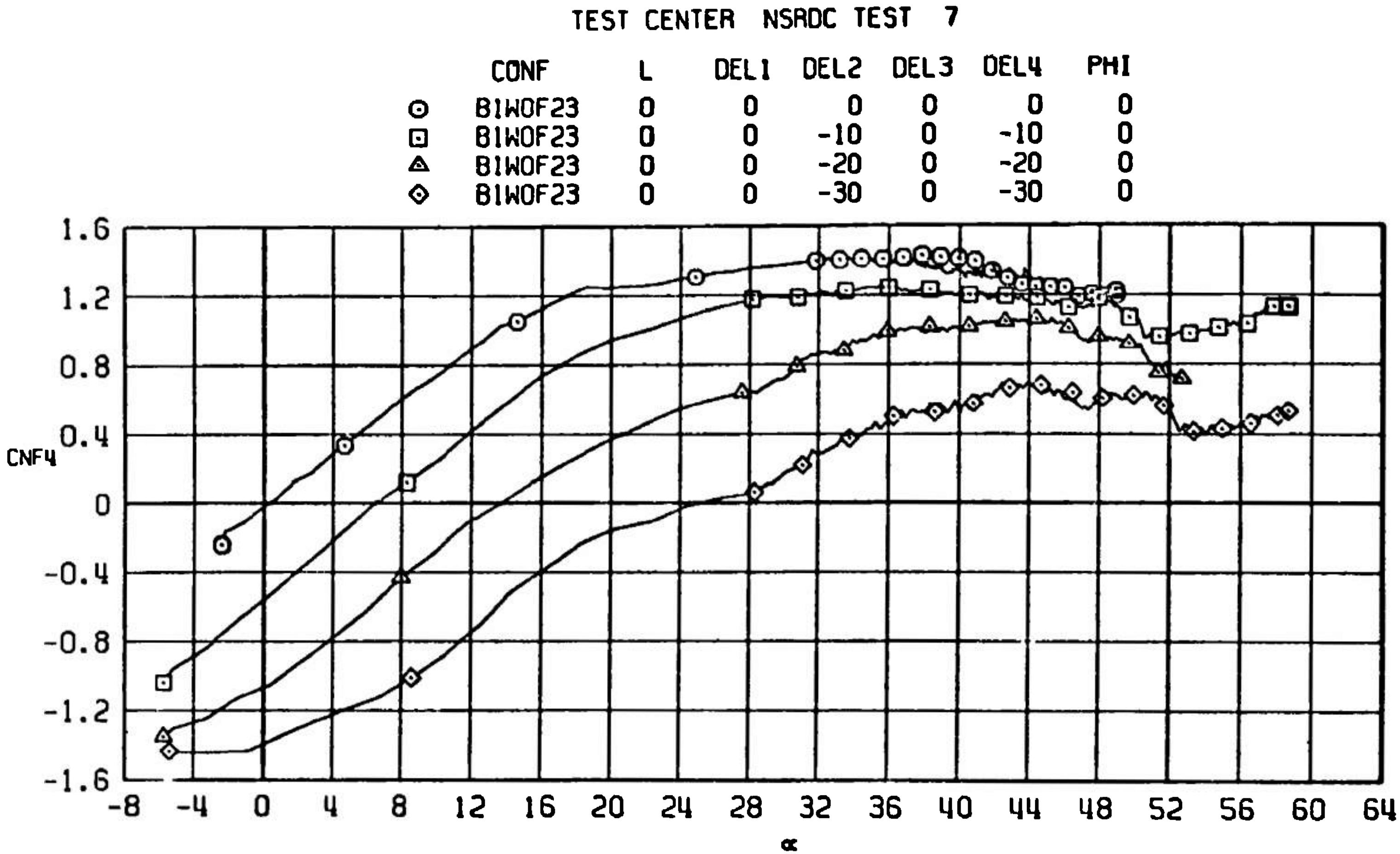

i. CNF4 versus α
Figure 54. Continued.

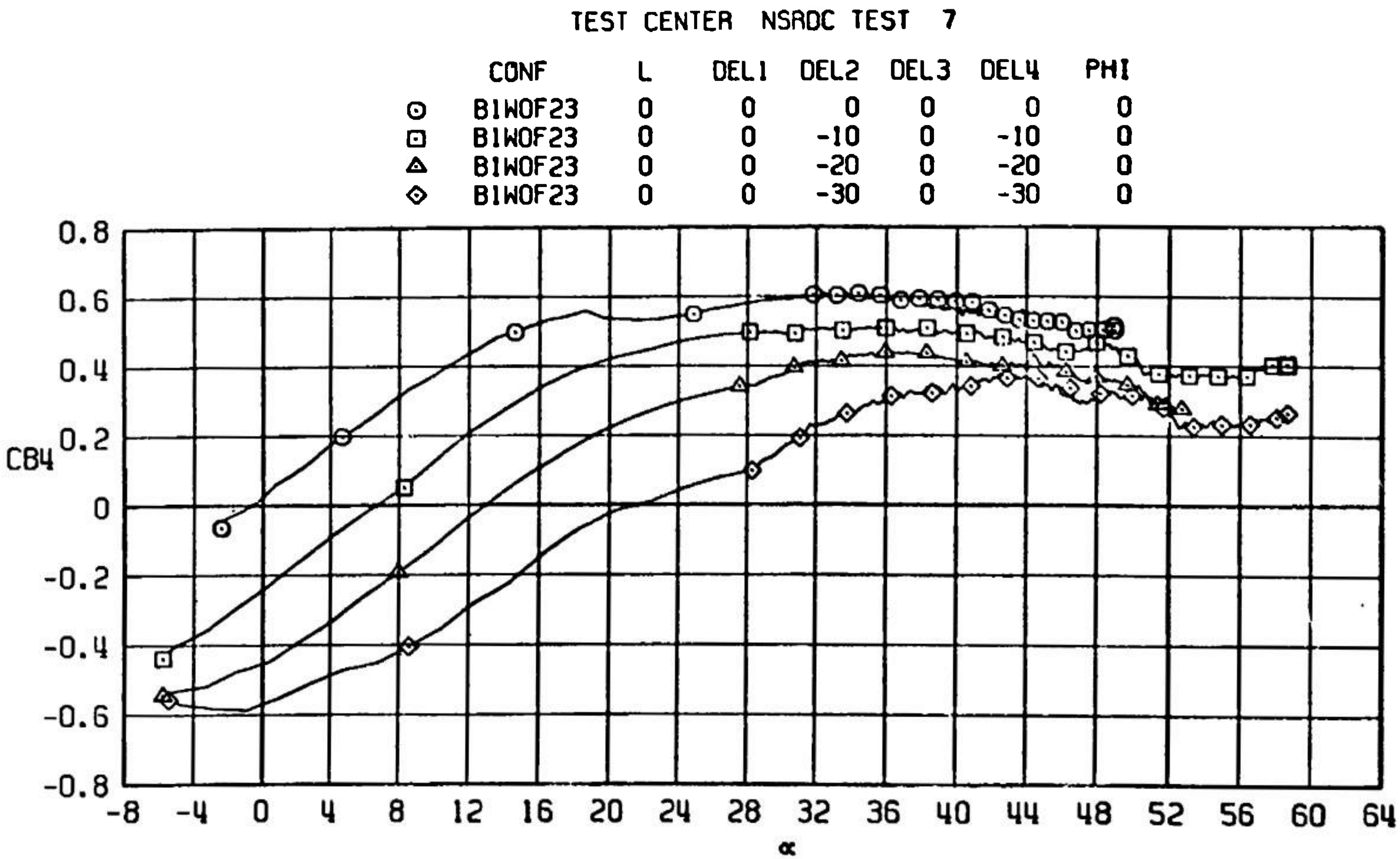

j. CB4 versus α
Figure 54. Continued.

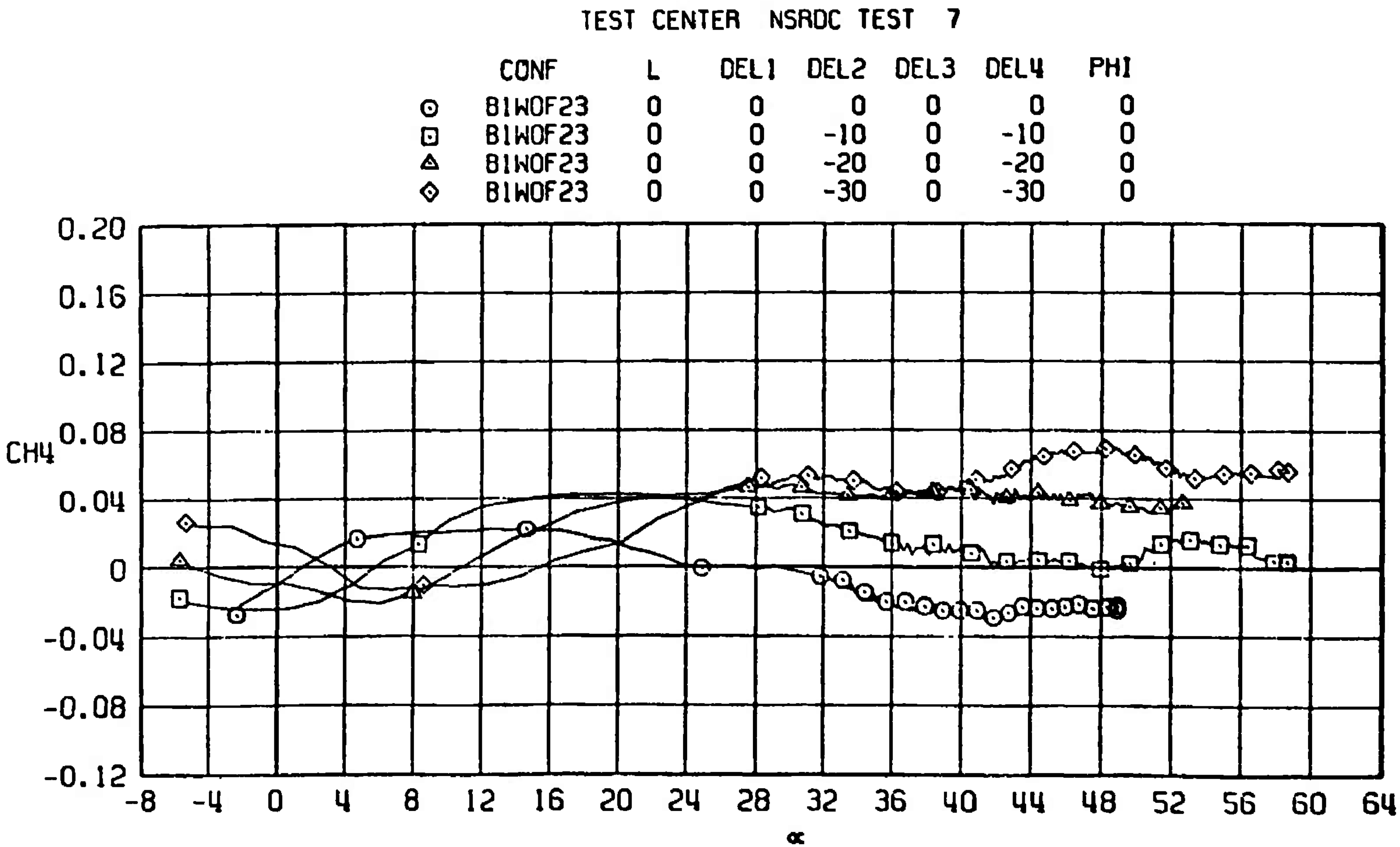

k. CH4 versus α

Figure 54. Concluded.

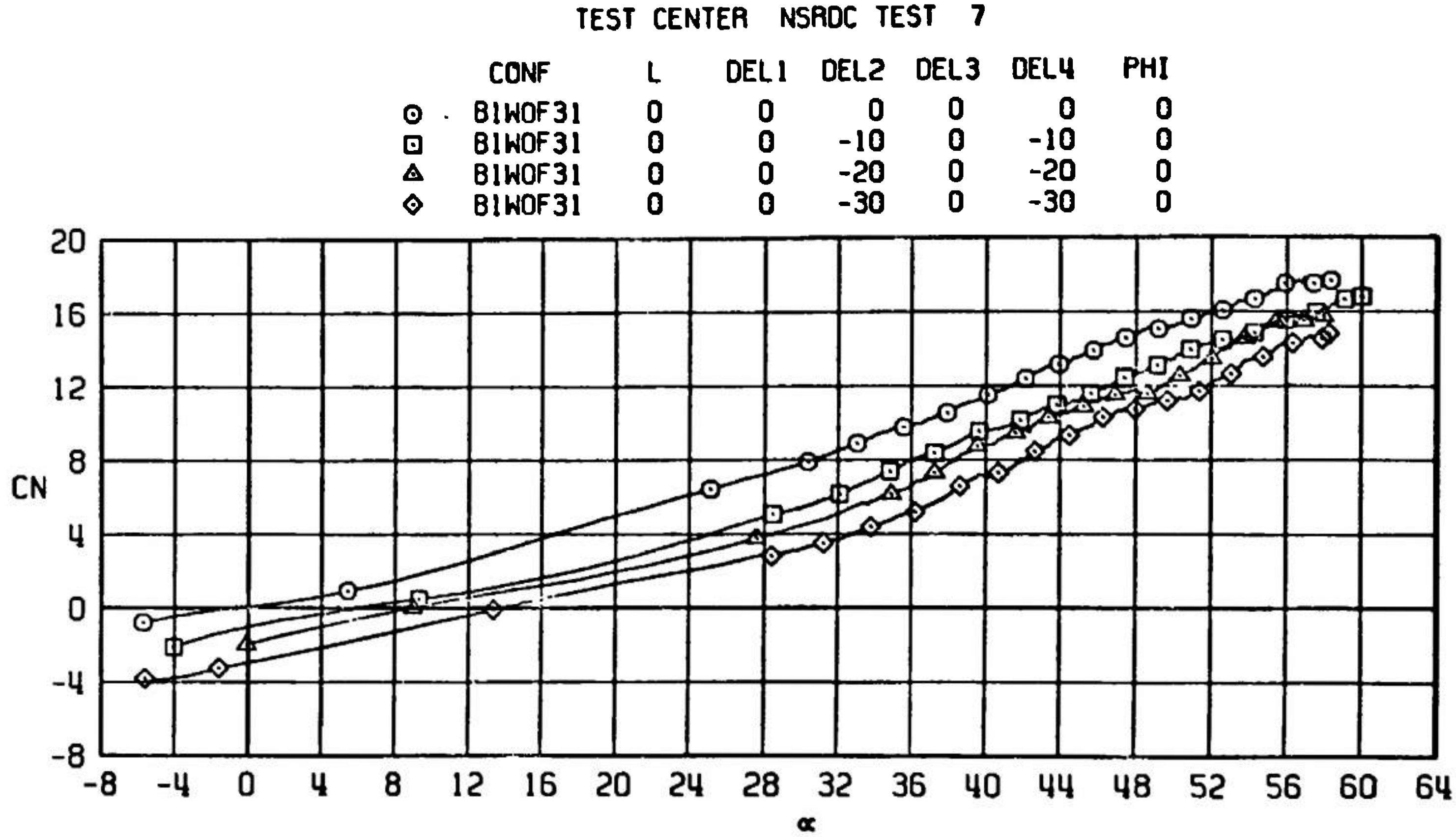

a. CN versus α

Figure 55. Test No. 7, comparison of aerodynamic coefficients of configuration B1W0F31 for various deflections of tail fins No. 2 and 4 at M_∞ = 0.8.

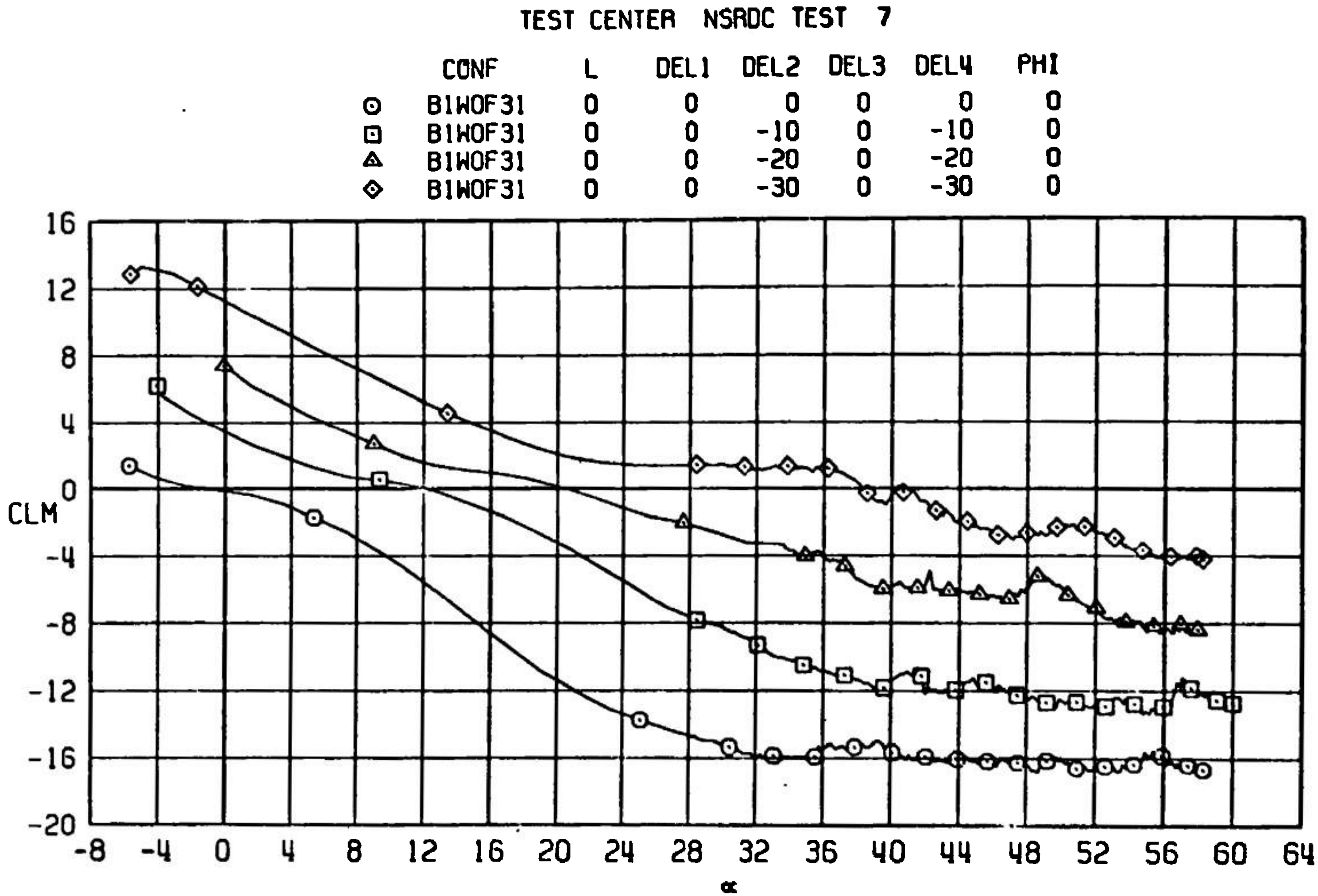

b. CLM versus α

Figure 55. Continued.

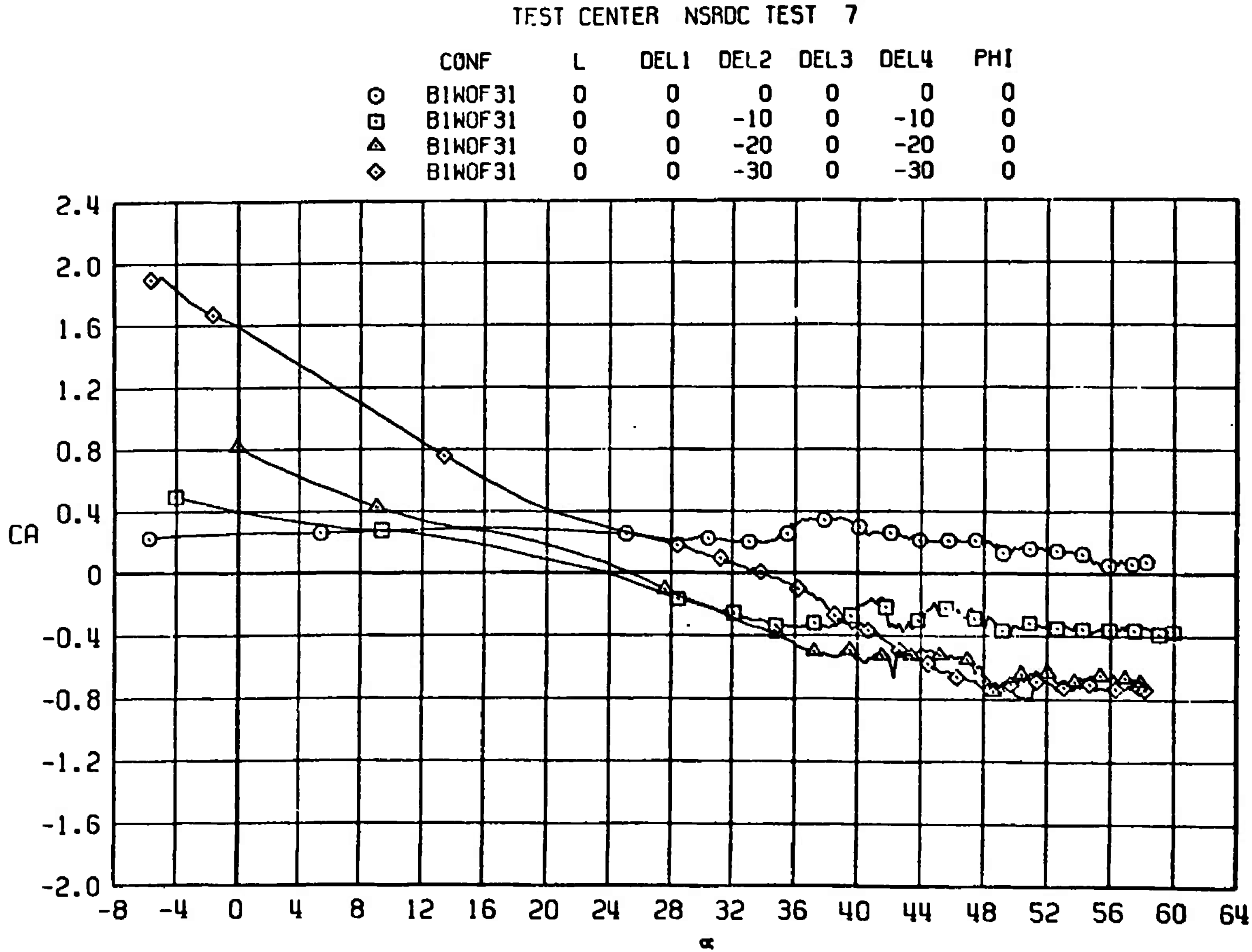

c. CA versus α

Figure 55. Continued.

TEST CENTER NSRDC TEST 7

	CONF	L	DEL1	DEL2	DEL3	DEL4	PHI
⊙	B1W0F31	0	0	0	0	0	0
⊡	B1W0F31	0	0	-10	0	-10	0
△	B1W0F31	0	0	-20	0	-20	0
◇	B1W0F31	0	0	-30	0	-30	0

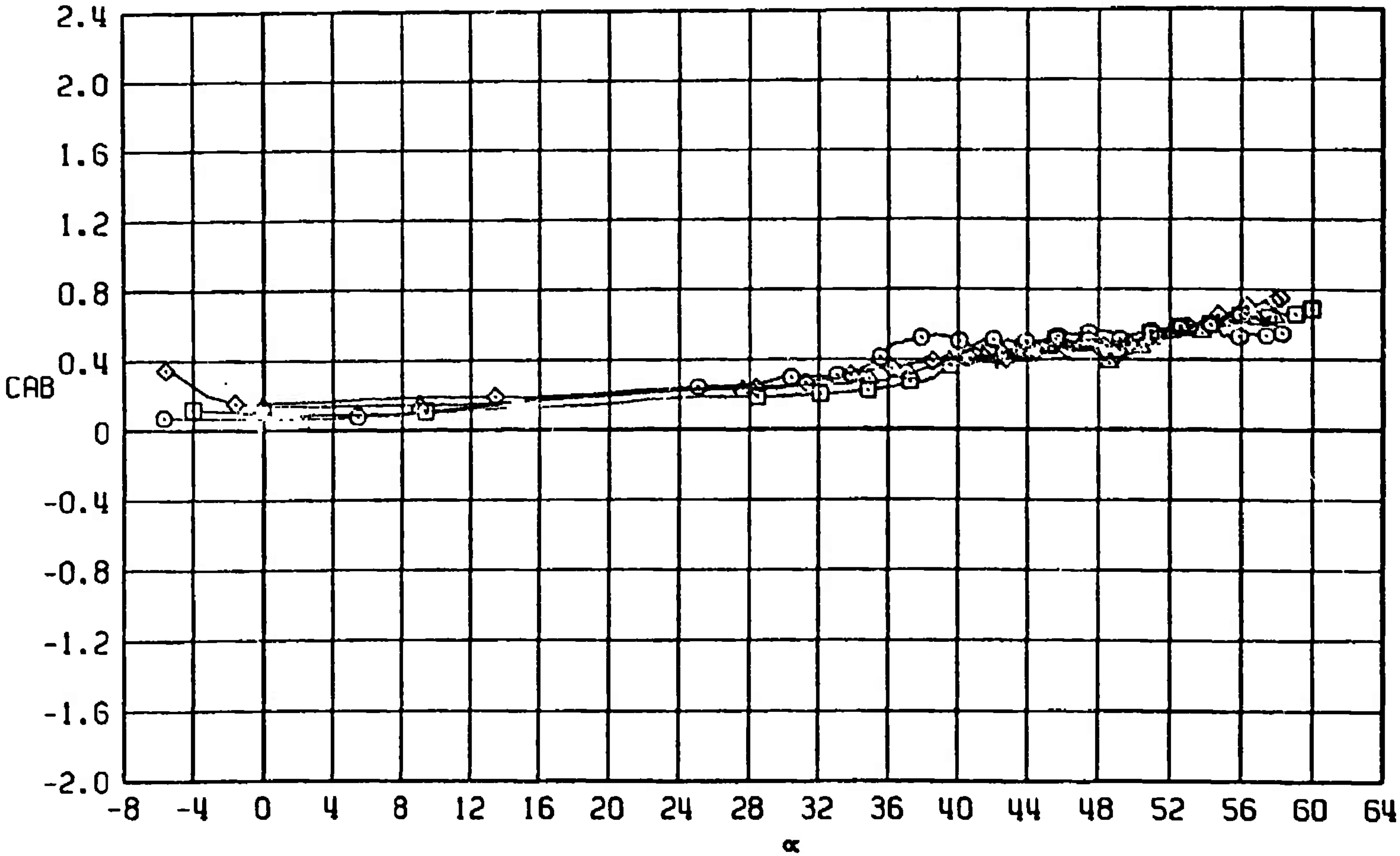

d. CAB versus α

Figure 55. Continued.

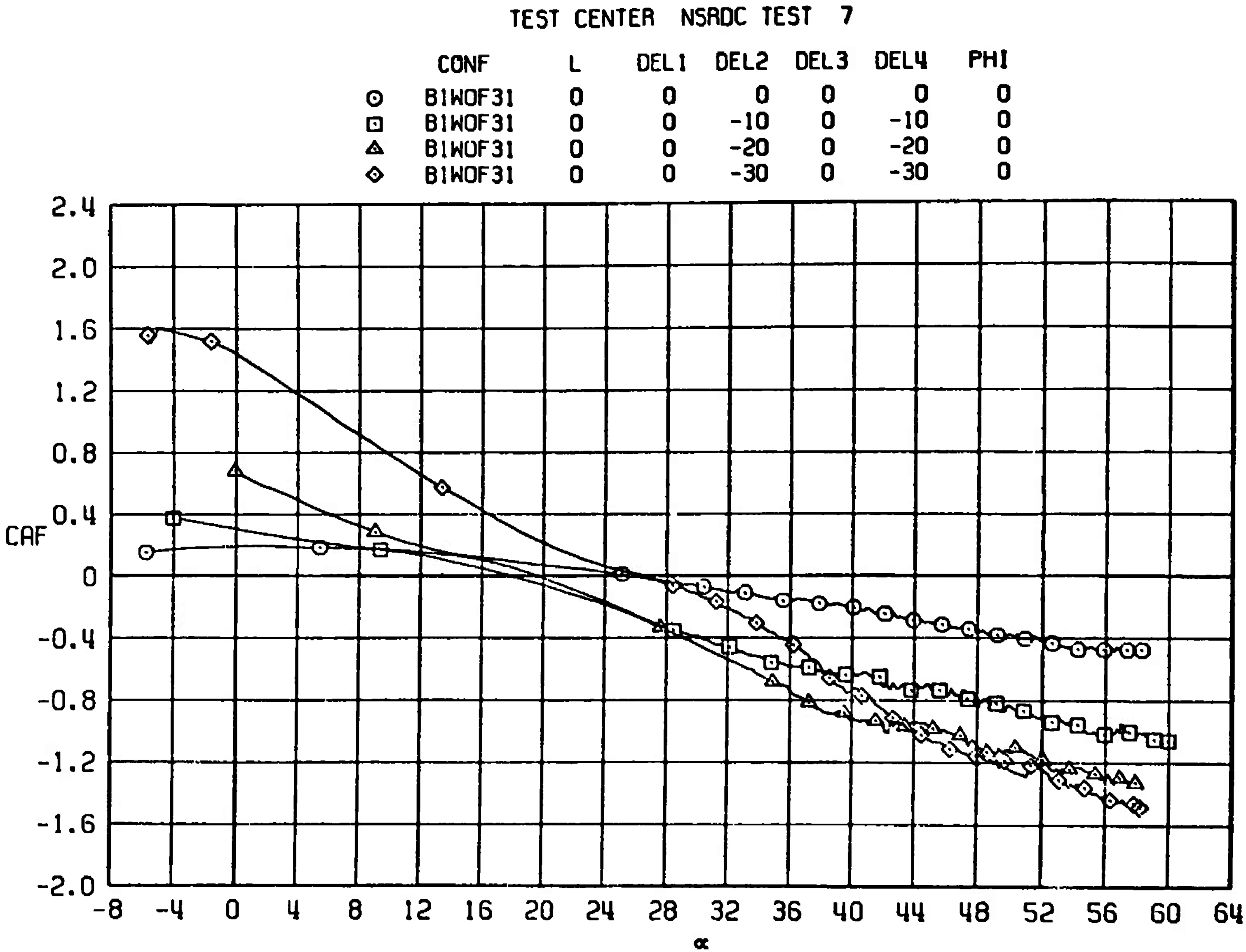

e. CAF versus α
Figure 55. Continued.

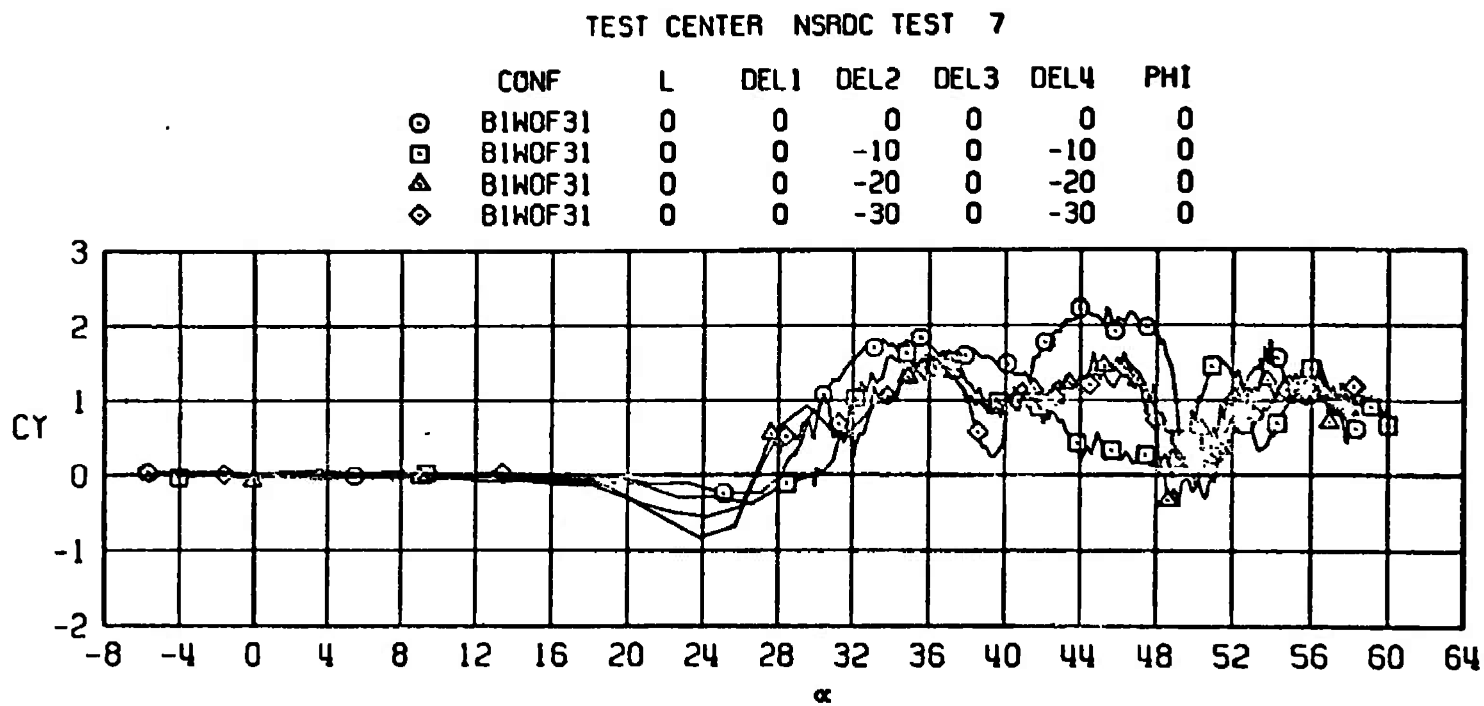

f. CY versus α
Figure 55. Continued.

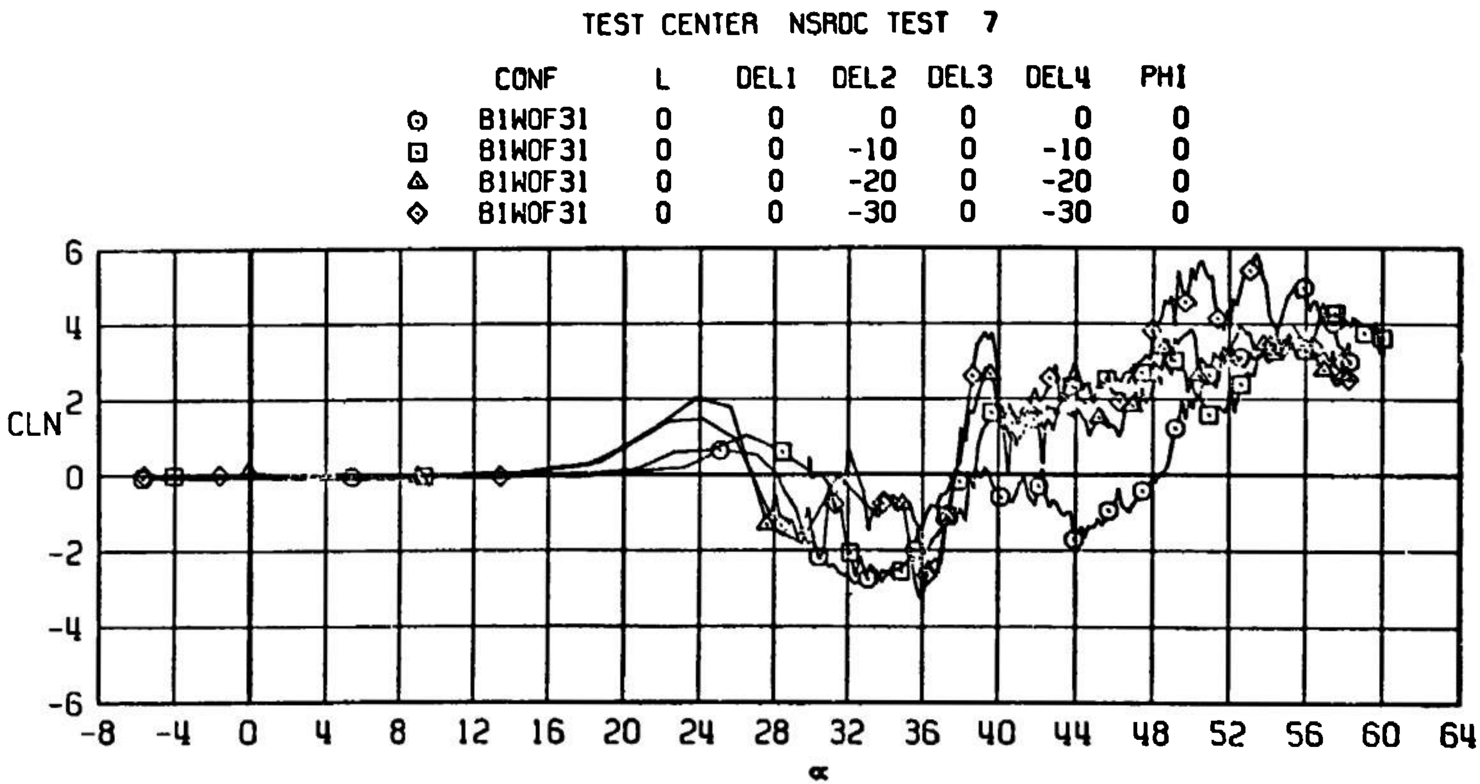

g. CLN versus α
Figure 55. Continued.

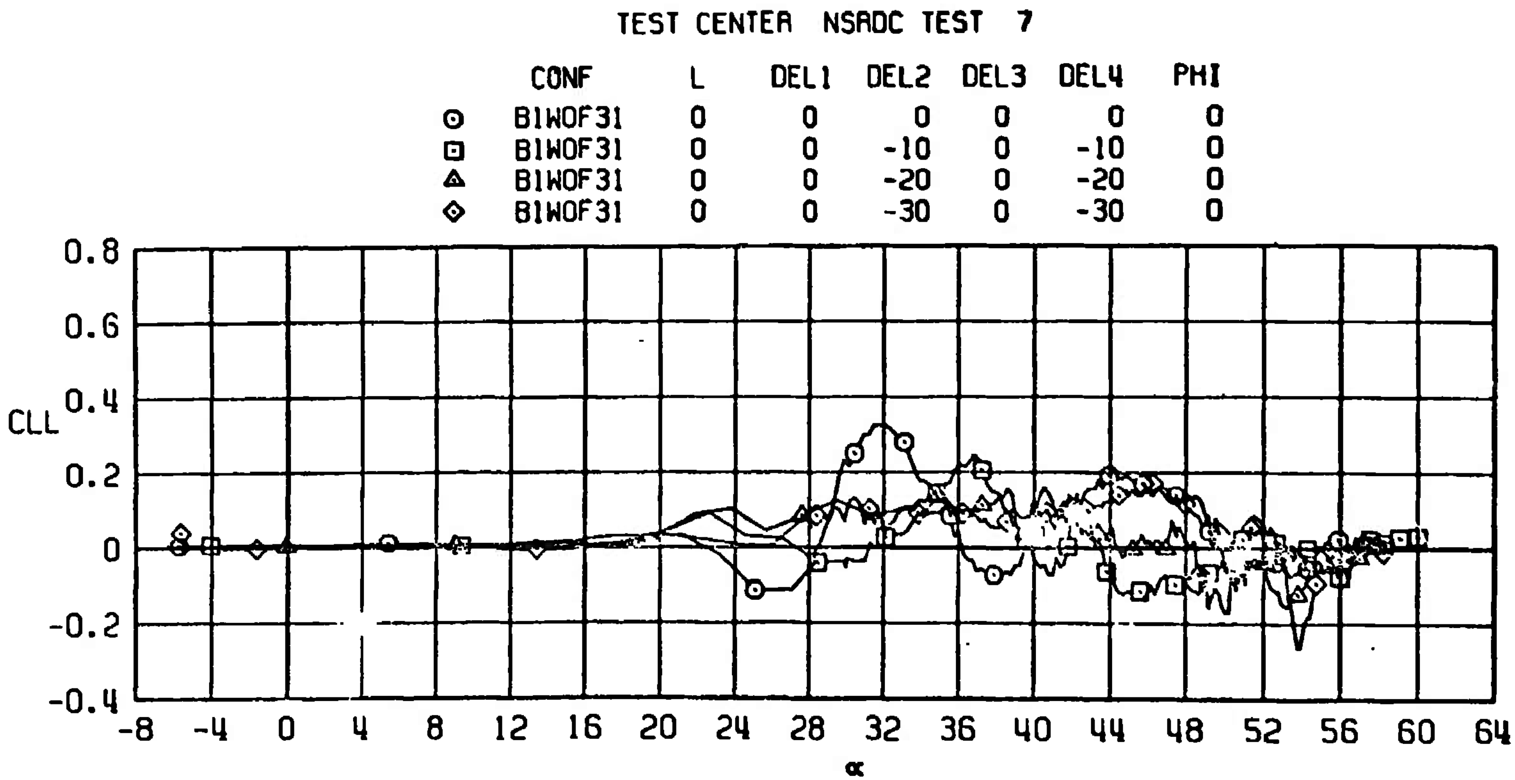

h. CLL versus α
Figure 55. Continued.

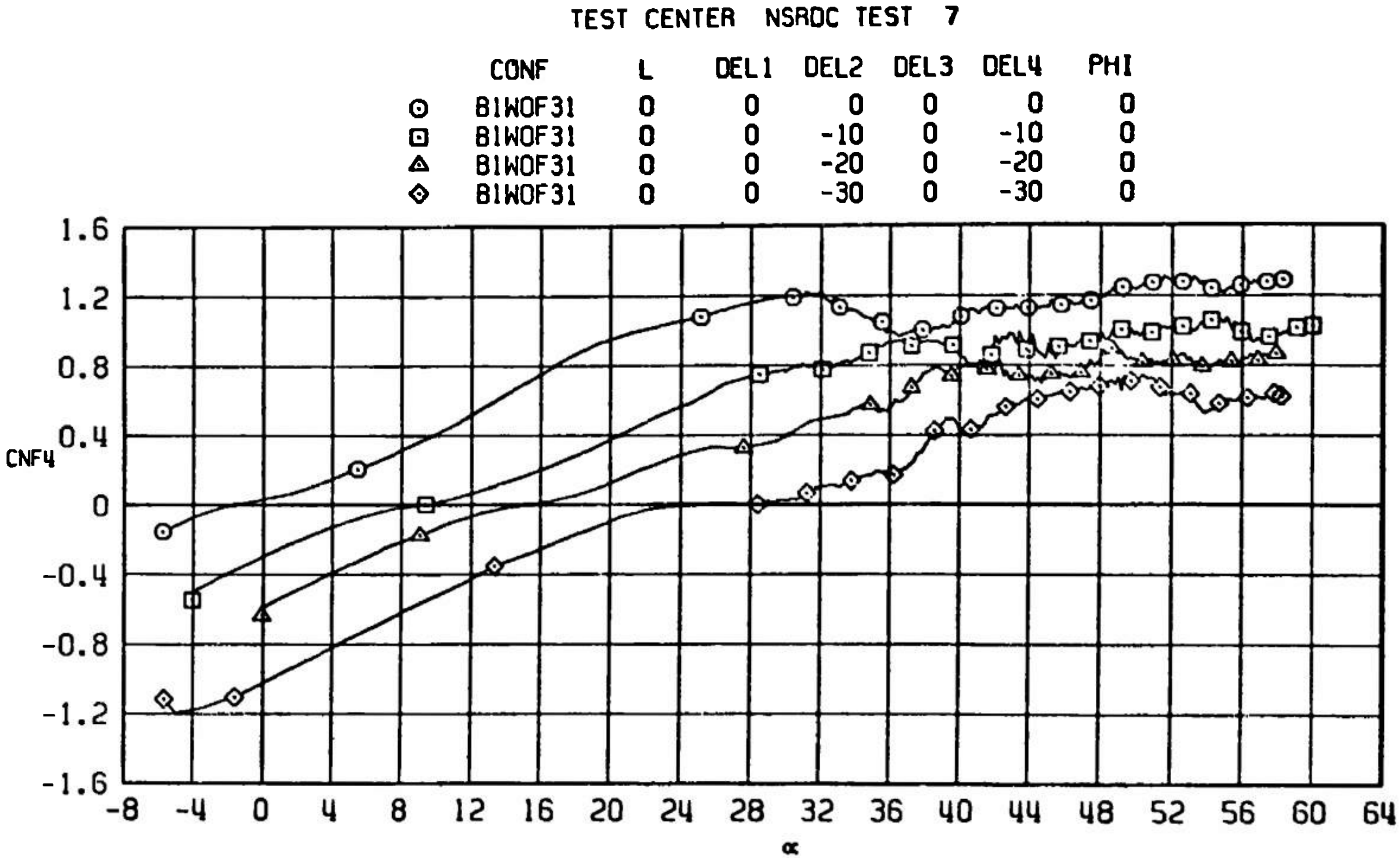

i. CNF4 versus α
Figure 55. Continued.

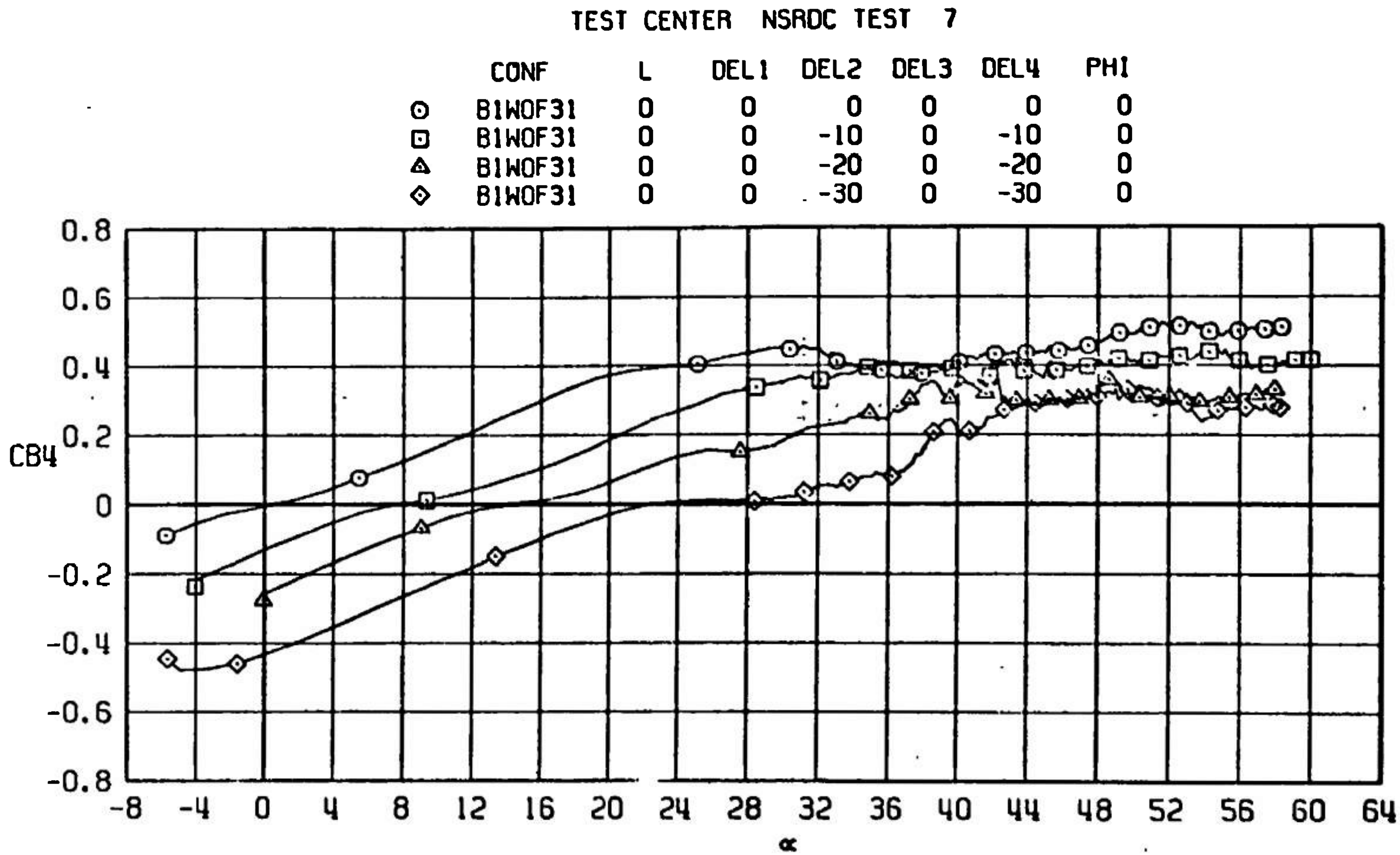

j. CB4 versus α
Figure 55. Continued.

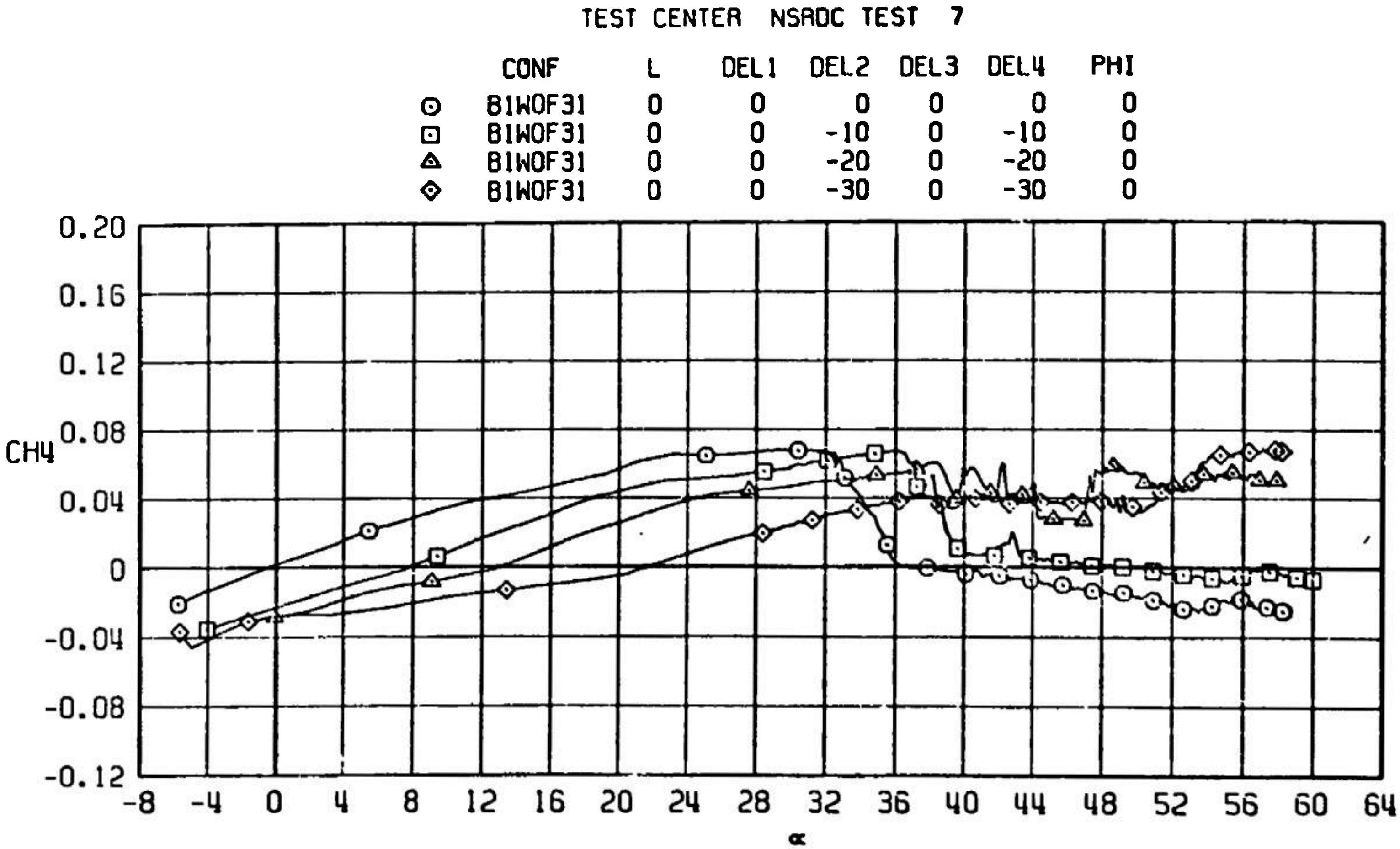

k. CH4 versus α
Figure 55. Concluded.

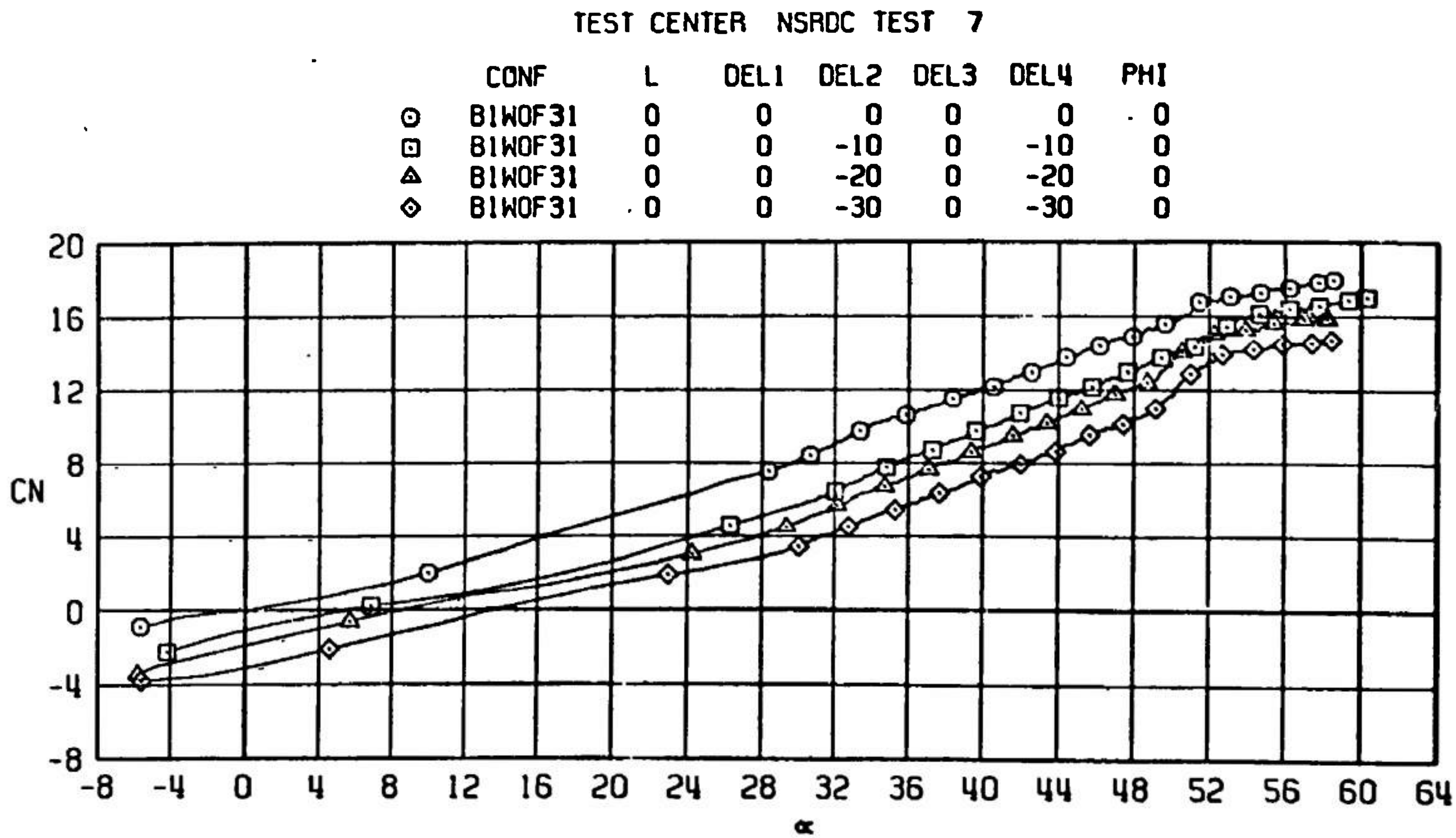

a. CN versus α

Figure 56. Test No. 7, comparison of aerodynamic coefficients of configuration B1W0F31 for various deflections of tail fins No. 2 and 4 at M_∞ = 0.9.

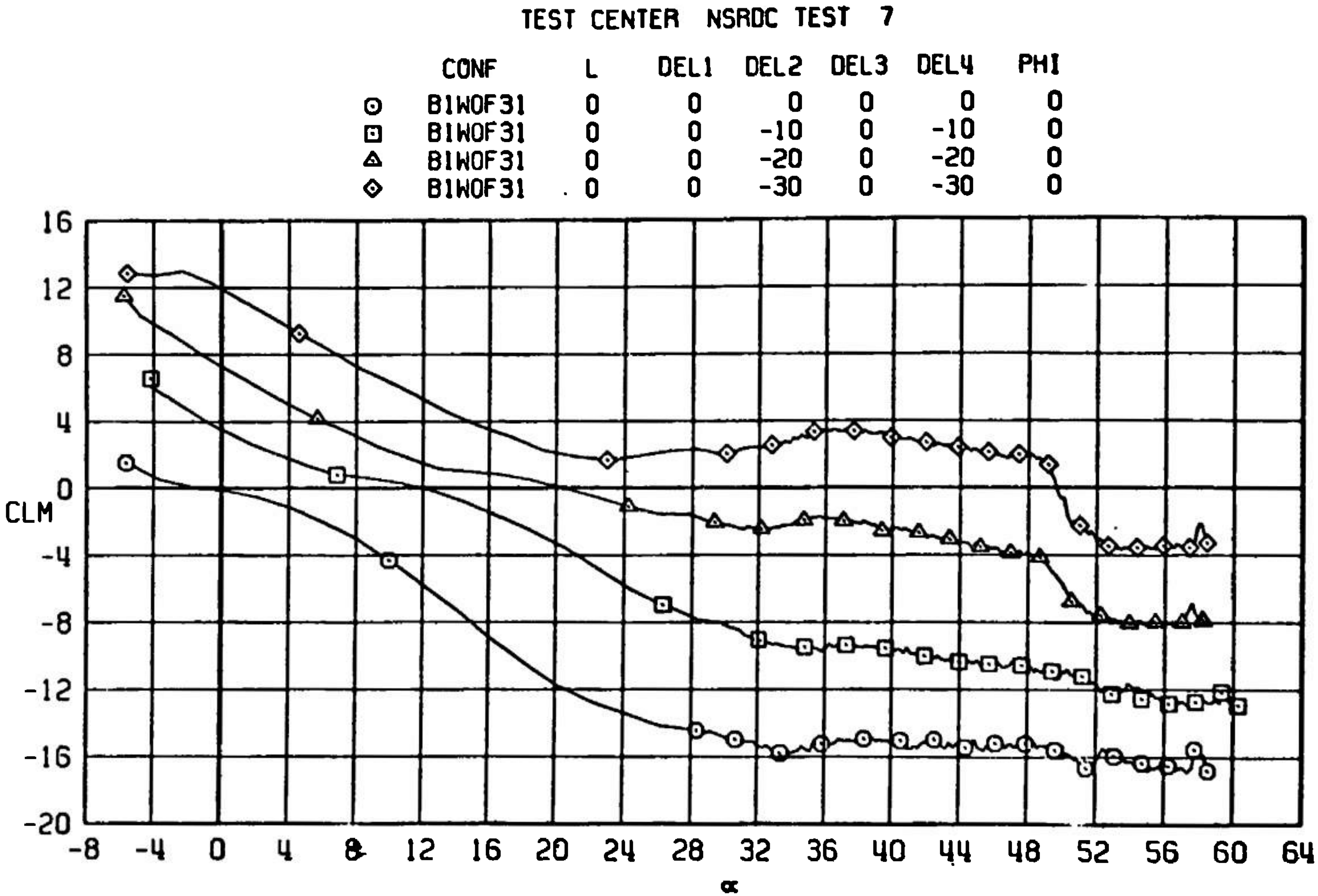

b. CLM versus a

Figure 56. Continued.

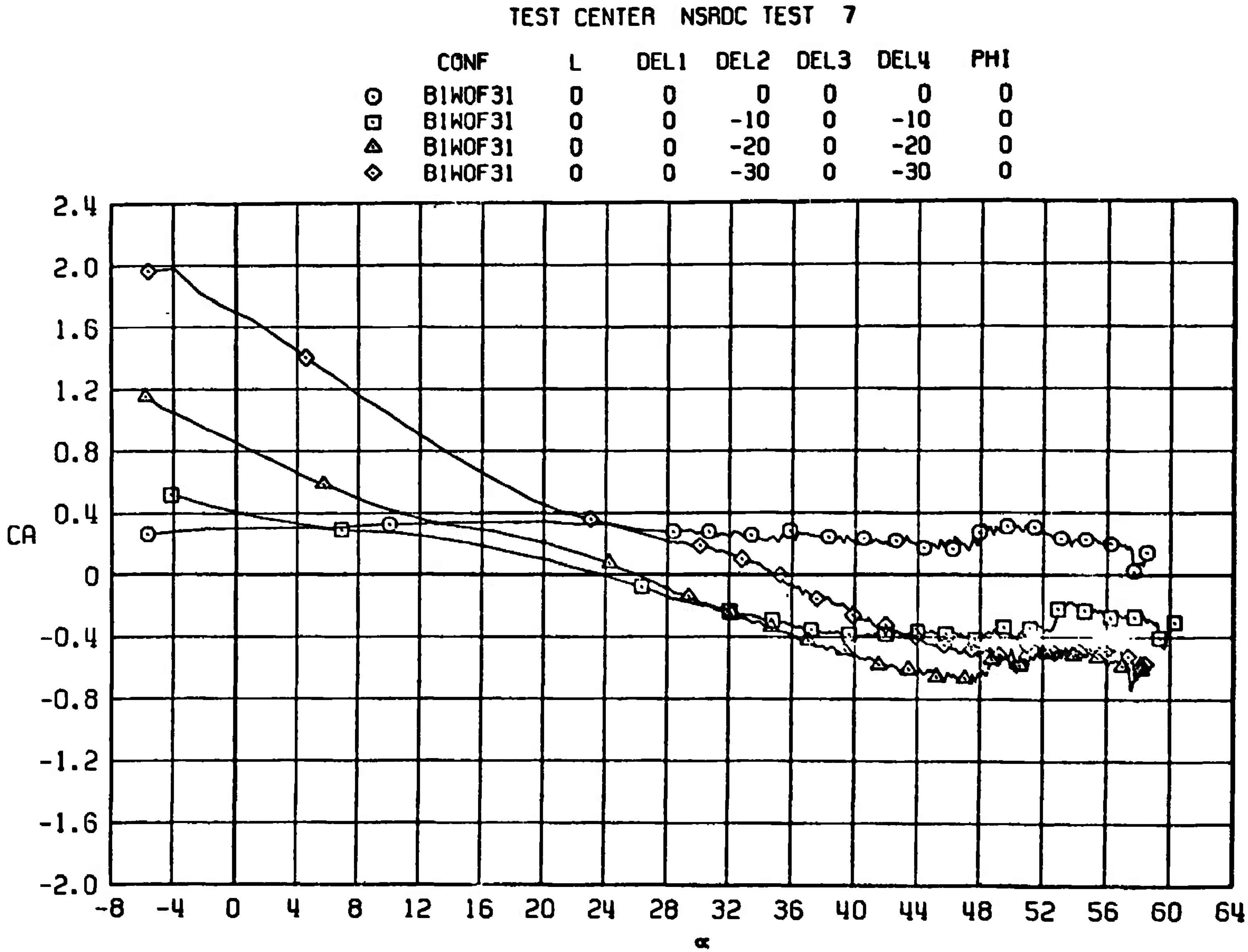

c. CA versus α
Figure 56. Continued.

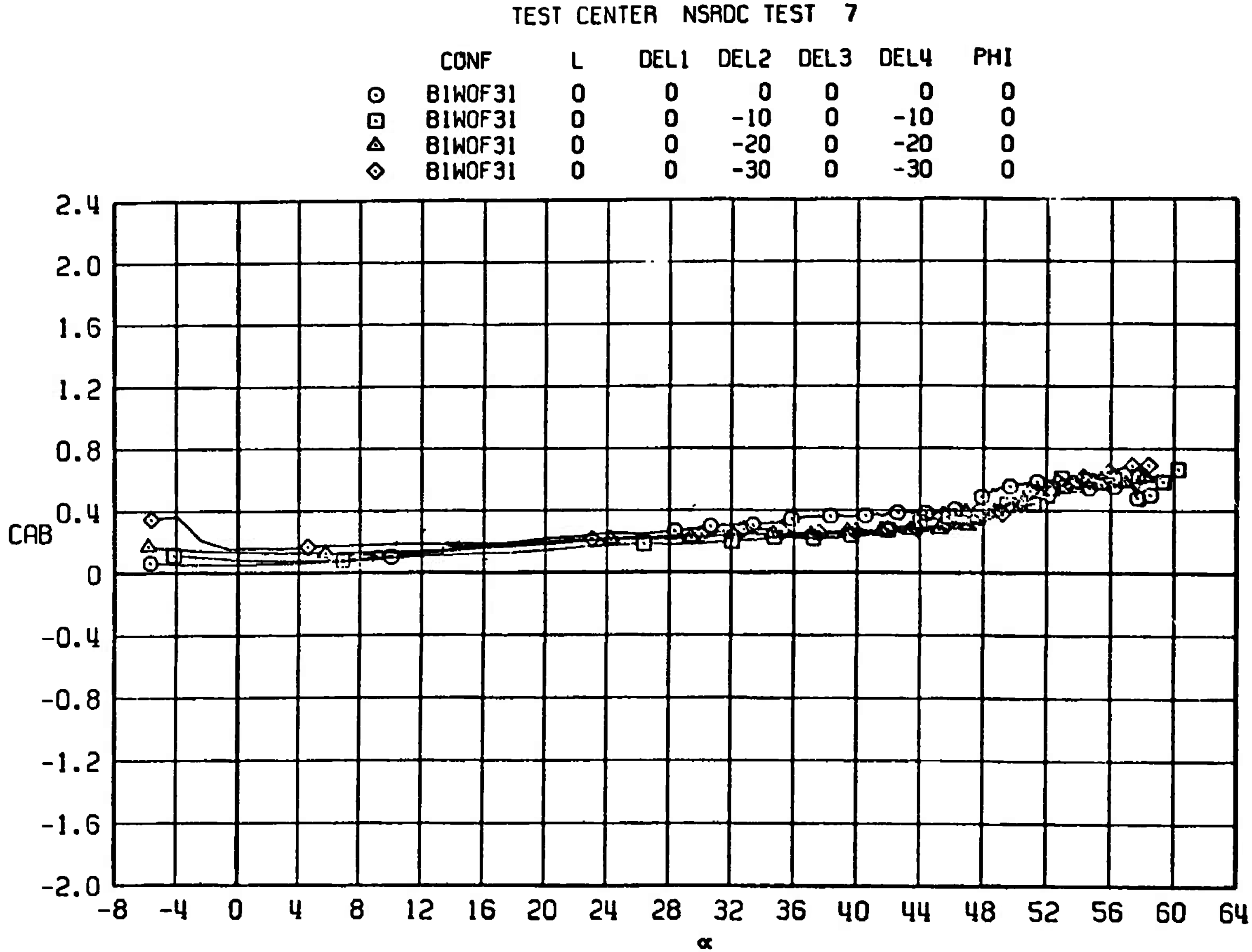

d. CAB versus α
Figure 56. Continued.

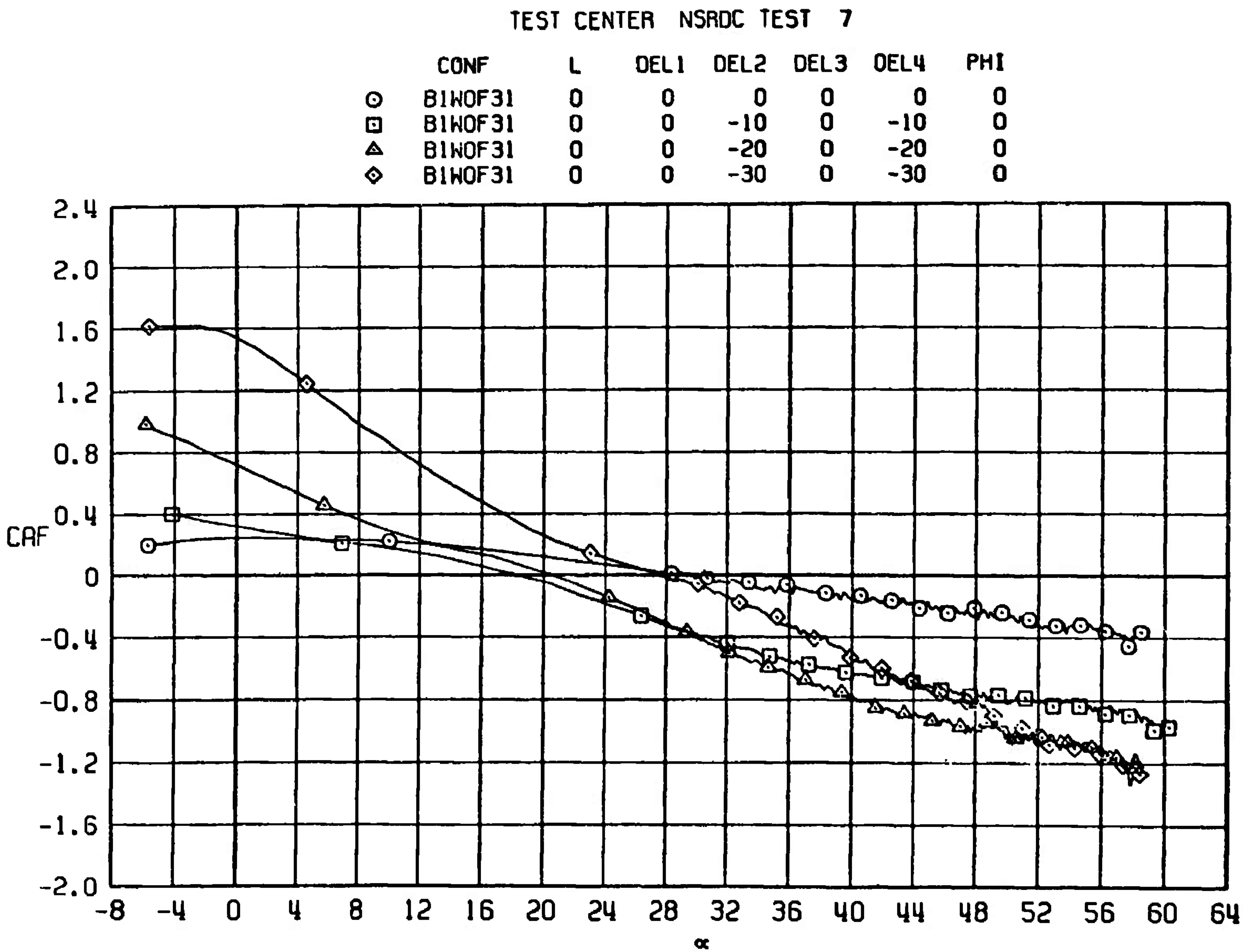

e. CAF versus α

Figure 56. Continued.

TEST CENTER NSRDC TEST 7

	CONF	L	DEL1	DEL2	DEL3	DEL4	PHI
⊙	B1WOF31	0	0	0	0	0	0
⊡	B1WOF31	0	0	-10	0	-10	0
△	B1WOF31	0	0	-20	0	-20	0
◇	B1WOF31	0	0	-30	0	-30	0

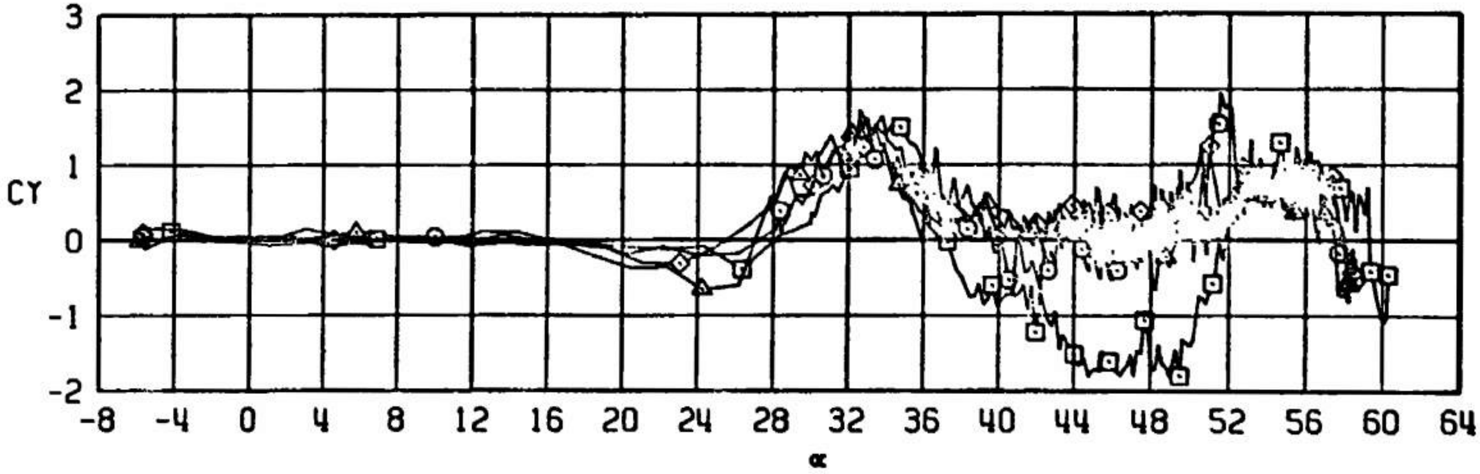

f. CY versus α
Figure 56. Continued.

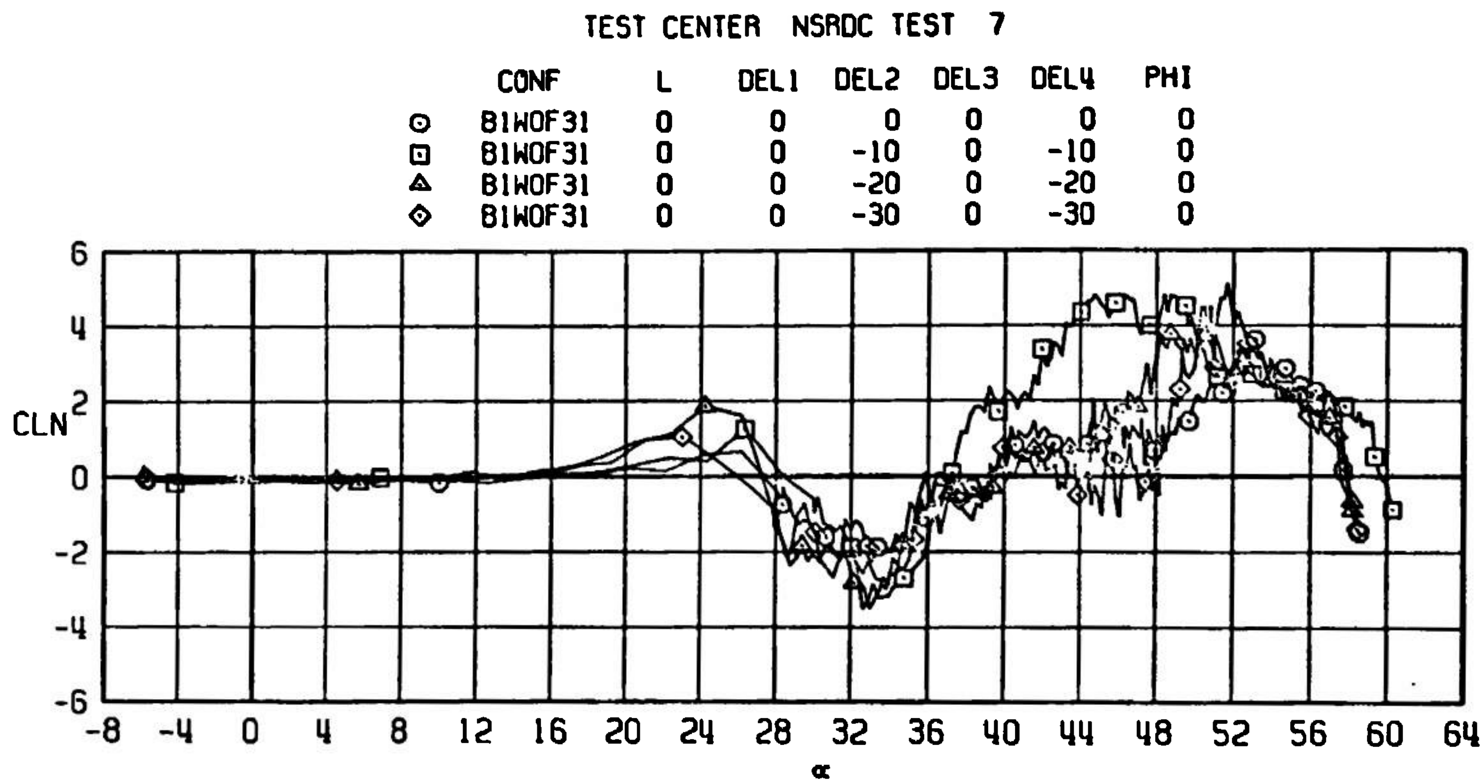

g. CLN versus α
Figure 56. Continued.

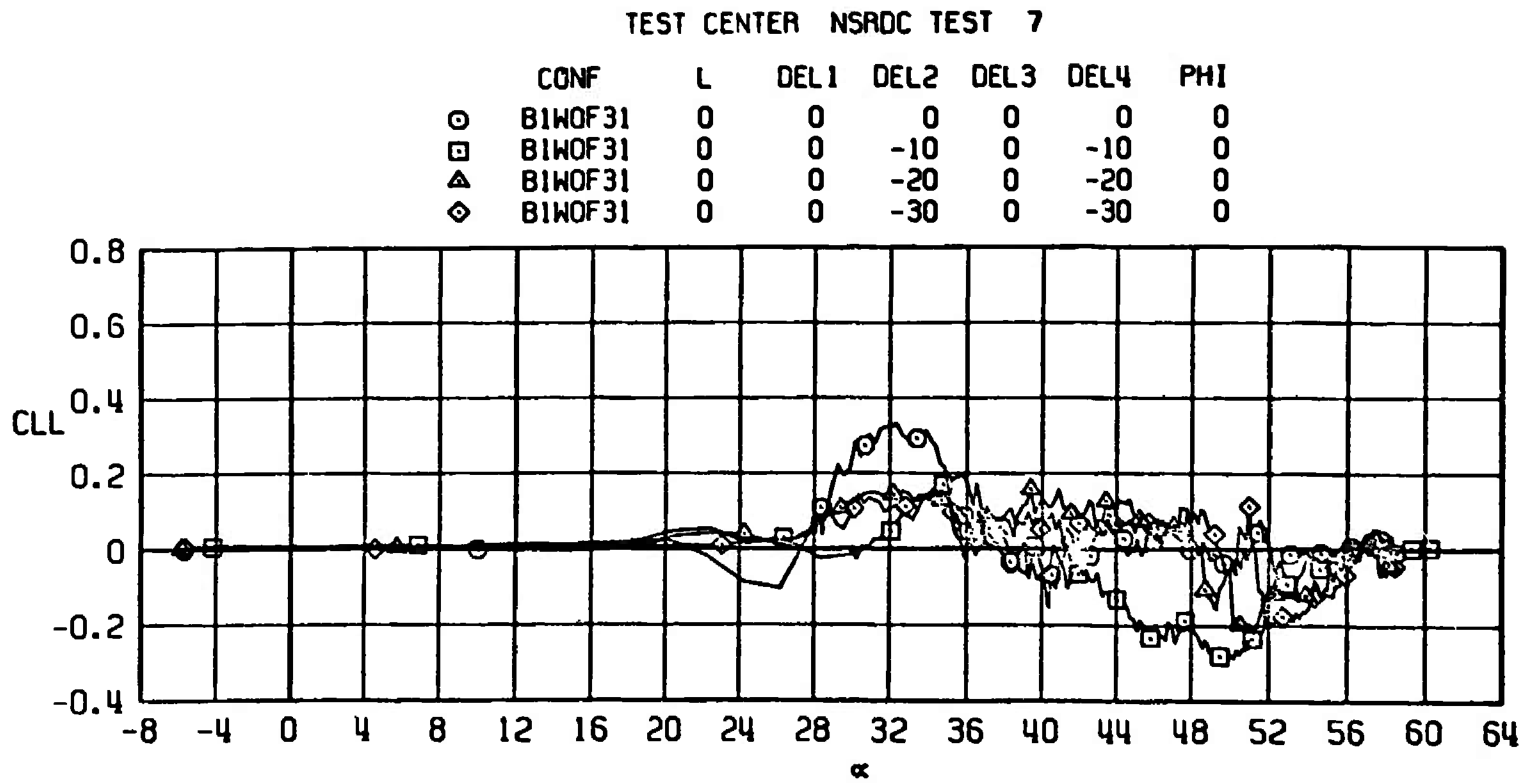

h. CLL versus α
Figure 56. Continued.

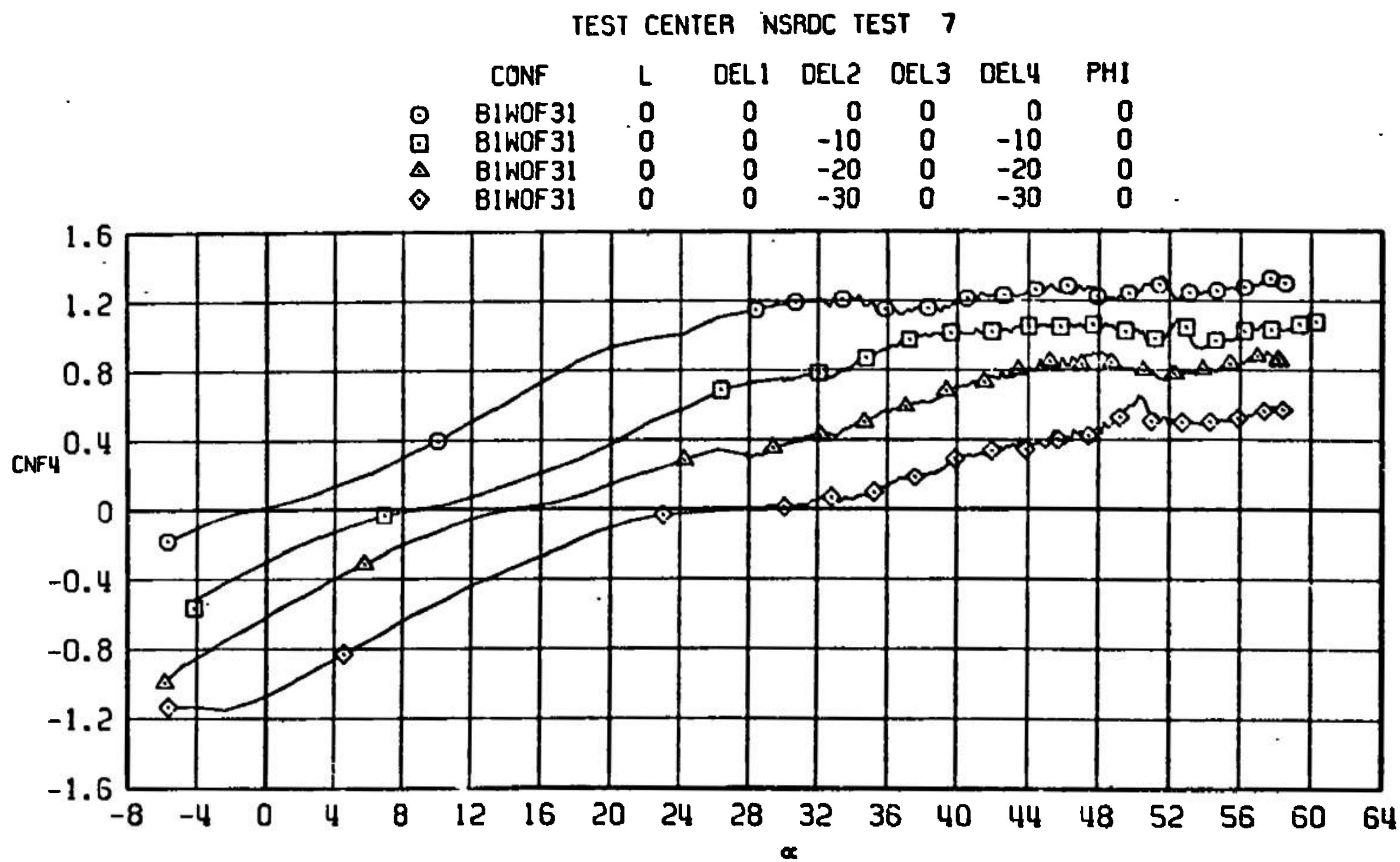

i. CNF4 versus α
Figure 56. Continued.

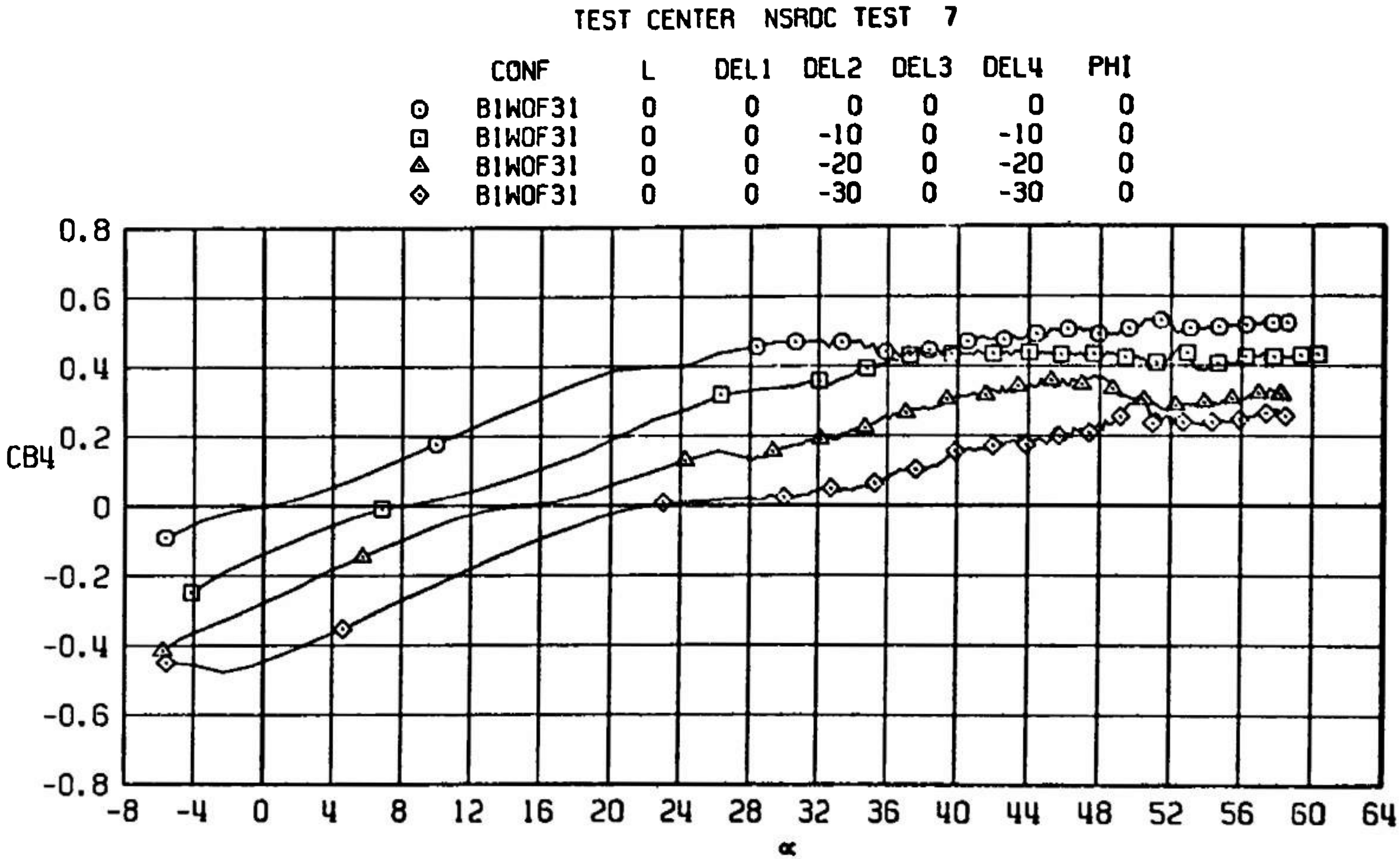

j. CB4 versus α

Figure 56. Continued.

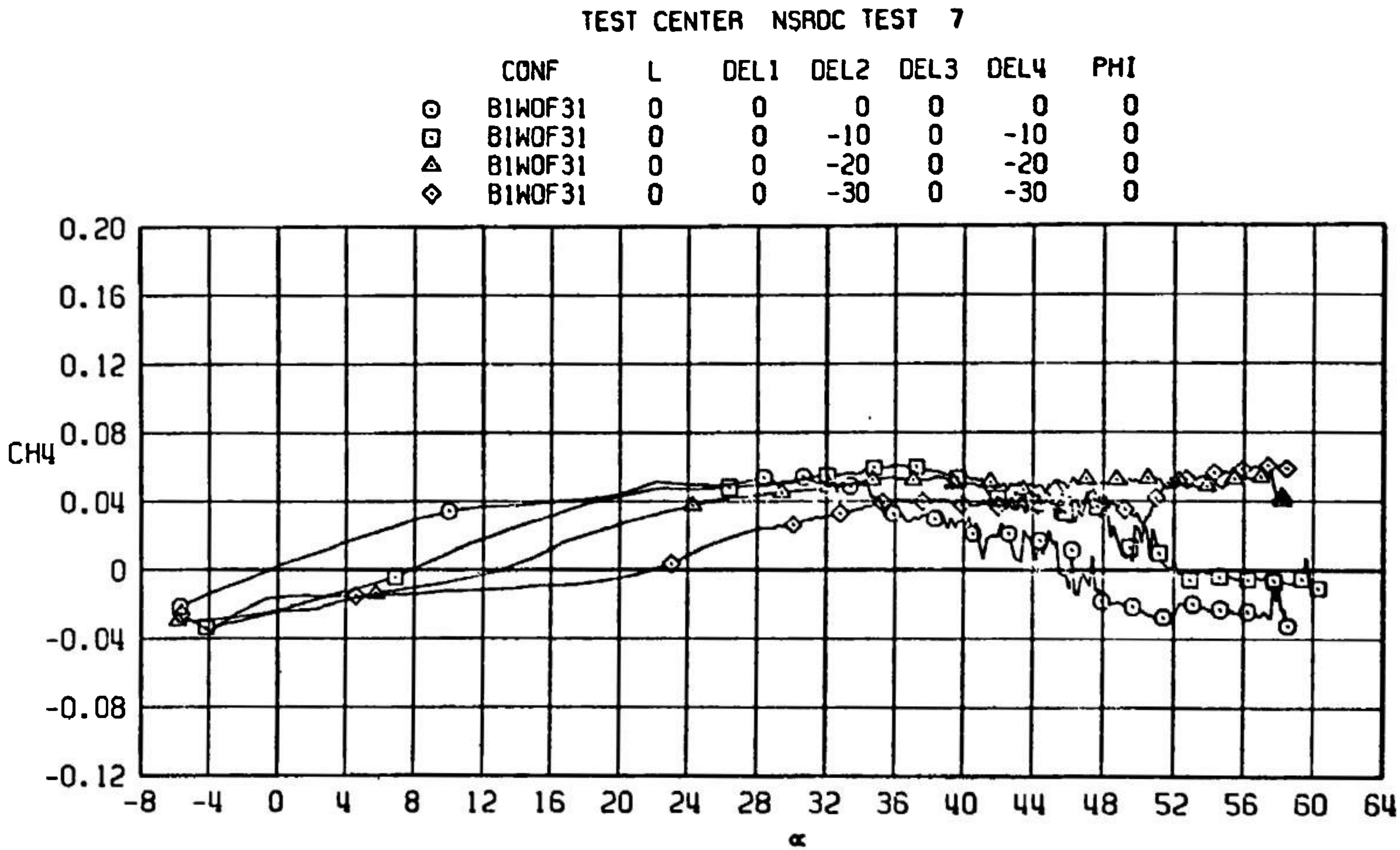

k. CH4 versus α
Figure 56. Concluded.

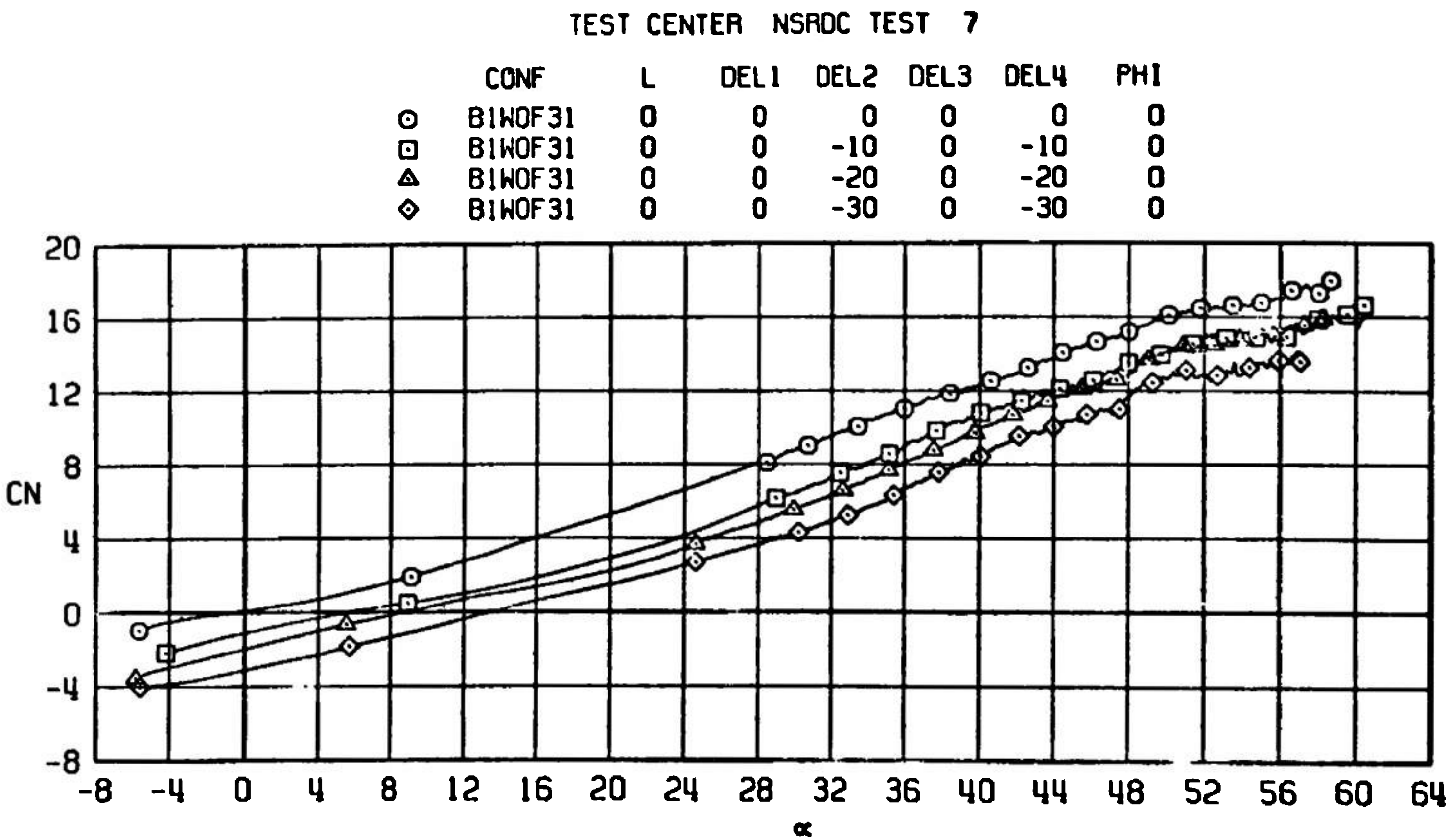

a. CN versus α

Figure 57. Test No. 7, comparison of aerodynamic coefficients of configuration B1W0F31 for various deflections of tail fins No. 2 and 4 at $M_\infty = 1.0$.

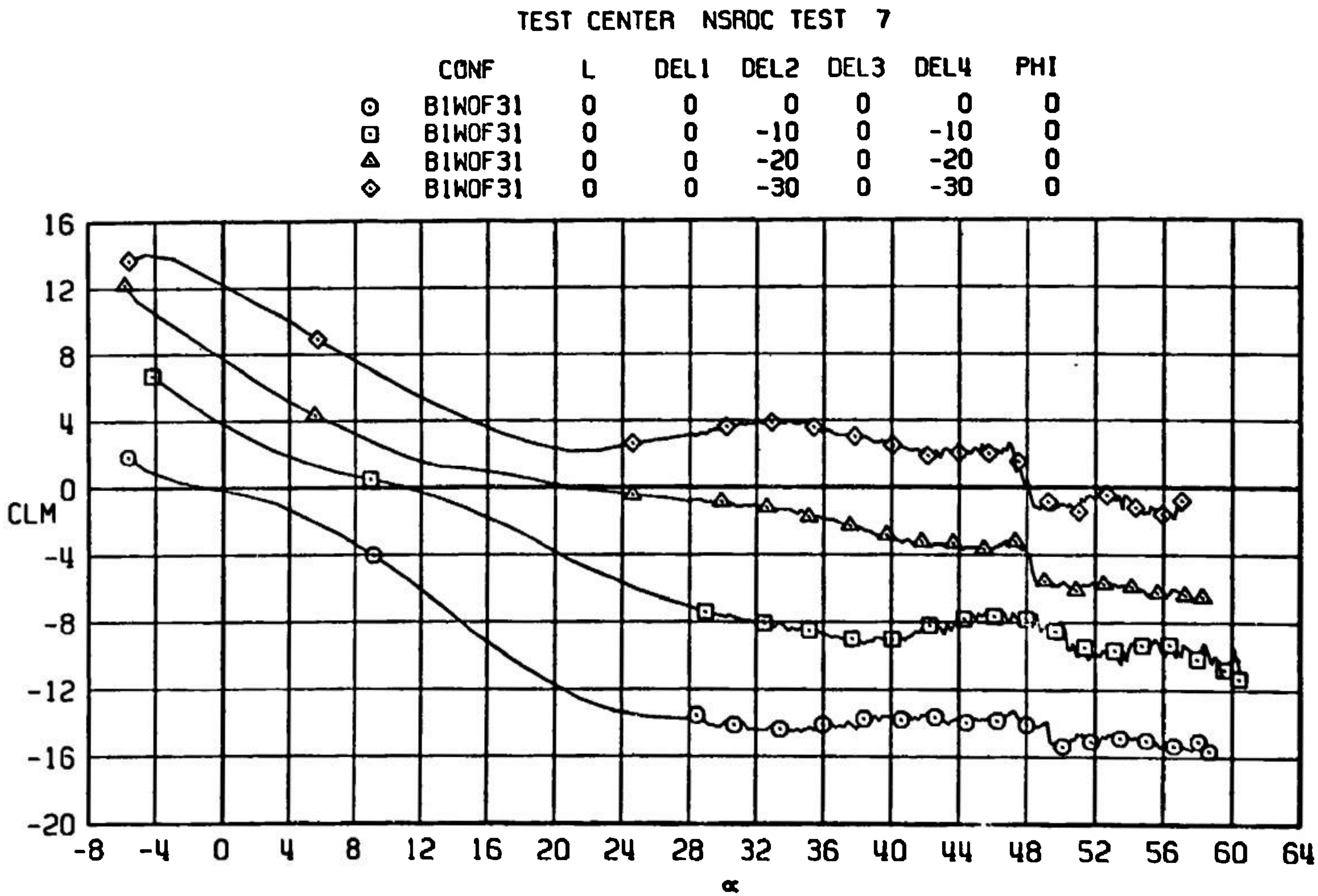

b. CLM versus α

Figure 57. Continued.

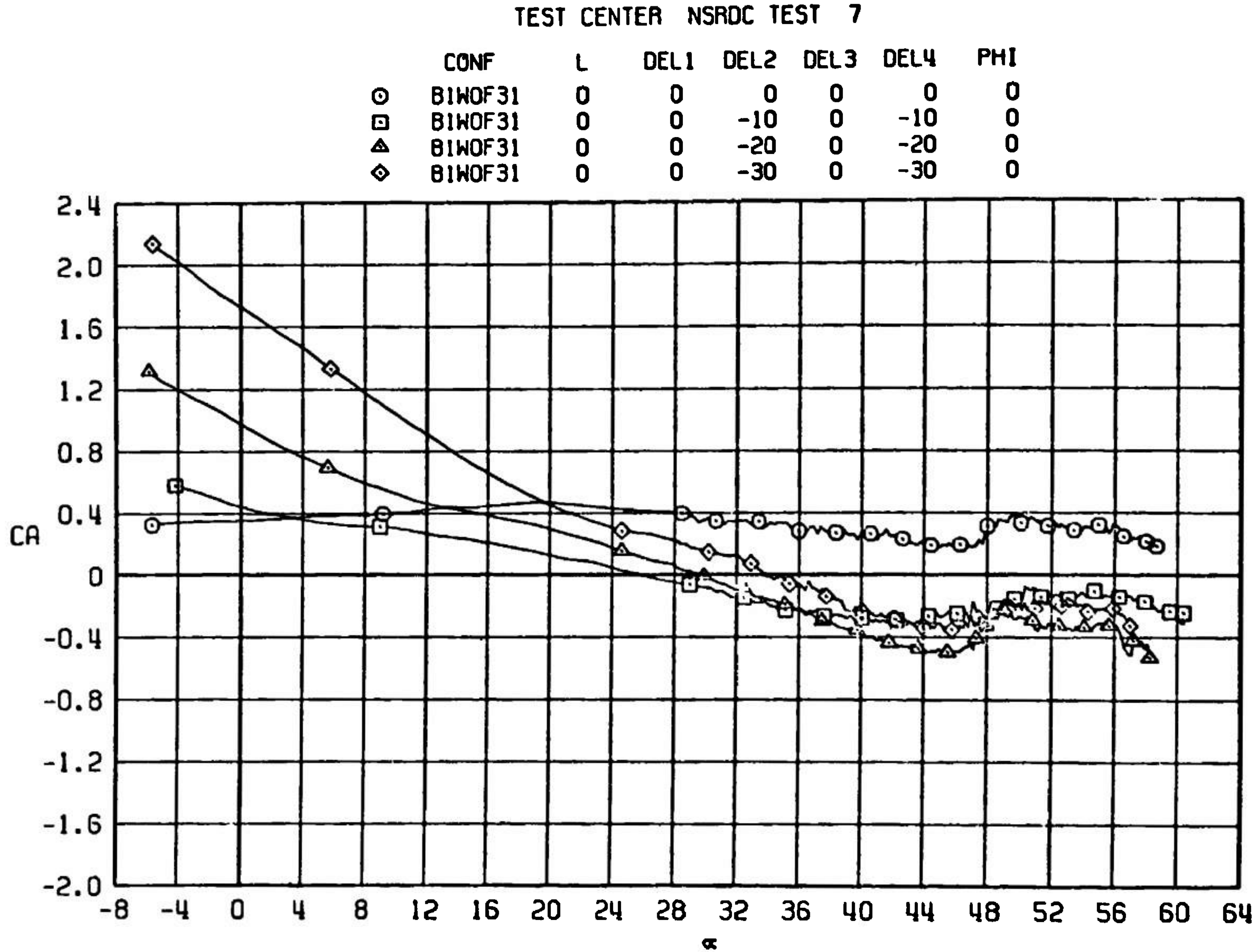

c. CA versus α
Figure 57. Continued.

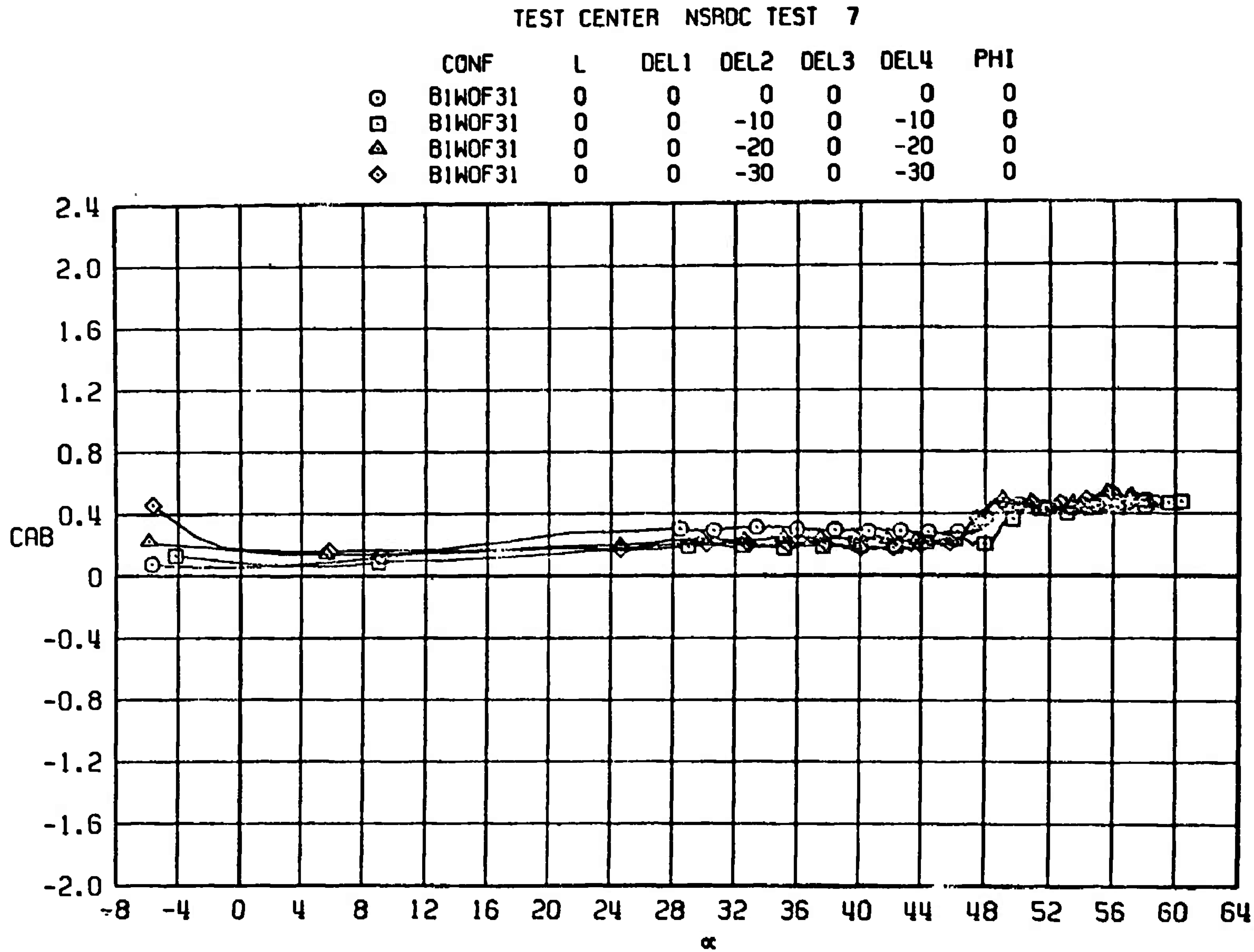

d. CAB versus α
Figure 57. Continued.

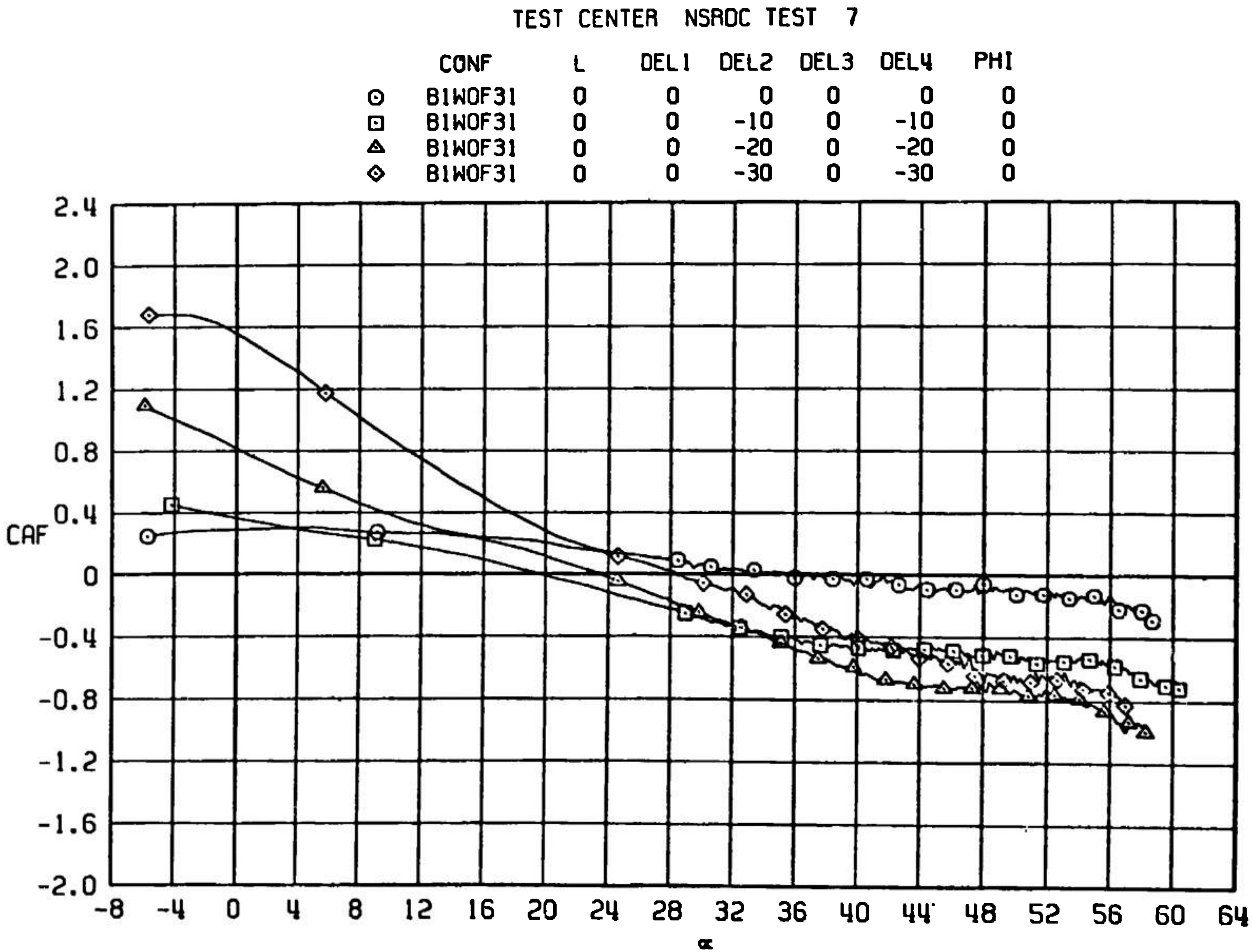

e. CAF versus α
Figure 57. Continued.

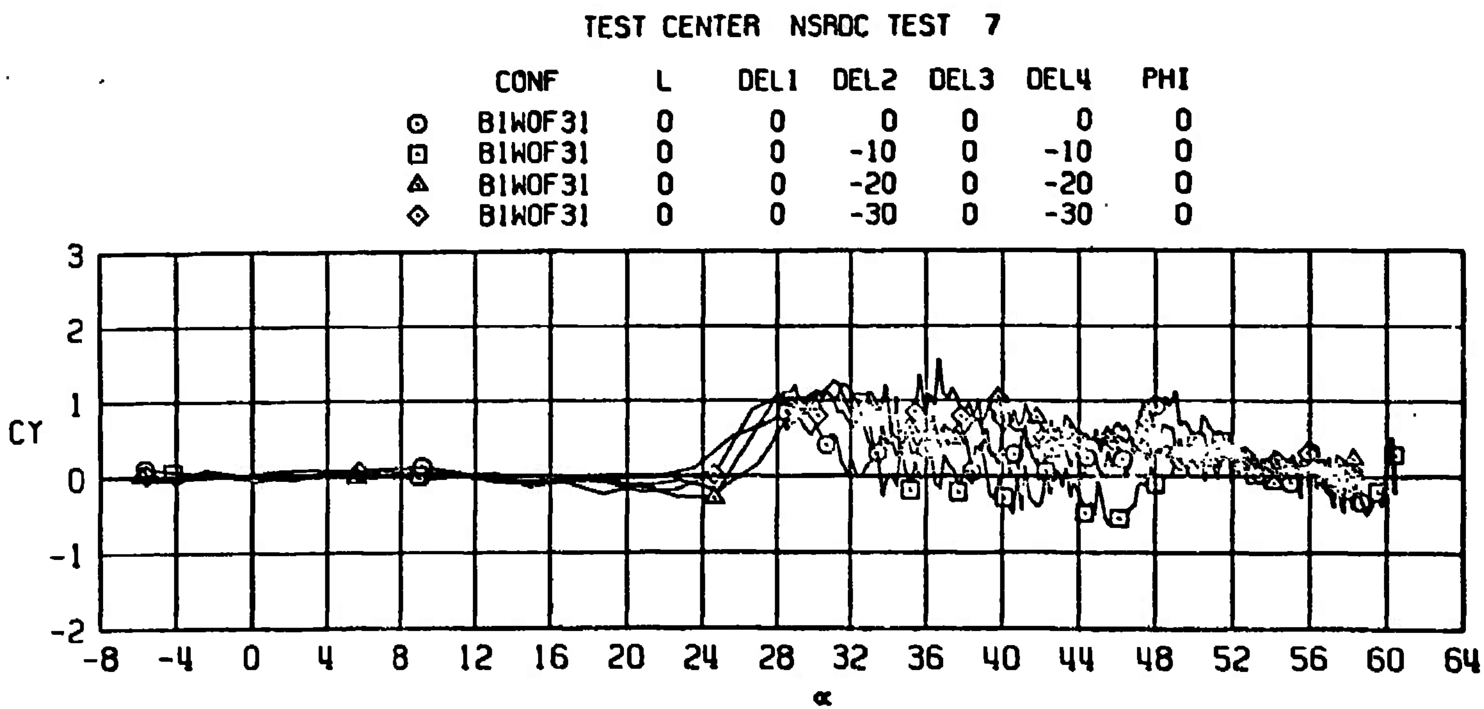

f. CY versus α

Figure 57. Continued.

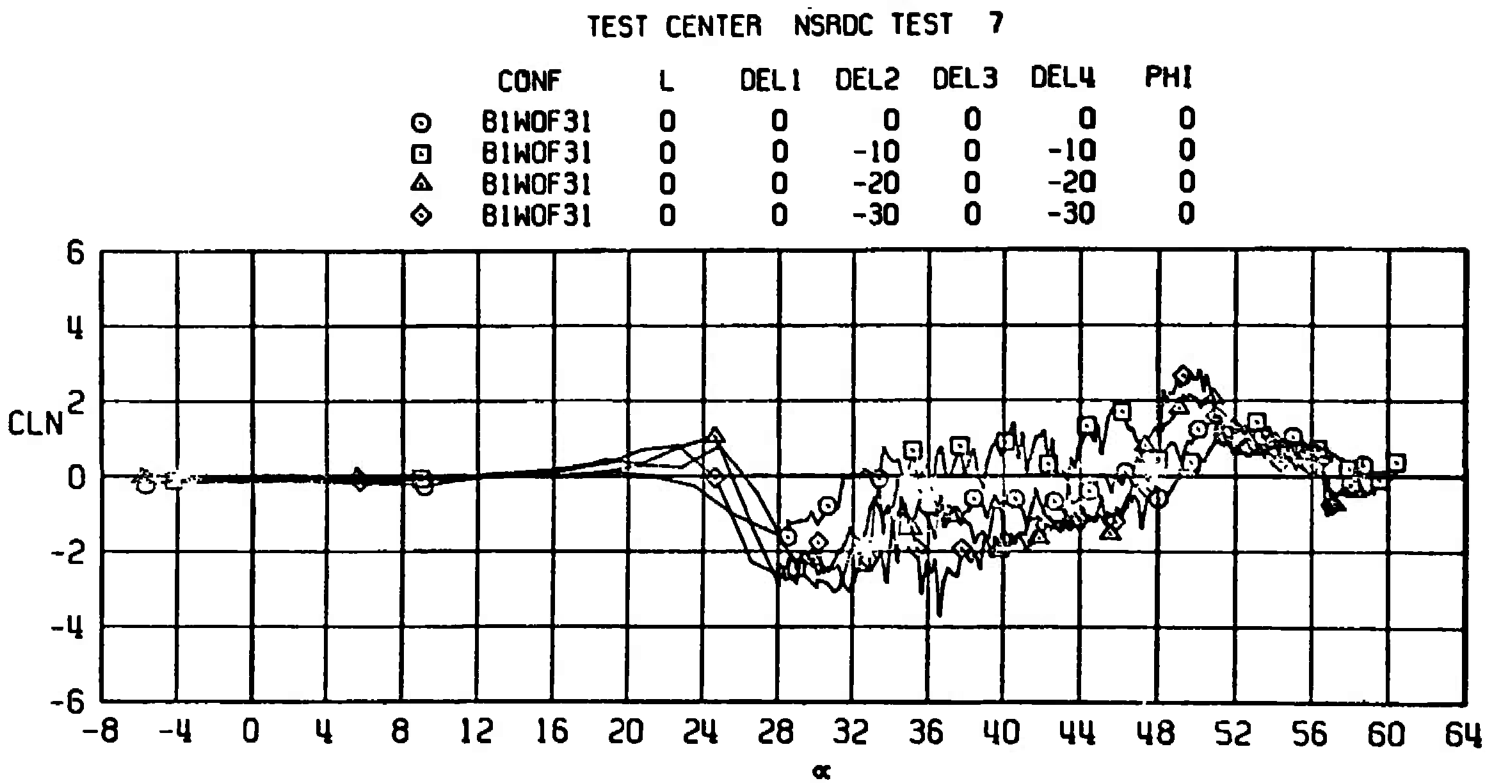

g. CLN versus α
Figure 57. Continued.

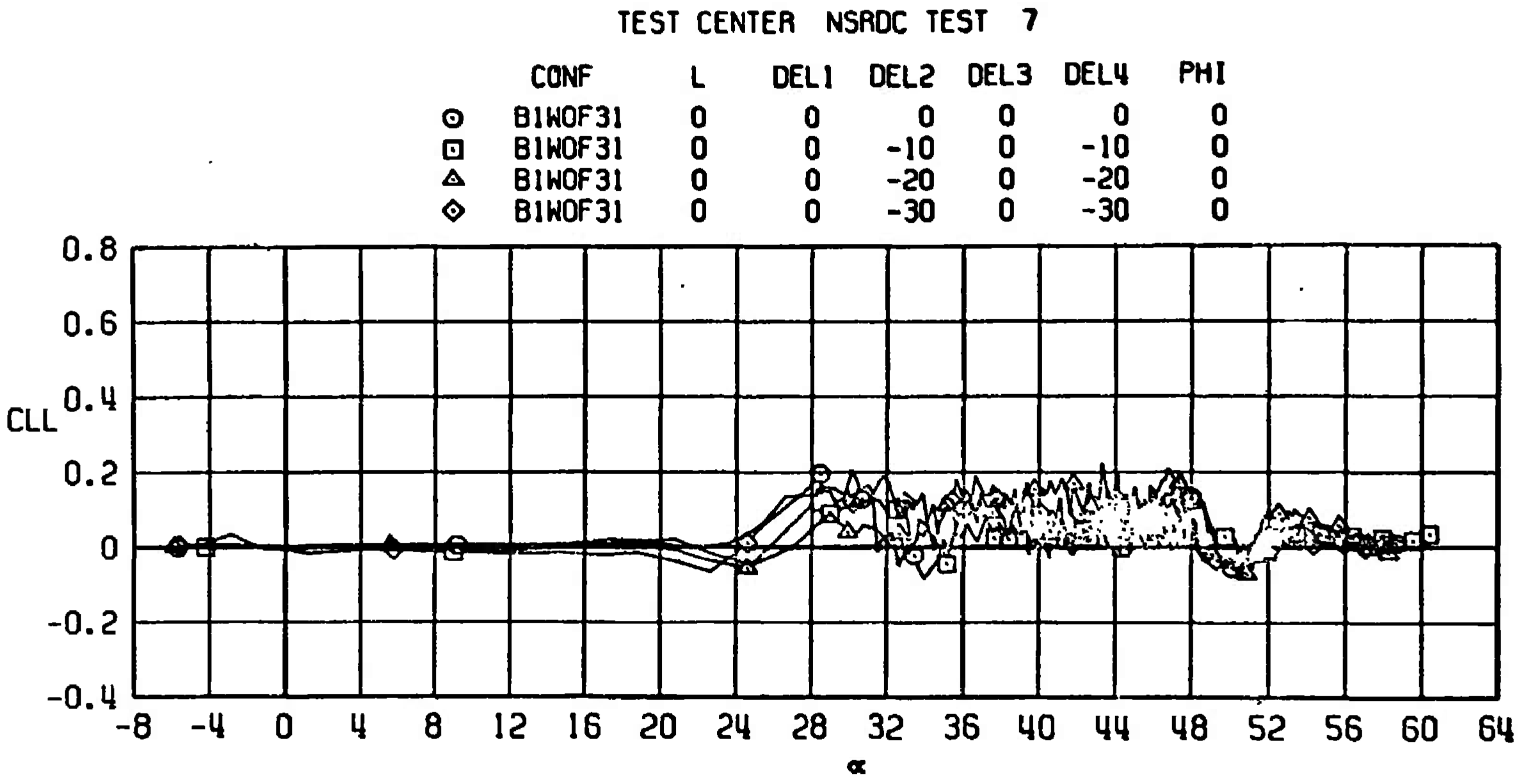

h. CLL versus α
Figure 57. Continued.

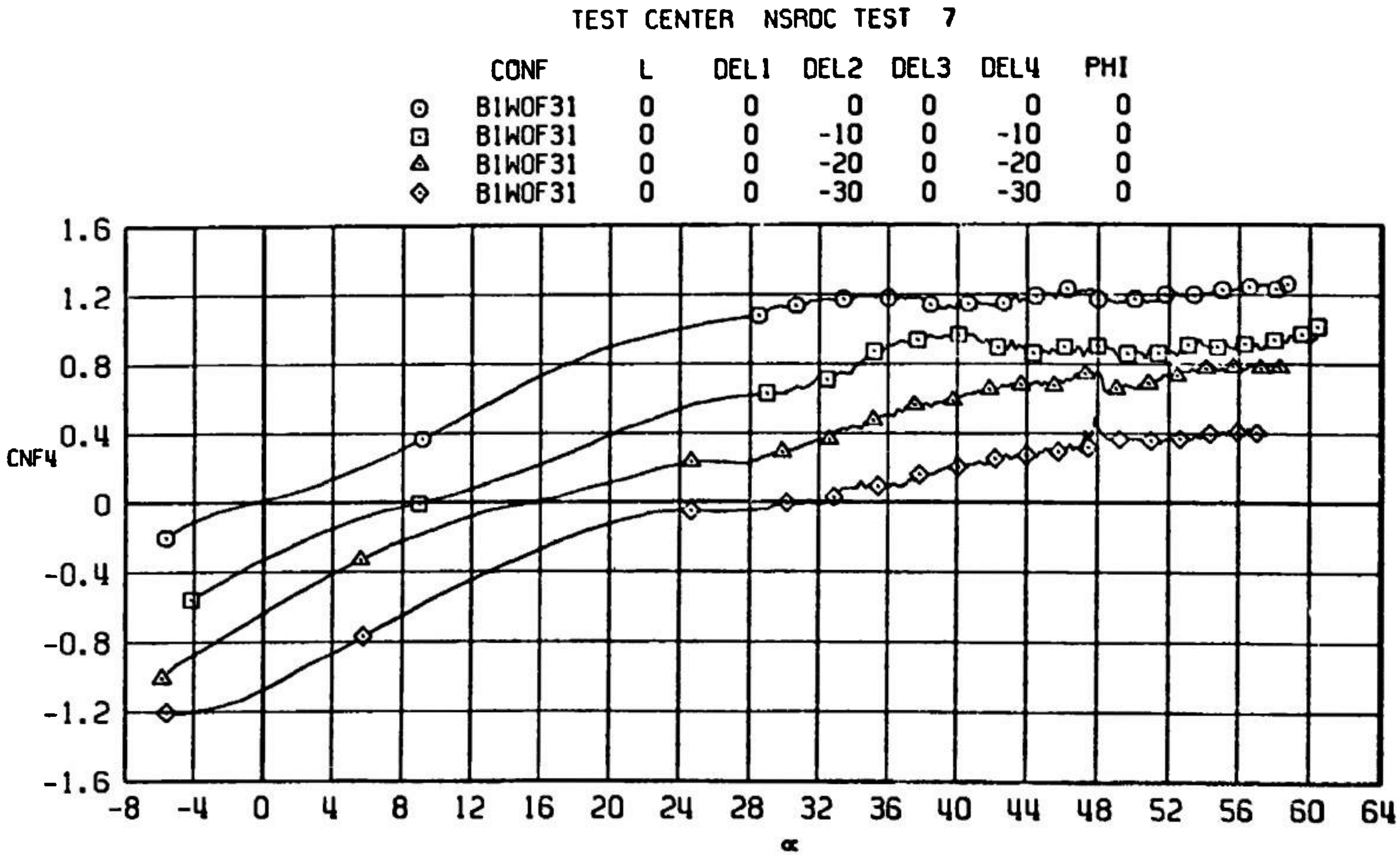

i. CNF4 versus α

Figure 57. Continued.

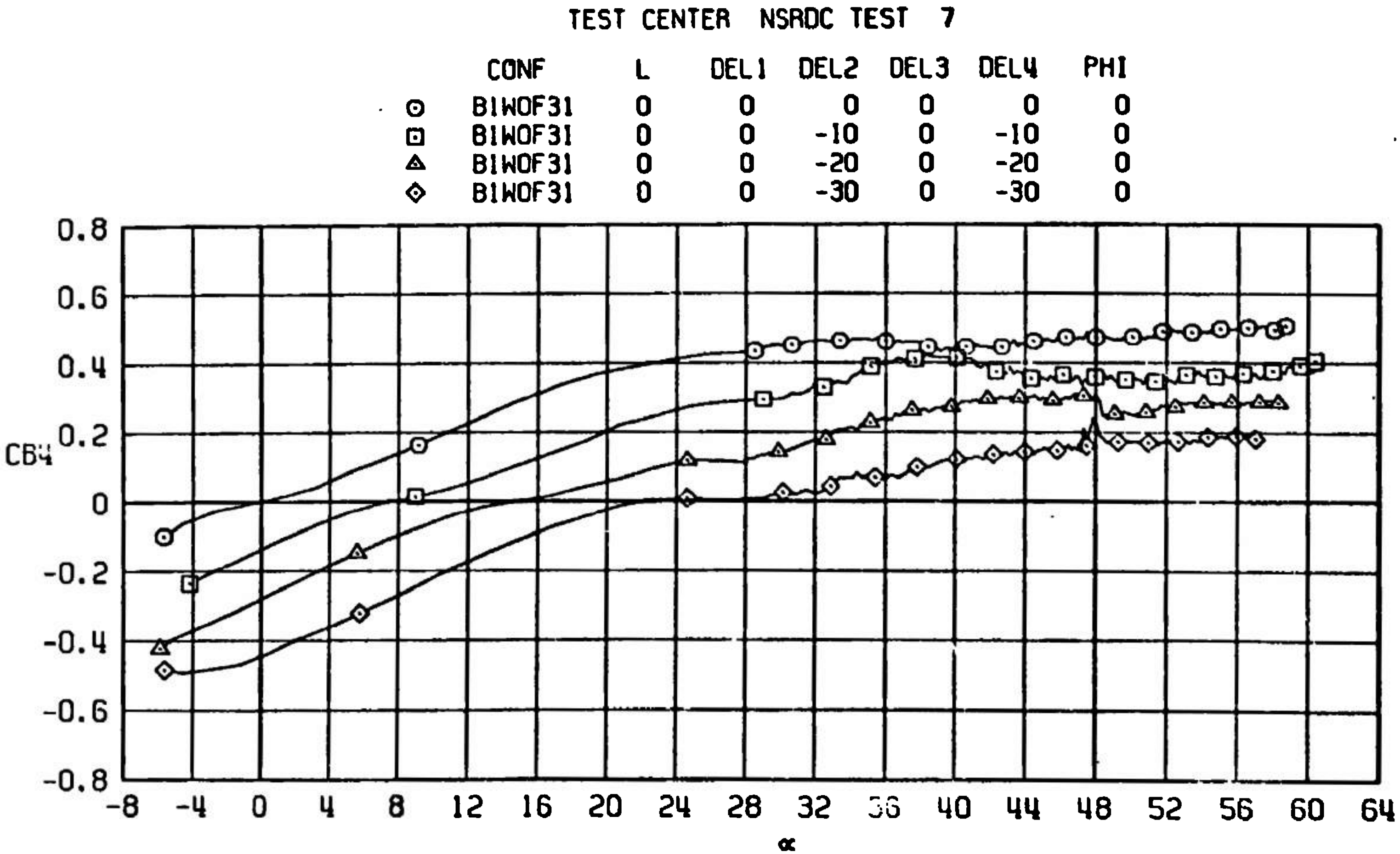

j. CB4 versus α
Figure 57. Continued.

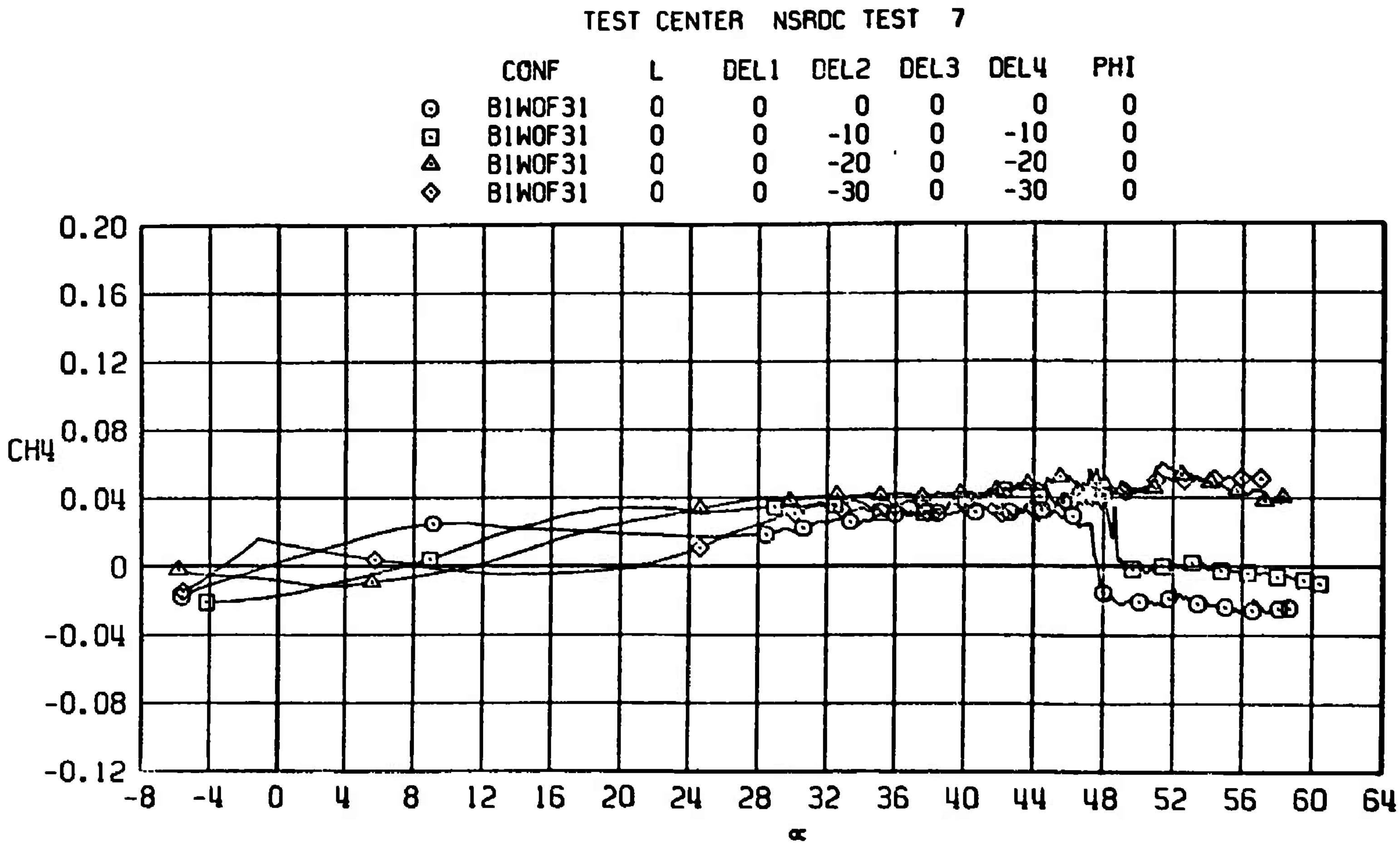

k. CH4 versus α

Figure 57. Concluded.

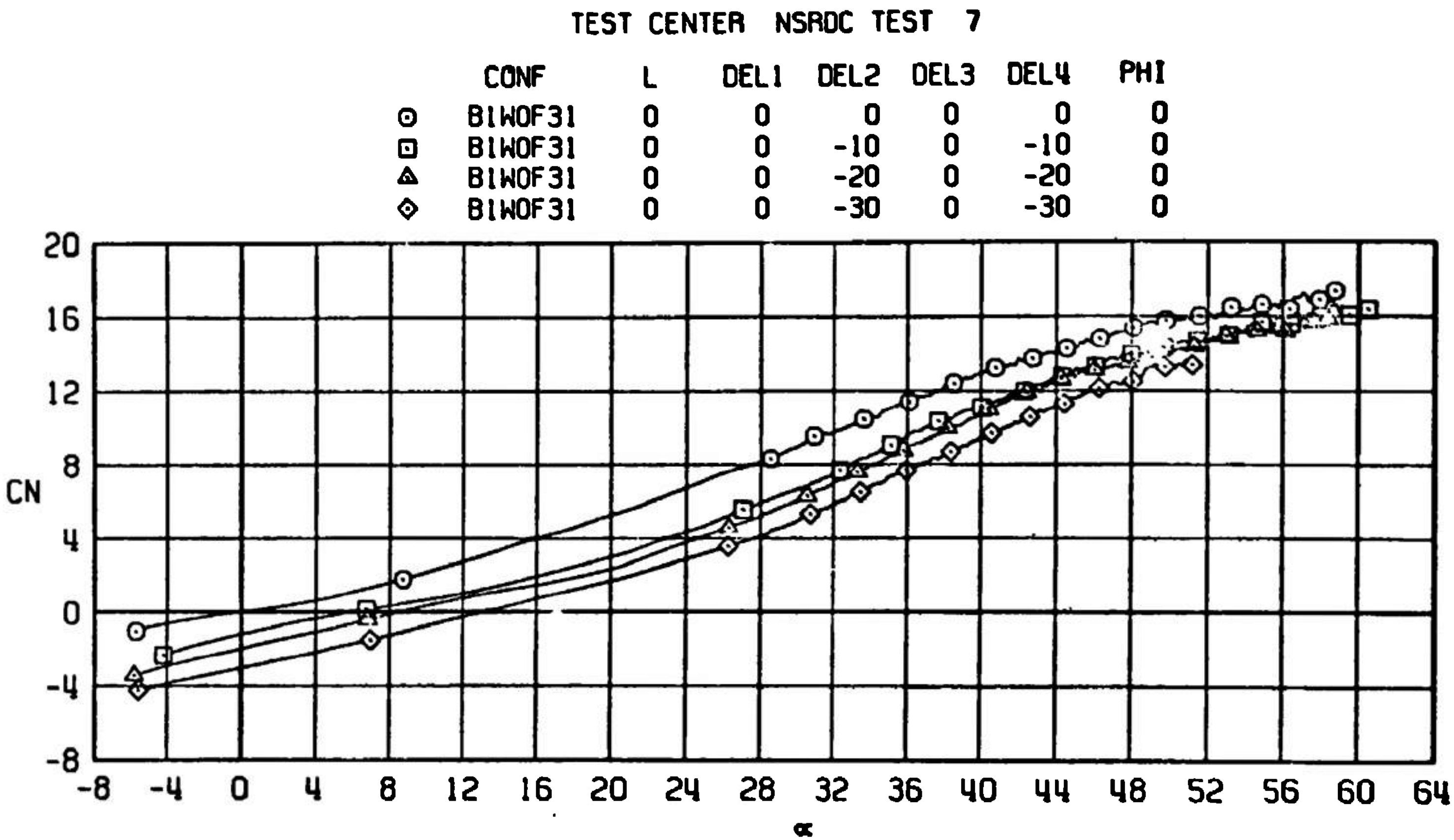

a. CN versus α

Figure 58. Test No. 7, comparison of aerodynamic coefficients of configuration B1W0F31 for various deflections of tail fins No. 2 and 4 at $M_\infty = 1.1$.

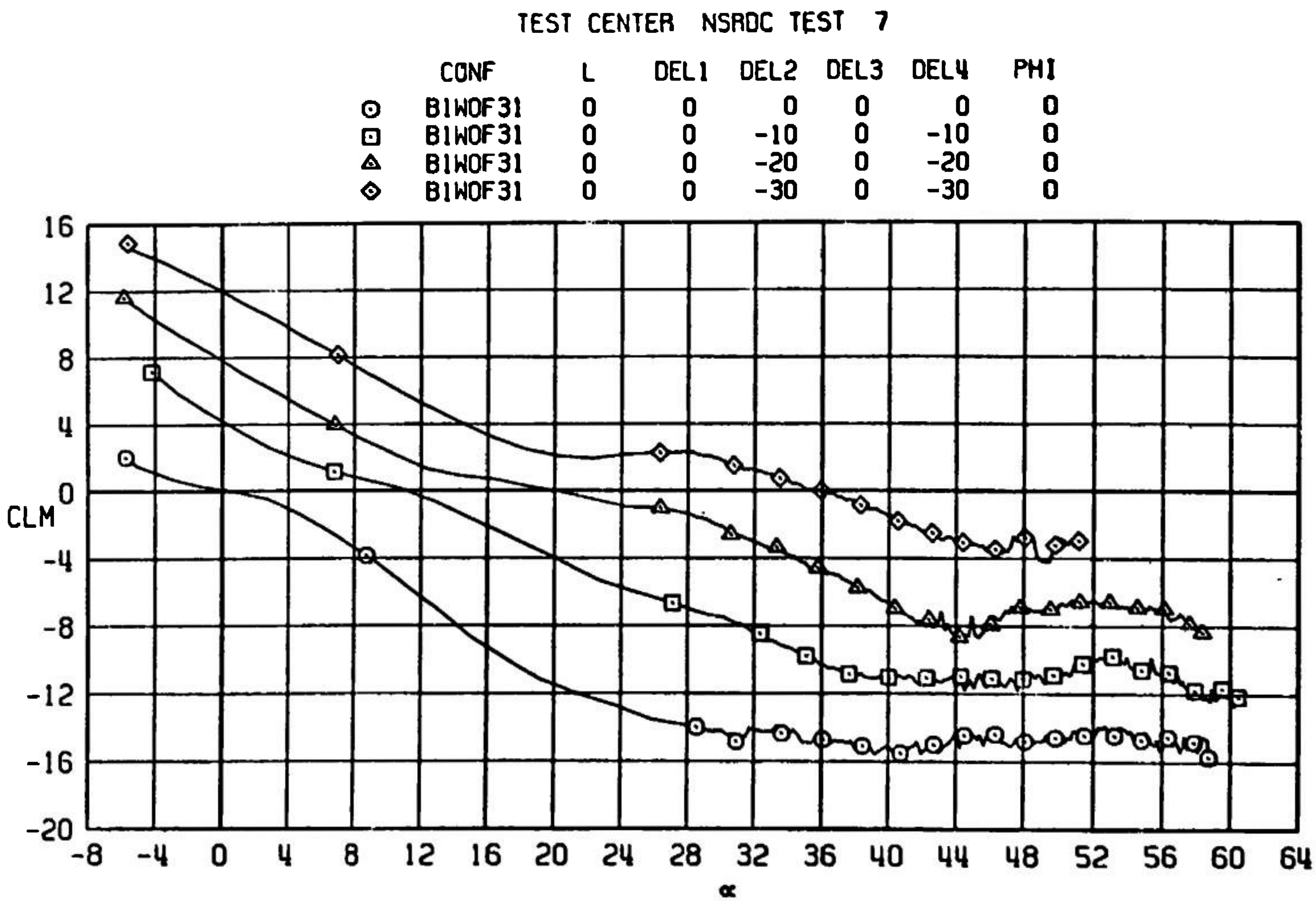

b. CLM versus α
Figure 58. Continued.

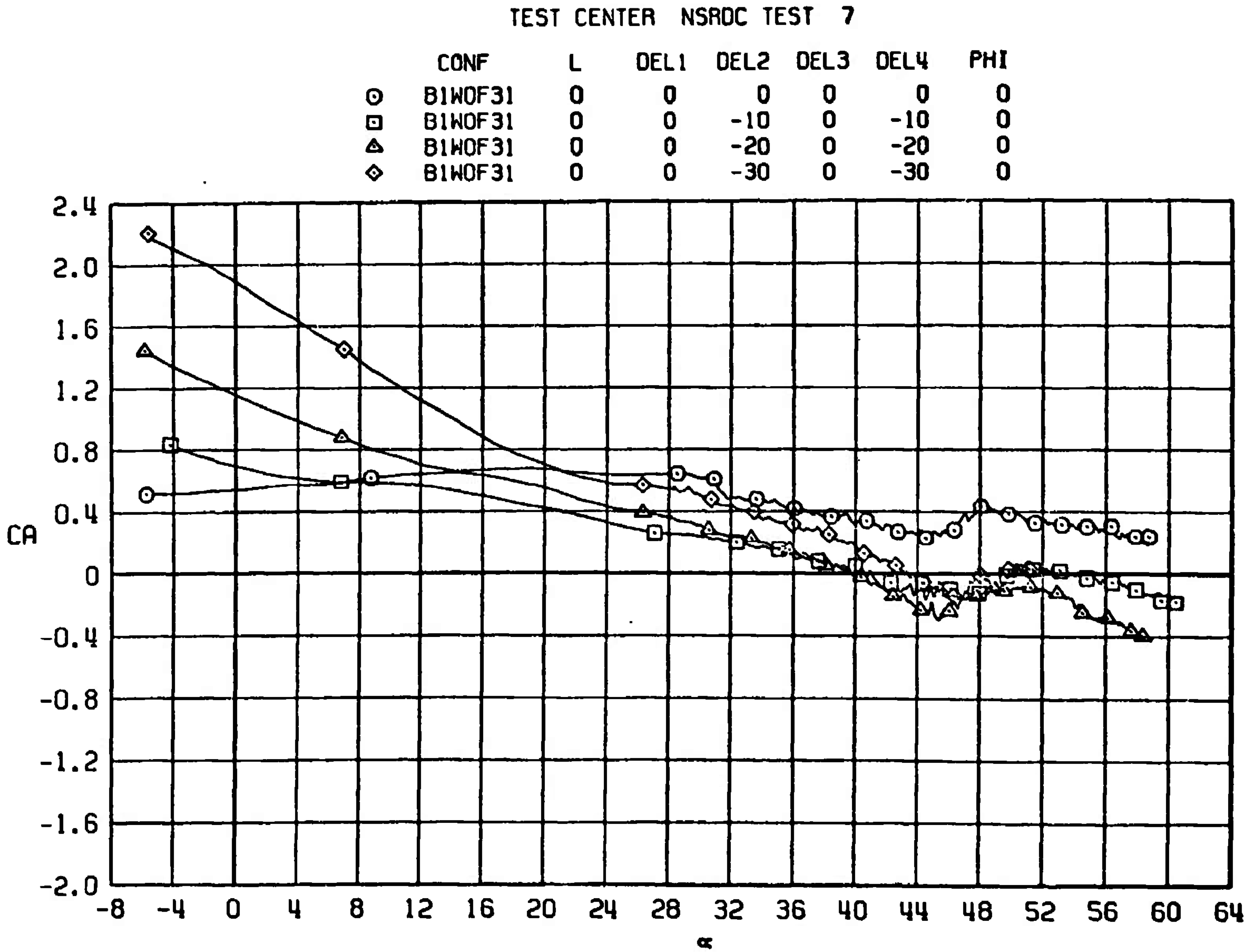

c. CA versus α

Figure 58. Continued.

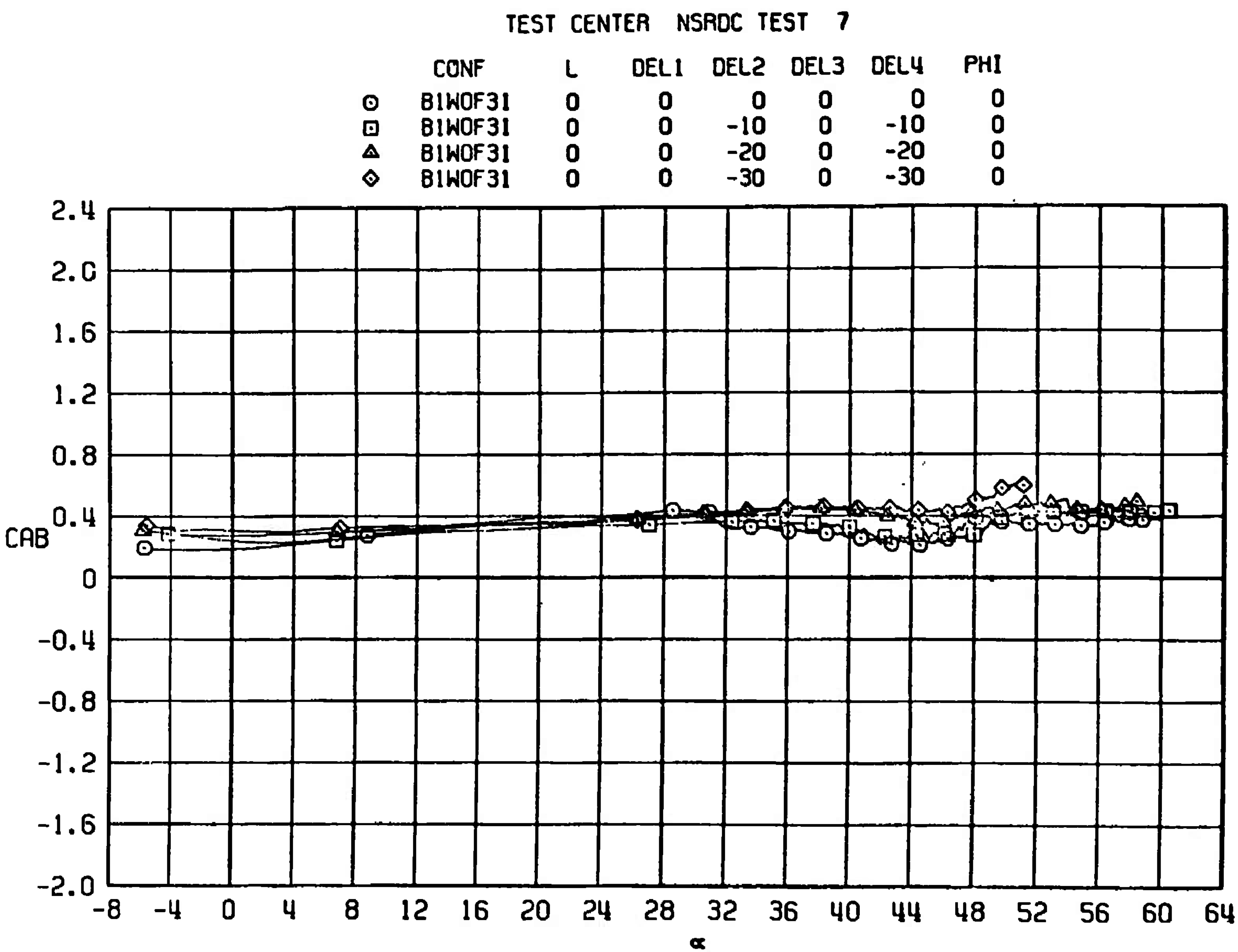

d. CAB versus α
Figure 58. Continued.

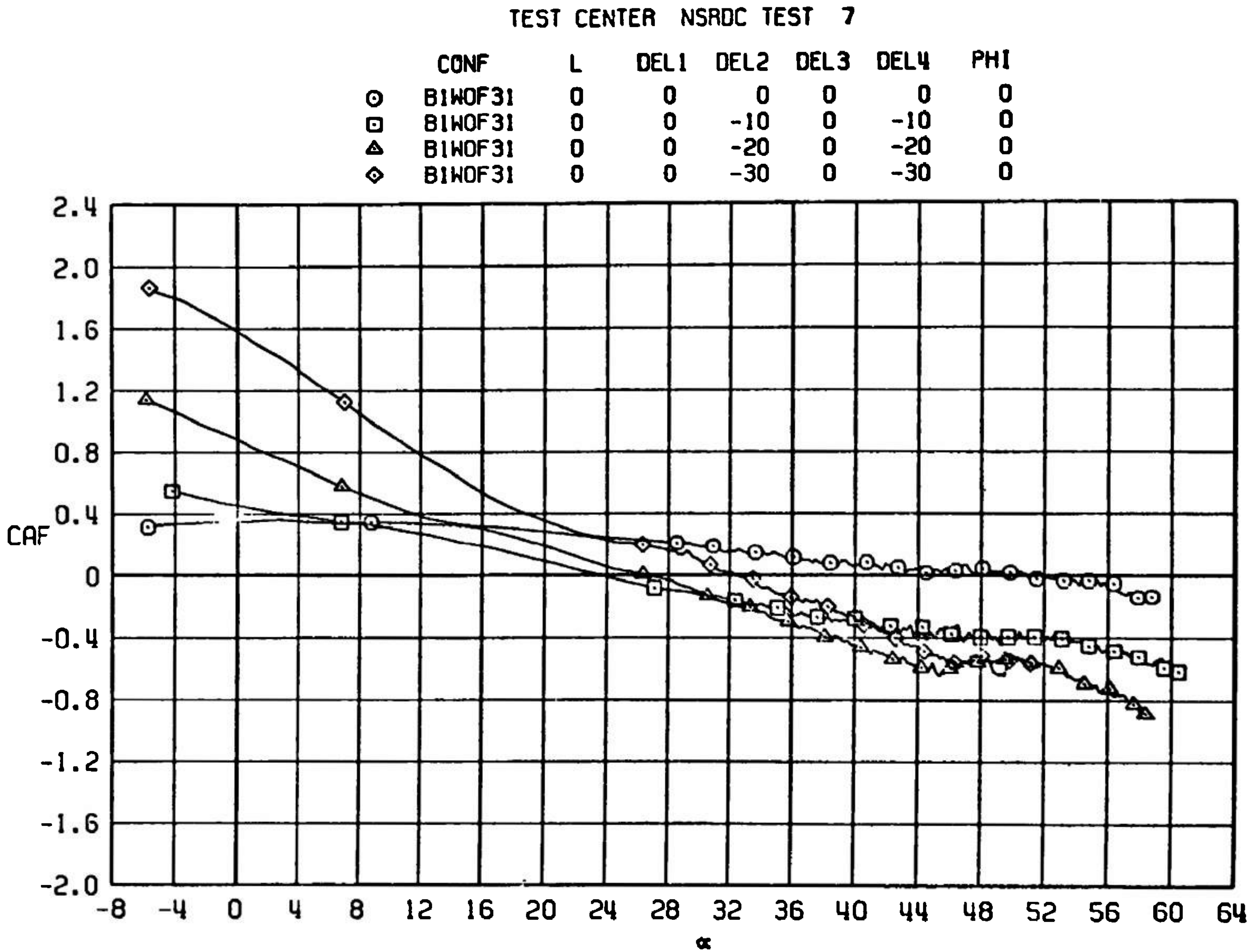

e. CAF versus α
Figure 58. Continued.

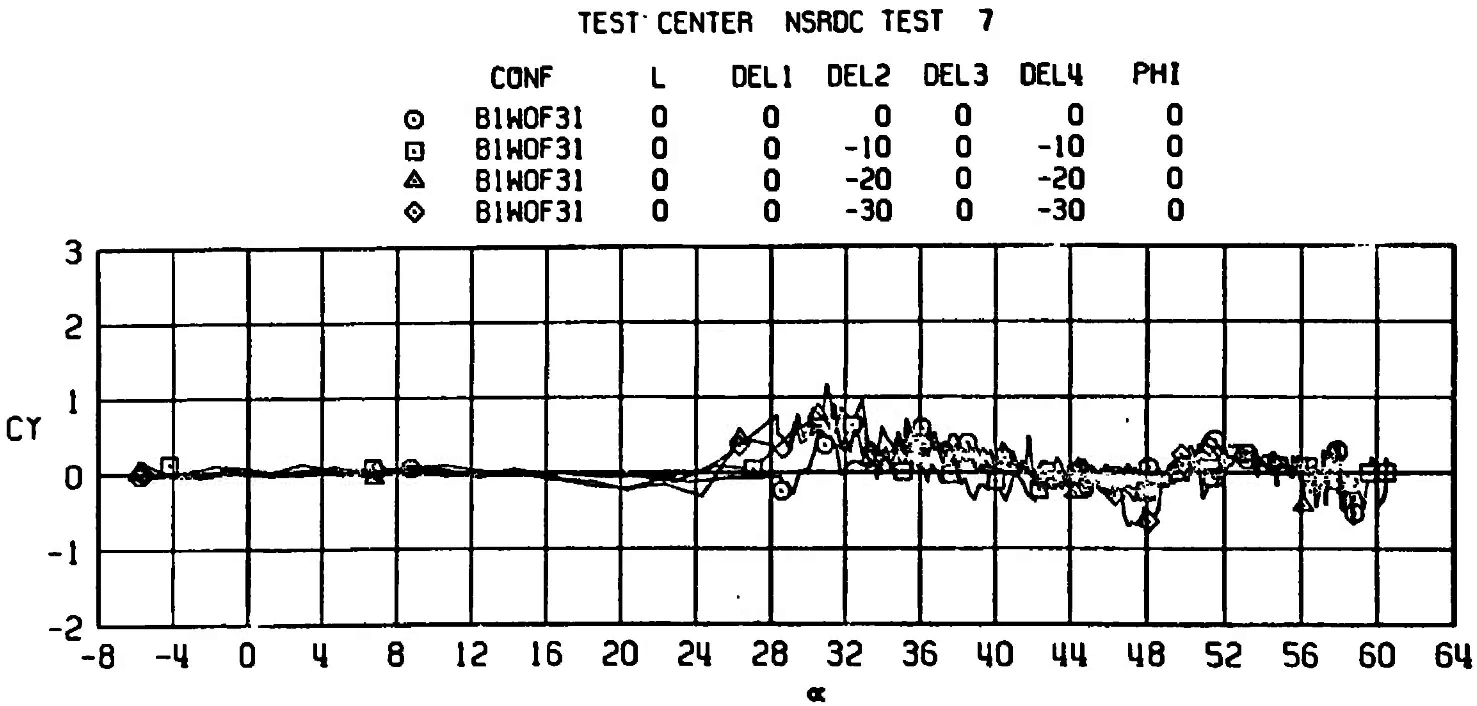

f. CY versus α
Figure 58. Continued.

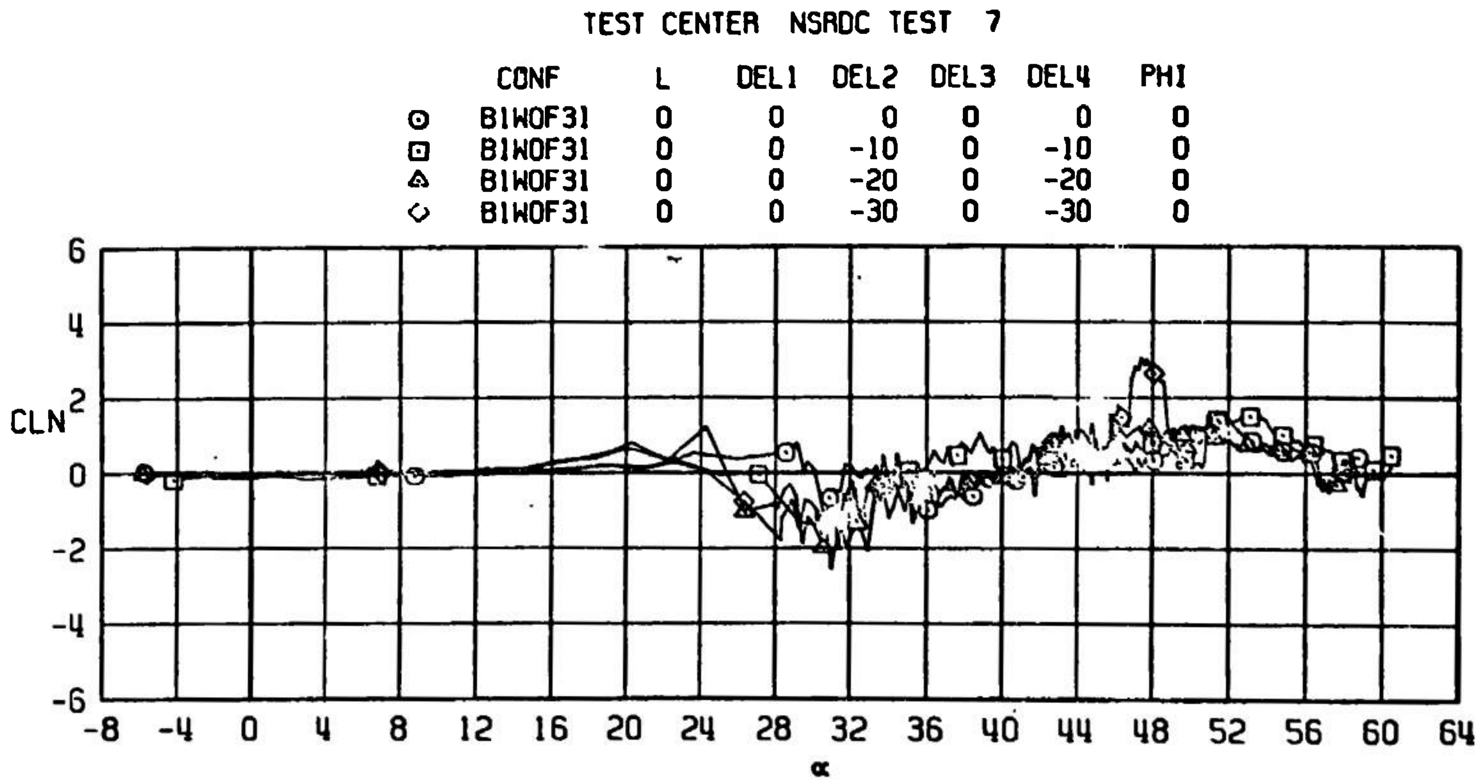

g. CLN versus α

Figure 58. Continued.

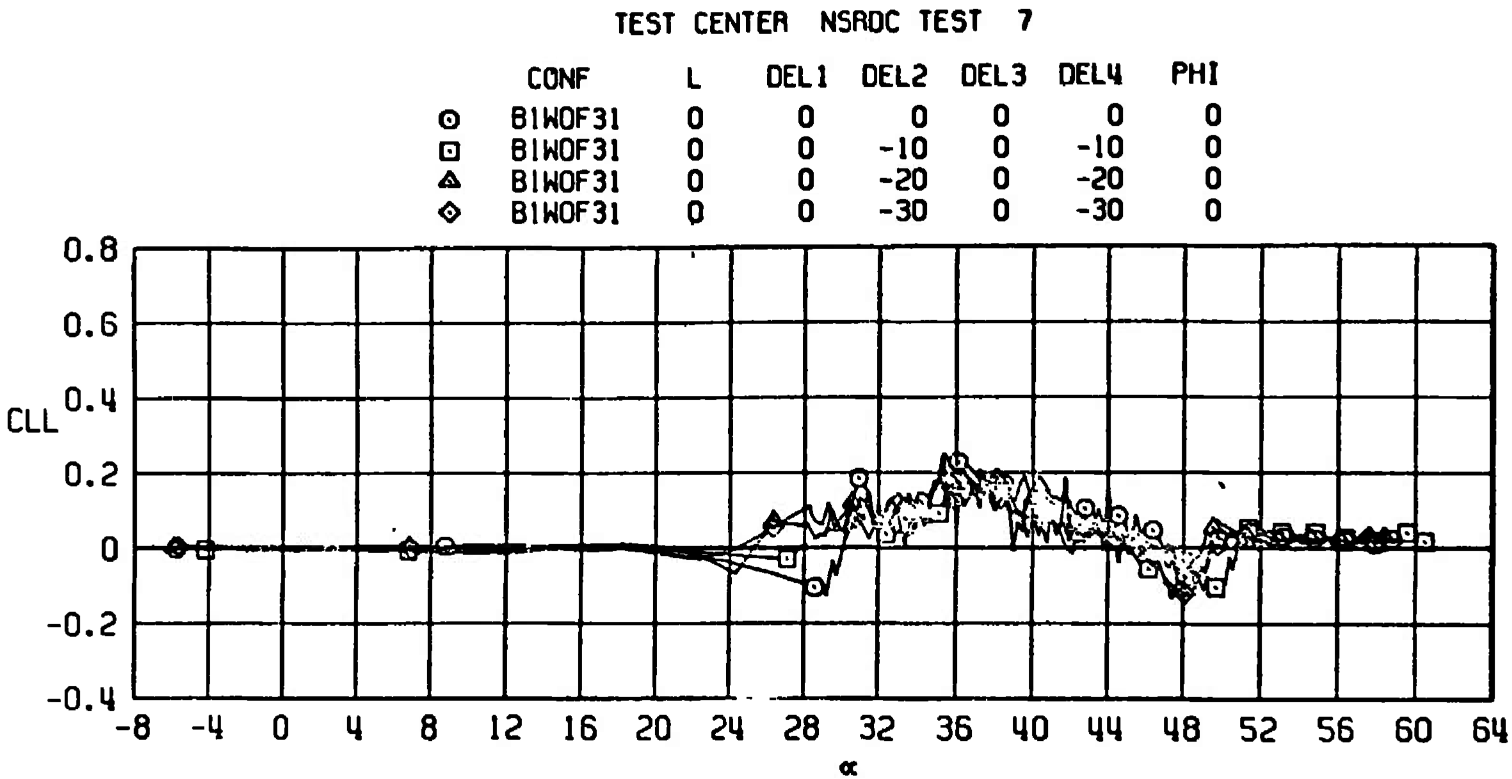

h. CLL versus α
Figure 58. Continued.

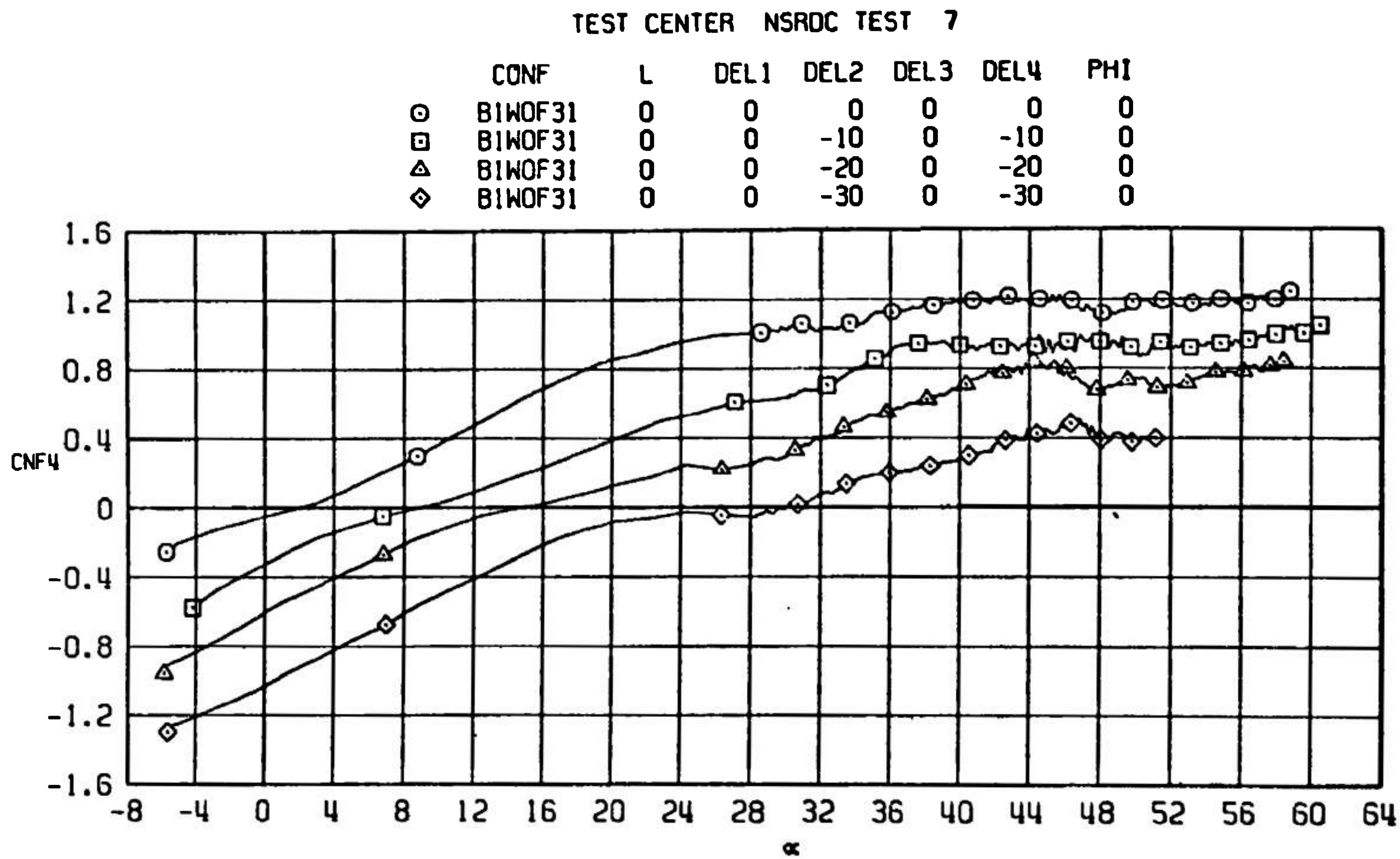

i. CNF4 versus α
Figure 58. Continued.

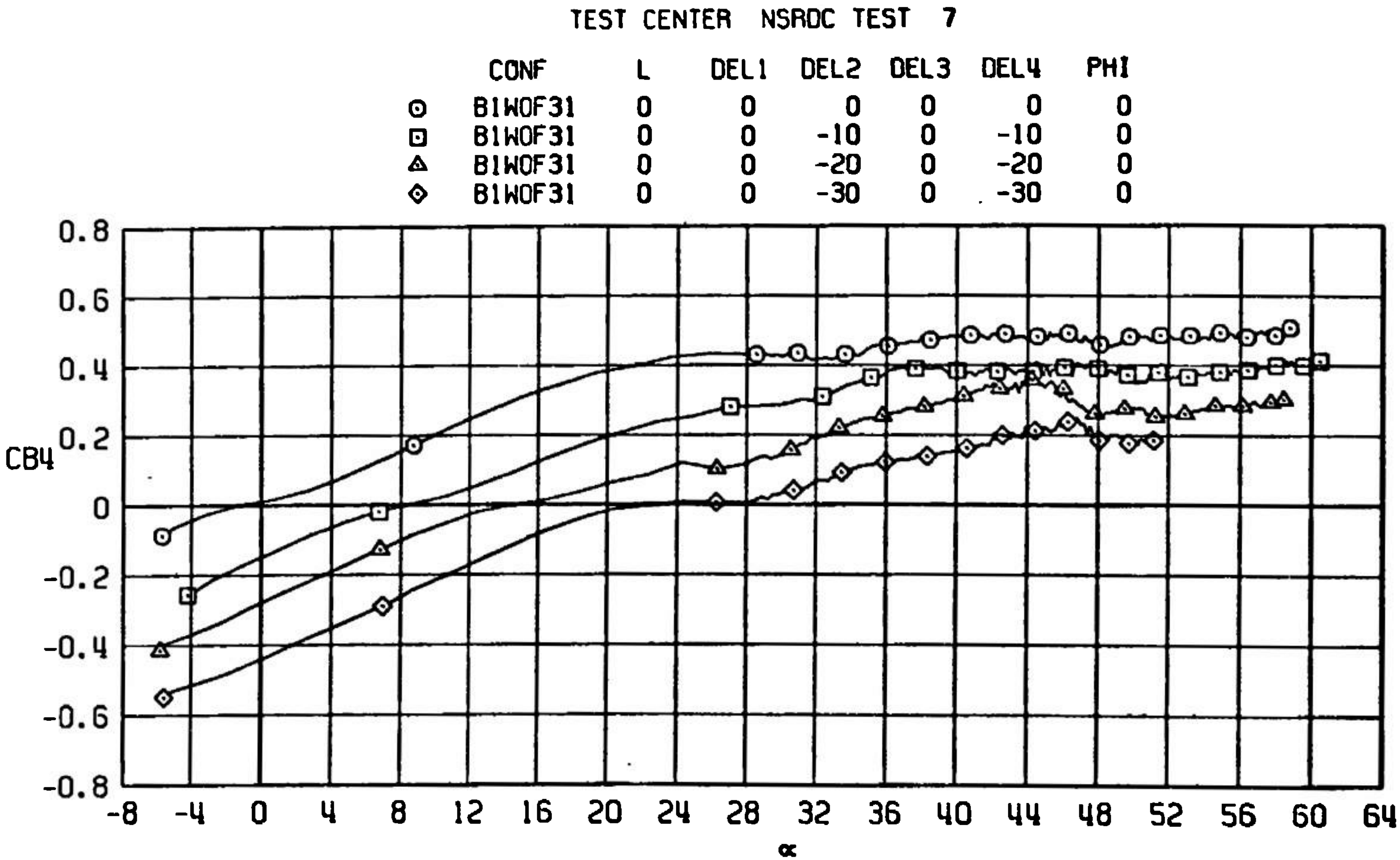

j. CB4 versus α

Figure 58. Continued.

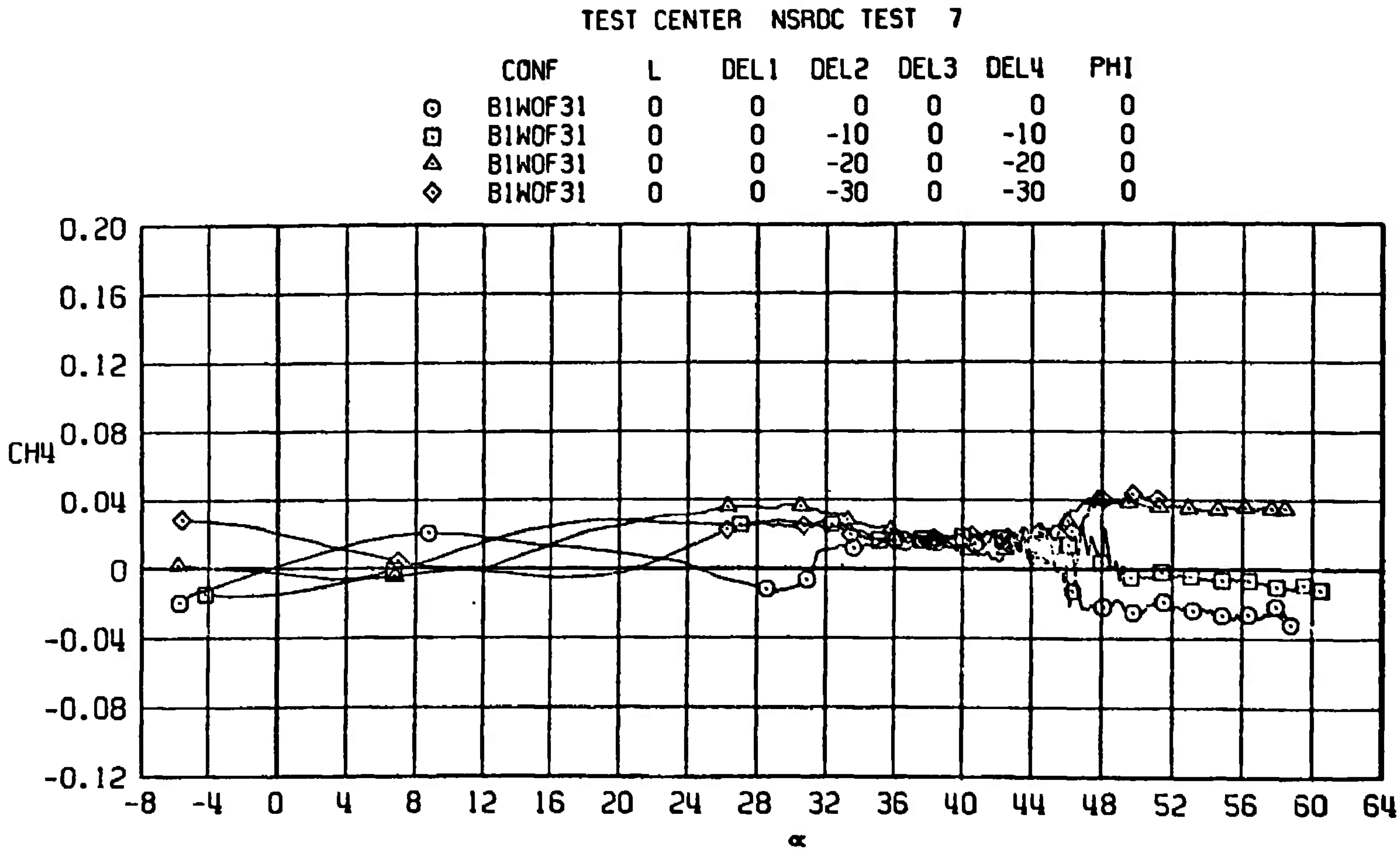

k. CH4 versus α
Figure 58. Concluded.

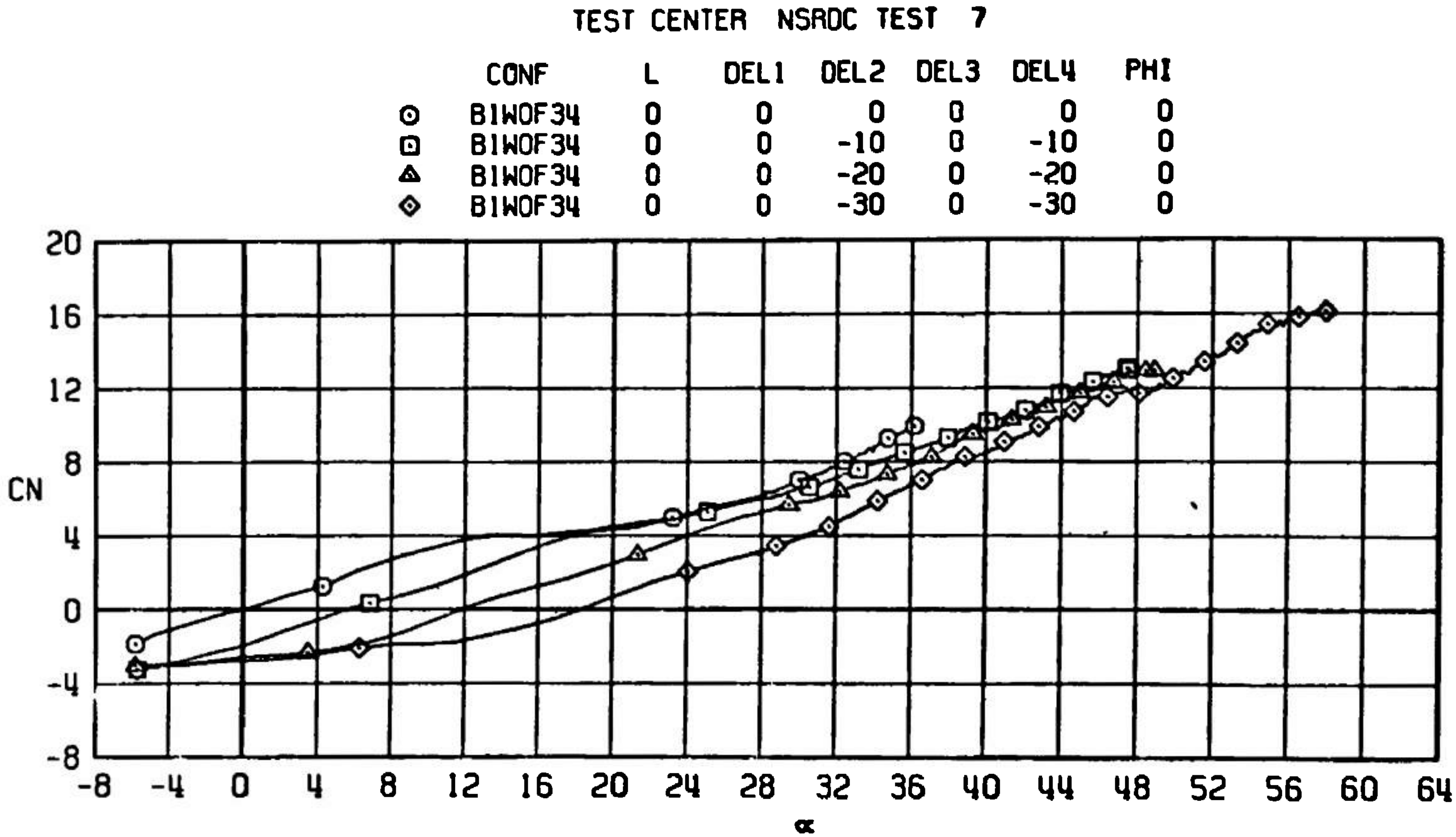

a. CN versus α

Figure 59. Test No. 7, comparison of aerodynamic coefficient of configuration B1W0F34 for various deflections of tail fins No. 2 and 4 at M_∞ = 0.8.

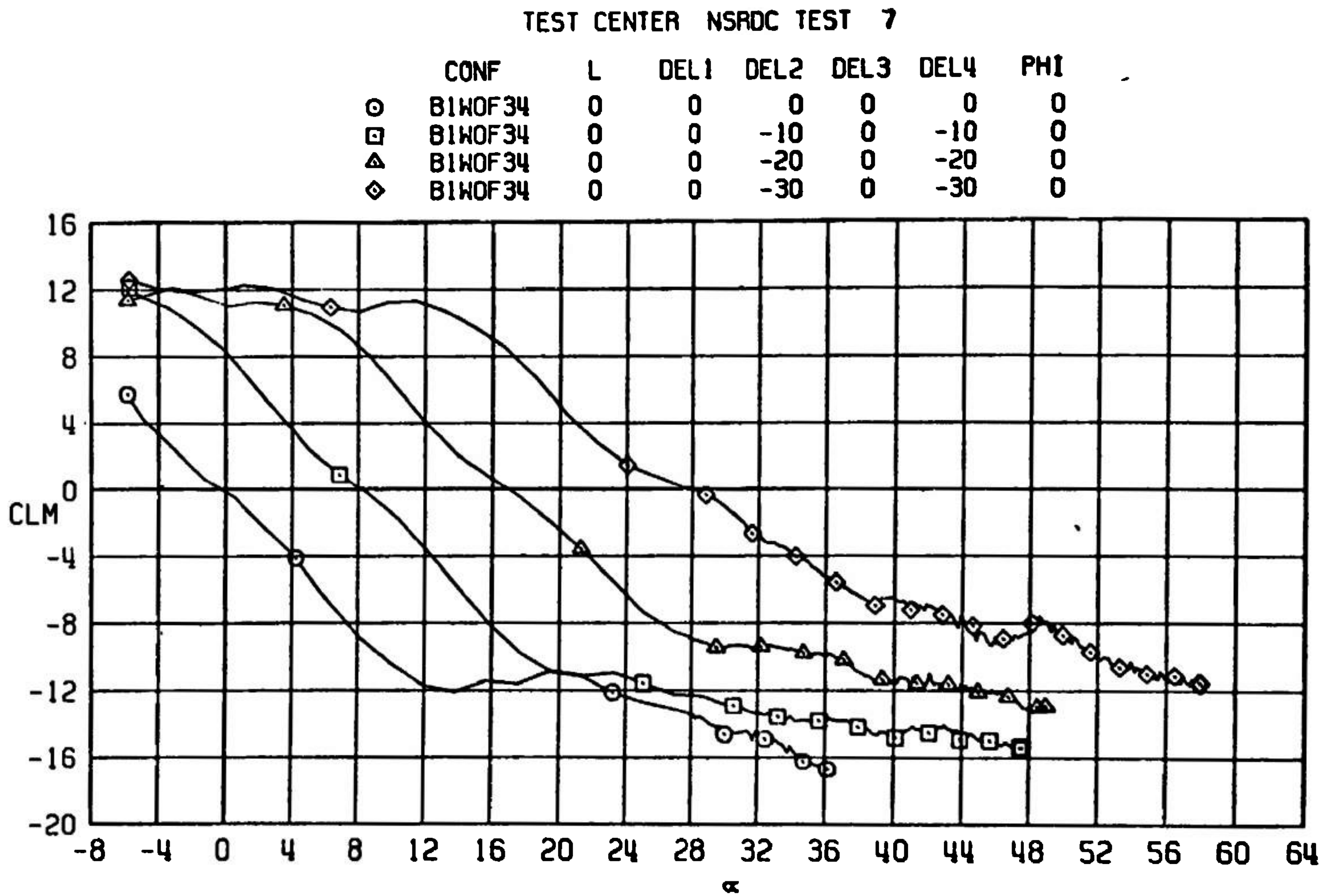

b. CLM versus α
Figure 59. Continued.

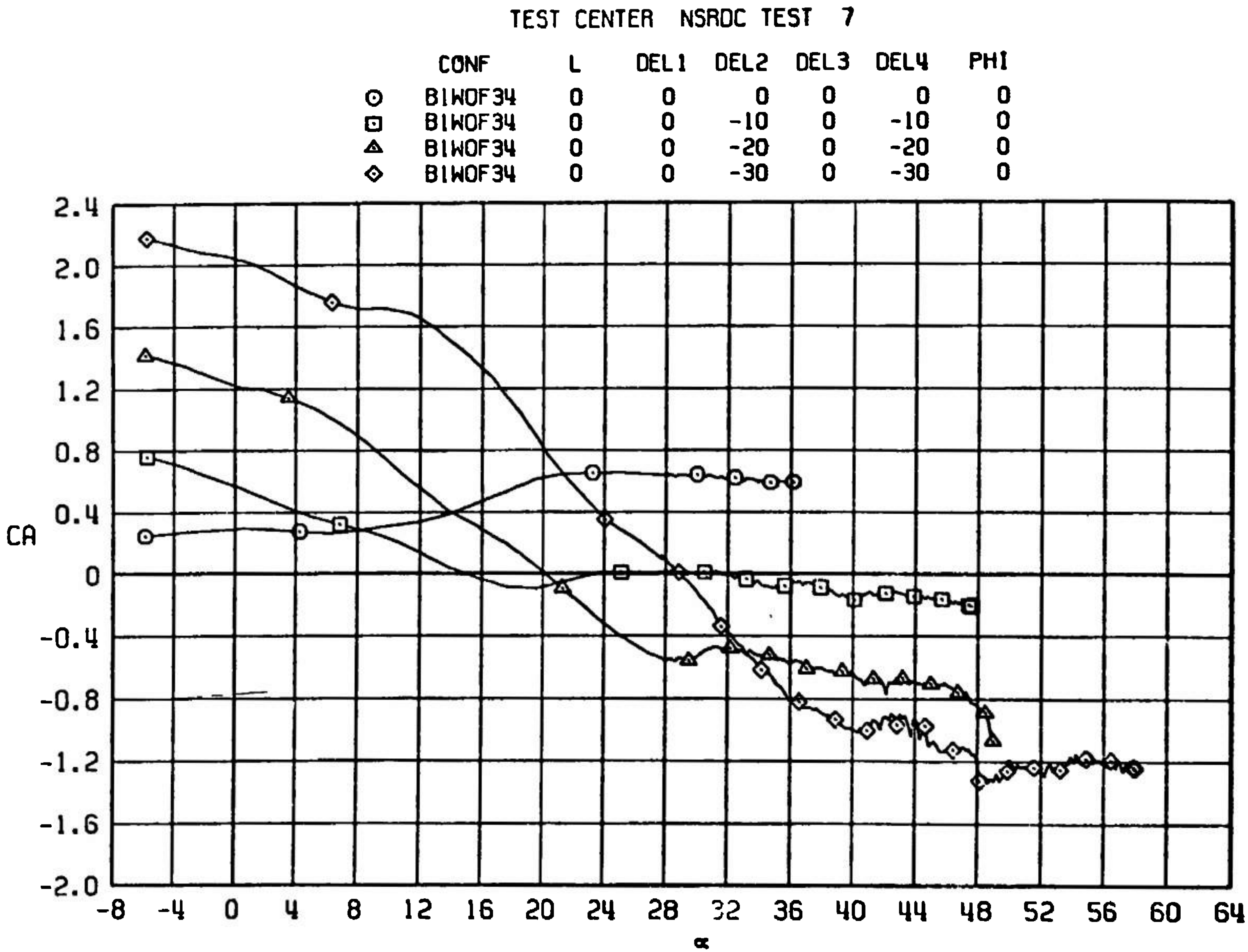

c. CA versus α
Figure 59. Continued.

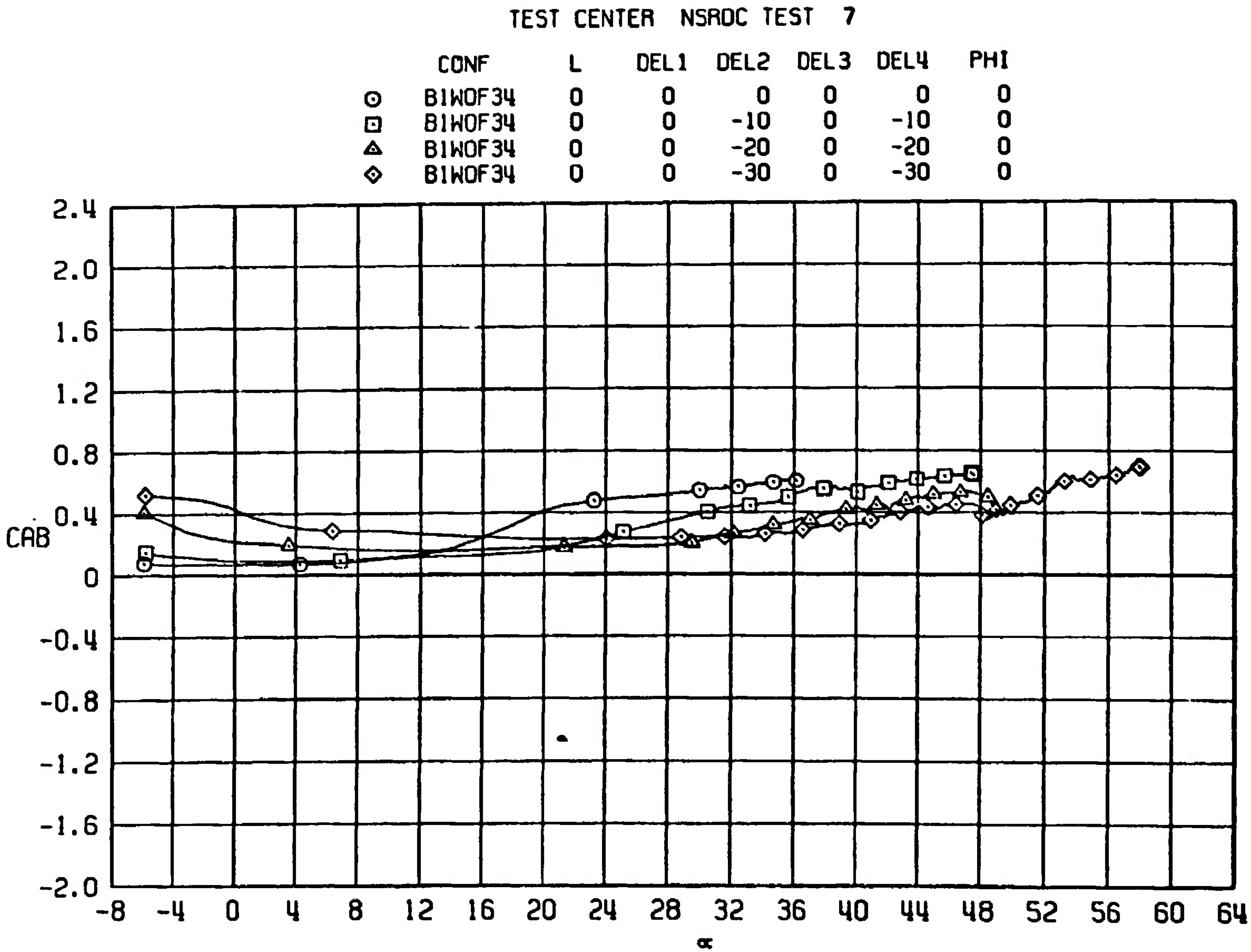

d. CAB versus α

Figure 59. Continued.

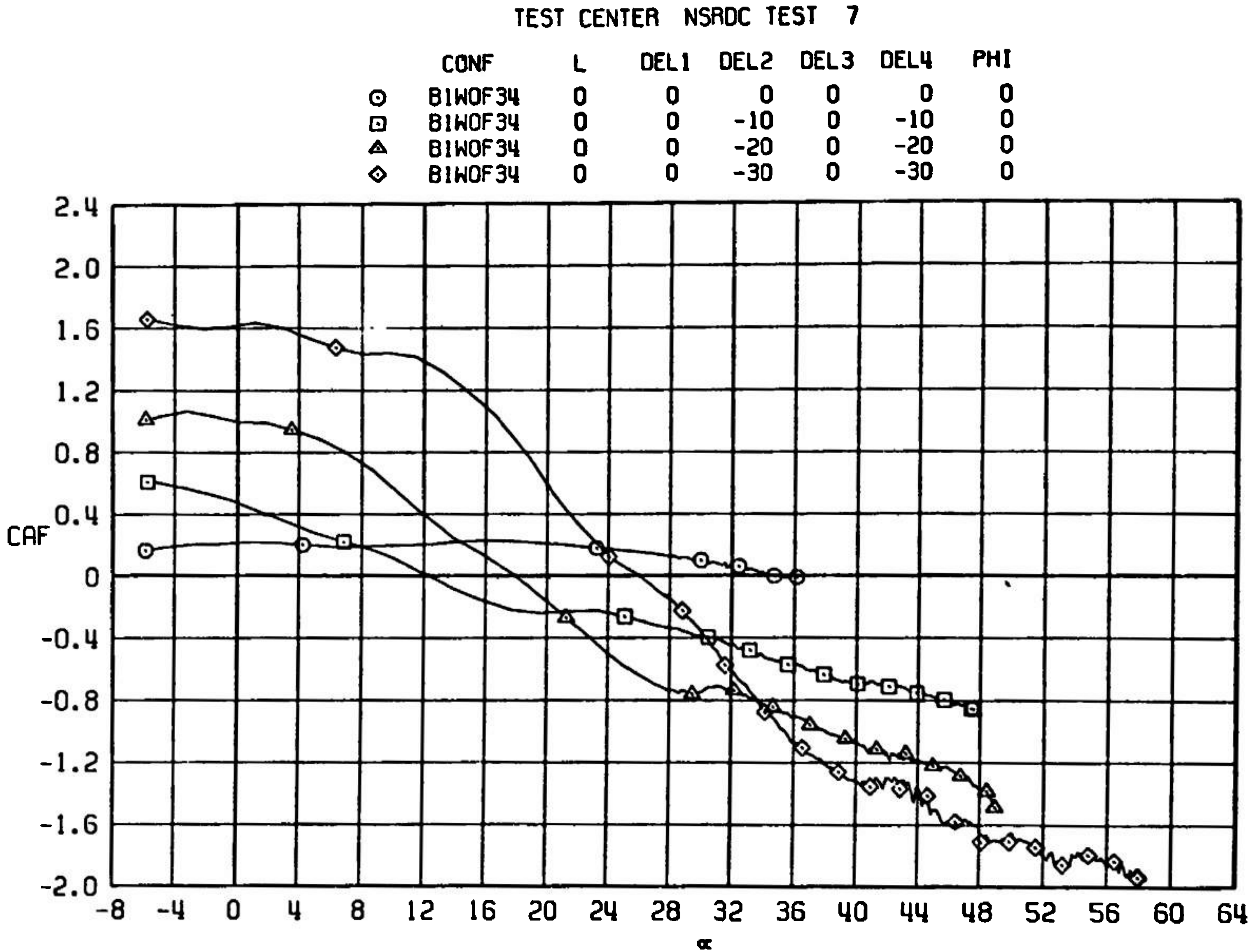

e. CAF versus α
Figure 59. Continued.

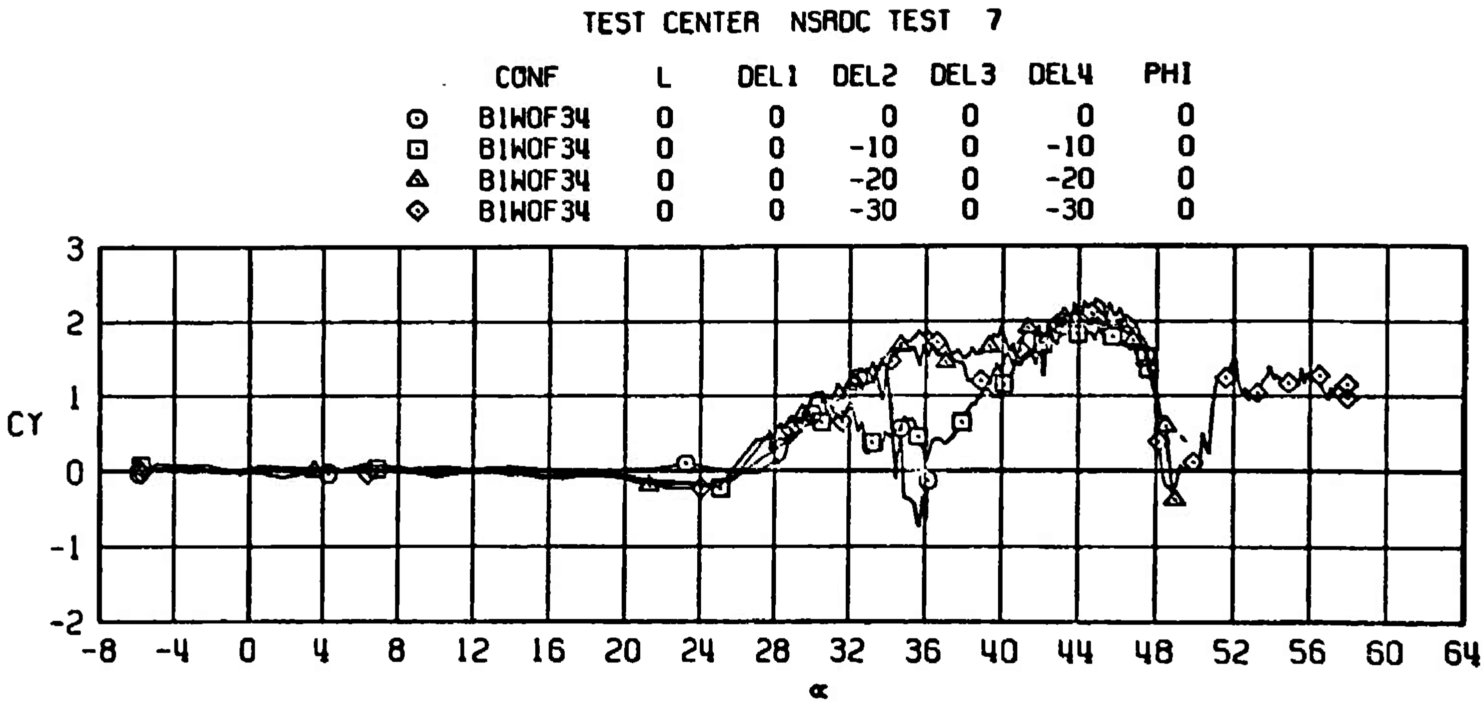

f. CY versus α

Figure 59. Continued.

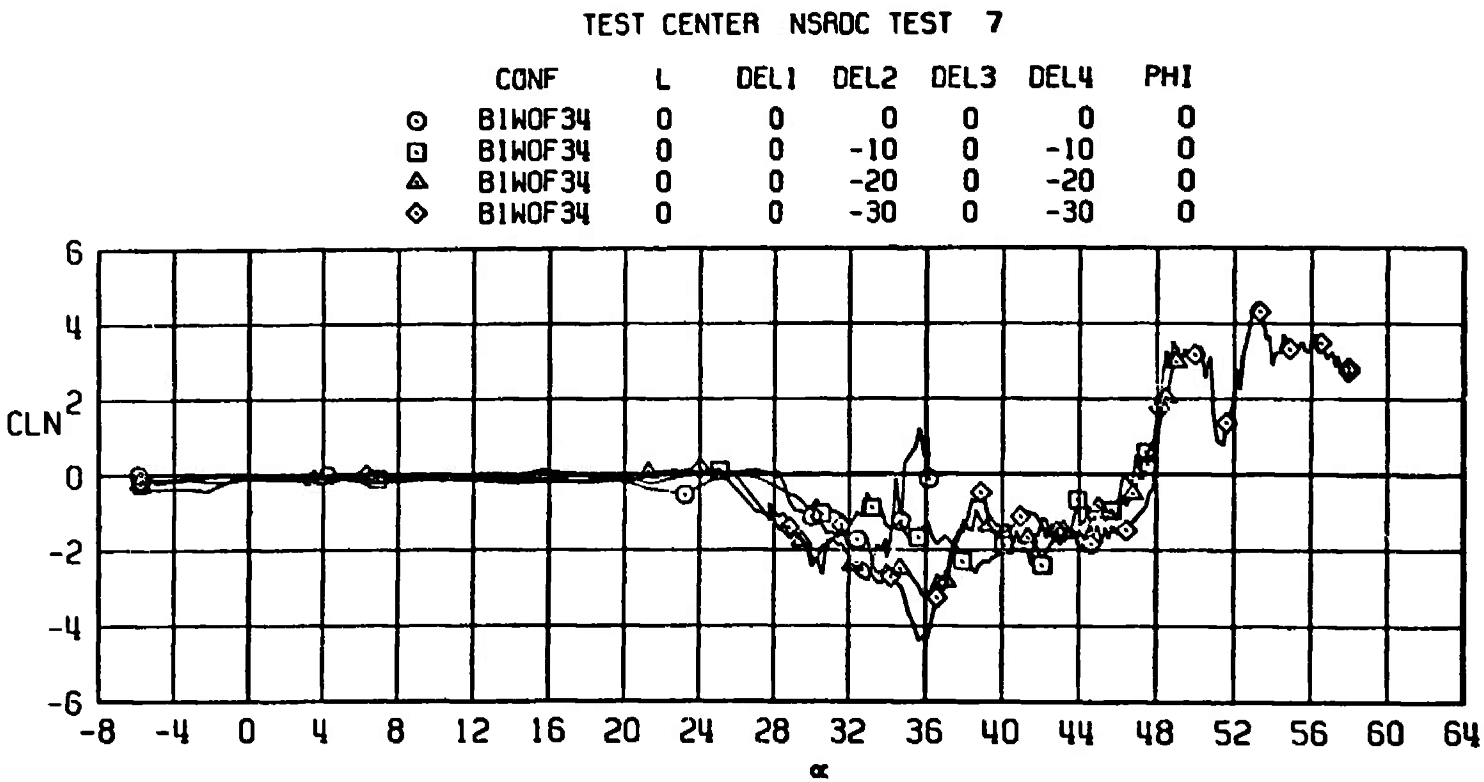

g. CLN versus α
Figure 59. Continued.

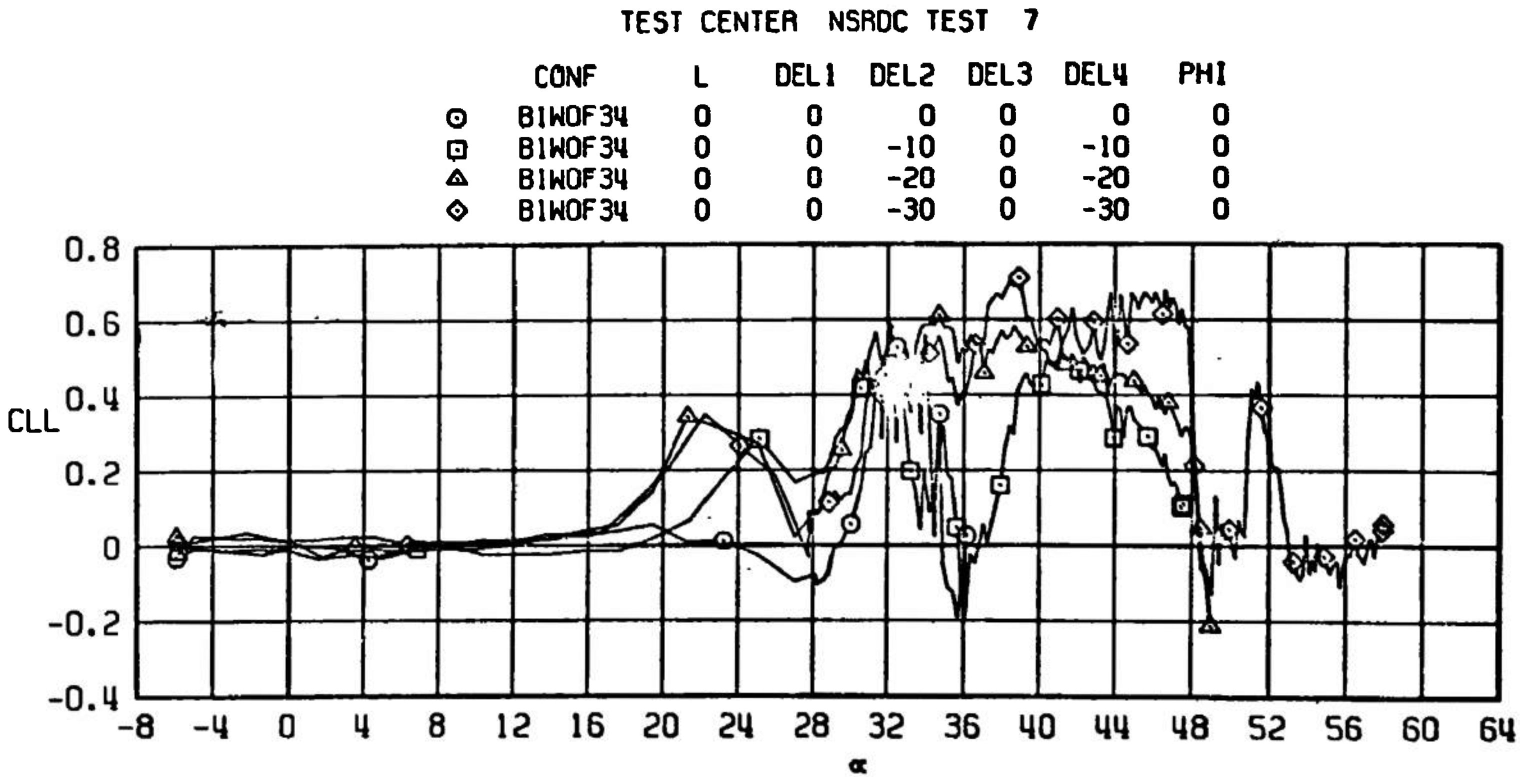

h. CLL versus α

Figure 59. Continued.

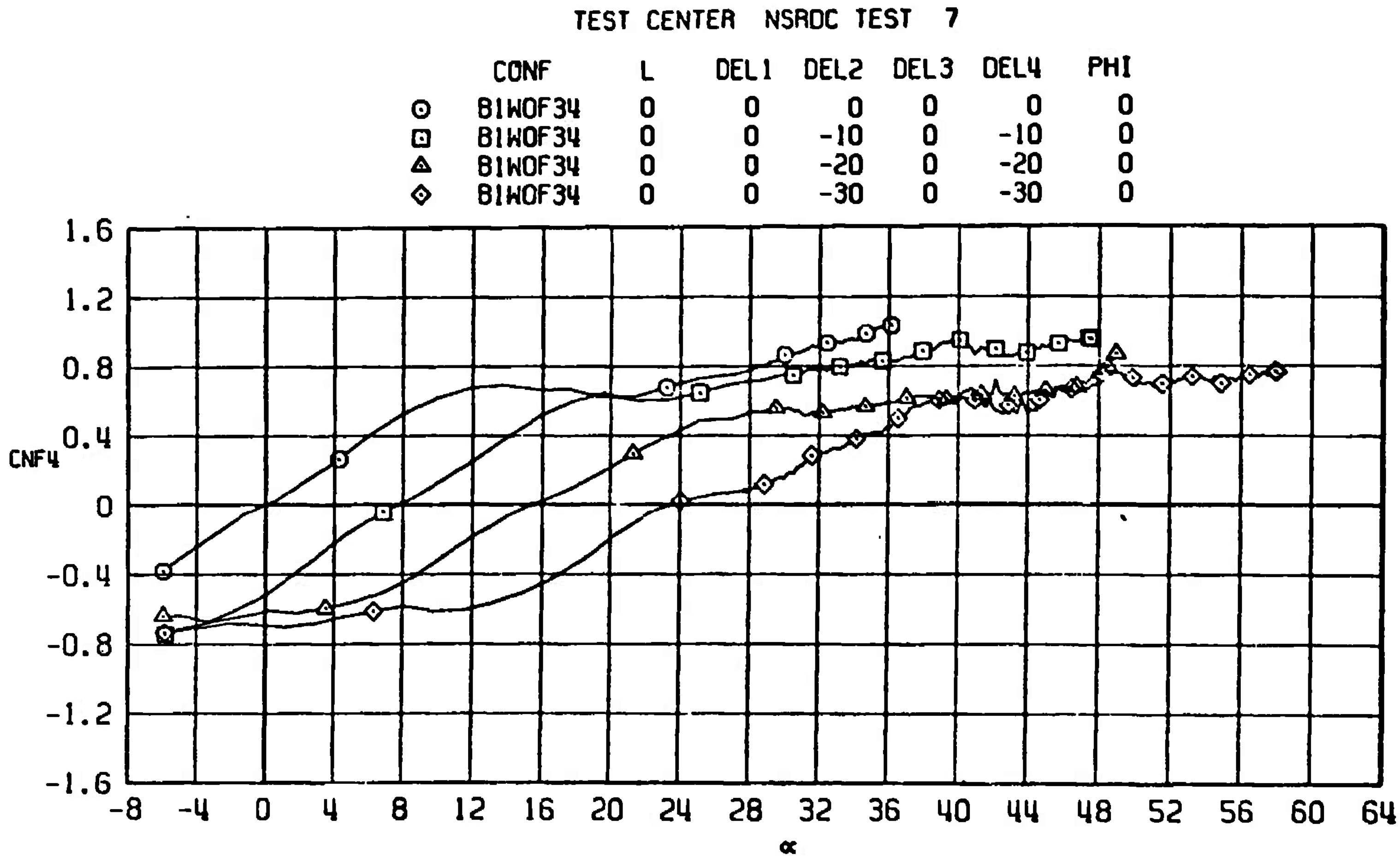

i. CNF4 versus α

Figure 59. Continued.

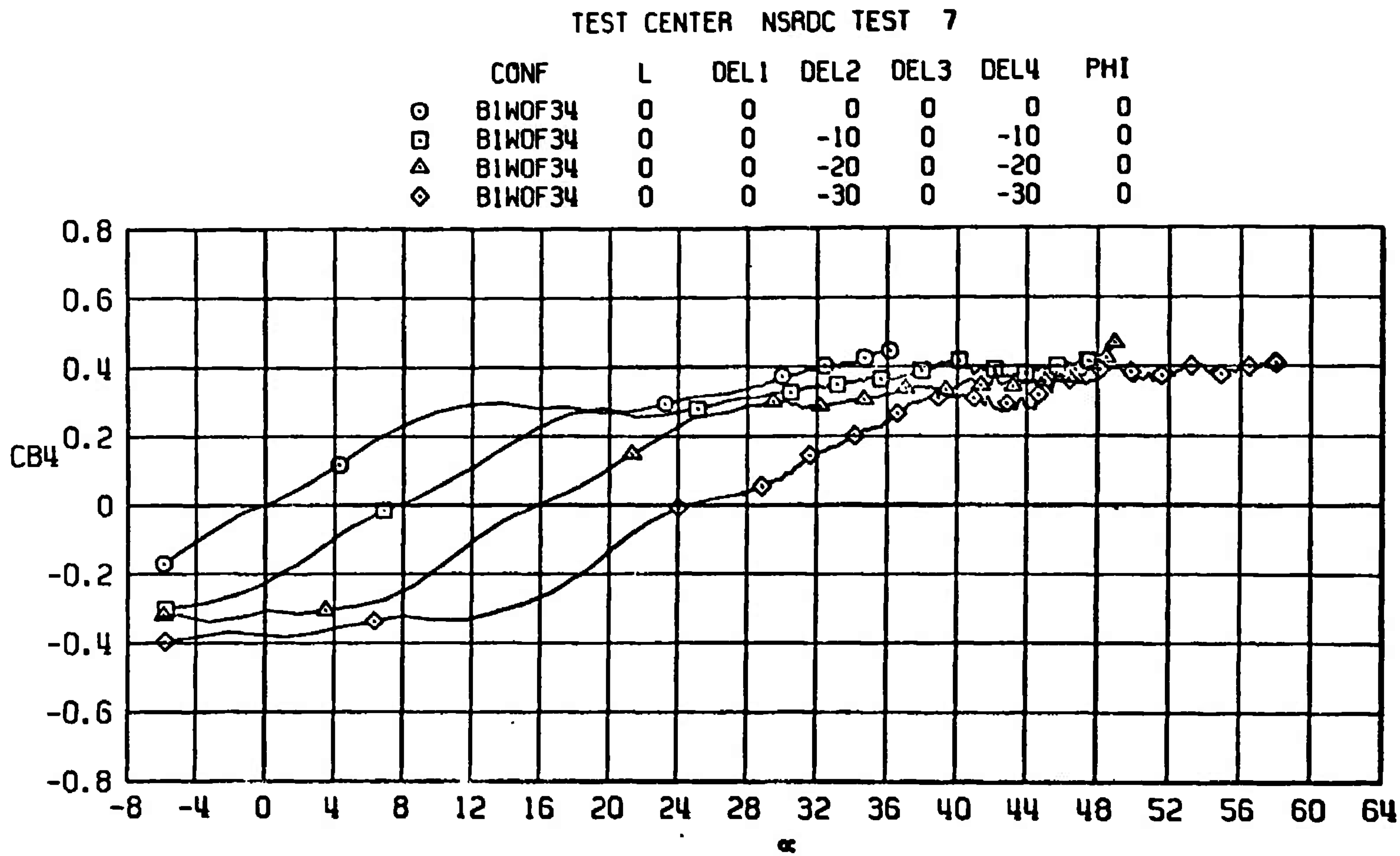

j. CB4 versus α

Figure 59. Continued.

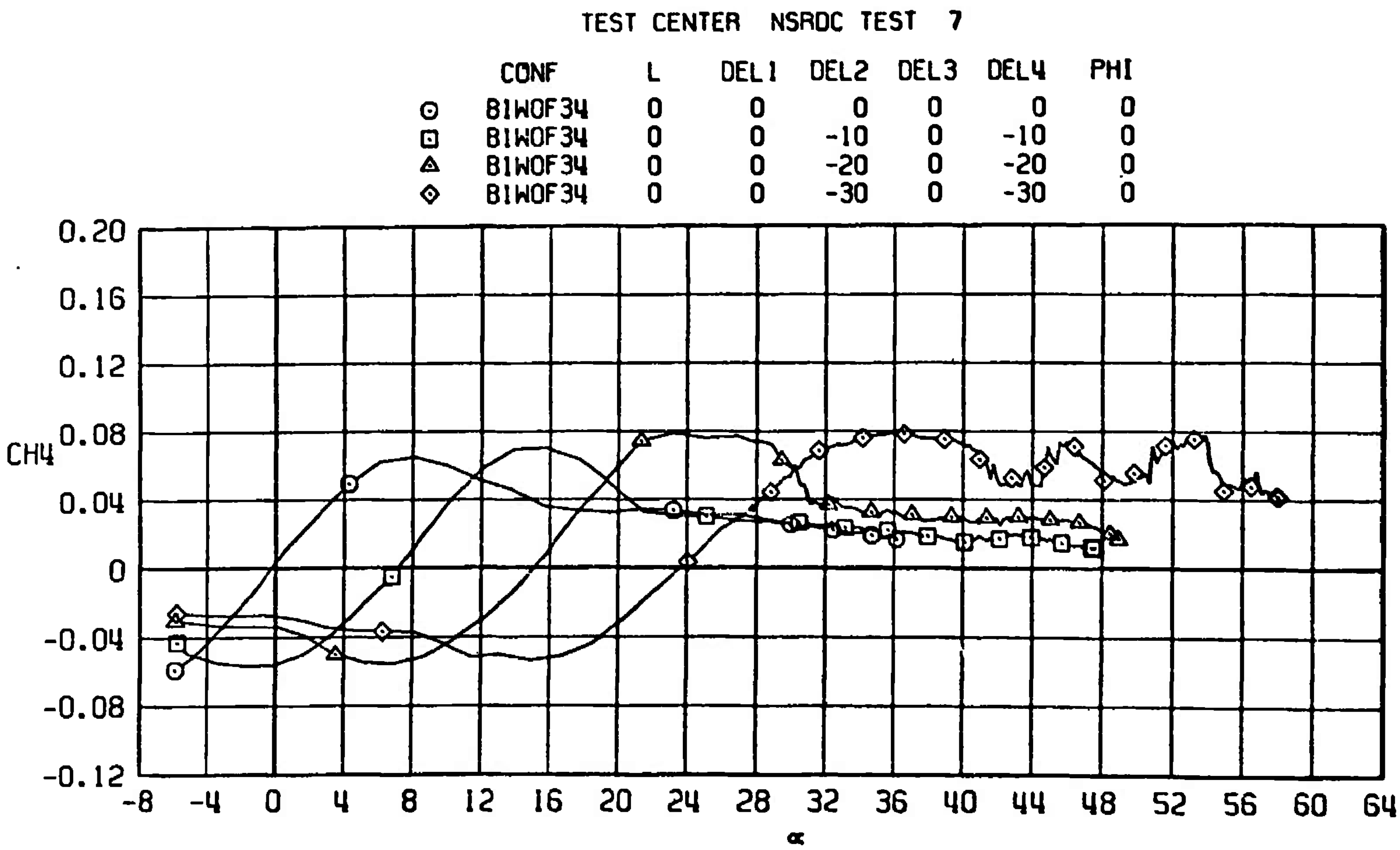

k. CH4 versus α
Figure 59. Concluded.

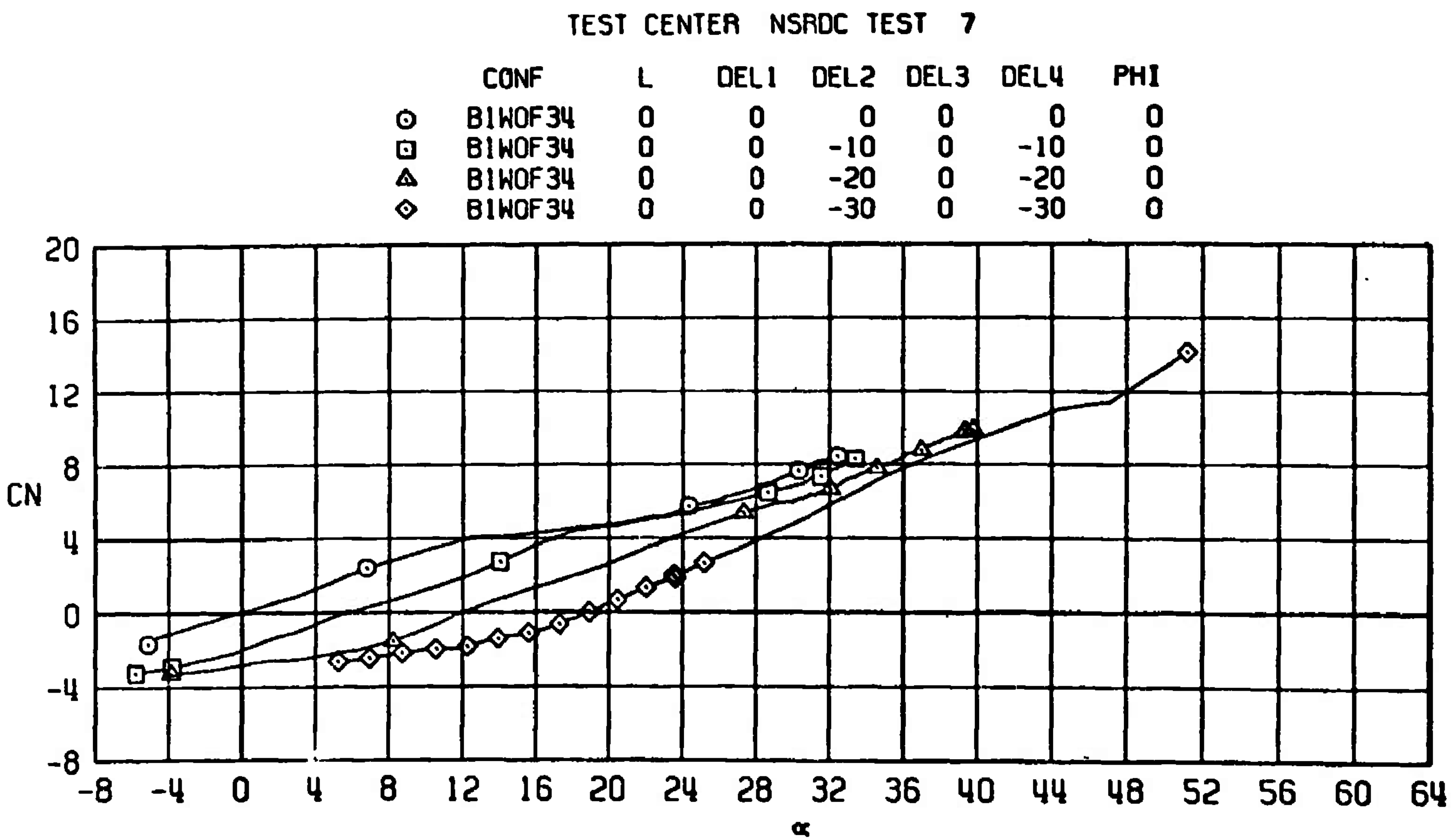

a. CN versus a

Figure 60. Test No. 7, comparison of aerodynamic coefficients of configuration B1W0F34 for various deflections of tail fins No. 2 and 4 at M_∞ = 0.9.

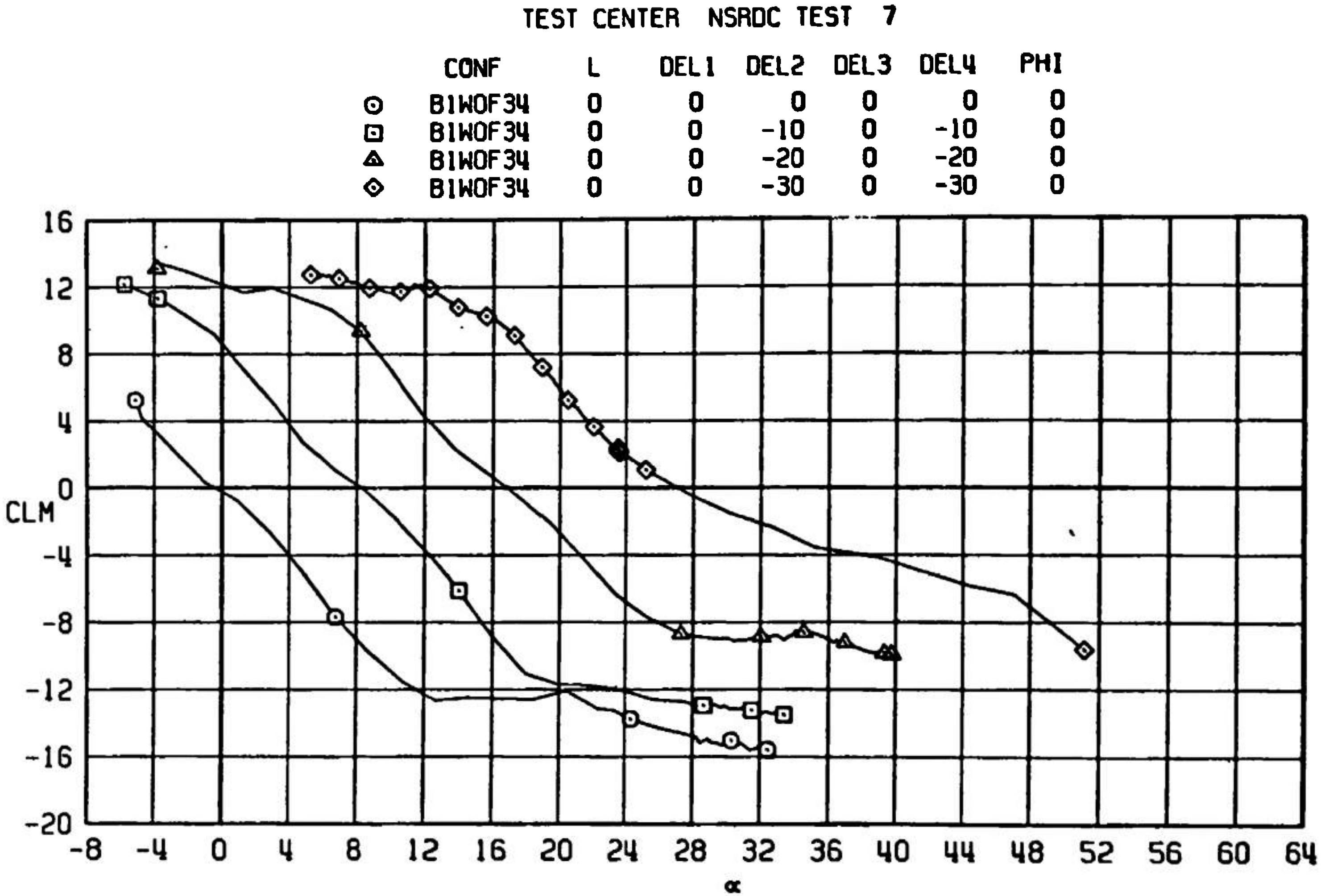

b. CLM versus α
Figure 60. Continued.

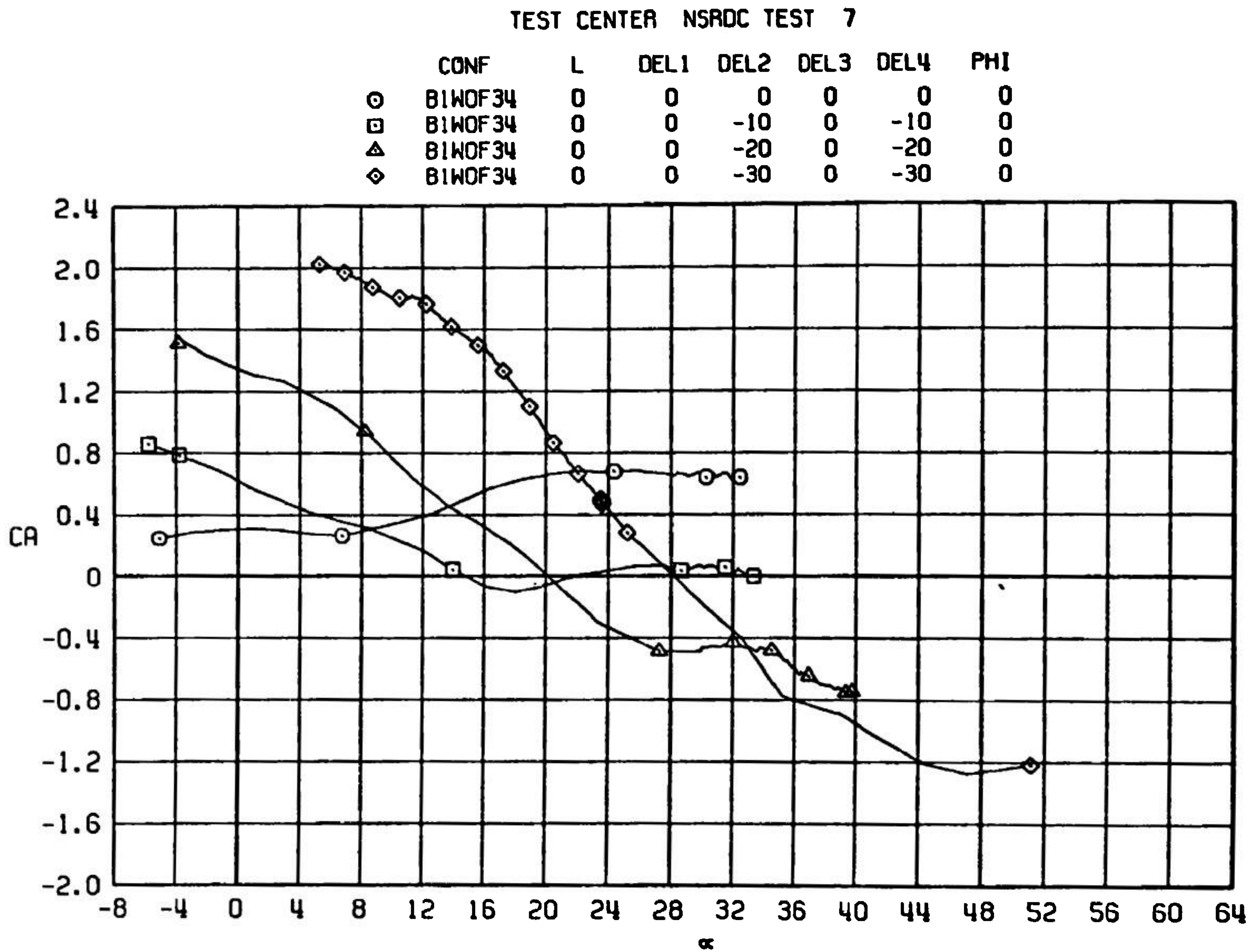

c. CA versus α
Figure 60. Continued.

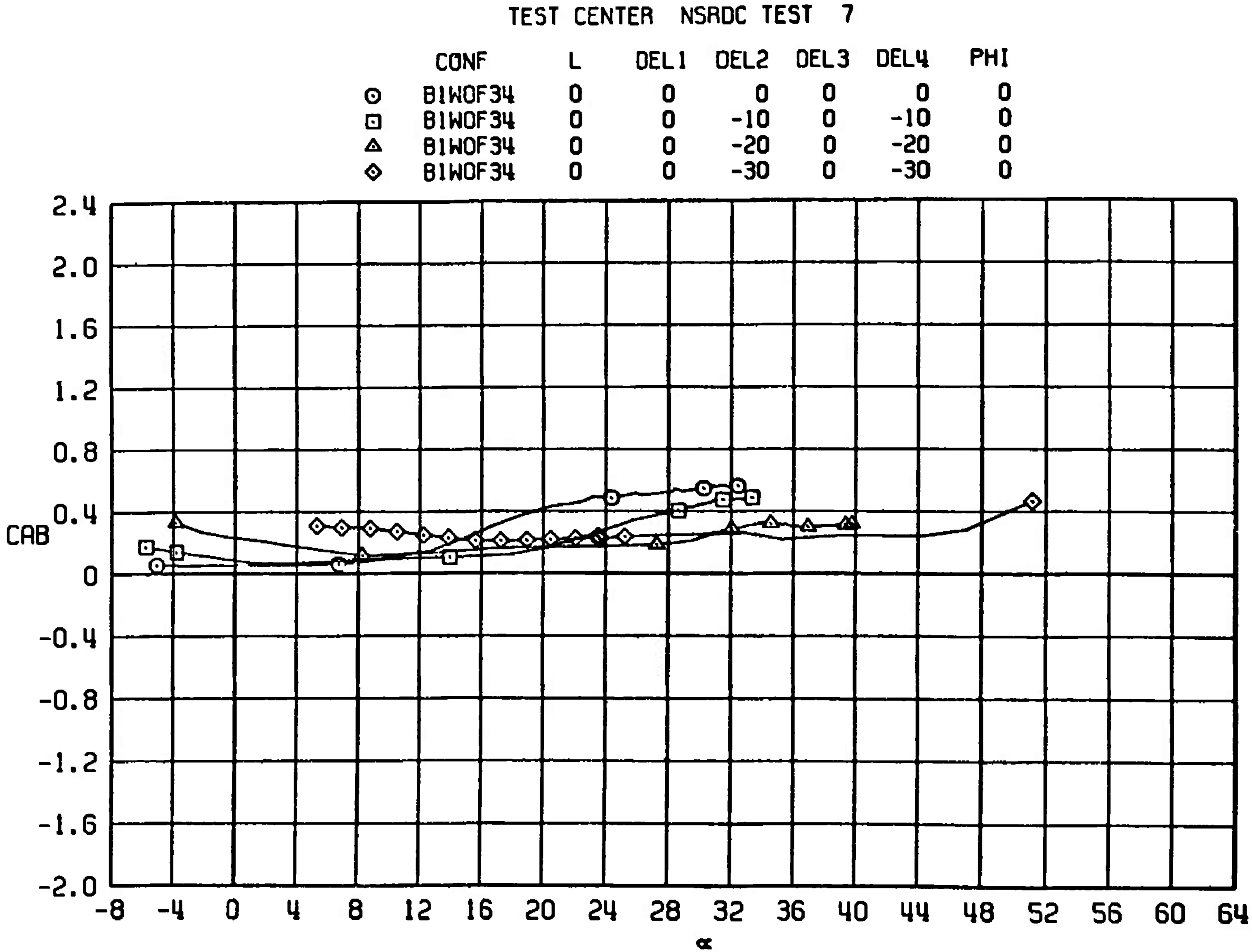

d. CAB versus α
Figure 60. Continued.

TEST CENTER NSRDC TEST 7

	CONF	L	DEL1	DEL2	DEL3	DEL4	PHI
⊙	BIWOF34	0	0	0	0	0	0
⊡	BIWOF34	0	0	-10	0	-10	0
△	BIWOF34	0	0	-20	0	-20	0
◇	BIWOF34	0	0	-30	0	-30	0

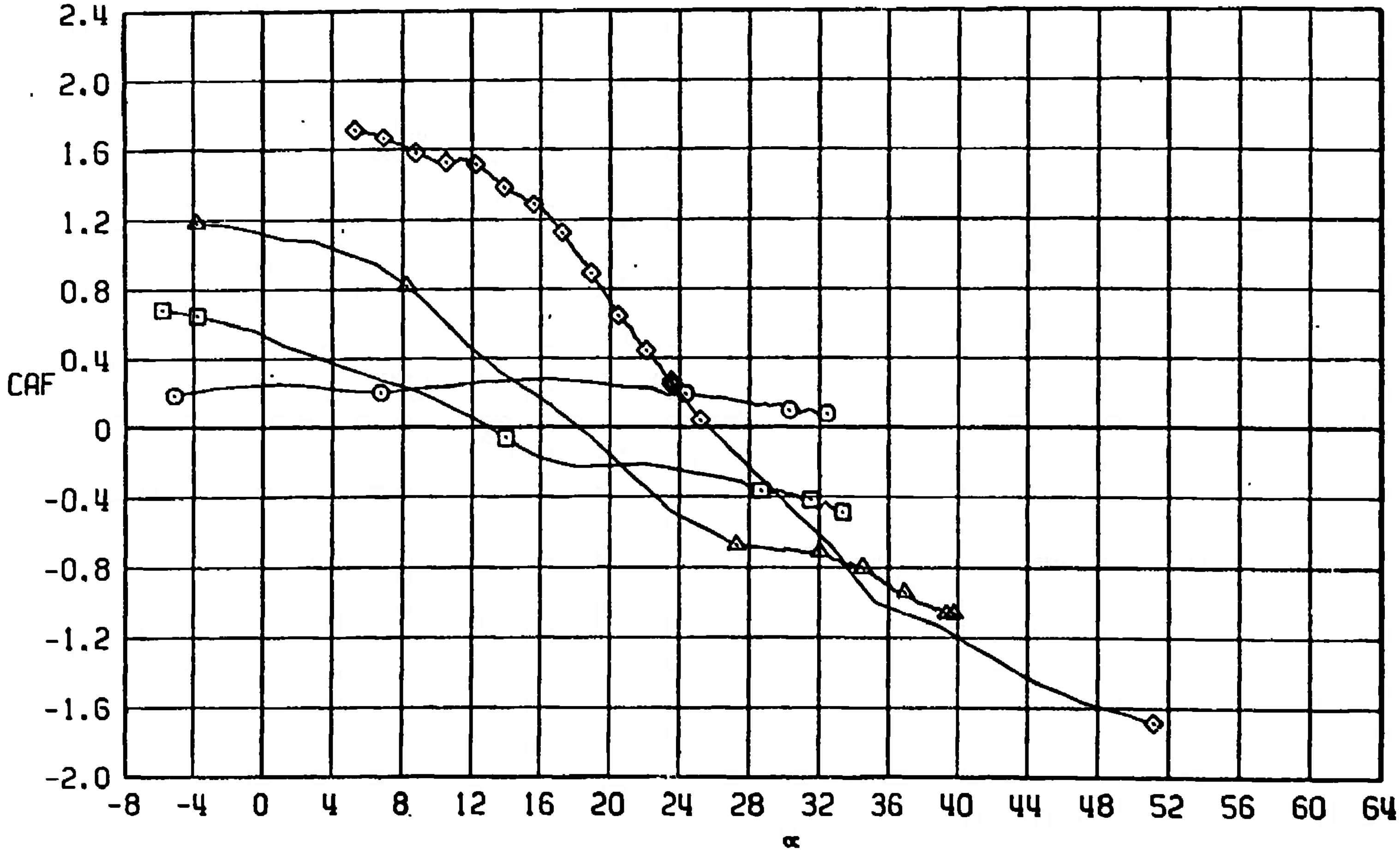

e. CAF versus α
Figure 60. Continued.

TEST CENTER NSRDC TEST 7

	CONF	L	DEL1	DEL2	DEL3	DEL4	PHI
⊙	B1W0F34	0	0	0	0	0	0
⊡	B1W0F34	0	0	-10	0	-10	0
◬	B1W0F34	0	0	-20	0	-20	0
◇	B1W0F34	0	0	-30	0	-30	0

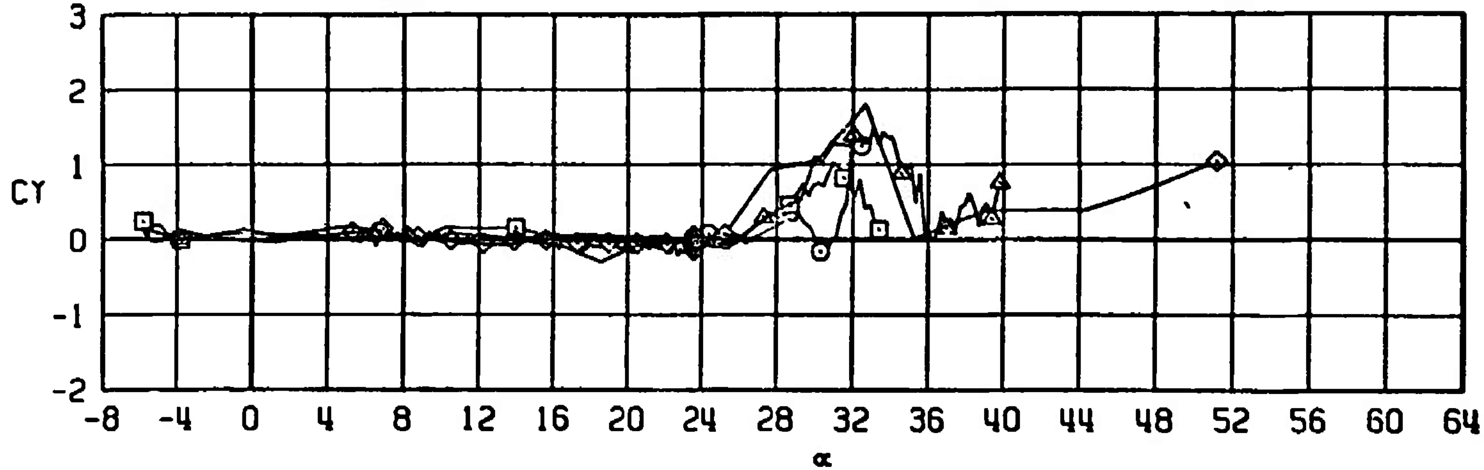

f. CY versus α
Figure 60. Continued.

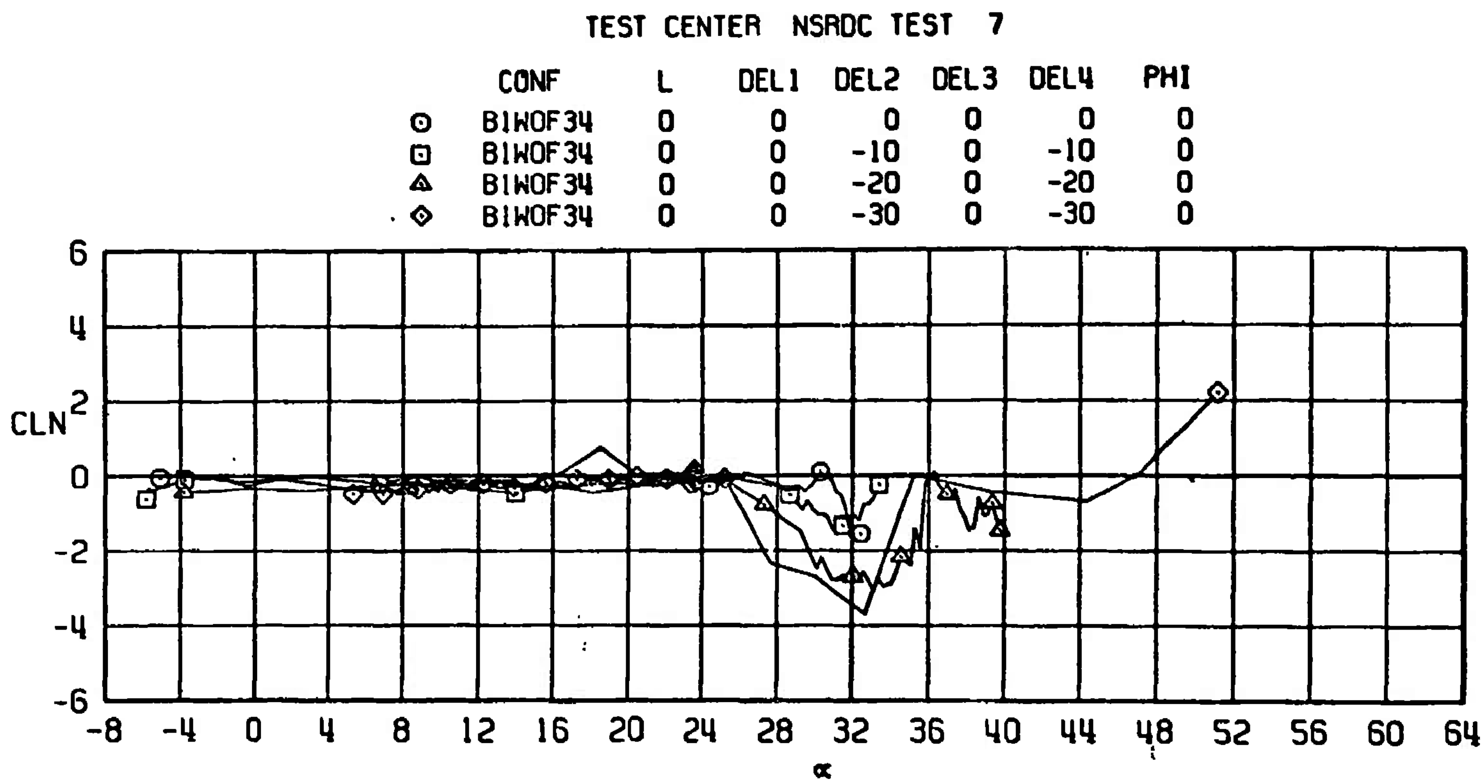

g. CLN versus α
Figure 60. Continued.

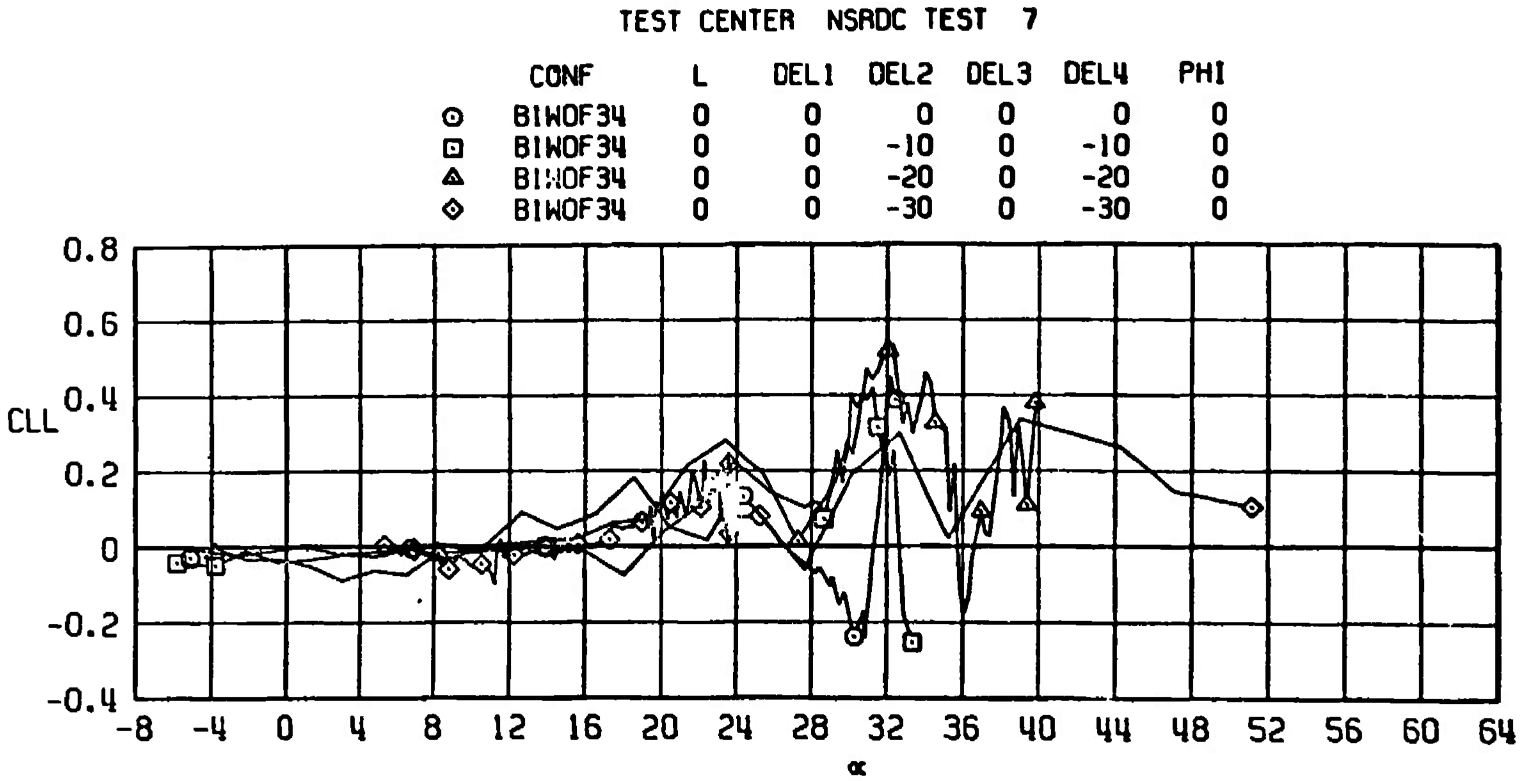

h. CLL versus α
Figure 60. Continued.

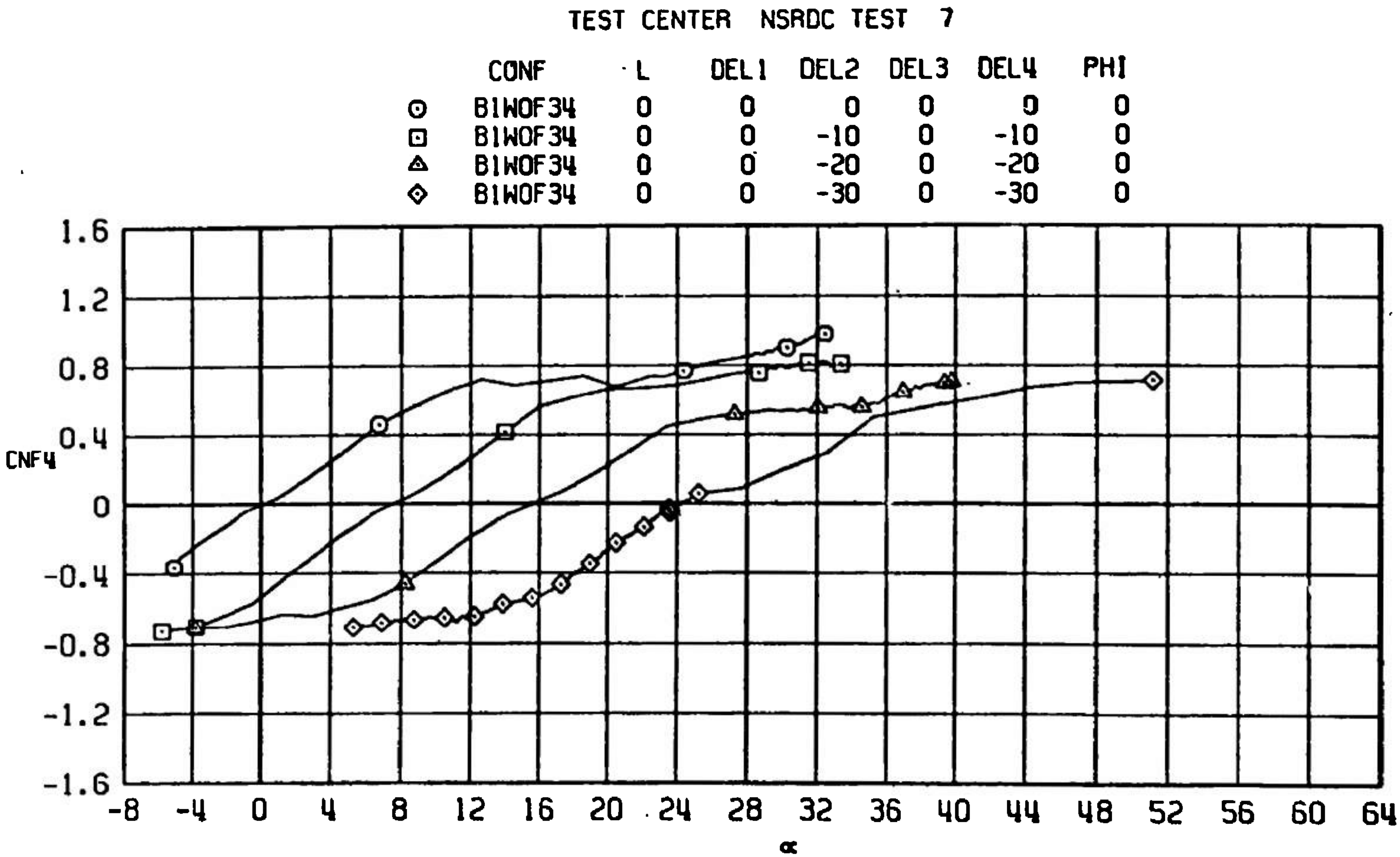

i. CNF4 versus α
Figure 60. Continued.

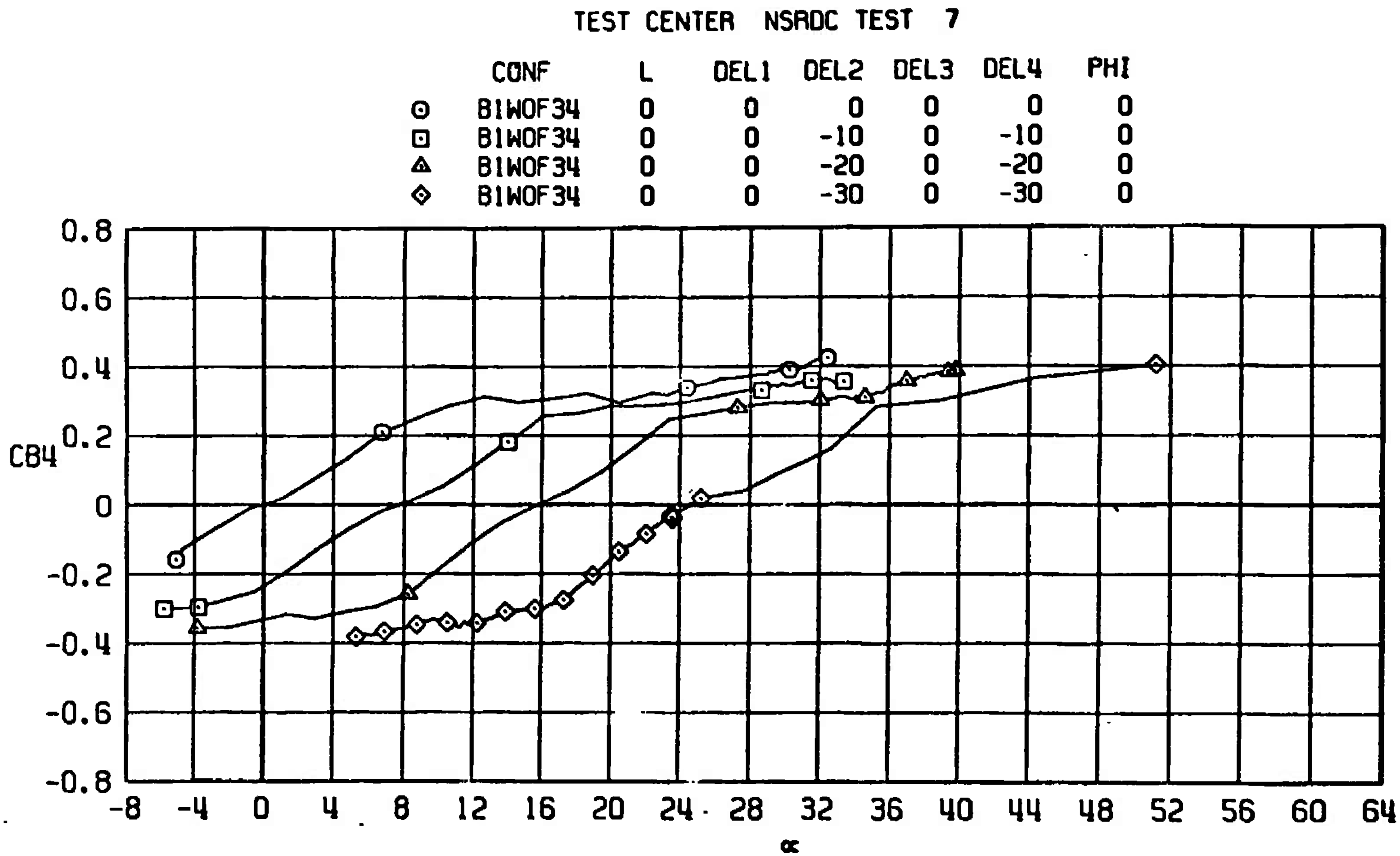

j. CB4 versus α
Figure 60. Continued.

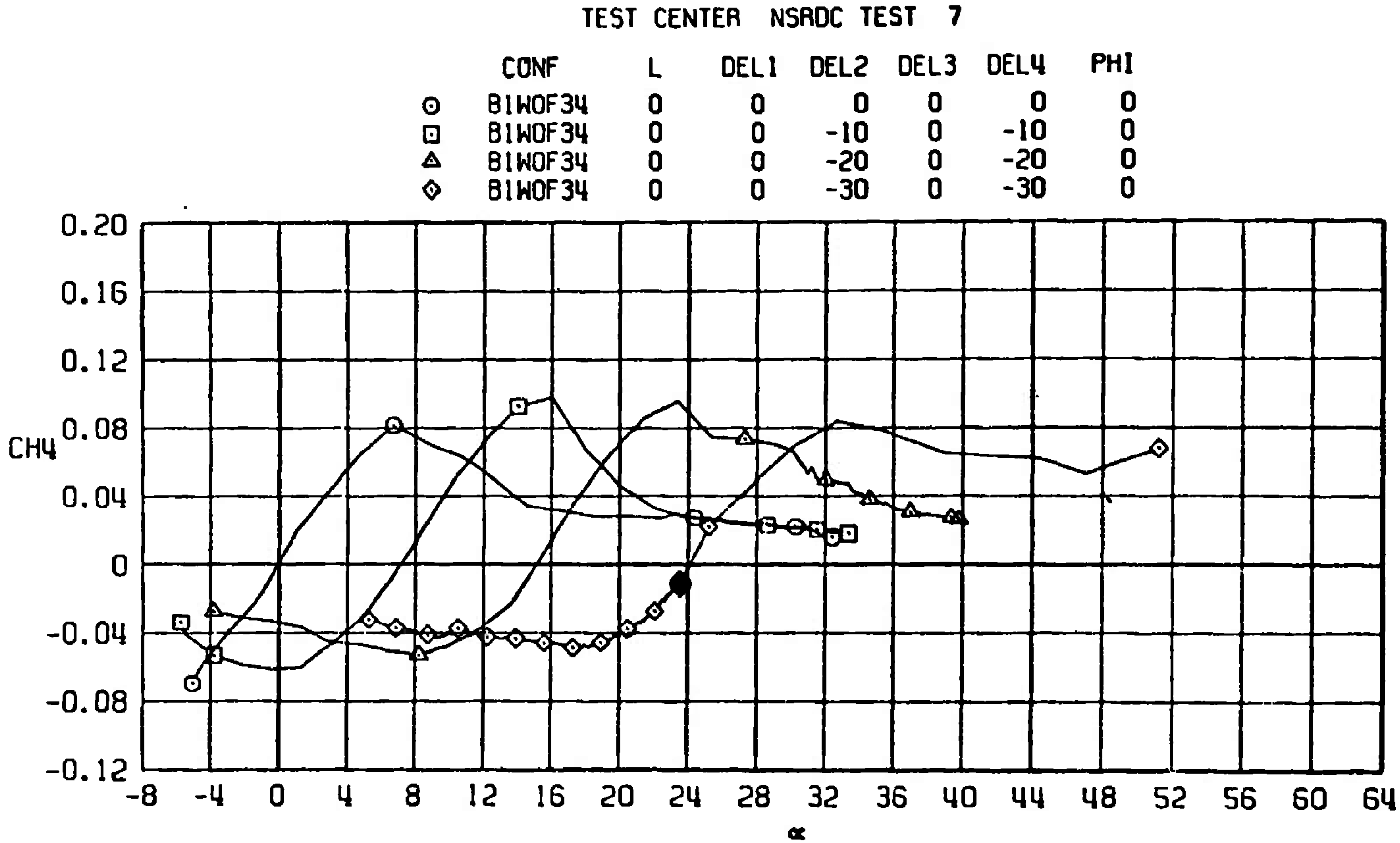

k. CH4 versus α
Figure 60. Concluded.

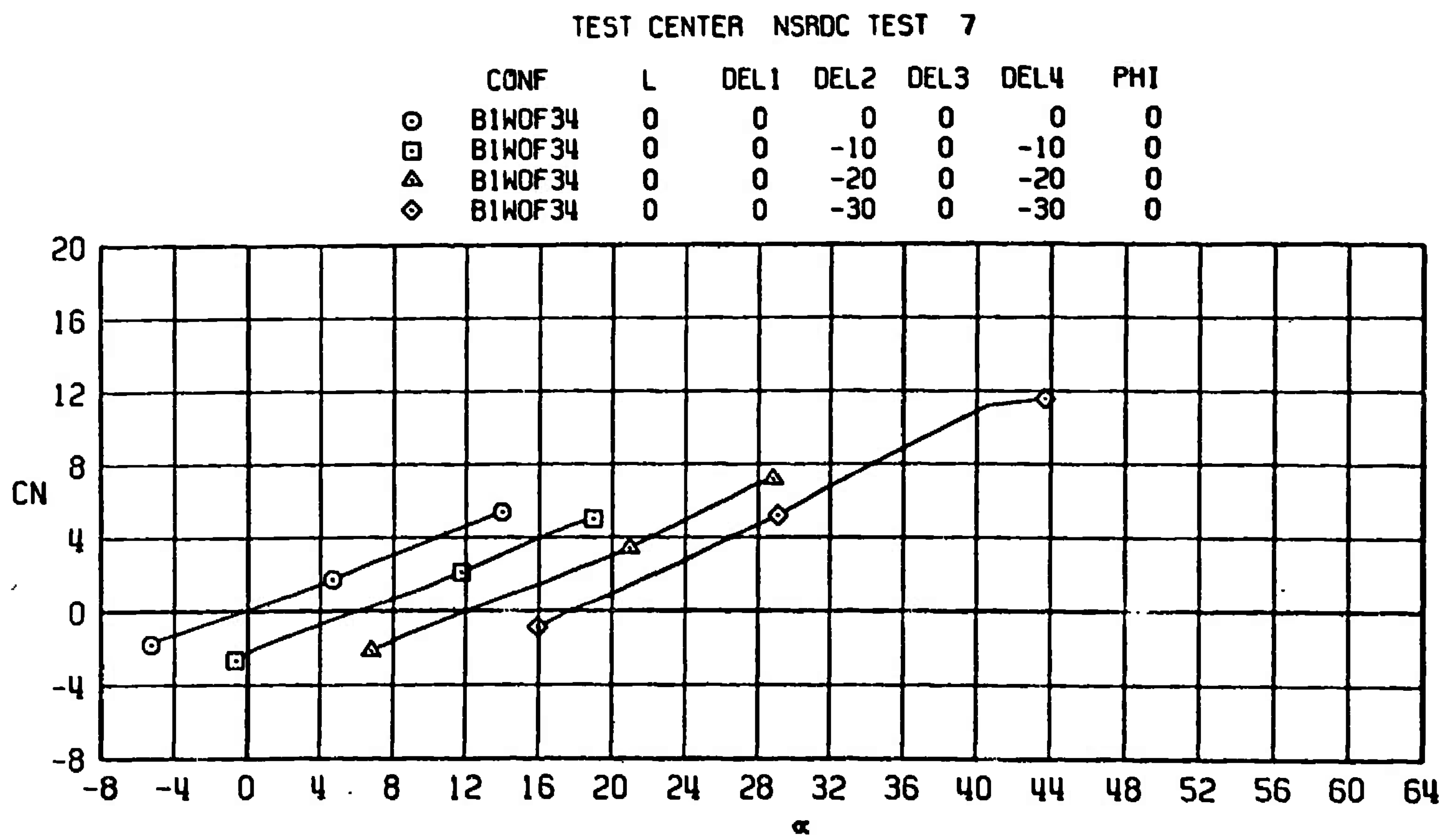

a. CN versus α

Figure 61. Test No. 7, comparison of aerodynamic coefficients of configuration B1W0F34 for various deflections of tail fins No. 2 and 4 at M_∞ = 1.0.

TEST CENTER NSRDC TEST 7

	CONF	L	DEL1	DEL2	DEL3	DEL4	PHI
⊙	B1W0F34	0	0	0	0	0	0
⊡	B1W0F34	0	0	-10	0	-10	0
△	B1W0F34	0	0	-20	0	-20	0
◇	B1W0F34	0	0	-30	0	-30	0

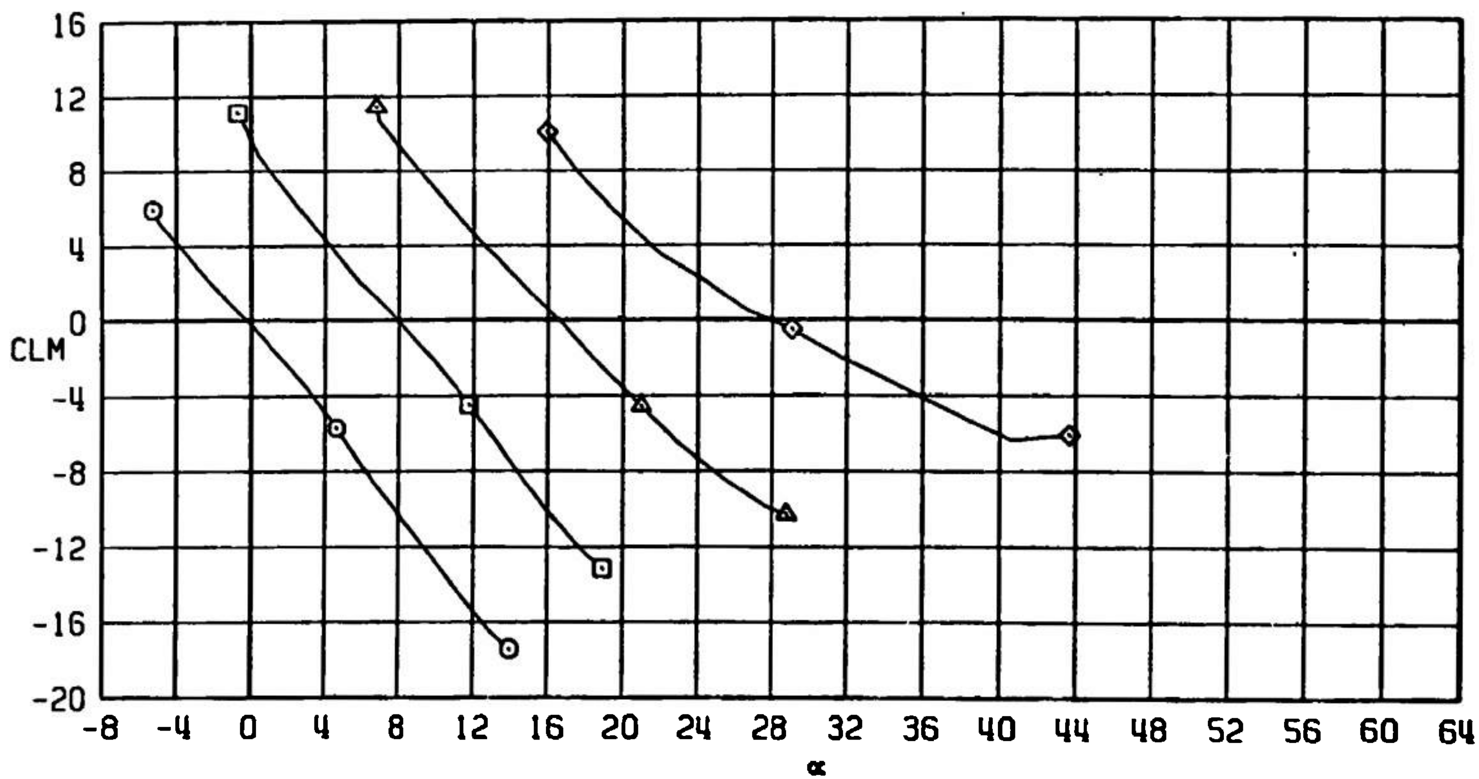

b. CLM versus α

Figure 61. Continued.

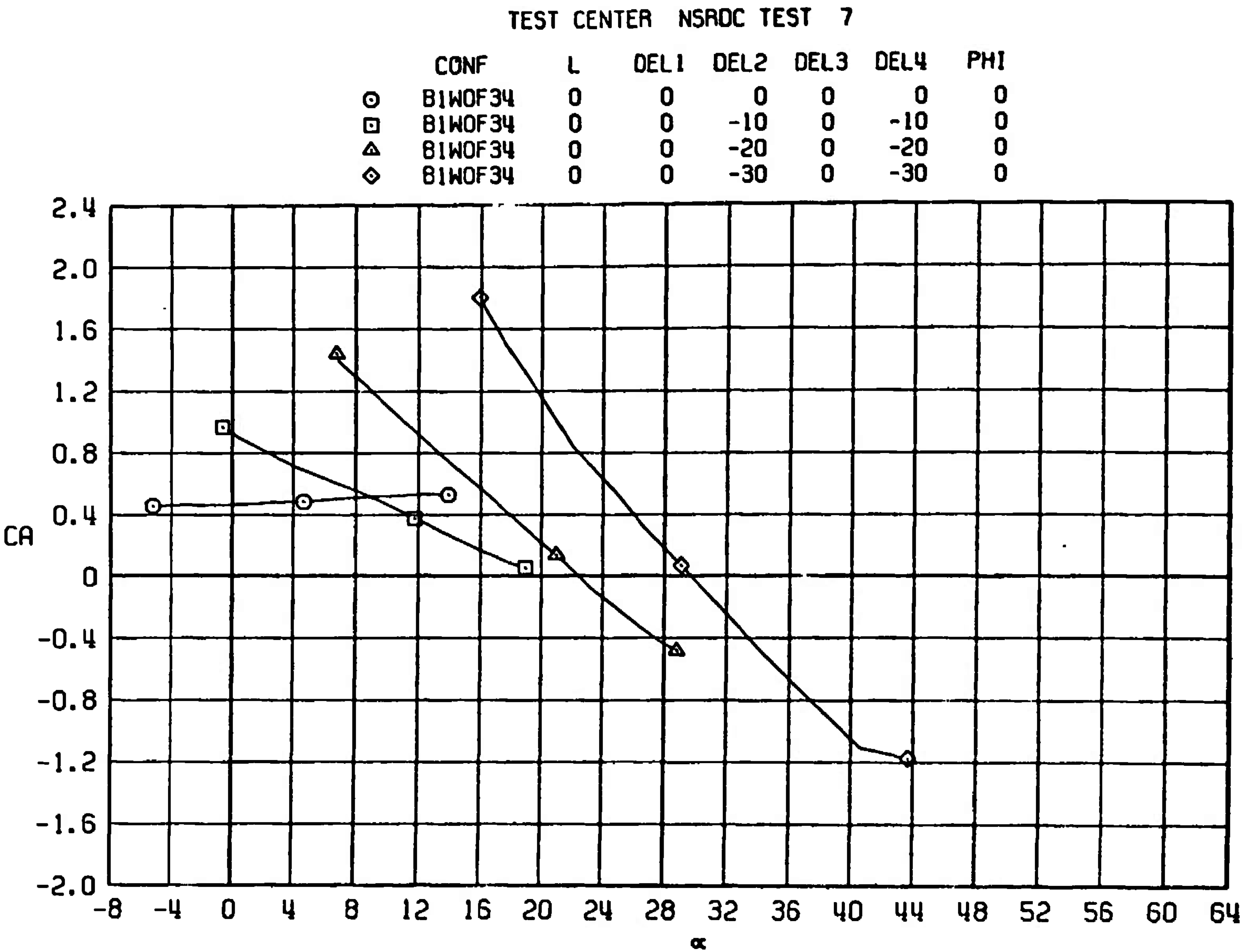

c. CA versus α

Figure 61. Continued.

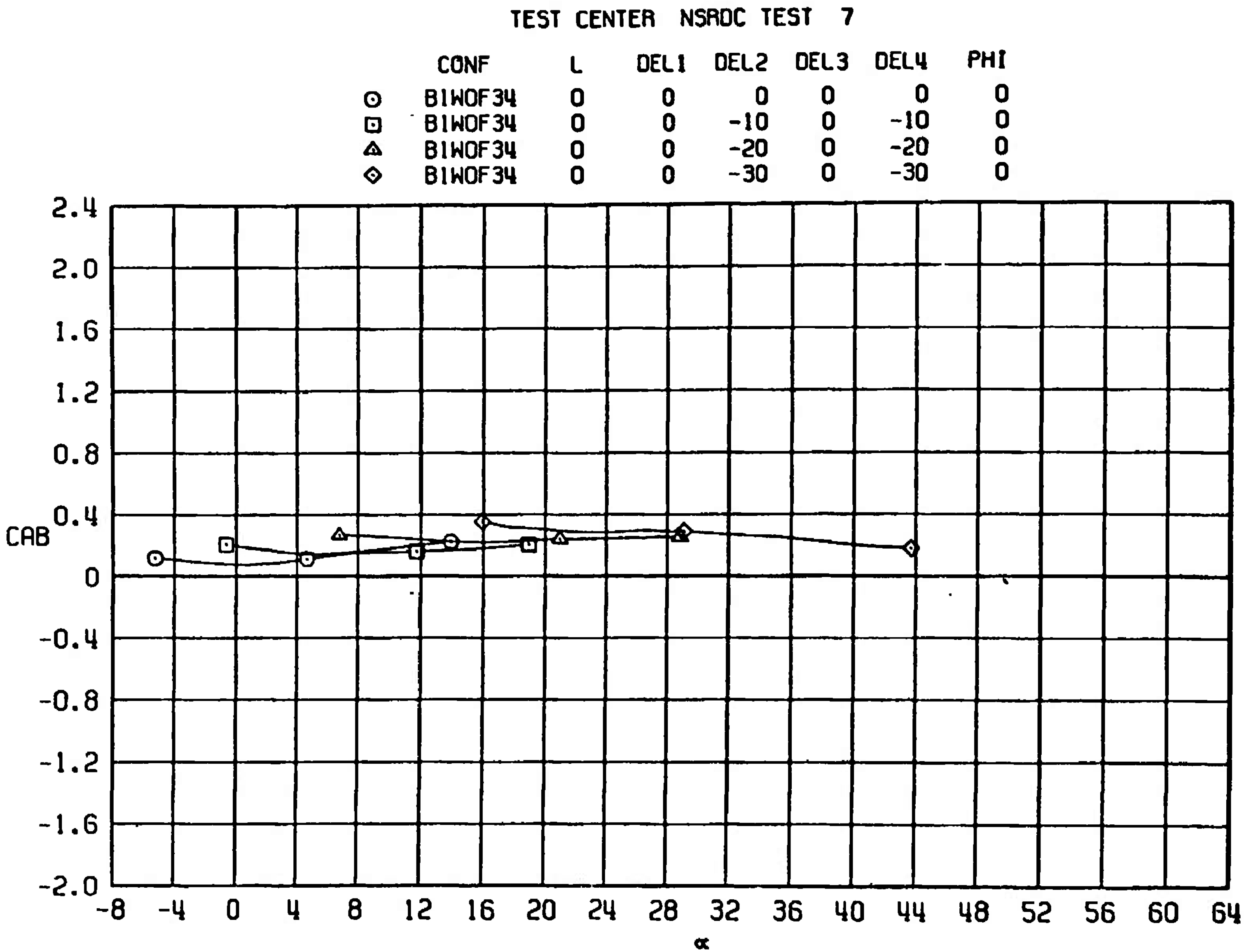

d. CAB versus α

Figure 61. Continued.

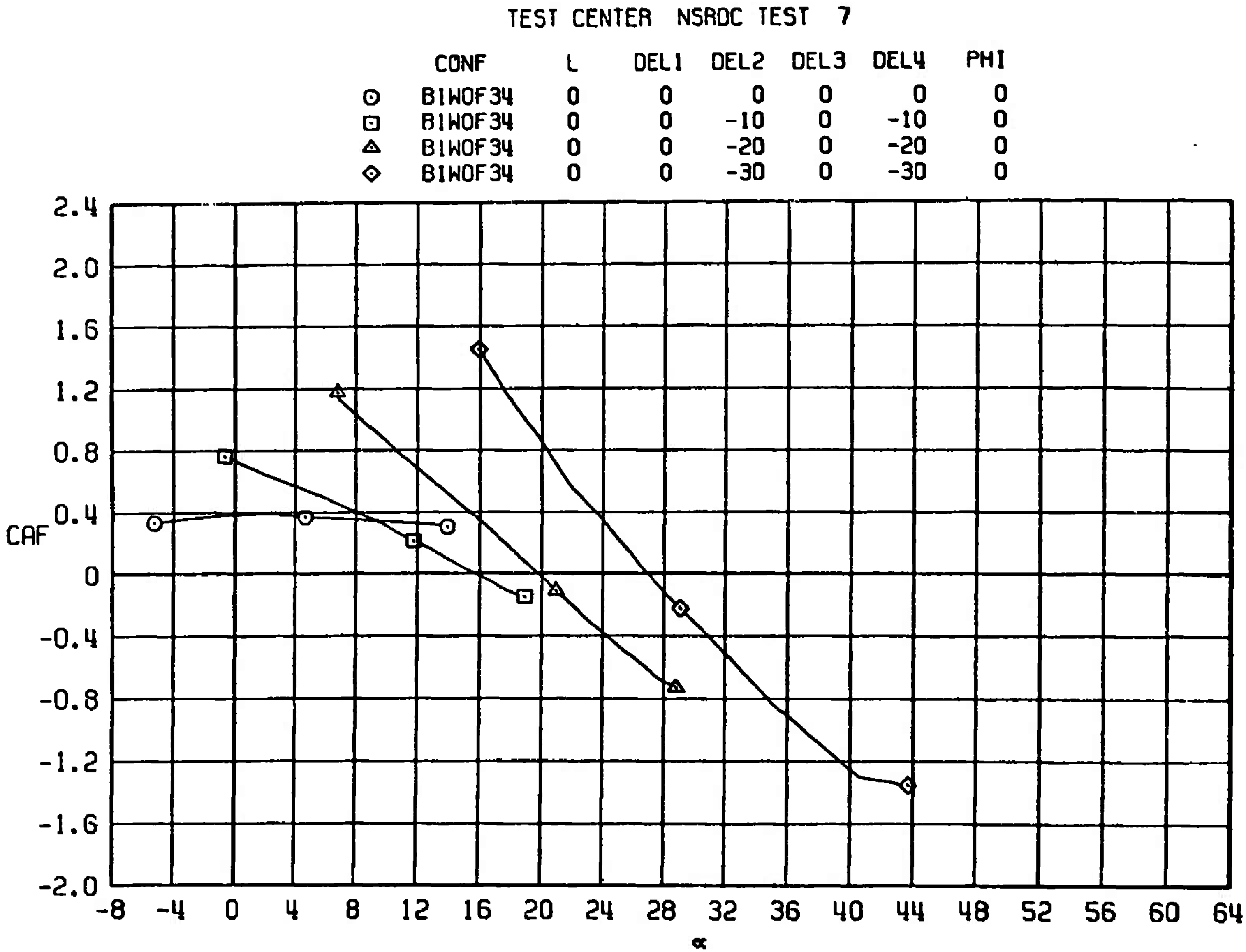

e. CAF versus α

Figure 61. Continued.

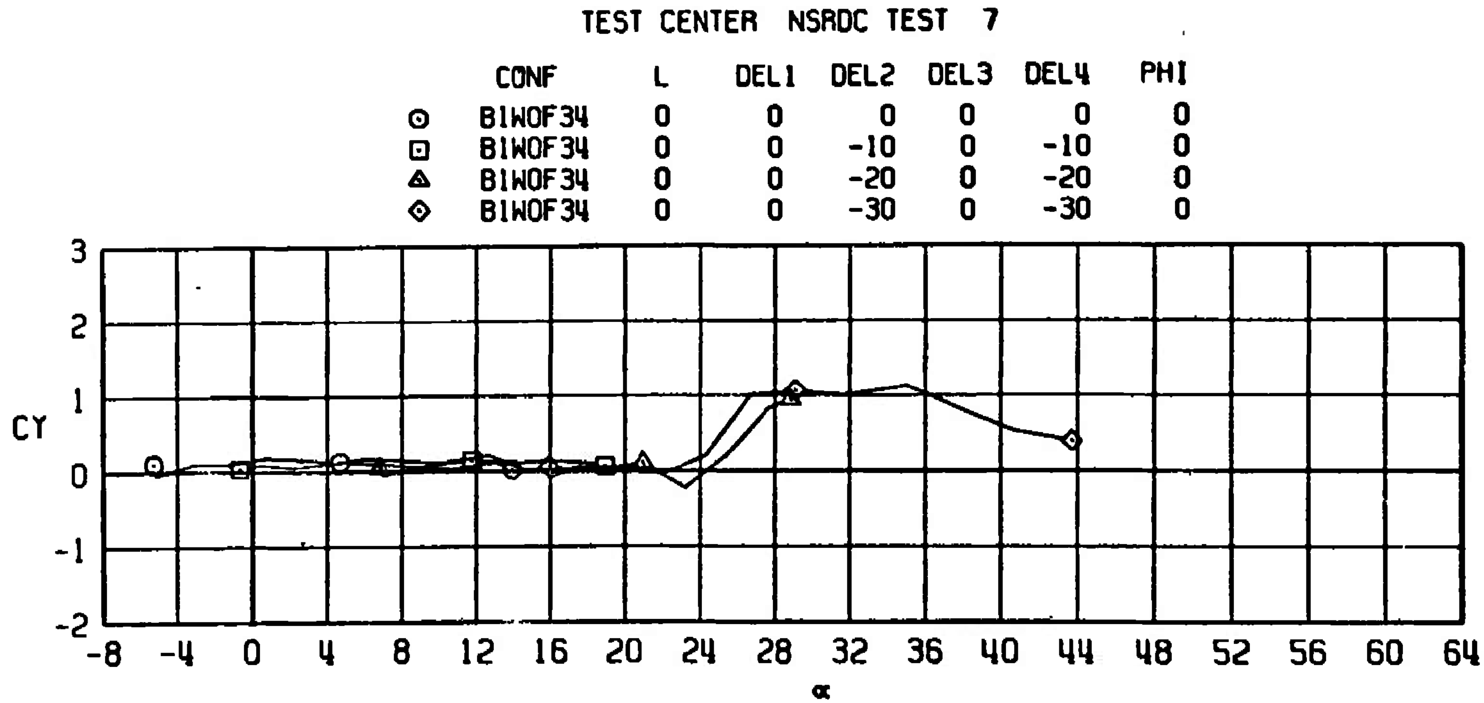

f. CY versus α
Figure 61. Continued.

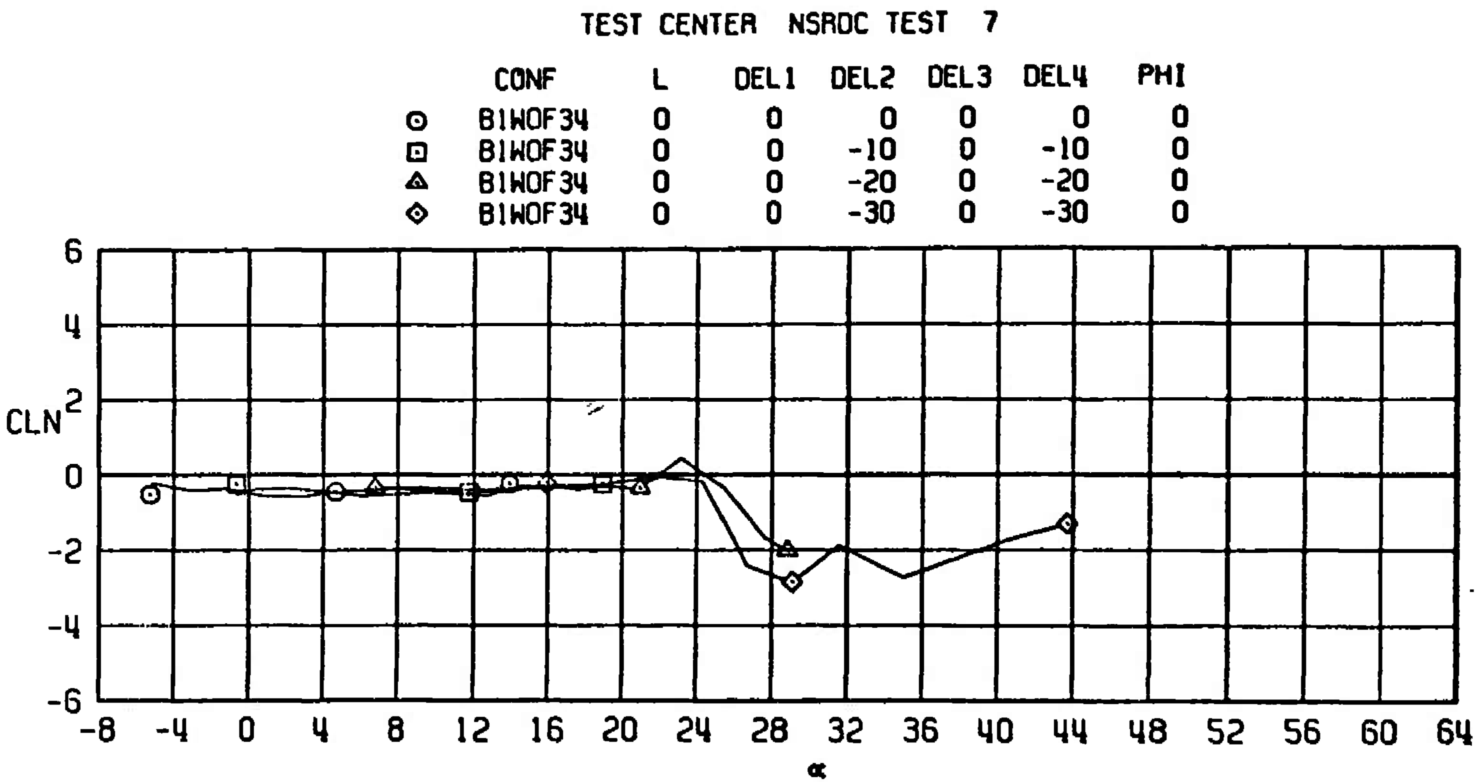

g. CLN versus α
Figure 61. Continued.

TEST CENTER NSRDC TEST 7

	CONF	L	DEL1	DEL2	DEL3	DEL4	PHI
⊙	B1W0F34	0	0	0	0	0	0
⊡	B1W0F34	0	0	-10	0	-10	0
△	B1W0F34	0	0	-20	0	-20	0
◇	B1W0F34	0	0	-30	0	-30	0

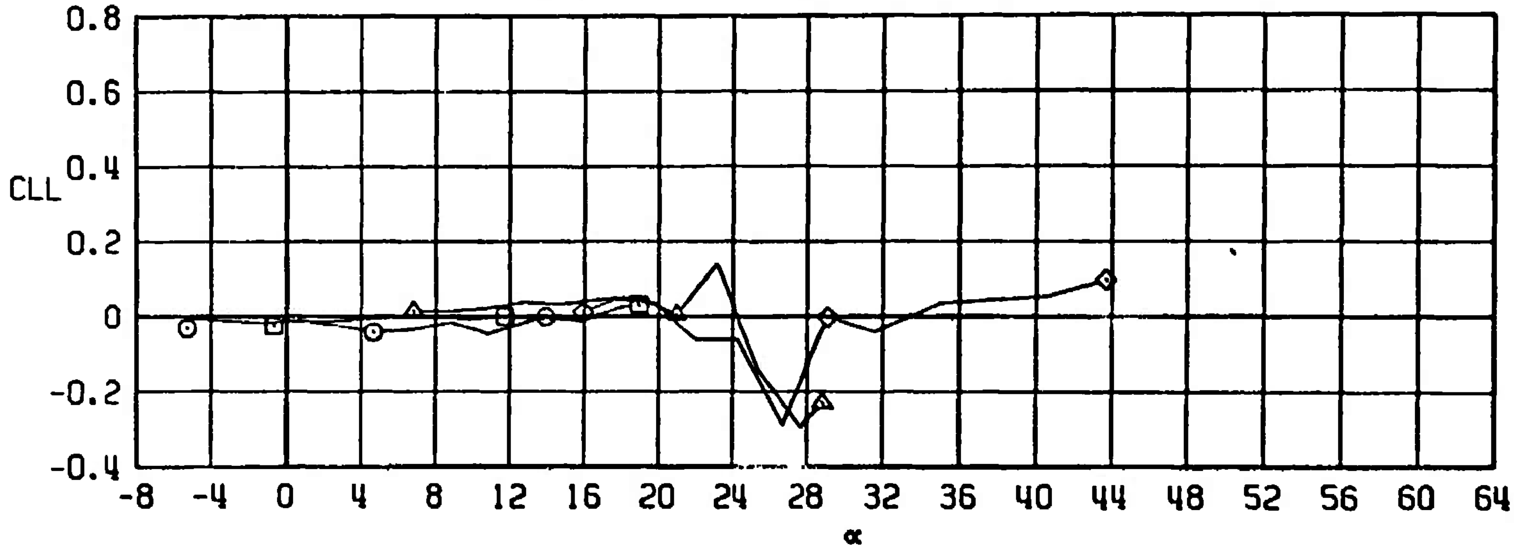

h. CLL versus α
Figure 61. Continued.

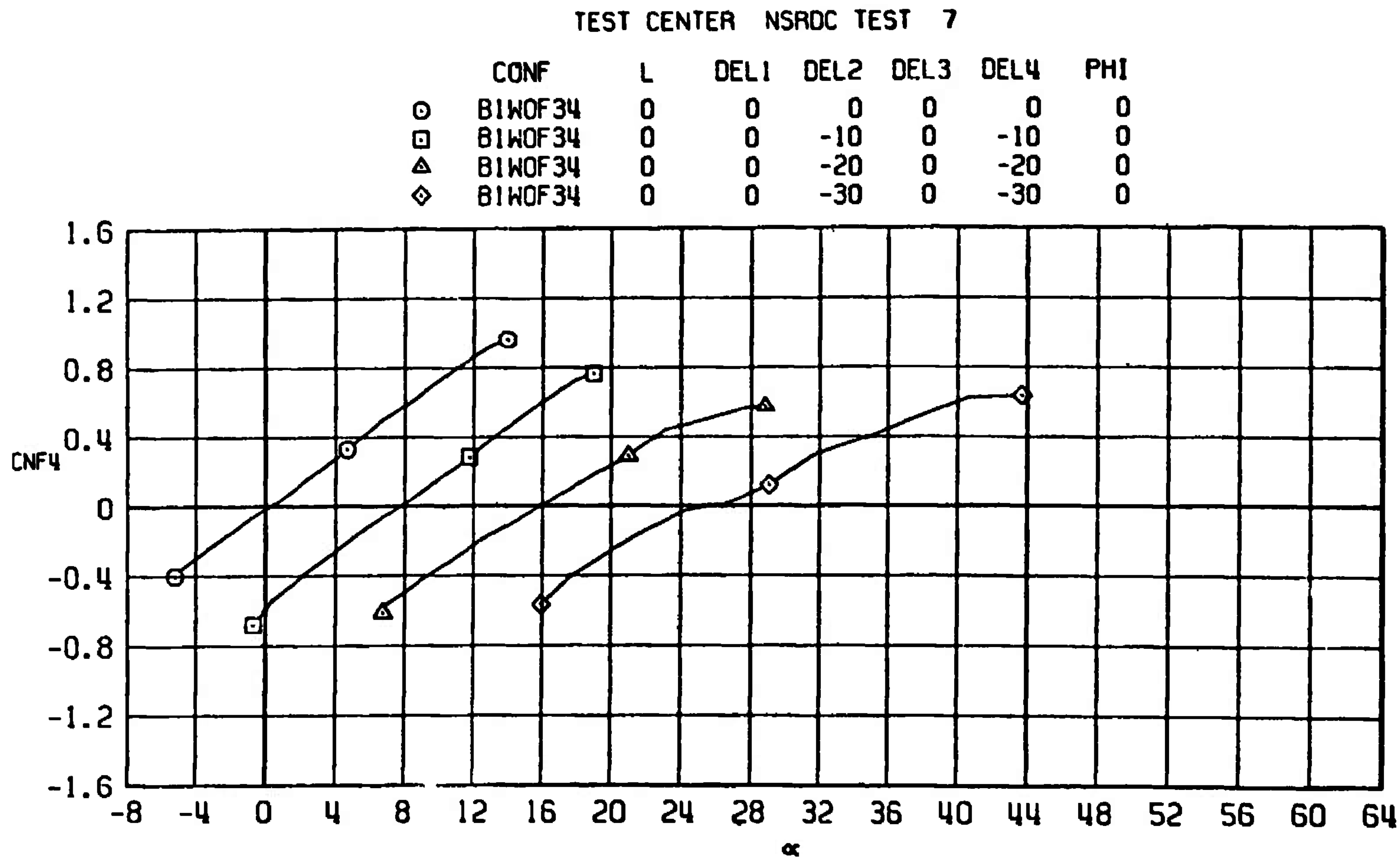

i. CNF4 versus α
Figure 61. Continued.

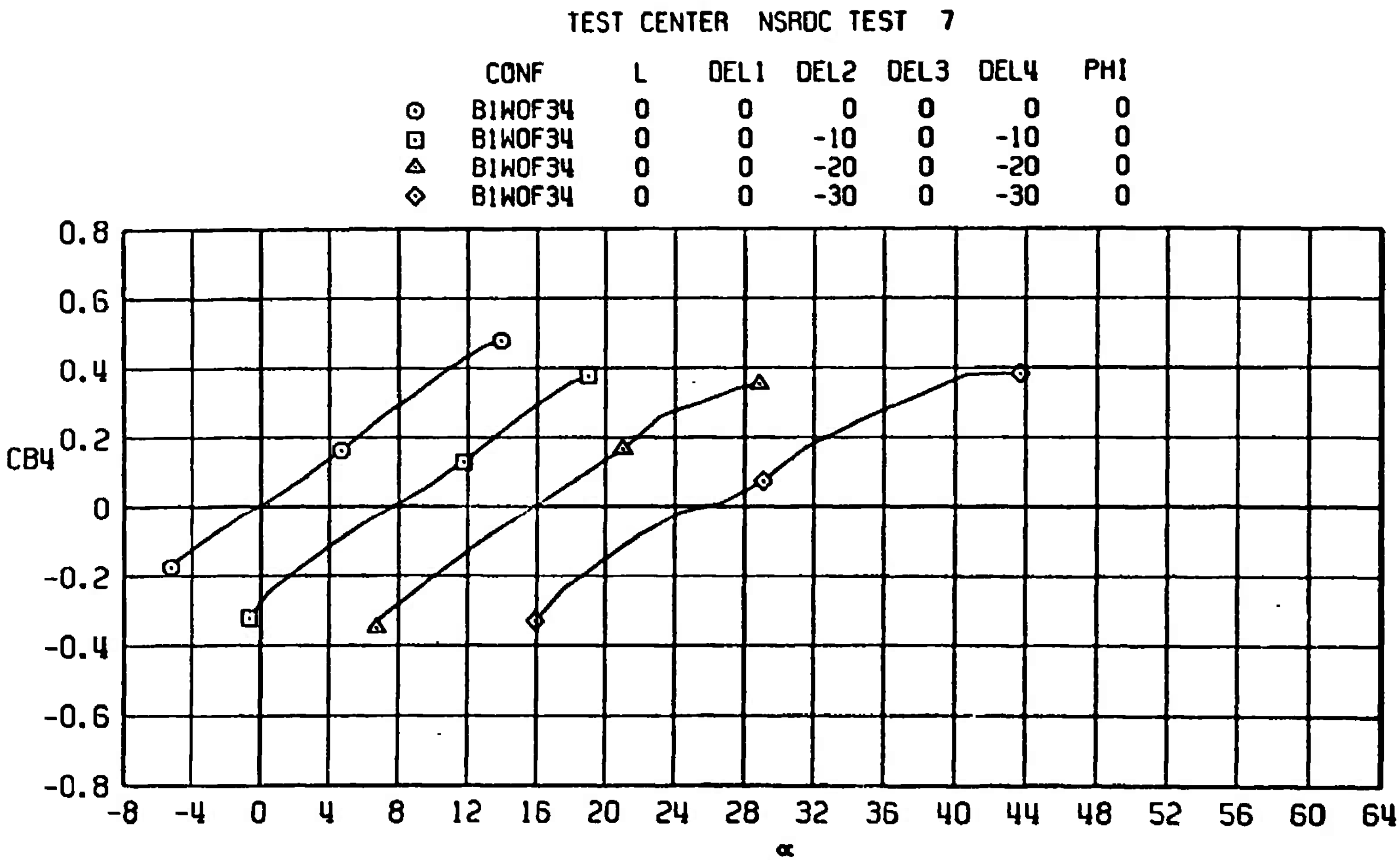

j. CB4 versus α
Figure 61. Continued.

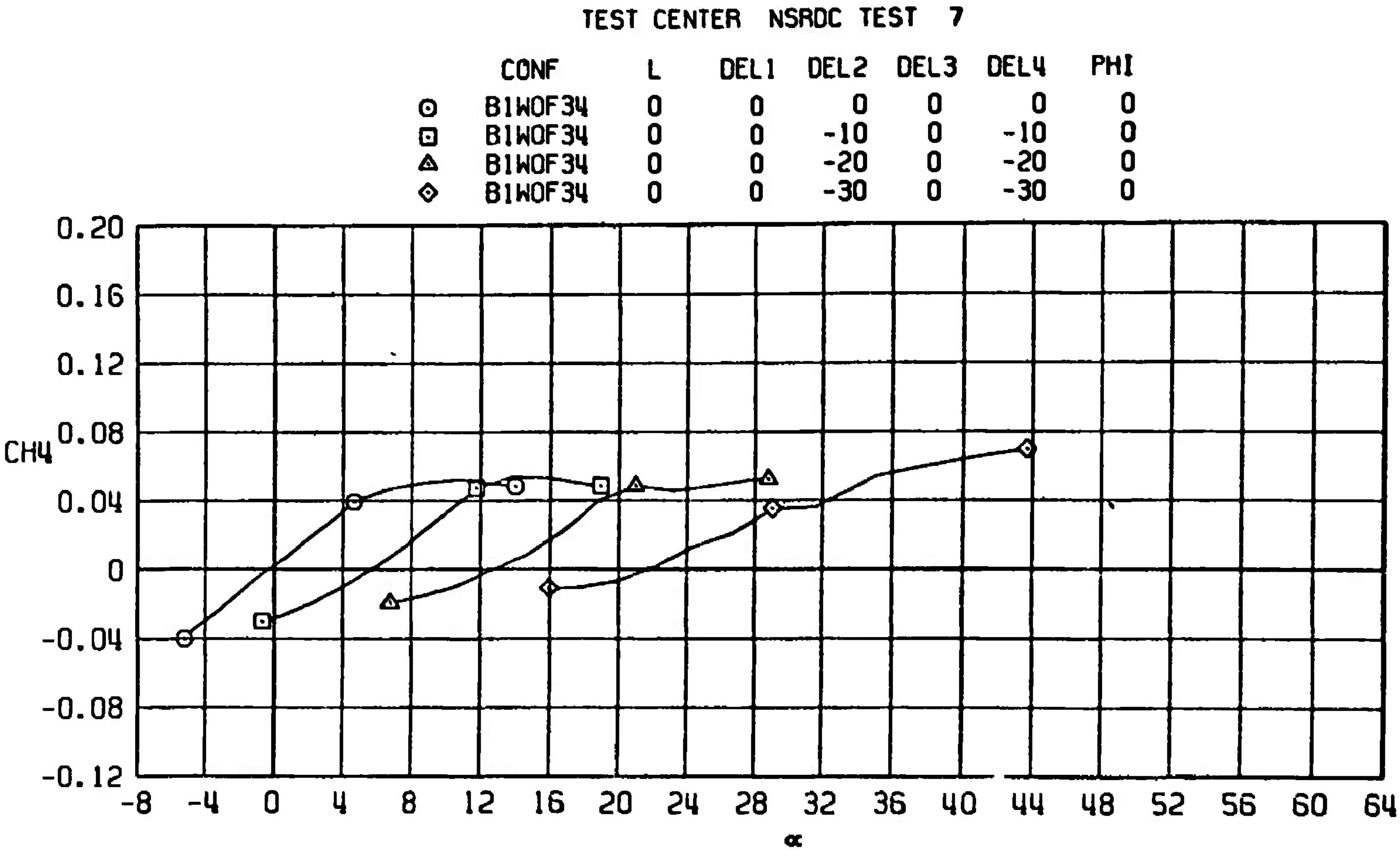

k. CH4 versus α
Figure 61. Concluded.

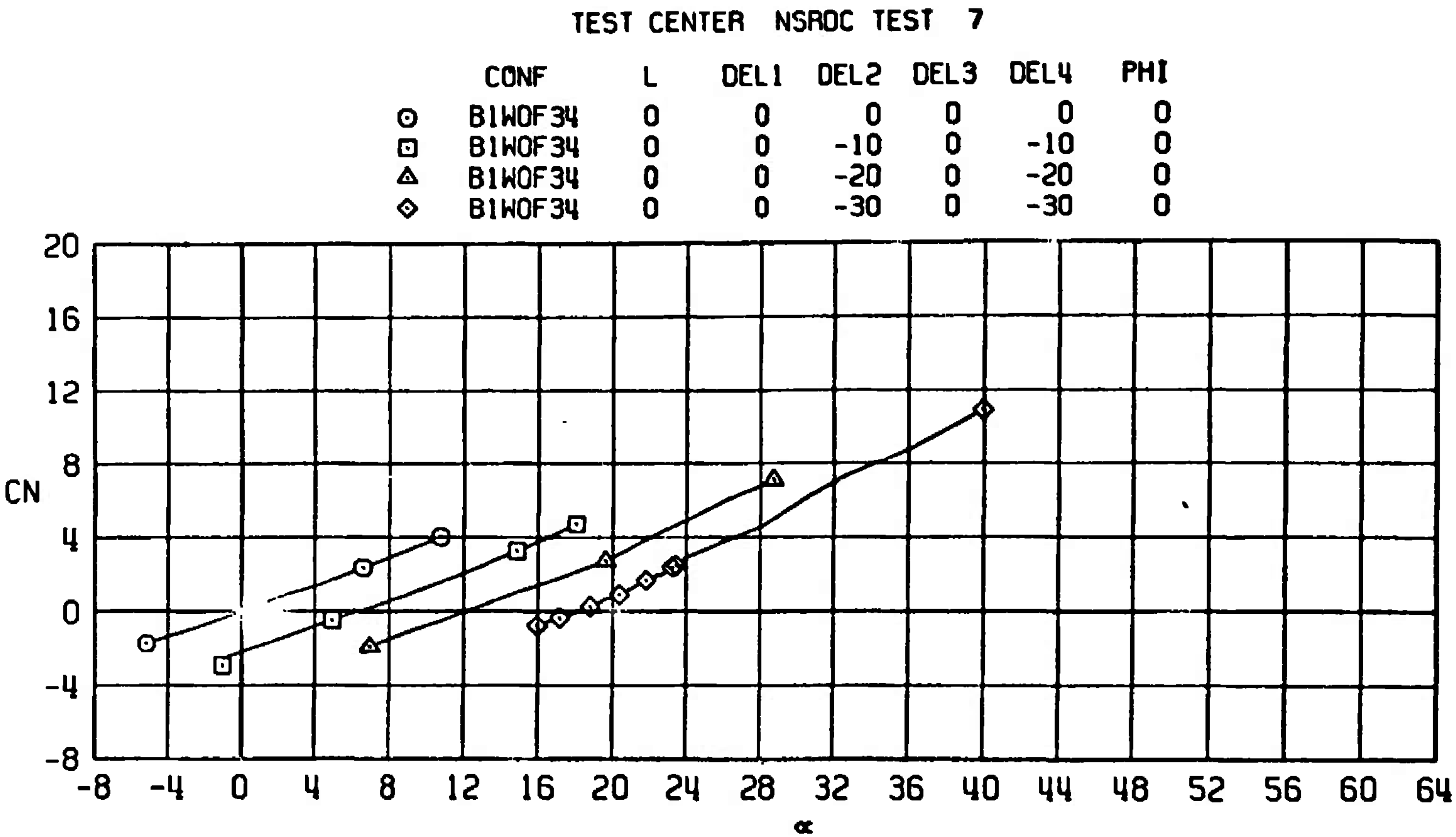

a. CN versus α

Figure 62. Test No. 7, comparison of aerodynamic coefficients of configuration B1W0F34 for various deflections of tail fins No. 2 and 4 at M_∞ = 1.0.

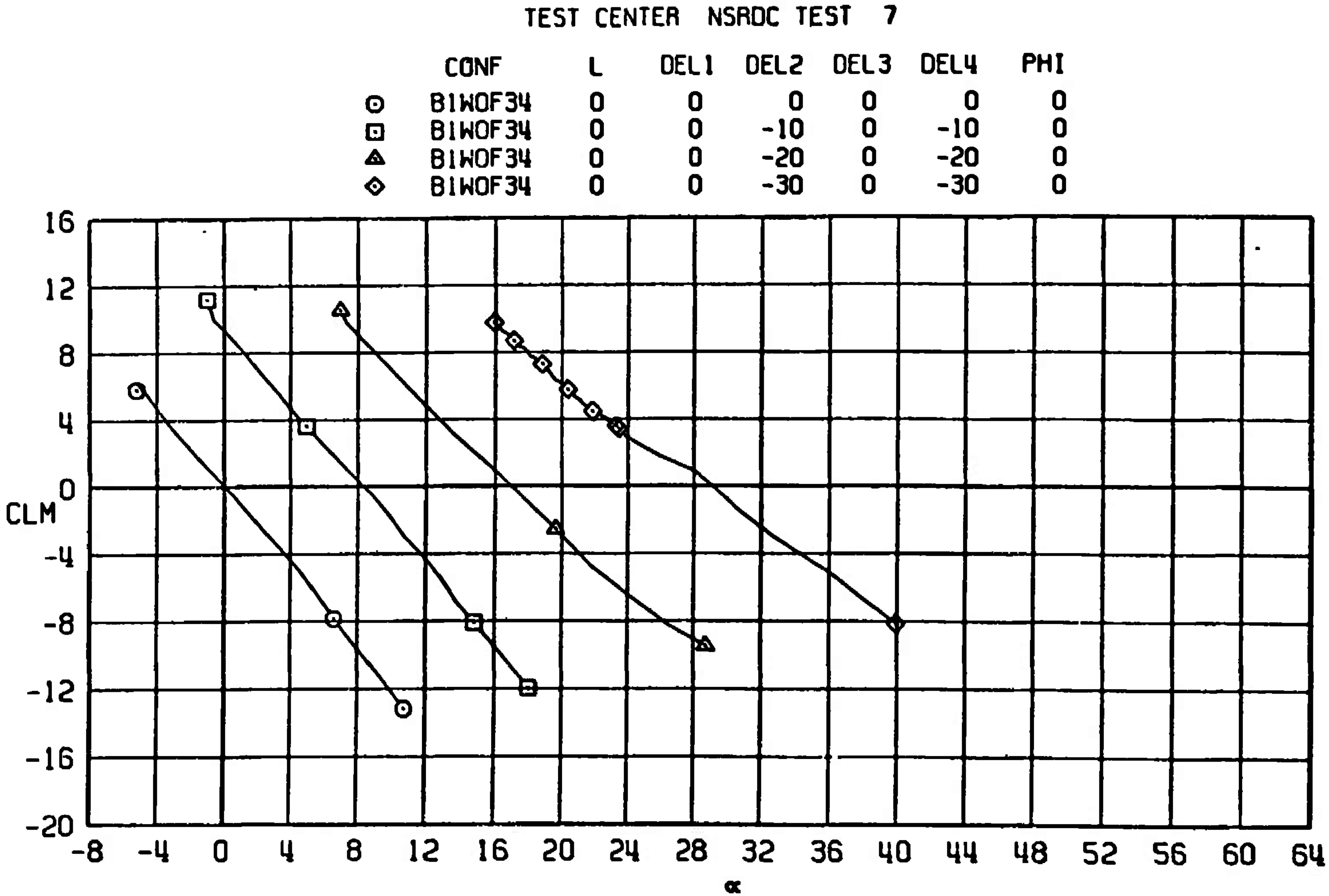

b. CLM versus α
Figure 62. Continued.

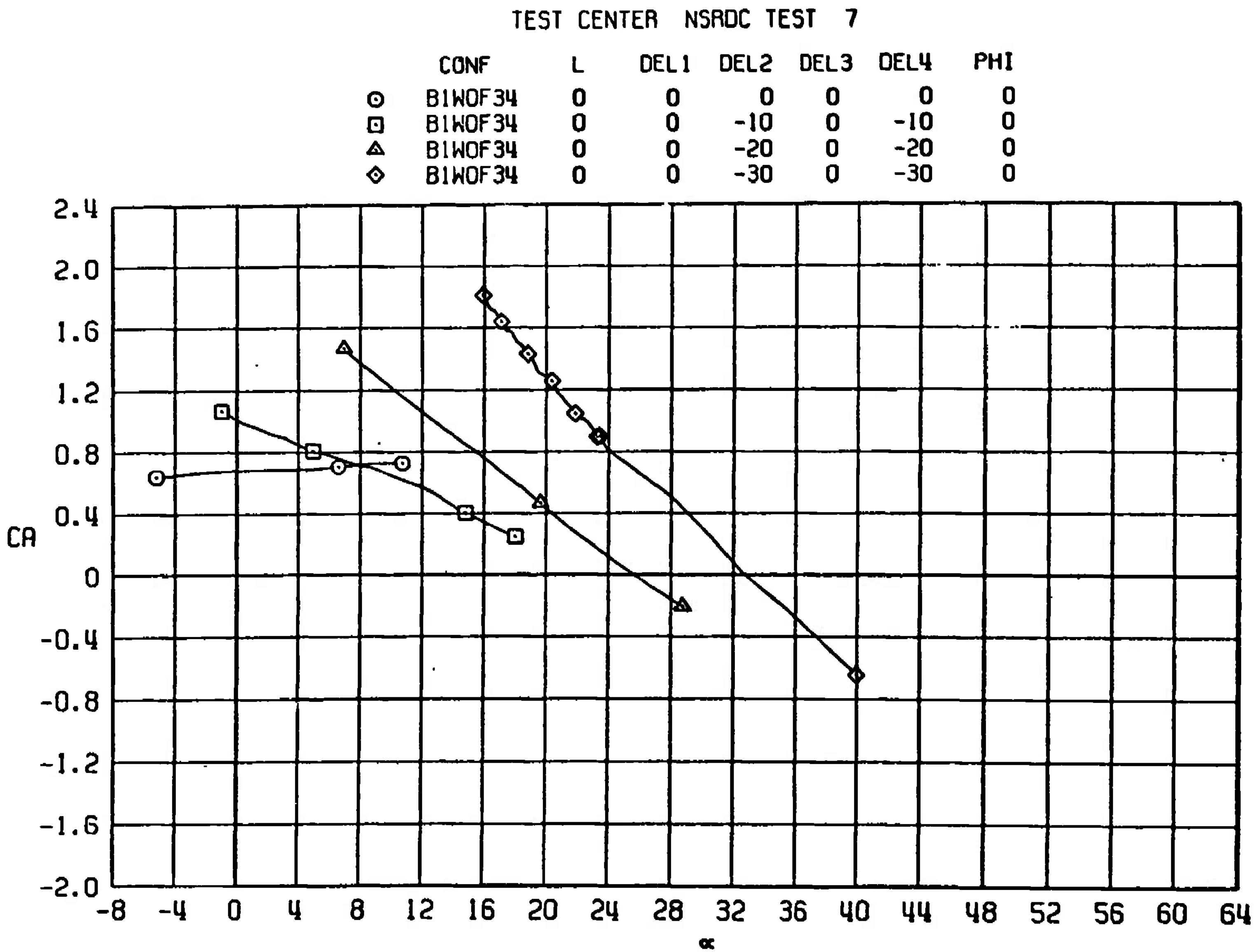

c. CA versus α

Figure 62. Continued.

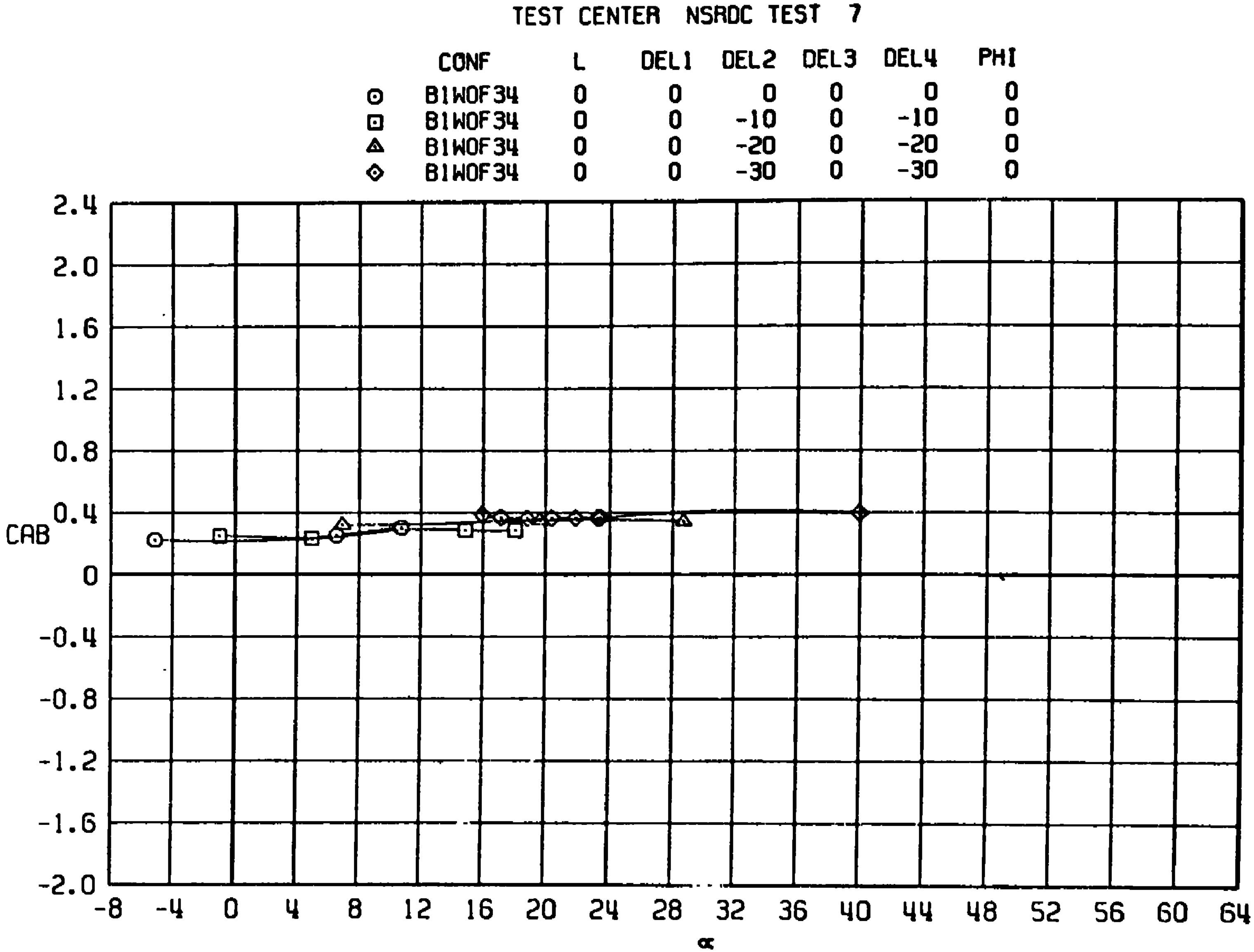

d. CAB versus α
Figure 62. Continued.

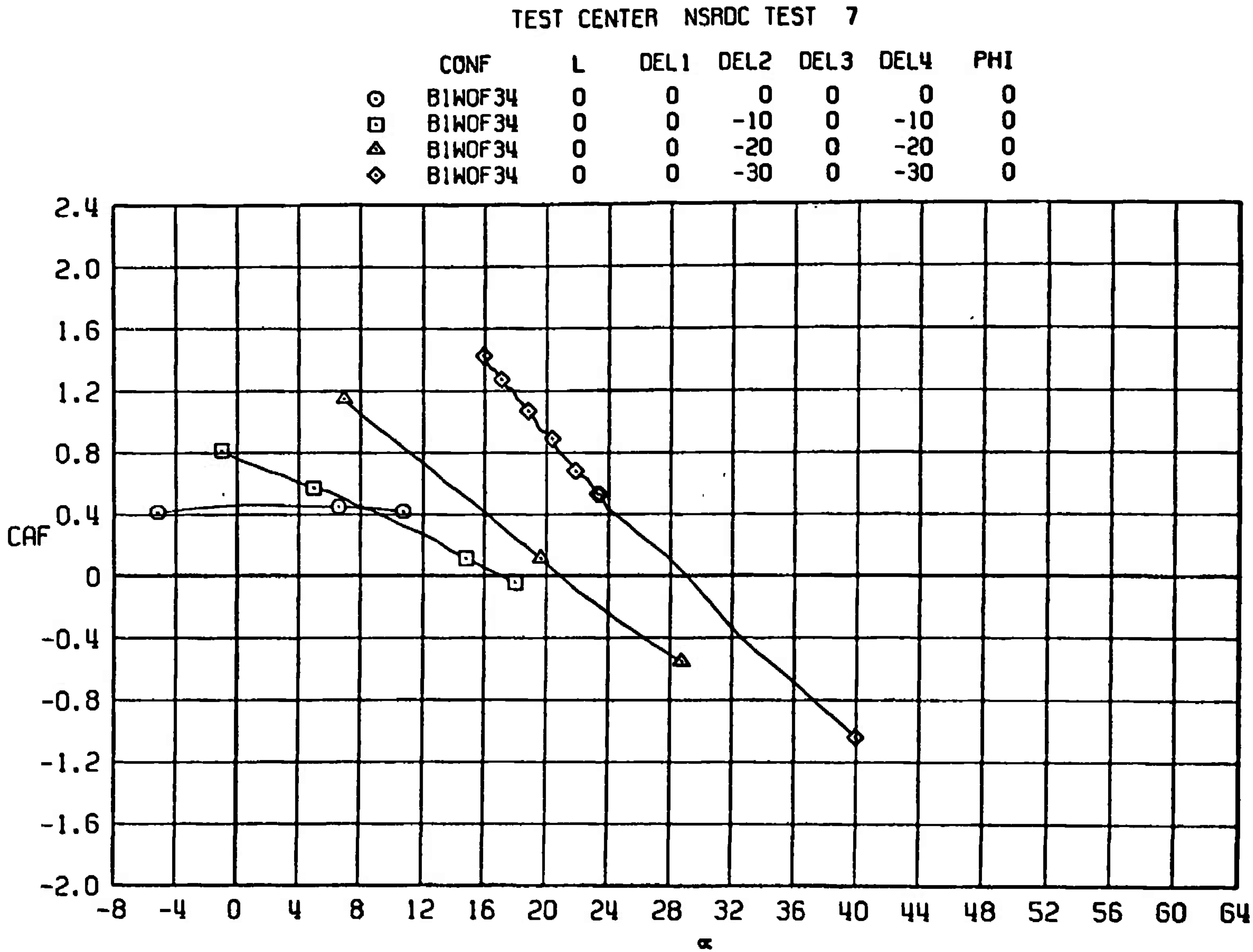

e. CAF versus α

Figure 62. Continued.

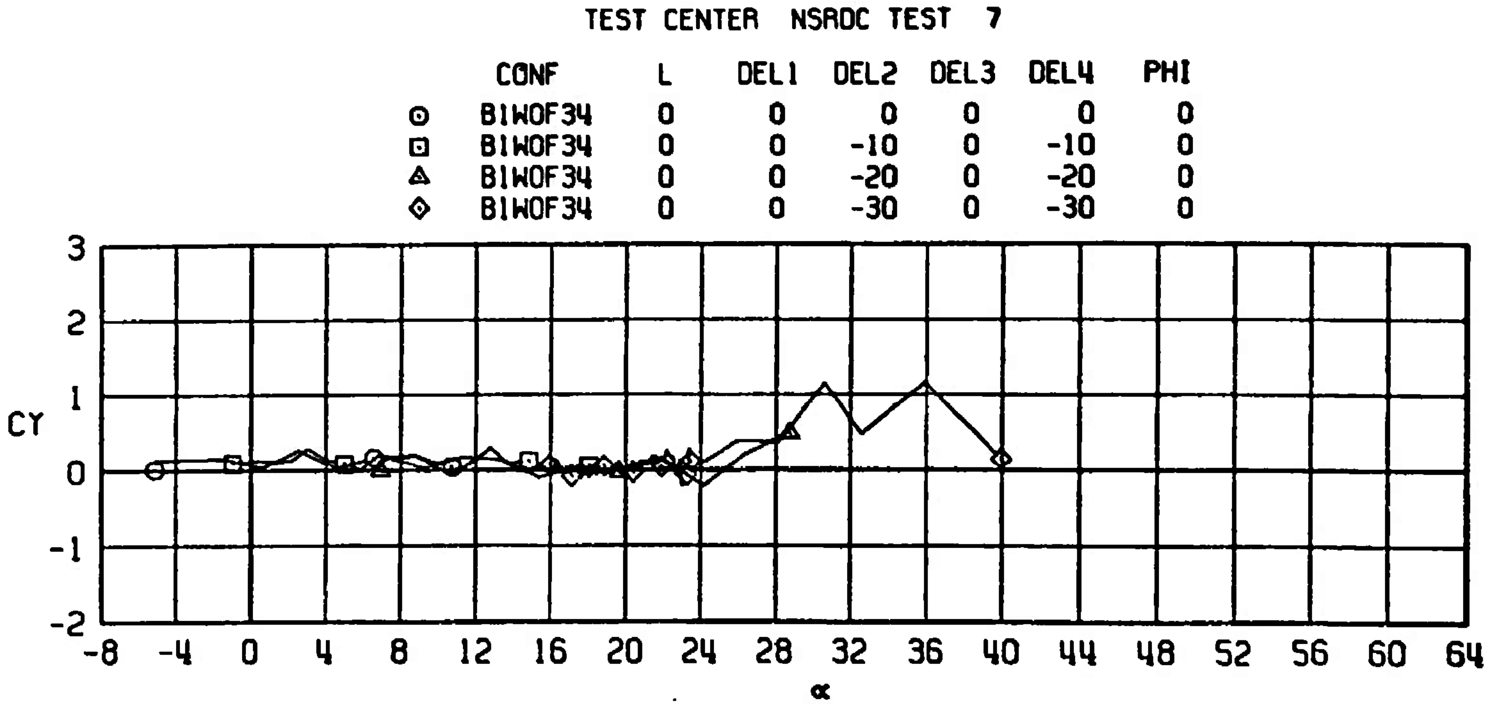

f. CY versus α

Figure 62. Continued.

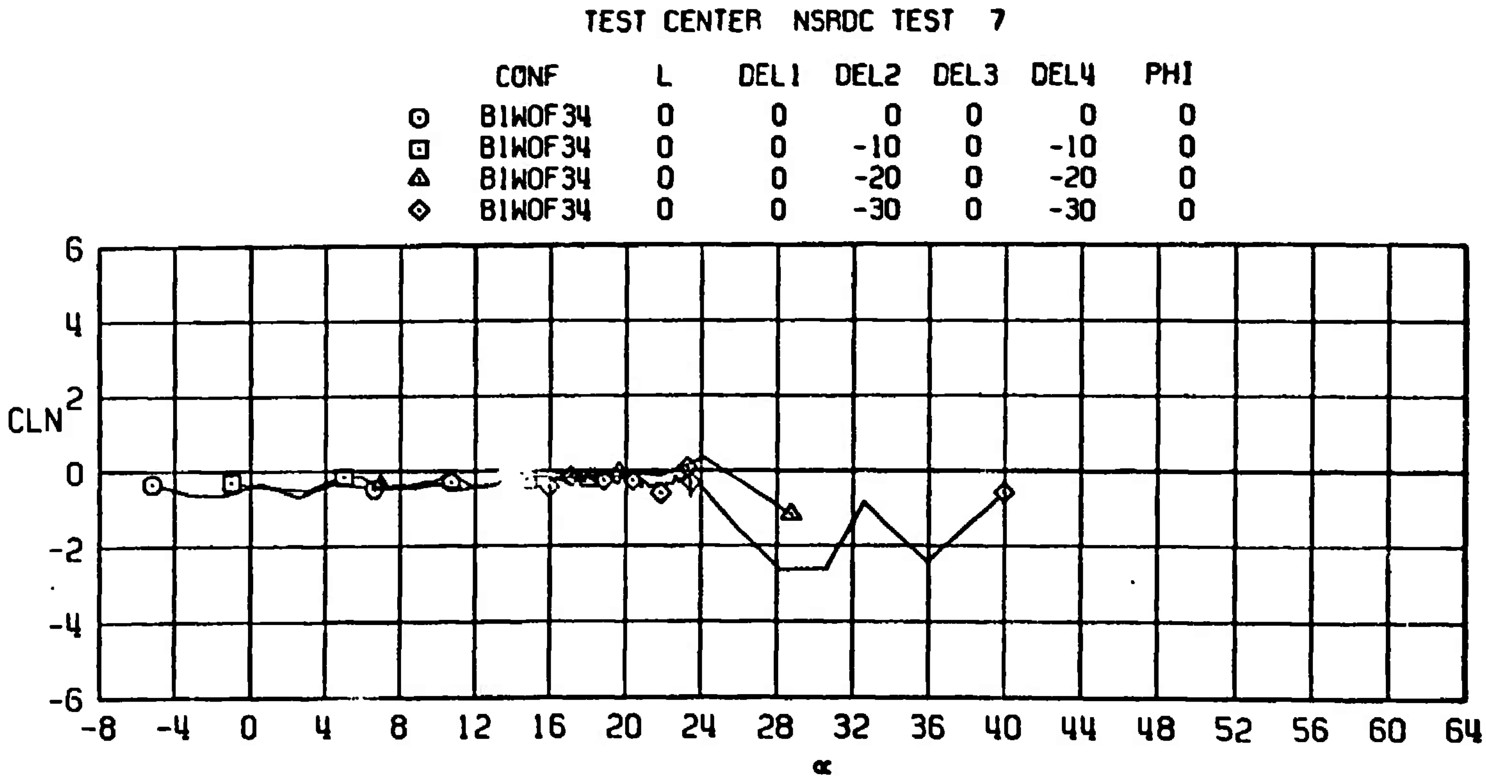

g. CLN versus α
Figure 62. Continued.

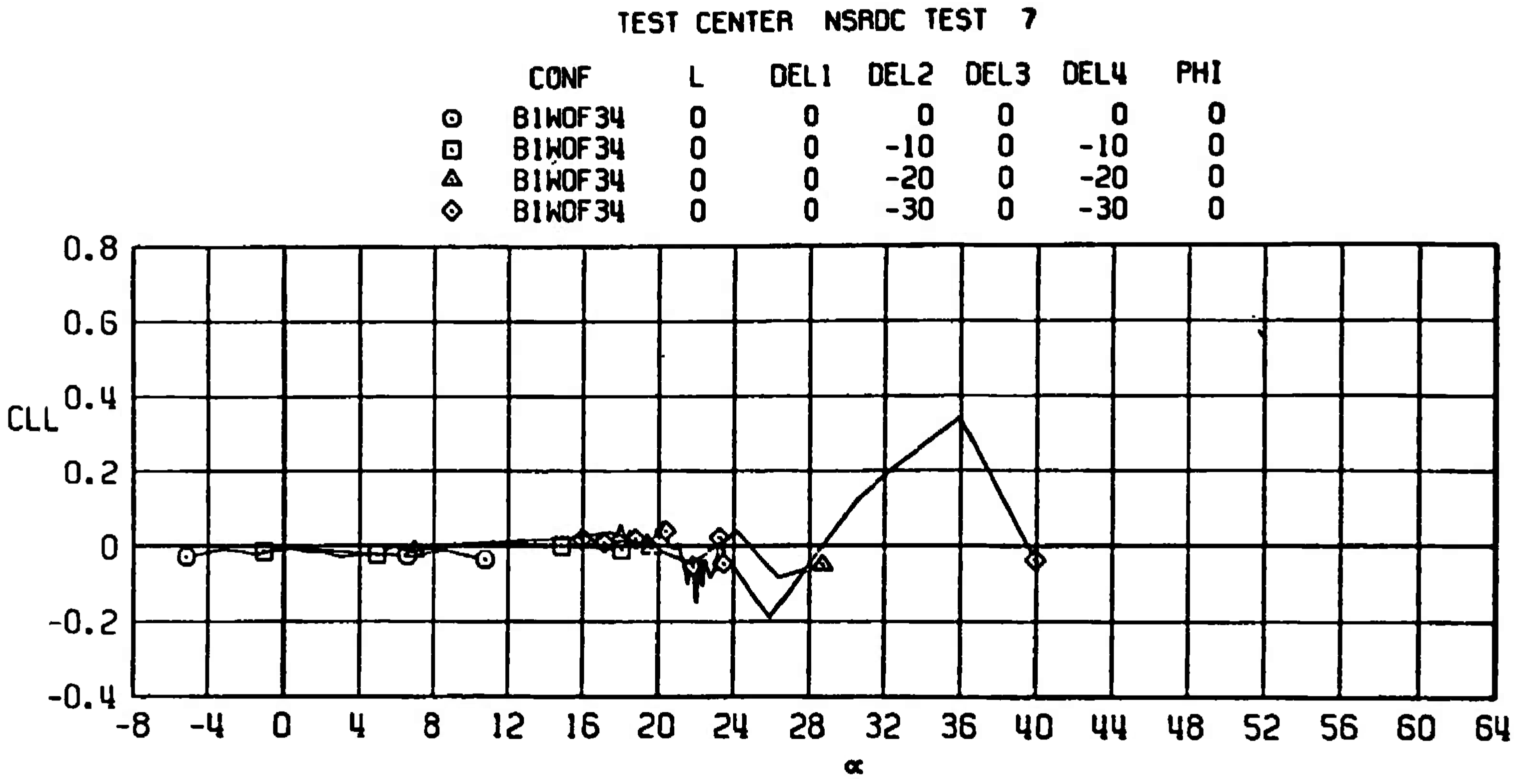

h. CLL versus α

Figure 62. Continued.

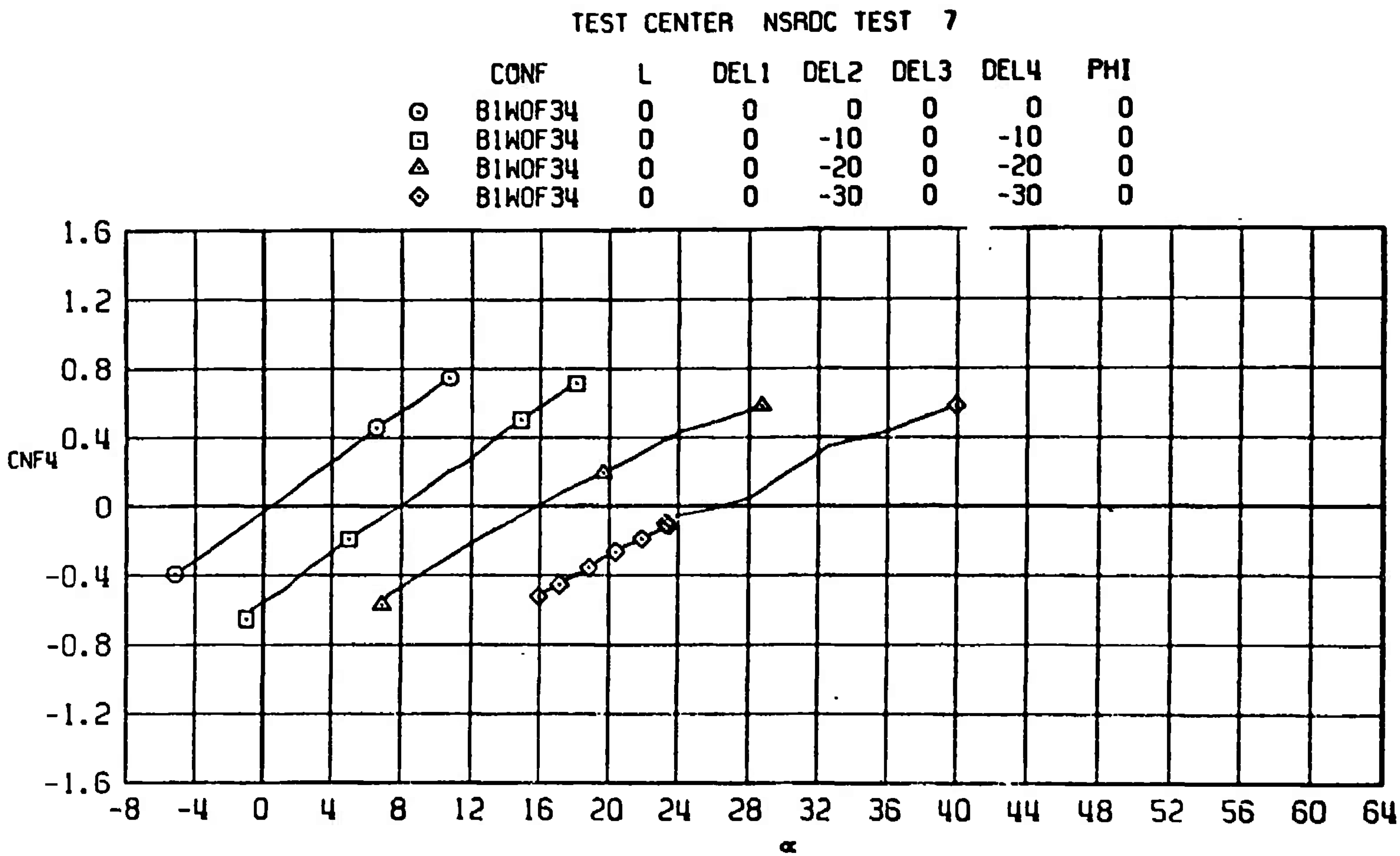

i. CNF4 versus α
Figure 62. Continued.

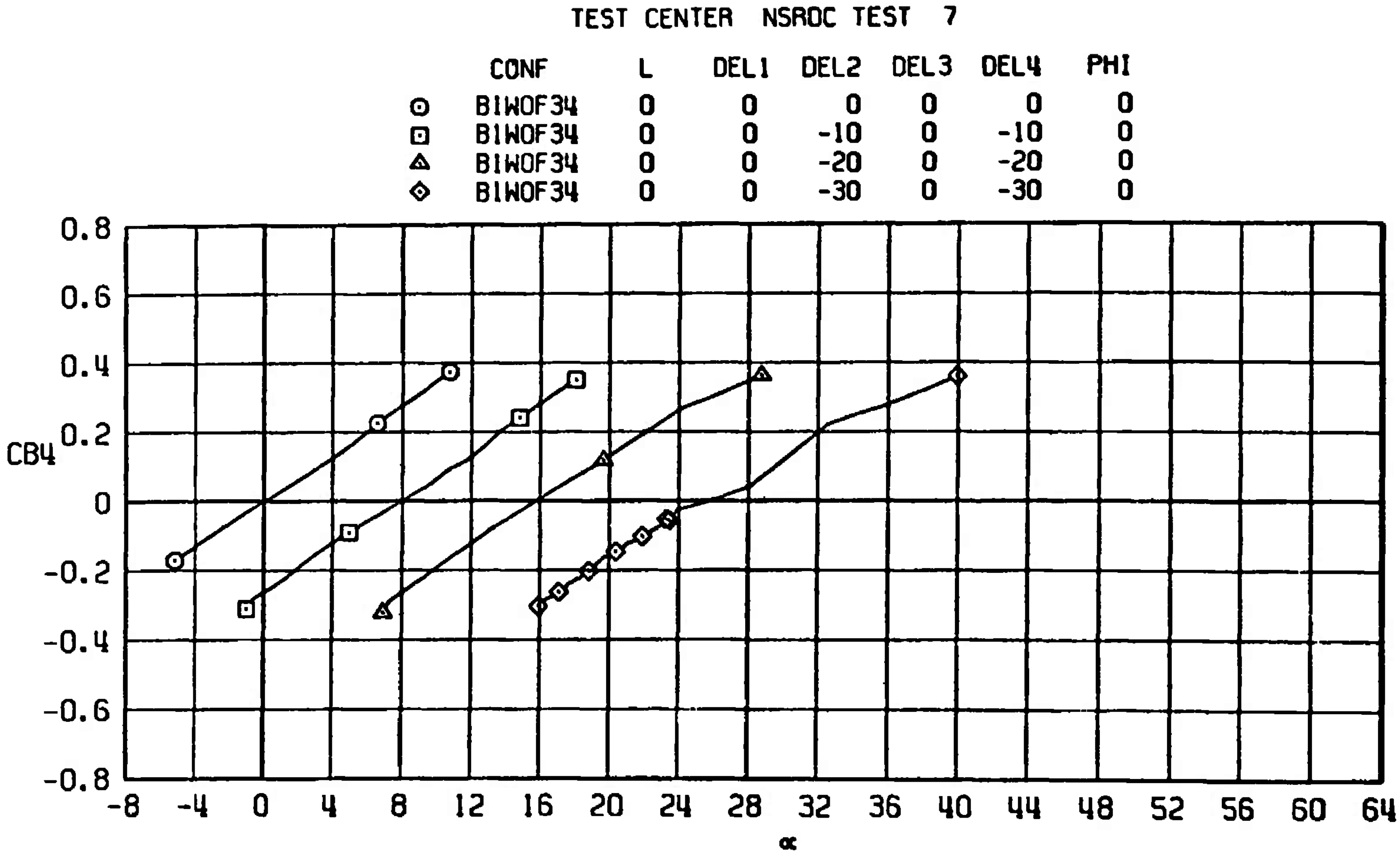

j. CB4 versus α
Figure 62. Continued.

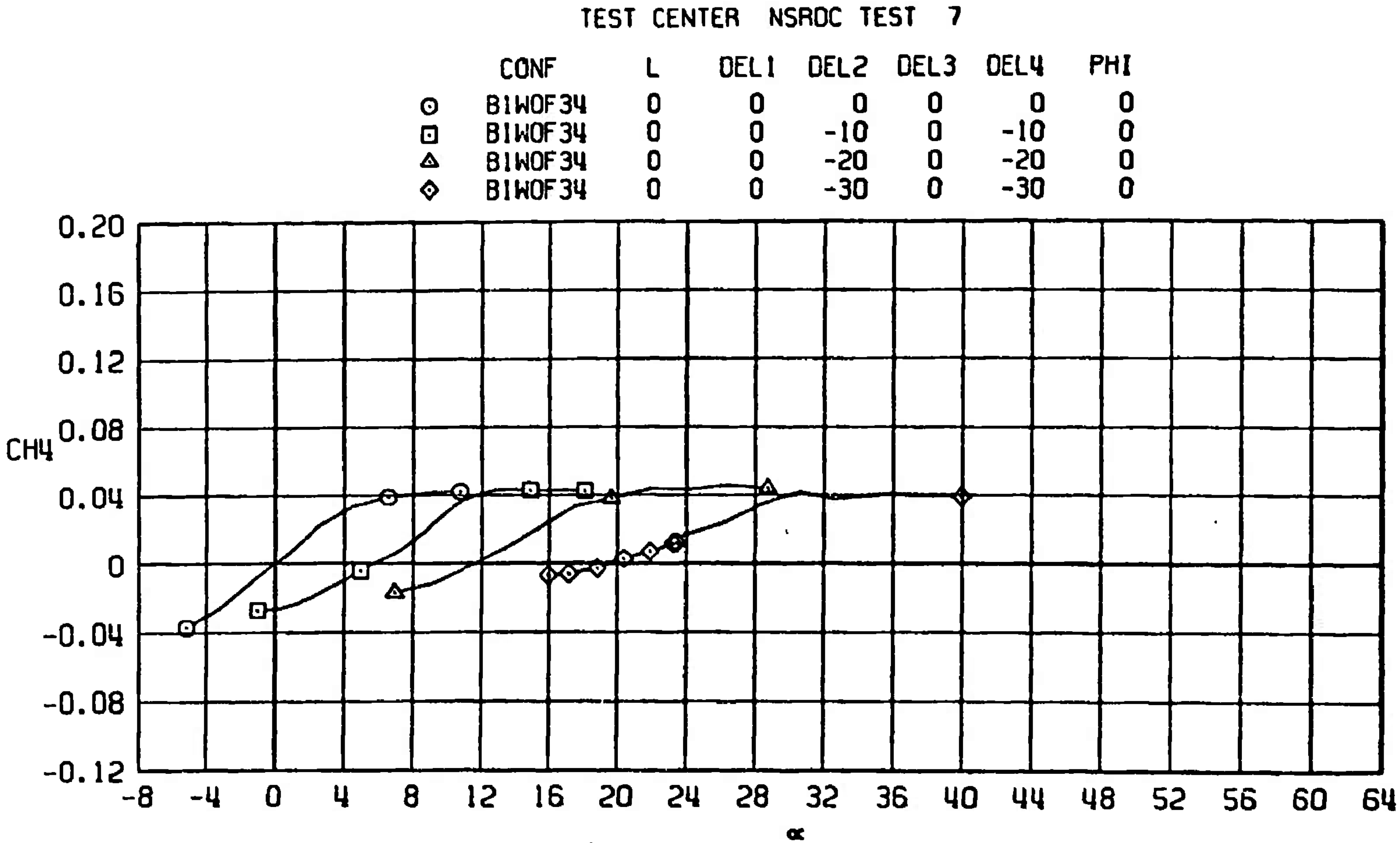

k. CH4 versus α

Figure 62. Concluded.

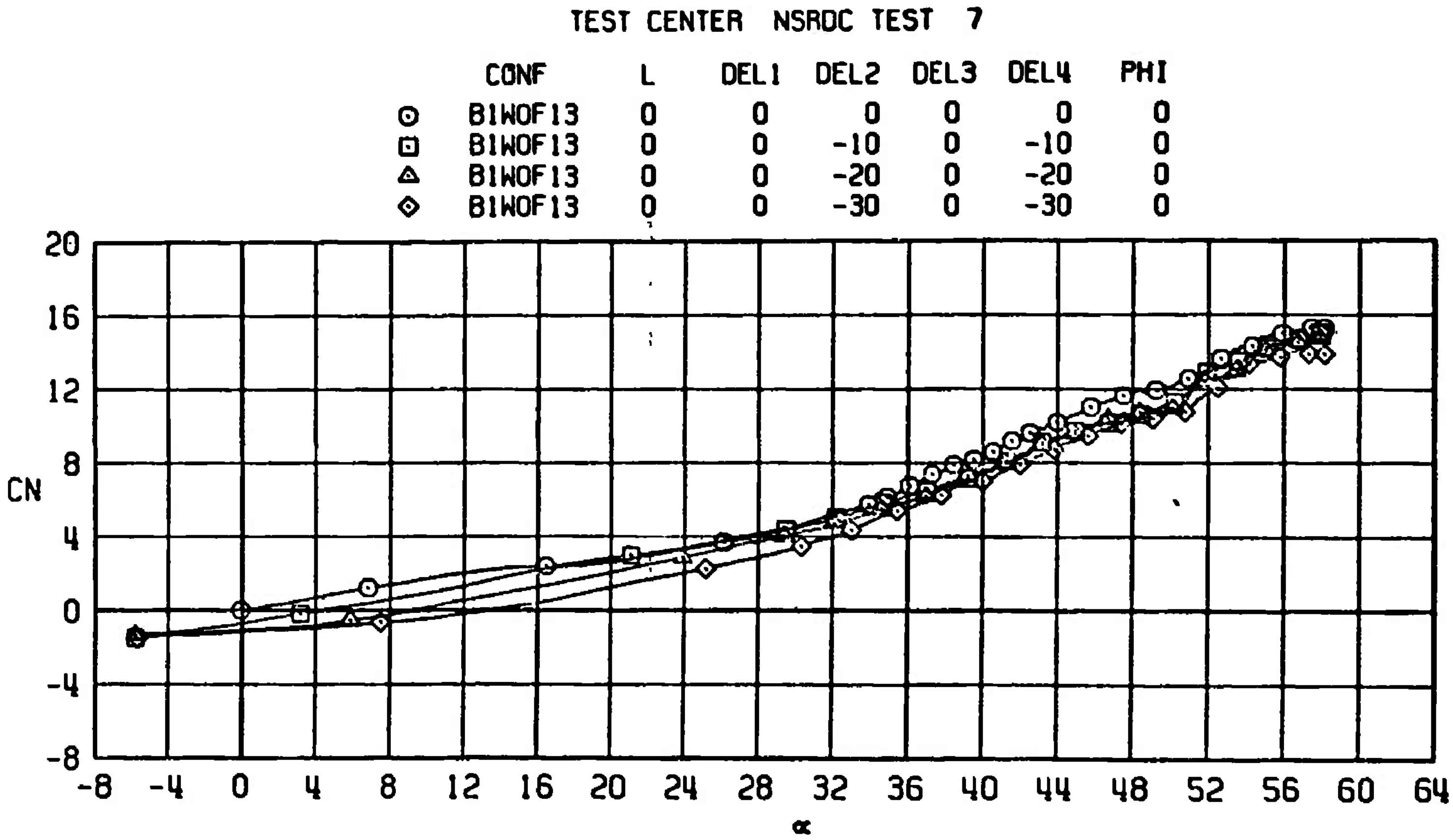

a. CN versus α

Figure 63. Test No. 7, comparison of aerodynamic coefficients of configuration B1W0F13 for various deflections of tail fins No. 2 and 4 at $M_\infty = 0.8$.

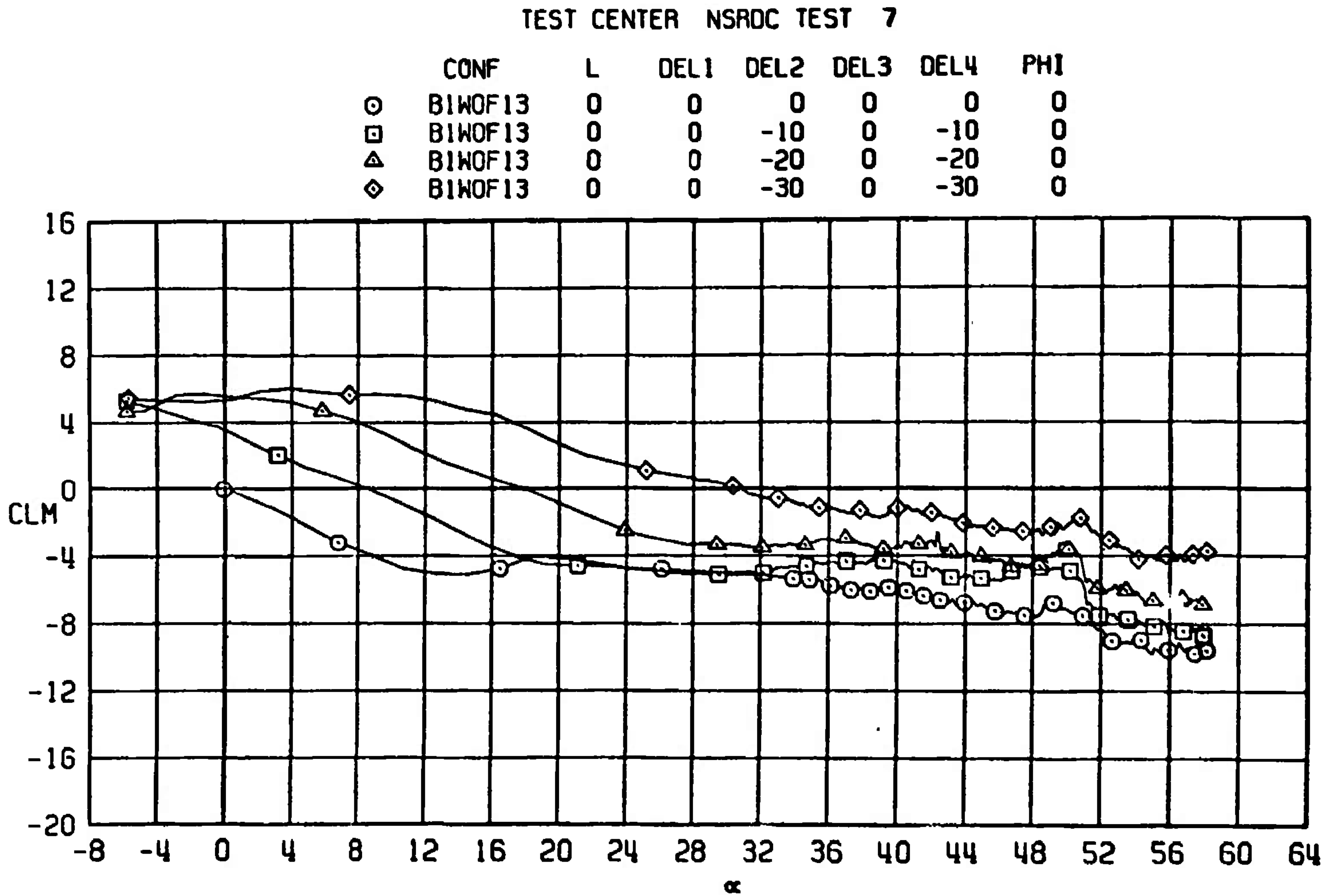

b. CLM versus α

Figure 63. Continued.

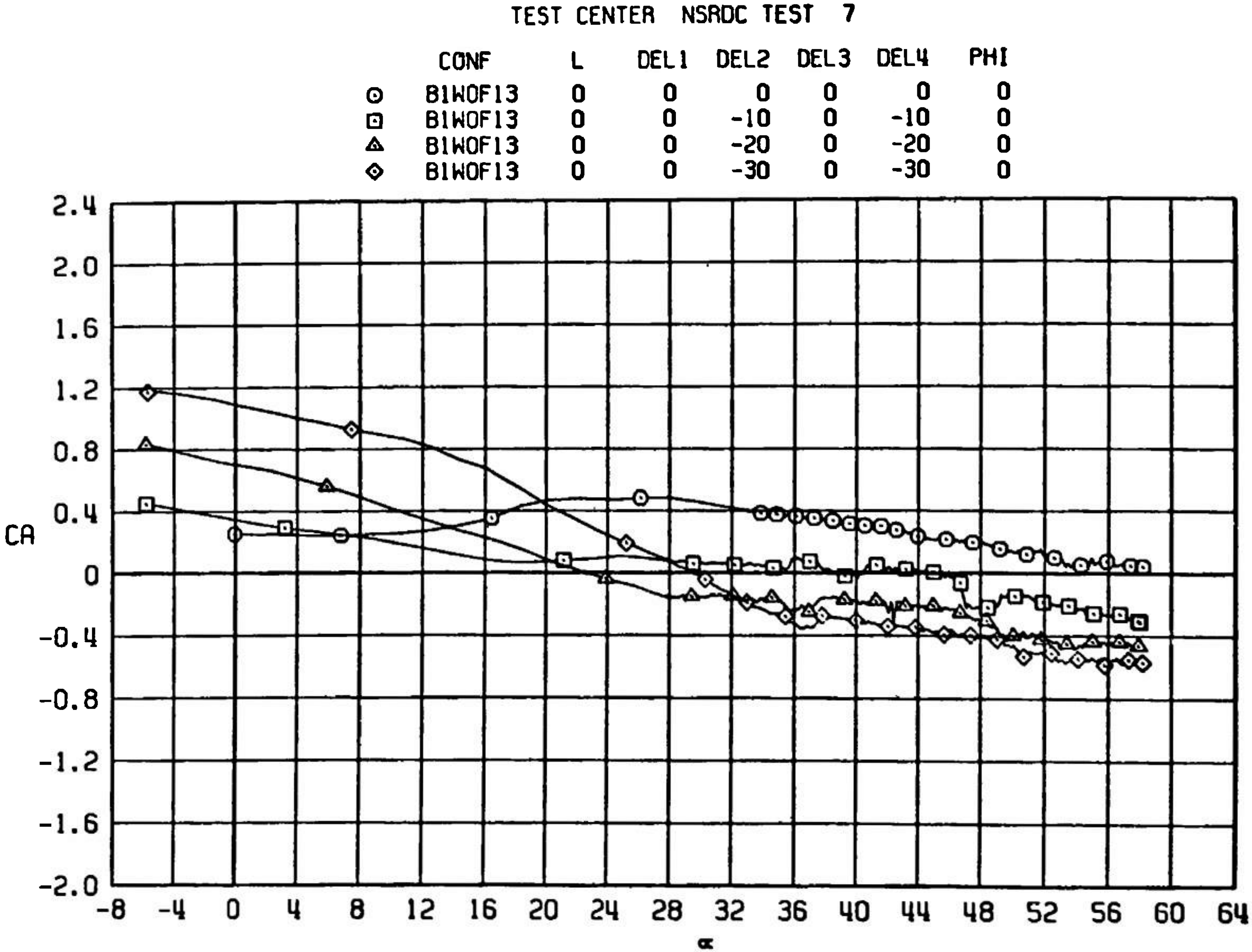

c. CA versus α
Figure 63. Continued.

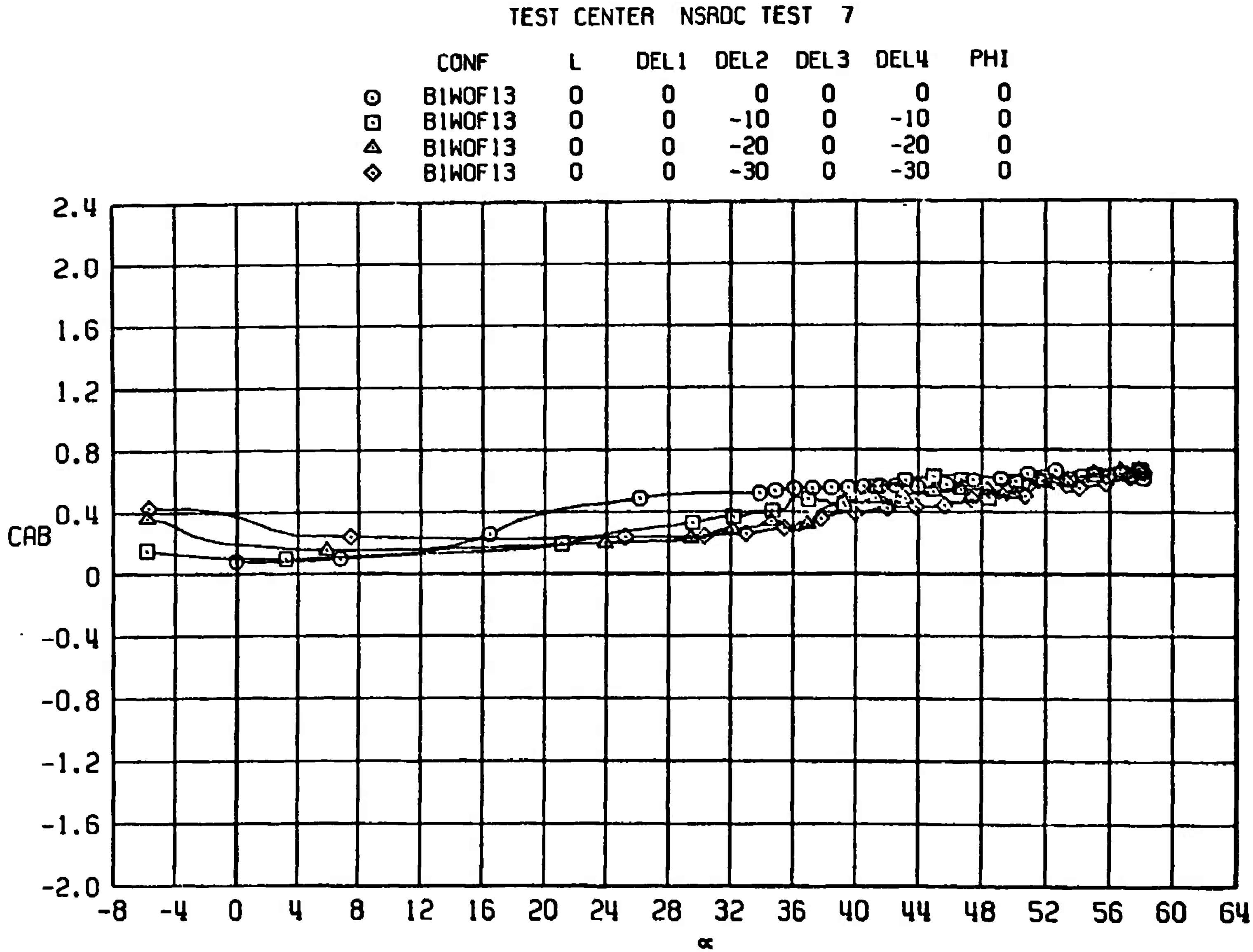

d. CAB versus α

Figure 63. Continued.

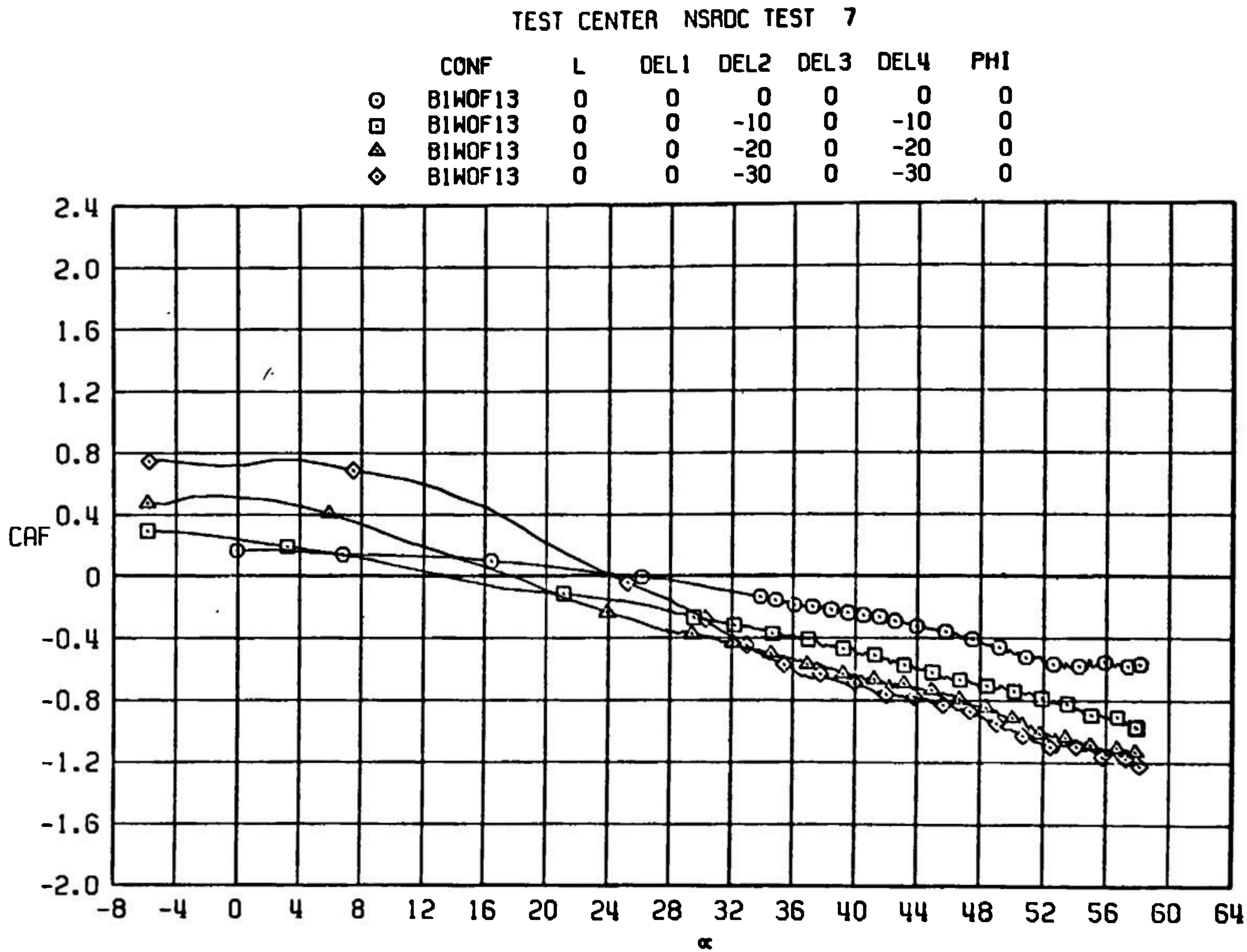

e. CAF versus α
Figure 63. Continued.

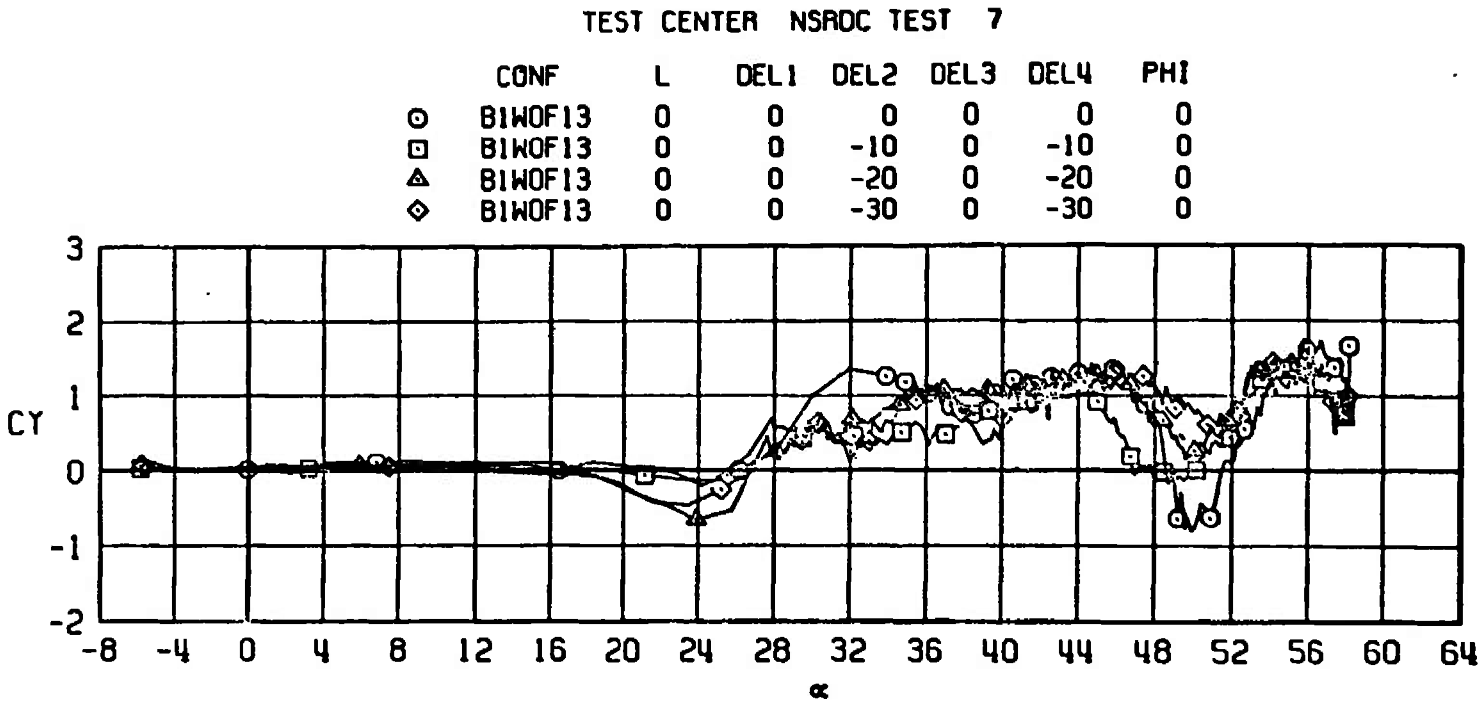

f. CY versus α
Figure 63. Continued.

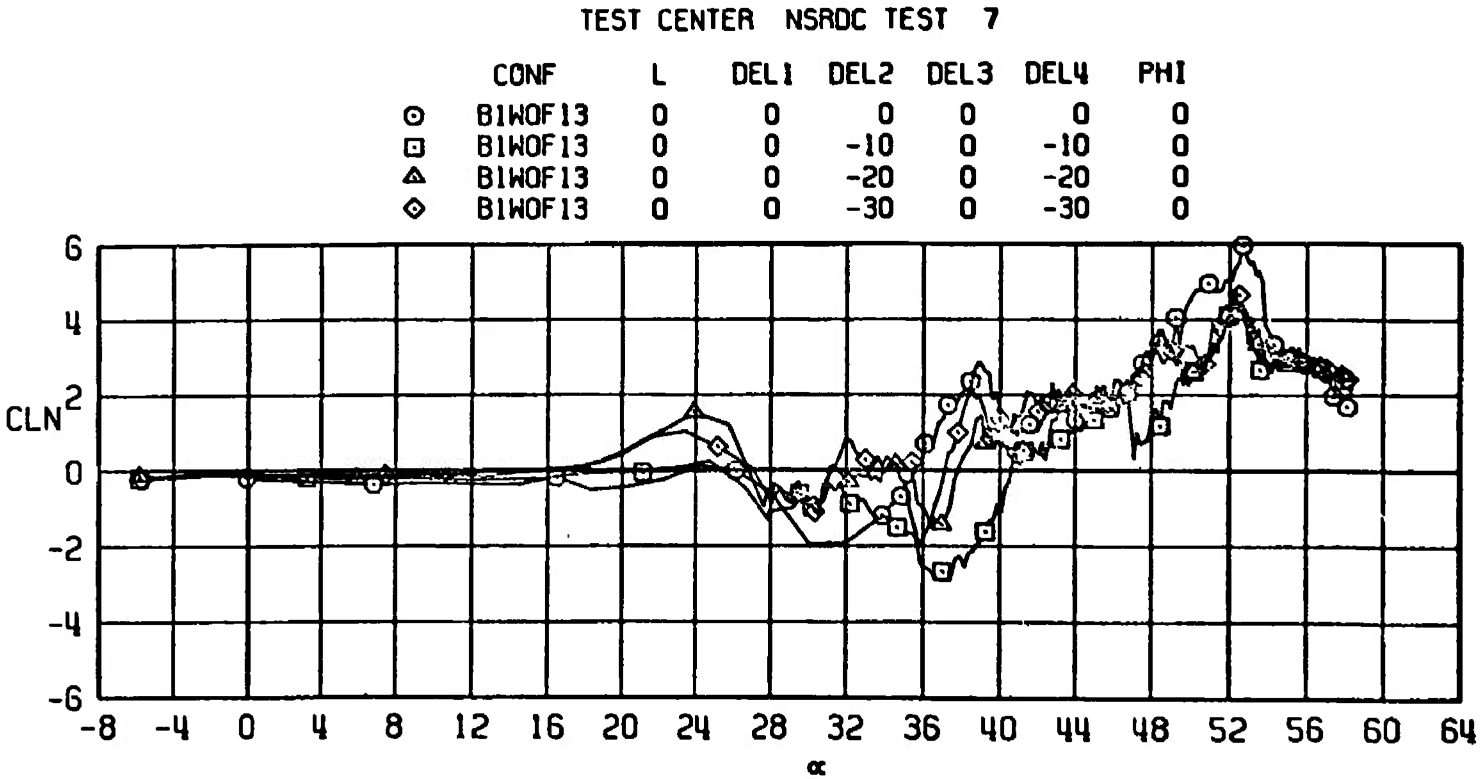

g. CLN versus α

Figure 63. Continued.

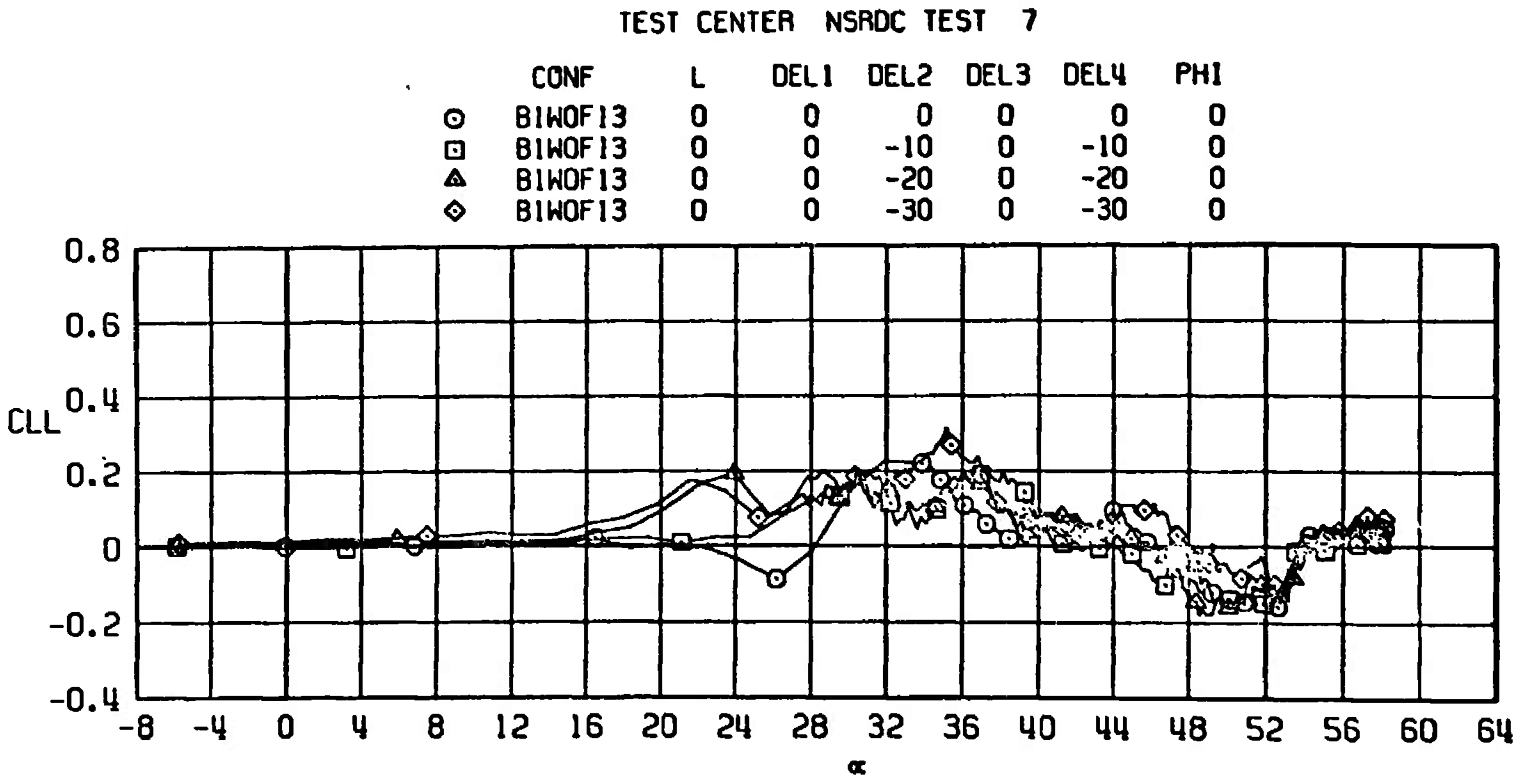

h. CLL versus α
Figure 63. Continued.

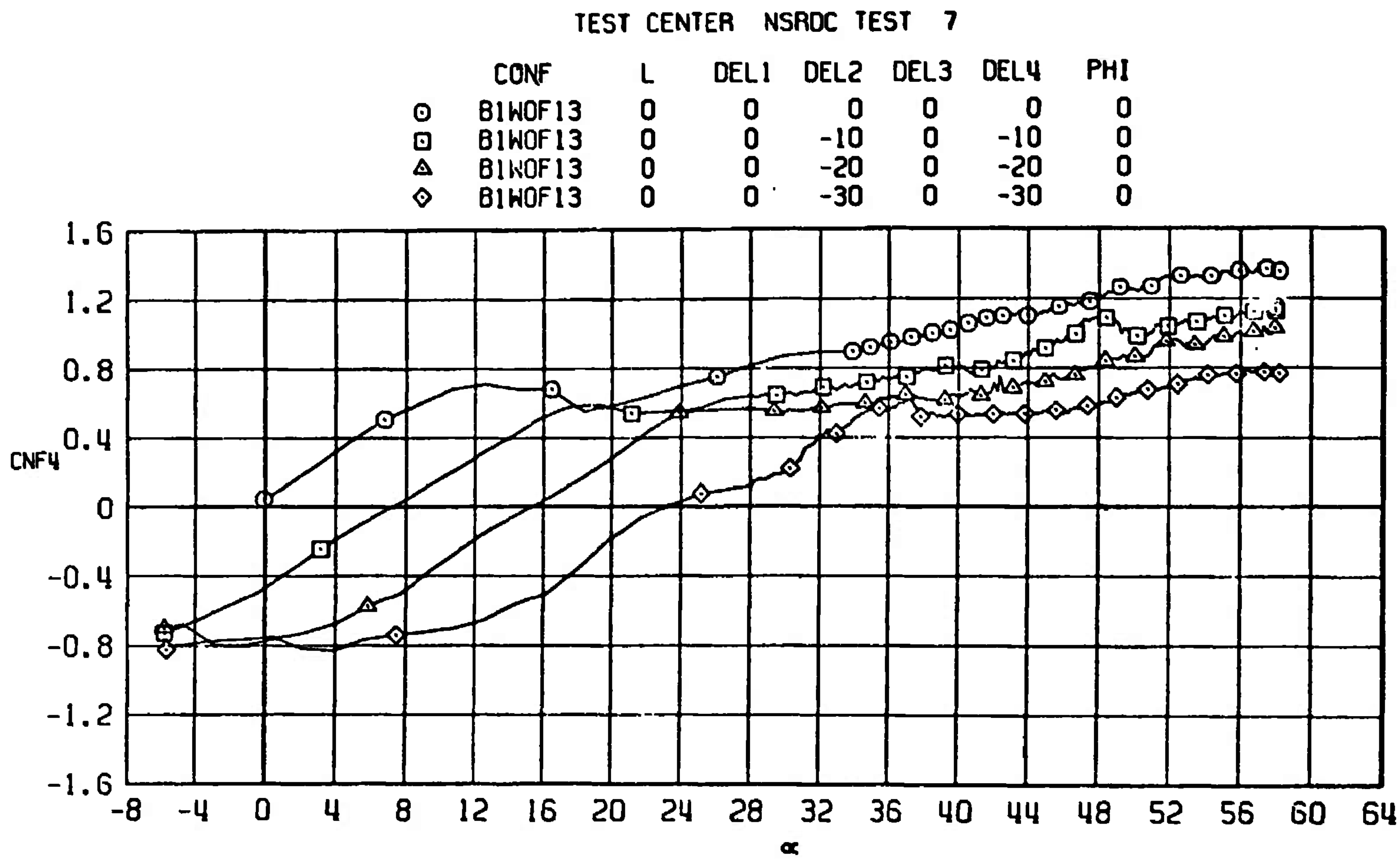

i. CNF4 versus α
Figure 63. Continued.

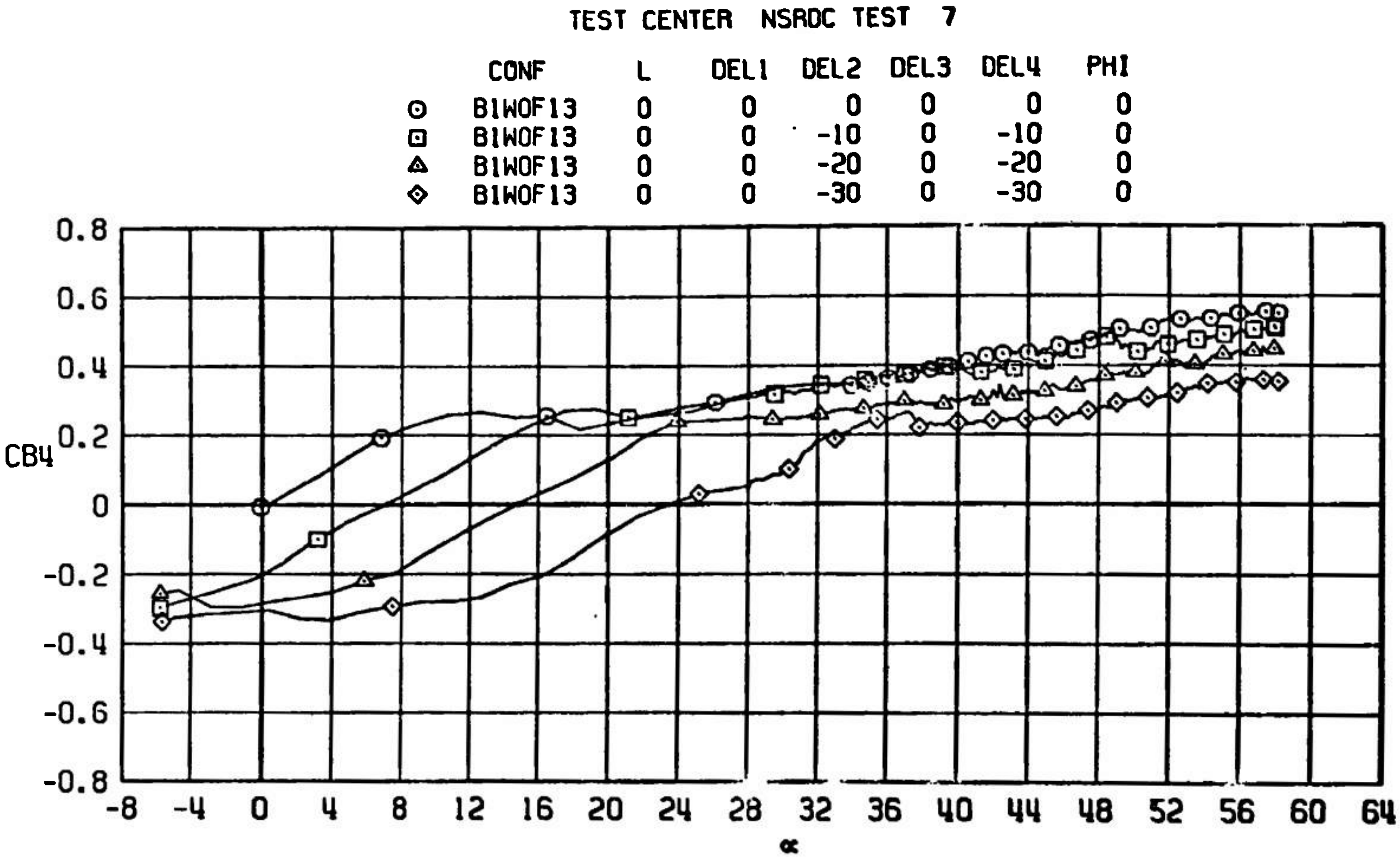

j. CB4 versus α
Figure 63. Continued.

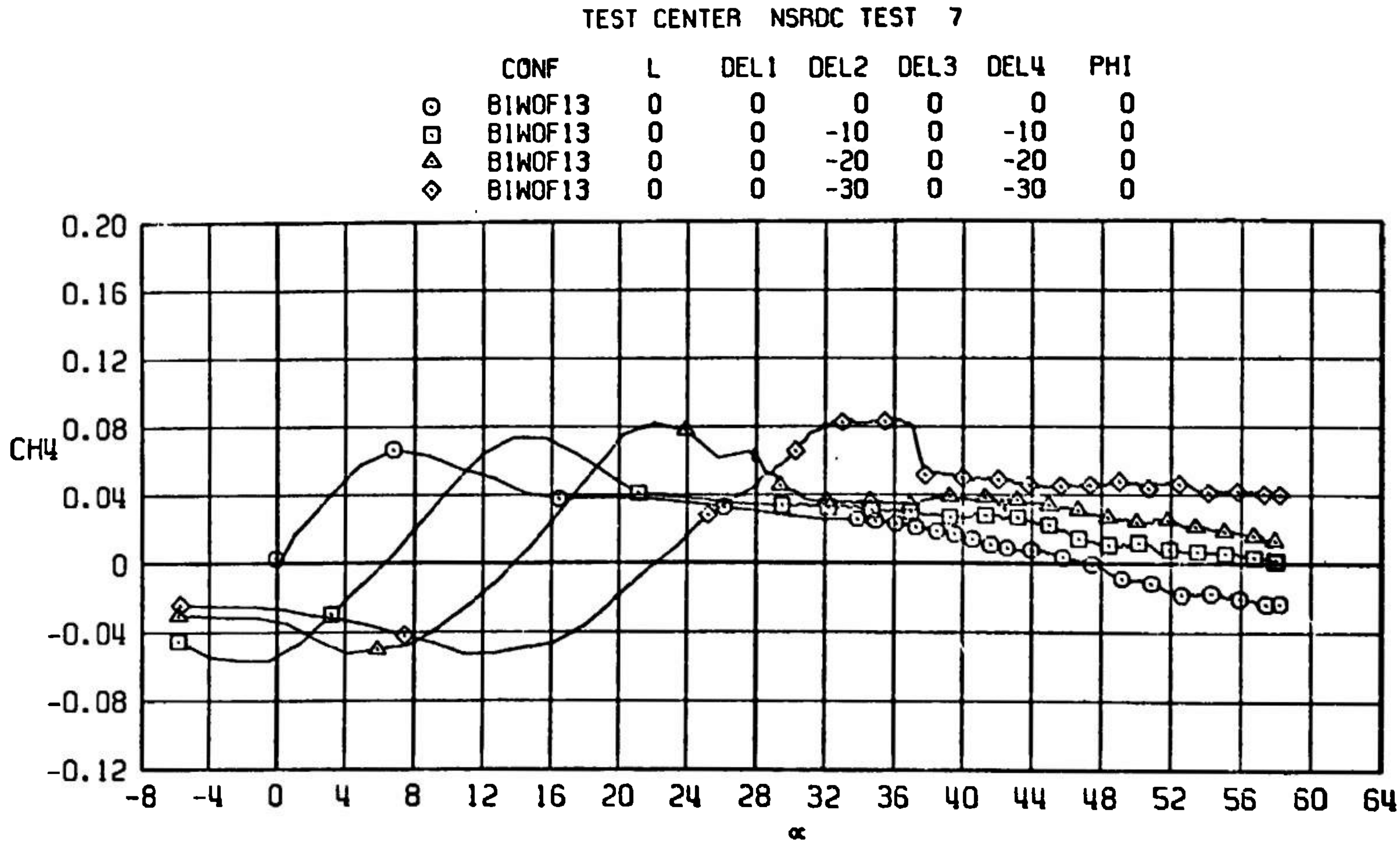

k. CH4 versus α

Figure 63. Concluded.

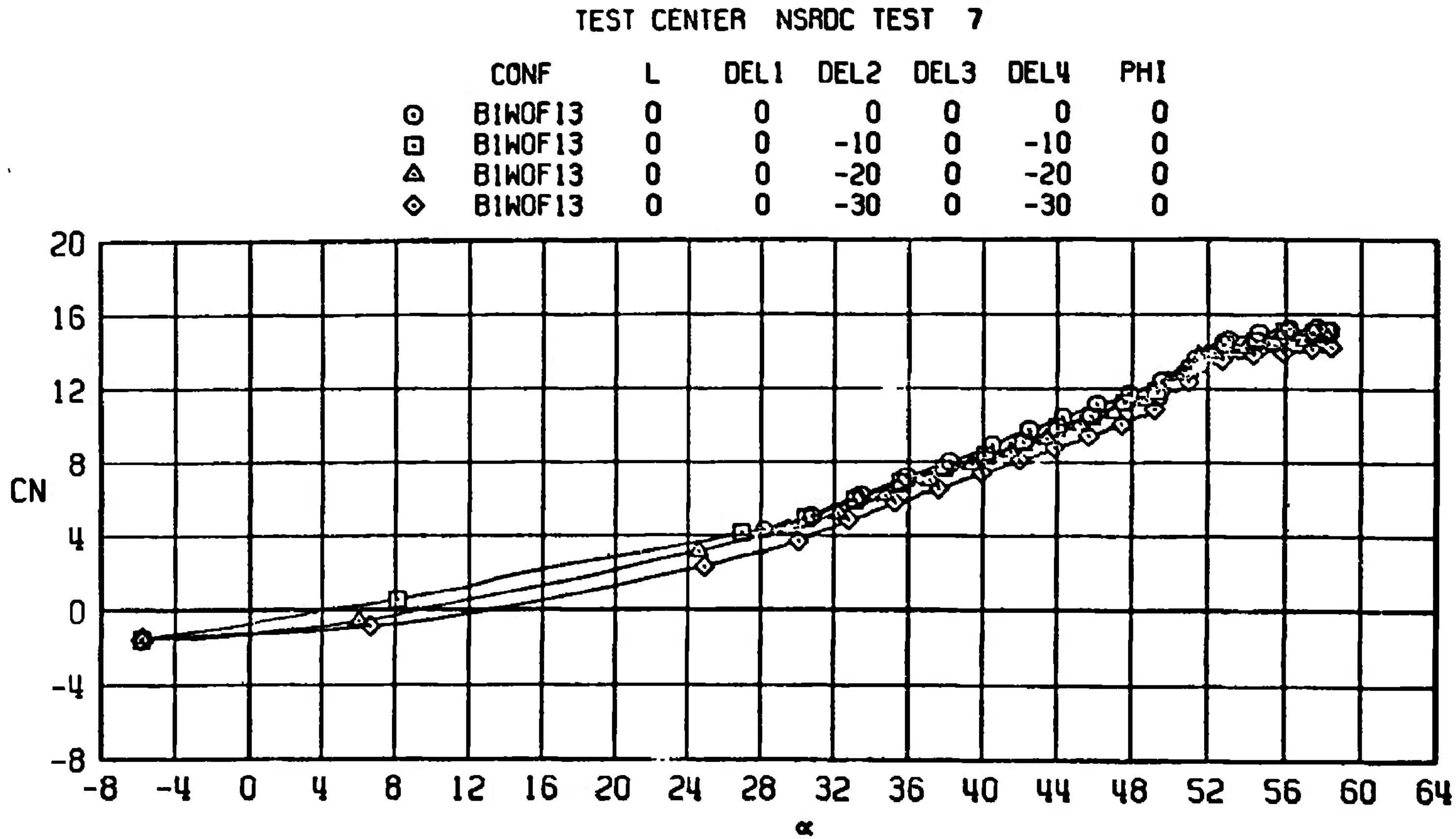

a. CN versus α

Figure 64. Test No. 7, comparison of aerodynamic coefficients of configuration B1W0F13 for various deflections of tail fins No. 2 and 4 at M_∞ = 0.9.

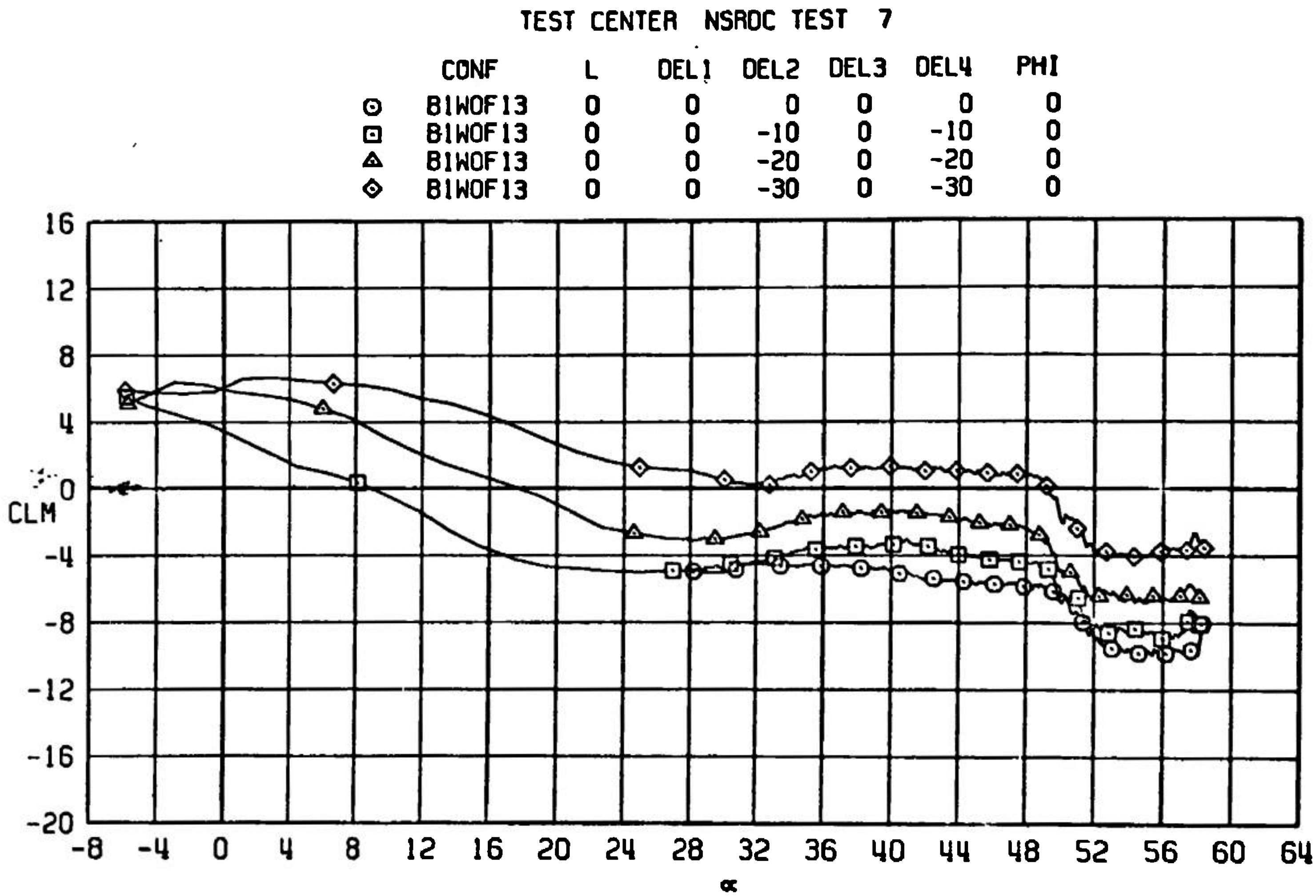

b. CLM versus α

Figure 64. Continued.

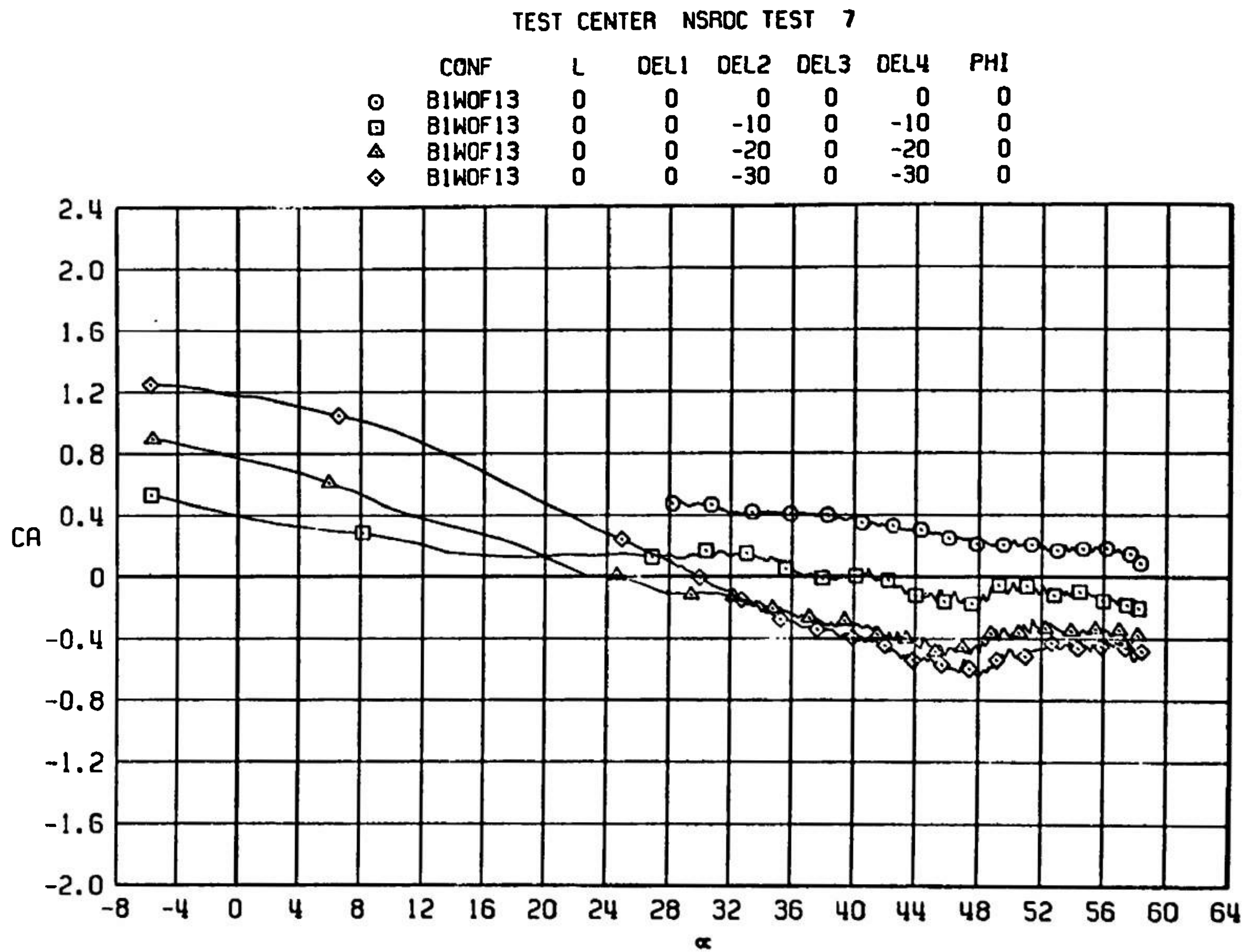

c. CA versus α
Figure 64. Continued.

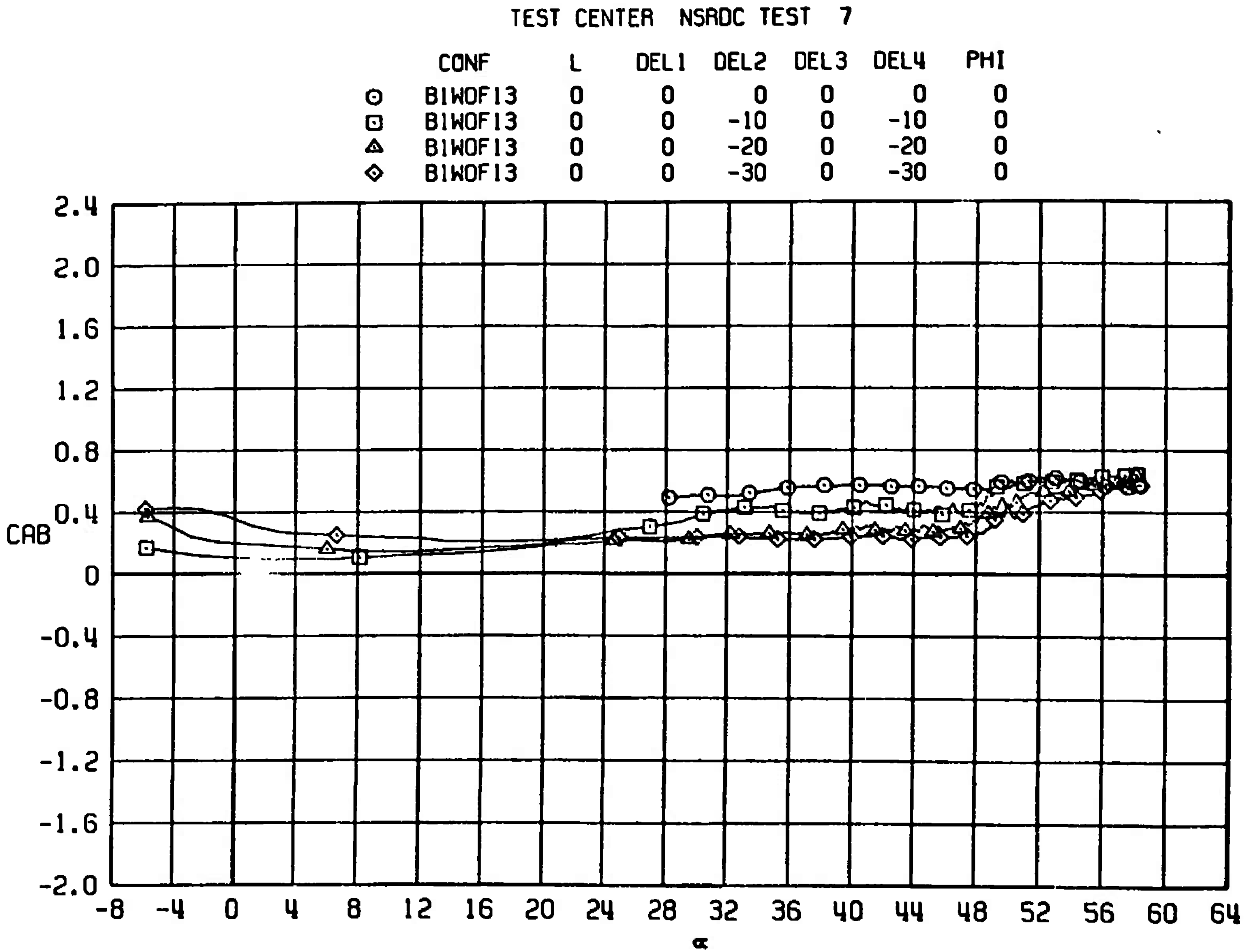

d. CAB versus α
Figure 64. Continued.

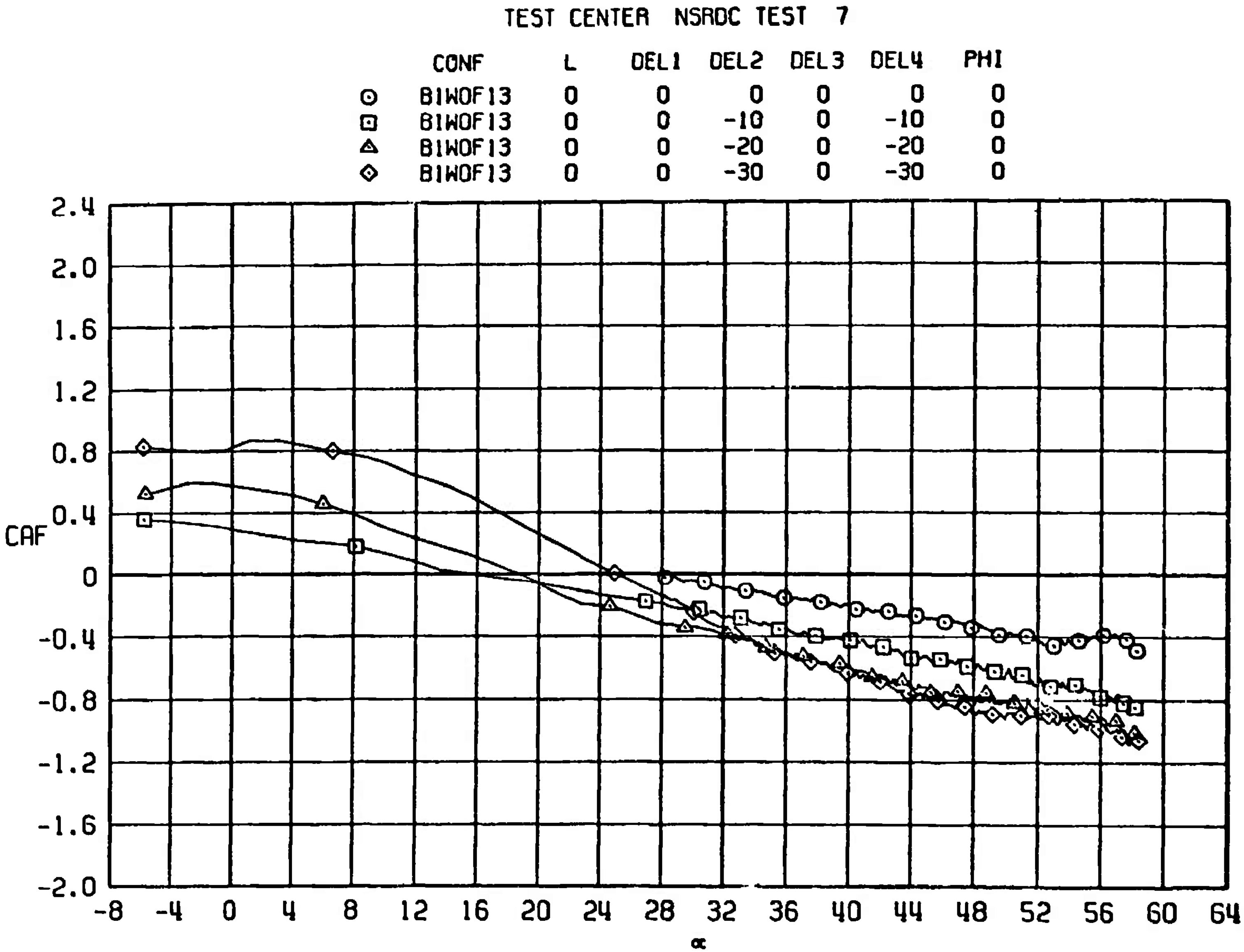

e. CAF versus α
Figure 64. Continued.

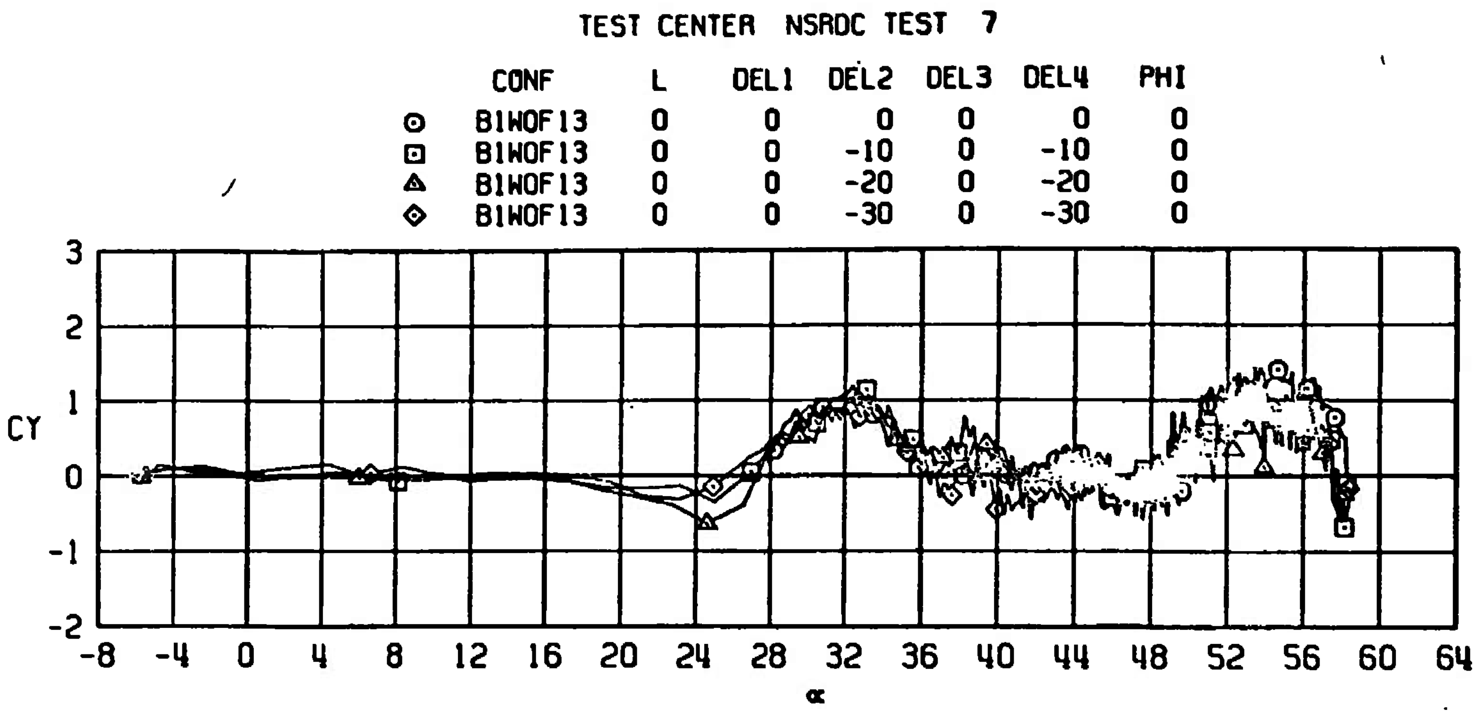

f. CY versus α
Figure 64. Continued.

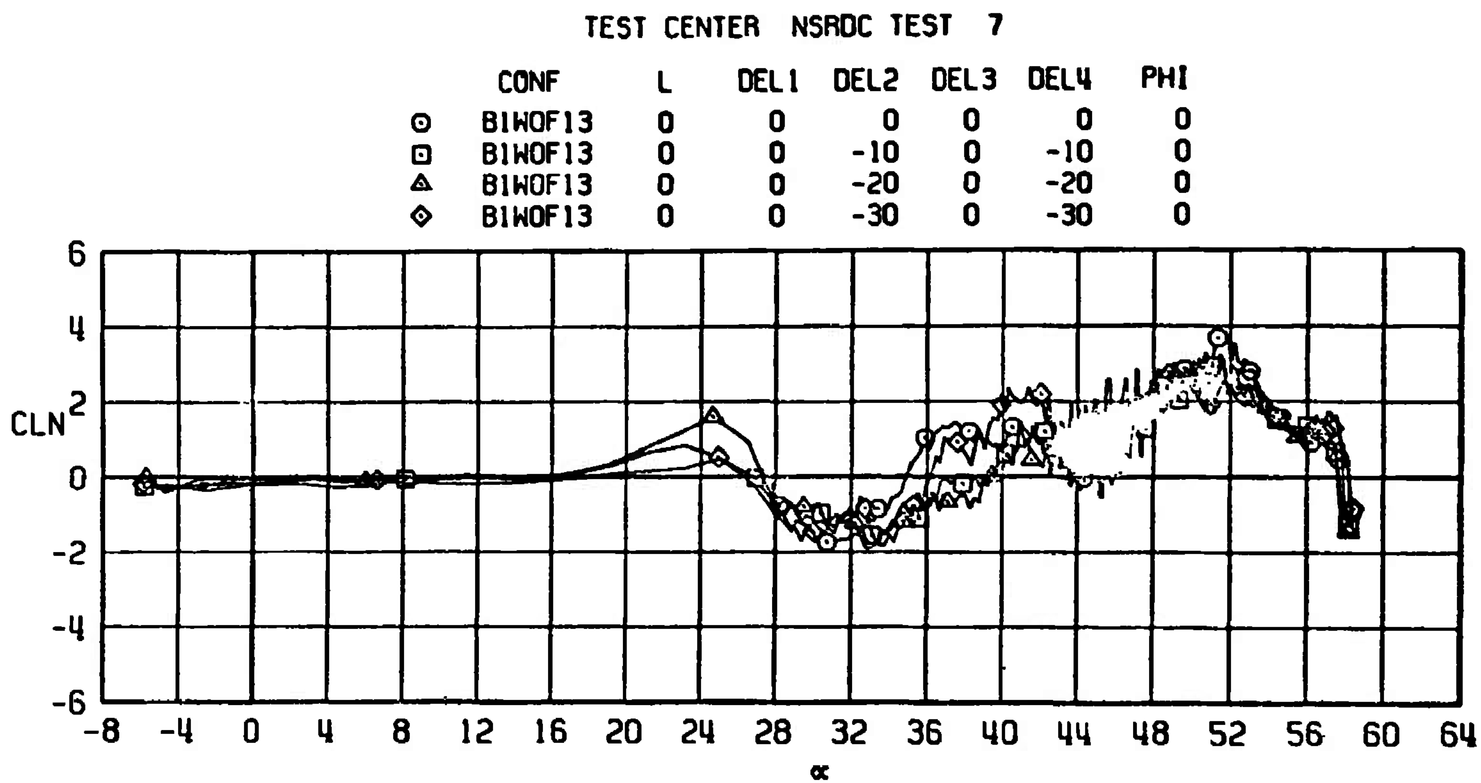

g. CLN versus α

Figure 64. Continued.

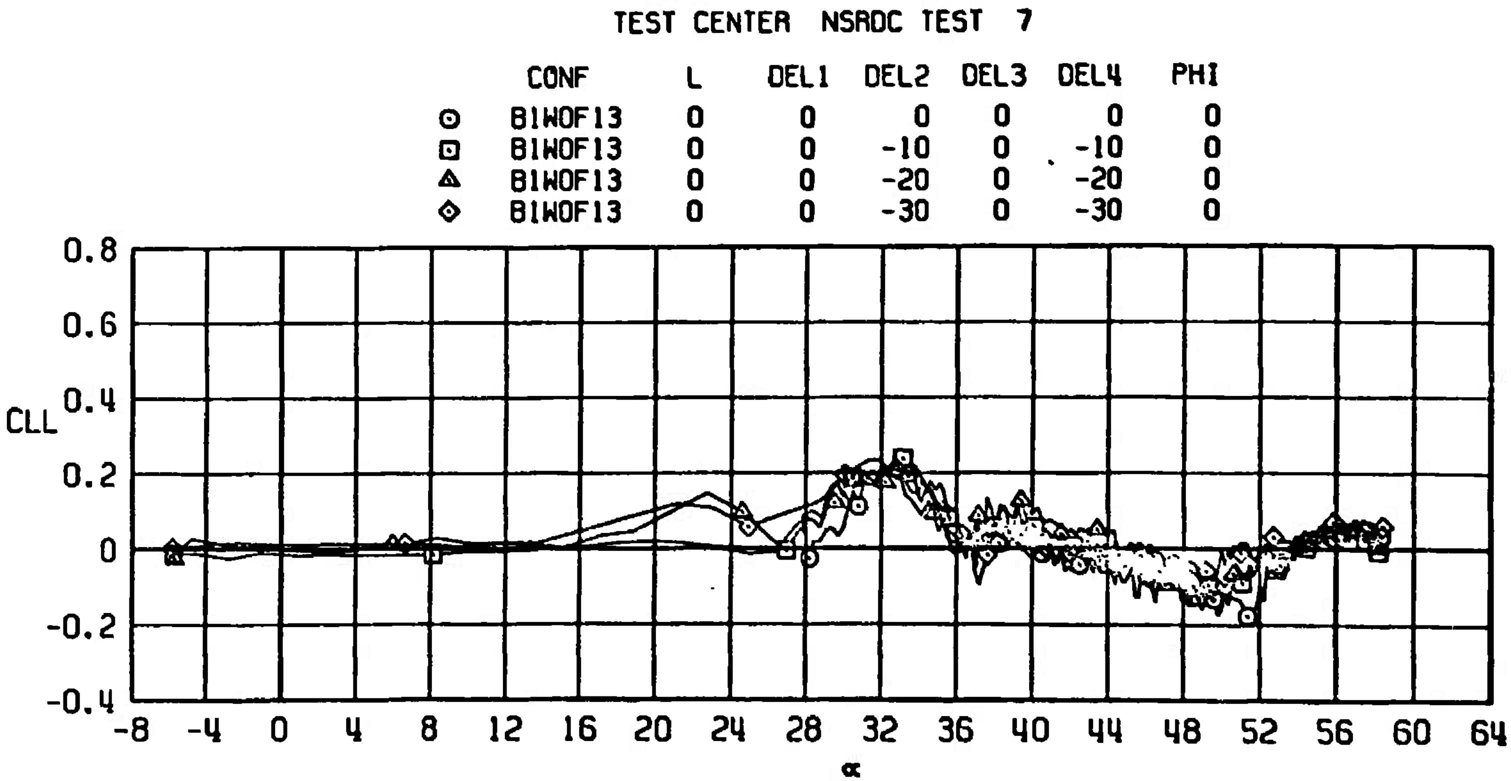

h. CLL versus α
Figure 64. Continued.

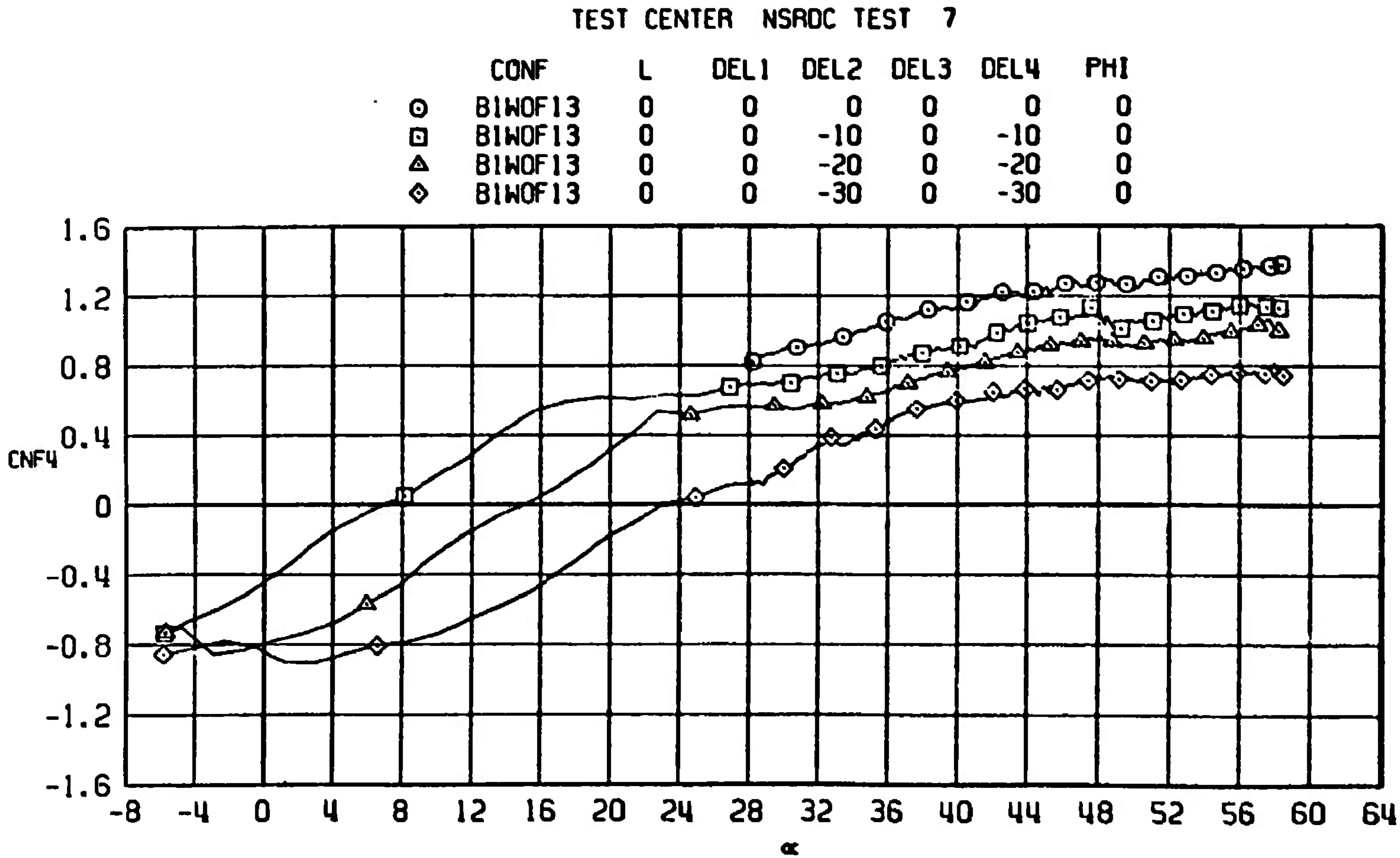

i. CNF4 versus α
Figure 64. Continued.

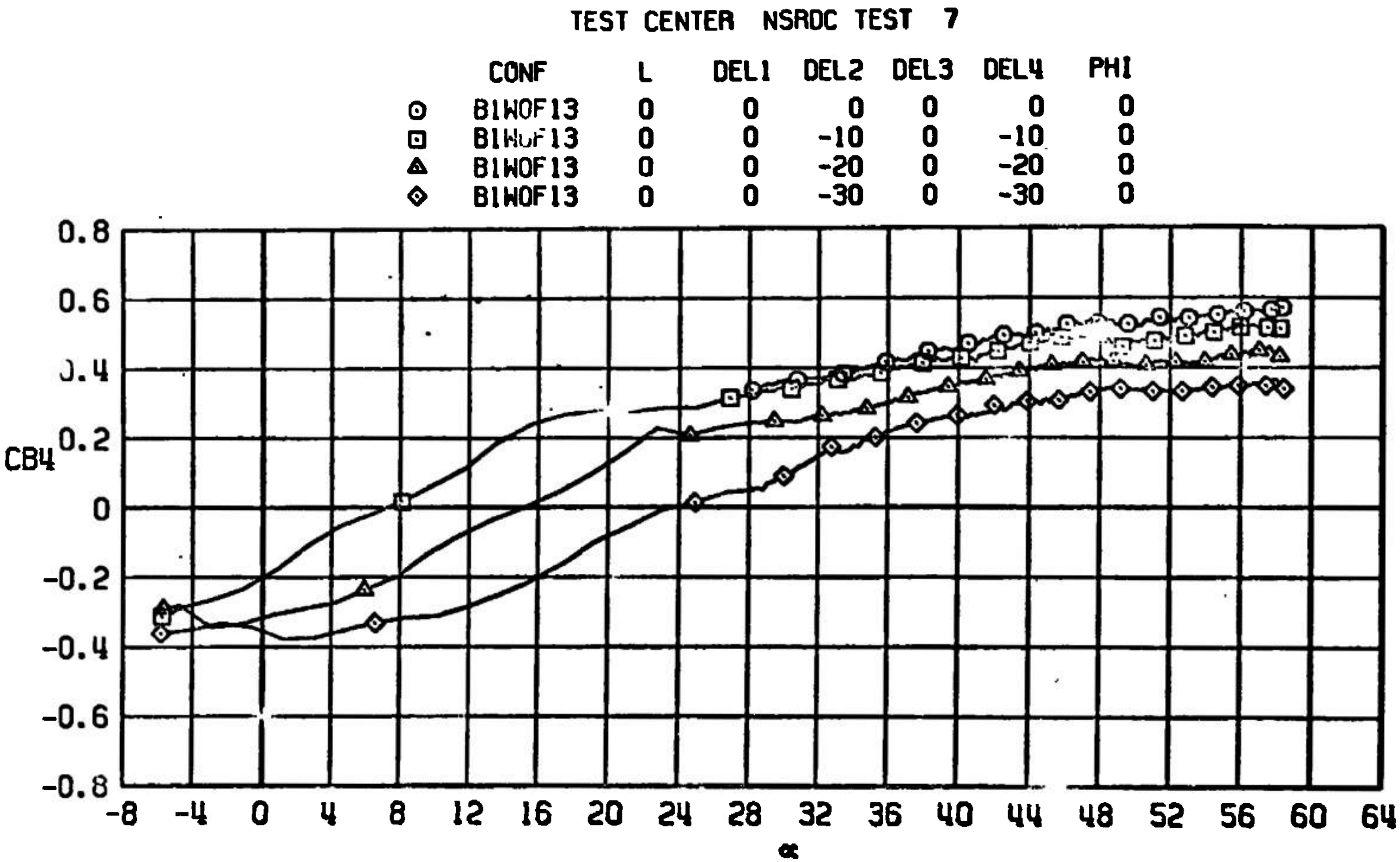

j. CB4 versus α
Figure 64. Continued.

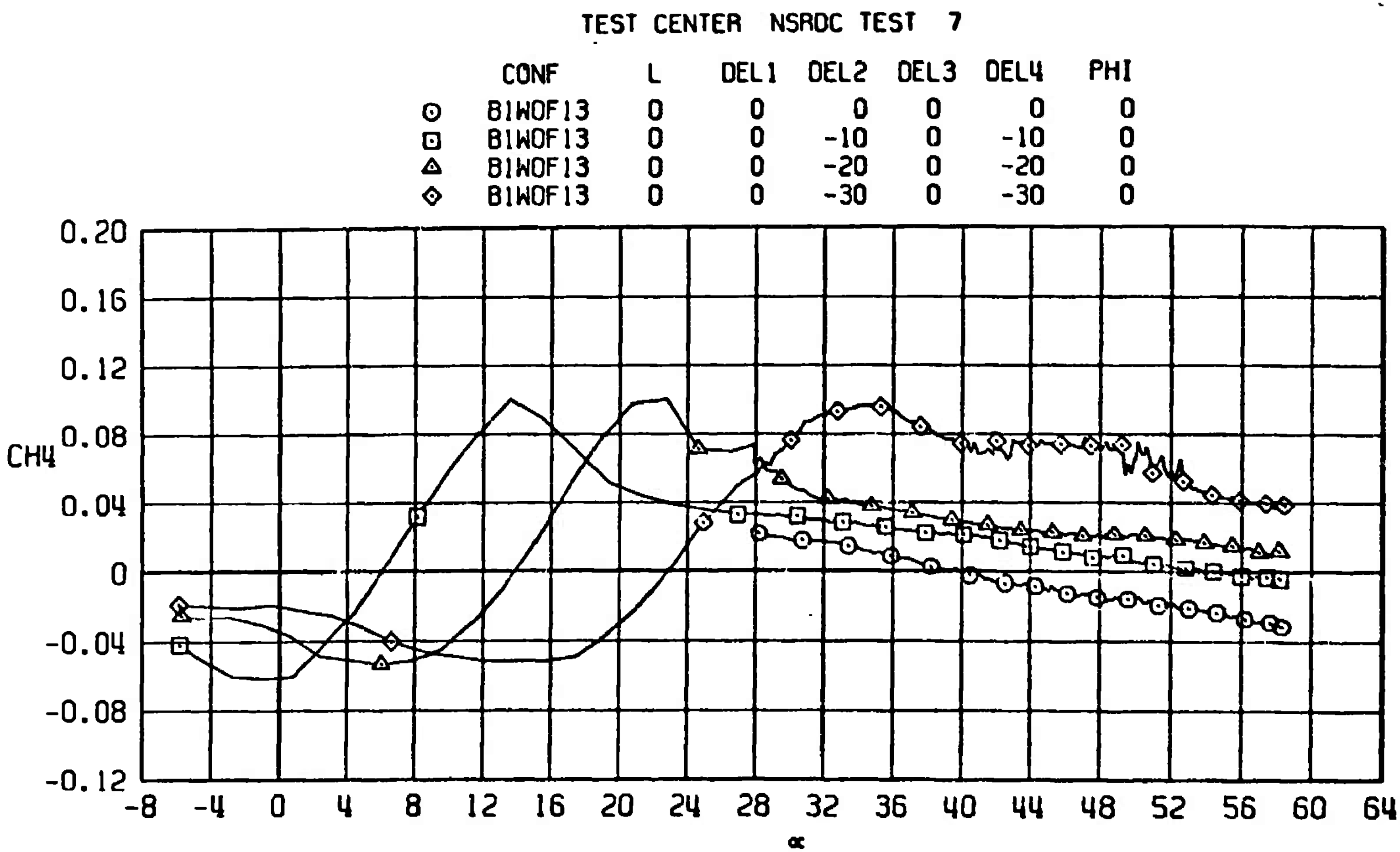

k. CH4 versus α

Figure 64. Concluded.

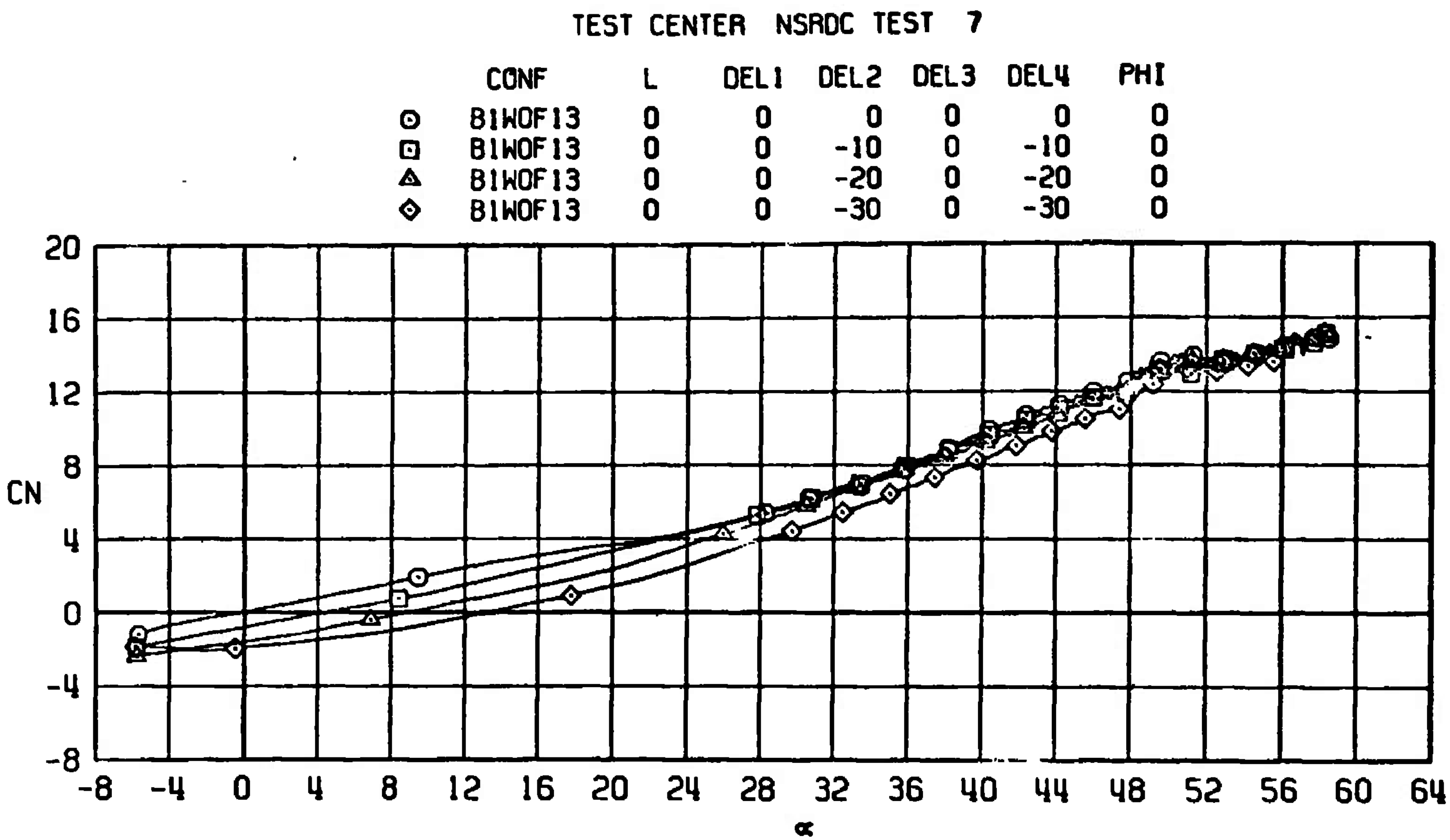

a. CN versus α

Figure 65. Test No. 7, comparison of aerodynamic coefficients of configuration B1W0F13 for various deflections of tail fins No. 2 and 4 at M_∞ = 1.0.

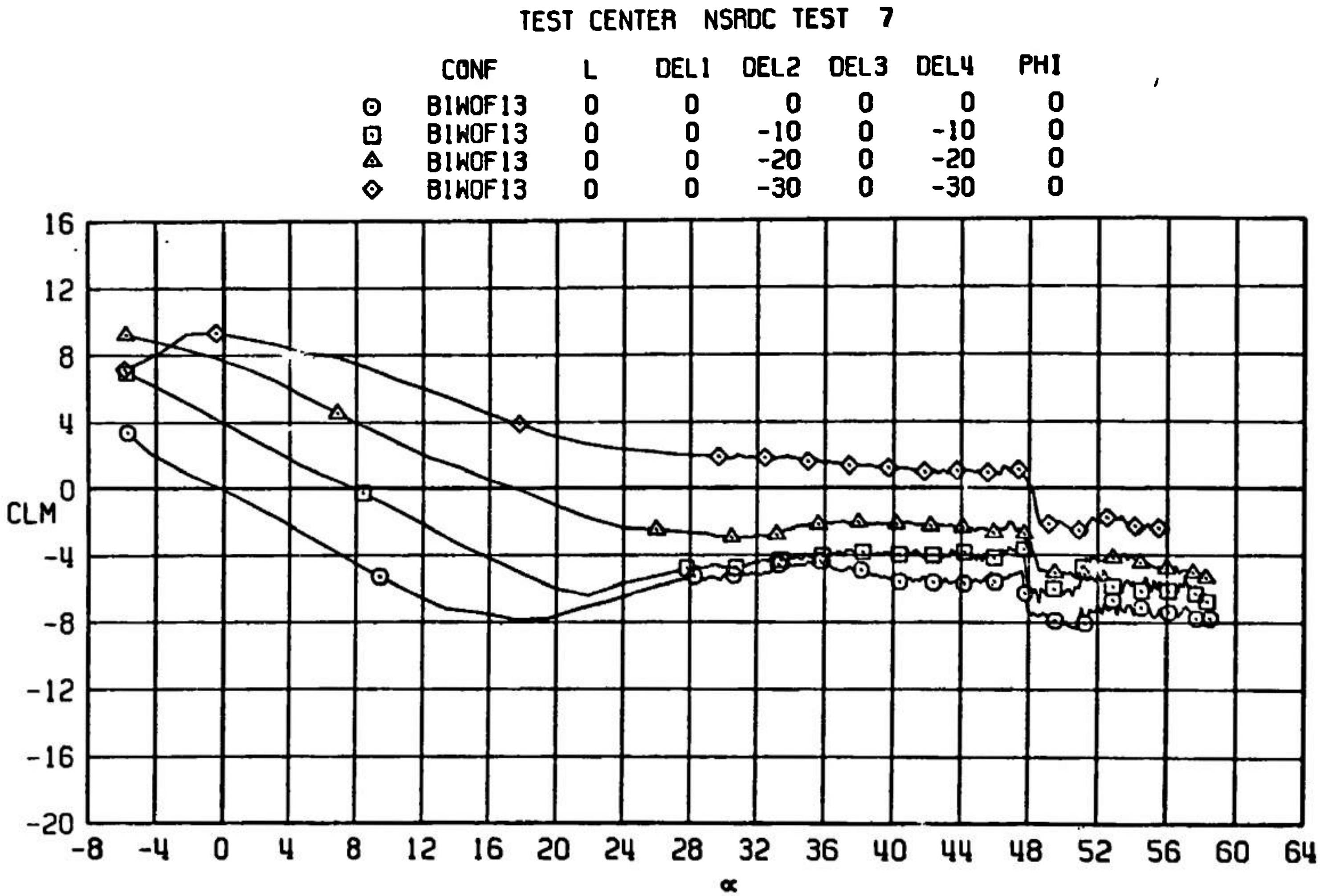

b. CLM versus α
Figure 65. Continued.

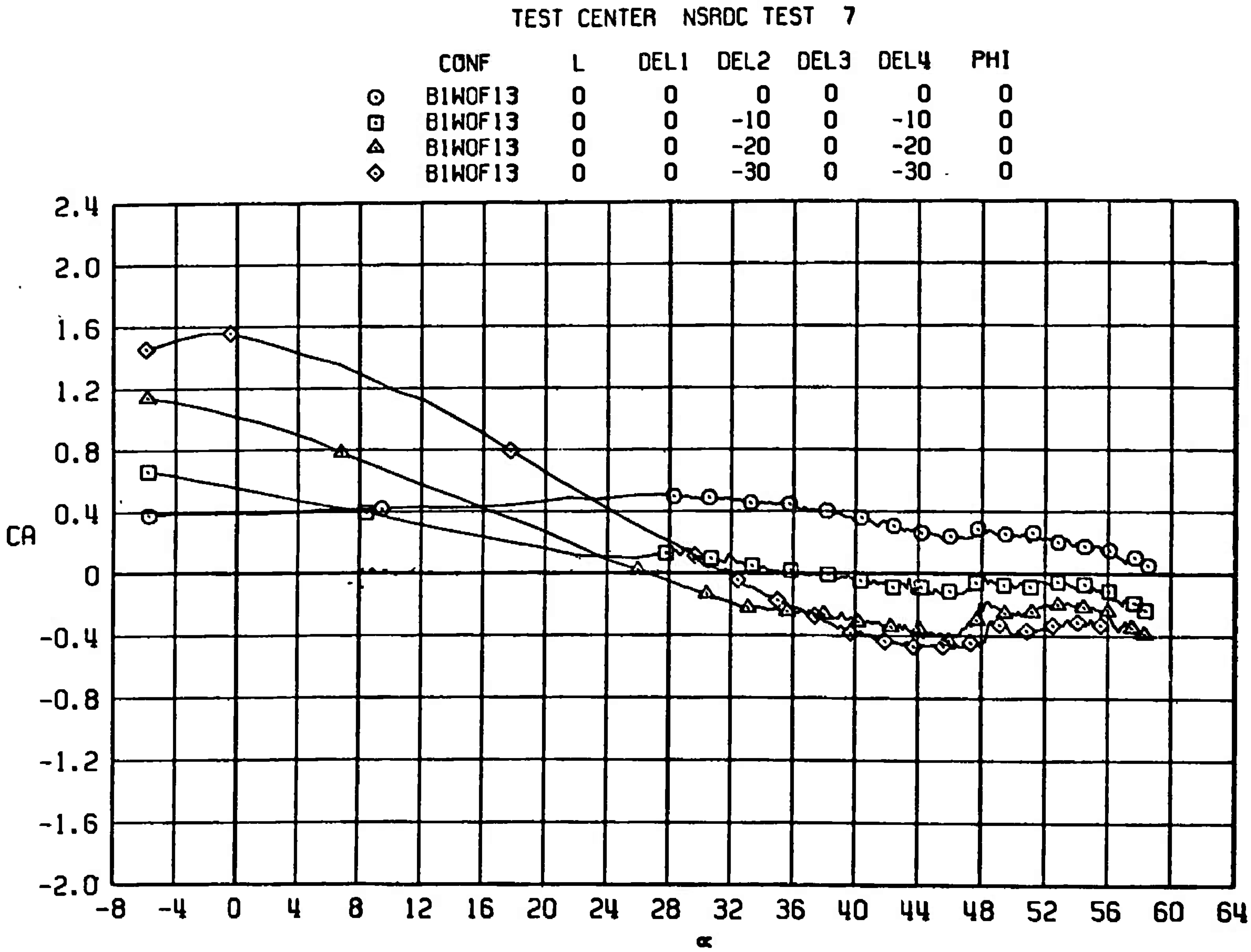

c. CA versus α

Figure 65. Continued.

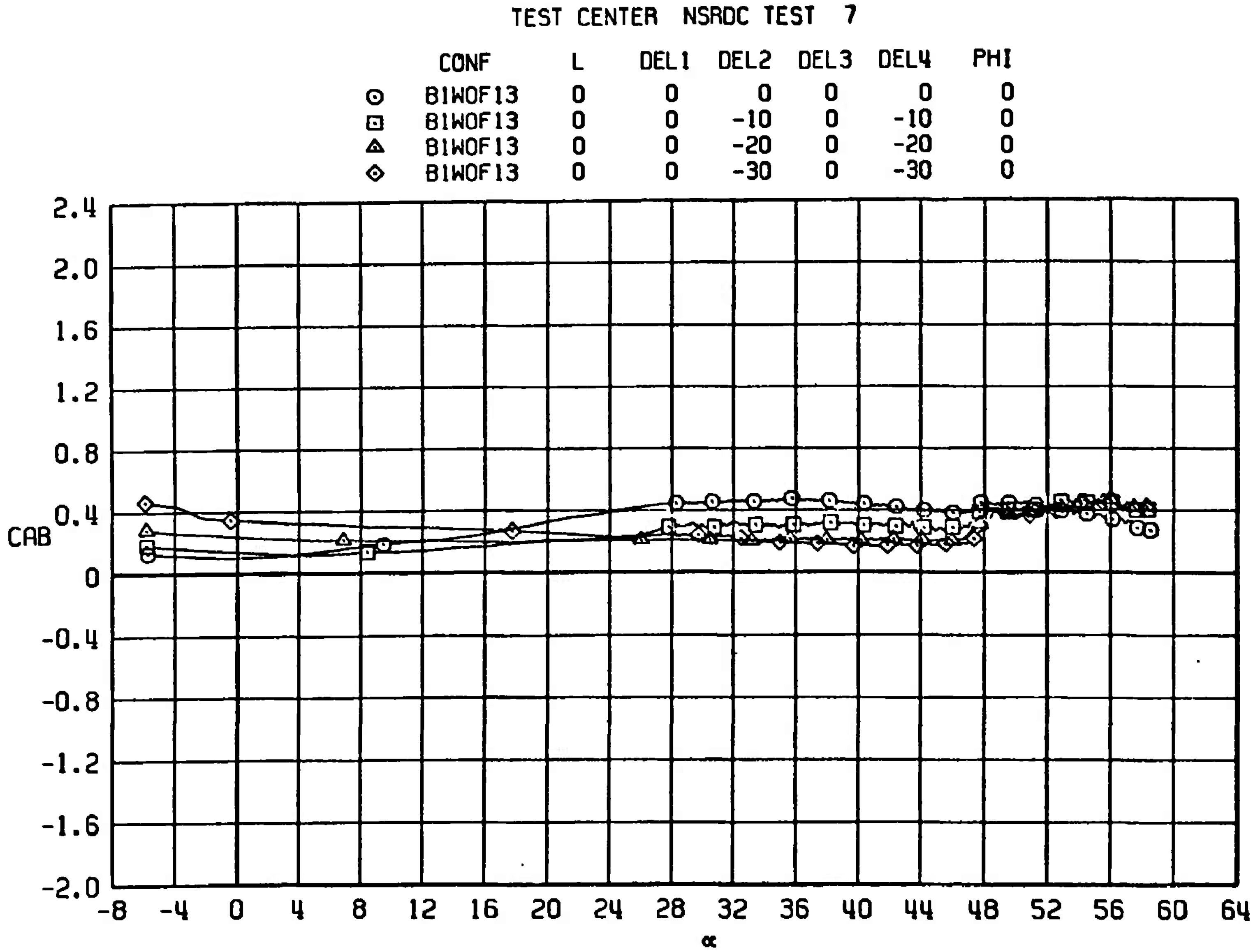

d. CAB versus α
Figure 65. Continued.

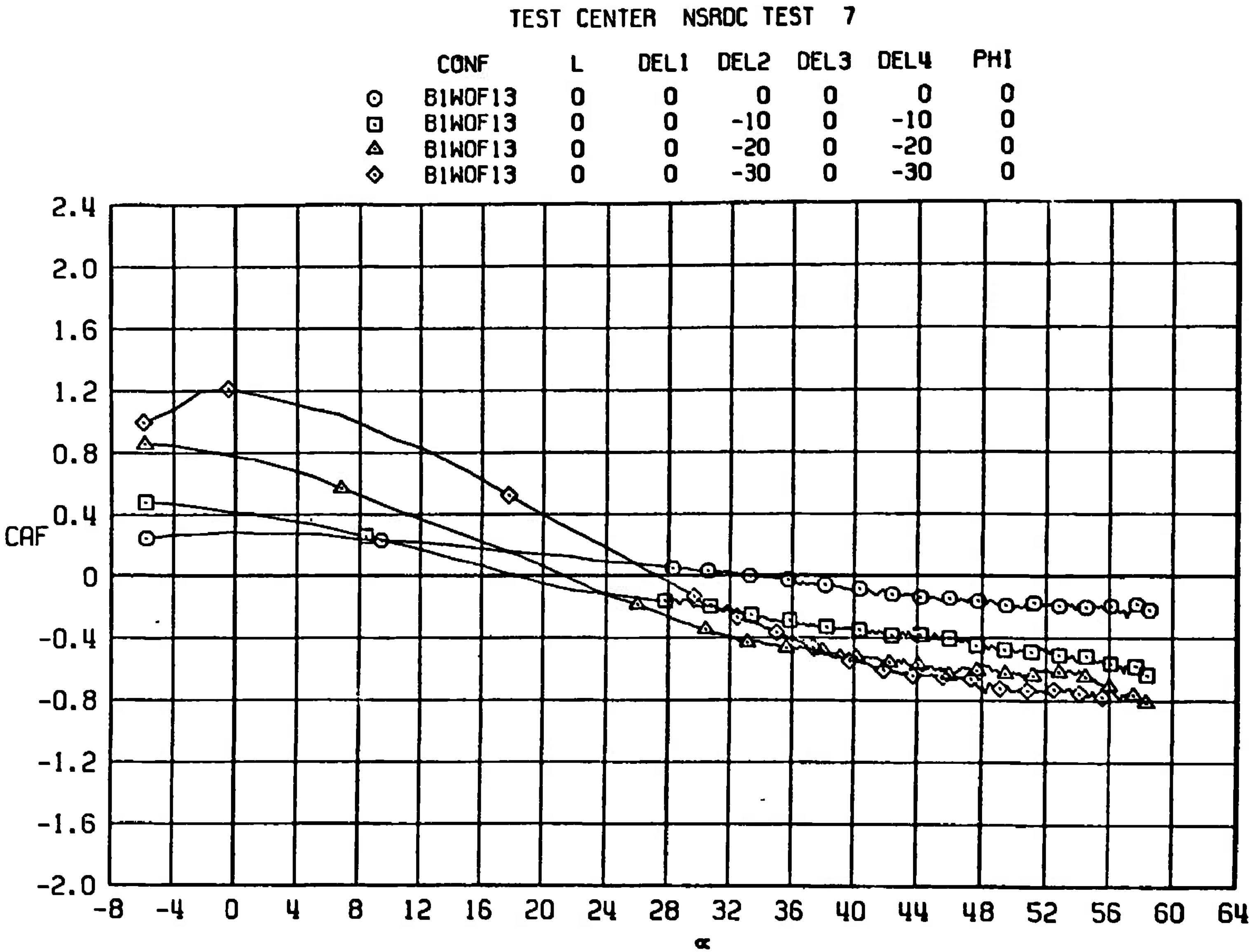

e. CAF versus α
Figure 65. Continued.

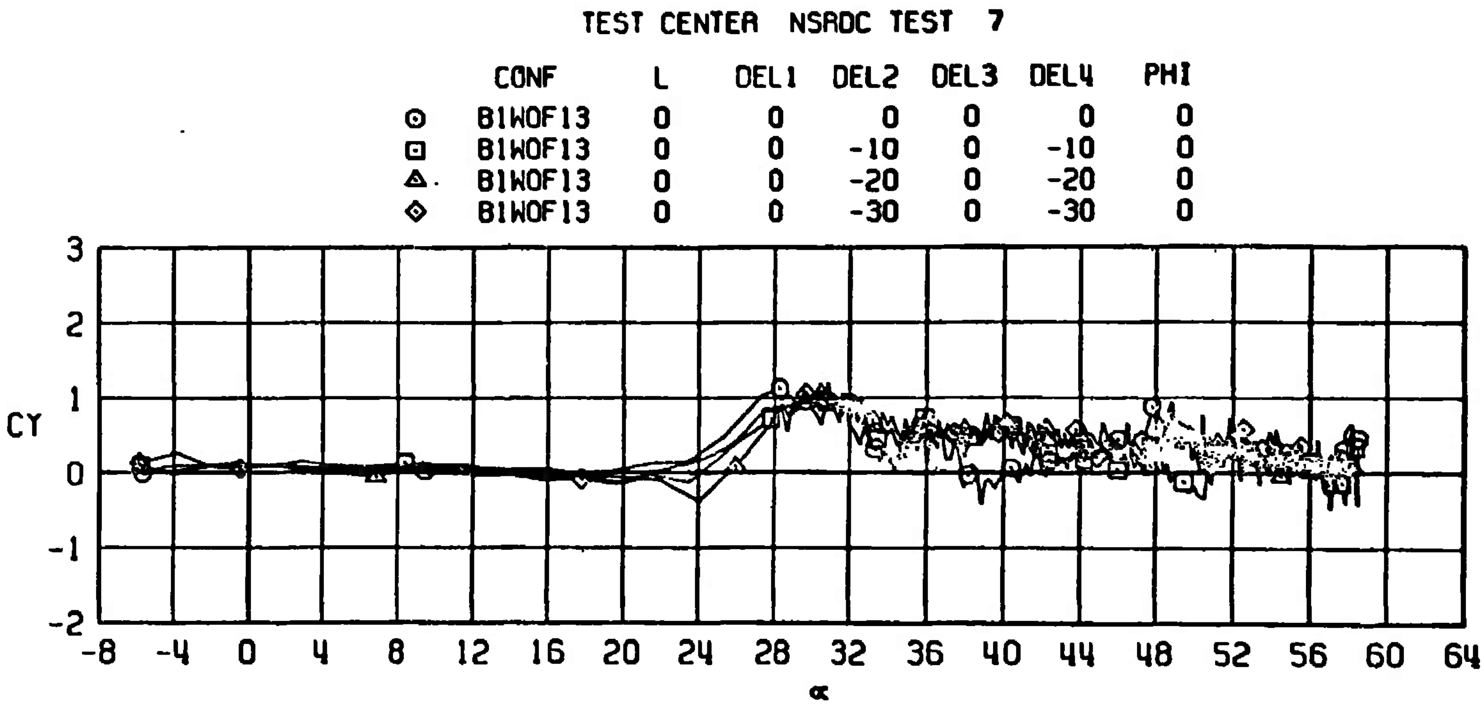

f. CY versus α
Figure 65. Continued.

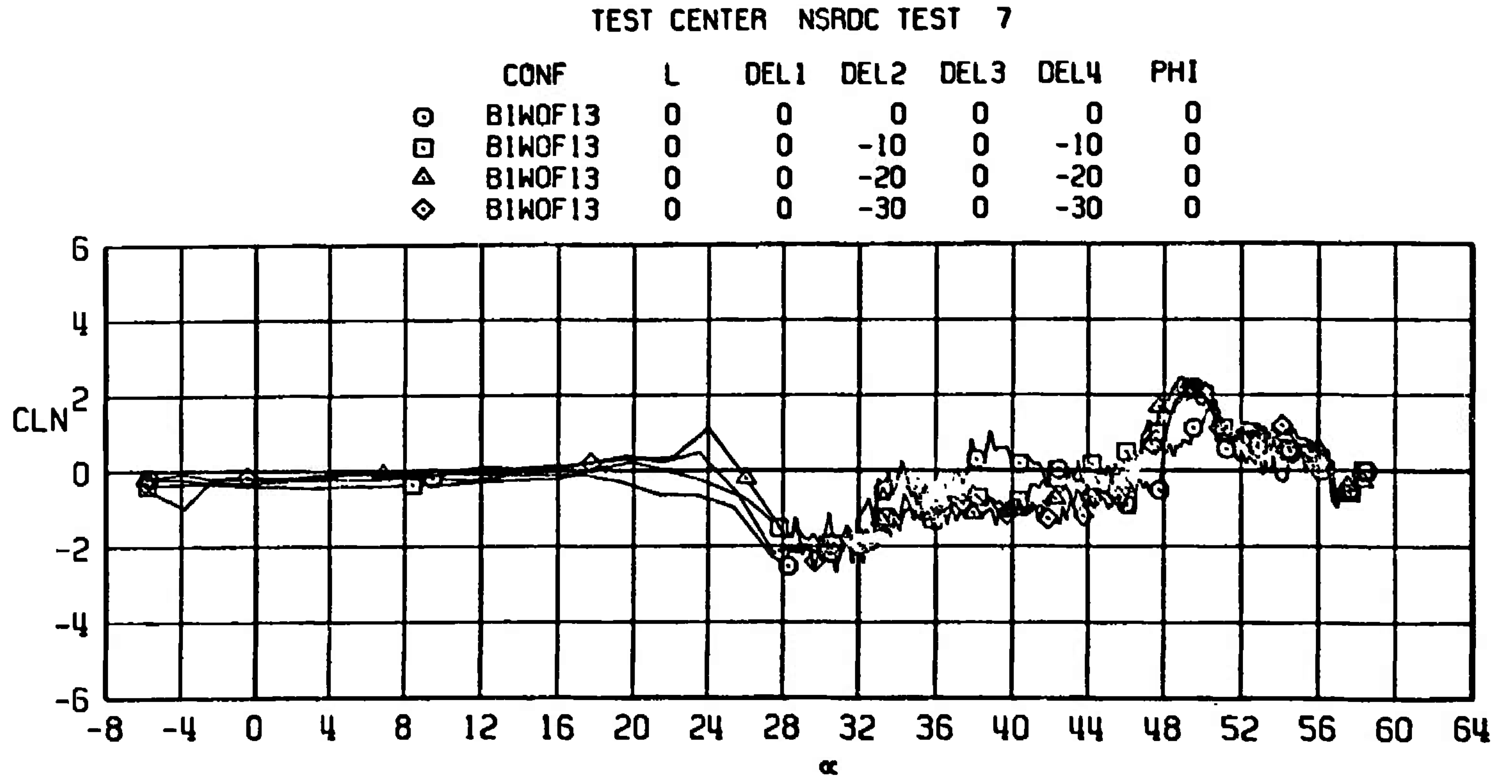

g. CLN versus α
Figure 65. Continued.

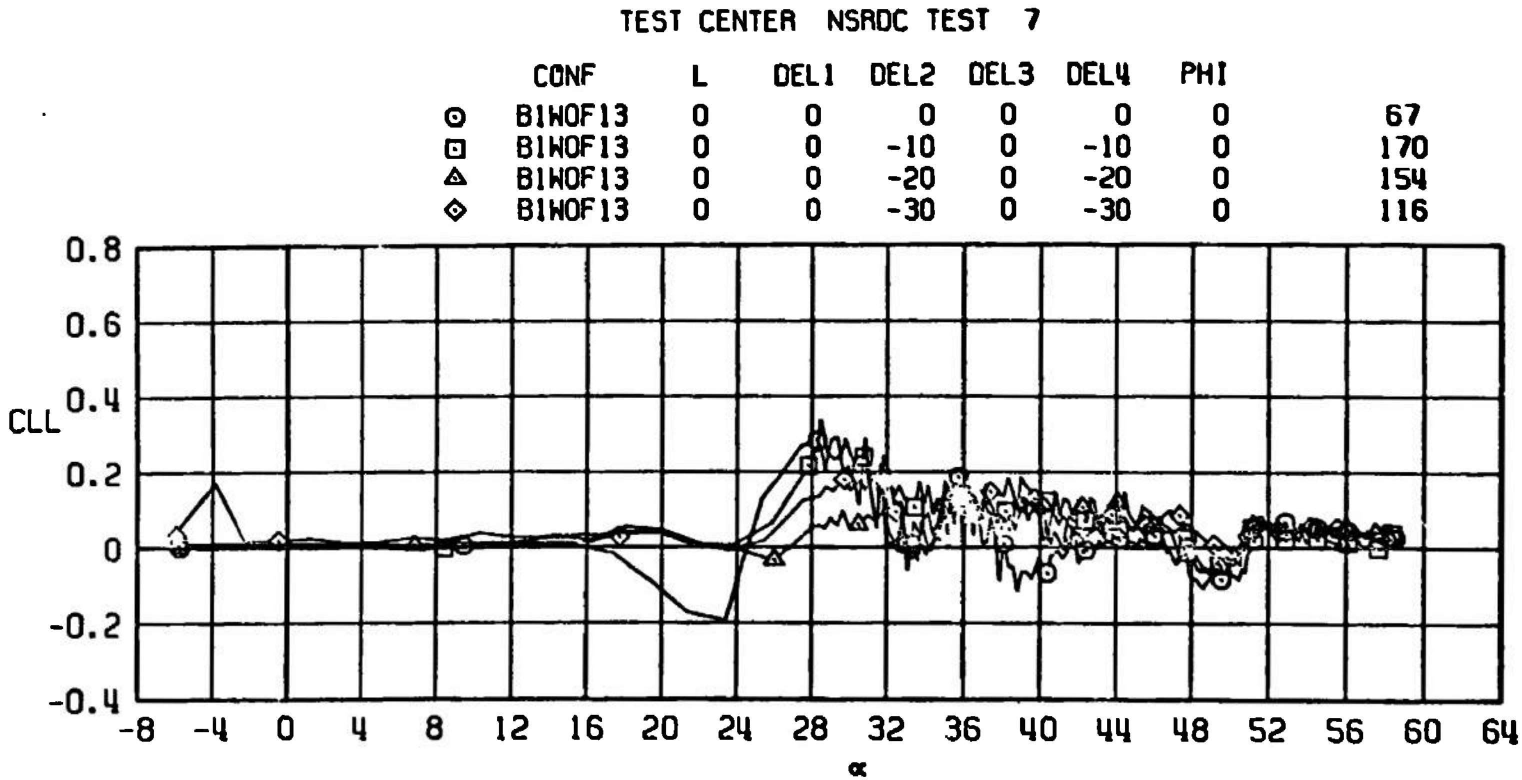

h. CLL versus α
Figure 65. Continued.

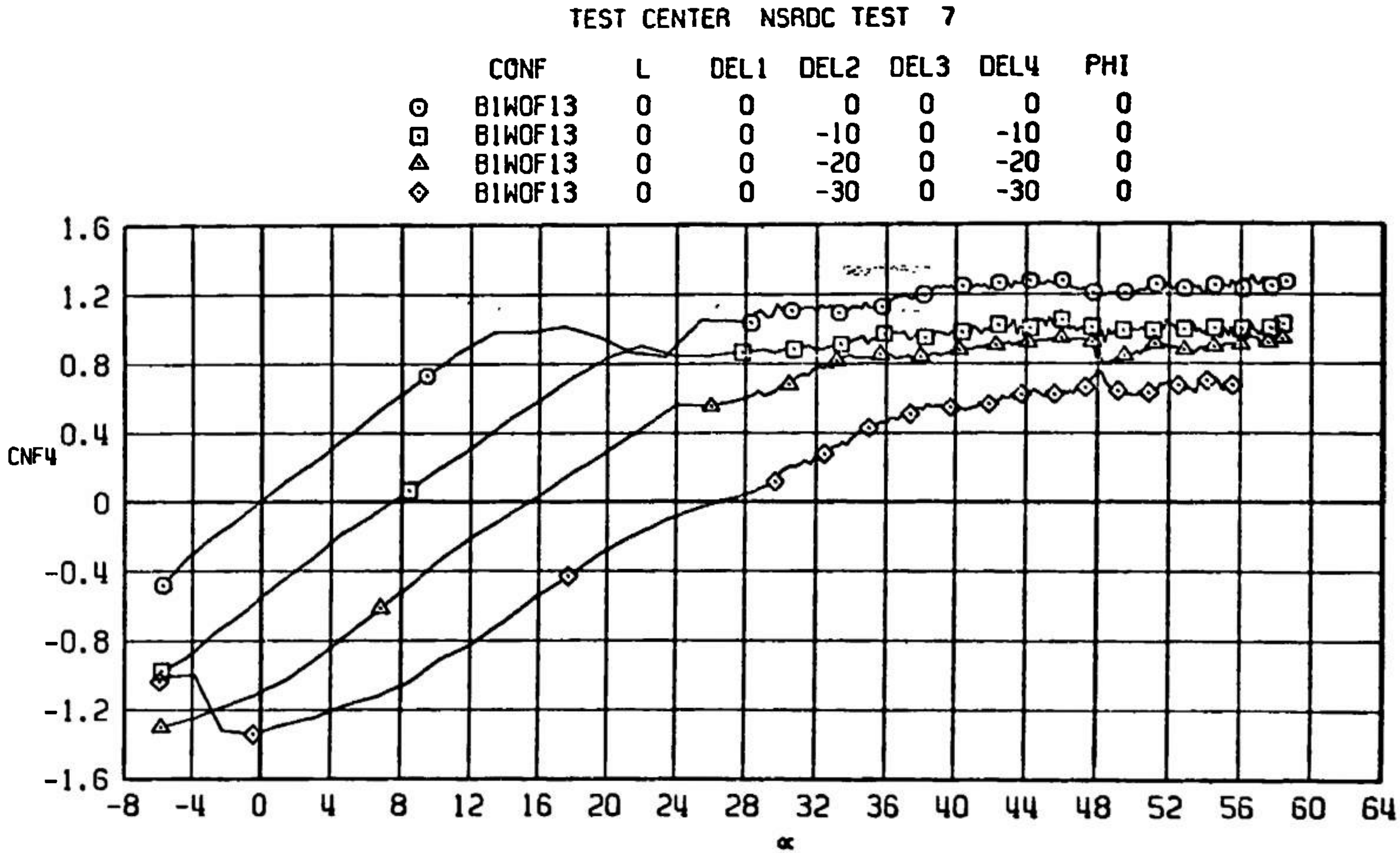

i. CNF4 versus α
Figure 65. Continued.

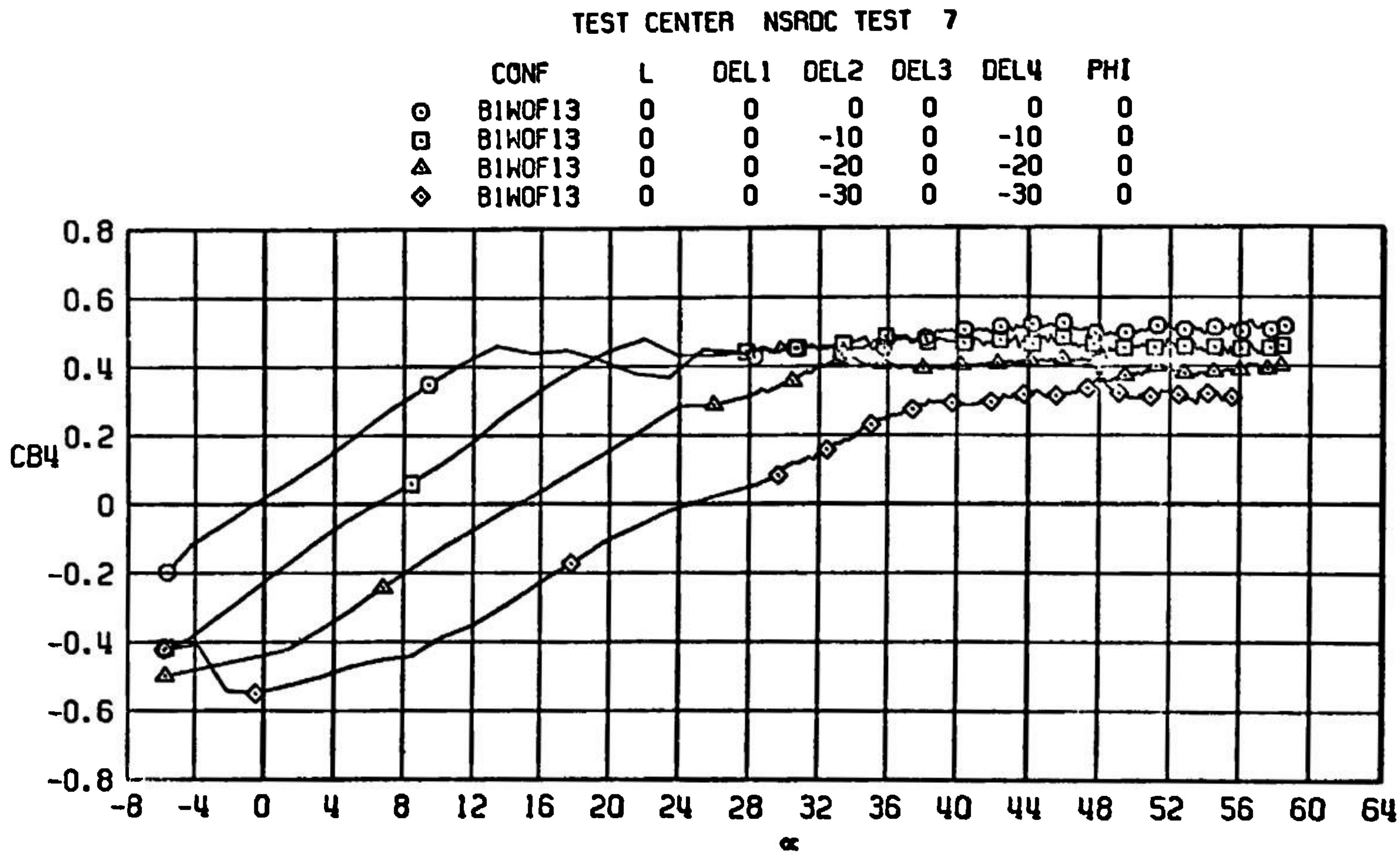

j. CB4 versus α
Figure 65. Continued.

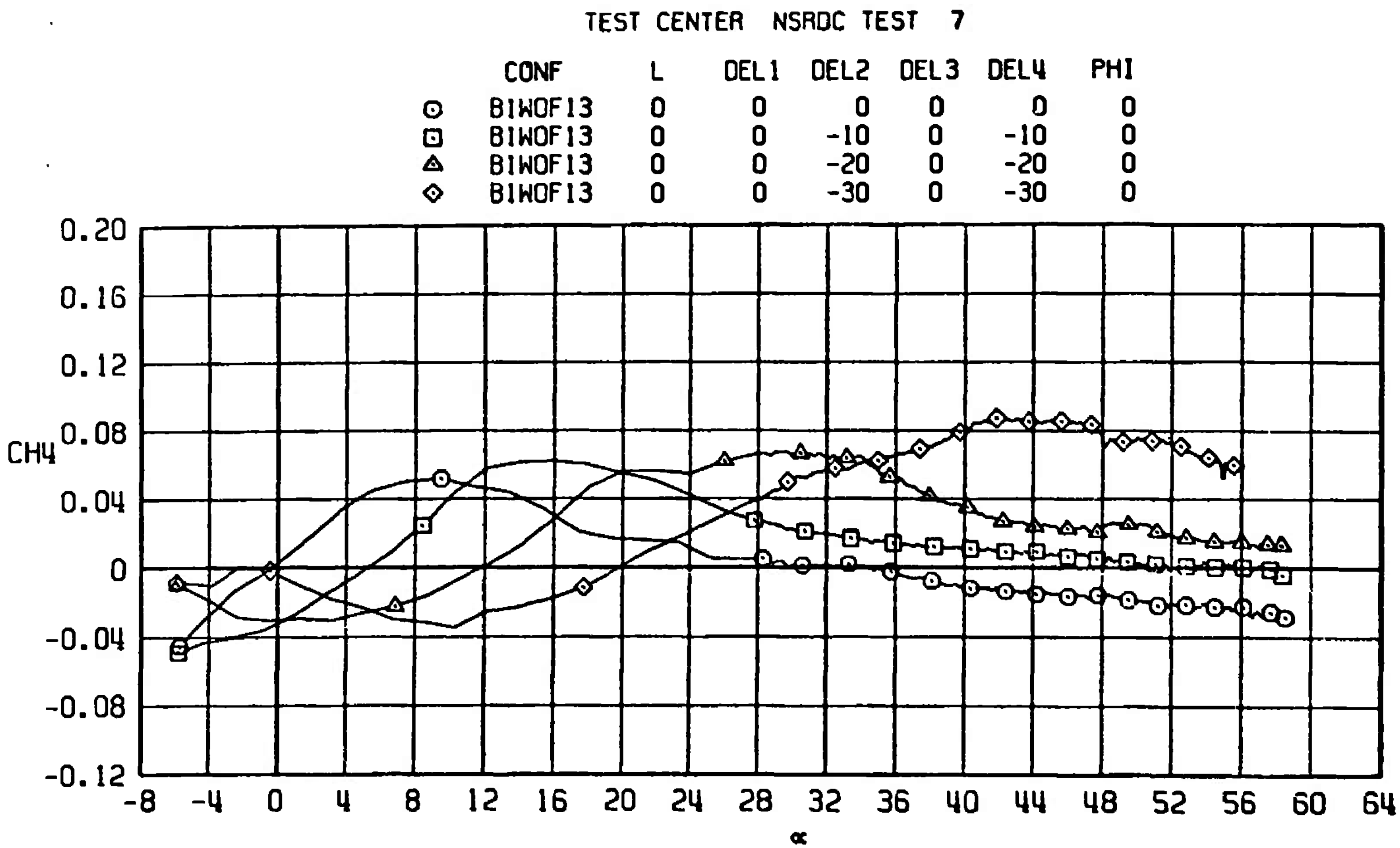

k. CH4 versus a
Figure 65. Concluded.

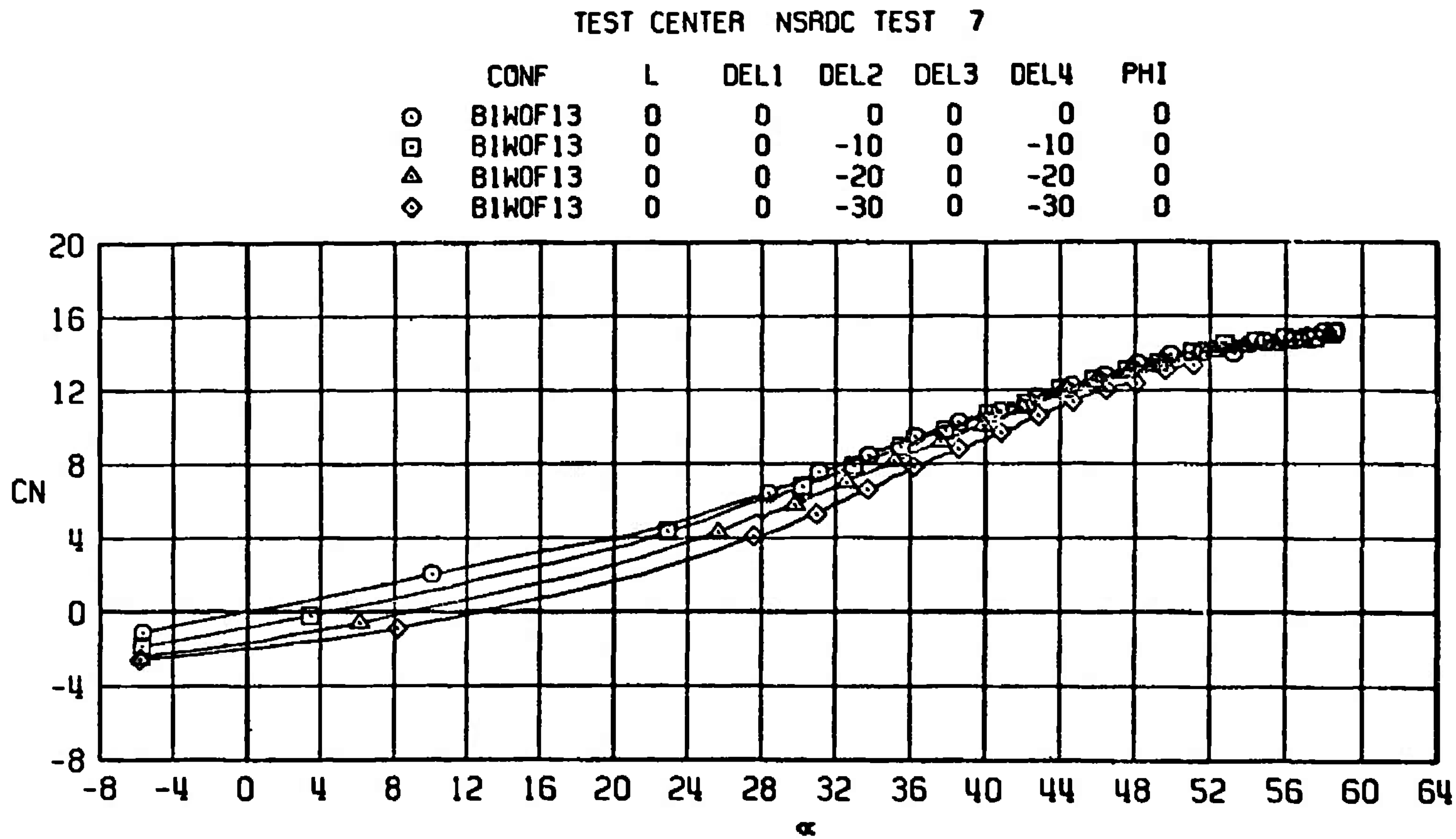

a. CN versus α

Figure 66. Test No. 7, comparison of aerodynamic coefficients of configuration B1W0F13 for various deflections of tail fins No. 2 and 4 at M_∞ = 1.1.

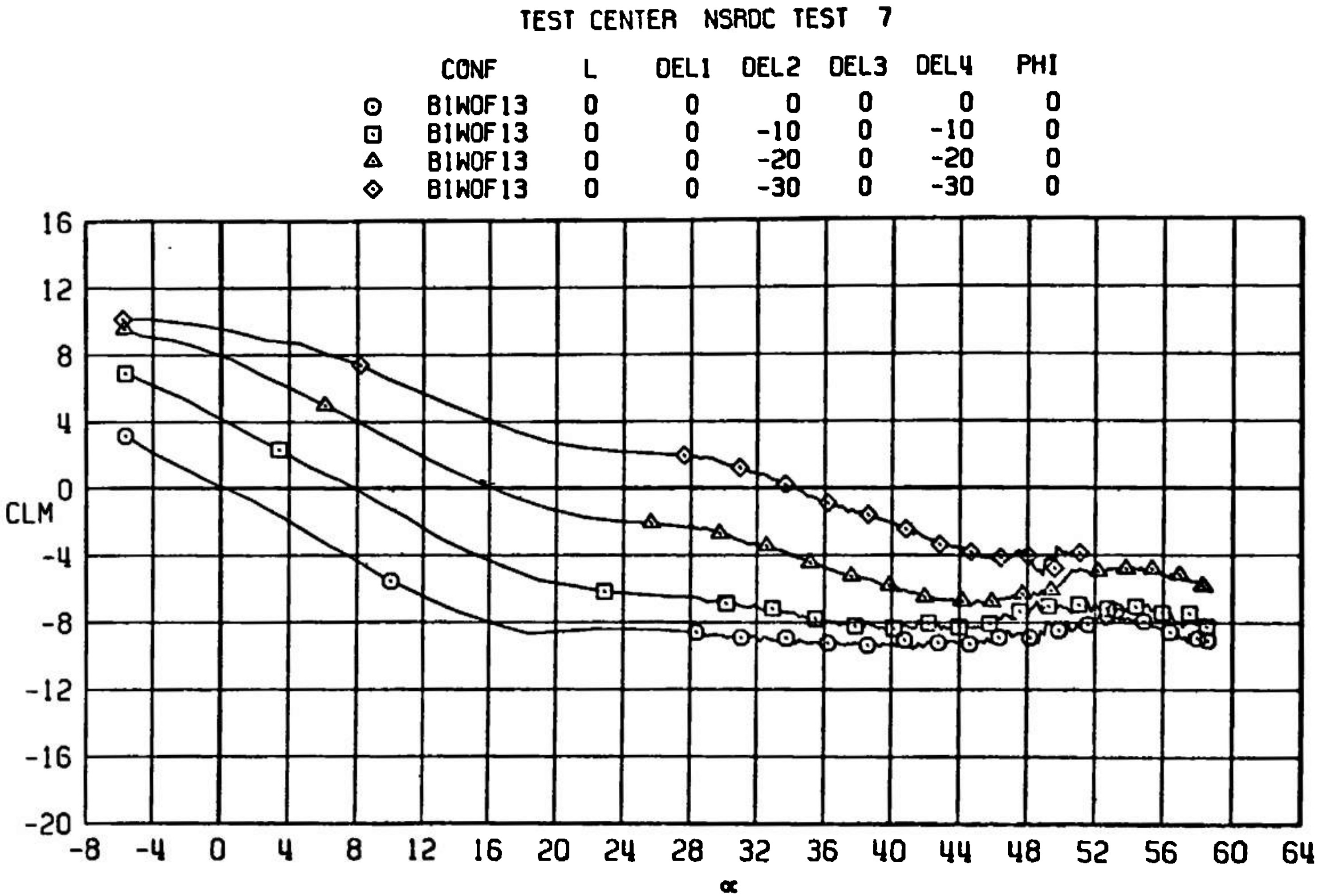

b. CLM versus α
Figure 66. Continued.

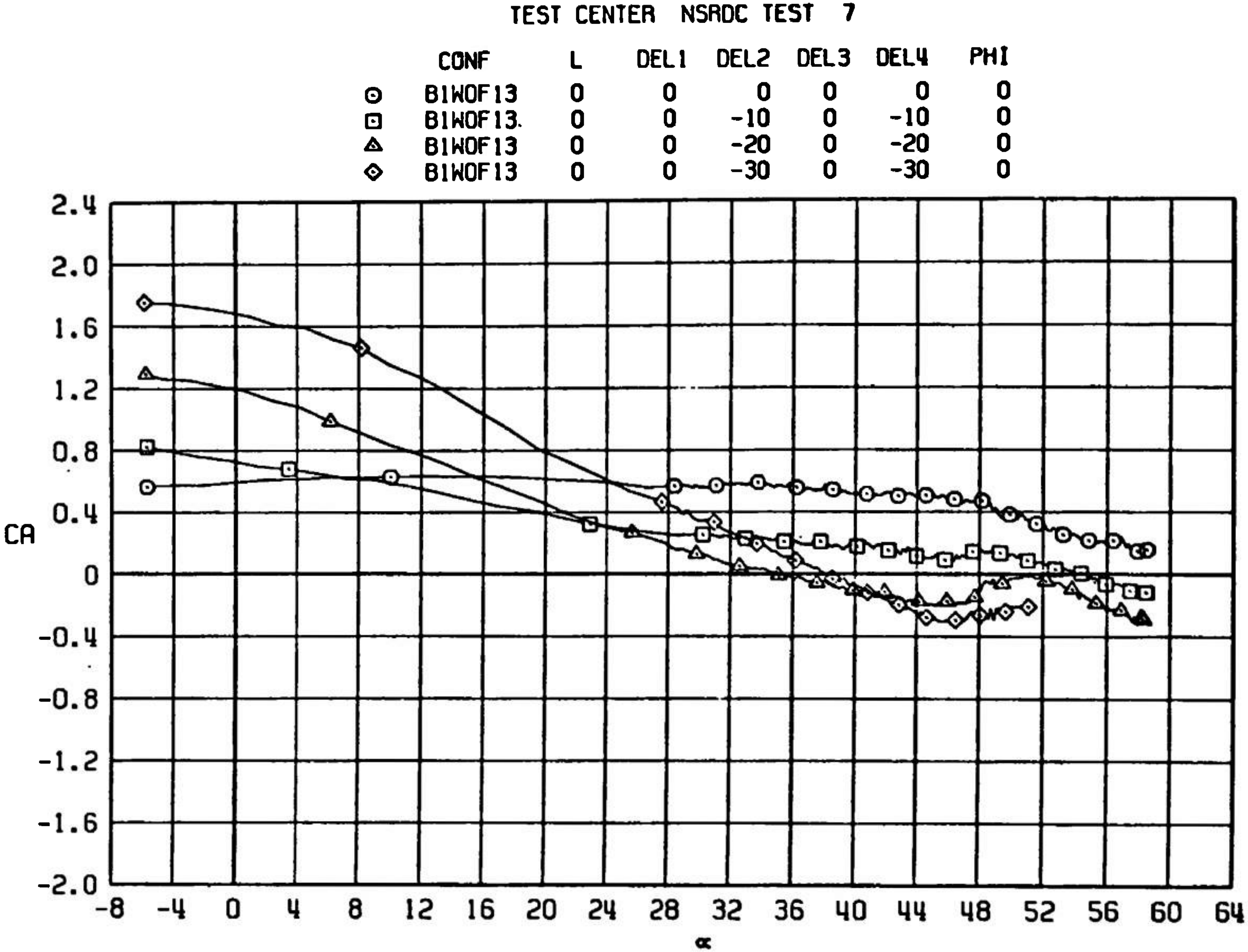

c. CA versus α
Figure 66. Continued.

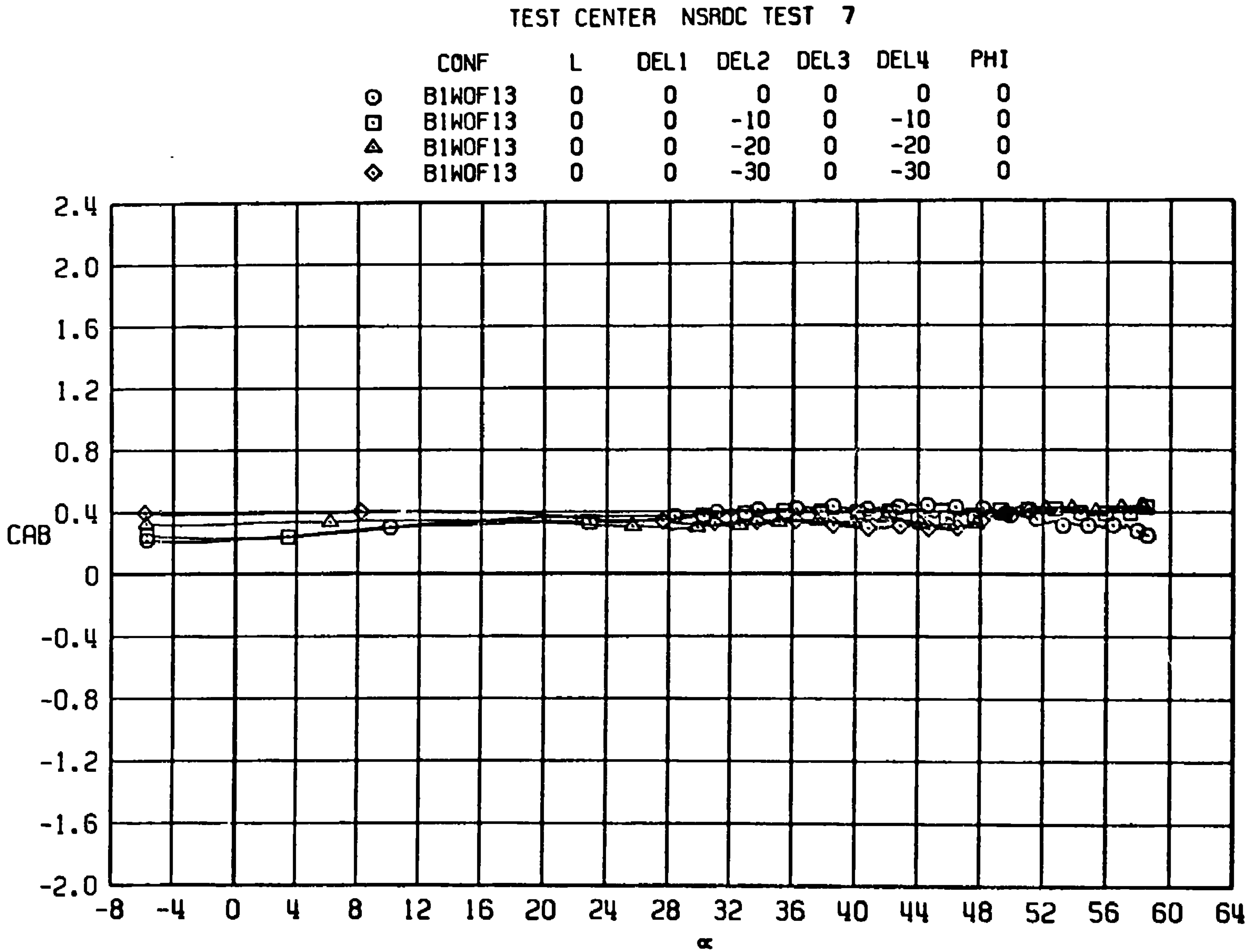

d. CAB versus α
Figure 66. Continued.

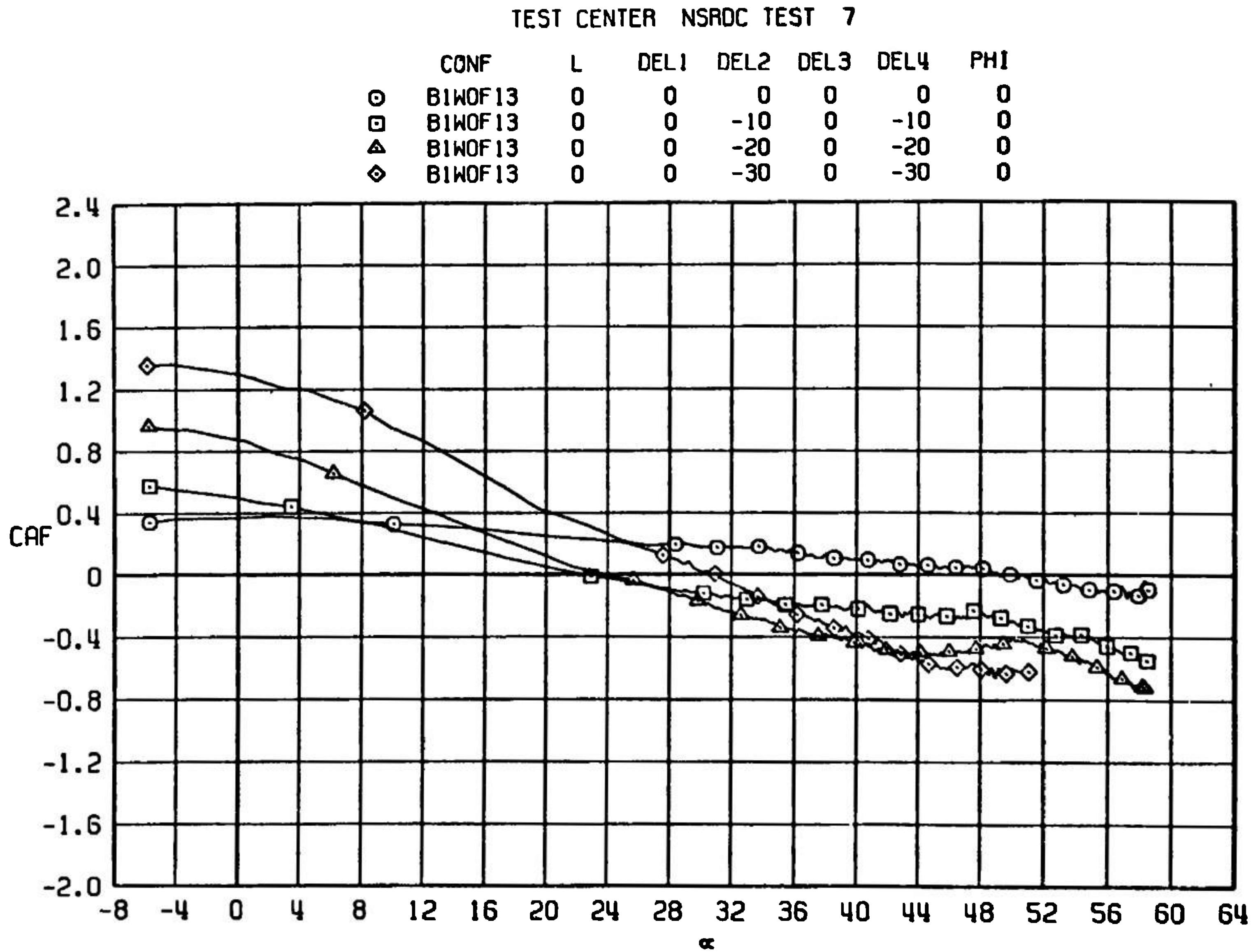

e. CAF versus α
Figure 66. Continued.

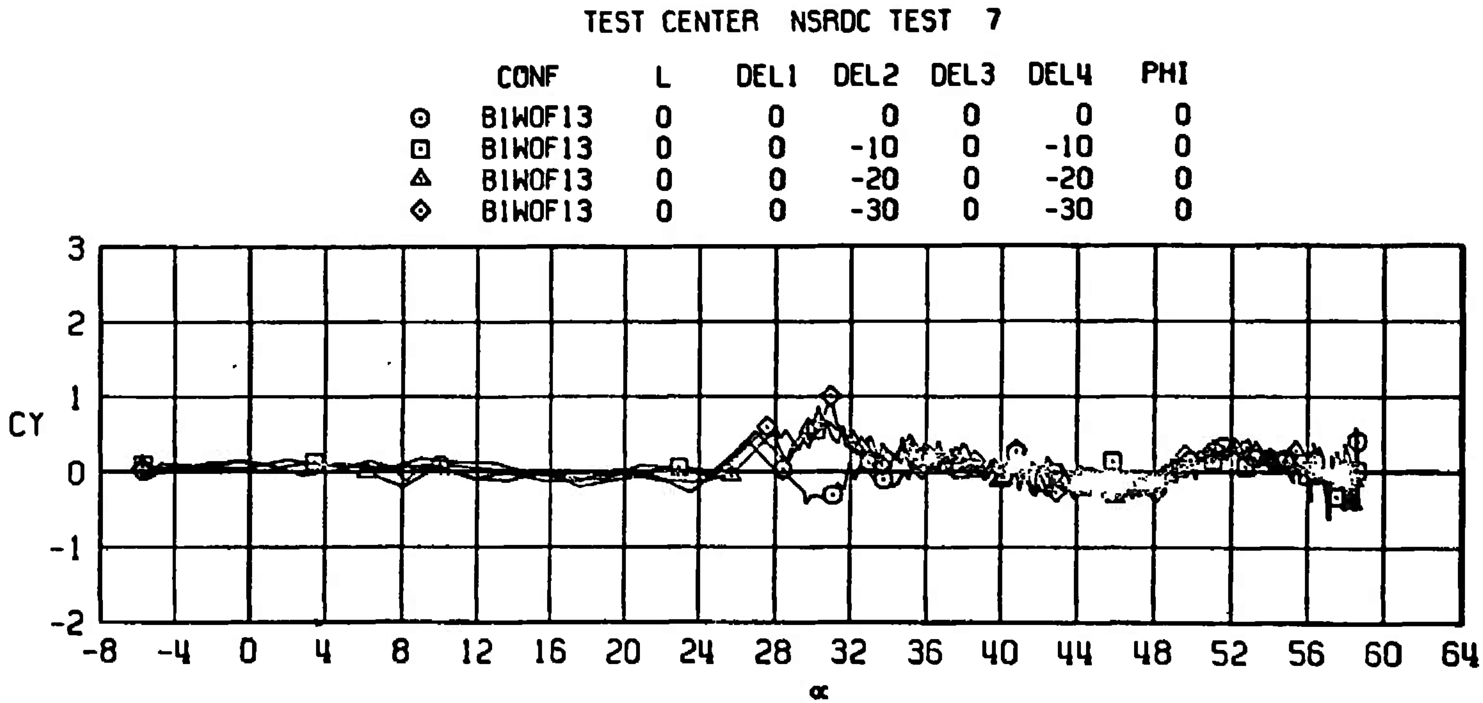

f. CY versus α

Figure 66. Continued.

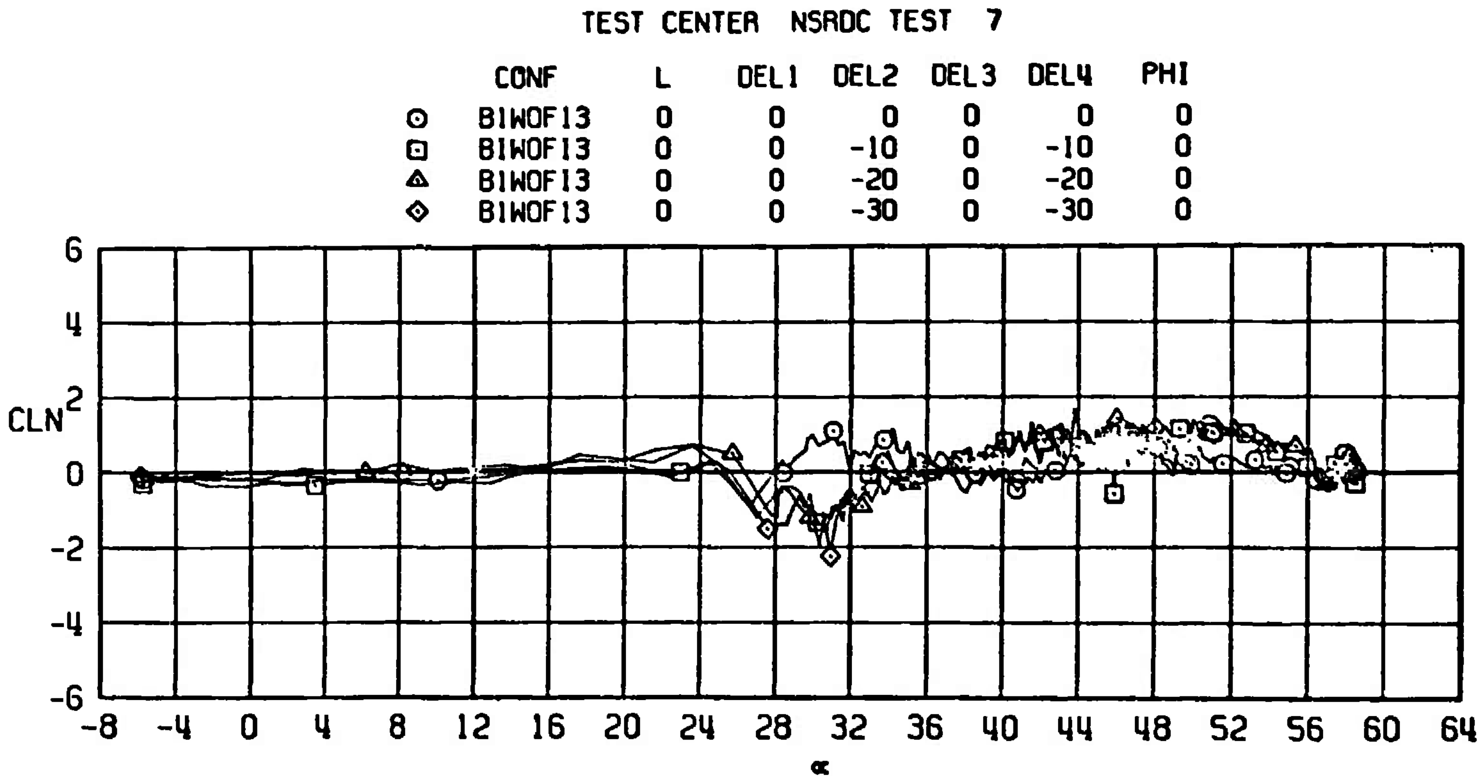

g. CLN versus α
Figure 66. Continued.

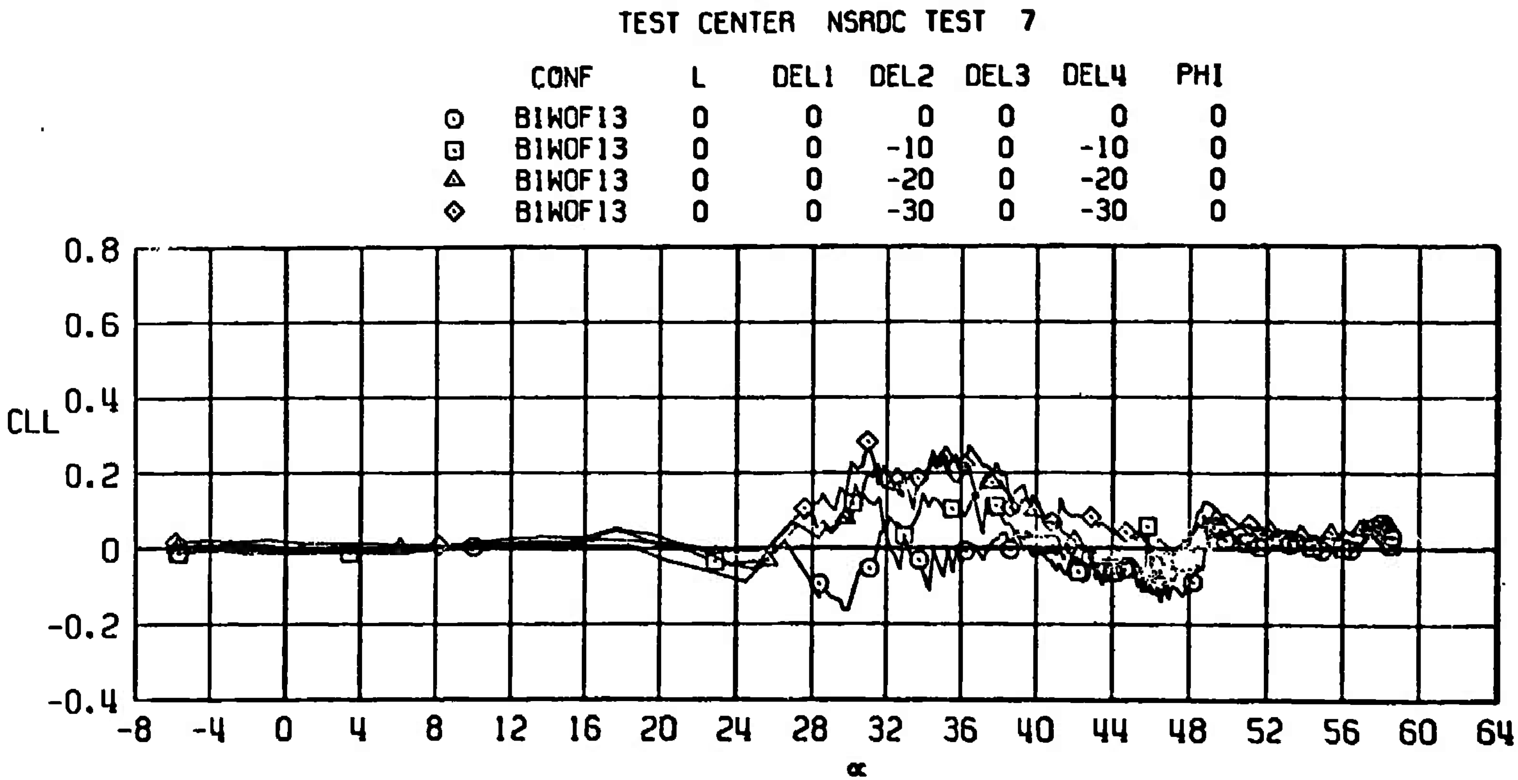

h. CLL versus α

Figure 66. Continued.

TEST CENTER NSRDC TEST 7

	CONF	L	DEL1	DEL2	DEL3	DEL4	PHI
⊙	B1W0F13	0	0	0	0	0	0
⊡	B1W0F13	0	0	-10	0	-10	0
△	B1W0F13	0	0	-20	0	-20	0
◇	B1W0F13	0	0	-30	0	-30	0

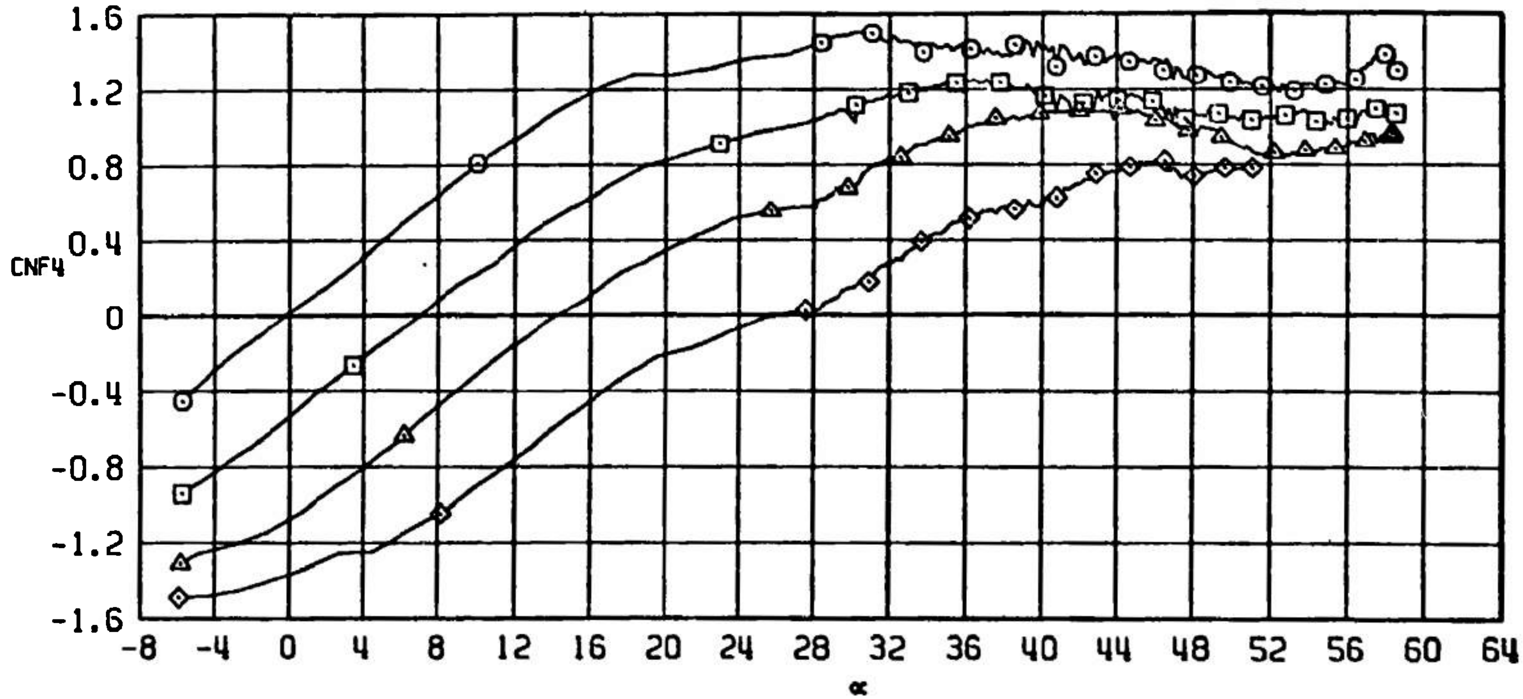

i. CNF4 versus α
Figure 66. Continued.

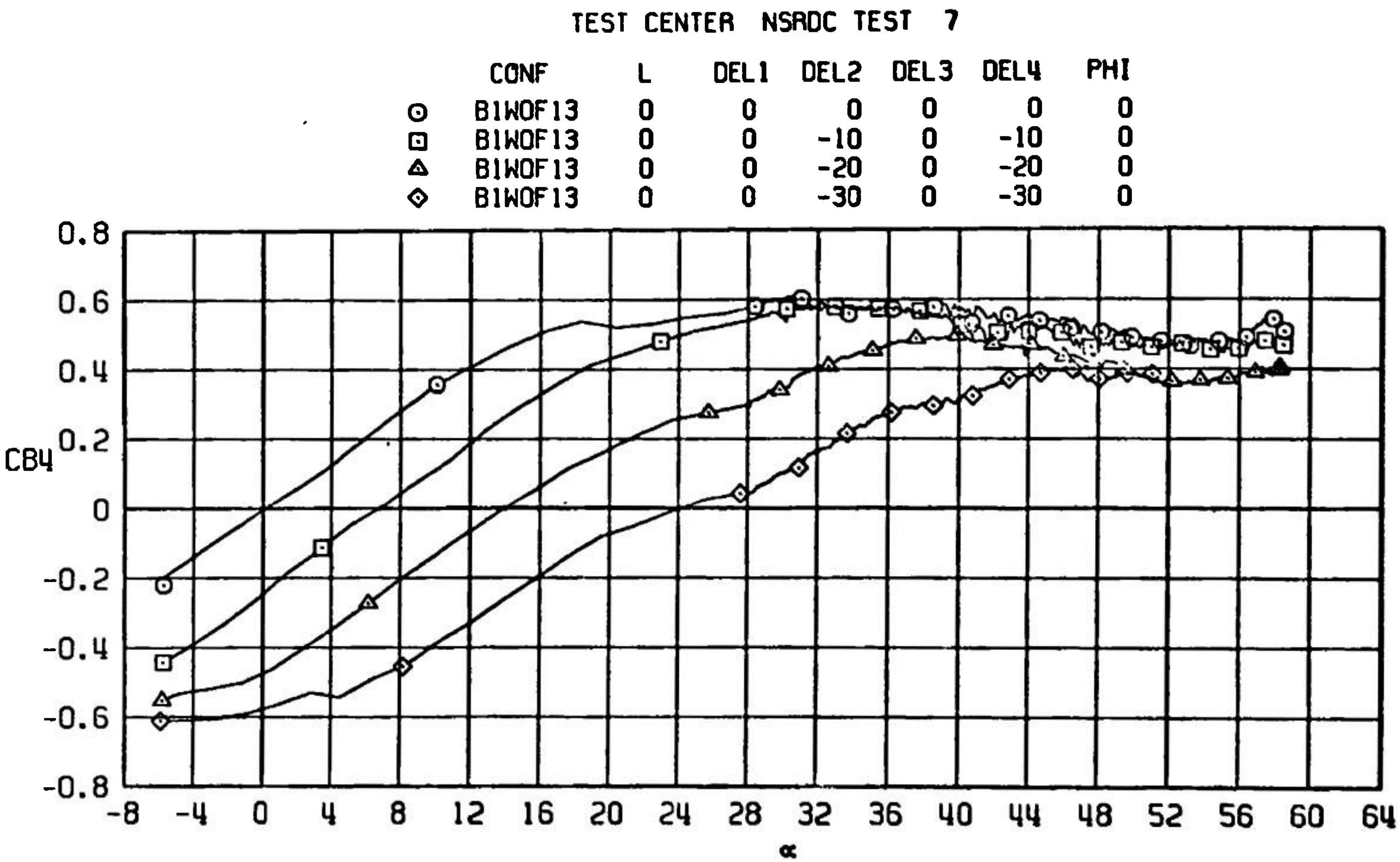

j. CB4 versus α
Figure 66. Continued.

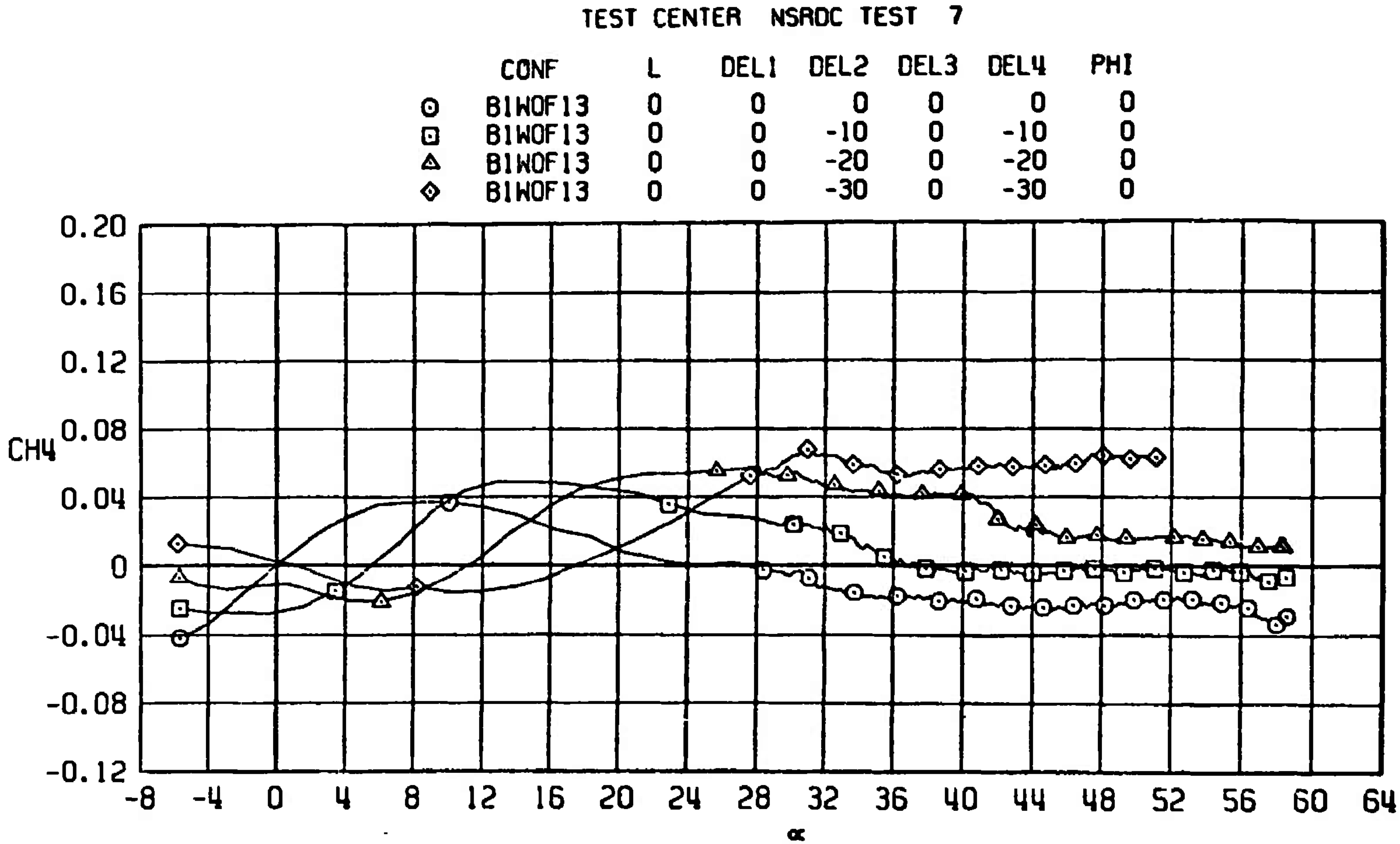

k. CH4 versus α
Figure 66. Concluded.

Table 1. Measured Dimensions of Each Tail Fin Configuration (All Fins)

Tail Fin No.	Conf.	b	C_R	C_T	X
1	F11	1.8784	3.7474	3.7474	1.6884
2	↓	1.8797	3.7477	3.7477	1.6859
3	↓	1.8768	3.7505	3.7505	1.6891
4	↓	1.8788	3.7516	3.7516	1.6903
Average	↓	1.8784	3.7493	3.7493	1.6884
1	F12	2.8050	5.6090	0	3.4703
2	↓	2.8135	5.6103	0	3.4712
3	↓	2.8127	5.6184	0	3.4794
4	↓	2.8068	5.6215	0	3.4852
Average	↓	2 8095	5.6148	0	3.4765
1	F13	2.8076	3.7472	1.8840	2.0533
2	↓	2.8141	3.7479	1.8720	2.0512
3	↓	2.8103	3.7514	1.8750	2.0586
4	↓	2.8124	3.7446	1.8950	2.0476
Average	↓	2.8111	3.7478	1.8815	2.0527
1	F14	1.8756	7.5193	0	4.6662
2	↓	1.8802	7.5394	0	4.6831
3	↓	1.8748	7.5098	0	4.6523
4	↓	1.8790	7.5305	0	4.6747
Average	↓	1.8774	7.5248	0	4.6690
1	F15	1.8735	4.9938	2.4990	2.7453
2	↓	1.8732	4.9951	2.4990	2.7489
3	↓	1.8755	4.9931	2.4930	2.7459
4	↓	1.8740	4.9925	2.5030	2.7431
Average	↓	1.8741	4 9936	2.4985	2.7458

Tail Fin No.	Conf.	b	C_R	C_T	X
1	F16	2.8072	2.8325	2.8305	1.2762
2	↓	2.8067	2.8319	2.8232	1.2767
3	↓	2.8069	2.8260	2.8256	1.2691
4	↓	2.8045	2.8292	2.8244	1.2732
Average	↓	2.8063	2.8299	2.8272	1.2738
1	F21	1.8760	1.8730	1.8730	0.8432
2	↓	1.8744	1.8741	1.8741	0.8423
3	↓	1.8728	1.8743	1.8743	0.8434
4	↓	1.8709	1.8726	1.8726	0.8427
Average	↓	1.8735	1.8735	1.8735	0.8429
1	F22	1.8794	3.7560	0	2.3279
2	↓	1.8803	3.7555	0	2.3265
3	↓	1.8736	3.7563	0	2.3274
4	↓	1.8749	3.7527	0	2.3232
Average	↓	1.8771	3.7551	0	2.3263
1	F23	1.8731	2.5600	1.3000	1.4036
2	↓	1.8589	2.5933	1.3220	1.4160
3	↓	1.8696	2.5593	1.2960	1.4018
4	↓	1.8765	2.5929	1.2900	1.4106
Average	↓	1.8695	2.5764	1.3020	1.4080
1	F31	1.8740	9.9490	5.0010	5.4553
2	↓	1.8675	9.8540	4.9800	5.4550
3	↓	1.8785	9.9327	4.9520	5.4419
4	↓	1.8666	9.9435	4.9750	5.4534
Average	↓	1.8717	9.9198	4.9770	5.4514

Tail Fin No.	Conf.	b	C_R	C_T	X
1	F32	1.8725	7.5008	7.5008	3.3758
2	↓	1.8274	7.4992	7.4992	3.3768
3	↓	1.8731	7.4973	7.4973	3.3729
4	↓	1.8761	7.5005	7.5005	3.3747
Average	↓	1.8623	7.4995	7.4995	3.3751
1	F33	4.3962	4.3971	4.3971	1.9791
2	↓	4.3723	4.3974	4.3956	1.9843
3	↓	4.3851	4.3967	4.3924	1.9829
4	↓	4.3788	4.3971	4.3960	1.9795
Average	↓	4.3831	4.3971	4.3953	1.9815
1	F34	4.3953	5.5601	2.8080	3.0384
2	↓	4.3962	5.5616	2.8020	3.0399
3	↓	4.3858	5.5685	2.7900	3.0496
4	↓	4.3939	5.5779	2.8140	3.0563
Average	↓	4.3928	5.5670	2.8035	3.0461
1	F35	4.3542	8.7100	0	5.3676
2	↓	4 3454	8.6789	0	5.3418
3	↓	4.3523	8.6914	0	5.3531
4	↓	4.3912	8.7273	0	5.3859
Average	↓	4.3608	8.7019	0	5.3621
1	F36	1.8890	14.9558	0	9.2537
2	↓	1 8817	14.9738	0	9.2716
3	↓	1.8850	14.9805	0	9.2790
4	↓	1.8553	15.0044	0	9.3025
Average	↓	1.8778	14.9786	0	9.2767

Table 2. Test Number 1 Data Uncertainties

ΔCN	ΔCLM	ΔCA	$\Delta\alpha$	ΔM_∞
±0.067	±0.078	±0.014	±0.1°	±0.005 for $M_\infty \leq 0.95$ ±0.010 for $0.95 < M_\infty \leq 1.3$

Table 3. Test Number 6 Data Uncertainties

ΔCN	ΔCLM	$\Delta CNF4$ $\Delta CNFI$	$\Delta CH4$ ΔCHI	$\Delta CB4$ ΔCBI	$\Delta\alpha$	ΔM_∞
±0.100	±0.020	±0.050	±0.007	±0.050	0.1°	±0.01

Table 4. Test Number 2 Body plus Fin Data Uncertainties

M_∞	Model Body			Fin F14			Fin F15			Fin F21			Fin F32			Fin F36		
	ΔCN	ΔCLM	ΔCA	ΔCNF4	ΔCH4	ΔCB4	ΔCNF4	ΔCH4	ΔCB4	ΔCNF4	ΔCH4	ΔCB4	ΔCNF4	ΔCH4	ΔCB4	ΔCNF4	ΔCH4	ΔCB4
0.80	0.021	0.105	0.012	0.015	0.004	0.008	0.015	0.005	0.008	0.020	0.026	0.013	0.013	0.002	0.007	0.013	0.002	0.007
0.85	0.019	0.100	0.012	0.013	0.003	0.008	0.013	0.005	0.008	0.019	0.025	0.012	0.011	0.002	0.006	0.011	0.002	0.006
0.92	0.017	0.094	0.011	0.011		0.007	0.011	0.005	0.007	0.018	0.024	0.012	0.009	0.002	0.005	0.009	0.001	0.005
0.98	0.015	0.089	0.010	0.010		0.006	0.010	0.004	0.006	0.016	0.023	0.011	0.008	0.002	0.004	0.008		0.003
1.10	0.014	0.083	0.010	0.008		0.005	0.008		0.005	0.014	0.021	0.010	0.006	0.001	0.003	0.006		0.002
1.20	0.012	0.079	0.009	0.007		0.005	0.007		0.005	0.013	0.021	0.009	0.005	0.001	0.003	0.005		0.002
1.30	0.012	0.077	0.009	0.007		0.005	0.007		0.005	0.013	0.020	0.009	0.004	0.001	0.002	0.004		0.002

Table 5. Test Number 2 Fin-Alone Data Uncertainties

M_∞	Fin F11			Fin F14			Fin F36		
	ΔCNF	ΔCH	ΔCB	ΔCNF	ΔCH	ΔCB	ΔCNF	ΔCH	ΔCB
0.80	0.026	0.015	0.013	0.026	0.008	0.013	0.026	0.004	0.013
0.85	0.024	0.015	0.012	0.024	0.007	0.012	0.024	0.004	0.012
0.92	0.022	0.014	0.011	0.022	0.007	0.011	0.022	0.004	0.011
0.98	0.021	0.013	0.011	0.021	0.007	0.011	0.021	0.003	0.011
1.10	0.019	0.012	0.010	0.019	0.006	0.010	0.019	0.003	0.010
1.20	0.018	0.012	0.009	0.018	0.006	0.009	0.018	0.003	0.009
1.30	0.018	0.012	0.009	0.018	0.006	0.009	0.018	0.003	0.009

Table 6. Test Number 2 Reynolds Number Study Data Uncertainties

M_∞	$R \times 10^{-6}$	Model Body			Fin F15		
		ΔCN	ΔCLM	ΔCA	ΔCNF4	ΔCH4	ΔCB4
0.59	0.3	0.160	1.072	0.124	0.089	0.053	0.062
	0.4	0.110	0.750	0.087	0.064	0.037	0.044
	0.7	0.069	0.439	0.051	0.041	0.021	0.027
	1.1	0.052	0.307	0.036	0.032	0.015	0.020
	1.3	0.044	0.244	0.028	0.029	0.012	0.017
	2.5	0.032	0.130	0.015	0.023	0.006	0.013
	3.5	0.029	0.105	0.012	0.022	0.005	0.012

Table 7. Listing of Part Numbers for the Tabulated Data of Test Number 1*

CONF	L	DEL1	DEL2	DEL3	DEL4	PHI	TRANSITION	R x 10^{-6}	α	β	Part Number															
											M_∞ 0.20	M_∞ 0.40	M_∞ 0.50	M_∞ 0.60	M_∞ 0.80	M_∞ 0.35	M_∞ 0.92	M_∞ 0.94	M_∞ 0.95	M_∞ 0.96	M_∞ 0.98	M_∞ 1.00	M_∞ 1.05	M_∞ 1.10	M_∞ 1.20	M_∞ 1.30
B4WOF12	0	0	0	0	0	0	Unknown	2.3	Vary	0					4	5	8	9 19		10	14		15	16	17	18
B4WOF13															22	24	30	31		32	33		34	35	36	37
B4WOF16															42	43	44	45		46	47		48	49	50	51
B4WOF22															57	58	61				62			64	65	66
B4WOF23															71	72	73				74			75	76	77
B4WOF21															82	83	84				87			90	91	92
B4WOF35															97	98 106	99				100			103	104	105
B4WOF34															111	112	115				117			118	119	120
B4WOF33															125	126	127	128		129	131			132	133	134
B4WOF32															139	140	141	142		143	144			150	151	152
B4WOF31															156	157	158				159			160	161	162
B4WOF11															166	167	168	169		170	171			172	173	174
B2WOF0		OFF	OFF	OFF	OFF										178	179	180				181			182	183	184
B5WOF0															187	188	189				190			191	192	193
B4WOF0															196	197	198				199			200	201	202
								Vary	23.5				205													
									12.0										206							
									9.0																	207
								3.9	30.0			210		211	212							213			214	
								2.0			220	219		218	217								216	215		
								3.8	Vary			223														

*No Tail Fin Data Presented

Table 8. Listing of Part Numbers for the Tabulated Data of Test Number 2*

CONF	L	OEL1	OEL2	OEL3	OEL4	PHI	TRANSITION	$R \times 10^{-6}$	α	β	Part Number								
											M_∞	M_∞	M_∞	M_∞	M_∞	M_∞	M_∞	M_∞	M_∞
											0.59	0.80	0.85	0.92	0.98	1.10	1.20	1.29	1.30
B3WOF0	0	OFF	OFF	OFF	OFF	0	Free	0.3	Vary	0	5								
								0.4			7								
								0.7			8								
								1.1			9								
								1.3			10								
								1.8			11								
								2.6			12								
								3.5			14								
								4.3			15								
								4.9			16								
B3WOF15		0	0	0	0		Fixed	0.3			24								
								0.4			26								
								0.7			27								
								1.1			31								
								1.3			32								
								3.4			33								
						180		0.3			36								
								0.4			37								
								0.7			38								
								1.1			39								
								1.3			40								
								3.4			41								
						0	Free	0.4			47								
								0.7			48								
								1.1			49								
								3.4			50								
								2.5				57	58	59	60	61	62	63	
83WOF14												69	70	71	72	73	74		75
83WOF21												80	81	82	83	84	85		86
83WOF36												91	92	93	94	95	96		98
83WOF32												105	106	107	108	109	110		111
						Splitter Plate Offset Angle													
B0WOF14	—	—	—	—	—	0	Free	2.5	Vary	—		123	155	162	171	130	144		137
						15								163					
						30						124	156	164	172	131	145		138
						60						125	157	166	173	132	146		139
						90						126	158	167	174	133	147		140
						120						127	159	168	175	134	148		141
						150						128	160	169	176	135	149		142
						180						129	161	170	177		150		143
B0WOF11						0						184	194	201	272	279	287		294
						30						185	195	202	273	280	288		295
						60						186	196	203	274	281	289		296
						90						187	197	204	275	282	290		297
						120						188	198	269	276	283	291		298
						150						189	199	270	277	284 285	292		299
						180						190	200	271	278	286	293		300
B0WOF36						0						208	215	223	230	240	247		257
						15													258
						30						209	217	224	231	241	248		259
						60						210	218	225	234	242	249		260
						90						211	219	226	235	243	250		261
						120						212	220	227	236	244	251		262
						150						213	221	228	237	245	252		263
						180						214	222	229	238	246	253		264

*After Part Number 111, Only Splitter Plate Oata Presented

Table 9. Listing of Part Numbers for the Tabulated Data of Test Number 3*

CONF	L	DEL1	DEL2	DEL3	DEL4	PHI	TRANSITION	R x 10^{-6}	α	β	Part Number M_∞ 2.36	M_∞ 2.86	M_∞ 3.95	M_∞ 4.63
BIWOF35	0	0	0	0	0	0	Fixed	3.0	Vary	0	19	22	24	25
			↓		↓	45					20	21	23	26
		↓	-20	↓	-20	0		↓			27	28	29	30
		20		20		45		2.5			31			
↓								3.0				32	33	34
BIWOF34								2.5			35			
		↓		↓		↓		3.0				36	37	38
↓		0		0		0					39	40	41	42
BIWOF33		↓		↓		↓		↓			43	44	45	46
		20		20		45		2.5			47			
		↓	↓	↓	↓	↓		3.0				48	49	50
		0	0	0	0	0		2.9			51			
						45		↓			52			
						↓		3.2				53		
						0		↓				54		
						45		3.0					55	58
↓						0							56	57
BIWOF34											59	62	64	65
↓	↓					45					60	61	63	66
BIWIF34	15.42					↓					68	69	71	74
		↓	↓	↓	↓	0					67	70	72	73
		0	-20	0	-20	↓		↓			75	76	77	78
		20		20		45		2.5			79			
↓		↓	↓	↓	↓			3.0				80	81	82
BIWIF0		OFF	OFF	OFF	OFF	↓					84	85	89	92
↓	↓					0					83	86	90	91
BIWOF0	0	↓	↓	↓	↓	↓	↓	↓	↓	↓	93	94	95	

* No Tail Fin Data Presented

Table 10. Listing of Part Numbers for the Tabulated Data of Test Number 4*

CONF	L	DEL1	DEL2	DEL3	DEL4	PHI	TRANSITION	$R \times 10^{-6}$	α	β	Part Number M_∞ 2.36	M_∞ 2.86	M_∞ 3.95	M_∞ 4.63
B2W0F34	0	0	0	0	0	0	Fixed	3.0	Vary	0	2	5	7	8
↓						-90					3	4	6	9
B2W0F35						0					12	11	13	10
B2W0F33			↓		↓						16	17	14	15
B2W0F34			-20		-20						18	19	20	21
B2W0F35											22	23	24	25
B2W0F33		↓	↓	↓	↓	↓						26		
		20	0	20	0	-90		↓				28	29	30
↓								2.0			27			
B2W0F31								3.0			34	35	36	37
B2W0F32											38	39	40	41
B2W0F36	↓	↓	↓	↓	↓	↓	↓	↓	↓	↓	43	42	44	45

* No Tail Fin Data Presented

Table 11. Listing of Part Numbers for the Tabulated Data of Test Number 5*

CONF	L	DEL1	DEL2	DEL3	DEL4	PHI	TRANSITION	$R \times 10^{-6}$	α	β	Part Number M_∞ 1.50	Part Number M_∞ 1.80	Part Number M_∞ 2.16
B0W0F35	—	—	—	—	—	—	Fixed	1.8	Vary	—	2	3	
↓								2.5					4
B0W0F34								1.8			5	6	
↓								2.5					7
B0W0F31								1.8			8	9	
↓								2.5					10
B0W0F32								1.8			11	12	
↓								2.5					13
B0W0F36								1.8			14	15	
↓								2.5					16
B0W0F11								1.8			17	18	
↓								2.5					19
B0W0F15								1.8			20	21	
↓								2.5					22
B0W0F14								1.8			23	24	
↓								2.5					25
B0W0F13								1.8			26	27	
↓								2.5					28
B0W0F16								1.8			29	30	
↓	↓	↓	↓	↓	↓	↓	↓	2.5	↓	↓			31

* Only Splitter Plate Data Presented

Table 12. Listing of Part Numbers for the Tabulated Data of Test Number 6

CONF	L	DEL1	DEL2	DEL3	DEL4	PHI	TRANSITION	R x 10^{-6}	α	β	Part Number M_∞ 0.85	M_∞ 0.92	M_∞ 0.97	M_∞ 1.01	M_∞ 1.05	M_∞ 1.10
B2W0F16	0	0	0	0	0	0	Fixed	1.7	Vary	0	1	2	3	4	5	6
B2W0F13											7	8	9	10	11	12
B2W0F12											13	14	15	16	17	18
									3	Vary	19					
									6		20					
									9		21					
									12		22					
									15		23					
									18		24					
B2W2F0	16.75	OFF	OFF	OFF	OFF				Vary	0	25	26	27	28	29	30
B2W1F0	15.40										31	32	33	34	35	36
B2W3F0	16.75										37	38	39	40	41	42
B2W3F12		0	0	0	0						43	44	46	47	48	49
B2W2F12											57	50	51	52 56	53 55	54
B2W1F12	15.40										58	59	60	61	62	63
B2W0F13	0	30	0	30					0	Vary	64	65	66	67	68	69
B2W0F12													71	72	73	74
B2W0F16											75	76	77	78	79	80
		20		20							81	82	83	85	86	87
		10		10							88		91	92	93	94
B2W0F0		OFF	OFF	OFF	OFF				Vary	0	95	96	97	98	99	100
B2W0F13		10	0	10	0				0	Vary	102	103	104	105	106	107
		20		20							108	109	110	111	112	113
B2W0F12											114	115	116	117	118	119
		10		10							120	121	122	123	124	125
		0		0							140	148	156	164	172	180
									3		141	149	157	165	173	181
									6		142	150	158	166	174	182
									9		143	151	159	167	175	183
									12		144	152	160	168	176	184
									15		145	153	161	169	177	185
									18		145	154	162	170	178	186
									21		147	155	163	171	179	187

Table 13. Listing of Part Numbers for the Tabulated Data of Test Number 7

CONF	L	DEL1	DEL2	DEL3	DEL4	PHI	TRANSITION	$R \times 10^{-6}$	α	β	Part Number M_∞ 0.80	Part Number M_∞ 0.90	Part Number M_∞ 1.00	Part Number M_∞ 1.10
BIWOF23	0	0	0	0	0	0	Unknown	1.7	Vary	0	2	5	8	10
↓						45					4	6	9	11
BIWOF11						0					28	30	33 34	37
↓						45					29	32	35	36
BIWOF34						0					39	41	44	45
↓						45					40	42	43	46
BIWOF14						0					47	50	51	54
↓						45					48	49	52	53
BIWOF15						0					55	58	59	62
↓						45					56	57	60	61
BIWOF13						0					63	66	67	70
↓						45					64	65	68	69
BIWOF31						0					71	74	75	79
↓						45					72	73	76	77
BIWOF0		OFF	OFF	OFF	OFF	0					85	86	87	
BIWOF31		0	-10	0	-10						90	91	92	93
BIWOF23											94	95	96	97
BIWOF11											98	99	100	101
BIWOF14											102	103	104	105
↓			-30		-30						106	107	108	109
BIWOF15											110	111	112	113
BIWOF13											114	115	116	117
BIWOF31											118	119	120	121
BIWOF34											122	123	124	125
BIWOF23											126	127	128	129
BIWOF11											130	131	132	133
↓			-20		-20						135	136	137	138
BIWOF14											140	141	142	143
BIWOF15											144	145	146	147
BIWOF23											148	149	150	151
BIWOF13											152	153	154	155
BIWOF31											156	157	158	159
BIWOF34											160	161	162	163
↓			-10		-10						164	165	166	167
BIWOF13											168	169	170	171
BIWOF15											172	173	174	175

NOMENCLATURE

A	Streamwise length of beveled portion of fin leading edge, in. (see Fig. 6)
ALPHA (α)	Model angle of attack, deg
AR	Fin aspect ratio, b^2/S_F
B	Streamwise length of beveled portion of fin trailing edge, in. (see Fig. 6)
BETA (β)	Model angle of sideslip, deg
b	Tail fin span, measured from the root chord to the tip, in. (see Fig. 6)
CA	Axial-force coefficient, measured axial force/$q_\infty S$
CAB	Base axial-force coefficient, $(p_\infty - p_b)/q_\infty$
CAF	Forebody axial-force coefficient, CA - CAB
CB	Splitter plate tail fin root bending-moment coefficient, fin bending moment/$q_\infty S_F b$
CB1, CB2, CB3, CB4	Root bending-moment coefficient of tail fins No. 1, 2, 3, and 4, respectively, fin bending moment/$q_\infty S_F b$
CH	Splitter plate tail fin hinge-moment coefficient, hinge moment/$q_\infty S_F C_R$
CH1, CH2, CH3, CH4	Hinge-moment coefficients of tail fins No. 1, 2, 3, and 4, respectively, fin hinge moment/$q_\infty S_F C_R$
CLL	Rolling-moment coefficient, rolling moment/$q_\infty Sd$
CLM	Pitching-moment coefficient, pitching moment/$q_\infty Sd$ (moment reference point located on centerline at 50 percent of model body length)
CLN	Yawing-moment coefficient, yawing moment/$q_\infty Sd$
CN	Normal-force coefficient, normal force/$q_\infty S$

CNF	Splitter plate tail fin normal-force coefficient, fin normal force/$q_\infty S_F$
CNF1, CNF2, CNF3, CNF4	Normal-force coefficient of tail fins No. 1, 2, 3, and 4, respectively, fin normal force/$q_\infty S_F$
CONF	Model configuration identification
C_R	Tail fin root chord, in. (see Fig. 6)
C_T	Tail fin tip chord, in. (see Fig. 6)
C_Y	Side-force coefficient, side force/$q_\infty S$
d	Model body maximum diameter, in. (see Fig. 3)
DEL1, DEL2, DEL3, DEL4	Deflection of tail fins No. 1, 2, 3, and 4, respectively, deg
L	Distance between model nose and the intersection of the wing leading edge with the body (measured parallel to the body centerline), in.
MACH (M_∞)	Nominal free-stream Mach number
PART	Data indexing number
PHI	Model roll angle, deg
POINT	Data indexing number per part number
p_b	Average static pressure at model base, psfa
p_∞	Free-stream static pressure, psfa
q_∞	Free-stream dynamic pressure, psf
R	Nominal Reynolds number per foot
S	Maximum body cross-sectional area, ft^2
S_F	Tail fin planform area, ft^2 (see Fig. 6)
TEST	Test identification number
T_R	Tail fin root thickness, in. (see Fig. 6)

TRANSITION	Transition identification
X	Distance from fin root chord leading edge to fin hinge line, in. (see Fig. 6)
XCP	Missile body center-of-pressure location, CLM/CN
XCPF	Splitter plate fin longitudinal center-of-pressure location, CH/CNF
XCPF1, XCPF2 XCPF3, XCPF4	Longitudinal center-of-pressure location of tail fins No. 1, 2, 3, and 4, respectively, hinge moment/fin normal force
YCPF	Splitter plate fin lateral center-of-pressure location, CB/CNF
YCPF1, YCPF2 YCPF3, YCPF4	Lateral center-of-pressure location of tail fins No. 1 2, 3, and 4. respectively, root bending moment/fin normal force
Λ	Tail fin leading-edge sweep angle (see Fig. 6)
λ	Tail fin taper ratio, C_T/C_R